Fifth Symposium

NAVAL HYDRODYNAMICS

SHIP MOTIONS
DRAG REDUCTION

PROFESSOR J. K. LUNDE
STANLEY W. DOROFF
EDITORS

Office of Naval Research
Department of the Navy
ACR-112

Fifth Symposium on

NAVAL HYDRODYNAMICS

SHIP MOTIONS AND DRAG REDUCTION

Sponsored by the

OFFICE OF NAVAL RESEARCH

and the

SKIPSMODELLTANKEN

September 10-12, 1964

Bergen, Norway

ACR-112

OFFICE OF NAVAL RESEARCH—DEPARTMENT OF THE NAVY

Washington, D.C.

PREVIOUS REPORTS IN THE NAVAL HYDRODYNAMICS SERIES

1. "First Symposium on Naval Hydrodynamics," National Academy of Sciences - National Research Council, Publication 515, 1957, Washington, D.C.; $5.00.

2. "Second Symposium on Naval Hydrodynamics," Office of Naval Research, Department of the Navy, ACR-38, 1958; Superintendent of Documents, U.S. Government Printing Office, Washington, D.C., Catalog No. D210.15:ACR-38; $4.00.

3. "Third Symposium on Naval Hydrodynamics," Office of Naval Research, Department of the Navy, ACR-65, 1960; Superintendent of Documents, U.S. Government Printing Office, Washington, D.C., Catalog No. D210.15:ACR-65; $3.50.

4. "Fourth Symposium on Naval Hydrodynamics," Office of Naval Research, Department of the Navy, ACR-92, 1962; Superintendent of Documents, U.S. Government Printing Office, Washington, D.C., Catalog No. D210.15:ACR-92; $6.75.

5. "The Collected Papers of Sir Thomas Havelock on Hydrodynamics," Office of Naval Research, Department of the Navy, ONR/ACR-103, 1963; Superintendent of Documents, U.S. Government Printing Office, Washington, D.C., Catalog No. D210.15:ACR-103; $4.50.

For sale by the Superintendent of Documents, U.S. Government Printing Office
Washington, D.C., 20402 - Price $7.25

PREFACE

This Symposium is the fifth in a series each of which has been concerned with various aspects of Naval Hydrodynamics. The first (held in September 1956) presented critical surveys of Hydrodynamics that are of significance in naval science. Subsequent meetings were to be devoted to one or more topics selected on the basis of importance and need for research stimulation, or of particular current interest.

In keeping with this objective, the second symposium (August 1958) had for its subject the areas of hydrodynamic noise and cavity flow; the third (September 1960) was concerned with the area of high performance ships; and the fourth (August 1962) emphasized the topics of propulsion and hydroelasticity.

Still continuing with the original plan, the present symposium selected for its dual theme the areas of ship motions and drag reduction, thus emphasizing, among other things, the interest in the current problems and latest accomplishments associated with: theoretical and experimental determination of the coefficients of the equations governing the motions of ships in a seaway; the characteristics and design of motion stabilizers; the reduction of frictional resistance by the introduction of additives; and the design of bulbous bows to reduce wave drag.

The international flavor of these meetings continues to be an outstanding feature, and in this case, has been enhanced by virtue of the setting, the participation, and most particularly by the joint sponsorship by the Skipsmodelltanken of Trondheim, Norway and the U.S. Office of Naval Research.

The address of welcome by Dr. Weyl and the speech opening this symposium by H.R.H. Crown Prince Harald more than adequately describe the background and objectives of this meeting, thus leaving little more to be said other than to express our gratitude to all those who contributed so much to the success of this symposium. However, taking the liberty of speaking both for the Office of Naval Research as well as the international scientific community of hydrodynamicists, I should like once again to express our deepest appreciation to Professor J. K. Lunde, to his associates Dr. H. Aa. Walderhaug and Mr. O. Skjetne, and to the Norwegian Ship Model Experiment Tank, Trondheim for their outstanding efficiency and care in managing the many varied aspects of this symposium.

Ralph D. Cooper

RALPH D. COOPER, Head
Fluid Dynamics Branch

CONTENTS

ADDRESS OF WELCOME

F. J. Weyl
Deputy and Chief Scientist
Office of Naval Research
Washington, D.C.

Your Royal Highness, Professor Lunde, fellow wayfarers on the road to Bergen: It is my pleasure in the name of the Norwegian Ship Model Experiment Tank and the United States Office of Naval Research to bid you welcome at this our goal. We are most appreciative for this opportunity of descending, maybe a bit disorganized but full of friendliness, upon your country; and we look forward to discovering more of its social fabric, its forests and fjords. Perhaps we are, inadvertently, redressing in these latter days a long term balance by the confusion we may cause in your hostelries and shops in return for that caused by visits which were made from these parts to very nearly the whole of the here-represented world during the centuries of Norway's birth. Most deeply grateful we are to the staff of Skipsmodelltanken, its distinguished director, Professor Lunde, and his associates, for having taken on the task of being host for the Symposium, and thus to look after our well-being, both temporal and spiritual, during our days in Bergen. We shall express our thanks in work reported and new endeavors initiated, in legends told and traditions started.

The ocean is a strange and wondrous thing, not only to the historian who traces the role which it has played in the fates of men and people, but no less to the scientist. Let us first give a look at its geometry. Its characteristic horizontal dimension exceeds its depth by three orders of magnitude. Bounded by the atmosphere above, it presents a mightily agitated surface. Massive currents and huge eddies characterize the motion of the basins, driven by gravity and the rotation of the earth. Unexplored heat transfer phenomena across its bottom vitally influence the energy balance. In short, it is all boundary and yet presents itself so unbounded.

To a technology peculiarly matched to life in the atmosphere where the signal speed is that of light and even the fastest form of locomotion constitutes but one thousandth of one percent of this speed, the ocean again presents a radically different concert of parameters. Opaque to electromagnetic radiation, the characteristic mode of signal transmission is acoustic. Complicated reflection and refraction phenomena are caused by the layer structure, multipath phenomena obscure reception, and scattering is a fact of life rather than being encountered at the very fringe of usefulness of the information carrier. Moreover, measured in terms of signal speed, locomotion is now two orders of magnitude faster than in our wonted atmospheric medium.

Lastly, let me point out the tremendous range of time scales encountered in the dynamic behavior of the oceans. The waves and wave patterns on the surface cover a range from minutes to days. The large currents and the eddies which they generate show an erratic behavior whose large scale changes are measured in weeks and months. Seasonal variations characterize the major features of stratification; and finally, in the deepest layer of the oceans, memory appears to be measured in centuries.

All of this presents us with engineering challenges and tasks of tremendous scope, of which those so ingeniously solved with ever increasing competence by the designers and developers of ships are but a small yet highly characteristic part. Reaching out towards an ultimate goal, where we can freely traffic and go about such business as we may choose throughout the volume of the oceans, an exciting spectrum of new problems and opportunities opens up to scientist and engineer alike. The integrity of the hull requires that new ground be broken in the physics of materials, in the ingenious invention of geometries, and in advancing processes of fabrication. Propulsion and maneuver control place demands on the marine engineer which force him to look to the very boundaries of science and in many instances beyond before he will be confidently able to meet them. And, finally, there are the pioneering adventures in experimentation and instrumentation which alone can secure for us the scientific knowledge and the operational experiences that are prerequisite for ultimate mastery of the medium. Viewed in this light, the preoccupations, past and future, which will constitute the substance of our discussions here during the next few days, appear as an advanced salient of an onward sweeping front of competence and knowledge which we shall surely see broadened with great vigor during our lifetimes.

In short, to quote with slight adaptation the modern American lyric poet, E. E. Cummings: "There's a hell of a nice universe out there, let's go!"

His Royal Highness, the Crown Prince of Norway, has graciously accepted our invitation to come here and to open this the 5th Symposium on Naval Hydrodynamics. We are most particularly appreciative of the fact that, even with the duties and responsibilities of Head of State on his shoulders now during the King's absence, he has consented to be with us this morning, giving added significance to the occasion. I have, therefore, the honor at this time to call on His Royal Highness to open the proceedings.

OPENING ADDRESS

H.R.H. Crown Prince Harald of Norway

Mr. Chairman,
Ladies and Gentlemen,

May I firstly thank Dr. Weyl for his kind words of welcome. Perhaps it is typical of the universality and internationalism of our times – and indeed a promising feature – that an American scientist should address us here in Bergen, Norway, in his capacity as Host.

My father, His Majesty The King, who addressed a similar symposium – the 7th International Conference on Ship Hydrodynamics – ten years ago in Oslo, has asked me to bring you all his greetings and best wishes for a successful and enjoyable stay – both beneficial to science and conducive to pleasure.

As a user – one of those who benefit, or suffer, as a result of your findings – I am particularly happy to be here today. I have no doubts that the great majority of ideas tested are found not suitable – perhaps even dangerous – and thereby you spare us anxiety and economic losses. On the other hand, we live in a competitive world – in politics, in economics and in sports. When a new idea is thought of and found fruitful, we, the users, would like to keep it to ourselves. You have the scientific attitude; you like to share your findings, for the betterment of mankind, to develop your findings, and indeed to further the science you represent.

The world has come a long way from pieces of wood drifting in rivers and on the sea, thereby giving man the idea to try to float himself on the first raft or boat.

Sturdiness and stability, particularly in the serious and often fatal question of top-weight, were the first problems to be solved. Then followed a long epoch of the shipbuilder as an artist, and now science has more and more taken over. The modern shipbuilder is no more a fifth generation artist in his field with a saw and axe, but a serious, studious mathematician with drawingboard and slide rule.

Perhaps we have come too far; perhaps we shall have to take one or several steps back, searching for something important overlooked in the rapid development. That in itself may be one of the findings, here or elsewhere.

I wish you all every success in your endeavours to improve ships and boats for the benefit of all. May your discussions be fruitful and not too long.

When you leave may you feel that you have benefited technically, and also that you have made good contacts and established friendships.

With every good wish to all of you for a useful, successful and pleasant congress and stay, I declare the Fifth Symposium on Naval Hydrodynamics to be opened.

INTRODUCTORY REMARKS

G. P. Weinblum
Institut für Schiffbau der Universität
Hamburg, Germany

Ten years ago the International Towing Tank Conference held a meeting in Oslo. At that time, I had the privilege of lecturing on the subject, ship motions, before His Royal Highness Crown Prince Olaf now His Majesty the King. It is a highlight of my professional career that today in your Royal Highness' presence a team of gifted younger scientists will report on the impressive progress reached in our field during the recent years. They will prove the well established fact that we, in engineering sciences, usually overestimate what can be accomplished within one year but fortunately underrate what can be done within ten years.

Now that your Royal Highness has graciously opened the session we shall start immediately with our work.

Our kind hosts have carefully included short curricula of the lecturers in the abstracts. Thus the need for introducing the speakers to the auditorium is eliminated. There is another reason why it is perhaps not so important to follow this well established habit of introduction: although our young speakers have already reached a high scientific reputation, their future is still more important to our profession than their past.

Calling now Dr. Ogilvie, the head of the Free Surface Phenomena Branch of the David Taylor Model Basin in Washington, D.C., to deliver his lecture. It is my pleasant duty to emphasize that during his stay as liaison scientist of the Office of Naval Research in London he has earned universal esteem and friendship.

Thursday, September 10, 1964

Morning Session

SHIP MOTIONS

Chairman: G. P. Weinblum

Institut für Shiffbau der Universität
Hamburg, Germany

221-249 O - 66 - 2

RECENT PROGRESS TOWARD THE UNDERSTANDING AND PREDICTION OF SHIP MOTIONS

T. Francis Ogilvie
David Taylor Model Basin
Washington, D.C.

ABSTRACT

Since the Symposium on the Behavior of Ships in a Seaway (Wageningen, 1957), many papers have been published on the theory of ship motions. The present paper is a survey, collation, and evaluation of those contributions which have led toward a rational theory for predicting ship motions.

During this period, evidence has accumulated which demonstrates the validity of the superposition principle for ship motions in a seaway. This concept was stated as hypothesis eleven years ago by St. Denis and Pierson (and also sixty years ago by R. E. Froude); its validity may now be considered as proven, beyond the fondest hopes of earlier investigators.

With this principle established, attention once again returns to the prediction of motions in small-amplitude regular waves. The best practical approach to making ship motions predictions is probably still through use of strip theory. However, the two-dimensions assumptions of strip theory are so pervasive that the validity of the resulting analysis is always questionable except in the most routine problems.

In the past decade, the concept of the thin ship has been extensively applied to ship motions problems. Many elements in the complete picture have been developed on this basis, and in addition, thin-ship theory has been highly systematized. This latter effort, involving the establishment of a rigorous development of the theory on a set of carefully stated assumptions, has pointed up some basic shortcomings in applying thin ship ideas to motions problems.

Very recently, much attention has been devoted to developing a slender ship theory for predicting motions. The motivation and basic ideas are discussed; more thorough consideration will be found in other papers at this symposium.

INTRODUCTION

Background

The hydrodynamic theory of ships was born in the last half-decade of the nineteenth century, and it was a spectacular beginning, for within three years there appeared three papers by Krylov and the famous paper by Michell. Unfortunately, the response to these papers was not what they deserved, and many years passed before naval architects again considered their problems as scientific problems. We look back and see a few hardy souls struggling to progress against the apathy of their own profession. Not until almost 1950 was there a general renaissance of interest in the possibility of finding scientific solutions to the naval architect's hydrodynamics problems.

Then, in 1953-4, there was another spectacle comparable to the one over fifty years earlier. In these two years there appeared the papers by St. Denis and Pierson (1953) and Peters and Stoker (1954). The former suggested the procedure for relating to reality the highly idealized hydrodynamic theory of ship motions (as it then existed). The latter provided a logical foundation for this idealized theory and, in particular, it set forth clearly the hypotheses involved.

Neither of these two papers presented the final words on the subject; on the contrary, each raised more questions than it answered. But these authors were more fortunate than Krylov and Michell, for their papers were followed by an explosion of activity. By 1957, it was possible for the Netherlands Ship Model Basin to sponsor a symposium on seakeeping at which there were presented nearly fifty papers, some on the most basic scientific aspects of seakeeping problems.

Now, seven years later, we have again come together to (1) assess our progress, (2) discuss our latest findings, and (3) orient ourselves toward further discoveries on "the way of a ship in the midst of the sea." My own purpose is concerned primarily with the first of these three, viz., to look back over the last few years and attempt to evaluate our progress. I shall be discussing already published work almost exclusively. Of course, I cannot ignore work that is in progress, but a few words on such will suffice, for other speakers here are ready and willing to present their latest findings. Neither can I ignore the future, and in fact my whole presentation will be somewhat biased towards what I consider the most auspicious recent trends in research in our field.

Scope

In naval architecture, as in all branches of engineering, the designer is faced with immediate demands. During the past decade it has become evident that it would be not only desirable but perhaps even feasible to calculate the motions of a ship, given only a geometrical description of the ship and adequate information about its sea environment. Of course, shipbuilders and shipowners want this information now, and so it has been incumbent on the naval architecture profession to produce techniques as good as the state of the art allows.

Some important results have been obtained in this effort. However, my presentation is not very closely related to these efforts, for I shall discuss progress toward what I call a "scientific solution" of the problems of ship motions.

Perhaps I should be more specific in defining a "scientific solution." By this I mean that one starts with a mathematical model of the fluid. It may be — and in fact must be — a highly idealized model, but the implications of the idealization are probably well-understood in a general sense. To this mathematical model, one must add a set of boundary conditions and also possibly initial conditions, all of which should be stated as precisely and accurately as possible. Even though the fluid is represented by an idealized model, the resulting problem is always intractable. Therefore one must put forth a set of additional assumptions which reduces the problem to manageable proportions. When this analytical problem has been solved, one makes calculations and compares them with experimental data. There will be discrepancies, and so one goes all the way back to the beginning and tries to relax one of the restrictive assumptions, find a more general solution, etc., etc.

Two parts of this process qualify it as a "scientific solution" by my definition, viz., all of the assumptions are stated at the beginning, and improvements are made by modifying the assumptions rather than by trying empirically to patch up faulty results.

In practice, the engineer may not have the time to do all of this, or it may be simply impossible. Still, he must make predictions. So, if he is a good engineer, he improves his first poor predictions in any way he sees fit. This progress requires great ingenuity and skill, and its accomplishment is an essential element in the working of our technocracy. However, I shall not discuss such attempts, important though they may be. Other speakers here are much better qualified for this, and I leave it to them.

Summary of Contents

Generally speaking, we wish ultimately to supply certain statistical information to the ship designer. We may justify such an approach either by reasoning that he cannot really use more precise information or by accepting the fact that we cannot hope to provide anything better. In either case, we begin with a statistical description of the sea, assuming that the water motion can be described as the sum of many simple sinusoidal waves, each of which is described separately by the classical Airy formulas of linearized water wave theory. It was the great contribution of St. Denis and Pierson (1953) to suggest (a) that the statistical nature of the sea could be expressed by allowing the phases of these components to take on random values and (b) that the response of a ship to the sea was the sum of its responses to the various components. They only suggested these hypotheses, and it may be claimed that both had been made earlier, but these authors were the first to state them in precise, quantitative terms. Their suggestion (a) relates more to the oceanographer's problem, and so I shall not consider it here. However, (b) will be discussed in some detail, for it has received much attention in recent years and it is at the heart of our problem.

Today we may consider that it has been confirmed, for most practical purposes; some of the evidence will be presented.

St. Denis and Pierson used an extremely primitive set of equations of motion, and we must now conclude that those equations are quite unacceptable. They were the best available ten years ago, but we can now do much better. The use of second order ordinary differential equations to describe the rigid body motions of a ship is quite artificial. Under appropriate conditions and with proper interpretation, they provide a valid representation, but such equations certainly cannot have constant coefficients in the usual sense. The form of the equations of motion can now be stated with considerable confidence, and this will be done.

Actually, the discussion of rigid body equations of motion is somewhat of a digression. Basically, having accepted the linear superposition principle, we need only to find a means of determining the transfer function (or frequency response function) of the ship. This may be done experimentally, in which case the whole subject of equations of motion need not be introduced, or it may be done by the use of hydrodynamic theory, in which case the information provided by the equations of motion comes out automatically.

Nevertheless there are important reasons for studying the equations of motion per se. On the one hand, the direct experimental procedure treats only input (the exciting waves) and output (the motions). It provides no insight into the particular ship characteristics which cause different ships to respond differently in a given seaway. On the other hand, the hydrodynamic theory of ship motions is not yet highly enough developed to tell us comprehensively which ship characteristics are most important in seakeeping and why they are so important.

Perhaps the largest portion of the literature on ship motions during the past decade has been concerned with the calculation of individual elements in the equations of motion. Some of the methods used have been quite sound scientifically, and some of the results have shown quantitative agreement with experiments. For example, the damping (due to wave radiation) in heave or pitch can be analyzed straightforwardly in certain situations, and recently it has been demonstrated how to calculate the added mass or added moment of inertia through knowledge of the damping.

Although some of these analyses have led to remarkable results, there is also a basic difficulty of principle in using them, and this problem was already clearly pointed out by Peters and Stoker (1954). Since the free surface problems involved must all be linearized before any progress can be made, these authors set out to perform the linearization in a clearly stated, rational way and to investigate the logical consequences of the simplification. They obtained the linear mathematical model from a systematic perturbation analysis, ship beam being the small parameter. The results were disappointing, for they obviously do not correspond to reality: In the lowest order motion solution, there appear undamped resonances in heave and pitch. The physical interpretation of this result is that the wave damping is of higher order (in powers of the small parameter) than the exciting force, restoring force, and inertial reaction force.

Attempts were subsequently made to correct this situation by reformulating the perturbation problem. In particular, the Peters-Stoker assumption that the ship beam can be used as the sole characteristic small parameter is open to question; the amplitude of the incident waves is a small quantity which is quite independent of beam. A multiple-parameter perturbation scheme takes care of this problem theoretically, but it does not lead to practicable results. The theory for motions of a thin ship still stands in this unsatisfactory condition.

There seem to be at least two logical ways out of this predicament. We must have at least one small parameter associated with the hull geometry, in order that the ship travelling at finite speed may cause only a very small disturbance. (This is necessary for any linearization to be valid.) We could try to select this small parameter so that the damping due to vertical motions is increased in size by an order of magnitude. Such a result is realized, for example, in a flat-ship theory. But there are at least two objections to this; first, the practical solution of the flat-ship approximation is very difficult, involving a two-dimensional integral equation, and, second, the original difficulty would pop up again in consideration of horizontal modes of motion, namely, in surge, yaw, and sway.

The second logical escape is to use a small parameter which leads to no resonance at all in the lowest order non-trivial solution. This is accomplished by assuming that the ship is both shallow and narrow, i.e., slender. Then it can be shown that the inertia becomes an order of magnitude smaller than in the thin-ship theory, whereas the damping order of magnitude is unchanged. But slender body theory for ships also has its problems. In particular, a theory for ship motions should be part of a general theory which includes steady translation as a special case. We now know that slender body theory in fact gives poor results for the wave resistance of a ship in steady motion.

Nevertheless, slender body theory appears promising for predictions of ship motions. I shall only outline the ideas involved, for, if I presented the detailed modern theory as it stands in the published literature, I would be out-of-date before this morning session is over. The following speakers will present some of the evidence which suggests the promise of the approach.

It is obvious that much remains to be done in the theory of ship motions. There is still a problem of developing a logical approach which gives answers agreeing with experiments. Furthermore, most of my discussion relates only to motions in the longitudinal plane of the ship; we have barely begun to attack the corresponding problems involving yaw, sway, and roll.

SHIP MOTIONS IN CONFUSED SEAS

It has long been recognized that the sea is a complicated thing, but it was only with the war-time and post-war development of random noise theory that the means became available for providing a realistic description of it.

The kind of statistical description to be employed in describing the sea depends on the specific aspect of the ship motions problem which happens to be of immediate interest. The engineer who must evaluate the likelihood of fatigue failures is obviously concerned with different data and different theoretical formulations from the engineer who must design equipment for helping aircraft to land on a carrier. One might say that the ship captain will not be satisfied with statistical descriptions at all; he sets an absolute standard: the safety of the ship. So we must state carefully what problem concerns us before we choose a statistical model.

Long term phenomena, such as the fatigue problem, must still be treated on a strictly phenomenological basis. At present, we cannot hope to specify ship motions or any other ship-related variables for the whole variety of conditions which a ship encounters in its lifetime. Even if we could suddenly obtain perfect oceanographic prediction data, such an enterprise would be out of sight in the future — and probably not even desirable.

Also beyond the scope of this paper is the problem at the other extreme, that is, the prediction of the specific short-time motions of a ship, given its immediate, detailed history.

We shall here be concerned with a problem somewhere between these, namely, to predict the probability of occurrence of various phenomena when a ship is travelling in certain well-defined environments. Since we are limited by the available tools of probability theory, we restrict ourselves to the case of a stationary random sea. Such an environment is probably highly non-typical, but its study does give valuable information and it is in any case the best we can do at present.

Following St. Denis and Pierson (1953) and others, we first describe the seaway by the energy spectrum of the wave height. This function specifies the fraction of the total energy which is associated with any given band of wave frequencies. The assumption of an energy spectrum description implies nothing about the possibility of linearly superposing wave trains on each other. It simply means that one measures the wave height at a point for an (in principle) infinitely long time and then calculates the spectrum by a standard technique which is found in many textbooks.

Next, one generalizes the spectral description at the point so as to obtain a description valid over an area of the sea. It is here that the assumption is introduced that the sea can be represented as the linear sum of elementary waves, each travelling in the manner described by the classical Airy formulas of linearized water wave theory. If one starts with a wave height record at only a single point, many possibilities are available for making the generalization. Of all these possibilities, two have special meaning for us, because they correspond to situations of physical interest:

1. We may assume that all of the wave components travel in the same direction. Such a thing does not happen in nature, of course, but it is the situation which many towing tank operators have attempted to produce.

2. We may assume that the energy in any bandwidth is distributed among wave components travelling in a continuous distribution of directions. Insofar

as the sea can sometimes be described as a stationary random process, such an assumption can lead to a description of a real sea if the angular distribution is properly chosen. Without question, such a description can represent the short-crestedness of the sea. The particular distribution of energy as a function of angle will vary greatly with sea conditions, and it is not clear at present if there is a standard distribution which will lead to generally useful results in connection with ship motions predictions.

Our knowledge of the hydrodynamics of ship motions is such that we are well-advised to limit our attention to the first of the two choices above, although it is unrealistic. Stated bluntly, the fact is that we have far to go on the simpler problem, and we cannot hope to understand ship motions in multi-directional seas until we first understand what happens in artificially-produced uni-directional seas. This statement need not apply if we are content to obtain frequency response functions strictly by experiment. But the principle purpose of this paper is to consider the prospects for entirely analytical predictions of ship motions. With such a goal in mind, we must accept that we cannot solve all of our problems at once. Therefore I shall restrict myself generally to long-crested seas, recognizing that a broader outlook is desirable and will ultimately be necessary.

In calculating the energy spectrum from a given wave height record, one effectively discards the information which relates to relative phases of the various component waves. The energy spectrum gives us information only about about the amplitude of the components. From the point of view of probability theory, all wave height records which yield the same energy spectrum are equivalent.* Then, if one wants a general representation of the surface elevation corresponding to a particular energy spectrum, one must allow complete ambiguity in the relative phases of the frequency components. For the long-crested sea, St. Denis and Pierson (1953) proposed the representation:

$$\zeta(x,t) = \int_0^\infty \cos\left[Kx - \omega t - \epsilon(\omega)\right]\sqrt{[\zeta(\omega)]^2\,d\omega}\,, \tag{1}$$

where

$\zeta(x,t)$ = surface elevation at position x, time t,

$[\zeta(\omega)]^2$ = energy spectrum of $\zeta(x,t)$, a function of frequency, ω,

$K = \omega^2/g$,

g = acceleration of gravity, and

$\epsilon(\omega)$ = a random variable, with equal probability of realizing any value between 0 and 2π.†

*That is, they are all members of an ensemble which is characterized by a single energy spectrum. We assume not only that the processes are stationary but also that an ergodic hypothesis is valid.

†A more precise definition is that $P[\alpha_1 < \epsilon(\omega) < \alpha_2] = (\alpha_2 - \alpha_1)/2\pi$.

Such a representation yields the same energy spectrum for all values of x and all functions $\epsilon(\omega)$. It is supposed that any particular stationary long-crested sea can be represented by such a formula and conversely that any realization of this formula (through an arbitrary choice of $\epsilon(\omega)$) can occur. It should be noted that the relationship between wave number and frequency is just that which obtains for small-amplitude deep-water waves.

The "integral" in Eq. (1) has needlessly caused much controversy and confusion. St. Denis and Pierson carefully defined it as the limit of a sequence of partial sums, in a manner common in noise theory, in the theory of gust-loading on airplanes, etc. The conventional integral sign is always symbolic, denoting a limiting operation on a sequence of partial sums. In the present situation, the operation is not the usual Riemann integration, but it is quite properly defined provided that one is certain of the existence of the limit (or of the convergence) of the defining sequence. Proof of this point is a problem in the calculus of probability and will not be discussed here.

In the theory of random noise, there is another standard representation of the time history of a random variable with a given spectrum. Instead of using a cosine function with random phase (as in (1)), one uses a sum of sine and cosine functions of $(Kx - \omega t)$, with random amplitudes which are uncorrelated with each other. This stochastic model was applied to sea waves by Cote (1954). It is entirely equivalent to the random phase model, the choice between the two depending primarily on the relative convenience of deriving various probability properties of the sea.

From these stochastic models, one can derive all kinds of interesting conclusions about the sea, some of which will be true. But our interest is primarily with the ship. St. Denis and Pierson suggested that, looking at (1) as a sum of many sinusoidal waves, we should determine the response of the ship to each component, and then the response of the ship to the actual sea would be just the sum of the responses to the component waves. The process of finding the response to a regular sinusoidal wave is a completely deterministic process, of course, but in summing (or integrating) these responses we carry the stochastic nature of the seaway over to the ship motions. In particular, if we use the random phase model for the sea, the ship response should be expressible by an integral like that in (1).

The remainder of this section will be devoted to an investigation of the evidence for accepting this supposition of St. Denis and Pierson, i.e., that the ship response to a random sea is just the sum of its responses to the various frequency components. The accumulation of such evidence during the last few years is striking, and, prejudging the case somewhat, I believe that the chapter which was opened by St. Denis and Pierson in 1953 is now almost concluded.

The most straightforward approach to verifying the superposition principle for ship responses is to conduct model tests in different sea conditions. In each test the wave height and motions spectra are measured, and, from these, the amplitude of the frequency response (f.r.) functions of the ship can be calculated. If different conditions yield the same f.r. functions, then the ship can be described as responding "separately" to each frequency component, the total response being the sum of the responses to the various frequencies. Alternately, one may use the f.r. function amplitudes obtained from one test, together with the wave height spectrum in a second test, to predict the motion spectra in the second test. Comparison of these predictions with measured spectra then provides an indication of the degree of validity of superposing responses.

Let us be more specific. Suppose that the energy spectrum of the wave height at the center of gravity of the ship* is given by $\Phi_{ww}(\omega)$ and that the f.r. function in heave is given by $T_h(\omega)$. Then the energy spectrum of the heave motion will be:

$$\Phi_{hh}(\omega) = |T_h(\omega)|^2 \Phi_{ww}(\omega) .$$

If both energy spectra are known, this formula yields the magnitude of $T_h(\omega)$.[†] In a single test, the quantity $|T_h(\omega)|$ can always be found from this equation; defining such a ratio of two energy spectra implies nothing about the physical processes involved. However, in a second test with a different $\Phi_{ww}(\omega)$, the same $|T_h(\omega)|$ will be obtained only if the ship responds "separately" and linearly to each frequency component. Thus a simple direct means is provided for checking the principle of superposition and thus for checking the linearity of the whole process.

Only the amplitude of $T_h(\omega)$, that is $|T_h(\omega)|$, is found by the above procedure. Such a result is to be expected of course, for the calculation of an energy spectrum from a given test record washes out all phase information. But for some purposes it is necessary to know the actual complex value of $T_h(\omega)$. For example, if we want to predict bow emergence, the occurrence of slamming, deck wetness, etc., we must be able to relate the instantaneous ship position and attitude to the simultaneous free surface shape.

The complete evaluation of $T_h(\omega)$ can be made from random seas tests, through measurement of cross-spectra. For example, if $\Phi_{hw}(\omega)$ is the cross-power spectrum of heave and wave height, then

$$\Phi_{hw}(\omega) = T_h(\omega) \Phi_{ww}(\omega) .$$

Since $\Phi_{ww}(\omega)$ is a real quantity, this equation states that the cross-spectrum has the same argument in the complex plane as the f.r. function.

A remarkable series of such experiments has been performed at the Davidson Laboratory in recent years, in which the limits of validity of the linearity hypothesis have been extended more and more. (See Dalzell (1962a,b).) Long-crested random seas were created for a great range of degrees of severity. Figure 1, taken from Dalzell (1962b), shows the wave height power spectra

*The spectrum must be properly adjusted so that "frequency" is really "frequency of encounter." See St. Denis and Pierson (1953) for the frequency mapping.

†In general, the f.r. function will depend on the angle of incidence of the waves, as well as on ω. I am now assuming long-crested waves, moving parallel to the ship center plane.

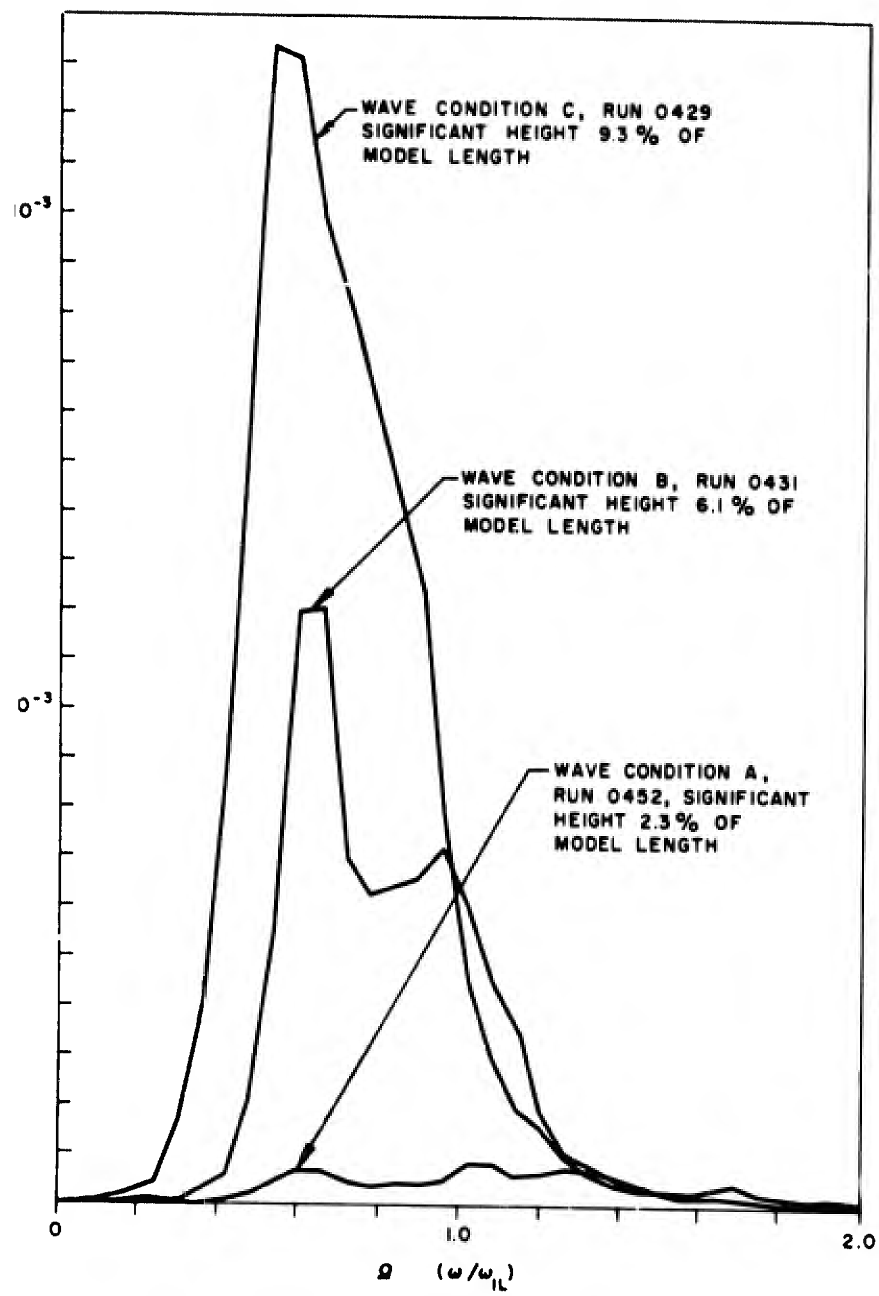

Fig. 1 - Wave power spectra used in Dalzell's tests (from Dalzell (1962b))

which were used. When the 5.82 ft ship model is scaled up to a 392 ft prototype length, wave conditions A, B, and C correspond respectively to sea states 5, low 7, and high 7. The hull form used was that of a DD692 destroyer. Wave condition C was the most severe that could be produced in the Davidson Laboratory tank; from Fig. 1 it may be noted that the significant wave height for wave C was 9.3% of the model length.

Figures 2-4 show typical results from Dalzell (1962b). They present the pitch f.r. function, both amplitude and phase, for three speeds which correspond to $\underline{F}$ = 0, 0.18, 0.37. The abscissa of these curves is a non-dimensional frequency, obtained by dividing the actual frequency of encounter by the frequency of a wave with wavelength equal to model length. The ordinate for f.r. function amplitude is $|T_p(\omega)|L/\pi$ and for phase the ordinate gives the lag of maximum bow-up pitch after the wave crest at the longitudinal center of gravity (LCG), in degrees. These quantities were calculated from wave and motion records by standard spectral techniques, although some manipulating of the wave height record was necessary, since the probe was located ahead of the model bow, and surface elevation was required at the LCG.*

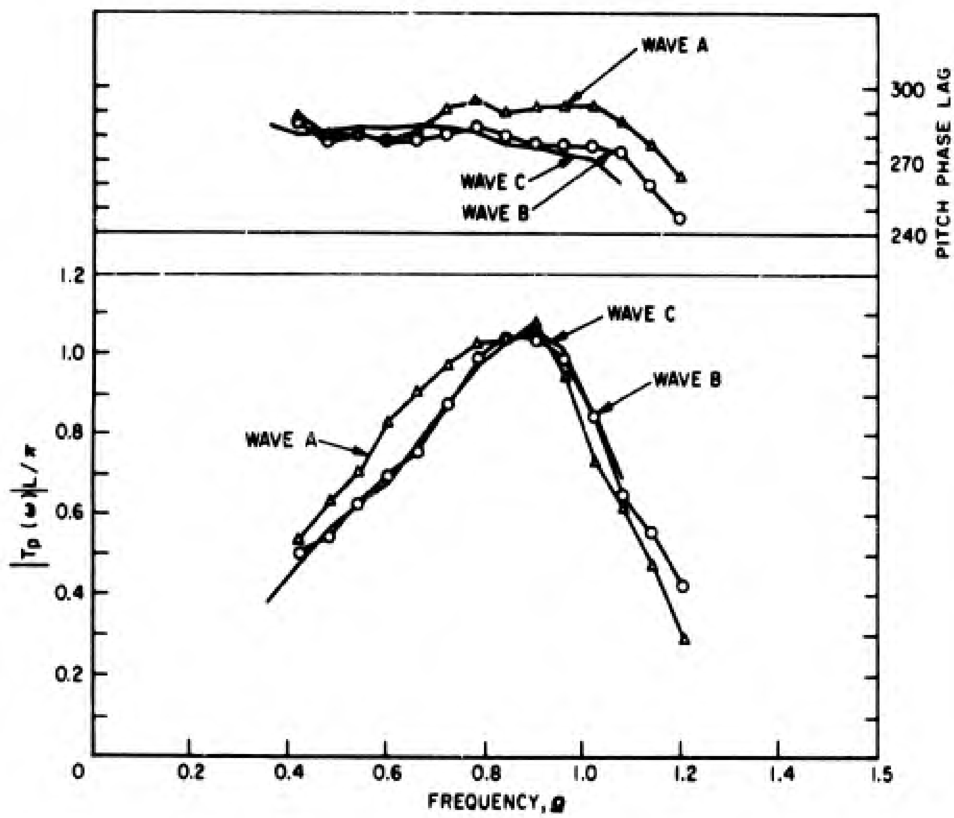

Fig. 2 - Dalzell's pitch frequency response function, Model DD 692 Froude number = 0 (from Dalzell (1962b))

*The reference elevation at the LCG was the wave height which would have occurred there in the absence of the model.

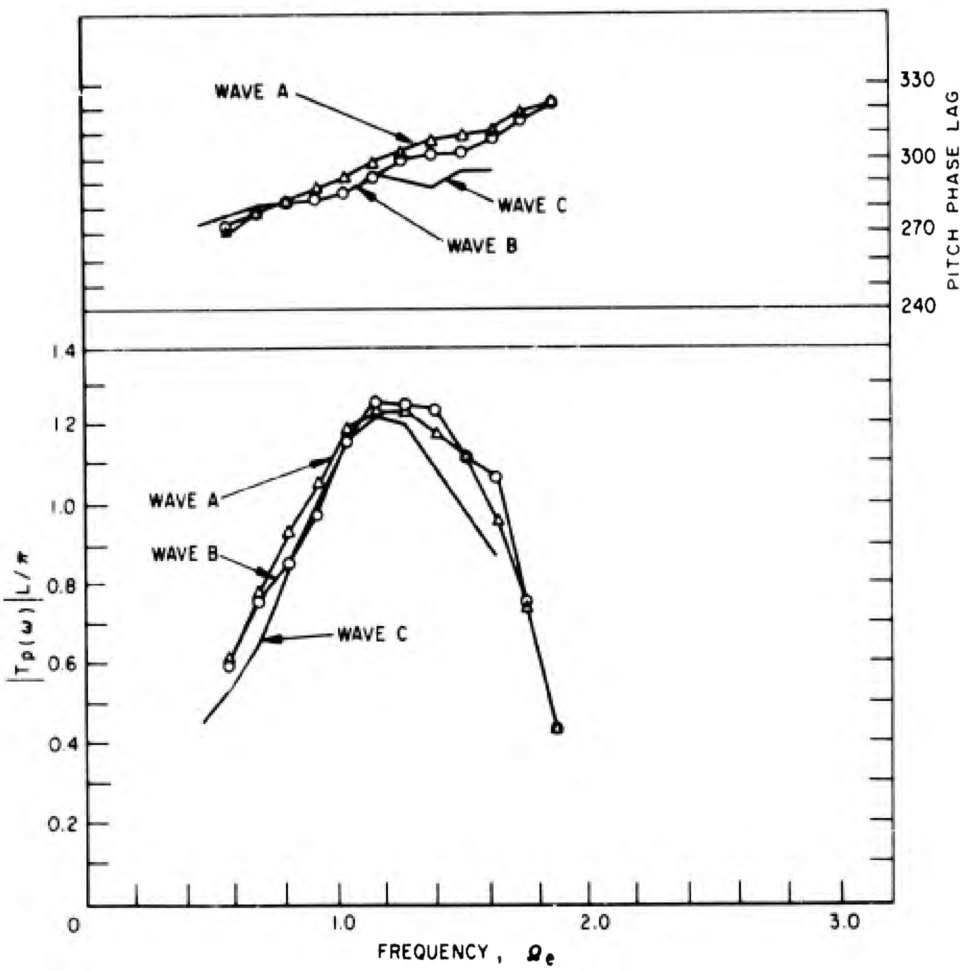

Fig. 3 - Dalzell's pitch frequency response function, Model DD 692 Froude number = 0.18 (from Dalzell (1962b))

From Fig. 2, it is seen that the f.r. function for $\underline{F} = 0$ is practically the same for each wave condition. The statistical design and analysis of the experiment will not be considered here; it will suffice to point out that the confidence to be attached to the f.r. function drops at the ends of the curves. No results were presented at all for cases in which either spectral density dropped below a certain value (10% of its peak).

Figure 3 shows the same results for $\underline{F} = 0.18$ and Fig. 4 for $\underline{F} = 0.37$. In the latter, it is clear that nonlinearities are making themselves felt. In particular, the pitch amplification factor decreases as wave conditions become more severe; this is the trend which one usually expects when nonlinearities become non-negligible.

It must be appreciated that Fig. 4 represents an extraordinarily severe condition. In fact, one must really stretch his imagination to conceive of a destroyer captain maintaining a speed such that $\underline{F} = 0.37$ in a high state 7 sea. The fact that our hypothesis about superposition is not so good in this case should not cause us too much unhappiness. At moderate speed ($\underline{F} = 0.18$) it is still rather good for the high-7 sea state, and the breakdown occurs only as speed increases beyond this. Five years ago, the most sanguine investigators did not dare to hope that the hypothesis could ever be pushed as far as Dalzell has done.

Similar results can be observed for heave and bending moment f.r. functions. The respective figures of Dalzell will not be reproduced here. For

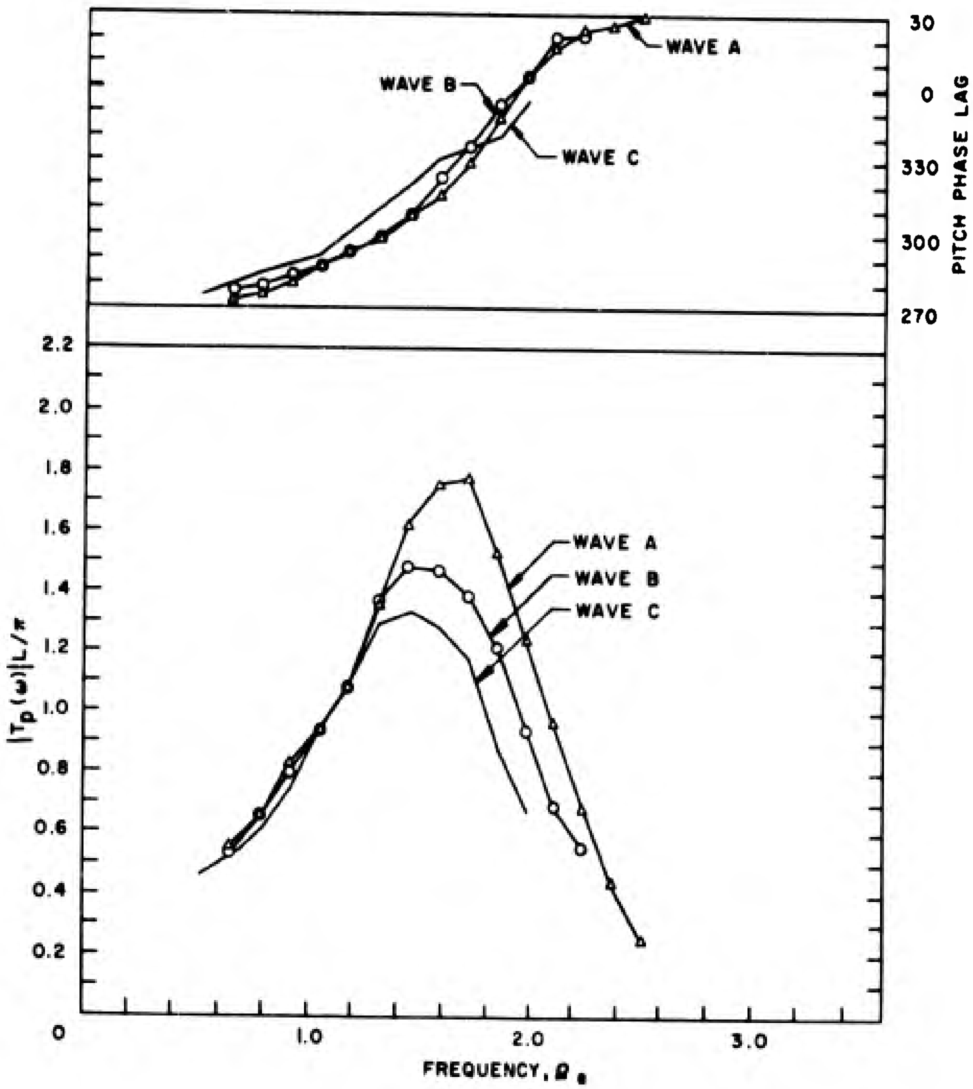

Fig. 4 - Dalzell's pitch frequency response function, Model DD 692
Froude number = 0.37 (from Dalzell (1962b))

bending moment the hypothesis of superposability proves somewhat poorer than for pitch and heave motions. At $\underline{F} = 0.18$ there is already considerable discrepancy in bending moment f.r. functions computed from spectra in different sea states, and coherency is found to run much lower in general.

Gerritsma (1960) arrived at similar conclusions in tests with Series 60 models. His approach was somewhat different from Dalzell's. Gerritsma found the f.r. functions in heave and pitch by three different methods: (1) a direct determination from measured ship responses in small amplitude regular waves; (2) calculation from the second order ordinary differential equations of motion, after an experimental determination of coefficients in the equations; (3) tests in irregular waves, in the manner of Dalzell.

Most of Gerritsma's regular-wave experiments were performed with a wave amplitude 1/48 of the model length, L. He also tried larger amplitude waves, 1/40L and 1/30 L, for the $C_B = 0.70$ and $C_B = 0.80$ models. There was generally excellent agreement among responses to the waves of various amplitudes, but a reduction in response appeared in some cases for the 1/30L wave. There was no pattern to the lack of linearity which could be associated systematically with either speed or wavelength. (Froude number was varied between 0.15 and 0.30, λ/L between 0.75 and 1.75.)

These regular waves were much less steep and much smaller in amplitude than the severe irregular waves used by Dalzell. It appears that nonlinearities make themselves felt more easily in regular waves than in irregular waves. This has also been observed recently by Ochi (1964),* who showed that f.r. functions must be obtained from small amplitude waves, if regular waves are to be used at all for their determination. These f.r. functions can then be used in confused seas of much greater severity. One is tempted to argue that in a confused sea the amplitude of a wave of any particular frequency is infinitesimally small and so the f.r. functions for infinitesimal amplitudes should be used — even though the actual wave heights and steepnesses may be very large. Of course, such an argument is illogical and explains nothing. For the moment, we must simply accept the phenomenological observations described above.

Gerritsma also performed a series of tests in which he determined the coefficients (i.e., added mass, added moment of inertia, damping, buoyancy, and couplings) in the differential equations of motion for heave and pitch. This was done by forcing the model to oscillate in various ways in calm water. Then the model was restrained and towed in regular waves, measurements being made of the heave force and pitch moment. With all of these quantities known, he solved the equations to obtain the f.r. functions.

---

*Ochi has also pointed out that acceleration measurements are much more sensitive to nonlinearities than are displacement measurements. This is simple to explain. In regular waves with frequency of encounter ω, we could represent the effects of nonlinearities by expressing the vertical displacement of a ship reference point by a Fourier series, the terms being sinusoidal with frequency $n\omega$, $n = 1, 2, \ldots$. If acceleration can be expressed by differentiating this series twice, then the terms in the Fourier series for acceleration will be multiplied respectively by n^2, so that the higher order terms are relatively larger than in the displacement Fourier series.

Finally, he conducted a few tests with the $C_B = 0.70$ model in irregular waves and obtained the f.r. functions in exactly the way Dalzell did.

Figure 5 is drawn from data in Gerritsma's paper and shows pitch and heave f.r. functions for the Series 60 model ($C_B = 0.70$) at $\underline{F} = 0.20$. Heave amplitude, z_o, has been divided by wave amplitude, r, and pitch amplitude, ψ_o, has been divided by the maximum wave slope of the sinusoidal wave, α_w. θ is the relative phase between heave and pitch (positive for heave lagging pitch). Five curves appear in each section of Fig. 5:

1. Response measured in regular waves.

2. Response calculated from the equations of motion, with coefficients determined experimentally and forcing functions determined from tests of restrained models in regular waves.

3. Response calculated as in (2), but with all coupling coefficients arbitrarily set equal to zero.

4. Response from wave and motions spectra.

5. Response from wave and motions cross-spectra.

(Of course, (4) does not apply to the figure for phases, since no information on phase is obtainable from ordinary power spectra.) It is seen that the f.r. functions are practically identical except for those of (3). At the moment, the effect of couplings is of only incidental interest, and these results (i.e., (3)) are presented here primarily for later convenience.

It must be emphasized that Gerritsma's tests do not go so far as Dalzell's in proving the validity of the superposition hypothesis. The irregular waves used by Gerritsma are very mild by comparison. However, Gerritsma's use of three methods of measurement — with his demonstration of their equivalence — is of far-reaching importance. In a direct way he has proved the usefulness and validity of the old procedures of testing in regular waves. Secondly, since these ordinary frequency response investigations are appropriate tools for studying ship motions in random seas, other methods of characterizing the system should be equally valid if such methods are equivalent to finding the f.r. functions. In particular, the measured response of a ship to a single transient wave can yield as much information as a long sequence of regular wave tests. Moreover, such a test is purely deterministic, and there are none of the special difficulties which are so characteristic of tests in random seas (real or artificial).

I have been consistently restricting myself to consideration of heave and pitch motions, but this section would be lacking without some mention of recent work on the problem of superposing ship roll responses. One is inclined to believe intuitively that roll motion will involve stronger nonlinearities than other ship motions, and regular wave experiments seem to confirm this intuitive feeling. Nevertheless, at least two papers have appeared which present irregular wave test data indicating that roll responses can indeed be superposed in the same sense as heave and pitch responses.

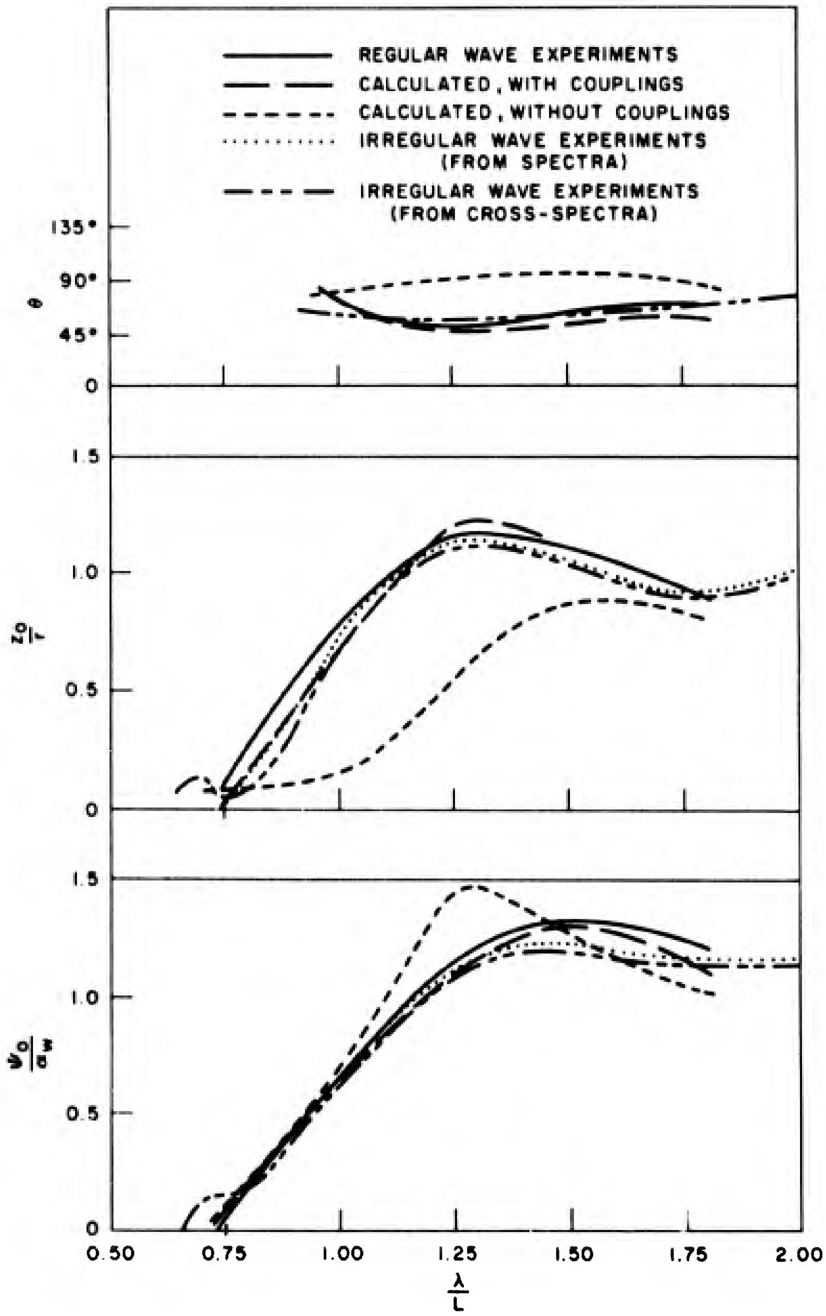

Fig. 5 - Gerritsma's pitch and heave frequency response functions, Model: Series 60, c_B = 0.70 Froude number = 0.20 (from Gerritsma (1960))

The first of these papers was presented at the Wageningen meeting by Kato, Motora, and Ishikawa (1957). They restrained their model to remain in a beam seas attitude, with natural confused waves. The model had zero forward speed. Its roll amplification factor, $|T_r(\omega)|$, was determined in tank tests with regular waves, and this operator was used with the measured wave height energy spectra to predict roll response energy spectra in random waves. The calculations were then compared with measured energy spectra for roll, with good agreement being found. The wave and roll amplitudes were rather small, and so the results were not conclusive. Also, the paper lacked certain model details, and so one does not know, for example, whether the model had bilge keels. Nevertheless, these experiments were among the first to be conducted for checking the superposition hypothesis, and the authors' general conclusions have since been corroborated.

Earlier this year, Lalangas (1964) published a report on some Davidson Laboratory experiments directed toward the same goal. A Series 60, $C_B = 0.60$, model (with bilge keels) was used, and the statistical design of the experiments was quite similar to Dalzell's. Only beam seas were studied, but forward speed was included, up to a Froude number of 0.156. Essentially the result was the same as in the tests of Kato, et al., viz., superposition does work for roll responses. The irregular waves in Lalangas's tests varied in severity up to a low state 7.

In a certain sense, we are back where we were eleven years ago, that is, we now turn our attention again to the behavior of ships in sinusoidal waves. There is, of course, one major change: We now know that the study of such idealized environments has a real relevance to the physical problem which occurs in nature. Moreover, regular wave problems have not been ignored during this decade. There has been much progress, although unfortunately it will not be possible to make such definitive statements in this area as in the area of random sea phenomena.

THE EQUATIONS OF MOTION

Equations in the Frequency Domain

A ship in a seaway can be completely characterized (for studies of its motions) by a set of six frequency response functions depending on ship speed, wave encounter, and angle of wave encounter. If these f.r. functions are known, the ship can be treated as a "black box." An input wave system is selected which is a sum (or integral) of many sinusoidal waves, and the output is calculated by multiplying each input wave amplitude by the appropriate value of the f.r. functions and adding all of the responses. The experiments cited in Chapter II have demonstrated the validity of these statements at least with respect to heave and pitch motions in head seas and roll motions in beam seas. We may perhaps expect difficulties in following seas (see Grim (1951)) and also with the other modes of motion. In the case of following seas, it is well-known that nonlinearities are important, and for yaw and sway we simply do not have much data. We shall proceed on the premise that the same laws of linearity apply in these other conditions, but it must be recognized that our conclusions may be valid only for those modes which have been extensively studied experimentally.

The f.r. functions may be found by a straightforward set of experiments in regular waves, by experiments in irregular waves (as by Dalzell (1962a,b) and others), or by tests in transient waves (Davis and Zarnick (1964)).

The regular wave tests are the simplest in principle, but there are objections against them: (1) A separate test must be run for each frequency of interest, at each speed and at each heading. (2) With most wavemaking installations there is a question about the regularity of "regular waves." Harmonics may be non-negligible, causing large errors if ignored. (3) The amplitudes must be kept very small, to avoid nonlinear distortion of the f.r. functions.

The irregular wave tests are better in each of these three respects. In particular, the whole frequency spectrum is covered in a single well-designed test. However, here there is another objection: The test run must be long enough for the records to be analyzed statistically. In most tanks this is impossible, and so several test runs are made and the records are patched together.

Tests in transient waves, that is, in wave pulses or wave packets, avoid the difficulties of both regular and confused sea tests in that a single record of reasonable length provides all of the information necessary for finding the f.r. functions. The price one pays here is in meeting the stringent requirements on measurement accuracy.

Sometimes it is desirable to characterize the ship in a more detailed manner than is possible with the "black box" methods. A procedure has been developed for this purpose by several investigators, and, although it requires more testing than any of the above mentioned procedures, it also provides more information. In mathematical terms it may be described as follows:

A sinusoidal wave system exerts on the ship a force and moment, which can be represented by the expressions $F_j \mathrm{Re}\{e^{i(\omega t+\epsilon_j)}\}$, $j = 1, 2, \ldots, 6$. There may be other external forces and moments as well, such as oscillatory propeller thrust, control surface forces, and artificial constraint forces on the model. Let these be represented by $G_j \mathrm{Re}\{e^{i(\omega t+\theta_j)}\}$. Finally, there will be forces which are induced by the motions of the ship itself. If the instantaneous displacement in the k-th mode is represented by $X_k \mathrm{Re}\{e^{i(\omega t+\delta_k)}\}$, then we assume that the motion-induced forces and moments are proportional to the amplitudes X_k, but of course they may have phases which are quite different from the motion phases, δ_k. This troup of forces includes inertial reactions.

It must generally be accepted that all modes of motion interact with each other and with all of the force and moment components. The simplest possible relationship is a linear one, and so we assume that the excitations, external constraints, inertial reactions, and hydrodynamic and hydrostatic motion-induced forces are linearly related:

$$\mathrm{Re}\left\{\sum_{k=1}^{6} A_{jk} X_k e^{i(\omega t+\delta_k)}\right\} = \mathrm{Re}\left\{F_j e^{i(\omega t+\epsilon_j)}\right\} + \mathrm{Re}\left\{G_j e^{i(\omega t+\theta_j)}\right\}, \quad j = 1, \ldots, 6.$$

where A_{jk} is a complex matrix of coefficients.

The above set of equations can be solved for the quantities $X_k e^{i\delta_k}$, provided that the matrix, A_{jk}, and the forcing functions are known. Such a solution then effectively expresses a set of six f.r. functions, and so it is entirely equivalent to the previous approaches. Of course, this method requires knowledge of the matrix, A_{jk}, and of the forcing functions. These can be obtained by a straightforward but tedious set of experiments, as suggested by Haskind and Riman (1946) and as carried out partially or completely with specific models by Golovato (1957), Gerritsma (1960), and others. Such experiments are in effect set up to correspond to special cases of the above equations, as follows:

1. If the model is completely restrained, then $X_k = 0$ for all k, and so

$$G_j e^{i\theta_j} = -F_j e^{i\epsilon_j}.$$

Such an experiment provides measurements of the wave excitation force and moment; the quantities $G_j e^{i\theta_j}$ are obtained from dynamometers in the structure which restrains the model.

2. If there are no incident waves, then $F_j = 0$ for all k, and so

$$\sum_{k=1}^{6} A_{jk} X_k e^{i\delta_k} = G_j e^{i\theta_j}, \quad j = 1, \ldots, 6.$$

The model can be forced to oscillate in selected modes only, so that the A_{jk} can be determined. For example, if $k = 3$ corresponds to the vertical velocity or force component, and if the model is forced to oscillate in heave only, the set of equations reduces to

$$A_{j3} X_3 e^{i\delta_3} = G_j e^{i\theta_j}, \quad j = 1, \ldots, 6.$$

which allows the determination of $A_{13}, \ldots, A_{63}$.

3. If the model is completely free to respond to incident wave excitations, and if there are no extraneous sinusoidal forces (such as oscillatory propeller thrust), then $G_k = 0$ for all k, and

$$\sum_{k=1}^{6} A_{jk} X_k e^{i\delta_k} = F_j e^{i\epsilon_j}, \quad j = 1, \ldots, 6.$$

This experiment is redundant if performed with (1) and (2) above, and so it can be taken as a check on the validity of the whole approach. This was done in the experiments of Gerritsma (1960) described in the preceding chapter.

This method is similar to the method of finding f.r. functions by direct measurement in regular waves, in that the ship behavior is determined at discrete frequencies and the data are then smoothed to provide continuous curves of the frequency dependence on all variables. In particular, the forcing functions,

$F_j e^{i\epsilon_j}$, and the system parameters, A_{jk}, are all functions of frequency,* so that the outputs, $X_k e^{i\delta_k}$, and the f.r. functions are explicitly functions of frequency.

Such an approach is often described as "working in the frequency domain." The basic set of equations above is valid only if all variables depend sinusoidally on time, at a fixed, given frequency. The utility of this approach follows from two further conditions: (1) The frequency domain analysis can be used for non-sinusoidal motions through use of Fourier transform techniques (for transient disturbances of limited duration) or generalized harmonic analysis (for stationary random disturbances). (2) Some of the coefficients, A_{jk}, can be interpreted physically in such ways that engineering estimates can be made of the importance for motions of some ship parameters. The first of these points has been discussed at some length in the previous chapter. The second will be considered further here.

For simplicity, let us consider the experiment in which the model is forced to oscillate sinusoidally in heave only, at angular frequency ω. We would measure the amplitude of heave, X_3, the six force and moment amplitudes, G_j, and the six relative phases, $(\theta_j - \delta_3)$. Then we would calculate the six coefficients:

$$A_{j3} = (G_j/X_3)\, e^{i(\theta_j - \delta_3)} .$$

Each of these would be generally a complex number, the value depending on ω.

In particular, let us look at A_{33}. It is related to the f.r. function describing the ship; it equals heave force divided by heave response. We do not know at this point the equations of motion of the ship, but it is an elementary problem to write down an ordinary first order differential equation with constant coefficients which would yield the value $(1/A_{33})$ for its f.r. function <u>at a particular frequency</u>. In fact, if we set $A_{33} = i\omega b + c$, with b and c real, then the equation

$$b\dot{x}_3 + c x_3 = f(t) \tag{2}$$

yields exactly $(1/A_{33})$ as its f.r. function. By considering $b = b(\omega)$ and $c = c(\omega)$, one could use this equation as a description of the pure heave motion of the ship. Such an approach is quite objectionable mathematically, for in simply stating the differential equation above we have implied that we have described the system response for any input, $f(t)$, whereas actually Eq. (2) has no meaning unless $f(t)$ is a sinusoidal function of time. To quote Tick (1959), "Differential equations with frequency-dependent coefficients are very odd objects." The equation has significance only inasmuch as it yields the proper frequency response. In other words, it is not a differential equation at all but is simply another way of writing down the frequency domain properties of the system.

The naval architect would generally raise a different objection to the use of the above equation: The physical problem involves the dynamics of a rigid body, to which Newton's law is applicable, and, since this law relates the forces to the

*They are also functions of relative wave heading, unless we consider only head seas. This point will not be repeated every time it comes up.

second derivative of displacement, the equation should be of second order. In other words, it should contain a term $m\ddot{x}_3$, where m is the mass of the ship. The differential equation to be chosen is now not unique, without further considerations, whereas Eq. (2) above was uniquely determined by the value of $A_{33}(\omega)$. Now, any equation of the form

$$a\ddot{x}_3 + b\dot{x}_3 + cx = f(t) \tag{3}$$

will suffice, provided only that

$$A_{33} = i\omega b + (c - \omega^2 a) .$$

The only a priori restriction on the values of a and c is that the linear combination $(c - \omega^2 a)$ should have the proper value.

It is here that a physical idea is introduced. We know that if a ship is given a steady displacement in heave from its equilibrium position, there will be a steady restoring force approximately proportional to the amplitude of the displacement. We let the quantity cx denote this steady force component, and we note that c is independent of frequency, ω. Then the parameter a can be uniquely determined from A_{33}.

Quite often the quantity cx is referred to as a buoyancy force, but it must be recognized that this is not entirely true. It is easily shown experimentally that c varies with speed, and it does in fact include hydrodynamic as well as hydrostatic effects.

The quantity a will usually (but not always!) be found to be larger than the ship mass, m. It is then common to define an "added mass" equal to $(a - m)$; this is the apparent increase in inertia which the ship experiences because it is accelerating the surrounding water. Of course, it is not a quantity which is characteristic of the ship, for in fact it depends on frequency.

Finally, the quantity b, which is uniquely determined from the value of A_{33}, can be considered as a damping coefficient. This is easily seen from Eq. (3). At least in the case of heave motion, most of the damping will appear physically in the form of radiated waves, and this quantity can be more reliably calculated than any of the other parameters considered here.

The major advantage of this approach is that to some extent the dynamics of the ship itself can be separated from the hydrodynamic problem. This appears most clearly when the above ideas are extended to include all six degrees of freedom. In the rotational modes, in particular, the moments of inertia can be varied easily without changing the hull shape or the hydrodynamic forces or moments. If the coefficients A_{jk} are all known and if they have been broken down into hydrodynamic and ship inertial components, the changes in A_{jk} (and thus in the motions) due to variations in mass distribution can be calculated.

Furthermore, ship motions are often most critical near resonance, for then they are largest in amplitude. Near resonance, the amplitude is very largely controlled by the amount of damping, and it is the damping which is most readily calculated in the above framework.

It is apparent that there can be considerable utility in representing the motion by a set of second order equations, generalized from (3),

$$\sum_{k=1}^{6} \left\{ a_{jk}\ddot{x}_k + b_{jk}\dot{x}_k + c_{jk}x_k \right\} = f_j(t) + g_j(t), \quad j = 1, \ldots, 6, \tag{4}$$

where the $f_j(t)$ represent wave-induced excitations and the $g_j(t)$ represent all other external forces and constraints. However, it is worth reiterating that these are not really equations of motion in a proper sense. They are valid only if the right hand sides all vary sinusoidally at a single frequency and if the constant coefficients on the left have the values appropriate to that frequency. As stated earlier, these equations describe the frequency-domain characteristics of the system, and a non-conventional derivation was presented here to emphasize this point.

Golovato (1959) gave direct experimental proof that these second order equations cannot be used to describe non-sinusoidal motions. He conducted transient tests with a ship model, giving the model an initial pitch inclination and allowing it then to undergo a transient motion, returning to its equilibrium attitude. He found that the response could not be represented as that of a simple damped spring-mass system, which would have been appropriate to a second order ordinary differential equation with constant coefficients. An even more startling result has recently been produced by Ursell (1954). For a heaving body which is released from a position above its equilibrium height and allowed to come to rest, he found analytically that there are only a finite number of oscillations, after which the body gradually approaches its equilibrium position in a non-oscillatory manner. This cannot be explained in terms of equations such as (4), but it will be shown presently that the true equations are integro-differential equations, and these do allow of such solutions.

In the full generality of six degrees of freedom, the ordinary differential equations are still not simple to work with. There are 108 "constants" on the left, each being a function of frequency. Also, all of the parameters in general depend on wave heading as well as frequency.

In order to make the system manageable, several simplifications have been tried by various investigators. The most straightforward is to limit consideration to head and following seas. This means that three degrees of freedom can be eliminated,* and the number of coefficients is reduced to 27 — these not being functions of heading. Of course, there is nothing wrong with this simplification, provided one is satisfied with results valid only in head or following waves.

Frequent attempts have also been made to neglect couplings between modes. This was done, for example, by St. Denis and Pierson (1953), and it has appealed to many investigators since then. However, Gerritsma (1960) has shown this is dangerous. He calculated responses using experimentally obtained frequency-dependent coefficients, both with and without couplings. Some of his results were

*We are neglecting phenomena such as the unstable rolling which occurs in following seas when frequency of encounter equals twice the natural frequency of roll. See Grim (1952), Kerwin (1955), Kinney (1963).

already reproduced here in Fig. 5. The effects of couplings between pitch and heave modes are clearly not negligible. Couplings of pitch and heave with surge may be negligible.

Much effort has been devoted to calculating some of the coefficients in these equations, and in fact the following chapters will be concerned with this problem. We defer consideration of such analyses for the moment, until we have discussed the nature of the true equations of motion in the time domain.

Equations in the Time Domain

We would like to find equations of motion which are valid whatever the nature of the seaway; we want to avoid the difficulty encountered with Eq. (4), viz., that the forcing functions had to depend sinusoidally on time. From the nature of Eq. (4), in particular from the frequency dependence of the coefficients, Tick (1959) suggested that the true equations would involve convolution integrals. In fact, this had already been demonstrated many years earlier by Haskind (1946). Unfortunately, there were some errors in Haskind's work, but this basic conclusion was correct.

If we are to obtain the actual equations of motion, we must start by formulating the complete mathematical problem involving the dynamics of the ship (as a rigid body), the description of the sea, and the hydrodynamics of the ship-water interactions. This general problem will be treated to some extent in later chapters, and other authors at this meeting will devote their papers to it. For present purposes, we shall look simply at the form of the equations, and for this we follow closely the work of Cummins (1962). The net result will be a set of equations analogous to (4) in that there will be several undetermined parameters and functions. These must be determined either from experiments or from separate hydrodynamic analyses.

Cummins makes one major assumption: linearity of the system. This means much more than the linearity of Eq. (4). In that case, linearity implied that if the ship were subjected to a sum of two excitations, both sinusoidal at the same frequency, the total response would be the sum of the separate responses. Now the assumption is extended to cover excitations of any nature. In particular, if a ship is given an impulse of some kind, it will have a certain response lasting much longer than the duration of the impulse. If the ship experiences a succession of impulses, its response at any time is assumed to be the sum of its responses to the individual impulses, each response being calculated with an appropriate time lag from the instant of the corresponding impulse. These impulses can be considered as occurring closer and closer together, until finally one integrates the responses, rather than summing them.

This is an approach to water wave problems which was very popular in the days of Kelvin, but which is generally out of style today. However, modern understanding of analogous problems in control theory makes this approach more useful than ever. In a sense, we find that the existence of the free surface causes the physical system to have a "memory": What happens at one instant of time affects the system for all later times. This, of course, is very obvious;

for example, if we drop a pebble into a pond, waves continue to move about for a very long time. If the fluid were not viscous, the waves would appear forever. This is in considerable contrast to the common situation in which a body moves through an ideal fluid filling all space. In such cases, all motion stops instantly if the body stops. Thus it can be seen that the impulse response method exhibits very clearly the basic contribution of the free surface to the problem.

Following Cummins, we consider first the case of a ship with no forward speed. Let $\underline{x}$ denote the position vector of a point on the hull surface, S, measured in a fixed reference system, and let $\underline{x}'$ be the position vector of the same point on the hull surface, measured in a reference system moving with the hull. The two systems of axes are assumed to coincide when the ship is in its equilibrium position. When the hull is displaced from equilibrium, the deflection of any point of the hull can then be expressed:

$$\underline{x} - \underline{x}' = \sum_{k=1}^{6} \underline{a}\,(\underline{x}, t)\,,$$

where

$$\underline{a}_k(\underline{x}, t) = \begin{cases} a_k(t)\,\underline{i}_k\,, & k = 1, 2, 3, \\ a_i(t)\,[\underline{i}_{k-3} \times \underline{x}]\,, & k = 4, 5, 6. \end{cases} \tag{5}$$

$a_k(t)$ is a deflection in surge, sway, or heave, respectively, for $k = 1, 2$, or 3, or a rotation in roll, pitch, or yaw, respectively, for $k = 4, 5$, or 6. It is assumed that all $a_k(t)$ are small enough that only second order errors are incurred in the vector addition of rotations. Also, we can use $\underline{x}'$ as the first argument of $\underline{a}_k$, causing thereby only second order differences in the results.

The velocity potential, $\Phi(\underline{x}, t)$, must satisfy the following conditions:*

a) $\dfrac{\partial\Phi}{\partial n} = \underline{n} \cdot \sum_{k=1}^{6} \dot{\underline{a}}_k(\underline{x}, t)$ on the hull,

b) $\dfrac{\partial^2\Phi}{\partial t^2} + g\dfrac{\partial\Phi}{\partial x_3} = 0$ on $x_3 = 0$, (6)

c) a radiation condition for $x_1^2 + x_2^2 \to \infty$,

d) $|\nabla\Phi| \to \infty$, as $x_3 \to -\infty$.

It is easily seen that only second order errors arise if the body boundary condition is applied at the mean position of the hull, rather than on its actual moving surface;† all of the boundary conditions are then applied on fixed domains.

---

*I am defining Φ such that its gradient equals the velocity vector. For a thorough derivation of the free surface conditions, see Stoker (1957) or Wehausen and Laitone (1960).

†This will not be the case when forward speed is included.

Cummins proposed a solution in the following form:

$$\Phi(\underline{x}, t) = \sum_{k=1}^{6} \dot{\alpha}_k(t)\, \psi_k(\underline{x}) + \sum_{k=1}^{6} \int_{-\infty}^{t} \chi_k(\underline{x}, t-\tau)\, \dot{\alpha}_k(\tau)\, d\tau\,, \tag{7}$$

where $\psi_k(\underline{x})$ satisfies:

$$\left.\begin{array}{lll} \text{a)} & \psi_k = 0 & \text{on } x_3 = 0\,, \\ \text{b)} & \dfrac{\partial \psi_k}{\partial n} = \begin{cases} \underline{n} \cdot \underline{i}_k\,, & k = 1, 2, 3\,, \\ \underline{n} \cdot \underline{i}_{k-3} \times \underline{x}\,, & k = 4, 5, 6\,, \quad \text{on } S_o\,, \end{cases} & \end{array}\right\} \tag{8}$$

with S_o the mean position of the hull, and where $\chi_k(\underline{x}, t)$ satisfies:

$$\left.\begin{array}{lll} \text{a)} & \dfrac{\partial^2 \chi_k}{\partial t^2} + g \dfrac{\partial \chi_k}{\partial x_3} = 0\,, & \text{on } x_3 = 0\,, \\ \text{b)} & \dfrac{\partial \chi_k}{\partial n} = 0\,, & \text{on } S_o\,, \\ \text{c)} & \dfrac{\partial \chi_k}{\partial t} = -g \dfrac{\partial \psi_k}{\partial x_3}\,, & \text{on } x_3 = 0, \text{ for } t = 0\,, \\ \text{d)} & \chi_k = 0 & \text{for all } \underline{x} \text{ when } t = 0\,, \end{array}\right\} \tag{9}$$

There is no particular difficulty in showing that (7), along with conditions (8) and (9), does satisfy (6a) and (6b). The verification will not be carried out here. In any case, Cummins did not suggest how to find any of the twelve functions, ψ_k and χ_k, and it is simply assumed that they can be found and that they will satisfy the other conditions of the problem, namely, (6c) and (6d). It is much more interesting to investigate the meaning of the different parts of the solution.

The functions $\psi_k(\underline{x})$ are the velocity potentials for separate, much simpler problems. These functions are originally defined only in the fluid region, that is, outside the body and in $x_3 < 0$. But condition (8a) implies that ψ_k is antisymmetric with respect to the $x_3 = 0$ plane, and so we can interpret it physically in a much larger region. For example, consider the case of the heaving ship. That is, let $\alpha_3(t)$ be the only non-zero motion variable. We can think of the body being extended by having its reflection in the free surface added to it, the whole space outside of the body now being filled with fluid. If the extended body now moves as a unit, the velocity potential for the hydrodynamic problem will be just $\dot{\alpha}_3(t)\, \psi_3(x)$, with $\psi_3(\underline{x})$ satisfying (8a) and (8b). This is a classical Neumann problem, and the same picture fits the pitch and roll modes.

For the other three degrees of freedom, the physical problem to which $\psi_k(\underline{x})$ pertains is not so clear. For $k = 1$ (surge), for example, the body must be completed by having its reflection added to it, but the reflected half-body must move oppositely to the real body. The same situation obtains for sway and yaw.

The condition (8a) is the appropriate free surface condition for problems of oscillations at high frequencies. Flows under such conditions are characterized by having no horizontal component of velocity at the undisturbed free surface. A more important property of the ψ_k-flows is the fact that they represent the instantaneous fluid response to the motion of the body. If the body is moving and then suddenly stops, the entire fluid motion associated with the ψ_k potentials stops.

As was suggested earlier, the integral terms of the proposed form of solution represent the effects of the free surface. For example, let the ship be at rest until, at $t = 0$, it moves impulsively with a large velocity in the k-th mode for a short time. We may idealize this situation by setting

$$\dot{a}_k(t) = \delta(t), \quad \text{the Dirac function.}$$

For all $t \geq 0$,

$$\Phi(\underline{x}, t) = \delta(t)\, \psi_k(\underline{x}) + \int_{-\infty}^{t} \chi_k(\underline{x}, t-\tau)\, \delta(\tau)\, d\tau$$

$$= \delta(t)\, \psi_k(\underline{x}) + \chi_k(\underline{x}, t).$$

This result shows that, for $t > 0$, $\chi_k(\underline{x}, t)$ is just the velocity potential of the motion which results from the impulse of body velocity at $t = 0$. Furthermore, χ_k satisfies the ordinary free surface condition, (9a), and a homogeneous Neumann condition on the body, (9b). Thus $\chi_k(\underline{x}, t)$ represents the dispersion of waves caused by the impulse, and this dispersion takes place in the presence of the unmoving ship hull.

The potentials for the instantaneous response, $\psi_k(\underline{x})$, provide initial conditions on the potentials which describe the later motion, $\chi_k(\underline{x}, t)$. If we set $\dot{a}_k(t) = \delta(t)$, the fluid particles which initially made up the free surface, $x_3 = 0$, are given a vertical displacement,

$$\int_{-\infty}^{0+} \delta(t) \left.\frac{\partial \psi_k}{\partial x_3}\right|_{x_3=0} dt = \left.\frac{\partial \psi_k}{\partial x_3}\right|_{x_3=0}.$$

In the linearized theory of free surface waves, the surface elevation is given by

$$-\frac{1}{g} \left.\frac{\partial \chi_k}{\partial t}\right|_{x_3=0},$$

and, at $t = 0+$, this quantity must equal the surface elevation due to the impulse. This, in fact, is the meaning of Eq. (9c).

The solution, (7), of the free surface problem is of just the form commonly used in control theory. The motion of the body is considered to be made up of a sequence of impulsive motions; for each impulse there is an immediate fluid response (due to the incompressibility of the fluid) and an extended response, the latter lasting much longer than the impulse itself. The quantities $\dot{\alpha}_k(t)$ are the inputs and quantities $\chi_k(\underline{x}, t)$ are the impulse response functions for the velocity potential.

If the ship has forward speed, the situation is more complicated in practice, but in principle the approach is the same. Let us again use two coordinate systems, one moving steadily with velocity $\underline{V}$, where $|\underline{V}|$ equals the mean speed of the ship, the other system being fixed to the ship. We can then define the vector displacement of a hull point by the same expressions as in (5).

Let the potential be represented generally by:

$$\Phi(\underline{x}, t) = -Vx_1 + \varphi_0(\underline{x}) + \varphi_1(\underline{x}, t),$$

where $[-Vx_1 + \varphi_0(\underline{x})]$ is the potential for steady flow past the ship fixed in its undisturbed position, that is, $\varphi_0(\underline{x})$ satisfies:

$$V^2 \frac{\partial^2 \varphi_0}{\partial x_1^2} + g \frac{\partial \varphi_0}{\partial x_3} = 0 \qquad \text{on } x_3 = 0,$$

$$\underline{n} \cdot \underline{v}_0 = 0 \qquad \text{on } S_0,$$

where

$$\underline{v}_0(\underline{x}) = \nabla[-Vx_1 + \varphi_0(\underline{x})].$$

Again S_0 is the surface of the undisturbed hull. Then the free surface condition on $\varphi_1(\underline{x}, t)$ is readily found:

$$\frac{\partial^2 \varphi_1}{\partial t^2} - 2V \frac{\partial^2 \varphi_1}{\partial t \partial x_1} + V^2 \frac{\partial^2 \varphi_1}{\partial x_1^2} + g \frac{\partial \varphi_1}{\partial x_3} = 0 \qquad \text{on } x_3 = 0. \tag{10a}$$

The body boundary condition on $\varphi_1(\underline{x}, t)$ is not so readily determined, for it may be shown that the body condition must be satisfied on the exact, instantaneous surface* of the hull. However, Timman and Newman (1962) have proved that a consistent first order theory results if the following condition is used:

$$\underline{n} \cdot \nabla\varphi_1 = \underline{n} \cdot \left\{ \frac{\partial \underline{\alpha}(\underline{x}, t)}{\partial t} + \nabla \times [\underline{\alpha}(\underline{x}, t) \times \underline{v}_0(\underline{x})] \right\}. \tag{10b}$$

If we tried to apply the time-dependent boundary condition directly on the mean surface of the hull, we would have only the first term in the braces. The second

*This has not been done properly by such eminent authors as Havelock and Haskind, and it has led to some long-standing wrong ideas. For a thorough discussion, see Timman and Newman (1962).

term may be considered as a correction for two effects: (1) The steady velocity potential satisfies a condition on the wrong surface, viz., on the undisplaced hull surface. (2) Rotational displacements of the ship interact with the steady flow to produce an additional cross-flow. Both of these effects yield contributions of the same order of magnitude as the desired perturbation effects.

Now we state that a solution can be written in the form (cf. Eq. (7)):

$$\Phi(\underline{x}, t) = -Vx_1 + \varphi_0(\underline{x}) + \sum_{k=1}^{6} \dot{a}_k(t)\, \psi_{1k}(\underline{x}) + \sum_{k=1}^{6} a_k(t)\, \psi_{2k}(\underline{x})$$

$$+ \sum_{k=1}^{6} \int_{-\infty}^{t} \chi_{1k}(\underline{x}, t-\tau)\, \ddot{a}_k(\tau)\, d\tau + \sum_{k=1}^{6} \int_{-\infty}^{t} \chi_{2k}(\underline{x}, t-\tau)\, a_k(\tau)\, d\tau , \quad (11)$$

where the new unknown functions, $\psi_{jk}(\underline{x})$, $\chi_{jk}(\underline{x}, t)$ satisfy:

$$\psi_{jk} = 0, \qquad \text{on } x_3 = 0 ;$$

$$\frac{\partial \psi_{1k}}{\partial n} = \begin{cases} \underline{n} \cdot \underline{i}_k , & k = 1, 2, 3, \\ \underline{n} \cdot \underline{i}_{k-3} \times x , & k = 4, 5, 6, \end{cases} \qquad \text{on } S_0 ;$$

$$\frac{\partial \psi_{2k}}{\partial n} = \begin{cases} \underline{n} \cdot \nabla \times \left[\underline{i} \times \underline{v}_0(x)\right] , & k = 1, 2, 3, \\ \underline{n} \cdot \nabla \times \left[(\underline{i}_{k-3} \times \underline{x}) \times \underline{v}_0(\underline{x})\right] , & k = 4, 5, 6, \end{cases} \qquad \text{on } S_0 ;$$

$$\frac{\partial^2 \chi_{jk}}{\partial t^2} - 2V \frac{\partial^2 \chi_{jk}}{\partial t\, \partial x_1} + V^2 \frac{\partial^2 \chi_{jk}}{\partial x_1^2} + g \frac{\partial \chi_{jk}}{\partial x_3} = 0, \qquad \text{on } x_3 = 0 ;$$

$$\frac{\partial \chi_{jk}}{\partial n} = 0, \qquad \text{on } S_0 ;$$

$$\chi_{jk} = 0, \qquad \text{for } t = 0 ;$$

$$\frac{\partial \chi_{jk}}{\partial t} = -g \frac{\partial \psi_{jk}}{\partial x_3} , \qquad \text{for } t = 0,\ x_3 = 0.$$

This solution is quite analogous to the zero-speed solution. In fact, if $V = 0$, the functions $\psi_{1k}(\underline{x})$ and $\chi_{1k}(\underline{x}, t)$ reduce to the corresponding functions introduced previously and the functions $\psi_{2k}(\underline{x})$ and $\chi_{2k}(\underline{x}, t)$ become identically zero. It has been necessary here to introduce an extra double set of functions to take care of the Timman-Newman boundary condition correction. It can be checked straightforwardly that this solution does satisfy (10a) and (10b). (In addition, there should be further conditions at infinity — which the solution is assumed to satisfy.)

As before, the quantities

$$\dot{a}_k(t)\,\psi_{1k}(\underline{x}) + \int_{-\infty}^{t} \dot{a}_k(\tau)\,\chi_{1k}(\underline{x},\, t-\tau)\, d\tau$$

can be interpreted in terms of the instantaneous and subsequent response to a sequence of velocity impulses. However, more care is now necessary. If the ship is given a unit velocity impulse in the k-th mode, it will afterwards have a unit displacement in that mode, and the potential for the fluid motion subsequent to the impulse will be

$$-Vx_1 + \varphi_o(\underline{x}) + \chi_{1k}(\underline{x},t) + \psi_{2k}(\underline{x}) + \int_0^t \chi_{2k}(\underline{x},\, t-\tau)\, d\tau\,.$$

The last two terms clearly represent the disturbance due to the steady displacement. If, on the other hand, we think of an impulse of displacement (which is rather difficult to picture), the potential for the later stages of the motion will be:

$$-Vx_1 + \varphi_o(\underline{x}) + \frac{\partial \chi_{1k}(\underline{x},t)}{\partial t} + \chi_{2k}(\underline{x},t)\,.$$

Thus it would not be proper to consider $\chi_{2k}(\underline{x},t)$ as the response to a unit impulse of displacement.

So far, we have found only the form of the velocity potential. Before we can write the equations of motion, we must know the pressure distribution on the ship hull and we must then integrate this appropriately to obtain the six components of force and moment.

The pressure anywhere in the fluid is given by Bernoulli's Equation:

$$\frac{p}{\rho} = -\frac{\partial \Phi}{\partial t} - gx_3 + \frac{1}{2}V^2 - \frac{1}{2}(\nabla\Phi)^2\,.$$

To first order in the small motion variables, this can be approximated by:

$$\frac{p}{\rho} = -gx_3 + \left[V\frac{\partial \varphi_o}{\partial x_1} - \frac{1}{2}(\nabla\varphi_o)^2\right] + \left[-\frac{\partial \varphi_1}{\partial t} + V\frac{\partial \varphi_1}{\partial x_1} - \nabla\varphi_o \cdot \nabla\varphi_1\right].$$

When we substitute into this equation the expression (11) for the velocity potential, we obtain, after some reduction,

$$
\begin{aligned}
\frac{p}{\rho} = & - g x_3 + \left[V \frac{\partial \varphi_o}{\partial x_1} - \frac{1}{2} (\nabla \varphi_o)^2 \right] \\
& - \sum_{k=1}^{6} \ddot{\alpha}_k(t)\, \psi_{1k}(\underline{x}) \\
& - \sum_{k=1}^{6} \dot{\alpha}_k(t) \left\{ \psi_{2k}(\underline{x}) + \left(-V \frac{\partial}{\partial x_1} + \nabla \varphi_o \cdot \nabla \right) \psi_{1k}(\underline{x}) \right\} \\
& - \sum_{k=1}^{6} \alpha_k(t) \left\{ \left(-V \frac{\partial}{\partial x_1} + \nabla \varphi_o \cdot \nabla \right) \psi_{2k}(\underline{x}) \right\} \\
& - \sum_{k=1}^{6} \int_{-\infty}^{t} \dot{\alpha}_k(\tau) \left[\frac{\partial}{\partial t} + \left(-V \frac{\partial}{\partial x_1} + \nabla \varphi_o \cdot \nabla \right) \right] \chi_{1k}(\underline{x}, t - \tau)\, d\tau \\
& - \sum_{k=1}^{6} \int_{-\infty}^{t} \alpha_k(\tau) \left[\frac{\partial}{\partial t} + \left(-V \frac{\partial}{\partial x_1} + \nabla \varphi_o \cdot \nabla \right) \right] \chi_{2k}(\underline{x}, t - \tau)\, d\tau .
\end{aligned}
$$

The first line on the right-hand side represents a steady pressure. The second, third, and fourth lines, respectively, depend on the acceleration, velocity, and displacement in the six modes of motion. The last two lines are convolution integrals, involving the whole past history of the velocity and displacement in the six modes.

The computation of force and moment components has been relegated to Appendix A, because it is rather tedious and does not add much perspicuity to the result. There are two problems which may be mentioned here:

1. The pressure must be evaluated on the instantaneous position of the ship hull and not on the mean position. Similarly, the instantaneous extent of the wetted hull surface must be calculated and used as the domain over which the pressure is integrated.

2. Since we wish to use the force and moment results to write down equations of motion, we must express these quantities in terms of an inertial reference frame. The geometry of the ship is most easily described in a reference frame attached to the ship, but this is accelerating and therefore it is not acceptable. The procedure adopted in Appendix A is to calculate the force and moment components with respect to the moving axes and then to use standard transformations to express them in the steadily translating Newtonian system.

The six components of force and moment are written out in Eqs. (A1) - (A10) of the Appendix A. The form of these components is as follows:

$$X_j(t) = X_{jo} - \sum_{k=1}^{6} \mu_{jk}\ddot{a}_k(t) - \sum_{k=1}^{6} b_{jk}\dot{a}_k(t) - \sum_{k=1}^{6} c_{jk}a_k(t)$$

$$- \sum_{k=1}^{6} \int_{-\infty}^{t} \dot{a}_k(\tau)\, K_{jk}(t-\tau)\, d\tau , \tag{12}$$

where X_{jo} is a steady force component, μ_{jk} is a constant depending only on ship geometry, b_{jk} and c_{jk} are constants which depend on ship geometry and forward speed, and $K_{jk}(t)$ is a function of time, geometry, and speed. None of these quantities depends on the past history of the unsteady motion. X_j represents the total hydrodynamic and hydrostatic force and moment on the ship due to its own motions, plus the static buoyancy and drag forces on the ship in its equilibrium position. In order to obtain the equations of motion, we must add to $X_j(t)$ the other forces acting on the ship, viz., the wave-induced forces, body (gravity) force, artificial restraints, propulsive force, etc., and set this sum equal to the inertial reactions, in accordance with Newton's Law.

First, we note that X_{jo} will be exactly offset by the steady propulsive force and by the gravity force on the ship, for we assume that the perturbations occur in a system which is otherwise in equilibrium. Therefore we can omit both of these external forces if we also set X_{jo} equal to zero.

Let us denote by $F_j(t)$ the six components of force and moment due to incident waves and by $G_j(t)$ the six components of all other external forces and moments (except the two steady components of force). Then the equations of motion are:

$$\sum_{k=1}^{6} m_{jk}\ddot{a}_k(t) = X_j(t) + F_j(t) + G_j(t) - \beta_j mg\, a_j(t) , \tag{13}$$

where

$\beta_j = x_3^*$, for $k = 4, 5$,

$= 0$, otherwise;

x_3^* = vertical distance of center of gravity below the origin of the coordinate system in the equilibrium position,

m_{jk} = generalized mass such that, if T = kinetic energy of the ship,

$$\sum_{k=1}^{6} m_{jk}\ddot{a}_k(t) = \frac{d}{dt}\frac{\partial T}{\partial \dot{a}_k} .$$

If the ship has lateral symmetry, it is readily found that:

$$m_{jk} = \begin{bmatrix} m & 0 & 0 & 0 & -mx_3^{\bullet} & 0 \\ 0 & m & 0 & mx_3^{\bullet} & 0 & 0 \\ 0 & 0 & m & 0 & 0 & 0 \\ 0 & mx_3^{\bullet} & 0 & I_4 & 0 & -I_{46} \\ -mx_3^{\bullet} & 0 & 0 & 0 & I_5 & 0 \\ 0 & 0 & 0 & -I_{46} & 0 & I_6 \end{bmatrix}$$

where

m = mass of ship,

I_j = moment of inertia in j-th mode, and

I_{jk} = product of inertia.

The only product of inertia which appears, I_{46}, vanishes if the ship has fore-and-aft symmetry. The other non-diagonal elements all vanish if the coordinate origin coincides with the center of gravity of the ship.

The last term in (13) arises because we allow the origin to be taken at a point other than the center of gravity of the ship. Such generality is introduced only as a convenience in hydrodynamic studies, where it is often simplest to take the coordinate origin in the free surface directly above the center of gravity. Specifically, we assume the center of gravity is located at $\underline{x}' = (0, 0, -x_3^{\bullet})$.

Equation (13), together with the associated definitions, is essentially Cummins' final form of the equations of motion, although the detailed derivation here differs somewhat from his. Some aspects are worth further note. Let us rewrite (13):

$$\sum_{k=1}^{6} (m_{jk} + \mu_{jk})\, \ddot{\alpha}_k(t) + \sum_{k=1}^{6} b_{jk}\, \dot{\alpha}_k(t) + \sum_{k=1}^{6} c_{jk}\, \alpha_k(t)$$

$$+ \sum_{k=1}^{6} \int_{-\infty}^{t} \dot{\alpha}_k(\tau)\, K_{jk}(t-\tau)\, d\tau$$

$$= F_j(t) + G_j(t) - \beta_j\, mg\, \alpha_j(t)\,. \qquad (13)$$

It is clear that μ_{jk} has the nature of an added mass. Cummins has pointed out that this is a "genuine" added mass, in the sense that it depends only on the body; it is neither frequency nor speed dependent. In heave, pitch, and roll (and their couplings), it is actually one-half of the infinite-fluid added mass of the double body. However, in surge, yaw, and sway (and their couplings), it is the added mass that corresponds to the case of the upper half-body moving oppositel to the lower half-body. In couplings between heave, pitch, or roll, on the one hand, and surge, yaw, or sway, on the other hand, it is a hybrid added mass coefficient. The physical situation was described above in the discussion of the meaning of the functions $\psi_k(\underline{x})$.

It should be mentioned that b_{jk} is not a damping coefficient and c_{jk} is not a buoyancy coefficient. The situation with respect to b_{jk} will become clearer presently. The statement about c_{jk} is obvious from Eqs. (A5) and (A6) of Appendix A.

Relations Between Time- and Frequency-Domain Descriptions

So long as we had only the ordinary differential equations to describe ship motions, it could never be clear how a ship in a confused sea would be able to respond to each frequency component as if the wave of that frequency existed separately. The experiments described in Chapter II showed that indeed the ship did respond in this way. But certainly we had no basis for expecting, in a random process, that a different differential equation could validly be used for each of the uncountably many frequency components. Such an idea makes nonsense of the whole concept of differential equations of motion. The difficulty, as already pointed out, was that the differential equations were not really differential equations at all, but simply a frequency-domain description.

Now we have a system of integro-differential equations which purport to describe the ship in a seaway, regardless of the nature of the seaway. This system of equations should, first of all, be capable of representing the ship motions if everything varies sinusoidally. In fact, it is very easy to show that it does. Let us suppose that the exciting forces, whether due to waves $[F_j(t)]$ or other external causes $[G_j(t)]$, are sinusoidal at frequency ω. After a long enough time, it is reasonable to expect that all motions will also be sinusoidal in time, so that we can write

$$a_k(t) = \alpha_k \cos(\omega t + \epsilon_k) ,$$

where α_k and ϵ_k are constants. We substitute this into (13'), noting that the convolution integral can be written

$$\int_{-\infty}^{t} \dot{a}_k(\tau)\, K_{jk}(t-\tau)\, d\tau = \int_0^{\infty} \dot{a}_k(t-\tau)\, K_{jk}(\tau)\, d\tau$$

$$= \omega\alpha_k \left\{\cos(\omega t+\epsilon_k)\int_0^{\infty} K_{jk}(\tau)\sin\omega\tau\, d\tau\right.$$

$$\left. - \sin(\omega t+\epsilon_k)\int_0^{\infty} K_{jk}(\tau)\cos\omega\tau\, d\tau\right\} ,$$

thus obtaining for the left-hand side of (13'):

$$\sum_{k=1}^{6} \alpha_k \cos(\omega t + \epsilon_k) \left\{ -\omega^2 (m_{jk} + \mu_{jk}) + c_{jk} + \omega \int_0^\infty K_{jk}(\tau) \sin \omega\tau \, d\tau \right\}$$

$$+ \sum_{k=1}^{6} \alpha_k \sin(\omega t + \epsilon_k) \left\{ -\omega b_{jk} - \omega \int_0^\infty K_{jk}(\tau) \cos \omega\tau \, d\tau \right\}$$

$$= \sum_{k=1}^{6} \ddot{\alpha}_k(t) \left\{ m_{jk} + \mu_{jk} - \frac{1}{\omega} \int_0^\infty K_{jk}(\tau) \sin \omega\tau \, d\tau \right\}$$

$$+ \sum_{k=1}^{6} \dot{\alpha}_k(t) \left\{ b_{jk} + \int_0^\infty K_{jk}(\tau) \cos \omega\tau \, d\tau \right\} + \sum_{k=1}^{6} \alpha_k(t)\, c_{jk} . \tag{14}$$

We can identify this expression directly with the left-hand side of (4), and furthermore it is clear that the right-hand side of (13') will be identical with the right-hand side of (4).* Thus Eq. (13') reduces to (4) in the special case of sinusoidal oscillations.

We note specifically that the term

$$\omega \int_0^\infty K_{jk}(\tau) \sin \omega\tau \, d\tau$$

in (14) could just as well have been combined with the term c_{jk} as with μ_{jk}. However, as mentioned previously, this ambiguity is usually resolved by including in the displacement force (i.e., in the sum over $\alpha_k(t)$) only the zero-frequency contributions. The only part of the coefficient of $\cos(\omega t + \epsilon_k)$ which is non-zero when $\omega \to 0$ is c_{jk}, and so we let it stand alone.

Thus we have seen that the time- and frequency-domain descriptions are equivalent if all functions depend sinusoidally on time. The same is true for non-sinusoidal disturbances. We show this simply by taking Fourier transforms of Eq. (13'). Suppose first that the disturbance is a transient such that all motions die out after a reasonable time and all displacements approach zero (at least asymptotically). Then we can take Fourier transforms of (13'), obtaining:

$$\sum_{k=1}^{6} \left[-\omega^2 (m_{jk} + \mu_{jk}) + i\omega b_{jk} + (c_{jk} + mg\,\beta_k\,\delta_{jk}) + i\omega \mathcal{F}\{K_{jk}\} \right] \mathcal{F}\{\alpha_k\}$$

$$= \mathcal{F}\{F_j + G_j\} ,$$

where

*The definitions of c_{jk} are slightly different in (4) and (13'), the effect of the "pendulum" terms, $mg\,\beta_j\,\alpha_j(t)$, being included in $c_{jj}\alpha_j(t)$ in (4).

$\mathfrak{F}\{f\}$ = Fourier transform of $f(t)$

$$= \int_{-\infty}^{\infty} e^{-i\omega t} f(t)\, dt\ .$$

If $f(t) = 0$ for $t < 0$, then

$$\mathfrak{F}\{f\} = \mathfrak{F}_c\{f\} - i\mathfrak{F}_s\{f\}\ ,$$

where

$\mathfrak{F}_c\{f\}$ = Fourier cosine transform $= \int_0^{\infty} f(t) \cos \omega t\, dt$,

$\mathfrak{F}_s\{f\}$ = Fourier sine transform $= \int_0^{\infty} f(t) \sin \omega t\, dt$.

The functions $K_{jk}(t)$ have this property, and so we can rewrite the transform of (13'):

$$\sum_{k=1}^{6} \left\{ \left[-\omega^2 \left(m_{jk} + \mu_{jk} - \frac{1}{\omega} \mathfrak{F}_s\{K_{jk}\} \right) + (c_{jk} + mg\beta_k \delta_{jk}) \right] \right.$$

$$\left. + i\left[\omega b_{jk} + \omega \mathfrak{F}_c\{K_{jk}\} \right] \right\} \mathfrak{F}\{a_k\} = \mathfrak{F}\{F_j + G_j\}\ . \tag{15}$$

If we multiply this equation by $e^{i\omega t}$ and, in (4), let

$$x_k(t) = e^{i\omega t}\, \mathfrak{F}\{a_k\}\ ,$$

$$f_j(t) + g_j(t) = e^{i\omega t}\, \mathfrak{F}\{F_j + G_j\}\ ,$$

then this equation is clearly equivalent to (4). In words, this means that taking the Fourier transforms of the equations of motions (that is, of the true equations in the time domain) is equivalent to breaking the forcing function into its frequency components and determining the response to each of these components. Such a result can hardly be considered as surprising, in view of what is common knowledge in control theory about the relationship between time- and frequency-domain descriptions of a linear system, but it was, until recently, a missing link in our arguments about ship motions in non-sinusoidal waves.

It was assumed above that the disturbances were transients such that, for all k, $a_k(t) \to 0$ as $t \to \infty$, so that all transforms existed in the conventional sense. The character of a ship is such that this assumption may well not be warranted, and for generality a modification of the results is necessary. In Appendix B, it is shown that if the ship system is stable, that is, if all $a_k(t)$ remain bounded for all time, then Eq. (15) is still valid even if the transform of

$\alpha_k(t)$ does not exist, provided only that we replace $\mathcal{F}\{\alpha_k\}$ by $\mathcal{F}\{\alpha_k\}/i\omega$. There will also be a singularity at $\omega = 0$, and so the modified (15) is not valid for $\omega = 0$. It is also shown in Appendix B that $\alpha_k(\infty)$ will generally be zero unless some of the c_{jk}'s are zero. This is, of course, quite reasonable, since the c_{jk}'s are restoring force coefficients (even though they are not hydrostatic restoring force coefficients).

We have now shown that the two types of equations of motion are equivalent for both sinusoidal and transient motions, provided only that the system is stable. In the third situation of interest to us, viz., a ship moving in a stationary random sea, the usual arguments of generalized harmonic analysis can be used to show that the two descriptions are again equivalent. Actually, in order to carry out the conventional spectral analysis, we need only to be certain that the assumption of linearity is valid, and evidence was presented in Chapter II to show that it is indeed valid in at least certain modes of motion. The value here of having equations of motion is in the capability which they provide for predicting the effects of various parameters on the spectral properties of the ship. They also enable us to develop test procedures, which have been called "pulse techniques," which are an order of magnitude more efficient than regular wave tests in determining the frequency domain characteristics of a ship hull. See Cummins and Smith (1964).

From (14) or (15), it is natural to define the following quantities:

$$\begin{aligned} \mu^*_{jk}(\omega) &= \text{added mass coefficient} = \mu_{jk} - \frac{1}{\omega}\int_0^\infty K_{jk}(t)\sin\omega t\,dt\,; \\ b^*_{jk}(\omega) &= \text{damping coefficient} = b_{jk} + \int_0^\infty K_{jk}(t)\cos\omega t\,dt\,. \end{aligned} \tag{16}$$

Of course, following Cummins, we previously defined μ_{jk} as an added mass. This situation merely shows how arbitrary the definition of this quantity is. The added mass defined in (16) depends on frequency and speed, and so in one sense it is not so natural as the previous definition. However, for the special case of sinusoidal oscillations, it is as reasonable a definition as the other.

In the time-domain equations, it was not possible to identify any one quantity as a "damping coefficient"; some or all of the damping was included in the forces represented by the convolution integral of (13'). In the case of sinusoidal motions, we can readily pick out certain quantities which we identify as "damping coefficients," but we must be careful in interpreting the label thus applied. If there is sinusoidal motion in just one mode, say the k-th mode, then the average rate at which the ship performs work on the water depends only on the component of force which is in phase with the velocity in that mode; in other words, the dissipation of energy depends only* on b^*_{kk}, which is properly a damping coefficient. The force components in phase with acceleration or displacement

*This is true only in the reference frame in which the water is streaming past the ship. Otherwise ship resistance is involved with the work done.

may be called "reactive" forces; they are associated with the local disturbance of the water, but they are not related to the average rate of transfer of energy.

If there are two or more modes of motion occurring simultaneously, then, as we have seen, there will be coupling between modes, and we may expect that there will be, say, j-component forces in phase with $\dot{x}_j(t)$ which result from the accelerations and displacements in the k-th mode. This will be demonstrated explicitly in the next chapter. This means that the damping in the case of coupled motions will involve the coefficients μ^*_{jk} and c_{jk}. It is still convenient to refer to the coefficients μ^*_{jk}, b^*_{jk}, and c_{jk}, for $k \neq j$, respectively, as added mass, damping, and restoring force coefficients, but it must be remembered that all are involved in the damping.

In the two expressions appearing in (16), the frequency dependence enters only through the integral terms, and it is important to note that these integrals are, respectively, the sine and cosine transforms of the same function, $K_{jk}(t)$. This fact will lead to the establishment in the next chapter of a formula relating added mass and damping coefficients.

In concluding this chapter, I would comment much as I did at the end of the previous chapter. We can now continue to use the old second order differential equations, as we did years ago. But now we know that we can, when desirable, turn to the true equations of motion, for it is these which give broader meaning physically to the equations which are valid only for sinusoidal motions. We also know that we <u>must</u> allow the "constants" in the differential equations to be functions of frequency. And finally we have obtained from this study of the equations of motion some powerful new tools: pulse methods of testing, which are an order of magnitude more efficient than the older methods, and an extremely valuable relation between added mass and damping (to be proved presently).

PROPERTIES OF TERMS IN THE EQUATIONS OF MOTION

This chapter will be devoted to some special relationships for the various terms and coefficients in the equations of motion. Specifically, the following facts will be proven:

1. The added mass matrix can be determined from the matrix of damping coefficients, and vice versa.

2. The exciting forces at zero speed can be deduced from knowledge of the far-field potential for the problem of the ship oscillating in calm water, i.e., the diffraction problem can be avoided.

3. The diagonal elements of the damping coefficient matrix can be calculated from the same far-field potentials used in (2) above. If the ship has zero speed, <u>all</u> elements of this matrix can in principle be found in this way.

In other words, if we can find velocity potentials for the six problems corresponding to the sinusoidal oscillations of a ship in calm water, we can evaluate these potentials far away from the ship (effectively at infinity) and from the resulting simplified functions determine some of the damping coefficients. From the same asymptotic forms of the potentials we can also find the forces on a ship due to sinusoidal incident waves from any direction, without having to solve the problem of determining the diffracted waves around the ship. In both problems we avoid the necessity of integrating the pressure over the ship hull. It is only necessary to integrate over a simplified mathematical surface far away from the ship. Finally, in any case for which we know the damping coefficients, we can find the corresponding added mass coefficients.

These relationships all depend on our use of a linear model to describe the ship and fluid motions, but they do not depend on a specific mathematical representation of the ship. In general, we shall be talking about the frequency-domain equations of motion; the concept of "damping coefficient" has no meaning in the time-domain equations which were developed in the last chapter.

In order to use any of the relations proved in this chapter, we must be able to find the velocity potentials for the oscillating ship problems, or at least the far-field asymptotic forms of these potentials. Finding these functions requires the assumption of a particular mathematical model for the ship, for the velocity potentials cannot be found until we have formulated appropriate boundary conditions for the whole problem, and this obviously requires some statements about the flow near the ship. Two general methods of finding the velocity potentials will be discussed in the following chapters.

It may perhaps be argued that all of these relations are academic, for there are several important gaps. To fill these gaps requires the integration of the pressure over the hull, and thus the complete potential, including the complicated local flow, must be considered. It then follows that perhaps one may as well solve the whole problem by evaluating the local potential and integrating pressure over the hull to find the forces. This may turn out to be true, but the simplicity of using the far-field potentials is so attractive that I have considered it desirable to present these partial results, hoping that someone may be able to fill the gaps in an equally simple manner.

Relation Between Added Mass and Damping Coefficients

It was pointed out previously that the frequency-dependent parts of the added mass and damping coefficients, as defined in (16), are proportional to the sine and cosine transforms of a single function, $K_{jk}(t)$. From the theory of Fourier transforms, it is well-known that, if $K_{jk}(t)$ is well-enough behaved, either of these transforms uniquely determines the inverse transform. Therefore, if <u>either</u> transform is known, the function $K_{jk}(t)$ can be found, and from this the other transform can be determined.

In the language of the ship motions problem, this means that if we know $\mu^*_{jk}(\omega)$ for any single frequency and the damping coefficients for all frequencies, we can obtain the added mass for any frequency. This result is sufficiently important that it deserves to be stated explicitly in formulas.

If

$$\int_0^\infty K_{jk}(\tau)\, d\tau$$

is absolutely convergent, then the Riemann-Lebesgue lemma* says that

$$\lim_{\omega\to\infty}\int_0^\infty K_{jk}(\tau)\sin\omega\tau\, d\tau = \lim_{\omega\to\infty}\int_0^\infty K_{jk}(\tau)\cos\omega\tau\, d\tau = 0 .$$

Then, from (16), it is evident that

$$b_{jk} = b^*_{jk}(\infty) ,$$

so that we know the constant term b_{jk} if we know $b^*_{jk}(\omega)$ for all ω (as assumed).

The inverse of the cosine transform is given by:

$$K_{jk}(t) = \frac{2}{\pi}\int_0^\infty \left[b^*_{jk}(\omega) - b_{jk}\right]\cos\omega t\, d\omega .$$

Then the added mass is:

$$\mu^*_{jk}(\omega) = \mu_{jk} - \frac{2}{\pi\omega}\int_0^\infty \sin\omega t\int_0^\infty \left[b^*_{jk}(\omega') - b_{jk}\right]\cos\omega' t\, d\omega'\, dt .$$

The last formula would be rather awkward for purposes of computations, and indeed a much simpler formula is possible. For the moment, let the upper limit of the outer integral be a large positive number, M, and interchange the order of integrations. Then we can use the Riemann-Lebesgue lemma again in letting $M\to\infty$, finding:

$$\begin{aligned}
\mu^*_{jk}(\omega) - \mu_{jk} &= -\frac{2}{\pi\omega}\lim_{M\to\infty}\int_0^\infty d\omega'\left[b^*_{jk}(\omega') - b_{jk}\right]\int_0^M \sin\omega t\cos\omega' t\, dt \\
&= \frac{1}{\pi\omega}\lim_{M\to\infty}\left\{\int_0^\infty \left[b^*_{jk}(\omega') - b_{jk}\right]\left[\frac{\cos(\omega'+\omega)M}{\omega'+\omega} - \frac{1}{\omega'+\omega}\right]d\omega'\right. \\
&\qquad \left. - \int_0^\infty \left[b^*_{jk}(\omega') - b_{jk}\right]\left[\frac{\cos(\omega'-\omega)M}{\omega'-\omega} - \frac{1}{\omega'-\omega}\right]d\omega'\right\} \\
&= \frac{1}{\pi\omega}\int_0^\infty \left[b^*_{jk}(\omega') - b_{jk}\right]\left[\frac{1}{\omega'-\omega} - \frac{1}{\omega'+\omega}\right]d\omega' = \frac{2}{\pi}\int_0^\infty \left[b^*_{jk}(\omega') - b_{jk}\right]\frac{d\omega'}{\omega'^2-\omega^2} .
\end{aligned} \tag{17a}$$

*See, for example, Whittaker and Watson (1927), p. 172.

$\displaystyle -\!\!\!\!\!\!\int_0^\infty$ indicates that a Cauchy principal value is to be used. Similarly, we find:

$$b^*_{jk}(\omega) - b_{jk} = -\frac{2}{\pi} -\!\!\!\!\!\!\int_0^\infty \left[\mu^*_{jk}(\omega') - \mu_{jk}\right] \frac{\omega'^2\, d\omega'}{\omega'^2 - \omega^2}\,. \tag{17b}$$

Equation (17a) is useful if we know $\mu_{jk} = \mu^*_{jk}(\infty)$, but it is easily shown that knowledge of $\mu^*_{jk}(\omega)$ for any single frequency is sufficient. The same comment applies to (17b) with respect to $b^*_{jk}(\omega)$. The values at $\omega = \infty$ are most likely to be amenable to calculation, although in some cases it may be easier to calculate the values at $\omega = 0$. In either of these two limiting cases, the free surface problem degenerates into a much simpler problem, and in fact numerical solutions for quite complicated geometries are possible by methods such as that of Hess and Smith (1962).

Equations (17a) and (17b) have been proven by Kotik and Mangulis (1962) for the special case of heave disturbances at zero forward speed, and these authors surmised that a similar result would be valid for all modes, with or without forward speed. Their argument was based on the observation in other fields of science* that such formulas are obtainable whenever the system response obeys a linear law and there is a clear causality relation between input and output. In the ship motions problem, linearity has been demonstrated for certain types of motion, as described in Chapter II, and Cummins' analysis was based on a linearity hypothesis. Therefore it is not surprising that the formulas can be derived from Cummins' results and the experiments indicate that we should expect the formulas to be valid. Also, there can hardly be any question about the validity of the causality assumption.†

An alternative derivation of these relations is presented in Appendix C, wherein we avoid the double transform operations which were used to derive (17a) and (17b). It is seen in the Appendix that the formulas are really just corollaries of Cauchy's Integral Formula.

Two points should be made with respect to use of these formulas:

1. Contrary to statements by Kotik and Mangulis, it does not follow that an approximate formula for, say, a damping coefficient can be used in (17a) to obtain an approximate formula for the corresponding added mass coefficient. The reason for this is that an approximate formula for damping coefficient may give good results in the range of interest for damping coefficients (especially near resonance) but the asymptotically wrong at extreme values of the frequency.

---

*Such relations are known as the "Kramers-Kronig relations" in statistical mechanics. They may be interpreted as Hilbert transforms.

†Davis and Zarnick (1964) have questioned this, because in their experiments they observed a response before $t = 0$ when an impulse occurred at $t = 0$. However, I consider their paradox a result of their choice of time coordinates and their definition of an impulse. Certainly there can be no ship disturbance until the ship encounters a free surface disturbance, and so a causality hypothesis is valid.

Since (17a) depends on the value of the damping coefficient over the whole spectrum, one may expect that the added mass will be incorrectly predicted unless $b^*_{jk}(\omega)$ is approximately correct over the entire frequency spectrum. The "Hi-Fi" approximation espoused by Kotik and Mangulis has proper asymptotic limits, and so this effect does not vitiate their calculations. However, an example to the contrary may be found in slender body theory, where added mass and damping coefficient predictions both break down at high frequency. Equations (17a) and (17b) cannot be used with predictions based on slender body theory.

2. Throughout this survey, I assume that the amplitude of all disturbances is bounded for all time, and this assumption is necessary for taking Fourier transforms of (13'). If there is an instability such as static divergence (which can occur in yaw with an inadequately controlled ship) or if there is negative damping at any frequency (which can in principle occur at high speeds), then these formulas are invalid for all modes unless the modes of difficulty are constrained to have zero amplitude.

Exciting Forces

One of the most difficult parts of using any equations of motion for analytical predictions of ship motions is calculating the forcing functions, that is, finding the force and moment exerted by the incident waves on a restrained ship. Quite often in the past, the practice has been advocated of using the pressure in the undisturbed wave and integrating it over the actual surface of the ship. In other words, it is assumed that the presence of the ship does not affect the pressure in the water. This assumption, often referred to as the "Froude-Krylov" assumption, is obviously not generally correct, although under certain circumstances it may not be grossly in error. Properly, one must formulate a boundary value problem in which there are included both the incident waves and the diffracted waves. The two systems of waves must be such that the total fluid velocity on the ship surface satisfies the correct boundary condition there.

In addition, there will be waves generated by the motions of the ship. From a hydrodynamic point of view, this presents an easier problem than the incident-diffracted wave problem, because the normal velocity component on the hull is a fairly simple, known function, depending only on the shape of the hull and on the six rigid body modes of motion. Therefore Haskind (1957) made a considerable contribution to our problem when he showed that the forces due to incident waves could be calculated from solutions of the forced oscillation problem. Specifically, he showed that if we can solve the hydrodynamic problems involved in the oscillation of a ship in an otherwise calm sea, then we can also compute the force and moment on a ship restrained in incident waves.

Haskind proved his result only for the case of a ship at zero speed. His solution is rederived in a paper by Newman (1962). Recently, Newman has shown that an analogous result can be obtained for the case of a ship with forward speed. However, there is a logical difficulty in such case, for it is not certain that the diffraction-wave potential should satisfy the ordinary linear free surface condition. This problem is discussed in the next chapter in connection with thin ship theory. We shall limit our discussion here to the published case of a ship at zero speed.

Suppose that the ship oscillates sinusoidally in the j-th mode. Let the potential be the real part of

$$v_j \varphi_j(x_1, x_2, x_3)\, e^{i\omega t} ,$$

where v_j is a real amplitude. Then φ_j satisfies the usual free surface boundary condition, a radiation condition, and a condition on the hull,

$$\frac{\partial \varphi_j}{\partial n} = f_j(x_1, x_2, x_3) \qquad \text{on } S , \tag{18a}$$

where f_j depends only on the geometry of the hull and on the mode being considered. We may look on the quantities f_j as modal weighting functions. For example, $f_1 = \cos(\underline{n}, \underline{i}_1)$. If the ship surges, the fluid disturbance due to an element of the hull surface is proportional to this direction cosine. Haskind's formula arises because this same quantity, f_1, plays a role in the inverse problem: If there is an external disturbance to the fluid, the surge-force contribution of the pressure on this element will again be proportional to f_1. (See Chertock (1962).)

To see how this works out, we must consider the potential function for the diffraction problem. Let

$$\varphi_o(x_1, x_2, x_3)\, e^{i\omega t} , \qquad \varphi_d(x_1, x_2, x_3)\, e^{i\omega t}$$

be the functions of which the real parts are the potentials, respectively, for the incident wave and the diffracted wave. (The ship is fixed in this problem.) The functions φ_o and φ_d satisfy the same free surface condition as φ_j, and φ_d satisfies the radiation condition as well. φ_o is known everywhere, but it clearly does not satisfy the radiation condition, since it represents a wave which is incident on the ship. These two potentials yield normal velocity components on the hull surface which are equal and opposite, since the hull is not moving; that is,

$$\frac{\partial \varphi_o}{\partial n} = -\frac{\partial \varphi_d}{\partial n} , \qquad \text{on } S . \tag{18b}$$

The force in the j-th mode on an element of the surface of the hull is just proportional to f_j, so that we may write for the generalized force

$$X_j = -\int_S p\, f_j\, dS ,$$

where p is the hydrodynamic pressure:

$$p = -\rho \frac{\partial}{\partial t} \operatorname{Re}\left\{(\varphi_o + \varphi_d)\, e^{i\omega t}\right\} = -\operatorname{Re}\left\{i\omega\rho(\varphi_o + \varphi_d)\, e^{i\omega t}\right\} .$$

We substitute this expression into the previous equation, and we also make use of (18a):

$$X_j = \operatorname{Re}\left\{i\omega\rho\, e^{i\omega t} \int_S (\varphi_o + \varphi_d) \frac{\partial \varphi_j}{\partial n}\, dS\right\} .$$

Since φ_j and φ_d satisfy the same radiation condition and the same free surface condition, Green's theorem yields the fact that

$$\int_S \varphi_d \frac{\partial \varphi_j}{\partial n}\, dS = \int_S \varphi_j \frac{\partial \varphi_d}{\partial n}\, dS$$

$$= - \int_S \varphi_j \frac{\partial \varphi_o}{\partial n}\, dS\,.$$

The second equality follows from (18b). With this formula, we can eliminate φ_d from the expression for X_j:

$$X_j = \mathrm{Re}\left\{ i\omega\rho\, e^{i\omega t} \int_S \left[\varphi_o \frac{\partial \varphi_j}{\partial n} - \varphi_j \frac{\partial \varphi_o}{\partial n} \right] dS \right\}. \tag{19}$$

Green's Theorem can be used again to show that the integral need not be evaluated over the actual hull surface, S, but may be evaluated over any control surface enclosing the ship. In particular, we may choose a surface arbitrarily far away, say a cylindrical surface extending from the free surface far down into the water, closed on the bottom by a horizontal surface. (The latter, as its depth becomes infinite, will contribute nothing to the value of the integral.) This is a particularly valuable result, because we avoid considering all of the local disturbance effects in φ_j. In fact, we need only asymptotic expressions for φ_j, valid far away from the ship, and such expressions will represent simply the radiated waves in the forced oscillation problem. These asymptotic forms of the potential will be the same functions which are needed to predict the damping coefficients, as will be seen in the next section.

Calculation of Damping Coefficients

In an oscillating ship problem, the existence of damping implies that the ship is performing work on the water, that is, energy is being put into the water. Since we consider always a nonviscous fluid, this energy cannot be converted into heat but must be radiated in outgoing surface waves. Thus we expect to find a relationship between the damping coefficients and the outgoing waves far away from the oscillating ship, and this relationship will be based on the law that there can be no non-zero average rate of accumulation of energy in any region of the fluid. In the derivation which follows, due to Newman (1959), it will be shown that there is a simple formula giving the diagonal elements of the damping coefficient matrix in terms of the velocity potential at infinity. Also, it will be possible to obtain a formula which relates the sum of symmetric pairs of the same matrix to the potential at infinity, but it has not yet been found possible to determine these off-diagonal elements completely separately except in the special case of zero forward speed.

We establish formulas for three energy flow rates. First, we assume that the ship is being forced to oscillate sinusoidally in some mode or combination of modes, by means of an artificial external system of forces. From knowledge of the force and the ship velocity in each mode, we can calculate the average rate at which the external force system performs work on the ship. Since the ship cannot absorb energy steadily over a long period of time, this energy is then transmitted to the surrounding water, and we calculate the average rate at which work is performed on the water. Finally, we visualize a large fixed mathematical surface far away from the ship which completely encloses the ship. There can be no average rate of accumulation of energy in the fluid region between the two surfaces, and so the rate of flow of energy out of this control surface must equal the two previous rates of energy flow.

First, suppose that the forces $F_j \cos(\omega t + \delta_j)$ are applied to the ship by some external means (there are no incident waves), and let the motions be designated by $\alpha_j(t) = a_j \cos(\omega t + \epsilon_j)$. (We suppose further that there is a superimposed steady flow past the ship at speed V. Of course, there will be a net drag force, but there will be no work done by the drag force, since the ship has no forward speed in the coordinate system chosen.) Let the equations of motion be:

$$\sum_{k=1}^{6} \left\{ \left[m_{jk} + \mu^*_{jk}(\omega) \right] \ddot{\alpha}_k(t) + b_{jk}(\omega)\, \dot{\alpha}_k(t) + c_{jk}\, \alpha_k(t) \right\} = F_j \cos(\omega t + \delta_j) .$$

The rate at which work is done on the ship by the external forces will then be

$$\begin{aligned} W &= \sum_{j=1}^{6} \dot{\alpha}_j(t)\, F_j \cos(\omega t + \delta_j) \\ &= -\omega \sum_{j=1}^{6} \sum_{k=1}^{6} a_j\, a_k \sin(\omega t + \epsilon_j) \\ &\quad \times \left\{ \left[-\omega^2 (m_{jk} + \mu^*_{jk}) + c_{jk} \right] \cos(\omega t + \epsilon_k) - \omega b^*_{jk} \sin(\omega t + \epsilon_k) \right\} . \end{aligned}$$

The average value, $\overline{W}$, over a whole cycle will be

$$\overline{W} = \frac{1}{2}\omega \sum_{j=1}^{6} \sum_{k=1}^{6} a_j\, a_k \left\{ \left[\omega^2 (m_{jk} + \mu^*_{jk}) - c_{jk} \right] \sin(\epsilon_k - \epsilon_j) + \omega b^*_{jk} \cos(\epsilon_k - \epsilon_j) \right\} .$$

We note that $m_{jk} = m_{kj}$, and so the generalized mass terms cancel each other, due to the presence of the antisymmetric factor $\sin(\epsilon_k - \epsilon_j)$. Thus

$$\overline{W} = \frac{1}{2}\omega \sum_{j=1}^{6} \sum_{k=1}^{6} a_j\, a_k \left\{ \left[\omega^2 \mu^*_{jk} - c_{jk} \right] \sin(\epsilon_k - \epsilon_j) + \omega b^*_{jk} \cos(\epsilon_k - \epsilon_j) \right\} .$$

The rate of increase of energy of the fluid within a closed surface can be written:

$$\frac{dE}{dt} = \int_S \left[\rho \Phi_t (\Phi_n - V_n) - p V_n \right] dS .$$

(See p. 14 of Stoker (1957).) Here, $\underline{n}$ is an outward unit normal vector, and V_n is the velocity component of the surface normal to itself. The surface may be a physical surface, always containing the same fluid particles, in which case $\Phi_n = V_n$, it may be a mathematical surface following an arbitrary prescribed law, or it may be a combination of real and mathematical boundaries. The same formula may be interpreted as the energy flux rate across a non-closed surface. However, one must be careful to note that a positive flux rate is to be taken in the direction opposite to the standard normal vector.

On the ship hull, which is a physical surface, we have $\Phi_n = V_n$, and so the average rate at which the ship does work on the water is:

$$\overline{W} = -\overline{\int_S pV_n \, dS}\,.$$

As a control surface far away, we take a vertical right circular cylinder extending from the free surface far down into the water, capped on the bottom by a flat horizontal surface. This is a fixed (mathematical) surface on which $V_n = 0$. Furthermore, we assume that all disturbances vanish sufficiently rapidly with increasing depth so that there is no contribution at all from the deep horizontal surface. Then the average rate at which energy passes outward through the control surface is:

$$\overline{W} = -\overline{\int_\Sigma \rho \Phi_t \Phi_n \, dS}\,,$$

where Σ denotes the cylindrical control surface. (Physically it is clear that no energy can pass through the free surface. Mathematically this statement follows from the fact that the free surface is both a physical surface, so that $\Phi_n = V_n$, and a zero-pressure surface.)

We now have three expressions for $\overline{W}$. Actually, we do not need the second one, for the desired result comes from equating the first and third:

$$\frac{1}{2}\omega \sum_{j=1}^{6} \sum_{k=1}^{6} \alpha_j \alpha_k \left\{\left[\omega^2 \mu_{jk}^* - c_{jk}\right] \sin(\epsilon_k - \epsilon_j) + \omega b_{jk}^* \cos(\epsilon_k - \epsilon_j)\right\} = -\rho \overline{\int_\Sigma \Phi_t \, \Phi_n \, dS}\,. \tag{20}$$

We have here one equation relating all of the hydrodynamic coefficients in the equations of motion with an integral of the velocity potential far away (at "infinity," for talking purposes). The problem still remains of separating as far as possible the various coefficients in (20). At the beginning of this derivation, it was assumed that the ship was forced to oscillate in an arbitrary mode or combination of modes by an external force system. Because of this arbitrariness we can separate a number of special cases of (20), by selecting the amplitudes α_j and the phases ϵ_j in appropriate ways.

First, let us assume that only one particular α_j is non-zero. If Φ_j is the velocity potential for such motion, then

$$\overline{W} = \frac{1}{2}\omega^2 \alpha_j^2 b_{jj}^* = -\rho \int_\Sigma \Phi_{jt}\,\Phi_{jn}\,dS\,.$$

Thus the diagonal damping coefficients can be calculated from the velocity potential at infinity for this mode of oscillation.

Next, let just two α_j's, say α_a and α_b, be non-zero. We can choose the relative phases so that $\epsilon_a - \epsilon_b = \pi/2$ or 0. In these two cases, then, from the respective potentials at infinity we can calculate respectively

$$\overline{W} = \frac{\omega}{2}\alpha_a\alpha_b\left[\omega^2(\mu_{ab}^* - \mu_{ba}^*) - (c_{ab} - c_{ba})\right]. \tag{21}$$

$$\overline{W} = \frac{1}{2}\omega^2 \alpha_a \alpha_b (b_{ab}^* + b_{ba}^*)\,. \tag{22}$$

From the latter, we obtain the sum of any symmetric pair of coupling damping coefficients, but it is not generally possible to find them separately.

If the ship has zero forward speed, then c_{jk} is just the hydrostatic coupling coefficient, which is easily calculated from the ship lines. In this case we can use such a calculation, together with (21), to find $\mu_{ab}^* - \mu_{ba}^*$, and from the equations (previously proved) relating added mass and damping coefficients we can in principle calculate the difference between the two damping coefficients:

$$b_{ab}^* - b_{ba}^* = -\frac{2}{\pi}\int_0^\infty \left[\mu_{ab}^*(\omega') - \mu_{ba}^*(\omega')\right]\frac{\omega'^2\,d\omega'}{\omega'^2 - \omega^2}\,.$$

(It may be recalled that $b_{ab} = b_{ab}^*(\infty) = 0$ for zero forward speed, and also $\mu_{ab} = \mu_{ab}^*(\infty) = \mu_{ba}$.) In this special case, we now have both the sum and the difference of $b_{ab}^*(\omega)$ and $b_{ba}^*(\omega)$, from which they can be individually calculated.

These formulas are useful generally only when we have found the appropriate velocity potentials for the oscillatory ship motions. The problem of finding these potentials will be taken up in the next two chapters. In the meantime, it may again be pointed out that all of the results of the present chapter require the knowledge of the potentials only at a great distance from the ship. Furthermore, there are no problems here in deciding whether the pressure must be evaluated on the actual hull position or the mean hull position. This is a great simplification in carrying out computations, but, as has been seen, there are several gaps in the results. In particular, the coupling damping coefficients cannot be found in the case of non-zero forward speed, and therefore the added mass coupling coefficients cannot be determined either. These gaps would not exist if we could calculate the c_{jk}'s, but doing this is a rather formidable undertaking; it must be recalled that these coefficients are not just the hydrostatic coupling coefficients, but, rather, they depend strongly on hydrodynamics and they involve the complicated local flow around the ship.

$$R_{Bs} = -\int_0^{\pi/2} \left\{ S_1(0)\left[S_1(1)\cos(k_1 \sec\theta) + S_2(1)\sin(k_1\sec\theta)\right]\right.$$

$$\left. - S_2(0)\left[S_1(1)\sin(k_1\sec\theta) - S_2(1)\cos(k_1\sec\theta)\right]\right\} K^2 \cos^3\theta \, d\theta \qquad (25)$$

$$K \quad 8\left[1 - \exp(-k_o \sec^2\theta)\right] .$$

From (23) we can see that the bow wave resistance consists of the sum of the wave resistance due to sine elementary waves and that due to cosine elementary waves. The same is true of the stern wave resistance in (24). The expression for the interference resistance (25) shows that there is no interference between the elementary sine waves and the elementary cosine waves starting from the same point either at the bow or the stern. The humps and hollows of the wave resistance are due to the interference resistance, and this is usually very difficult to evaluate. However, if the bow or stern wave resistance is small, the interference resistance is also small. The idea of bulbous bows or bulbous sterns is therefore to reduce the bow or stern wave resistance.

MECHANISM OF BULBOUS BOWS

We consider the bow wave (9), and the bow wave resistance (23) due to a sine ship with its source distribution

$$m_1(x) = \cos(\pi x) \qquad \text{in} \quad 0 \le x \le 1, \quad 0 \ge z \ge -1 \qquad (26a)$$

which has no cosine elementary waves but only positive sine waves from the bow in all direction of propagation. Namely $S_2(0) = 0$ in (9) and (23) and $S_1(0) \ge 0$, or we may write

$$\zeta_{sB} = \int_{-\pi/2}^{\pi/2} A(\theta) \sin\omega(0)\, d\theta \qquad (26b)$$

with $A(\theta) \ge 0$, for $|\theta| \le \pi/2$. Now we observe the regular wave height due to a point doublet of strength $-\mu$ at $(0, 0, z_1)$, which was calculated by Havelock (1928),

$$\zeta_B \sim -4k_o^2 \int_{-\pi/2}^{\pi/2} \mu \exp(-k_o z_1 \sec^2\theta) \sec^4\theta \sin\left[k_1 \sec^2\theta\,(x\cos\theta + y\sin\theta)\right] d\theta$$

$$\equiv \int_{-\pi/2}^{\pi/2} B(\theta) \sin\omega(0)\, d\theta . \qquad (27)$$

Inui, Takahei, and Kumano (1960) noticed these doublet waves also consist of sine elementary waves and that the amplitude function $B(\theta)$ is purely negative for all θ which is in $|\theta| \leq \pi/2$. Therefore the superposition of two waves (26) and (27) becomes

$$\zeta_{sB} \sim \int_{-\pi/2}^{\pi/2} [A(\theta) - B(\theta)] \sin \omega(0) \, d\theta \tag{28}$$

and the bow wave resistance is

$$R_B = \int_{-\pi/2}^{\pi/2} [A(\theta) - B(\theta)]^2 \cos^3\theta \, d\theta . \tag{29}$$

By matching $B(\theta)$ to $A(\theta)$ graphically to make $[A(\theta) - B(\theta)]$ as small as possible, especially for small θ, Takahei (1960) found the most favorable doublet strength μ and the position of the doublet z_1 in (27). They built cosine ship models according to Inui's method, observed the wave patterns by the method of stereo photographs, and tested numerous spherical bulbs faired at the cosine ship. Finally they obtained the models C-201F2 with the so-called waveless bow. Namely, they observed a remarkable reduction in the bow wave heights due to the bulb at the design speed. If we notice in (7) and (11)

$$m^{(n)}(0) = n! \; a_n \tag{30}$$

we can readily see in (9) that the bow waves consist purely of sine waves if the source distribution (7) is an even power series and consists purely of cosine waves if (7) is an odd power series. If we consider (7) with only an even power series and in addition,

$$(-1)^n \, a_{2n} \geq 0 \text{ in } (7) \tag{31}$$

(as in the cosine series) the waves will always be positive sine waves. (However, (31) is a necessary but not a sufficient condition.) Yim (1963) showed that these positive sine bow waves due to a source distribution of even power series can be completely eliminated by a doublet distribution along a semi-infinite line $x = 0$, $y = 0$, $-\infty > z \geq 0$, with the doublet strength in the negative x direction,

$$\left.\begin{aligned} \mu(z_1) &= \sum_{n=0}^{\infty} \frac{b_n z_1^{n+1}}{n+1} \qquad \text{for } 0 \leq z_1 \equiv -z \leq 1 \\ &= \sum_{n=0}^{\infty} \frac{b_n}{n+1} \left[z_1^{n+1} - (z_1 - 1)^{n+1}\right] \qquad \text{for } z_1 \geq 1 \end{aligned}\right\} \tag{32}$$

having the relation

$$b_n = (-1)^n \frac{(2n)!}{n!} \frac{k_o^{\,n}}{k_1^{\,2n+1}} a_{2n} . \tag{33}$$

Namely the amplitude function of the elementary waves from the bow for all angle θ in (28) can be made zero by attaching at the bow a concentrated doublet line which extends to infinite depth. Since the deeply submerged part does not influence too much the surface waves (Yim, 1963) this clarifies the mechanism of the bulb and backs up the approach made by Inui (1962).

SHIPS WITH ZERO BOW WAVE RESISTANCE

Krein (1955) proved that there is no finite ship which has zero wave resistance. Therefore it was essential for the latter to have an infinite doublet line. Nevertheless, ships of zero resistance is not only of academic interest but also gives us a good physical insight and directs us in practical usage.

Although a doublet is good to cancel positive sine waves, it is not applicable to cosine bow waves. Yim (1963) considered one step higher order singularities than a doublet, which is called a quadrupole. The wave height due to a point quadrupole with the strength λ_o (in x direction) at $x = 0$, $y = 0$, $z = -z_1$ in the uniform flow V generates the wave heights

$$\zeta_q \sim -8k_o^3 \int_0^{\pi/2} \lambda \exp(-k_o z_1 \sec^2\theta) \sec^5\theta \cos(k_1 x \sec\theta) \times \cos(k_1 y \sin\theta \sec^2\theta)\, d\theta \tag{34}$$

where

$$\lambda = \lambda_o/(H^3 LV) . \tag{35}$$

We notice here that (34) consists of cosine elementary waves with the same sign, $-\lambda$ in all direction θ. It was found that the cosine waves due to the source distribution (7) of odd power series can be completely eliminated by a distribution of quadrupoles along the semi-infinite line $x = 0$, $y = 0$, $-\infty > z \geq 0$ with the strength

$$\left.\begin{aligned} \lambda &= \sum_{n=0}^{\infty} b_{n+1} \frac{z_1^{n+2}}{n+2} \quad \text{in } 0 \leq z_1 \equiv -z \leq 1 \\ &= \sum_{n=0}^{\infty} b_{n+1} \frac{\left[z_1^{n+2} - (z_1 - 1)^{n+2}\right]}{n+2} \quad \text{in } 1 \leq z_1 \leq \infty \end{aligned}\right\} \tag{36}$$

and

$$b_{n+1} = \frac{(-1)^{n+1} k_o^{n+1} (2n+1)!}{(n+1)!\, k_1^{2n+3}} a_{2n+1} . \tag{37}$$

A quadrupole itself in a uniform stream does not produce a closed body, but it may, when combined with the doublet line. Therefore these quadrupoles could

221-249 O - 66 - 70

be used to improve the bulb form used to decrease the cosine wave heights as well as to cancel the sine waves.

Another idea to cancel negative cosine waves is to use a source line. In the same way as we found the infinite doublet or quadrupole line to cancel sine or cosine ship waves, we can find the line source distribution

$$\left.\begin{aligned} m(z_1) &= \sum_{n=0}^{\infty} \frac{b_n z_1^{n+1}}{n+1} \qquad \text{for} \quad 0 \le z_1 \le 1 \\ &= \sum_{n=0}^{\infty} \frac{b_n}{n+1} \left[z_1^{n+1} - (z_1 - 1)^{n+1}\right] \qquad \text{for} \quad z_1 \ge 1 \end{aligned}\right\} \tag{38}$$

with

$$b_n = (-1)^n \frac{(2n+1)!\ k_o^{n+1}}{n!\ k_1^{2(n+1)}} a_{2n+1} \tag{39}$$

which completely eliminates cosine bow waves due to the source distribution (7), of odd power series. Of course, we have to take care to employ a sink distribution at the ship afterbody in order to have a closed body.

Bulbs at ship sterns can be dealt with exactly in the same manner as for ship bows in an ideal fluid, neglecting the effect of propellers and other attachments. However, the influence of the viscosity and the wake near the stern is so important that the stern problem should really be considered separately. Therefore we deal here only with bulbous bows and bow waves. Henceforth we may omit the word "bow" except to avoid ambiguities.

In all three kinds of bulbs mentioned above, the strength of concentrated singularities along the vertical line increases with the depth, starting with zero strength at the free surface. This suggests the shape of a bulb to be used for a practical ship.

PRACTICAL APPLICATION OF THE THEORY OF WAVE CANCELLATION

In understanding the mechanics of cancelling regular ship waves through the concept of elementary waves and for the practical application we can note here three important characteristics of an elementary wave in each direction of propagation between the angles $-\pi/2$ and $\pi/2$: (1) the point where the wave starts, (2) the phase of the wave, (3) the amplitude. In general, regular bow waves consist of elementary waves which have different characteristics in each direction of propagation, despite the fact that point or line singularities by themselves produce negative sine elementary waves (pt. doublet) and cosine elementary waves (pt. source or quadrupole) in all directions of propagation from the point of the singularity's location. Therefore it is impossible to match in all directions the aforementioned three characteristics of elementary waves from bulbs with those from a <u>general</u> ship bow so that all waves are cancelled everywhere. Indeed, we have to choose carefully the ship shapes or the source distributions (7) for ships for which we adopt bulbs: namely ship shapes for which the bow waves are either positive sine waves ($a_{2n+1} = 0$, $(-1)^n a_{2n} \geq 0$) for the application of a doublet bulb, negative cosine waves ($a_{2n} = 0$, $(-1)^n a_{2n+1} \geq 0$) for a source bulb, or strong positive cosine waves plus weak (positive or negative) sine waves for a doublet bulb combined with either a source (sink) or a quadrupole bulb.

Since no waves from a finite singularity distribution for the bulb can cancel the bow (or stern) waves completely, the best bulb is such a distribution of singularities which produces waves so as to minimize amplitudes in all directions (statistically). This is equivalent to minimizing the bow (stern) wave resistance. In fact, it is not very difficult to obtain the optimum distribution of concentrated singularities in a power series of z along a finite vertical line at the bow such that minimum bow wave resistance is obtained corresponding to a given power series for the ship source distribution.

Indeed, the bow wave resistance (23) can be represented in a quadratic form in a_n of (7) and b_n (coefficients in z for the distribution of singularities as in (32), (36), or (38)) with coefficients represented in terms of Bessel functions. Therefore we have only to solve the simultaneous equations,

$$\frac{\partial R}{\partial b_n}(b_1, b_2, \ldots;\ a_1, a_2, a_3, \ldots) = 0 \qquad n = 1, 2, \ldots \tag{40}$$

for b_n when a_n are given. Since the bow resistance due to sine waves and that due to cosine waves are additive as shown in (23), the concentrated singularities for each case can be dealt with separately.

The optimum distribution of the concentrated singularities at the finite stern line for several given ship source distributions are calculated (Yim 1963) and shown in Figs. 3-7. These indicate that the strength of the singularities at the deepest point (the same level as the keel) is the largest. Especially for the higher Froude numbers, the optimum distributions appear to be almost concentrated at the keel. This rather supports Wigley's fourth rule. However the optimum size of the bulb is extremely sensitive to the Froude number. We notice in Figs. 3-7 almost a linear distribution of the doublet for the low Froude numbers. If we were given the volume of the bulb, the optimum distribution would be also sensitive to the Froude number and the displacement of the bulb would gradually move from the keel closer to the surface as the Froude number increases, since the effect of a bulb is stronger at a smaller depth. This would clarify the difference in the opinions of Wigley and Weinblum mentioned before in our introduction. However, in actual ships, the wave resistance is not the only problem.

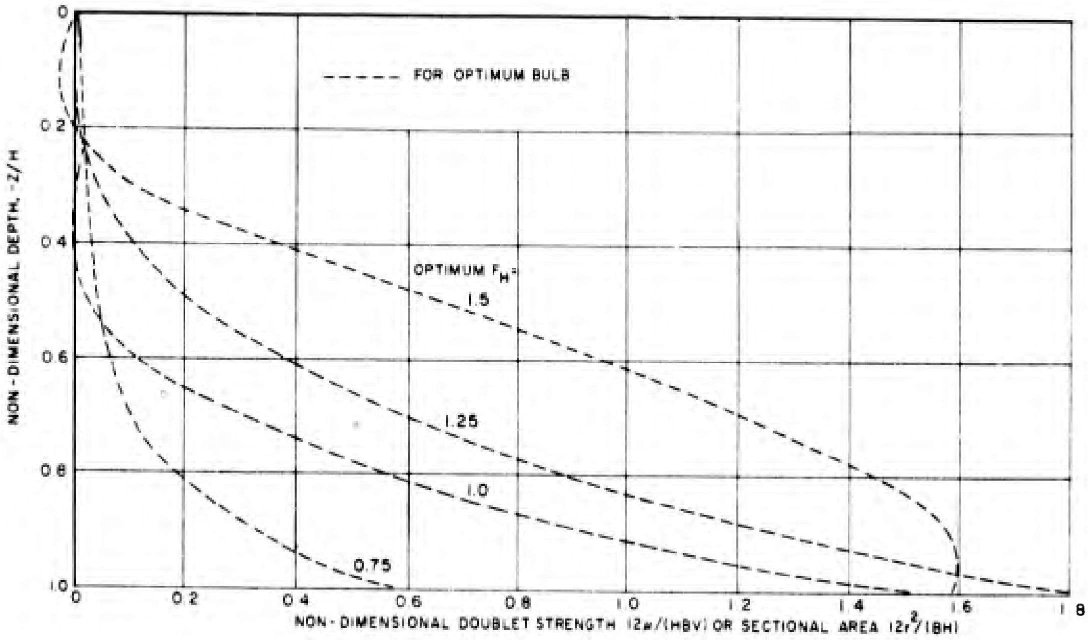

Fig. 3a - Doublet distribution for sine ship (L/H = 16)

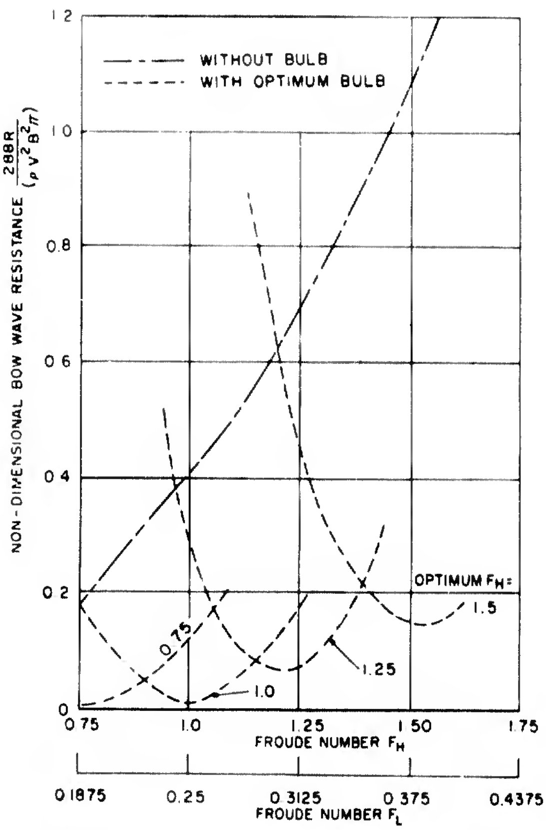

Fig. 3b - Bow wave resistance of sine ship (L/H = 16)

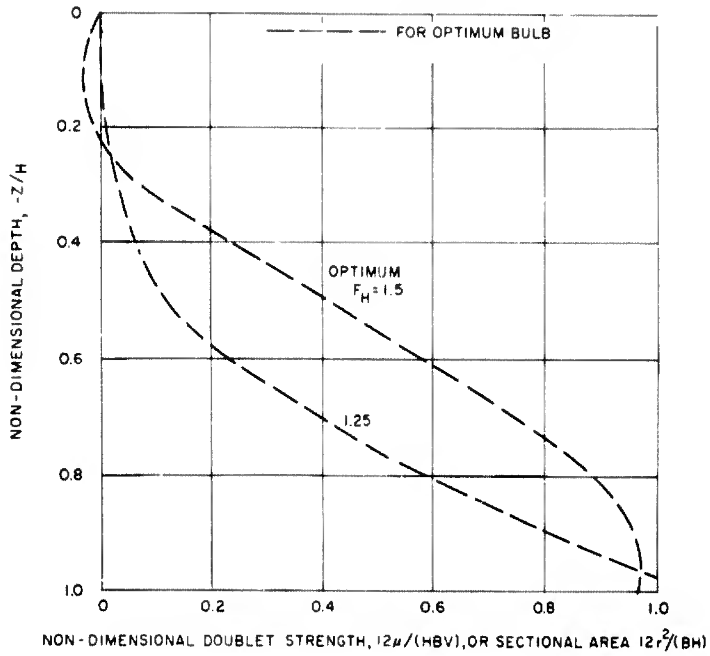

Fig. 4a - Doublet distribution for sine ship (L/H = 24)

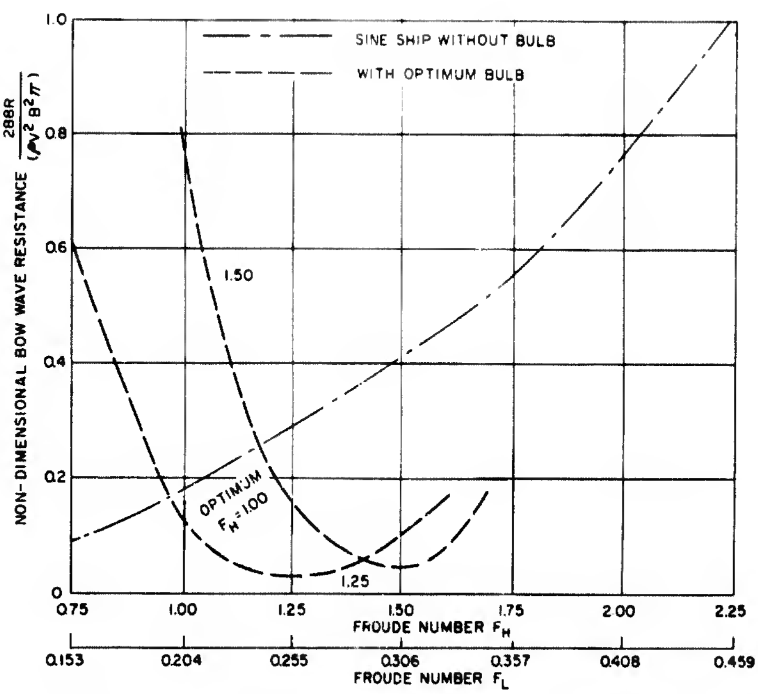

Fig. 4b - Bow wave resistance of sine ship (L/H = 24)

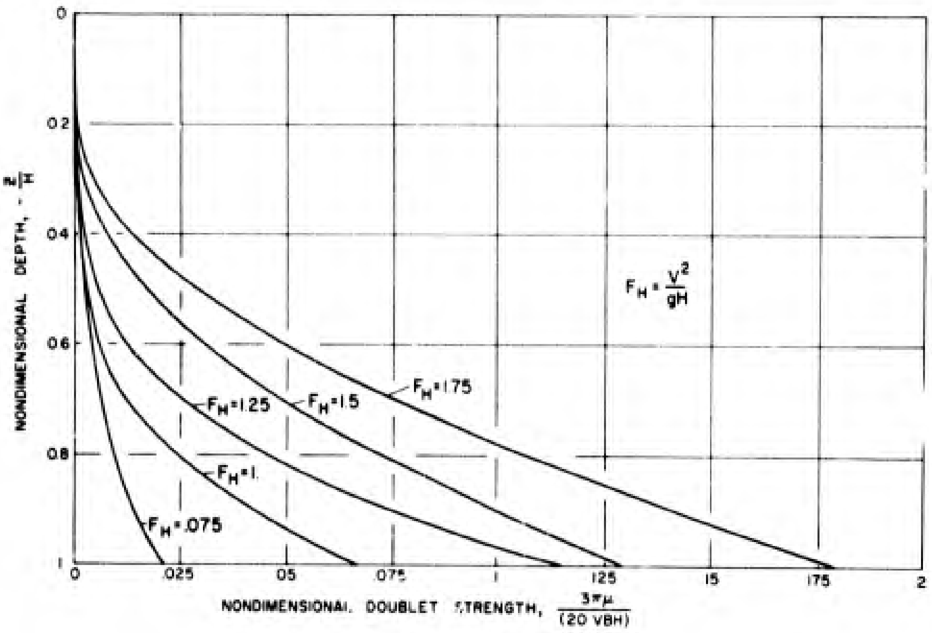

Fig. 5a - Doublet distribution for a parabolic ship $Y = 2B/L \times (X - X^2)$, $(L/H = 16)$

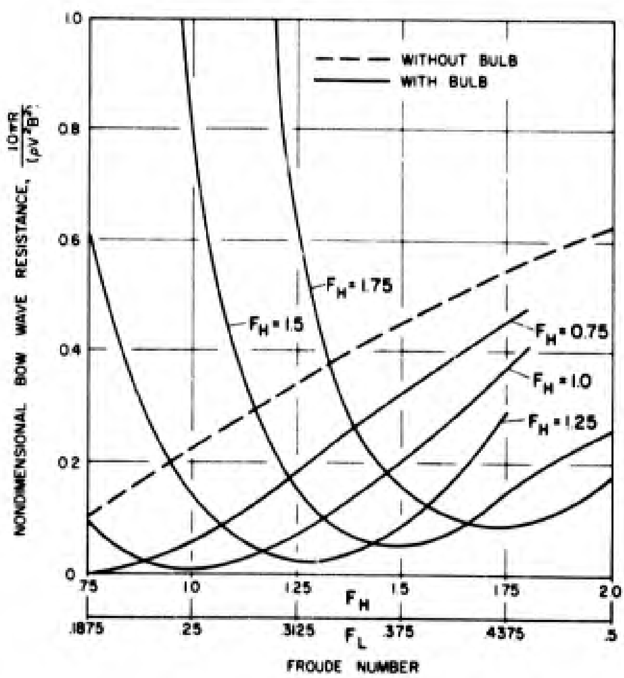

Fig. 5b - Bow wave resistance due to the first term in the source distribution of a parabolic ship, $m = 1/\pi\ B/L \times (1 - 2X)$, $(L/H = 16)$

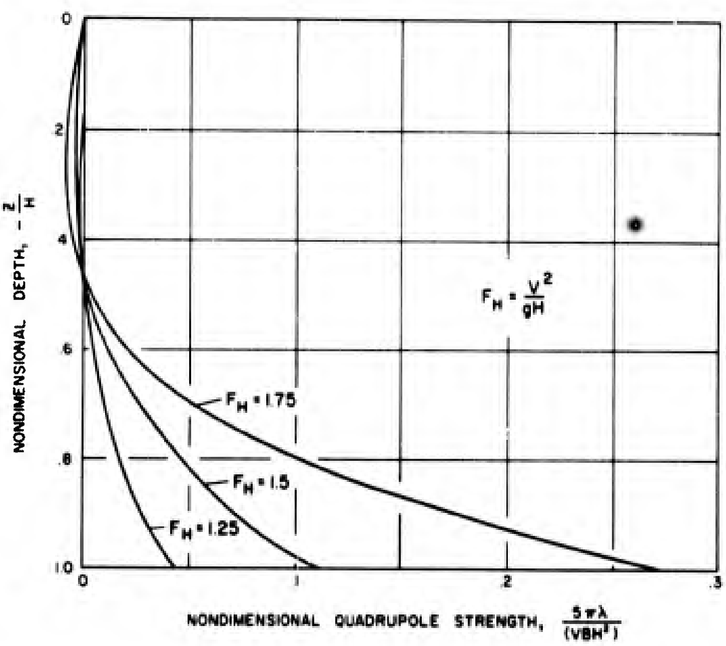

Fig. 6a - Quadrupole distribution for a parabolic ship $Y = 2B/L \times (X - X^2)$, $(L/H = 16)$

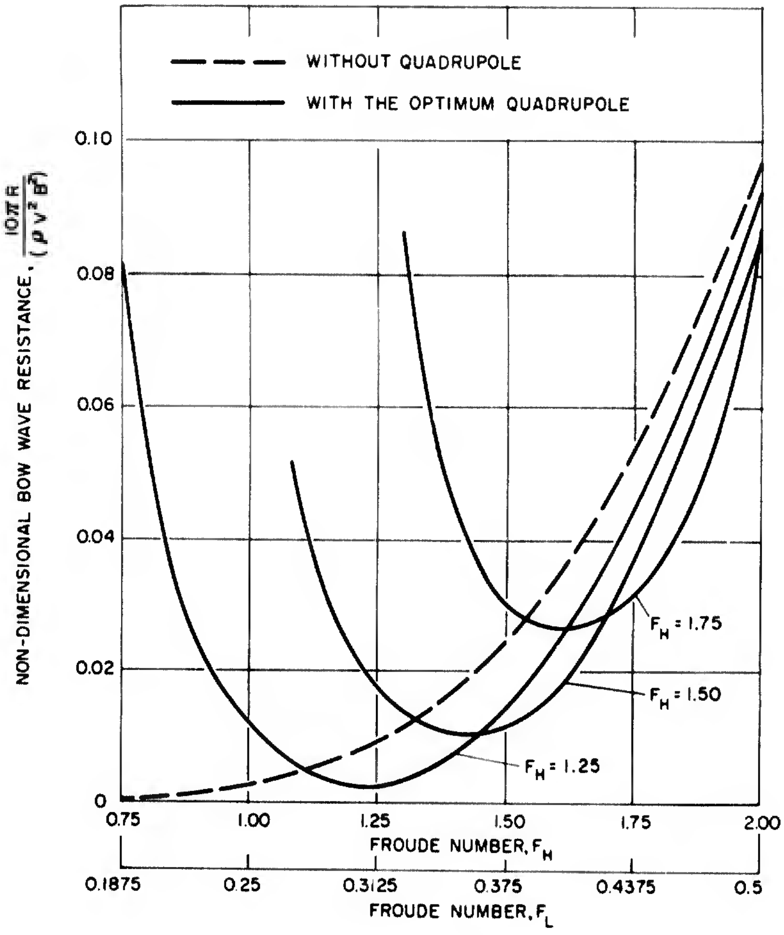

Fig. 6b - Bow wave resistance due to the second term in the source distribution of a parabolic ship, $m = 1/\pi \; B/L \times (1 - 2X)$, $(L/H = 16)$

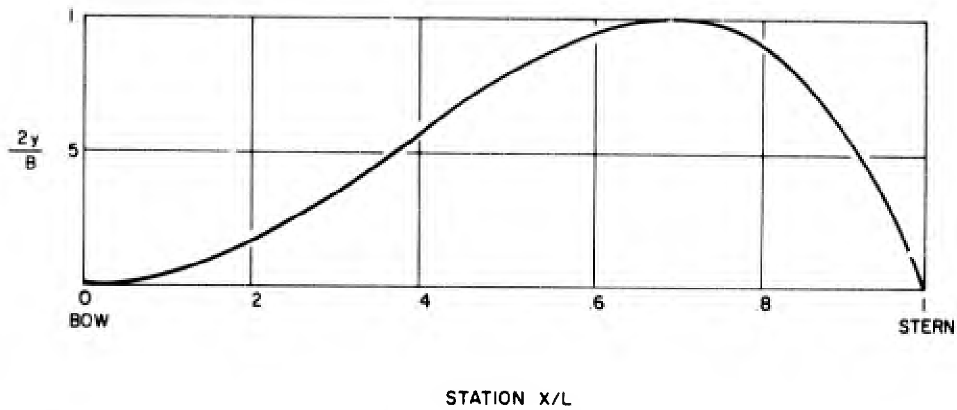

Fig. 7a - Graphical representation of a hollow ship

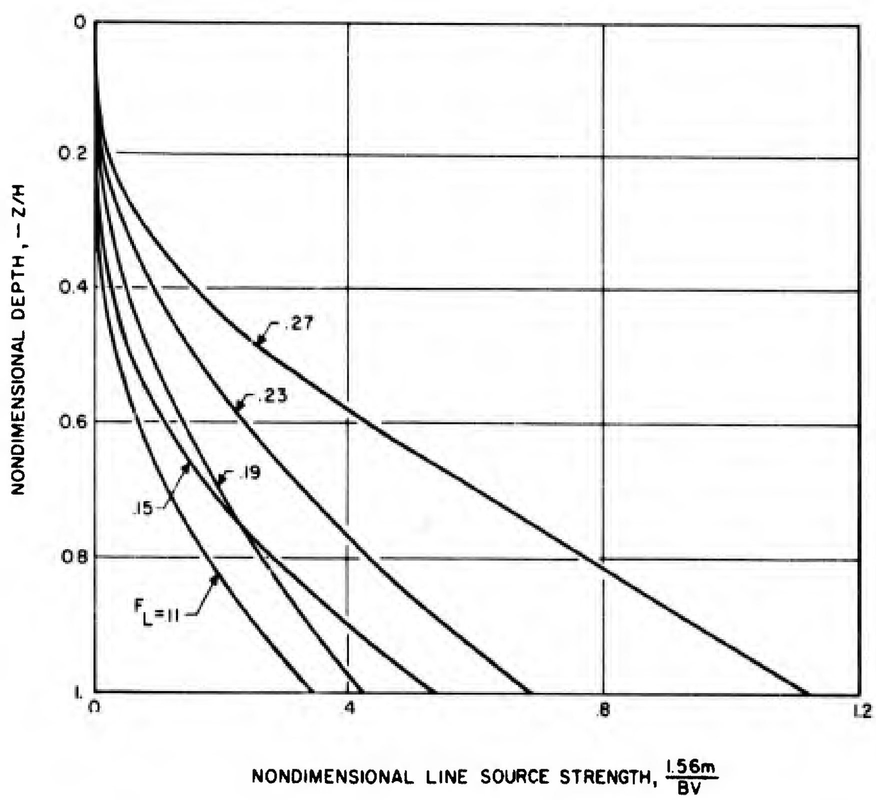

Fig. 7b - Optimum line source distribution
for the hollow ship

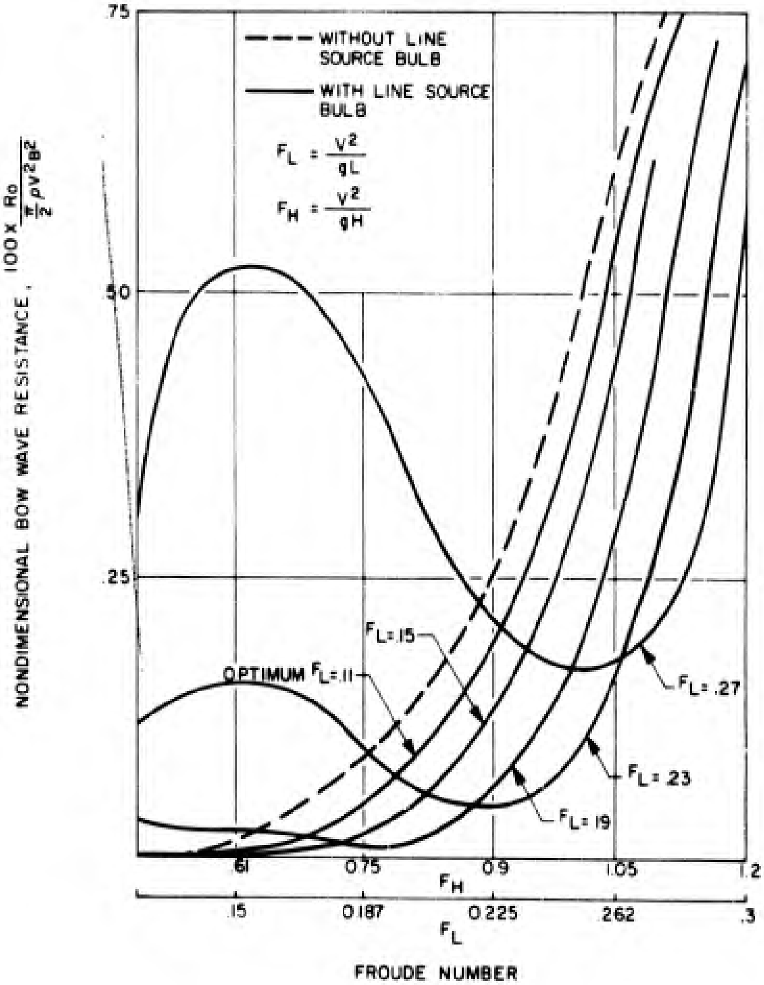

Fig. 7c - Bow wave resistance of the hollow ship

There are many side problems even with the bulbous bow alone, i.e., spray, slamming, cavitation, form drag due to separation, etc. In this respect, the bulb made of a source line for a hollow ship seems to be more favorable than a doublet bulb, especially for lower Froude numbers, since the source bulb will not produce any marked swan neck shape. It may be worth noting here again that the bulb is not necessarily made of a doublet, but it can be a concentrated source at the bow near the keel, or a doublet plus a source or a quadrupole depending upon the original hull shape.

Of course it is possible to consider the adjustment of the location of bulbs instead of considering only the shapes of bulbs with a fixed location. However, in this case, it is not easy to find the best location from the theory of wave cancellation only, since cancellation of elementary waves in one direction of propagation does not mean that cancellation occurs in the other directions. Yim (1962) considered a most simple case of a point source and a doublet in a uniform stream under a free surface as in Fig. 8. As mentioned already, a point source produces positive cosine waves while a point doublet produces negative sine waves. By using Lagalley's theorem, he obtained forces at the doublet point and the source point separately as shown in Fig. 8 corresponding to the optimum distance "a" between the two points (shown in Fig. 9), which was calculated so as to minimize the total force in the x direction. If we consider only the wave phases along the centerline through the two points, the distance "a" should always be one quarter of the wavelength λ_o for cancellation of phases,

$$\frac{\lambda_o}{4} = \frac{V}{4} \times \frac{2\pi V^2}{gr} = \frac{\pi}{2} F_r^2 .$$

However, it is shown in Fig. 9 that the optimum "a" is always less than $\lambda_o/4$. Figure 8 shows the remarkable reduction of the total wave resistance in this case. In addition, the negative force at the doublet is rather an interesting phenomena. The shape of bulbs made of these singularities can be produced by plotting the body streamlines as Inui does for his double model, or we may use an approximate sphere for a point doublet and the head of a Rankine ovoid for a point source.

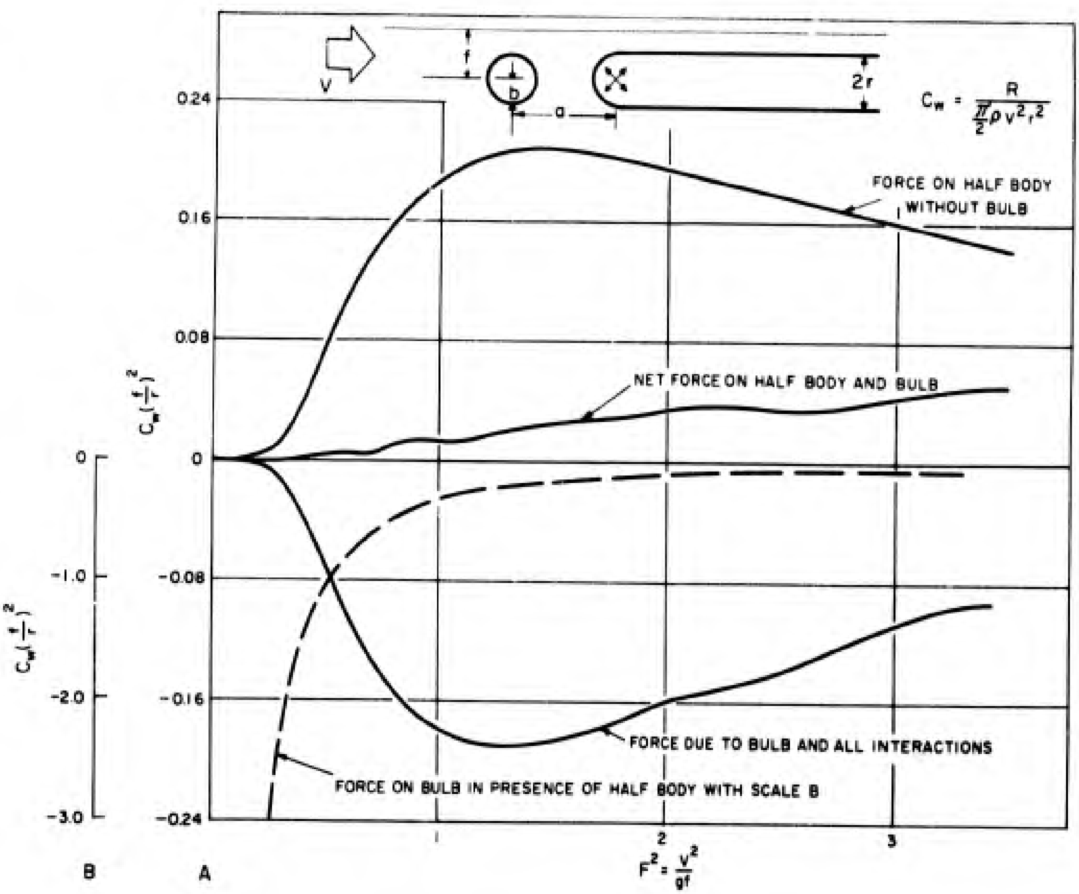

Fig. 8 - Wave resistance of half body with optimized bulb

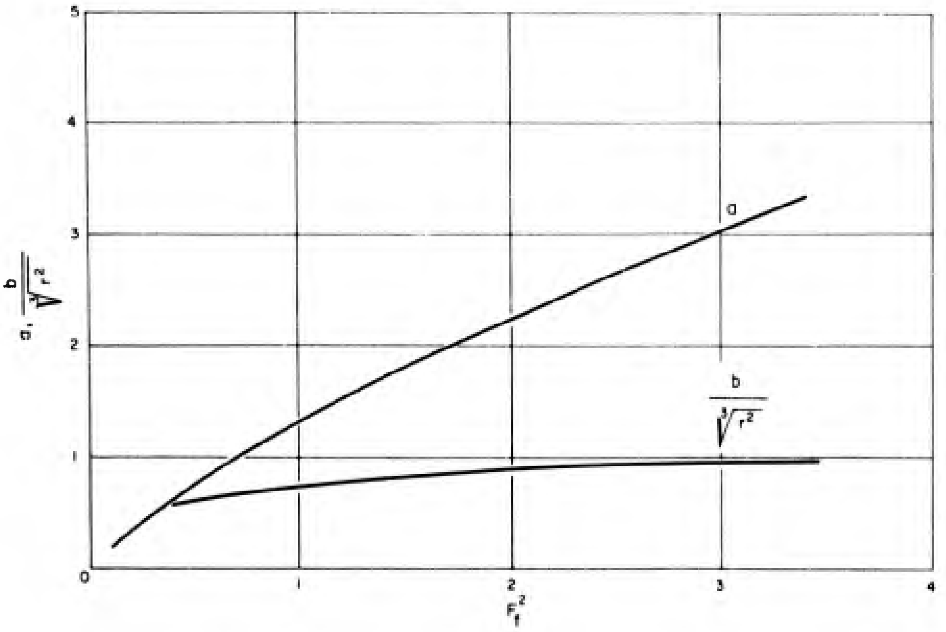

Fig. 9 - Optimum distance between source and doublet, optimum radius of bulb (a, b, r are non-dimensionalized with respect to the depth f)

HIGHER ORDER EFFECT ON THE ELEMENTARY WAVES

In the case of a sine ship (26a) which has theoretically only positive sine waves starting from the bow and the stern, Inui and his colleagues observed in their experiment with Inui's model of the sine ship a forward shifting of the wave phase. Therefore, they had to stick their bulb quite a bit forward of the bow instead of locating the bulb center at the stern. They seem to have had a serious concern about this discrepancy between the theory and the experiment. It has been speculated in Japan that the explanation may be in the orbital wave motion on the ship boundary (Takahei, 1960), or in the non-zero Froude number effect (Inui, 1962), since Inui's model is exactly right for his source distribution only in the case of zero Froude number. Inui used two correction factors which are determined by experiments to correct this observed effect together with the influence of viscosity. We will now discuss an explanation for Inui's observations which are based on higher order wave theory.

For a long time since Havelock's representation of a ship by a singularity distribution, people have been very curious about the exact ship form generated by these singularities which satisfy all the conditions including the linearized free surface condition for a non-zero Froude number. Havelock (1936) and Bescho (1957) considered submerged simple bodies including the free surface effect on body representation, and indicated this effect could be large. Sisov (1961) formulated a higher order theory of wave resistance on surface ships.

However the calculations involved are so complicated that no one seems to have succeeded yet in producing a significant result from this higher order theory of surface ships.

Recently, in connection with the theory of wave cancellation in bulbous bowed ships, Yim (1964) considered the Froude number effect on the ship representation near the free surface, and its influence on the regular wave far behind the ship.

We consider a uniform source distribution whose strength

$$m = a_o \tag{41}$$

in $0 \le x \le 1$, $y = 0$, $-\infty < z < 0$, in the uniform flow considered in this report.

The y component of velocity at (x, y, z) is

$$v_y = \int_0^1 \int_0^\infty d\zeta\, d\xi\, a_0 \frac{\partial}{\partial y} \left[\frac{1}{r_1} + \frac{1}{r_2} - \frac{1}{\pi} \operatorname{Re} \int_{-\pi}^{\pi} \int_0^\infty \frac{k e^{k(i\omega - |z+\zeta|)}}{k - k_o \sec^2\theta - i\mu \sec\theta}\, dk\, d\theta \right] \tag{42}$$

where

$$\begin{aligned} r_1 &= \left[(x-\xi)^2 + y^2 + (z-\zeta)^2 \right]^{1/2} \\ r_2 &= \left[(x-\xi)^2 + y^2 + (z+\zeta)^2 \right]^{1/2} \\ \omega &= (x-\xi) \cos\theta + y \sin\theta . \end{aligned} \tag{43}$$

At a point (x, y, o) which is not on the singularity plane, the last quadruple integral $J(x, y, o; \xi)$, say, can be written

$$\begin{aligned} J(x,y,o;1) - J(x,y,o;0) = {} & \frac{1}{\pi} \operatorname{Re} \int_{-\pi}^{\pi} \int_0^\infty \frac{\sec\theta \sin\theta\, e^{ik[(x-1)\cos\theta + y\sin\theta]}}{k - k_o \sec^2\theta - i\mu \sec\theta}\, dk\, d\theta \\ & - \frac{1}{\pi} \operatorname{Re} \int_{-\pi}^{\pi} \int_0^\infty \frac{\sec\theta \sin\theta\, e^{ik(x\cos\theta + y\sin\theta)}}{k - k_o \sec^2\theta - i\mu \sec\theta}\, dk\, d\theta . \end{aligned} \tag{44}$$

When we consider the limiting case of $y \to 0$ in $J(x, y, o; 1)$, this becomes zero for any k_o since the integrand is antisymmetric in θ. Now if we change the variable $k \to k_o k$

$$J(x,y,o;1) = \frac{1}{\pi} \operatorname{Re} \int_{-\pi}^{\pi} \int_0^\infty \frac{\sec\theta \sin\theta\, e^{ikk_o(x\cos\theta + y\sin\theta)}}{k - \sec^2\theta - i\mu \sec\theta}\, dk\, d\theta . \tag{45}$$

This is a function of only $k_o x$ and $k_o y$. The case when $x \to 0$, $y \to 0$ for a certain k_o is exactly the same as the case when $k_o \to 0$ for certain fixed values of x and y. For $k_o \to 0$, or the case of infinite Froude number,

$$\phi_y = 0 \quad \text{on} \quad z = 0 .$$

Therefore, for any k_o

$$\lim_{\substack{x \to 0 \\ y \to 0}} \phi_y = 0 \quad \text{on } z = 0 \tag{46}$$

The above argument can also hold for a point $(1 + x, y, o)$ as $x \to 0$, $y \to 0$.

Although we considered points only on $z = 0$, we notice from the potential theory that physical quantities change continuously into the potential flow field from the boundary. This indicates that every surface ship which is represented by a centerplane source distribution has as strong an influence of the free surface on the shape of the ship in a certain neighborhood of the free surface as in the case of infinite Froude number.

The influence of the free surface can be explained much more eloquently by Green's formula for the velocity potential ϕ which satisfies the Laplace equation (2) with the boundary conditions (3), (4) and

$$\phi_n = \frac{\partial \phi}{\partial n} = - \bar{n} \bar{V} . \tag{47}$$

($\bar{n}$ is the normal vector at the ship hull surface into the fluid.) On a given ship hull,

$$\phi = \frac{1}{4\pi} \iint_S \left[\phi(\xi,\eta,\zeta)\, G_n(\xi,\eta,\zeta,x,y,z) - \phi_n(\xi,\eta,\zeta)\, G(\xi,\eta,\zeta,x,y,z)\right] dS \tag{48}$$

where S includes the free surface S_F and the ship surface S_s (see Fig. 2). G is the well known Green's function (see e.g., Stoker 1957) which is a harmonic function for $\zeta < 0$ except at (x, y, z) where it has the singularity

$$1/\left[(\xi - x)^2 + (\eta - y)^2 + (\zeta - z)^2\right]^{1/2} ;$$

and G satisfies the boundary conditions (3), (4) and

$$G_\eta = 0 \quad \text{on} \quad \eta = 0 .$$

The integral on the free surface S_F in (48) can be written by using (3)

$$I = \iint_{S_F} [\phi G_n - \phi_n G]\, dS = - \iint_{z=0} [\phi G_z - G\phi_z]\, d\xi\, d\eta$$

$$= \frac{1}{k_o} \iint_{z=0} \left[\frac{\partial}{\partial \xi}(\phi G_\xi) - \frac{\partial}{\partial \xi}(\phi_\xi G)\right] d\xi\, d\eta$$

$$= -\frac{1}{k_o} \oint_{\Gamma} (\phi G_\xi - \phi_\xi G)\, d\eta \tag{50}$$

where Γ is the intersection of the ship surface and the $z = 0$ plane. Since the ship beam length ratio $B/L = \epsilon$ is considered to be small, in general, (50) is omitted in the first order theory.

Wehausen (1962) considered a systematic, formal, yet thorough estimation of the order of magnitude in the Green's formula with the exact boundary conditions of the potential. For a ship with the draft H as small as the beam B, he estimated I in (50) is $O(\epsilon^3)$ while the main integral around the ship hull in (48) is $O(\epsilon^2)$. In fact it has been known that the effect of the draft behaves like $\exp(-CH)$ where C is a function of Froude number and even for the case $H/B = 2$, the wave heights was comparable to the case $H \to \infty$ (Wigley, 1931). Therefore the above estimation may be true even for the case of an infinite draft ship, and the line integral I, in this case will be the most important contribution to the higher order terms which have been previously neglected. Indeed, in (50), I is the influence of the free surface on the potential.

However, it is extremely difficult to understand the higher order effect just by the formal estimation of the magnitude and without actual evaluation, since the property of Green's function is very complicated particularly near the free surface. As a simplest case for the evaluation of the line integral, Yim (1964) considered a source distribution

$$m = a_o \quad \text{in} \quad 0 \le x \le a, \quad y = 0, \quad -\infty < z \le 0$$

on the forebody of a semi-infinite wedge shaped strut,

$$y = x \tan \alpha \quad \text{in} \quad 0 \le x \le a$$

$$-\infty \le z \le 0$$

$$y = \tan \alpha \quad \text{in} \quad 0 \le x \le \infty$$

$$-\infty \le z \le 0 .$$

For ϕ or ϕ_ξ inside the line integral (50) he used the first order solution obtained by Havelock (1932),

$$\zeta_1 = -\frac{\pi}{k_o}\frac{a_o}{V}\left[\int_0^{k_o \xi} [H_o(t) + 3Y_o(t)]\, dt - \int_0^{k_o(a-\xi)} [H_o(t) - Y_o(t)]\, dt\right]$$

where H is the Struve function and Y is the Bessel function of the second kind. If we use the relation from the pressure condition on the free surface

$$_1 \quad \frac{}{k_o}$$

and the Green's function represented on the free surface

$$G_x(\ ,0,0,x,0,0) \quad -\frac{k_o}{} \mathrm{Re} \int \int_0 \frac{ik \sec \ e^{ki}}{k - k_o \sec^2 \ - i \ \sec} \, dk\, d$$

$$\left[-4 k_o^2 \frac{d}{dt} Y_1(t) + k_o^2 \frac{d^2}{dt^2} \left[H_o(t) - Y_o(t)\right]\right]_{t \ k_o(x-)}$$

we can evaluate the line integral (50) at large x and $y \ 0$ neglecting higher order terms,

$$_1 \quad \frac{I_x}{k_o} \quad - 2 \tan \left[(k_o x - t) \frac{d}{dt} Y_1(t)\right]_{t \ k_o x}^{k_o(x-a)}$$

$$+ 4 \tan k_o \int_0^a \ _1 \left[\frac{d}{dt} Y_1(t)\right]_{t=k_o(x-)} d \ .$$

If we take only the lower limit of the above equation, it can be considered from the equation for the surface wave to represent a regular wave starting from the bow due to the influence of the free surface. From here Yim (1964) calculated the amplitude and the phase of the regular bow wave $_1$ far behind the ship on $y \ 0$ due to the line integral,

$$_1 \quad P \sin\left(k_o x + \frac{}{4} + \ \right) .$$

It is easy to see from Havelock's result that the regular bow wave $_1$ from the first order theory is,

$$_1 \quad Q \sin\left(k_o x + \frac{}{4}\right)$$

$$Q \quad \frac{4}{k_o} \frac{a_o}{V} \sqrt{\frac{2}{k_o x}} .$$

In Fig. 10 are shown the phase difference and

$$\frac{P}{Q \tan \alpha} = f(k_o a)$$

which are functions of only $k_o a$. The amplitude of the total wave ζ_t

$$\zeta_t = \zeta_1 + \zeta_{1'}$$

$$= \sqrt{Q^2 + P^2 + 2QP \cos \beta} \, \sin\left(k_o x + \frac{\pi}{4} + \delta\right)$$

and the phase difference δ between the total wave ζ_t and the first order wave ζ_1 are shown in Figs. 11 and 12. β and δ are shown in radian, considering that one wave length $(2\pi/k_o)$ is just 2π.

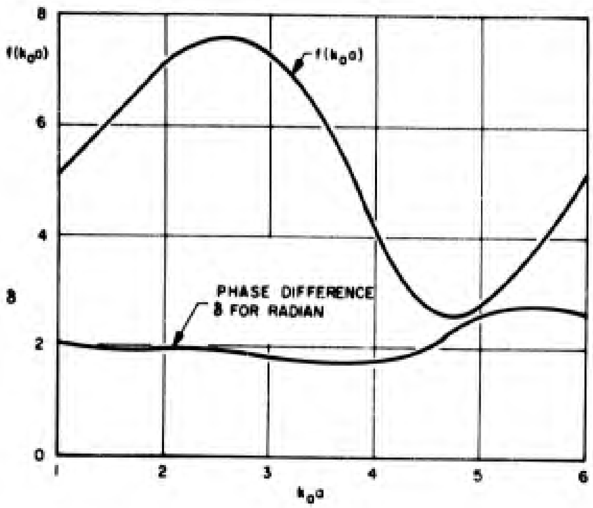

Fig. 10 - Phase difference between the first and the higher order waves δ, and the amplitude ratio/half entrance angle, $f(k_o a)$

These show that the total wave phase is indeed advanced considerably compared with the first order wave, while the amplitude of the total wave height does not differ too much from that of the first order wave. Namely the second order effect is quite large. It is proportional to the slope of the entrance on the free surface, for a given run, a. Therefore, the smaller the entrance slope near the free surface is, the less the second order effect to be expected. As we see in the integrand of the line integral (50), this effect mainly depends on the potential and the wave on the free surface waterline where the waterline slope is large. Since the local effect is usually big near the bow and the shoulder, the influence of the local effect on the second order wave may be quite important.

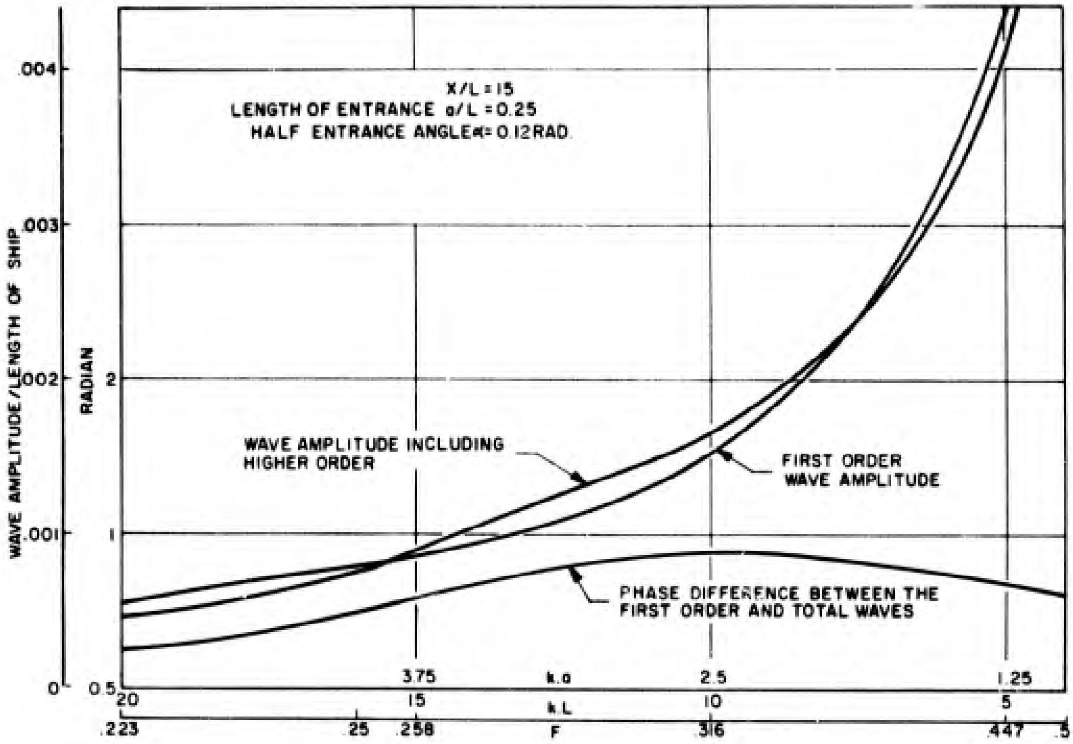

Fig. 11 - Comparison between the first order wave and the total wave (α = 0.12 rad)

THIN SHIP THEORY

Historically, the thin ship idealization was introduced by Michell in his famous study of ship wave resistance. In order to formulate a consistent linearized free surface problem for a ship moving at finite speed, it is necessary to assume that there is some identifiable property of the ship which makes the ship produce a very small disturbance, in spite of its moving at an arbitrary finite speed. Michell chose to consider "thin ships," that is, ships with such a small beam/length ratio that they may be pictured as knife-like.

If we were concerned only with ship motions at zero speed of advance, such problems would not concern us. However, we certainly do not want to restrict ourselves in such a way. Furthermore, a rational theory of ship motions which includes forward speed effects should include the special case of steady forward motion (without time-dependent perturbations). Therefore we are forced to give consideration to the linearization problems which have so disturbed mathematicians working on wave resistance theory.

Michell assumed that, in addition to linearizing the free surface condition, he could replace the boundary condition on the hull by a requirement that there be a certain anti-symmetrical component of velocity normal to the ship center plane. In recent years it has been demonstrated that the latter simplification <u>follows</u> logically from the assumption of small beam, if only we assume that the potential flow can be continued analytically into the hull up to the center plane; it is not a separate linearization.* See, for example, Wehausen (1957) or Stoker (1957). There has been much discussion of this point in recent years, naval architects arguing that there ought to be an improvement in predictions if the hull boundary condition is satisfied exactly — even though the free surface condition remains linearized.

At the risk of offending both naval architects and mathematicians, I must insist that this remains an open question. Certainly, from the point of view of thin ship theory, such a patching-up of procedures is at least inconsistent and could give misleading results, but the grounds for accepting the thin ship idealization are not very secure either. I would hope that some day <u>numerical</u> results may be presented which are based on such a hybrid approach.† Then it may be possible to compare these results with the predictions of the strict thin ship theory and with experiments, to find out whether the present apparent shortcomings of the theory can be laid to the simplification of the hull boundary condition.‡ If such appears to be the case, then we shall have to presume that the premises of thin ship theory are at fault.

---

*Newman has claimed that even the assumption of the possibility of analytic continuation is not needed. See p. 39, Newman (1961).

†We had had hopes of obtaining just such results from the work at the Douglas Aircraft Co. See Smith, Giesing, and Hess (1963). Apparently the problem is still too complicated for present day methods, even with computers such as the IBM 7090.

‡Before this is possible, there will have to be a tremendous improvement in our understanding of the experiments as well.

Some of this controversy has been stimulated by the observations, largely in Japan and Germany, that if a centerplane source distribution for a thin body in an infinite fluid is determined by the recipe of thin ship theory, and if the streamlines which result from this source distribution are actually traced, it is found that the body which is generated is quite different from that which was originally prescribed. This observation certainly suggests that one should be more careful than heretofore about satisfying the body boundary condition.

However, I can only assume that the investigators who discovered this fact have never tried to trace streamlines in a linearized free surface problem. Figure 6 shows the results of tracing streamlines in a very simple linearized free surface problem. A dipole is located at (0,0) in the figure, and there is a steady superimposed flow from left to right. Of course, a dipole exactly generates a circle in the flow of an infinite fluid (in two dimensions). For the flow depicted, the dipole potential has been modified to satisfy the linearized free surface condition on $y = 2$. We would expect that under these conditions, the "free surface dipole" might generate a somewhat distorted circle. However, we note first of all that it does not even generate a closed body; the forward and after stagnation points lie on different streamlines! The streamline containing the after stagnation point passes right out of the lower half-space, as if it were part of a vertical jet flow. This is immediately followed by a downward jet, as the same streamline re-enters the lower half-space. The double-jet pattern repeats every cycle of the wave behind the "body." On the other hand, the ordinary linearized-theory free surface condition gives the broken line as the free surface shape — a not unreasonable looking wave, although its amplitude is rather extraordinary.

This figure was prepared by Dr. E. O. Tuck, to whom I am indebted for allowing its use here. He will be publishing a paper soon which will include a discussion of the problems pointed up by this calculation. Here it must suffice to say that, although the case depicted is so severe that one would be suspicious of linearized theory, one would not expect the streamlines to do such ridiculous

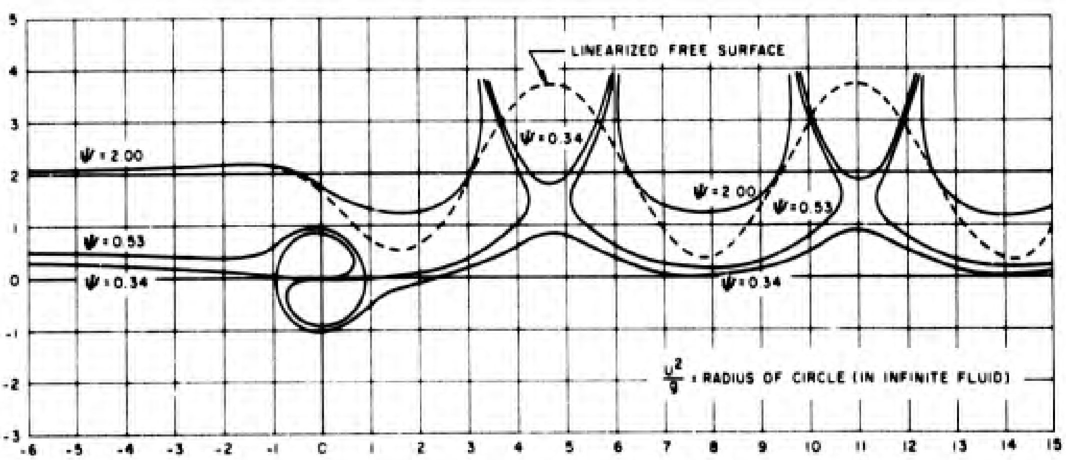

Fig. 6 - Streamlines around a dipole under a free surface (linearized problem) (by courtesy of Dr. E. O. Tuck)

things. The non-existence of a closed body can be rationalized easily. However, the manner in which the streamlines cross the linearized free surface curve appears to be most unreasonable. At the least, it suggests that much more study must be devoted to these streamlines before we jump to far-reaching conclusions about how best to improve satisfaction of the body boundary conditions. Perhaps it is more important to satisfy the free surface condition exactly. Tuck has made force calculations which suggest that this may be the case.

It must be emphasized that the strange behavior of the streamlines depicted in Fig. 6 has nothing to do with nonlinearities, except inasmuch as we are neglecting them. The streamlines shown are those which result from solution of the first order (linearized) problem. We usually accept the idea that solutions of linearized free surface problems may be physically invalid just because the problems are linearized, that is, because we have omitted and/or simplified some terms in the boundary conditions. This example demonstrates that the linearized solution can be meaningless because it is internally physically contradictory.

Regardless of these problems, we can formulate a self-consistent mathematical theory for the motions of a thin ship, and the theory will include the Michell-Havelock wave resistance theory as a special case. This was first done in a general way by Peters and Stoker (1954). Their work is quite well known in our field, especially since most of it was reproduced by Stoker (1957) in his monograph on wave problems. Only a very brief discussion of it will be presented here.

Peters and Stoker first formulate the exact nonlinear problem of a ship performing arbitrary motions in a nonviscous, incompressible fluid with a free surface not able to sustain surface tension. They then assume that all variables can be expanded in perturbation series in powers of β, a small parameter which may be considered as the beam/length ratio. Some quantities must be allowed to have a zero-order term; in particular, ship speed is assumed to have the expansion:

$$s(t) = s_0(t) + \beta s_1(t) + \beta^2 s_2(t) + \dots .$$

However, most of the variables are assumed to represent small disturbances, and so their expansions start with terms linear in β. For example, the disturbance potential is written:

$$\Phi(x,y,z,t) = \beta\varphi_1(x,y,z,t) + \beta^2\varphi_2(x,y,z,t) + \dots .$$

The free surface elevation, the motion variables, the thrust, etc., all have similar expansions.

These expansions are all substituted into the various conditions and equations, and the terms are all arranged according to powers of β. Before solving any boundary value problems, Peters and Stoker make a number of observations. For example, $ds_0/dt = 0$, which means that $s(t)$ represents a steady forward speed with perturbations superposed on it, the perturbations being of order β. The usual conditions for hydrostatic equilibrium are also obtained.

The equations of motion in the longitudinal plane are all found to contain only second and higher order terms.

They then restrict their attention to the case of a ship in sinusoidal head waves. These incident waves have an amplitude with order of magnitude β. The resulting second order problem is then straightforwardly separated into a time-independent problem and a time-dependent problem. The solution of the former leads to the Michell-Havelock solution of the resistance problem, unaffected by the incident waves or the motions. The solution of the latter, the time-dependent problem of lowest order, is carried out without the necessity of treating any more boundary value problems. The resulting ordinary differential equations of motion represent simply a two-degree-of-freedom coupled spring-mass system, without damping. Even the coupling is removed if we assume that the centroid of the waterplane is in the same cross section as the center of gravity of the ship. In this case, the solution predicts an undamped resonance in heave and in pitch. In the heave mode, the spring constant is the hydrostatic restoring force per unit deflection, and, in the pitch mode, the spring constant is the hydrostatic restoring moment per unit pitch angle (plus a non-hydrodynamic contribution which results from the condition that the center of gravity is generally below the origin, i.e., below the pitch axis). The resonance frequencies are then obtained as the square roots of spring constants divided by mass and moment of inertia, respectively. The disturbing force is just a "Froude-Krylov" force. That is, the heave or pitch excitation is obtained simply by integrating the pressure in the incident wave over the hull, with direction cosines and lever arms as weighting functions, as appropriate. The presence and motion of the hull do not affect the values to be used for the pressure.

Obviously, some of these results must be rejected on physical arguments, especially the prediction of undamped resonances and thus of infinite amplitudes of motion. Unfortunately, heave and pitch resonance frequencies quite often occur within the important range of wave excitation frequencies, and, if this happens, it is evident that the narrow spectral band around resonance covers the frequencies of most interest. Even if this theory is valid for other frequencies, it is not of much help in predicting real phenomena.

In spite of these difficulties, the results come directly out of the hyptheses. There can be no arguing with the logic used by Peters and Stoker in deriving conclusions from their formulation of the problem, and so the difficulty must be sought in the formulation. This situation will be resolved presently, but for the moment let us note that the anomalous behavior at resonance can be explained non-mathematically. There are three types of quantities which are assumed to be of order β, and we can start a catalog of orders of magnitude by listing these:

ship beam, waterplane area, volume, mass	β
amplitude of incident waves	β
amplitude of oscillations of the ship	β

Speaking in terms of orders of magnitude, we can say that: (a) exciting force = (amplitude of incident waves) $\times$ (waterplane area); (b) restoring force = (amplitude of ship motions) $\times$ (waterplane area); (c) ship inertial reactions = (amplitude of ship motions) $\times$ (ship mass); (d) amplitude of motion-generated waves =

(amplitude of ship motions) × (waterplane area); (e) motion-generated fluid force = (amplitude of motion-generated waves) × (waterplane area). We can now add to our catalog of orders of magnitude:

excitation by incident waves	β^2
hydrostatic restoring force	β^2
ship inertial reactions	β^2
added mass and damping force	β^3

At resonance, the restoring force and inertial reaction add up to zero, and there are no second order forces to counter the excitation force. Therefore the response amplitudes are unbounded to this order of approximation. This violates the assumption that motions are of order β, but it would not be proper in the perturbation analysis to try to modify the resonance prediction through use of higher forces, simply because they are of higher order and therefore small by comparison.

Peters and Stoker criticized Haskind for assuming a priori the orders of magnitude of the various kinds of forces, but it can be seen a fortiori that Peters and Stoker have done essentially the same thing, for they also assumed the orders of magnitude of certain quantities (not the forces) and arrived at untenable conclusions.

These authors recognized and noted this anomaly, and they suggested several escapes from this predicament. For example, they discussed the "flat ship" linearization. However, such an approach simply shifts the same difficulty to the lateral motion modes. They also considered a "yacht-type" ship, which would avoid the trouble in all modes except surge. Such a mathematical model is quite artificial, but it might produce successful results if it could be worked out.

However, the basic difficulty with thin-ship theory may be looked at in another way which suggests a totally different method. It was assumed that ship beam, ship motions, and incident waves were all small, of the same order of magnitude. However, it was found that motions near resonance could be very large — to an extent that invalidated the assumptions. Newman (1960) proposed that there should be more than one small parameter in the statement of the problem, and he worked out a development in terms of three parameters. He retained β, the beam/length ratio, and he added a parameter γ which indicates the order of magnitude of the unsteady motions and another parameter δ which indicates the order of magnitude of the incident waves. Such a triple expansion allows for consideration of two important points: 1) There is no reason at all to assume that ship beam is related in size to the amplitude of the incident waves; 2) it is not necessary to make any a priori assumptions about the magnitude of ship motions relative to the magnitude of ship beam or incident waves. With regard to point 1), we note that ship beam and incident wave amplitude remain as independent parameters throughout the problem, whereas, with regard to point 2), we expect that the solution of the problem will provide us with information about the actual amplitudes of motion.

Newman expands each of the dependent variables in multiple series expressions. For example, the potential is made to depend on all three small parameters:

$$\varphi(x, y, z, t) = \sum_{i, j, k} \beta^i \gamma^j \delta^k \varphi_{ijk}(x, y, z, t),$$

whereas the motions are represented by double series, e.g., for heave,

$$z_o(t) = \sum_{i, j} \beta^i \gamma^j z_{ij}(t).$$

(The unsteady motions depend on γ, by the definition of this parameters, but we also expect steady displacements, which will depend on β. This is the reason for including both parameters in the expansion here.)

Since Newman develops his analysis on the assumption that it will be necessary to include higher than first order effects, he carefully introduces other needed expansions, which will not be written out here. For example, he transforms from a body-fixed coordinate system to a steadily translating system, both for calculation of the potential functions and for calculation of the pressure and forces; this transformation involves the parameters β and γ. Finally he obtains a sequence of problems, each homogeneous in each of the small parameters, and he solves explicitly for the following potential functions: φ_{100}, the potential for the steady translation problem; φ_{001}, the potential for incident waves; φ_{110}, the potential for small motions of the ship in an otherwise undisturbed ocean; φ_{101}, the diffraction potential. The first is just the Michell-Havelock potential, and the second is the classical potential for sinusoidal waves on an infinitely deep ocean. The third and fourth potential functions are somewhat more interesting and deserve some further comment.

If a ship model is forced to perform small oscillations of order of magnitude γ, perhaps by being driven by a mechanical oscillator, then the appropriate potential function is φ_{110}. The one complication of interest here lies in the specification of the body boundary condition. In the initial formulation of this problem, it is necessary to state the boundary condition on the actual, instantaneous position of the body surface. Then, by a systematic procedure, this condition can be translated into a (different) condition on the mean position of the body. This problem has already been mentioned; see the discussion accompanying Eq. (10b). There is an interaction between the ship oscillations and the steady flow past the ship which produces effects in the lowest order unsteady solution. This interaction is lost if we assume immediately that the body boundary condition can be satisfied on the mean position of the hull. Such an error has occurred frequently in work in this field; the first correct treatment is apparently due to Hanaoka (1957). Newman (1961) discusses the problem quite explicitly and shows that the difference in the potential functions, corresponding to the two methods of satisfying the hull condition, is equivalent to the potential of a line distribution of oscillating sources located on the mean keel line. It must be emphasized that this is not a higher order effect, and the problem is not related, for example, to the arguments about how to satisfy the body boundary condition in the steady motion (resistance) problem. The elegant formulation of the boundary condition by Timman and Newman (1962) provides the most convenient procedure for handling this difficulty. Again, see Eq. (10b).

The potential φ_{101}, as found by Newman (1961), points up an interesting difficulty which is still not well understood or appreciated. This potential represents the diffracted flow around the translating restrained ship. It satisfies a straightforward boundary condition on the hull, providing a normal component of velocity which just offsets the corresponding velocity component of the incident wave system. However, its boundary condition on the free surface is unique among the potential problems formulated by Newman. When the series expansions are substituted into the free surface condition and the resulting conditions are modified so as to apply on the undisturbed free surface, the potentials φ_{100}, φ_{001}, and φ_{110} all satisfy a homogeneous condition:

$$g \frac{\partial\varphi}{\partial z} + \frac{\partial^2\varphi}{\partial t^2} - 2V \frac{\partial^2\varphi}{\partial x \partial t} + V^2 \frac{\partial^2\varphi}{\partial x^2} = 0 .$$

However, φ_{101}, must satisfy a nonhomogeneous condition; there is a nonzero right-hand side in the corresponding equation, and this right side contains terms which are essentially products of φ_{001} and φ_{100}. This situation is somewhat analogous to the problem of satisfying the body boundary condition. There is an interaction between the incident wave system and the steady Kelvin wave system such that an apparent pressure distribution is applied to the free surface, and this apparent pressure gives rise to an unexpected addition to the diffracted wave.

This complication with the diffracted wave is an excellent example of the value of systematic perturbation analyses. We could have set up the diffraction problem much more easily. It would have seemed quite reasonable to assume that the usual linearized free surface condition would apply, and so we would have found a potential function which satisfied that condition and which also offset the normal component of the incident wave system on the ship hull. Newman's systematic approach shows that this is not proper. We need another contribution to the potential which satisfies a homogeneous condition on the hull and a non-homogeneous condition on the mean free surface. This extra part will be of the same order of magnitude as the potential which we would obtain by the more naive approach. We should note specifically that, since this effect is due to interaction of the incident waves with the steady wave system of the translating ship, this is a problem only when the ship has non-zero forward speed.

The effects of this difficulty may be quite pervasive. In particular, the Haskind relations for predicting wave-induced forces (discussed in Chapter IV) were derived only for a ship at zero forward speed, and the extension of these relations to ships with non-zero forward speed will depend on a further satisfactory resolution of the problem discussed here.

For the thin ship moving through sinusoidal waves, Newman's solution is complete to first order in β, and he obtained a set of formulas for the coefficients in the force expansions, complete to second order in β. The expressions are quite unwieldy, and one can not be very optimistic about being able to use them for practical calculations. However, it is of some interest to point out how they resolve the problem left over from the work of Peters and Stoker: How do we explain away the predicted infinite amplitudes of motion at resonance?

In Newman's formulation, the lowest order forces have the following orders of magnitude:

excitation by incident wave,	$\beta\delta$;
hydrostatic restoring force,	$\beta\gamma$;
ship inertial reactions,	$\beta\gamma$;
added mass and damping forces,	$\beta^2\gamma$.

Away from resonance, the excitation must be equal to the sum of hydrostatic plus ship inertia forces. Under these circumstances, it is clear that we can set:

$$\gamma = \delta + \text{smaller terms.}$$

At resonance, the forces of order $\beta\gamma$ total zero, and so the excitation force must equal the added mass and damping forces, which are the lowest order non-vanishing forces. Therefore, at resonance

$$\gamma = \frac{\delta}{\beta} + \text{smaller terms.}$$

Since γ must still be a small parameter, we must require that $\delta \ll \beta$, if the perturbation analysis is to remain valid. Such a requirement appears reasonable.

As a practical approach, if we were to try to use Newman's formulas for the forces, we could now follow the procedure which is usual in perturbation analyses, viz., absorb the small parameters into the force and motion variables. We would then calculate the forces, including the higher order added mass and damping forces, and from these calculate the motions. Away from resonance, the higher order contributions should be negligible (if the conditions of the theory are really satisfied), and the results should reduce to those of Peters and Stoker. At and near resonance, the higher order forces should dominate the lower order forces and control the predicted responses.

This approach is logical, at least insofar as a ship may really be considered as thin, but the results are not very useful because of their complexity. The damping coefficients are the only elements of the problem which fall out in a fairly simple fashion, and it has already been seen that at least some of these can be calculated in a much simpler manner, from radiation considerations. In order to evaluate the potential usefulness of the thin ship idealization in predicting ship motions, some calculations of damping coefficients have been made for Series 60 models and compared with experiments by Gerritsma, Kerwin, and Newman (1962). Figure 7 shows some typical results from their paper. The heave damping coefficient (b_{33}^*) is plotted against frequency for a sequence of values of Froude number. The ship concerned is the $C_B = 0.60$ form of the Series 60. The agreement is at least qualitatively good.

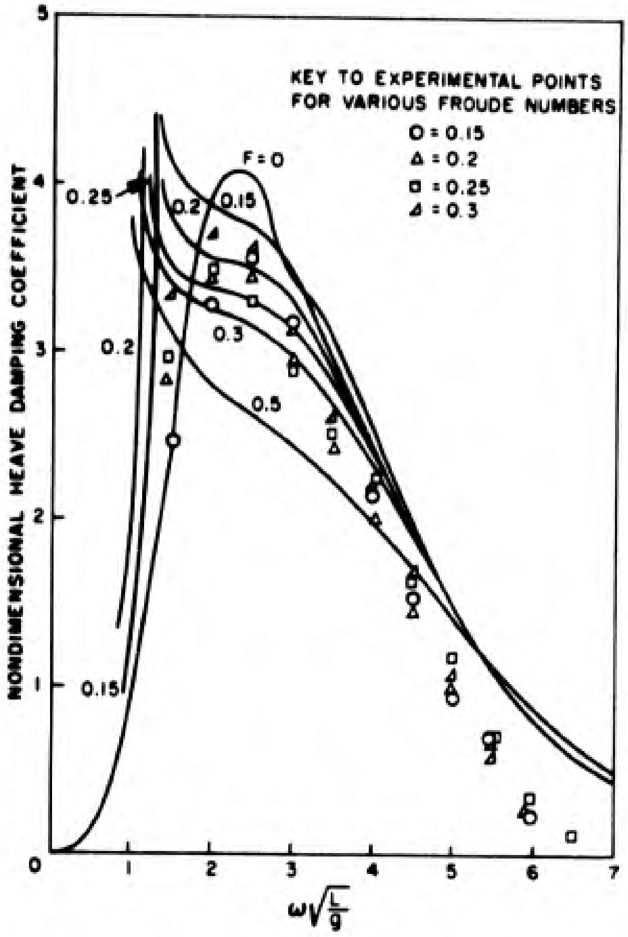

Fig. 7 - Heave damping coefficient for series 60, C_B = 0.60, Model at various Froude numbers, experiments and calculations (from Gerritsma, Kerwin, and Newman (1962))

SLENDER SHIP THEORY

A slender body theory, whether for aircraft or for ships, is formulated on the assumption that all dimensions in a cross section of the body are small compared to the length of the body. Also, the rate of change of transverse dimensions (with respect to the lengthwise coordinate) must be small in a similar sense. Such an approximation appears attractive for ship problems, since ships generally fit such a qualitative description. Nevertheless, the application of slender body theory to ship problems has been long in coming, in spite of the fact that the aerodynamic version of the theory is forty years old.

There are probably several reasons for this long delay, and a quick inspection of these reasons will suggest something about the nature of slender body theory. One important problem arises immediately which distinguishes the slender body approach from thin ship analysis. If we introduce the slenderness parameter into the formulation of the boundary value problem, the effects of the free surface are generally lost and we are left with an infinite fluid problem. This is clearly quite unsatisfactory, because we seek primarily a description of just those phenomena which result from the presence of the free surface. Furthermore, such a formulation turns out to be equivalent to a set of two-dimensional problems, and the effects of interactions between various cross sections are apparently quite ambiguous. These problems can be resolved by a reformulation which is altogether different from the thin ship approach, but then the final formulas depend on the geometry of the ship in an elementary way — which is offensive to the naval architect, for it implies that the complicated geometry of a hull is of little importance for ship motions.

These difficulties all demand that our attempts to apply slender body theory in ship problems be done with great care, by a systematic procedure. Using a perturbation analysis, we can answer to all of these problems, even the last, for, by being systematic, we can (in principle) proceed to higher approximations which involve more and more details of the hull geometry.

Before proceeding to the logical development of slender body theory, we should note that Grim (1957, 1960) anticipated much that would later come out of the theory. He pointed out that there were apparently two general approaches to representing the ship in studies of ship motions: (1) The ship can be represented by a set of three-dimensional singularities which clearly predict three-dimensional effects but which are loosely connected to ship geometry. (2) The exact shape of the ship in each cross section can be generated as if that cross section were part of an infinitely long body of uniform shape, with no account taken of three-dimensional effects (either interactions or forward speed effects). In order to combine the advantages of both, he proposed to solve the potential problem corresponding to the second approach, representing the potential as a two-dimensional multipole expansion about a line in the centerplane, and then at each section to replace the two-dimensional singularities by three-dimensional singularities of the same strength. The resulting potential would then be used to calculate pressure and force. In other words, he proposed to use strip theory only to find singularities for representing the ship and then to use truly three-dimensional potential functions to represent the flow. Grim (1960) published the details of the analysis and some calculations, all for the case of zero forward speed. He also stated that the theory had been worked out for forward speed cases as well, but apparently he has not yet published that.

There is considerable similarity between Grim's procedure and the rules for calculation which follow from slender body theory. However, the two are not identical, and it is obscure as to what meaning should be attributed to the differences. It will appear that slender body theory actually gives simpler results than Grim's, and one may say that the slender body results fall into the category which Grim criticized for not providing a realistic representation of the ship geometry. But the systematic approach is logical if the assumptions are correct, and, if they are correct, then there is no need to use Grim's more complicated formulas. The questions raised here can not yet be answered.

The first comprehensive attack on ship motions problems by slender body theory was by Vossers (1962a), and I shall follow his approach in essence. (However, other methods are possible. See, for example, Ursell (1962), Tuck (1964).) After formulating the problem exactly, we must introduce the slenderness approximation and this proves to be a difficult task. Vossers's analysis and results are very complicated and moreover they are somewhat suspect. Newman (1964) has had more success in obtaining approximations, at least for the case of no forward speed, and his first numerical results are very encouraging. However, the calculations are still at a very rudimentary stage, and it is too early to predict the quality of the outcome. Whether all of this effort will lead to valid and useful formulas is not yet known. I leave the two following authors (and their discussers) the opportunity to speculate on the future of slender body theory for predicting ship motions.

In formulating the slender body problem for ships, Vossers assumes that the ratio (ship beam)/(ship length) is a very small quantity, which we call ϵ. The purpose of his investigation is to find solutions which become more and more accurate as ϵ becomes smaller and smaller. Vossers expands various quantities as perturbation series in powers* of ϵ, substitutes these into the various mathematical conditions of the problem, and non-dimensionalizes all quantities and equations. In the last process, a number of special non-dimensional ratios arise, and the nature of problem and solution depends on the relative sizes of these quantities. The important non-dimensional quantities are, besides ϵ,

$\omega L/2V$, a reduced frequency,

$2V^2/gL$, a forward speed parameter, proportional to (wavelength of waves travelling at speed V)/(ship length),

$\omega^2 L/2g$, proportional to (ship length)/(wavelength of waves with frequency ω),

$\omega^2 B/2g$, proportional to (ship beam)/(wavelength of waves with frequency ω),

$\omega V/g$, a parameter for describing the pattern of radiated waves (usually called "τ" in the American literature),

where

L = ship length,
B = ship beam,
ω = circular frequency of exciting or motion-generated waves, and
V = forward speed.

*This is really not correct, and it shows the danger of loose assumptions. One should, as it turns out, use double series containing factors $\epsilon^m(\log \epsilon)^n$. It is also possible to avoid this trap altogether by assuming only that the potential can be expanded: $\phi = \Sigma\phi_n$, with $\phi_{n+1} = 0(\phi_n)$. By such an approach, one must determine in turn the actual order of magnitude of each term.

The nature of the free surface problem depends primarily on the length of waves (of frequency ω) compared with the ship dimensions. If these waves have length comparable with ship length, that is, $\omega^2 B/2g = O(\epsilon)$, then Vossers shows that the free surface condition reduces to the rigid wall (low frequency) condition. If the waves are short compared with ship beam, the high frequency degenerate boundary condition applies. Only if the waves are comparable in length with ship beam does one obtain an interesting problem, for then the free surface condition becomes (in dimensional form):

$$\frac{\partial^2 \varphi}{\partial t^2} + g \frac{\partial \varphi}{\partial x_3} = 0 \qquad \text{on } x_3 = 0 , \tag{23}$$

and Laplace's Equation reduces from

$$\frac{\partial^2 \varphi}{\partial x_1^2} + \frac{\partial^2 \varphi}{\partial x_2^2} + \frac{\partial^2 \varphi}{\partial x_3^2} = 0$$

to

$$\frac{\partial^2 \varphi}{\partial x_2^2} + \frac{\partial^2 \varphi}{\partial x_3^2} = 0 . \tag{24}$$

In words, the problem reduces to a set of two-dimensional problems; for each cross section, we must find, in two dimensions only, a solution of Laplace's Equation satisfying (23), the usual free surface condition, and (as Vossers shows) the usual boundary condition on the body.

This problem should be quite familiar, for it corresponds exactly to "strip theory." There is no effect of forward speed and no interaction between cross sections. Vossers' formulation shows clearly then that strip theory is a natural consequence of assuming that the disturbance waves and ship beam are comparable in size, and accordingly it should be valid in problems of ship rolling in short beam waves, for example, but not for problems of pitching and heaving in waves comparable with ship length.

It should be noted specifically that solutions which satisfy (23) and (24) are functions of x_1, since the body boundary condition depends on x_1. Moreover we can add to such solutions any other function of x_1 which we desire, without violating (23), (24), or the body condition. This arbitrary additive function may be interpreted as expressing the interaction between sections. But it is unknown. In this formulation of the problem, we can do only as in strip theory, namely, assume that there is no interaction.

If we are interested in pitch and heave problems (and most of this paper is concerned with just these problems), then we must consider wavelengths comparable with ship length, and it is apparent that we do not obtain a satisfactory formulation by the above procedure. Therefore Vossers proposed a different tack, viz., that we write down the solution in a general way by using Green's theorem and then use the slenderness approximation to simplify the resulting integral equation. In other words, we effectively establish an integral equation for the solution of the problem involving a general body (not a slender body); we cannot solve this equation, but we simplify it for the special case of the slender body, and the resulting equation can be solved. It turns out that the integral equation which must be solved relates to a set of two-dimensional problems again, but this time we obtain an additional part of the solution which explicitly represents interaction effects between sections.

It seems to be desirable at this point to restrict ourselves to the case of zero forward speed, since it has been worked out in detail and we can be reasonably confident of the results. In detail, the approach which follows is that of Newman (1964); the general concept is still Vossers'.

In order to simplify matters, let us assume immediately that all disturbances are sinusoidal in time. For the potential we write $\mathrm{Re}\,\{\phi(\underline{x})\,e^{-i\omega t}\}$, and we have similar expressions for all other variables. This is not necessary and perhaps not desirable, but it is certainly convenient. We also stipulate that $\phi(\underline{x})$ represents the potential for motion-induced diffraction waves, but not for incident waves.

By Green's theorem, we can write an expression for the potential at any point in the interior of the fluid:

$$\phi(\underline{x}) = \frac{1}{4\pi}\int_{\Sigma}\left\{G(\underline{x},\underline{\xi})\,\frac{\partial\phi(\underline{\xi})}{\partial n} - \phi(\underline{\xi})\,\frac{\partial G(\underline{x},\underline{\xi})}{\partial n}\right\}d\sigma\,. \tag{25}$$

$G(\underline{x},\underline{\xi})$, a Green's function, is any function which satisfies Laplace's Equation (in three dimensions) except at $\underline{x} = \underline{\xi}$, where it has the behavior:

$$G(\underline{x},\underline{\xi}) = (1/|\underline{x}-\underline{\xi}|) + \ldots\,.$$

The domain of integration, Σ, must be a closed surface with $\underline{x}$ in its interior, and $\underline{\xi}$ is the dummy variable which ranges over Σ. Under these conditions, (25) is a very general equation, and its usefulness for us depends on our selecting $G(\underline{x},\underline{\xi})$ in a meaningful way.

We choose $G(\underline{x},\underline{\xi})$ as the potential function of a pulsating source located at $\underline{\xi}$, the potential satisfying the linearized free surface condition on $x_3 = 0$ and an appropriate radiation condition at infinity. Also, we define the closed surface Σ as $S_0 + S_f + S_\infty$, where S_0 is the wetted surface of the ship, S_f is the mean free surface, that is, the plane $x_3 = 0$ outside the ship, and S_∞ is a closing surface far away from the ship, at "infinity." If now we assume that $\phi(\underline{x})$ satisfies the linearized free surface condition and a radiation condition, the integrals over S_f and S_∞ vanish, leaving only the integral over S_0 in (25).

We have left a gap in our logic by assuming that we can use the linearized free surface conditions. However, we get away with it in the case of zero forward speed, for we actually have two means of supporting the linearization: If there are incident waves, we may assume them small, so that the ship motions will also be small (even if it is a "fat ship"), or we can concentrate on the assumption of slenderness of the ship, in which case even finite amplitude motions will produce small amplitude disturbances. It is evident that the linearized condition will be appropriate and we proceed to use it without further justification. However, the forward speed problem would require much more care.

With Σ now replaced by S_o, Eq. (25) is much simpler, but we still can do nothing with it in its present form. We assume that $\partial\phi/\partial n$ is a known quantity on S_o, but $\phi(\underline{x})$ is not known, and so this is an integral equation for $\phi(\underline{x})$ on S_o.* To reduce it to a simpler integral equation, Newman now introduces the slenderness parameter. This is essentially a rather tedious exercise in estimating the relative sizes of various quantities, and I shall be satisfied here to state his result. He finds that $\phi(\underline{x})$ can be written as the sum of two terms plus an error:

$$\phi(\underline{x}) = [\phi_{2D}(\underline{x}) + f(\underline{x})]\,[1 + O(\epsilon \log \epsilon)]\,. \tag{26}$$

where ϕ_{2D} is the solution of the two-dimensional problem in which the body cross section performs its motions in the presence of a rigid wall at $x_3 = 0$. The function $f(x_1)$ is obtained explicitly:

$$f(x_1) = \frac{K}{4}\int_{-L/2}^{L/2} F(\xi_1)\left\{-\mathbf{H}_o(K|x_1-\xi_1|) - Y_o(K|x_1-\xi_1|) + 2iJ_o(K|x_1-\xi_1|)\right\} d\xi_1$$

$$+ \frac{1}{2\pi}\int_{-L/2}^{L/2} \log\frac{2|x_1-\xi_1|}{L}\ \mathrm{sgn}\,(x_1-\xi_1)\ \frac{\partial}{\partial\xi_1}F(\xi_1)\, d\xi_1\,,$$

where

$$F(x_1) = \int_C \frac{\partial\phi}{\partial n}\, dl\,,$$

C is the contour around the hull in the cross section at x_1,

$K = \omega^2/g$,

J_o = Bessel function of the first kind,

Y_o = Bessel function of the second kind, and

$\mathbf{H}_o$ = Struve function.

It is easily seen that $F(x_1)$ is just the fluid flux through the hull surface at the cross section at x_1; it is zero for yaw and sway motions but not for heave, pitch, and roll motions. (We avoid mention of surge motions. They can be analyzed by slender body theory just as well as the other kinds of motion, but the results can be expected to be rather special with respect to orders of magnitude. To some extent this is true for roll also.)

*In order to obtain the integral equation on S_o, we must let $\underline{x}$ approach S_o, and then the factor $1/4\pi$ changes to $1/2\pi$.

In the formula for $f(x_1)$ we have two integrals over the length of the hull, and we should distinguish between their meanings. The first integral, involving the Struve and Bessel functions, represents a free surface effect. It can also be looked upon as expressing an interaction between sections — an interaction caused by the presence of the free surface. The second integral also represents an interaction, but it would exist even in the absence of the free surface. We could combine the latter with ϕ_{2D} and look on the sum as the slender body approximation for the three-dimensional body in the presence of a rigid wall, with the first integral supplying a correction to account for the free surface effect on the three-dimensional body.

We note that the interaction, due to either term of $f(x_1)$, involves the ship geometry in a very simple way. In fact, $F(x_1)$ depends only on the ship beam at section x_1, and thus $f(x_1)$ depends only on the waterplane shape. However, ϕ_{2D} depends on the detailed shape of the cross section. (Fortunately, the finding of ϕ_{2D} is not too difficult, since it is not really the solution of a free-surface problem.) Thus, the solution does depend on the hull geometry in a detailed manner, but this dependence is shunted off to the mathematically easier field of problems with fixed, rigid boundaries.

We should now refer back to the earlier statements which resulted from various assumptions about orders of magnitude. We have assumed here that wave length is comparable with ship length. Under these conditions, Vossers showed that the three-dimensional boundary value problem would reduce to a set of two-dimensional problems in the cross sections, with the free surface condition replaced by a rigid wall condition. This is exactly what Newman obtains. However, we now have an explicit formula for the interaction term, $f(x_1)$.

Perhaps it should be emphasized that (26) is valid only very near to the ship hull, at distances which are of order of magnitude ϵL. However, this is just where we need to evaluate the potential in order to find the force on the ship, and we do not need to be concerned about complications far away. The expression for ϕ given by (26) presumably does not even satisfy the three-dimensional Laplace's Equation, except in an approximate sense very near to the body. Far away from the body, the potential would have quite a different form from that given in (26).

Without finding explicit formulas for the forces, we can immediately reach some conclusions of importance. For the transverse oscillations, that is, yaw and sway, the flux, $F(x_1)$, vanishes and so $f(x_1)$ vanishes also. In other words, the theory predicts no interaction between cross sections in these modes. If this holds for the potential, it must be true for the forces too, and so the lowest-order slender body theory for ship motions reduces to strip theory for the transverse modes. However, to the same degree of approximation, there will be non-negligible interactions between cross sections in the heave, pitch, and roll modes. It is interesting to note that many years ago the same conclusions were reached by Grim (1957) on the basis of physical arguments.

In order to calculate the force and moment on the ship, we must add the potential for the incident waves to the function represented in (26), and from this sum we find the pressure, which we integrate over the submerged part of the hull in the usual way, with direction cosines and lever arms for weighting functions, as appropriate. We can distinguish three separate parts of this force: (1) the force due to the incident waves, which is a Froude-Krylov force, (2) the hydrostatic restoring force due to the disturbed position of the hull, (3) the hydrodynamic force due to the ship motions and to the diffraction wave. The sum of all these is set equal to the inertial reaction of the ship, in accordance with Newton's Law, to yield the equation of motion.

These different kinds of forces involve various functions of ϵ. We obtain the lowest order theory by considering only those forces which are homogeneous in the lowest order of ϵ. The precise form of these expressions is not particularly interesting except to someone who wants to make quantitative predictions. The details can be found in Newman (1964). The qualitative conclusions which can be drawn are, however, worthy of some comment.

In yaw and sway, there is no hydrostatic restoring force or moment. The other three kinds of forces, that is, inertial, excitation (Froude-Krylov), and motion-induced forces, are all of order ϵ^2, and so all must be included in the equations of motion for these modes. It may be noted that there are no free surface effects in the motion-induced forces (except inasmuch as the rigid wall may be considered as a free surface condition). Also, it has already been pointed out that there are no interaction effects between sections in these modes. So here the theory becomes exceptionally simple: The excitation is calculated from the Froude-Krylov formula, the body inertia comes from the ordinary theory of the dynamics of a rigid body, and the hydrodynamic reaction is obtained from the solution of a fairly simple two-dimensional problem. In fact, since there can be no radiation of waves in the presence of a rigid wall at $x_3 = 0$, the motion-induced hydrodynamic force is simply the added mass force for the simplified two-dimensional problem. Therefore the whole resistance to the yaw and sway excitation force has the nature of an inertial reaction.

In pitch and heave, the Froude-Krylov excitation force and the hydrostatic restoring force provide the leading terms in the equations of motion; these forces are both of order ϵ, and all other forces are of higher order. The lowest order theory is accordingly even simpler than for yaw and sway. There is no hydrodynamic force (except the excitation) in the first approximation. Also, the inertia does not enter into the calculation. The response is entirely controlled by the "spring" term.

However, in heave and pitch, it is fairly straightforward to derive higher order forces, and Eq. (26) leads directly to formulas for the next approximation. It can be shown that the interaction term in (26) yields a force of order $\epsilon^2 \log \epsilon$ in the heave and pitch equations of motion. This force includes added mass, damping, and diffraction effects. The inertia of the ship itself is of order ϵ^2 in these modes, and the calculation can be extended to take this into account. This is a much more interesting situation, for the system now has the properties of a damped spring-mass system. However, it must be recognized that the occurrence of a resonance is a higher order effect superimposed on the simple effects described in the previous paragraph. If the amplitudes of response are very large near resonance, or if there are large phase shifts, then we can hardly pretend that these are higher order effects, and the theory is of questionable validity. Fortunately, the experiments of Davis and Zarnick (1964) with a pitching and heaving aircraft carrier at zero speed show good agreement with calculations based on the very simple, lowest order theory developed by Newman, and there is some hope that the higher order theory outlined here will still give good results even when resonance phenomena become more important.

It may be well to recall again (see the Introduction) how the slender body approach rectifies the difficulty of the Peters-Stoker thin ship model. In the latter, the Froude-Krylov excitation, the hydrostatic restoring force, and the ship inertia force were all of the same order of magnitude, and damping and added mass forces were of higher order of magnitude. Because of the presence of "spring forces" and inertia forces and the absence of damping, the system had resonances with unbounded amplitudes of motion. In the slender body theory, the mass and thus the inertial reactions are raised to a higher order in terms of the small parameter, while the restoring forces are unchanged in order of magnitude. Without the inertia terms, there is no resonance at all in the lowest order theory, and when inertia does appear in higher order terms, damping also enters in.

There is one other difference between this slender body approach and the Peters-Stoker theory which may be mentioned. In the latter, it was assumed that the slope of the incident waves was small, of the same order of magnitude as the (small) beam/length ratio. In the slender body theory, wave height (or slope) remains an independent parameter, and all of the above results may be considered as part of a homogeneous first order theory in terms of such a parameter. However, this parameter must be small compared with ϵ, the slenderness parameter.

REFERENCES

The references listed here are limited to those mentioned in the text, with a few exceptions. Five of the publications are marked with an asterisk; these have extensive bibliographies which may be of further interest to the reader.

G. Chertock, 1962. General Reciprocity Relation. J. of the Acoustical Society of America, 34, 989. Reprinted as David Taylor Model Basin Report 1663

L. J. Cote, 1954. Certain Problems Connected with the Short Range Prediction of Sea Surface Height. New York University College of Engineering Research Division Technical Report No. 4

W. E. Cummins, 1962. The Impulse Response Function and Ship Motions. Schiffstechnik, 9, 101-109. Reprinted as David Taylor Model Basin Report 1661

W. E. Cummins and W. E. Smith, 1964. Pulse Methods for Determining Ship Motions. Fifth ONR Symposium on Naval Hydrodynamics, to be published

J. F. Dalzell, 1962a. Cross-Spectral Analysis of Ship Model Motions: A Destroyer Model in Irregular Long-Crested Head Seas. Stevens Institute of Technology-Davidson Laboratory Report No. 810

J. F. Dalzell, 1962b. Some Further Experiments on the Application of Linear Superposition Techniques to the Responses of a Destroyer Model in Extreme Long-Crested Head Seas. Stevens Institute of Technology-Davidson Laboratory Report No. 918

M. C. Davis and E. E. Zarnick, 1964. Testing Ship Models with Transient Waves. Fifth ONR Symposium on Naval Hydrodynamics, to be published

J. Gerritsma, 1960. Ship Motions in Longitudinal Waves. International Shipbuilding Progress, 7, 49-76.

J. Gerritsma, J. E. Kerwin, J. N. Newman, 1962. Polynomial Representation and Damping of Series 60 Hull Forms. International Shipbuilding Progress, 9, 295-304. Reprinted as David Taylor Model Basin Report 1694

P. Golovato, 1957. The Forces and Moments on a Heaving Surface Ship. J. of Ship Research, 1, No. 1, 19-26

P. Golovato, 1959. A Study of the Transient Pitching Oscillations of a Ship. J. of Ship Research, 2, No. 4, 22-30

O. Grim, 1951. Das Schiff in von achtern auflaufender See. Jahrbuch der Schiffbautechnischen Gesellschaft, 45, 264-287

O. Grim, 1952. Rollschwingungen, Stabilität, und Sicherheit im Seegang. Schiffstechnik, 1, 10-21

O. Grim, 1957. Durch Wellen an einem Schiffskörper erregte Kräfte. Symposium on the Behaviour of Ships in a Seaway, Netherlands Ship Model Basin, Wageningen, 232-265

O. Grim, 1960. A Method for a More Precise Computation of Heaving and Pitching Motions Both in Smooth Water and in Waves. Third ONR Symposium on Naval Hydrodynamics, Office of Naval Research ACR-65, 483-518

T. Hanaoka, 1957. Theoretical Investigation Concerning Ship Motion in Regular Waves. Symposium on the Behavior of Ships in a Seaway, Wageningen, 266-285

M. D. Haskind, 1946. Oscillation of a Ship on a Calm Sea. (In Russian.) Izvestia Akademii Nauk S.S.S.R., Otdelenie Tekhinicheskikh Nauk, No. 1, 23-34. English Translation: Technical and Research Bulletin No. 1-12, The Society of Naval Architects and Marine Engineers, 1953

M. D. Haskind, 1957. The Exciting Forces and Wetting of Ships. (In Russian.) Izvestia Akademii Nauk S.S.S.R., Otdelenie Teckhnicheskikh Nauk, No. 7, 65-79. English Translation: David Taylor Model Basin Translation No. 307, March 1962

M. D. Haskind and I. S. Riman, 1946. A Method of Determining the Pitching and Heaving Characteristics of Ships. (In Russian.) Izvestia Akademii Nauk S.S.S.R., Otdelenie Tekhicheskikh Nauk, No. 10, 1373-1383. English Translation: David Taylor Model Basin Translation No. 253, 1955

J. L. Hess and A. M. O. Smith, 1962. Calculation of Non-Lifting Potential Flow About Arbitrary Three-Dimensional Bodies. Douglas Aircraft Co., Inc., Report No. E.S. 40622

H. Kato, S. Motora, and K. Ishikawa, 1957. On the Rolling of a Ship in Irregular Wind and Wave. Symposium on the Behaviour of Ships in a Seaway, Netherlands Ship Model Basin, 43-58

J. E. Kerwin, 1955. Notes on Rolling in Longitudinal Waves. International Shipbuilding Progress, 2, 597-614

W. D. Kinney, 1963. The Effect of Nonlinear Static Coupling on the Motion Stability of a Ship Moving in Oblique Waves. University of California (Berkeley) Institute of Engineering Research Report No. NA-63-3

*B. V. Korvin-Kroukovsky, 1961. Theory of Seakeeping. The Society of Naval Architects and Marine Engineers, New York.

J. Kotik and V. Mangulis, 1962. On the Kramers-Kronig Relations for Ship Motions. International Shipbuilding Progress, 9, 361-368

P. A. Lalangas, 1964. Application of Linear Superposition Techniques to the Roll Response of a Ship Model in Irregular Beam Seas. Stevens Institute of Technology-Davidson Laboratory Report No. 983

M. J. Lighthill, 1960. Fourier Analysis and Generalized Functions. Cambridge University Press

J. N. Newman, 1959. The Damping and Wave Resistance of a Pitching and Heaving Ship. J. of Ship Research, 3, No. 1, 1-19

J. N. Newman, 1961. A Linearized Theory for the Motion of a Thin Ship in Regular Waves. J. of Ship Research, 5, No. 1, 34-55

J. N. Newman, 1962. The Exciting Forces on Fixed Bodies in Waves. J. of Ship Research, 6, No. 3, 10-17. Reprinted as David Taylor Model Basin Report No. 1717

J. N. Newman, 1964. A Slender-Body Theory for Ship Oscillations in Waves. J. of Fluid Mechanics, 18, 602-618

M. K. Ochi, 1964. Prediction of Occurrence and Severity of Ship Slamming at Sea. Fifth ONR Symposium on Naval Hydrodynamics, to be published

A. S. Peters and J. J. Stoker, 1954. The Motion of a Ship, as a Floating Rigid Body, in a Seaway. Institute of Mathematical Sciences, New York University, Report No. IMM-203. Also: Comm. Pure and Applied Mathematics, 10 (1957), 399-490

M. St. Denis and W. J. Pierson, 1953. On the Motions of Ships in Confused Seas. Transactions, Society of Naval Architects and Marine Engineers, 61, 280-332 (with discussion on pp. 332-357)

A. M. O. Smith, J. P. Giesing, and J. L. Hess, 1963. Calculation of Waves and Wave Resistance for Bodies Moving on or Beneath the Surface of the Sea. Douglas Aircraft Co., Inc., Report No. 31488A

J. J. Stoker, 1957. Water Waves. Interscience Publishers

L. J. Tick, 1959. Differential Equations with Frequency-Dependent Coefficients. J. of Ship Research, 3, No. 2, 45-46

R. Timman and J. N. Newman, 1962. The Coupled Damping Coefficients of a Symmetric Ship. J. of Ship Research, 5, No. 4, 1-7

E. O. Tuck, 1964. A Systematic Asymptotic Expansion Procedure for Slender Ships. J. of Ship Research, 8, No. 1, 15-23

F. Ursell, 1962. Slender Oscillating Ships at Zero Forward Speed. J. of Fluid Mechanics, 14, 496-516

F. Ursell, 1964. The Decay of the Free Motion of a Floating Body. J. of Fluid Mechanics, 19, 305-319

G. Vossers, 1962a. Some Applications of the Slender Body Theory in Ship Hydrodynamics. Dissertation, Technical University of Delft. Publication No. 214, Netherlands Ship Model Basin

*G. Vossers, 1962b. Behavior of Ships in Waves. Vol. IIC, Resistance, Propulsion and Steering of Ships. De Technische Uitgeverij J. Stam N. V. (The Technical Publishing Company H. Stam N. V.) Haarlem (The Netherlands)

J. V. Wehausen, 1957. Wave Resistance of Thin Ships. First ONR Symposium on Naval Hydrodynamics. National Academy of Sciences-National Research Council Publication 515, 109-137

*J. V. Wehausen and E. V. Laitone, 1960. Surface Waves. Encyclopedia of Physics, Vol. IX, 446-778. Springer-Verlag, Berlin

*J. V. Wehausen, 1963. Recent Developments in Free-Surface Flows. University of California (Berkeley) Institute of Engineering Research Report No. NA-63-5

E. T. Whittaker and G. N. Watson, 1927. A Course of Modern Analysis. Cambridge University Press

*E. T. Whittaker and G. N. Watson, 1963. Researches on Seakeeping Qualities of Ships in Japan. Vol. 8, 60th Anniversary Series, The Society of Naval Architects of Japan, Tokyo

APPENDIX A

Calculation of Force and Moment

It has been remarked several times that, in order to calculate force and moment on the ship, the pressure must be evaluated on the actual instantaneous position of the ship hull. However, it is quite inconvenient to have a changing domain of integration, especially since finding the domain is part of the problem. (A priori, the location and orientation of the ship at any instant are unknown, and so one does not know where to evaluate the pressure.) Therefore we choose to express the pressure at a point of the hull surface, S, in terms of the pressure at the corresponding point of S_o, the undisturbed position of the hull. The resulting expressions will involve the unknown motion variables, but they will appear in an explicit manner and not as arguments of functions.

The pressure at any point in the fluid can be expressed as follows:

$$p = -\rho g x_3 + p_s + p_m ,$$

where

$$p_s = \rho V \frac{\partial \varphi_o}{\partial x_1} - \frac{1}{2}\rho(\nabla\varphi_o)^2 ,$$

$$p_m = -\rho \frac{\partial \varphi_1}{\partial t} + \rho V \frac{\partial \varphi_1}{\partial x_1} - \rho \nabla\varphi_o \cdot \nabla\varphi_1 - \frac{1}{2}\rho(\nabla\varphi_1)^2 .$$

We assume that the steady motion and the unsteady motion problems have both been linearized in some way, and so we neglect certain quadratic terms,* retaining only the following simplified expressions:

$$p_s = \rho V \frac{\partial \varphi_o}{\partial x_1} ,$$

$$p_m = -\rho \frac{\partial \varphi_1}{\partial t} + \rho V \frac{\partial \varphi_1}{\partial x_1} - \rho \nabla\varphi_o \cdot \nabla\varphi_1 .$$

It would not generally be proper to assume also that we could neglect the term $-\rho\nabla\varphi_o \cdot \nabla\varphi_1$ in p_m, although in practice this quantity may be quite small. The reason for this is discussed in detail in Chapter V: The steady motion problem

*This step may not be proper in certain cases, e.g., a deeply submerged body or a slender body.

and the oscillation problem should generally be linearized in terms of different small parameters, say β and γ, and we may neglect terms in β^2 compared with terms in β, or terms in γ^2 compared with γ, but we cannot make any arbitrary assumptions about the relative size of β and γ.

We assume that the pressure is given by a function which can be expressed as a Taylor series about a point on S_o. Let us describe the motion of the ship by the two vectors:

$$\underline{\xi}(t) = \sum_{k=1}^{3} \alpha_k(t)\, \underline{i}_k ,$$

$$\underline{\theta}(t) = \sum_{k=1}^{3} \alpha_{k+3}(t)\, \underline{i}_k .$$

$\underline{\xi}(t)$ specifies the linear displacement of the ship and $\underline{\theta}(t)$ the angular displacement (which is assumed to be small enough that a vector representation is approximately valid). The displacement from equilibrium of a point $\underline{x}$ on the hull is then given by $\underline{\xi} + \underline{\theta} \times \underline{x}$. The pressure at a point on S can be expressed in terms of the pressure (and its derivatives) at the corresponding point of S_o:

$$p\big|_S = p\big|_{S_o} + [\underline{\xi} + \underline{\theta} \times \underline{x}] \cdot \nabla p\big|_{S_o} + \ldots .$$

In addition to expressing the pressure appropriately, we need to be able to write down a set of direction cosines for calculating the effects of the pressure on an element of the hull. For calculating the moments, we shall need furthermore a set of appropriate lever arms.

Let us look first just at the force components, resolved along the steady axes:

$$X_j = \int_S p(\underline{n} \cdot \underline{i}_j)\, dS .$$

We could just as well resolve forces along the unsteady (body) axes:

$$X_j' = \int_S p(\underline{n} \cdot \underline{i}_j')\, dS .$$

The two sets of force components are related by:

$$\underline{X} = \underline{X}' + \underline{\theta} \times \underline{X}' .$$

where $\underline{X} = (X_1, X_2, X_3)$, and so the determination of either set is sufficient. We note that the factors $(\underline{n} \cdot \underline{i}_j')$ have the values which we associate with the undisturbed ship, whereas the factors $(\underline{n} \cdot \underline{i}_j)$ vary with time. Therefore we find it somewhat easier to calculate the components X_j' directly.

To the expression for X_j' we add and subtract a quantity, as follows:

$$X_j' = \left\{ \int_S (\underline{n} \cdot \underline{i}_j')p \, dS - \int_L (\underline{n} \cdot \underline{i}_j') d\ell \int_{(\underline{\xi}+\underline{\theta}\times\underline{x})\cdot\underline{i}_3}^{\zeta(x_1,x_2,t)} p \, dx_3 \right\}$$

$$+ \int_L (\underline{n} \cdot \underline{i}_j') d\ell \int_{(\underline{\xi}+\underline{\theta}\times\underline{x})\cdot\underline{i}_3}^{\zeta(x_1,x_2,t)} p \, dx_3 \, .$$

where L is the line of intersection of the ship hull at any instant with the undisturbed free surface, and $\zeta(x_1, x_2, t)$ is the free surface elevation. I have assumed that the ship is wall-sided near the free surface. It can now be recognized that the quantity in braces is just an integral over that part of the hull surface which is wetted when there are no waves and no ship motions. It has the same shape and size as S_o, but it is displaced from the equilibrium position. The direction cosines, $(\underline{n} \cdot \underline{i}_j')$, in fact have the values appropriate to S_o itself, but the pressure must be evaluated on the actual position of S. However, we can use the Taylor expansion of the pressure to convert it into a function to be evaluated on S_o. The quantity in braces is then just:

$$\int_{S_o} (\underline{n} \; \underline{i}_j) \left\{ p + (\underline{\xi} + \underline{\theta} \times \underline{x}) \cdot \nabla p + \ldots \right\} \Big|_{S_o} dS \, .$$

The correction term, the integral over L, is expressed partly in terms of each of the two coordinate systems. It is perhaps easier to retain the quantity $(\underline{n} \cdot \underline{i}_j')$ as it stands, and so we must express the inner integral in terms of the primed coordinates. From the geometry, it is found that this correction term can be written:

$$\int_{L_o} (\underline{n} \cdot \underline{i}_j) d\ell \int_0^{\zeta - (\underline{\xi}+\underline{\theta}\times\underline{x})\cdot\underline{i}_3} dx_3 \left\{ p + (\underline{\xi} + \underline{\theta} \times \underline{x}) \cdot \nabla p + \ldots \right\} ,$$

where L_o is the intersection of the undistrubed free surface with the hull surface, the latter being in its undisturbed position. The upper limit of x_3 is in error by a small quantity which does not affect the result. If we now work out this integral, systematically keeping only lowest order small quantities, we obtain

$$\rho V \int_{L_o} d\ell \, (\underline{n} \cdot \underline{i}_j) \left[\frac{\partial \varphi_o}{\partial x_1} \left\{ -\frac{1}{g} \frac{\partial \varphi_1}{\partial t} + \frac{V}{g} \frac{\partial \varphi_1}{\partial x_1} - (\xi_3 + x_2\theta_1 - x_1\theta_2) \right\} \right]_{x_3 = 0}$$

The complete result for X_j' is:

$$X_j' = \rho \int_{S_o} dS(\underline{n} \cdot \underline{i}_j) \left\{ -gx_3 - g(\xi_3 + x_2\theta_1 - x_1\theta_2) - \frac{\partial \varphi_1}{\partial t} + V \frac{\partial \varphi_1}{\partial x_1} - \nabla\varphi_o \cdot \nabla\varphi_1 \right.$$

$$\left. + V\left[1 + (\underline{\xi} + \underline{\theta} \times \underline{x}) \cdot \nabla\right] \frac{\partial \varphi_o}{\partial x_1} \right\} - \rho V \int_{L_o} d\ell(\underline{n} \cdot \underline{i}_j) \frac{\partial \varphi_o}{\partial x_1} \left\{ \frac{1}{g} \frac{\partial \varphi_1}{\partial t} - \frac{V}{g} \frac{\partial \varphi_1}{\partial x_1} + (\xi_3 + x_2\theta_1 - x_1\theta_2) \right\} .$$

We can interpret the various terms here readily. The first term of the first integrand is just the hydrostatic pressure at equilibrium, and the second term yields the hydrostatic disturbance force. The following three terms are unsteady force contributions, and the last term in the first integral yields the resistance and the unsteady force which results from interaction between the steady flow and the displaced position of the hull. The line integral represents an interaction force arising from the superposition of steady and unsteady motions; the factor $\partial\varphi_o/\partial x_1$ can be recognized as being proportional to the wave height in the steady motion problem, and

$$\left[\frac{\partial\varphi_1}{\partial t} - V\,\frac{\partial\varphi_1}{\partial x_1}\right]$$

is proportional to the unsteady wave height (omitting a term containing both φ_o and φ_1).

It may be noted that the line integral is zero for $j = 3$. This follows from the assumption that the ship is wall-sided near the waterline, which means that $\underline{n}$ lies in the plane of $\underline{i}_1$ and $\underline{i}_2$ for points on L_o. Furthermore, if we consider only motions in the longitudinal plane, then the line integral is also zero for $j = 2$. Finally, if the steady motion problem is linearized in any of the usual ways (thin, flat, or slender ship approximations), then $\underline{n}\cdot\underline{i}_1$ is small, of the same order as φ_o, and the whole integral is of second order in terms of the perturbation parameter for the steady motion problem.

The moments acting on the hull can be calculated in a similar manner, with only slight complications appearing. Let us again choose to work directly with the moments about the unsteady (body) axes:

$$X'_{j+3} = \int_S (\underline{n}\cdot\underline{i}'_j \times \underline{x}')\, p\, dS\,.$$

Then the moments about the steady axes will be given by:

$$\underline{M} = \underline{M}' + \underline{\theta}\times\underline{M}' + \underline{\xi}\times\underline{X}'\,,$$

where $\underline{M} = (X_4, X_5, X_6)$ and $\underline{X} = (X_1, X_2, X_3)$, and similarly for the primed quantities.

We proceed to calculate X'_{j+3} in the same manner as we did X'_j and so the details will not be repeated. The factor $(\underline{n}\cdot\underline{i}'_j\times\underline{x}')$ must initially be kept within the inner integral in the correction term, since $\underline{x}'$ depends on x'_3, but if we set $x_3 = 0$ in this factor, we cause only higher order errors, as is easily verified. The result is:

$$X'_{j+3} = \rho\int_{S_o} dS\,(\underline{n}\cdot\underline{i}_j\times\underline{x})\left\{-g x_3 - g(\xi_3 + x_2\theta_1 - x_1\theta_2) - \frac{\partial\varphi_1}{\partial t} + V\,\frac{\partial\varphi_1}{\partial x_1} - \nabla\varphi_o\cdot\nabla\varphi_1\right.$$

$$\left. + V\left[1 + (\underline{\xi}+\underline{\theta}\times\underline{x})\cdot\nabla\right]\frac{\partial\varphi_o}{\partial x_1}\right\} - \rho V\int_{L_o} d\ell\,(\underline{n}\cdot\underline{i}_j\times\underline{x})\,\frac{\partial\varphi_o}{\partial x_1}\left\{\frac{1}{g}\,\frac{\partial\varphi_1}{\partial t} - \frac{V}{g}\,\frac{\partial\varphi_1}{\partial x_1} + (\xi_3 + x_2\theta_1 - x_1\theta_2)\right\}.$$

Since we set $x_3 = 0$ in the line integral, the vector $\underline{x}$ now lies in the $x_1 - x_2$ plane, as does $\underline{n}$ also. Therefore the correction term is non-zero only for $j = 3$. That is, it contributes only to the yawing moment. For motions limited to the longitudinal plane, the correction term is clearly zero.

To conclude this appendix, we write down the complete expressions for force and moment components in the steady coordinate system, using the potential function in essentially the form proposed by Cummins, Eq. (11):

$$X_j(t) = X_{jo} - \sum_{k=1}^{6} \mu_{jk}\, \ddot{\alpha}_k(t) - \sum_{k=1}^{6} b_{jk}\, \dot{\alpha}_k(t) - \sum_{k=1}^{6} c_{jk}\, \alpha_k(t)$$

$$- \sum_{k=1}^{6} \int_{-\infty}^{t} \dot{\alpha}_k(\tau)\, L_{jk}(t-\tau)\, d\tau - \sum_{k=1}^{6} \int_{-\infty}^{t} \alpha_k(\tau)\, M_{jk}(t-\tau)\, d\tau \,, \tag{A1}$$

where

$$X_{jo} = \rho \int_{S_o} \frac{\partial \psi_{1j}(\underline{x})}{\partial n} \left[-g x_3 + V \frac{\partial \varphi_o}{\partial x_1} \right] dS \,, \tag{A2}$$

$$\mu_{jk} = \rho \int_{S_o} \frac{\partial \psi_{1j}(\underline{x})}{\partial n}\, \psi_{1k}(\underline{x})\, dS \,, \tag{A3}$$

$$b_{jk} = \rho \int_{S_o} \frac{\partial \psi_{1j}(\underline{x})}{\partial n} \left[\psi_{2k}(\underline{x}) - V \frac{\partial \psi_{1k}(\underline{x})}{\partial x_1} + \nabla\varphi_o \cdot \nabla\psi_{1k}(\underline{x}) \right] dS \,, \tag{A4}$$

$$c'_{jk} = \rho \int_{S_o} \frac{\partial \psi_{1j}(\underline{x})}{\partial n} \left[-V \frac{\partial \psi_{2k}(\underline{x})}{\partial x_1} + \nabla\varphi_o \cdot \nabla\psi_{2k}(\underline{x}) + g\, \underline{i}_3 \cdot \underline{h}_k(\underline{x}) \right.$$

$$\left. - V \underline{h}_k(x) \cdot \nabla \frac{\partial \varphi_o}{\partial x_1} \right] dS + \rho V \int_{L_o} \frac{\partial \psi_{1j}(x)}{\partial n} \left[\frac{\partial \varphi_o}{\partial x_1} \left(\underline{i}_3 \cdot \underline{h}_k(\underline{x}) \right) \right] d\ell \,, \tag{A5}$$

$$c_{jk} = c'_{jk} + \begin{bmatrix} 0 & 0 & 0 & 0 & +X_{3_o} & -X_{2_o} \\ 0 & 0 & 0 & -X_{3_o} & 0 & +X_{1_o} \\ 0 & 0 & 0 & +X_{2_o} & -X_{1_o} & 0 \\ 0 & +X_{3_o} & -X_{2_o} & 0 & +X_{6_o} & -X_{5_o} \\ -X_{3_o} & 0 & +X_{1_o} & -X_{6_o} & 0 & +X_{4_o} \\ +X_{2_o} & -X_{1_o} & 0 & +X_{5_o} & -X_{4_o} & 0 \end{bmatrix} , \tag{A6}$$

$$\underline{h}_k(\underline{x}) = \begin{cases} \underline{i}_k , & k = 1, 2, 3 , \\ \underline{i}_{k-3} \times \underline{x} , & k = 4, 5, 6 , \end{cases} \tag{A7}$$

$$L_{jk}(t) = \rho \int_{S_o} \frac{\partial \psi_{1j}(\underline{x})}{\partial n} \left(\frac{\partial}{\partial t} - V \frac{\partial}{\partial x_1} + \nabla \varphi_o \cdot \nabla \right) \chi_{1k}(\underline{x}, t)\, dS$$

$$+ \frac{\rho V}{g} \int_{L_o} \frac{\partial \psi_{1j}(\underline{x})}{\partial n} \frac{\partial \varphi_o(\underline{x})}{\partial x_1} \left(\frac{\partial}{\partial t} - V \frac{\partial}{\partial x_1} \right) \chi_{1k}(\underline{x}, t)\, d\ell , \tag{A8}$$

$$M_{jk}(t) = \rho \int_{S_o} \frac{\partial \psi_{1j}(\underline{x})}{\partial n} \left(\frac{\partial}{\partial t} - V \frac{\partial}{\partial x_1} + \nabla \varphi_o \cdot \nabla \right) \chi_{2k}(\underline{x}, t)\, dS$$

$$+ \frac{\rho V}{g} \int_{L_o} \frac{\partial \psi_{1j}(\underline{x})}{\partial n} \frac{\partial \varphi_o(\underline{x})}{\partial x_1} \left(\frac{\partial}{\partial t} - V \frac{\partial}{\partial x_1} \right) \chi_{2k}(\underline{x}, t)\, d\ell . \tag{A9}$$

It may be noted that the quantities $(c_{jk} - c'_{jk})$ arise from the transformation of force and moment components from the unsteady to the steady reference frames.

There is some ambiguity in choosing the best representation of the convolution integral terms. There would be no basic difficulty in carrying along both sums, but it would lead to much extra writing later on, and so we choose to combine the two sums of convolution integrals into a single sum. We can partially integrate the sum containing the L_{jk}'s:

$$\int_{-\infty}^{t} \dot{\alpha}_k(\tau)\, L_{jk}(t-\tau)d\tau = \alpha_k(\tau)\, L_{jk}(t-\tau) \Big|_{-\infty}^{t} + \int_{-\infty}^{t} \alpha_k(\tau) \frac{\partial}{\partial t} L_{jk}(t-\tau)d\tau ,$$

and then this sum has the same appearance as the other one, since the integrated part vanishes. However, for reasons of convenience later, we choose now to handle these integrals in the opposite way: We assume that a partial integration can be performed on the sums containing the M_{jk}'s and that the integrated terms will vanish, so that we can write the last two sums in Eq. (A1) as follows:

$$\sum_{k=1}^{6} \int_{-\infty}^{t} \dot{\alpha}_k(\tau)\, L_{jk}(t-\tau)d\tau + \sum_{k=1}^{6} \int_{-\infty}^{t} \alpha_k(\tau)\, M_{jk}(t-\tau)d\tau = \sum_{k=1}^{6} \int_{-\infty}^{t} \dot{\alpha}_k(\tau)\, K_{jk}(t-\tau)d\tau . \tag{A10}$$

A further discussion of this point appears in Appendix B.

APPENDIX B

Systems Lacking Some Restoring Forces

We want to treat here the case that, after a transient disturbance, some of the $\alpha_k(t)$ may not return to zero. As explained in the main text, we specifically exclude the case that any $\alpha_k(t)$ may continue to grow indefinitely, for then the linear analysis must certainly break down and there is no meaning to applying Fourier transforms to the equations of motion – even though they may be valid in the initial stages of the motion.

If $\alpha_k(t) \to \alpha_k(\infty) \neq 0$, as $t \to \infty$, the Fourier transform of α_k does not exist in the classical sense. However, we can still treat it by using the concepts of generalized function theory. (See Lighthill (1958).) Let

$$\alpha_k(t) = \left[\alpha_k(t) - \alpha_k(\infty)\, H(t)\right] + \alpha_k(\infty)\, H(t)\,.$$

where

$$H(t) = \begin{cases} 0 & \text{for } t < 0\,, \\ 1 & \text{for } t > 0\,. \end{cases}$$

The Fourier transform of the quantity in brackets exists in the usual sense and is easily shown to be:

$$\mathfrak{F}\left\{\alpha_k(t) - \alpha_k(\infty)\, H(t)\right\} = \frac{1}{i\omega}\left[\bar{\dot{\alpha}}_k(\omega) - \alpha_k(\infty)\right],$$

where, for brevity, I have introduced the notation

$$\bar{\dot{\alpha}}_k(\omega) = \mathfrak{F}\left\{\dot{\alpha}_k(t)\right\}.$$

We also note that

$$\bar{\dot{\alpha}}_k(0) = \int_{-\infty}^{\infty} \dot{\alpha}_k(t)\, dt = \alpha_k(\infty)\,.$$

In the language of generalized functions (see page 43 of Lighthill),

$$\mathfrak{F}\left\{H(t)\right\} = \bar{H}(\omega) = \frac{1}{2}\,\delta(\omega) + \frac{1}{i\omega}\,.$$

Therefore,

$$\mathfrak{F}\left\{\alpha_k(t)\right\} = \bar{\alpha}_k(\omega) = \frac{1}{2}\,\alpha_k(\infty)\,\delta(\omega) + \frac{\bar{\dot{\alpha}}_k(\omega)}{i\omega}\,.$$

Since we assume that $\alpha_k(t)$ remains bounded, there is no difficulty about taking transforms of the terms containing $\ddot{\alpha}_k$ or $\dot{\alpha}_k$, but the convolution integrals in the equations of motion, (13), require care. Rather than attempt to transform these terms as they appear in Eqs. (13), I find it desirable to retrace steps somewhat. Equation (A1) of Appendix A states that the j-th component of the motion induced force is:

$$X_j = X_{jo} - \sum_{k=1}^{6} \mu_{jk}\, \ddot{\alpha}_k(t) - \sum_{k=1}^{6} b_{jk}\, \dot{\alpha}_k(t) - \sum_{k=1}^{6} c_{jk}\, \alpha_k(t)$$

$$- \sum_{k=1}^{6} \int_{-\infty}^{t} \dot{\alpha}_k(\tau)\, L_{jk}(t-\tau)d\tau - \sum_{k=1}^{6} \int_{-\infty}^{t} \alpha_k(\tau)\, M_{jk}(t-\tau)d\tau . \qquad \text{(B1)}$$

The last two sums are compressed into the single sum of convolution integrals in (13). However, it is now more perspicuous to consider the two separate kinds of integrals.

In order to study the behavior of the kernels in these integrals, let us assume that there is a velocity impulse in the k-th mode, so that

$$\dot{\alpha}_k(t) = \alpha_{ko}\, \delta(t) .$$

Then, for $t > 0$,

$$X_j = X_{jo} + \alpha_{ko} \left[c_{jk} + L_{jk}(t) + \int_0^t M_{jk}(\tau)d\tau \right] .$$

The term $L_{jk}(t)$ represents the actual unsteady force due to the velocity impulse itself. Physically, this must approach zero for large t, since the impulse motion generates only a finite-energy wave system, and these waves rapidly radiate away. The terms

$$\left[c_{jk} + \int_0^t M_{jk}(\tau)d\tau \right]$$

represent the force which results from the steady deflection of the translating ship after $t = 0$. The integral term of this expression must approach zero eventually, because c_{jk}, by definition, is the constant of proportionality between steady perturbation force and displacement. Obviously, if the integral of M_{jk} approaches zero as t becomes infinite, then M_{jk} itself approaches zero.

We can now find the Fourier transforms of the convolutions. For the first, involving L_{jk} and the disturbance velocity, we have from the convolution theorem:

$$\mathfrak{F}\left\{ \int_{-\infty}^{t} \dot{\alpha}_k(\tau)\, L_{jk}(t-\tau)d\tau \right\} = \bar{\dot{\alpha}}_k(\omega)\, \bar{L}_{jk}(\omega) .$$

For the other convolution, we must perform a little manipulation:

$$\mathfrak{F}\left\{\int_{-\infty}^{t} \alpha_k(\tau)\, M_{jk}(t-\tau)d\tau\right\} = \mathfrak{F}\left\{\int_{-\infty}^{t} [\alpha_k(\tau) - \alpha_k(\infty)\, H(\tau)]\, M_{jk}(t-\tau)d\tau\right\} + \alpha_k(\infty)\mathfrak{F}\left\{\int_{0}^{t} M_{jk}(\tau)d\tau\right\}$$

$$= \overline{M}_{jk}(\omega) \times \mathfrak{F}\{\alpha_k(t) - \alpha_k(\infty)\, H(t)\} + \alpha_k(\infty) \times \frac{\overline{M}_{jk}(\omega)}{i\omega}$$

$$= \overline{M}_{jk}(\omega) \times \frac{\bar{\dot{\alpha}}_k(\omega) - \alpha_k(\infty)}{i\omega} + \alpha_k(\infty) \times \frac{\overline{M}_{jk}(\omega)}{i\omega}$$

$$= \overline{M}_{jk}(\omega)\, \frac{\bar{\dot{\alpha}}_k(\omega)}{i\omega} .$$

The two kinds of convolution integrals can now be combined, as in Eq. (A10), and their sum will have as its Fourier transform

$$\frac{\bar{\dot{\alpha}}_k(\omega)}{i\omega}\left[\overline{M}_{jk}(\omega) + i\omega\, \overline{L}_{jk}(\omega)\right] .$$

The above derivation amounts to a demonstration that the integrals in (13),

$$\int_{-\infty}^{t} \dot{\alpha}_k(\tau)\, K_{jk}(t-\tau)d\tau ,$$

do indeed exist and have conventional transforms.

The transform of $(X_j - X_{jo})$ can now be written out explicitly:

$$\mathfrak{F}\{X_j - X_{jo}\} = -\frac{1}{2}\,\delta(\omega) \sum_{k=1}^{6} c_{jk}\, \alpha_k(\infty)$$

$$- \sum_{k=1}^{6} \left\{-\omega^2 \mu_{jk} + i\omega b_{jk} + c_{jk} + i\omega\, \overline{L}_{jk}(\omega) + \overline{M}_{jk}(\omega)\right\} \frac{\bar{\dot{\alpha}}_k(\omega)}{i\omega} . \quad \textbf{(B2)}$$

This can be substituted into the transform of (13), and we recover (15) — with three changes:

1. $\bar{\dot{\alpha}}_k(\omega)/i\omega$ replaces $\bar{\alpha}_k(\omega)$.

2. $\overline{L}_{jk}(\omega) + \overline{M}_{jk}(\omega)/i\omega$ replaces $\overline{K}_{jk}(\omega)$.

3. There is an extra sum on the left-hand side:

$$\frac{1}{2}\,\delta(\omega) \sum_{k=1}^{6} c_{jk}\, \alpha_k(\infty) .$$

Item (1) is of no consequence if $\bar{a}_k(\omega)$ exists, for it then equals $\bar{\dot{a}}_k(\omega)/i\omega$. Even if $\bar{a}_k(\omega)$ does not exist, our assumptions imply that $\bar{\dot{a}}_k(\omega)$ does exist, and so the applicability of (15) has been extended.

Item (2) is also of no consequence, for we have just shown that the two expressions are equivalent. Also, $\bar{M}_{jk}(\omega)/i\omega$ exists even when $\omega = 0$, because of the fact that

$$\int_0^\infty M_{jk}(\tau)d\tau = 0 .$$

Item (3) is not quite so easily disposed of. We note that, if the external forces represented in (15) are well-behaved transients, then

$$\omega\left[\bar{F}_j(\omega) + \bar{G}_j(\omega)\right] \to 0 \qquad \text{as} \quad \omega \to 0 .$$

Also, $\omega\delta(\omega) = 0$, for all . Therefore, if we multiply Eq. (15) (as now modified) by ω and let $\omega \to 0$, we are left with:

$$\sum_{k=1}^{6} c_{jk}\,\bar{\dot{a}}_k(0) = \sum_{k=1}^{6} c_{jk}\,a_k(\infty) = 0 .$$

This result is hardly unexpected, for it says simply that c_{jk} must be zero if $a_k(\infty) \neq 0$, unless two or more $a_k(\infty)$ are non-zero in such a way that this sum vanishes without the individual terms all vanishing.

It is now evident that the above sum can be omitted from (B2) and thus from the modified (15). However, the equation will not apply when $\omega = 0$. With this exception, Eq. (15) remains valid even when $\bar{a}_k(\omega)$ does not exist, provided only that we replace $\bar{a}_k(\omega)$ by $\bar{\dot{a}}_k(\omega)/i\omega$.

APPENDIX C

Alternative Derivation of (17a) and (17b)

Equations (17a) and (17b), relating the added mass and damping coefficients, can be derived in a way which avoids inverting one of the transforms and using the inversion to find the other transform. Thus it also avoids the double integration and the interchange of limiting operations (which were not proved valid) in the derivation of (17a). The proof which follows is not entirely rigorous either, but it shows some of the physical bases on which the final formulas stand.

The kernels $K_{jk}(t)$ in the convolution integrals all have the property that $K(t) = 0$ for $t < 0$. (I shall omit the subscripts hereafter.) Furthermore, they approach zero as $t \to \infty$. Therefore the Fourier transform of $K(t)$ can be written:

$$\bar{K}(\omega) = \int_0^\infty K(t)\, e^{-i\omega t}\, dt = \bar{K}_c(\omega) - i\, \bar{K}_s(\omega)\,.$$

Also,

$$\bar{K}(-\omega) = \int_0^\infty K(t)\, e^{i\omega t}\, dt = \bar{K}_c(\omega) + i\bar{K}_s(\omega) = \overline{\bar{K}(\omega)}\,.*$$

These relations depend quite explicitly on the condition that $K(t) = 0$ for $t < 0$; this has frequently been described as an effect of "causality," i.e., the system does not respond before $t = 0$ if the disturbance comes at $t = 0$.

If now we consider ω as a complex variable, it is clear from the definition of the Fourier integral $\bar{K}(\omega)$ that the convergence of the integral can only be quickened when $\mathrm{Im}\ \omega < 0$. Then $\bar{K}(\omega)$ cannot have any singularities in the lower half of the ω-plane. But for an analytic function we can use Cauchy's integral formula:

$$\bar{K}(\omega) = -\frac{1}{2\pi i} \int_C \frac{\bar{K}(\omega')\, d\omega'}{\omega' - \omega}\,.$$

See the figure.

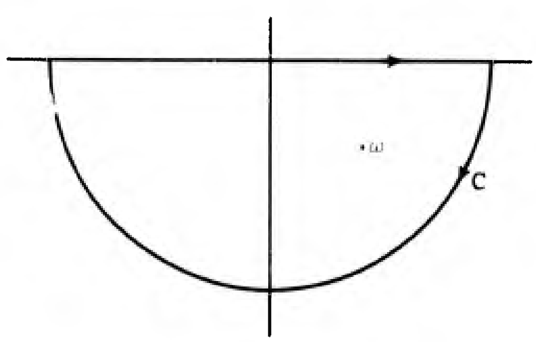

If $\bar{K}(\omega)$ vanishes far from the origin in the lower half-plane (no matter how slowly), the contribution from the semi-circle vanishes as the radius grows to infinity, and so we can replace the integral over the closed contour C by a contour integral along the real axis from $-\infty$ to $+\infty$.

Now we let ω approach the real axis (from below), and we indent the contour above the real axis, so that for real ω

$$\bar{K}(\omega) = -\frac{1}{2\pi i}\left\{ ⨍_{-\infty}^{\infty} \frac{\bar{K}(\omega')\, d\omega'}{\omega' - \omega} - \pi i\, \bar{K}(\omega) \right\} = -\frac{1}{\pi i} ⨍_{-\infty}^{\infty} \frac{\bar{K}(\omega')\, d\omega'}{\omega' - \omega}\,.$$

*The long bar denotes the complex conjugate quantity.

Furthermore,

$$\overline{K}(-\omega) = -\frac{1}{\pi i}\int_{-\infty}^{\infty}\frac{\overline{K}(\omega')d\omega'}{\omega' + \omega} = \overline{\overline{K}(\omega)} .$$

Finally, we express the real and imaginary parts of these equations separately

$$\overline{K}_c(\omega) = \frac{1}{2}\left[\overline{K}(\omega) + \overline{\overline{K}(\omega)}\right] = -\frac{1}{\pi i}\int_{-\infty}^{\infty}\frac{\omega'\overline{K}(\omega')d\omega'}{\omega'^2 - \omega^2}$$

$$= \frac{2}{\pi}\int_{0}^{\infty}\frac{\omega'\overline{K}_s(\omega')d\omega'}{\omega'^2 - \omega^2} .$$

$$\overline{K}_s(\omega) = \frac{i}{2}\left[\overline{K}(\omega) - \overline{\overline{K}(\omega)}\right] = -\frac{\omega}{\pi}\int_{-\infty}^{\infty}\frac{\overline{K}(\omega')d\omega'}{\omega'^2 - \omega^2}$$

$$= -\frac{2\omega}{\pi}\int_{0}^{\infty}\frac{\overline{K}_c(\omega')d\omega'}{\omega'^2 - \omega^2} .$$

From (16), we substitute the definitions:

$$\overline{K}_c(\omega) = b^*(\omega) - b ; \qquad \overline{K}_s(\omega) = -\omega\left[\mu^*(\omega) - \mu\right] ;$$

and this leads immediately to (17).

* * *

PROBLEM AREAS IN SHIP MOTION RESEARCH

Willard J. Pierson, Jr.
New York University
New York, New York

INTRODUCTION

There are a number of subjects that were not covered by the various papers on ship motions given at this symposium. Three of the subjects are: (1) Ships in short crested waves, (2) coherency and resolvability of spectral and cross spectral shapes, and (3) the solutions of specific problems that are nonlinear. It is the purpose of these comments to discuss these subjects and their relationship to the papers that were presented so as to complete the record of this symposium. These comments apply in particular to the papers by Dr. Ogilvie, Dr. Ochi, and Drs. Breslin, Savitsky, and Tsakonas.

The papers by Fuchs and MacCamy (1953) and by St. Denis and Pierson (1953) have been cited as initiating the study of the motions of ships in real waves, the first from the time domain viewpoint and the second from a spectral viewpoint. The first is often thought of as deterministic and as having little to do with the Gaussian properties of real waves. The second is thought of as highly dependent on the assumption of Gaussian behavior for the waves and on the principle of linear superposition.

The first is nevertheless highly dependent on many of the same assumptions of St. Denis and Pierson. Since waves are very nearly Gaussian, it is useful to get the spectra and cross spectra that describe the response of a ship to long crested waves in order to obtain an accurate time domain operator for the application of the procedures of Fuchs and MacCamy. Their model is just as linear and just as dependent on a linear hypothesis as that of St. Denis and Pierson.

In actuality the work of Fuchs and MacCamy is much more restrictive than the work of St. Denis and Pierson, and much of the work described at this symposium is too restrictive for direct application to real ships in real waves. The work of Fuchs and MacCamy is strictly applicable only to ships in long crested waves. Long crested waves are an abstraction not met in nature. The work of St. Denis and Pierson, and its completion so as to include co- and quadrature spectra, by Pierson (1957) is applicable to actual ships in actual waves and provides valuable guidance in the study of ships and other floating objects in real waves. Studies such as those of Canham, Cartwright, Goodrich, and Hogben (1962) and O'Brien and Muga (1965) show the value of spectral and cross-spectral analysis. More can be done in a full utilization of these results, however.

The concept of linearity invoked by St. Denis and Pierson is not as essential to their theory as it seemed at the time although even for such extreme conditions as slamming, the theory yields useful results as in the work of Tick (1958) and in the paper of this symposium by Dr. Ochi. Recent work has extended the linear model of the seaway to a number of nonlinear models, and for specific problems nonlinear models concerning waves and the effect of waves on ships and some other objects have been developed.

SHIPS IN A SHORT CRESTED SEAWAY

If $\eta(x, y, t)$ is the sea surface, and if $S(\omega, \theta)$ is the variance spectrum of the waves, one can write that

$$\eta(x, y, t) = \int_0^\infty \int_{-\pi}^{\pi} \cos\left(\frac{\omega^2}{g}(x\cos\theta + y\sin\theta) - \omega t + \epsilon(\omega, \theta)\right) \sqrt{2S(\omega, \theta)\, d\omega\, d\theta}\,. \quad (1)$$

Consider a point moving in the negative x direction with the velocity, v. The coordinates of this point are given by Eq. (2) as x_e, y_e.

$$x_e = x + vt$$
$$y_e = y_e . \tag{2}$$

Such a coordinate system moving with this velocity would record or see a sea surface given by Eq. (3) as a function of position and time with reference to the moving origin.

$$\eta(x_e, y_e, t) = \int_0^\infty \int_{-\pi}^{\pi} \cos\left[\frac{\omega^2}{g}(x_e \cos\theta + y_e \sin\theta) - \left(\omega - \frac{\omega^2}{g} v \cos\theta\right) t - \epsilon\right] \sqrt{2S(\omega, \theta)\, d\omega\, d\theta} . \tag{3}$$

For region I of St. Denis and Pierson, the spectrum, $S(\omega, \theta)$ becomes the spectrum of encounter as given by

$$S_e(\omega_e, \theta_e)_I = \frac{S\left(\dfrac{1 - \sqrt{1 - 4\omega_e v \cos\theta_e/g}}{2\omega_e v \cos\theta_e/g}, \omega_e, \theta_e\right)}{\sqrt{1 - 4\omega_e v \cos\theta_e/g}} \tag{4}$$

and the seaway of encounter is given by

$$\eta_{eI}(x_e, y_e, t) = \iint_{\text{Region I}} \cos\left\{(\omega_e t + \epsilon) - \left[(\omega(\omega_e))^2/g\right](x_e \cos\theta_e + y_e \sin\theta_e)\right\}$$
$$\times \sqrt{2S_{eI}(\omega_e, \theta_e)\, d\omega_e\, d\theta_e} . \tag{5}$$

The above steps can be repeated with appropriate modifications for regions II and III with the result that

$$\eta_e(x_e, y_e, t) = \eta_{eI}(x_e, y_e, t) + \eta_{eII}(x_e, y_e, t) + \eta_{eIII}(x_e, y_e, t). \tag{6}$$

If the center of gravity of a ship is located at the point $x_e = y_e = 0$ Eq. (5) can be written as

$$\eta_{eI}(t) = \Sigma\Sigma \cos(\omega_e t + \epsilon) \sqrt{2S_e(\omega_e, \theta_e)\, \Delta\omega_e\, \Delta\theta_e} \tag{7}$$

where a partial sum is indicated as an approximation to (5). The important point to note at this stage of the derivation is that the same frequency of encounter, ω_e, can result from many different waves coming from many directions, θ_e, and can be associated with many different wavelengths.

In practice for a given θ_{e1} and ω_{e1}, given the wavelength, the region can be determined. One single term in the double partial sum of (7) is thus sensed as in Eq. (8) by a wave recorder located at the moving origin.

$$\eta_{e1}(t) = a \cos(\omega_{e1} t + \epsilon) . \tag{8}$$

In Eq. (8) the other important parameter for the waves, that is, the direction of encounter, θ_e, is no longer in evidence.

If ω_e and θ_e and the region of definition for that portion of the spectrum are known then a particular wave, $\eta_{e1}(t)$ can be associated with the motion of a ship as caused by this one sinusoidal wave. The concept of a transfer function as evaluated at a particular frequency for a particular direction is then valid and the response of the ship can be considered as a part in phase with the forcing waves or 180 degrees out of phase and a part in quadrature with the forcing waves having a phase of either 90° or 270° with the forcing waves. The functions, $c_z(\omega_e, \theta_e)$, $q_z(\omega_e, \theta_e)$, and so on, can be determined either by means of experiments or by theories. The response to a single forcing wave is therefore given by Eqs. (9), (10), and (11) for heave, pitch, and roll.

$$z_1(t) = ac_z(\omega_{e1}, \theta_{e1}) \cos (\omega_{e1}t + \epsilon) + aq_z(\omega_{e1}, \theta_{e1}) \sin (\omega_{e1}t + \epsilon) \tag{9}$$

$$\psi_1(t) = ac_\psi(\omega_{e1}, \theta_{e1}) \cos (\omega_{e1}t + \epsilon) + aq_\psi(\omega_{e1}, \theta_{e1}) \sin (\omega_{e1}t + \epsilon) \tag{10}$$

$$\phi_1(t) = ac_\phi(\omega_{e1}, \theta_{e1}) \cos (\omega_{e1}t + \epsilon) + aq_\phi(\omega_{e1}, \theta_{e1}) \sin (\omega_{e1}t + \epsilon) . \tag{11}$$

The difference between short crested waves and long crested head seas is most striking here. In general, if θ_e is changed, c_z, q_z, c_ϕ, and q_ϕ may or may not change but they can change even for the same frequency of encounter. For example, one wave at +30° into the course of the vessel and another at -30° to the course of the vessel will look the same at the center of gravity of the vessel, but they will produce rolling motions that are 180° out of phase with each other.

From Eqs. (9), (10), and (11) by means of the definition of the seaway of encounter given by Eq. (5), it is possible now to write down the vector Gaussian process that describes the time histories that would be recorded for the forcing seaway (at the center of gravity of the vessel if it could be observed there) and the heaving motion, the pitching motion, and the rolling motion.

$$\eta_e(t) = \Sigma\Sigma \cos (\omega_e t + \epsilon) \sqrt{2S_e(\omega_e, \theta_e) \Delta\omega_e, \Delta\theta_e}$$

$$\begin{aligned} z(t) &= \Sigma\Sigma \left[\cos (\omega_e t + \epsilon)\, c_z(\omega_e, \theta_e) + \sin (\omega_e t + \epsilon)\, q_z(\omega_e, \theta_e)\right] \sqrt{2S_e(\omega_e, \theta_e) \Delta\omega_e, \Delta\theta_e} \\ \psi(t) &= \Sigma\Sigma \left[\cos (\omega_e t + \epsilon)\, c_\psi(\omega_e, \theta_e) + \sin (\omega_e t + \epsilon)\, q_\psi(\omega_e, \theta_e)\right] \sqrt{2S_e(\omega_e, \theta_e) \Delta\omega_e, \Delta\theta_e} \\ \phi(t) &= \Sigma\Sigma \left[\cos (\omega_e t + \epsilon)\, c_\phi(\omega_e, \theta_e) + \sin (\omega_e t + \epsilon)\, q_\phi(\omega_e, \theta_e)\right] \sqrt{2S_e(\omega_e, \theta_e) \Delta\omega_e, \Delta\theta_e} . \end{aligned} \tag{12}$$

These double summation partial sums are to be evaluated over the same net in ω_e and θ_e for the same random phases. If there is any "phase relationship" between the various motions and the forcing seaway these phase relationships will be preserved. However, by virtue of the remarks made above in connection with Eqs. (9), (10), and (11), it is not necessary for a particular phase relationship to manifest itself. Indeed, in general, there are cases where no phase relationship exists and there are other cases where a phase relationship appears to exist.

An ensemble of such vector processes as defined by Eqs. (12) can be generated by choosing different sets of the ϵ's at random in a large number of partial sums. One can then compute ten different expected values of various time lagged products of different combinations of these motions.

$$E\left[\eta_e(t), \eta_e(t+\tau)\right] \quad E\left[z(t), z(t+\tau)\right] \quad E\left[\psi(t), \psi(t+\tau)\right] \quad E\left[\phi(t), \phi(t+\tau)\right]$$

$$E\left[\eta_e(t), z(t+\tau)\right] \quad E\left[\eta_e(t), \psi(t+\tau)\right] \quad E\left[\eta_e(t), \phi(t+\tau)\right]$$

$$E\left[z(t), \psi(t+\tau)\right] \quad E\left[z(t), \phi(t+\tau)\right]$$

and

$$E\left[\psi(t), \phi(t+\tau)\right] .$$

One of these expectations as evaluated is Eq. (13):

$$E\left[\eta_e(t), z(t+\tau)\right] = \int S(\omega_e, \theta_e)\left[c_z(\omega_e, \theta_e)\cos\omega_e\tau + q_z(\omega_e, \theta_e)\sin\omega_e\tau\right] d\theta_e . \quad (13)$$

The cospectrum between the forcing waves and heaving motion is thus given by Eq. (14) as this is the even part of the Fourier transform of Eq. (13).

$$\overline{C}_{\eta z}(\omega_e) = \int S(\omega_e, \theta_e)\, c_z(\omega_e, \theta_e)\, d\theta_e . \quad (14)$$

The quadrature spectrum is given by Eq. (15).

$$\overline{Q}_{\eta z}(\omega_e) = \int S(\omega_e, \theta_e)\, q_z(\omega_e, \theta_e)\, d\theta_e . \quad (15)$$

It is to be noted that the cospectrum and the quadrature spectrum still involve an integration over θ_e. The way in which $c_z(\omega_e, \theta_e)$ and $q_z(\omega_e, \theta_e)$ vary as a function of θ_e for a fixed ω_e can evidently have a marked effect on the cross spectra.

A complete analysis yields four spectra, six co-spectra, and six quadrature spectra. The spectrum for the heave, for example, is given by Eq. (16).

$$S_z(\omega_e) = \int S(\omega_e, \theta_e)\left[\left(c_z(\omega_e, \theta_e)\right)^2 + \left(q_z(\omega_e, \theta_e)\right)^2\right] d\theta_e . \quad (16)$$

The co-spectrum between heave and the waves and the quadrature spectrum between heave and the waves are given by Eqs. (17) and (18).

$$\overline{C}_{\eta z}(\omega_e) = \int S(\omega_e, \theta_e)\left[c_z(\omega_e, \theta_e)\right] d\theta_e \quad (17)$$

$$\overline{Q}_{\eta z}(\omega_e) = \int S(\omega_e, \theta_e)\left[q_z(\omega_e, \theta_e)\right] d\theta_e . \quad (18)$$

The cross spectra between heave and pitch are given by Eqs. (19) and (20).

$$\bar{C}_{z\psi}(\omega_e) = \int S(\omega_e, \theta_e) \left[c_z(\omega_e, \theta_e)\, c_\psi(\omega_e, \theta_e) + q_z(\omega_e, \theta_e)\, q_\psi(\omega_e, \theta_e)\right] d\theta_e \tag{19}$$

$$\bar{Q}_{z\psi}(\omega_e) = \int S(\omega_e, \theta_e) \left[c_z(\omega_e, \theta_e)\, c_\psi(\omega_e, \theta_e) - q_z(\omega_e, \theta_e)\, q_\psi(\omega_e, \theta_e)\right] d\theta_e . \tag{20}$$

The response amplitude operator defined by St. Denis and Pierson is seen to be given by Eq. (21) in terms of the spectrum for the heaving motion and the spectrum of the seaway of encounter. This is simply the square of the response of the vessel to a unit sine wave at a particular frequency of encounter and direction of encounter.

$$T(\omega_e, \theta_e) = \left[c_z(\omega_e, \theta_e)\right]^2 + \left[q_z(\omega_e, \theta_e)\right] . \tag{21}$$

The coherency for short crested waves takes on a new and essentially different feature, however. Consider, for example, the coherency between the forcing waves and the heave. It is given by Eq. (22).

$$\bar{K}_{\eta z}(\omega_e) = \frac{\left[\bar{C}_{\eta z}(\omega_e)\right]^2 + \left[\bar{Q}_{\eta z}(\omega_e)\right]^2}{S_e(\omega_e)\; S_z(\omega_e)} . \tag{22}$$

This can be rewritten in full as Eq. (23), and the top expression can be shown to satisfy the relationship given by Eq. (24).

$$\bar{K}_{\eta z}(\omega_e) = \frac{\left[\int S_e(\omega_e, \theta_e)\, c_z(\omega_e, \theta_e)\, d\theta_e\right]^2 + \left[\int S_e(\omega_e, \theta_e)\, q_z(\omega_e, \theta_e)\, d\theta_e\right]^2}{\int S_e(\omega_e, \theta_e)\, d\theta_e \cdot \int S_e(\omega_e, \theta_e) \left[\left(c_z(\omega_e, \theta_e)\right)^2 + \left(q_z(\omega_e, \theta_e)\right)^2\right] d\theta_e} \tag{23}$$

$$\left[\int S_e(\omega_e, \theta_e)\, c_z(\omega_e, \theta_e)\, d\theta_e\right]^2 \le \int S_e(\omega_e, \theta_e)\, d\theta_e \int S_e(\omega_e, \theta_e) \left[c_z(\omega_e, \theta_e)\right]^2 d\theta_e . \tag{24}$$

For a particular ship headed in a particular direction through a particular forcing seaway it is quite possible for the numerator of the expression for the coherency to be zero. The function under the integrand which is integrated over direction through 2π radians can change sign in such a way that the integral is very small or zero. The denominator of this expression for the coherency is composed of terms that are everywhere positive, and it must be large.

In St. Denis and Pierson (1953), these "phase relationships" were not considered, and since cross spectra were not considered, the effects just discussed did not enter into the problem. The spectra of heave, pitch, and roll were properly predicted.

In 1957, the writer wrote the following three paragraphs (with a change of notation to conform to these comments) in connection with the interpretation of coherency and spectra and cross spectra for ships in short crested waves:

> Consider a ship in head seas such that $S(\omega_e, \theta_e)$ is exactly symmetrical, i.e., $S_e(\omega_e, \theta_e) = S_e(\omega_e, -\theta_e)$. Under these conditions, $\eta_e(t)$,

$z(t)$, and $\psi(t)$ will probably have values for their coherency which are appreciable, perhaps, 0.6 to 0.8. However, the oncoming apparent waves will at one time be high on the port side and at another time be high on the starboard side causing the vessel to roll first one way and then the other for the same apparent wave form in $\eta_e(t)$. More precisely, $c_\phi(\omega_e, \theta_e)$ and $q_\phi(\omega_e, \theta_e)$ in (11) will be odd as a function of θ_e. Hence both $\bar{C}_{\eta\phi}(\omega_e)$ and $\bar{Q}_{\eta\phi}(\omega_e)$ will be zero. This implies that the coherencies between $\eta(t)$ and $\phi(t)$, $z(t)$ and $\phi(t)$, and $\psi(t)$ and $\phi(t)$ will all be near zero in a practical case when the motions are observed in head seas.

During storms, when in a hove to condition, ship masters prefer to take the seas a few points off the bow instead of from directly ahead. As explained to the author by a naval officer, this is because the vessel tends to roll in a more favorable way so that less green water is shipped over the bow. The side of the vessel toward the oncoming sea as explained by the above considerations will roll away from an oncoming crest as the bow rises and thus less water will be shipped. Stated another way, the coherency between $\eta_e(t)$ and $\phi(t)$ will be increased in a way favorable to drier decks.

A similar analysis can be carried out for a ship underway in beam seas. Roll, heave, and $\eta_e(t)$ will have fairly high coherencies. Pitch will be nearly incoherent with the other three components of the vector process.

Since these statements in 1957, our knowledge of the directional wave spectrum has been improved by the results of Longuet-Higgins, Cartwright and Smith (1963), by the results of Cartwright and Smith (1964) and by the results that I have described in another paper in this volume. The above conclusions have been verified by two papers that have been written since the report was prepared. The first paper that verified these conclusions is one by Canham, Cartwright, Goodrich, and Hogben (1962). In this paper, the ship was operated on an octagonal course. The forcing seaway was measured on this ship, not exactly at the center of gravity but this is irrelevant, and the various motions were also measured. It was indeed a fact that the coherency of roll and the forcing seaway was very small in head seas and that the coherency of pitch with the forcing seaway was very small for beam seas as predicted.

The important point is that this is to be expected. It is a basic feature of the probability model. The result does not mean that there is something wrong with the records of roll and pitch under these circumstances, and it does not mean that the theory is in error. For short crested waves the situation is more complicated than it is for ships in long crested waves.

In another study, O'Brien and Muga (1965) measured the response of a moored aircraft carrier to forcing waves and obtained spectra and co-spectra that yielded coherencies consistent with the above conclusions.

The above results on spectral and co-spectral coherencies can be analyzed in such a way as to provide an understanding of many features of ship motions in waves. They can also be compared with the much simpler case of long crested head seas in which for heaving motions, for example,

$$
\begin{aligned}
\eta_e(t) &= \Sigma \cos(\omega_e t + \epsilon)\sqrt{2S(\omega_e)\,\Delta\omega_e} \\
z_e(t) &= \Sigma\left[\cos(\omega_e t + \epsilon)\, c_z(\omega_e) + \sin(\omega_e + \epsilon)\, q_z(\omega_e)\right]\sqrt{2S(\omega_e)\,\Delta\omega_e}\,.
\end{aligned}
\tag{25}
$$

The cross spectra are given by

$$
\begin{aligned}
C_z(\omega_e) &= S(\omega_e)\, c_z(\omega_e) \\
Q_z(\omega_e) &= S(\omega_e)\, q_z(\omega_e)\,.
\end{aligned}
\tag{26}
$$

It therefore follows that the coherency is one.

These conclusions about the behavior of ships in both short crested and long crested waves bring up one of the main points that needs to be made. The method of Fuchs and MacCamy has not yet been extended to the point where it can describe the motions of actual ships in actual waves. In fact, the simple measurement of the forcing waves at one point as a function of time is insufficient for the prediction of the complete behavior of a ship in these waves. This is true whether or not the ship is underway just as long as the waves are short crested.

The essential reason for this difference between short crested waves and long crested waves is that in the above relationships an integration over direction is still involved in the definition of each function of frequency that is obtained by the analysis of a time history. An extra dimension is added to the problem when short crested waves occur. This dimension can conceivably be removed by recording the forcing waves along a line as a function of time with this line moving with the vessel. Or, a sufficiently dense network of points surrounding the moving ship should provide that kind of data that would make it possible to recover functions such as $c_z(\omega_e, \theta_e)$. However, the problem is one of a double Fourier analysis and not a single Fourier analysis properly generalized in terms of time series and probabilistic concepts. Some suggestions were given by Pierson (1957) as to how to do this.

Nevertheless, the spectral theory is complete for ships in short crested waves. It has not been fully exploited. Experimentation with actual ships in short crested waves should provide useful design information today in this connection.

COHERENCY AND RESOLVABILITY OF SPECTRAL AND CROSS SPECTRAL SHAPES

Poor resolution of rapidly varying cross spectra is likely to be reflected in a computation of low coherency. Such apparent low coherencies are not actually low coherencies, and great care must be taken in interpreting experimental results for long and (especially) short crested waves in this connection. Low coherencies between ship motions and the forcing waves in long crested waves are an indication of poor experimental design and interpretation, and they are not an indication of the failure of the linear theory.* For short crested waves the coherencies could be low both because of poor experimental design and because they really ought to be low.

The rapid variation in the cross spectral estimates that are sometimes obtained is the first indication that something is amiss. Such rapidly varying cross spectral estimates suggest that the coherency will be low because of the lack of adequate resolution.

An interesting example of this is given by the study of observations at two points in long crested random waves. Let the long crested random waves be given by Eq. (27).

$$\eta(x,t) = \int_0^\infty \cos\left(\frac{\omega^2 x}{x} - \omega t + \epsilon\right)\sqrt{2S(\omega)d\omega}\,. \tag{27}$$

By definition the co- and quadrature spectra are given by Eqs. (28) and (29) when (27) is observed at $x = 0$ and $x = L$.

$$C(\omega) = \cos\frac{\omega^2 L}{g}\,S(\omega) \tag{28}$$

$$Q(\omega) = \sin\frac{\omega^2 L}{g}\,S(\omega)\,. \tag{29}$$

The coherency is one.

$$K(\omega) = \frac{[C(\omega)]^2 + [Q(\omega)]^2}{[S(\omega)]^2} = 1\,. \tag{30}$$

Pierson and Dalzell (1960) studied two records that were taken in long crested waves. One record was about five feet away from the other record. The spectra and cross spectra were computed. Figure 1 shows the estimated spectrum as indicated by the histogramic presentation. One number centered at the center of each step in the histogram was the number that describe the particular spectrum. There were two spectra and the circle and the diamond indicate how these two spectral estimates differed over a separation of five feet in long crested waves. The co- and quadrature spectra were also computed. These spectra are shown in Fig. 2 by the black diamonds. They look fairly reasonable in comparison with Eqs. (28) and (29).

However, the computation of the coherency led to the results shown by the black diamonds in Fig. 3. The coherency is high near a value of $h = 7$ and it falls of steadily to values of 0.5, 0.4, 0.3 for larger values of h. This is quite disturbing as certainly the model proposed by Eq. (27) for the free surface and

*In most cases.

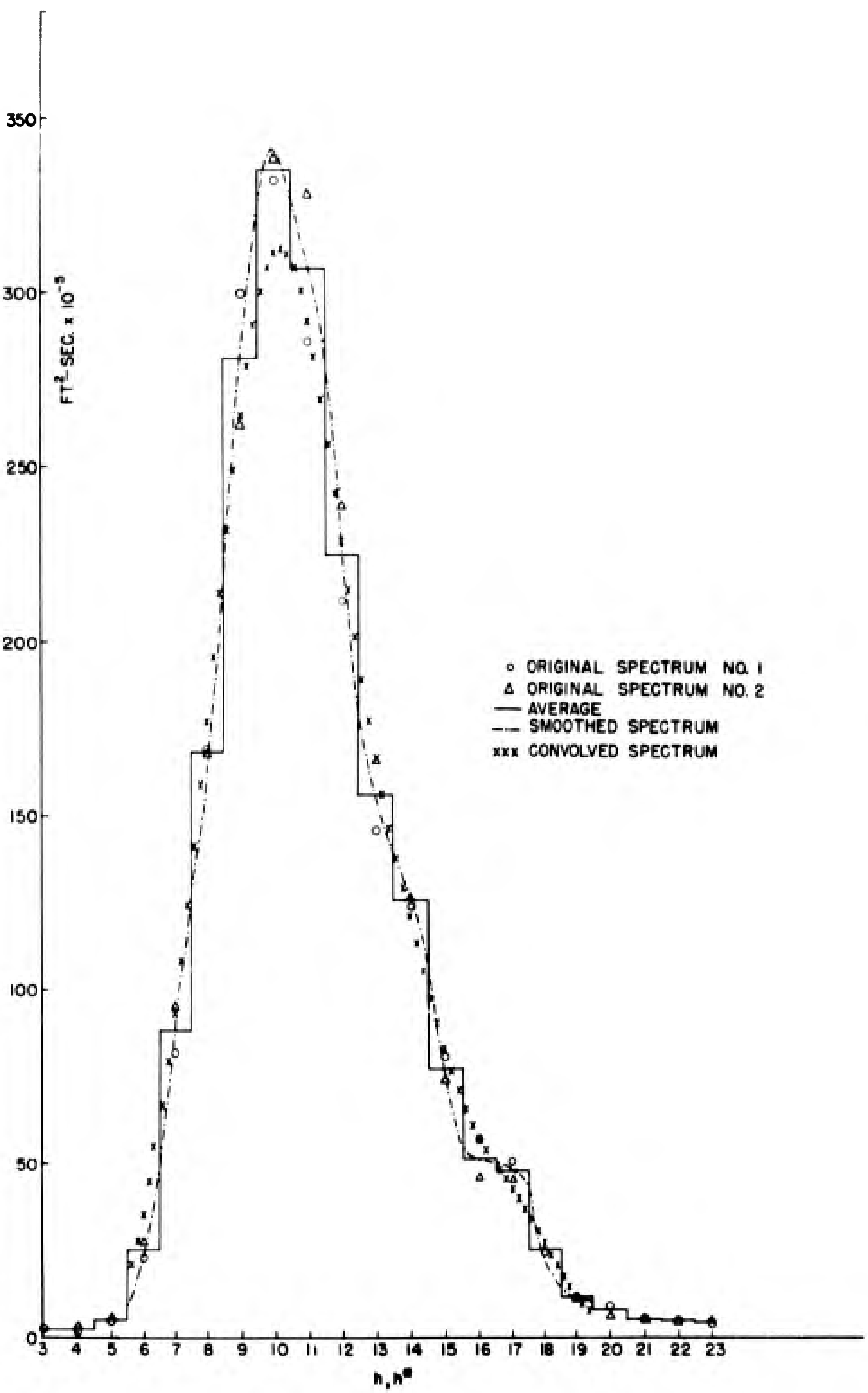

Fig. 1 - Comparison of original spectra
and spectra derived therefrom

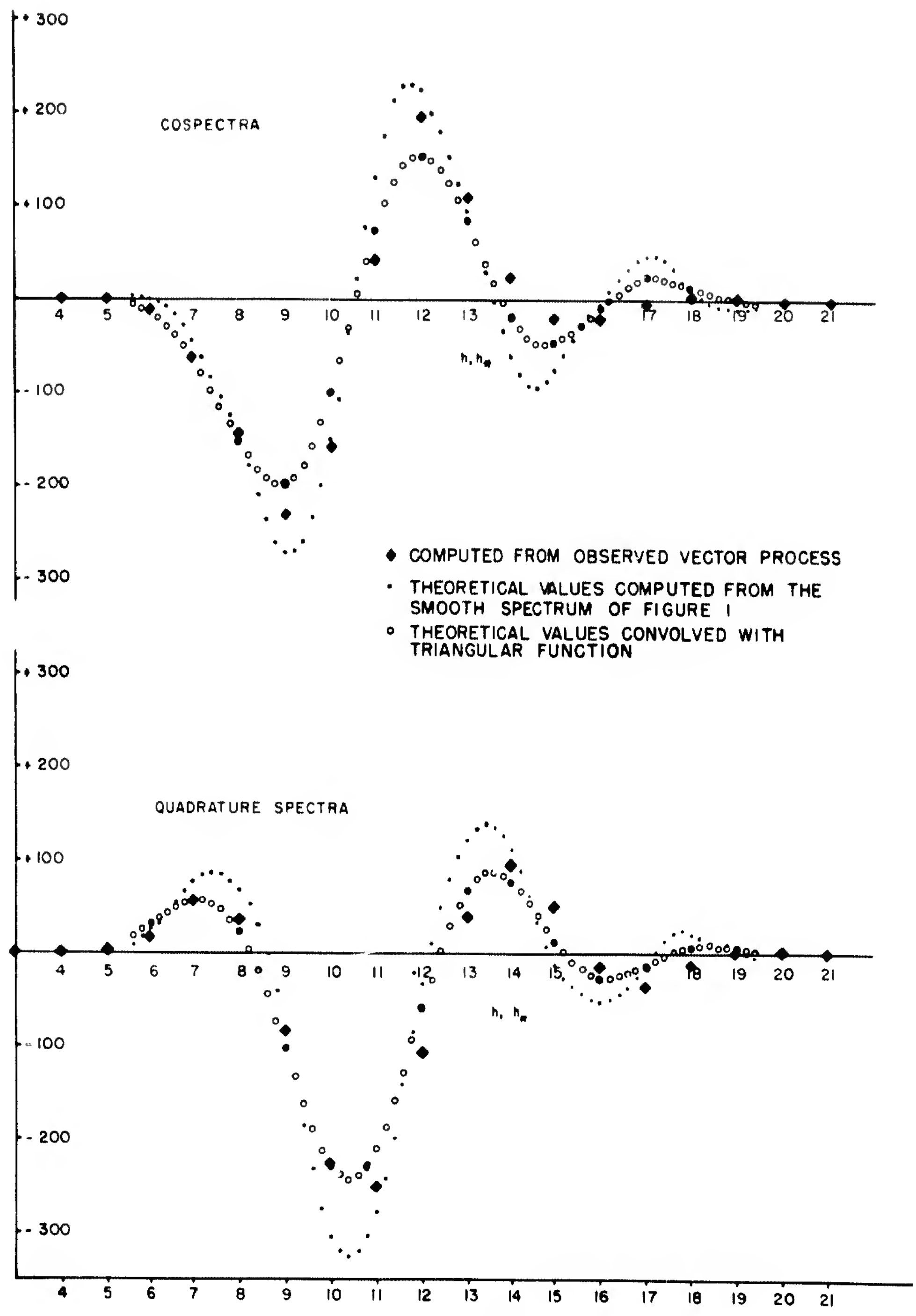

Fig. 2 - Cross spectra obtained by varous procedures

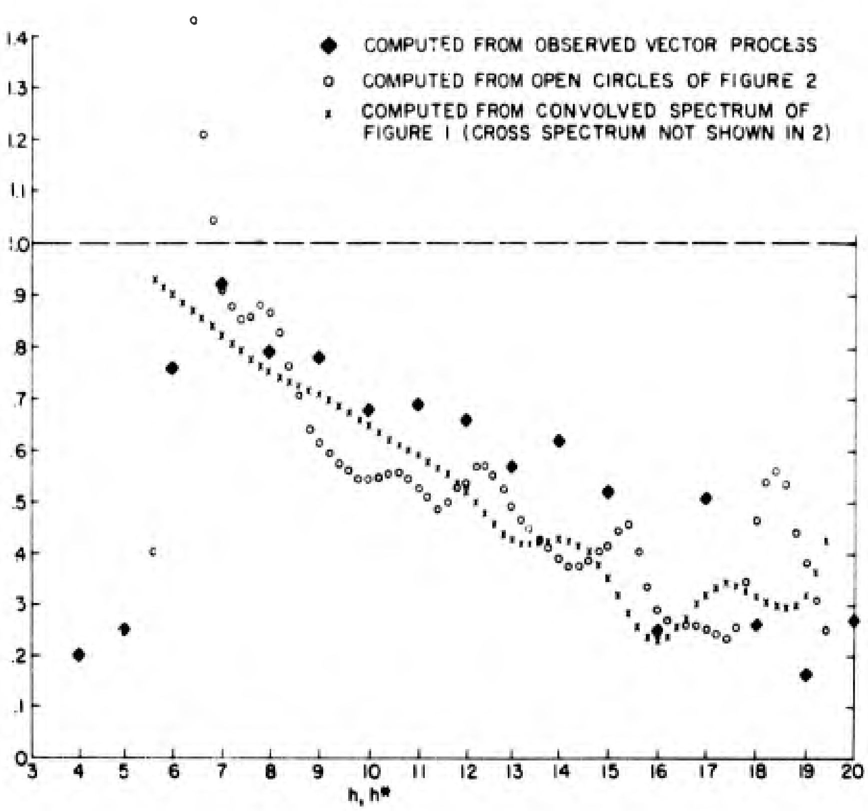

Fig. 3 - Coherencies obtained by various procedures

the cross spectra given in Eqs. (28) and (29) when substituted in the equation for the computation of coherency should yield one. The problem then is why are the computed coherencies so much lower than the theoretical coherencies?

To find out, the spectrum shown in Fig. 1 was smoothed and points were read from it at five times the spacing of the h values indicated on the horizontal scale of the figure. The smoothed higher resolution curve is shown by the dash-dot curve. Total variance was preserved with reference to the area under the smoothed curve. It was then possible to take Eqs. (28) and (29) and from them compute what the co-spectrum and the quadrature spectrum should have been. These values are shown by the small black dots in Fig. 2. By definition they would yield the coherency of one.

Now the window through which the co-spectra are viewed is roughly triangular in shape, and if, for example, it were peaked at the value $h = 9$ on one of these figures, it would fall approximately linearly to zero at the values $h = 7$ and $h = 11$. A linear combination of seventeen of the values given by the black dots thus represents the value given by a diamond. This operation is called a convolution and the results of a seventeen-point centered convolution with a linear growth to the middle value and a linear descent from the middle value is shown by the open circles in Fig. 2. More points are available than were available in the spectral estimates. The black circles are those points that correspond to the diamonds as far as the horizontal axis of the figure is concerned. This approximation to the spectral window yields values for the black dots that compare favorably with the values of the black diamonds that were obtained directly from the spectral computations. The results show that both the shapes of the cross spectra and the location of the zeros in the cross spectra are lost due to poor resolution. The rapid variation in the values indicated by the black dots when convolved with a broad triangular weighting function results in a decrease of the peaks of the estimates for the cross spectra and shifts the zeros to erroneous values. In Fig. 3 the coherencies as computed from the open circles are shown in order to compare them with the black diamonds. The loss of coherency caused by the shape of the window is confirmed.

The above computations were based on the assumption that the spectrum as smoothed in Fig. 1 was the true spectrum. It is in fact, an estimate of the true spectrum that also has been convolved with a window of roughly the same shape. The original spectrum cannot be recovered and hence the computations do not completely describe the full effect. An attempt was made to determine what the effect of the convolution is by convolving the true spectral estimate once more and then computing the coherencies that would be obtained by using this new spectrum and the spectra and cross spectra obtained from the open circles and the filled circles of Fig. 2. The result of the computation is shown by the crosses in Fig. 3. Some of the rapid variations in the circles have been removed but the same general trend is evident.

There are two ways to avoid the low coherencies that were obtained in this example. The first requires that a considerably longer record be obtained and that the resolution of the analysis be anywhere from five to ten times greater than that used in this example. The rule is, of course, that the convolution operator, which spreads over four frequency intervals, must operate on a portion of a curve that is slowly varying. The work of Dr. Yamanouchi is important in this connection. The computations illustrated by Pierson and Dalzell (1960) show that when the resolution is increased in such spectral and cross spectral estimates the peaks become much higher and the coherencies improve. A second procedure is to require that, for the same resolution, the estimates of the cross spectra be less rapidly varying. This can be achieved by a "false" time shift of one record with reference to the other. For example, the cross variance function obtained by computing all lag products of $\eta(x, t)$ and $\eta(x + L, \ t + \tau)$ for L fixed yields a function that has a maximum at a certain value of τ, say, τ_1. If the covariance function is then considered to be time shifted so that the value of τ_1 is zero, one achieves a very nearly even function about this new time origin. The co-spectrum and quadrature spectrum computed from this new time origin in general have the property that the co-spectrum is quite large and the quadrature spectrum is near zero. The coherency between these cross spectra and the original spectrum is then quite large. Pierson and Dalzell have illustrated these ideas by studying both higher resolution spectra analyzed in the same way and by studying time-shifted covariance estimates. Coherencies that fell from 0.9 to 0.5 over a range of six or seven ordinate values were raised by these techniques to from 0.8 to 0.9 by higher resolution and to values greater than 0.9 by a time shift.

The high coherencies that should actually occur in an adequately resolved properly designed analysis of a vector Gaussian process associated with a long crested random seaway are reflected finally in the papers of the symposium in which the motion of the ship was predicted from the forcing waves. Accurate transfer functions are needed to construct the time domain operators for such predictions. These so-called "predictions" are not strictly predictions in that they use data from the future to a certain extent in order to compute the motions of the ship. A true prediction would be one in which the forcing waves were known only up to a certain time, $t = t_0$ and the motions of the vessel in all degrees of freedom were known up to this same time. The problem would then be to predict the observed value of one of the motions at a time, say, 10 seconds into the future, based on just the amount of data available at $t = t_0$. It is evident that this true prediction problem can be solved more accurately for models in long crested waves. From a discussion in this section and from the results on short crested waves it should prove to be more difficult to predict the motions of an actual ship in actual waves 10 seconds into the future. Nevertheless, the ability to do this is still needed, and an adequate investigation of this problem needs to be made. The past history of the motions of the vessel and the past history of the waves as observed at some point near the vessel can be combined to provide a prediction of the motion of the vessel at some future time.

THE SOLUTION OF SPECIFIC PROBLEMS THAT ARE NOT LINEAR

From different assumptions, a large number of linear models to describe ships in waves have been developed. The more advanced models may even be nonlinear in the beam parameter and still linear in the forcing wave systems. Nevertheless, roll and certain extreme motions will eventually have to be treated by nonlinear equations.

A number of realistic problems have been formulated in wave theory and in ship motion theory that are not linear. These problems have been solved. The assumption of linearity by St. Denis and Pierson and by Pierson (1957) is no longer a restriction due to the lack of techniques for solving problems that are not linear.

An interesting example of a procedure that does not get too deeply involved in the intransigent aspects of the subject is the analysis of the forces due to waves on a vertical piling as given by Pierson (1963) and by Pierson and Holmes (1965).

Consider a pile in water with long crested waves passing it. The velocity field due to the waves in the water will exert a force on a small segment of the pile given by Eq. (31).

$$f(t) = k_1 U(t)|U(t)| + k_2 \dot{U}(t) . \tag{31}$$

Given the depth of the water, the spectrum of the waves, and the depth of the pile segment at which the force is measured, the spectra of $U(t)$ and $\dot{U}(t)$ can be found. Also the variance of $U(t)$ and $\dot{U}(t)$ can be found and designated as ψ_1 and ψ_2.

Then the joint probability density function U and $\dot{U}$ can be given by

$$P(U,\dot{U}) = \frac{1}{2\pi\sqrt{\psi_1\psi_2}} e^{-U^2/2\psi_1 - \dot{U}^2/2\psi_2} . \tag{32}$$

Given this equation, the probability density function for f can be derived. It is given by

$$P(f)dt = \frac{1}{2\pi\sqrt{\psi_1\psi_2}} \int_0^\infty e^{-\frac{\alpha}{2\psi_1}} \left(e^{-\left(\frac{k_1\alpha}{k_2} + \frac{f}{k_2}\right)^2 2\psi_2} + e^{-\left(\frac{k_1\alpha}{k_2} - \frac{f}{k_2}\right)^2 2\psi_2} \right) \frac{d\alpha}{2k_2\sqrt{\alpha}} \, df . \tag{33}$$

The time history of f is not given. The time history could be obtained by generating U and $\dot{U}$ as functions of time given the free surface $\eta(t)$ in a manner quite similar to that of some of the other papers in this symposium. The non-linear operation corresponding to $U(t)\,|U(t)|$ could then be carried out in the time domain and the time history of the force on the pile could be constructed. This has in fact been done by Reid (1958). In this analysis, however, the only thing desired is knowledge about the probability density structure of $f(t)$. This density structure can be obtained simply by reading off equally spaced values of this force and plotting the histogram of the values that are read.

This probability density function as given by Eq. (33) has been compared with values obtained directly from measurements of the forces on an actual pile. Though there appear to be a number of parameters involved in Eq. (33) there are really only two, the second moment and the fourth moment, since $P(f)$ is an even function.

When these two parameters are determined from the data consisting of a twenty-minute long record of the fluctuations in this force, and used to construct $P(f)$, the resulting probability density function agrees remarkably well with the observations. The probability density is not Gaussian; in fact, it predicts probabilities about ten times those of the normal distribution, three standard deviations from the origin.

It is also interesting to comment that the computation of the bi-spectrum of $f(t)$ would not have been particularly revealing because the bi-spectrum resolves the third moment of a distribution into frequency pairs. The third moment of this distribution is essentially zero.

Work described by Tick (1963) has shown that it is possible to take a linear Gaussian model for the long crested seaway and construct the model that would satisfy the equations of motion in the Eulerian frame of reference to second order. One result is that there is a correction to the frequency spectrum. A second result is that the profile of the waves changes as a function of time at a fixed point. The crests become higher and sharper and the troughs become shallower. The density function for the waves observed as a function of time at a fixed point will then have a certain amount of skewness that could be investigated in terms of bi-spectra.

Wind waves have been carefully measured by Kinsman (1960) and found to be non-Gaussian. His data have been used by Longuet-Higgins (1963) to verify a theory for the probability structure of the waves and this probability structure has been adequately represented by a modified Gram-Charlier series. The mathematical techniques of Longuet-Higgins would be applicable to the study of the nonlinear aspects of certain ship motions.

Another example of great interest to this symposium is the example provided in the comments of Dr. Yamanouchi. He has solved the very complicated problem of the nonlinear damping of the rolling motion of a ship in irregular waves in terms of a random process and second order nonlinear correction to the motions. Just as the work of Dalzell was cited by Dr. Ogilvie as establishing the principle of linear superposition assumed by St. Denis and Pierson, some investigator now needs to study the rolling motion of a ship in long crested beam seas in order to see if it is possible to verify the nonlinear probabilistic theory of roli damping propounded by Dr. Yamanouchi. It is quite likely that this nonlinear theory will verify quite well and that the spectra of the rolling motion as predicted by this theory will agree with the observations. Nonlinear roll in short crested waves requires very careful control of resolution, sampling variability, and coherency calculations in the analysis of the time series that would be recorded. Still missing is the probability structure of the rolling motion. Perhaps the techniques of Longuet-Higgins (1963) could be applied here to obtain it.

CONCLUDING REMARKS

The essential feature of the work of St. Denis and Pierson now appears to be that of expressing the short crested waves and the resulting ship motions in terms of a probabilistic description instead of in terms of a deterministic one. The assumption of linearity so convenient in order to obtain results on the probability structure of the resulting ship motions is no longer absolutely essential toward the further understanding of the motions of ships at sea. Insofar as the actual waves that force the ship satisfy nonlinear differential equations, it should be possible to model these waves with these essential non-linear features as accurately as desired by means of continued efforts along the path outlined by Tick in the work cited above. At the same time whenever it should turn out that the differential equations that describe a particular phenomenon are nonlinear, a perturbation technique such as the one described by Dr. Yamanouchi should make it possible to obtain the spectra of these motions and certain of the statistical properties of these motions. Even at times the probability density functions that provide considerable information about the phenomenon can be obtained by analogy to the results on the forces of waves on a pile. The strength of the techniques that have been developed quite obviously then lies in the assumption of randomness and the use of the very powerful tool of probability for the derivation of results and the very powerful tool of statistics in the analysis and interpretation of observations.

ACKNOWLEDGMENTS

The work by the writer described in these comments was supported at various times by the Office of Naval Research, Geophysics Branch, by the David Taylor Model Basin, and by the U.S. Naval Civil Engineering Laboratory.

REFERENCES

Canham, H. J. S., D. E. Cartwright, G. J. Goodrich, and N. Hogben (1962): Seakeeping trials on OWS "Weather Reporter." Trans. Roy. Institution of Naval Architects, London, v. 104, pp. 447-492.

Cartwright, D. E., and N. D. Smith (1964): Buoy Techniques for Obtaining Directional Wave Spectra. Trans. Buoy Technology Symposium, Marine Technology Soc., Washington, D.C.

Fuchs, P. A., and R. C. MacCamy (1953): A linear theory of ship motion in irregular waves. Tech. Rept., Series 61, Issue 2, Inst. of Engineering, Univ. of California, July 1963.

Kinsman, B. (1960): Surface waves at short fetches and low wind speeds - a field study. Tech. Rept. XIX, vols. 1, 2, and 3, ref. 60-1, Chesapeake Bay Institute, The Johns Hopkins Univ.

Longuet-Higgins, M. S. (1963): The effect of non-linearities on statistical distributions in the theory of sea waves. J. Fluid Mech., v. 17, Part 3.

Longuet-Higgins, M. S., D. E. Cartwright, and N. D. Smith (1963): Observations of the directional spectrum of sea waves using the motions of a floating buoy. Ocean Wave Spectra, Prentice-Hall, Inc.

O'Brien, J. T., and B. Muga (1965): Sea test of a spread moored landing craft. (To appear in the Proc. of the 9th Conference on Coastal Engineering, approx. Feb. 1965.)

Pierson, W. J. (1957): On the phases of the motions of ships in confused seas. Tech. Rept. No. 9, contr. Nonr 285(17), New York University, College of Engineering, Research Div.

Pierson, W. J. (1963): Methods for the time series analysis of water wave effects on piles. U.S. Naval Civil Engineering Lab., Pt. Hueneme, Cal.

Pierson, W. J., and J. F. Dalzell (1960): The apparent loss of coherency in vector Gaussian processes due to computational procedures with application to ship motions and random seas. Tech. Rept. contr. Nonr 285(17), New York University, College of Engineering, Research Division.

Pierson, W. J., and P. Holmes (1965): The force on a pile due to irregular waves. (Submitted for publication to ASCE, Journal Waterways and Harbor Division.)

Reid, R. O. (1958): Correlation of water level variations with wave forces on a vertical pile for non-periodic waves. Proc. Sixth Conf. on Coastal Engineering, Gainesville, Florida (1957).

St. Denis, M., and W. J. Pierson (1953): On the motions of ships in confused seas. Trans. Soc. of Naval Architects and Marine Engineers, v. 61, pp. 280-357.

Tick, L. T. (1958): Certain probabilities associated with bow submergence and ship slamming in irregular seas. JSR SNAME, v. 2, no. 1, June (p. 30).

Tick, L. J. (1959): A nonlinear random model of gravity waves. J. Math. and Mech., VIII, 643-652.

Tick, L. J. (1963): Nonlinear probability models of ocean waves. Ocean Wave Spectra, Prentice-Hall, Inc.

* * *

SOME REMARKS ON THE STATISTICAL ESTIMATION OF RESPONSE FUNCTIONS OF A SHIP

Yasufumi Yamanouchi
Ship Research Institute
Tokyo, Japan

INTRODUCTION

In connection with the papers by Dr. Ogilvie, Prof. Lewis, Mr. Smith and Dr. Cummins, Drs. Breslin, Savitsky and Tsakonas, I would like to make several comments on three problems concerning the statistical estimation of the response functions of ship. The first problem concerns the statistical considerations that occur in estimating the frequency response function, which no paper has referred to in this symposium and which still has several difficulties to be solved. The second problem is about the impulse response of ship motion which has been one of the main topics in this symposium. The third problem is about the effect of nonlinearity on the response of motion, on the computation of spectrum, and on the estimation of the frequency response itself.

1. A PROCESSING SCHEME FOR THE ESTIMATION OF FREQUENCY RESPONSE FUNCTIONS

Beginning with the work of Blackman and Tukey [1], many contributions have been made to the problem of the estimation of the statistical characteristics of time series. Most of them, however, treat mainly the estimation of the spectrum, and very few have been concerned with the frequency response itself. For the sake of establishing a standard procedure for obtaining the frequency response, our group did some work [2] that followed the results of Dr. Akaike and myself [3].

Skipping over the items that are already commonly clear in text books, several items closely related to the selection of parameters in the estimation of the frequency response function will be mentioned and examples for the case of ship oscillations will be given.

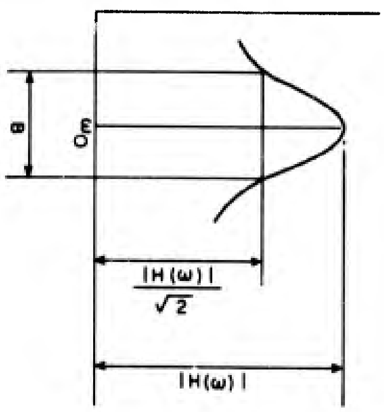

Figure 1

Choice of m

If m is the maximum number of lags in the correlation function used for the computation of the estimates, then m should be chosen so as to satisfy

$$m\Delta t \geq 2\pi/B ,$$

where B is the bandwidth of the peak of $|H(\omega)|$ of main concern as defined by Fig. 1.

An excessively large m implies an increase of sample variance, and an excessively small m implies that bias occurs and usually gives an underestimate of $|H(\omega)|$. Also, the amount of shift, mentioned later, should be taken into account in choosing m.

For the case of ship rolling where

$$\ddot{\phi} + 2\kappa\omega\dot{\phi} + \omega_o^2\phi = \omega_o^2\phi_w ,$$

under the condition where $\kappa \ll 1$, the bandwidth of the peak of $|H(\omega)|$ is calculated as $B \cong 2\kappa\omega_o$.

The Effect of Windows

Before starting to discuss the choice of the amount of shift, the effect of various windows is examined approximately.

Assume that the output $y(t)$ and input $x(t)$, as well as the noise $n(t)$ that contaminates the output $y(t)$, have the Fourier transform. Then

$$Y\left(\frac{2\pi}{2T}\mu\right) = H\left(\frac{2\pi}{2T}\mu\right) \times X\left(\frac{2\pi}{2T}\mu\right) + N\left(\frac{2\pi}{2T}\mu\right).$$

Accordingly, the estimate of $H(\omega)$ at $\omega = (2\pi/2T)\mu$ evaluated from the cross spectrum is

$$\hat{H}\left(\frac{2\pi}{2T}\mu\right) = \frac{\sum_\nu W_\nu Y_{\mu-\nu} \cdot \bar{X}_{\mu-\nu}}{\sum_\nu W_\nu X_{\mu-\nu} \cdot \bar{X}_{\mu-\nu}}$$

$$= \frac{\sum_\nu W_\nu H\left\{\frac{2\pi}{2T}(\mu-\nu)\right\} X_{\mu-\nu} \cdot \bar{X}_{\mu-\nu}}{\sum_\nu W_\nu X_{\mu-\nu} \cdot \bar{X}_{\mu-\nu}} + \frac{\sum_\nu W_\nu H_{\mu-\nu} \cdot \bar{X}_{\mu-\nu}}{\sum_\nu W_\nu X_{\mu-\nu} \cdot \bar{X}_{\mu-\nu}},$$

where W_ν are the weight factors that describe various windows. The noise and the input can be considered as mutually uncorrelated. Therefore

$$E\left[H\left(\frac{2\pi}{2T}\mu\right)\right] \doteq E\,\frac{\sum_\nu W_\nu H\left\{\frac{2\pi}{2T}(\mu-\nu)\right\} \cdot X_{\mu-\nu} \cdot \bar{X}_{\mu-\nu}}{\sum_\nu W_\nu X_{\mu-\nu} \cdot \bar{X}_{\mu-\nu}}$$

$$\doteq \frac{E\left[\sum_\nu W_\nu H\left\{\frac{2\pi}{2T}(\mu-\nu)\right\} |X_{\mu-\nu}|^2\right]}{\frac{1}{2T} S_{xx}\left(\frac{2\pi}{2T}\mu\right)}$$

$$\doteq \frac{\sum_\nu W_\nu H\left\{\frac{2\pi}{2T}(\mu-\nu)\right\} \cdot S_{xx}\left(\frac{2\pi}{2T}\mu\right)}{S_{xx}\left(\frac{2\pi}{2T}\mu\right)}.$$

Here the variation of $S_{xx}(\omega)$ around $\omega = (2\pi/2T)\mu$ is assumed to be smaller than that of $H(\omega)$. Accordingly

$$E\left[H\left(\frac{2\pi}{2T}\mu\right)\right] \doteq \sum_\nu W_\nu H\left\{\frac{2\pi}{2T}(\mu-\nu)\right\}.$$

Now let us consider the case where $H(\omega)$ in the form $|H(\omega)|e^{j\sigma(\omega)}$ has the local approximation

$$H\left\{\frac{2\pi}{2T}(\mu-\nu)\right\} = H\left(\frac{2\pi}{2T}\mu\right)\left\{1 + \alpha\left(\frac{2\pi}{2T}\nu\right) + \beta\left(\frac{2\pi}{2T}\nu\right)^2\right\} e^{j\frac{2\pi}{2T}\nu k_\mu},$$

where $k_\mu = -d\sigma(\omega)/d\omega$ as in Fig. 2. We have assumed that $|H(\omega)|$ varies locally as a 2nd order curve, and that the phase $\sigma(\omega)$ increases linearly with frequency. Then,

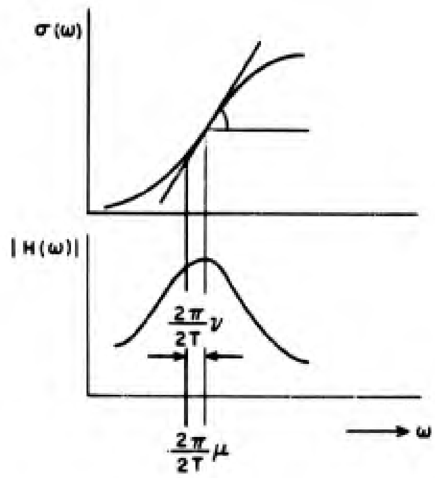

Figure 2

$$\sum_{\nu} W_\nu H\left\{\frac{2\pi}{2T}(\mu-\nu)\right\} = H\left(\frac{2\pi}{2T}\mu\right)\left\{\sum_{\nu} W_\nu\, e^{j\frac{2\pi}{2T}\nu k_\mu} + \alpha \sum_{\nu} W_\nu \left(\frac{2\pi}{2T}\nu\right) e^{j\frac{2\pi}{2T}\nu k_\mu} + \beta \sum_{\nu} W_\nu \left(\frac{2\pi}{2T}\nu\right)^2 e^{j\frac{2\pi}{2T}\nu k_\mu}\right\}$$

$$= H\left(\frac{2\pi}{2T}\mu\right)\left\{w(k_\mu) + \frac{\alpha}{2\pi j}\dot{w}(k_\mu) + \frac{\beta}{(2\pi j)^2}\ddot{w}(k_\mu)\right\},$$

where

$$\dot{w}(k_\mu) = \frac{d}{d\tau} w(\tau)\Big|_{\tau=k_\mu}$$

$$\ddot{w}(k_\mu) = \frac{d^2}{d\tau^2} w(\tau)\Big|_{\tau=k_\mu}.$$

This shows, through the averaging effects of the weights, W_ν, that the estimated frequency response is much affected by the variation of phase angle $d\sigma(\omega)/d\omega$ around that particular frequency. This fact was entirely disregarded in the paper by Goodman [4], which treated the confidence limit of the frequency response. For example, if the k_μ has values that are shown in Fig. 3, even if $\alpha \doteqdot 0$, and $\beta = 0$

$$E\left[H\left(\frac{2\pi}{2T}\mu\right)\right] \to \sum_{\nu} W_\nu H\left\{\frac{2\pi}{2T}(\mu-\nu)\right\} \to H\left(\frac{2\pi}{2T}\mu\right) w(\tau),$$

and $w(k_\mu)$ is much less than 1. As the result, the estimated frequency response becomes much less than the true value. This has been the reason for the low coherencies obtained in some experiments as already pointed out by Mr. Dalzell and me [5]. As an extreme case, when $k_\mu > T_m$,

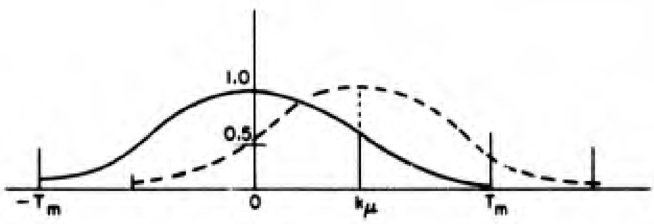

Figure 3

$$\sum_{\nu} W_{\nu} H \left\{ \frac{2\pi}{2T} (\mu - \nu) \right\} \doteq 0 .$$

This window also causes bias in phase estimation. Generally, however, β is much larger than α, when $|H(\omega)|$ has a peak, and then $d\sigma(\omega)/d\omega$ usually has a large value. Accordingly the effect of $(\alpha/2\pi)\dot{w}(k_\mu)$ is rather small compared to that of $w(k_\mu)$ and $[\beta/(2\pi)^2]\ddot{w}(k_\mu)$. This shows that the effect of a window on the phase shift, $\sigma(\omega)$, is rather small compared to the effect on the amplitude gain, $|H(\omega)|$.

If we shift the data window by K_μ and bring the origin of the window to k_μ, then $w(\tau) = 0$ and $\dot{w}(\tau) = 0$. Moreover if we can choose the shape of the window so as to have $\ddot{w}(\tau) = 0$, then, as the result, the bias due to phase shift can be eliminated completely.

As the natural results of the above-mentioned considerations, the following results are obtained. In these results $s\Delta t$ is the amount of shift of the data window for the computation of the sample cross spectra.

Choice of $s\Delta t$

To compensate for the bias due to the phase shift, $s\Delta t$ should be chosen so that we have

$$\left| s\Delta t - \left\{ -\frac{d(\omega)}{d\omega} \right\} \right| \leq \begin{Bmatrix} 0.15\ m\Delta t \\ 0.30\ m\Delta t \\ 0.40\ m\Delta t \end{Bmatrix} \quad \text{for} \quad \begin{matrix} W_1 \\ W_2 \\ W_3 , \end{matrix}$$

namely if

$$\left| -\frac{d\sigma(\omega)}{d\omega} \right| \leq \begin{Bmatrix} 0.15\ m\Delta t \\ 0.30\ m\Delta t \\ 0.40\ m\Delta t \end{Bmatrix} \quad \text{for} \quad \begin{matrix} W_1 \\ W_2 \\ W_3 , \end{matrix}$$

we do not need to shift the data window or the output. W_1, W_2 and W_3 are the windows which are explained later. Otherwise, $|H(\omega)|$ will be underestimated by more than 5%. $s\Delta t$ should also be chosen so as to satisfy

$$|s\Delta t| \leq 0.05\, N\Delta t\ .$$

Otherwise, adopt $y(t + s\Delta t)$ as $y(t)$. This is the clear solution for the elimination of the effect of windows on frequency response function.

For example for roll, expressed by the equation of motion,

$$\ddot{\phi} + 2\kappa\omega_o\dot{\phi} + \omega_o^2\phi = \omega_o^2\gamma(\omega)\frac{\omega^2}{g}\zeta(\omega)\, e^{j\frac{\pi}{2}},$$

where

$\gamma(\omega)$ is the effective wave slope coefficient and

$\frac{\omega^2}{g}\zeta(\omega)\, e^{j\frac{\pi}{2}}$ is the wave slope expressed by the wave height $\zeta(\omega)$ measured at the C.G. of the ship.

The amount of time shift is computed as follows:

$$|H(\omega)|^2 = \frac{\omega_o^4(\gamma\omega^2/g)^2}{(\omega^2 - \omega_o^2) + (2\kappa\omega_o\omega)^2}$$

$$\sigma(\omega) = \tan^{-1}\left(\frac{-2\kappa\omega_o\omega}{\omega_o^2 - \omega^2}\right) + \frac{\pi}{2}$$

$$\frac{d\sigma(\omega)}{d\omega} = \frac{d}{d\omega}\left[\tan^{-1}\left(\frac{-2\kappa\omega_o\omega}{\omega_o^2 - \omega^2}\right)\right] = \frac{-2\kappa\omega_o(\omega_o^2 + \omega^2)}{(\omega_o^2 - \omega^2)^2 + (2\kappa\omega_o\omega)^2}\ ;$$

therefore

$$\left.\frac{d\sigma(\omega)}{d\omega}\right|_{\omega=\omega_o} = -\frac{1}{\kappa\omega_o}\ .$$

Namely if we want a good estimate (with small bias) of $H(\omega)$, the amount of shift $s\Delta t$ is

$$s\Delta t = \frac{1}{\kappa\omega_o}\ .$$

This shows that the output of roll $y(t + s\Delta t)$ should be taken as $y(t)$. When the wave height $\zeta(\omega)$ is measured at the distance, D, as is shown in Fig. 4, the phase difference between

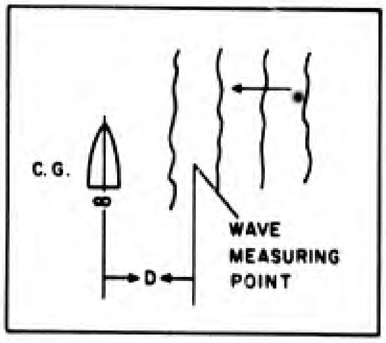

Figure 4

the measured wave height and the wave slope at the C.G. of ship is $\pi/2 - (\omega^2/g)D$, and this gives

$$\sigma(\omega) = \tan^{-1}\left(\frac{-2\kappa\omega_o\omega}{\omega_o^2 - \omega^2}\right) + \frac{\pi}{2} - \frac{\omega^2}{g} D ,$$

and therefore,

$$s\Delta t = -\left.\frac{d\sigma(\omega)}{d\omega}\right|_{\omega=\omega_o} = \frac{1}{\kappa\omega_o} + \frac{2\omega_o}{g} D .$$

When the character of the frequency response, $H(\omega)$, is known before we start the computation, the above-mentioned value can be estimated. This is, however, not the case usually. At that time, as is shown in Fig. 5, T_p can be taken as a good estimate of $s\Delta t$. This value can be decided after computing the cross covariance function. Namely, in the case where the input is considered to be fairly white in the range of our concern, we can obtain a fairly good overall estimate of $H(\omega)$ by shifting the center of the lag window or the origin of the time axis of the cross covariance function to that time point T_p where the maximum of the absolute value of the sample cross covariance function occurs. Pierson and Dalzell [6] showed very interesting analyses for two cases, one for wave measurements where the apparent low coherency between two wave measurements was improved and another in which the coherency between the waves and the ship response was improved. I have also described [7] the intuitive and practical method to find the amount of shift. The above-mentioned theory shows more generally the way to find the proper amount of shift. A large bias because of the large phase shift which usually occurs at the peak of the amplitude gain, induced by the use of windows, is prevented in this way.

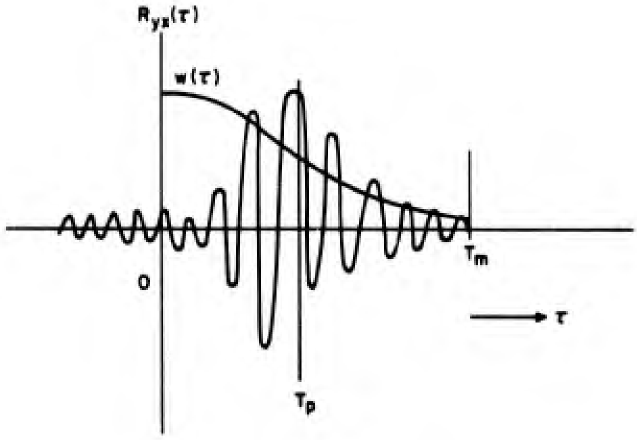

Figure 5

w, W_ν: Windows

Several papers have been written on the design of windows so as to provide spectral estimates with various properties. Hamming and the hanning windows are the most popular ones commonly used. Just a few comments will be made here on this subject.

Putting X as the Fourier transform of $x(t)$ $(-T < t < T)$, the smoothing effect of the windows of the trigonometric sum type is expressed as follows (see Fig. 6):

$$\sum_\nu 2T|X_{\mu-\nu}|^2 W_\nu = \frac{1}{2\pi}\int_{-T}^{T} e^{-2\pi j\frac{\mu}{2T}\tau}\left(\sum_\nu e^{2\pi j\frac{\mu}{2T}} W_\nu\right)\hat{\hat{R}}^*_{xx}(\tau)\, d\tau$$

$$= \frac{1}{2\pi}\int_{-T}^{T} e^{-2\pi j\frac{\mu}{2T}\tau} w(\tau)\,\hat{\hat{R}}^*_{xx}(\tau)\, d\tau\,,$$

$$w(\tau) = \sum_{n=-k}^{k} a_n e^{2\pi j\frac{n}{2T_m}\tau} \qquad |\tau| < T_m$$

$$= \frac{1}{2}\sum_{n=-k}^{k} a_n e^{2\pi j\frac{n}{2T_m}\tau} \qquad \tau = \pm T_m$$

$$= 0 \qquad |\tau| > T_m\,.$$

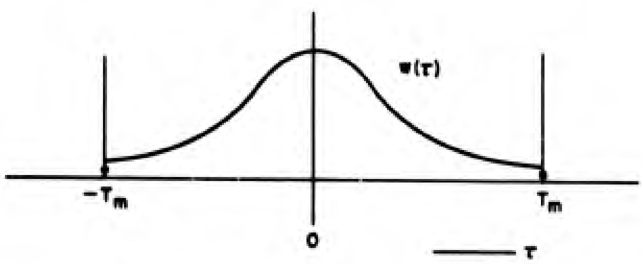

Figure 6

Many windows have been designed [8], and have been checked [3] for the case of simple oscillations like linear rolling in waves. The following windows, W_1, W_2, W_3; which have been designed, are the optimum as the 1st, 2nd and the 4th order type and are free from biases up to the 1st, 2nd and the 4th order respectively.

	W_1	W_2	W_3	θ	Hamming	Hanning
a_0	0.5132	0.6398	0.7029	0.64	0.54	0.50
a_1	0.2434	0.2401	0.2228	0.24	0.23	0.25
a_2		-0.0600	-0.0891	-0.06		
a_3			0.0149			

As an example, these windows can be applied to the estimation of the frequency response of a simple oscillation such as linear rolling.

$$H(\omega) = \frac{\omega_o^2}{(\omega_o^2 - \omega^2) + 2j\kappa\omega_o\omega} .$$

W_1, W_2, W_3 have been checked to be adequate for use if

$$\rho = \frac{\pi}{\kappa\omega_o} \frac{1}{m\Delta t}$$

is kept less than 1. (Usually this is satisfied if $m\Delta t \geq 2\pi/B$, where

$$B = 2\kappa\omega_o , \qquad \rho = \frac{\pi}{\kappa\omega_o} \frac{1}{m\Delta t} \leq \frac{\pi}{\kappa\omega_o} \frac{B}{2\pi} = 1) .$$

The window Q, which is a modification of W_2, is generally recommended for the estimation of the power spectra, cross spectra and of the frequency response function of a linear time-invariant system.

If the very careful estimation is necessary, the following is recommended. Apply the windows W_1, W_2 and W_3 successively, and if there is a significant difference, say, of order greater than 10% between the results, it is advisable to repeat the whole computing process using $2m$ in place of m, and, at the same time, use a correspondingly increased N, if necessary. W_3 tends to produce the deepest troughs and highest peaks, W_2 the next deepest and highest, and W_1 the shallowest.

$R(\omega)$: RELATIVE ERROR OF $H(\omega)$; CONFIDENCE BAND

The relative error of the estimation of $H(\omega)$, obtained by the procedure mentioned above was evaluated relative to the estimated value of coherency. The results are as follows: Assuming that

$$Y(\omega) = X(\omega)\, H(\omega) + N(\omega)$$

$$S_{yy}(\omega) = S_{xx} |H(\omega)|^2 + S_{nn}(\omega) ,$$

$$\text{Coherency } \gamma^2(\omega) = \frac{|H(\omega)|^2 S_{xx}(\omega)}{S_{yy}(\omega)} \to 1 - \frac{S_{nn}(\omega)}{S_{yy}(\omega)} .$$

Then

$$R(\omega) = \sqrt{\frac{1}{n-1}\left(\frac{1}{\hat{\gamma}^2(\omega)} - 1\right) F[\delta, 2, 2(n-1)]}$$

where n is the integer nearest to

$$\left(\frac{N}{m}\right) \Big/ 2 \sum_{n=-k}^{K} a_n^2 ;$$

also $F[\delta, 2, 2(n-1)]$ is defined as

$$\text{Prob.} \left\{F^2_{2(n-1)} \leq F[\delta, 2, 2(n-1)]\right\} = \delta .$$

At $\omega = 0$, and $2\pi/2\Delta t$, $F[\delta, 2, 2(n-1)]$ should be replaced by $F[\delta, 1, (n-1)]$. Accordingly, the confidence band is drawn as

$$\text{Prob.} \left\{|\hat{H}(\omega) - H(\omega)| \leq R(\omega) \, |\hat{H}(\omega)|\right.$$

and

$$\left.|\text{Arg}\left[\hat{H}(\omega)\right] - \sigma(\omega)| \leq \sin^{-1} R(\omega)\right\} \geq \delta.$$

$R(\omega)$ should be put equal to 1.00 to indicate the relative error greater than 100%, when the value inside the square root of the definition of $R(\omega)$ is greater than 1 or less than 0. The value $\delta = 0.95$ is used usually in our group. When $R(\omega)$ had the value, 1.00, the estimate of $\sigma(\omega)$ often showed sudden change of magnitude $\pm\pi$, which shows unreliability of the results.

The following approximation formula for F-values can be conveniently used for computer application:

$$F(2, n, 0.95) = 3.00 + \frac{10.00}{n - 1.40}$$

$$F(1, n, 0.95) = 3.84 + \frac{10.00}{n - 1.40} .$$

Figures 7 through 14 are the examples of the results obtained by this procedure. The cross correlograms of wave-roll and wave-heave in Figs. 7 and 8 are the ones where the origin was shifted by $9\Delta t$ and $7\Delta t$ respectively. Correlations were computed to very large lag number ± 200, however, m, the largest lag number was taken as 90 in the analysis. All windows W_1, W_2 and W_3 were applied to the calculation of the spectra; however, the results came out so close that it is difficult to show on one sheet. Accordingly, in Figs. 7 through 13, only

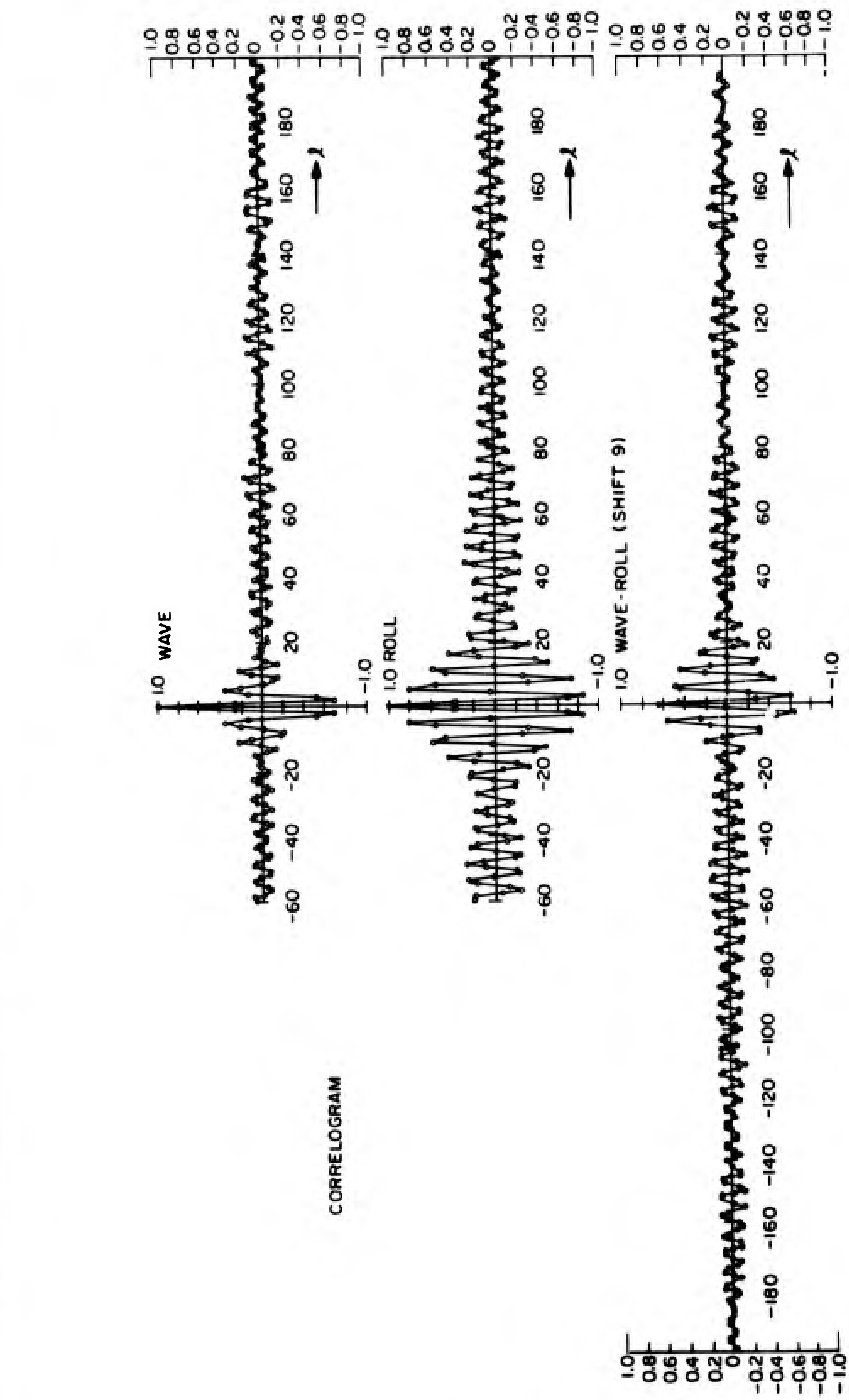

Figure 7

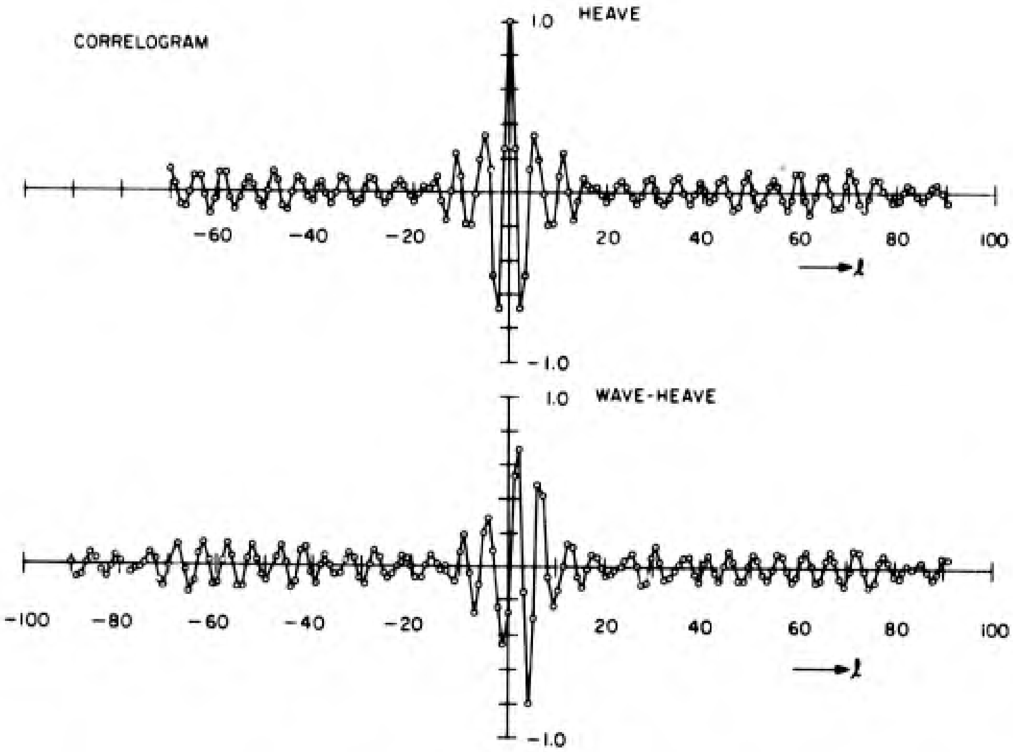

Figure 8

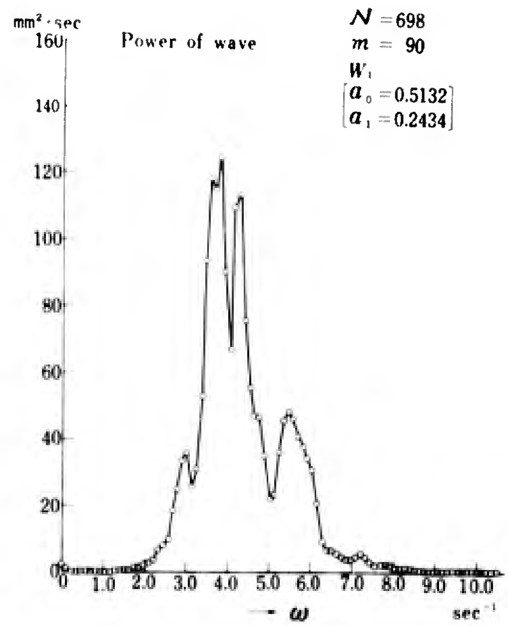

Figure 9

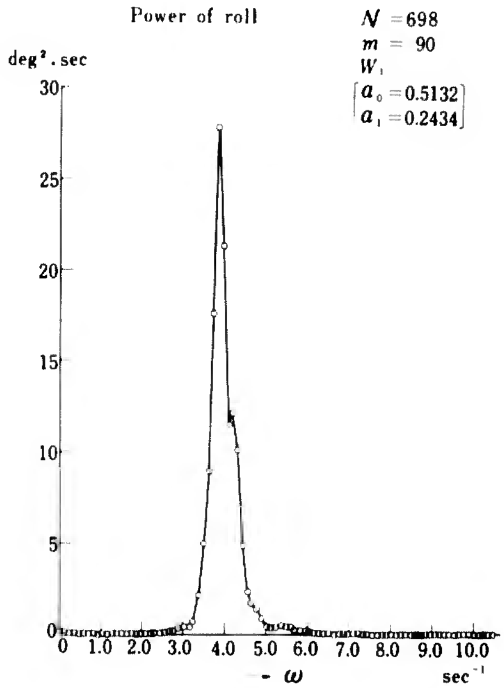

Figure 10

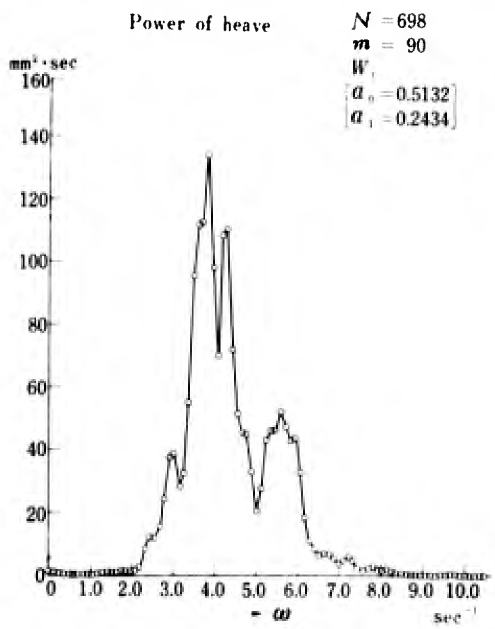

Figure 11

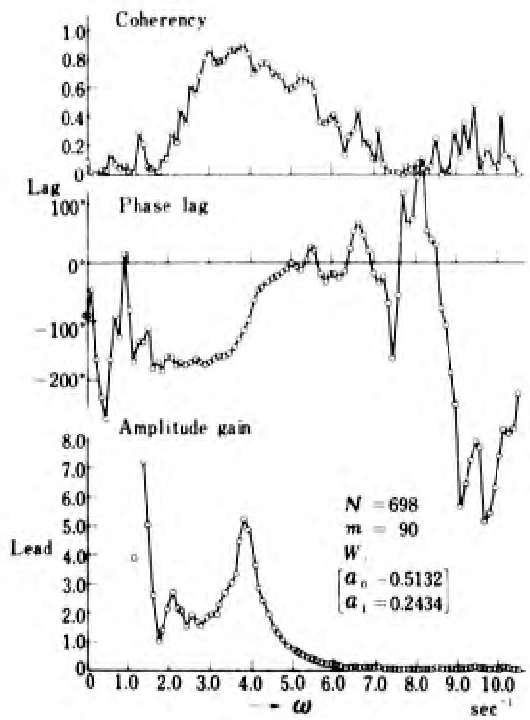

Figure 12

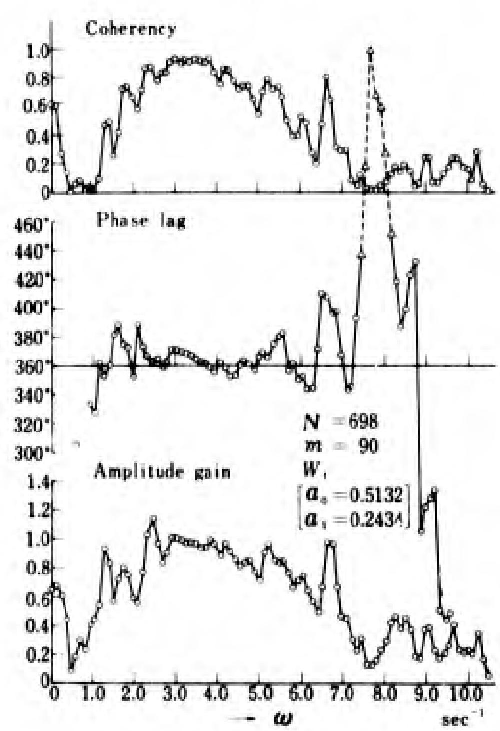

Figure 13

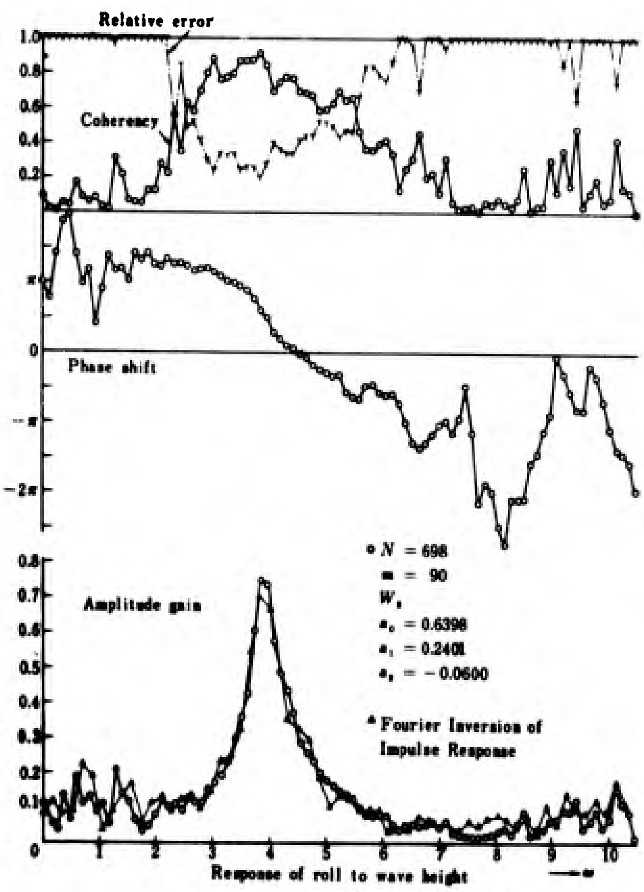

Figure 14

the results obtained by using W_1 are shown here as examples. The amplitude gain in roll was calculated as the ratio of the roll angle to the wave slope in Fig. 12, from the original results of gain of roll angle to wave height as is shown in Fig. 14, where the result obtained by using W_2 is shown as an example. The relative error is shown in Fig. 14.

2. ON THE EVALUATION OF THE IMPULSE RESPONSE FUNCTION

The impulse response function is one of the forms by which the character of the response of a linear system is expressed completely. This has long been used very conveniently in many engineering fields. However, it has been rather unfamiliar to naval architects. Fuchs and MacCammy [9] wrote a paper in 1953 and made it clear that the time history of the heave and pitch can be synthesized by the convolution of impulse response and the time history of the waves. They computed the impulse response function theoretically for a cylinder, and as the Fourier inversion of the frequency response function obtained from tank experiments for a ship form. The present author [10] has already called attention to this function and has also made clear the way to get the impulse function from a free damping test.

Mr. Smith and Dr. Cummins insisted in their paper that the step compulsory input is not applicable to get the impulse response function, because the step function includes components of very wide range of frequency, theoretically from zero to infinitive, and this incurs the noise which comes from the resonance of model itself, guide, restraining frame or others to high frequency component of input. However, if we are careful on a few points, this author believes, we can obtain the impulse response even from the inclining test, especially if the response has very low natural frequency as that of rolling. This author obtained successfully the very complicated frequency response function of a ship with Flume type anti-rolling tank as the Fourier inversion of the impulse response obtained by free damping test. The results show that this method is a useful way to guess the frequency response just by a simple free oscillation test. The impulse response function is also useful in this example, and here some topics related to the statistical estimation of the impulse response will be described.

When the system is linear and time invariant,

$$y(t) = \int_{-\infty}^{\infty} h(\tau)\, x(t-\tau)\, d\tau = \int_{-\infty}^{\infty} h(t-\tau)\, x(\tau)\, d\tau = h(t) * x(t)$$

where * represents the convolution operation. The impulse response function $h(\tau)$ and the frequency response function $H(\omega)$ are related to each other by Fourier transformation as

$$H(\omega) = \int_{-\infty}^{\infty} h(\tau)\, e^{-j\omega\tau} d\tau\,, \qquad h(\tau) = \frac{1}{2\pi}\int_{-\infty}^{\infty} H(\omega)\, e^{j\omega\tau} d\omega\,.$$

The Fourier transforms of output and input are connected by the frequency response $H(\omega)$ as

$$Y(\omega) = H(\omega) \cdot X(\omega)\,.$$

Through manipulation, we will get

$$R_{yy}(\tau) = \int_{-\infty}^{\infty}\int_{-\infty}^{\infty} h(\mu)\, h(\nu)\, R_{xx}(\tau - \mu + \nu)\, d\nu\, d\mu$$

$$= h(\tau) * \overline{h(\tau)} * R_{xx}(\tau)\,.$$

This corresponds to the relation in frequency domain

$$S_{yy}(\omega) = H(\omega)\, \overline{H(\omega)}\, S_{xx}(\omega) = |H(\omega)|^2\, S_{xx}(\omega)\,.$$

In the same way

$$R_{yx}(\tau) = \int_{-\infty}^{\infty} h(\mu)\, R_{xx}(\tau-\mu)\, d\mu = \int_{-\infty}^{\infty} h(\tau-\mu)\, R_{xx}(\mu)\, d\mu$$

$$= h(\tau) * R_{xx}(\tau) .$$

This corresponds to

$$S_{yx}(\omega) = H(\omega) \cdot S_{xx}(\omega) .$$

Namely $R_{yx}(\tau)$ is connected with $R_{xx}(\tau)$ by the impulse response function $h(\tau)$ just as $y(t)$ with $x(t)$. As is very clear, the relation between $R_{yx}(\tau)$ and $R_{xx}(\tau)$ is much stabler from the statistical point of view than that between $y(t)$ and $x(t)$.

When the computation is carried out digitally from the sample of data taken at interval Δt,

$$R_{yx}(\tau) = \sum_{\mu} h(\mu)\, R_{xx}(\tau - t)\, \Delta t .$$

Putting Δt as 1 for the purpose of simplification

$$R_{yx}(\tau) = \sum_{\mu} h(\mu)\, R_{xx}(\tau-\mu) .$$

The impulse response can be obtained discretely as the form of a weight function, for example as $h_{-n}, h_{-n+1}, \ldots h_o, \ldots h_{n-1}, h_n$, by solving the simultaneous equations

$$\begin{bmatrix} R_{yx}(-n) \\ R_{yx}(-n+1) \\ \vdots \\ R_{yx}(0) \\ \vdots \\ R_{yx}(n-1) \\ R_{yx}(n) \end{bmatrix} \begin{bmatrix} R_{xx}(0) & R_{xx}(1) & \ldots R_{xx}(n) & \ldots R_{xx}(2n) \\ R_{xx}(1) & R_{xx}(0) & \ldots R_{xx}(n-1) & \ldots R_{xx}(2n-1) \\ \vdots & \vdots & \vdots & \vdots \\ R_{xx}(n) & R_{xx}(n-1) & \ldots R_{xx}(0) & \ldots R_{xx}(n) \\ \vdots & \vdots & \vdots & \vdots \\ R_{xx}(2n-1) & R_{xx}(2n-2) & \ldots R_{xx}(n-1) & \ldots R_{xx}(1) \\ R_{xx}(2n) & R_{xx}(2n-1) & \ldots R_{xx}(n) & \ldots R_{xx}(0) \end{bmatrix} \begin{bmatrix} h_{-n} \\ h_{-n+1} \\ \vdots \\ h_o \\ \vdots \\ h_{n-1} \\ h_n \end{bmatrix} .$$

Figure 15 shows the impulse response function obtained by solving a 59th order simultaneous equations from R_{yx} at $\tau = -29 \sim +29$ and R_{xx} at $\tau = 0 \sim 58$ of roll and wave height correlation, shown in Fig. 7. In the same figure, the impulse response function, calculated as the Fourier inversion of $H(\omega)$ that was obtained through the spectrum analysis as in Fig. 14, is drawn. The latter was calculated as $h_{-90} \sim h_{90}$, and the figure shows the main part of it. The two weight functions are not necessarily the same. To our surprise, however, inversely, the frequency

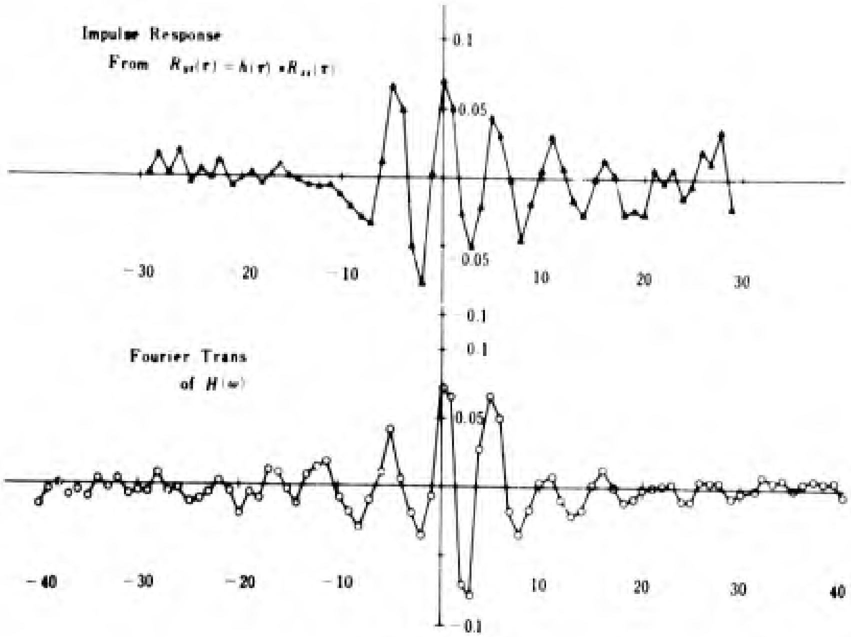

Figure 15

response function obtained as the Fourier transform of this impulse response function calculated through the simultaneous equation shows just about the same values as the frequency response (amplitude gain) obtained from the results of spectrum analysis as is demonstrated in Fig. 14.

The example of synthesis of $y(t)$ from the history of $x(t)$ using this impulse response functions is shown in Fig. 16 which shows pretty good agreement with the actual observation of $y(t)$, whichever impulse response function is used.

Attention should be paid on the fact, however, that an analysis in the time domain by means of $R_{yx}(\tau)$ and $R_{xx}(\tau)$ is inferior to the analysis in the frequency domain in the following reasons:

1. The choices of Δt, m, and N are difficult from the statistical point of view. This makes it difficult to decide on the really important part of the correlogram to be used for analysis as that part must include enough information.

2. The evaluation of error is not easy as in the frequency response function. In the frequency domain, the coherency plays a big role, and makes the estimation of relative error practicable.

We have to be very careful because of the above-mentioned defects. After these points have been made clear once, however, we can utilize the method to obtain the impulse response function from the correlations directly and use that to predict the future response. For this purpose, some special type computer

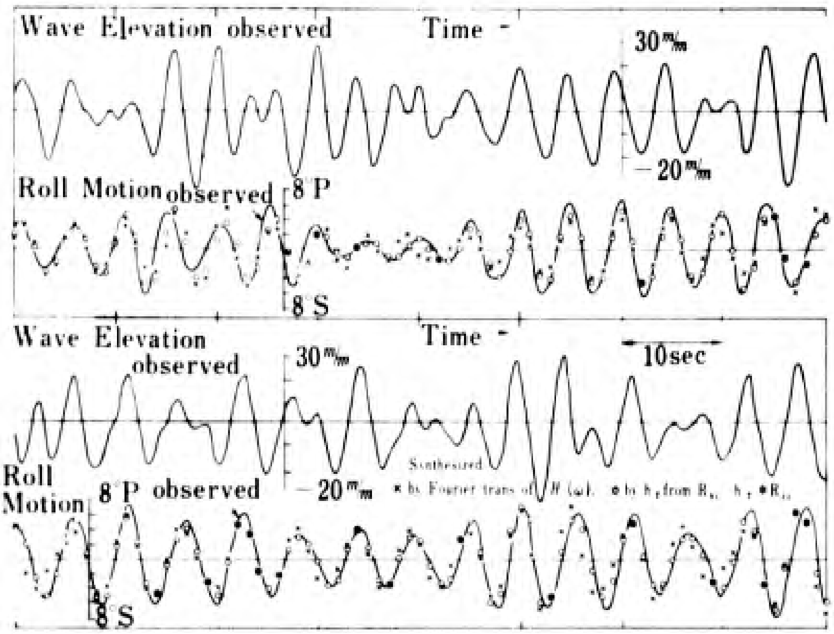

Figure 16

such as an analogue computer can be used in addition to the general purpose computer.

3. ON THE EFFECTS OF NON-LINEAR DAMPING ON CALCULATION OF THE SPECTRUM [11]

When the irregular input, for example the sea waves for the ship, can be considered as a Gaussian process, the output of a linear system, such as the linear oscillation of ship, is also a Gaussian process and can be expressed using the spectral expression.

$$y(t) = \int_{-\infty}^{\infty} e^{j\omega t}\, dZ(\omega)$$

$$E[dZ(\omega)\, dZ(\omega')] = dS_{yy}(\omega)\ \delta(\omega - \omega')$$

$$S_{yy}(\omega) = |H(\omega)|^2\ S_{xx}(\omega)\ .$$

When a non-linear component is included in the response character, the output is no longer Gaussian, and cannot be expressed by the spectral form which premises the superposition theory.

Even for that kind of case, the autocorrelation function as

$$R_{yy}(\tau) = E[y(t+\tau)\,\overline{y(t)}] \doteq \frac{1}{2T}\int_{-T}^{T} y(t+\tau)\,\overline{y(t)}\,dt$$

can be calculated. Accordingly if we adopt the definition of a spectrum in a wide sense as the Fourier transform of the correlation function, we can compute the spectrum. Here a trial has been made to show how the non-linear element — here non-linear damping as described by velocity square damping has been considered — affects the computed spectrum, using an approximation method. For example, for rolling, the equation of motion with velocity square damping is

$$I\ddot{\phi} + N_1\dot{\phi} + N_2\dot{\phi}|\dot{\phi}| + K_1\phi = M(\omega)\,e^{j\omega t}. \tag{3.1}$$

Now for the purpose of simplicity, all coefficients on the left-hand side of this equation are considered to be constant and do not vary with frequency. Then for input of a general irregular moment, the equation is

$$\ddot{\phi} + 2\alpha\dot{\phi} + \beta\dot{\phi}|\dot{\phi}| + \omega_o^2\phi = g(t). \tag{3.2}$$

As the zero order approximation ϕ_o, the solution of the linear equation without velocity square damping is taken as

$$\ddot{\phi}_o + 2\alpha\dot{\phi}_o + \omega_o^2\phi_o = g(t). \tag{3.3}$$

Then

$$\phi_o = \int_{-\infty}^{\infty} h_g(t-\tau)\,g(t)\,d\tau = \int_{-\infty}^{\infty} h_g(\tau)\,g(t-\tau)\,d\tau \tag{3.4}$$

$h_g(\tau)$, being the unit impulse response function of this linear system to the compulsory moment g. $h_g(\tau)$ is decided from Eq. (3.3) and, of course, is connected to the frequency response function $H(\omega)$ by a Fourier transformation and its inverse.

Here Eq. (3.2) is modified and the compulsory force $g(t)$ is assumed to change to $\{g(t) - \beta\dot{\phi}|\dot{\phi}|\}$. On substitution of ϕ_o into this ϕ, the 1st order approximation is taken as the solution of the equation

$$\ddot{\phi}_1 + 2\alpha\dot{\phi}_1 + \omega_o^2\phi_1 = g(t) - \beta\dot{\phi}_o|\dot{\phi}_o|. \tag{3.5}$$

The left-hand side of this equation is just the same as that of Eq. (3.3). Therefore using the same response $h_g(\tau)$,

$$\phi_1(t) \doteq \int_{-\infty}^{\infty} h_g(t-\mu)\,\{g(\mu) - \beta\dot{\phi}_o(\mu)\cdot|\dot{\phi}_o(\mu)|\}\,d\mu = \int_{-\infty}^{\infty} h_g(t-\mu)\,g(\mu)\,d\mu$$

$$-\beta\int_{-\infty}^{\infty} h_g(t-\mu)\,\{\dot{\phi}_o(\mu)\cdot|\dot{\phi}_o(\mu)|\}\,d\mu = \phi_o(t) - \phi_1'(t). \tag{3.6}$$

$\phi_1'(t)$ being the modification term and is

$$\phi_1'(t) = \beta \int_{-\infty}^{\infty} h_g(t-\mu) \{\dot{\phi}_o(\mu) \cdot |\dot{\phi}_o(\mu)|\} \, d\mu . \tag{3.7}$$

Of course the convergence of this approximation should be certified strictly at first; however, here the convergence is assumed as far as the linear damping α/ω_o' is rather large and the non-linear damping β is pretty small.

The autocorrelation function of this 1st approximation $\phi_1(t)$ is then,

$$\begin{aligned}
R_{\phi_1\phi_1}(\tau) &= E\left[\phi_1(t+\tau)\cdot\overline{\phi_1(t)}\right] \\
&= E\left[\phi_o(t+\tau) - \phi_1'(t+\tau)\right] \left[\overline{\phi_o(t) - \phi_1'(t)}\right] \\
&= E\left[\phi_o(t+\tau)\,\overline{\phi_o(t)}\right] - E\left[\phi_o(t+\tau)\,\overline{\phi_1'(t)}\right] \\
&\quad - E\left[\phi_1'(t+\tau)\,\phi_o(t)\right] + E\left[\phi_1'(t+\tau)\,\overline{\phi_1'(t)}\right] \\
&= E\left[\phi_o(t+\tau)\,\overline{\phi_o(t)}\right] - 2\,R E\left[\phi_o(t+\tau)\,\overline{\phi_1'(\tau)}\right] + E\left[\phi_1'(t+\tau)\,\overline{\phi_1'(t)}\right] .
\end{aligned} \tag{3.8}$$

Accordingly the spectrum $S_{\phi_1\phi_1}(\omega)$ of the 1st approximation, $\phi_1(t)$, is

$$\begin{aligned}
S_{\phi_1\phi_1}(\omega) &= S_{\phi_o\phi_o}(\omega) - \frac{1}{2\pi}\int_{-\infty}^{\infty} e^{-j\omega\tau}\, 2\,R E\left[\phi_o(t+\tau)\,\overline{\phi_1'(t)}\right] dt \\
&\quad + \frac{1}{2\pi}\int_{-\infty}^{\infty} e^{-j\omega\tau}\, E\left[\phi_1'(t+\tau)\cdot\overline{\phi_1'(t)}\right] d\tau .
\end{aligned} \tag{3.9}$$

The substitution of Eq. (3.7) into this equation yields

$$\begin{aligned}
&= S_{\phi_o\phi_o}(\omega) - \frac{\beta\cdot 2R}{2\pi}\int_{-\infty}^{\infty}\int_{-\infty}^{\infty} \overline{h_g(t-\alpha)}\, e^{-j\omega\tau}\, E\left[\phi_o(t+\tau)\cdot\dot{\phi}_o(\mu)\,|\dot{\phi}_o(\mu)|\right] d\mu\, d\tau \\
&\quad + \frac{1}{2\pi}\beta^2 \int_{-\infty}^{\infty}\int_{-\infty}^{\infty}\int_{-\infty}^{\infty} h_g(t+\tau-\mu)\,\overline{h_g(t-\nu)} \\
&\quad \times e^{-j\omega\tau}\, E\left[\dot{\phi}_o(\mu)\cdot|\dot{\phi}_o(\mu)|\cdot\dot{\phi}_o(\nu)\cdot|\dot{\phi}_o(\nu)|\right] d\mu\, d\nu\, d\tau \\
&= S_{\phi_o\phi_o}(\omega) - \frac{R\beta}{\pi}\int_{-\infty}^{\infty} \overline{h_g(t-\mu)}\, e^{j\omega(t-\mu)}\, d\mu \int_{-\infty}^{\infty}
\end{aligned}$$

(3.10)
(Cont.)

$$\times\ e^{-j\omega(\tau+t-\mu)}\ E\left[\dot\phi_o(t+\tau)\ \dot\phi_o(\mu)\cdot|\dot\phi_o(\mu)|\right]\ d\tau$$

$$+\ \frac{1}{2\pi}\beta^2 \int_{-\infty}^{\infty} h_g(t+\tau-\mu)\ e^{-j\omega(t+\tau-\mu)}\ d\tau \int_{-\infty}^{\infty} \overline{h_g(t-\nu)}\ e^{j\omega(t-\nu)}\ d\nu \int_{-\infty}^{\infty}$$

$$\times\ e^{-j\omega(\mu-\nu)}\ E\left[\dot\phi_o(\mu)\cdot|\dot\phi_o(\mu)|\cdot\dot\phi_o(\nu)\cdot|\dot\phi_o(\nu)|\right]\ d\mu$$

$$= S_{\phi_o\phi_o}(\omega) - 2\Re\left[\beta\overline{H_g(\omega)}\cdot S_{\dot\phi_o\cdot\dot\phi_o\cdot|\dot\phi_o|}(\omega)\right]$$

$$+\ \beta^2|H_g(\omega)|^2\ S_{\dot\phi_o\cdot|\dot\phi_o|\cdot\dot\phi_o\cdot|\dot\phi_o|}(\omega)\ . \qquad (3.10)$$

Now $g(t)$ is the compulsory moment that comes from the waves, and, so, if the waves are Gaussian, $g(t)$ is also a Gaussian process. From Eq. (3.4), $\phi_o(t)$ is also Gaussian, and

$$\dot\phi_o(t) = \int_{-\infty}^{\infty} h_g(t-s)\ g(s)\ ds\ . \qquad (3.11)$$

This shows $\dot\phi_o(t)$ is also a Gaussian process.

Here in order to calculate (3.10), we have to evaluate the expected value of $[\dot\phi_o(a)\cdot\dot\phi_o(b)\cdot|\dot\phi_o(b)|]$ and $[\dot\phi_o(\mu)\cdot|\dot\phi_o(\mu)|\cdot\dot\phi_o(\nu)\cdot|\dot\phi_o(\nu)|]$ concerning two Gaussian process $\phi_o(t)$ and $\dot\phi_o(t)$. $\phi_o(t)$ and $\dot\phi_o(t)$ are correlated to each other, of course by the correlation coefficient ρ.

Here, two Gaussian variables ξ and η, connected by the correlation coefficient ρ are assumed. The two-variable Gaussian probability distribution function is

$$p(\xi,\eta) = \frac{1}{2\pi\sigma_\xi\sigma_\eta\sqrt{1-\rho^2}} \exp -\left[\frac{\sigma_\eta^2\xi^2 - 2\sigma_\xi\sigma_\eta\xi\eta + \sigma_\xi^2\eta^2}{2\sigma_\xi^2\sigma_\eta^2(1-\rho^2)}\right]. \qquad (3.12)$$

It is necessary to evaluate $E[\xi,\eta\cdot|\eta|]$ and $E[\xi\cdot|\xi|\cdot\eta\cdot|\eta|]$ by means of this distribution function. The absolute values are what make the problem somewhat intricate. These evaluations could not be found in any text books and papers, and so were calculated by this author. The results are

$$E[\xi,\eta\cdot|\eta|] = \sqrt{\frac{2}{\pi}}\rho\sigma_\xi\cdot\sigma_\eta^2 = \sqrt{\frac{2}{\pi}}R_{\xi,\eta}(\tau)\,\sigma_\eta \qquad (3.13)$$

$$
\begin{aligned}
E[\xi\cdot|\xi|\cdot\eta\cdot|\eta|] &= \frac{2\sigma_\xi^2\sigma_\eta^2}{\pi}\left[\sqrt{1-\rho^2}\times 3\rho + 2(1+2\rho^2)\tan^{-1}\left\{\frac{\sqrt{1+\rho}-\sqrt{1-\rho}}{\sqrt{1+\rho}+\sqrt{1-\rho}}\right\}\right] \\
&\doteq \frac{2\sigma_\xi^2\sigma_\eta^2}{\pi}\left[4\rho + \frac{2}{3}\rho^3 + \frac{1}{30}\rho^5 - \frac{3}{80}\rho^7 \dots\right] \\
&= \frac{8}{\pi}\sigma_\xi\sigma_\eta R_{\xi\eta}(\tau) + \frac{4}{3}\frac{1}{\sigma_\xi\sigma_\eta}R^3_{\xi\eta}(\tau) + \frac{1}{15\pi}\frac{1}{\sigma_\xi^3\sigma_\eta^3}R^5_{\xi\eta}(\tau) + \dots,
\end{aligned}
\tag{3.14}
$$

where

$$
\rho = \frac{R_{\xi\eta}}{\sigma_\xi\sigma_\eta}.
$$

From these results and the relations

$$
S_{\phi_o\dot{\phi}_o}(\omega) = (-j\omega)\, S_{\phi_o\phi_o}(\omega) \tag{3.15}
$$

$$
S_{\dot{\phi}_o\dot{\phi}_o}(\omega) = \omega^2\, S_{\phi_o\phi_o}(\omega)\,, \tag{3.16}
$$

the result is

$$
\begin{aligned}
S_{\phi_o\cdot\dot{\phi}_o|\dot{\phi}_o|}(\omega) &= \frac{1}{2\pi}\int_{-\infty}^{\infty} e^{-j\omega(\tau+t-\mu)}\, E\left[\phi_o(t+\tau)\cdot\dot{\phi}_o(\mu)\cdot|\dot{\phi}_o(\mu)|\right] d\tau \\
&= \sqrt{\frac{2}{\pi}}\,\sigma_{\dot{\phi}_o}\,\frac{1}{2\pi}\int_{-\tau}^{\infty} R_{\phi_o\dot{\phi}_o}(\tau)\, e^{-j\omega t}\, d\tau \\
&= \sqrt{\frac{2}{\pi}}\,\sigma_{\dot{\phi}_o}\, S_{\phi_o\dot{\phi}_o}(\omega) = \sqrt{\frac{2}{\pi}}\,\sigma_{\dot{\phi}_o}\,(-j\omega)\, S_{\phi_o\phi_o}(\omega)\,.
\end{aligned}
\tag{3.17}
$$

Accordingly the 2nd term of the Eq. (3.10) is

$$
\begin{aligned}
2R\left[\beta\overline{H_g(\omega)}\right] S_{\phi_o\cdot\dot{\phi}_o|\dot{\phi}_o|}(\omega) &= 2\sqrt{\frac{2}{\pi}}\,\sigma_{\dot{\phi}_o}\,\beta S_{\phi_o\phi_o}(\omega)\, R\left\{-j\omega\,\overline{H_g(\omega)}\right\} \\
&= -2\sqrt{\frac{2}{\pi}}\,\sigma_{\dot{\phi}_o}\,\beta S_{\phi_o\phi_o}(\omega)\times\omega\, q_g(\omega)\,,
\end{aligned}
\tag{3.18}
$$

where

$$
q_g(\omega) = Q\{H_g(\omega)\} = -\frac{2\alpha\omega}{(\omega_o^2-\omega^2)^2 + 4\alpha^2\omega^2}\,. \tag{3.19}
$$

Also

$$E\left[\dot{\phi}_o(\mu)\cdot|\dot{\phi}_o(\mu)|\cdot\dot{\phi}_o(\nu)\cdot|\dot{\phi}_o(\nu)|\right] \doteq \frac{8}{\pi}\sigma^2_{\dot{\phi}_o} R_{\dot{\phi}_o\dot{\phi}_o}(\tau) + \frac{4}{3\sigma^2_{\dot{\phi}_o}} R^3_{\dot{\phi}_o\dot{\phi}_o}(\tau)$$

$$+ \left[\frac{1}{15\pi\sigma^6_{\dot{\phi}_o}} R^5_{\dot{\phi}_o\dot{\phi}_o}(\tau) + \ldots\right] . \tag{3.20}$$

The 3rd term of the Eq. (3.10) is the Fourier transform of the functions that is the product of Eq. (3.20) and some other function. The following relation is used, in this calculation:

$$\frac{1}{2\pi}\int_{-\infty}^{\infty} R(\tau)\, e^{-j\omega\tau} = S(\omega)\,, \qquad R(\tau) = \int_{-\infty}^{\infty} S(\omega)\, e^{j\omega t}\, d\omega \tag{3.21}$$

$$\frac{1}{2\pi}\int_{-\infty}^{\infty} R^3(\tau)\, e^{-j\omega\tau}\, d\tau = \frac{1}{2\pi}\int_{-\infty}^{\infty} e^{-j\omega\tau} R^2(\tau)\int_{-\infty}^{\infty} S(\omega')\, e^{j\omega'\tau}\, d\omega' d\tau$$

$$= \frac{1}{2\pi}\int_{-\infty}^{\infty}\left[e^{-j(\omega-\omega')\tau} R(\tau)\int_{-\infty}^{\infty} e^{j\omega''\tau} S(\omega'')\, d\omega'' \int_{-\infty}^{\infty} S(\omega')d\omega'\right] d\tau$$

$$= \int_{-\infty}^{\infty} S(\omega')\int_{-\infty}^{\infty} S(\omega'')\left[\frac{1}{2\pi}\int_{-\infty}^{\infty} e^{-j(\omega-\omega'-\omega'')\tau} R(\tau)d\tau\right] d\omega' d\omega''$$

$$= \int_{-\infty}^{\infty} S(\omega')\int_{-\infty}^{\infty} S(\omega'')\, S(\omega-\omega'-\omega'')\, d\omega' d\omega'' . \tag{3.22}$$

Similarly

$$\frac{1}{2\pi}\int_{-\infty}^{\infty} R^5(\tau)\, e^{-j\omega\tau}\, d\tau = \int_{-\infty}^{\infty} S(\omega_1)\int_{-\infty}^{\infty} S(\omega_2)\int_{-\infty}^{\infty} S(\omega_3)\int_{-\infty}^{\infty} S(\omega_4)$$

$$\times\, S(\omega-\omega_1-\omega_2-\omega_3-\omega_4)\, d\omega_1\, d\omega_2\, d\omega_3\, d\omega_4 . \tag{3.23}$$

However, because of the small value of the coefficient of $R^5(\tau)$, Eq. (3.23) was omitted in further analysis. Then, the 3rd term of Eq. (3.10) is

$$\beta^2 |H_g(\omega)|^2 \left[\frac{8}{\pi} \sigma_{\dot{\phi}_o} S_{\dot{\phi}_o \dot{\phi}_o}(\omega) + \frac{4}{3\sigma^2_{\dot{\phi}_o}} \int_{-\infty}^{\infty}\int_{-\infty}^{\infty} S_{\dot{\phi}_o\dot{\phi}_o}(\omega_1) S_{\dot{\phi}_o\dot{\phi}_o}(\omega_2) S_{\dot{\phi}_o\dot{\phi}_o}(\omega-\omega_1-\omega_2) d\omega_1 d\omega_2\right]$$

$$= \beta^2 |H_g(\omega)|^2 \left[\frac{8}{\pi} \sigma^2_{\dot{\phi}_o} \omega^2 S_{\phi_o\phi_o}(\omega) + \frac{4}{3\sigma^2_{\dot{\phi}_o}} S(\omega)\right] . \tag{3.24}$$

where

$$S(\omega) = \int_{-\infty}^{\infty}\int_{-\infty}^{\infty} S_{\dot{\phi}_o\dot{\phi}_o}(\omega_1) \cdot S_{\dot{\phi}_o\dot{\phi}_o}(\omega_2) \, S_{\dot{\phi}_o\dot{\phi}_o}(\omega - \omega_1 - \omega_2) d\omega_1 \, d\omega_2 . \tag{3.25}$$

By the substitution of Eqs. (3.19) and (3.24) into Eq. (3.10) and from

$$H_g(\omega) = \frac{\Phi(\omega)}{G(\omega)} = \frac{1}{-\omega^2 + \omega_o^2 + 2j\alpha\omega} = \frac{I\Phi(\omega)}{M(\omega)} = I \cdot H_o(\omega) ,$$

$$q_g(\omega) = -\frac{2\alpha\omega}{(\omega_o^2 - \omega^2)^2 + 4\alpha^2\omega^2} = Q\{H_g(\omega)\} ,$$

and also from

$$S_{\phi_o\phi_o}(\omega) = |H(\omega)|^2 S_{\zeta\zeta}(\omega) = \left\{H_o(\omega) I \cdot \frac{\omega^2}{g} \omega_o^2 \gamma(\omega)\right\}^2 S_{\zeta\zeta}(\omega)$$

$$= \left\{H_g(\omega) \frac{\omega^2}{g} \omega_o^2 \gamma(\omega)\right\} S_{\zeta\zeta}(\omega)$$

$$= \frac{\left\{\gamma(\omega)\, \omega_o^2 \frac{\omega^2}{g}\right\}^2}{\left\{(\omega_o^2 - \omega^2)^2 + 4\alpha^2\omega^2\right\}} \times \frac{1}{4} \left[A_\zeta(\omega)\right]^2 , \quad -\infty < \omega < \infty \tag{3.26}$$

$$S_{\dot{\phi}_o\dot{\phi}_o}(\omega) = \omega^2 S_{\phi_o\phi_o}(\omega)$$

$$\sigma^2_{\dot{\phi}_o} = 2\int_0^{\infty} S_{\dot{\phi}_o\dot{\phi}_o}(\omega)\, d\omega$$

the spectrum of the 1st order approximation $\phi_1(t)$ can be calculated.

As an example, the spectrum of the non-linear rolling of a model with $\omega_o = 3.85$ and $\alpha/\omega_o = \chi = 0.06705$, $\beta = 0.08$ has been calculated. For the waves, the Neumann shape spectrum which has its peak around $\omega_o = 3.85$ was used. In these kinds of computation which include the convolution of a spectrum, the spectrum should be defined in the range of $-\infty \sim +\infty$ of ω, and accordingly the definition which is usually used by oceanographers that define the spectrum only on $0 \sim +\infty$ range of ω is inconvenient. The spectrum of the waves, $|H_g(\omega)|^2$, $S_{\phi_0\phi_0}$, $S_{\dot{\phi}_0\dot{\phi}_0}$ and also the convolution S are shown in Figs. 17, 18 and 19. From Fig. 19, we can see the character of single and double convolutions. In the single convolution, a large power appears at $\omega = 0$ and at the frequency twice of that of the peak. In the double convolution, the large power appears again at the frequency of the peak of the original spectrum, and at the triple of that frequency. Because of the large decay of $|H(\omega)|^2$ at these high frequencies, the latter peak did not modify the spectrum. From these results, $S_{\phi_1\phi_1}$ was obtained as in Fig. 20. This is a pretty reasonable example of the effect of non-linear damping, which reduced the height of the peak that appeared in the spectrum of zero order approximation. There is the possibility that when the linear

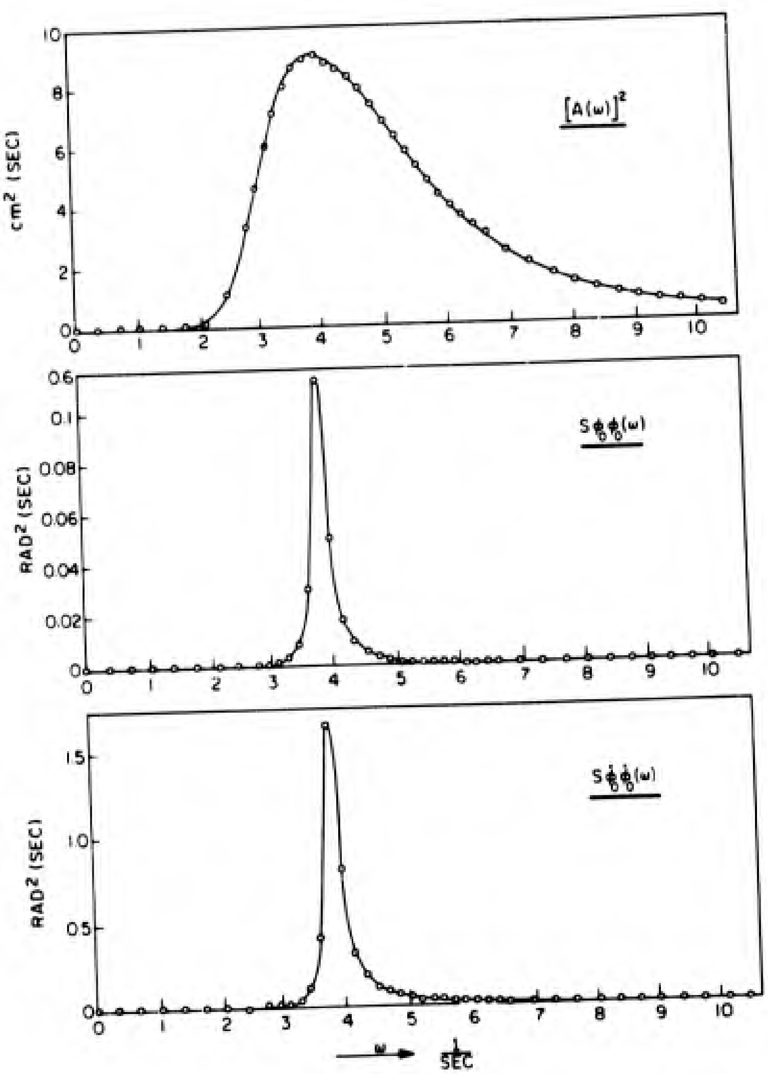

Fig. 17 - Spectra of wave, roll, and roll angular velocity

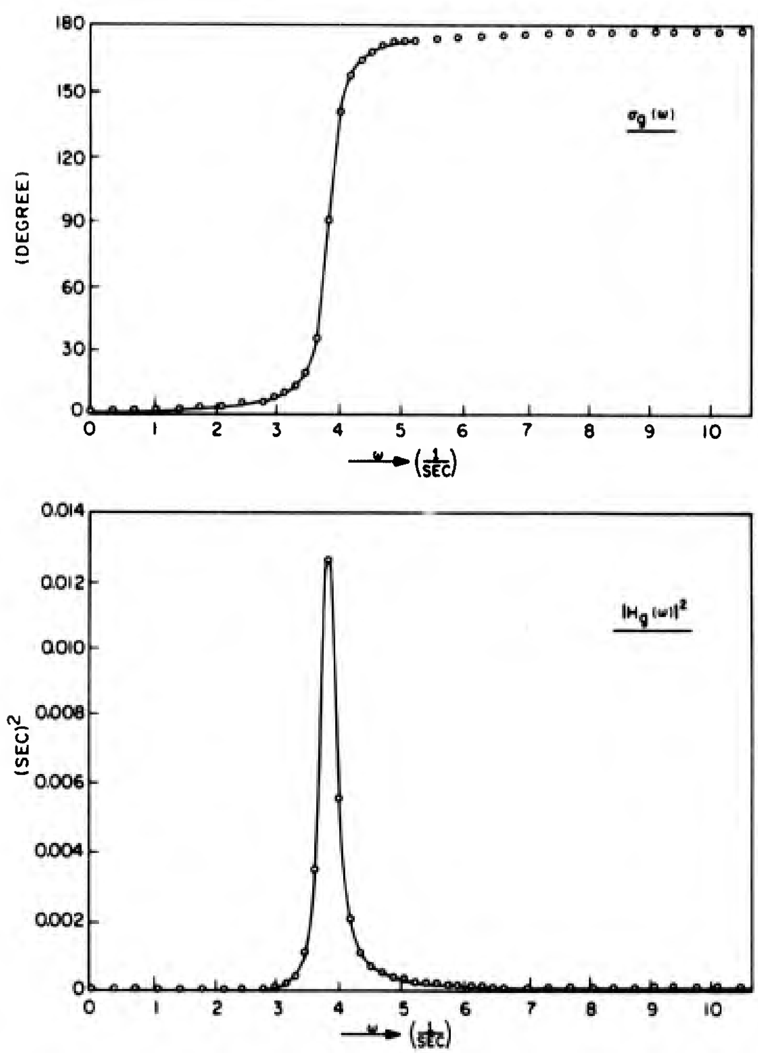

Fig. 18 - Linear response of roll
to the compulsory moment

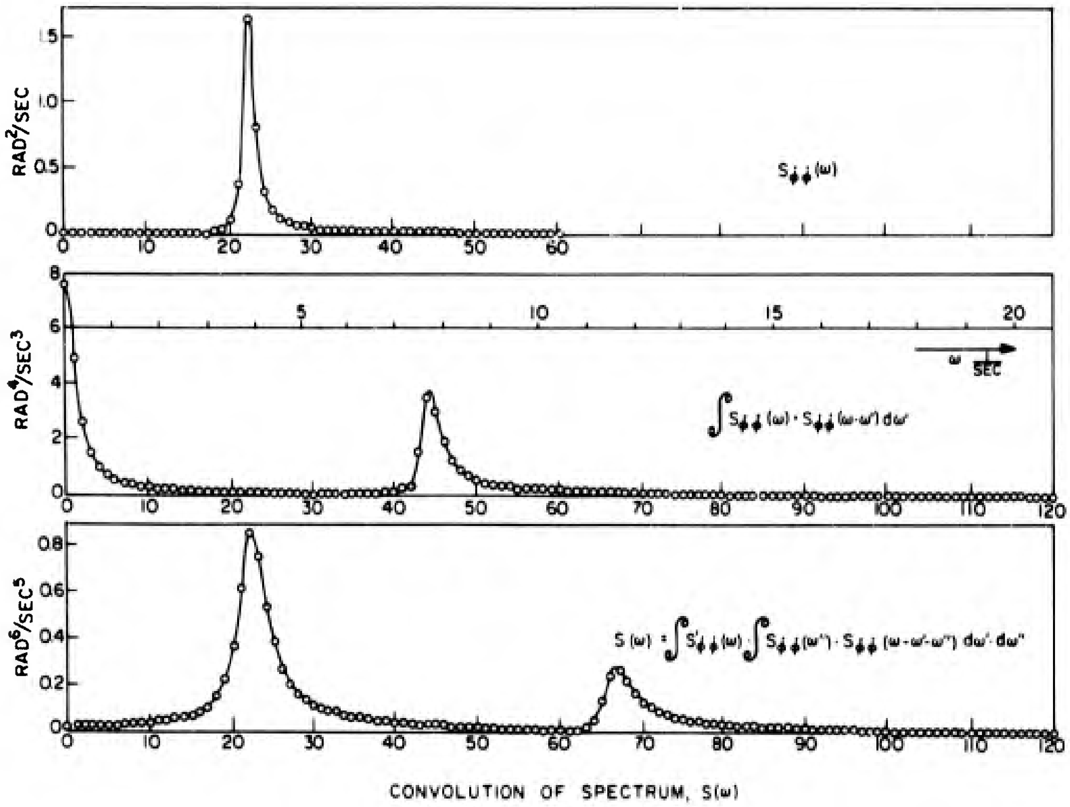

Figure 19

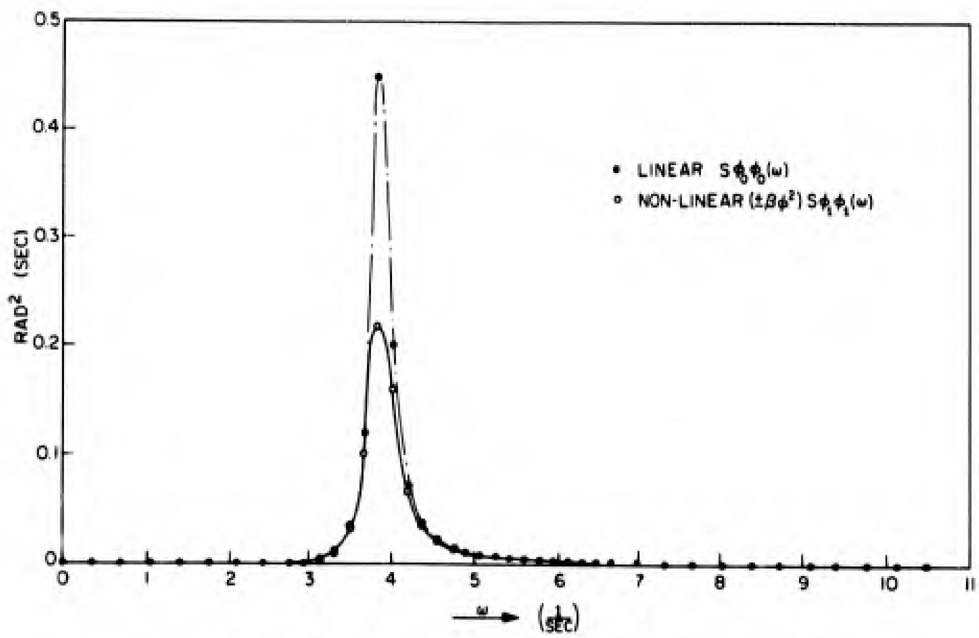

Fig. 20 - Computed spectrum of non-linear rolling

damping $\alpha/\omega = x$ is very large and $H(\omega)$ does not decay so much at $3\omega_0$, that a small peak will appear around $3\omega_0$, when the velocity square damping exists.

NOMENCLATURE

ω	circular frequency = $2\pi f$, f = frequency,
t	time,
Δt	time interval between adjacent data values (sampling time interval),
$x(t)$	input to the system, assumed to be a weakly stationary stochastic process,
$y(t)$	output of the system, under the input $x(t)$ and usually contaminated with noise $n(t)$,
$x(n)$	$x(n\Delta t)$,
$y(t)$	$y(n\Delta t)$,
$H(\omega)$	frequency response function of the system, when the system is linear and time-invariant; otherwise, that of the corresponding linearized system,
$\lvert H(\omega)\rvert$	amplitude gain,
$\sigma(\omega)$	$\mathrm{Arg}\,\{H(\omega)\}$, phase shift defined by $H(\omega) = \lvert H(\omega)\rvert \exp\{j\sigma(\omega)\}$ $(j^2 = -1)$,
$h(\tau)$	impulse response function of the system when the system is linear and time-invariant,
m	maximum number of lags of correlation computed, $T_m = m\Delta t$,
N	number of data used, $N\Delta t$ = total length of observation,
$R(\tau)$	covariance function,
$S(\omega)$	power spectrum function.

REFERENCES

1. Blackmann, R. B. and Tukey, John W., "The measurement of power spectra from the point of view of communications engineering," Part I and II, Bell System Tech. Jour., Vol. XXXVII, No. 1, Jan. 1958 and No. 2, March 1958.
2. Akaike, Hirotugu; Yamanouchi, Yasufumi; Kawashima, Rihei and others: "Studies on the statistical estimation of frequency response function," Annals of the Institute of Statistical Mathematics Supplement III, 1964.

3. Akaike, Hirotugu and Yamanouchi, Yasufumi, "On the statistical estimation of frequency response function, "Annals of the Institute of Statistical Mathematics, Vol. XIV, No. 1.

4. Goodman, N. R., "On the joint estimation of the spectra, cospectrum and quadrature spectrum of a two dimensional stationary Gaussian processes," Scientific Paper No. 10, Engineering Statistics Laboratory, New York Univ., March 1957.

5. Dalzell, John F. and Yamanouchi, Yasufumi, "The analysis of model test results in irregular head seas to determine the amplitude and phase relations of motions to the waves," ETT Report 708, Stevens Institute of Technology, 1958.

6. Pierson, Willard J., Jr. and Dalzell, John F., "The apparent loss of coherency in vector Gaussian process due to computational procedures with application to ship motions and random seas," Tech. Report, College of Engineering, Research Division, New York Univ., Sept. 1960.

7. Yamanouchi, Yasufumi, "On the analysis of the ship oscillations among waves, Part II," Journ. of the Society of Naval Architects of Japan, Vol. 110, Dec. 1961.

8. Akaike, Hirotugu, "On the design of lag window for the estimation of spectra," Annals of the Institute of Statistical Mathematics, Vol. XIV, No. 1.

9. Fuchs, R. A. and MacCammy, "A linear theory of ship motion in irregular waves," Tech. Report Series 61, Issue 2, Institute of Engineering Research, Wave Research Laboratory, Univ. of California, July 1953.

10. Yamanouchi, Yasufumi, "On the analysis of ship oscillations among waves, Part I," Journ. of the Society of Naval Architects of Japan, Vol. 109, June 1961.

11. Yamanouchi, Yasufumi, "On the effect of non-linear damping on the calculation of response spectrum," 24th general meeting of the Transportation Technical Research Institute, 1962.

* * *

RESPONSE TO COMMENTS BY WILLARD J. PIERSON, JR.

T. Francis Ogilvie
David Taylor Model Basin
Washington, D.C.

I appreciate Professor Pierson's comments very much. Since he was co-author of one of the most important papers ever written on the subject of ship motions, any worker in our field should listen carefully when he enters the discussion.

It is rather difficult to reply to his formal discussion, since his comments generally refer to what I did not say. My paper was too long as it was, and so a large amount of oceanographic data and statistical theory were omitted. In fact, Figs. 2-4 of my report, which I took from Dalzell's work, were modified to the extent that I cut out Dalzell's reported results on coherencies, since I wished to avoid detailed arguments about such matters. Perhaps this was wrong. Nolo contendere.

Furthermore, I have been very close to this whole subject for several years, and I have come to accept certain statements as being so obvious that one need no longer state them. For example, I would have been quite surprised if anyone were to suggest that the coherency between roll and wave height in head seas were not extremely small. However, if Professor Pierson considers that such facts should still be restated in 1964, I may have again committed a sin of omission.

The comments in the section, "Coherency and Resolvability of Spectral and Cross Spectral Shapes," do not seem to be relevant to my paper and so I shall not offer any response to them.

Professor Pierson's comments on nonlinear problems are relevant and I welcome them. It is very encouraging and stimulating to observe recent progress in the probabilistic treatment of nonlinear physical problems. It appears that the oceanographers and statisticians have in fact stepped far out ahead of the hydrodynamicists.

Unfortunately, there is much more to the prediction of ship motions than the establishment of statistical laws. Eventually, we would hope to be able to start with geometric and dynamic descriptions of the ship, add to this an adequate description of the seaway, and then predict any desired motions-related quantity. Professor Pierson's comments almost imply that all of this can now be done, because the oceanographers have supplied the tools. Actually, we cannot make very good predictions of heave and pitch in long-crested head seas, where the simplest concepts are most nearly valid. We are still lacking in basic methods for treating the hydrodynamics of such problems, and under such circumstances the statisticians' impressive accomplishments are of limited usefulness. Certainly their value must rest very largely on the use of empirical substitutes for hydrodynamic theory. It was for considerations such as this that my paper was totally lacking in discussion of short-crested-seas problems. How can we hope to solve such problems when we have not been able to solve the long-crested-seas problems?

Nevertheless, it is pleasant to anticipate the prospect that, if and when the hydrodynamicists make breakthroughs in the future, the statistical apparatus will all be waiting for them — ready to cover not only linear problems of short-crested seas but nonlinear ones as well.

CURRENT PROGRESS IN THE SLENDER BODY THEORY FOR SHIP MOTIONS

J. N. Newman and E. O. Tuck
David Taylor Model Basin
Washington, D.C.

ABSTRACT

This paper describes current work towards a complete systematic theory for the motions of a slender ship in a seaway. Part I contains an introduction and a general discussion of the results which are obtained, and presents calculations of pitch and heave response at zero speed. Part II contains a complete derivation of the zero speed theory for harmonic oscillations in the presence of oblique incident waves. Part III contains a derivation of a more general theory with forward speed, for arbitrary forced oscillations in calm water. A significant feature of this paper is the splitting of the velocity potential and forces into parts which are dependent on free surface effects, plus parts which correspond to the motion of the double body in infinite fluid or specifically to the case of a rigid free surface.

I. INTRODUCTION

A fundamental motivation of the theoretical physicist is his desire to bring a sense of order to the physical world, by means of mathematical models which are derived from the basic physical principles governing the problem at hand. Practical problems in ship hydrodynamics have resisted this ordering process, however, not because the basic physical principles were unknown, but because their mathematical representation has been comparatively intractable, at least by comparison with most other problems in classical mechanics. The prediction of ship motions in waves is typical of this situation, and in spite of concerted efforts we are still short of our desired goal of giving engineering predictions of ship motions from a rational theory.

It is generally accepted that, for most purposes at least, the desired theory can be attained by considering that the water around the ship to be an ideal (incompressible, inviscid) fluid, and by linearizing the unsteady motions (wave heights and ship motions). Within this framework there have been several different approaches, which can be distinguished according to the assumptions made concerning the hull shape and forward velocity (Table 1). At zero speed it is possible to proceed without any assumptions as to hull geometry, and we

Table 1
Rational Linear Theories for Oscillatory Surface Ships

Theory	B/L	T/L	λ/L	$\omega\sqrt{L/g}$	Froude No.
Fat Ship	$0(1)$	$0(1)$	$0(1)$	$0(1)$	0
Thin Ship	$0(\epsilon)$	$0(1)$	$0(1)$	$0(1)$	0 or $0(1)$
Slender Ship	$0(\epsilon)$	$0(\epsilon)$	$0(1)$	$0(1)$	0 or $0(1)$
Flat Ship	$0(1)$	$0(\epsilon)$	$0(1)$	$0(1)$	0 or $0(1)$
Strip	$0(\epsilon)$	$0(\epsilon)$	$0(\epsilon)$	$0(\epsilon^{-1/2})$	0

Nomenclature: B = beam, T = draft, λ = wavelength,
ω = radian frequency.

indicate this situation by the designation "fat ship theory"; this approach has the advantage that no assumptions are made concerning the hull geometry, but closed form solutions are not obtainable, and moreover the theory is restricted to zero speed by the requirement that the disturbance of the free surface be small.

The thin ship model, which is most familiar in wave resistance theory, has been applied to ship motions in longitudinal (head or following) waves and both first- and second-order theories have been developed; criticisms are first that conventional ships are not thin (B/T is usually greater than one), secondly that the first order theory contains an unbounded resonance in pitch and heave while the second order theory is extremely complex, and thirdly that the use of this model for oblique wave motions results in a lifting-surface type of integral equation.

The flat ship was proposed in order to overcome the objections of the thin ship, but its analysis is still incomplete, and one may note that it suffers from drawbacks similar to the thin ship, but with the vertical and transverse modes reversed.

The strip theory and slender ship theory are based upon identical geometrical assumptions, namely that the beam and draft are both small compared to the ship's length; intuitively this assumption seems reasonable for conventional ships. They differ however, in regard to the additional characteristic length of the problem, namely the length of the incident waves. The strip theory, which assumes two-dimensional flow in transverse planes at each section of the ship, is rational only if the wavelength is small compared to the ship length. If this is the case, interference between the bow and stern will be negligible, since they are many wavelengths apart, and the three-dimensional hydrodynamic problem can be reduced to a sequence of two-dimensional problems.* An additional drawback of the strip theory is that, by hypothesis, it cannot be rationally applied with forward speed. Slender body theory, on the other hand, attempts to account for longitudinal changes in the flow, either from interference effects or from the effects of forward motion, but at the expense of transverse interference phenomena since the beam is assumed small compared to a wavelength.

Thus it would seem natural to apply the techniques of slender body theory, which have been well established in aerodynamics, to the prediction of ship motions in waves. However, this seemingly obvious union was not consummated until recently. Now progress is being made by several workers and we can optimistically hope that a rational and successful theory for predicting ship motions in waves will be forthcoming in the near future.

This paper contains an outline of some recent developments toward the above goal. Our results are still incomplete, and to some extent disjoint, but they are sufficient to suggest the practical utility of a truly rational approach to ship motion predictions. To support this statement we will show numerical computations for practical ships which, at least in parts of the domain of interest, are as accurate as available experimental data. Our paper will be divided into three parts and these will be presented in the inverse order from that which is customary, so that the most important results are exhibited before we become engrossed in the details.

The Essential Features of Slender Ship Motions

Our theory assumes the ship to be long compared to its beam and draft, to be floating on the surface of an ideal incompressible fluid, and to be excited in unsteady motion either by external forces or by an incident plane progressive wave system. We assume moreover that the unsteady motions are of small amplitude compared to all of the other characteristic lengths (i.e., the ship dimensions and wavelength) so that linearization is possible. Finally we assume that the wavelength of the incident wave system or the waves radiated from the body is of the same order as or greater than the ship's length. The last assumption ensures that the transverse dimensions of the body are small compared to a wavelength and greatly simplifies the interference effects between points on the ship's surface.

It is convenient to introduce a small parameter ϵ, which may be defined as the beam-length ratio of the ship. The slender body solution of our problem is then developed by formulating a boundary value problem for the appropriate velocity potential, whose gradient represents the unsteady fluid velocity vector, and then finding an approximate solution of this boundary value problem which is asymptotically valid for small values of ϵ. The first order slender body

*However, if incident waves are present from any angle other than abeam, the resulting two-dimensional problem is governed by the wave equation rather than Laplace's equation. This complication is frequently overlooked in analysing the exciting forces from strip theory.

theory results from retaining only those contributions to the velocity potential and forces acting on the body which are of leading order in ϵ, and higher order approximations follow by systematically including the next-higher-order contributions, etc. However, our problem is complicated by the fact that a slender ship, oscillating in six degrees of freedom, will produce hydrodynamic disturbances in the various modes and encounter hydrodynamic, hydrostatic, and inertial forces in each mode, which are of different orders in ϵ. It is clear, for example, that the surging or rolling oscillations of a slender ship will not generate disturbances of the same order as pitching or heaving modes. Moreover, even within one given mode, say heave, certain types of forces will dominate others; for example the hydrostatic restoring force will be of the same order as the waterplane area, or $O(\epsilon)$, while the inertial force will be of the same order as the ship's displaced volume, or $O(\epsilon^2)$. As a result many of the accepted components to the total forces and moments acting on the ship are higher order, and do not appear in the first order theory for each mode. This situation is illustrated in Table 2, which shows the order of magnitude, for each mode of oscillation, of various physical quantities. These include the normal fluid velocity $\partial\phi_B/\partial n$ on the ship's surface induced by its oscillations and by the incident wave system, the corresponding body velocity potential ϕ_B representing the disturbance of the fluid by the ship, the hydrodynamic body force F_B due to this disturbance, the hydrodynamic force F_{FK} due to the pressure field of the undisturbed incident wave system (the "Froude-Krylov" force), the hydrostatic restoring force F_{HS}, and the inertial force F_I due to the body's own mass or moment of inertia. For each mode the forces of leading order are underlined, and the first order equation of motion is written symbolically in the last column. Conceptually this table can be derived most easily for uncoupled motions, but in fact the inclusion of coupling between modes does not affect the order of magnitude in each case (assuming that the origin is taken at the center of gravity).

Table 2
Relative Orders of Magnitude for each Degree of Freedom

Mode	$\partial\phi_B/\partial n$	ϕ_B	F_B	F_{FK}	F_{HS}	F_I	First Order Equation of Motion
Surge	ϵ	$\epsilon^2 \log \epsilon$	$\epsilon^4 \log \epsilon$	$\underline{\epsilon^2}$	0	$\underline{\epsilon^2}$	$F_{FK} + F_I = 0$
Sway	1	ϵ	$\underline{\epsilon^2}$	$\underline{\epsilon^2}$	0	$\underline{\epsilon^2}$	$F_{FK} + F_I + F_B = 0$
Heave	1	$\epsilon \log \epsilon$	$\epsilon^2 \log \epsilon$	$\underline{\epsilon}$	ϵ	ϵ^2	$F_{FK} + F_{HS} = 0$
Roll	ϵ	ϵ^2	ϵ^4	$\underline{\epsilon^3}$	$\underline{\epsilon^3}$	ϵ^4	$F_{FK} + F_{HS} = 0$
Pitch	1	$\epsilon \log \epsilon$	$\epsilon^2 \log \epsilon$	$\underline{\epsilon}$	$\underline{\epsilon}$	ϵ^2	$F_{FK} + F_{HS} = 0$
Yaw	1	ϵ	$\underline{\epsilon^2}$	$\underline{\epsilon^2}$	0	$\underline{\epsilon^2}$	$F_{FK} + F_B + F_I = 0$

To illustrate how the entries of Table 2 are obtained, consider the case of surge. The normal velocity on the ship's surface is proportional to the direction cosine in the longitudinal direction, which is $O(\epsilon)$ for a slender body. The magnitude of the potential can only be established rigorously by solving the problem, but it can be estimated heuristically by considering the corresponding two-dimensional problem in the transverse or "cross-flow" plane, where the ship's submerged area is pulsating at a rate proportional to the longitudinal rate of change of sectional area, and it is easily verified that a pulsating circular cylinder of radius R will have a potential, on its surface, of magnitude proportional to $R \log R$ times the normal velocity. The hydrodynamic forces follow from Bernoulli's equation and the fact that the longitudinal projected area of the ship is $O(\epsilon^2)$. (The potential of the incident wave is of course $O(1)$ since it doesn't depend on ϵ.) There is no hydrostatic restoring force in surge and the inertial force is proportional to the displaced volume, or $O(\epsilon^2)$. The leading order forces are the Froude-Krylov exciting force and the inertial restoring force. Thus the leading order equation of motion for surge oscillations does not depend on the hydrodynamic disturbance generated by the body. We note that a similar conclusion holds for heave, roll, and pitch. Thus, at least in these four modes, the familiar damping and added mass forces are secondary and the Froude-Krylov hypothesis has a rational basis.

Certain fundamental conclusions follow from Table 1:

1. In every mode the leading-order equations of motion are homogeneous in ϵ. Thus the response in each mode, to incident waves, will be $O(1)$ in terms of ϵ, and of the same order as the wave height.

2. For surge the dominant forces are inertial and Froude-Krylov, with the effects of the ship's own disturbance small by the factor $\epsilon^2 \log \epsilon$.

3. For sway and yaw the ship's hydrodynamic disturbance must be accounted for even in the first-order equations of motion.

4. For roll the Froude-Krylov exciting moment and hydrostatic restoring moment are dominant, with other effects small by the factor ϵ.

5. For pitch and heave the dominant forces are Froude-Krylov and hydrostatic, with effects from the ship's hydrodynamic disturbance small by a factor $\epsilon \log \epsilon$. It follows that the first-order equations of motion for pitch and heave will not contain resonance effects, but there will be a bounded resonance in the second-order equations.

At first glance the above conclusions may seem trivial, at variance with physical observation, and a step backward in our scientific development. One noted critic has even stated that "at least thin-ship theory predicts resonance." The best counter-argument is to show some results from the application of the first-order theory for pitch and heave (Figs. 1 and 2). These show the pitch and heave response of an aircraft carrier at zero speed. The solid curves are the results of solving the coupled first-order equations of motion, equating the Froude-Krylov exciting force and moment* to the hydrostatic restoring force

*Actually we employ the slender body limits of the Froude-Krylov force and moment, in which the surface integrals over the hull are replaced by simpler line integrals.

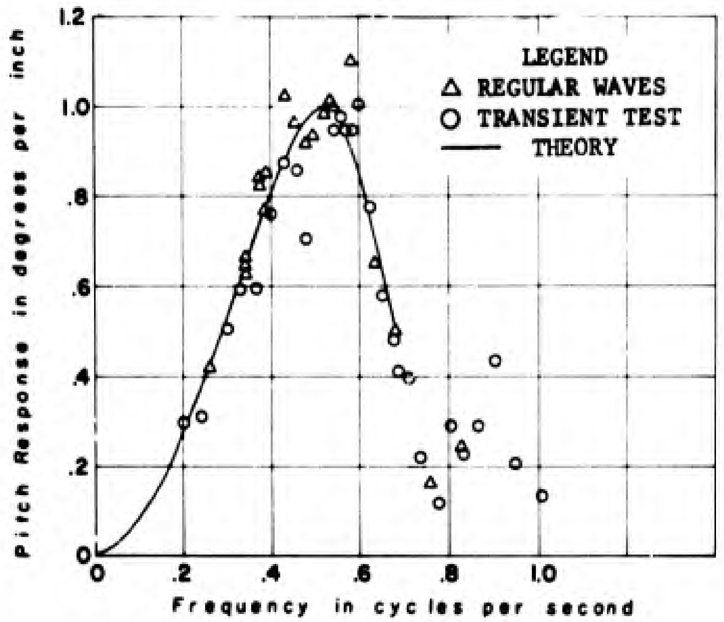

Fig. 1 - Pitch response calculated from first order theory and compared with zero speed experimental data

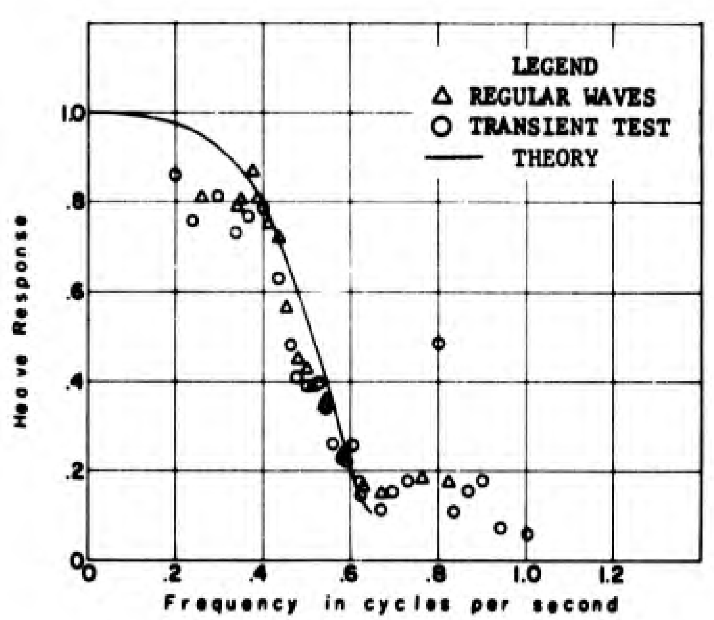

Fig. 2 - Heave response calculated from first order theory and compared with zero speed experimental data

and moment. The experimental points were obtained both from regular wave tests and from transient or "pulse" type tests, as described in the paper by Davis and Zarnick at the present Symposium; these experiments were made in the Maneuvering and Seakeeping Facility, so that wall effects are minimized. It is clear that under these conditions the seemingly crude first order slender body theory gives a very good prediction of pitch and heave, in fact much better than is usual in this field.

The above results are less surprising if we recall that they are for zero forward speed, and in this condition the resonant frequencies of conventional ships in pitch and heave correspond to very short wavelengths, on the order of 50-75% of the ship length, or much shorter than the range of practical significance. In other words, at zero speed with conventional ship forms the practical frequency range for heave and pitch is substantially below resonance. Clearly, however, the situation will change when forward speed is involved, at least in ahead waves, since the frequency of encounter will be increased. This is illustrated in Figs. 3 and 4, showing the same theoretical curves compared to experimental data with forward speed (at a Froude number 0.14). There is now a resonant peak within the domain of interest, although the data are essentially unchanged away from resonance. This suggests that a second order slender body theory, including the mass of the ship and all other effects of equal order, might be sufficient to give predictions with forward speed of the same accuracy as those shown for zero speed. It is for this reason that we have been examining the second order slender body theory for ship motions in waves, which includes

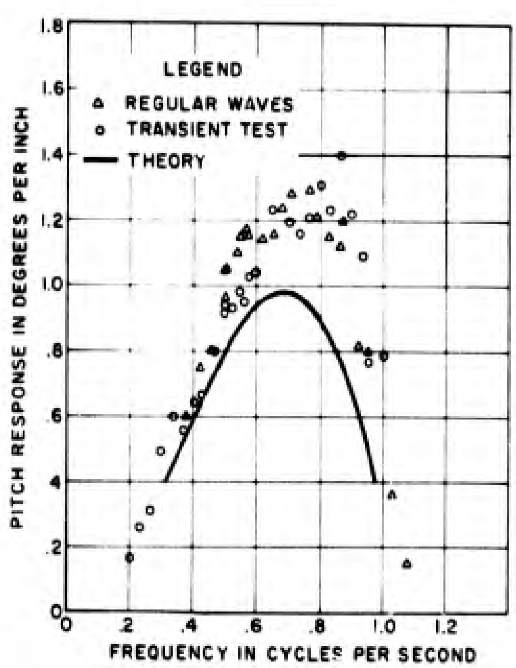

Fig. 3 - Pitch response calculated from first order theory and compared with experimental data at 0.14 Froude number

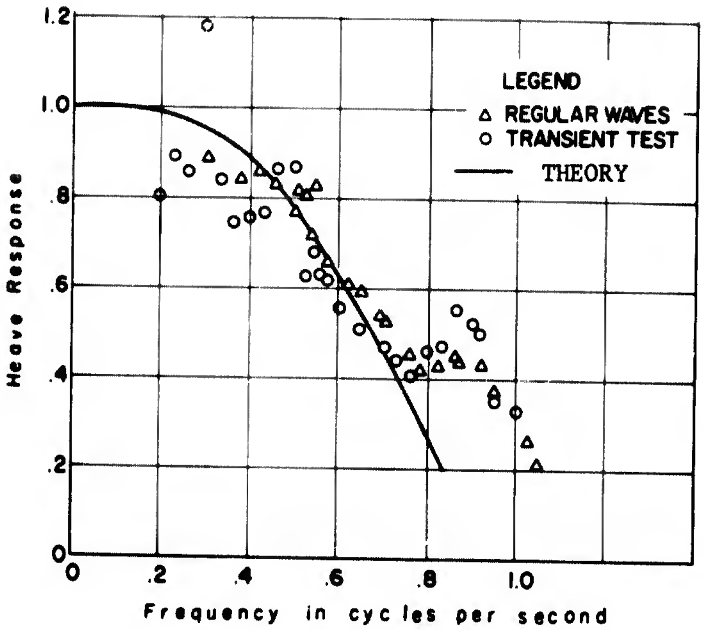

Fig. 4 - Heave response calculated from first order theory and compared with experimental data at 0.14 Froude number

all the familiar complications of damping, added mass, and the diffraction of the incident wave system by the presence of the ship.

The complete second order theory at zero speed is presented in Part II, this work being an extension of the results of Newman (1964). Figures 5 and 6 show the resulting pitch and heave response for the same conditions as Figs. 1 and 2. The first order theory and experimental data are repeated for comparison. It is apparent that there are only minor differences between the first- and second-order results.

At finite speed neither a complete theory nor calculated responses are as yet available; the theory is presented in Part III for the case of forced oscillations only, leaving the exciting forces still to be determined. The theoretical results of Part III (e.g., Eqs. 3.36) are presented in the form of double integrals involving the cross-sectional area curve $S(x)$ and/or the waterline beam curve $B(x)$ multiplied by a complicated kernel function $K(x, \omega, U)$ where ω is radian frequency and U forward speed. If $U = 0$, K reduces as in Part II to a combination of Bessel and Struve functions which are tabulated; on the other hand for non-zero U, K remains an untabulated function defined at the moment only in the form of a Fourier integral. More work is needed on investigation and tabulation of this function before computation of responses at finite speed can be carried out.

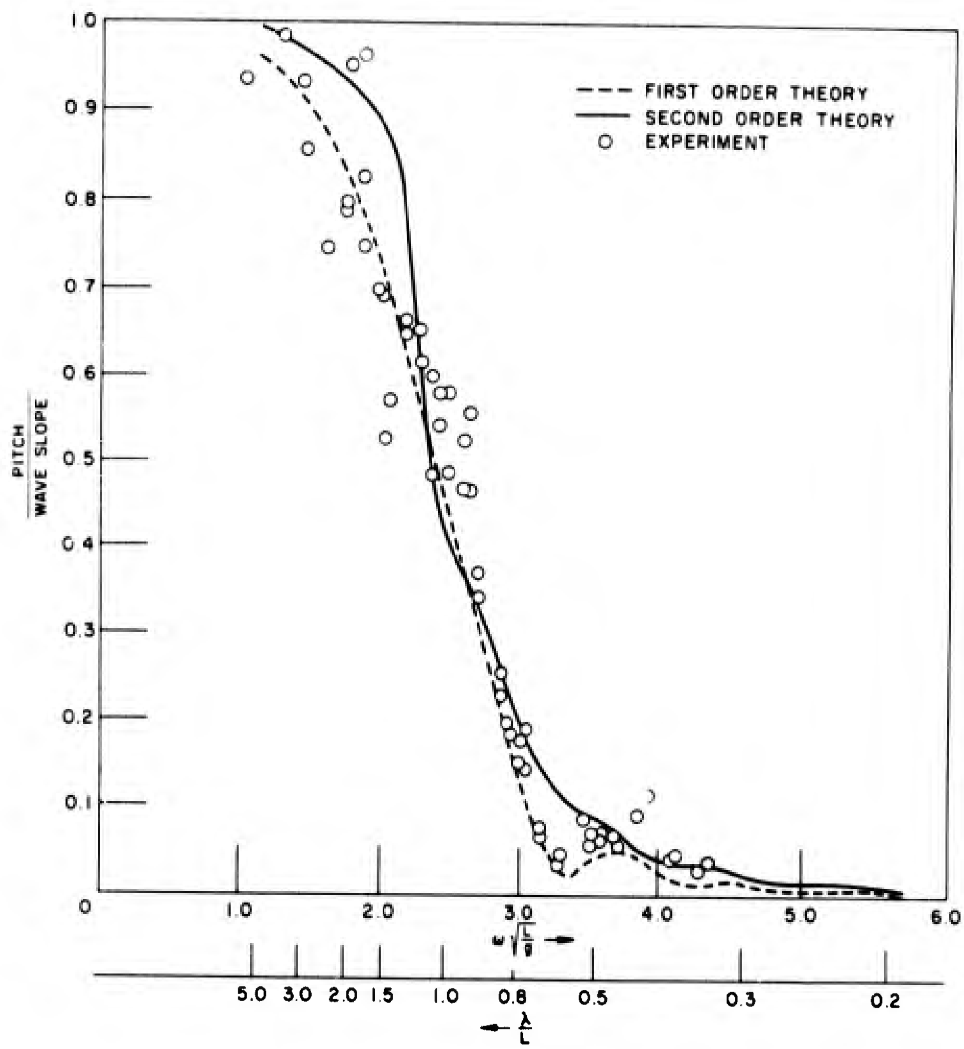

Fig. 5 - Pitch response from second order theory compared with first order theory and experiments

In deriving the second order theory, the fundamental result we use is that any velocity potential ϕ representing a regular disturbance of the fluid by the ship can, near the ship, be written in the form

$$\phi(x, y, z) = \phi^{(WALL)}(x, y, z) + f^{(FS)}(x) \tag{1.1}$$

where $\phi^{(WALL)}$ is the potential for the identical problem but with the free surface replaced by a rigid surface or "wall" (which is, by reflection, the problem for a double body consisting of the ship hull plus its image above the free surface in an infinite fluid). The function $f^{(FS)}(x)$ contains all the free surface effects (and in particular is dependent on the acceleration of gravity whereas $\phi^{(WALL)}$ is not), and is defined by an integral transform of the form

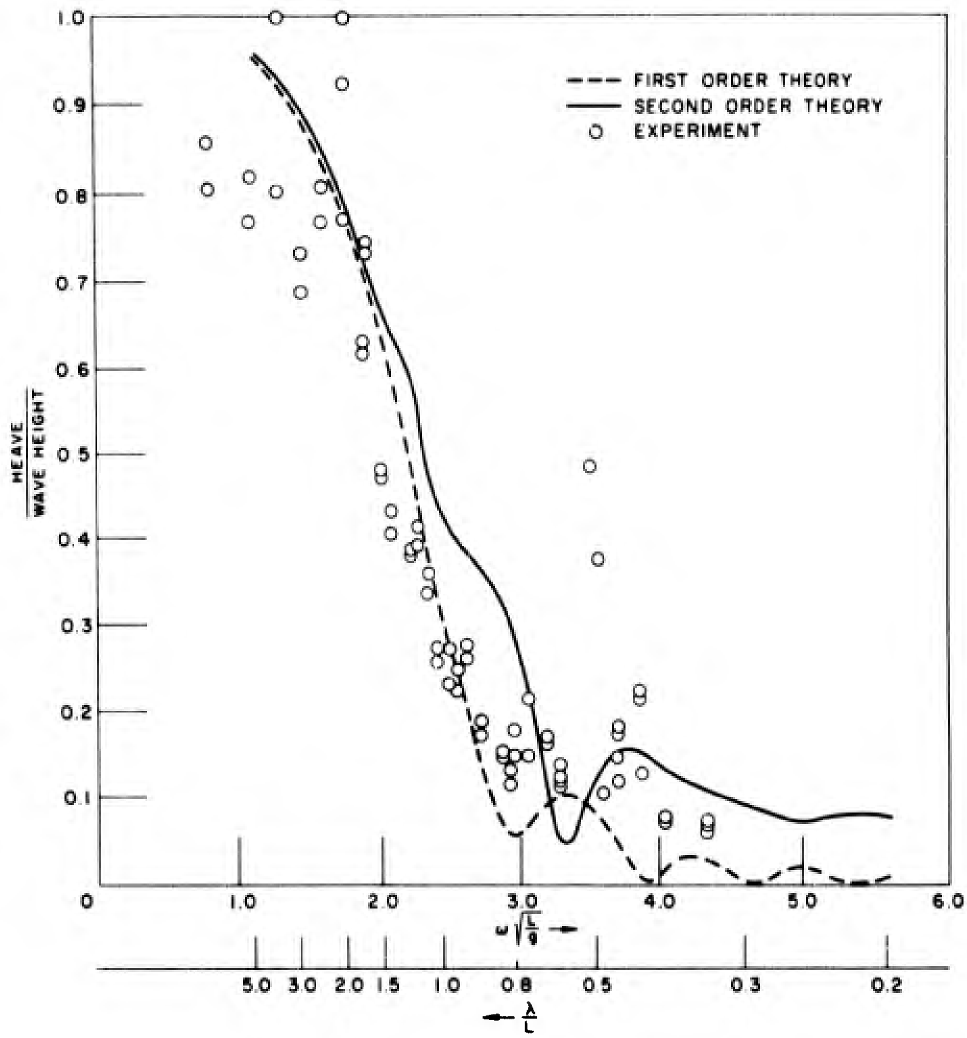

Fig. 6 - Heave response from second order theory compared with first theory and experiments

$$f^{(FS)}(x) = \int_L K(x - \xi, \omega)\, Q(\xi)\, d\xi \tag{1.2}$$

where

$$Q(x) = \int_C \frac{\partial \phi}{\partial n}\, d\ell \tag{1.3}$$

is the flux through the cross section C of the ship at the station x. Since $\partial\phi/\partial n$ is given from the hull boundary condition, Q is calculable as a function of hull geometry and the motion amplitudes. On the other hand the function K is a kernel function independent of hull geometry and of the motions, the calculation of which may be carried out once and for all, this being one of the chief objectives of the present theory. For sinusoidal oscillations K is a function of the radian frequency ω; for general motions, however, K may be interpreted in the usual sense of control theory as a transfer function.

Using this splitting up of the potential we may now calculate the hydrodynamic forces on the ship, which will be split up in a similar manner. In particular for sinusoidal oscillations we can define in the conventional manner a matrix of frequency dependent damping, added mass, and exciting force coefficients, each of which can be decomposed into "wall" and "free surface" portions. In this paper we shall focus attention on the latter half of the problem, although in Part II the classical slender body theory is used to find the "wall" forces for oscillations at zero speed.

II. THE ZERO-SPEED THEORY

Motions in Oblique Waves

We shall outline the general analysis for zero forward speed, constructing the velocity potential from Green's theorem in the manner suggested by Vossers (1962). Further details of the present analysis can be found in the recent paper by Newman (1964).

A slender rigid ship is floating with zero mean velocity in the presence of plane progressive incident waves, of amplitude A and angle of incidence β relative to the longitudinal x-axis. The resulting fluid velocity vector can be represented by the gradient of a velocity potential $\phi(x, y, z)\, e^{-i\omega t}$, including both the known incident wave potential

$$\phi_I(x, y, z) = \frac{gA}{\omega} \exp\,[K(z + ix\cos\beta + iy\sin\beta)] \tag{2.1}$$

and the unknown disturbance potential ϕ_B due to the presence of the body. Here ω denotes the circular frequency, g the gravitational acceleration, $K = \omega^2/g$ is the wave number, and the z-axis is positive upwards with $z = 0$ the plane of the undisturbed free surface. It follows from Green's theorem and the boundary conditions of the problem that the disturbance potential satisfies

$$\phi_B(x, y, z) = -\frac{1}{4\pi}\iint_S \left[G(x, y, z; \xi, \eta, \zeta)\,\frac{\partial\phi_B}{\partial n} - \phi_B(\xi, \eta, \zeta)\,\frac{\partial G}{\partial n}\right] dS\,, \tag{2.2}$$

where the integral is over the submerged surface S of the ship, the direction of the normal n is out of the ship, and the Green's function is defined (cf. Wehausen and Laitone, 1961) by the expression

$$G = G_0 + G_1\,, \tag{2.3}$$

$$G_0 = \left[(x-\xi)^2+(y-\eta)^2+(z-\zeta)^2\right]^{-1/2} + \left[(x-\xi)^2+(y-\eta)^2+(z+\zeta)^2\right]^{-1/2}, \tag{2.4}$$

$$G_1 = 2K\int_0^\infty \frac{dk}{k-K}\, e^{k(z+\zeta)}\, J_0\left(k\left[(x-\xi)^2+(y-\eta)^2\right]^{1/2}\right). \tag{2.5}$$

The contour of integration in the integral for G_1 is indented below the singularity $k = K$, in order to satisfy the radiation condition of outgoing waves at infinity. Physically the Green's function G represents the potential of an oscillatory source, located beneath the free surface at the point $x = \xi$, $y = \eta$, $z = \zeta$; the function G_0 is the elementary source function $1/R$ plus its image above the free surface, and the function G_1 represents the necessary correction to account for free-surface effects.

The above statement of the problem is exact, and Eq. (2.2) can be regarded as an integral equation for ϕ_B. If the body is slender, however, major reductions can be affected. It can be shown that the term $\phi_B(\partial G_1/\partial n)$ is small compared to the remainder of the integrand, by a factor $1 + O(\epsilon \log \epsilon)$, and the surface integral of the term $G_1(\partial\phi_B/\partial n)$ can, to the same degree of accuracy, be reduced to a line integral over the length. The resulting integral equation, for points (x, y, z) in the near field (i.e., a distance $O(\epsilon)$ from the ship), is then

$$\phi_B = -\frac{1}{4\pi}\iint\left(G_0\frac{\partial\phi_B}{\partial n} - \phi_B\frac{\partial G_0}{\partial n}\right)dS + f^{(FS)}(x), \tag{2.6}$$

where

$$f^{(FS)}(x) = -\frac{1}{4\pi}\int_L G_1(x,0,0,\xi,0,0)\left(\int_C \frac{\partial\phi_B}{\partial n}\,d\ell\right)d\xi$$

$$= -\frac{1}{4\pi}\int_L G_1(x,0,0,\xi,0,0)\,Q(\xi)\,d\xi. \tag{2.7}$$

Since G_0 is the Green's function for the rigid free surface problem, it can be shown that (2.6) is equivalent to

$$\phi_B = \phi_B^{(WALL)} + f^{(FS)}(x). \tag{2.8}$$

Thus, as stated in Eq. (1.1), we can express the velocity potential explicitly in terms of the solution of the corresponding wall problem plus a function $f^{(FS)}(x)$ containing the free surface effects. (The $f^{(FS)}(x)$ of (2.8) is in the form (1.2) with $-(1/4\pi)G_1$ for the kernel K.)

It is now a straightforward matter to find the hydrodynamic forces due to the disturbance of the fluid by the body. From Bernoulli's equation the linearized hydrodynamic pressure is

$$p = i\omega\rho\phi e^{-i\omega t}, \tag{2.9}$$

and thus the six forces and moments are

$$F_i = -i\omega\rho e^{-i\omega t} \iint \phi \cos(n, x_i)\, dS, \tag{2.10}$$

where $\cos(n, x_i)$ denotes the direction cosine for $i = 1, 2, 3$ and the generalized direction cosine

$$x_{i-2} \cos(n, x_{i-1}) - x_{i-1} \cos(n, x_{i-2})$$

for $i = 4, 5, 6$. Substituting (2.7) and (2.8) in (2.10) it follows that

$$F_i = F_i^{(WALL)} + F_i^{(FK)} + \frac{1}{4\pi} i\omega\rho\, e^{-i\omega t} \iint dS \cos(n, x_i)$$

$$\times \int_L Q(\xi)\, G_1(x, 0, 0; \xi, 0, 0)\, d\xi, \tag{2.11}$$

where $F_i^{(FK)}$ denotes the "Froude-Krylov" exciting force from the undisturbed incident wave potential ϕ_I. The last term in (2.11) contains all of the free surface effects due to the presence of the body. This can be reduced further by noting that

$$G_1(x, 0, 0; \xi, 0, 0) = -\pi K \{H_0(K|x-\xi|) + Y_0(K|x-\xi|) - 2iJ_0(K|x-\xi|)\}, \tag{2.12}$$

where H_0, Y_0, and J_0 are the Struve function, Bessel function of the second kind, and Bessel function of the first kind, respectively.

One important consequence of (2.11) is that for transverse oscillations (sway, roll, and yaw),

$$F_i = F_i^{(WALL)} + F_i^{(FK)} \qquad (i = 2, 4, 6). \tag{2.13}$$

Of course higher order terms including free surface effects could be retained. In particular the damping coefficients for sway, roll, and yaw can be found fairly easily from the energy flux at infinity (Newman, 1963), in the form

$$\left.\begin{array}{c} B_{22} \\ B_{44} \\ B_{66} \end{array}\right\} = \frac{1}{2\pi} \omega\rho K^3 \int_0^\pi d\theta \sin^2\theta \left| \int_L e^{iKx\cos\theta} \left\{ \begin{array}{c} S(x) + m_{22}(x)/\rho \\ S(x)\, z_0(x) + \frac{1}{12} B^3(x) - m_{24}(x)/\rho \\ \times\; S(x) + m_{22}(x)/\rho \end{array} \right\} dx \right|^2, \tag{2.14}$$

where $m_{22}(x)$ and $m_{24}(x)$ are the two dimensional added mass coefficients of the section for the sway force due to sway and the sway force due to roll, respectively, and for the rigid free surface condition, and where $S(x)$ is the sectional area, $z_0(x)$ is the vertical coordinate of the center of buoyancy at each section, and $B(x)$ is the beam of the section at the waterline. We note that B_{22} and B_{66} are $0(\epsilon^4)$ while $B_{44} = 0(\epsilon^6)$, and as indicated in Table 2, all three are of higher order compared with other terms in the equations of motion.

Pitch and Heave in Head Waves

We shall illustrate the above theory by considering in more detail the important case of pitch and heave motions in head waves. If ζ_3 and ζ_5 denote the (complex) amplitudes of heave and pitch, the boundary condition on the ship hull is

$$\frac{\partial\phi}{\partial n} = \frac{\partial}{\partial n}(\phi_I + \phi_B) = -i\omega\zeta_3 \cos(n,z) + i\omega\zeta_5 \left[x\cos(n,z) - z\cos(n,x)\right], \quad (2.15)$$

or, for the disturbance potential,

$$\begin{aligned}\frac{\partial\phi_B}{\partial n} &= -\omega A \exp\left[K(z+ix)\right]\left[\cos(n,z) + i\cos(n,x)\right] \\ &\quad - i\omega\zeta_3\cos(n,z) + i\omega\zeta_5\left[x\cos(n,z) - z\cos(n,x)\right] \\ &= -\omega\left[Ae^{ikx} + i\zeta_3 - ix\zeta_5\right]\cos(n,z) + 0(\epsilon)\,. \end{aligned}\quad (2.16)$$

The flux function is thus

$$Q(x) = \int_C \frac{\partial\phi_B}{\partial n}\, d\ell = \omega B(x)\left[Ae^{iKx} + i\zeta_3 - ix\zeta_5\right]. \quad (2.17)$$

The wall force $F_i^{(WALL)}$ can be analyzed from classical slender body theory. Thus the potential $\phi^{(WALL)}$ is given by

$$\phi^{(WALL)}(x,y,z) = \phi^{(2D)}(y,z;x) + f^{(WALL)}(x)\,, \quad (2.18)$$

where $\phi^{(2D)}$ is the two-dimensional "strip theory" potential satisfying the boundary condition (2.16) on the contour of the hull section and the rigid wall condition on the free surface, and the interaction term $f^{(WALL)}$ is

$$f^{(WALL)}(x) = -\frac{1}{2\pi}\int_L \log\frac{2|x-\xi|}{L}\,\operatorname{sgn}(x-\xi)\,Q'(\xi)\,d\xi\,. \quad (2.19)$$

From (2.10) the wall force is

$$\begin{aligned} F_i^{(WALL)} &= \int_L dx\, F_i^{(2D)}(x) - i\omega\rho e^{-i\omega t}\iint_S f^{(WALL)}(x)\cos(n,x_i)\,dS \\ &= -\omega^2 e^{-i\omega t}\int_L m_{ii}(x)\,dx - i\omega\rho e^{-i\omega t}\iint_S f^{(WALL)}(x)\cos(n,x_i)\,dS, \end{aligned}\quad (2.20)$$

where $m_{ii}(x)$ is the two-dimensional added mass coefficient with a rigid free surface condition.*

We can now write down the heave force F_3 and pitch moment F_5 from Eqs. (2.11), (2.12), (2.17), (2.19) and (2.20), using Eqs. (A1.3-6) of Appendix I to evaluate the surface integrals. Thus it follows that

$$\begin{pmatrix} F_3 \\ F_5 \end{pmatrix} = -\omega^2 e^{-i\omega t} \int_L m_3(x) \begin{pmatrix} 1 \\ -x \end{pmatrix} \left(\zeta_3 - x\zeta_5 - iAe^{ikx}\right) dx$$

$$- \frac{1}{2\pi} \omega^2 \rho e^{-i\omega t} \int_L \begin{pmatrix} 1 \\ -x \end{pmatrix} B(x) \int_L \log \frac{2|x-\xi|}{L} \operatorname{sgn}(x-\xi)$$

$$\times \frac{d}{d\xi} \left[B(\xi) \left(\zeta_3 - x\zeta_5 - iAe^{ikx}\right)\right] d\xi\, dx$$

$$- \frac{1}{4} \rho g K^2 e^{-i\omega t} \int_L \begin{pmatrix} 1 \\ -x \end{pmatrix} B(x) \int_L B(\xi) \left(\zeta_3 - x\zeta_5 - iAe^{ikx}\right) \left\{ H_0(K|x-\xi|)\right.$$

$$\left. + Y_0(K|x-\xi|) - 2iJ_0(K|x-\xi|)\right\} d\xi\, dx$$

$$+ i\rho g A e^{-i\omega t} \int_L \begin{pmatrix} 1 \\ -x \end{pmatrix} \left[B(x) - KS(x)\right] e^{ikx} dx + O(\epsilon^3)\,, \qquad (2.21)$$

where the last term represents the slender body approximation of the Froude-Krylov exciting force and moment, to second order in ϵ.

The total force and moment will include the hydrodynamic components, represented by (2.21), plus the conventional hydrostatic restoring force and moment (of first order in ϵ) and the inertial force and moment of the ship's own mass (of second order in ϵ). Setting the sum of these equal to zero yields a consistent set of equations of motion, accurate to second order in ϵ. We note that the first order contributions include only the hydrostatic terms plus the first order Froude-Krylov contributions. The solution of this first order system was illustrated in Figs. 1 and 2. There are various second order contributions in Eq. (2.21), each of which is interesting by itself. The first integral gives the "strip theory wall forces" involving the stripwise zero frequency added mass times the relative acceleration, including the incident wave height. The first double integral gives the corresponding "wall" three-dimensional correction to the added mass and exciting force. The second double integral contains the free surface effects, including an added mass contribution from the real part of the kernel $H_0 + Y_0$, and a damping contribution from the imaginary term $-2iJ_0$. Note that in all cases the relative displacement $\zeta_3 - x\zeta_5 - iAe^{ikx}$

*This is not a unique definition by itself. We may say that $m_i(x)$ is the coefficient of the force associated with the pressure $i\omega\rho\phi^{(2D)} e^{-i\omega t}$, and $\phi^{(2D)}$ must be of the form $\phi^{(2D)} \sim C \log(y^2+z^2)/L^2$ as $y^2+z^2 \to \infty$.

between the body and the undisturbed incident wave height is of principal importance; in this way the theory accounts for the diffraction effects, or the correction to the Froude-Krylov exciting force due to the presence of the ship. It is important to note that both double integrals contain truly three-dimensional effects, with the disturbance at one station of the ship (ξ) affecting the force at another (x).

III. FORCED OSCILLATIONS AT FINITE SPEED OF ADVANCE

Introduction

In this portion of the paper we suppose that the ship is being forced to make small oscillations about an equilibrium fixed position, while an otherwise uniform stream U flows past in the positive x direction. These forced oscillations, which need not in general be sinusoidal or even periodic, will be described by given functions of time $\zeta_1(t)$, $\zeta_2(t)$, $\zeta_3(t)$ for the linear displacements in surge, sway and heave, and $\zeta_4(t)$, $\zeta_5(t)$, $\zeta_6(t)$ for the roll, pitch, and yaw angles. Similarly we denote the resulting hydrodynamic force component in the ith mode by $F_i(t)$.

Under the usual control theory assumptions of linearity and causality there will be a linear relationship between F_i and all ζ_j, $j = 1, \ldots 6$, which we may write symbolically as

$$F_i = \sum_{j=1}^{6} C_{ij}\,\zeta_j \tag{3.1}$$

for some set of linear operators C_{ij}. Alternatively (3.1) may be interpreted literally as a linear algebraic relationship between the Fourier transforms of the variables F_i, ζ_j, with coefficients $C_{ij} = C_{ij}(\omega)$ called "transfer functions." Here the Fourier transform of $\zeta_j(t)$ is defined as

$$\zeta_j(\omega) = \int_{-\infty}^{\infty} dt\, e^{i\omega t}\,\zeta_j(t) \tag{3.2}$$

(the use of the same symbol for a function of time and for its Fourier transform is common and convenient, and will not cause confusion). Clearly $C_{ij}(\omega)$ is the Fourier transform of the force $C_{ij}(t)$ in the ith mode due to a unit impulse $\delta(t)$ of displacement in the jth mode, the actual relationship between $\zeta_j(t)$ and $F_i(t)$ being thus a convolution integral with $C_{ij}(t)$ as kernel.

In the case of sinusoidal motion at a real radian frequency ω, the real and imaginary parts of the functions $C_{ij}(\omega)$ define the frequency response of the forces to sinusoidal displacements of unit amplitude. Historically these quantities as used in ship problems have been calculated in the form of "added masses"

$$M_{ij}(\omega) = \mathrm{Re}\left[\frac{C_{ij}(\omega) - C_{ij}(0)}{(-i\omega)^2}\right] \tag{3.3}$$

in phase with the accelerations $(-i\omega)^2 \zeta_j$, and "damping coefficients"

$$B_{ij}(\omega) = \mathrm{Re}\left[\frac{C_{ij}(\omega)}{(-i\omega)}\right] \tag{3.4}$$

in phase with the velocities $(-i\omega)\zeta_j$.

Thus there are three interpretations of the linearity Eq. (3.1). When (3.1) is to be viewed as an operator equation we write $C_{ij} = C_{ij}(\omega)$ but reserve the combination "$-i\omega$" to mean the operator "$\partial/\partial t$." The second interpretation views $C_{ij}(\omega)$ as a transfer function with ω as a (complex) Fourier transform variable, while the third views $C_{ij}(\omega)$ as the frequency response for real ω. The following analysis may be given any of the three interpretations although it is mainly expressed in the language of the second of them; that is, we seek a set of 36 complex valued transfer functions $C_{ij}(\omega)$ of the complex variable ω. However, in practice one need calculate the C_{ij} only for real ω, so that added masses and damping coefficients would be obtained directly, as in the third interpretation.

Evaluation of the Velocity Potential Near the Ship

Firstly let us linearize with respect to the amplitudes $\zeta_j(t)$ of motion, which are assumed to be small of order α, for some small parameter α which measures the general size of the motions. Thus we expand the velocity potential in the form

$$\phi = \phi_{(0)}(x,y,z) + \phi_{(1)}(x,y,z,t) + \phi_{(2)}(x,y,z,t) + \ldots , \tag{3.5}$$

where $\phi_{(0)}$ is the steady flow due to a uniform stream U past the ship <u>fixed</u> in its equilibrium position, while $\phi_{(1)} = O(\alpha)$ is the first approximation to the unsteady potential for small oscillations of order α about this position. Further terms $\phi_{(2)} \ldots$ describe non-linear effects due to not-so-small oscillations and will not be investigated in this paper.

Now if the ship is slender, each of the potentials $\phi_{(0)}, \phi_{(1)}, \ldots$ may be further expanded in terms of the slenderness parameter ϵ, in a manner typified by the expansion of the steady term $\phi_{(0)}$ which has been obtained previously (Tuck, 1964). Thus near the ship we can write

$$\phi_{(0)} = Ux + \left[\phi_{(0)}^{(WALL)}(x,y,z) + f_{(0)}^{(FS)}(x)\right] + O(\epsilon^3 \log^2 \epsilon) , \tag{3.6}$$

where the term "Ux" represents the free stream and is of zero order in ϵ, while the contents of the square brackets are of order $\epsilon^2 \log \epsilon$ and represent the steady disturbance to the stream due to the presence of a fixed ship. This disturbance potential is of the class described in Part I, and the terms "$\phi_{(0)}^{(WALL)}$" and "$f_{(0)}^{(FS)}$" have the significance discussed after Eq. (1.1).

The "wall" potential can itself be further decomposed into

$$\phi_{(0)}^{(WALL)}(x,y,z) = \phi_{(0)}^{(2D)}(y,z;x) + f_{(0)}^{(WALL)}(x), \tag{3.7}$$

where, for constant x, $\phi_{(0)}^{(2D)}$ satisfies the two dimensional Laplace equation with respect to y and z. Both terms $f_{(0)}^{(WALL)}$ and $f_{(0)}^{(FS)}$ represent interactions between sections of the ship and were determined explicitly in Tuck, 1964, in the form

$$f_{(0)}^{(WALL)} = \int_{-\infty}^{\infty} d\xi\, K_{(0)}^{(WALL)}(x-\xi)\, US'(\xi), \tag{3.8}$$

$$f_{(0)}^{(FS)} = \int_{-\infty}^{\infty} d\xi\, K_{(0)}^{(FS)}(x-\xi)\, US'(\xi), \tag{3.9}$$

with

$$K_{(0)}^{(WALL)}(x) = -\frac{1}{2\pi}\frac{d}{dx}\left[\operatorname{sgn} x \log 2|x|\right], \tag{3.10}$$

$$K_{(0)}^{(FS)}(x) = -\frac{1}{4}\frac{d}{dx}\left[H_0\left(\frac{gx}{U^2}\right) + (2+\operatorname{sgn} x)\, Y_0\left(\left|\frac{gx}{U^2}\right|\right)\right]. \tag{3.11}$$

The above results are in the form of Eq. (1.2), since "$US'(\xi)$" is the flux through the cross section at ξ due to the steady motion, $S(\xi)$ being the immersed area of the cross section.

Now a similar analysis holds for the linear unsteady potential $\phi_{(1)}$ which can be written as

$$\phi_{(1)}(x,y,z,t) = \phi_{(1)}^{(WALL)}(x,y,z,t) + f_{(1)}^{(FS)}(x,t) + O(\epsilon^2 \log \epsilon), \tag{3.12}$$

with the wall potential further decomposed into

$$\phi_{(1)}^{(WALL)}(x,y,z,t) = \phi_{(1)}^{(2D)}(x,y,z,t) + f_{(1)}^{(WALL)}(x,t) \tag{3.13}$$

if desired. The interaction terms $f_{(1)}^{(WALL)}$ and $f_{(1)}^{(FS)}$ are not now simply related to the area curve as in (3.8) and (3.9) but, since the unsteady flow is produced by linear oscillations of the ship, will be linear functions of the magnitude of these motions. Thus we can write

$$f_{(1)}^{(FS)} = \sum_{j=1}^{6} f_j \zeta_j , \tag{3.14}$$

with $f_j = f_j(x, \omega)$ as the transfer function between motion in the jth mode and the free surface interaction potential at station x. A similar relationship would hold for the wall interaction $f_{(1)}^{(WALL)}$, which is not of interest to us in the present work.

The free surface interaction transfer functions f_j are obtained in Appendices I and II by the use of the hull boundary condition, the result being again in the form of Eq. (1.2), i.e.,

$$f_j = \int_{-\infty}^{\infty} d\xi \, K_{(1)}(x-\xi) \, Q_j(\xi) , \tag{3.15}$$

where

$$\begin{aligned}
Q_1(x) &= -\left(-i\omega + U\frac{d}{dx}\right) S'(x) \\
Q_2(x) &= 0 \\
Q_3(x) &= -\left(-i\omega + U\frac{d}{dx}\right) B(x) \\
Q_4(x) &= 0 \\
Q_5(x) &= +\left(-i\omega + U\frac{d}{dx}\right) x\,B(x) \\
Q_6(x) &= 0
\end{aligned} \tag{3.16}$$

are flux transfer functions, and $K_{(1)}$ is an absolute kernel independent of hull geometry and defined by

$$K_{(1)}(x) = \frac{1}{2\pi^2} \int_{-\infty}^{\infty} dk \, e^{-ikx} \beta(k) \coth \beta(k) , \tag{3.17}$$

where

$$\cosh \beta(k) = \frac{(-i\omega - ikU)^2}{g|k|}$$

(for the case ω real, see Eq. (A3.6)).

The kernel $K_{(1)}(x)$ depends on the frequency ω and speed U as parameters as well as the variable x, and will sometimes be written $K_{(1)}(x, \omega, U)$ to emphasize this. In particular for $U=0$, $K_{(1)}$ reduces to the zero speed kernel of Part II, Eq. (2.12), i.e.,

$$K_{(1)}(x,\omega,0) = -\frac{1}{4}\frac{\omega^2}{g}\left[H_0\left(\left|\frac{\omega^2 x}{g}\right|\right) + Y_0\left(\left|\frac{\omega^2 x}{g}\right|\right) - 2iJ_0\left(\left|\frac{\omega^2 x}{g}\right|\right)\right]. \tag{3.18}$$

On the other hand, for zero frequency, $K_{(1)}$ reduces (as it must) to the steady kernel $K_{(0)}^{(FS)}$ of Eq. (3.11), i.e.,

$$K_{(1)}(x,0,U) = -\frac{1}{4}\frac{d}{dx}\left[H_0\left(\frac{gx}{U^2}\right) + (2+\operatorname{sgn} x)\, Y_0\left(\left|\frac{gx}{U^2}\right|\right)\right]. \tag{3.19}$$

For non-zero values of ω and U, $K_{(1)}$ has not yet been tabulated, and further work is needed to investigate the properties of this function. We may note that by a suitable non-dimensionalization $K_{(1)}(x,\omega,U)$ may be expressed as a function of two dimensionless variables only, for instance

$$K_{(1)}(x,\omega,U) = \frac{\omega^2}{g},\ \text{function of}\ \left(\frac{\omega^2 x}{g},\ \frac{\omega U}{g}\right).$$

It is easy to see that $K_{(1)}$ has the familiar singularity when $\omega U/g = 1/4$, which may complicate the task of numerical evaluation of the kernel.

Pressure Calculation

From Bernoulli's equation the hydrodynamic portion of the pressure field is

$$p = -\rho\left[-i\omega\phi + \frac{1}{2}|\nabla\phi|^2 - \frac{1}{2}U^2\right] \tag{3.20}$$

(here "$-i\omega$" may best be interpreted simply as the operator "$\partial/\partial t$"), which gives on expanding with respect to α that

$$p = -\rho\left[\frac{1}{2}|\nabla\phi_{(0)}(x,y,z)|^2 - \frac{1}{2}U^2 - i\omega\phi_{(1)} + \nabla\phi_{(0)}(x,y,z) \cdot \nabla\phi_{(1)}(x,y,z,t) + O(\alpha^2)\right],$$

that is,

$$p = p_{(0)}(x,y,z) + p_{(1)}(x,y,z,t) + \dots,$$

where $p_{(0)}$ is the steady pressure field

$$p_{(0)} = -\rho\left[\frac{1}{2}|\nabla\phi_0|^2 - \frac{1}{2}U^2\right], \tag{3.21}$$

while $p_{(1)}$ is the term of first order in α, namely

$$p_{(1)} = -\rho\left[-i\omega\phi_{(1)} + \nabla\phi_{(0)} \cdot \nabla\phi_{(1)}\right] . \tag{3.22}$$

Equations (3.21) and (3.22) give the steady and linear unsteady pressure fields for an arbitrary body. Now if the body is slender, both pressures may be consistently approximated in the form

$$p_{(0)} = p_{(0)}^{(WALL)}(x, y, z) + p_{(0)}^{(FS)}(x) \tag{3.23}$$

$$p_{(1)} = p_{(1)}^{(WALL)}(x, y, z, t) + p_{(1)}^{(FS)}(x, t) , \tag{3.24}$$

as was done for the potentials. We shall not write down the "wall" pressures, which are not required for the present analysis; the free surface contributions are

$$p_{(0)}^{(FS)} = -\rho U f_{(0)}^{(FS)\prime}(x) \tag{3.25}$$

$$p_{(1)}^{(FS)} = -\rho\left(-i\omega + U\frac{\partial}{\partial x}\right) f_{(1)}^{(FS)}(x, t) . \tag{3.26}$$

These formulas give the free surface dependent part of the pressure everywhere in the field of flow. In particular from (3.14) we can express the unsteady pressure field as a sum of contributions from each mode of motion, with appropriate transfer functions.

In order to find the forces on the ship we require the pressure on the instantaneous hull surface. This is obtained by evaluating the pressure on the equilibrium hull surface and adding a correction term to account for the displacement of the ship in the non-uniform steady flow field. Thus if $p_{(1)}$ now denotes the unsteady pressure evaluated on the equilibrium hull surface, then the unsteady pressure on the actual hull is

$$p_{(1)} + \underline{\alpha} \cdot \nabla p_{(0)} + O(\alpha^2) ,$$

where $\underline{\alpha}$ is the vector displacement of the hull at any point. In particular the correction to the FS part of the pressure is

$$\underline{\alpha} \cdot \nabla p_{(0)}^{(FS)}(x) = \zeta_1 \frac{\partial}{\partial x} p_{(0)}^{(FS)}(x)$$

$$= -\zeta_1 U f_{(0)}^{(FS)\prime\prime}(x) , \tag{3.27}$$

where $\zeta_1(t)$ is the surge displacement (note from (A2.1) that the x component of $\underline{\alpha}$ also contains terms involving the pitch and yaw angles $\zeta_5(t)$ and $\zeta_6(t)$, but these contributions are negligibly small in ϵ compared with other retained terms). Thus the only contribution from this correction is in surge excited motion, and we can write for the pressure on the actual hull

$$p_{(1)}^{(FS)} = \sum_{j=1}^{6} p_j \zeta_j , \tag{3.28}$$

where the pressure transfer functions $p_j = p_j(x, \omega)$ are given by

$$p_1 = -\rho\left(-i\omega + U\frac{\partial}{\partial x}\right) f_1 - \rho U f_{(0)}^{(FS)\prime\prime}(x) ,$$
$$p_j = -\rho\left(-i\omega + U\frac{\partial}{\partial x}\right) f_j , \quad j = 2, 3, \ldots, 6 , \tag{3.29}$$

and where the f_j are those of Eq. (3.. ¯).

Forces and Moments

The forces and moments now follow directly by integrations over the hull from the formulas

$$\underline{i} F_1 + \underline{j} F_2 + \underline{k} F_3 = -\iint p \, \underline{n} \, dS$$
$$\underline{i} F_4 + \underline{j} F_5 + \underline{k} F_6 = -\iint p \, \underline{r} \times \underline{n} \, dS . \tag{3.30}$$

The splitting up of the pressure p into a wall and a free surface part leads to a similar splitting of the forces, viz.,

$$F_i = F_i^{(WALL)} + F_i^{(FS)} \tag{3.31}$$

for all $i = 1, \ldots 6$. But since $p_{(1)}^{(FS)}$ is a function of x (and time) only, the results of Appendix I, Eqs. (A1.3) and (A1.4), may be used to show that

$$F_1^{(FS)} = \int dx \, S'(x) \, p_{(1)}^{(FS)}(x, t)$$
$$F_2^{(FS)} = 0$$
$$F_3^{(FS)} = \int dx \, B(x) \, p_{(1)}^{(FS)}(x, t)$$
$$F_4^{(FS)} = 0 \tag{3.32}$$
$$F_5^{(FS)} = -\int dx \, x \, B(x) \, p_{(1)}^{(FS)}(x, t)$$
$$F_6^{(FS)} = 0 .$$

Now we view the force in each mode as the sum of contributions from displacements in all modes, with transfer functions c_{ij} as in Eq. (3.1), putting for the free surface portions:

$$F_i^{(FS)} = \sum_{j=1}^{6} c_{ij}^{(FS)} \zeta_j . \tag{3.33}$$

Thus

$$\begin{aligned}
c_{1j}^{(FS)} &= \int dx\, S'(s)\; p_j(x,\omega) \\
c_{2j}^{(FS)} &= 0 \\
c_{3j}^{(FS)} &= \int dx\, B(x)\; p_j(x,\omega) \\
c_{4j}^{(FS)} &= 0 \\
c_{5j}^{(FS)} &= -\int dx\, x\, B(x)\; p_j(x,\omega) \\
c_{6j}^{(FS)} &= 0 .
\end{aligned} \tag{3.34}$$

In terms of the f_j of Eq. (3.15), the non-zero $c_{ij}^{(FS)}$ are

$$\begin{aligned}
c_{11}^{(FS)} &= -\rho\int dx\; S'(x)\left(-i\omega + U\frac{\partial}{\partial x}\right) f_1 - \rho U\int dx\; S'(x)\; f_{(0)}^{(FS)\prime\prime}(x) \\
c_{13}^{(FS)} &= -\rho\int dx\; S'(x)\left(-i\omega + U\frac{\partial}{\partial x}\right) f_3 \\
c_{15}^{(FS)} &= -\rho\int dx\; S'(x)\left(-i\omega + U\frac{\partial}{\partial x}\right) f_5 \\
c_{31}^{(FS)} &= -\rho\int dx\; B(x)\left(-i\omega + U\frac{\partial}{\partial x}\right) f_1 - \rho U\int dx\; B(x)\; f_{(0)}^{(FS)\prime\prime}(x) \\
c_{33}^{(FS)} &= -\rho\int dx\; B(x)\left(-i\omega + U\frac{\partial}{\partial x}\right) f_3 \\
c_{35}^{(FS)} &= -\rho\int dx\; B(x)\left(-i\omega + U\frac{\partial}{\partial x}\right) f_5 \\
c_{51}^{(FS)} &= \rho\int dx\, x\, B(x)\left(-i\omega + U\frac{\partial}{\partial x}\right) f_1 + \rho U\int dx\, x\, B(x)\; f_{(0)}^{(FS)\prime\prime}(x)
\end{aligned} \tag{3.35 (Cont.)}$$

$$C_{53}^{(FS)} = \rho \int dx\, xB(x) \left(-i\omega + U \frac{\partial}{\partial x}\right) f_3$$
$$C_{55}^{(FS)} = \rho \int dx\, xB(x) \left(-i\omega + U \frac{\partial}{\partial x}\right) f_5 . \tag{3.35}$$

Finally, using the convolution integral representations (3.9) and (3.15) for $f_{(0)}^{(FS)}$ and f_j respectively, we have

$$C_{11}^{(FS)} = \rho \iint dx\, d\xi\; S'(x)\; S'(\xi)\; [\underline{K}(x-\xi,\omega,U) - \underline{K}(x-\xi,0,U)]$$
$$C_{13}^{(FS)} = \rho \iint dx\, d\xi\; S'(x)\; B(\xi)\; \underline{K}(x-\xi,\omega,U)$$
$$C_{15}^{(FS)} = -\rho \iint dx\, d\xi\; S'(x)\; \xi B(\xi)\; \underline{K}(x-\xi,\omega,U)$$
$$C_{31}^{(FS)} = \rho \iint dx\, d\xi\; B(x)\; S'(\xi)\; [\underline{K}(x-\xi,\omega,U) - \underline{K}(x-\xi,0,U)]$$
$$C_{33}^{(FS)} = \rho \iint dx\, d\xi\; B(x)\; B(\xi)\; \underline{K}(x-\xi,\omega,U) \tag{3.36}$$
$$C_{35}^{(FS)} = -\rho \iint dx\, d\xi\; B(x)\; \xi B(\xi)\; \underline{K}(x-\xi,\omega,U)$$
$$C_{51}^{(FS)} = -\rho \iint dx\, d\xi\; xB(x)\; S'(\xi)\; [\underline{K}(x-\xi,\omega,U) - \underline{K}(x-\xi,0,U)]$$
$$C_{53}^{(FS)} = -\rho \iint dx\, d\xi\; xB(x)\; B(\xi)\; \underline{K}(x-\xi,\omega,U)$$
$$C_{55}^{(FS)} = \rho \iint dx\, d\xi\; xB(x)\; \xi B(\xi)\; \underline{K}(x-\xi,\omega,U) ,$$

where

$$K(x,\omega,U) = \left(-i\omega + U \frac{\partial}{\partial x}\right)^2 K_{(1)}(x,\omega,U) . \tag{3.37}$$

This $\underline{K}$ is the kernel for all heave and pitch motions, but for surge induced motions the kernel is

$$\left(\underline{K} - \lim_{\omega \to 0} \underline{K}\right),$$

the additional correction being only of importance for non-zero forward speed and arising from the correction (3.27) to the pressure field due to displacement of the ship in the steady flow field. But we can easily see that without this correction the results for (say) $C_{11}^{(FS)}$ would be nonsensical, for as $\omega \to 0$, $C_{11}^{(FS)}$ must represent the restoring force in surge (i.e., change in wave resistance) due to a unit lengthwise displacement of the ship, and this is clearly zero. On the other hand, if $j \neq 1$ then $C_{ij}^{(FS)}$ does not in general vanish at zero frequency and yields for $\omega \to 0$ the trim forces and moments on the ship in steady motion. Since in evaluating added masses by (3.3) we must in any case subtract off these trim forces $C_{ij}(0)$, the kernel

$$"\underline{K} - \lim_{\omega \to 0} \underline{K}"$$

may be used for all $C_{ij}^{(FS)}$ whenever trim forces are not required.

At non-zero frequencies ω of purely sinusoidal motion we can split the 9 Eqs. (3.36) into their real and imaginary parts yielding 18 added masses and damping coefficients from Eqs. (3.3) and (3.4). In order to compute these 18 quantities we require just two functions $S(x)$ and $B(x)$ describing the geometry of the ship and one universal kernel function $\underline{K}(x, \omega, U)$ which can be computed once and for all. Of course the complete added masses and damping coefficients are the sum of the "wall" values plus the values obtained from Eqs. (3.36), but the determination of the former is, as described in Part I, a much less difficult task.

For the lateral modes of sway, roll, and yaw, where i or j takes the values 2, 4 or 6, the $C_{ij}^{(FS)}$ vanish, so that the remaining 54 added masses and damping coefficients are dominated by the "wall" values. Since the latter are frequency independent, this conclusion is equivalent to the conclusion that all lateral and damping coefficients are independent of frequency, to leading order in slenderness. Any frequency dependence must come from higher approximations in ϵ.

ACKNOWLEDGMENTS

The authors wish to thank Mr. Werner Frank and Miss Evelyn Woolley, who developed the computer programs used for the zero speed calculations.

REFERENCES

Newman, J. N., 1963, "Lectures on the Theory of Slender Ships," Unpublished notes, Department of Naval Architecture, Berkeley, California.

Newman, J. N., 1964, "A Slender Body Theory for Ship Oscillations in Waves," Journal of Fluid Mechanics, Vol. 8, Part 4, pp. 602-18.

Timman, R., and Newman, J. N., 1962, "The Coupled Damping Coefficients of a Symmetric Ship," Journal of Ship Research," Vol. 5, No. 4, Reprinted as David Taylor Model Basin Report 1672.

Tuck, E. O., 1964, "On Line Distributions of Kelvin Sources," Journal of Ship Research, Vol. 8, No. 2.

Vossers, G., 1962, "Some Applications of the Slender Body Theory in Ship Hydrodynamics," Unpublished Thesis, Delft.

Wehausen, J. V., and Laitone, E. V., 1961, "Handbuch der Physik," Vol. 9, Surface Waves, Berlin:Springer-Verlag.

APPENDIX I

SOME GEOMETRICAL IDENTITIES

Gauss's theorem applied to a closed surface consisting of the immersed hull surface S, together with the waterplane, indicates that

$$\iint_S p\,\underline{n}\,dS = \iiint_{\substack{\text{interior}\\ \text{of hull}}} \underline{\nabla} p\,dx\,dy\,dz - \iint_{\substack{\text{water}\\ \text{plane}}} p\,\underline{k}\,dx\,dy \tag{A1.1}$$

and

$$\iint p\,\underline{r}\times\underline{n}\,dS = \iiint \underline{r}\times\underline{\nabla} p\,dx\,dy\,dz - \iint p(y\underline{i} - x\underline{j})\,dx\,dy\,, \tag{A1.2}$$

for any sufficiently regular scalar $p(x,y,z)$, $\underline{n}$ being the outward unit normal and $\underline{r}$ the position vector $x\underline{i} + y\underline{j} + z\underline{k}$. The following identities are obtained from the above for some simple special choices of the function $p(x,y,z)$:

$$\iint p(x)\,\underline{n}\,dS = \int dx\;p(x)\left[\underline{i}(-S'(x)) + \underline{k}(-B(x))\right] \tag{A1.3}$$

$$\iint p(x)\,\underline{r}\times\underline{n}\,dS = \int dx\;p(x)\left[\underline{j}\left(xB(x) - \frac{d}{dx}\iint z\,dy\,dz\right)\right] \tag{A1.4}$$

$$\iint p(x)\;z\underline{n}\,dS = \int dx\;p(x)\left[\underline{i}\left(-\frac{d}{dx}\iint z\,dy\,dz\right) + \underline{k}S(x)\right] \tag{A1.5}$$

$$\iint p(x)\;z\,\underline{r}\times\underline{n}\,dS = \int dx\;p(x)\left[\underline{j}\left(-x\,S(x) - \frac{d}{dx}\iint z^2\,dy\,dz\right)\right] \tag{A1.6}$$

$$\iint p(x)\;y\,\underline{n}\,dS = \int dx\;p(x)\left[\underline{j}\,S(x)\right] \tag{A1.7}$$

$$\iint p(x)y\,\underline{r}\times\underline{n}\,dS = \int dx\;p(x)\left[\underline{i}\left(-\iint z\,dy\,dz - \frac{1}{12}B^3(x)\right.\right.$$
$$\left.\left. + \underline{k}\quad x\,S(x) + \frac{d}{dx}\iint y^2\,dy\,dz\right)\right]. \tag{A1.8}$$

For instance, to prove (A1.3) we note that

$$\iiint\limits_{\substack{\text{interior}\\\text{of}\\\text{hull}}} \nabla p(x)\, dx\, dy\, dz = \underline{i} \int\limits_{\substack{\text{length}\\\text{of}\\\text{ship}}} dx\, p'(x) \cdot \iint\limits_{\substack{\text{cross}\\\text{section}\\\text{at } x}} dy\, dz$$

$$= \underline{i} \int dx\; p'(x)\; S(x)$$

$$= -\underline{i} \int dx\; p(x)\; S'(x)\,,$$

where $S(x)$ is the area of the cross section at x and is for the last step assumed to vanish at both ends of the ship. On the other hand

$$-\underline{k} \iint\limits_{\substack{\text{water-}\\\text{plane}}} p(x)\, dx\, dy = -\underline{k} \int\limits_{\substack{\text{length}\\\text{of}\\\text{ship}}} dx\; p(x) \cdot \int\limits_{\substack{\text{width of}\\\text{waterplane}\\\text{at } x}} dy$$

$$= -\underline{k} \int dx\; p(x)\; B(x)\,,$$

where $B(x)$ is the waterplane beam at station x. The remaining identities (A1.4) to (A1.8) may be proved similarly.

The above identities are exact for a hull of arbitrary shape (providing it is symmetrical with respect to y) and for an arbitrary function $p(x)$. Their principal use, of course, is for evaluating the forces and moments on a slender ship, in which case $p(x)$, $z\,p(x)$, $y\,p(x)$, will be identified as terms in a Taylor series for the pressure on the hull. In addition, if the ship is slender, some of the terms in (A1.3) to (A1.8) may be dropped to a consistent order of approximation in ϵ. For instance, in (A1.4) the term

$$-\frac{d}{dx} \iint z\, dy\, dz$$

is of order ϵ^3 whereas $xB(x)$ is of order ϵ; the former will be neglected when (A1.4) is used in obtaining (2.21) and (3.32). Equations (A1.7) and (A1.8) are used to obtain the sway, roll and yaw damping coefficients (2.14).

It was not necessary to use explicit representations of the components of the unit normal $\underline{n}$ in the above, but for later reference we now derive these using a particular equation

$$z = Z(x, y)$$

describing the hull. Clearly then

$$\underline{n} = (\underline{i}\, Z_x + \underline{j}\, Z_y - \underline{k}) \left(1 + Z_x^2 + Z_y^2\right)^{-1/2}.$$

Also since in terms of this hull equation the magnitude of the element of surface area is

$$dS = dx\,dy\left(1 + Z_x^2 + Z_y^2\right)^{1/2},$$

we have for the outward vector element of surface area

$$\underline{n}\,dS = (\underline{i}\,Z_x + \underline{j}\,Z_y - \underline{k})\,dx\,dy\,.$$

This may be written in a manner not dependent on the choice $z = Z(x, y)$ of hull equation, viz.

$$\underline{n}\,dS = dx\left[\underline{i}\,\frac{\partial}{\partial x}(z\,dy) + \underline{j}\,dz - \underline{k}\,dy\right], \tag{A1.9}$$

where dy and $dz = Z_y\,dy$ denote components of arc length along the cross section curve. The area of a vertical strip from the free surface to the cross section curve is $-z\,dy$ so that the x component of $\underline{n}\,dS$ represents the decrease in the area of this strip in passing from station x to station $x + dx$. The integral identities (A1.3) to (A1.8) may also be proved directly using the expression (A1.9) for $\underline{n}\,dS$, but appear to be more easily derivable from Gauss's theorem, as indicated above.

APPENDIX II

EVALUATION OF FLUX TRANSFER FUNCTIONS Q_j AT FINITE SPEED

The hull boundary condition for $\phi_{(1)}$, on an arbitrary body with unit normal $\underline{n}$ at a point where the hull displacement is

$$\underline{\alpha} = \left[\underline{i}\,\zeta_1(t) + \underline{j}\,\zeta_2(t) + \underline{k}\,\zeta_3(t)\right] + \left[\underline{i}\,\zeta_4(t) + \underline{j}\,\zeta_5(t) + \underline{k}\,\zeta_6(t)\right] \times \underline{r}\,, \tag{A2.1}$$

can be written

$$\frac{\partial \phi_{(1)}}{\partial n} = \underline{n} \cdot \left[-i\omega\underline{\alpha} + \underline{\nabla} \times (\underline{\alpha} \times \underline{\nabla}\phi_{(0)})\right] \tag{A2.2}$$

(Timman and Newman, 1962). The second term inside the square brackets gives the induced normal velocity due to non-uniformity of the steady flow $\phi_{(0)}$ in which the body oscillates. On separating out the contributions due to each mode $\zeta_j(t)$, $j = 1, \ldots 6$, we can write (A2.2) as

$$\frac{\partial \phi_{(1)}}{\partial n} = \sum_{j=1}^{6} g_j(\omega)\,\zeta_j\,. \tag{A2.3}$$

where the hull velocity transfer functions $g_j(\omega)$ are given by

$$\underline{i}\, g_1 + \underline{j}\, g_2 + \underline{k}\, g_3 = -i\omega \underline{n} - \frac{\partial}{\partial n} \underline{\nabla}\phi_{(0)}$$

$$\underline{i}\, g_4 + \underline{j}\, g_5 + \underline{k}\, g_6 = \underline{r} \times (\underline{i}\, g_1 + \underline{j}\, g_2 + \underline{k}\, g_3) - \underline{n} \times \underline{\nabla}\phi_{(0)} . \tag{A2.4}$$

No slenderness assumptions have been made up to this point and the boundary condition (A2.3) is still valid for an arbitrary rigid body making arbitrary small motions in an arbitrary steady field $\phi_{(0)}$.

Now if the ship is slender $\underline{n}$ lies nearly in cross-sectional planes (or, more accurately, from (A1.9) we see that $n_1 = 0(\epsilon)\, n_2 = 0(\epsilon)\, n_3$) so that the g_j may be consistently approximated in the form

$$g_1 = -i\omega n_1 - \left(n_2 \frac{\partial}{\partial y} + n_3 \frac{\partial}{\partial z}\right) \phi^{(2D)}_{(0)_x}$$

$$g_2 = -i\omega n_2 - \left(n_2 \frac{\partial}{\partial y} + n_3 \frac{\partial}{\partial z}\right) \phi^{(2D)}_{(0)_y}$$

$$g_3 = -i\omega n_3 - \left(n_2 \frac{\partial}{\partial y} + n_3 \frac{\partial}{\partial z}\right) \phi^{(2D)}_{(0)_z} \tag{A2.5}$$

$$g_4 = y g_3 - z g_2 - \left(n_2 \frac{\partial}{\partial z} + n_3 \frac{\partial}{\partial y}\right) \phi^{(2D)}_{(0)}$$

$$g_5 = -x g_3 - U n_3$$

$$g_6 = x g_2 + U n_2$$

all with error a factor $1 + 0\,(\epsilon \log \epsilon)$ which is mainly due to the replacement of $\phi_{(0)}$ by its slender body approximation $Ux + \phi^{(2D)}_{(0)} + f^{(WALL)}_{(0)} + f^{(FS)}_{(0)}$ from (3.6) and (3.7); of these terms only $\phi^{(2D)}_{(0)}$ contributes to the g_j. Notice that in the expression for g_1 we have used the slender body approximation to the boundary condition for $\phi_{(0)}$, namely

$$\left(n_2 \frac{\partial}{\partial y} + n_3 \frac{\partial}{\partial z}\right) \phi^{(2D)}_{(0)} = -Un_1 .^{*} \tag{A2.6}$$

Notice also that the surge and roll velocity transfer functions g_1 and g_4 are smaller by a factor $0(\epsilon)$ than the other g_j, since a slender body is an inefficient exciter of motion in these modes.

*Recent investigation has shown that Eq. (A2.6) cannot legitimately be used to simplify g_1. The resulting values for the fluxes Q_1, Q_4 in these modes are unchanged, although the given derivation for Q_1 is no longer valid.

Now as a consequence of slenderness, $\partial\phi_{(1)}/\partial n$ as given by (A2.3) with the g_j of (A2.5), is the normal velocity across the cross-sectional curve in planes normal to the x axis. Hence, the net flux across this curve may be calculated in the form

$$Q_{(1)}dx = \int \frac{\partial\phi_{(1)}}{\partial n}\, dS = \sum_{j=1}^{6} \left(\int g_j\, dS\right)$$

$$= dx \sum_{j=1}^{6} Q_j \zeta_j , \tag{A2.7}$$

where

$$Q_j\, dx = \int g_j\, dS$$

is the flux transfer function for the jth mode, the integration proceeding around the equilibrium hull cross section curve beneath the plane $z = 0$, with dS obtained from (A1.9). Thus

$$Q_1 = \left(-i\omega + U\frac{\partial}{\partial x}\right)\frac{\partial}{\partial x}\int z\, dy$$

$$= -\left(-i\omega + U\frac{\partial}{\partial x}\right) S'(x) ,$$

where $S(x) = -\int z\, dy$ is the area of cross section below the equilibrium free surface $z = 0$.

$$Q_2 = -i\omega\int dz - \int\left(dz\, \phi^{(2D)}_{(0)_{yy}} - dy\, \phi^{(2D)}_{(0)_{yz}}\right) .$$

But since $\phi^{(2D)}_{(0)}$ satisfies the 2D Laplace equation

$$\phi^{(2D)}_{(0)_{yy}} + \phi^{(2D)}_{(0)_{zz}} = 0 ,$$

$$Q_2 = -i\omega[z]_{z=0} + \int\left(dz\, \phi^{(2D)}_{(0)_{zz}} + dy\, \phi^{(2D)}_{(0)_{yz}}\right)$$

$$= -i\omega[z]_{z=0} + \left[\phi_{(0)_z}\right]_{z=0} , \tag{A2.8}$$

where $[\ ]_{z=0}$ indicates that the difference between the values of the enclosed quantities at the two points of intersection of the cross section with the free surface is to be taken. But $\phi^{(2D)}_{(0)}$ is by definition the 2D double body potential, i.e., $\phi^{(2D)}_{(0)_z} = 0$ on $z = 0$, so that

$$[z]_{z=0} = \left[\phi^{(2D)}_{(0)_z}\right]_{z=0} = 0\,,$$

and thus, from (A2.8), $Q_2 = 0$.

Similarly

$$Q_3 = i\omega[y]_{z=0} - \left[\phi^{(2D)}_{(0)_y}\right]_{z=0}.$$

But now if the waterline of the ship is described by

$$y = \pm\frac{1}{2}B(x)\,,$$

then $[y]_{z=0} = B(x)$. Also it is clear that the boundary condition (A2.6) for $\phi^{(2D)}_{(0)}$ reduces to

$$\phi^{(2D)}_{(0)_y} = \pm\frac{1}{2}UB'(x)$$

at the free surface $z = 0$; i.e.,

$$\left[\phi^{(2D)}_{(0)_y}\right]_{z=0} = UB'(x)\,.$$

Thus

$$\begin{aligned} Q_3 &= +\,i\omega B(x) - UB'(x) \\ &= -\left(-i\omega + U\frac{\partial}{\partial x}\right)B(x)\,. \end{aligned}$$

Now

$$\begin{aligned} Q_4 &= i\omega\int y\,dy + i\omega\int z\,dz - \int dz\,\phi^{(2D)}_{(0)_z} - \int dy\,\phi^{(2D)}_{(0)_y} \\ &= \frac{1}{2}i\omega\left[y^2+z^2\right]_{z=0} - \left[\phi^{(2D)}_{(0)}\right]_{z=0} \\ &= 0\,, \end{aligned}$$

provided the ship (and hence the steady flow $\phi^{(2D)}_{(0)}$) has transverse symmetry, which is the case of interest.

Finally, by similar reasoning to that for Q_2, Q_3, we have that

$$Q_5 = \left(-i\omega + U \frac{\partial}{\partial x}\right) xB(x) ,$$

$$Q_6 = 0 .$$

These Q_j, $j = 1, \ldots 6$, are reproduced in Eq. (3.16) of the text. Note that the dominant flux transfer functions are those for heave and pitch, for which Q_3 and Q_5 are of the order of $B(x)$, i.e., $O(\epsilon)$. The flux in surge is of order $S'(x)$, i.e., $O(\epsilon^2)$, while the flux in transverse modes of sway, roll and yaw vanishes.

APPENDIX III

EVALUATION OF THE KERNEL FUNCTION $K_{(1)}$ AT FINITE SPEED

Now at any finite distance from the ship (i.e., such that $y^2 + z^2$ is large compared with the small lateral dimensions of the slender ship) the effect of the motions of the ship for vanishing slenderness is that of a line distribution of sources of strength $Q_{(1)}$ per unit length. These sources are "wave sources," i.e., ordinary sources modified to satisfy the linearized free surface condition

$$g \frac{\partial \phi}{\partial z} + \left(-i\omega + U \frac{\partial}{\partial x}\right)^2 \phi = 0 \quad \text{on} \quad z = 0 . \tag{A3.1}$$

This potential may be obtained from well-known results on such wave sources (e.g., Wehausen and Laitone, 1961). One way of writing the source potential is in the form of a Fourier transform with respect to x, putting

$$\phi_{(1)}(x, y, z, t) = \int_{-\infty}^{\infty} dk\, e^{-ikx} \phi^*_{(1)}(k; y, z, t)$$

$$Q_{(1)}(x, t) = \int_{-\infty}^{\infty} dk\, e^{-ikx} Q^*_{(1)}(k; t) ,$$

etc., where we have for the Fourier transformed potential $\phi^*_{(1)}$,

$$\phi^*_{(1)} = \frac{1}{\pi} Q^*_{(1)} \left[-K_0\left(|k| \sqrt{y^2 + z^2}\right) + \frac{1}{2} (-i\omega - ikU)^2 \int_{-\infty}^{\infty} \frac{d\lambda\, e^{-i\lambda y + z\sqrt{k^2+\lambda^2}}}{\sqrt{k^2+\lambda^2}\; g\sqrt{k^2+\lambda^2} + (-i\omega - ikU)^2} \right] . \tag{A3.2}$$

Here K_0 is a modified Bessel function of the third kind and gives the source behavior of $\phi_{(1)}$, while the integral with respect to λ is the correction required to satisfy the free surface condition (A3.1).

Now the interaction term in the potential near the ship is found by investigating the source potential near the line of sources, i.e., for $y^2 + z^2$ small, in which case

$$\phi^*_{(1)} = \frac{1}{\pi} Q^*_{(1)} \left[\log \sqrt{y^2 + z^2} + \log \frac{1}{2} C|k| \right.$$

$$\left. + \frac{1}{2} (-i\omega - ikU)^2 \int_{-\infty}^{\infty} \frac{d\lambda}{\sqrt{k^2 + \lambda^2}\,\left(g\sqrt{k^2 + \lambda^2} + (-i\omega - ikU)^2\right)} \right], \quad \text{(A3.3)}$$

($\log C = \gamma = 0.577\ldots$). The first term of (A3.3) corresponds to $\phi^{(2D)}_{(1)}$ in (3.13), the second to $f^{(WALL)}_{(1)}$ and the third to $f^{(FS)}_{(1)}$. The last is the quantity of interest here, and the λ integral involved can be integrated explicitly to give

$$f^{(FS)*}_{(1)} = \frac{1}{\pi} Q^*_{(1)} \, \beta(k) \coth \beta(k) \,, \qquad \text{(A3.4)}$$

where $\beta(k)$ is defined by

$$\cosh \beta(k) = \frac{(-i\omega - ikU)^2}{g|k|} \qquad \text{(A3.5)}$$

with $|\mathrm{Im}\,\beta| < \pi$. The last condition appears to fail for ω real, since then $\cosh \beta$ is real and negative. The correct interpretation is, however, obtained by taking $-i\omega$ to have a small positive real part (corresponding to decaying transients) which we may then let tend to zero, giving

$$\beta(k) = \begin{cases} i(\pi - \alpha(k)) \,, & \text{if} \quad \cos \alpha(k) = \dfrac{(\omega + kU)^2}{g|k|} \le 1 \,, \quad 0 \le \alpha(k) \le \dfrac{\pi}{2} \,, \\[2ex] i\pi - \alpha(k) \, \mathrm{sgn}\,(\omega + kU) \,, & \text{if} \quad \cosh \alpha(k) = \dfrac{(\omega + kU)^2}{g|k|} \ge 1 \,, \quad 0 \le \alpha(k) < \infty . \end{cases} \qquad \text{(A3.6)}$$

The inverse Fourier transform of (A3.4) may be taken by use of the convolution theorem, giving

$$f^{(FS)}_{(1)} = \int_{-\infty}^{\infty} d\xi \; K_{(1)}(x - \xi) \; Q_{(1)}(\xi) \,,$$

where

$$K_{(1)}(x) = \frac{1}{2\pi^2} \int_{-\infty}^{\infty} dk\, e^{-ikx} \beta(k) \coth \beta(k) ,$$

this being the kernel function of Eq. (3.17).

* * *

DISCUSSION

H. Maruo
National University of Yokohama
Yokohama, Japan

Dr. Newman and Dr. Tuck have achieved a rigorous and systematic development of the slender body theory in the problem of the motion of ships among waves. It must be one of the most important achievements in the theory of ship motion, because it enables a consistent formulation for the damping force and the added mass which cannot be realized by the thin ship theory. According to the results, the effect of the free surface by which the frequency dependence appears, is not important unless the finite speed of advance exists. Therefore the results with finite forward velocity seem to be more important. The ultimate aim of the formulation is to enable the prediction of the hydrodynamic forces by means of the theory. In this respect, the present analysis is not yet conclusive. The reason is that the formulas for the forces and moments given by the Eqs. (3.36) and (3.37) with the kernel function (3.17) are not convenient for the numerical computation. An important thing is that the final result should be given by a convergent form. However, the formulas given here involve divergent integrals. In order to obtain a formula which is suitable to the computation, another expression is needed. For this purpose, an expression for Green's function which was obtained by Hanaoka some ten years ago is recommended. It takes the following form:

$$G(x,y,z;x',y',z') = \frac{1}{r_1} + \frac{1}{r_2} + \frac{2}{\pi} \int_{-\infty}^{\infty} dm \int_0^{\infty} \frac{\exp\left[-|y-y'|\sqrt{m^2+n^2} - im(x-x')\right]}{\sqrt{m^2+n^2}}$$

$$\times \{\cos(nz+\epsilon)\cos(nz'+\epsilon) - \cos nz \cos nz'\}\, dn$$

$$+ \frac{2}{x}\int_{m_2}^{m_1} \exp\left[(z+z')(m-\omega_0)^2/x - |y-y'|K_1 - im(x-x')\right] (m-\omega_0)^2 \frac{dm}{K_1}$$

$$+ \frac{2}{x}\int_{m_4}^{m_3} \exp\left[(z+z')(m+\omega_0)^2/x - |y-y'|K_2 + im(x-x')\right] (m+\omega_0)^2 \frac{dm}{K_2}$$

(Cont.)

$$-\frac{2i}{x}\int_0^{m_2} \exp\left[(z+z')(m-\omega_0)^2/x - i|y-y'|K_1 - im(x-x')\right](m-\omega_0)^2\,\frac{dm}{K_1}$$

$$+\frac{2i}{x}\int_{m_1}^{\infty} \exp\left[(z+z')(m-\omega_0)^2/x + i|y-y'|K_1 - im(x-x')\right](m-\omega_0)^2\,\frac{dm}{K_1}$$

$$-\frac{2i}{x}\left[\int_0^{m_4}+\int_{m_3}^{\infty}\right]\exp\left[(z+z')(m+\omega_0)^2/x - i|y-y'|K_2 + im(x-x')\right](m+\omega_0)^2\,\frac{dm}{K_2}\,,$$

where

$$r_1 = \sqrt{(x-x')^2+(y-y')^2+(z-z')^2}$$

$$r_2 = \sqrt{(x-x')^2+(y-y')^2+(z+z')^2}$$

$$x = g/U^2 \qquad \omega_0 = \omega/U$$

$$\left.\begin{matrix}K_1\\ \\ K_2\end{matrix}\right\} = \sqrt{m^2-(m\mp\omega_0)^4/x^2}$$

$$\tan\epsilon = -(m-\omega_0)^2/xn$$

$$\left.\begin{matrix}m_1\\ \\ m_2\end{matrix}\right\} = \frac{1}{2}\left(x+2\omega_0 \pm \sqrt{x^2+4x\omega_0}\right)$$

$$\left.\begin{matrix}m_3\\ \\ m_4\end{matrix}\right\} = \frac{1}{2}\left(x-2\omega_0 \pm \sqrt{x^2-4x\omega_0}\right).$$

On applying the slender body approximation, the asymptotic expression for Green's function along the line $y = z = 0$ becomes

$$G(x,y,z;x',y',z') \approx \frac{1}{r_1}+\frac{1}{r_2}-\frac{2i}{\pi}\frac{d}{dx}\int_{-\infty}^{\infty} e^{im(x-x')}\,\frac{\Phi(m)}{m}\,dm$$

$$-\;2i\,\frac{d}{dx}\left[\int_{-m_1}^{-m_2}+\int_{m_4}^{m_3}\right] e^{im(x-x')}\,\frac{(m+\omega_0)^2}{m\sqrt{m^2x^2-(m+\omega_0)^4}}\,dm$$

(Cont.)

$$- 2 \frac{d}{dx} \left[- \int_{-\infty}^{-m_1} + \int_{-m_2}^{m_4} + \int_{m_3}^{\infty} \right] e^{im(x-x')} \frac{(m+\omega_0)^2}{m\sqrt{m^2 x^2 - (m+\omega_0)^4}} dm$$

where

$$\Phi(m) = \frac{(m+\omega_0)^2}{\sqrt{x^2 m^2 - (m+\omega_0)^4}} \cos^{-1} \frac{(m+\omega_0)^2}{x|m|} \qquad \text{when} \quad x|m| > (m+\omega_0)^2$$

$$= \frac{(m+\omega_0)^2}{\sqrt{(m+\omega_0)^4 - x^2 m^2}} \cosh^{-1} \frac{(m+\omega_0)^2}{x|m|} \qquad \text{when} \quad x|m| < (m+\omega_0)^2 .$$

Making use of the above, the hydrodynamic forces can be expressed by convergent forms. The component of the force in heave for instance, is given by the following form:

$$C_{33}^{(FS)} = \frac{\rho U^2}{2\pi^2} \left[\int_{-\infty}^{\infty} |P_z|^2 \, \Phi(m) \left(\frac{m+\omega_0}{m}\right)^2 dm \right.$$

$$+ \pi \left\{ \int_{-m_1}^{-m_2} + \int_{m_4}^{m_3} \right\} |P_z|^2 \frac{(m+\omega_0)^4 \, dm}{m^2 \sqrt{m^2 x^2 - (m+\omega_0)^4}}$$

$$\left. - i\pi \left\{ - \int_{-\infty}^{-m_1} + \int_{-m_2}^{m_4} + \int_{m_3}^{\infty} \right\} |P_z|^2 \frac{(m+\omega_0)^4 \, dm}{m^2 \sqrt{(m+\omega_0)^4 - m^2 x^2}} \right]$$

where

$$P_z = \int_{-L/2}^{L/2} \frac{dB(x)}{dx} e^{imx} dx .$$

This formula resembles Michell's integral for the wave resistance in uniform motion. Hanaoka has given a similar formula for the hydrodynamic forces and moments of an oscillating thin ship. The discussor wishes to propose that the above formula will be called Hanaoka's integral. There is another type of the expression, which is given by repeated integrals of a kernel function and has some resemblance to Vosser's formula for the wave resistance of a slender ship.

$$C_{33}^{(FS)} = \rho U^2 \left[B'(L/2)B'(-L/2)K(L) + B'(L/2)\int_{-L/2}^{L/2} B''(x)K(x-L/2)dx \right.$$

$$- B'(-L/2)\int_{-L/2}^{L/2} B''(x)K(x+L/2)dx$$

$$\left. - \frac{1}{2}\int_{-L/2}^{L/2}\int_{-L/2}^{L/2} B''(x)B''(x)K(x-x')dx\,dx' \right]$$

where

$$K(x) = \frac{1}{\pi^2} ⨍_{-\infty}^{\infty} \Phi(m)\left(\frac{m+\omega_0}{m}\right)^2 \frac{\cos mx - 1}{m^2} dm$$

$$+ \frac{1}{\pi}\left\{\int_{-m_1}^{-m_2} + \int_{m_4}^{m_3}\right\} \frac{(m+\omega_0)^4(\cos mx - 1)}{m^4\sqrt{m^2x^2 - (m+\omega_0)^4}} dm$$

$$+ \frac{i}{\pi}\left\{-\int_{-\infty}^{-m_1} + ⨍_{-m_2}^{m_4} + \int_{m_3}^{\infty}\right\} \frac{(m+\omega_0)^4(\cos mx - 1)}{m^4\sqrt{(m+\omega_0)^4 - m^2x^2}} dm .$$

Since the above expression involves divergent integrals, the finite part of the integral should be taken.

* * *

COMMENTS ON SLENDER BODY THEORY

E. V. Laitone
Professor and Chairman
University of California
Berkeley, California

It should be noted that the singularities noted in the integrals for the source distribution can be always evaluated by using Hadamard's concept of the "Finite Part" of the integral. This is a generalization of Cauchy's "Principal Value," and can usually (but not always) be most simply determined by "Integration by Parts."

Also the question arises as to how deep must the thin ship be in order to avoid the three-dimensional effects that correspond to the differences $(k_2 - k_1)$ in the virtual mass coefficients for a body of revolution (see Lamb: "Hydrodynamics," p. 155), or to avoid the fineness ratio effects corresponding to the complete elliptic integral (E) determination of the virtual mass of a thin plate (see Lamb, Eq. (16), p. 154).

* * *

REPLY TO DISCUSSION

J. N. Newman and E. O. Tuck
David Taylor Model Basin
Washington, D.C.

As Professor Maruo correctly points out, the kernel function $\underline{K}(x)$ of Eq. (3.37) (which is proportional to the 4th derivative of his function $K(x)$) has a high order singularity at $x = 0$, so that if Eqs. (3.36) were to be used as they stand to calculate the $C_{ij}^{(FS)}$, some juggling (such as integration by parts, as suggested by Professor Laitone) would be needed in order to get a finite answer. However, in presenting the results in the form (3.36), we did not imply a recommendation that this particular form of the integrals was suitable for direct computation. Just as Michell's integral can be manipulated into many different forms, so also can the integrals for the transfer functions $C_{ij}^{(FS)}$, and Professor Maruo has shown an alternative form due to Hanoaka which is clearly better for numerical computation than that given in (3.36), and which avoids the difficulty with the singularity. In fact our initial attempts at numerical computation have used precisely this form, which can be derived directly from Appendix III by use of the Fourier transform convolution theorem. The form in which we gave the results in the paper was chosen for pedagogical reasons, since it illustrates most clearly the simplicity of the formulas in their dependence on $B(x)$ and $S(x)$.

The three-dimensional effects mentioned by Professor Laitone are of smaller order of magnitude according to slender body theory than the contributions we calculate. As far as possible we have indicated by order of magnitude statements the size of the error in each equation, but there is probably no way other than comparison with experiment to test whether or not the ship is sufficiently slender for all the neglected terms (not only those mentioned by Professor Laitone) to be small.

SLENDER BODY THEORY FOR AN OSCILLATING SHIP AT FORWARD SPEED

W. P. A. Joosen
Netherlands Ship Model Basin
Wageningen, Netherlands

ABSTRACT

A linearized theory is developed for an oscillating slender body which is moving along a straight line on the free surface of an ideal fluid. Green's function is used to formulate the velocity potential. Some assumptions are made about the order of magnitude of the Froude number and the frequency with respect to the slenderness parameter.

The first order term of the potential is derived by asymptotic expansion.

INTRODUCTION

During the past few years several papers have been published on the subject of slender body theory for surface ships. In the slender body theory the beam-length ratio ϵ is supposed to be small with respect to unity and of the same order as the draft-length ratio. This is in contrast with the thin ship theory, where only the beam-length ratio is assumed to be small. The principal task of the theory is to provide the expansion of the velocity potential in terms of the slenderness parameter ϵ.

Ursell [1] has solved the problem of an oscillating slender body of revolution at zero forward speed for the case of small and moderate frequency parameter as well as for the case of large frequency. He derived two terms in the series expansion.

Newman [2] followed another approach, suggested by Vossers [3] starting from Green's theorem. He treated the problem of an oscillating slender body of arbitrary shape at small or moderate frequency in the presence of incoming waves. He derived the first order terms of the velocity potential and of the forces and moments.

A difficulty arises in the equation of motion for pitch and heave, because it appears that the force due to hydrostatic pressure and the Froude-Krylov force is of lower order than the hydrodynamic forces (added mass and damping). A similar result was obtained already by Peters and Stoker [4] in the thin ship theory.

Simultaneously Joosen [5] derived the solution of the same problem without waves, also using Green's function for two conditions. More precisely for the case where the frequency parameter is of order unity and for the case where the frequency parameter is of order ϵ^{-1}. In the first case the final formula for the velocity potential consists of two terms, one term corresponding to the problem of a pulsating double body in an infinite fluid and another term representing the longitudinal interference effects.

In the second case the result leads to the conclusion that the flow in each cross section is independent of the flow at other sections.

It is therefore a rigorous justification for the use of the two-dimensional strip theory such as is applied by Grim [6] and Tasai [7], who calculated the added mass and damping coefficient for a family of cross section curves. The agreement between theoretical values and experimental data is very good, of course, especially for the higher frequencies.

The problem of a slender body moving at a steady speed on the water surface has also drawn attention. Vossers was the first who attacked the problem starting from the three-dimensional formulation with Green's theorem. Using the method of inner and outer expansions, Tuck [8] solved the problem for a body of revolution. Starting from the formulation with Green's function Joosen [5] obtained the solution for a body of arbitrary shape under the condition of straight vertical lines at bow and stern. It appears that the influence of the end point terms is dominant and that the series expansion is not uniformly convergent for arbitrary shape of the bow and stern line. From the numerical value of the wave resistance it can be concluded that the results are not in closer agreement with the experiments than the Michell theory. The reason for this seems to be the behaviour near the end points and the fact that the Froude number is in most practical examples of the same order of magnitude as the slenderness parameter. The more satisfactory formulae for this case will be obtained as a by-product of the present work. The result contains only integrals along the bow and stern line.

In the following sections the full problem of an oscillating slender body at forward speed will be considered. In the usual strip theory forward speed effects and three-dimensional effects are not present. In the past several authors have considered the forward speed effect in damping and cross-coupling coefficients; see Grim [6], Korvin-Kroukovsky [9]. Although this work seems to be in good agreement with experimental data (Vassilopoulos [10]), a consistent theory, based on a rigorous asymptotic expansion of the three-dimensional formulae is still lacking.

Recent experimental work of Gerritsma [11] has shown the relatively small effect of forward speed on the total value of damping and added mass coefficient for heave and pitch, but an important influence on the distribution of the damping over the ship length. In order to verify these results an asymptotic theory is set up in this paper with the assumptions that the Froude number is of order $\epsilon^{1/2}$ and the frequency parameter of order ϵ^{-1}. It is expected that the result consists of that of the two-dimensional strip theory extended with some terms representing the three-dimensional and forward speed effects.

The case that both parameters are of order unity is also treated here. Although the same difficulties in the equations of motion can be expected as in the corresponding problem with Froude number equal to zero it is nevertheless worthwhile to carry out the calculations in order to get some insight in the range of validity of the theory.

FORMULATION OF THE PROBLEM

In the coordinate system used in the following the x_1, y_1 plane coincides with the free surface. The origin moves with the ship speed V in the same direction as the ship and the z_1 axis is taken positive in upward direction.

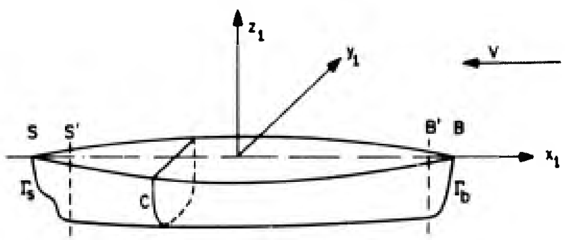

The hull surface in equilibrium position is assumed to be of the form

$$y_1 = f_1(x_1, z_1) \operatorname{sgn} y_1 . \tag{2.1}$$

As an additional condition the bow and the stern have the shape of sharp wedges. Between B^1 and S^1 the bottom of the ship is flat.

The length of the ship is L, the beam B and the draft T. A cross section contour is denoted by $C(x_1)$. The bow contour and the stern contour are denoted respectively by Γ_b and Γ_s. Only heaving and pitching motions of the ship are considered, which are harmonic in time with angular speed ω. The same procedure can be followed for swaying and yawing motions.

In the inviscid fluid a velocity potential exists defined by

$$\Phi(x_1, y_1, z_1, t) = -Vx_1 + \phi(x_1, y_1, z_1, t) , \tag{2.2}$$

$\phi(x_1, y_1, z_1, t)$ must satisfy the Laplace equation

$$\Delta\phi = 0 , \tag{2.3}$$

the linearized free surface condition for $z_1 = 0$

$$\phi_{tt} + V^2 \phi_{x_1 x_1} - 2V\phi_{t x_1} + g\phi_{z_1} = 0 \tag{2.4}$$

and the boundary condition on the hull

$$H_t - VH_{x_1} + \Phi_{x_1} H_{x_1} + \Phi_{y_1} H_{y_1} + \Phi_{z_1} H_{z_1} = 0 \tag{2.5}$$

where $H(x, y, z, t) = 0$ is the part of the ship under the water surface at the time t.

The following dimensionless quantities are introduced:

$$x_1 = \frac{L}{2}\xi_1, \quad y_1 = \epsilon\frac{L}{2}\eta_1, \quad z_1 = \epsilon\frac{L}{2}\zeta_1, \quad \epsilon = \frac{B}{L},$$
$$f_1(x_1, z_1)\,\mathrm{sgn}\,y_1 = \epsilon\frac{L}{2} f(\xi_1, \zeta_1), \quad \beta_0 = \frac{2V^2}{gL}, \quad \xi_L = \frac{\omega^2 L}{2g}, \quad \xi_B = \frac{\omega^2 B}{2g}, \quad \gamma = \frac{\omega V}{g}. \tag{2.6}$$

The displacements and rotations of the ship are supposed to be small and consequently the problem can be linearized.

$$\psi_0 = \sigma\bar{\psi}_0 e^{-i\omega t}, \qquad z_0 = \sigma\frac{L}{2}\bar{\zeta}_0 e^{-i\omega t}. \tag{2.7}$$

H can be written in dimensionless form as

$$H(\xi, \eta, \zeta, t) = \epsilon\{\eta - f(\xi, \zeta)\} - \sigma(\bar{\zeta}_0 - \bar{\psi}_0\xi) f_\zeta e^{-i\omega t} + 0(\epsilon\sigma). \tag{2.8}$$

Because of the linearity of the problem it is possible to split up $\Phi(x_1, y_1, z_1, t)$ in a time-dependent term and a term independent of t:

$$\Phi(x_1, y_1, z_1, t) = \epsilon^2\frac{gL}{2\omega}\bar{\varphi}_1(\xi_1, \eta_1, \zeta_1) + \epsilon^2\frac{gL}{2\omega}\bar{\varphi}_2(\xi_1, \eta_1, \zeta_1)e^{-i\omega t}. \tag{2.9}$$

After substitution of (2.8) and (2.9) into (2.3)-(2.5) and omitting higher order terms the conditions for $\bar{\varphi}_1$ and $\bar{\varphi}_2$ are obtained:

$$\Delta\bar{\varphi}_1 = 0, \qquad \Delta\bar{\varphi}_2 = 0 \tag{2.10}$$

for $\zeta_1 = 0$:

$$\epsilon\beta_0\bar{\varphi}_{1\xi_1\xi_1} + \bar{\varphi}_{1\zeta_1} = 0, \qquad -\epsilon\xi_L\bar{\varphi}_2 + \epsilon\beta_0\bar{\varphi}_{2\xi_1\xi_1} + 2i\epsilon\gamma\bar{\varphi}_{2\xi_1} + \bar{\varphi}_{2\zeta_1}; \tag{2.11}$$

for $\eta_1 = f(\xi_1, \zeta_1)$:

$$\sqrt{1 + f_{\zeta_1}^2}\,\frac{\partial\bar{\varphi}_1}{\partial\nu} = \bar{\varphi}_{1\eta_1} + \bar{\varphi}_{1\zeta_1} f_{\zeta_1} = \gamma f_{\xi_1},$$

$$\sqrt{1 + f_{\zeta_1}^2}\,\frac{\partial\bar{\varphi}_2}{\partial\nu} = \bar{\varphi}_{2\eta_1} + \bar{\varphi}_{2\zeta_1} f_{\zeta_1} = -i\frac{\sigma}{\epsilon}\xi_L(\bar{\zeta}_0 - \bar{\psi}_0\xi_1) f_{\zeta_1}$$
$$+ \frac{\sigma}{\epsilon}\gamma\{\bar{\psi}_0 f_{\zeta_1} - (\bar{\zeta}_0 - \bar{\psi}_0\xi_1) f_{\zeta_1\xi_1}\}. \tag{2.12}$$

Of primary interest is the leading term in the series expansion with respect to ϵ of $\bar{\varphi}_1$ and $\bar{\varphi}_2$. Before starting this derivation it is necessary to introduce some statements as to the order of magnitude of σ, β_0 and ξ_L with respect to ϵ. In this paper two cases will be considered.

$$\text{I.}\quad \sigma = \epsilon^2 , \quad \beta_0 = \epsilon\beta_1 , \quad \xi_L = \frac{\xi_B}{\epsilon} . \tag{2.13}$$

with $\beta_1 = O(1)$ and $\xi_B = O(1)$;

$$\text{II.}\quad \sigma = \epsilon , \quad \beta_0 = O(1) , \quad \xi_L = O(1). \tag{2.14}$$

The first case is related to the problem of low Froude number and high frequencies and one may expect that it corresponds with a ship moving in head waves with small wave length.

The second case deals with the problem of high Froude number and low or moderate frequencies and it seems to be a good approximation for a ship moving in following waves with moderate wave length.

As far as the magnitude of the frequency parameter is concerned it is of course evident that the ratio wave length to ship length is of much importance.

The potential $\bar{\varphi}_i$ can be written in the form

$$\bar{\varphi}_i = \int_{-1}^{1} d\xi \int_{c(\xi)} F(\xi,\zeta)\, \bar{G}_i(\xi_1,\eta_1,\zeta_1;\xi,\eta,\zeta)\, d\zeta$$

where $\bar{G}_i$ is Green's function for the free surface condition and $F(\xi,\zeta)$ is the source distribution to be determined from the boundary condition (2.12).

A further notation is introduced:

$$\bar{\varphi}_i = \varphi_0 + \varphi_i \tag{2.15}$$

with

$$\varphi_0 = \int_{-1}^{1} d\xi \int_{c(\xi)} F(\xi,\zeta)$$

$$\times \left\{ \frac{1}{\sqrt{(\xi_1-\xi)^2+\epsilon^2(\eta_1-f)^2+\epsilon^2(\zeta_1-\zeta)^2}} - \frac{1}{\sqrt{(\xi_1-\xi)^2+\epsilon^2(\eta_1-f)^2+\epsilon^2(\zeta_1+\zeta)^2}} \right\} d\zeta \tag{2.16}$$

and

$$\varphi_i = \int_{-1}^{1} d\xi \int_{c(\xi)} F(\xi,\zeta)\, G_i(\xi_1,\eta_1,\zeta_1;\xi,\eta,\zeta)\, d\zeta . \tag{2.17}$$

The formula for G_i can be found, e.g., in [4]:

$$G_2(\xi_1, \eta_1, \zeta_1; \xi, \eta, \zeta) =$$

$$- \frac{2}{\pi} \int_0^{\theta_\gamma} d\theta \int_0^\infty \frac{q\, e^{\epsilon(\zeta_1+\zeta)q + i(\xi_1-\xi)q \cos\theta} \cos\{\epsilon(\eta_1 - f)q \sin\theta\} dq}{\beta_0 q^2 \cos^2\theta + 2\gamma q \cos\theta + \xi_L - q}$$

$$- \frac{2}{\pi} \int_{\theta_\gamma}^{\pi/2} d\theta \int_{M_1} \frac{q\, e^{\epsilon(\zeta_1+\zeta)q + i(\xi_1-\xi)q \cos\theta} \cos\{\epsilon(\eta_1 - f)q \sin\theta\} dq}{\beta_0 q^2 \cos^2\theta + 2\gamma q \cos\theta + \xi_L - q}$$

$$- \frac{2}{\pi} \int_0^{\pi/2} d\theta \int_{M_2} \frac{q\, e^{\epsilon(\zeta_1+\zeta)q - i(\xi_1-\xi)q \cos\theta} \cos\{\epsilon(\eta_1 - f)q \sin\theta\} dq}{\beta_0 q^2 \cos^2\theta - 2\gamma q \cos\theta + \xi_L - q} \qquad (2.18)$$

with

$$\cos\theta_\gamma = \frac{1}{4\gamma},$$

$$G_1(\xi_1, \eta_1, \zeta_1; \xi, \eta, \zeta) = \left[G_2(\xi_1, \eta_1, \zeta_1; \xi, \eta, \zeta)\right]_{\xi_L = 0}. \qquad (2.19)$$

If the roots in the denominators are denoted by q_1, q_2, q_3, q_4, the contours M_1 and M_2 are defined by

$$\left.\begin{aligned} q_1 = \bar{q}_1 &= \frac{1 - 2\gamma\cos\theta + i\sqrt{4\gamma\cos\theta - 1}}{2\beta_0 \cos^2\theta} \\ q_2 = \bar{q}_2 &= \frac{1 - 2\gamma\cos\theta - i\sqrt{4\gamma\cos\theta - 1}}{2\beta_0 \cos^2\theta} \end{aligned}\right\} \cos\theta > \frac{1}{4\gamma},$$

$$q_3 = \frac{1 + 2\gamma\cos\theta - \sqrt{1 + 4\gamma\cos\theta}}{2\beta_0 \cos^2\theta}$$

$$\left.\begin{aligned} q_1 &= \frac{1 - 2\gamma\cos\theta - \sqrt{1 - 4\gamma\cos\theta}}{2\beta_0 \cos^2\theta} \\ q_2 &= \frac{1 - 2\gamma\cos\theta + \sqrt{1 - 4\gamma\cos\theta}}{2\beta_0 \cos^2\theta} \end{aligned}\right\} \cos\theta < \frac{1}{4\gamma}.$$

$$q_4 = \frac{1 + 2\gamma\cos\theta + \sqrt{1 + 4\gamma\cos\theta}}{2\beta_0 \cos^2\theta}$$

The first order term in φ_0 is well known, see [5]:

$$\varphi_0 = -2 \int_{c(\xi_1)} \left\{ \ln \sqrt{(\eta_1 - f)^2 + (\zeta_1 - \zeta)^2} - \ln \sqrt{(\eta_1 - f)^2 + (\zeta_1 + \zeta)^2} \right\} F(\xi_1, \zeta)\, d\zeta . \qquad (2.20)$$

In the next sections the corresponding term in φ_1 and φ_2 will be derived for the two cases (2.13) and (2.14).

THE CASE OF LOW FROUDE NUMBER AND HIGH FREQUENCY

First the potential φ_2 for this case will be considered. From that result the final form for φ_1 can easily be obtained. The Greens' function G_2 is transformed into a slightly different form by separating the poles and introducing a new variable.

$$G_2(\xi_1, \eta_1, \zeta_1; \xi, \eta, \zeta) =$$

$$\frac{2i}{\pi\epsilon} \int_0^{\theta_\gamma} \frac{d\theta}{\sqrt{4\gamma \cos\theta - 1}} \int_0^\infty \left(\frac{1}{q - \bar{q}_1} - \frac{1}{q - \bar{q}_2} \right) q\, e^{q(\zeta_1 + \zeta) + \frac{ig}{\epsilon}(\xi_1 - \xi)\cos\theta} \cos\left\{ q(\eta_1 - f)\sin\theta \right\} dq$$

$$- \frac{2}{\pi\epsilon} \int_{L_2} \frac{q\, dq}{q - 1} \int_{\theta_\gamma}^{\pi/2} e^{q_2(\zeta_1 + \zeta)q + \frac{i}{\epsilon} q_2(\xi_1 - \xi) q \cos\theta} \cos\left\{ q_2(\eta_1 - f) q \sin\theta \right\} \frac{q_2\, d\theta}{\sqrt{1 - 4\gamma\cos\theta}}$$

$$- \frac{2}{\pi\epsilon} \int_{L_1} \frac{q\, dq}{q - 1} \int_0^{\pi/2} e^{q_4(\zeta_1 + \zeta)q - \frac{i}{\epsilon} q_4(\xi_1 - \xi) q \cos\theta} \cos\left\{ q_4(\eta_1 - f) q \sin\theta \right\} \frac{q_4\, d\theta}{\sqrt{1 + 4\gamma\cos\theta}}$$

$$+ \frac{1}{\pi\epsilon} \int_{L_1} \frac{q\, dq}{q - 1} \int_{\theta_\gamma}^{\pi/2} e^{q_1(\zeta_1 + \zeta)q + \frac{i}{\epsilon} q_1(\xi_1 - \xi) q \cos\theta} \left\{ e^{iq_1(\eta_1 - f) q \sin\theta} + e^{-iq_1(\eta_1 - f) q \sin\theta} \right\} \frac{q_1\, d\theta}{\sqrt{1 - 4\gamma\cos\theta}}$$

$$+ \frac{1}{\pi\epsilon} \int_{L_1} \frac{q\, dq}{q - 1} \int_0^{\pi/2} e^{q_3(\zeta_1 + \zeta)q - \frac{i}{\epsilon} q_3(\xi_1 - \xi) q \cos\theta} \left\{ e^{iq_3(\eta_1 - f) q \sin\theta} + e^{-iq_3(\eta_1 - f) q \sin\theta} \right\} \frac{q_3\, d\theta}{\sqrt{1 + 4\gamma\cos\theta}} .$$

(3.1)

where L_1 and L_2 are defined by

By one time partial integration with respect to ξ after changing the order of integration the contribution of the first three integrals to the potential φ_2 becomes, if ϵ tends to zero:

$$\frac{2}{\pi} \left\{ \int_{\Gamma_s} - \int_{\Gamma_b} \right\} F(\xi, \zeta)\, d\zeta \int_0^{\theta_\gamma} \frac{d\theta}{\cos\theta \sqrt{4\gamma\cos\theta - 1}} \int_0^\infty \left(\frac{1}{q - \bar{q}_1} - \frac{1}{q - \bar{q}_2} \right)$$

$$\times\, e^{q(\zeta_1 + \zeta)} \; e^{\frac{i}{\epsilon} q(\xi_1 - \xi)\cos\theta} \cos\left\{ q(\eta_1 - f)\sin\theta \right\} dq$$

(3.2) (Cont.)

$$+ \frac{2i}{\pi}\left\{\int_{\Gamma_s} - \int_{\Gamma_b}\right\} F(\xi,\zeta)d\zeta \int_{L_2} \frac{dq}{q-1} \int_{\theta_\gamma}^{\pi/2}$$

$$\times\, e^{q_2(\zeta_1+\zeta)q - \frac{i}{\epsilon}q_2(\xi_1-\xi)q\cos\theta} \cos\{q_2(\eta_1 - f)q\sin\theta\} \frac{d\theta}{\cos\theta\sqrt{1-4\gamma\cos\theta}}$$

$$+ \frac{2i}{\pi}\left\{\int_{\Gamma_s} - \int_{\Gamma_b}\right\} F(\xi,\zeta)d\zeta \int_{L_1} \frac{dq}{q-1} \int_{0}^{\pi/2}$$

$$\times\, e^{q_4(\zeta_1+\zeta)q - \frac{i}{\epsilon}q_4(\xi_1-\xi)q\cos\theta} \cos\{q_4(\eta_1 - f)q\sin\theta\} \frac{d\theta}{\cos\theta\sqrt{1-4\gamma\cos\theta}} \; . \tag{3.2}$$

In this derivation the bow region BB^1 and the stern region SS^1 are assumed to be of order ϵ and therefore $\xi_1 - \xi/\epsilon$ is of order unity if ξ_1 is in the neighbourhood of bow or stern.

If these regions are of order unity the expression (3.2) becomes zero in the limiting case. This fact follows from the application of the method of stationary phase, which will be discussed somewhat later in this section.

From these results it must be concluded that the series expansion is not uniformly convergent in the neighbourhood of $|\xi_1| = 1$. In the following it is assumed that the ship is sharply pointed.

With this restriction the final results for φ_2 is only produced by the last two terms of (3.1). These integrals are of the form:

$$\mathfrak{J} = \int_{-1}^{1} d\xi \int_{c(\xi)} F(\xi,\zeta)d\zeta \int_{L_1} \frac{q\,dq}{q-1} \int^{\pi/2} B(q,\theta)\, e^{\frac{i}{\epsilon}D(\xi,\theta)}\, d\theta \tag{3.5}$$

where

$$D(\xi,\theta) = q\,q_k\{(\xi_1 - \xi)\cos\theta \pm \epsilon(\eta_1 - f)\sin\theta\}. \tag{3.6}$$

For this integral the method of stationary phase can be applied in the ξ,θ plane, ϵ^{-1} being the large parameter. The general theory of the method of stationary phase applied on multiple integrals can be found, e.g., in [12].

Here only the first order term in ϵ will be derived using the above mentioned theory for the case of a double integral with the point of stationary phase inside the integration domain.

Let this point be denoted by (ξ_0, θ_0); then $D_\xi(\xi_0,\theta_0) = 0$, $D_\theta(\xi_0,\theta_0) = 0$.

In the neighbourhood of (ξ_0, θ_0), $D(\xi,\theta)$ can be written as

$$D(\xi,\theta) = D(\xi_0,\theta_0) + \frac{1}{2}(\xi-\xi_0)^2 D_{\xi\xi}(\xi_0,\theta_0) + \frac{1}{2}(\theta-\theta_0)^2 D_{\theta\theta}(\xi_0,\theta_0)$$
$$+ (\xi-\xi_0)(\theta-\theta_0) D_{\xi\theta}(\xi_0,\theta_0) + \dots .$$

After a rotation of coordinates this becomes

$$D(\xi,\theta) = D(\xi_0,\theta_0) + (\xi-\xi_0)^2 P(\xi_0,\theta_0) - (\theta-\theta_0)^2 Q(\xi_0,\theta_0) + \dots$$

with

$$P(\xi_0,\theta_0) = \frac{1}{2}\left\{D_{\xi\xi} + D_{\theta\theta} + \sqrt{(D_{\xi\xi} - D_{\theta\theta})^2 + 4D_{\xi\theta}^2}\right\}$$

and

$$Q(\xi_0,\theta_0) = -\frac{1}{2}\left\{D_{\xi\xi} + D_{\theta\theta} - \sqrt{(D_{\xi\xi} - D_{\theta\theta})^2 + 4D_{\xi\theta}^2}\right\}. \tag{3.7}$$

The first order term in (3.5) originates from the neighbourhood of the stationary point and therefore if (ξ_0,θ_0) is an interior point, this term becomes:

$$\mathfrak{I} = \int_{c(\xi_0)} F(\xi_0,\zeta)d\zeta \int_{L_1} \frac{qB(q,\theta_0)e^{\frac{i}{\epsilon}D(\xi_0,\theta_0)}}{q-1}dq \int_{-\infty}^{\infty} e^{\frac{i}{\epsilon}P(\xi-\xi_0)^2} d\xi \int_{-\infty}^{\infty} e^{-\frac{i}{\epsilon}Q(\theta-\theta_0)^2} d\theta$$

$$= \pi\epsilon \int_{c(\xi_0)} F(\xi_0,\zeta)d\zeta \int_{L_1} \frac{B(q,\theta_0)\, e^{\frac{i}{\epsilon}D(\xi_0,\theta_0)}\, q\,dq}{(q-1)\sqrt{PQ}}, \quad \text{if } P > 0,\ Q > 0. \tag{3.8}$$

Inserting for $D(\xi,\theta)$ the expression (3.6) the result becomes

$$\begin{aligned} &\cos\theta_0 = O(\epsilon), \quad D_{\xi\xi} = O(\epsilon), \quad D_{\xi\theta} = q\xi_B + O(\epsilon^2), \\ &\xi_0 = \xi_1 + O(\epsilon), \quad D_{\theta\theta} = O(\epsilon), \quad D(\xi_0,\theta_0) = \pm q\xi_B\,\epsilon(\eta_1 - f). \end{aligned} \tag{3.9}$$

With (3.7), (3.8) and (3.9), for (3.5) the result

$$\mathfrak{I} = \frac{\pi\epsilon}{\xi_B} \int_{C(\xi_1)} F(\xi_1,\zeta)d\zeta \int_{L_1} B(q,\theta_0)\, e^{\pm i(\eta_1 - f)\xi_B q} \frac{dq}{q-1} \tag{3.10}$$

is obtained.

From (3.1) and (3.10) the first order term of φ_2 follows easily:

$$\varphi_2(\xi_1,\eta_1,\zeta_1) = 4\int_{c(\xi_1)} F(\xi_1,\zeta)d\zeta \int_{L_1} e^{\xi_B(\zeta_1+\zeta)q} \cos\{\xi_B(\eta_1-f)q\}\frac{dq}{q-1}\,. \qquad (3.11)$$

By changing the integration contour (3.11) is transformed into:

$$\varphi_2(\xi_1,\eta_1,\zeta_1) = 4\int_{c(\xi_1)} F(\xi_1,\zeta)d\zeta \left[-\ln\sqrt{(\eta_1-f)^2+(\zeta_1+\zeta)^2} + \pi i e^{\xi_B(\zeta_1+\zeta)+i\xi_B|\eta_1-f|}\right.$$

$$\left. + \int_0^\infty e^{-\xi_B\lambda} \ln\sqrt{(\eta_1-f)^2+(\zeta_1+\zeta+\lambda)^2}\,d\lambda\right]. \qquad (3.12)$$

Following the same procedure as discussed before it appears that the first three integrals of (3.1) with $\xi_B = 0$ produce no first order contribution to the value of φ_1 except for the case that bow and stern region are of order ϵ. The last two terms of (3.1) become with $\xi_B = 0$

$$G_1 = \frac{2}{\sqrt{(\xi_1-\xi)^2 + \epsilon^2(\eta_1-f)^2 + \epsilon^2(\zeta_1+\zeta)^2}}\,.$$

After expansion with respect to ϵ and with the condition of sharpness at the end-points for φ_1 is obtained:

$$\varphi_1(\xi_1,\eta_1,\zeta_1) = -4\int_{c(\xi_1)} F(\xi_1,\zeta)\,\ln\sqrt{(\eta_1-f)^2+(\zeta_1+\zeta)^2}\,d\zeta$$

$$= +4\int_{-1}^{1} \operatorname{sgn}(\xi_1-\xi)\,\ln 2|\xi_1-\xi|\,d\xi \int_{c(\xi)} F_\xi(\xi,\zeta)\,d\zeta\,. \qquad (3.13)$$

The function $\varphi_0 + \varphi_1$ can be considered as the potential associated with the translatory motion of a body in an unbounded medium.

The function $F(\xi,\zeta)$ can be determined by the boundary condition (2.12).

A discussion of the results of this section with a view to experimental results obtained elsewhere, will be postponed till section 6.

THE CASE OF HIGH FROUDE NUMBER AND MODERATE FREQUENCY

The velocity potential φ_1 for this case is already known (see e.g., [5], [8]).

$$\varphi_1 = -2 \int_{c(\xi_1)} F(\xi_1, \zeta) \left\{ \ln \sqrt{(\eta_1 - f)^2 + (\zeta_1 - \zeta)^2} + \ln \sqrt{(\eta_1 - f)^2 + (\zeta_1 + \zeta)^2} \right\} d\zeta$$

$$+ 2 \int_{-1}^{1} d\xi \int_{c(\xi)} F(\xi, \zeta) d\zeta \left\{ \operatorname{sgn}(\xi_1 - \xi) \ \ln 2 |\xi_1 - \xi| \right.$$

$$\left. + \frac{\pi}{2} H_0 \left(\frac{\xi_1 - \xi}{\beta_0} \right) - \frac{\pi}{2} \left[2 - \operatorname{sgn}(\xi_1 - \xi) \right] Y_0 \left(\frac{|\xi_1 - \xi|}{\beta_0} \right) \right\} . \tag{4.1}$$

The Greens function (2.18) associated with the potential φ_2 is written in the form:

$$G = \frac{2}{\sqrt{(\xi_1 - \xi)^2 + \epsilon^2(\eta_1 - f)^2 + \epsilon^2(\zeta_1 + \zeta)^2}} + \bar{G}_3 + \bar{G}_4 , \tag{4.2}$$

where

$$\bar{G}_n = \frac{-2}{\pi} \int_0^{\theta_\gamma} d\theta \int_0^{\infty} \frac{\bar{A}_n(q, \theta) \ e^{\epsilon(\zeta_1 + \zeta) q + i q (\xi_1 - \xi) \cos\theta} \cos \{\epsilon(\eta_1 - f) q \sin\theta\} \, dq}{\beta_0 q^2 \cos^2\theta + 2\gamma q \cos\theta + \xi_L - q}$$

$$\times \frac{-2}{\pi} \int_{\theta_\gamma}^{\pi/2} d\theta \int_{M_1} \frac{\bar{A}_n(q, \theta) \ e^{\epsilon(\zeta_1 + \zeta) q + i q (\xi_1 - \xi) \cos\theta} \cos \{\epsilon(\eta_1 - f) q \sin\theta\} \, dq}{\beta_0 q^2 \cos^2\theta + 2\gamma q \cos\theta + \xi_L - q}$$

$$\times \frac{-2}{\pi} \int_{0}^{\pi/2} d\theta \int_{M_2} \frac{\bar{B}_n(q, \theta) \ e^{\epsilon(\zeta_1 + \zeta) q - i q (\xi_1 - \xi) \cos\theta} \cos \{\epsilon(\eta_1 - f) q \sin\theta\} \, dq}{\beta_0 q^2 \cos^2\theta - 2\gamma q \cos\theta + \xi_L - q} \tag{4.3}$$

with $\bar{A}_3 = \bar{B}_3 = \xi_L$

$$A_4 = \beta_0 q^2 \cos^2\theta + 2\gamma q \cos\theta , \quad B_4 = \beta_0 q^2 \cos^2\theta - 2\gamma q \cos\theta . \tag{4.4}$$

The term containing $\bar{G}_4$ in φ_2 is integrated with respect to ξ. The first order term of φ_2 can easily be obtained by putting $\epsilon = 0$ in the formulae with $\bar{G}_n$, because all the integrals remain convergent. It is assumed that

$$\int_{c(1)} I(1, \zeta) d\zeta = \int_{c(-1)} F(-1, \zeta) d\zeta = 0 .$$

The result becomes:

$$\varphi_2(\xi_1,\eta_1,\zeta_1) = -4\int_{c(\xi_1)} F(\xi_1,\zeta)\ \ln\sqrt{(\eta_1-f)^2+(\zeta_1+\zeta)^2}\ d\zeta$$

$$+4\int_{-1}^{1}\operatorname{sgn}(\xi_1-\xi)\ \ln 2|\xi_1-\xi|d\xi\int_{c(\xi)}F(\xi,\zeta)d\zeta$$

$$+\int_{-1}^{1}d\xi\int_{c(\xi)}F(\xi,\zeta)\,G_3\,d\zeta-\int_{-1}^{1}d\xi\int_{c(\xi)}F_{\xi}(\xi,\zeta)\ G_4\,d\zeta\,, \tag{4.5}$$

where

$$G_n = \frac{-2}{\pi}\int_0^{\theta_\gamma}d\theta\int_0^\infty\frac{A_n(q,\theta)\,e^{-iq(\xi-\xi_1)\cos\theta}\,dq}{\beta_0q^2\cos^2\theta+2\gamma q\cos\theta+\xi_L-q}$$

$$\times\frac{-2}{\pi}\int_{\theta_\gamma}^{\pi/2}d\theta\int_{M_1}\frac{A_n(q,\theta)\,e^{-iq(\xi-\xi_1)\cos\theta}\,dq}{\beta_0q^2\cos^2\theta+2\gamma q\cos\theta+\xi_L-q}$$

$$\times\frac{-2}{\pi}\int_0^{\pi/2}d\theta\int_{M_2}\frac{B_n(q,\theta)\,e^{iq(\xi-\xi_1)\cos\theta}\,dq}{\beta_0q^2\cos^2\theta-2\gamma q\cos\theta+\xi_L-q} \tag{4.6}$$

with $A_3 = B_3 = \xi_L$

$$A_4 = -i(\beta_0 q\cos\theta+2\gamma)\,,\qquad B_4 = i(\beta_0 q\cos\theta-2\gamma)\,. \tag{4.7}$$

By changing the integration contour and introducing some new variables (4.6) can be transformed into a formula that is more convenient for computation:

$$G_n = G_n^{(1)}+G_n^{(2)}+G_n^{(3)}\,,$$

where

$$G_n^{(1)} = \sqrt{2}\int_0^\infty R_n(p)\left\{\left(\sqrt{m_1^2+m_2^2}+m_1\right)^{1/2}\right.$$

$$\left.-\,i\ \operatorname{sgn} m_2\left(\sqrt{m_1^2+m_2^2}-m_1\right)^{1/2}\right\}e^{-p|\xi_1-\xi|}\frac{dp}{\sqrt{m_1^2+m_2^2}}\,.$$

For $\xi-\xi_1<0$:

$$G_n^{(2)} = -8ih\int_0^1 H_n(\tau)\,e^{-i\frac{h}{2\beta_0}(\xi-\xi_1)\tau}\frac{d\tau}{\sqrt{(h\tau+2\gamma)^4-4h^2\tau^2}}\,.$$

For $\xi - \xi_1 > 0$:

$$G_n^{(2)} = -\delta i c \int_0^1 C_n(\tau)\, e^{i\frac{c}{2\beta_0}(\xi-\xi_1)\tau} \frac{d\tau}{\sqrt{(c\tau - 2\gamma)^4 - 4c^2\tau^2}}$$

$$- \delta i \ell \int_1^\infty L_n(\tau)\, e^{-i\frac{\ell}{2\beta_0}(\xi-\xi_1)\tau} \frac{d\tau}{\sqrt{(\ell\tau + 2\gamma)^4 - 4\ell^2\tau^2}}$$

$$- \delta i d \int_1^\infty D_n(\tau)\, e^{i\frac{d}{2\beta_0}(\xi-\xi_1)\tau} \frac{d\tau}{\sqrt{(d\tau - 2\gamma)^4 - 4d^2\tau^2}}$$

with

$$m_1 = (\xi_L - \beta_0 p^2)^2 - (4\gamma^2 - 1)p^2, \quad m_2 = -4\gamma p(\xi_L - \beta_0 p^2)\ \mathrm{sgn}\,(\xi - \xi_1),$$

$$R_3 = H_3 = C_3 = L_3 = D_3 = \xi_L,$$

$$R_4 = -\beta_0 p\ \mathrm{sgn}\,(\xi - \xi_1) - 2\gamma i, \qquad H_4 = -i\left(\frac{h}{2}\tau + 2\gamma\right),$$

$$L_4 = -i\left(\frac{\ell}{2}\tau + 2\gamma\right), \quad C_4 = i\left(\frac{c}{2}\tau - 2\gamma\right), \quad D_4 = i\left(\frac{d}{2}\tau - 2\gamma\right),$$

$$c = 1 + 2\gamma - \sqrt{1+4\gamma}, \qquad d = 1 + 2\gamma + \sqrt{1+4\gamma}.$$

For $\gamma < 1/4$:

$$h = 1 - 2\gamma - \sqrt{1-4\gamma},$$

$$\ell = 1 - 2\gamma + \sqrt{1-4\gamma}$$

and

$$G_n^{(3)} \equiv 0.$$

For $\gamma > 1/4$:

$$h = \ell = 2\gamma$$

and

$$G_n^{(3)} = -4\, e^{-\frac{i}{i\beta_0}(1-2\gamma)(\xi-\xi_1)} \int_0^1 N_n(\tau)\, e^{-\frac{|\xi_1-\xi|}{2\beta_0}\left\{\sqrt{\delta(\delta\tau+1)(1-\tau)} + i\delta\tau\ \mathrm{sgn}(\xi-\xi_1)\right\}}$$

$$\times \frac{d\tau}{\sqrt{(\delta\tau+2)(\delta\tau+1)(1-\tau)\tau}}$$

with

$$N_3 = \xi_L\,, \quad N_4 = -\sqrt{\delta(\delta\tau+1)(1-\tau)}\ \mathrm{sgn}(\xi-\xi_1) - \frac{i}{2}(\delta\tau + 2\gamma + 1)\,, \quad \delta = 4\gamma - 1\,. \tag{4.9}$$

For $\xi_L = 0$ these formulae become:

$$G_3 = 0\,, \qquad G_4 = \pi\left[H_0\left(\frac{\xi_1-\xi}{\beta_0}\right) - \{2 - \mathrm{sgn}(\xi_1-\xi)\}\ Y_0\left(\frac{|\xi_1-\xi|}{\beta_0}\right)\right]$$

which is in agreement with (4.1).

For $\beta_0 = 0$ the result is:

$$G_4 = 0\,, \quad G_3 = \pi\xi_L\ \{-H_0(\xi_L|\xi_1-\xi|) - Y_0(\xi_L|\xi_1-\xi|) + 2i\ J_0(\xi_L|\xi_1-\xi|)\}\,.$$

This has been obtained already in the papers [1], [2], [5].

THE ADDED MASS AND DAMPING COEFFICIENT

The varying part of the pressure exerted by the water on the body equals:

$$p(x,y,z,t) = \frac{\epsilon^2}{2}\, gL\rho i\left\{\bar{\varphi}_2(\xi,\eta,\zeta) - i\,\frac{\gamma}{\xi_L}\,\bar{\varphi}_{2\xi}(\xi,\eta,\zeta)\right\} e^{-i\omega t}\,. \tag{5.1}$$

Considering only the heaving motion the vertical force acting on the ship becomes:

$$\begin{aligned} F_0 &= \frac{\epsilon^4}{8}\, gL^3 \rho i\, e^{-i\omega t} \int_{-1}^{1} d\xi \int_{c(\xi)} f_\zeta(\xi,\zeta)\left\{\bar{\varphi}_2(\xi,\eta,\zeta) - i\,\frac{\gamma}{\xi_L}\,\bar{\varphi}_{2\xi}(\xi,\eta,\zeta)\right\} d\xi \\ &= m_z\, \ddot{z}_0 + n_z\, \dot{z}_0\,, \end{aligned} \tag{5.2}$$

where

$$M_z = \frac{8m_2}{\rho L^3} = \frac{\epsilon^4}{4\sigma\,\xi_L\,\overline{\zeta}_0}\ \mathrm{Im} \int_{-1}^{1} d\xi \int_{c(\xi)} f_\zeta\left(\bar{\varphi}_2 - i\,\frac{\gamma}{\xi_L}\,\bar{\varphi}_{2\xi}\right) d\zeta \tag{5.3}$$

$$N_z = \frac{4\sqrt{2}\,n_2}{\rho L^2\sqrt{gL}} = \frac{\epsilon^4}{4\sigma\sqrt{\xi_L}\ \overline{\zeta}_0}\ \mathrm{Re} \int_{-1}^{1} d\xi \int_{c(\xi)} f_\zeta\left(\bar{\varphi}_2 - i\,\frac{\gamma}{\xi_L}\,\bar{\varphi}_{2\xi}\right) d\zeta \tag{5.4}$$

are the coefficients for added mass and damping.

For the case I these coefficients are already calculated for a family of cross section curves, see [6], [7].

In order to obtain the three dimensional and forward speed effects the terms originating from (3.2) must be added to (3.12). A comparison of these results with Gerritsma's experimental data show a qualitative agreement. The influence of forward speed, as expressed in (3.2), involves $F(\xi, \zeta)$. This function assumes positive values at the bow, negative values at the stern. The deviations from the midship behaviour in Gerritsma's results show the same character.

For the case II the coefficients can be obtained by computation of the results of section 4. If the forward speed is zero M_z and N_z become:

$$M_z = \frac{\epsilon^3 i}{2\xi_L \bar{\zeta}_0} \int_{-1}^{1} d\xi_1 \int_{c(\xi_1)} f_{\zeta_1}(\xi_1, \zeta_1) d\zeta_1 \int_{\substack{c(\xi)+ \\ \bar{c}(\zeta)}} F(\xi,\zeta) \ln \sqrt{(\eta_1 - f)^2 + (\zeta_1 + \zeta)^2}$$

$$- \frac{\epsilon^3}{4\pi} \int_{-1}^{1} b(\xi_1) d\xi_1 \int_{-1}^{1} b_\xi(\xi) \operatorname{sgn}(\xi_1 - \xi) \ln 2|\xi_1 - \xi| d\xi$$

$$+ \frac{\epsilon^3 \xi_L}{16} \int_{-1}^{1} b(\xi_1) d\xi_1 \int_{-1}^{1} b(\xi) \{H_0(\xi_L|\xi_1 - \xi|) + Y_0(\xi_L|\xi_1 - \xi|)\} d\xi \tag{5.5}$$

$$N_z = \frac{\epsilon^3 \xi_L^{3/2}}{8} \int_{-1}^{1} b(\xi_1) d\xi_1 \int_{-1}^{1} b(\xi) J_0(\xi_L|\xi_1 - \xi|) d\xi . \tag{5.6}$$

Here $b(\xi)$ is the beam at the point ξ.

The damping coefficient and the part of the added mass that depends on the frequency is calculated and represented in the graph below. For $b(x)$ is taken

$$b(x) = 2 \cos \frac{\pi}{2} x \quad \text{and} \quad \epsilon = 0.2 .$$

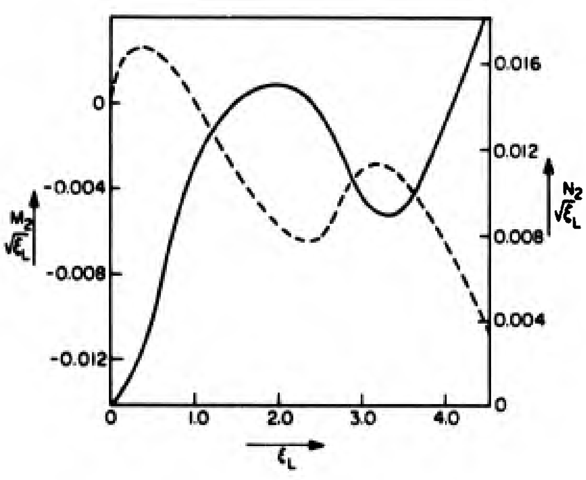

Up till $\xi \approx 2.5$ the curves have a character that can be expected for three-dimensional bodies. It can be compared, e.g., with the curves for a sphere calculated by Havelock [13]. Experimental data are only available for frequency parameters higher than 2.5, but there obviously the theory is not valid anymore.

CONCLUSIONS

It appears to be very useful, in dealing with the problem of a slender ship performing oscillatory motions at different forward speeds, to express the Froude number and the frequency parameter in terms of the slenderness parameter ϵ. For practical purposes the range of low Froude number and high frequency parameter is most interesting.

In this paper the first order term of the velocity potential is derived for the case where the Froude number is of order $\epsilon^{1/2}$ and the frequency parameter is of order ϵ^{-1}.

The theory presented here can easily be extended such as to determine the motion of a slender body in waves. Then a consistent pair of equations of motion for heave and pitch will follow.

The analysis of section 4 is resulting in the two dimensional strip theory if the slope of the bow- and stern-line is of order unity or smaller and the only problem then is to solve an integral equation for each cross section separately. If the slope is larger three dimensional and forward speed effects are present as well. The resulting integral equation can be solved by an iteration process, but an alternative method is to start the analysis from Greens' theorem instead of a source distribution on the hull.

Apart from the problem of the oscillatory motion of the ship an interesting result is obtained for the steady advancing slender ship.

For the case where the Froude number is of order $\epsilon^{1/2}$ the only first order contribution to the velocity potential and the wave resistance originates from the source distribution on bow- and stern-line. From this fact it becomes clear that it must be possible to affect the wave resistance by adding another singularity in the bow and stern region.

The strength of the singularity might be determined from a condition of minimum wave resistance. By adding a dipole at the bow the concept of a bulbous bow could be treated in the frame work of slender body theory.*

*See comments by Laitone on paper by Newman and Tuck.

REFERENCES

1. Ursell, F., "Slender Oscillating Ships at Zero Forward Speed," Journal of Fluid Mechanics, 1962.

2. Newman, J. N., "A Slender Body Theory for Ship Oscillations in Waves, Journal of Fluid Mechanics, 1964.

3. Vossers, G., "Some Applications of the Slender-Body Theory in Ship Hydrodynamics," Thesis, Delft, 1962.

4. Peters, A. S., and Stoker, J. J., "The Motion of a Ship," communication on pure and applied mathematics, Vol. X, 1957.

5. Joosen, W. P. A., "The Velocity Potential and Wave Resistance Arising from the Motion of a Slender Ship," Seminar on theoretical wave resistance, Ann Arbor, 1963.

6. Grim, O., "A Method for a More Precise Computation of Heaving and Pitching Motions Both in Smooth Water and in Waves," Third Symposium on Naval Hydrodynamics.

7. Tasai, F., "On the Damping Force and Added Mass of Ships Heaving and Pitching," Journal of Zosen Kiokai, July 1959.

8. Tuck, E. O., "The Steady Motion of a Slender Ship," Thesis, Cambridge, 1963.

9. Korvin-Kroukovsky, B. V., "Pitching and Heaving Motions of a Ship in Regular Waves," SNAME, 1957.

10. Vassilopoulos, L., "The Analytical Prediction of Ship Performance in Random Seas," Publ. Massachusetts Institute of Technology, 1964.

11. Gerritsma, J., and Beukelman, W., "Distribution of Damping and Added Mass Along the Length of a Ship Model," Publ. Shipbuilding Laboratory, Techn. University, Delft, 1963.

12. Jones, D. S., and Kline, M., "Asymptotic Expansion of Multiple Integrals and the Method of Stationary Phase," Journ. of Math. and Phys., 37, 1958.

13. Havelock, T., "Waves Due to a Floating Sphere Making Periodic Heaving Oscillations," Proc. Roy. Soc., London, A231, 1955.

Thursday, September 10, 1964

Afternoon Session

SHIP MOTIONS

Chairman: R. Brard

Bassin d'Essais des Carenes de la Marine
Paris, France

APPLYING RESULTS OF SEAKEEPING RESEARCH

Edward V. Lewis
Webb Institute of Naval Architecture
Glen Cove, Long Island, New York

ABSTRACT

Although developments in the theory of seakeeping are still continuing rapidly, this paper points out that presently available research results can be effectively applied to practical problems of ship design. The most useful tool is the method of superposition whereby almost any ship response to irregular short-crested seas may be predicted--provided the responses to regular waves are known. Pending the development of completely satisfactory methods of calculating these responses theoretically at all headings to waves, results of systematic model tests can be used.

A calculation procedure to be followed in making such predictions of ship behavior in irregular waves is outlined, and typical results of calculations are presented. These include trends of wave bending moments with ship size, speed, and heading. In the same manner, trends of relative bow motion are presented under the influence of similar factors.

Some general conclusions are drawn regarding the effects of ship size, proportions, speed, and heading on seagoing performance of ships. Needs for further oceanographic data, systematic model tests in waves, and advances in seakeeping theory are outlined. Future possibilities in the use of such research in developing improved naval ships are explored, with particular emphasis on the optimization of ship designs in relation to seagoing performance.

INTRODUCTION

Professor B. V. Korvin-Kroukovsky in the introduction to his classic paper on the theory of ship motions in regular waves [1] called attention to the need at times to apply "vigor" as well as "rigor." The emphasis of this symposium has been rightly placed on rigor — on refining and improving our theoretical tools for calculating the motions of ships in waves. This paper, along with certain other presentations, meanwhile, attempts to demonstrate that the application of vigor — even with our presently available tools — can yield valuable conclusions for the guidance of ship designers.

The basic theoretical tool available to us is the principle of superposition first applied by St. Denis and Pierson [2] to the study of ship responses to irregular seas. The essential empirical data that make it workable are systematic model tests, such as those of Vossers [3,4], and observational data on ocean wave spectra, such as those of Pierson and Moskowitz [5]. However, for practical application of even the best theory it is necessary to have a suitable calculation procedure. This may or may not be programed for electronic computer computation. Furthermore, for practical people to accept the results of such calculations it is necessary that they be able to visualize the factors involved and understand the trends obtained. It is the purpose of this paper to describe a convenient procedure whereby the performance of a ship in realistic irregular seas can be predicted and then to show the sort of trends and conclusions that can be obtained by the method.

The work discussed here has been carried out largely in connection with research sponsored by the American Bureau of Shipping and Society of Naval Architects and Marine Engineers. The paper itself has been prepared under ONR Grant Nonr(G)00063-64.

NON-DIMENSIONAL REPRESENTATION

It has been previously pointed out [6] that the dimensional characteristics of the conventional form of presenting sea spectra and ship response curves make it difficult to understand and interpret the results of the calculations, particularly when comparing geometrically similar ships of different size. Accordingly, a quasi-non-dimensional method of presentation was developed at Webb Institute based on a sea spectrum showing component wave slopes as a function of the logarithm of wave length [6]. Since the original proposal was made, it has been found that a suggestion of Dr. Y. Yamanouchi to use $\log_e \omega$ instead of $\log_e \lambda$ results in a truly non-dimensional representation which appears more suitable for general adoption. Here ω is circular frequency, $2\pi/T$, T is wave period, and λ is wave length. In this log-slope scheme not only is the sea spectrum independent of the units used, but geometrically similar ships will have similar response operators. Hence, it will be shown that the effect of ship size and form, sea spectrum shape, etc., can be clearly visualized. It is unnecessary to convert to frequency of encounter as originally proposed [2].

In order to explain the new form of presentation, reference is made first to Fig. 1 showing the transformation of a typical wave amplitude spectrum (a), $[r(\omega)]^2$ vs ω, to log-slope form (c). The first step is the transformation from ω to $\log_e \omega$ base. This is accomplished by finding the increment on $\log_e \omega$ scale, $\delta(\log_e \omega)$ that corresponds to $\delta\omega$, thus:

$$\delta(\log_e \omega) = \frac{d(\log_e \omega)}{d\omega}$$

$$= \frac{\delta\omega}{\omega} .$$

Hence, for an incremental area to be the same in both systems,

$$[r(\log_e \omega)]^2 = \omega[r(\omega)]^2 .$$

It so happens that the range of $\log_e \omega$ of general interest to us is negative in sign.

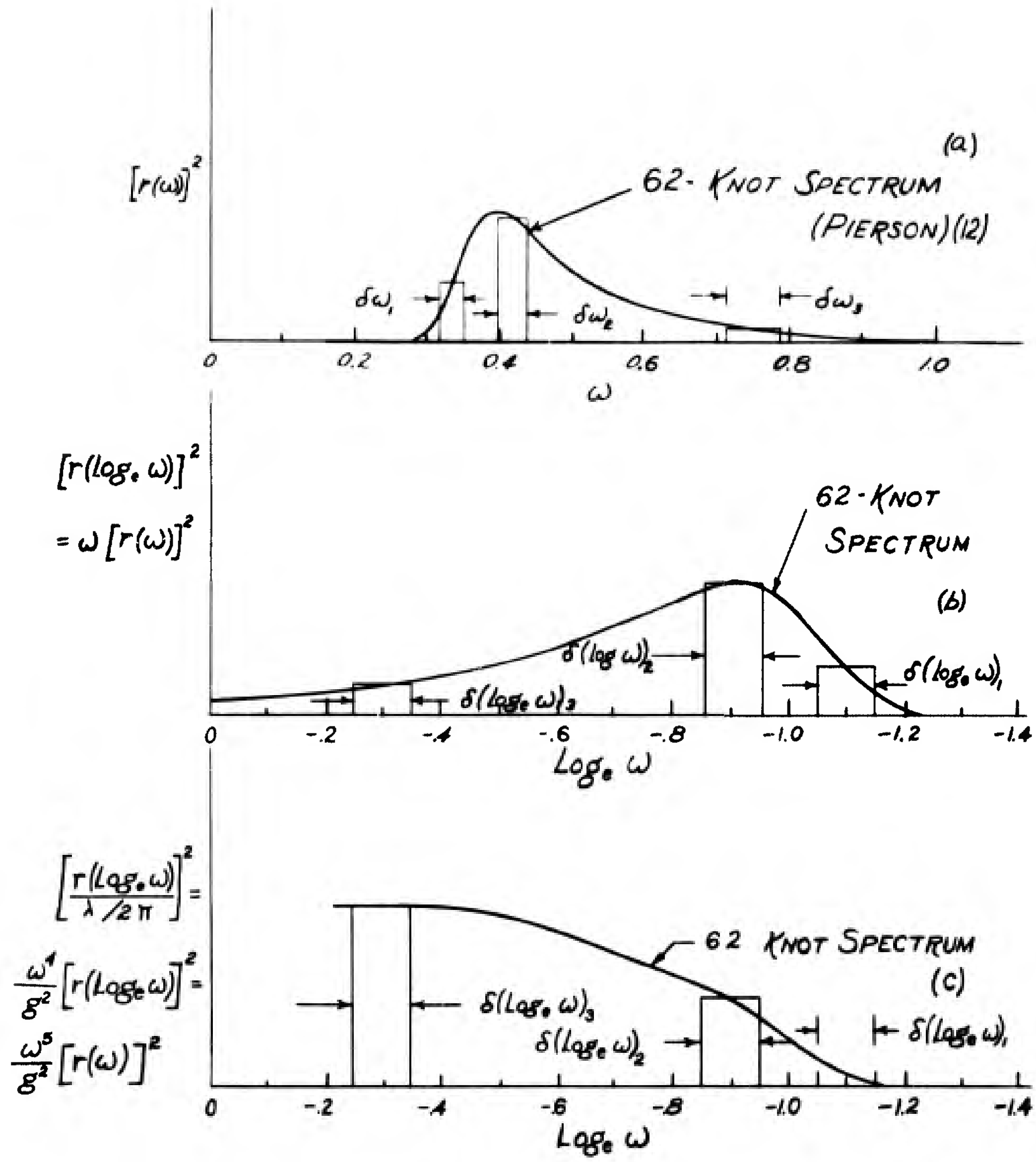

Fig. 1 - Transformations of sea spectrum

Finally, for the present purpose the spectrum must be transformed from amplitude (b) to slope (c) form. In general, maximum wave slope is $2\pi\zeta_a/\lambda$. Since $\lambda = 2\pi g/\omega^2$, maximum slope can be expressed in terms of ω,

$$\frac{\omega^2 \zeta_a}{g}$$

where ζ_a is wave amplitude. The square of the amplitude of a wave component is given by:*

$$[r(\log_e \omega)]^2 \, \delta \log_e \omega$$

where $[r(\log_e \omega)]^2$ represents the wave spectral ordinates on the $\log_e \omega$ base. Therefore, the square of the slope is given by:

$$\frac{\omega^4}{g^2} [r(\log_e \omega)]^2 \, \delta \log_e \omega .$$

Hence, if the spectral ordinate plotted in (c) represents

$$\frac{\omega^4}{g^2} [r(\log_e \omega)] ,$$

an incremental area will represent the square of a component wave slope. Furthermore, the area under the spectrum (with finite limits) can be interpreted as a mean wave slope.

The most obvious difference between the log-slope form and the conventional form of spectrum is the suppression of the spectrum peak which is so prominent in the conventional form of presentation. This calls attention to the fact that the wave components at the peak of a conventional spectrum are usually less steep than at the higher frequencies. It has been found that for many ship motions wave amplitude in relation to length, i.e., wave slope, is more important than wave amplitude directly, or energy. For such motions, the log-slope form is preferable for the study of ship behavior.

For example, pitch angle is directly related to maximum slope. In fact, as wave lengths become very long and the frequency of encounter is far from resonance with the ship's natural frequency, pitch amplitude will approach wave slope asymptotically.

The manner in which the new form of log-slope sea spectrum may be used in predicting ship responses is shown in Fig. 2 for the case of pitching motion. The figure shows the simple case of a ship heading directly into a long-crested

---

*The original concept of [2] is used here, in which the spectrum represents amplitude squared. In some systems a factor of 1/2 is introduced in order to represent wave energy.

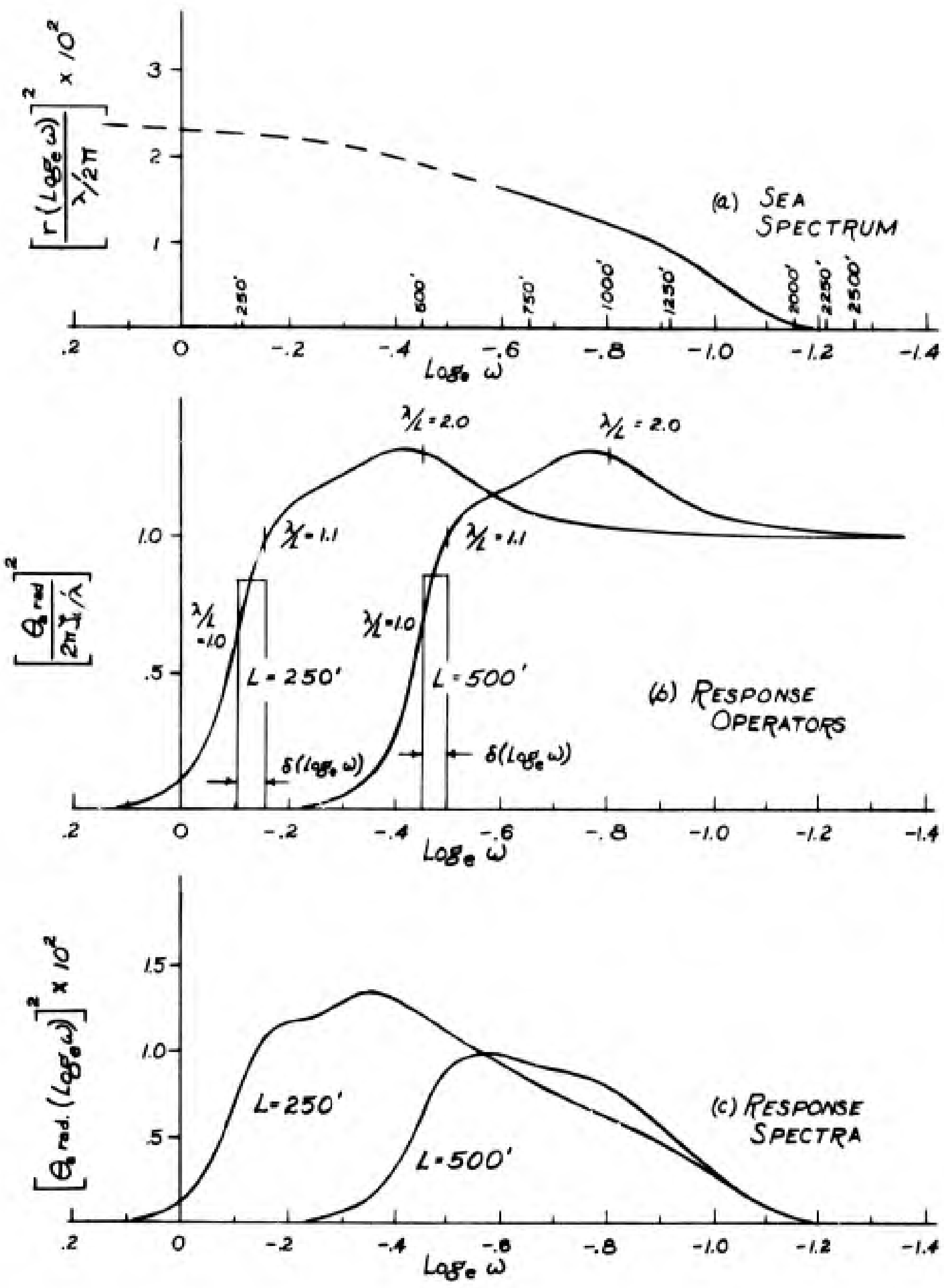

Fig. 2 - Non-dimensional representation of pitching response to irregular sea

irregular sea (a), but it will be shown later that a short-crested sea and different headings can also be taken into account. In determining the form of the response amplitude operators, it must be recognized that the parameters describing ship performance should be non-dimensional. Pitch angle is a satisfactory measure of angular motion, for it will be the same for ships of different size in comparable situations as well as being related to wave slope. Fig. 2(b) shows the pitching response amplitude operator in the form

$$\frac{\theta_a}{\frac{2\pi\zeta_a}{\lambda}} = \frac{\theta_a}{\frac{\omega^2}{g}\zeta_a}$$

with θ_a in radians. It is clear that if the response operator curves are expressed non-dimensionally — here pitch angle/wave slope — they will be identical in shape for geometrically similar ships at the same Froude Number. However, they are separated horizontally by an amount equal to $\log_e \omega_1/\omega_2$. Furthermore, points at corresponding values of λ/L will have the same ordinates, where L is ship length.

If, as in this case, one ship is twice the length of the other, we have $L_2 = 2L_1$, and at equal values of λ/L, $\lambda_2 = 2\lambda_1$. Hence, $\omega_1 = \sqrt{2}\,\omega_2$, and the separation of corresponding points is $\log_e \omega_1 - \log_e \omega_2 = \log_e \omega_1/\omega_2 = \log_e \sqrt{2} = 1/2 \log_e 2 = 0.3468$.

Finally, we may multiply the wave slope spectrum (Fig. 2a) by the pitch response operators (Fig. 2b) to give the non-dimensional response spectra (Fig. 2c). These non-dimensional response spectra are of direct quantitative significance, since they represent (pitch amplitude)^2 and the mean pitch amplitudes will be a function of the areas under the curves.

Similarly heaving acceleration — or vertical acceleration at any point along the length of the ship — is properly referred to wave slope. For in long waves, if we neglect forward speed, the vertical motion of the ship will approach that of the surface wave particles, whose vertical acceleration is, when expressed non-dimensionally, $(\omega^2/g)\,\zeta_a$. Maximum wave slope at any particular frequency is the same, for

$$\frac{2\pi\zeta_a}{\lambda} = 2\pi\zeta_a \frac{\omega^2}{2\pi g} = \frac{\omega^2}{g}\zeta_a .$$

Hence, if vertical acceleration is referred to wave slope, this is equivalent to relating it to the wave particle accelerations at the particular wave frequency. The response amplitude operator for heaving acceleration (or vertical acceleration at any point) can therefore be expressed as

$$\left[\frac{\ddot{Z}_a/g}{2\pi\zeta_a/\lambda}\right]^2 = \left[\frac{\ddot{Z}_a}{\omega^2\zeta_a}\right]^2 .$$

Heaving motion is somewhat different. If one is concerned with the absolute value of heaving, then the conventional wave amplitude spectrum is appropriate, with a response amplitude operator in the form:

$$\left[\frac{\text{Heave amplitude}}{\text{Wave amplitude}}\right]^2 = \left[\frac{Z_a}{\zeta_a}\right]^2 .$$

But when a non-dimensional relationship is appropriate, one may divide by a ship dimension such as length, giving a ratio, Z_a/L. This means that we consider two ships to have equivalent heaving behavior in comparable conditions if the ratios of heave amplitude to ship length are the same. (This is in contrast to the conventional procedure to comparing heave amplitudes directly.) The parameter Z_a/L will be the same for geometrically similar ships in similar waves. The response amplitude operator may be obtained by dividing by the wave slope, which is also non-dimensional, thus:

$$\left[\frac{Z_a/L}{2\pi\zeta_a/\lambda}\right]^2 = \left[\frac{Z_a/L}{\frac{\omega^2}{g}\,\zeta_a}\right]^2 .$$

This operator goes to infinity as wave length becomes very long and Z_a approaches infinity.

Similarly, vertical velocity, $\dot{Z}_a = \omega_e Z_a$, can be non-dimensionalized by multiplying $\dot{Z}_a/L$ by $\sqrt{L/g}$, giving $\dot{Z}_a/\sqrt{gL}$ which is a sort of Froude number. The response amplitude operator is then,

$$\left[\frac{\dot{Z}_a/\sqrt{gL}}{2\pi\zeta_a/\lambda}\right]^2 = \left[\frac{\dot{Z}_a/\sqrt{gL}}{\frac{\omega^2}{g}\,\zeta_a}\right]^2 .$$

This operator also goes to infinity as wave lengths become very long, but not so rapidly as the above.

Multiplying the non-dimensional velocity $\dot{Z}_a/\sqrt{gL}$ again by $\omega_e\sqrt{L/g}$ gives the non-dimensional acceleration previously discussed, $\ddot{Z}_a/g$.

Similarly, any other response that is non-dimensional may be related to wave slope. For example, relative bow motion, S_a, in relation to length, L, is more significant than the absolute value, S_a, and therefore S_a/L is an appropriate non-dimensional parameter. Although similar in appearance to the heave parameter, it tends toward zero in very long waves.

The response amplitude operator for relative vertical velocity between bow and wave, which is of significance in relation to slamming, can be obtained by multiplying S_a/L by $\omega_e\sqrt{L/g}$, giving

$$\frac{S_a\omega_e}{\sqrt{gL}} = \frac{\dot{S}_a}{\sqrt{gL}}$$

which is a non-dimensional relative velocity. The response amplitude operator then is,

$$\left[\frac{\dot{S}_a/\sqrt{gL}}{2\pi\zeta_a/\lambda}\right]^2 = \left[\frac{\dot{S}_a/\sqrt{gL}}{\frac{\omega^2}{g}\zeta_a}\right]^2$$

Also wave bending moment, if expressed in non-dimensional form, may be divided by wave slope, giving [11]:

$$\left[\frac{h_e/L}{2\pi\zeta_a/\lambda}\right]^2$$

where h_e is effective wave height and h_e/L is a non-dimensional bending moment coefficient,

$$\frac{M_w}{c\rho g L^3 B C_w}$$

where

M_w is wave bending moment in irregular sea (such as average or highest expected value in 10,000 cycles),

c is a static bending moment coefficient = static wave bending moment in $L/20$ wave$/\rho g L^2 B(L/20) C_w$,

ρ is mass density of water,

g is acceleration of gravity,

L is ship length,

B is ship breadth,

C_w is waterplane coefficient.

An important step in the application of the superposition principle to ship behavior was taken by Gerritsma [7] when he showed that the added resistance, power, torque, or propeller revolutions in waves could also be handled in this way. However, the work of Maruo [8] had indicated that these quantities are roughly proportional to the square of wave amplitude and therefore should not be squared as are motion amplitude operators. The non-dimensional coefficient of power increase, ΔP, used by Gerritsma was

$$\pi_r = \frac{\Delta P}{\rho g \zeta_a^2 V B^2/L}$$

which is also the response amplitude operator. Swaan has applied the superposition procedure to predicting trends of power and speed in waves [9], using this coefficient and a conventional amplitude or energy spectrum.

For use with a slope spectrum it is convenient to adopt the modified coefficient,

$$\pi = \frac{\Delta P\ (\lambda/L)^2}{\rho g \zeta_a^2 V B}\ .$$

Study of Gerritsma's model results [7] shows that the trend with λ/L indicated by this coefficient is roughly correct for values of λ/L greater than about 1.0, but it reverses for $\lambda/L < 1.0$. Nevertheless, the coefficient appears to be entirely suitable for use with a wave slope spectrum.

So far mention has been made only of the simple case of ship response to long-crested irregular head seas. The method of presenting data can easily be extended to the case of short-crested seas and any ship heading — provided, of course, that model test results in oblique seas are available. The short-crested sea is represented by a family of curves showing the magnitude of wave components coming from different directions. Response amplitude operator curves are also prepared for different wave directions, and each of the directional spectrum curves must be multiplied by the appropriate response amplitude operator curve. The resulting family of response spectral components can be integrated to obtain a single response spectrum on a base of $\log_e \omega$. This procedure will be illustrated in the section on results.

The computations required to obtain the curves that have been discussed can be conveniently carried out by slide rule or desk computer with the use of a suitable computation form. The form and procedure developed at Webb Institute of Naval Architecture, mainly in connection with work for the American Bureau of Shipping, is described in [10]. It has also been programed for solution on an IBM 1620 computer.

RESULTS — WAVE BENDING MOMENTS

The application of the procedures discussed above can be illustrated first by considering trends of wave-induced bending moments for a series of ships for which model results in regular waves were available [3]. This work was carried out under the sponsorship of the American Bureau of Shipping.

Figure 3 has been prepared to show graphically the calculation for the case of the 0.80 block ship heading into short-crested irregular seas. The upper portion of the figure shows a spectrum based on the average of the 13 worst records reported by Pierson [5], with directional components obtained by applying a "spreading function" of $2/\pi \cos^2 \mu_w$ to approximate the effect of short-crestedness. The second part of the figure shows the family of curves representing the response amplitude operators derived from the model test results, each curve for the 600-foot ship length defining the response of the model to the waves coming from a particular angle. The curves are labeled with the angles μ indicating the responses to the same angular wave components as those shown in the sea spectrum. Each of these component response curves was derived from the model tests at a particular angle to the waves by picking off the results at the appropriate angles.

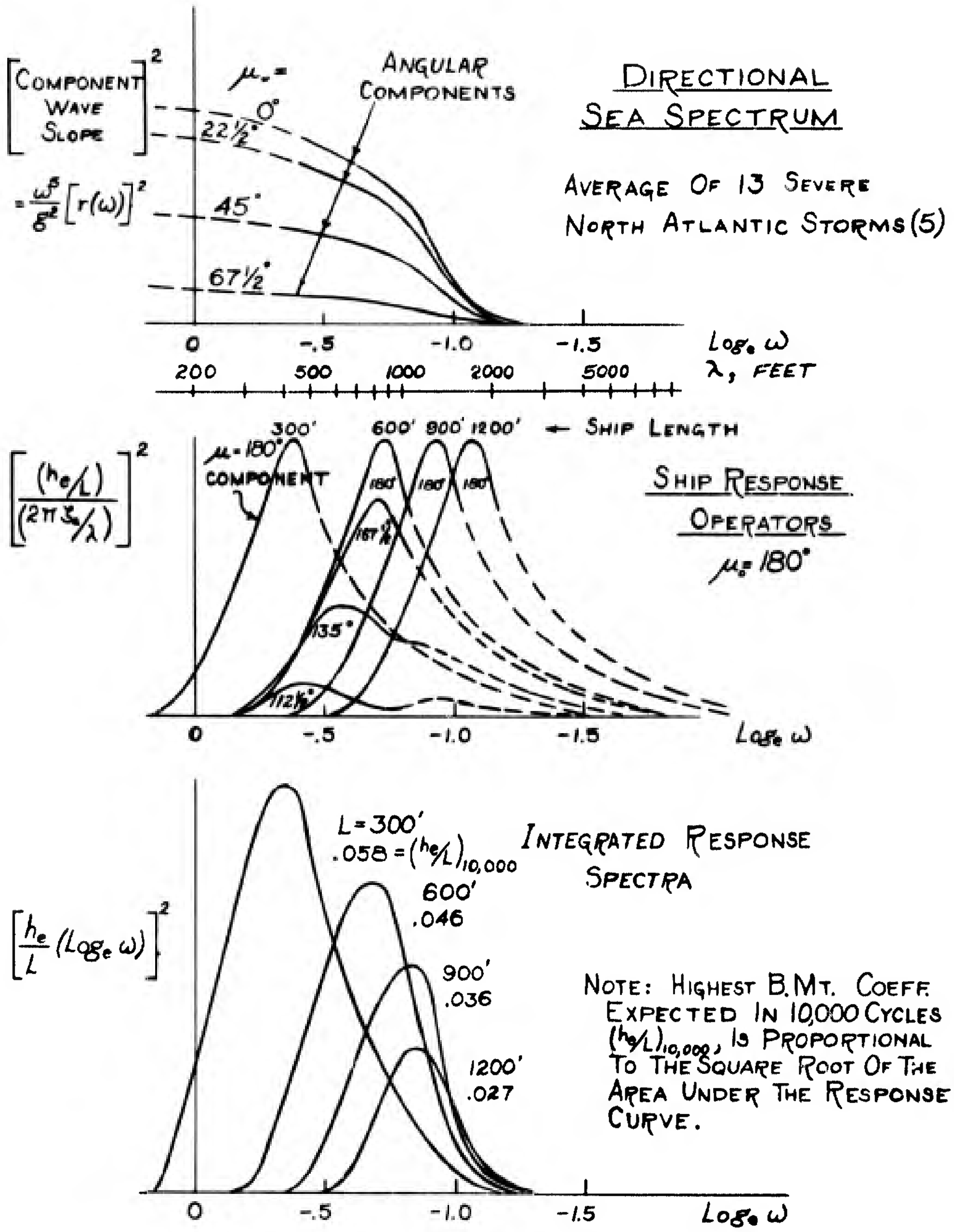

Fig. 3 - Bending moment prediction for c_B = 0.80 ships

Also shown in this plot are the head sea response operators expanded to ship lengths of 900 and 1,200 feet, and reduced to 300 feet. The other angular components for these lengths have been omitted from the figure for clarity. A comparison of the operator curves for different ship lengths demonstrates the advantage of the form of presentation used in these calculations — the response operators for any series of geometrically similar ships plot as a set of identically shaped curves, shifted on the $\log_e \omega$ axis according to the absolute sizes of the ships. Portions of the curves shown by broken lines are extrapolated beyond the measured data.

The product of a sea spectrum component for a certain angle μ_w, and the response amplitude operator component associated with that wave direction gives a response spectrum component curve. The family of curves obtained in this way (one curve for each wave component) is then integrated over direction (angle) to obtain a single response curve. Four such integrated response curves for the four ship lengths are shown in the lower plot of Fig. 3. The angular components of the response spectra have not been plotted.

Finally, the integration of a response spectrum curve over wave frequency gives the cumulative energy density, R, for the bending moment coefficient. From values of R for each ship size statistical parameters, such as the average value of the highest expected wave bending moment coefficient out of a total of N oscillations, may be calculated from the expression, $h_e/L = C\sqrt{R}$ where the multiplier C takes different values depending on the number of oscillations considered. For example, assuming a Rayleigh distribution,

Average h_e/L	$= 0.866\sqrt{R}$
Average of 1/10 highest h_e/L	$= 1.800\sqrt{R}$
Highest expected h_e/L in 100 oscillations	$= 2.280\sqrt{R}$
Highest expected h_e/L in 1,000 oscillations	$= 2.730\sqrt{R}$
Highest expected h_e/L in 10,000 oscillations	$= 3.145\sqrt{R}$.

The variation of wave bending moment with ship speed is shown in Fig. 4 for a ship heading directly into a severe 62-knot spectrum [12]. It is evident that increasing the speed of a ship does not in general increase the wave bending moments. Decreasing speed can, in fact, increase the wave bending moments slightly. No consideration is given here to two other effects of speed, namely the increase in the bending moment caused by ship-produced waves as speed increases and the effect of speed on slamming which may increase midship hull stresses. The former causes a shift of the mean value; the magnitude of the effect of slamming requires further detailed study.

The vertical wave bending moment is also influenced by the direction of the ship's travel relative to the waves. In a short-crested sea the wave components come from various directions simultaneously, so that regardless of its heading the ship reacts to waves coming from many angles. The heading of a ship is defined here as the angle between the direction of ship's motion and that of the

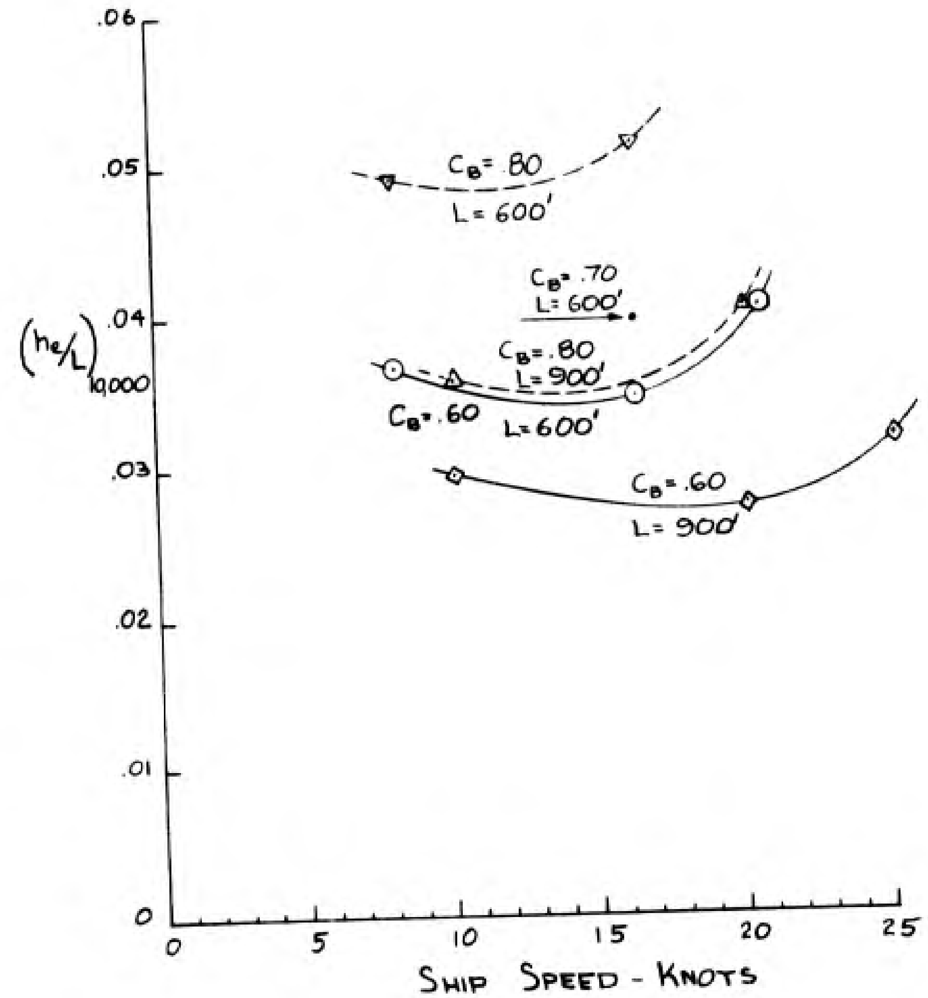

Fig. 4 - Bending moment for series 60 ships in Pierson 62-knot spectrum as a function of speed (highest expected value of h_e/L in 10,000 cycles)

dominant waves, i.e., of the wind. The calculated bending moments are the result of superimposing the ship's response to all wave components present for each heading.

The effect on wave bending moment of ship heading is shown in Fig. 5 for ships of 600-foot length in both short and long-crested seas, corresponding to the 62-knot spectrum [11]. This figure indicates that maximum bending moments are reached in head seas, as expected, and are then less in realistic short-crested than in hypothetical long-crested seas. It also shows the reduction in bending moments in beam seas is comparatively small when the waves are short-crested, especially for fine ships.

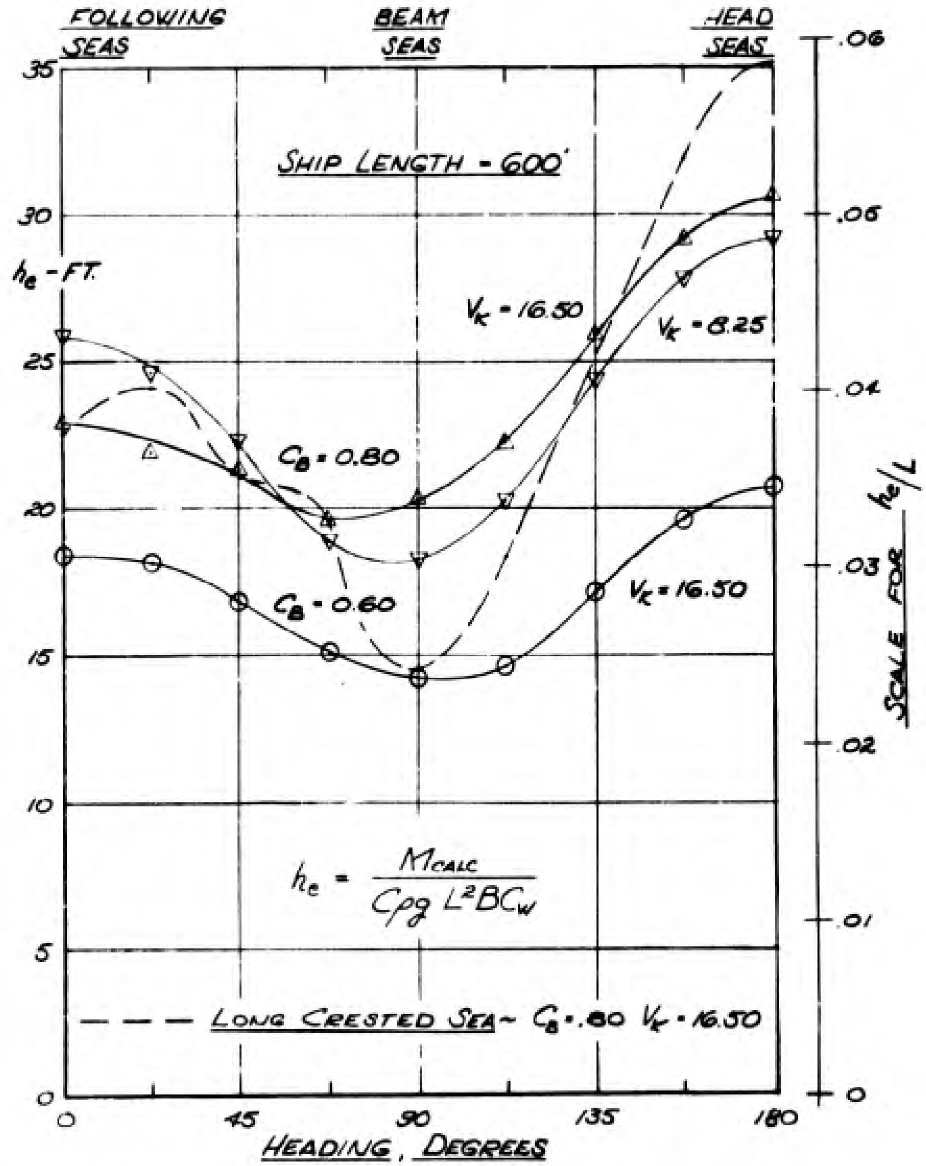

Fig. 5 - Variation of effective wave height and bending moment coefficient with heading (vertical bending only)

The comparatively high values of bending moment calculated in beam seas seems reasonable on the basis of the principle of superposition. However, it should be noted that the application of this principle to ship behavior in short-crested seas has not yet been confirmed through model tests. It is to be hoped that facilities for generating realistic short-crested seas in a model tank will be developed by some laboratory in order to check and confirm the superposition principle.

The results of the calculations for tanker type vessels with $C_B = 0.80$ in the average severe spectrum (Fig. 3) are shown in Fig. 6, which gives effective wave height as a function of length [11]. A low ship speed of Froude number = 0.10 (8.25 knots for a 600-foot ship) was considered to be a reasonable maximum speed in an extremely rough sea. The curve crosses the $L/20$ line at $L = 500$ feet, and coincides with the $0.6L^{0.6}$ wave that has been proposed from about 500 feet to 650 feet. The matching of the calculated trend with these other criteria thus provides a sound basis for the comparison of the larger ships with those of 500 to 650 feet, even if the absolute significance of the statistical parameter is doubtful. The calculated trend indicates that at lengths greater than 600 feet the increase in effective wave height with length is less rapid than is shown by the other criteria.

The results for the finer ships are also shown in Fig. 6. A somewhat higher speed (Froude number = 0.15; 12.4 knots for a 600 foot ship) was used since the finer ships could be expected to make better speed in rough seas. Possible increased stresses caused by slamming were not included. The trend with length is similar to that for the fuller ships, and from 15 to 20% lower. Thus the bending moment coefficient is not quite proportional to block coefficient, since in that case the reduction would have been 25%. However, it should be noted that fullness is already taken into account in the bending moment coefficient h_e/L which includes the waterplane coefficient.

RESULTS — BOW MOTIONS

The trends of ship motions in irregular seas have also been investigated, with particular reference to relative bow motion. This work has been carried out under the sponsorship of the Society of Naval Architects and Marine Engineers, Panel H-7 of the Hydrodynamics Committee. Calculations are based on Vosser's Series 60 model tests in regular waves [4], showing the effect of both speed and proportion.

Figure 7 shows the results for a ship of $C_B = 0.70$ and $L/H = 17.5$ at various speeds in short-crested head seas, using one of the severe sea spectra used in the bending moment study [12]. It may be seen that the response amplitude operator peaks increase steadily with speed. They also move to the right with increasing speed, which has a favorable effect — because of the downward slope of the wave spectrum. However, the overall effect of speed is unfavorable, as shown by the response spectra at the bottom of the figure.

Figure 8 shows in a similar way the effect of varying the L/H ratio when heading into the same sea at constant speed. It may be seen that the reduction in height of the response amplitude operator peaks with increasing L/H results in a corresponding reduction in response spectra.

The trend with ship speed is shown more clearly in the upper part of Fig. 9. Also shown in the figure are two points from Fig. 8 for ships of different length/draft ratio at the same speed.

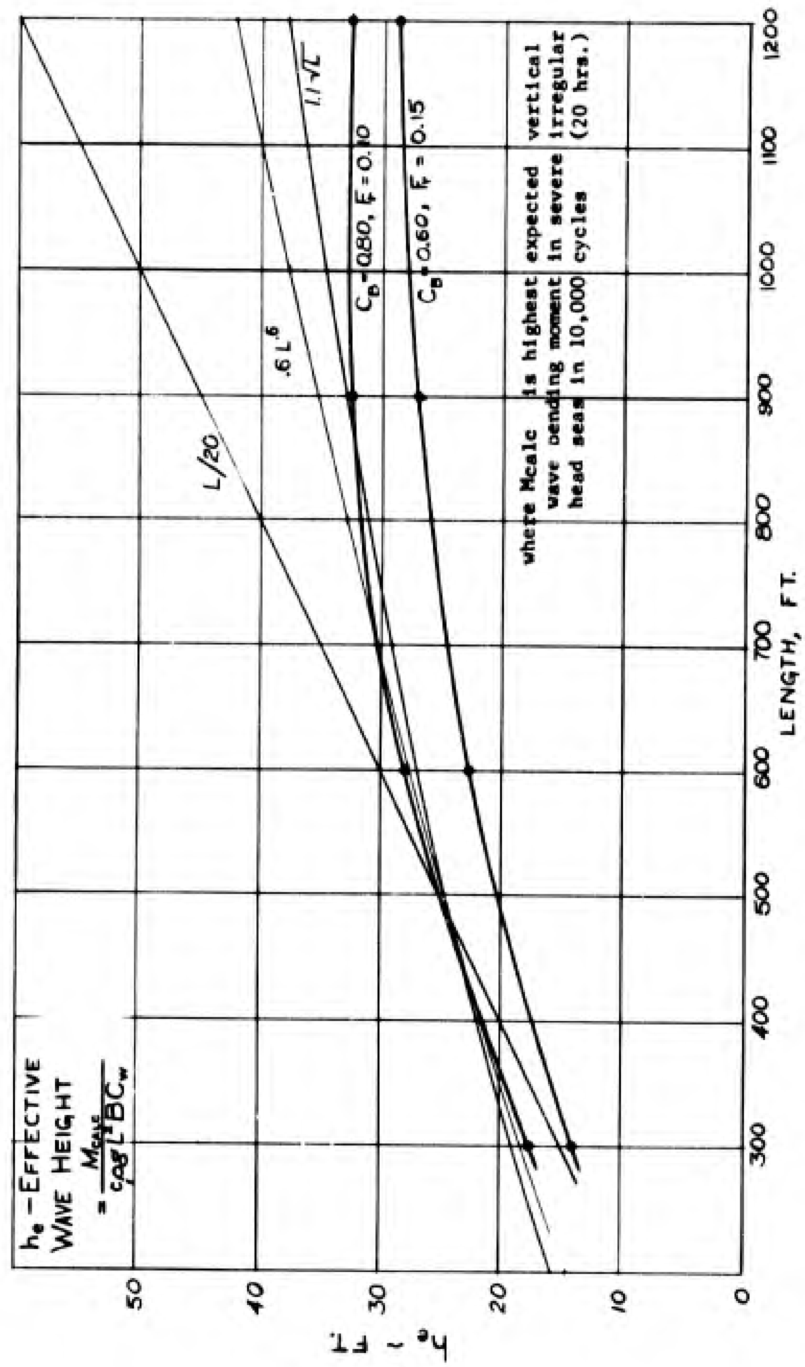

Fig. 6 - Trend of effective wave height h_e with ship length computed for ships of 0.60 and 0.80 block coefficient in severe short-crested irregular head seas, in comparison with other wave height formulations

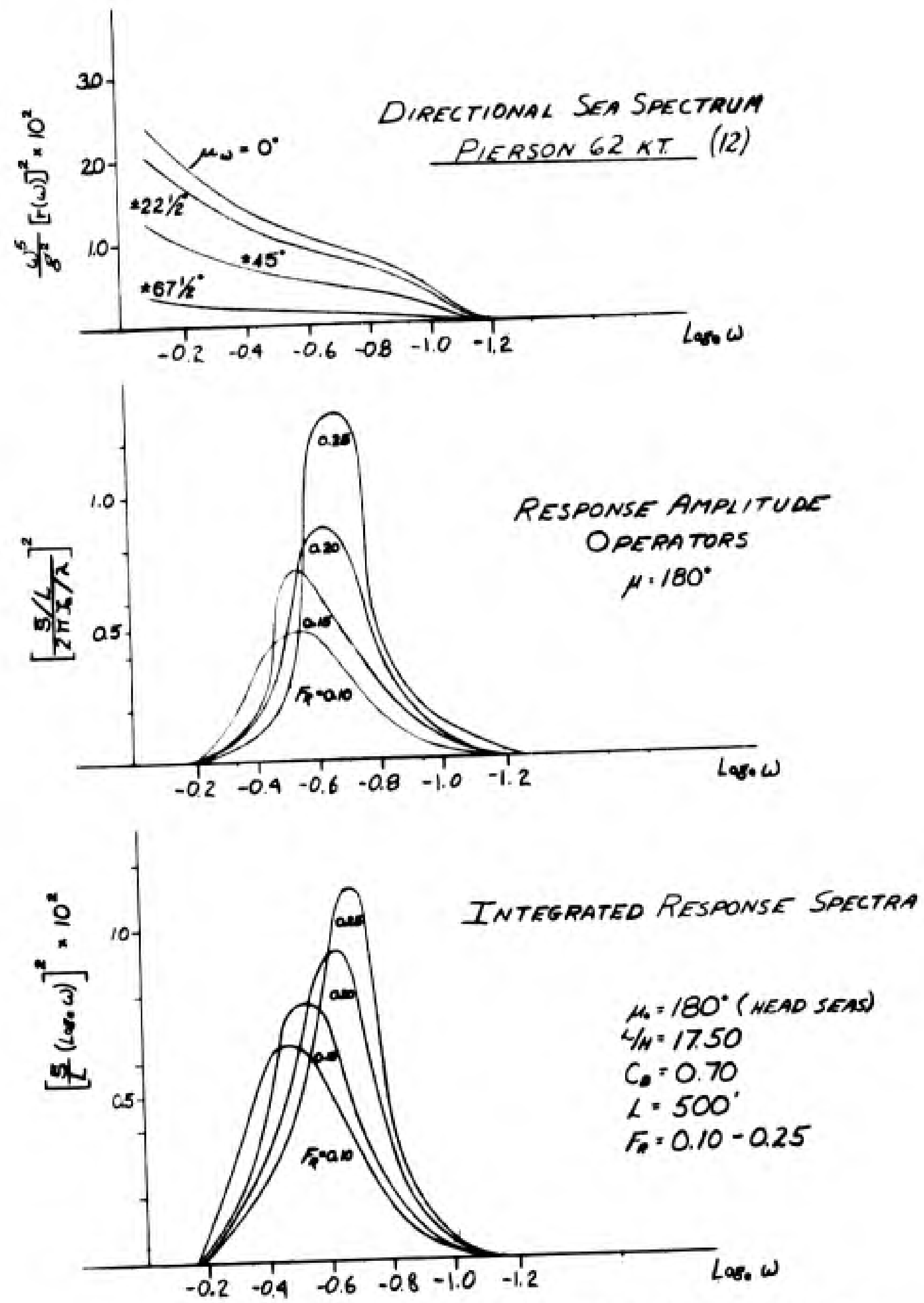

Fig. 7 - Relative bow motion, series 60 ship in Pierson 62-knot spectrum at various speeds

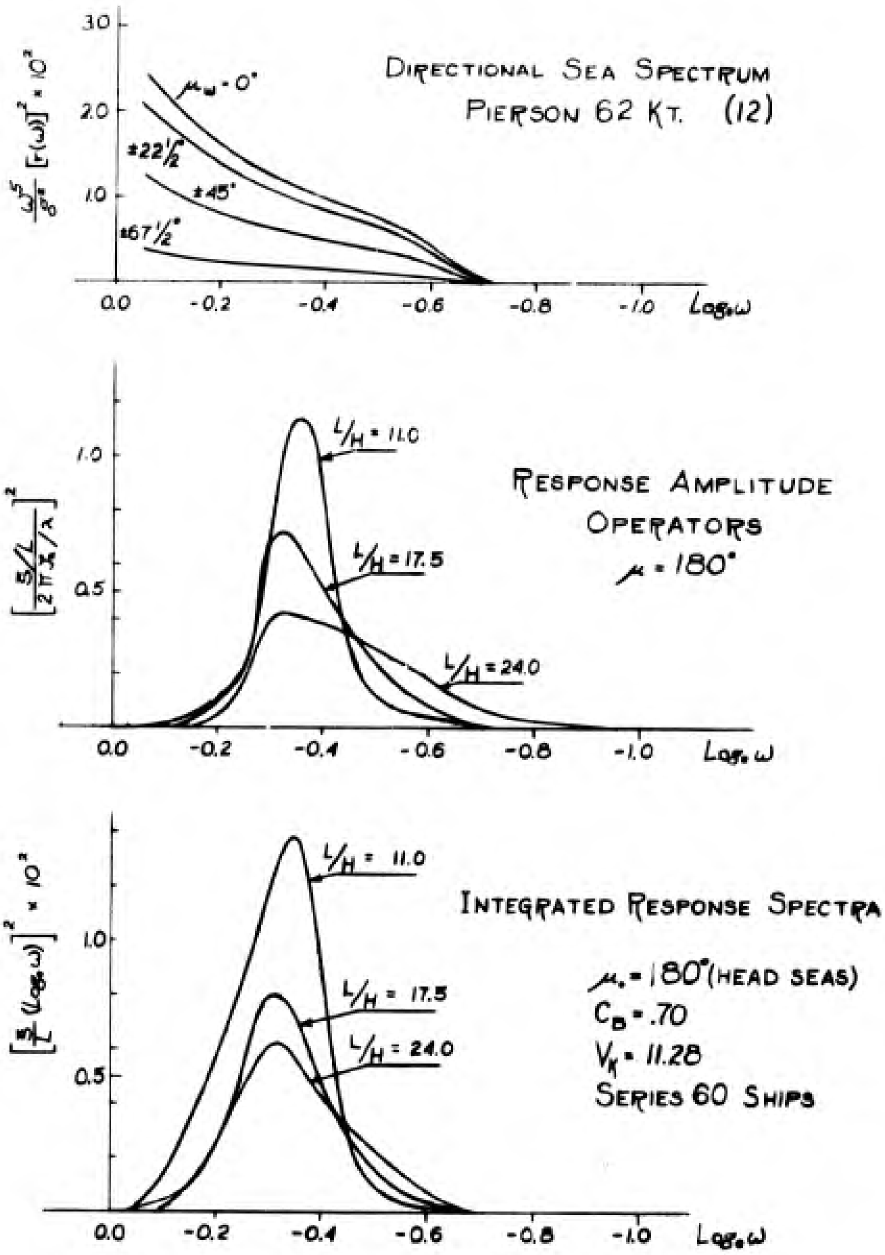

Fig. 8 - Relative bow motion of series 60 ships in Pierson 62-knot spectrum showing effect of L/H

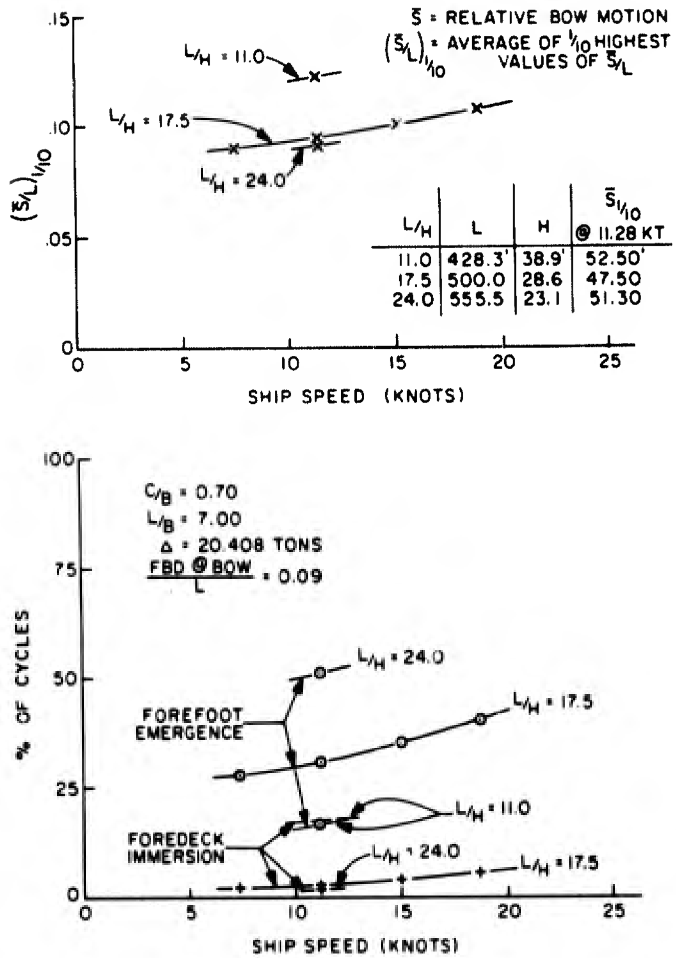

Fig. 9 - Relative bow motion for series 60, C_B = 0.70 ship in Pierson 62-knot spectrum, trends with speed

Of more direct interest in evaluating a ship's seagoing performance than relative bow motion are two derived quantities:

(a) Foredeck immersion, as an index of shipping water.

(b) Forefoot emergence, as a rough indicator of possibility of slamming.

For a particular forward freeboard or draft these quantities can easily be worked out statistically from the response spectra. A convenient form of presentation is in terms of percentages of cycles of motion in which the foredeck is immersed or the forefoot emerges, as shown in the lower part of Fig. 9.

It is interesting to see from this figure that increasing speed is even more unfavorable to wet decks than was suggested in the upper part of Fig. 9. For increasing the speed from 7-1/2 to 20 knots almost doubles the frequency of foredeck immersion. It also shows a big advantage of L/H = 17.5 over L/H = 11.0. In all cases bow freeboard is 9% of length.

Considering the question of forefoot emergence, Fig. 9 shows again a disadvantage in speed. Conversely, it shows that slowing down will always ameliorate the situation. However, it also shows a distinct disadvantage for a slender ship with high L/H value. This is because, although the shorter ships have more relative bow motion, their greater draft serves to reduce the frequency of bow emergence. Definite conclusions regarding slamming cannot be drawn, however, because the form of the more slender ships involves less flat of bottom and therefore less tendency to slam when the bow does emerge. Further investigation is clearly needed, but the calculation procedure described does indicate the trends of forefoot emergence.

Finally, the effect of ship heading can be considered. Figure 10 shows the trend of relative bow motion with ship heading for the case of one particular ship at one speed. The improvement shown in behavior as the bow falls away from the sea is to be expected, but it is perhaps surprising to see such small changes for all headings between a beam and a following sea.

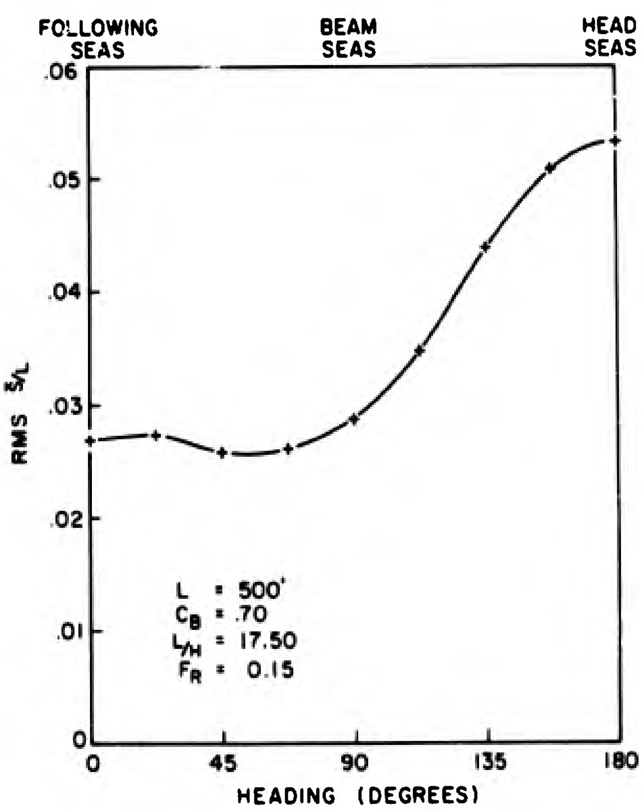

Fig. 10 - Relative bow motion effect of heading in Pierson 62-knot spectrum series 60, C_B = 0.70 ships

CONCLUSIONS

A method of computing the response of a ship to irregular waves is available which is non-dimensional and convenient for graphical presentation. Use of this log-slope form of plotting shows that for most ship responses the wave components at the peak of the wave spectrum may be less significant than the shorter wave components. It also shows that the cut-off point, or maximum wave length present, is of considerable importance.

Samples of the application of the procedure lead to certain general conclusions:

Non-dimensional wave bending moment coefficients in very severe seas show a distinct downward trend as ship size increases.

Wave-induced bending moments in severe storm seas are affected relatively little by increase of speed, but relative motion between bow and wave is appreciably affected. High values of length/draft ratio show a distinct advantage in this respect which leads to less shipping of water forward with a given freeboard/length ratio. But possible danger of slamming from greater forefoot emergence should be considered.

Change of heading has a significant effect on wave bending moments, but much more so in long-crested than in short-crested seas. Relative bow motion is greatly reduced by a change from head to beam seas.

FUTURE POSSIBILITIES

It is of interest to consider some of the further possibilities in the application of results of seakeeping research. One of the obvious steps being undertaken at M.I.T. [13] and elsewhere is to make use of calculated response amplitude operators instead of model test values. This requires perhaps some further refinement in ship theory along the line of work by Grim [14] and Gerritsma [15]. It also requires that the theory be extended to oblique seas in order that short-crestedness can be properly taken into account. Preliminary investigation of this important problem indicates that it may not be too difficult [16]. Lalangas [17] has shown that pitching and heaving motions in oblique seas can be predicted quite well simply by allowing for the effect of heading on effective wave length, frequency of encounter, and ship-wave interaction effects such as "Smith effect." In due course it will be possible to evaluate the seagoing performance of any number of alternative designs entirely by electronic computer.

Meanwhile, systematic model tests at all headings to regular waves can provide the needed inputs (response amplitude operators) into our calculations. For ships of very unusual characteristics, such as semi-submerged types for supercritical operation [18], model tests are the only reliable basis for the calculations. The excellent work of Vossers [3] should be extended to cover a wider range of ship characteristics and speeds. From the viewpoint of naval ship design, the need for systematic model tests is particularly great, for very little complete information is now available. For example, many reports on naval ship motions give pitch and heave amplitudes in regular head seas, but no information of phase angles that would permit relative motion between bow and wave to be computed, or vertical acceleration at any point along the length of the ship. Furthermore, motions in oblique seas are unknown. It is to be hoped that vigor will be applied here in systematic experimental work.

A related development of great importance is the application of electronic computers to the preliminary "feasibility study" stage of ship design. Pioneering work in the field of merchant ship design [19] is now being applied to the naval design problem. The outstanding result of this work to date is the clear demonstration that, insofar as the ship design problem for ideal, calm water conditions is concerned, there are many possible technical solutions. Assuming certain required characteristics, such as payload, range, and speed, the principal technical requirements to be met, which can be expressed in equation form, are: displacement, volume, stability, and freeboard. But the number of ship variables to choose from — as dimensions, fullness, power, etc. — is much greater. In short, there are more unknowns than there are equations, a situation which is disturbing to a mathematician but intriguing to the naval architect who discovers he has a wider freedom of choice than he had previously realized. Following the traditional trial and error approach, the designer was apt to feel, when a satisfactory compromise of all the factors was reached, that this was the only possible design solution — or at least that he could not depart far from it. But results show [19] that very wide variations in overall dimensions are possible with only slight changes in the cost criterion used (capital charges plus fuel).

The significance of all this to the seakeeping problem is that the availability of a method of realistically evaluating the seagoing performance of widely different alternative ship designs opens the door to definite improvements in the economic efficiency of merchant ships and the military effectiveness of naval vessels. The procedure is visualized as follows for the case of a destroyer-type ship whose primary mission is patrol duty in the North Atlantic, for example. A wide range of possible ships is determined, each of which has the required speed, payload, and range. The potential performance of each design is then predicted on the basis of some criterion such as percentage of time that a stated speed or speeds can be attained at sea without shipping water. Cost factors and operations research techniques must finally be brought into the picture to ascertain which design is best from the viewpoint of military effectiveness. It is my firm belief that the optimum ship designed in this way will not be the same as that designed for minimum displacement, minimum power on trial, or other purely technical criteria. In short, vigorous application of techniques now at hand should lead to better ships for the Navy.

These future developments will be greatly enhanced in value if much more complete information on ocean wave spectra encountered on various trade routes becomes available. The excellent work of Pierson [5] is only a beginning. Furthermore, there is a real need for additional short-crested sea spectra, such as those obtained by the National Institute of Oceanography in Britain [20]. Here again vigor in obtaining and analyzing ocean wave data is the most urgent need.

Finally, progress in applying results of seakeeping research requires much more complete information on criteria of seagoing performance for different types of ships. What values of acceleration are acceptable? How much water can be shipped over the bow before speed must be reduced? How severe can slamming be in terms of hull stress or local pressures before remedial action must be taken? For being able to predict ship performance at sea is not enough. We must be able to determine at what speeds and in what seas any particular design is satisfactory or unsatisfactory.

In conclusion, it is felt that valuable tools are now available to determine significant trends of ship behavior in realistic sea conditions. It is urged that in planning research in the field of seakeeping vigorous efforts be applied to the systematic accumulation of basic data on the sea, model series results in waves, and criteria of seagoing performance. Then our future improved theories and computation techniques can be verified and applied rather than set to gather dust on library shelves.

ACKNOWLEDGMENTS

The assistance of various members of the Webb staff is gratefully acknowledged, particularly Professor Robert B. Zubaly and Mr. Roger H. Compton. Mr. Larry Liddle, Student Assistant, prepared the figures. The courtesy of American Bureau of Shipping and Panel H-7, SNAME, in permitting reproduction of research results is appreciated.

REFERENCES

1. Korvin-Kroukovsky, B. V., "Investigation of Ship Motions in Regular Waves," TRANSACTIONS OF SNAME, Vol. 63, 1955.

2. St. Denis, M. and Pierson, W. J., "On the Motions of Ships in Confused Seas," TRANSACTIONS OF SNAME, Vol. 61, 1953.

3. Vossers, G., Swaan, W. A., and Rijken, J., "Experiments with Series 60 Models in Waves," TRANSACTIONS OF SNAME, Vol. 68, 1960.

4. Vossers, G., Swaan, W. A., and Rijken, J., "Vertical and Lateral Bending Moment Measurements on Series 60 Models," INTERNATIONAL SHIPBUILDING PROGRESS, Vol. 8, No. 83, July, 1961.

5. Moskowitz, L., Pierson, W. J., and Mehr, E., "Wave Spectra Estimated from Wave Records Obtained by the O. W. S. WEATHER EXPLORER and the O. W. S. WEATHER REPORTER," New York University Research Division Report, Part I, November, 1962, and Part II, March, 1963.

6. Lewis, E. V. and Bennet, Rutger, "Lecture Notes on Ship Motions in Irregular Seas," Webb Report, October, 1963.

7. Gerritsma, J., Van Den Bosch, J. J., and Beukelman, W., "Propulsion in Regular and Irregular Waves," INTERNATIONAL SHIPBUILDING PROGRESS, Vol. 8, No. 82, June, 1961.

8. Maruo, H., "The Excess Resistance of a Ship in Rough Seas," INTERNATIONAL SHIPBUILDING PROGRESS, Vol. 4, No. 35, July, 1957.

9. Swaan, W. A. and Rijken, H., "Speed Loss at Sea as a Function of Longitudinal Weight Distribution," TRANSACTIONS OF SNAME, Vol. 79, January, 1963.

10. Zubaly, R. B. and Compton, R. H., "A Computation Procedure for Determination of Ship Responses to Irregular Seas," Webb Spring Seminar on Ship Behavior at Sea, May, 1964.

11. Zubaly, R. B. and Lewis, E. V., "Ship Bending Moments in Irregular Seas Predicted from Model Tests," Webb Report, December, 1963.

12. Pierson, W. J., "A Study of Wave Forecasting Methods and of the Height of a Fully Developed Sea on the Basis of Some Wave Records Obtained by the O. W. S. WEATHER EXPLORER During a Storm at Sea," Deutsche Hydrographische Zeitschrift, Band 12, Heft 6, 1959.

13. Vassilopoulos, Lyssimachos, "The Analytical Prediction of Ship Performance in Random Seas," M.I.T. Department of Naval Architecture and Marine Engineering Report, February, 1964.

14. Grim, O., "Die Deformation Eines Regelmassigen, In Langsrichtung Laufenden Seeganges Durch Ein Fahrendes Schiff," Symposium Uber Schiffstheorie Am Institut Fur Schiffbau Der Universitat Hamburg, 25-27 January, 1962.

15. Gerritsma, J. and Beukelman, W., "Distribution of Damping and Added Mass Along the Length of a Shipmodel," TNO Report No. 49S, March, 1963.

16. Lewis, E. V. and Mumata, Edward, "Ship Motions in Oblique Seas," TRANSACTIONS OF SNAME, Vol. 68, 1960.

17. Lalangas, Petros, "Theoretical Determination of the Pitching and Heaving Motions of a Ship at Oblique Headings," Thesis, Stevens Institute of Technology, 1960.

18. Lewis, E. V. and Breslin, J. P., "Semi-Submerged Ships for High Speed Operation in Rough Seas," Third Symposium on Naval Hydrodynamics, Scheveningen, Netherlands, September 19-22, 1960.

19. Murphy, Sabat, and Taylor, "Least Cost Ship Characteristics by Computer Techniques," Chesapeake Section, SNAME, October 23, 1963.

20. Canham, H. J. S., Cartwright, D. E., Goodrich, G. J., and Hogben, N., "Seakeeping Trials on O. W. S. WEATHER REPORTER," TRANSACTIONS OF RINA, Vol. 104, 1962.

* * *

DISCUSSION

G. Aertssen
University of Gent
Gent, Belgium

This paper is an excellent approach to the trend of the wave-induced moments in extreme seas and the investigation comes at the right moment. It is known that in extreme seas some waves are exceptionally high (heights of 80 ft have been recorded in the North Atlantic). But on the other hand strain gages applied to the stringer plating of the main deck of usual cargo ships of 500 ft showed in these extreme seas bending moments which were not greater than the calculated bending moment, the ship being poised on a trochoidal wave of a length L_{pp} and a height $L_{pp}/12$, i.e., a height of about 25 ft. It has been argued that the reason for this was the ability of the ship to adapt herself to the actual shape of the sea, especially when it is considered that in this extreme sea the ship of 500 ft is hove to at a speed of about 5 knots.

Prof. Lewis comes to a better explanation when applying to the bending moments the superposition principle and accepting a spreading function for the energy of the assumed short-crested sea. The surprising result is that for the 500 ft cargo ship having $C_B = 0.8$ the wave induced bending moments are then quite the same as the conventional static bending moments.

A second important result of this work is the deviation from the $L/20$ law for long ships. It was known that for these ships a smaller wave height must be taken and a wave height $0.6L^{0.6}$ was proposed. This again, as Prof. Lewis shows in Fig. 6, is a very good approximation for all bulk carriers and tankers now under construction and ranging from 500 to 800 ft.

There is an old rule limiting the bending stresses calculated on a basis $L/20$ to $5L + 500$ Kg. per sq mm, L is ship length in m. This rule holds good for $L = 150$m where the allowable stress is 1250 Kg. per sq cm and for the largest bulk carriers up to $L = 200$m where the allowable stress is 1500 Kg. per sq cm, which means 20 percent more for the longer ship. This allowance of 20 percent is exactly — as Prof. Lewis shows in Fig. 6 — the error in excess when applying for large bulk carriers the static method on a base $L/20$. This is a support for the static calculation based on $L/20$, even for ships up to 200m, provided the allowable stress is given by the formula $5L + 500$ Kg. per sq cm.

There are other remarkable results emerging from Prof. Lewis' paper. Stresses and bow motions in the realistic short-crested sea are reduced in beam and in following seas as compared with head seas but less than would be expected and this is especially true for the stresses. The relative bow motions are roughly the same in beam and in following seas. The writer recently, in a paper to the North East Coast Institution of Engineers and Shipbuilders,* gave the results of observations on two trawlers in rough seas. It is evident from Fig. 8 of this paper that in rough seas pitching is the same in beam seas and in following seas. Rolling of these trawlers in extreme seas is roughly the same in bow seas and in beam seas, as is evident from Fig. 11 of the same paper. Altogether the short-crestedness of extreme seas has in a certain way a smoothening effect on stresses and on motions. These irregularities — and others — of random seas allow in certain circumstances to turn a cargo ship of 12,000 tons even in a sea $\bar{H}1/10$ = 35 ft of which some waves are as high as 50 ft.

Finally a question. A speed of 12 knots of the fine 600 ft ship ahead in an extreme sea is somewhat surprising. Has Prof. Lewis some information as to what extent this 600 ft ship was able to maintain this speed in such a severe sea?

* * *

DISCUSSION

G. J. Goodrich
National Physical Laboratory
Teddington, England

Prof. Lewis has, as usual, produced an extremely practical paper. It is obvious to us all that research in seakeeping, to be of worth, must ultimately produce design data for the improvement of ship performance.

I would question the practical use of pitch and heave response operators in regular waves, for such waves never exist. Uni-directional long-crested seas are rare and even one node two dimensional spectra are few and far between. The sea in general consists of multi-nodal spectra and predictions should ultimately be made for such conditions. However, full scale sea data on such spectra are almost non-existent and it is probably sufficient for the present time to consider the one node two dimensional spectrum.

There is no doubt that ship operators look to those of us working in the field of seakeeping, for help in assessing new designs and we must look extremely closely at what we consider to be the important features of a design which should influence the choice of such a design. Prof. Lewis has suggested in the closing paragraph of his paper some of the important criteria which should be considered.

*Aertssen, Ferdinande and De Lembre: Service Performance and Sea Keeping Trials on Two Conventional Trawlers, Trans. North East Coast Institution of Engineers and Shipbuilders, November 1964.

I would suggest that for the merchant ship the loss in speed to be expected is of prime importance; other factors such as accelerations, bow wetness and slamming, are others that will influence the captain in reducing power and hence producing a further reduction in ships speed.

It is not enough however to consider such criteria for single sea states. Predictions must be made on a long term basis, for after all, the more severe sea states occur at low probability and the consequences of high seas may be negligible in relation to the all year round operation of the ship.

In conclusion I think the method of analysis and presentation in terms of $\log \omega$ used by the author is useful for visualizing what is happening to the responses of the ship as various parameters are varied.

* * *

DISCUSSION

H. Lackenby
British Ship Research Association
London, England

The subject of Professor Lewis' paper is of particular interest to me, namely the application of results of seakeeping research. A considerable amount of work has been carried out on this subject over the past few years, but it has not always been very clear as to the design applications in many instances. A contributory factor in this has doubtless been the apparent complexity of the subject. Against this background Professor Lewis' paper is very timely, and I would just like to raise a point of principle which was touched on this morning.

As I understand it, the essence of the theory and analysis is based on the principle of superposition and the principle of linearity, that is, relatively small angular displacements, wall-sidedness of the model or ship within the range of the motions and so on. From the practical point of view, however, I think it is the larger angles and the question of whether or not water breaks over the decks which are the more important. This state of affairs appears to be well outside the linear range, but from the discussion this morning it seems that the principle of linearity applies beyond the range that one would expect. The instances quoted however have referred particularly to model tests on a destroyer form and I should be glad if Professor Lewis would care to comment on this aspect, more particularly as far as the fuller merchant ship is concerned. In other words, to what extent can we use — or perhaps one should say abuse — the linear principle and get away with it for practical design purposes?

* * *

DISCUSSION

W. A. Swaan
Netherlands Ship Model Basin
Wageningen, Netherlands

The paper gives a clear review of the possibilities of applying the results of presently available and future seakeeping research. I do agree with the author in his conclusion about the need for more data on the sea, model series in waves and criteria for seagoing performance. Especially the lack of sea data is a great obstacle in providing useful behaviour predictions for new ship designs.

It appears doubtful to use the expression "response amplitude operator" for the power coefficients because it is something essentially different from the "response amplitude operator" for ship motions. In the case of the power coefficient the result of the described procedure is a mean value; the zero frequency component of the power in irregular seas. In the case of ship motions and bending moments the results have an oscillatory character with a zero mean. Therefore it might be better to indicate the power coefficient as "response operator" and leave the expression "response amplitude operator" for oscillating phenomena.

The comparison of the wave bending moment in Fig. 5 for short-crested and long-crested seas is very illuminating. It can serve as a warning against using long-crested irregular seas in an overconfident way.

Figure 6 shows the highest expected vertical bending moment in 10,000 cycles. Because the ships in this diagram have lengths between 300 ft and 1300 ft and speeds from 6 knots to 18 knots one would expect the time interval covered by these 10,000 cycles to be a function of ship length. This involves a different risk when small and large ships are compared. Because the author does not convert the spectrum to the frequency of encounter it is not quite obvious in which way one can reach some definite conclusion about the time covered by 10,000 cycles.

There is another difficulty involved in using the highest expected value in 10,000 cycles. The relation given in the paper between the spectrum area and the value of the average highest amplitude is only valid for a narrow band spectrum in which no negative maxima and positive minima occur when the zero level is taken at the mean position. It seems therefore much easier to discard the use of bending moment amplitudes altogether and return to the Gaussian distribution of the bending moment values when they are determined at constant time intervals. Because the variance of this Gaussian distribution is equal to the area of the spectrum it is not difficult to determine the percentage of time in which a certain bending moment is exceeded. From this it follows that for a narrow spectrum the average highest amplitude in 10,000 oscillations is equivalent to the deviation (absolute value) which will be exceeded during 0.0009% of the time or 3/4 seconds per day. The number of times it occurs is left undefined in this way so there is indeed no reason to use a frequency of encounter spectrum. For a broad spectrum, containing negative maxima and positive minima, only the number of times may be different but not the percentage of time. This makes it superfluous to make any assumption on the shape of the spectrum. Therefore the interpretation of the results in this manner is more rigorous without being less vigorous.

* * *

DISCUSSION

L. Vassilopoulos
Massachusetts Institute of Technology
Cambridge, Massachusetts

I cannot help but basically disagree with the philosophy behind this paper as well as the alleged usefulness of the procedures which Professor Lewis proposes. The points of the paper, which bear directly to the profession's real needs at present, are unfortunately obscured and are only very briefly treated while the author mainly reiterates his recently proposed technique for interpreting results of seakeeping research rather than applying them.

Despite the fact that we are almost ready to commence an evaluation of the importance of seaworthiness considerations in preliminary ship design, there still exists a definite need for: (a) a scrutiny of the validity and applicability of the basic procedures with which the results of ten years active research have been obtained, and (b) the establishment of a generalized philosophy for applying our knowledge to the actual design process of all ship types.

With respect to the first item, one notes that members of the profession on occasion fail to adhere to the fundamental notions and implications behind the St. Denis - Pierson approach. It is the writer's opinion that the present paper introduces unnecessary confusion and complication. The author seems to believe that our present procedures rest on such sure principles that we are in a position to modify and transform these principles. It is with this belief that I disagree.

Professor Lewis has actually recast, without any formalism, the basic Wiener-Kintchine relation of the theory of random processes to suit what he terms the needs of the ship designer. He forcedly transforms the components of the equation

$$\Phi_{oc}(\omega_e) = |H(\omega_e)|^2 \, \Phi_{ii}(\omega_e) \tag{1}$$

where

$\Phi_{ii}(\omega_e)$ = input function amplitude density spectrum,

$H(\omega_e)$ = system complex frequency response (system transfer function), and

$\Phi_{oo}(\omega_e)$ = output function amplitude density spectrum

into a so-called non-dimensional form, but in so doing forgets the precise notions behind each quantity and assumptions and reasoning behind the derivation of Eq. (1).

Let us examine the problem more carefully by fixing attention on the independent variable involved in Eq. (1). The frequency domain analysis of linear systems in other engineering fields is precise in the sense that the analysis involves a single, unambiguous "frequency." Unfortunately, in ship work this is not the case, for we have two "frequencies" to play with; the absolute wave frequency and the encounter frequency. This adverse fact causes much trouble and the ensuing complications, especially in astern seas are, of course, due to the fact that sea wave celerity is a function of wavelength. The question which arises is which is our fundamental variable and why? Professor Lewis arbitrarily employs the logarithm of the absolute wave frequency and states that it is "unnecessary to convert to frequency of encounter as originally proposed."

The writer disagrees with this choice and suggests that the frequency of encounter is the basic variable because of the following reasons:

(a) The frequency of encounter is the frequency which the ship feels and to which it responds.

(b) The ship-system is "non-stationary" and furthermore "directional." Hence, ship speed and wave direction are not simply labels to families of graphs but must be embedded in the encounter frequency.

(c) The mathematical model of the ship system involves the frequency of encounter and not the absolute wave frequency.

(d) Equation (1) is strictly applicable only to system functions derived from the mathematical model and relates them via the actual input density spectrum to the actual response spectrum.

There is, furthermore, a delicate point in the statistical process which merits some attention. First of all there is an ambiguity as to what constitutes the actual input function to the ship system. Is it the <u>wave</u> or is it the <u>load</u> (force or moment) caused by the wave? The answer depends on the definition of the system. The physical system (the ship model), presents no difficulty and what we measure in say a unit amplitude wave system is definitely related via Eq. (1) to the <u>wave</u>. The mathematical system needs special care however; if the Korvin-Kroukovsky type differential equations are used, then strictly speaking, the calculated response must be related to the <u>load</u>, whereas if the Cummins-type differential equations are used the calculated response must be related to the <u>wave</u>. Whichever the case, however, the important point is that <u>as regards "inputs," wave amplitude or wave-induced load</u> amplitudes have a definite physical meaning whereas "wave slopes" do not. Incidentally, the area under the

Lewis log-type spectrum is equal to the mean squared wave slope and not the mean slope which presumably must be zero just like the mean wave amplitude is considered to be zero.

There is next, a definite and precise meaning attached to the complex frequency response and I suggest that arbitrary interpretations had better be avoided. What the meaning of the now accepted word-response amplitude operator should be, is simply the square of the response amplitude measured in its own units due to a unit amplitude of the excitation, be it wave or wave-induced load. In advocating his non-dimensional procedure, Professor Lewis is forced, on account of the large number of ship responses, to examine and adopt different parameters which will non-dimensionalize each individual response. Hence, the cause of such confusing statements like "wave slope is more important for pitch motion than wave amplitude." What Professor Lewis means is that if one wants to non-dimensionalize an angular displacement he had better divide by a (dimensionless) angle such as maximum wave slope. Clearly then, because we have many and different "responses" in the ship-system case, non-dimensionalization is of no real use and only adds to undue complication.

I also fail to see the legitimacy of multiplying two arbitrarily derived functions in order to get a response spectrum, unless these functions indeed represent quantities which specifically relate themselves to the fundamental notions behind the theory of linear systems. The advantage that the author claims is that the effects of ship size can be readily shown. But by size, Professor Lewis limits himself to length only. What about variations in say breadth or draft or water-plane coefficient when the "useful shift" of the curves doesn't take place? Do we have to start all over again with new non-dimensionalizing?

An important final point is that in the end of our analysis, we should not be satisfied with simple families of curves. The trends, once established, are only a palliative; the really useful information to the designer is rather numbers like the ones Dr. Ochi has discussed in his paper. The author presumably makes a plea at the end of his paper that we should avoid masses of dusty information. Personally, I can think of no better way to fill drawers than by attempting to collect curves for all possible variables.

The last section of the paper is the most interesting and it is a pity that the author did not amplify the basic problem. As I see it, there are now three things to be done before we can really say that we are incorporating our knowledge in ship design.

The first thing is related to the oceanographers and here we must wait for their answer to the basic question. In a given year (or even better in a period of years) and over a specified ship route what are the sea spectra encountered by a ship and what is their individual time occurrence?

The second thing is to determine in numerical terms exactly what ship operators mean by unacceptable wetness, untolerable number of slams or unbearable acceleration.

Third and final, we must attempt to devise an approach which will discriminate between a family of ships all meeting the owner's requirements, and will choose the one that exhibits the best capacity for sustaining a preassigned speed in rough water.

* * *

REPLY TO THE DISCUSSION

E. V. Lewis
Webb Institute of Naval Architecture
Glen Cove, Long Island, New York

Mr. Lackenby's comments are appreciated. In reply to his question, I would expect to find linearity apply to merchant ships as well as to destroyers. He is quite correct in pointing out that the larger angles are most important, when water is shipped over the bow or slamming occurs. However, since we are interested mainly in identifying when these non-linear events occur, rather than to determine how deep the bow is immersed or how far out of the water it emerges, we do not need to push the assumption of linearity too far.

Mr. Goodrich suggests that uni-directional sea spectra are adequate for the present. However, we have found in our calculations at Webb that short-crestedness has a significant effect, and therefore even an approximate allowance for it is better than none. Mr. Goodrich is quite right in pointing out that to draw significant conclusions one must take into effect the combined effect of different sea states based on their probabilities, and he has illustrated this further step very clearly in his own paper before this Symposium.

Professor Aertssen has called attention to particular features of the paper and indicated their possible implications for ship design. His comments based on his own wide experience in making measurements on ships at sea is greatly appreciated. As for the speed of 12 knots for the 600 ft ship, this was simply the lowest speed for which model test data were available, and I doubt very much that it would be maintained in an extremely rough sea.

Mr. Swaan has made a number of good points, and I concur with all of them. It is certainly true that different numbers of cycles should be used for large and small ships when comparing them over the same long period of time. However, the difference in predicted stress will not be great. Although most ship motion spectra seem to be narrow enough to make predictions of the highest expected value from a Rayleigh distribution reasonable, working directly with the Gaussian distribution of points in the record is a useful and simple approach.

I feel that Mr. Vassilopoulos has given a little too much emphasis to following strictly the mathematics of linear systems theory without recognizing the peculiarities of the ship-wave problem. In particular, we must recognize that frequencies of encounter can vary either with ship speed or wave length, and this leads to a great deal of confusion. The procedure outlined in the paper, if properly used, gives the same numerical results as the conventional procedure and therefore cannot be incorrect. Moreover, the graphs that can be prepared in the course of the work are much more meaningful than the numbers alone, as one finds with practice. Mathematics should be a tool, not a straitjacket.

It is correct that the area under the log-slope wave spectrum is equal to the mean squared wave slope rather than the mean slope. I agree entirely with Mr. Vassilopoulos' closing paragraphs and have been working in the directions he suggests for a long time.

Dr. Yamanouchi has made a valuable contribution* which can stand on its own as an important paper. Therefore, I shall simply thank him for presenting it to the Symposium.

I wish to thank all of the discussers for their interest in my paper and for their very valuable comments.

* * *

*See remarks by Yamanouchi on paper by Ogilvie.

THE DISTRIBUTION OF THE HYDRODYNAMIC FORCES ON A HEAVING AND PITCHING SHIPMODEL IN STILL WATER

J. Gerritsma and W. Beukelman
Technological University
Delft, Netherlands

ABSTRACT

Forced oscillation tests are carried out with a segmented shipmodel to investigate the distribution of the hydrodynamic forces along the hull for heaving and pitching motions.

The vertical forces on each of the seven sections of the shipmodel are measured as a function of forward speed and frequency. By using the in-phase and quadrature components of these forces, an analysis is made of their distribution along the length of the shipmodel.

The experimental results are compared with the results of a simple strip theory, taking into account the effect of forward speed.

The comparison shows a satisfactory agreement between theory and experiment.

INTRODUCTION

The calculation of shipmotions in regular head waves by using a strip theory, has been discussed in a number of papers. Recent contributions were given by Korvin-Kroukovsky and Jacobs [1], Fay [2], Watanabe [3] and Fukuda [4].

In these papers the influence of forward speed on the hydrodynamic forces is considered and dynamic cross-coupling terms are included in the equations of motion, which are assumed to describe the heaving and pitching motions.

In earlier work [5] it was shown that a relatively small influence of speed exists on the damping coefficients, the added mass and the exciting forces, at least for the case of head waves and for speeds which are of practical interest. On the other hand, forward speed has an important effect on some of the dynamic cross-coupling coefficients. Although, at a first glance these terms could be regarded as second order quantities, it was pointed out by Korvin-Kroukovsky [1] and also by Fay [2] that they can be very important for the amplitudes and phases of the motions. This has been confirmed in [5] where the coupling terms are neglected in a calculation of the heaving and pitching motions. In this calculation we used coefficients of the motion equations, which were determined by forced oscillation tests. In comparison with the calculation where the cross-coupling terms are included and also in comparison with the measured motions, an important influence is observed, as shown in Fig. 1, which is taken from Ref. [5]. Further analysis showed that the discrepancies between the coupled and uncoupled motions were mainly due to the damping cross-coupling terms.

The influence of forward speed has been discussed to some extent in Vossers' thesis [6]. From a first order slender body theory it was found that the distribution of the hydrodynamic forces along an oscillating slender body is not influenced by forward speed. Vossers concluded that the inclusion of speed dependent damping cross-coupling terms is not in agreement with the use of a

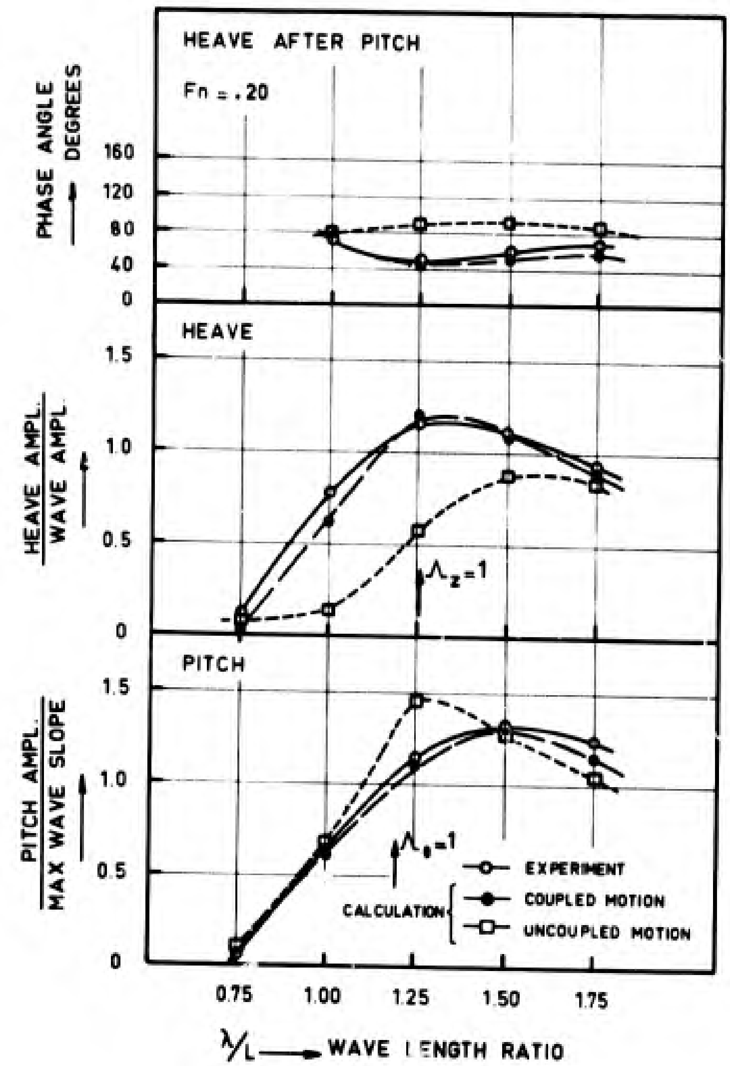

Fig. 1 - Influence of cross-coupling

strip theory. In view of the above mentioned results such a simplification does not hold for actual shipforms.

For symmetrical shipforms at forward speed, it was shown by Timman and Newman [7] that the damping cross-coupling coefficients for heave and pitch are equal in magnitude, but opposite in sign. Their conclusion is valid for thin or slender submerged or surface ships and also for non-slender bodies.

Golovato's work [8] and some of our experiments [5] on oscillating shipmodels confirmed this fact for actual surface ships to a certain extent.

The effects of forward speed are indeed very important for the calculation of shipmotions in waves. The two-dimensional solutions for damping and added mass of oscillating cylinders on a free surface, as given by Grim [9] and Tasai [10] show a very satisfactory agreement with experimental results. When the effects of forward speed can be estimated with sufficient accuracy, such two-dimensional values may be used to calculate the total hydrodynamic forces and moments on a ship, provided that integration over the shiplength is permissible.

In order to study the speed effect on an oscillating shipform in more detail, a series of forced oscillating experiments was designed. The main object of these experiments was to find the distribution of the hydrodynamic forces along the length of the ship as a function of forward speed and frequency of oscillation.

THE EXPERIMENTS

The oscillation tests were carried out with a 2.3 meter model of the Sixty Series, having a block coefficient $C_B = 0.70$. The main dimensions are given in Table 1. The model is made of polyester, reinforced with fibreglass, and consists of seven separate sections of equal length. Each of the sections has two end-bulkheads. The width of the gap between two sections is one millimeter. The sections are not connected to each other, but they are kept in their position by means of stiff strain-gauge dynamometers, which are connected to a longitudinal steel box girder above the model. The dynamometers are sensitive only for forces perpendicular to the baseline of the model.

By means of a Scotch-Yoke mechanism a harmonic heaving or pitching motion can be given to the combination of the seven sections which form the shipmodel. The total forces on each section could be measured as a function of frequency and speed.

A non-segmented model of the same form was also tested in the same conditions of frequency and speed to compare the forces on the whole model with the sums of the section results. A possible effect of the gaps between the sections could be detected in this way. The arrangement of the tests with the segmented model and with the whole model is given in Fig. 2.

The mechanical oscillator and the measuring system is shown in Fig. 3. In principle the measuring system is similar to the one described by Goodman [11]: the measured force signal is multiplied by $\cos \omega t$ and $\sin \omega t$ and after

Table 1
Main Particulars of the Shipmodel

Length between perpendiculars	2.258 m
Length on the waterline	2.296 m
Breadth	0.322 m
Draught	0.129 m
Volume of displacement	0.0657 m^3
Block coefficient	0.700
Coefficient of mid-length section	0.986
Prismatic coefficient	0.710
Waterplane area	0.572 m^2
Waterplane coefficient	0.785
Longitudinal moment of inertia of waterplane	0.1685 m^4
L.C.B. forward of $L_{pp}/2$	0.011 m
Centre of effort of waterplane after $L_{pp}/2$	0.038 m
Froude number of service speed	0.20

integration the first harmonics of the in-phase and quadrature components can be found with distortion due to vibration noise. In some details the electronic circuit differs somewhat from the description in [11]. In particular synchro resolvers are used instead of sine-cosine potentiometers, because they allow higher rotational speeds.

The accuracy of the instrumentation proved to be satisfactory which is important for the determination of the quadrature components, which are small in comparison with the in-phase components of the measured forces.

Throughout the experiments only first harmonics were determined. It should be noted that non-linear effects may be important for the sections at the bow and the stern where the ship is not wall-sided. The forced oscillation tests were carried out for frequencies up to ω = 14 rad/sec and four speeds of advance were considered, namely: Fn = 0.15, 0.20, 0.25 and 0.30. Below a frequency of ω = 3 to 4 rad/sec the experimental results are influenced by wall effect due to reflected waves generated by the oscillating model.

The motion amplitudes of the shipmodel covered a sufficiently large range to study the linearity of the measured values (heave ~4 cm, pitch ~4.6 degrees). An example of the measured forces on section 2, when the combination of the seven sections performs a pitching motion, is given in Fig. 4.

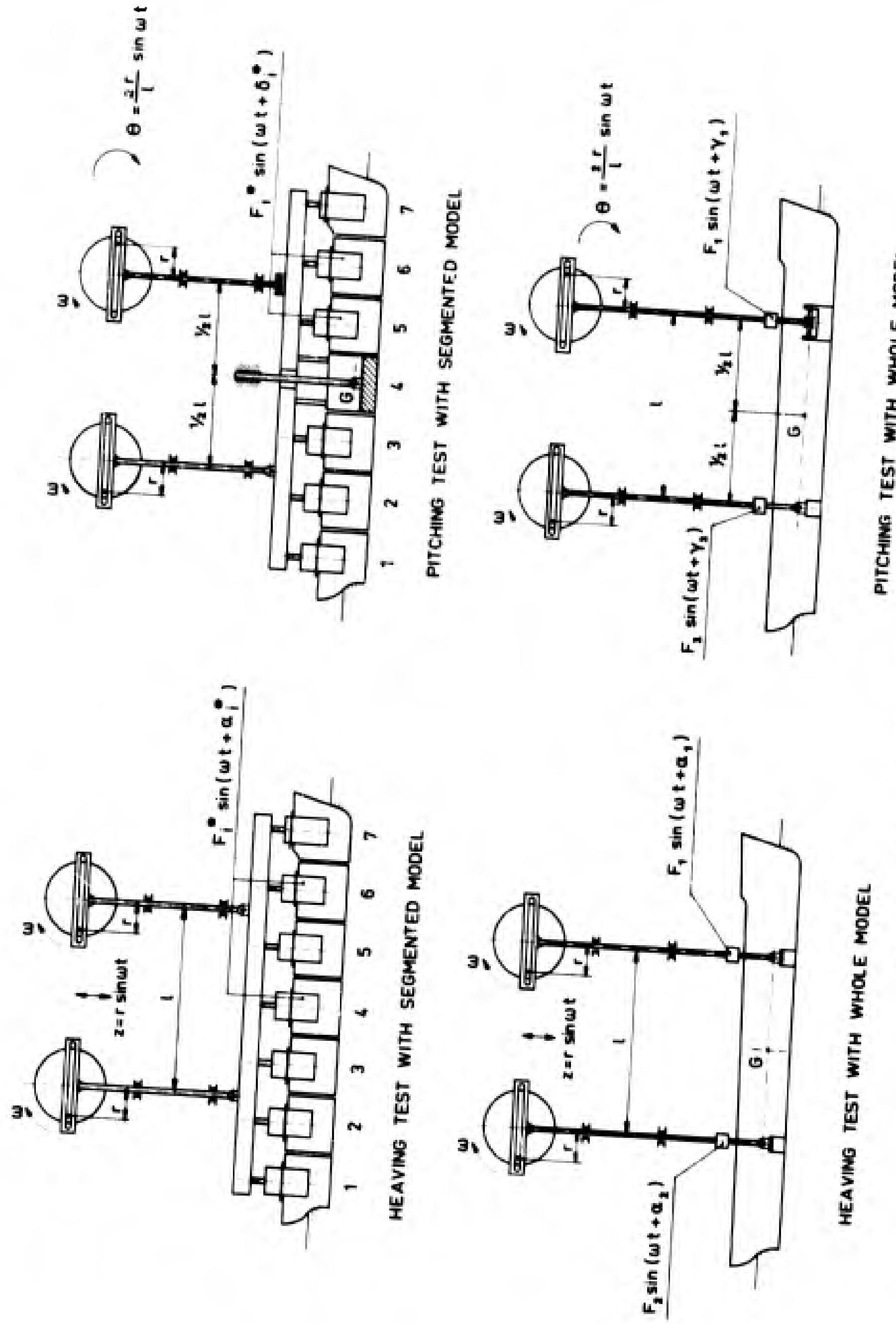

Fig. 2 - Arrangement of oscillation tests

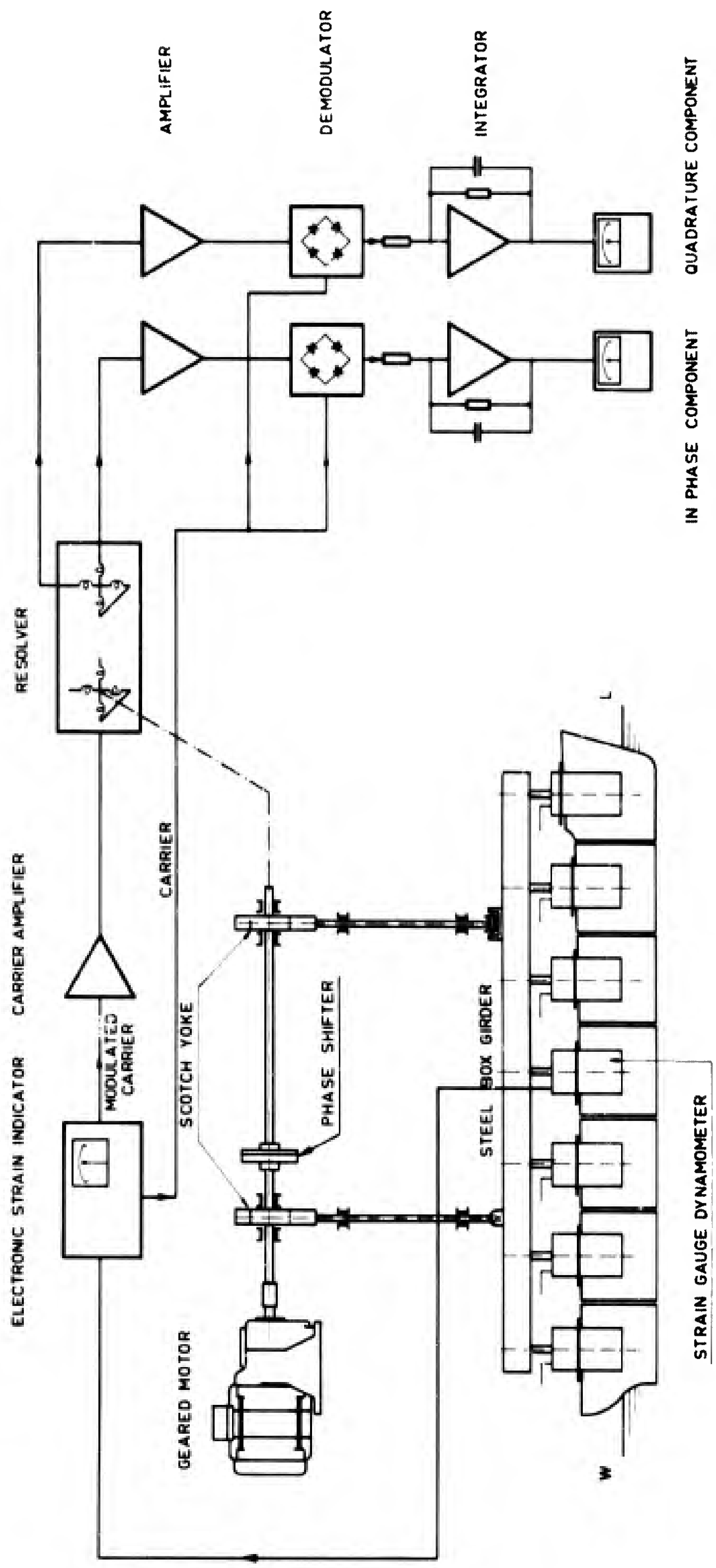

Fig. 3 - Principle of mechanical oscillator and electronic circuit

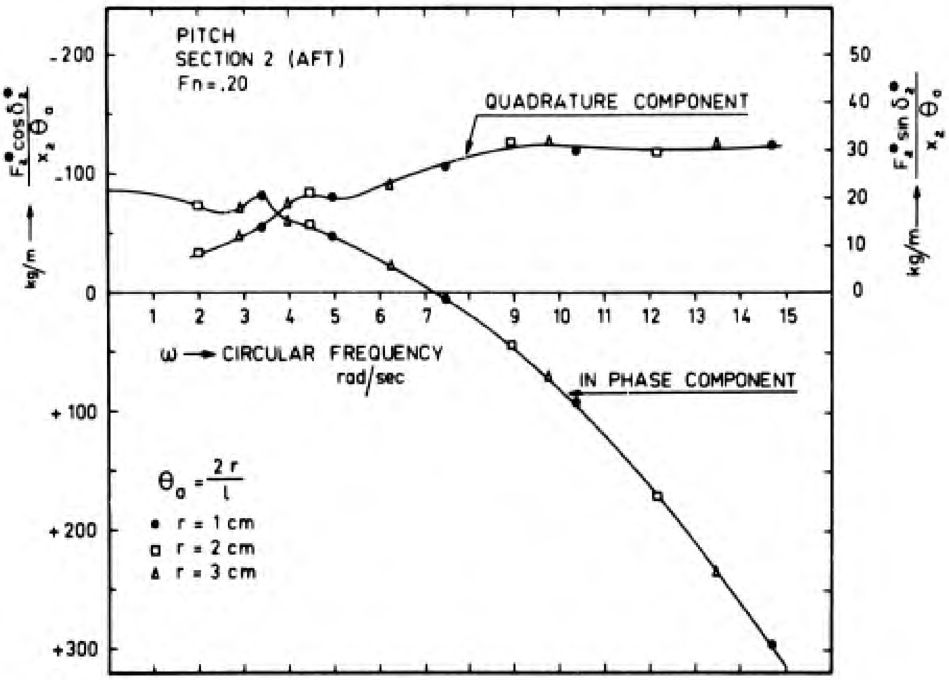

Fig. 4 - Components of force on section 2, pitching motion

PRESENTATION OF THE RESULTS

Whole Model

It is assumed that the force F and the moment M acting on a forced heaving or pitching shipmodel can be described by the following equations:

<u>Heave</u>

$$\left.\begin{aligned}(a+\rho\nabla)\,\ddot{z}_o + b\dot{z}_o + cz_o &= F_z \sin(\omega t + \alpha)\\ D\ddot{z}_o + E\dot{z}_o + Gz_o &= -M_z \sin(\omega t + \beta)\end{aligned}\right\}. \qquad (1)$$

<u>Pitch</u>

$$\left.\begin{aligned}\left(A + k_{yy}^2\rho\nabla\right)\ddot{\theta} + B\dot{\theta} + C\theta &= M_\theta \sin(\omega t + \gamma)\\ d\ddot{\theta} + e\dot{\theta} + g\theta &= -F_\theta \sin(\omega t + \delta)\end{aligned}\right\}. \qquad (2)$$

For a given heaving motion $z_o = z_a \sin \omega t$, it follows that:

$$\left.\begin{aligned} b &= \frac{F_a \sin\alpha}{z_a\omega} & E &= \frac{-M_z \sin\beta}{z_a\omega}\\ a &= \frac{cz_a - F_z\cos\alpha}{z_a\omega^2} - \rho\nabla & D &= \frac{gz_a + M_z\cos\beta}{z_a\omega^2}\end{aligned}\right\}. \qquad (3)$$

Similar expressions are valid for the pitching motion. The determination of the damping coefficients b and B and the damping cross-coupling coefficients e and E is straightforward: for a given frequency these coefficients are proportional to the quadrature components of the forces or moments for unit amplitude of motion. For the determination of the added mass, the added mass moment of inertia, a and A, and the added mass cross-coupling coefficients d and D it is necessary to know the restoring force and moment coefficients c and C, and the statical cross-coupling coefficients g and G.

The statical coefficients can be determined by experiments as a function of speed at zero frequency. For heave the experimental values show very little variation with speed; they were used in the analysis of the test results.

In the case of pitching there is a considerable speed effect on the restoring moment coefficient C. C decreases approximately 12% when the speed increases from $Fn = 0.15$ to 0.30. This reduction is due to a hydrodynamic lift on the hull when the shipmodel is towed with a constant pitch angle. Obviously this lift effect also depends on the frequency of the motion. Consequently, the coefficient of the restoring moment, as determined by an experiment at zero frequency, may differ from the value at a given frequency.

As it is not possible to measure the restoring moment and the statical cross-coupling as a function of frequency, it was decided to use the calculated values at zero speed. This is an arbitrary choice, which affects the coefficients of the acceleration terms: for harmonic motions a decrease of C by ΔC results in an increase of A by $\Delta C/\omega^2$ when C is used in the calculation.

The results for the whole model are given in the Figs. 5 and 6. The results for the heaving motion were already published in [13]; they are presented here for completeness.

Results for the Sections

The components of the forces on each of the seven sections were determined in the same way as for the whole model. As only the forces and no moments on the sections were measured two equations remain for each section:

Heave

$$(a^* + \rho\nabla^*)\,\ddot{z}_o + b^*\dot{z}_o + c^*z_o = F_z^* \sin(\omega t + \alpha^*)\,,$$

Pitch

$$(d^* + \rho\nabla^* x_i)\,\ddot{\theta} + e\dot{\theta} + g\theta = -F_\theta^* \sin(\omega t + \delta^*)\,, \tag{4}$$

where $\rho\nabla^* x_i$ is the mass-moment of the section i with respect to the pitching axis. The star (*) indicates the coefficients of the sections. The section coefficients divided by the length of the sections give the mean cross-section coefficients, thus:

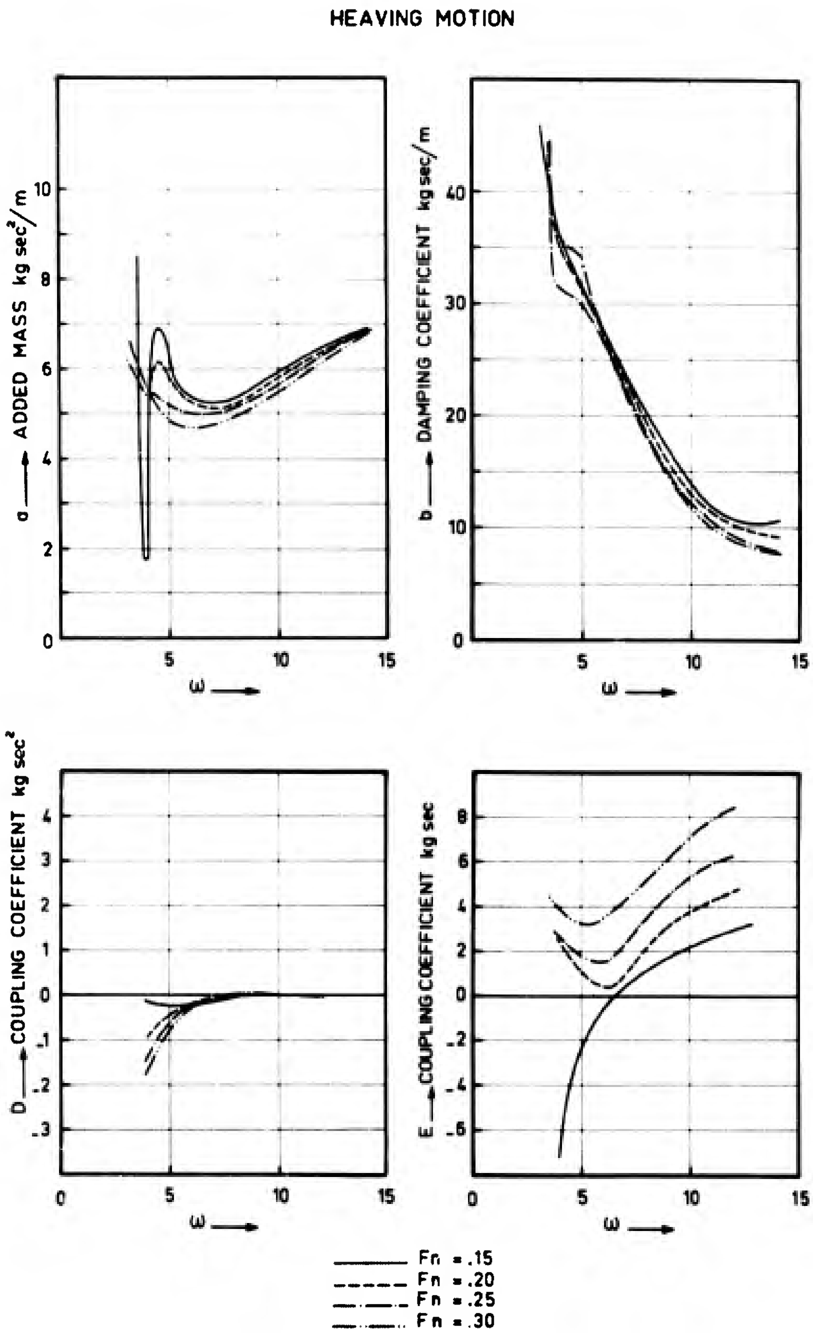

Fig. 5 - Experimental results for whole model

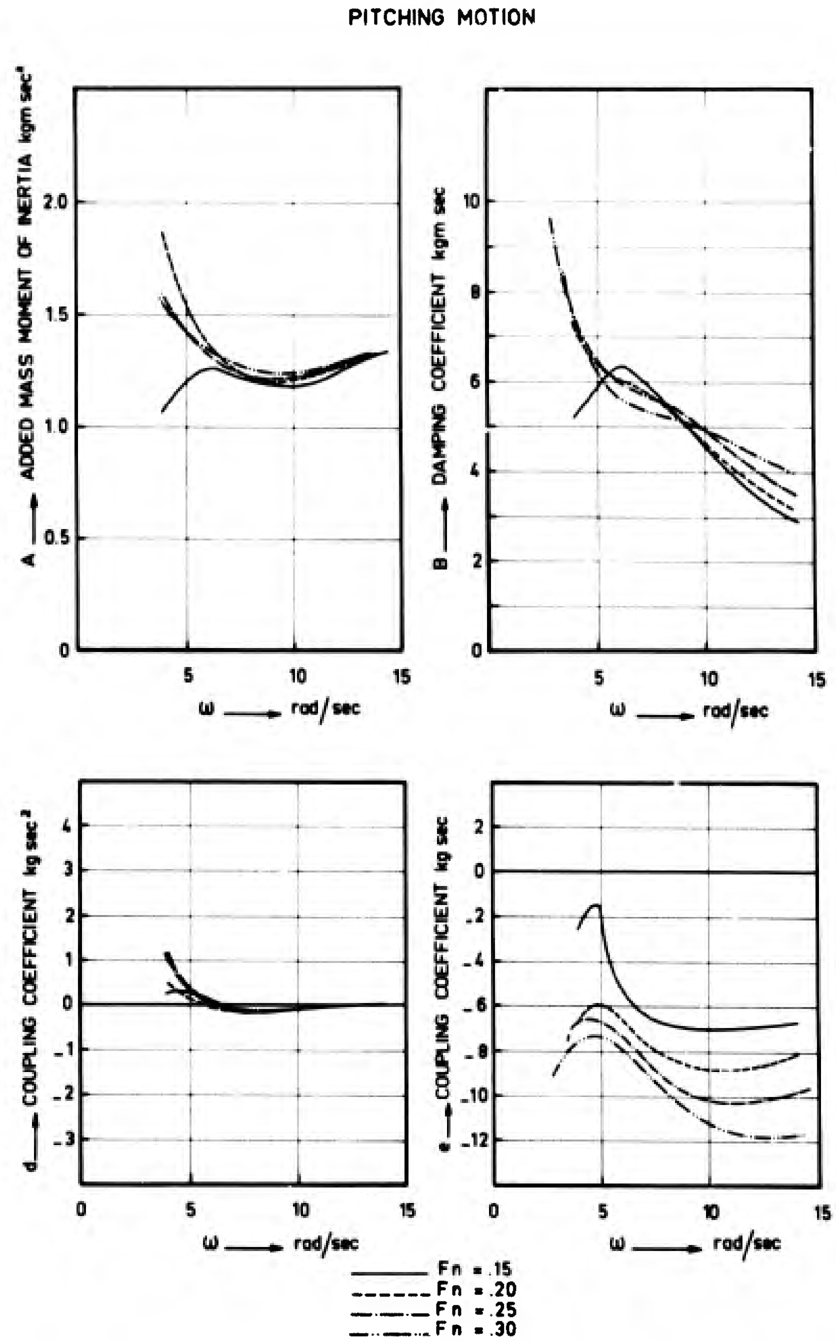

Fig. 6 - Experimental results for whole model

$$\frac{a^*}{L_{pp}/7} = \bar{a}',$$

and so on. Assuming that the distributions of the cross-sectional values of the coefficients a', b', etc., are continuous curves, these distributions can be determined from the seven mean cross-section values. In the Figs. 7, 8, 9 and 10 the distributions of the added mass a, the damping coefficient b and the cross-coupling coefficients d and e are given as a function of speed and frequency. Numerical values of the section results, a^*, b^*, etc., are summarized in the Tables 2, 3, 4 and 5.

Table 2
Added Mass for the Sections and the Whole Model
kg sec ^{2}/m

Fn = 0.15

ω rad/sec	a^* 1	2	3	4	5	6	7	a Sum of Sections	Whole Model
4	-1.21	0.59	-	0.54	0.87	0.41	-0.17	-	1.84
6	0.31	0.66	1.08	1.38	1.26	0.65	0.02	5.36	5.37
8	0.24	0.60	1.09	1.37	1.28	0.76	0.10	5.44	5.26
10	0.20	0.69	1.29	1.48	1.34	0.85	0.14	5.99	5.91
12	0.18	0.78	1.40	1.60	1.45	0.90	0.17	6.48	6.39

Fn = 0.20

4	0.59	0.83	1.29	1.59	1.15	0.22	-0.27	5.40	5.63
6	0.32	0.65	1.00	1.40	1.23	0.64	0	5.24	5.19
8	0.21	0.55	1.08	1.38	1.21	0.75	0.12	5.30	5.18
10	0.19	0.65	1.23	1.49	1.33	0.83	0.14	5.86	5.78
12	0.20	0.77	1.37	1.60	1.45	0.88	0.17	6.44	6.32

Fn = 0.25

4	0.86	1.09	1.26	1.66	1.20	0.16	-0.32	5.91	4.99
6	0.33	0.65	1.01	1.38	1.19	0.55	-0.02	5.09	4.89
8	0.20	0.54	1.03	1.39	1.26	0.68	0.08	5.18	5.13
10	0.18	0.62	1.19	1.48	1.34	0.77	0.12	5.70	5.65
12	0.20	0.76	1.37	1.60	1.45	0.83	0.16	6.37	6.21

Fn = 0.30

4	0.70	0.91	1.49	1.58	1.07	-0.10	-0.22	5.43	5.59
6	0.25	0.44	1.15	1.39	1.07	0.45	0.07	4.82	4.51
8	0.16	0.42	1.14	1.45	1.08	0.58	0.13	4.96	4.93
10	0.15	0.55	1.26	1.47	1.22	0.68	0.17	5.50	5.48
12	0.17	0.69	1.41	1.57	1.35	0.81	0.19	6.19	6.18

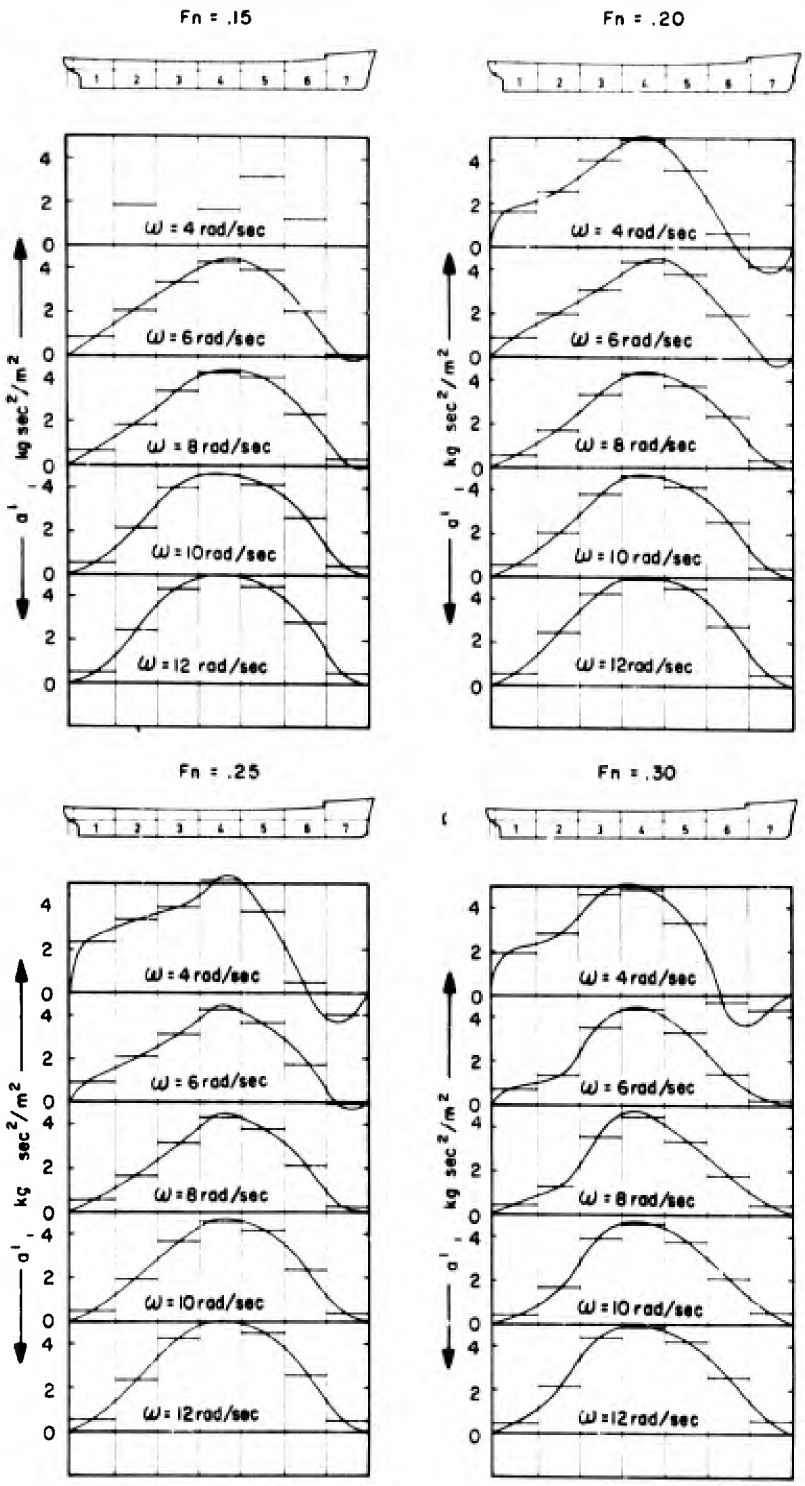

Fig. 7 - Distribution of a over the length of the shipmodel

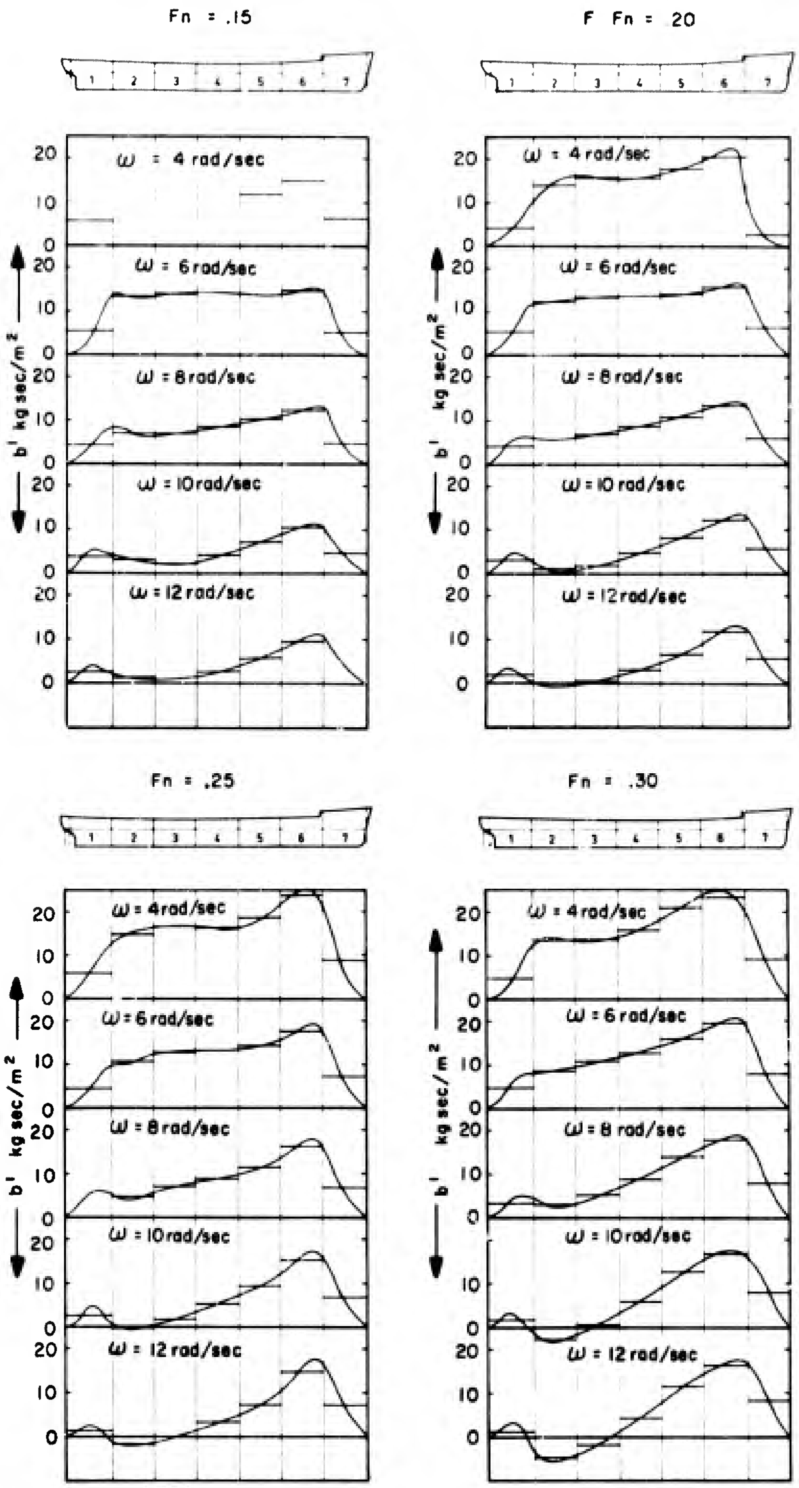

Fig. 8 - Distribution of b over the length of the shipmodel

In Fig. 8 it is shown that the distribution of the damping coefficient b depends on forward speed and frequency of oscillation. The damping coefficient of the forward part of the shipmodel increases when the speed is increasing. At the same time a decrease of the damping coefficient of the afterbody is noticed. For high frequencies negative values for the cross-sectional damping coefficients are found.

Table 3
Damping Coefficients for the Sections and the Whole Model
kg sec/m

Fn = 0.15

ω rad/sec	b*							b	
	1	2	3	4	5	6	7	Sum of Sections	Whole Model
4	2.03	9.78	-	5.78	3.80	4.80	2.00	-	35.63
6	1.82	4.42	4.55	4.58	4.52	4.78	1.67	26.34	26.53
8	1.61	2.31	2.26	2.75	3.35	3.94	1.53	17.75	17.49
10	1.36	1.08	0.76	1.39	2.36	3.43	1.49	11.87	11.63
12	0.95	0.47	0.44	0.87	1.89	3.09	1.50	9.21	8.54

Fn = 0.20

ω rad/sec	1	2	3	4	5	6	7	Sum of Sections	Whole Model
4	1.53	4.53	5.08	5.05	5.73	6.63	2.50	31.05	31.33
6	1.95	3.95	4.32	4.45	4.52	5.07	2.07	26.33	26.15
8	1.50	1.91	2.25	2.81	3.49	4.38	1.94	18.28	17.78
10	1.10	0.37	0.62	1.54	2.70	4.01	1.90	12.24	12.14
12	0.74	-0.15	0.21	1.01	2.18	3.84	1.93	9.76	9.03

Fn = 0.25

ω rad/sec	1	2	3	4	5	6	7	Sum of Sections	Whole Model
4	2.13	4.80	5.38	5.20	5.98	7.63	2.85	33.97	35.88
6	1.97	3.43	4.17	4.23	4.62	5.68	2.35	26.45	27.63
8	1.48	1.58	2.28	2.83	3.68	5.21	2.19	19.25	18.75
10	0.95	-0.06	0.60	1.68	3.00	4.96	2.20	13.33	12.69
12	0.52	-0.56	-0.03	1.03	2.63	4.74	2.29	10.62	9.78

Fn = 0.30

ω rad/sec	1	2	3	4	5	6	7	Sum of Sections	Whole Model
4	1.78	4.40	4.40	5.15	6.78	7.60	2.98	33.09	38.10
6	1.75	2.77	3.50	4.10	5.18	6.32	2.55	26.17	28.45
8	1.21	0.99	1.70	2.81	4.50	5.73	2.51	19.45	20.40
10	0.64	-0.87	0.17	1.88	4.07	5.42	2.59	13.90	13.95
12	0.42	-0.56	-0.63	1.37	3.72	5.28	2.66	11.26	10.42

The added mass distribution, as shown in Fig. 7, changes very little with forward speed but there is a shift forward of the distribution curve for increasing frequencies.

Negative values for the cross-sectional added mass are found for the bow sections at low frequencies. For higher frequencies the influence of frequency becomes very small.

Table 4
Added Mass Cross-Coupling Coefficients
for the Sections and the Whole Model
$kg\ sec^2$

Fn = 0.15

ω rad/sec	d^*							d	
	1	2	3	4	5	6	7	Sum of Sections	Whole Model
4	-	-	-	-	+0.59	+0.28	-	-	-
6	-0.42	-0.47	-0.33	+0.02	+0.46	+0.57	+0.13	-0.04	+0.09
8	-0.27	-0.44	-0.40	-0.01	+0.38	+0.50	+0.13	-0.11	-0.16
10	-0.19	-0.43	-0.40	-0.01	+0.37	+0.49	+0.15	-0.02	-0.10
12	-0.19	-0.45	-0.40	-0.01	+0.40	+0.51	+0.15	+0.01	-0.04

Fn = 0.20

4	-0.57	-0.67	-	-	-	+0.78	+0.32	-	-
6	-0.39	-0.52	-0.34	+0.01	+0.46	+0.59	+0.13	-0.06	-0.06
8	-0.24	-0.45	-0.40	-0.01	+0.39	+0.51	+0.11	-0.09	-0.14
10	-0.20	-0.45	-0.40	-0.01	+0.38	+0.51	+0.13	-0.04	-0.08
12	-0.20	-0.47	-0.41	-0.01	+0.40	+0.53	+0.14	-0.02	-0.03

Fn = 0.25

4	-0.62	-0.59	-0.01	+0.12	+0.72	+0.86	+0.21	+0.69	+0.15
6	-0.39	-0.50	-0.32	+0.02	+0.46	+0.59	+0.13	-0.01	0.00
8	-0.23	-0.48	-0.40	-0.01	+0.39	+0.52	+0.14	-0.07	-0.13
10	-0.18	-0.46	-0.42	-0.01	+0.38	+0.51	+0.13	-0.05	-0.08
12	-0.20	-0.46	-0.42	-0.01	+0.40	+0.51	+0.15	-0.03	-0.05

Fn = 0.30

4	-0.62	-0.61	+0.13	+0.08	+0.64	+0.93	+0.20	+0.75	+1.09
6	-0.29	-0.47	-0.36	+0.01	+0.43	+0.59	+0.21	+0.12	+0.01
8	-0.21	-0.47	-0.44	-0.01	+0.38	+0.53	+0.16	-0.06	-0.11
10	-0.19	-0.46	-0.44	-0.02	+0.38	+0.51	+0.15	-0.07	-0.10
12	-0.20	-0.46	-0.44	-0.02	+0.39	+0.52	+0.16	-0.05	-0.06

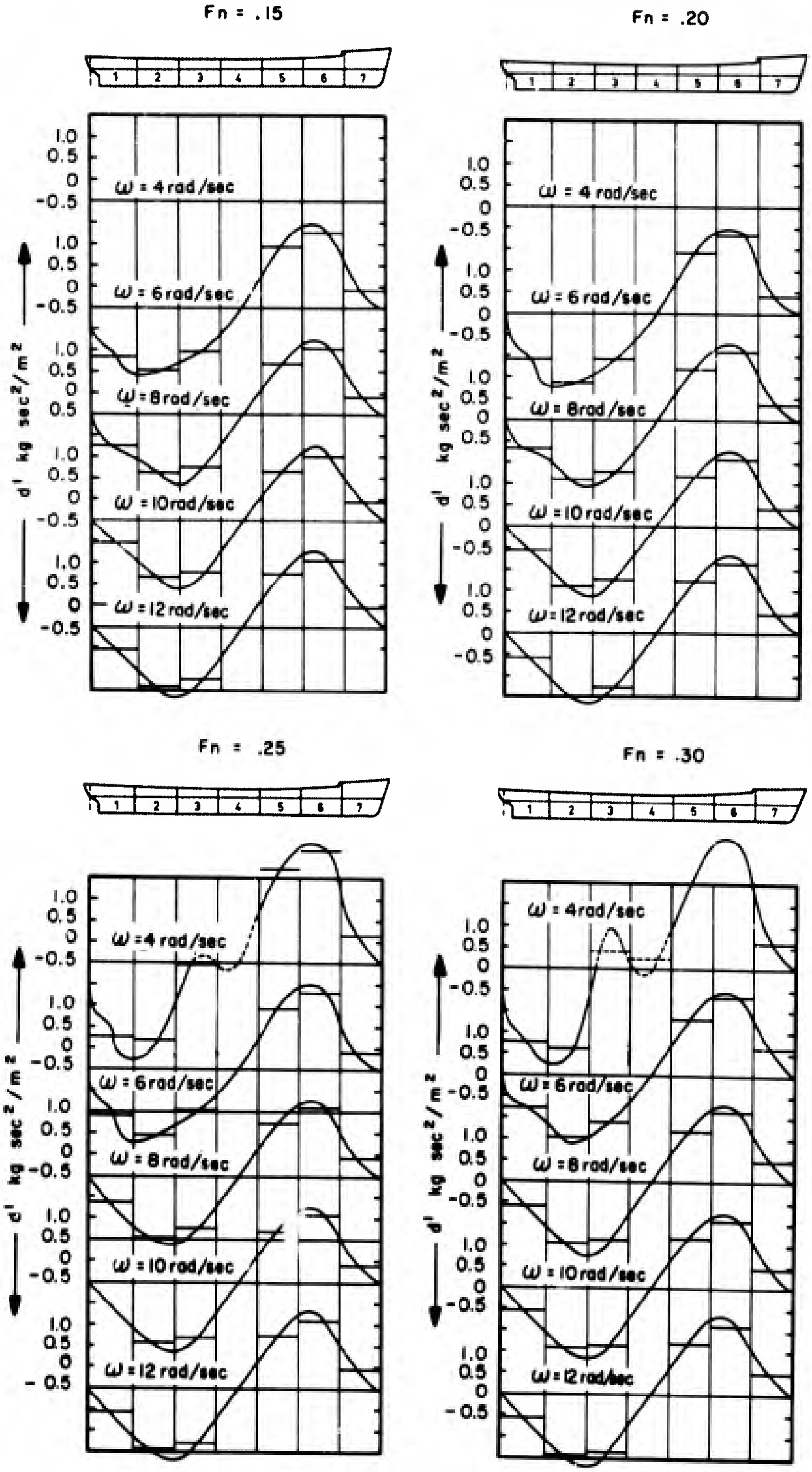

Fig. 9 - Distribution of d' over the length of the shipmodel

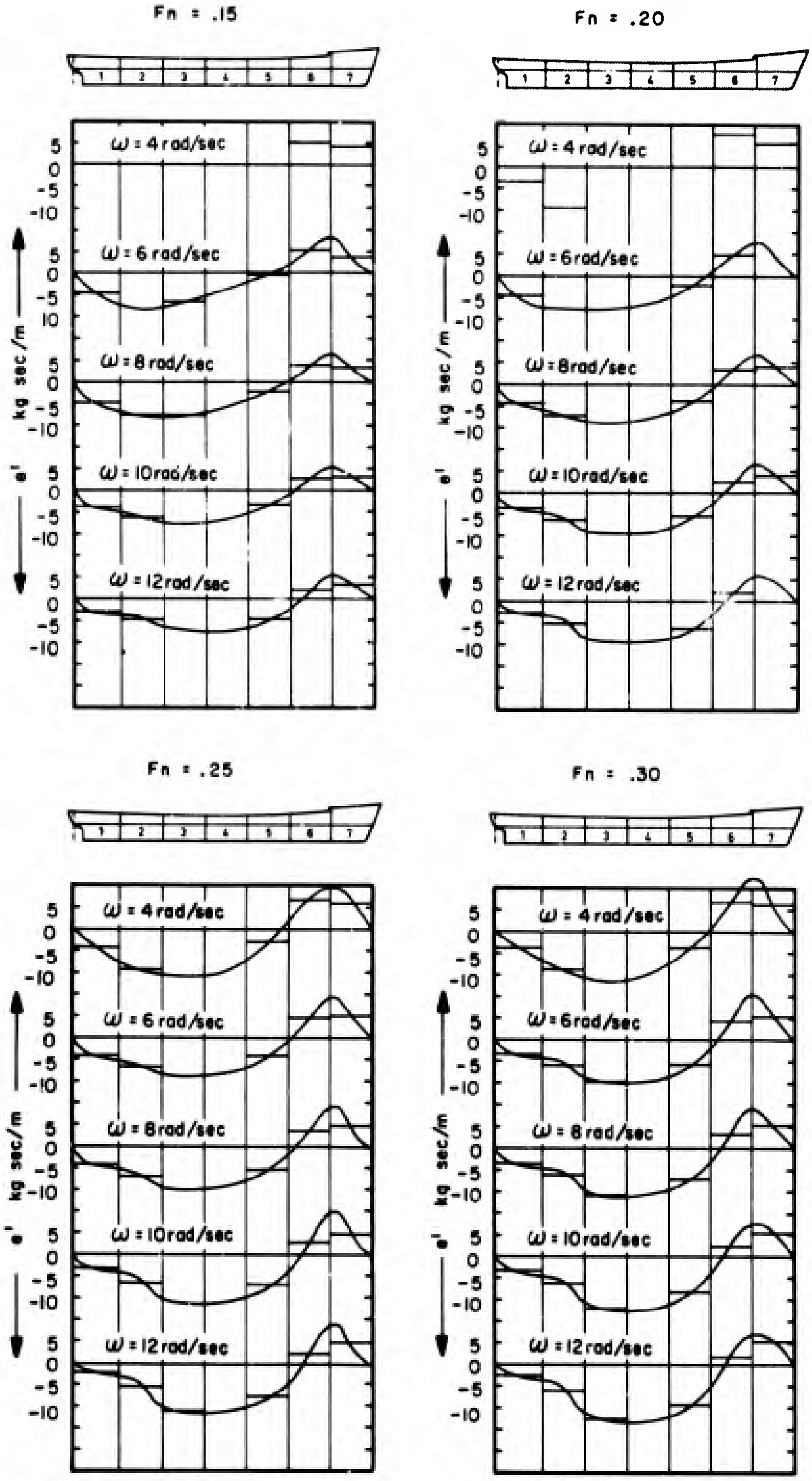

Fig. 10 - Distribution of e over the length of the shipmodel

Table 5
Damping Cross-Coupling Coefficients for the Sections and the Whole Model
kg sec

Fn = 0.15

ω rad/sec	e^* 1	2	3	4	5	6	7	e Sum of Sections	Whole Model
4	-	-	-	-	+1.63	+1.34	-	-	-2.43
6	-1.65	-2.58	-2.12	-1.19	-0.09	+1.70	+1.21	-4.72	-5.32
8	-1.71	-2.49	-2.45	-1.81	-0.68	+1.20	+1.09	-6.84	-6.75
10	-1.40	-2.01	-2.43	-2.10	-1.21	+0.88	+1.05	-7.22	-7.04
12	-1.07	-1.55	-2.28	-2.39	-1.52	+0.63	+1.05	-7.13	-6.88

Fn = 0.20

ω rad/sec	e^* 1	2	3	4	5	6	7	e Sum of Sections	Whole Model
4	-1.22	-3.07	-	-	-	+2.39	+1.77	-	-6.63
6	-1.68	-2.43	-2.40	-2.06	-0.68	+1.52	+1.42	-6.31	-6.65
8	-1.59	-2.36	-2.83	-2.50	-1.25	+1.11	+1.32	-8.10	-8.23
10	-1.29	-2.04	-3.02	-2.87	-1.75	+0.82	+1.29	-8.86	-8.86
12	-0.98	-1.65	-2.99	-2.97	-2.06	+0.61	+1.30	-8.74	-8.75

Fn = 0.25

ω rad/sec	e^* 1	2	3	4	5	6	7	e Sum of Sections	Whole Model
4	-1.52	-3.04	-3.47	-3.03	-0.96	+2.16	+1.91	-7.95	-6.70
6	-1.50	-2.21	-2.85	-2.66	-1.36	+1.47	+1.61	-7.50	-7.38
8	-1.50	-2.26	-3.21	-2.97	-1.79	+1.11	+1.51	-9.11	-9.30
10	-1.22	-2.14	-3.56	-3.39	-2.27	+0.86	+1.49	-10.23	-10.18
12	-0.85	-1.81	-3.66	-3.58	-2.53	+0.66	+1.47	-10.30	-10.31

Fn = 0.30

ω rad/sec	e^* 1	2	3	4	5	6	7	e Sum of Sections	Whole Model
4	-1.37	-2.82	-3.61	-3.06	-1.22	+2.19	+1.98	-7.91	-7.55
6	-1.23	-1.93	-3.16	-3.06	-1.84	+1.43	+1.72	-8.07	-7.95
8	-1.30	-1.96	-3.55	-3.42	-2.32	+1.03	+1.67	-9.85	-9.81
10	-1.19	-2.06	-3.94	-3.90	-2.70	+0.76	+1.67	-11.36	-11.25
12	-0.91	-1.97	-4.08	-4.19	-2.97	+0.56	+1,69	-11.87	-11.84

The distribution of the damping cross-coupling coefficient e varies with speed and frequency as shown in Fig. 10. From Fig. 9 it can be seen that the added mass cross-coupling coefficient depends very little on speed. For higher frequencies the influence of frequency is small.

As a check on the accuracy of the measurements the sum of the results for the sections were compared with the results for the whole model. The following relations were analysed:

$$\Sigma a^* = a \qquad \int_L d' \, x \, dx = A$$

$$\Sigma b^* = b \qquad \int_L e' \, x \, dx = B$$

$$\Sigma d^* = d \qquad \int_L a' \, x \, dx = D$$

$$\Sigma e^* = e \qquad \int_L b' \, x \, dx = E\,.$$

The results are shown in Fig. 11 for a Froude number Fn = 0.20. For the other Speeds a similar result was found. A numerical comparison is given in the Tables 2, 3, 4 and 5. It may be concluded that the section results are in agreement with the values for the whole model. No influence of the gaps between the sections could be found.

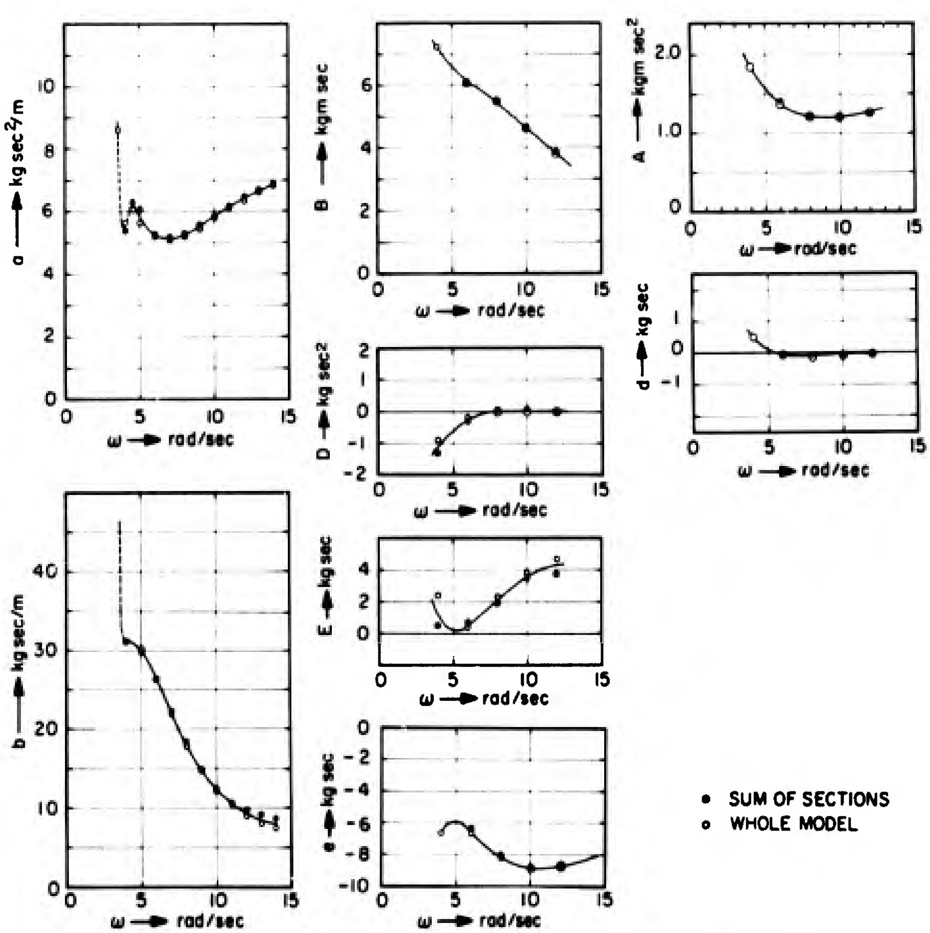

Fig. 11 - Comparison of the sums of section results and the whole model results for Froude number Fn = 0.20

ANALYSIS OF THE RESULTS

The experimental values for the hydrodynamic forces and moments on the oscillating shipmodel will now be analysed by using the strip theory, taking into account the effect of forward speed. For a detailed description of the strip theory the reader is referred to [1], [2] and [3]. For convenience a short description of the strip theory is given here. The theoretical estimation of the hydrodynamic forces on a cross-section of unit length is of particular interest with regard to the measured distributions of the various coefficients along the length of the shipmodel.

Strip Theory

A right hand coordinate system $x_o y_o z_o$ is fixed in space. The z_o-axis is vertically upwards, the x_o-axis is in the direction of the forward speed of the vessel and the origin lies in the undisturbed water surface. A second right hand system of axis xyz is fixed to the ship. The origin is in the centre of gravity. In the mean position of the ship the body axis have the same directions as the fixed axis.

Consider first a ship performing a pure harmonic heaving motion of small amplitude in still water. The ship is piercing a thin sheet of water, normal to the forward speed of the ship, at a fixed distance x_o from the origin.

At the time t a strip of the ship at a distance x from the centre of gravity is situated in the sheet of water. From $x_o = Vt + x$ it follows that $\dot{x} = -V$, where V is the speed of the ship.

The vertical velocity of the strip with regard to the water is $\dot{z}_o$, the heaving velocity. The oscillatory part of the hydromechanical force on the strip of unit length will be

$$F'_H = -\frac{d}{dt}(m'\dot{z}_o) - N'\dot{z}_o - 2\rho g y z_o ,$$

where m' is the added mass and N' is the damping coefficient for a strip of unit length and y is the half width of the strip at the waterline. Because

$$\frac{dm'}{dt} = \frac{dm'}{dx} \times \dot{x} ,$$

it follows that

$$F'_H = -m'\ddot{z}_o - \left(N' - V\frac{dm'}{dx}\right)\dot{z}_o - 2\rho g y z_o . \tag{5}$$

For the whole ship we find, because

$$\int_L \frac{dm'}{dx}\, dx = 0:$$

$$F_H = -\left(\int_L m'dx\right)\ddot{z}_o - \left(\int_L N'dx\right)\dot{z}_o - \rho g A_w z_o \tag{6}$$

where A_w is the waterplane area. The moment produced by the force on the strip is given by

$$M_H' = -xF_H' = (xm')\ddot{z}_o + \left(N'x - Vx\frac{dm'}{dx}\right)\dot{z}_o + 2\rho gxyz_o\,. \tag{7}$$

Because

$$\int_L x\frac{dm'}{dx}dx = -m\,,$$

we find for the whole ship

$$M_H = \left(\int_L xm'dx\right)\ddot{z}_o + \left(\int_L N'x\,dx + Vm\right)\dot{z}_o + \rho g S_w z_o \tag{8}$$

where S_w is the statical moment of the waterplane area.

For a pitching ship the vertical speed of the strip at x with regard to the water will be $-x\dot{\theta} + V\theta$, and the acceleration is $-x\ddot{\theta} + 2V\dot{\theta}$. The vertical force on the strip will be

$$F_p' = -\frac{d}{dt}m'(-x\dot{\theta} + V\theta) - N'(-x\dot{\theta} + V\theta) - 2\rho gyx\theta\,,$$

or

$$F_p' = m'x\ddot{\theta} + \left(N'x - 2Vm' - xV\frac{dm'}{dx}\right)\dot{\theta} + \left(2\rho g\,yx + V^2\frac{dm'}{dx} - N'V\right)\theta\,. \tag{9}$$

The total hydromechanical force on the pitching ship will be

$$F_p = \left(\int_L m'x\,dx\right)\ddot{\theta} + \left(\int_L N'x\,dx - Vm\right)\dot{\theta} + \left(\rho g S_w - V\int_L N'dx\right)\theta\,. \tag{10}$$

The moment produced by the force on the strip is given by

$$M_p' = -xF_p' = -m'x^2\ddot{\theta} - \left(N'x^2 - 2Vm'x - x^2V\frac{dm'}{dx}\right)\dot{\theta} - \left(2\rho gyx^2 + V^2x\frac{dm'}{dx} - N'Vx\right)\theta\,. \tag{11}$$

The total moment on the pitching ship will be

$$M_p = -\left(\int_L m'x^2dx\right)\ddot{\theta} - \left(\int_L N'x^2dx\right)\dot{\theta} - \left(\rho g I_w - V^2m - V\int_L N'x\,dx\right)\theta\,, \tag{12}$$

because

$$\int_L x^2 V \frac{dm'}{dx}\, dx = -2V \int_L m'x\, dx \, .$$

A summary of the expressions for the various coefficients for the whole ship according to the notation in Eqs. (1) and (2) is given in Table 6.

Table 6
Coefficients for the Whole Ship
According to the Strip Theory

$a = \int_L m'dx$	$d = \int_L m'x\, dx + \frac{Vb}{\omega^2}$
$b = \int_L N'dx$	$e = \int_L N'x\, dx - Vm$
$c = \rho g A_w$	$g = \rho g S_w$
$A = \int_L m'x^2 dx + \frac{VE}{\omega^2}$	$D = \int_L m'x\, dx$
$B = \int_L N'x^2 dx$	$E = \int_L N'x\, dx + Vm$
$C = \rho g I_w$	$G = \rho g S_w$

(13)

For the cross-sectional values of the coefficients similar expressions can be derived from the Eqs. (5) to (12). For the comparison with the experimental results two of these expressions are given here, namely:

$$b' = N' - V \frac{dm'}{dx} \, ,$$

$$e' = N'x - 2Vm' - xV \frac{dm'}{dx} \, . \tag{14}$$

Also it follows that

$$A = \int d'x\, dx$$

and

$$B = \int e'x\, dx \, . \tag{15}$$

Comparison of Theory and Experiment

For a number of cases the experimental results are compared with theory. First of all the damping cross-coupling coefficients are considered. From Eqs. (13) it follows that:

$$E = \int_L N' x \, dx + Vm$$
$$e = \int_L N' x \, dx - Vm \,. \qquad (16)$$

The first term in both expressions is the cross-coupling coefficient for zero forward speed. For a fore and aft symmetrical ship this term is equal to zero. For such a ship the resulting expressions are equal in magnitude but have opposite sign, which is in agreement with the result found by Timman and Newman [7]. The experiments confirm this fact as shown in Fig. 13 where e and E are plotted on a base of forward speed as a function of the frequency of oscillation. The magnitude of the speed dependent parts of the coefficients is equal within very close limits. Extrapolation to zero speed shows that the e and E lines intersect in one point which should represent the zero speed cross-coupling coefficient.

Using Grim's two-dimensional solution for damping and added mass at zero speed [9] the coefficients e and E were also calculated according to the Eqs. (16). The distribution of added mass and damping coefficient for zero speed is given in Fig. 12 and the calculated damping cross-coupling coefficients are shown in Fig. 13.

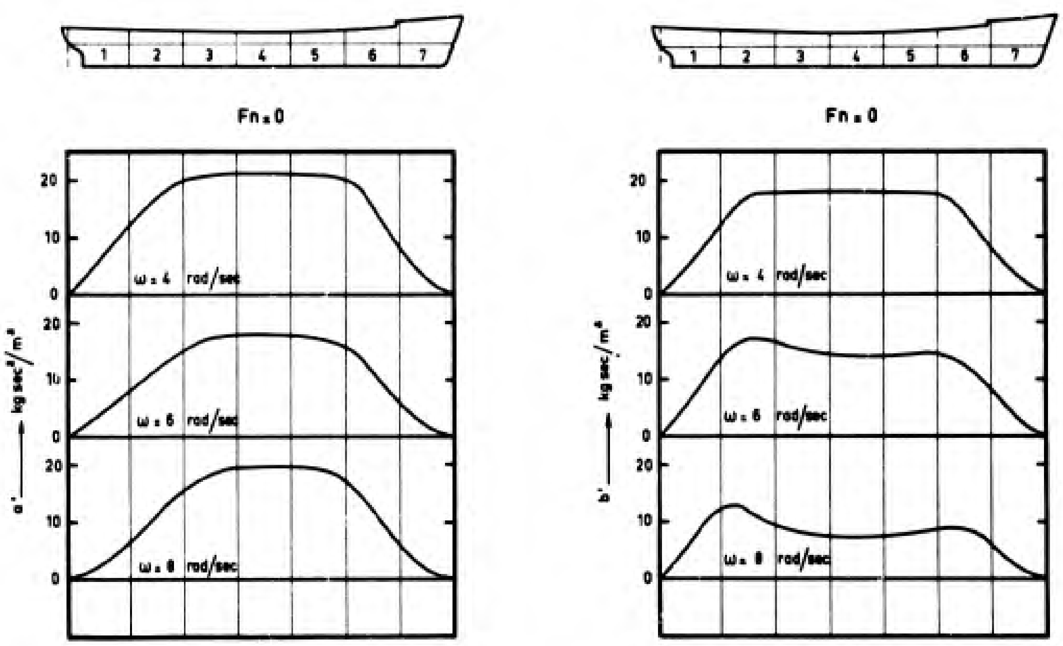

Fig. 12 - Calculated distribution of a and b for zero speed

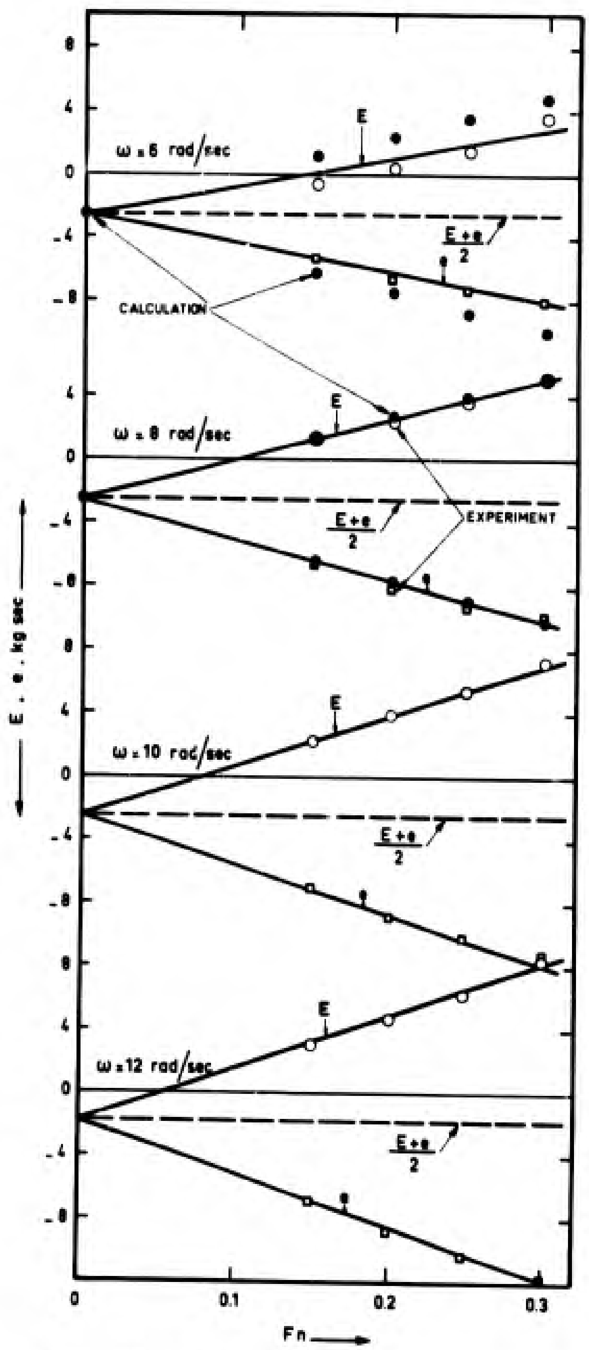

Fig. 13 - Comparison of calculated and measured values for e and E

The calculated values are in line with the experimental results. The natural frequencies for pitch and heave are respectively ω = 7.0/6.9 rad/sec and in this important region the calculation of the damping cross-coupling coefficients is quite satisfactory. The zero speed case will be studied in the near future by oscillating experiments in a wide basin to avoid wall influence.

Another comparison of theory and experiment concerns the distribution along the length of the shipmodel of the damping coefficient and of the damping cross-coupling coefficient e. From Eq. (14):

$$b' = N' - V\frac{dm'}{dx} ,$$

$$e' = N'x - 2Vm' - xV\frac{dm'}{dx} .$$

Again using Grim's two-dimensional values for N' and m', these distributions could be calculated. An example is given in Fig. 14. Also in this case the agreement between the calculation and the experiment is good. For high speeds negative values of the cross-sectional damping in the afterbody can be explained on the basis of the expression for b', because in that region dm'/dx is a positive quantity.

Finally the values for the coefficients A, B, a and b for the whole model, as given by the Eqs. (13) were calculated and compared with the experimental results. Figure 15 shows that the damping in pitch is over-estimated for low frequencies. The other coefficients agree quite well with the experimental results.

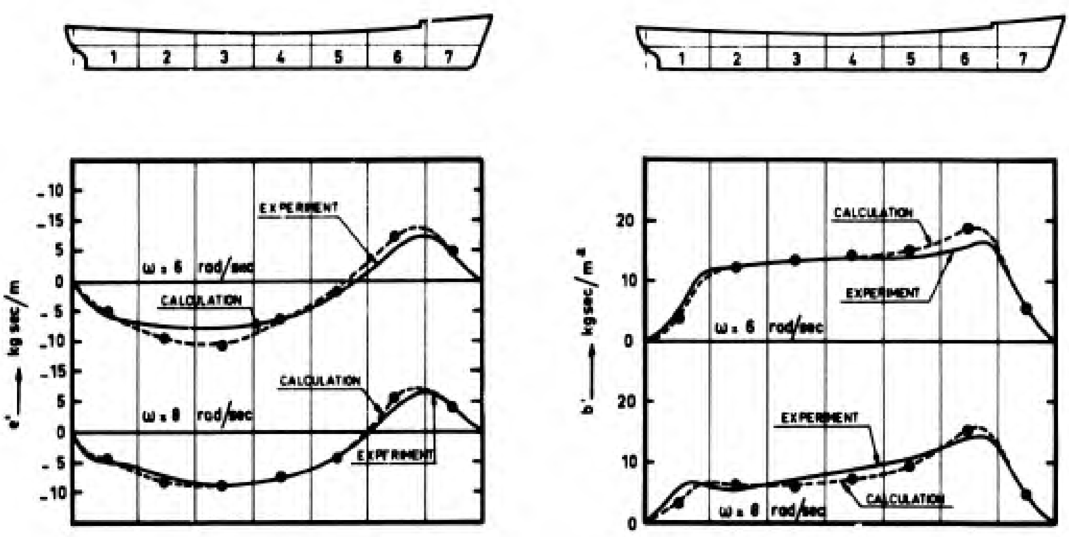

Fig. 14 - Comparison of the calculated distribution of e and b with experimental values for Froude number 0.20

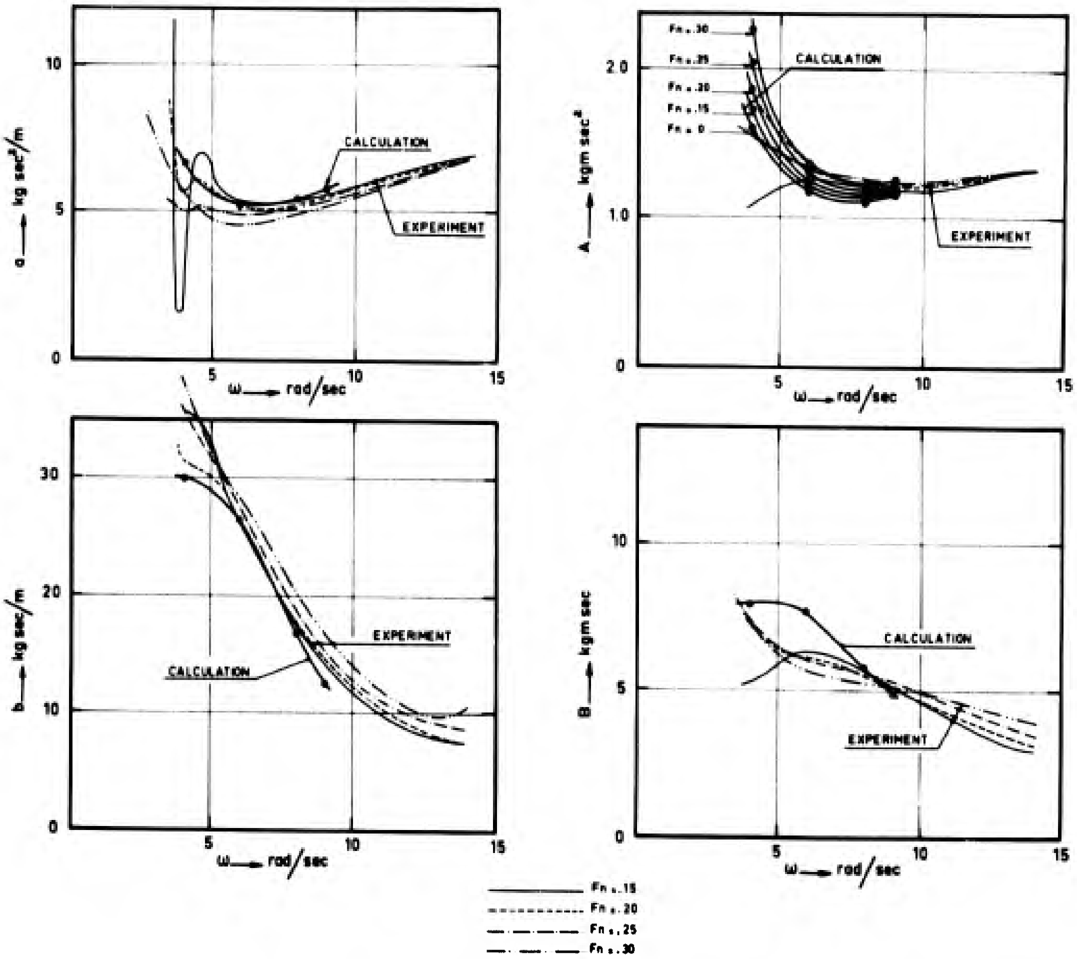

Fig. 15 - Comparison of calculated and measured values for a, b, A and B (whole model)

LIST OF SYMBOLS

$\left.\begin{matrix} a \ldots g \\ A \ldots G \end{matrix}\right\}$ coefficients of the motion equations (hydromechanical part),

$\left.\begin{matrix} a^* \ldots g^* \\ A^* \ldots G^* \end{matrix}\right\}$ the same for a section of the ship,

$\left.\begin{matrix} a' \ldots g' \\ A' \ldots G' \end{matrix}\right\}$ the same for a cross-section of the ship,

C_B Block coefficient,

Fn Froude number

F_z, F_θ amplitude of vertical force on a heaving or pitching ship,

F_H, F_p oscillatory part of the hydromechanical force on a heaving or pitching ship,

g acceleration of gravity,

k_{yy} longitudinal radius of inertia of the ship,

L_{pp} length between perpendiculars,

M_z, M_θ amplitude of moment on a heaving or pitching ship,

M_H, M_p oscillatory part of the hydromechanical moment on a heaving or pitching ship,

m' added mass of a cross-section (zero speed),

N' damping coefficient of a cross-section (zero speed),

t time,

V forward speed of ship,

$x\ y\ z$ right hand coordinate system, fixed to the ship,

x_o, y_o, z_o right hand coordinate system, fixed in space,

z_o vertical displacement of ship,

x_i distance of centre of gravity of a section to the pitching axis,

$\alpha, \beta, \gamma, \delta$ phase angles,

θ pitch angle,

ρ density of water,

ω circular frequency,

∇ volume of displacement of ship, and

∇^* volume of displacement of section.

REFERENCES

1. Korvin-Kroukovsky, B. V. and Jacobs, W. R., "Pitching and heaving motions of a ship in regular waves," S.N.A.M.E., 1957.

2. Fay, J. A., "The motions and internal reactions of a vessel in regular waves," Journal of Ship Research, 1958.

3. Watanabe, Y., "On the theory of pitch and heave of a ship," Technology Reports of the Kyushu University, Vol. 31, No. 1, 1958, English translation by Y. Sonoda, 1963.

4. Fukuda, J., "Coupled motions and midship bending moments of a ship in regular waves," Journal of the Society of Naval Architects of Japan, No. 112, 1962.

5. Gerritsma, J., "Shipmotions in longitudinal waves," International Shipbuilding Progress, 1960.

6. Vossers, G., "Some applications of the slender body theory in ship hydrodynamics," Thesis, Delft, 1962.

7. Timman, R. and Newman, J. N., "The coupled damping coefficient of a symmetric ship," Journal of Ship Research, 1962.

8. Golovato, P., "The forces and moments on a heaving surface ship," Journal of Ship Research, 1957.

9. Grim, O., "A method for a more precise computation of heaving and pitching motions both in smooth water and in waves," Third Symposium of Naval Hydrodynamics, Scheveningen, 1960.

10. Tasai, F.,

    a. "On the damping force and added mass of ships heaving and pitching,"

    b. "Measurements of the waveheight produced by the forced heaving of the cylinders,"

    c. "On the free heaving of a cylinder floating on the surface of a fluid,"

    Reports of Research Institute for Applied Mechanics, Kyushu University, Japan, Vol. VIII, 1960.

11. Goodman, A., "Experimental techniques and methods of analysis used in submerged body research," Third Symposium on Naval Hydrodynamics, Scheveningen, 1960.

12. Zunderdorp, H. J. and Buitenhek, M., "Oscillator techniques at the Shipbuilding Laboratory," Report No. 111, Shipbuilding Laboratory, Technological University, Delft, 1963.

13. Gerritsma, J. and Beukelman, W., "Distribution of damping and added mass along the length of a shipmodel," International Shipbuilding Progress, 1963.

* * *

DISCUSSION

E. V. Lewis
Webb Institute of Naval Architecture
Glen Cove, Long Island, New York

This is a noteworthy paper in an important series by Professor Gerritsma and his colleagues that is of vital importance to ship motion theory. This continuing work has been characterized by unerring choice of the right research subjects and by extraordinary experimental skill. The results have served to clarify the so-called "strip theory" of ship motion calculations and to provide step by step confirmation of the different elements of the theory. Thus the tremendous power of this comparatively simple approach to the problems of ship motions is being reinforced and the value of the pioneering insight of Korvin-Kroukovsky and others confirmed.

It may not be generally realized that this type of experiment, in which forces on seven different sections are measured, is of unusual difficulty, not only because of the many simultaneous readings to be taken, but in the need for accurate determination of in-phase and out-of-phase force components in spite of extraneous noise. The authors have mastered this difficult problem.

The particular value of the resulting research is in showing that when the ship velocity terms are included, excellent predictions of the longitudinal distribution of damping forces are obtained. Furthermore, the nature of the cross-coupling coefficients, E and e, has been clarified by the demonstration that they should be equal at zero speed and differ only by the term $\pm Vm$ at forward speeds. (Incidentally, m is not defined, but is apparently equal to $-a$.)

Incidental features of the paper are simplifications in the coefficients, which are not immediately obvious. It is mentioned that

$$\int x^2 V \frac{dm'}{dx}\, dx = -2V\int m' x\, dx ,$$

which makes the B coefficient, Eq. (13), much simpler than given in (1). Also

$$\int x \frac{dm'}{dx}\, dx = \int x\, dm' = \int m'\, dx = -m \ (= a) ,$$

and therefore the e coefficient is also simplified [Eq. (13)]. Hence, the simple relationship between e and E emerges in Eq. (16) and Fig. 13.

It is hoped that this important work strengthening the strip theory approach will be continued, including oscillation tests at zero speed and restrained tests in waves. My congratulations to the authors for a beautiful piece of research.

* * *

DISCUSSION

J. N. Newman
David Taylor Model Basin
Washington, D.C.

First of all let me congratulate the authors on yet another in the series of excellent papers which we have come to expect from Delft.

Certainly one of the most valuable results obtained recently is the very simple forward speed correction to the strip theory, as outlined in the strip theory paragraph, and the correlation of this theory with experiments. It would seem that all important speed effects are taken into account simply by replacing the time derivative in a fixed coordinate system by that for a moving coordinate system, or

$$\frac{d}{dt} \rightarrow \frac{\partial}{\partial t} - V \frac{\partial}{\partial x} .$$

As a result, the added mass coefficient contributes both to the acceleration and velocity terms of the equations of motion, since

$$\frac{d}{dt}(m'\dot{z}_o) \rightarrow m'\ddot{z}_o - V \frac{dm'}{dx} \dot{z}_o .$$

However this process seems rather arbitrary; why not repeat it for the second time derivative, so that

$$F_H' = -\frac{d^2}{dt^2} m' z_o - \frac{d}{dt} N' z_o - 2\rho g y z_o$$

$$= -m'\ddot{z}_o - \left(N' - 2V \frac{dm'}{dx}\right) \dot{z}_o - \left(2\rho g y + V^2 \frac{d^2 m'}{dx^2} - V \frac{dN'}{dx}\right) z_o \,?$$

It is clear from the experimental results that too much cross-coupling would result, and thus that the last equation is ridiculous both in appearance and in practical utility, but I am left wondering why the equation used in the paper is so much better. Is it possible to give any rational explanation for this?

Finally, since Professor Vossers is not here to defend himself, let me point out that, in general, forward speed <u>will</u> have an effect on the distribution of hydrodynamic forces along an oscillating slender body. Vossers reached the opposite conclusion only for the special case of high frequencies of encounter and very slow speeds.

* * *

DISCUSSION OF THE PAPERS BY GERRITSMA AND BEUKELMAN AND BY VASSILOPOULOS AND MANDEL

T. R. Dyer
Technological University
Delft, Netherlands

The paper by Vassilopoulos and Mandel rigorously examined seakeeping theory, with valuable emphasis on practical ship design. The paper by Gerritsma and Beukelman contains significant experimental results and a clear concise strip theory, thus relating theory and physical phenomena. However, the paper by Vassilopoulos and Mandel agrees only partially with Gerritsma and Beukelman, and with Korvin-Kroukovsky.

The papers were examined by this discusser with the following results:

1. Complete agreement exists as to (a) which motion derivatives appear in each coefficient, and (b) the appearance of velocity dependent terms arising purely from the mechanics of a fixed axis system.

2. Disagreement exists as to the importance of the effect of forward speed on strip theory, but this is the only point of disagreement.

This disagreement led to different evaluations of some motion derivatives. Direct comparison of the coefficients in the two papers does not reveal all disagreement, because of the cancellation of terms due to strip theory by terms due to the mechanics of a fixed axis system. The disagreement in the strip theory specifically arose in two ways: (1) Gerritsma and Beukelman consider sectional added mass to be a function of time, as suggested by Korvin-Kroukovsky. This is a "three-dimensional correction" and is justified experimentally by a velocity dependence in the b' term for the three-dimensional end sections of Gerritsma and Beukelman's model. (2) Gerritsma and Beukelman consider the distance x, between the body axis origin and the hypothetical sheet of water, to be a function of time. This is independent of dimensionality. The second difference is confusing; for Vassilopoulos and Mandel do implicitly take x as function of time when converting from movable to fixed axes, but do not when applying the strip theory.

The strip theory of Gerritsma and Beukelman was re-derived, eliminating these disagreements. The results agreed completely with those of Vassilopoulos and Mandel. Application of integrals quoted by Gerritsma and Beukelman showed agreement between that paper and Korvin-Kroukovsky. This therefore showed no errors in Korvin-Kroukovsky's work, only disagreement with Vassilopoulos and Mandel as to the role of forward speed on the strip theory. Conversion of Gerritsma and Beukelman results to a movable axis system revealed no difficulties, but clearly showed which speed terms result from mechanics and which from strip theory.

The differences, therefore, are seen to be completely a result of a different assumption of the importance of forward speed on strip theory, independent of what axis system is used. The assumption of Gerritsma and Beukelman seems to be justified by experiment. The derivation of the equations of motion by Vassilopoulos and Mandel, due to Abkowitz, seems the most rigorous and satisfying. However, the evaluation of the motion derivatives by Gerritsma and Beukelman, due in part to Korvin-Kroukovsky, seems to yield better results.

This discusser therefore feels it most practical to use the former work to study the mathematics of motion and the latter to evaluate the motion derivatives.

* * *

REPLY TO THE DISCUSSION BY E. V. LEWIS

J. Gerritsma and W. Beukelman
Technological University
Delft, Netherlands

The authors are grateful to have Professor Lewis' comments on their paper.

The definition of m, which is omitted in the paper, is given by

$$\int_L m' dx = m = a .$$

It should be noted that

$$\int_L x\, dm' = - \int_L m' dx$$

and not

$$\int_L x\, dm' = \int_L m' dx ,$$

as suggested by Professor Lewis.

The work reported in this paper was recently extended for the zero forward speed case.

These tests were carried out in a wide basin to avoid wall influence, due to reflected waves. The results support the conclusions of the present paper.

Within the very near future the restrained tests in waves with the segmented model will be carried out in our Laboratory. The results will be compared with calculated values.

* * *

REPLY TO THE DISCUSSION BY J. N. NEWMAN

J. Gerritsma and W. Beukelman
Technological University
Delft, Netherlands

For a fully submerged slender body of revolution in unsteady motion, the total hydrodynamic force on a transverse section is equal to the negative time rate of change of fluid momentum. By taking the time derivative in the moving body axis system the expression

$$\frac{d}{dt}(m'\dot{z}_o) = m'\ddot{z}_o - V\frac{dm'}{dx}\dot{z}_o,$$

is found.

For the surface ship, it is assumed that the flow over the submerged portion of the ship is similar to the flow over the lower half of a fully submerged body with circular cross sections.

Corrections are then necessary for the shape of the sections and for free surface effects. It is assumed that these corrections are introduced by using Grim's values for the sectional damping and added mass coefficients of cylinders having ship-like cross sections oscillating at a free surface. It is admitted that this assumption is more or less intuitive and it was clearly necessary that the assumptions being made had to be verified by experiments, as shown in the paper.

The authors cannot give a similar physical interpretation of the procedure put forward in Dr. Newman's discussion; they have therefore no rational explanation why such an approach is not successful. In addition, the result would certainly not agree with the experiments.

Vossers' results are discussed too shortly in our paper, and the authors are grateful to Dr. Newman for his additional comments.

However, for the actual ship form, as tested in our case, the forward speed effect cannot be neglected, even at quite low speeds, say $Fn = 0.15$.

For pitch, the method, as given in our paper, is valid for such combinations of forward speed and frequency that the motion of the ship in the stationary sheet of water does not depart too much from a harmonic motion (see Ref. [2]).

* * *

A NEW APPRAISAL OF STRIP THEORY

Lyssimachos Vassilopoulos and Philip Mandel
Massachusetts Institute of Technology
Cambridge, Massachusetts

ABSTRACT

After a brief historical review, this paper presents the results of the broad comparison between experimentally measured and theoretically computed ship motions and phase angles first reported in Ref. [6]. Tank data for a wide range of Series 60 models in regular waves were extracted from N.S.M.B. publications and correlated with model responses calculated by a digital computer program which is based on the Korvin-Kroukovsky linear theory of ship motions in conjunction with Grim's latest results on added mass and damping. Seas from both directly ahead and astern are considered and emphasis is paid to the effects of variations in hull form shape and weight distribution.

Methods which will improve the applicability of strip theory and advantages to be gained by modifying its analytical description are next presented in anticipation of further development of the theory. New theoretical data on added mass and damping are also discussed. Although no definite statements are as yet made with regard to some apparent inconsistencies in the Korvin-Kroukovsky analysis, there is reason to believe that certain modifications and corrections can be made which will generally improve the procedure and render it more useful.

INTRODUCTION

About seventy years ago, Captain Kriloff laid the foundation of what today is known to be the strip theory for computing pitching and heaving motions of a ship in regular waves [1,2]. Yet, it was only in 1950 when Weinblum and St. Denis launched a new era in seakeeping research [3] that Kriloff's seldom read paper received the recognition it deserved. During the last decade, Korvin-Kroukovsky addressed himself to the problem of improving and refining the analytical procedure and in this work he was assisted by numerous complementary studies made by other researchers. The culmination of all this activity led to the publication in 1960 of a guide by Jacobs et al. [5] making possible the ready application of strip theory as it was understood at that time.

In a recent report [6], one of the present authors utilized strip theory essentially as it was set forth by Jacobs et al., with a view towards evaluating seaworthiness performance in random seas along analytical lines. The present paper rests heavily on the results reported in Part I of Ref. [6] which includes an extensive correlation of results of strip theory calculations with model results for a wide range of hull forms. The present paper also reports on the further analysis made and experience gained since the publication of Ref. [6].

In contrast to the more rigorous thin-ship, raft and slender body theories, strip theory is undoubtedly the crudest and relies on the most limiting assumptions. However, in advocating a less rigorous approach, the proponents of strip theory were presenting to the profession a procedure for immediate practical application, something which more rigorous approaches to the ship motion problem have still failed to fulfill adequately. In the words of the quotation selected by Korvin-Kroukovsky [9], the advocates of strip theory have had to truly sacrifice rigor in favor of vigor.

Strip theory has reached its present state through a series of distinct stages during which significant contributions and corrections were advanced from time to time. In fact, a perusal of its evolution indicates that the method was built on a series of estimations, adjustments, and tedious accounting. Too many approximations which were neglected for "obvious" reasons in the beginning had to be incorporated at a later stage and many "essential" truths had to be finally neglected.

The fact that the strip theory procedure was not initially developed on a rigorous physical and analytical basis caused, and still causes, much doubt as to its validity in practical applications. For example, Cummins has referred to it [7] as a "shoe that doesn't really fit." On the other hand, at this stage of progress in seakeeping research, we cannot yet afford to reject a useful device which simulates nature fairly effectively, albeit, by force.

In support of the previous statement, one of the objectives of the work reported in Ref. [6] was to assess the degree of correlation between strip theory and experiment. It is mandatory to note that since both experimental and theoretical approaches contain sources of systematic errors, this comparison attempt was characterized by the absence of a distinct norm. Thus, it is only to be interpreted as being an attempt to match the products of strip theory and experiment in the hope that further light will be shed.

After a brief historical review, this paper presents the results of the broad comparison between experimentally measured and theoretically computed ship motions and phase angles first reported in Ref. [6]. Tank data for a wide range of Series 60 models in regular waves were extracted from N.S.M.B. publications and correlated with model responses calculated by a digital computer program which is based on the Korvin-Kroukovsky linear theory of ship motions in conjunction with Grim's latest results on added mass and damping. Seas from both directly ahead and astern are considered and emphasis is paid to the effects of variations in hull form shape and weight distribution.

Methods which will improve the applicability of strip theory and advantages to be gained by modifying its analytical description are next presented in anticipation of further development of the theory. New theoretical data on added mass and damping are also discussed. Although no definite statements are as yet made with regard to some apparent inconsistencies in the Korvin-Kroukovsky analysis, there is reason to believe that certain modifications and corrections can be made which will generally improve the procedure and render it more useful.

It is important to note that the prime objective of the authors' research effort is to ascertain the importance of seaworthiness considerations in preliminary design. Since, however, strip theory of all suggested theoretical approaches had been brought closest to practical application, the decision was made that it was the most appropriate building block upon which to erect further structure. This report constitutes the authors' thoughts as to the accuracy of the strip theory as currently understood and suggestions for improvements.

HISTORICAL NOTES

The earliest and least refined version of strip theory was presented in Ref. [8], where the authors essentially amplified the studies of Kriloff, Weinblum, St. Denis and other pioneers in the field of ship oscillations. The major advancement in Ref. [8] was the inclusion of some of the cross-coupling coefficients in the equations of motion. The first complete presentation of the procedure followed in 1955 [9] and was subsequently corrected and improved two years later [10]. In this effort, various discussers of Ref. [10] and in particular Kaplan [11] and Abkowitz [12] were instrumental in pointing out certain mistakes of the 1955 exposition, while Fay's analysis [13] motivated a more accurate definition of the velocity dependent terms in the equations of motion. Finally, Jacobs [14] at the suggestion of several discussers of Ref. [9] presented a more precise expression for the exciting force (and moment) and hence extended the procedure to the analytical calculation of ship bending moments, as a result of which a unified computational approach was outlined in [5]. The most recent discussion on the coefficients of the equations of motion and excitation terms appears in Ref. [15], whereas for a complete summary of the whole problem as it was understood by Korvin-Kroukovsky the interested reader is referred to Ref. [4].

Since the appearance of Ref. [6], the inclusion of hull-shape nonlinearities was achieved by Parissis [16]. This latter work represents a further refinement of strip theory and provides, with the aid of Kerwin's polynomial hull representation [17], some interesting answers with regard to the validity of linearity and effect of hull-shape non-linearities on ship responses. Although this quasi-nonlinear work is valuable in its own right, it is of no direct use in statistical analysis which is solidly tied to linear systems.

STRIP THEORY VERSUS EXPERIMENT

The first objective of the investigation reported in Ref. [6] was to attempt to assess the accuracy of the strip theory in the form it existed at the time of writing, Ref. [5]. This was accomplished by correlating theoretical computations to experimental data published by the Netherlands Ship Model Basin in Refs. [18] and [19]. The results reported in the latter publications were chosen as the main source for the comparison attempt because they contained the most systematic experimental data in seakeeping obtained to date and also because they dealt with the effects of extensive variations of hull form shape and hull weight distributions on model motions. The experimental data contained in the NSMB reports covered variations in:

1. block coefficient (c_b),

2. length to beam ratio (L/B),

3. length to draft ratio (L/H),

4. longitudinal radius of gyration (k_θ)

for motion in regular waves of height (double amplitude) equal to 1/50 the model length at four different speeds (Froude number of 0.10, 0.15, 0.20 and 0.25) and several heading angles.

To accomplish the extensive calculations involved in strip theory, a computer program was written, debugged and used on the IBM 7094 digital computer of the Computation Center at M.I.T. For a detailed description of the program and its use, the interested reader is referred to Ref. [6]. The basic steps involved in the digital computation are essentially similar to the ones proposed in Ref. [5]. Thus, the whole computation is broken down into suitable packages which can be easily modified or extended if this is deemed necessary. The ship hull, however, and certain of the coefficients of the equations of motion are more accurately defined in the M.I.T. computer program than in Ref. [5]. Also, a subroutine based on Grim's theory for calculating damping and added mass coefficients was incorporated, in preference to the graphical data presented in Ref. [5].

The results of the theoretical computations were compared with only a part of the results reported in Refs. [18] and [19]. In particular, consideration was given to non-dimensional pitching and heaving amplitudes together with their associated phase angles which correspond approximately to directly ahead and astern seas. The word "approximately" is used, since the experimental results of Refs. [18] and [19] referred to actual heading angles of $10°$ and $170°$, and therefore some corrections had to be made for direct comparison at $\chi = 0°$ and $\chi = 180°$. These corrections were based on a suggestion of the authors of Ref. [3] in which the model is considered to move at a modified speed in a fictitious train of waves of the same amplitude but different wavelength. This suggestion was recently justified by Lewis and Numata [20] for the case of small heading angles.

The correlation between theory and experiment was considered in two distinct phases. The first phase dealt solely with the effects of variation of hull shape geometry and was accomplished for the range of hull parameters shown schematically in Fig. 1. Table 1 indicates the main particulars of the family of models chosen for the correlation. Further information required for the computations, such as sectional area coefficients and load waterline shape were obtained from Tables 4, 6, and 8 of the original paper on the Series 60 models [21].

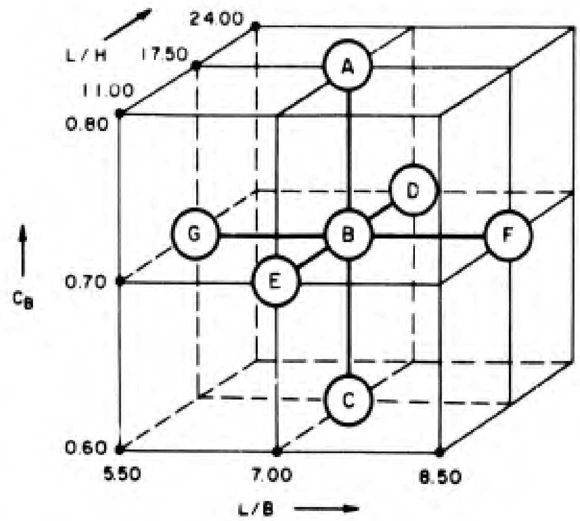

Fig. 1 - Three-dimensional configuration of model hull parameters under examination

Table 1
Series 60 Model Characteristics

Model	L (feet)	B (feet)	H (feet)	L/B	L/H	B/H	C_B	C_P	C_W	LCB (from % L)	Δ* (lbs)
A	10.00	1.429	0.571	7.00	17.50	2.50	0.800	0.805	0.871	2.50F	407.14
B	10.00	1.429	0.571	7.00	17.50	2.50	0.700	0.710	0.787	0.55A	356.25
C	10.00	1.429	0.571	7.00	17.50	2.50	0.600	0.614	0.706	1.50A	305.36
D	10.00	1.429	0.417	7.00	24.00	3.43	0.700	0.710	0.787	0.55A	260.17
E	10.00	1.429	0.909	7.00	11.00	1.57	0.700	0.710	0.787	0.55A	567.13
F	10.00	1.176	0.571	8.50	17.50	2.06	0.700	0.710	0.787	0.55A	293.17
G	10.00	1.818	0.571	5.50	17.50	3.18	0.700	0.710	0.787	0.55A	453.22

*As calculated for fresh water based on above particulars.

All models have a radius of gyration $k_\theta = 0.24L = 2.4$ feet.

The results of the first phase of the correlation are reported herein in the form of graphs of non-dimensional motion amplitudes versus wave length to ship length ratio for constant Froude number (Figs. 2-57). Heave is divided by the wave amplitude h_o and is considered positive upwards; pitch in radian measure is divided by the maximum wave slope $(2\pi/\lambda)h_o$ and is defined positive when the bow is up. Amplitudes of motions are considered positive for both ahead and astern wavelengths. Phase angles are superimposed on the same graphs and are defined as lags when referred to the maximum wave elevation amidships; their range is restricted to ±0-180° only.

The second phase of the correlation was concerned with the effect of longitudinal weight distribution on ship motions. The experimental data required in this case were obtained from Figs. 16 and 17 of Ref. [19]. In the latter work, Model C of Fig. 1 was ballasted in four additional ways so as to yield non-dimensional radii of gyration of k_θ = 0.21, 0.225, 0.255 and 0.270. The previous discussion with regard to presentation of data applies also in this phase of the investigation with the following exceptions due to insufficient model data:

a. Only amplitudes of pitch and heave were compared.

b. Only directly ahead seas (χ = 180°) were considered.

c. The results are given for only three Froude numbers of 0.15, 0.20, and 0.25.

Since Figs. 2-57 all pertain to the case of k_θ = 0.24, Figs. 58-65 deal with the remaining four values of k_θ only.

Wherever the wavelengths for resonance came within the range of values shown on Figs. 2-65, arrows are drawn to indicate their critical values.

KEYS TO FIGURES 2-65

Motion Non-Dimensional Amplitude		Motion Phase Angle (Lag)	
Theoretical	Experimental	Theoretical	Experimental
————	o	– – – – –	●

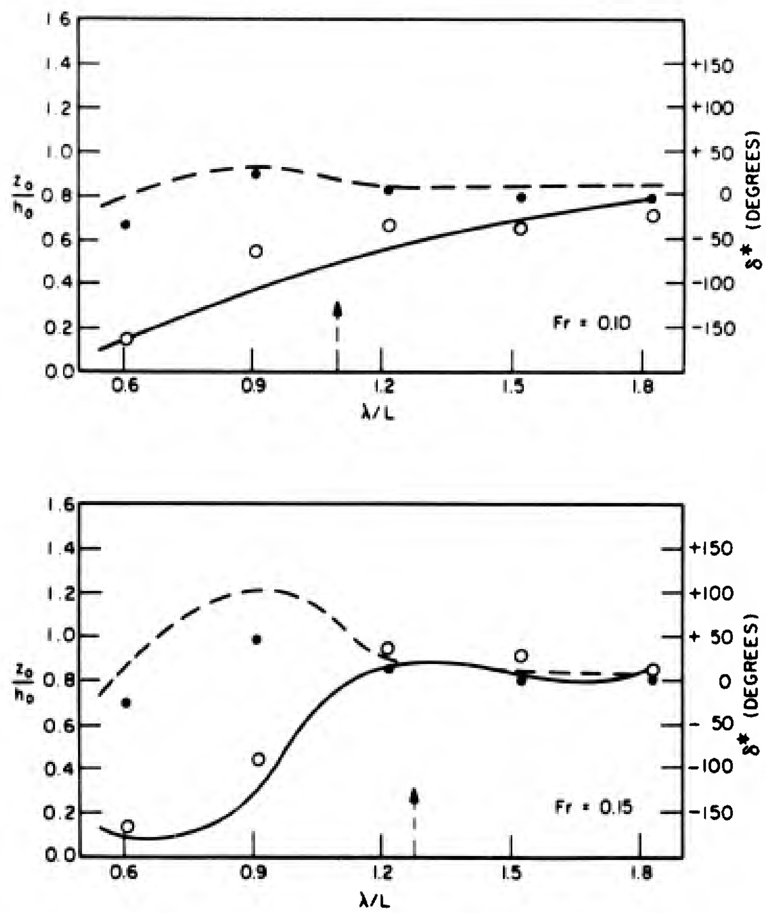

Fig. 2 - Model A in directly ahead seas, heaving non-dimensional amplitude and phase angle vs wavelength to shiplength ratio

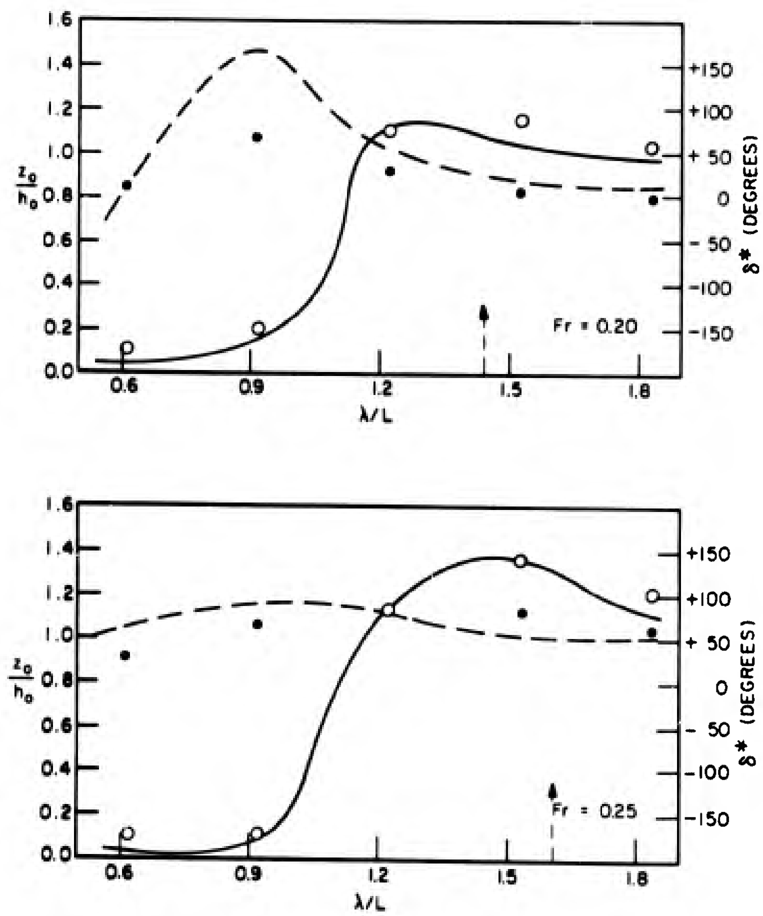

Fig. 3 - Model A in directly ahead seas, heaving non-dimensional amplitude and phase angle vs wavelength to shiplength ratio

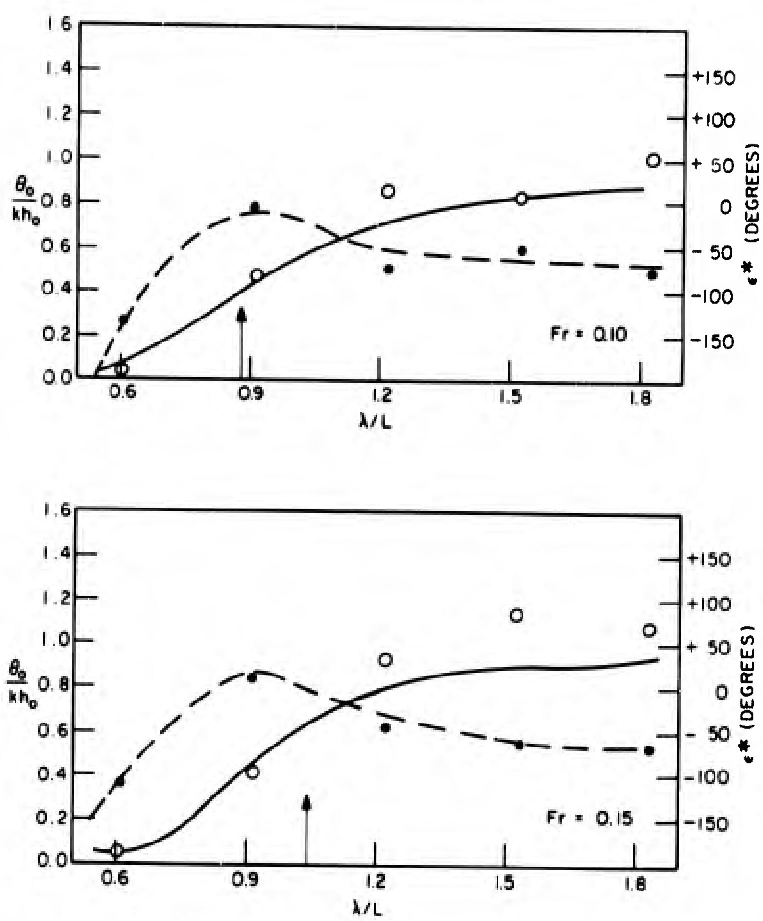

Fig. 4 - Model A in directly ahead seas, pitching non-dimensional amplitude and phase angle vs wavelength to shiplength ratio

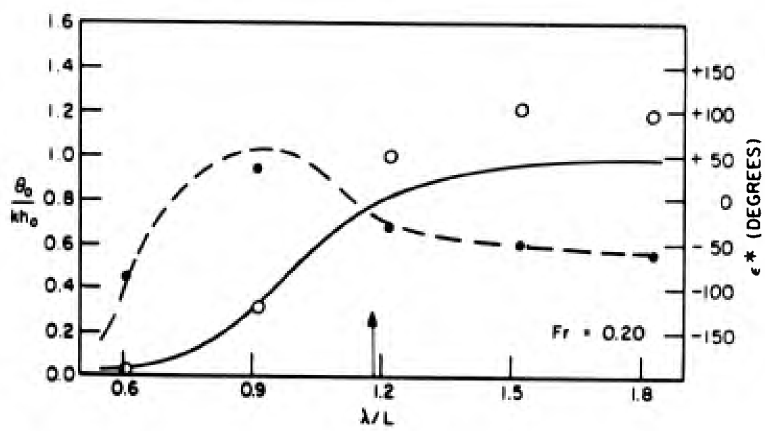

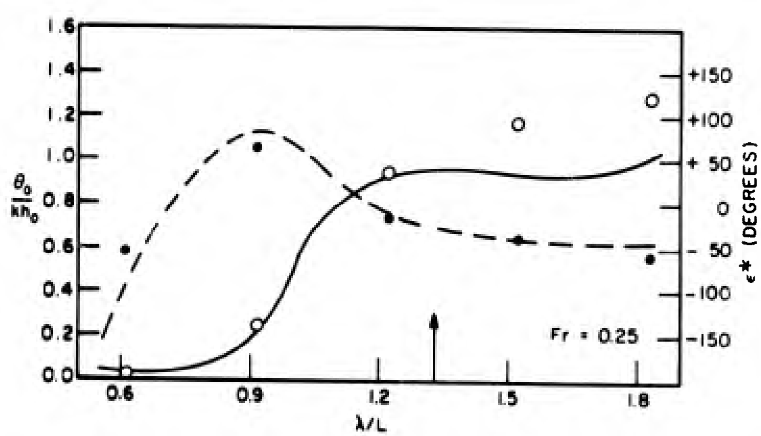

Fig. 5 - Model A in directly ahead seas, pitching non-dimensional amplitude and phase angle vs wavelength to shiplength ratio

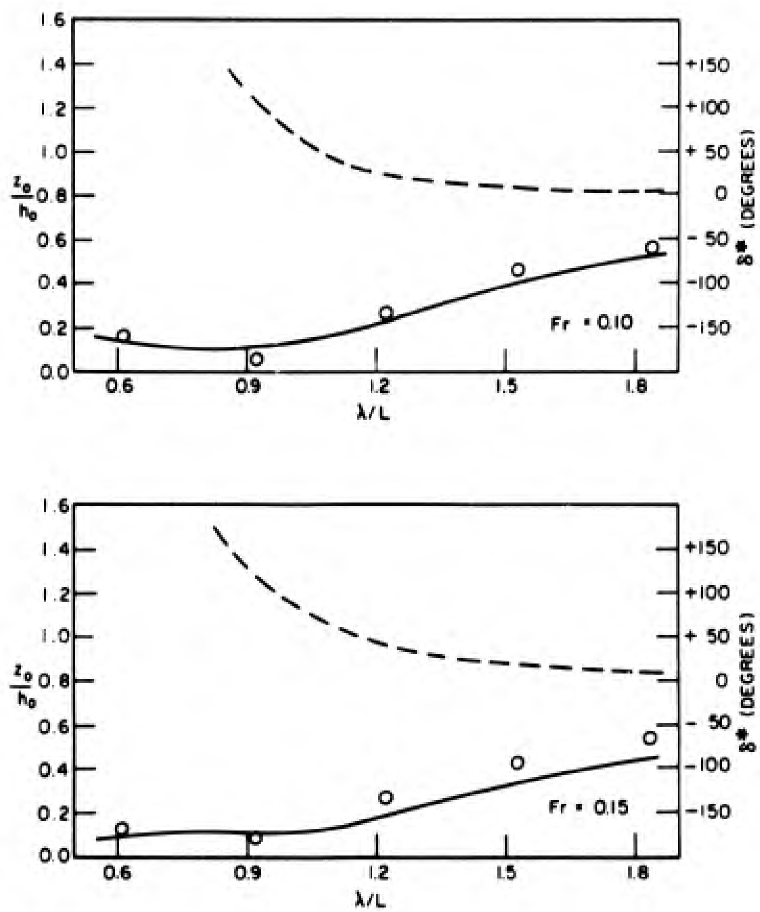

Fig. 6 - Model A in directly astern seas, heaving non-dimensional amplitude and phase angle vs wavelength to shiplength ratio

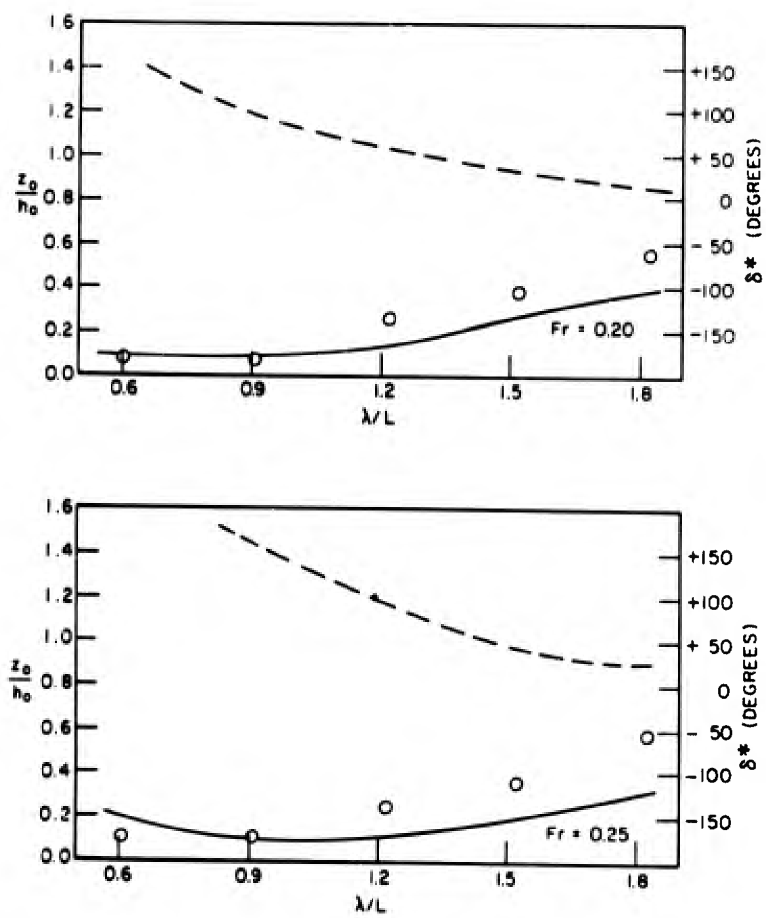

Fig. 7 - Model A in directly astern seas, heaving non-dimensional amplitude and phase angle vs wavelength to shiplength ratio

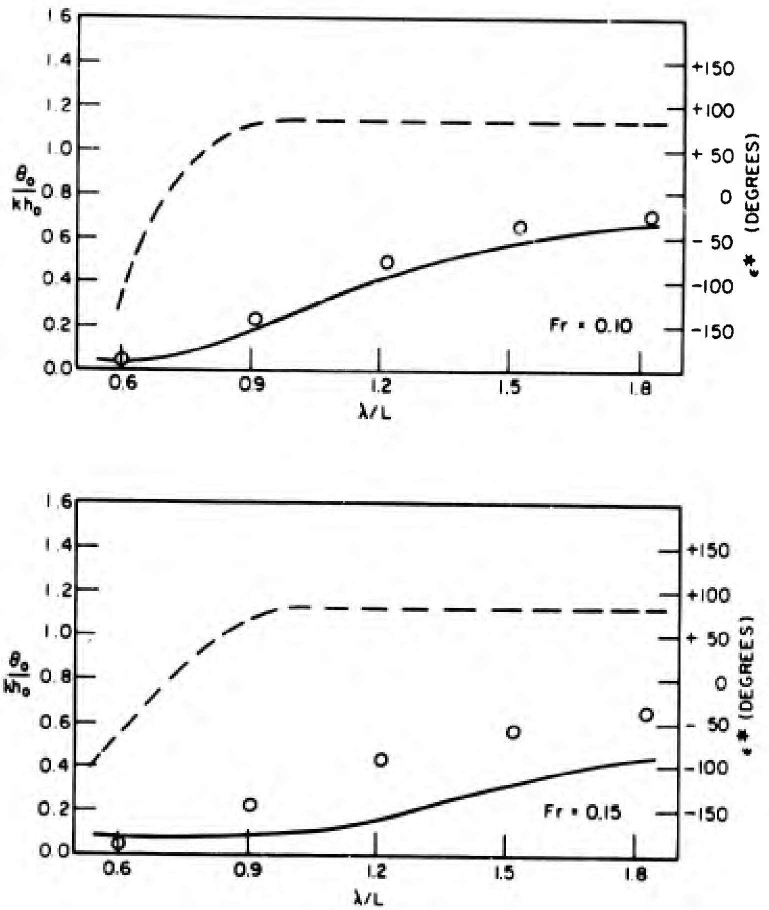

Fig. 8 - Model A in directly astern seas, pitching non-dimensional amplitude and phase angle vs wavelength to shiplength ratio

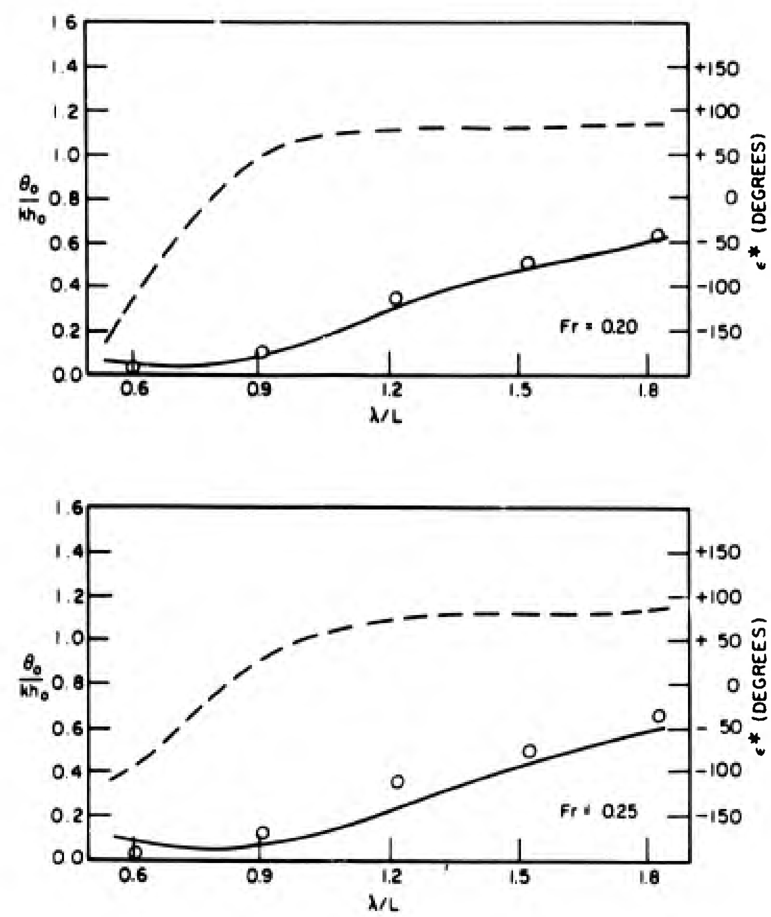

Fig. 9 - Model A in directly astern seas, pitching non-dimensional amplitude and phase angle vs wavelength to shiplength ratio

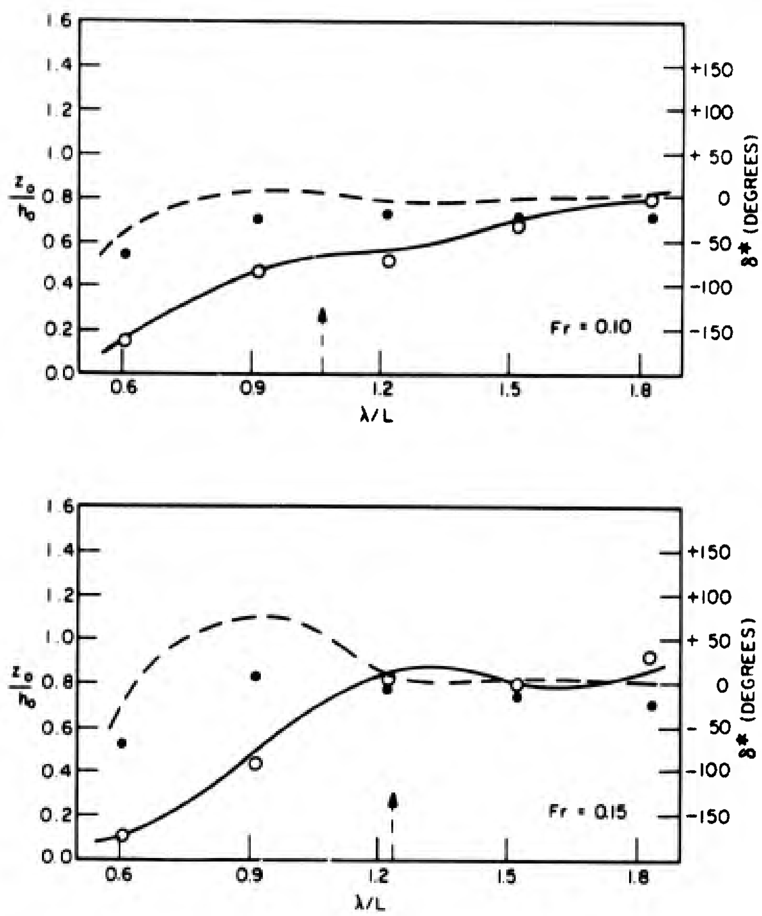

Fig. 10 - Model B in directly ahead seas, heaving non-dimensional amplitude and phase angle vs wavelength to shiplength ratio

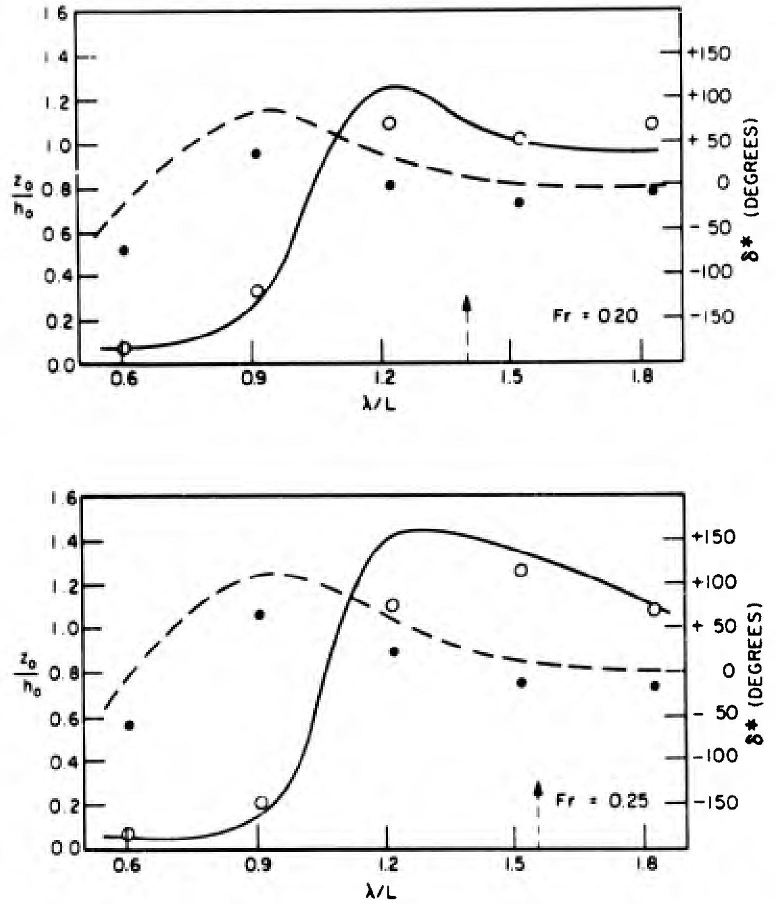

Fig. 11 - Model B in directly ahead seas, heaving non-dimensional amplitude and phase angle vs wavelength tc shiplength ratio

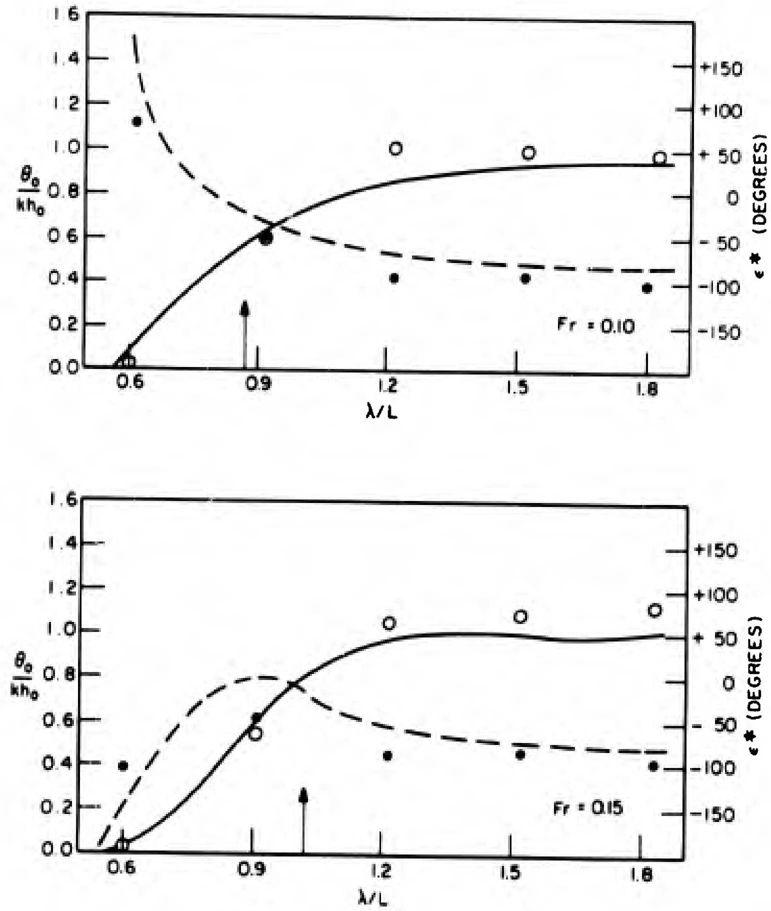

Fig. 12 - Model B in directly ahead seas, pitching non-dimensional amplitude and phase angle vs wavelength to shiplength ratio

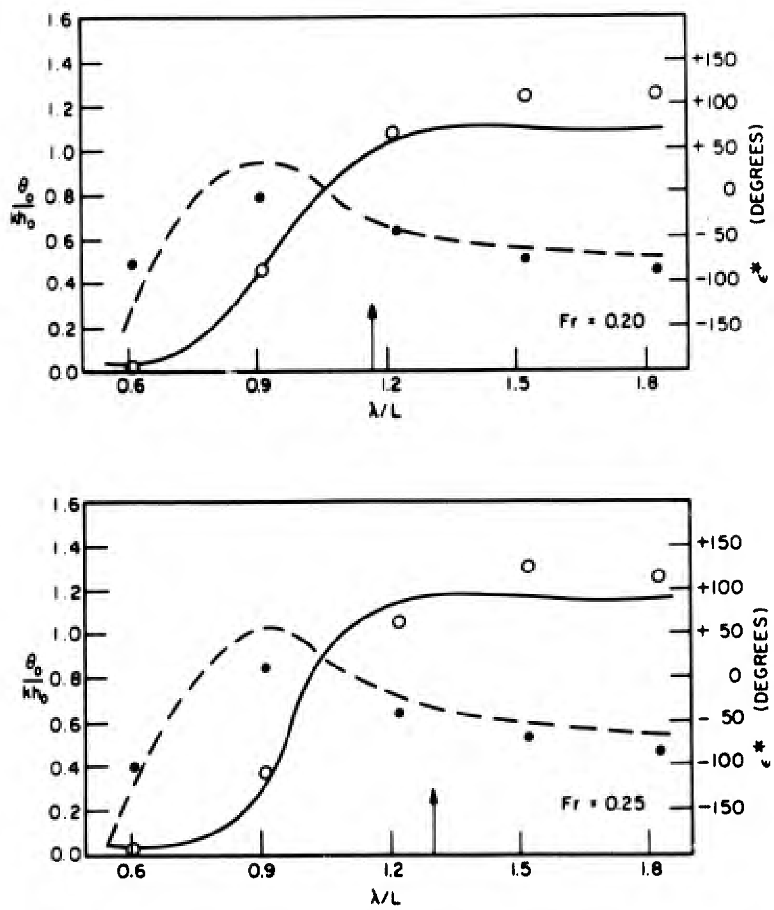

Fig. 13 - Model B in directly ahead seas, pitching non-dimensional amplitude and phase angle vs wavelength to shiplength ratio

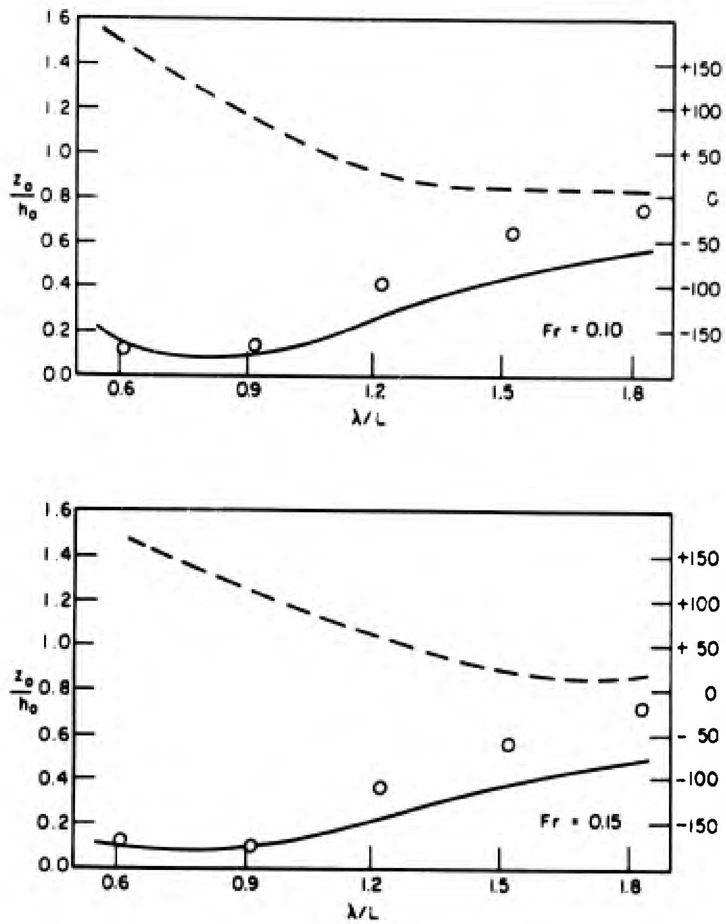

Fig. 14 - Model B in directly astern seas, heaving non-dimensional amplitude and phase angle vs wavelength to shiplength ratio

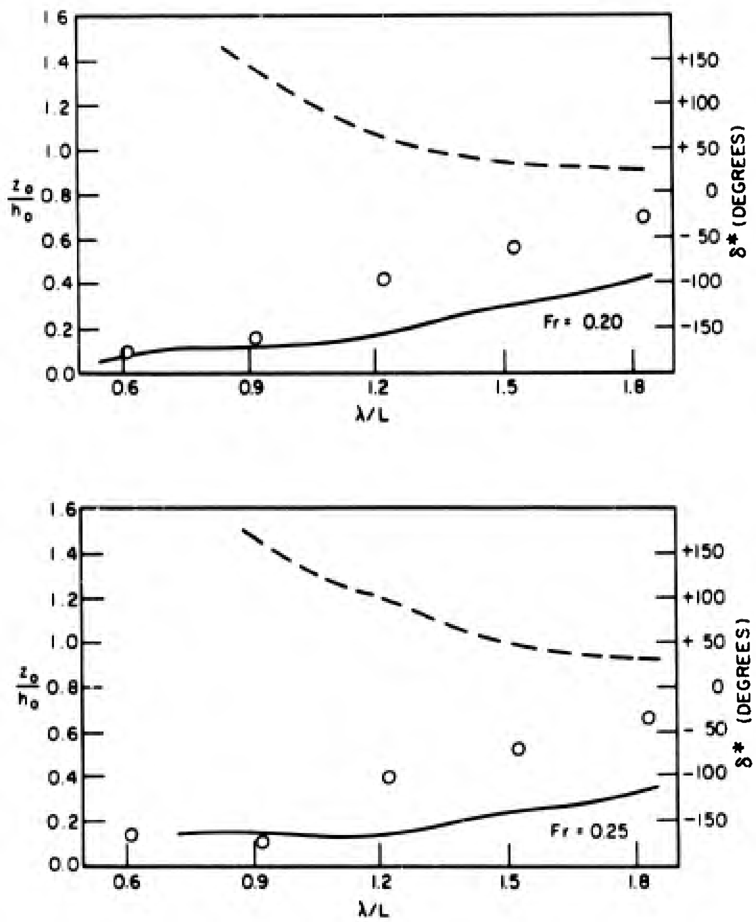

Fig. 15 - Model B in directly astern seas, heaving non-dimensional amplitude and phase angle vs wavelength to shiplength ratio

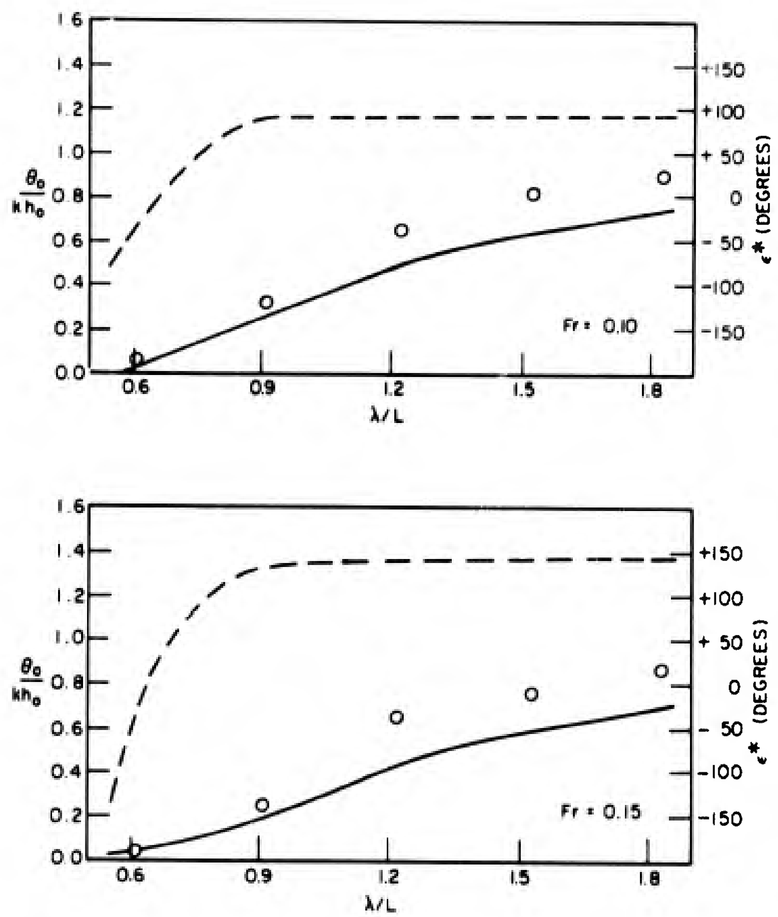

Fig. 16 - Model B in directly astern seas, pitching non-dimensional amplitude and phase angle vs wavelength to shiplength ratio

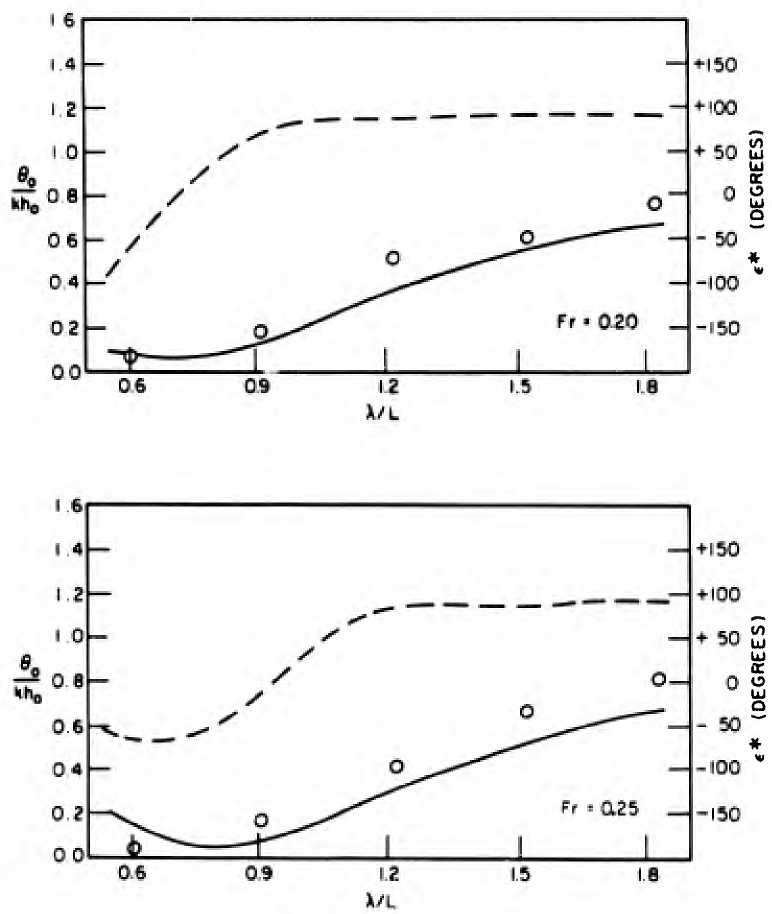

Fig. 17 - Model B in directly astern seas, pitching non-dimensional amplitude and phase angle vs wavelength to shiplength ratio

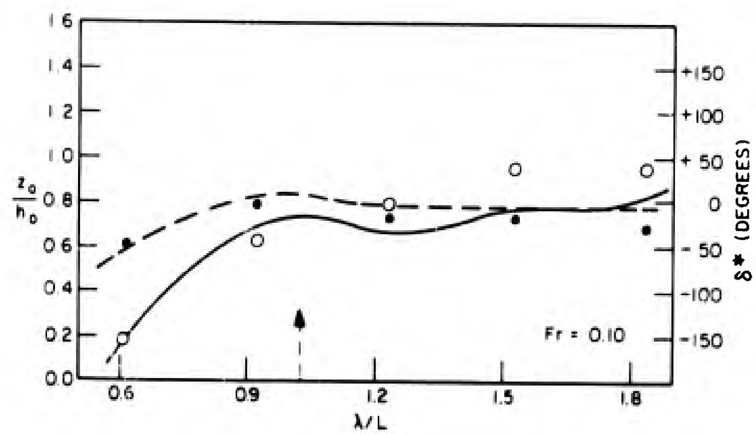

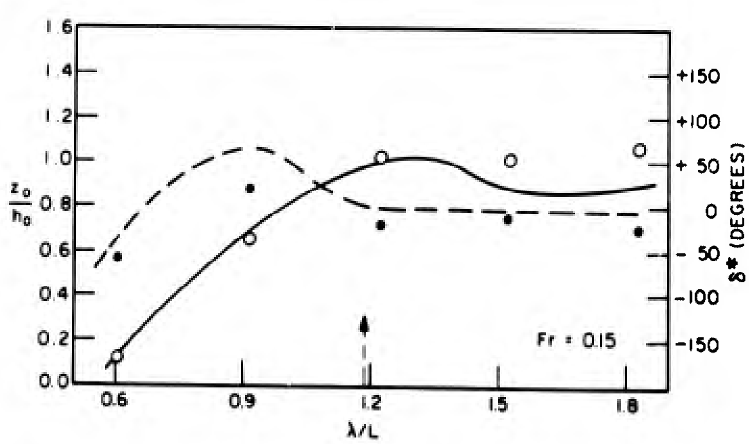

Fig. 18 - Model C in directly ahead seas, heaving non-dimensional amplitude and phase angle vs wavelength to shiplength ratio

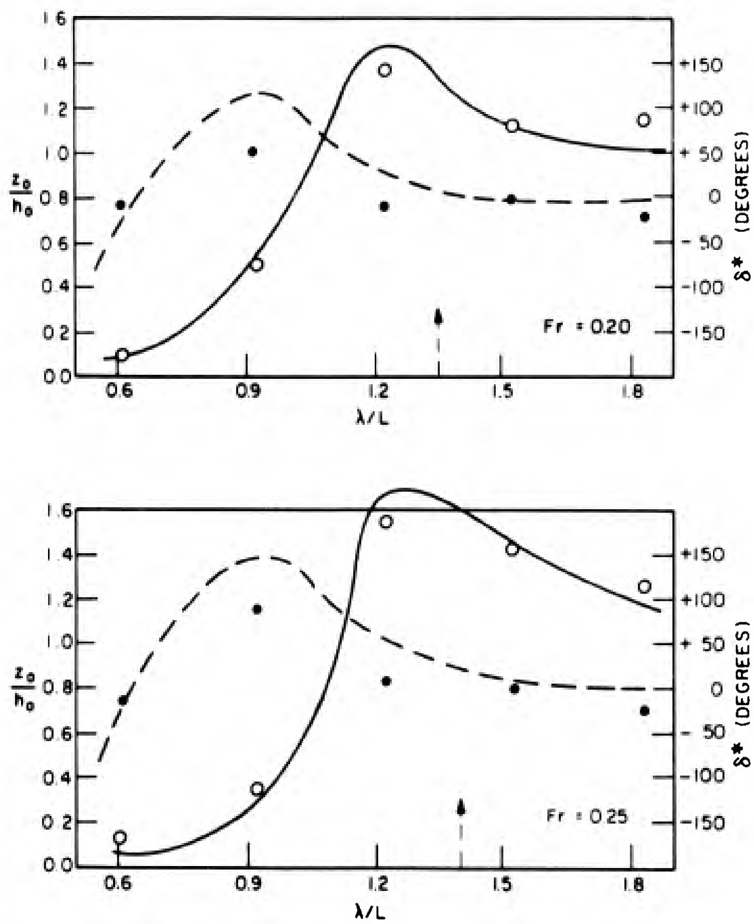

Fig. 19 - Model C in directly ahead seas, heaving non-dimensional amplitude and phase angle vs wavelength to shiplength ratio

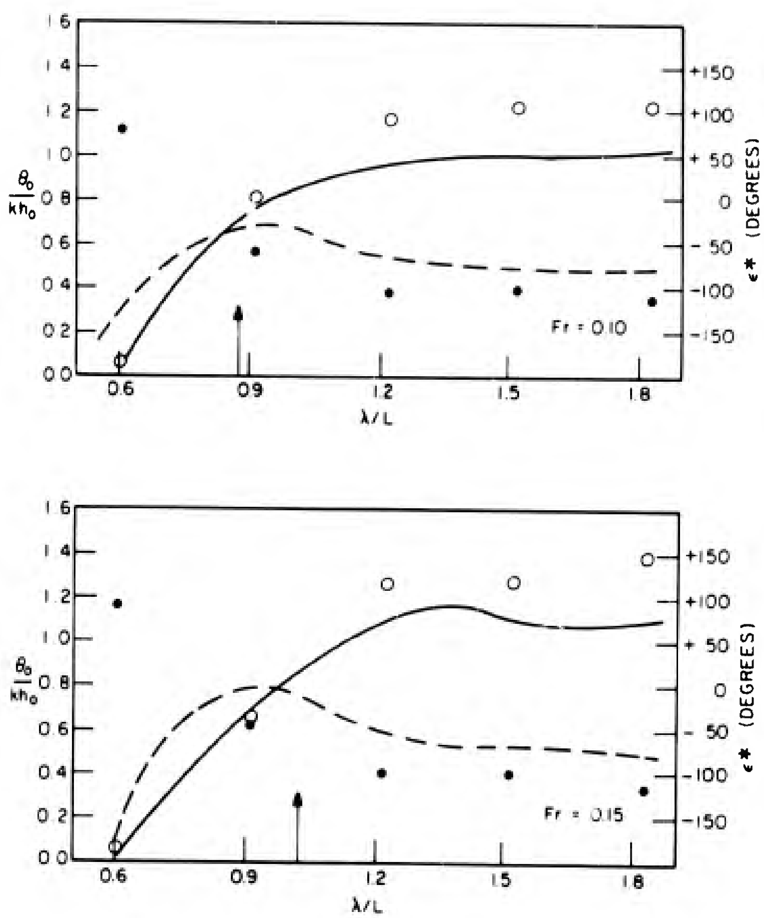

Fig. 20 - Model C in directly ahead seas, pitching non-dimensional amplitude and phase angle vs wavelength to shiplength ratio

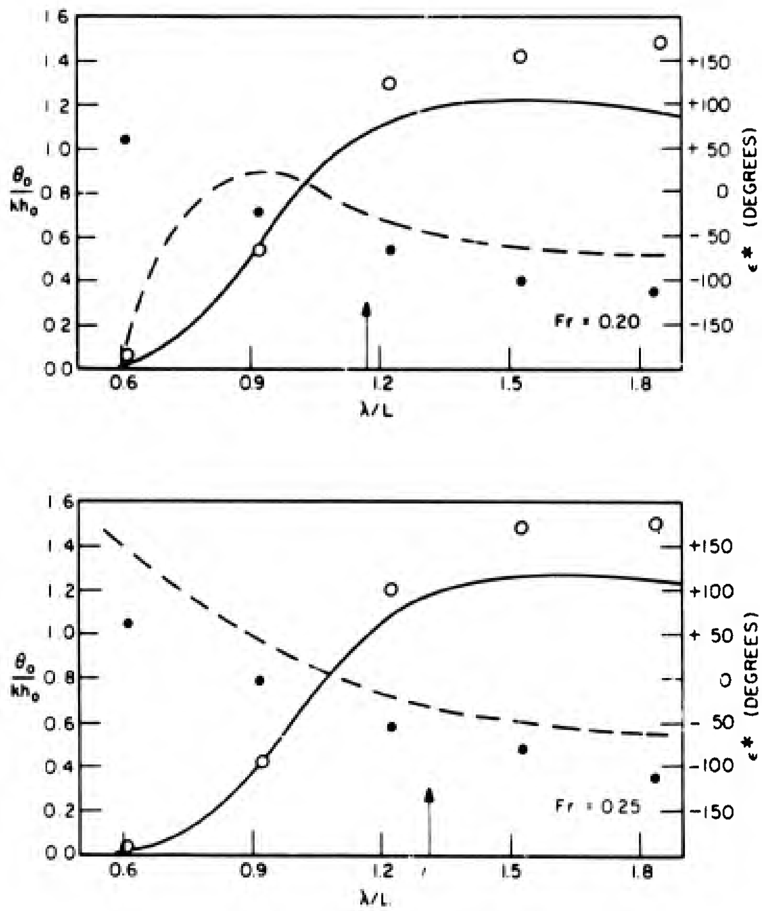

Fig. 21 - Model C in directly ahead seas, pitching non-dimensional amplitude and phase angle vs wavelength to shiplength ratio

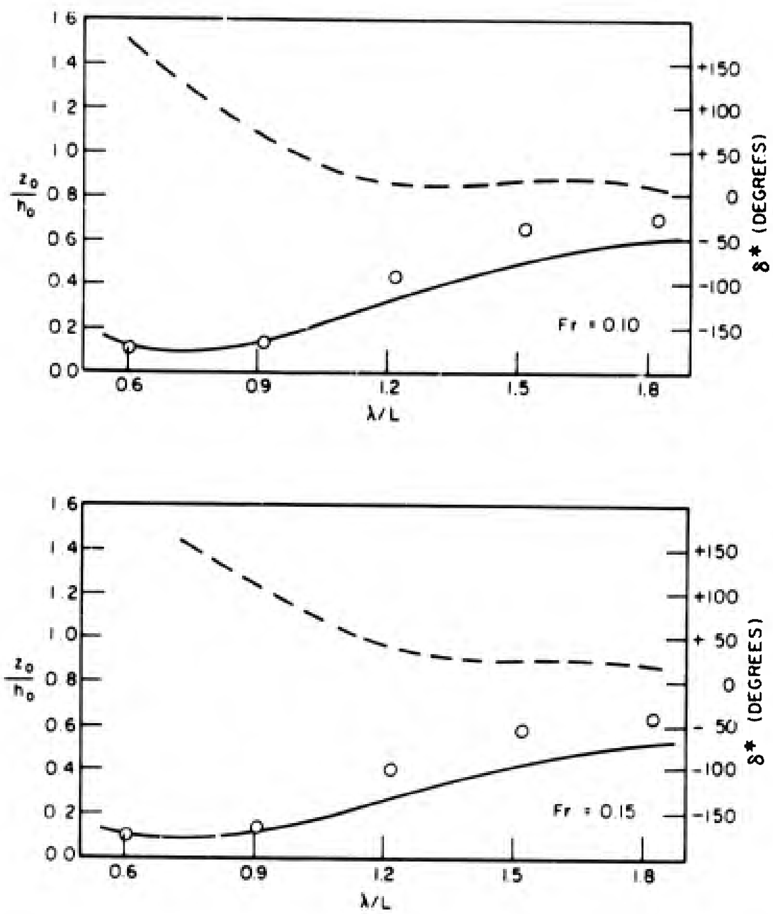

Fig. 22 - Model C in directly astern seas, heaving non-dimensional amplitude and phase angle vs wavelength to shiplength ratio

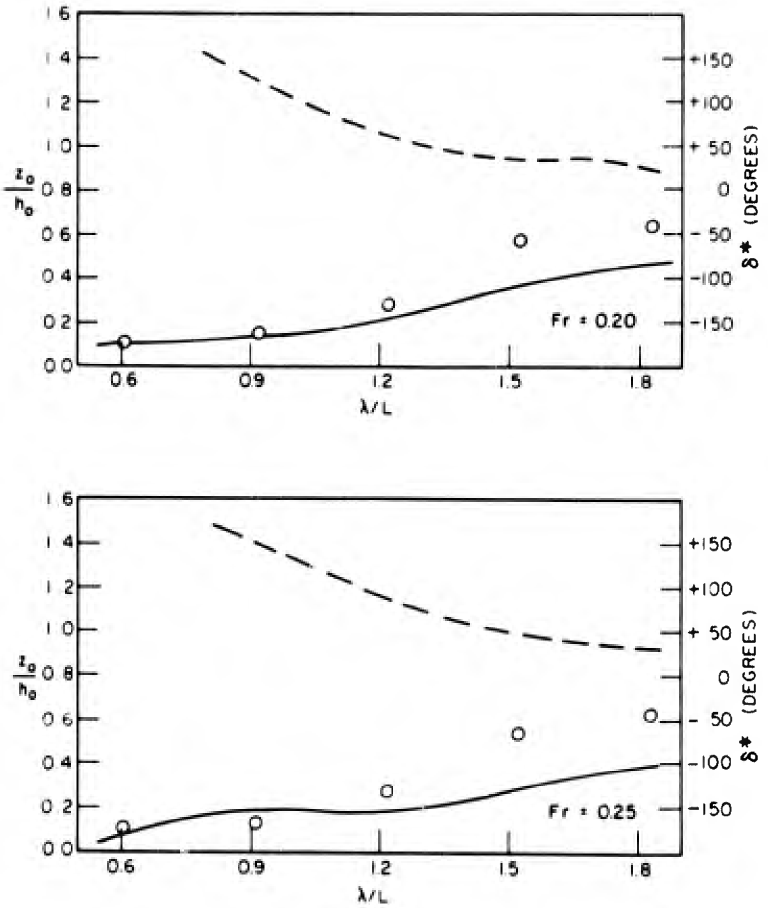

Fig. 23 - Model C in directly astern seas, heaving non-dimensional amplitude and phase angle vs wavelength to shiplength ratio

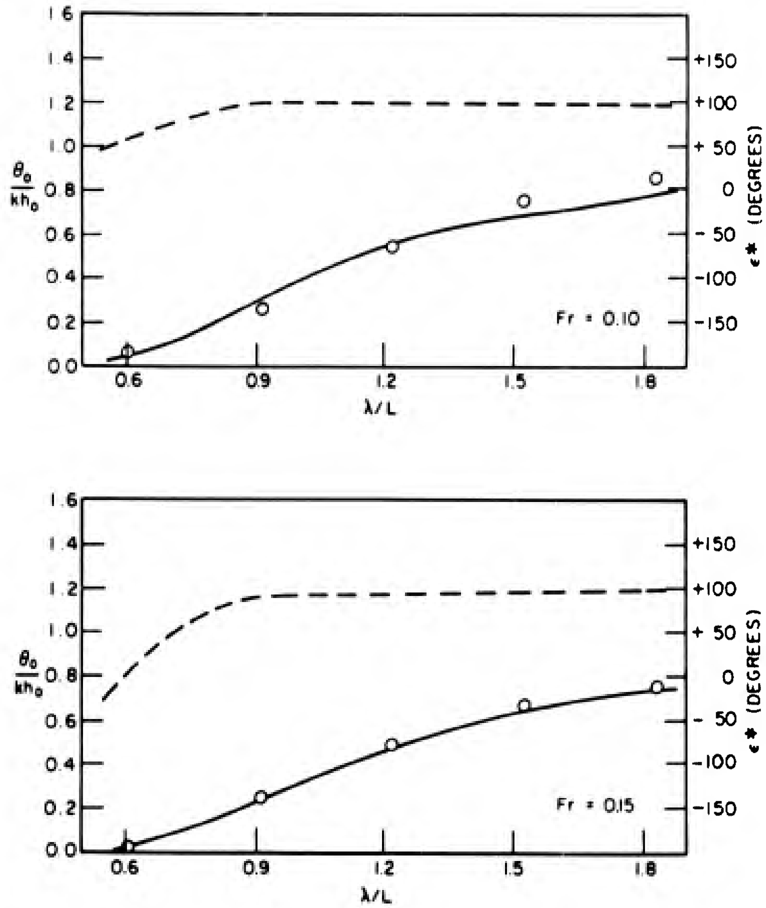

Fig. 24 - Model C in directly astern seas, pitching non-dimensional amplitude and phase angle vs wavelength to shiplength ratio

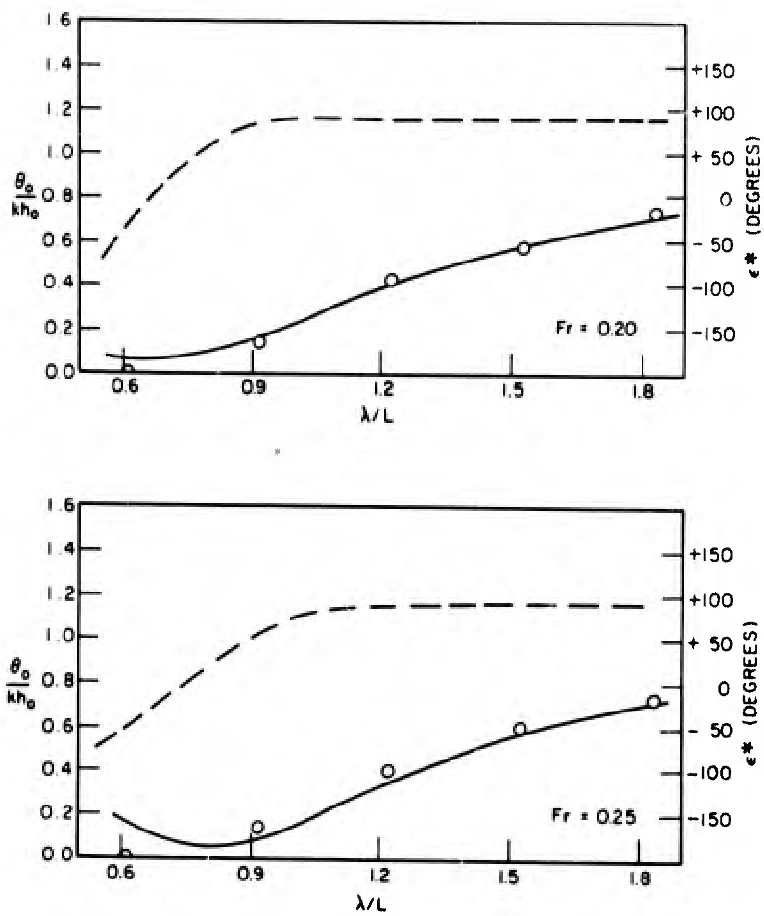

Fig. 25 - Model C in directly astern seas, pitching non-dimensional amplitude and phase angle vs wavelength to shiplength ratio

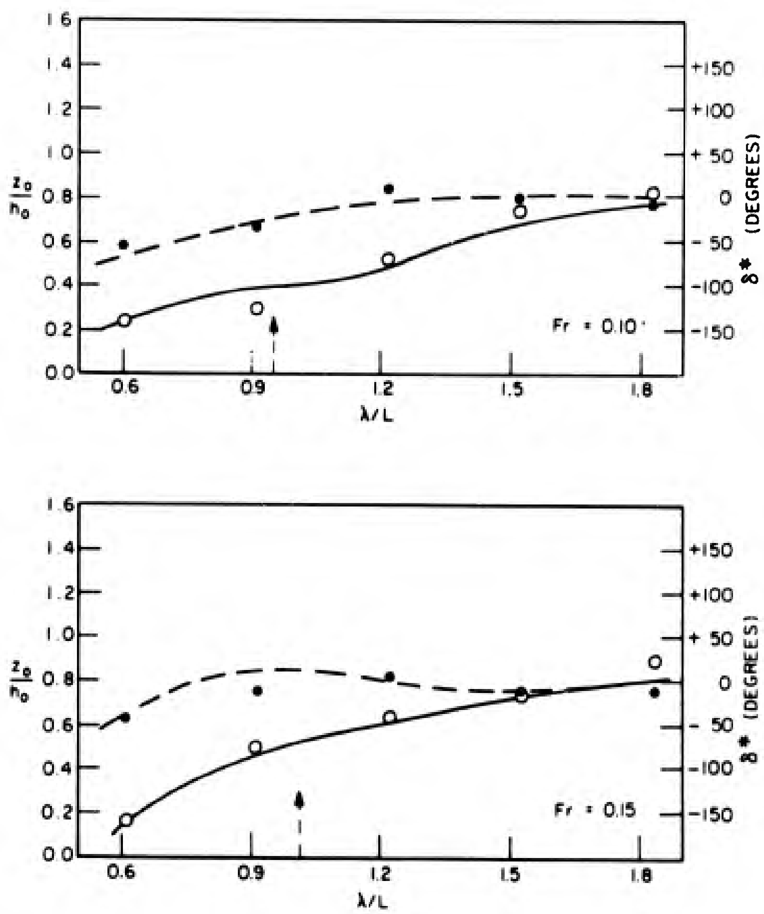

Fig. 26 - Model D in directly ahead seas, heaving non-dimensional amplitude and phase angle vs wavelength to shiplength ratio

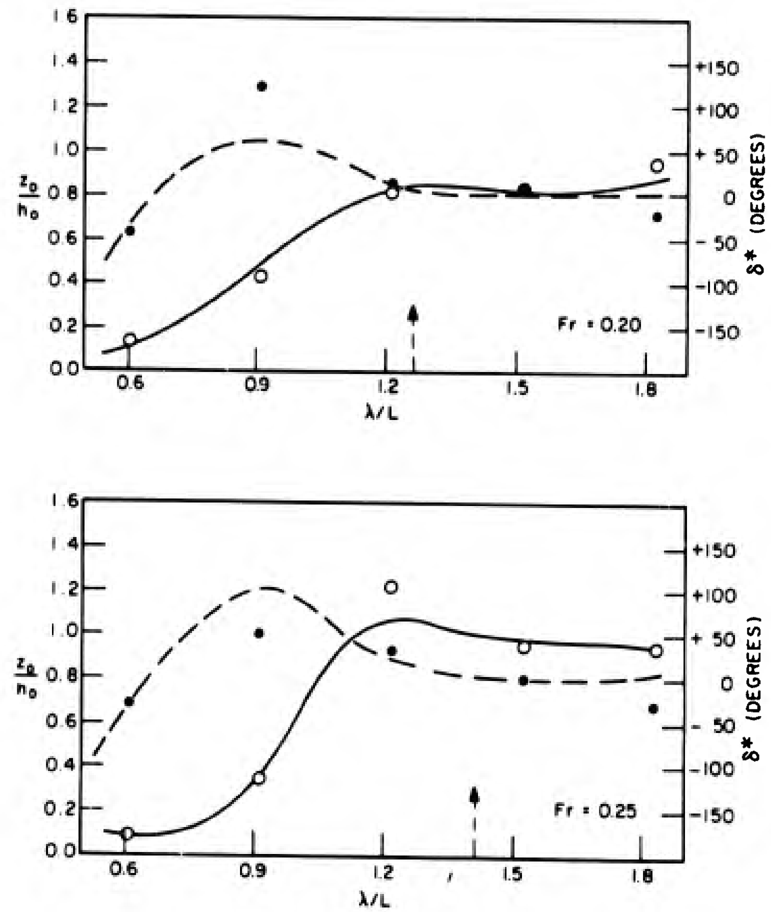

Fig. 27 - Model D in directly ahead seas, heaving non-dimensional amplitude and phase angle vs wavelength to shiplength ratio

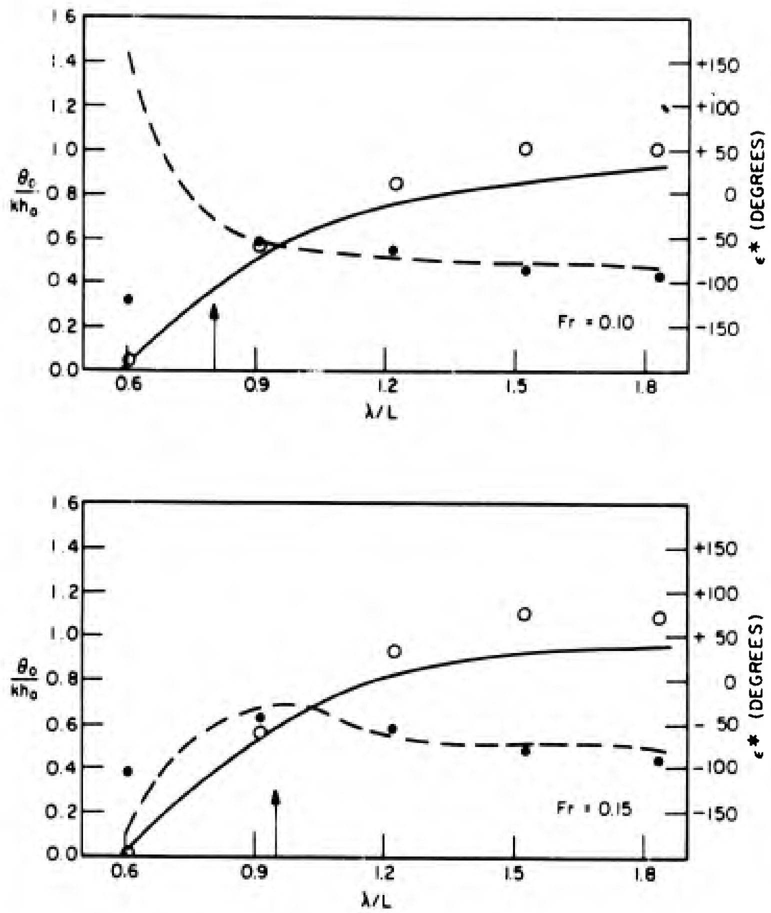

Fig. 28 - Model D in directly ahead seas, pitching non-dimensional amplitude and phase angle vs wavelength to shiplength ratio

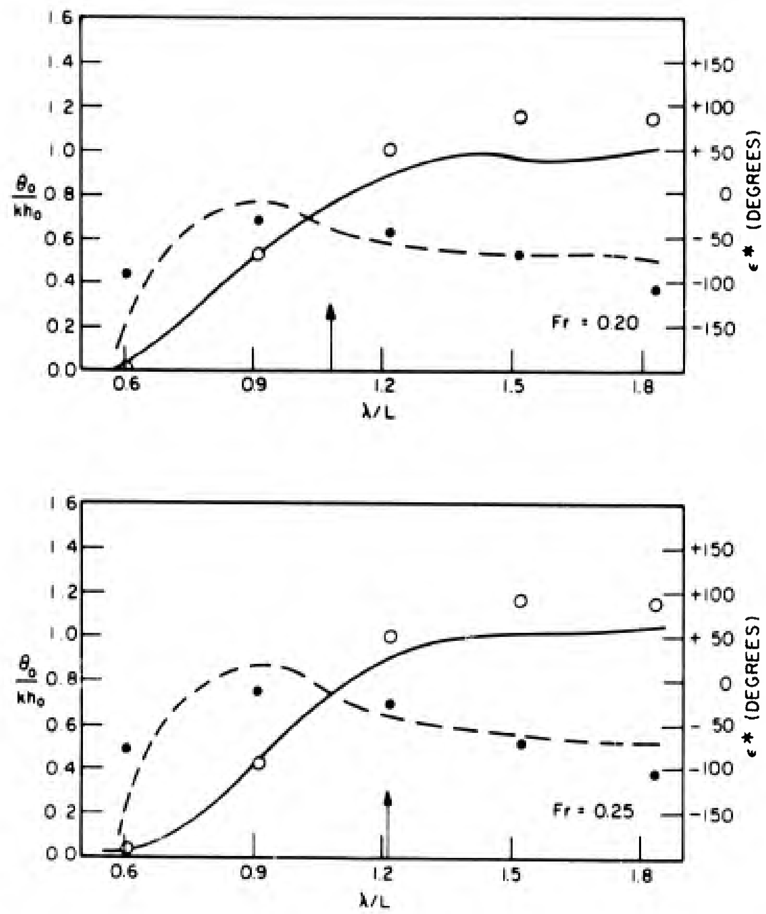

Fig. 29 - Model D in directly ahead seas, pitching non-dimensional amplitude and phase angle vs wavelength to shiplength ratio

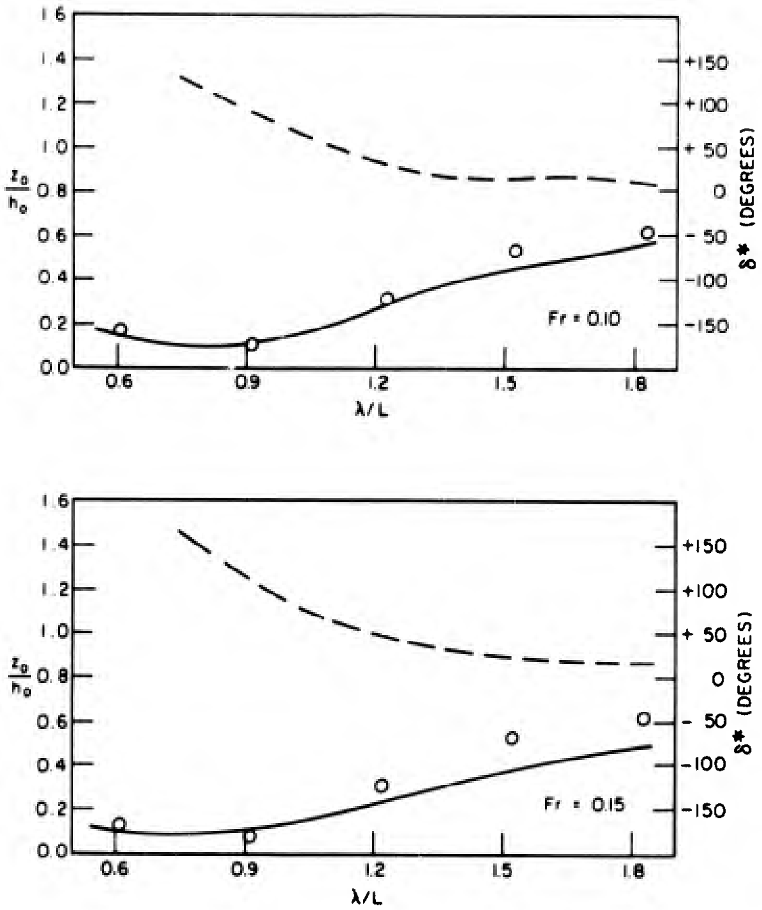

Fig. 30 - Model D in directly astern seas, heaving non-dimensional amplitude and phase angle vs wavelength to shiplength ratio

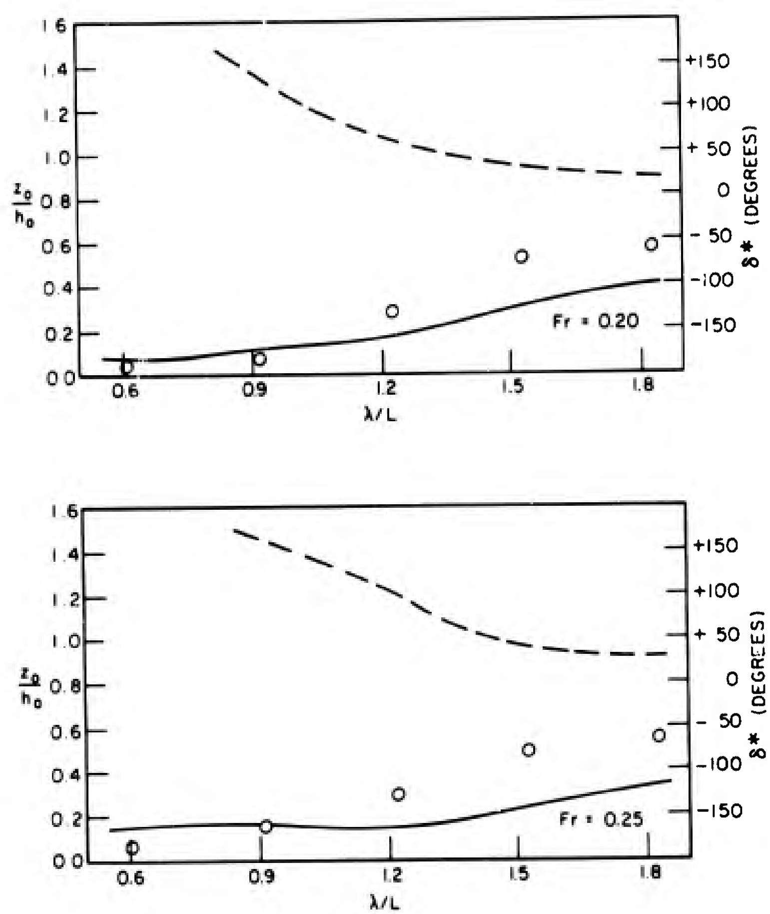

Fig. 31 - Model D in directly astern seas, heaving non-dimensional amplitude and phase angle vs wavelength to shiplength ratio

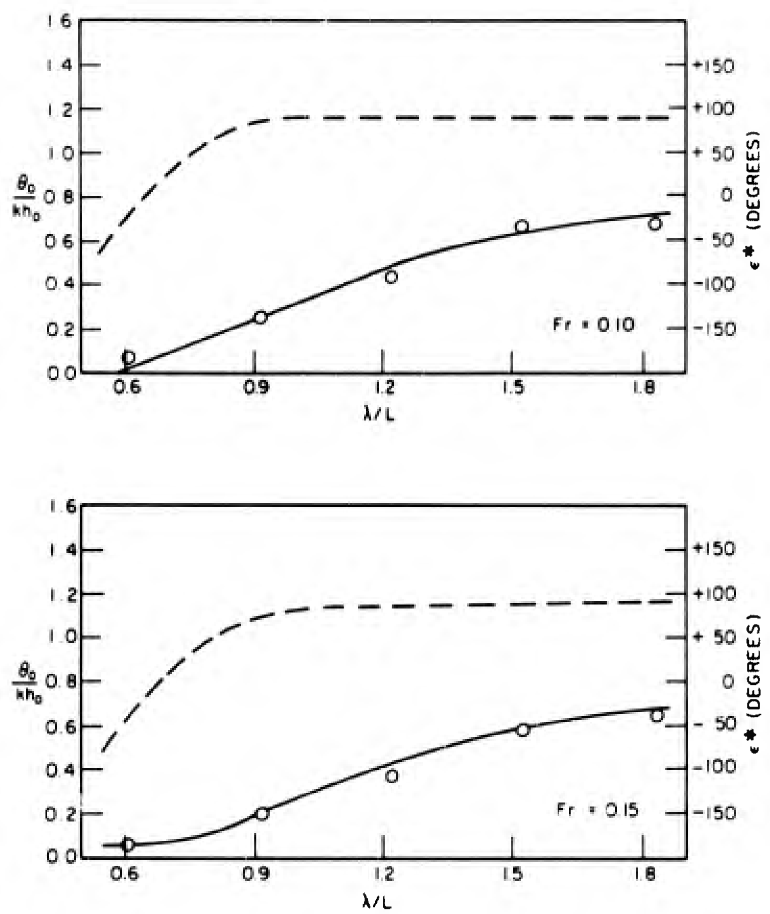

Fig. 32 - Model D in directly astern seas, pitching non-dimensional amplitude and phase angle vs wavelength to shiplength ratio

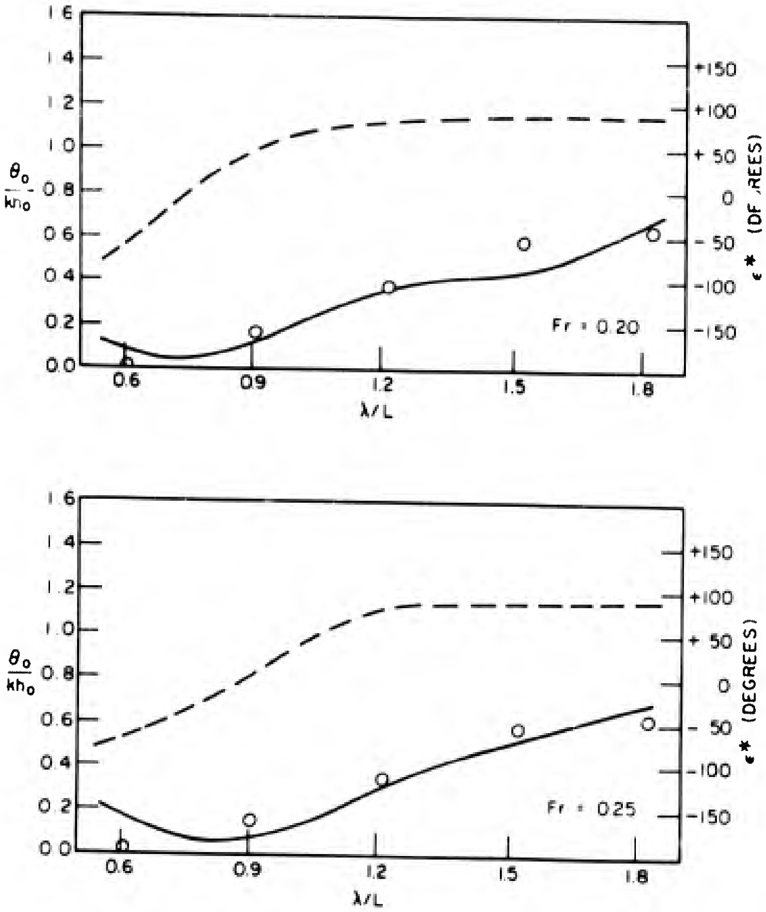

Fig. 33 - Model D in directly astern seas, pitching non-dimensional amplitude and phase angle vs wavelength to shiplength ratio

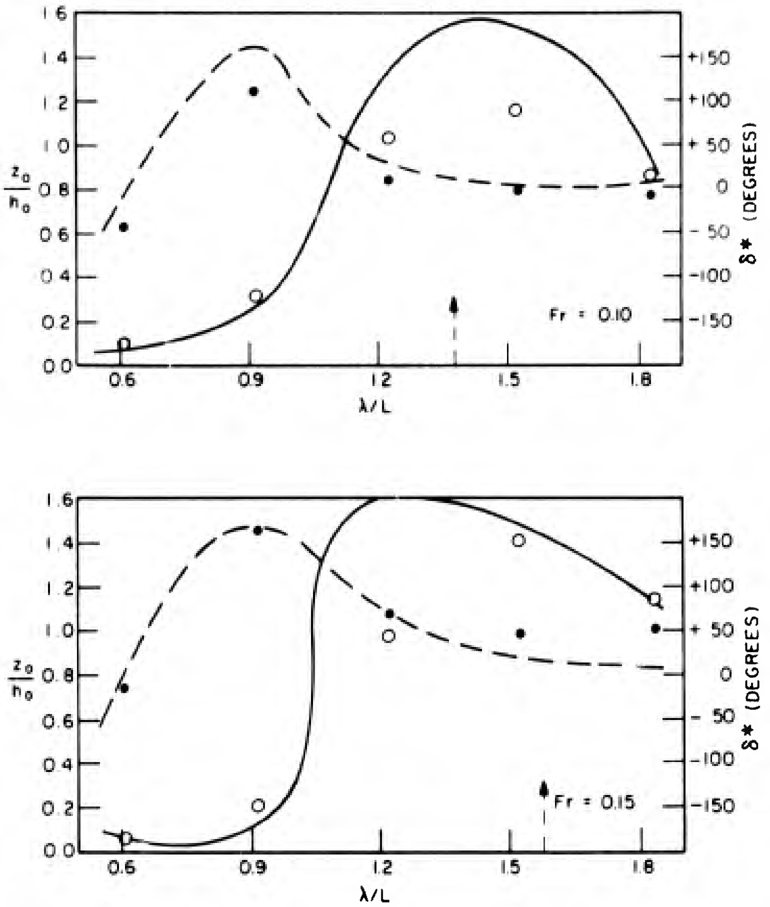

Fig. 34 - Model E in directly ahead seas, heaving non-dimensional amplitude and phase angle vs wavelength to shiplength ratio

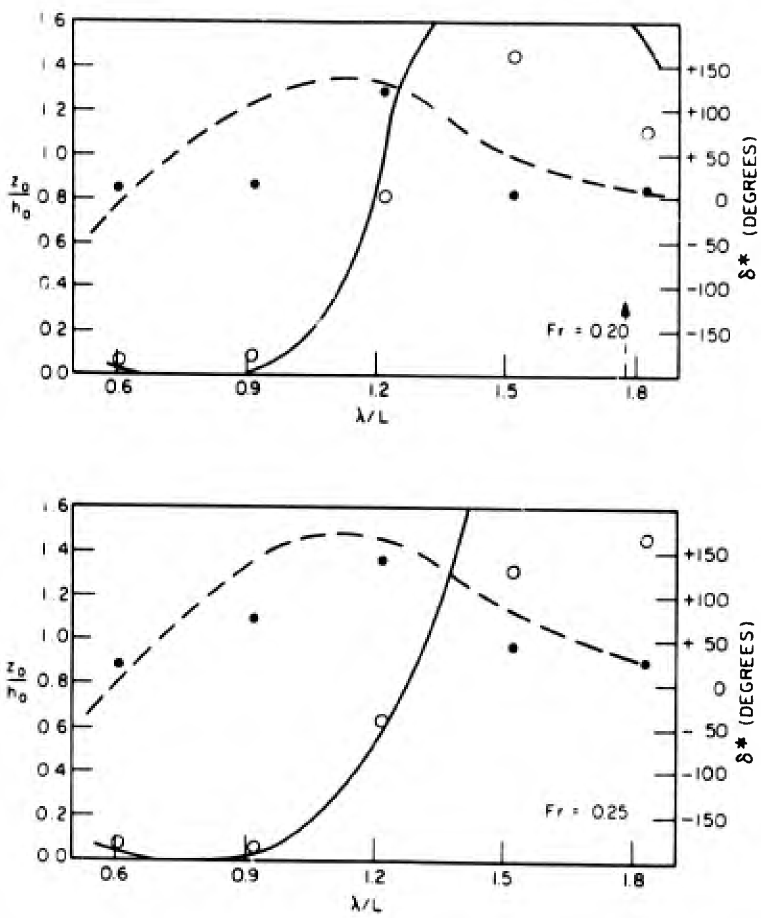

Fig. 35 - Model E in directly ahead seas, heaving non-dimensional amplitude and phase angle vs wavelength to shiplength ratio

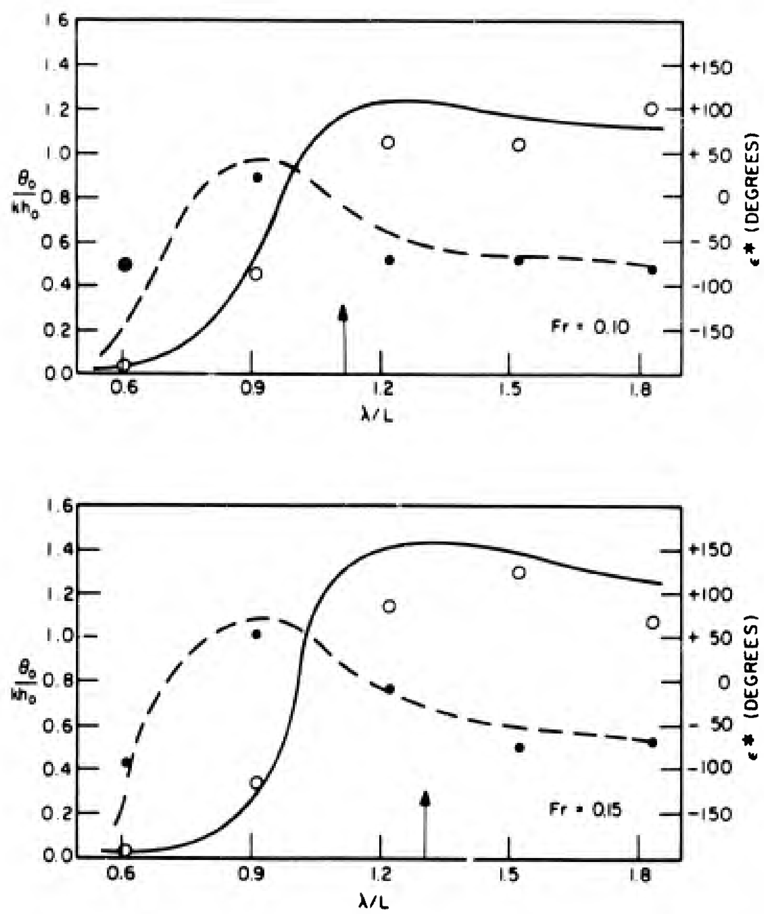

Fig. 36 - Model E in directly ahead seas, pitching non-dimensional amplitude and phase angle vs wavelength to shiplength ratio

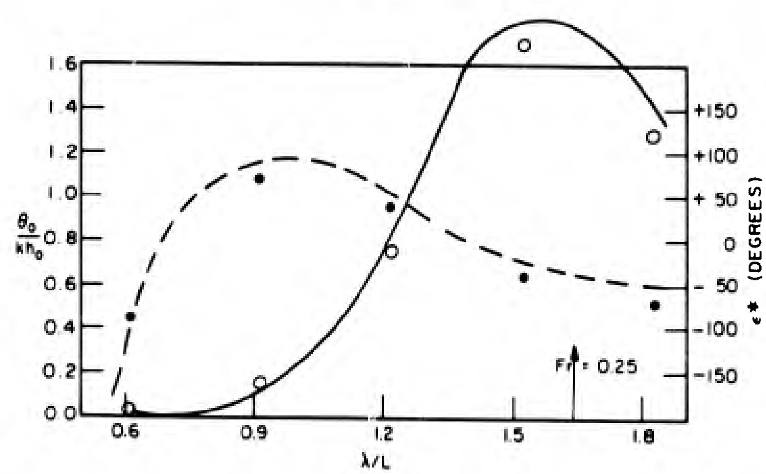

Fig. 37 - Model E in directly ahead seas, pitching non-dimensional amplitude and phase angle vs wavelength to shiplength ratio

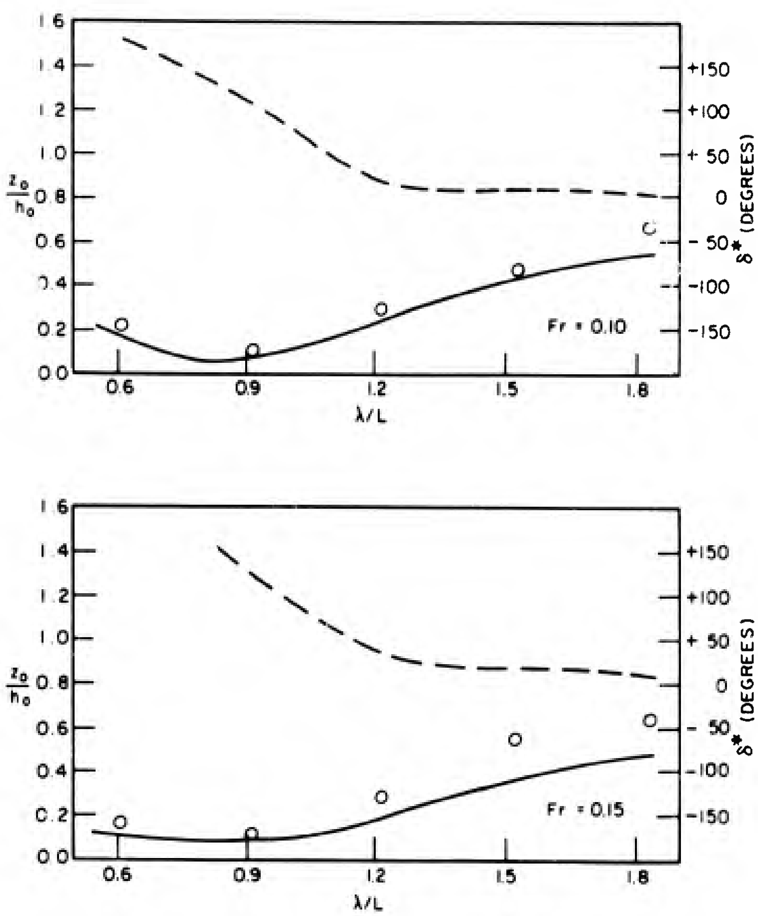

Fig. 38 - Model E in directly astern seas, heaving non-dimensional amplitude and phase angle vs wavelength to shiplength ratio

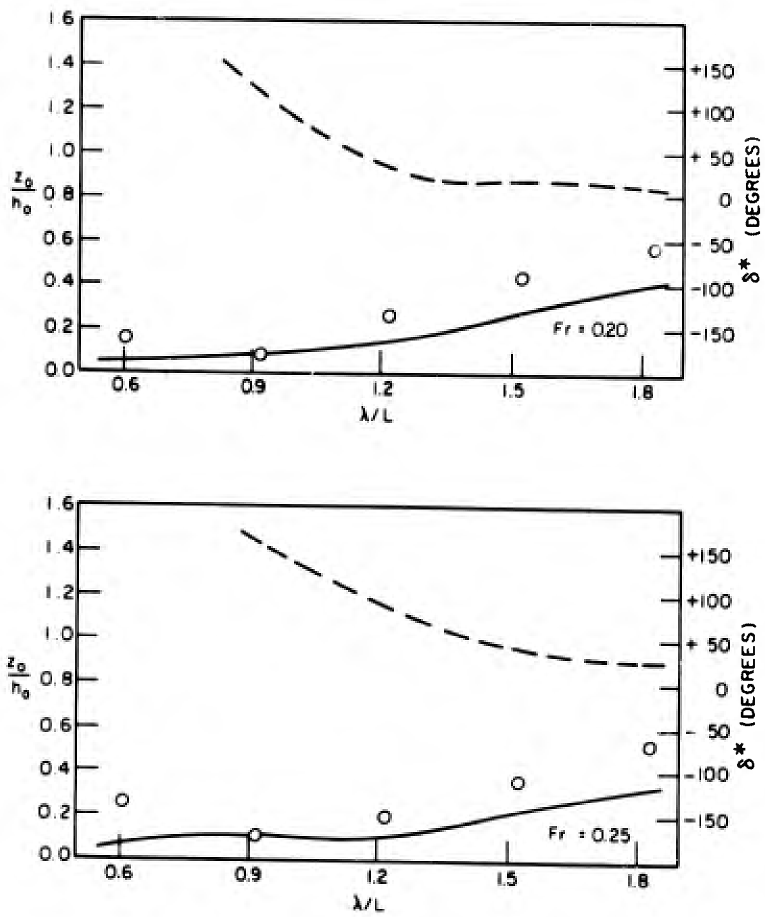

Fig. 39 - Model E in directly astern seas, heaving non-dimensional amplitude and phase angle vs wavelength to shiplength ratio

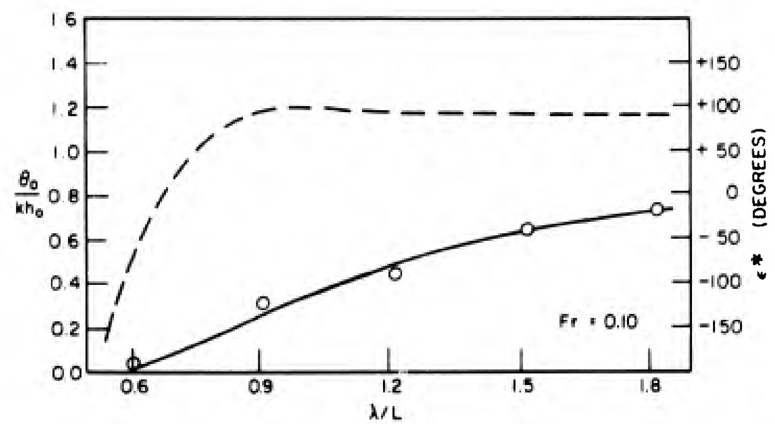

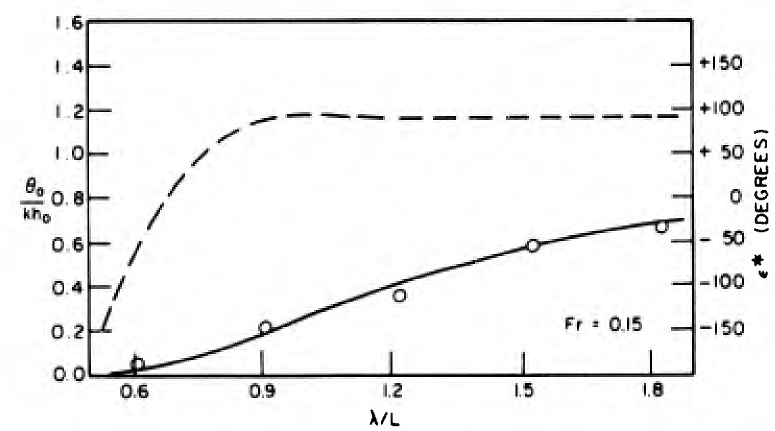

Fig. 40 - Model E in directly astern seas, pitching non-dimensional amplitude and phase angle vs wavelength to shiplength ratio

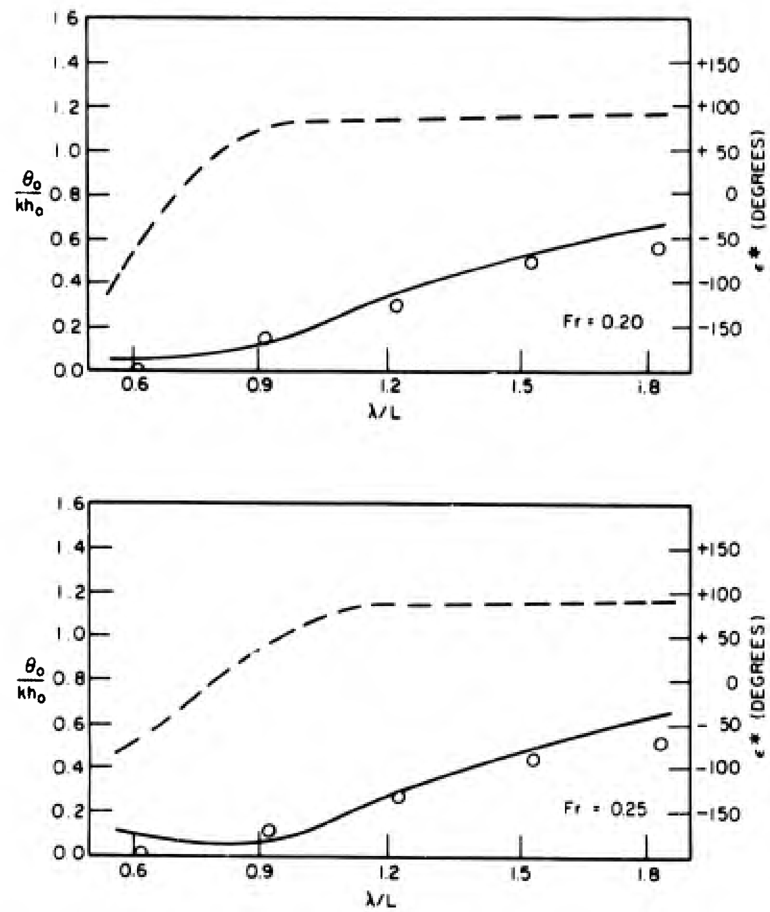

Fig. 41 - Model E in directly astern seas, pitching non-dimensional amplitude and phase angle vs wavelength to shiplength ratio

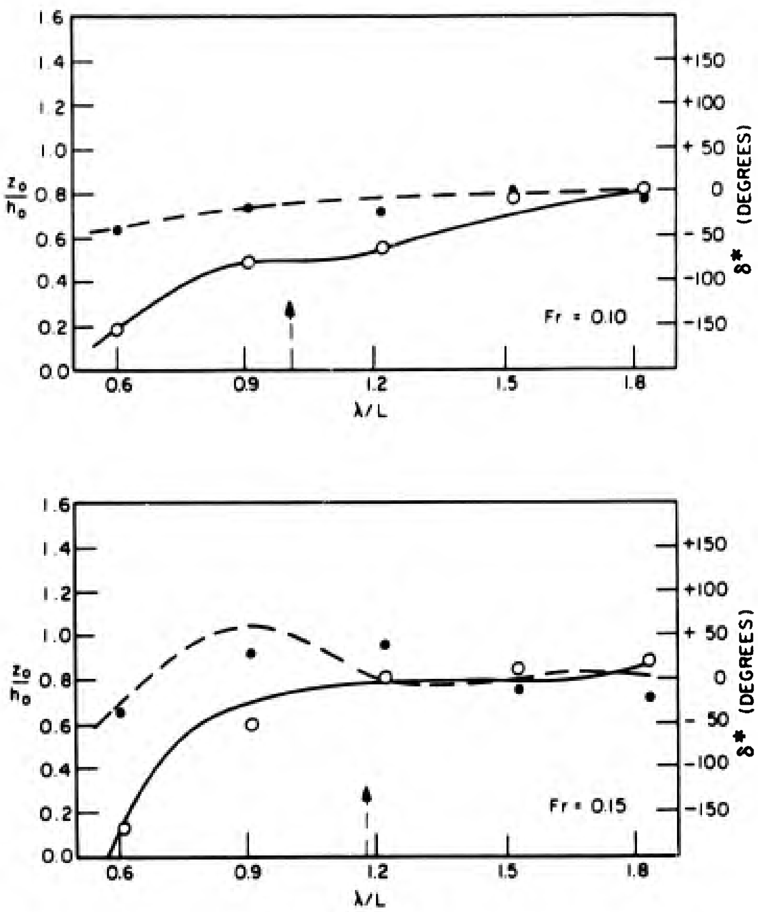

Fig. 42 - Model F in directly ahead seas, heaving non-dimensional amplitude and phase angle vs wavelength to shiplength ratio

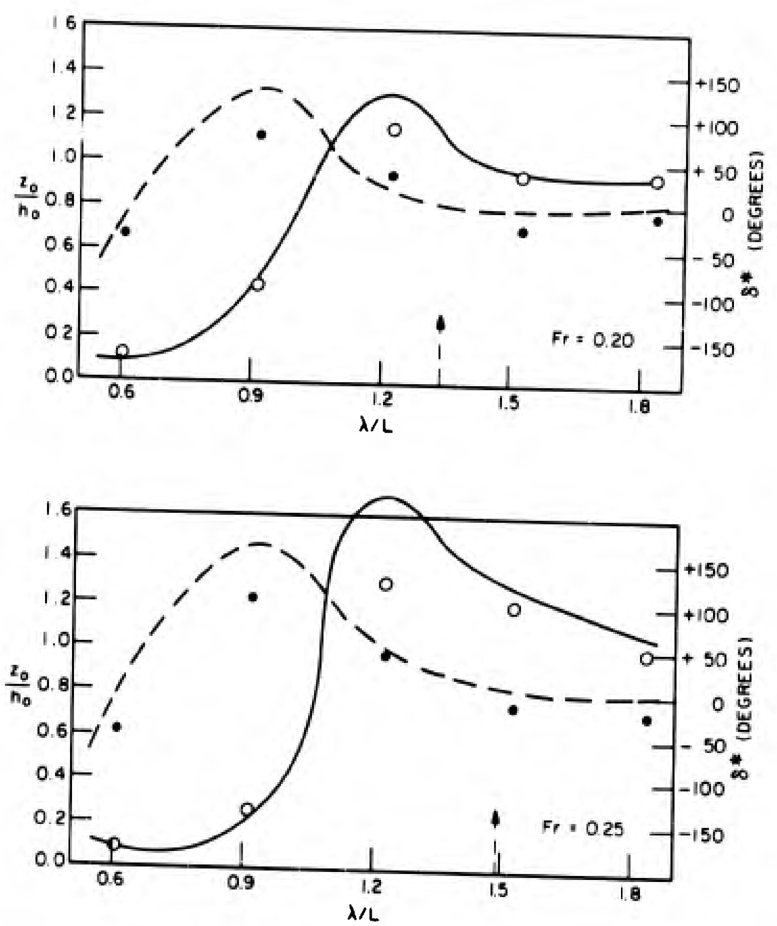

Fig. 43 - Model F in directly ahead seas, heaving non-dimensional amplitude and phase angle vs wavelength to shiplength ratio

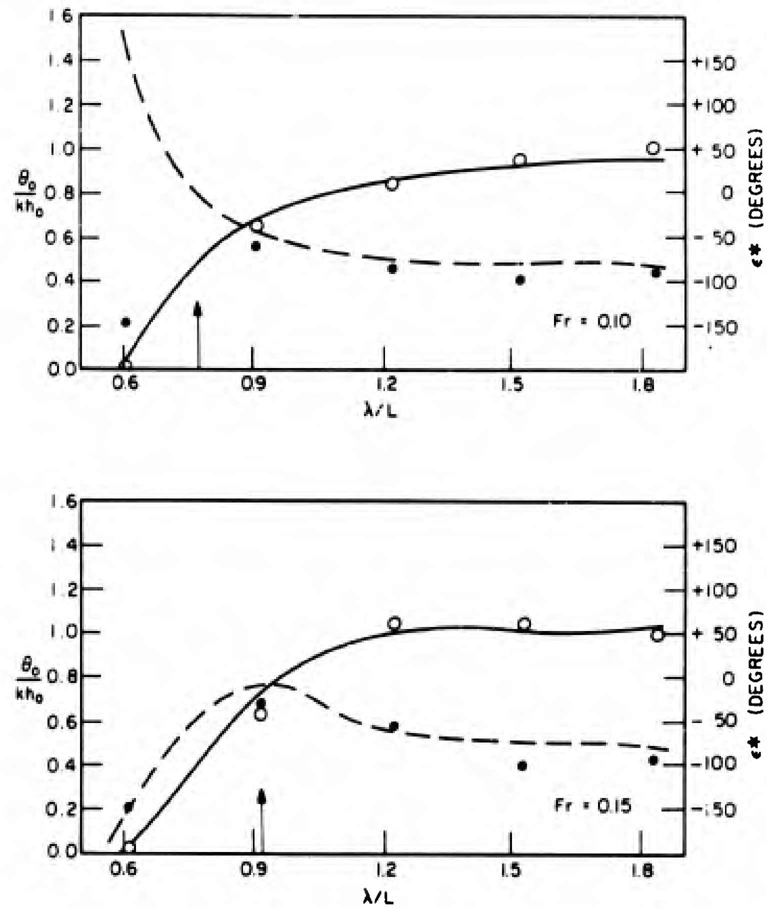

Fig. 44 - Model F in directly ahead seas, pitching non-dimensional amplitude and phase angle vs wavelength to shiplength ratio

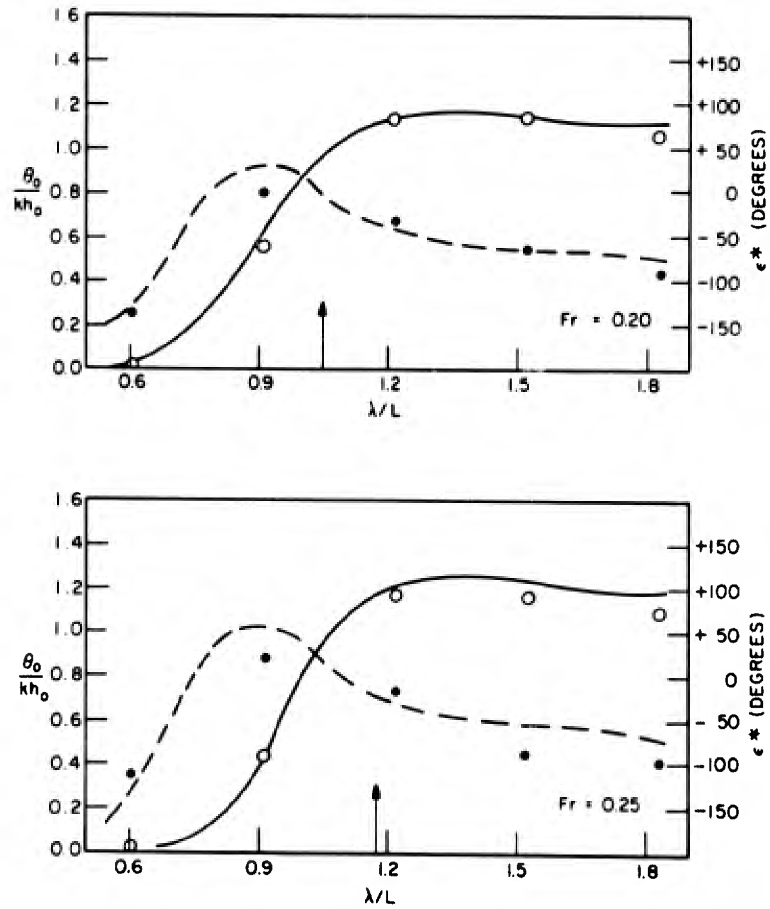

Fig. 45 - Model F in directly ahead seas, pitching non-dimensional amplitude and phase angle vs wavelength to shiplength ratio

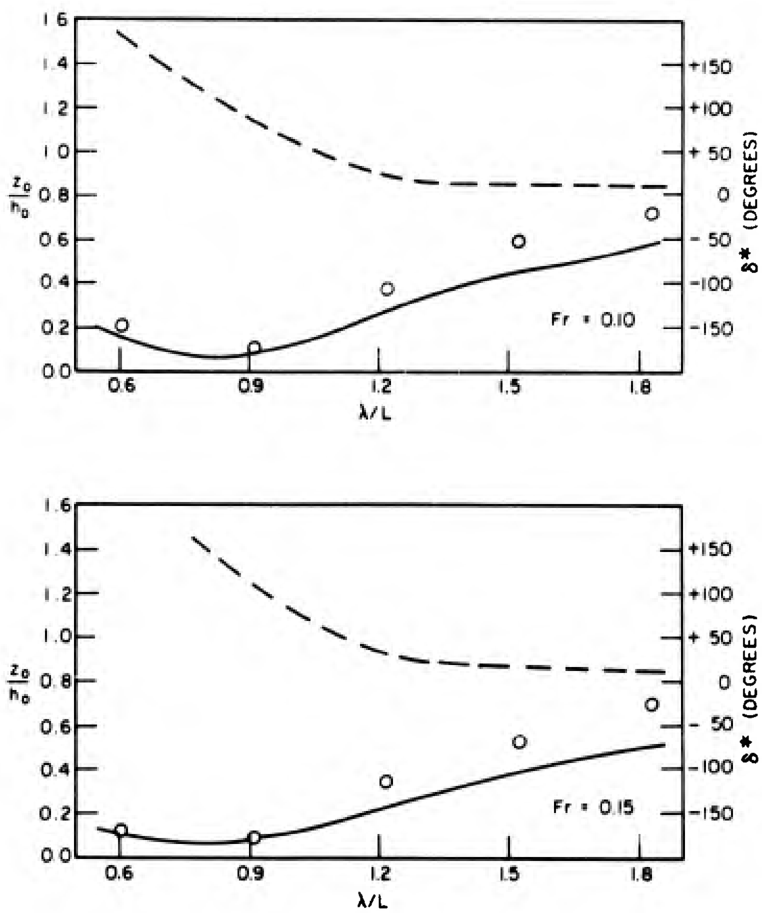

Fig. 46 - Model F in directly astern seas, heaving non-dimensional amplitude and phase angle vs wavelength to shiplength ratio

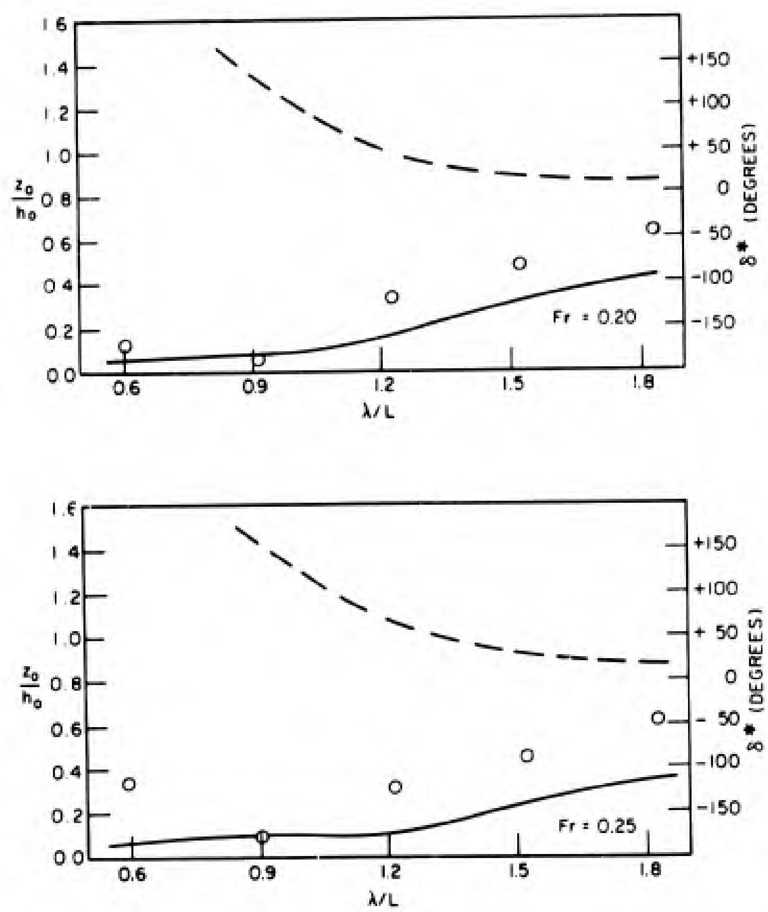

Fig. 47 - Model F in directly astern seas, heaving non-dimensional amplitude and phase angle vs wavelength to shiplength ratio

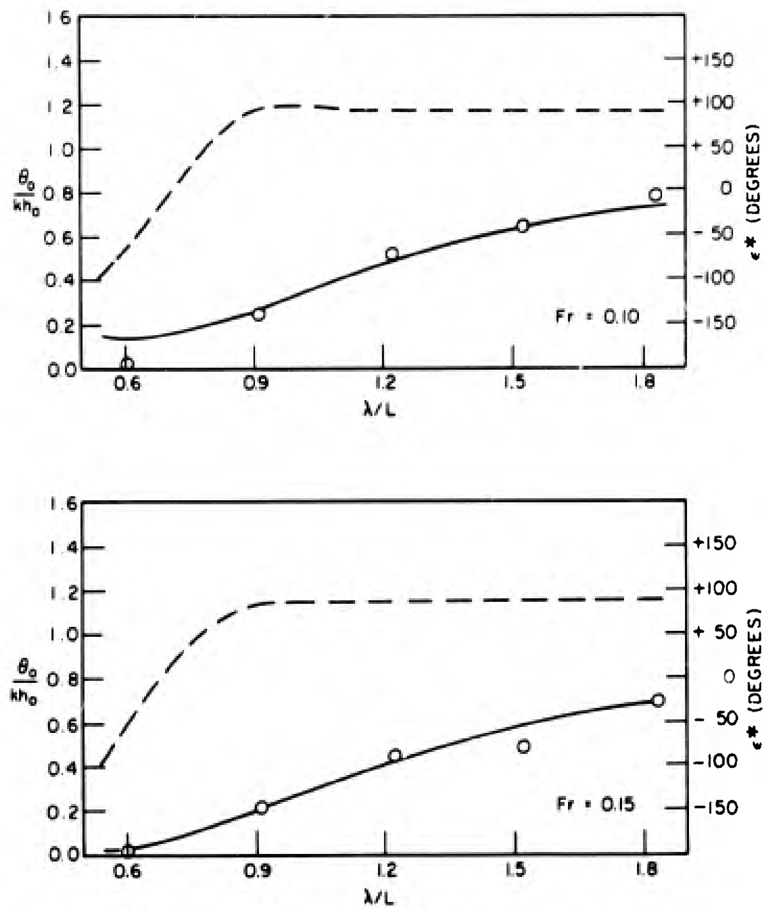

Fig. 48 - Model F in directly astern seas, pitching non-dimensional amplitude and phase angle vs wavelength to shiplength ratio

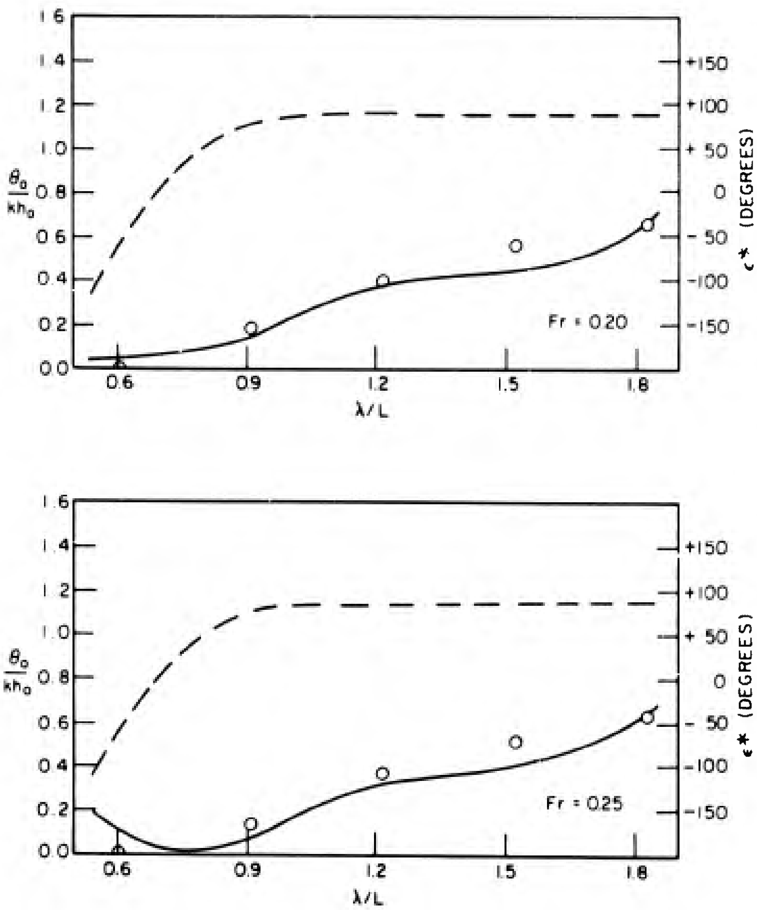

Fig. 49 - Model F in directly astern seas, pitching non-dimensional amplitude and phase angle vs wavelength to shiplength ratio

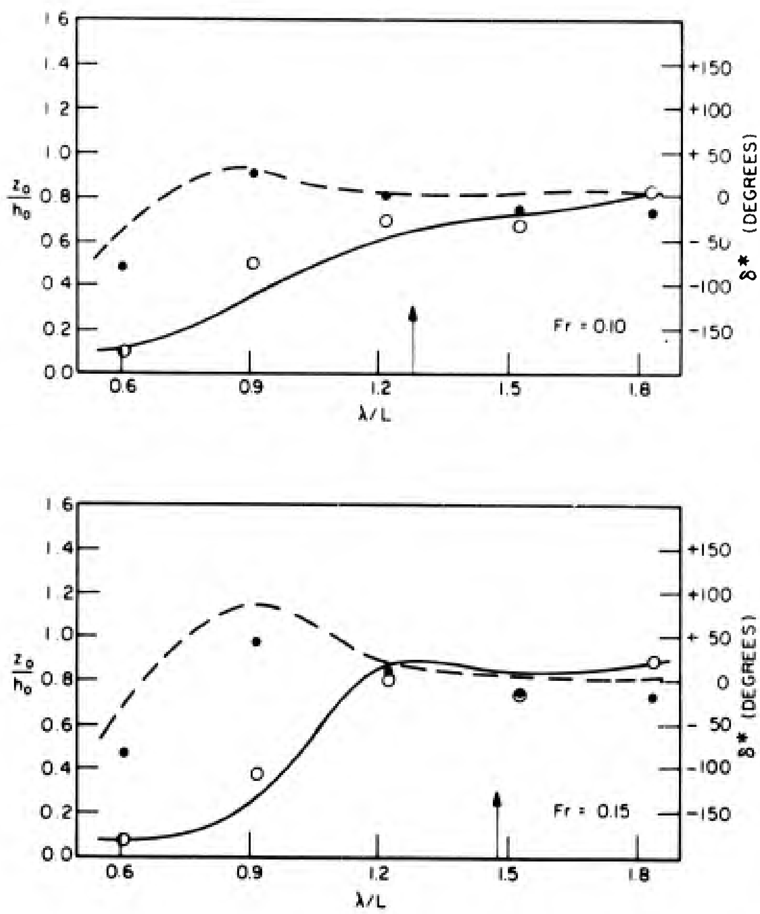

Fig. 50 - Model G in directly ahead seas, heaving non-dimensional amplitude and phase angle vs wavelength to shiplength ratio

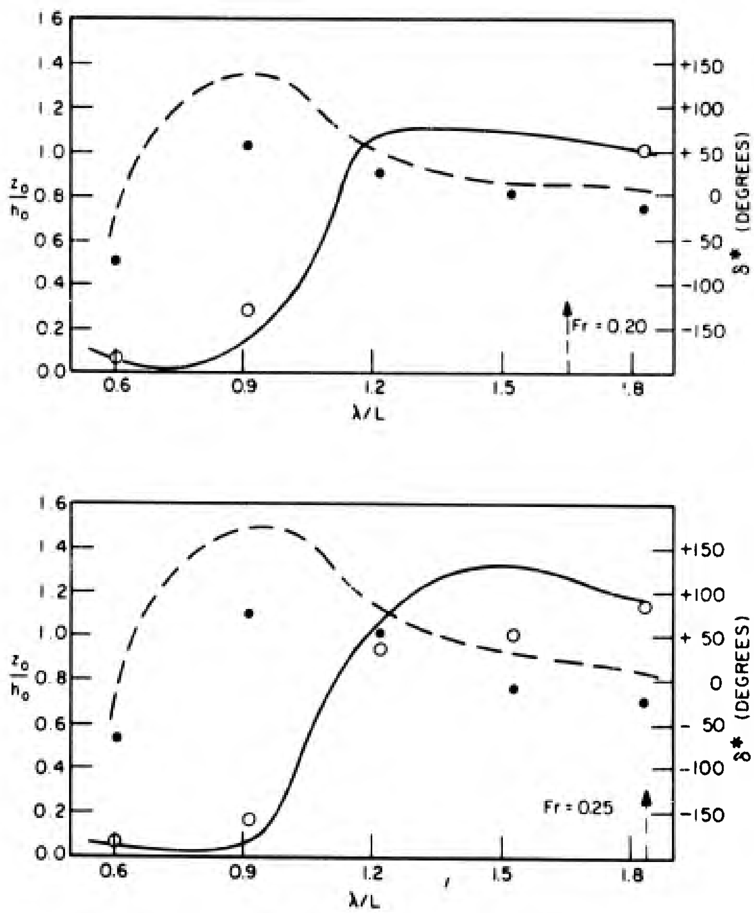

Fig. 51 - Model G in directly ahead seas, heaving non-dimensional amplitude and phase angle vs wavelength to shiplength ratio

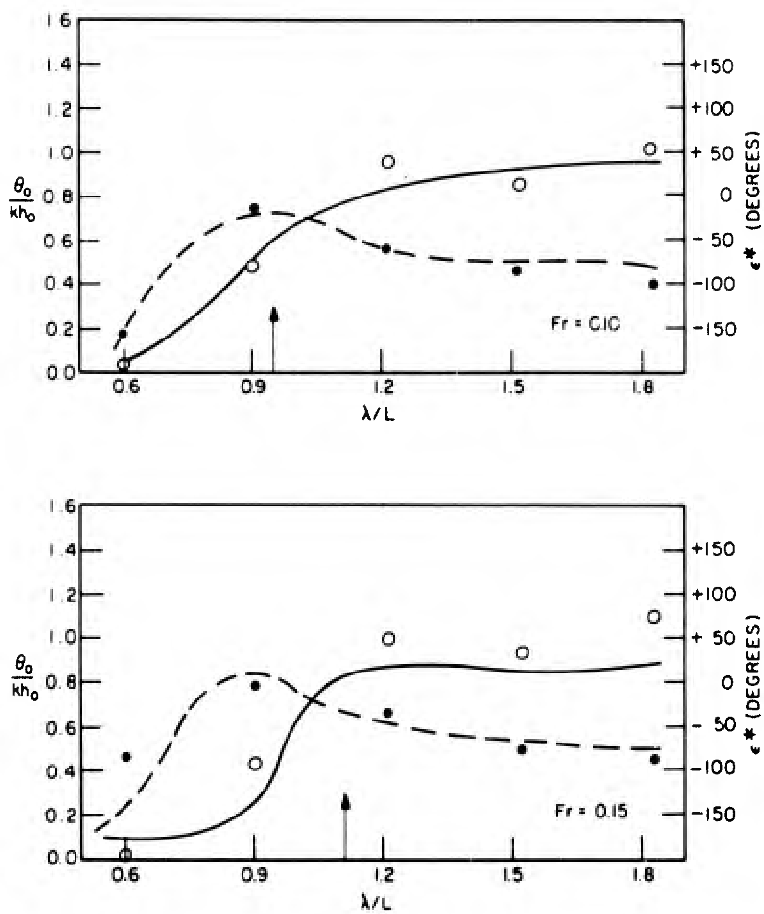

Fig. 52 - Model G in directly ahead seas, pitching non-dimensional amplitude and phase angle vs wavelength to shiplength ratio

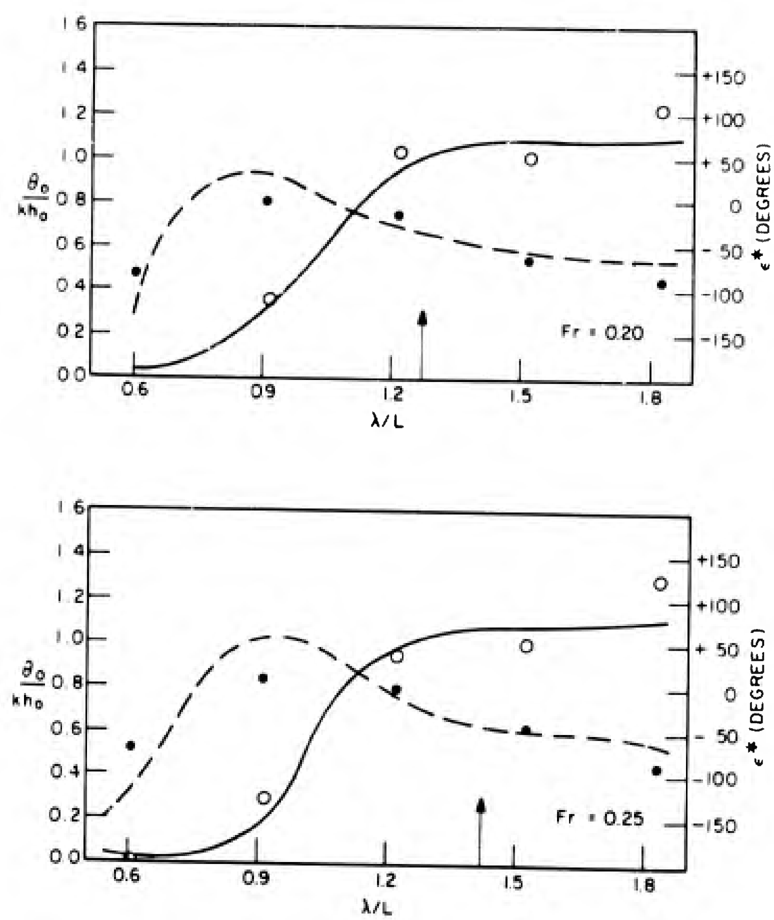

Fig. 53 - Model G in directly ahead seas, pitching non-dimensional amplitude and phase angle vs wavelength to shiplength ratio

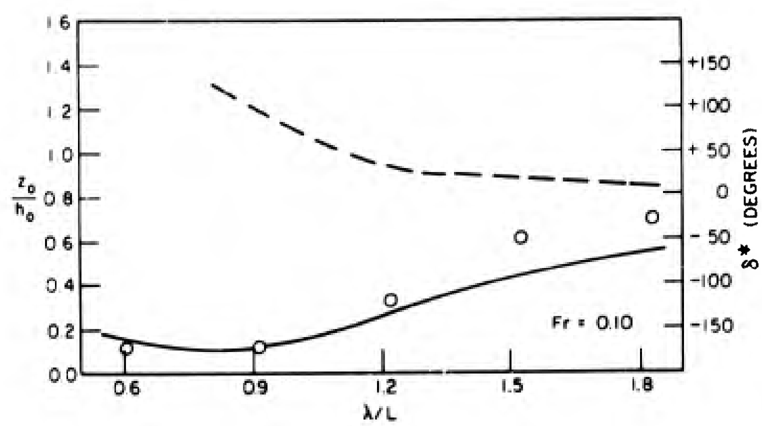

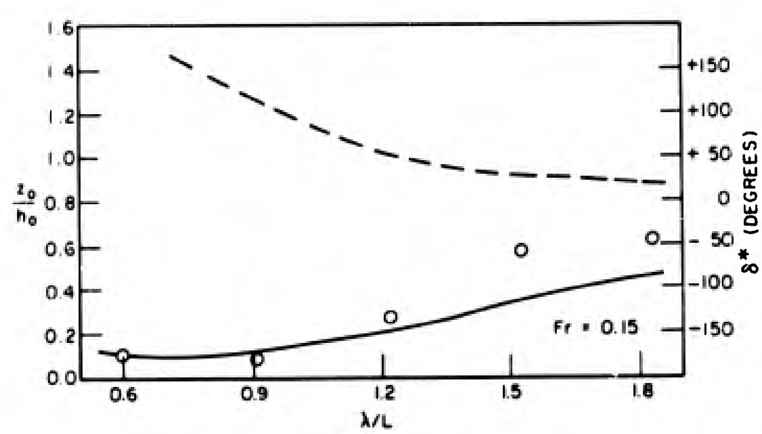

Fig. 54 - Model G in directly astern seas, heaving non-dimensional amplitude and phase angle vs wavelength to shiplength ratio

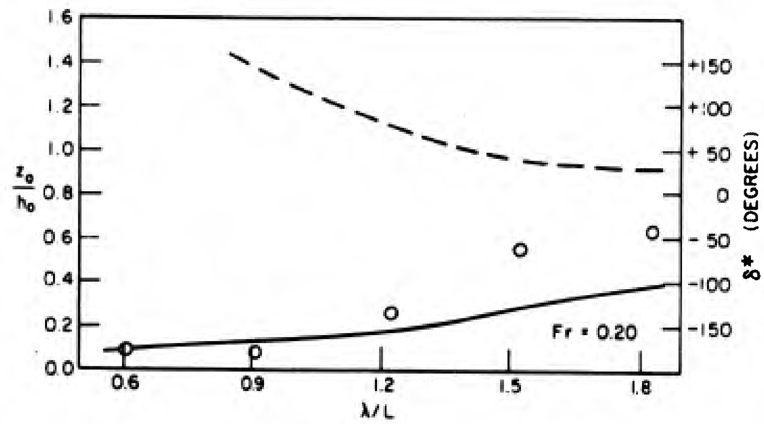

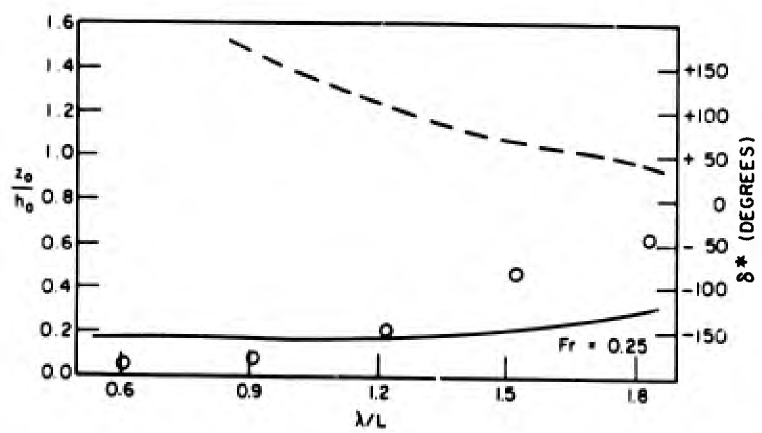

Fig. 55 - Model G in directly astern seas, heaving non-dimensional amplitude and phase angle vs wavelength to shiplength ratio

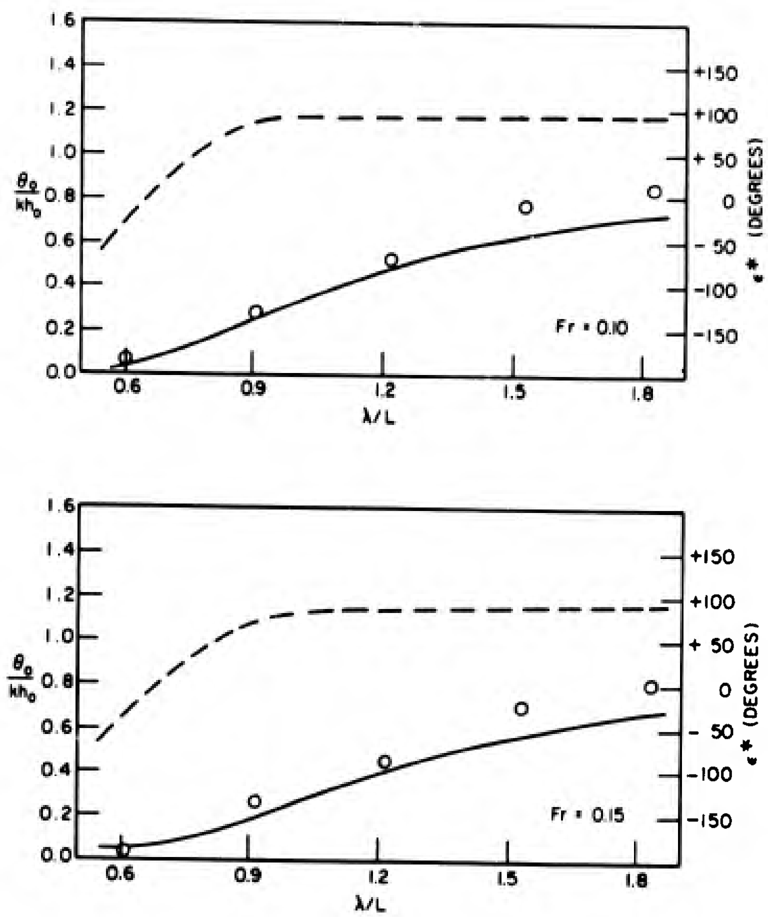

Fig. 56 - Model G in directly astern seas, pitching non-dimensional amplitude and phase angle vs wavelength to shiplength ratio

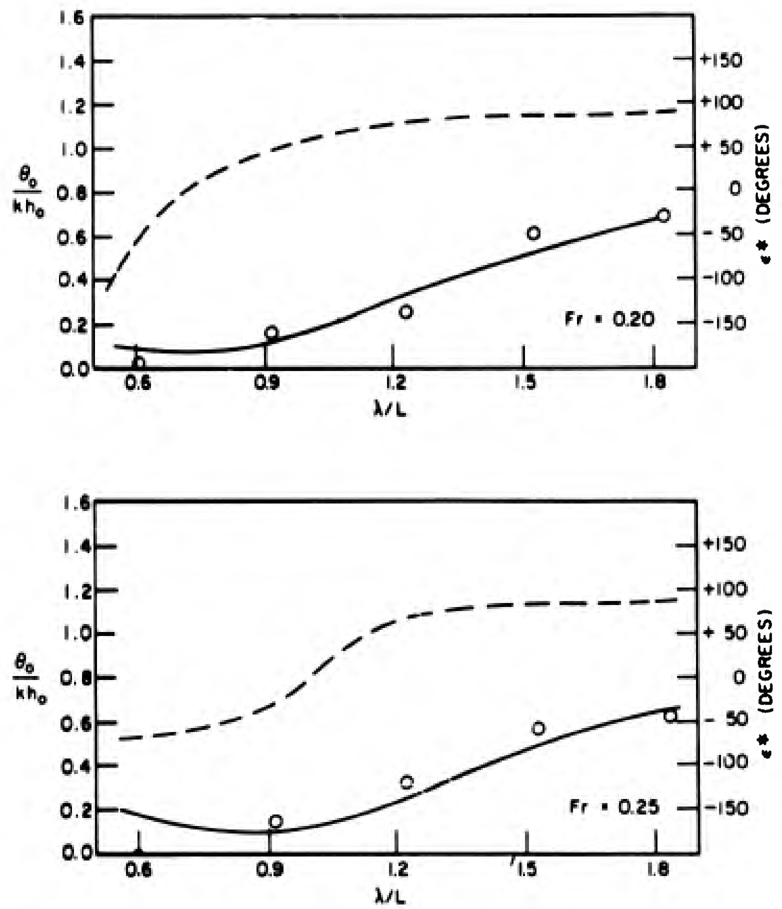

Fig. 57 - Model G in directly astern seas, pitching non-dimensional amplitude and phase angle vs wavelength to shiplength ratio

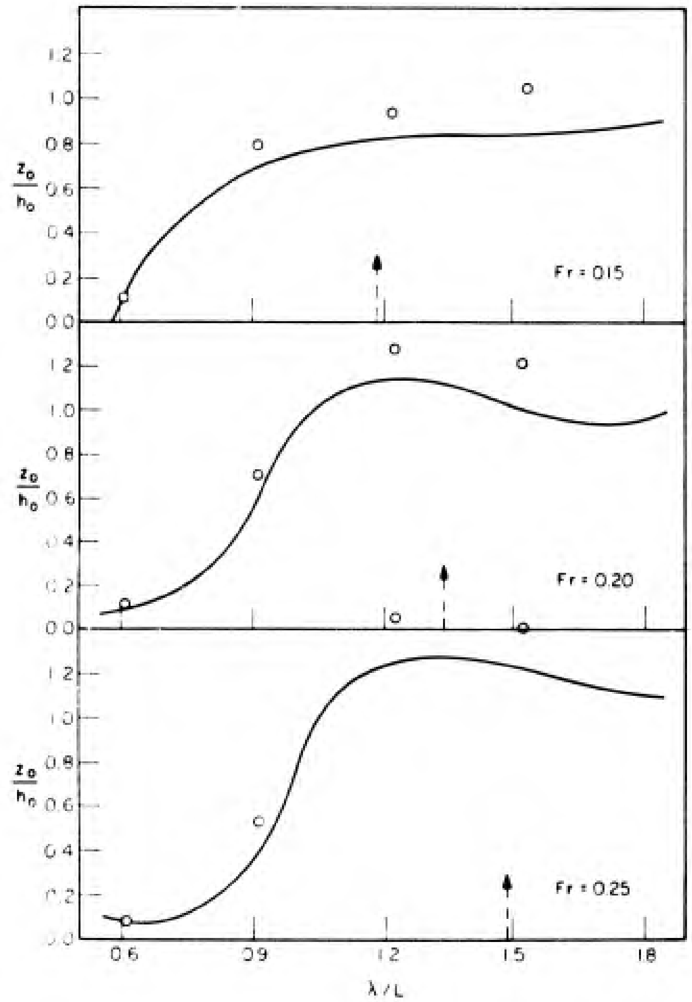

Fig. 58 - Model C (k_θ = 0.210) in directly ahead seas, heaving non-dimensional amplitude vs wavelength to shiplength ratio

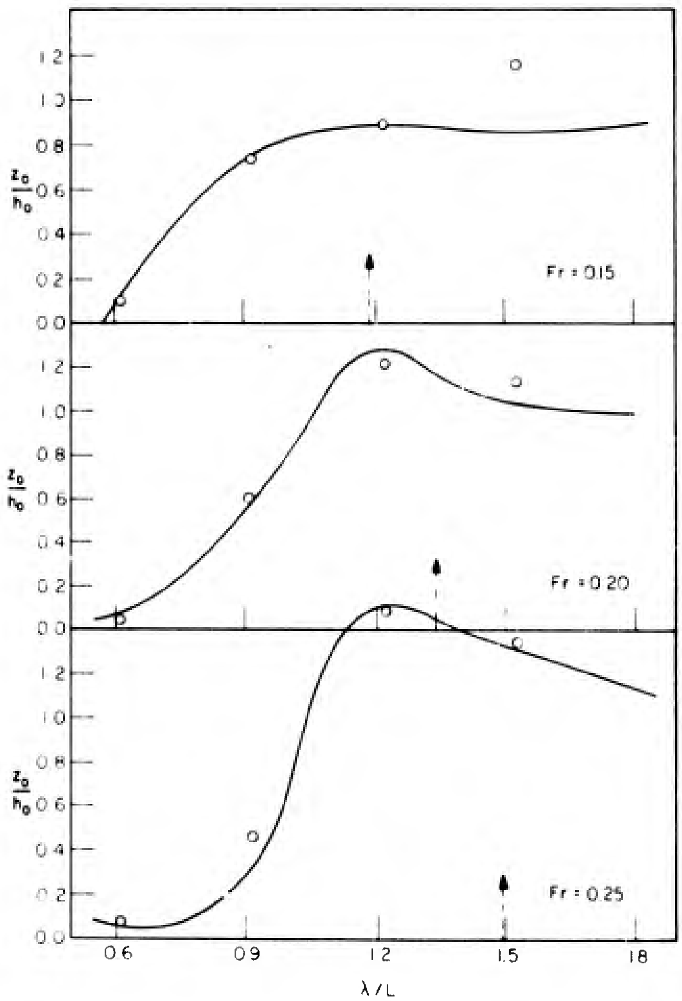

Fig. 59 - Model C (k_θ = 0.225) in directly ahead seas, heaving non-dimensional amplitude vs wavelength to shiplength ratio

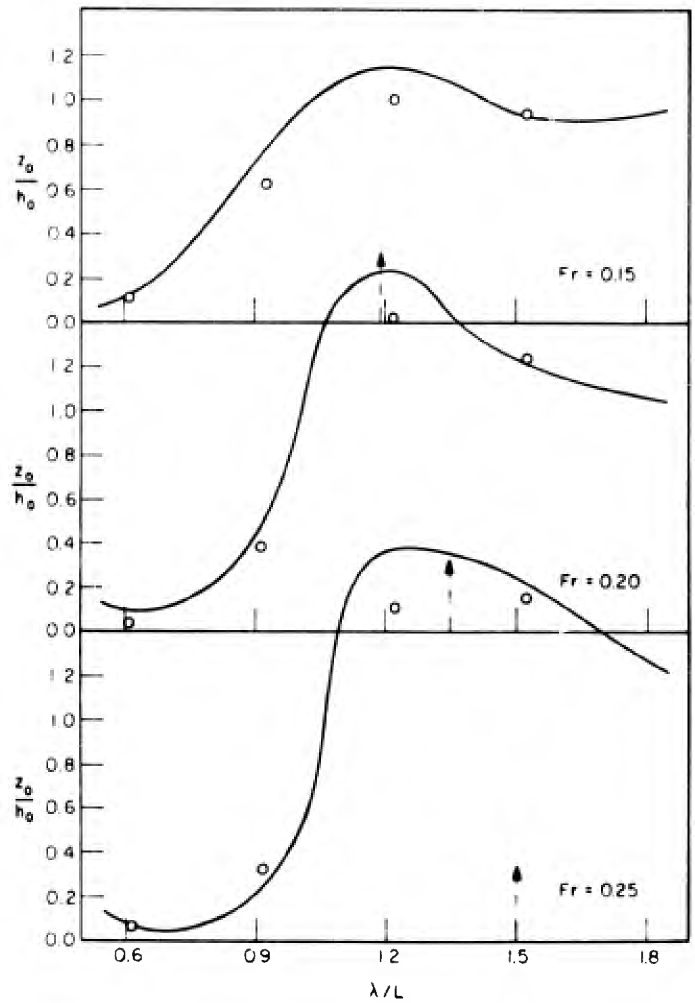

Fig. 60 - Model C (k_θ = 0.255) in directly ahead seas, heaving non-dimensional amplitude vs wavelength to shiplength ratio

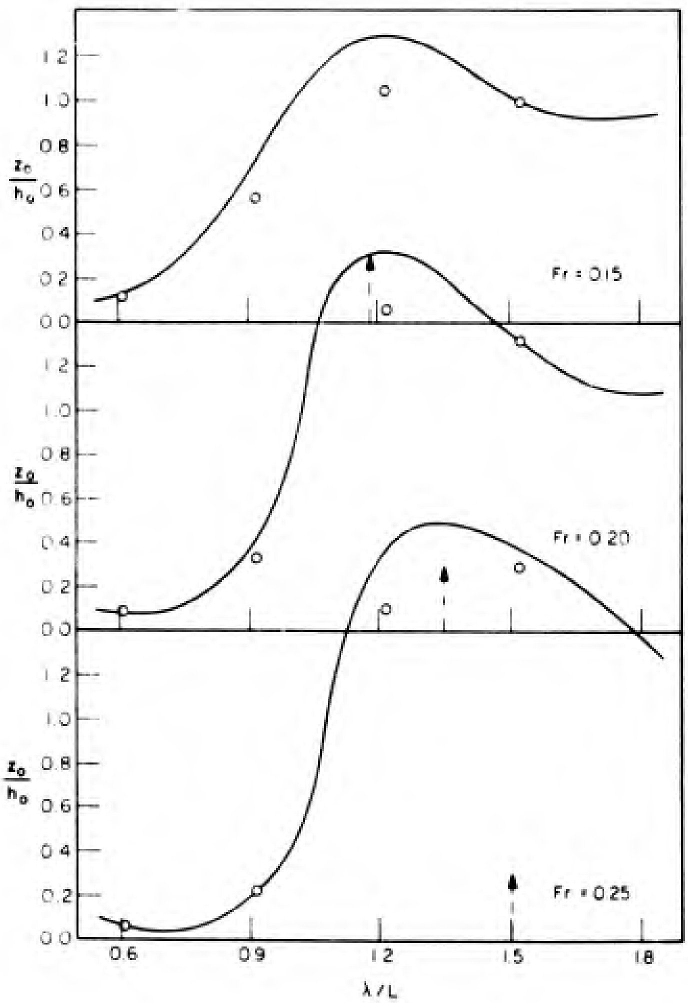

Fig. 61 - Model C (k_θ = 0.270) in directly ahead seas, heaving non-dimensional amplitude vs wavelength to shiplength ratio

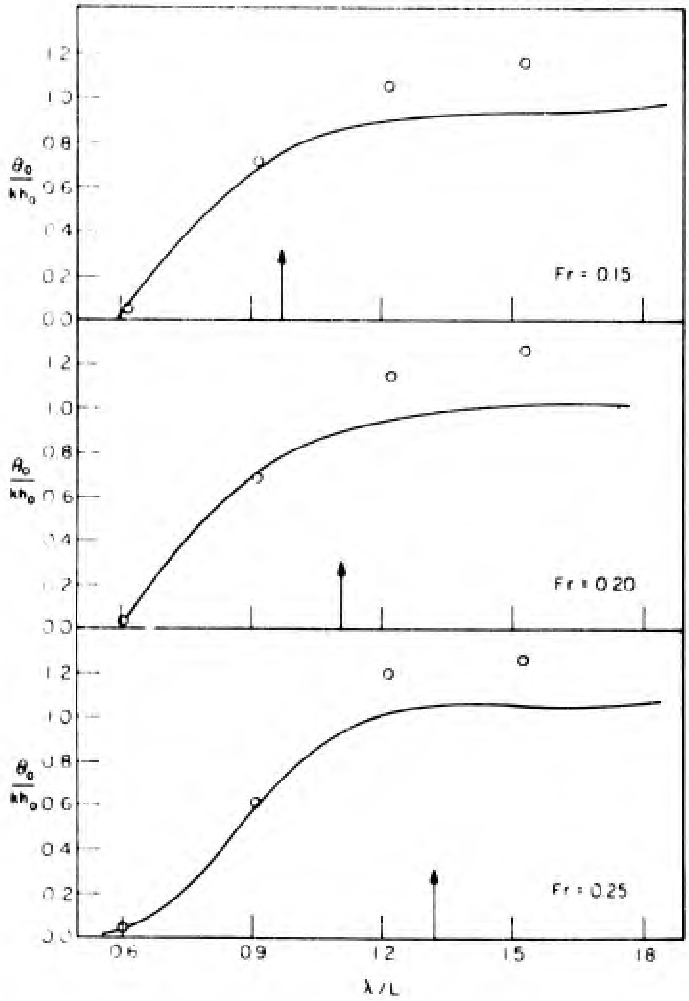

Fig. 62 - Model C (k_θ = 0.210) in directly ahead seas, pitching non-dimensional amplitude vs wavelength to shiplength ratio

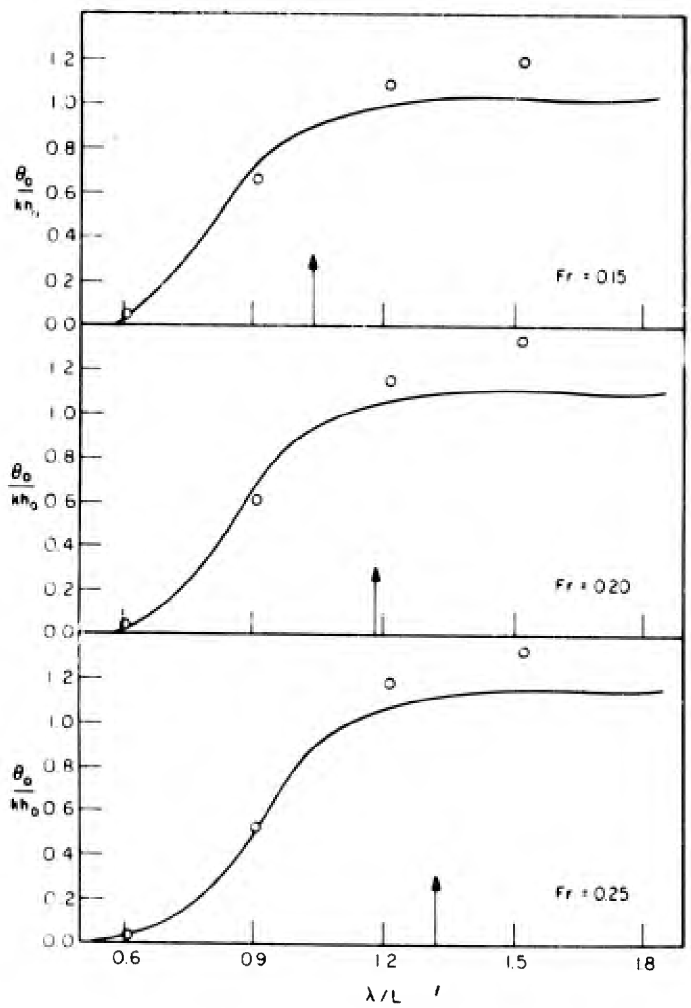

Fig. 63 - Model C (k_θ = 0.225) in directly ahead seas, pitching non-dimensional amplitude vs wavelength to shiplength ratio

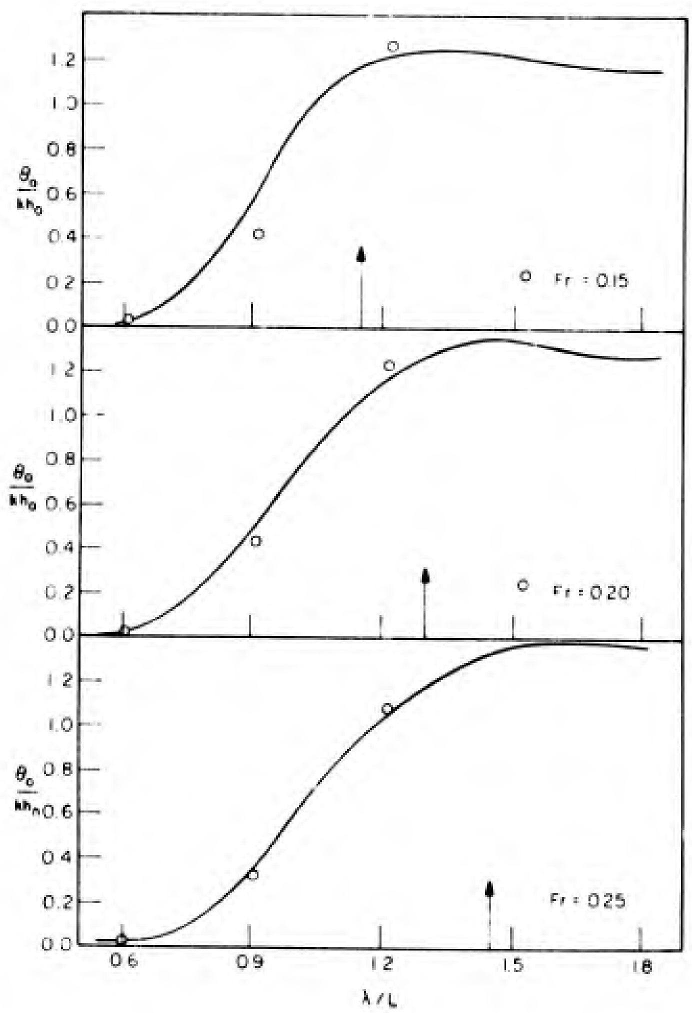

Fig. 64 - Model C (k_θ = 0.255) in directly ahead seas, pitching non-dimensional amplitude vs wavelength to shiplength ratio

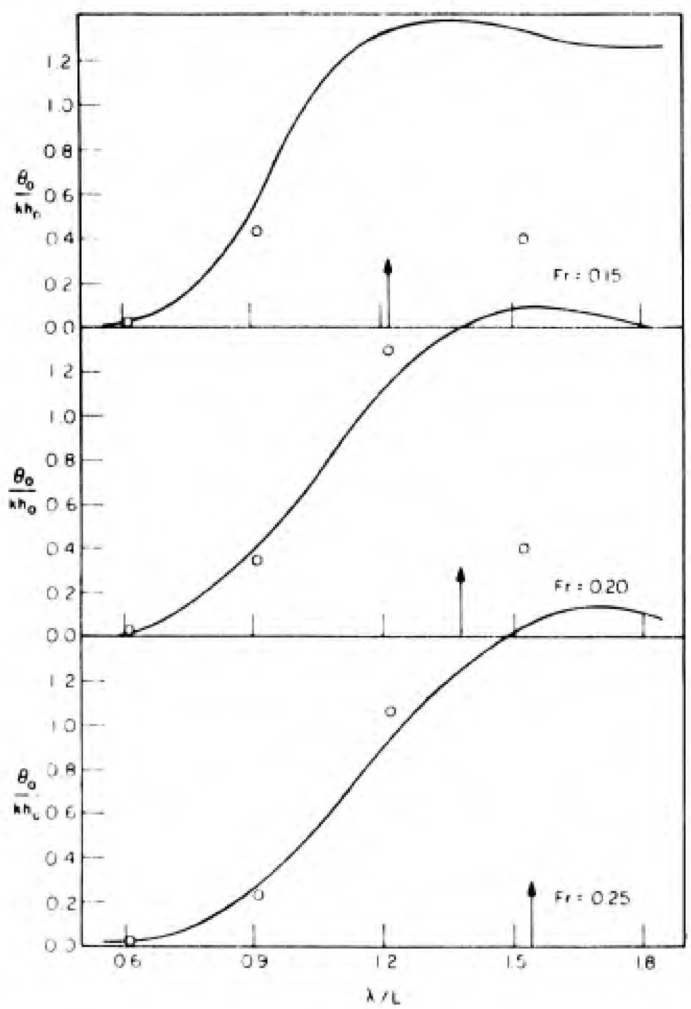

Fig. 65 - Model C (k_θ = 0.270) in directly ahead seas, pitching non-dimensional amplitude vs wavelength to shiplength ratio

DISCUSSION OF RESULTS

Previous correlations between strip theory and experiment shown in Refs. [10,14,22,23] were for the case of ahead seas only and the agreement was described as very satisfactory. No direct comparison can be made however between the results reported in the above references and the ones described herein, since the earlier correlations were based on more approximate hand computations and in some cases different formulations and/or experimental data for the coefficients and excitation terms were used.

The current comparison for models of different hull shapes, shown in Figs. 2-57 indicates that, in directly ahead seas, reasonably good correlation is achieved for heave amplitude. An exception is found in the case of Model E, $C_b = 0.70$, $B/H = 1.57$ (Figs. 34 and 35), where theory fails to reveal the correct trends and grossly exceeds measured values. At the time Ref. [6] was published, it was suspected that this was due to numerical errors which probably arose for low B/H ratios in the subroutine of the computer program which calculates damping and added mass according to Grim's theory. As discussed in a later section, this suspicion was confirmed by subsequent analysis. Apart from this discrepancy and for all wavelengths, except those corresponding to resonance, agreement can be termed satisfactory. For wavelengths corresponding to resonance, theory overestimates experimental heaving amplitudes by 15-20%. The above deviations are due to underestimation of heave damping by the analytical approach which is in accord with previous findings [10,14,23].

Agreement in directly ahead seas is much better for pitch than for heave although the trends are not the same for different models. For models A, B, C, and D (Figs. 2-33) at all speeds, theoretical results are below the experimental data and the effect is more pronounced as the wavelength is increased. In the case of Model E (Figs. 36-37) large discrepancies are not observable as with heaving motions. The best agreement in this case is found in the case of Model F (Figs. 44-45).

With respect to phase angles in directly ahead seas, it will be seen that the theoretical predictions are usually higher than experiment and this is true for both pitch and heave. Since phase angles are more susceptible to both computational and experimental errors, agreement should perhaps be interpreted as satisfactory whenever deviations are less than about 15-20%. Discrepancies usually occur at wavelengths equal to model length. Apparent disagreement is also observable at very short wavelengths, but this is mainly due to the manner in which experimental data have been presented in Ref. [18]. Pitching phase angles as computed by theory are much closer to the experimental data than heaving phase angles and this is particularly obvious in the case of Models F and G (Figs. 44-45 and 52-53).

In the case of directly astern seas, heaving motion is underestimated by theory and the deviations increase with wavelength. For most models, agreement of pitching motion amplitudes in directly astern seas is excellent, although in the case of Models A and B (Figs. 8-9 and 16-17) theory is considerably lower than experiment. No comparisons have been made of phase angles in astern seas, but general indications are that theory reveals the expected trends.

The second part of the current correlation which is concerned with the effect of weight distribution is illustrated in Figs. 58-65. For small radii of gyration, theoretical heaving motion amplitudes are slightly less than the experimental ones, but the situation is reversed and slightly worsened as k_θ is increased. Agreement in pitching motion appears to be similar and the tendency here is for the experimental data to be 15-20% higher, particularly at high wavelengths.

All figures for ahead seas indicate that for wavelengths less than about half the length of the model, both pitching and heaving motions are negligible while for wavelengths higher than about twice the model length, heaving becomes equal to the wave amplitude and pitching corresponds to the maximum wave slope. The range $0.9L < \lambda < 1.5L$ excites the models the most. On the contrary, astern seas do not induce large responses in heave or pitch and amplitudes tend to increase in a linear fashion with wavelength. These findings are in accord with those of earlier investigations [24] which showed that for all wavelengths and speeds, conventional ships suffer only small responses in astern seas in contrast to the more severe resonant responses that do occur in ahead seas.

It was noted in the introduction that both experiment and strip theory, as they were utilized for the purposes of this paper, are replete with errors. The inadequacies of the strip theory as it was employed so far in this paper will be discussed in the next section. Some of the shortcomings of the experimental approach, particularly as they relate to a comparison with theory (not to a comparison with a full scale ship responding to hypothetical regular waves) are as follows:

1. The models used by Vossers et al. [18], were free to move in all six degrees of freedom. Theory treats motion in the longitudinal plane of symmetry only and furthermore presumes the absence of surge.

2. All models tested at NSMB were equipped with bilge keels and were furthermore self-propelled. Bilge keel damping and propeller thrust fluctuations are ignored by theory.

3. Errors in measurement of wave heights.

4. Wall effects especially at low speeds and small wavelengths.

THE EQUATIONS OF MOTION FOR A SURFACE SHIP MOVING IN WAVES

General Remarks

A constructive appraisal of a given theory is best accomplished by examining the issue from different points of view. In this case, many such different points of view exist. We will therefore examine the validity of the linearized theory of ship motions as developed by Korvin-Kroukovsky by using a different approach which is backed by physical reasoning. The approach will involve two cardinal steps:

1. Develop rigorously the linearized equations of motion.

2. Use the strip theory technique to compute the values of the coefficients of equation of motion as well as the excitation terms from elementary arguments based on the results of two-dimensional flow theory.

In fulfilling the latter step, the reason why strip techniques are employed, the assumptions implicit in strip techniques, as well as the upper limit of accuracy that can be expected from strip techniques will be considered.

We will start from the basic concepts of the mechanics of rigid bodies following Abkowitz [12,25,26]. His approach, similar to those used by aerodynamicists, provides a concise statement of the kinematical and kinetic problem and readily identifies all of the physical mechanisms involved. After the equations of motion have been developed in an accurate manner, all that remains to be done is to determine the values of the coefficients of the equations as well as the forcing functions. It is here that use will be made of the cross-flow hypothesis and two-dimensional hydrodynamic theory.

The reader may well at this juncture question the consistency of the paper; first an extensive investigation using an existing theory is presented and then the very foundation upon which the theory rests is questioned. This is true. However, it is only after using a certain procedure that one can really appreciate and question it. Furthermore, it is suspected that the inconsistencies which seem to exist in the Korvin-Kroukovsky approach will not radically affect the final result. This is probably due to the fortunate cancellation of errors, but this remains to be verified.

A basic difference between the approach formulated by Korvin-Kroukovsky and the approach proposed in this paper is that hydrodynamics will be employed after dynamics have been utilized. Furthermore no attempt will be made to force fit the mathematical model to conform to experimental results, but rather a rational approach will be developed with the hope that eventually, refined experiment will agree with refined theory.

Derivation of Equations of Motion

In this section the mathematical model describing the six-degree of freedom motion of a surface ship in regular waves will be developed first and the results will then be specialized for the case of pitching and heaving motions. The following assumptions will be made in developing the equations:

1. The ship will be considered as a rigid body. The high-frequency vibration modes of the hull excited by the low-frequency wave encounters will not be considered here.

2. The size, geometry, mass and mass distribution of the ship are assumed known and invariant in time.

3. Rudders and other control surfaces and mechanisms are assumed "locked" in zero position.

4. In deriving the equations of motion for pitch and heave the coupling between the latter two and the other degrees of freedom is totally neglected. For seas from directly ahead or astern, this is a reasonably valid assumption. In particular, surge effects are ignored which in turn implies that propeller thrust fluctuations are negligible.

5. As a consequence of the last statement in 4., the ship speed is assumed to be constant.

6. Forces and moments due to wind action, tow-lines, etc., are not considered. The external excitation is to be that due to waves only.

7. Since a linear theory will be developed, the translatory and angular departures of the ship from and about an inertial reference are assumed to be very small (first order).

8. The ship is assumed to be originally on an even keel.

9. Motion of the ship is assumed to take place in a given, idealized fluid which is unbounded in all directions.

10. The wave excitation is that due to uniform, infinitely long-crested sinusoidal waves of small amplitude which come from directly ahead or astern, i.e., the direction of ship motion is taken to be normal to the wave crests.

Two orthogonal, right-handed systems of coordinates will be employed in the development of the coupled pitching and heaving equations of motion. Consistent use of right-handed systems is advantageous because it allows a convenient check in the analysis by simply permuting the terms of various expressions. The first system of axes will be fixed in space with its origin located at an arbitrary point on the still water level. This will be regarded as a Newtonian frame of reference with respect to which the wave configuration and body orientation in space will be referred. The second system of axes, usually referred to as "body" axes, will be fixed in the ship with a convenient point as origin. In rigid body dynamics, the origin of the "body" axes is usually chosen to be the center of gravity of the body. However, in the ship problem case it is usually advantageous to fix the origin of the "body" axes at the intersection of the midship section, the longitudinal vertical plane of symmetry and the waterplane through G. This not only simplifies the computation of the hydrostatic and hydrodynamic forces but is also convenient because the midsection plane is fixed in a ship, whereas the position of the center of gravity is variable.

It is pertinent to note at this point that, from 1954 [8] onwards, Korvin-Kroukovsky assumed for simplicity in all his analyses that the vertical plane of the center of gravity and midship section coincided. Whereas, it is true that the LCG is usually a small fraction of the ship length, this simplification is sometimes responsible for wrong interpretations of phase angles, leading to errors up to 10° for certain ships in short wavelengths.

For reasons of consistency and systemization in future analyses, we herein suggest the use of and shall adhere to the nomenclature of Bulletin No. 1-5 of SNAME [25]. Following the above definitions it is shown in Refs. [12,26,27] that in order to obtain separate vector force and moment equations, the principles of linear and angular momentum must be used for the center of gravity of the ship, but must be measured relative to the "body" axes fixed about the point defined previously. If we therefore denote by $\mathbf{F}$ the total external force and by $\mathbf{G}$ the total moment of the external forces about the center of gravity, then, the principles of linear and angular momentum give,

$$\mathbf{F} = \frac{d}{dt}(m\mathbf{U}_G) \tag{1}$$

and

$$\mathbf{G} = \frac{d}{dt}(\mathbf{H}_G), \tag{2}$$

where

$$\mathbf{F} = \hat{i}X + \hat{j}Y + \hat{k}Z, \tag{3}$$

$$\mathbf{G} = \hat{i}K + \hat{j}M + \hat{k}N. \tag{4}$$

Following the principles of dynamics and carrying out the operations indicated above, it may be shown [26] that the complete six-degree of freedom motion of the ship is characterized by:

$$X = m\left[\dot{u} + qw - rv - x_G(q^2 + r^2) + y_G(pq - \dot{r}) + z_G(pr + \dot{q})\right] \tag{5}$$

$$Y = m\left[\dot{v} + ru - pw - y_G(r^2 + p^2) + z_G(qr - \dot{p}) + x_G(qp + \dot{r})\right] \tag{6}$$

$$Z = m\left[\dot{w} + pv - qu - z_G(p^2 + q^2) + x_G(rp - \dot{q}) + y_G(rq + \dot{p})\right] \tag{7}$$

$$K = I_x\dot{p} + (I_z - I_y)qr + m\left[y_G(\dot{w} + pv - qu) - z_G(\dot{v} + ru - pw)\right] \tag{8}$$

$$M = I_y\dot{q} + (I_x - I_z)rp + m\left[z_G(\dot{u} + qw - rv) - x_G(\dot{w} + pv - qu)\right] \tag{9}$$

$$N = I_z\dot{r} + (I_y - I_x)pq + m\left[x_G(\dot{v} + ru - pw) - y_G(\dot{u} + qw - rv)\right] \tag{10}$$

where the various symbols are defined in Ref. [25]. From this general approach, it may be seen that if G, the center of gravity, is identified with the origin of the "body" axes, then the above equations reduce to the well known Euler equations:

$$X = m(\dot{u} + qw - rv) \tag{11}$$

$$Y = m(\dot{v} + ru - pw) \tag{12}$$

$$Z = m(\dot{w} + pv - qu) \tag{13}$$

$$K = I_x\dot{p} + (I_z - I_y)\,qr \tag{14}$$

$$M = I_y\dot{q} + (I_x - I_z)\,rp \tag{15}$$

$$N = I_z\dot{r} + (I_y - I_x)\,pq\,. \tag{16}$$

If all other degrees of freedom except pitch and heave are now ignored from Eqs. (5)-(10) and if the center of gravity is assumed to be located on the longitudinal body axis at a distance x_G from the origin of the "body" axes, then, the problem reduces to the examination of the coupled pitch and heave equations as given by:

$$m(\dot{w} - qu - x_G\dot{q}) = Z \tag{17}$$

$$I_y\dot{q} + m x_G \dot{w} = M\,. \tag{18}$$

By the same token, the equivalent set corresponding to Eqs. (11)-(16) becomes,

$$m(\dot{w} - qu) = Z \tag{19}$$

$$I_y\dot{q} = M\,, \tag{20}$$

where the mqu term in Eq. (19) represents the main distinction between the ordinary Newtonian equation with axes fixed in space and the equation of motion with axes fixed in the ship.

Turning now to the examination of the loads, we note that in the most general case, the total external force F and moment G about the center of gravity must depend on:

1. The characteristics of the body

2. The properties of the fluid

3. The parameters which describe the relative motion between the body and the fluid.

These may be listed as follows:

1. <u>Characteristics of Body</u>

Characteristic length (size)
Geometry
Mass and its distribution

2. Properties of Fluid

Density
Viscosity
Surface tension
Elasticity
Vapor pressure
Pressure

Also thermal, electric, magnetic properties, etc.

3. Relative Motion Parameters

Orientation parameters: $x_o, y_o, z_o, \theta, \varphi, \psi, h$.

Dynamic parameters: $u, v, w, p, q, r, \dot{u}, \dot{v}, \dot{w}, \dot{p}, \dot{q}, \dot{r}, \dot{h}, \ddot{h}$.

For a surface ship of fixed geometry, mass and mass distribution moving at constant speed in a sufficiently idealized fluid, the total force and moment depend only on the parameters describing the relative motion between the body and the fluid. For pitch and heave motions of a surface ship, these are:

a. Body and fluid orientation parameters: z_o, θ, h .

b. Body and fluid dynamic parameters: $w, q, \dot{h}, \dot{w}, \dot{q}, \ddot{h}$.

The most convenient way of defining an unknown function is in terms of its multivariable Taylor expansion about some convenient equilibrium point. Since we will be content with developing a linear theory, only the linear terms in the expansion need be retained. A convenient equilibrium point about which to expand the total force and moment and hence their components Z and M is that characterized by: (a) constant ahead speed, $u = u_o$, and (b) zero orientation and dynamic parameters. The Taylor expansions for the heaving and pitching forces then result in:

$$Z = Z_e(h, \dot{h}, \ddot{h}, t) + \left(\frac{\partial Z}{\partial z_o}\right)_o \left(z - z_o\right) + \left(\frac{\partial Z}{\partial \theta}\right)_o (\theta - \theta_o) + \left(\frac{\partial Z}{\partial w}\right)_o (w - w_o)$$

$$+ \left(\frac{\partial Z}{\partial q}\right)_o (q - q_o) + \left(\frac{\partial Z}{\partial \dot{w}}\right)_o (\dot{w} - \dot{w}_o) + \left(\frac{\partial Z}{\partial \dot{q}}\right)_o (\dot{q} - \dot{q}_o) , \tag{21}$$

$$M = M_e(h, \dot{h}, \ddot{h}, t) + \left(\frac{\partial M}{\partial z_o}\right)_o \left(z - z_o\right) + \left(\frac{\partial M}{\partial \theta}\right)_o (\theta - \theta_o) + \left(\frac{\partial M}{\partial w}\right)_o (w - w_o)$$

$$+ \left(\frac{\partial M}{\partial q}\right)_o (q - q_o) + \left(\frac{\partial M}{\partial \dot{w}}\right)_o (\dot{w} - \dot{w}_o) + \left(\frac{\partial M}{\partial \dot{q}}\right)_o (\dot{q} - \dot{q}_o) , \tag{22}$$

where the zero subscript denotes the dynamic equilibrium condition and, for reasons to be subsequently discussed, the wave action forces and moments have been lumped conveniently in $Z_e(h, \dot{h}, \ddot{h}, t)$ and $M_e(h, \dot{h}, \ddot{h}, t)$. Such a linearization indicates that the forces and moments acting on a pitching and heaving ship may be conveniently considered to be of two sorts:

a. Wave-induced forces and moments acting on a restrained ship, and

b. Forces and moments brought about by the motion of the ship in calm water.

Noting that $z_{o_o} = \theta_o = w_o = \dot{w}_o = q_o = \dot{q}_o = 0$ and using the notation

$$Z_w = \left(\frac{\partial Z}{\partial w}\right)_o ,$$

etc., Eqs. (21) and (22) become,

$$Z = Z_e(h, \dot{h}, \ddot{h}, t) + Z_{z_o} z_o + Z_\theta \theta + Z_w w + Z_q q + Z_{\dot{w}} \dot{w} + Z_{\dot{q}} \dot{q} , \tag{23}$$

$$M = M_e(h, \dot{h}, \ddot{h}, t) + M_{z_o} z_o + M_\theta \theta + M_w w + M_q q + M_{\dot{w}} \dot{w} + M_{\dot{q}} \dot{q} . \tag{24}$$

Since it is desirable to express the differential equations in terms of the orientation parameters z_o and θ and their first and second time derivatives, an expression must be found for w and $\dot{w}$ in terms of z_o and θ. From the following sketch,

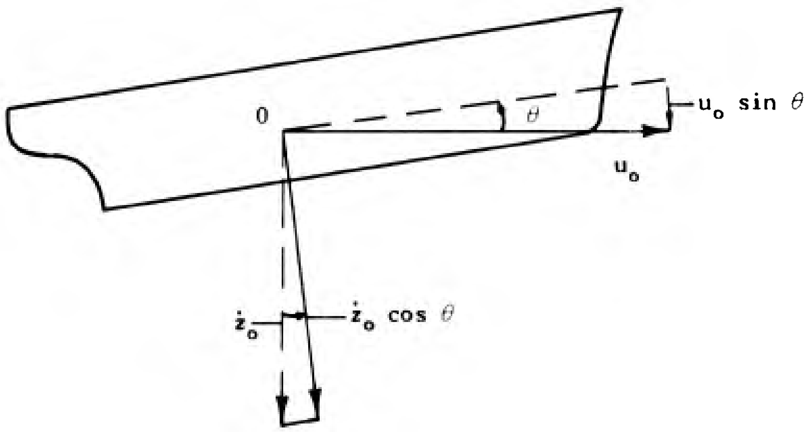

it follows that,

$$w = \dot{z}_o \cos \theta + u_o \sin \theta \tag{25}$$

or since within linearity, $\cos \theta \doteq 1$ and $\sin \theta \doteq \theta$, we get

$$w = \dot{z}_o + u_o \theta , \tag{26}$$

$$\dot{w} = \ddot{z}_o + u_o \dot{\theta} . \tag{27}$$

Substituting Eqs. (26) and (27) in Eqs. (23) and (24), calling $q = \dot{\theta}$ and $\dot{q} = \ddot{\theta}$ and rearranging terms in Eqs. (17) and (18), we finally obtain the coupled pitching and heaving equations of motion in the form:

$$(m - Z_{\dot{w}}) z_o + Z_w \dot{z}_o - Z_{z_o} z_o - (Z_{\dot{q}} + mx_G) \ddot{\theta} - (Z_q + u_o Z_{\dot{w}}) \dot{\theta}$$
$$- (Z_\theta + u_o Z_w) \theta = Z_e(h, \dot{h}, \ddot{h}, t) , \tag{28}$$

$$(I_y - M_{\dot{q}}) \theta - (M_q + u_o M_{\dot{w}}) \theta - (M_\theta + u_o M_w) \theta - (M_{\dot{w}} + mx_G) \ddot{z}_o - M_w \dot{z}_o$$
$$- M_{z_o} z_o = M_e(h, \dot{h}, \ddot{h}, t) . \tag{29}$$

If the above set were developed on the basis of Eqs. (19) and (20), i.e., for the origin of the "body" axes at the center of gravity, then the resulting equations would differ in form from Eqs. (28) and (29) only in that the mx_G term would be missing in the coefficients of pitch and heave accelerations in Eqs. (28) and (29).

CALCULATION OF THE COEFFICIENTS

The solutions to Eqs. (28) and (29) are in principle easily obtained provided that the twelve coefficients and the two forcing functions are known. Although, rational treatment of the problem does provide a precise identification of each term, the present state of art permits only rough approximations on the basis of theory and it is to this end that resource will be made to strip techniques. Deferring the discussion of the exciting terms until the next section, attention is here focused on the forces and moments brought about by the ship's oscillatory motion in calm water, and which are identified as the terms on the left hand side of Eqs. (28) and (29).

In order to exhibit the relationship between the new approach and that of Korvin-Kroukovsky, we shall, without loss of generality, substitute for each coefficient of Eqs. (28) and (29) a letter and thus obtain the set:

$$a(\omega_e) \ddot{z}_o + b(\omega_e) \dot{z}_o + c z_o + d(\omega_e) \ddot{\theta} + e(\omega_e) \dot{\theta} + f\theta = Z_e(h, \dot{h}, \ddot{h}, t) \tag{30}$$

$$A(\omega_e) \ddot{\theta} + B(\omega_e) \dot{\theta} + C\theta + D(\omega_e) \ddot{z}_o + E(\omega_e) \dot{z}_o + F z_o = M_e(h, \dot{h}, \ddot{h}, t) \tag{31}$$

where ω_e is the frequency of encounter with sinusoidal exciting waves and hence the frequency of the forced responses also.

In the interest of brevity and since the assumptions and steps to be followed in the computations by strip theory will be similar for all coefficients, we shall next examine in detail the manner in which one of the coefficients of the equation of motion can be computed on the basis of a strip technique. The extension of this approach to the other coefficients will be fairly apparent so that the values of the other coefficients will be given without derivation.

Equation (28) indicates that, after linearization, the coefficient of the heave acceleration term $a(\omega_e)$ consists in fact of two additive terms; the mass of the ship, m, which is known and is constant with time and the partial derivative of the total vertical hydrodynamic force with respect to heave acceleration, $Z_{\dot{w}}$. This is the force that is exerted on the body when oscillating in smooth water and its derivative is computed at the equilibrium condition characterized by a constant ship speed $u = u_o$, and by $z_o = \theta = w = q = \dot{w} = \dot{q} = 0$.

The statement of the problem has been given but the exact solution for the complete three-dimensional body is available only for special mathematically defined forms. Theoretical results are however available from two-dimensional theory; hence, it will be assumed that an arbitrary three-dimensional body can be replaced by the sum of a large number of two dimensional segments or strips. This is the essence of strip theory. It involves the following simplifications:

a. The underwater hull geometry is defined by an arbitrary number of typical sections.

b. These sections are arbitrarily assumed to be equally spaced.

c. To date, these sections are defined in terms of two geometrical parameters; the sectional area coefficient, $\sigma(x)$ and the beam/draft, $B(x)/H(x)$, ratio of section or its reciprocal.

d. Each of the strips is assumed to belong to a specific infinite cylinder oscillating at zero forward speed and its behavior is assumed independent and isolated from the neighboring strip.

e. Longitudinal perturbation velocities which exist in the three dimensional problem are totally neglected.

f. Since the available theoretical data to be used are based on an ideal fluid, viscosity is ignored.

Following strip theory,

$$Z_{\dot{w}} = - \int_{-L/2}^{+L/2} Z_{\dot{w}}(\omega_e, x)\, dx \tag{32}$$

where the integrand is the partial derivative of the force on the strip, which on the basis of extensive theoretical data is defined as

$$Z_{\dot{w}}(\omega_e, x) = k_2 k_4 c\, B(x)^2 . \tag{33}$$

The integrand is more commonly known as the added mass of the section or strip where the constant $c = \pi\rho/8$.

By similar reasoning, Z_w, the coefficient of the heave velocity term is approximated by

$$Z_w = -\int_{-L/2}^{+L/2} N(x)\, dx \tag{34}$$

where the integrand is the damping coefficient of the section and is calculated by the Havelock-Holstein [4] formula

$$N(x) = \frac{(\bar{A})^2 \rho g^2}{\omega_e^3} \tag{35}$$

where $\bar{A}$ = ratio of the amplitude of the wave created by the oscillation of the body to the amplitude of the oscillation of the body.

With the exception of the restoring coefficients c, C, f, F which can be evaluated on the basis of elementary hydrostatics, the remaining hydrodynamic derivatives of the equations of motion can be computed based on the knowledge of added mass and damping coefficients of cylinders of various shapes. The proposed expressions are summarized in Table 2 and compared to those developed by Korvin-Kroukovsky and his associates. Since the equations of Korvin-Kroukovsky were developed with the origin of the body axes fixed at the center of gravity of the ship, the new coefficients refer to the modified set of equations in which x_G is set equal to zero. Proper consideration was also given to the different definition of the total vertical force existing between the two approaches. Thus the expressions of Korvin-Kroukovsky have been corrected to allow for the fact that the total force is to be taken positive downwards.

Table 2 shows that the expressions for four of the newly proposed coefficients do not agree with those derived by Korvin-Kroukovsky. The differences in the Korvin-Kroukovsky coefficients $e(\omega_e)$, $B(\omega_e)$, C and $E(\omega_e)$ appear to be mainly due to an erroneous time differentiation of a fixed body coordinate with the result that: (a) a factor of 2 appears in the velocity dependent terms of $e(\omega_e)$ and $B(\omega_e)$, and (b) a pseudo-three-dimensional term is introduced in coefficients $e(\omega_e)$, $B(\omega_e)$, C and $E(\omega_e)$.

It would also appear that the introduction of terms dependent on the rate of change of added mass over the ship length is inconsistent with the use of two-dimensional theory. Despite these discrepancies however, it is expected that the final values of these coefficients will not be seriously modified since it has been shown by Jacobs et al. [5] that most of these terms which appear in the Korvin-Kroukovsky approach but not in the new approach are numerically small. It is hoped that in the near future these inconsistencies will be examined more carefully and their implications assessed on the basis of experimental data.

Since most of the coefficients of the equations of motion depend on the theoretically computed added mass and damping coefficients for two-dimensional cylinders, this matter will next be considered in some detail. The first solution of the potential problem of an infinite circular cylinder oscillating at zero forward speed in an ideal fluid was given by Ursell [28] and his results for added

Table 2
Comparison of Coefficients of Equations of Motion

Coefficient		New Approach	Korvin-Kroukovsky Approach
$a(\omega_e)$	$m - Z_{\dot{w}}$	$m + \int \mu(x)\,dx$ *	same
$b(\omega_e)$	$-Z_w$	$\int N(x)\,dx$	same
c	$-Z_{z_o}$	$\rho g \int B(x)\,dx$	same
$d(\omega_e)$	$-Z_{\dot{q}}$	$-\int \mu(x)\,x\,dx$	same
$e(\omega_e)$	$-(Z_q + u_o Z_{\dot{w}})$	$-\int N(x)\,x\,dx + u_o \int \mu(x)\,dx$	$-\int N(x)\,x\,dx + 2u_o \int \mu(x)\,dx + u_o \int \frac{d\mu(x)}{dx}\,x\,dx$
f	$-(Z_\theta + u_o Z_w)$	$-\rho g \int B(x)\,x\,dx + u_o \int N(x)\,dx$	same
$A(\omega_e)$	$I_y - M_{\dot{q}}$	$I_y + \int \mu(x)\,x^2\,dx$	same
$B(\omega_e)$	$-(M_q + u_o M_{\dot{w}})$	$\int N(x)\,x^2\,dx - u_o \int \mu(x)\,x\,dx$	$\int N(x)\,x^2\,dx - 2u_o \int \mu(x)\,x\,dx - u_o \int \frac{d\mu(x)}{dx}\,x^2\,dx$
C	$-(M_\theta + u_o M_w)$	$\rho g \int B(x)\,x^2\,dx - u_o \int N(x)\,x\,dx$	$\rho g \int B(x)\,x^2\,dx - u_o \int N(x)\,x\,dx + u_o^2 \int \frac{d\mu(x)}{dx}\,x\,dx$
$D(\omega_e)$	$-M_{\dot{w}}$	$-\int \mu(x)\,x\,dx$	same
$E(\omega_e)$	$-M_w$	$-\int N(x)\,x\,dx$	$-\int N(x)\,x\,dx + u_o \int \frac{d\mu(x)}{dx}\,x\,dx$
F	$-M_{z_o}$	$-\rho g \int B(x)\,x\,dx$	same

*For brevity $\mu(x) = k_2 k_4 \frac{\rho B^2(x)}{8}$.

mass were assumed by Korvin-Kroukovsky [10] and Jacobs et al. [5] to apply to more general cylinders. However, different results were used in Refs. [10] and [5] for computing the damping coefficients; the first utilized an approximate expression for A, whereas the second introduced and employed the graphical data computed by Grim in 1953 [29]. Since the publication of Ref. [30] which reviewed the state of art up to about 1955, the important problem of the oscillating cylinder of arbitrary section has been examined and solved in greater detail, both theoretically and experimentally. For example, Grim [29], Tasai [31] and, more recently Porter [32] have extended the Ursell problem to more general cylinders, and have provided added mass and damping as a function of the frequency of oscillation. Damping coefficients for extreme V sections were also evaluated by Kaplan [33] using a Green's function technique, whereas TRG [34] presented their approximate method for evaluating these quantities. These theoretical studies were supplemented and verified by experimental work carried out by Tasai [31], Porter [32], and Paulling and Richardson [36] and Watson [35].

These studies were of course concerned with the small oscillatory motion of two-dimensional bodies where the effect of frequency on the distribution of damping and added mass, the effect of forward speed, and nonlinear effects are ignored. These important effects have been discussed on the basis of experiment in part by Golovato [37] and in part by Gerritsma [38], and Gerritsma and Beukelman [39] and others. Reference [39] has shown for example that the distribution of damping along the length of a ship is appreciably affected by frequency and forward speed whereas the added mass distribution appears to be less affected by these parameters. Another very important point, which was anticipated from Newman's theoretical work [40] was the occurrence of negative sectional damping and added mass at certain speeds. Two-dimensional theory cannot of course predict such effects. Hence, strip theory fails to compute exactly the responses but more especially the bending moments in regular waves.

The computer program described and used in Ref. [6] made use of a subroutine which was based on more recent work by Grim, as outlined in Ref. [41]. His numerical results however appeared to be erroneous for certain combinations of sectional area coefficient and beam-to-draft ratio. This issue assumed great importance when disagreement was noted in the case of Model E as discussed earlier in this paper. Furthermore, his results, as well as those of Tasai [31], are restricted to Lewis shape sections only. However, as far back as 1947, Prohaska [42] indicated that the definition of a ship section in terms of two parameters is unsufficient. This inadequacy has since been clearly demonstrated by Landweber and Macagno [43], in connection with high-frequency added mass calculations.

The above points and the availability of a complete and exact analysis of the problem by Porter [32], launched a systematic examination of the problem which is currently still under way at M.I.T. by Porter and others. Some preliminary results of this work are herein included and discussed. Comparison of k_4 and $\bar{A}$ as calculated by two computer programs, one based on Grim [41] and another due to Porter [32], are shown in (a) Figs. 66 and 67 for semicircular cylinders of varying beam to draft ratio and, (b) Figs. 69 and 70 for the typical ship sections illustrated in Fig. 68. The latter figure and Table 3 are reproduced from Ref. [44].

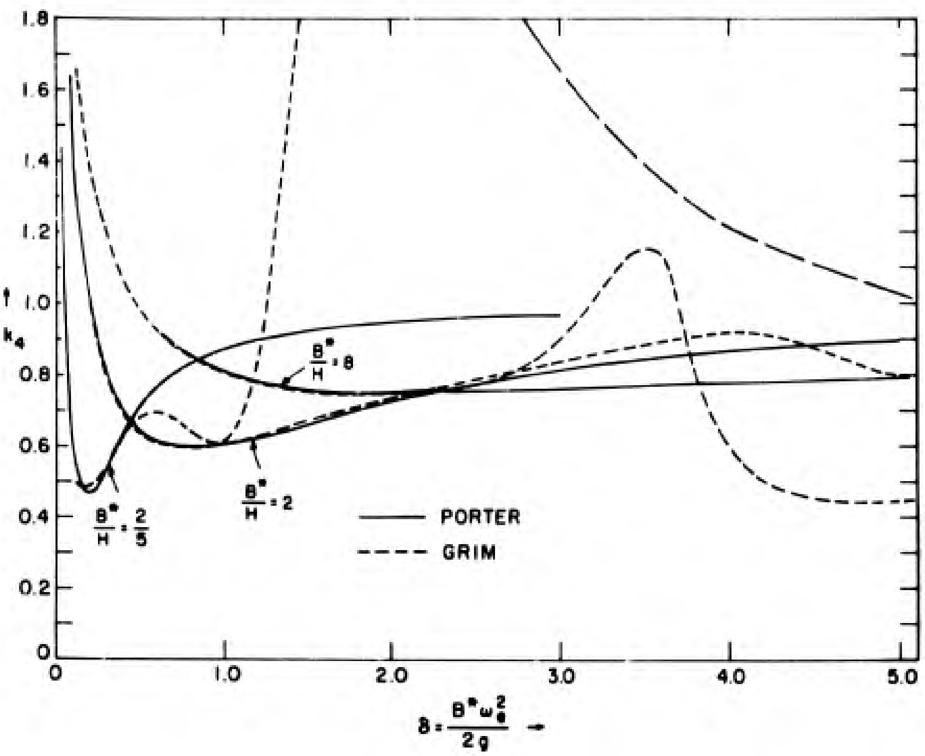

Fig. 66 - k_4 versus δ

Table 3
Particulars of Ship Model Sections

Model No.	Type	$B^*/2$ (in.)	B^*/H	$\sigma(x)$
2	Full-Form	8	2.00	0.9405
3	Wide Vee	8	0.80	0.700
4	Narrow Vee	4	0.40	0.644
5	Bulb-Form	4	0.40	0.695

Figures 66-70 indicate first of all that the computer algorithm of Porter is extremely accurate whereas that of Grim suffers from severe numerical breakdown, especially at high values of the non-dimensional frequency

$$\delta = \frac{B^* \omega_e^2}{2g} .$$

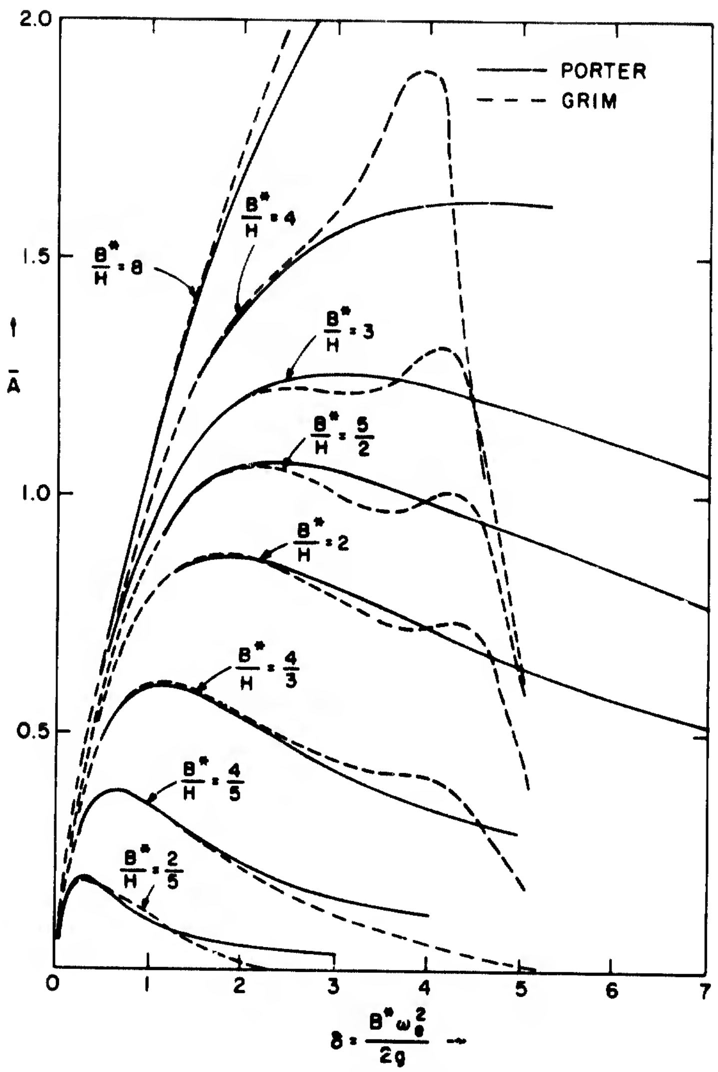

Fig. 67 - $\bar{A}$ versus δ

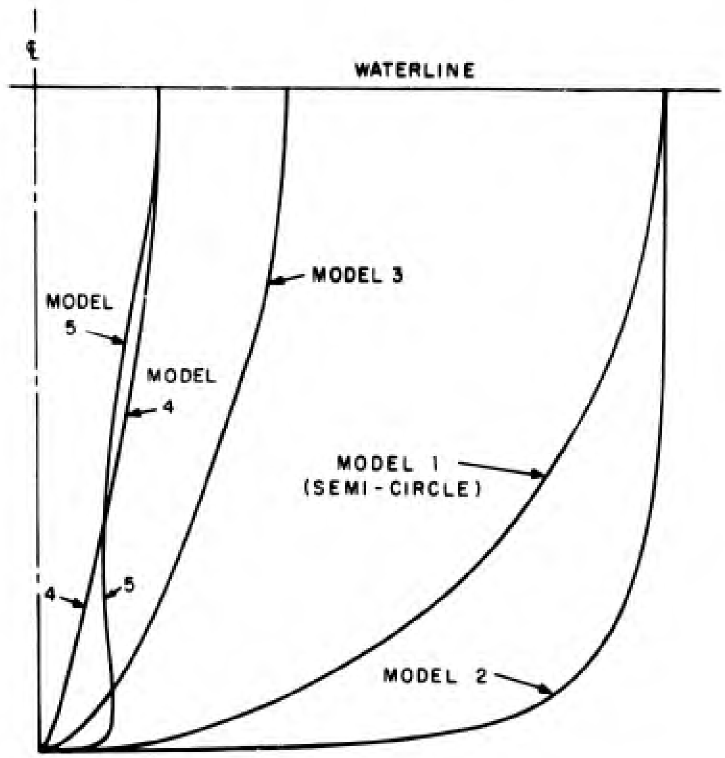

Fig. 68 - Model sections

It is important to note, however, that in the important ship range of the frequency parameter (0-1.5), the disagreement is minimum. Generally speaking, in the case of the semicircular cylinders, Figs. 66 and 67, the free-surface correction factor, k_4, as computed by Grim is less accurate than $\bar{A}$, the amplitude ratio. Also, for a given δ, the discrepancies for both k_4 and $\bar{A}$ increase with decreasing beam to draft ratio. This is particularly noticeable for the low beam to draft bulb-section (Model 5 of Fig. 68) as plotted in Fig. 70. This, in turn, causes underestimations of heave and pitch damping and consequently forces the strip theory to overestimate responses, particularly at resonance, as shown for example by Model E. However, it has not yet been possible to examine, in detail, the overall effect these differences will have for a particular ship model in a given condition.

The most important reasons why efforts are now being made to incorporate a version of Porter's work in our computer program are as follows:

a. His solution of the theoretical problem is considered more exact and by far the most general to date.

b. His numerical scheme is much more stable although, at present, more time-consuming than that of Grim.

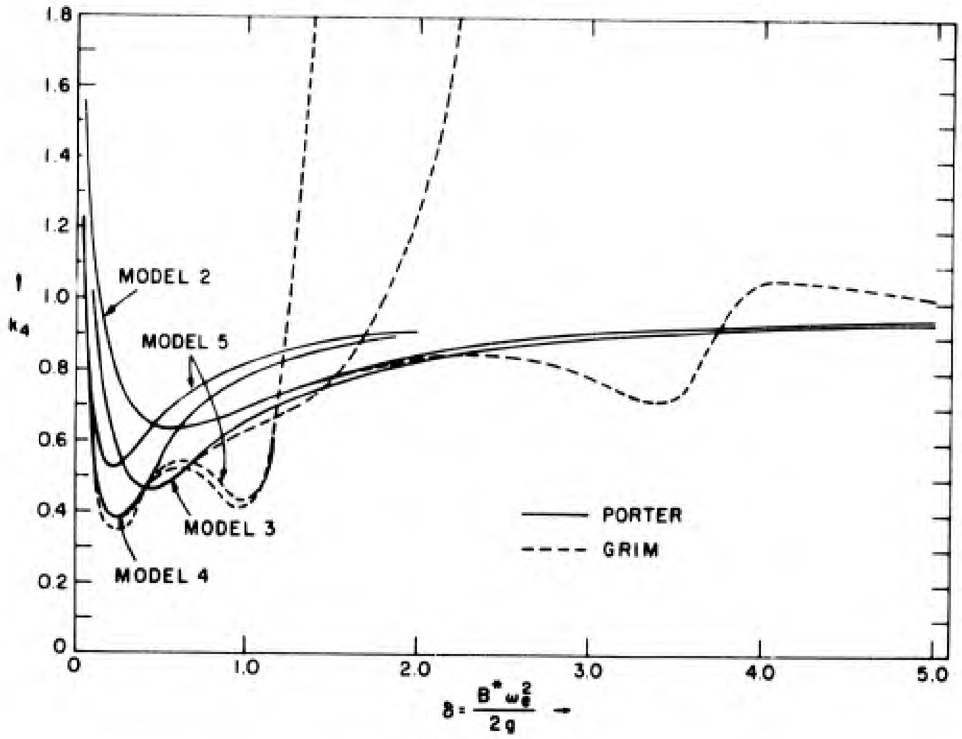

Fig. 69 - k_4 versus δ

c. His program can handle any arbitrary ship section which can be defined by either (1) an arbitrary number of parameters or, even better (2) a set of offsets for the section [45].

d. Extension to the problem of horizontal oscillation can also be made for lateral ship motions.

It follows from c. that Porter's program will discriminate between the added mass and damping of two sections of identical section coefficients and beam-draft ratio but differing in detailed section shape. Thus it should prove more flexible than programs tied to particular section families such as the Lewis or Landweber sections.

CALCULATION OF EXCITATION FORCE AND MOMENT

The second main category of the loads imposed on the ship hull are those due to wave action. As a result of the linearization of the problem, these forces and moments can be assumed to act independently on the ship which is moving at constant speed but is otherwise restrained from any translatory or angular displacements.

Since there is no distinction, as far as hydrodynamic forces and moments are concerned, between a restrained ship in a vertically oscillating fluid and an

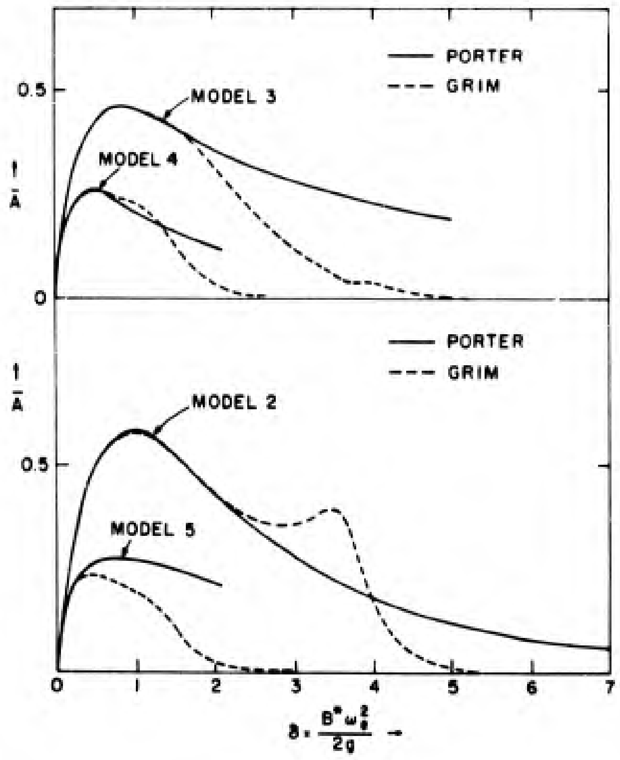

Fig. 70 - $\bar{A}$ versus δ

oscillating ship in a stationary fluid, the excitation forces and moments can be determined by exactly the same arguments used in the calculation of the coefficients of the equations. There are, however, two distinct points of difference which must be allowed for in the computation of the exciting loads:

a. Whereas in the calculation of the coefficients of the equations of motion the total force and moment are obtained by summing up strip contributions for sections in identical flow, in the case of wave excitation loads consideration must be given to the distinct flow which each section sees when the wave pattern encounters it. In other words, differential exciting forces depend on the ship section properties as well as the local static and dynamic state of the wave.

b. At every section and hence on the whole ship, an extra force and moment is brought about on account of the fact that the relative water flow at a given section involves a pressure gradient which is typical of gravity waves. This so-called "Smith effect" is due to the orbital motion of the water particles and must be allowed for since the differential exciting forces at a given section depend on whether the section is instantaneously on a wave crest or trough. The best approximate way of allowing for this effect is to consider in the calculations the static and dynamic state of an "effective subsurface" rather than the actual wave surface. Havelock has suggested [46] that the effective subsurface is located at a mean draught equal to ∇/A_w or $(C_B/C_W)H$, a result which is accurate for wall-sided ships. Since we shall compute the loads on the basis of two-dimensional flow theory, the equivalent mean draft at a specific ship station, which belongs to an infinite cylinder, becomes $\sigma(x)\ H(x)$. An overall correction factor such as

$$e^{-\left[\frac{2\pi}{\lambda}\sigma(x)\ H(x)\right]}$$

will therefore be employed in the calculation of the excitation force at a given section. It must be noted however that the Smith effect should, strictly speaking, be a single correction to the wave acceleration force only.

Since the exact calculation of the total exciting force is a formidable hydrodynamic problem, the following usual assumptions will be made in the approximate computation:

a. At each point on the submerged hull surface there is a pressure acting which is the same as the pressure that would occur at the corresponding point in the wave in the absence of the ship. This pressure is computed after the centripetal acceleration of the water particles has been accounted for (Smith effect).

b. The wave geometry and dynamic state is not affected by the presence of the ship, i.e., any diffraction effects are neglected.

Assumptions a. and b. constitute the well-known Froude-Kriloff hypothesis.

c. The effect of the forward speed of the ship is neglected.

It is surmised that the differential heaving force as felt by the ship section depends on the instantaneous elevation, velocity and acceleration of the effective subsurface measured relative to the body coordinate system. Thus,

$$\frac{dZ_e}{dx} = Z(h,\dot{h},\ddot{h})\ \exp\left[-\frac{2\pi}{\lambda}\zeta(x)\right] \tag{36}$$

where $\zeta(x) = \sigma(x)\ H(x)$. For small motions, we can expand the function $Z(h,\dot{h},\ddot{h})$ in a Taylor series about the condition of no wave, i.e., $h_o = \dot{h}_o = \ddot{h}_o = 0$ and $u = u_o$ and retain only linear terms. Noting that $Z(h_o,\dot{h}_o,\ddot{h}_o) = 0$, we finally get,

$$\frac{dZ_e}{dx} = \left[\left(\frac{\partial Z_e}{\partial h}\right)_x h(x,t) + \left(\frac{\partial Z_e}{\partial \dot{h}}\right)_x \dot{h}(x,t) + \left(\frac{\partial Z_e}{\partial \ddot{h}}\right)_x \ddot{h}(x,t)\right] \exp\frac{2\pi}{\lambda}\sigma(x)\ H(x) \tag{37}$$

where the wave elevation is measured positive downwards. The subscript x denotes that the derivatives $(\partial Z_e/\partial h)_x$ etc., correspond to the section under consideration only. Since the coefficients of each term are readily computed as

$$\frac{\partial Z_e}{\partial h} = Z_{z_o(x)}, \quad \frac{\partial Z_e}{\partial \dot{h}} = Z_{w(x)} \quad \text{and} \quad \frac{\partial Z_e}{\partial \ddot{h}} = Z_{\dot{w}(x)},$$

the total exciting force due to sinusoidal waves is simply obtained by summing up the individual contributions of each strip, i.e.,

$$Z_e(h,\dot{h},\ddot{h},t) = \int_{-L/2}^{+L/2} \left(\frac{\partial Z_e}{dx}\right)_x dx = Z_o e^{i\omega_e t} \tag{38}$$

and the total pitching moment is given by

$$M_e(h,\dot{h},\ddot{h},t) = \int_{-L/2}^{+L/2} \left(\frac{dZ_e}{dx}\right)_x x\,dx = M_o e^{i\omega_e t} . \tag{39}$$

It is interesting to compare the above expressions with those of Jacobs [14]. Following the same initial steps as Korvin-Kroukovsky [10] but pursuing a slightly different approach, Jacobs [14] modified and improved the excitation force expression as compared with the one given in Ref. [10]. In our notation, the formula as given by Jacobs [5] and as used in the existing computer program, reads as follows:

$$\frac{dZ_e}{dx} = \left\{ \rho g B(x)\; h(x,t) + \left[N(x) - u_o \frac{d\mu(x)}{dx}\right] \dot{h}(x,t) + \mu(x)\; \ddot{h}(x,t)\right\}$$

$$\times \exp\left[-\frac{2\pi}{\lambda}\sigma(x)\; H(x)\right] . \tag{40}$$

Equation (40) differs from (37) in that the wave velocity term includes an extra pseudo-three-dimensional term which is furthermore speed dependent. The contribution of the latter term is small in comparison with the other terms and predicts a decrease of the exciting force and moment, a finding which, as discussed by Vossers [47], contradicts that of Hanaoka. It is contended that the more rationally derived Eq. (37) will give almost similar results as Eq. (40) but this remains to be verified.

As justification of using the cross-flow hypothesis in computing excitation loads, Fay [13] provides an intuitive criterion which requires that

$$\frac{\omega_e^2 H}{g} > 1 .$$

The best criteria however of the success with which strip theory predicts the forcing function is the degree of correlation with experimental measurements and more sophisticated theoretical analyses. As far as the authors are aware, the only experimental data obtained with actual ship models is that of Jinnaka [48], Schultz [49], and Gerritsma [22], whereas Gersten [50] and Lee [51] measured excitation forces and moments on mathematically defined bodies. Correlation between experimentally measured and theoretically computed exciting forces and moments have been presented by Vossers [47], Gersten [50], and Lee [51], but the theoretical expressions used for the exciting loads differed from the one presented in Ref. [5]. These studies have shown that in general the Froude-Kriloff hypothesis (modified for Smith effect) supplemented by approximate corrections for the body-wave interference provide reasonable predictions of the excitation force and moment. The lack of severe dependence on speed has also been noted in these studies.

To supplement these correlations, the results of a preliminary analysis are shown in Figs. 71 and 72. Theoretical forces and moments based on Jacobs' formula, Eq. (40), have been compared with the experimental values given by Gerritsma in Ref. [22] for an 8-foot, Series 60, $C_B = 0.60$ model. The amplitudes of the heave exciting force compare more favorably than those of the pitching moment, although there are some discrepancies at low wavelengths. This finding seems to be in accord with Fay's statement [13] that the cross-flow hypothesis will be more valid for wavelengths equal to or greater than the ship length. Although results computed from Eq. (37) are not shown on Figs. 71 and

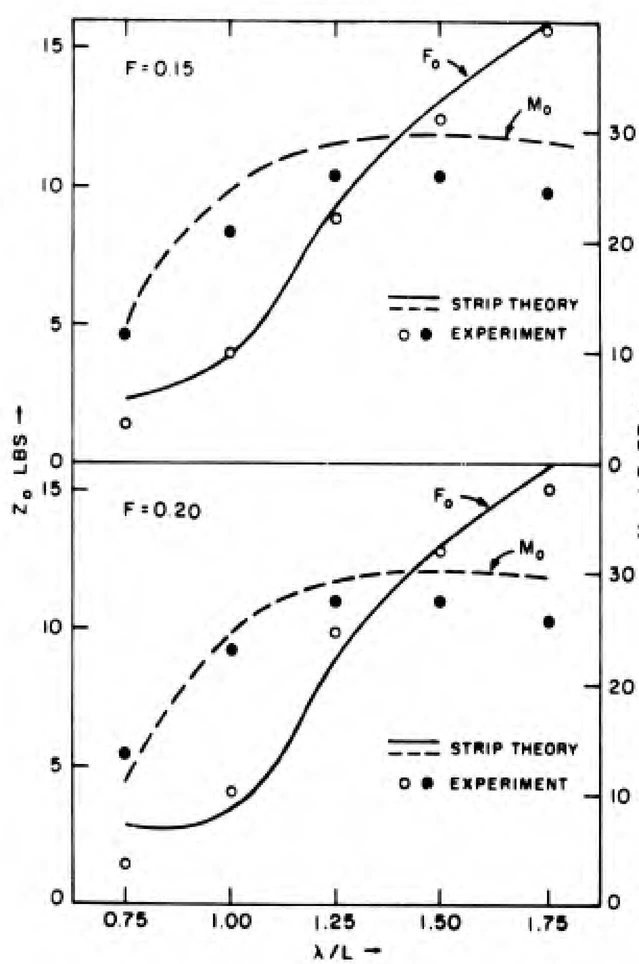

Fig. 71 - Comparison of excitation force and moment amplitudes

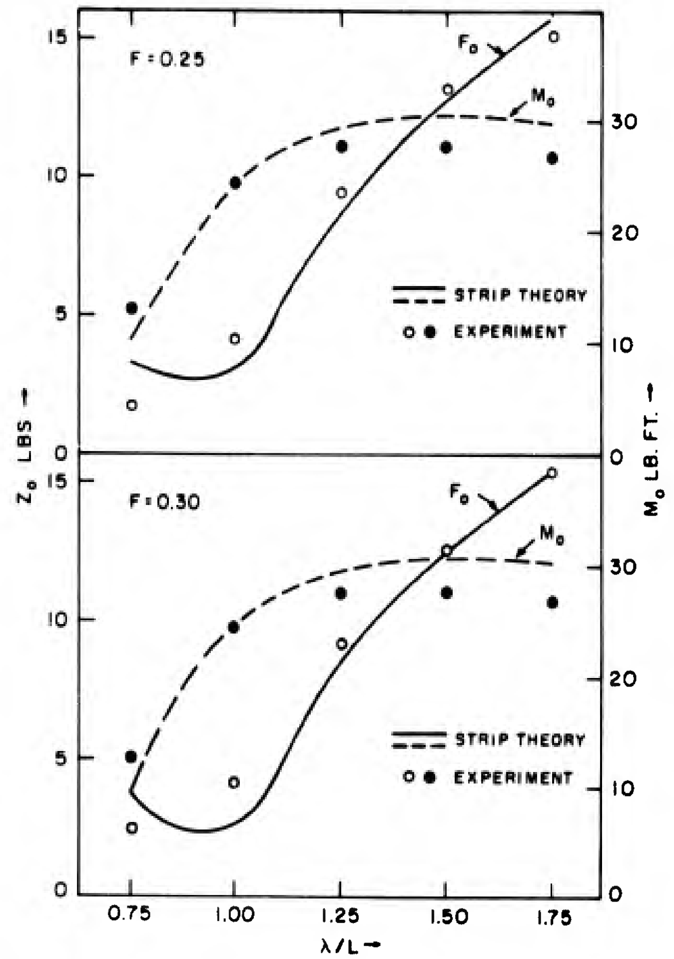

Fig. 72 - Comparison of excitation force and moment amplitudes

72, as previously noted, it is expected that these expressions will not yield answers significantly different from Jacobs' Eq. (40).

The discrepancies which are brought about by assuming that the body and wave do not interfere need also to be examined. Grim's [52] theoretical work, supplemented by Spens' [53] experimental work point out the considerable decrease in wave elevation as the wave passes along the ship length as well as the presence of a bow-induced wave. There is no doubt that such interference effects, especially in astern seas [53], will sensibly modify the theoretical exciting force and especially the pitching moment, which, at present, seem to be overestimated. It is not yet known whether a convenient correction may be applied in Eq. (37) to allow for this discrepancy, but the matter will be considered more carefully in the future.

The diffraction problem has also been investigated more recently by Neumann [54] on the basis of Haskind's theory. He presents a remarkably simple relationship between the wave-induced force on a fixed body and the amplitude of the progressive wave caused by the motion of the body in still water. Although his analysis does not provide the phase between force and wave, his expressions ought to be compared and evaluated on the basis of strip techniques. Using our notation, it can be shown that for a ship hull, his final formulations reduce to:

$$Z_o = \rho \left(\frac{g}{\omega_e}\right)^2 \int_{-L/2}^{+L/2} \bar{A}(x)\ h(x)\ dx \tag{41}$$

and

$$M_o = \rho \left(\frac{g}{\omega_e}\right)^2 \int_{-L/2}^{+L/2} \bar{A}(x)\ h(x)\ x\, dx\ . \tag{42}$$

Finally, three-dimensional corrections deserve comment. The work of Spens [53] and others has suggested that a three-dimensional correction to allow for end effects, etc., tends to worsen agreement between theory and experiment. Further analysis on this point is needed, however, because there is recent experimental evidence at M.I.T. to suggest that neglect of three-dimensional effects may not be in order for certain ship forms. Provided that the other neglected effects are allowed for, it may well be that a three-dimensional correction will improve agreement between theory and experiment.

CONCLUSIONS

1. Following Abkowitz [12,26,27], the more rigorous development of the equations of motion shown in this report along with the more systematic and symbolic notation of the SNAME Bulletin 1-5 [25] lead more quickly and simply to an accurate definition of the various parts of the coefficients of the equations of motion than the Korvin-Kroukovsky approach.

2. The quantitative evaluation of the coefficients of the equations of motion using strip theory developed in this report leads to agreement with Korvin-Kroukovsky in the case of eight of the coefficients and disagreement in the case of four of the coefficients.

3. Figures 2-65 show that pitching and heaving amplitudes as well as phase angles as computed by Korvin-Kroukovsky's procedure using Grim's section damping and added mass [41] correlate reasonably well with existing experimental data which however also include sources of possible error.

4. Substitution of the Porter method [32] for computing section damping and added mass should improve the discrimination amongst differing section shapes compared to Grim [41] and also removes the difficulties associated with oscillating nature of Grim's coefficients shown in Figs. 66, 67 and 69.

5. While it has been hypothesized that the correlation shown in Figs. 2-65 may be due to fortunate cancellation of substantial errors, it is not believed that

the errors shown to exist in the Korvin-Kroukovsky procedure using Grim's section added mass and damping are large. This remains to be further investigated however.

RECOMMENDATIONS

While the present report represents a start, much more can be done to assess the reliability and usefulness of an improved strip theory. The following list of recommendations cover suggestions for correcting the work already accomplished as well as suggestions for future work.

1. There is a strong need for phase angles to be uniformly and unambiguously defined. There are essentially three different ways for phase angles to be presented:

   a. Amplitude positive throughout and phase angles from 0°-360°.

   b. Amplitude positive throughout and phase angles ±0-180°.

   c. Amplitude both positive and negative and phase angles from 0°-180°.

The last was used by Vossers et al. [18,19] while the second way has been used in this report and in Ref. [6]. It is believed that the first way is the least ambiguous and that this should be used in the future. In the definition of phase, the maxima of response amplitudes should be referred to the maxima of the wave amplitude and not to the maxima of the wave slope as was done by Korvin-Kroukovsky. Furthermore, the reference point should be the mid-section of the ship or model rather than the longitudinal center of gravity since the former can be readily and precisely located.

2. The importance of the neglect of surge in the theory remains to be determined. The current work of Shen Wang at M.I.T. will help with the formulation of a system with the needed three degrees of freedom.

3. The assumption of wall sidedness as far as damping, added mass, and wave excitation is concerned is an important possible source of unrealism in the strip theory. The current work of Parissis [16] is important in this regard. Unfortunately, while success in coping with this problem should improve correlation between theory and experiment in regular waves, it will not be possible to incorporate this refinement in the prediction of statistical responses in random seas. The latter is strongly tied to a completely linear system.

4. Further refinements of strip theory should include the use of Porter [32] for computing section damping and added mass.

5. Correlations between the strip techniques and other theories for predicting ship motions should continue. For example, Fig. 73 shows a comparison between the non-dimensional pitch and heave amplitudes for a $C_B = 0.60$, Series 60 model at zero speed using Grim's three-dimensional theory [55] and those predicted for Model D at zero speed by the program of Ref. [6]. It is seen that

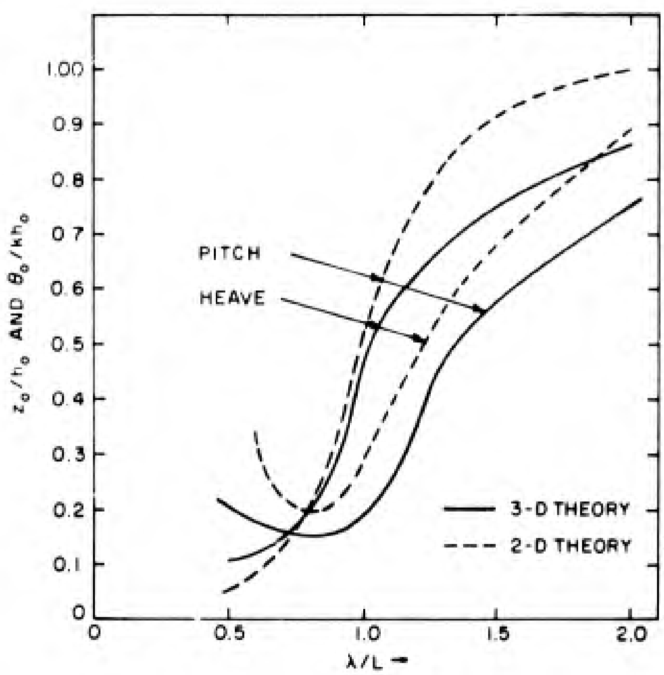

Fig. 73 - Comparison of motion amplitudes of Model D at zero speed

this agreement for heave is better than the agreement for pitch but that the comparisons are reversed for the two motions. No further comment can be made on these comparisons at this time.

6. Because of the absence of a firm basis for assessing the accuracy of any method for predicting ship motions, efforts toward refinement of existing theories and experimental techniques as well as the development of new theories and experimental techniques such as will be discussed by Davis and Zarnick at this Symposium should continue.

In the meantime, in order to show more clearly than it has been shown in the past, the importance of ship motions to the process of selecting dimensions and hull shape for ships, to the earning power of ships and to their economical operation, the effort begun in Ref. [6] towards assessing the performance of ships in random seas will be continued at M.I.T. This work will perforce have to rely on the most workable tool currently available to the profession. In the authors' opinion, this is strip theory.

ACKNOWLEDGMENTS

The authors are deeply grateful to Professors M. A. Abkowitz and W. Porter of M.I.T. for their freely given advice and counsel during the preparation of this paper. Those familiar with the history of the development in the United States of the equations of motion will immediately recognize the guiding philosophy of Professor Abkowitz in the discussion of the equations of motion contained in this paper. Most of the material used in the analysis of added mass and damping was kindly provided by Professor Porter.

Mrs. Barbara Allen of our Department at M.I.T. was most patient and co-operative in typing the manuscript of this paper. To her we extend our deep thanks.

NOMENCLATURE

English Letters

a = coefficient of equation of motion

A = coefficient of equation of motion

$\bar{A}$ = amplitude ratio

b = coefficient of equation of motion

B = breadth of ship or model

B = coefficient of equation of motion

B^*, $B(x)$ = station breadth of ship or model at designed waterline

c = a constant $= \pi\rho/8$

c = coefficient of equation of motion

C = coefficient of equation of motion

C_B = block coefficient of ship or model

C_P = prismatic coefficient of ship or model

C_W = waterplane area coefficient

d = coefficient of equation of motion

D = coefficient of equation of motion

e = coefficient of equation of motion

E = coefficient of equation of motion

Fr = Froude number

F = total external force

g = gravitational acceleration

g = coefficient of equation of motion

$\mathbf{G}$ = moment vector of external forces

G = coefficient of equation of motion

G = center of gravity

h, $h(t)$ = instantaneous wave elevation referred to absolute system

$h(x)$ = instantaneous wave elevation referred to relative (moving) system

$h(x)$ = instantaneous wave velocity referred to relative (moving) system

$h(x)$ = instantaneous wave acceleration referred to relative (moving) system

h_o = amplitude of sinusoidal wave (half wave-height)

H = draft of ship or model

$\mathbf{H}_G$ = angular momentum vector about G relative to fixed axes

I_x, I_y, I_z = moments of inertia about x, y, z axes respectively

K = rolling moment

k = wave number, $2\pi/\lambda$

k_θ = non-dimensional longitudinal radius of gyration

k_2 = high-frequency added mass coefficient of section (Lewis)

k_4 = low-frequency added mass correction factor (Grim-Porter)

L = length of ship or model

LCB = longitudinal distance of center of buoyancy from amidships

LCG = longitudinal distance of center of gravity from amidships

m = mass of ship or model

$\mu(x)$ = sectional added mass $= k_2 k_4 \pi\rho \dfrac{B^2(x)}{8}$

M = pitching moment

M_e = wave exciting pitching moment

M_o = amplitude of exciting pitching moment

N = yawing moment

$N(x)$ = sectional damping coefficient

O = origin of body axes

p = angular velocity of roll

$\dot{p}$ = angular acceleration of roll

q = angular velocity of pitch

$\dot{q}$ = angular acceleration of pitch

$\mathbf{R}_G$ = position vector of G relative to O

$\dot{r}$ = angular acceleration of yaw

r = angular velocity of yaw

t = time

u = longitudinal velocity component of origin of body axes relative to fixed axes

$\dot{u}$ = longitudinal acceleration component

$\mathbf{U}_G$ = velocity vector of G relative to fixed axes

v = transverse velocity component of origin of body axes relative to fixed axes

$\dot{v}$ = transverse acceleration component of origin of body axes relative to fixed axes

$\forall$ = underwater volume of ship

w = normal velocity component of origin of body axes relative to fixed axes

$\dot{w}$ = normal acceleration component of origin of body axes relative to fixed axes

x = longitudinal body axis or coordinate of a point relative to body axes

x_o = fixed longitudinal axis or longitudinal coordinate of a point relative to fixed axes

x_G = longitudinal coordinate of center of gravity relative to body axes

X = longitudinal component of hydrodynamic force on body

Y = lateral component of hydrodynamic force on body

y_o = transverse body axis or coordinate of a point relative to body axes

y_G = transverse coordinate of center of gravity relative to body axes

y = transverse body axis or coordinate of a point relative to body axes

z = normal body axis or coordinate of a point relative to body axes

z_o = fixed vertical axis or vertical coordinate of a point relative to fixed axes

z_G = vertical coordinate of center of gravity relative to body axes

$\dot{z}$ = heaving velocity of ship or model

z = heaving acceleration of ship or model

z_o = amplitude of heaving motion (for Figs. 2-65)

Z = vertical component of hydrodynamic force on body

Z_e = wave exciting heaving force

Z_o = amplitude of wave exciting heaving force

Greek Letters

δ = non-dimensional frequency parameter

δ^* = heaving phase angle (lag) after wave

Δ = displacement of ship or model

ϵ^* = pitching phase angle (lag) after wave

θ = pitch angle

θ_o = amplitude of pitching motion (for Figs. 2-65)

λ = wavelength

ρ = water density

$\sigma(x)$ = sectional area coefficient

φ = roll angle

χ = heading angle

ψ = yaw angle

ω_e = frequency of encounter

REFERENCES

1. Kriloff, A., "A New Theory of the Pitching Motions of Ships on Waves and the Stresses Produced by This Motion," Transactions of Institution of Naval Architects, Vol. 37, 1896, pp. 326-368 and plates 54-57.

2. Kriloff, A., "A General Theory of the Oscillations of a Ship on Waves," and "On Stresses Experienced by a Ship in a Seaway," Transactions of Institution of Naval Architects, Vol. 40, 1898, pp. 135-212 and plates 32 to 36.

3. Weinblum, G. and St. Denis, M., "On the Motions of Ships at Sea," Transactions of SNAME, Vol. 58, 1950, pp. 184-231.

4. Korvin-Kroukovsky, B. V., "Theory of Seakeeping," SNAME, New York, 1961.

5. Jacobs, W. R., Dalzell, J., and Lalangas, P., "Guide to Computational Procedure for Analytical Evaluation of Ship Bending Moments in Regular Waves," Davidson Laboratory Report No. 791, October 1960, Stevens Institute of Technology.

6. Vassilopoulos, L., "The Analytical Prediction of Ship Performance in Random Seas, Including a New Correlation of Theoretical and Experimental Motions in Regular Waves," M.I.T., Department of Naval Architecture and Marine Engineering, February 1964.

7. Cummins, W. E., "The Impulse Response Function and Ship Motions," Schiffstechnic, H.47, B.9, June 1962 and David Taylor Model Basin Report 1661, October 1962.

8. Korvin-Kroukovsky, B. V. and Lewis, E. V., "Ship Motions in Regular and Irregular Seas," Technical Memorandum No. 106, July 1954, Experimental Towing Tank, Stevens Institute of Technology.

9. Korvin-Kroukovsky, B. V., "Investigation of Ship Motions in Regular Waves," Transactions of SNAME, Vol. 63, 1955, pp. 386-435.

10. Korvin-Kroukovsky, B. V., and Jacobs, W. R., "Pitching and Heaving Motions of a Ship in Regular Waves," Transactions SNAME, Vol. 65, 1957, pp. 590-632.

11. Kaplan, P., "Application of Slender-Body Theory to Forces Acting on Submerged Bodies and Surface Ships in Regular Waves," Jour. of Ship Research, Vol. 1, No. 3, November 1957, pp. 40-49.

12. Abkowitz, M. A., "The Linearized Equations of Motion for the Pitching and Heaving of Ships," Proceedings, Symposium on the Behavior of Ships in a Seaway, Netherlands Ship Model Basin, Wageningen, 1957, pp. 178-189 and 883.

13. Fay, J. A., "The Motions and Internal Reactions of a Vessel in Regular Waves," Jour. of Ship Research, Vol. 1, No. 4, March 1958, pp. 5-13, 67.

14. Jacobs, W. R., "The Analytical Calculation of Ship Bending Moments in Regular Waves," Jour. of Ship Research, Vol. 2, No. 1, June 1958, pp. 20-29.

15. Korvin-Kroukovsky, B. V., "Theory of Ship Motions in Regular Head Seas," Notes of 4th Bi-Annual Seminar, Ship Behavior at Sea, Davidson Laboratory, Stevens Institute of Technology, January 1963, pp. 1-12.

16. Parissis, G., "The Effect of Hull Shape Non-Linearities on the Calculation of Heave and Pitch of a Ship," M.I.T., Department of Naval Architecture and Marine Engineering, Report No. 64-6, June, 1964 (to be published).

17. Kerwin, J. E., "Polynomial Surface Representation of Arbitrary Ship Forms," Jour. of Ship Research, Vol. 4, No. 1, June 1960.

18. Vossers, G., Swaan, W. A., and Rijken, H., "Experiments with Series 60 Models in Waves," Transactions of SNAME, Vol. 68, 1960, pp. 364-450.

19. Swaan, W. A. and Rijken, H., "Speed Loss at Sea as a Function of Longitudinal Weight Distribution," Transactions of NECIES, Vol. 79, 1962-63, pp. 165-188.

20. Lewis, E. V. and Numata, E., "Ship Motions in Oblique Seas," Transactions SNAME, Vol. 68, 1960, pp. 510-547.

21. Todd, F. A., "Some Further Experiments on Single Screw Ship Forms — Series 60," Transactions SNAME, Vol. 61, 1953, pp. 516-574.

22. Gerritsma, J., "An Experimental Analysis of Ship Motions in Longitudinal Regular Waves," International Shipbuilding Progress, Vol. 5, No. 52, December 1958, pp. 533-542.

23. Gerritsma, J., "Shipmotions in Longitudinal Waves," International Shipbuilding Progress," Vol. 7, No. 66, February 1960, pp. 49-76.

24. Mandel, P., "Subcritical and Supercritical Operation of Ships in Waves," Journal of Ship Research, Vol. 4, No. 1, June 1960.

25. "Nomenclature for Treating the Motions of a Submerged Body Through a Fluid," Bulletin No. 1-5, The Society of Naval Architects and Marine Engineers.

26. Abkowitz, M. A., "1963 Lecture Notes on Ship Hydrodynamics," Hydro-Og, Aerodynamisk Laboratorium, Lyngby, Copenhagen, Denmark (to be published).

27. Abkowitz, M. A., "The Dynamical Stability of Submarines," David Taylor Model Basin, 1949 (limited publication).

28. Ursell, F., "On the Heaving Motions of a Circular Cylinder on the Surface of a Fluid," Quarterly Journal of Mechanics and Applied Mathematics, Vol. 2, June 1949, pp. 218-231.

29. Grim, O., "Bereehnung der durch Schwingungen eines Schiffskorper erzeugten hydrodynamischen Krafte," Jahrbuch der Schiffbautechnischen Gessellschaft, 1953.

30. Korvin-Kroukovsky, B. V., "Brief Review of Ship Damping in Heaving and Pitching Oscillations," Stevens Institute of Technology, Experimental Towing Tank Note No. 328, February 1955.

31. Tasai, F., "On the Damping Force and Added Mass of Ships Heaving and Pitching," Univ. of California, Inst. of Eng. Research, Series No. 82, Issue No. 15, July 1960.

32. Porter, W., "Pressure Distributions, Added Mass, and Damping Coefficients for Cylinders Oscillating in a Free Surface," Univ. of California, Inst. of Eng. Research, Series No. 82, Issue No. 16, July 1960.

33. Kaplan, P. and Jacobs, W., "Two-Dimensional Damping Coefficients from Thin Ship Theory" and "Theoretical Motions of Two Yacht Models in Regular Head Seas on the Basis of Damping Coefficients Derived from Wide V-Forms," Davidson Laboratory Notes No. 586 and 593, June 1960.

34. Kaplan, P. and Kotik, J., "Report on a Seminar on the Hydrodynamic Theory Associated with Ship Motion in Waves," Technical Research Group, Report 140-FR.

35. Watson, T. C., "Experimental Investigation of the Vertical Forces Acting on Prolate Spheroids in Sinusoidal Heave Motion," Univ. of California, Inst. of Eng. Research, Series No. 82, Issue No. 18, April 1961.

36. Paulling, J. R. and Richardson, R. K., "Measurement of Pressures, Forces, and Radiating Waves for Cylinders Oscillating in a Free Surface," Univ. of Calif., Inst. of Eng. Research, Series No. 82, Issue No. 23, June 1962.

37. Golovato, P., "The Forces and Moments on a Heaving Surface Ship," Jour. of Ship Research, Vol. 1, No. 1, April 1957, pp. 19-26.

38. Gerritsma, J., "Experimental Determination of Damping Added Mass and Added Moment of Inertia of a Shipmodel," Inter. Shipbuilding Progress, Vol. 4, No. 38, October 1957, pp. 505-519.

39. Gerritsma, J. and Beukelman, W., "Distribution of Damping and Added Mass Along the Length of a Shipmodel," Report No. 49S, Netherlands Research Centre T.N.O. for Shipbuilding and Navigation, March 1963.

40. Newman, J. N., "The Damping of an Oscillating Ellipsoid Near a Free Surface," Jour. of Ship Research, Vol. 5, No. 3, December 1961, p. 44.

41. Grim, O., "A Method for a More Precise Computation of Heaving and Pitching Motions in Both Smooth Water and in Waves," Proc. of Third Symposium on Naval Hydrodynamics, Office of Naval Research, Dept. of the Navy, ACR-55, 1960, pp. 483-524.

42. Prohaska, C. W., "Vibration Verticales de Navire," Assoc. Technique Maritime et Aeronautique, Vol. 46, 1947, pp. 171-219.

43. Landweber, L. and Macagno, M., "Added Mass of a Rigid Prolate Spheroid Oscillating Horizontally in a Free Surface," Jour. of Ship Research, Vol. 3, No. 4, March 1960, pp. 30-36.

44. Paulling, J. R. and Porter, W. R., "Analysis and Measurement of Pressure and Force on Heaving Cylinders in a Free Surface," Proc. of the Fourth U.S. National Congress of Applied Mechanics, 1962, p. 1369.

45. Plant, J. B., "An Application of Linear Programming to the Problem of Inverting a Conformal Transformation," M.I.T., Department of Naval Architecture and Marine Engineering, January 1964 (unpublished document).

46. Havelock, T. H., "Notes on the Theory of Heaving and Pitching," Transaction of Institution of Naval Architects, Vol. 87, 1945, p. 109.

47. Vossers, G., "Resistance, Propulsion and Steering of Ships - Part IIC - Behavior of Ships in Waves," The Technical Publishing Company, H. Stam N.V., Haarlem, The Netherlands, 1962.

48. Jinnaka, T., "Some Experiments on the Exciting Forces of Waves on the Fixed Ship Model," J. Zosen Kiokai, Vol. 103, 1958, pp. 47-57.

49. Schultz, F. H., Forces and Moments on a Restrained Model in Regular Waves," Colorado State Univ., Research Foundation, Report CER 61 EFS72, March 1961.

50. Gersten, A., "A Comparison of Experimental and Theoretical Forces and Moments Acting on a Restrained Surface Ship in Regular Waves," Jour. of Ship Research, Vol. 6, No. 4, April 1963.

51. Lee, C. M., "Heaving Forces and Pitching Moments on a Semisubmerged and Restrained Prolate Spheroid Proceeding in Regular Head Waves," Inst. of Engineering Research, Univ. of California, Report No. NA-64-2, Contract Nonr-222(93), January 1964.

52. Grim, O., "The Deformation of Regular Head and Following Waves by a Moving Ship," Stevens Institute of Technology, Davidson Laboratory, Technical Translation by P. G. Spens and A. Winzer, November 1963.

53. Spens, G. P., "Experimental Measurements of the Deformation of Regular Head and Following Seas by a Ship Model," Stevens Institute of Technology, Davidson Laboratory Report No. 966, June 1963.

54. Newman, J. N., "The Exciting Forces on Fixed Bodies in Waves," Jour. of Ship Research, Vol. 6, No. 3, December 1962.

55. Grim, O., "The Influence of the Main Parameters of the Ship Form on the Heaving and Pitching Motions in Waves," Hamburg Model Basin, H.S.V.A., Report No. 1253, September 1961.

* * *

DISCUSSION

Winnifred R. Jacobs
Stevens Institute of Technology
Hoboken, New Jersey

I am belatedly aware of your criticism of the Korvin-Kroukovsky linear theory of ship motions. I wasn't at Bergen and therefore missed your presentation and Dr. Kaplan's defense as well as the counter-attacks.

Since I am equally responsible for what you consider erroneous in the analysis, I should like to discuss your paper with you, in particular two statements which, I believe, epitomize your criticism. (I hope I am correct in not considering as criticism the paragraph which states the fact that certain added mass and damping coefficients were used in one study, while different coefficients were used in other studies at Davidson Laboratory. Professor Korvin and, indeed, everyone involved in this work at Davidson Laboratory have repeatedly said that when more suitable hydrodynamic coefficients are available, they will be used.)

In one instance you say "Table 2 shows that the expressions for four of the newly proposed coefficients do not agree with those derived by Korvin-Kroukovsky. The differences in the Korvin-Kroukovsky coefficients $e(\omega_e)$, $B(\omega_e)$, C and $E(\omega_e)$ appear to be mainly due to an erroneous time differentiation of a fixed body coordinate with the result that

a. a factor of 2 appears in the velocity dependent terms of $e(\omega_e)$ and $B(\omega_e)$, and

b. a pseudo-three-dimensional term is introduced in coefficients $e(\omega_e)$, $B(\omega_e)$, C and $E(\omega_e)$.

"It would also appear that the introduction of terms dependent on the rate of change of added mass over the ship length is inconsistent with the use of two-dimensional theory. Despite these discrepancies, however, it is expected that the final values of these coefficients will not be seriously modified since it has been shown by Jacobs et al [5] that most of these terms which appear in the Korvin-Kroukovsky approach but not in the new approach are numerically small. It is hoped that in the near future these inconsistencies will be examined more carefully and their implications assessed on the basis of experimental data."

Several pages later you say "...In our notation, the formula [for the excitation force] as given by Jacobs [5] and as used in the existing computer program [at M.I.T.], reads as follows:

$$\frac{dZ_e}{dx} = \left\{\rho g B(x)\ h(x,t) + \left[N(x) - u_0 \frac{d\mu(x)}{dx}\right] \dot{h}(x,t) + \mu(x)\ \ddot{h}(x,t)\right\}$$

$$\times \exp\left[-\frac{2\pi}{\lambda}\sigma(x)\ H(x)\right] . \tag{40}$$

Equation (40) differs from (37) [the new approach] in that the wave velocity term includes an extra pseudo-three-dimensional term which is furthermore speed dependent. The contribution of the latter term is small in comparison with the other terms and predicts a decrease of the exciting force and moment, a finding which, as discussed by Vossers [47], contradicts that of Hanaoka. It is contended that the more rationally derived Eq. (37) will give almost similar results as Eq. (40) but this remains to be verified."

I should like to take up a few points.

1. It appears to me that this criticism boils down to one ingredient: we differentiated a "fixed" coordinate ξ with respect to time and hence inevitably the "fixed" radius r of the circular section associated with ξ. The latter derivative

$$\frac{dr}{dt} = \frac{dr}{d\xi}\frac{d\xi}{dt} = -V\frac{dr}{d\xi}$$

would then give terms, dependent on a rate of change of r (and hence of added mass) over the ship length, and also speed-dependent.

In our approach, the ξ-axis fixed in the ship is time-dependent with respect to the wave. Our strip method treated each ship section strip as if fixed in a frame of an animated cartoon with the strips changing from frame to frame and the frames changing from time to time.

In support of your contention that our approach is incorrect, you cite the work of Professor Fay among others. May I quote Professor Fay's discussion of Korvin-Kroukovsky's 1955 SNA paper? In that paper the forces due to body motions are developed through the following equations:

The potential

$$\varphi_{bm} = (V\theta - \dot{z} - \xi\dot{\theta})\, r \cos\alpha \tag{37}$$

and since

$$\frac{dr}{dt} = V \tan\beta \quad \text{and} \quad \frac{d\xi}{dt} = V\,,$$

the pressure

$$\frac{p}{\rho} = \frac{\partial\varphi}{\partial t} = \cos\alpha\,(\dot{\theta}Vr + \theta V^2 \tan\beta - \ddot{z}r - \dot{z}V\tan\beta - \dot{\theta}Vr - \xi\ddot{\theta}r - \dot{\theta}\xi V \tan\beta)\,. \tag{38}$$

The vertical force increment per unit length

$$\frac{dF}{dx} = 2r\int_0^{\pi/2} p\cos\alpha\, d\alpha$$

becomes

$$\frac{dF}{dx} = \left(\rho\frac{\pi}{2}r^2V\right)\dot{\theta} + \left(\rho\frac{\pi}{2}rV^2\tan\beta\right)\theta - \left(\rho\frac{\pi}{2}r^2\right)\ddot{z}$$

$$- \left(\rho\frac{\pi}{2}rV\tan\beta\right)\dot{z} - \left(\rho\frac{\pi}{2}r^2V\right)\dot{\theta} - \left(\rho\frac{\pi}{2}r^2\xi\right)\ddot{\theta} - \left(\rho\frac{\pi}{2}r\xi V\tan\beta\right)\dot{\theta}\,. \tag{39}$$

Professor Fay said: "If θ is positive when measured clockwise, z is positive in the downward direction, and V positive for motion in the positive x-direction then Eq. (37) is correctly stated. However, $d\xi/dt$ should equal $-V$, and terms (1) and (5) in (39) do not cancel but add. This term is the most important coupling term in the equations of motions and exists even for a symmetrical vessel." He also commented, with regard to the terms in dr/dt, that, since the method is a linear approximation, "the carrying of terms of higher order in subsequent equations does not seem justified."

In the 1957 SNA paper by Korvin-Kroukovsky and myself, we corrected the sign of V, and reinstated the velocity-dependent terms, which had been omitted in the 1955 paper on the assumption that these terms in the potential theory development merely implied damping and could be replaced by damping terms determined on the basis of energy dissipation by waves, as a quid pro quo. A study of Haskind (1946) and Havelock (1955) confirmed what Fay had said in his discussion about the coupling terms. The Korvin-Kroukovsky approach now has values for the coefficients $e(\omega_e)$ and $E(\omega_e)$, as shown in your Table 2, which contain the identical dynamic coupling terms derived by Havelock for a long half-immersed spheroid and by Haskind for a thin "Michell" ship.

2. This brings me to the second point I wish to raise. Why is

$$u_o \int \frac{d\mu(x)}{dx}\, x\, dx\,,$$

"pseudo-three-dimensional," whereas its equivalent $-u_o \int \mu(x)\,dx$ is not?

As shown in our 1957 SNA paper, if one integrates by parts

$$\int_L \frac{d\mu(x)}{dx}\, x\, dx = \int_L x\, d\mu(x) = -\int_L \mu(x)\, dx$$

and therefore

$$e(\omega_e) = -\int N(x)\, x\, dx + 2u_o \int \mu(x)\, dx + u_o \int \frac{d\mu(x)}{dx}\, x\, dx$$

$$= -\int N(x)\, x\, dx + u_o \int \mu(x)\, dx$$

which is equivalent to the value of $e(\omega_e)$ in your "new approach," as well as to Havelock's and Haskind's coefficient of θ in the heaving force equation.

In the Korvin-Kroukovsky approach, the coefficient of $\dot{z}$ in the pitching moment equation is

$$E(\omega_e) = -\int N(x)\, x\, dx + u_o \int \frac{d\mu(x)}{dx}\, x\, dx$$

$$= -\int N(x)\, x\, dx - u_o \int \mu(x)\, dx$$

the second term of which is missing in your "new approach," but is present in Havelock's and in Haskind's developments. Similarly, it can be shown that the Korvin-Kroukovsky coefficients $B(\omega_e)$ and C, after integrating by parts, become

$$B(\omega_e) = \int N(x)\, x^2\, dx - 2u_o \int \mu(x)\, x\, dx - u_o \int \frac{d\mu(x)}{dx}\, x^2\, dx$$

$$= \int N(x)\, x^2\, dx$$

$$C = \rho g \int B(x)\, x^2\, dx - u_o \int N(x)\, x\, dx + u_o^2 \int \frac{d\mu(x)}{dx}\, x\, dx$$

$$= \rho g \int B(x)\, x^2\, dx - u_o \int N(x)\, x\, dx - u_o^2 \int \mu(x)\, dx\,.$$

These are the three coefficients which are different from yours. The difference is negligible in the case of $B(\omega_e)$ and small in the case of C. However, the second term of E is of the same order of magnitude as the first term.

The reason for not substituting

$$-\int \mu(x)\,dx \quad \text{for} \int \frac{d\mu(x)}{dx}\,x\,dx$$

in our definitions of the coefficients is that the unit force and moment coefficients are required in the computations of bending moments.

3. You criticize the Jacobs formula for unit exciting force, given in your Eq. (40), because the coefficient of the damping component contains, in addition to $N(x)$, a term

$$-u_o \frac{d\mu(x)}{dx}$$

a "pseudo-three-dimensional" term which predicts a decrease of the exciting force and moment as forward speed u_o increases, whereas Hanaoka's calculations, as shown in Vossers' articles, predict an increase. This criticism would be valid only if the damping coefficient $N(x)$ were invariable with forward speed. However, $N(x)$ is a function of speed through its dependence on frequency of encounter, and itself contributes to the decrease in exciting force with speed. As you say, the contribution of the disputed term is small and your Eq. (37) which omits this term "will give almost similar results as Eq. (40) but this remains to be verified."

4. But why not verify it? Since the computer program at M.I.T. follows the computational procedure of Davidson Laboratory Report 791, it should be quite easy to drop the offending terms and test your new approach.

If the Korvin-Kroukovsky approach is devoid of vitality, why keep flogging a dead horse?

* * *

DISCUSSION

Martin A. Abkowitz
Massachusetts Institute of Technology
Cambridge, Massachusetts

I should like to discuss specifically the nature of the various coefficients in the coupled linearized equations of motion for pitch and heave as tabulated in Table 2 of the paper.

In the column headed "Coefficient" are the coefficients of the linear terms of each of the motion variables. On the left side of this column, the coefficients are merely expressed arbitrarily as letters in alphabetical sequence. On the right-hand side of this column, the coefficients are expressed in the nomenclature of Bulletin 1-5 of The Society of Naval Architects and Marine Engineers, which system is developed with reference to axes fixed in the ship, which provides the advantage of centerline plane symmetry in any hydrodynamic calculations. The appearance of double terms in the right-hand part of the column, arises from the rigorous treatment of transferring from axes oriented in the ship to axes (specifically heave) oriented relative to fixed space. The linear coefficients in this form are valid independent of any method one wishes to determine them — whether theoretically by strip theory, slender body theory, thin ship theory or by model experiments.

Under the column designated "New Approach" is listed the formulation for calculating these coefficients by a "pure strip theory" — i.e., each section treated as a cylindrical section and completely independent of the shape of other ship sections. Since the terms are calculated by integrals over the various ship sections, in a geometry fixed in the ship, the forward speed effect on some of the coefficients very neatly falls in place, such as in the terms

$$-u_o Z_{\dot{w}} = u_o \int \mu(x)\,dx$$

since by strip method

$$-Z_{\dot{w}} = \int \mu(x)\,dx\,.$$

$$-u_o Z_w = u_o \int N(x)\,dx$$

since by strip method

$$-Z_w = \int N(x)\,dx\,.$$

In the column headed "Korvin-Kroukovsky Approach" are listed formulations as attributed to the strip theory of Korvin-Kroukovsky. Perhaps a great deal of difficulty and confusion results from semantics in that what is often referred to as Korvin-Kroukovsky strip theory is in reality not a pure strip theory, but a rather crude slender body theory which takes into account three-dimensional effects in a rather rough way. Nevertheless, because of the physical realities of the situation, any method of calculation of the coefficients should be consistent with the terms listed in the right-hand side of the coefficient column. Hence, the Korvin-Kroukovsky terms given below in the coefficient $e(\omega_e)$ should reduce to $-u_o Z_{\dot{w}}$ (or $u_o \int \mu(x)\,dx$)

$$2u_o \int \mu(x)\,dx + u_o \int \frac{d\mu}{dx}(x)\,x\,dx \to u_o \int \mu(x)\,dx\,.$$

It has been indicated by others, that integrating the expression on the left by parts will reduce it to the right-hand expression provided the sectional area curve goes to zero (continuously) at the ship ends. Since this is a requirement of slender body theory, the left-hand terms can be written in the simpler form of the right-hand term. Similarly, it can be shown that the two terms under the Korvin Approach for Coefficient "B", and indicated by the dotted block in the attached figure, reduce to the one term, indicated by the dotted block under "New Approach." Some ships, such as those with transom sterns, need not have sectional area curves which are zero at the stern end, hence the possibility of an error in Korvin Approach for this hull shape. On the other hand the Korvin Approach gives a distribution of the effect along the length, which is desirable when bending moments are being considered.

There are only two additional coefficients in the tabulations which take different forms under "New Approach" and "Korvin Approach"—these are coefficients C and E. For coefficient E, (or $-M_w$), the Korvin approach has the additional term

$$u_o \int \frac{d\mu(x)}{dx}\, x\, dx$$

as compared to the "New Approach" and this term reduces to $-u_o \int \mu(x)\, dx$ or $u_o Z_{\dot{w}}$. Since the Korvin approach is a slender-body theory involving some pseudo three-dimensional effects, it will be shown below that this additional term can result from three-dimensional considerations. As introduced by Korvin, coefficient b (or $-Z_w$) is expressed by $\int N(x)\, dx$ which is purely a frequency dependent effect (surface wave effect) since in potential theory, for a deeply submerged body b (or Z_w), would be zero—i.e., no lift force with angle of attack in the absence of circulation. Hence, in the attached table the term zero has been added to indicate the addition of a three-dimensional potential solution. If we include in the pure strip approach or "New Approach" column, the other three-dimensional potential solutions in the appropriate terms, the following terms are added to the expressions in the "New Approach" column:

Coefficient	Additional Term for Three-Dimensional Solution
e	$-X_{\dot{u}}\, u_o$
E	$u_o(Z_{\dot{w}} - X_{\dot{u}})$
C	$u_o^2\,(Z_{\dot{w}} - X_{\dot{u}})$

where $-X_{\dot{u}}$ is the added mass for longitudinal acceleration.

These additional terms appear in the attached table as encircled by a dotted line. The $Z_{\dot{w}}$ terms are equivalent to the terms enclosed by dotted rectangles under the Korvin approach. However, we now find terms in $X_{\dot{u}}$ in the "New Approach" brought about by the rough three-dimensional correction based on the results of potential theory calculation. Since $X_{\dot{u}}$ can be estimated for a given

Table 2
Comparison of Coefficients of Equations of Motion

Coefficient		New Approach	Korvin-Kroukovsky Approach
$a(\omega_e)$	$m - Z_{\dot{w}}$	$m \boxed{+ \int \mu(x)\,dx}$ *	same
$b(\omega_e)$	$- Z_w$	$\int N(x)\,dx + \boxed{0}$	same
c	$- Z_{z_o}$	$\rho g \int B(x)\,dx$	same
$d(\omega_e)$	$- Z_{\dot{q}}$	$- \int \mu(x)\,x\,dx$	same
$e(\omega_e)$	$-(Z_q + u_o Z_{\dot{w}})$	$- \int N(x)\,x\,dx + \boxed{u_o \int \mu(x)\,dx}\ \boxed{- X_{\dot{u}} u_o}$	$- \int N(x)\,x\,dx \boxed{+ 2u_o \int \mu(x)\,dx + u_o \int \frac{d\mu(x)}{dx}\,x\,dx}$
f	$-(Z_\theta + u_o Z_w)$	$- \rho g \int B(x)\,x\,dx + u_o \int N(x)\,dx$	same
$A(\omega_e)$	$I_y - M_{\dot{q}}$	$I_y + \int \mu(x)\,x^2\,dx$	same
$B(\omega_e)$	$-(M_q + u_o M_{\dot{w}})$	$\int N(x)\,x^2 dx \boxed{- u_o \int \mu(x)\,x\,dx}$	$\int N(x)\,x^2 dx \boxed{- 2u_o \int \mu(x)\,x\,dx - u_o \int \frac{d\mu(x)}{dx}\,x^2 dx}$
C	$-(M_\theta + u_o M_w)$	$\rho g \int B(x)\,x^2\,dx - u_o \int N(x)\,x\,dx \boxed{+ u_o^2 (Z_{\dot{w}} - X_{\dot{u}})}$	$\rho g \int B(x)\,x^2\,dx - u_o \int N(x)\,x\,dx + \boxed{u_o^2 \int \frac{d\mu(x)}{dx}\,x\,dx}$
$D(\omega_e)$	$- M_{\dot{w}}$	$- \int \mu(x)\,x\,dx$	same
$E(\omega_e)$	$- M_w$	$- \int N(x)\,x\,dx + \boxed{u_o (Z_{\dot{w}} - X_{\dot{u}})}$	$- \int N(x)\,x\,dx + \boxed{u_o \int \frac{d\mu(x)}{dx}\,x\,dx}$
F	$- M_{z_o}$	$- \rho g \int B(x)\,x\,dx$	same

*For brevity $\mu(x) = k_2 k_4 \frac{\rho B^2(x)}{8}$.

hull shape, using the "New Approach" with the additional three-dimensional terms should be more realistic than the Korvin approach. Physically, the slender body assumption assumes such a large length-beam or length-diameter ratio that forward effects are neglected. The new approach corrected as indicated above, would hold better for the fuller ships. As an extreme, the deeply submerged sphere should have a coefficient E (or $-M_w$) equal to zero; the corrected new approach would give zero for this case, whereas the Korvin slender body approach gives a relatively large quantity. (Of course a sphere significantly violates the slender body assumption.)

It should be pointed out that the corrected coefficients, listed under "New Approach" in the attached figure, have the symmetry required by the Timman-Newman analysis, i.e., $d = D$, $e = E$.

* * *

DISCUSSION

O. Grim
University of Hamburg
Hamburg, Germany

Coefficients for added mass and damping force for some sections are shown in the paper. They are computed using Porter's and my own method. The results found by both methods are compared and discrepancies have been ascertained. However, these discrepancies appear not disturbing to me. The reason is very simple. The computer program used for my method was not designed for such a wide range of frequencies but only for the range important for the motions in a seaway. In the meantime the program has been supplemented which is valid for any arbitrary frequency and consequently the discrepancies have vanished.

* * *

DISCUSSION

William R. Porter
Massachusetts Institute of Technology
Cambridge, Massachusetts

These comments will be relative to the calculation of added-mass and damping coefficients for two-dimensional cylinders. The numerical results for all elliptic cylinders and for Models 2, 3, and 4, obtained by the procedures used by the authors and attributed to Grim should agree with my results, because all these forms can be uniquely defined by their beam/draft ratio and area coefficient. Professoı Grim has privately supplied to the original authors his values calculated by a different program, and my work is in much closer agreement with these later results.

Model 5, however, cannot be defined by its beam/draft ratio and section area coefficient alone. Therefore, calculations which define the cylinders by only these two parameters will not agree with more correct predictions. This is illustrated by the following figures.

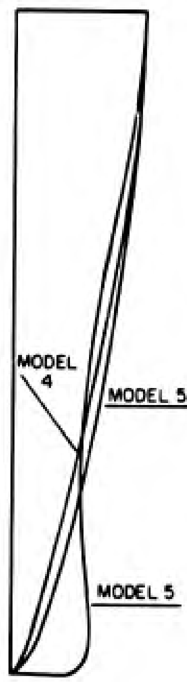

Fig. 1 - Three shipform cylinders with the same beam/draft ratio; Models 5 and 5G have the same area coefficients; Model 5G is a Lewis form similar to Model 4 but slightly more full

Figure 1 shows sections of three cylinders with the same beam/draft ratio. These are Model 4, Model 5, and a Model 5G which has the same area coefficient as Model 5. Model 5G can be described by its beam/draft ratio alone, Model 5 cannot.

Figure 2 shows values of the waveheight ratio A for these three cylinders. The values attributed to Grim are taken from his values as subsequently reported to the authors. The results of Grim and my results show only small differences for Model 4. The results do not agree for Model 5; however, it is clear that my results for Model 5G would agree with Grim's Model 5 to small differences. The difference between my values for Models 5 and 5G is due to the different vertical distribution of area. This difference is not one in theory alone as shown by the results of experiments with Models 4 and 5 as reported by Paulling and Porter in Ref. [44] or in Ref. [36] of the original paper. The conclusion is that two parameters alone are not sufficient to define the cylinder geometry.

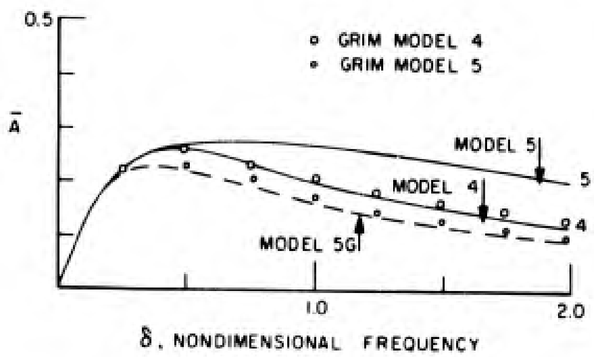

Fig. 2 - Waveheight ratio A for Models 4, 5, and 5G

* * *

DISCUSSION A

THE INFLUENCE OF THE ADDED MASS FORMULATION UPON THE COMPUTER MOTION PREDICTIONS

Peter A. Gale
Bureau of Ships
Washington, D.C.

To this discusser's knowledge, the significant differences between the Bureau of Ships computer program and the author's Massachusetts Institute of Technology (M.I.T.) program as of January 1964, are: first, the Bureau of Ships program is based upon ten station spaces while the M.I.T. program is flexible in this respect and it is believed that twenty station spaces are commonly used; second, the Bureau of Ships computer program uses the Prohaska added mass coefficients with Ursell's free surface corrections as presented in Davidson Laboratory Report No. 791 while the M.I.T. program uses Grim's 1959 added mass coefficients. Both programs use Grim's 1959 damping coefficients.

In order to assess the influence of the added mass formulation upon the predicted ship motions, the motions of the DD 710 (this discusser's ship "A") were computed using both the Bureau of Ships program and the M.I.T. program with ten station spaces. The resulting motion predictions are plotted in Fig. 1 for a wave length to ship length ratio of 1.25. This figure gives an indication of the influence of the change in added mass formulation described above for a particular set of conditions. For other wave length to ship length ratios the influence was found to be of the same or a lesser order of magnitude.

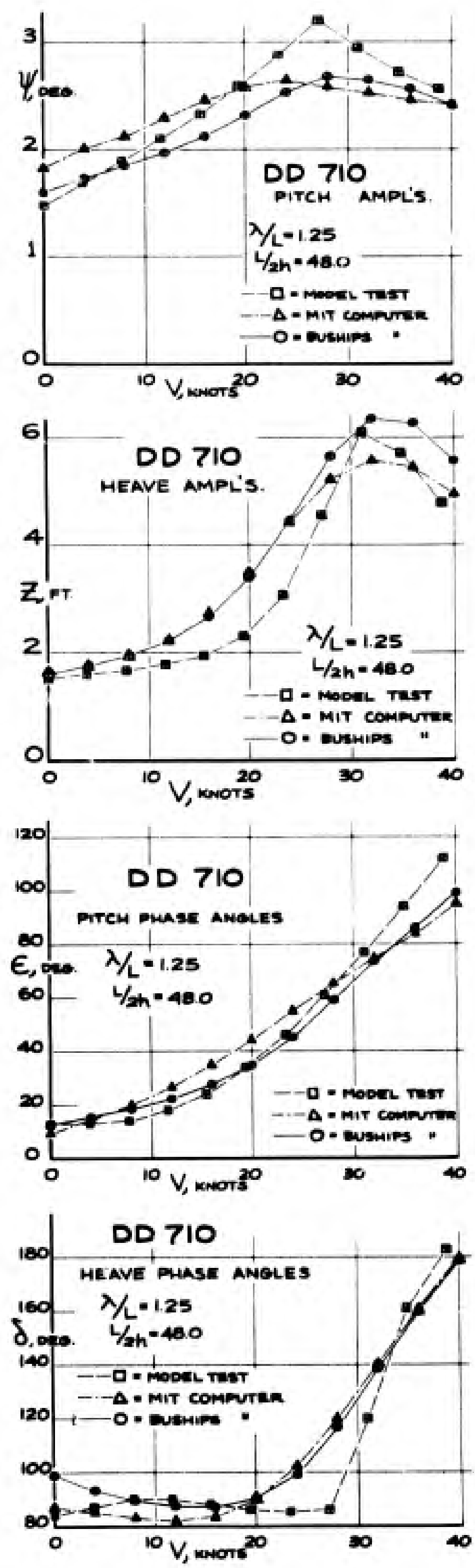
DD 710
PITCH AMPL'S.
λ/L = 1.25
L/2h = 48.0
□ = MODEL TEST
Δ = MIT COMPUTER
O = BUSHIPS "
ψ, DEG.
V, KNOTS
DD 710
HEAVE AMPL'S.
λ/L = 1.25
L/2h = 48.0
□ = MODEL TEST
Δ = MIT COMPUTER
O = BUSHIPS "
Z, FT.
V, KNOTS
DD 710
PITCH PHASE ANGLES
λ/L = 1.25
L/2h = 48.0
□ = MODEL TEST
Δ = MIT COMPUTER
O = BUSHIPS "
ε, DEG.
V, KNOTS
DD 710
HEAVE PHASE ANGLES
λ/L = 1.25
L/2h = 48.0
□ = MODEL TEST
Δ = MIT COMPUTER
O = BUSHIPS "
δ, DEG.
V, KNOTS

Figure 1

DISCUSSION B

THE PITCH AND HEAVE OF TEN SHIPS OF DESTROYER-PREDICTIONS COMPARED WITH MODEL TEST RESULTS

COMPUTER PREDICTIONS COMPARED WITH MODEL TEST RESULTS

Peter A. Gale
Bureau of Ships
Washington, D.C.

NOTES

1. Regular wave model test results were collected for ten destroyer-like ships. The data for five of the ships (F-K) were classified. By coincidence, model test phase angle results were not available for these same five ships. Due to the above, data sources, ship identifications and dimensions, body plans, and phase angle comparisons are not presented for ships F-K.

2. For ships, F and G the longitudinal gyradius of the model was not known. In order to use the computer to predict the motions of these two ships, κ_ψ was assumed to be 0.25L for both. These facts make the comparisons presented for ships F and G of dubious value.

3. The hull dimensions and coefficients presented in the Table of Ship Particulars are those used for the computer motion calculations. In general they also apply to the model test hull forms. In a few cases there are minor differences between the forms model tested and those used for the motion computations as, for example, when the model tested did not float on an even keel. Motion computations were always made for the even keel case.

4. In the graphs, the circles connected by lines represent the computer calculations. The model test results are represented by symbols other than circles. Ship K was model tested in regular waves of several heights and all of the test results are presented necessitating the use of a different ordinate than used for the other plots.

5. The following reports were the sources of the model test data for ships A-E.

a. For ships A and B:

"An Experimental Study of the Effect of Extreme Variations in Proportions and Form on Ship Model Behavior in Waves," by Numata and Lewis, ETT Report No. 643, December 1957.

b. For ships C, D, and E:

"The Influence of Shipform and Length on the Behavior of Destroyer-Type Ships in Head and Beam Seas," by Muntjewerf, International Shipbuilding Progress, Vol. 10, No. 102, February 1963.

6. The computer program used to calculate the ship motions presented here was written in the Bureau of Ships and is based upon a theoretical method developed by Korvin-Kroukovsky for computing the coupled pitch and heave of a surface ship in regular head waves. The step-by-step computational procedure followed by the computer is essentially that presented in Davidson Laboratory Report No. 791, "Guide to Computational Procedure for Analytical Evaluation of Ship Bending Moments in Regular Waves," by Jacobs, Dalzell, and Lalangas dated October 1960. The computer program uses the Prohaska added mass coefficients with Ursell's free surface corrections and Grim's 1959 damping coefficients, all published in D. L. Report No. 791. It is recognized that it would be more logical to use Grim's 1959 added mass and damping coefficients or perhaps even more recent data; this was not done for several practical reasons. The Bureau of Ships computer program divides the hull into ten station spaces for the computations. It has been found that the use of a greater number of station spaces has a negligible effect on the computed results.

NOMENCLATURE

ψ maximum single amplitude of pitching motion,

z maximum single amplitude of heaving motion of ship's center of gravity,

ϵ phase lead of maximum pitch up measured with respect to the instant when the wave node preceding the wave crest is at the ship's longitudinal center of gravity location,

δ phase lead of maximum heave up defined as for pitch phase angle above,

λ regular wave length,

L waterline length of ship,

h regular wave amplitude,

$2h$ regular wave height (twice wave amplitude),

K_ψ longitudinal radius of gyration of ship.

Table of Ship Particulars

	Ship									
	A	B	C	D	E	F	G	H	J	K
LWL (ft)	383.0	482.3	368.8	442.9	442.9					
B on WL (ft)	40.50	36.00	38.52	35.17	42.19					
H to WL (ft)	14.00	12.74	13.12	12.11	12.04					
Δ to WL LTSW	3393	3396	3017	3027	3041					
L/B	9.46	13.40	9.57	12.59	10.50	10.02	9.78	9.10	8.24	9.90
B/H	2.89	2.83	2.94	2.90	3.50	3.39	2.90	2.96	3.54	2.96
L/H	27.36	37.86	28.10	36.59	36.78	34.00	28.41	26.92	29.17	29.26
$\Delta/(0.01L)^3$	60.4	30.3	60.2	34.8	35.0	41.5	47.0	55.4	61.7	50.2
C_P	0.647	0.647	0.688	0.683	0.624	0.611	0.573	0.579	0.570	0.624
$C_{\boxtimes}$	0.845	0.845	0.822	0.823	0.759	0.800	0.785	0.792	0.910	0.813
C_b	0.547	0.547	0.565	0.563	0.473	0.489	0.450	0.459	0.519	0.507
C_w	0.770	0.770	0.805	0.805	0.791	0.745	0.716	0.725	0.717	0.771
LCG % L aft $\boxtimes$	2.04	2.45	1.23	1.32	1.41	1.70	2.42	1.50	0.88	0.64
$K\psi/L$	0.236	0.240	0.233	0.233	0.233	0.250*	0.250*	0.240	0.235	0.211
Identification:			Lengthened DD-710		Dutch Model B	Dutch Model D	Dutch Model E			

*Assumed value.

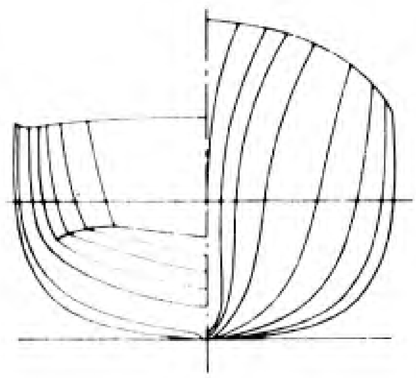

SHIP A

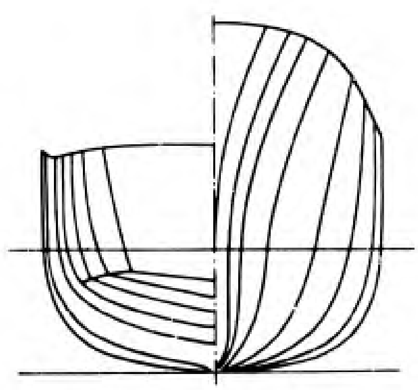

SHIP B

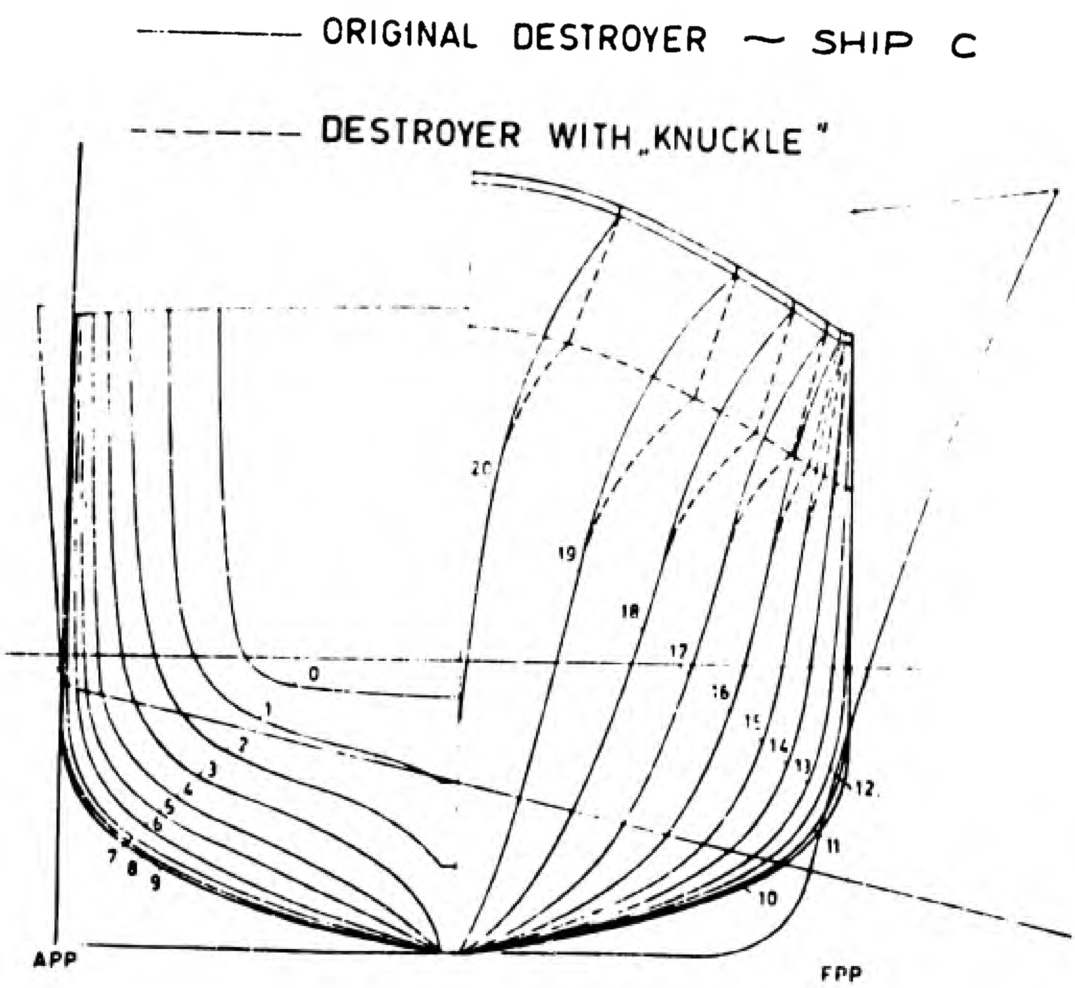
ORIGINAL DESTROYER ~ SHIP C
DESTROYER WITH „KNUCKLE"
0
1
2
3
4
5
6
7
8
9
10
11
12
13
14
15
16
17
18
19
20
APP
FPP

LENGTHENED DESTROYER ~ SHIP D

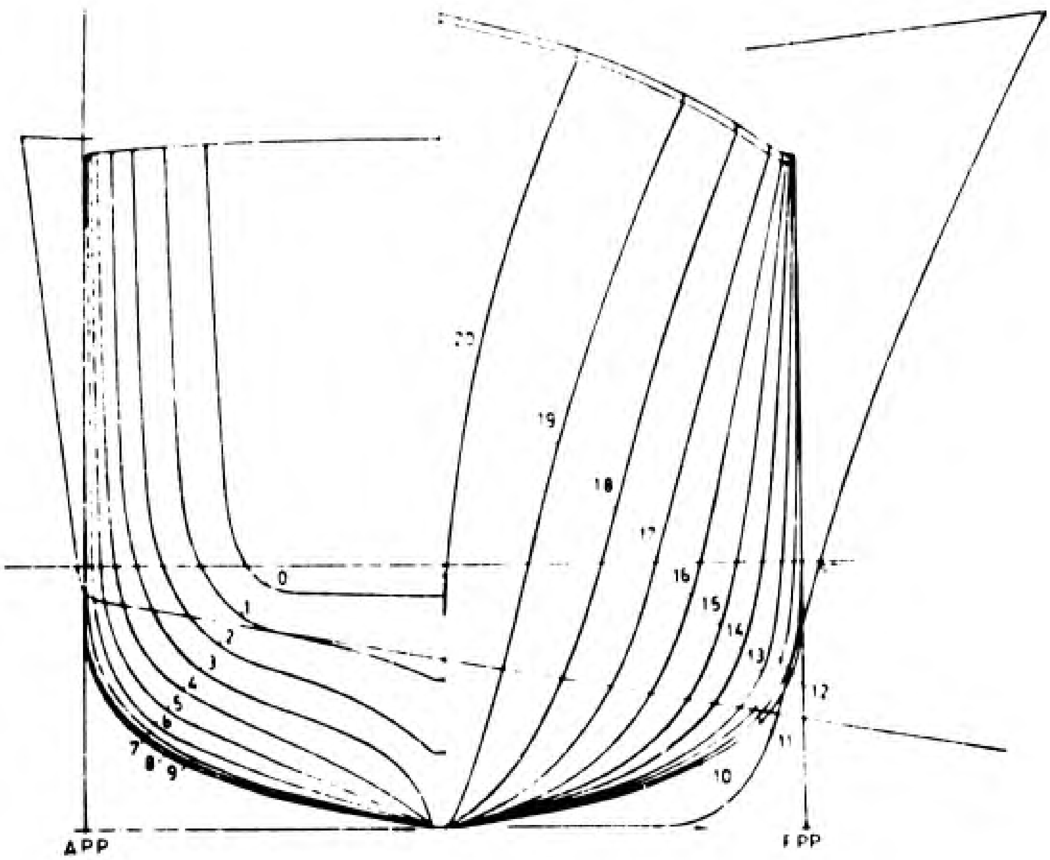

SHIP E
LENGTHENED DESTROYER WITH INCREASED BEAM

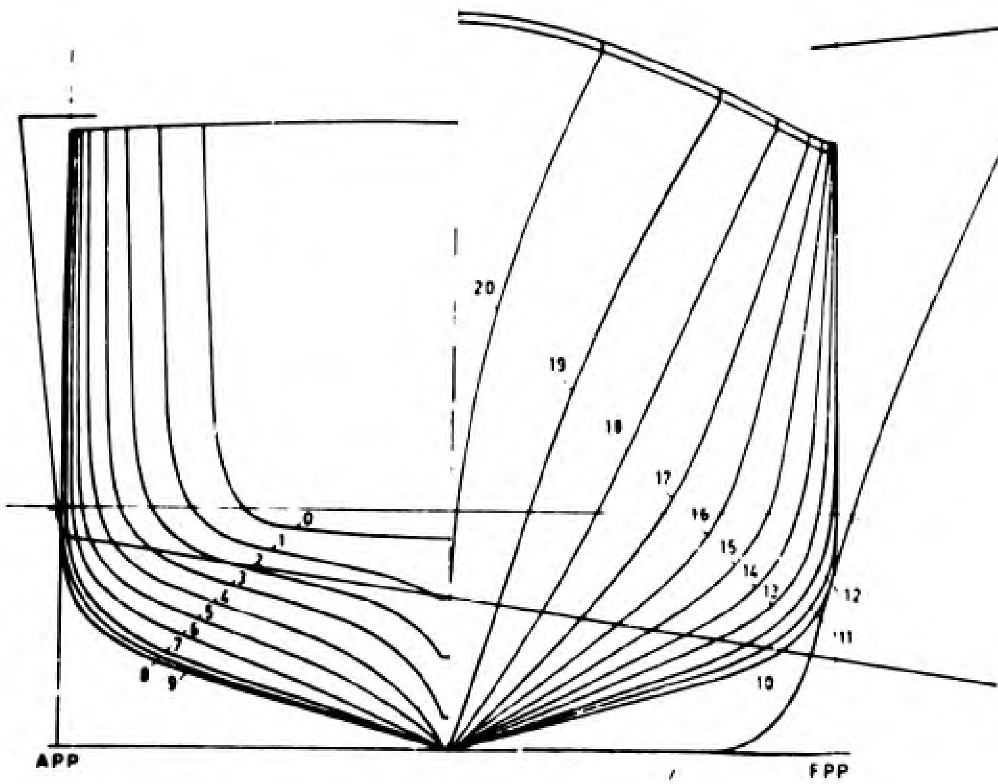

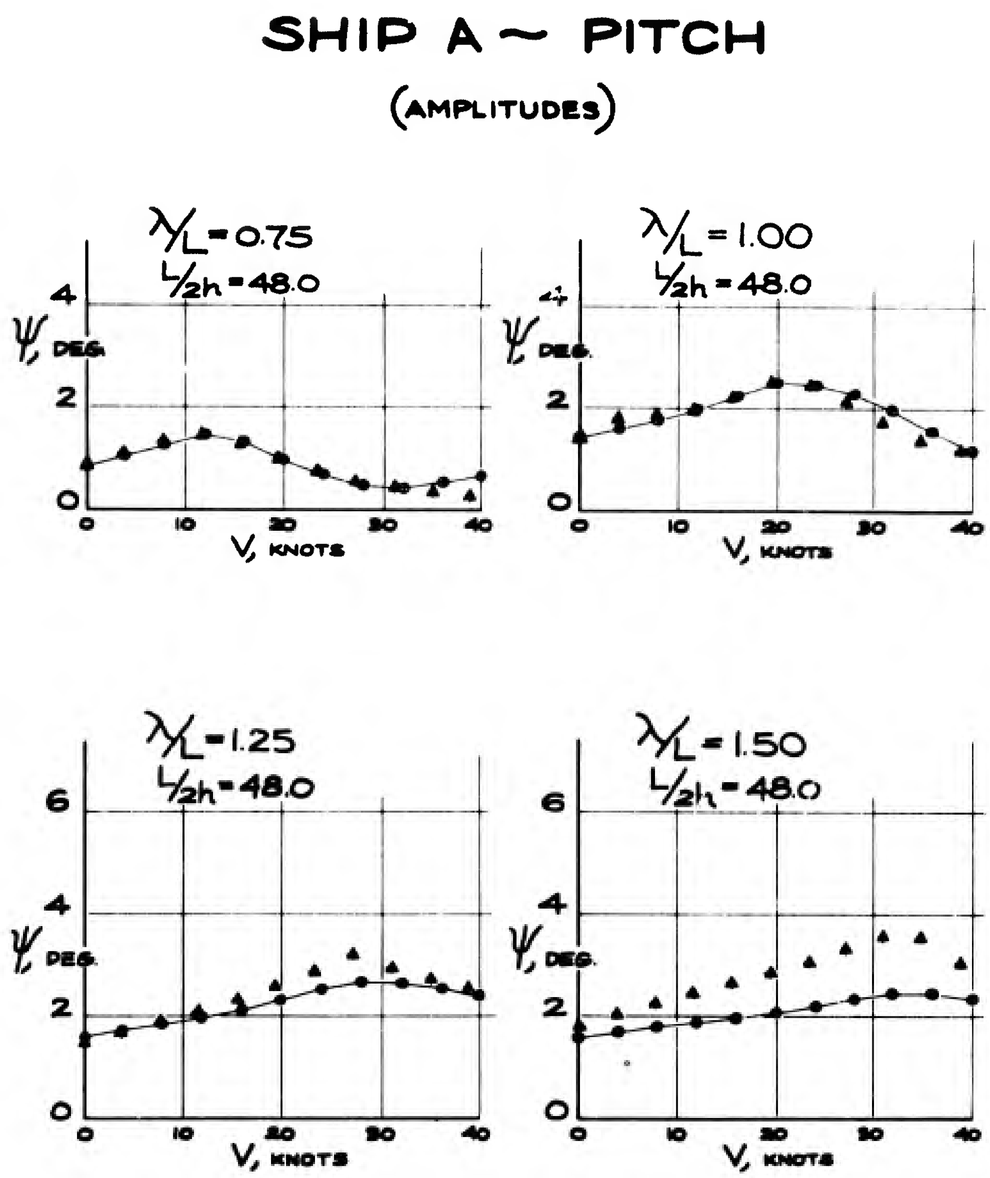
SHIP A ~ PITCH
(AMPLITUDES)
λ/L = 0.75
L/2h = 48.0
ψ, DEG.
V, KNOTS
λ/L = 1.00
L/2h = 48.0
ψ, DEG.
V, KNOTS
λ/L = 1.25
L/2h = 48.0
ψ, DEG.
V, KNOTS
λ/L = 1.50
L/2h = 48.0
ψ, DEG.
V, KNOTS

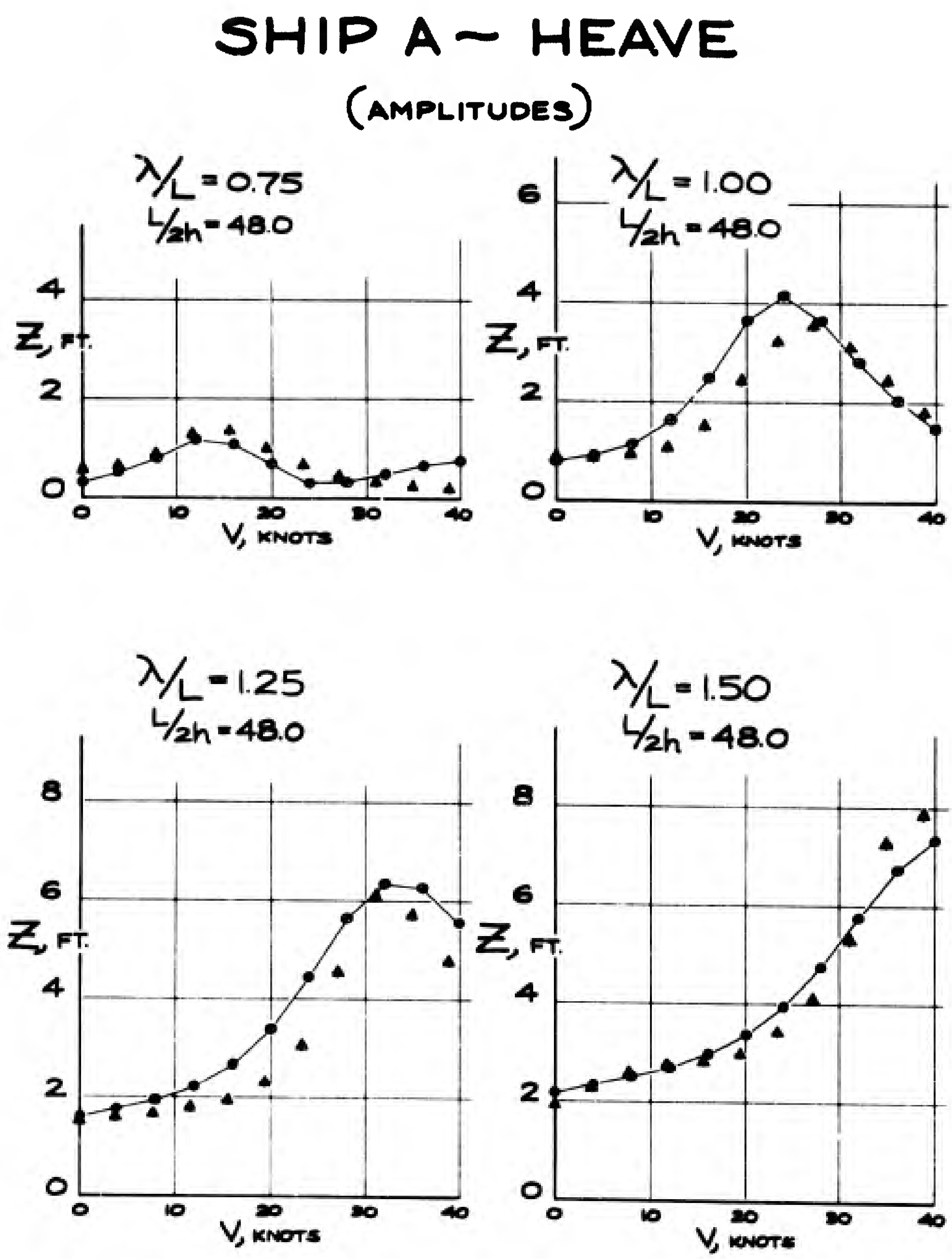
SHIP A ~ HEAVE
(AMPLITUDES)
λ/L = 0.75
L/2h = 48.0
λ/L = 1.00
L/2h = 48.0
λ/L = 1.25
L/2h = 48.0
λ/L = 1.50
L/2h = 48.0
Z, FT.
V, KNOTS
0
2
4
6
8
10
20
30
40

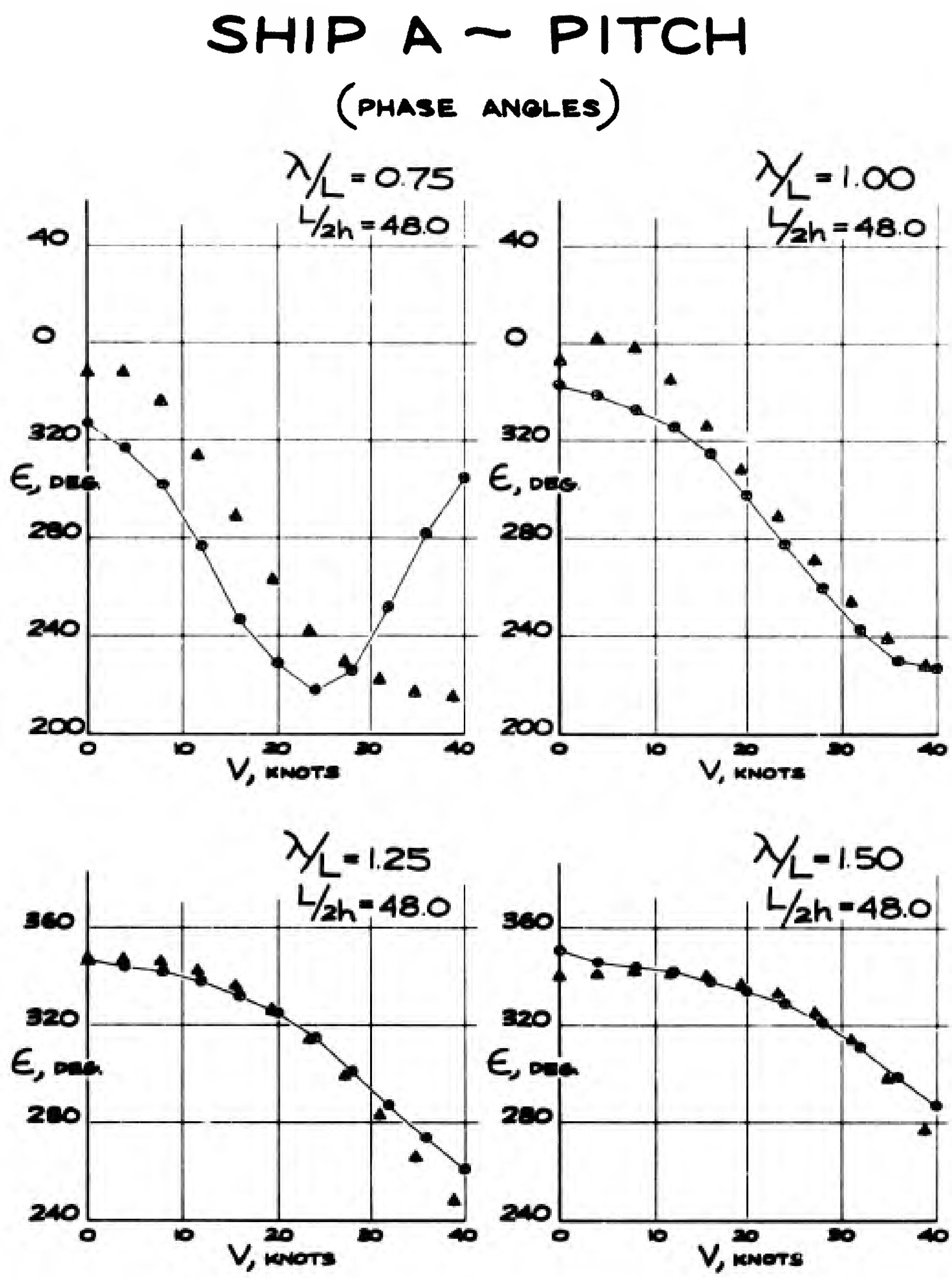
SHIP A ~ PITCH
(PHASE ANGLES)
λ/L = 0.75
L/2h = 48.0
λ/L = 1.00
L/2h = 48.0
λ/L = 1.25
L/2h = 48.0
λ/L = 1.50
L/2h = 48.0
ε, DEG.
V, KNOTS
40
0
320
280
240
200
360
0
10
20
30
40

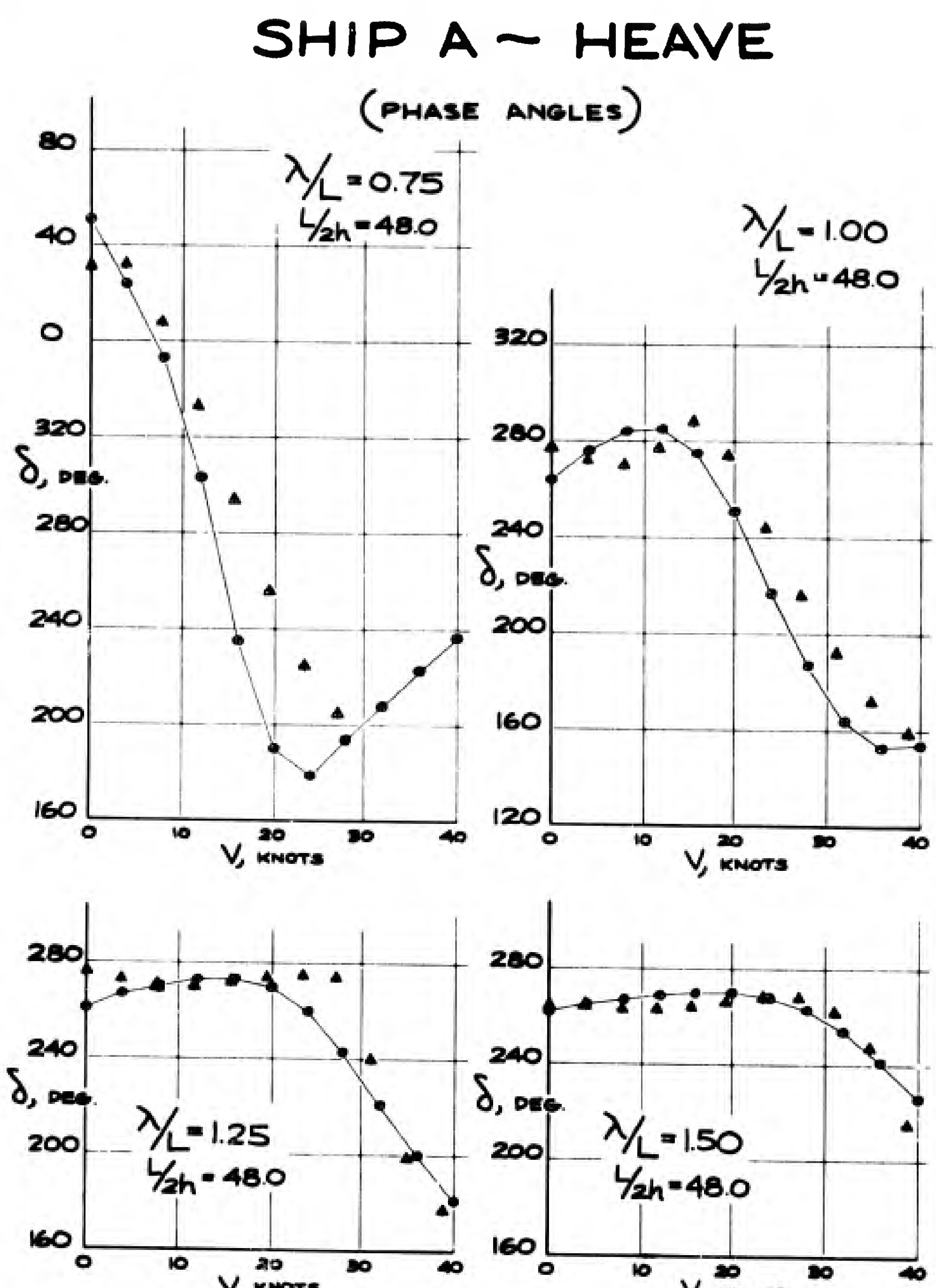
SHIP A ~ HEAVE
(PHASE ANGLES)
λ/L = 0.75
L/2h = 48.0
λ/L = 1.00
L/2h = 48.0
λ/L = 1.25
L/2h = 48.0
λ/L = 1.50
L/2h = 48.0
δ, DEG.
V, KNOTS
80
40
0
320
280
240
200
160
120
0
10
20
30
40

SHIP B ~ PITCH

(AMPLITUDES)

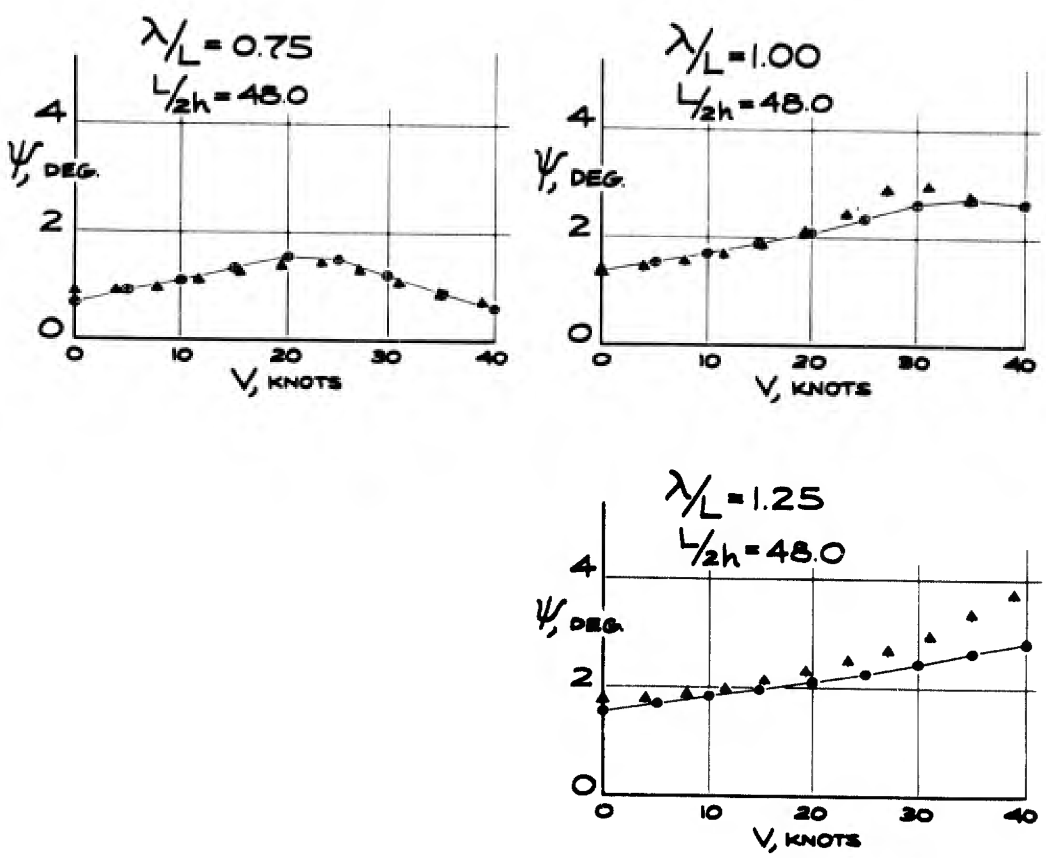

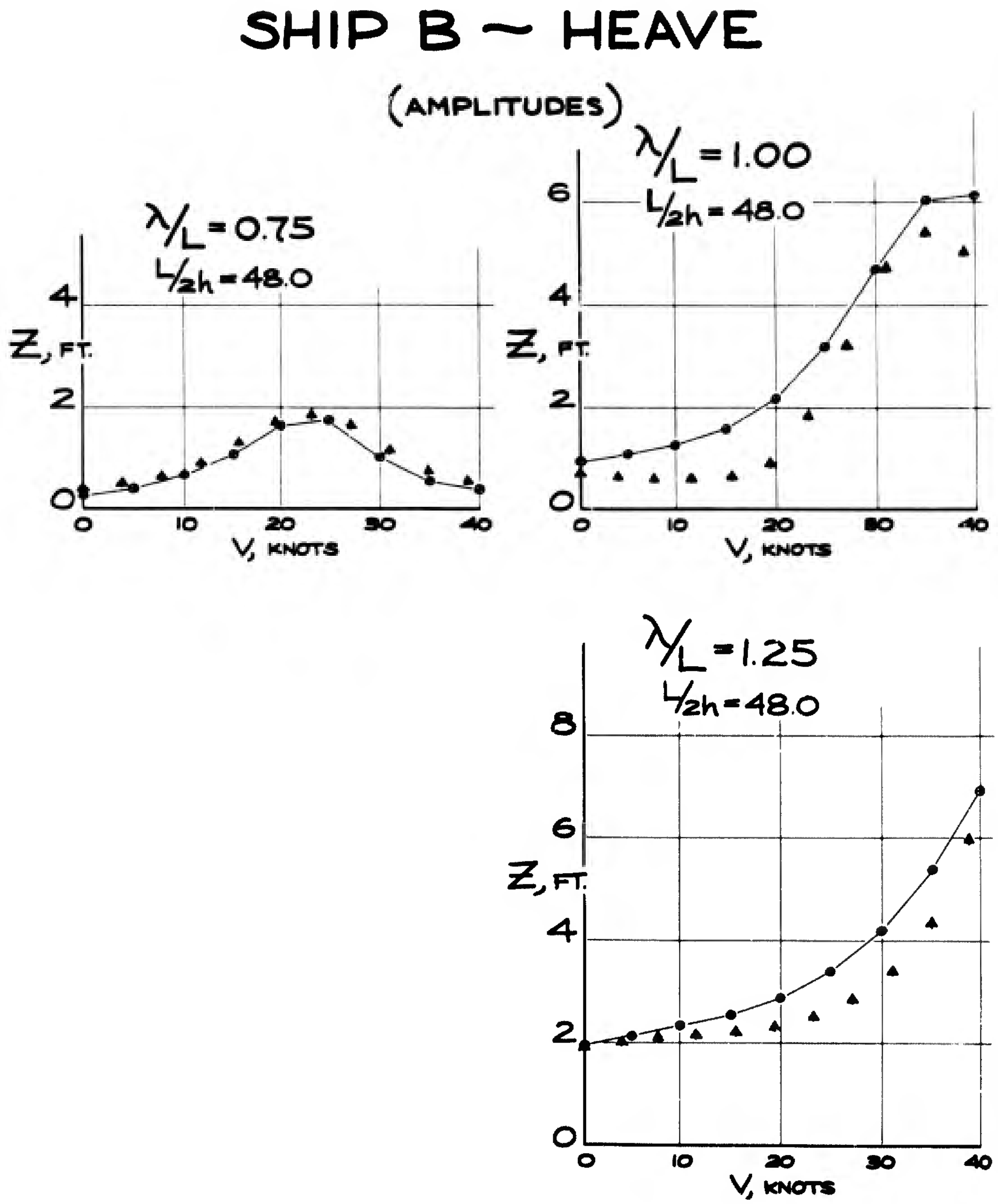
SHIP B ~ HEAVE
(AMPLITUDES)
λ/L = 0.75
L/2h = 48.0
Z, FT.
V, KNOTS
λ/L = 1.00
L/2h = 48.0
Z, FT.
V, KNOTS
λ/L = 1.25
L/2h = 48.0
Z, FT.
V, KNOTS

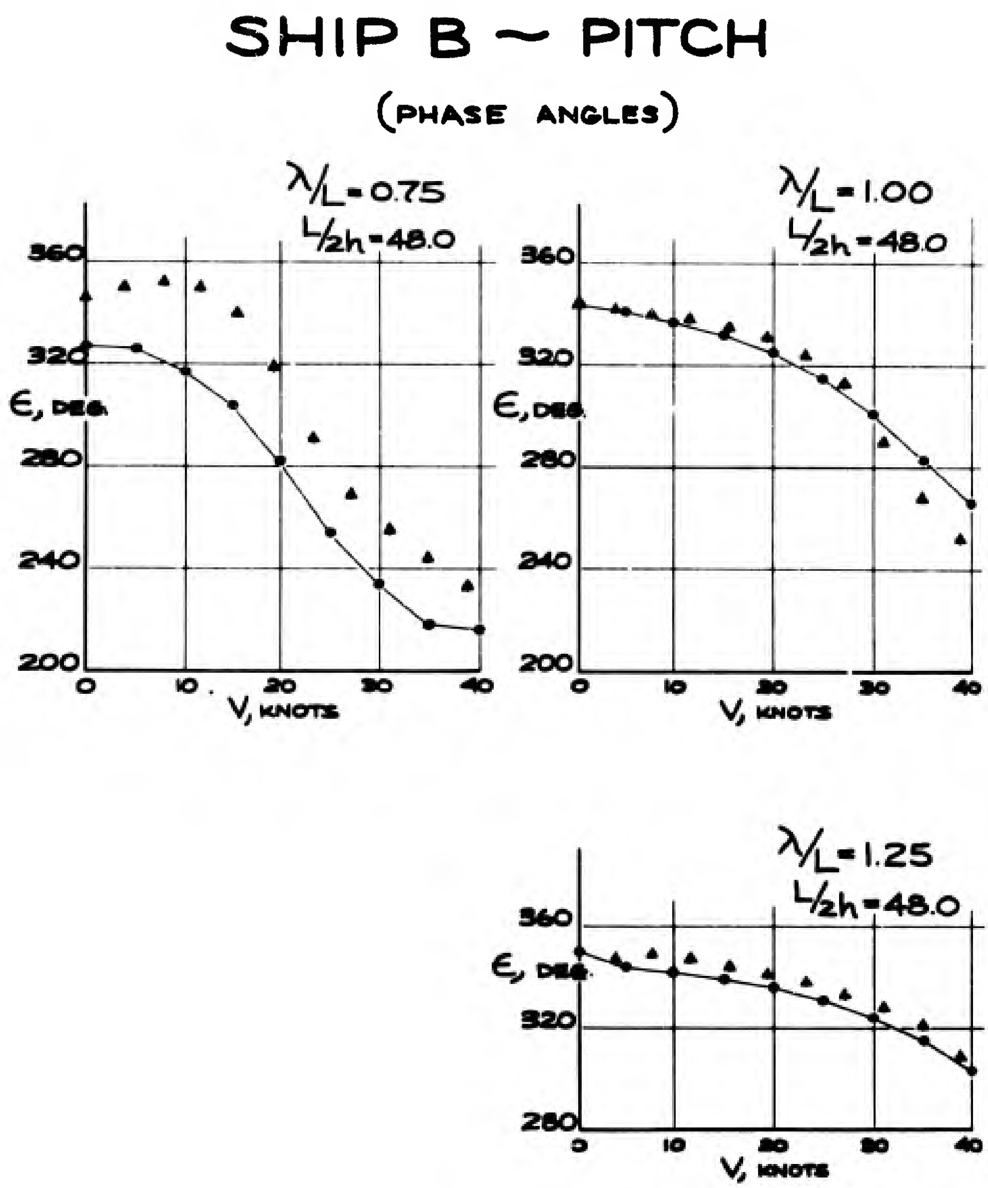
SHIP B ~ PITCH
(PHASE ANGLES)
λ/L = 0.75
L/2h = 48.0
λ/L = 1.00
L/2h = 48.0
λ/L = 1.25
L/2h = 48.0
ε, DEG.
360
320
280
240
200
0
10
20
30
40
V, KNOTS

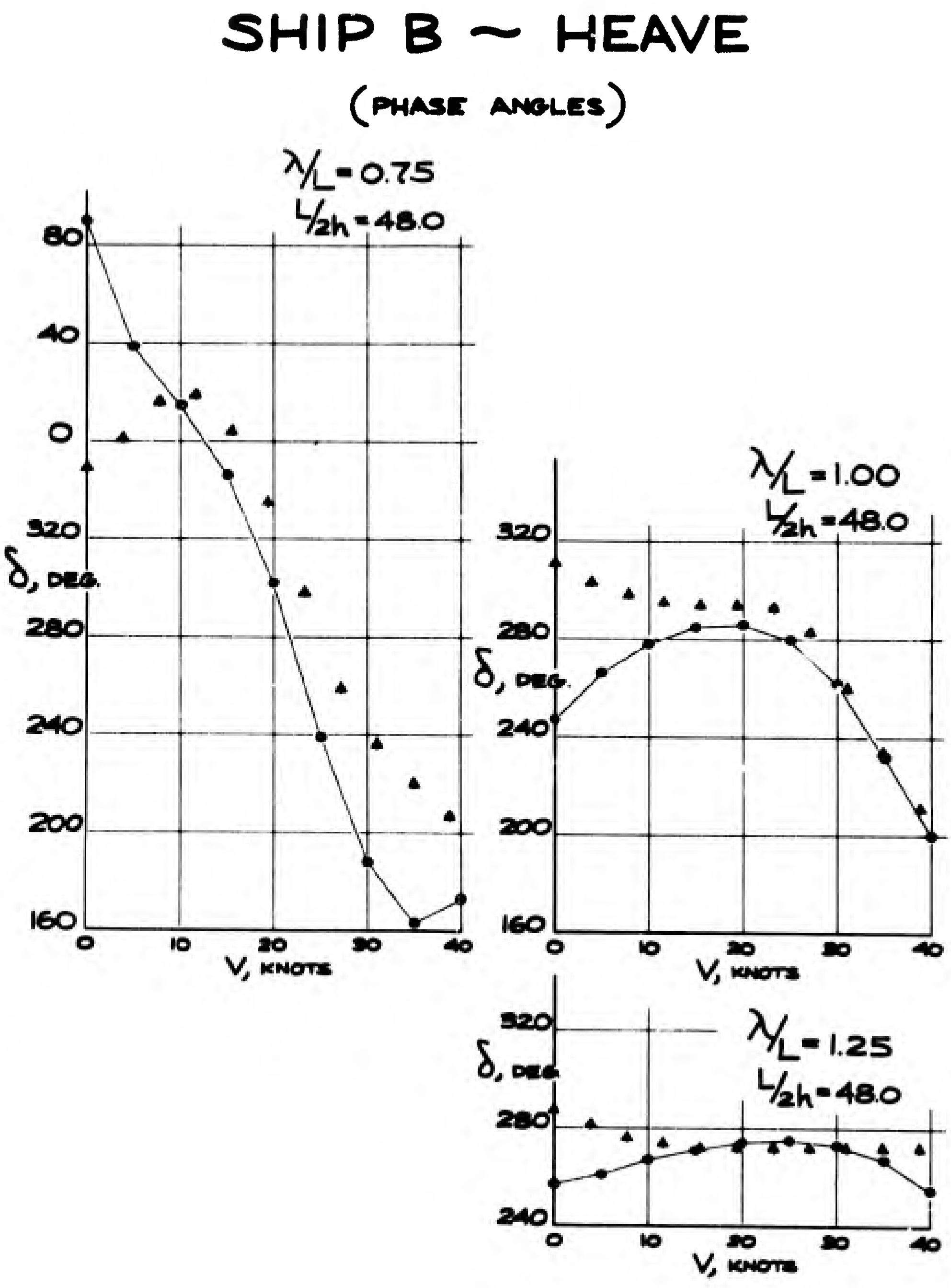
SHIP B ~ HEAVE
(PHASE ANGLES)
λ/L = 0.75
L/2h = 48.0
λ/L = 1.00
L/2h = 48.0
λ/L = 1.25
L/2h = 48.0
δ, DEG.
V, KNOTS
80
40
0
320
280
240
200
160
0
10
20
30
40

SHIP C ~ PITCH

(AMPLITUDES)

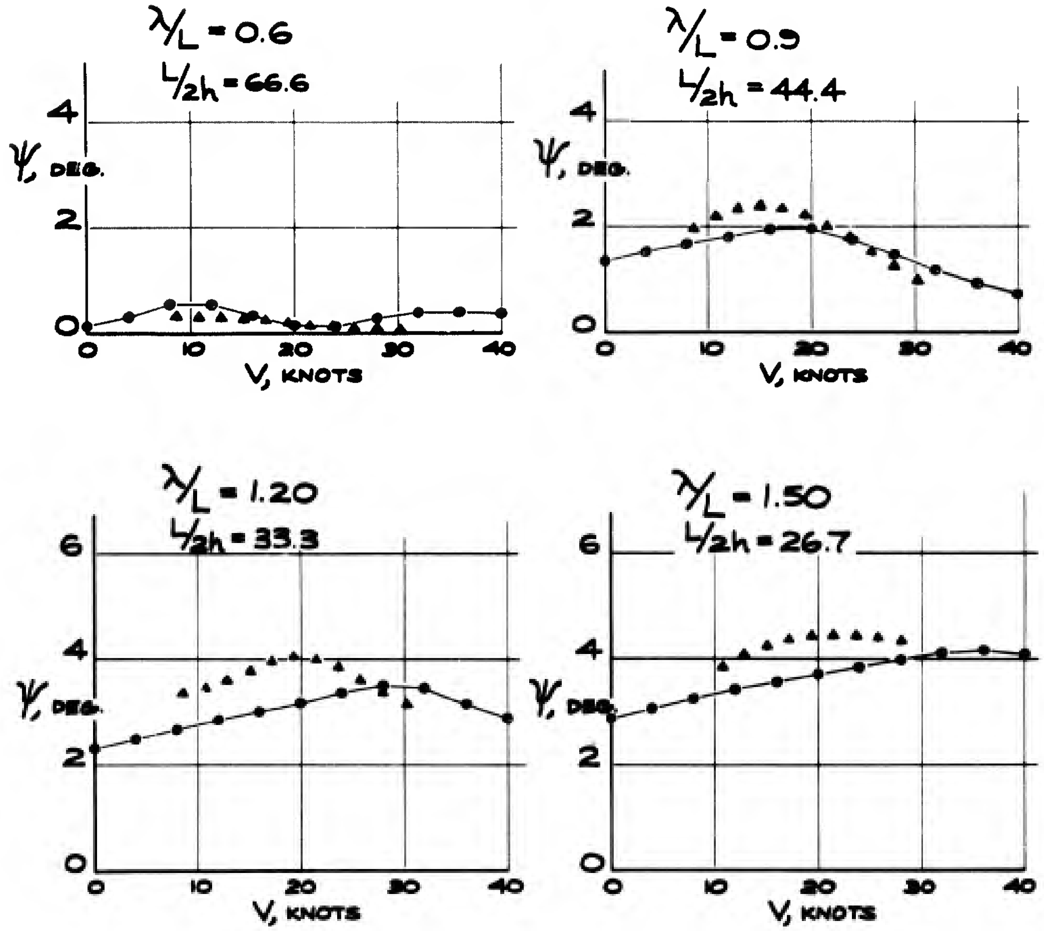

SHIP C ~ HEAVE

(AMPLITUDES)

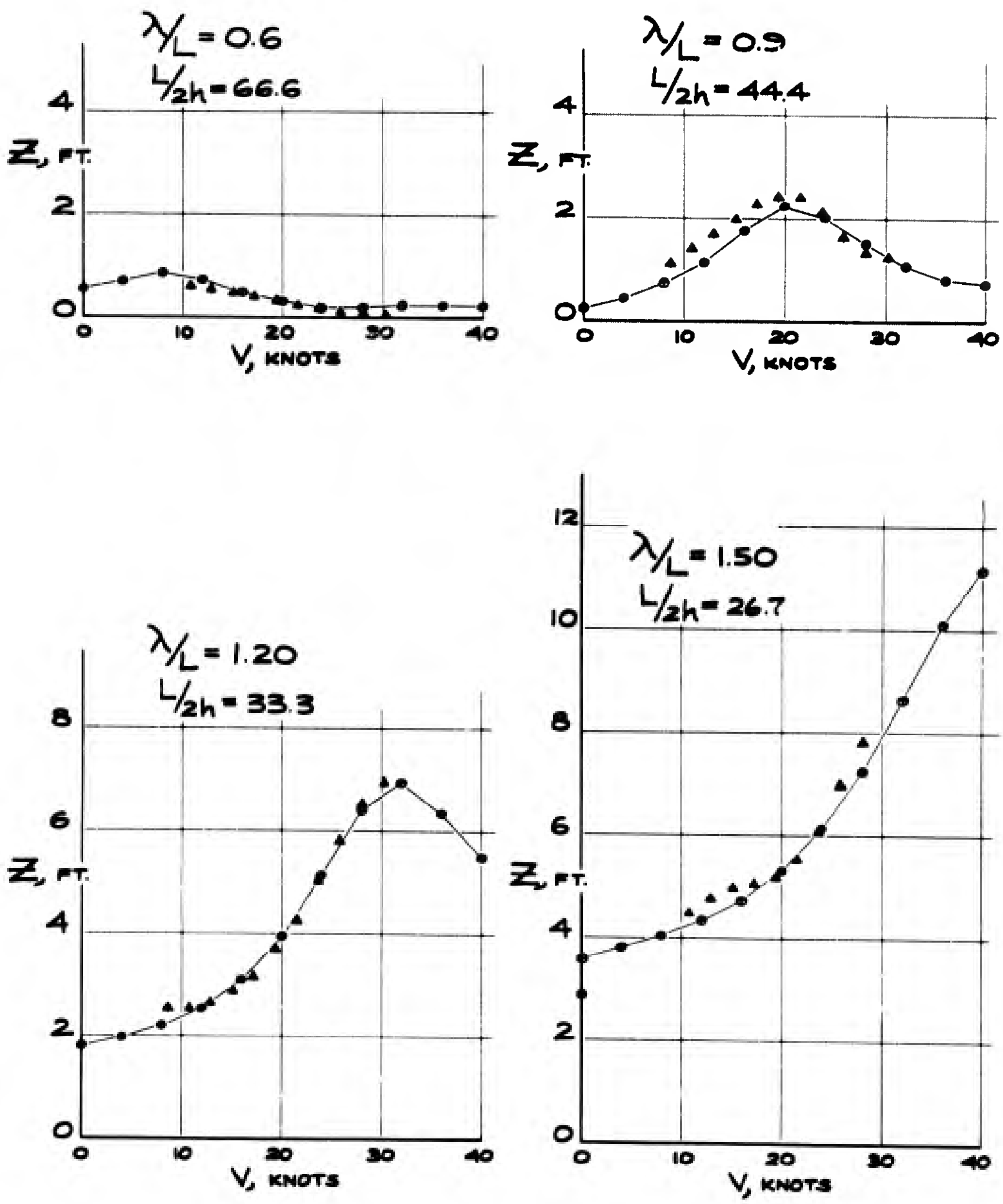

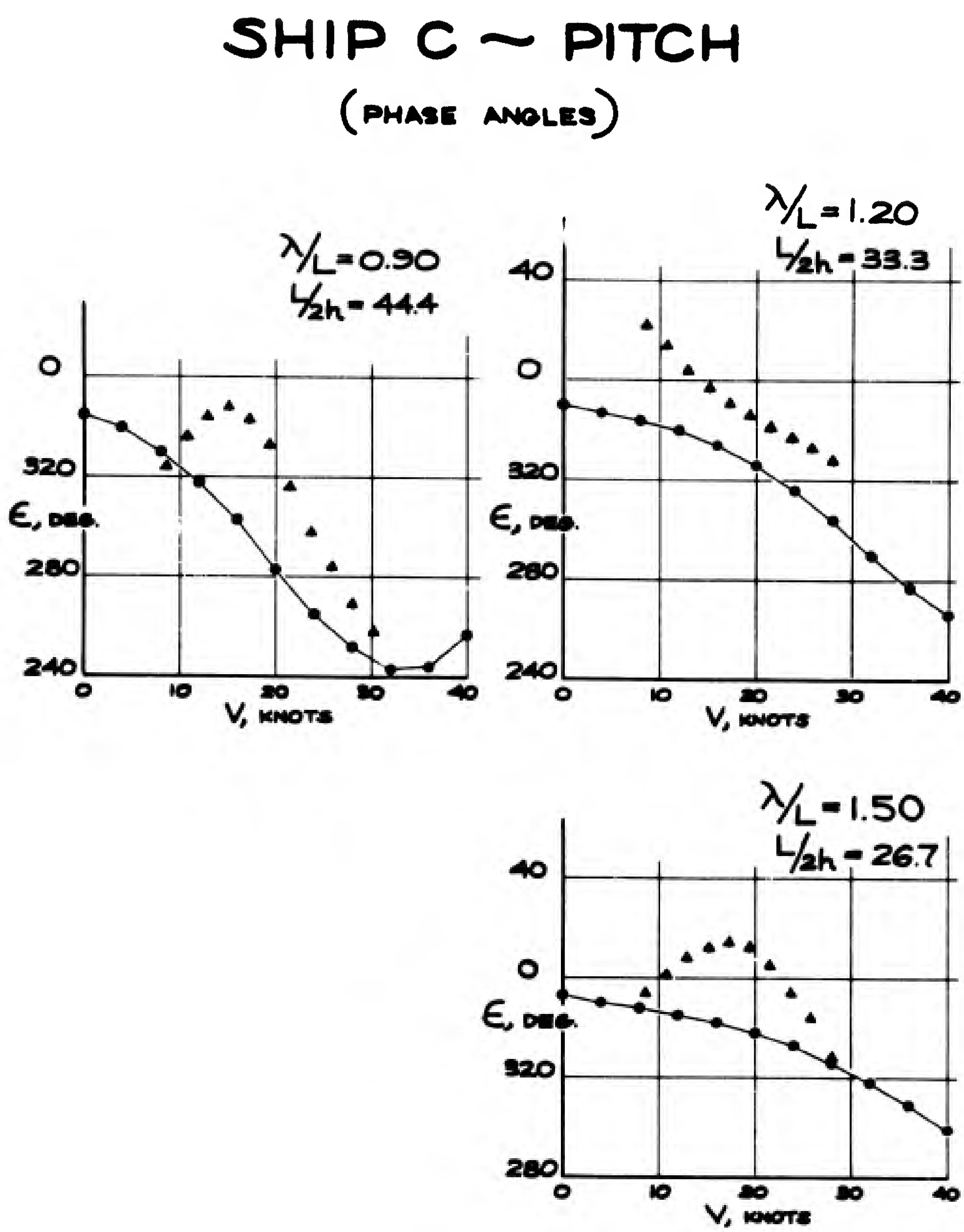
SHIP C ~ PITCH
(PHASE ANGLES)
λ/L = 0.90
L/2h = 44.4
λ/L = 1.20
L/2h = 33.3
λ/L = 1.50
L/2h = 26.7
ε, DEG.
V, KNOTS
0
10
20
30
40
240
280
320

SHIP C ~ HEAVE

(PHASE ANGLES)

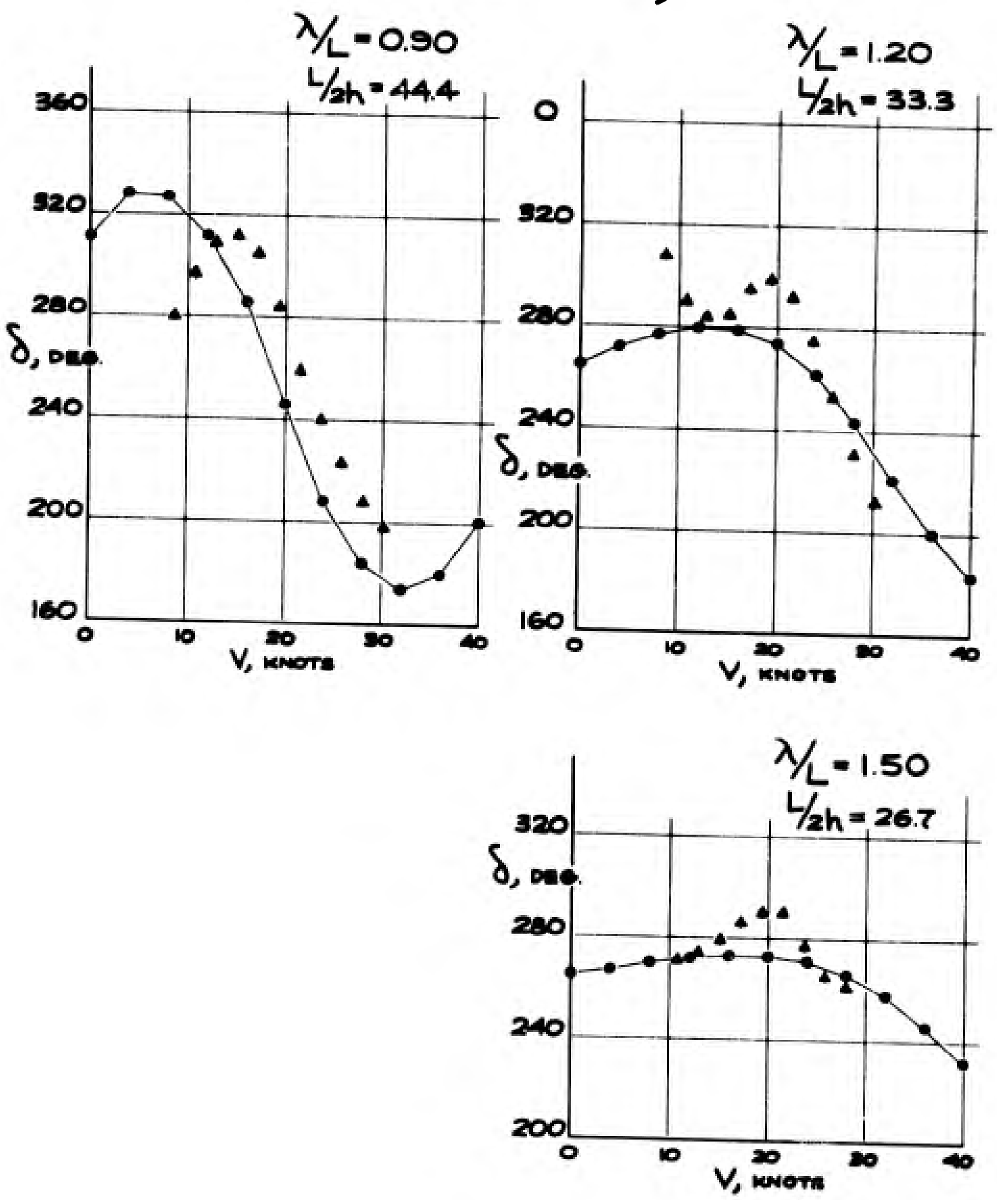

SHIP D ~ PITCH

(AMPLITUDES)

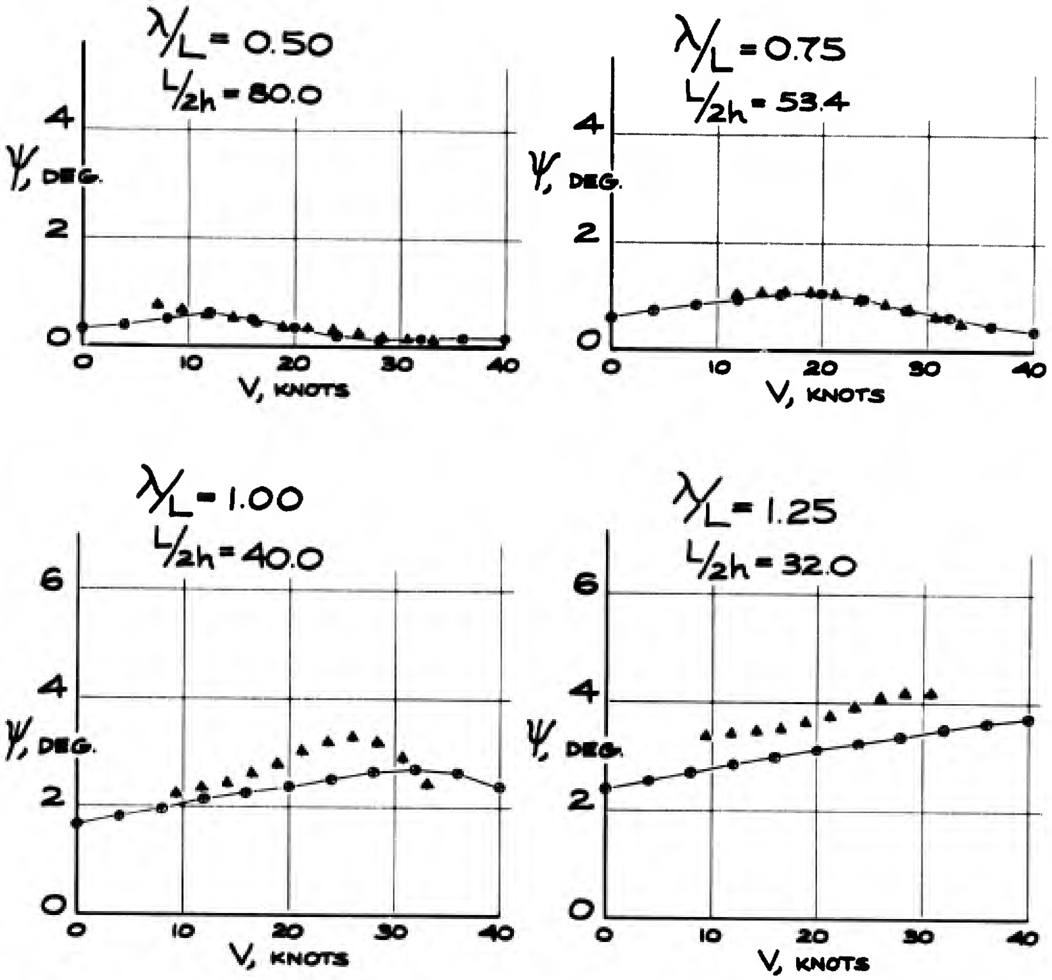

SHIP D ~ HEAVE

(AMPLITUDES)

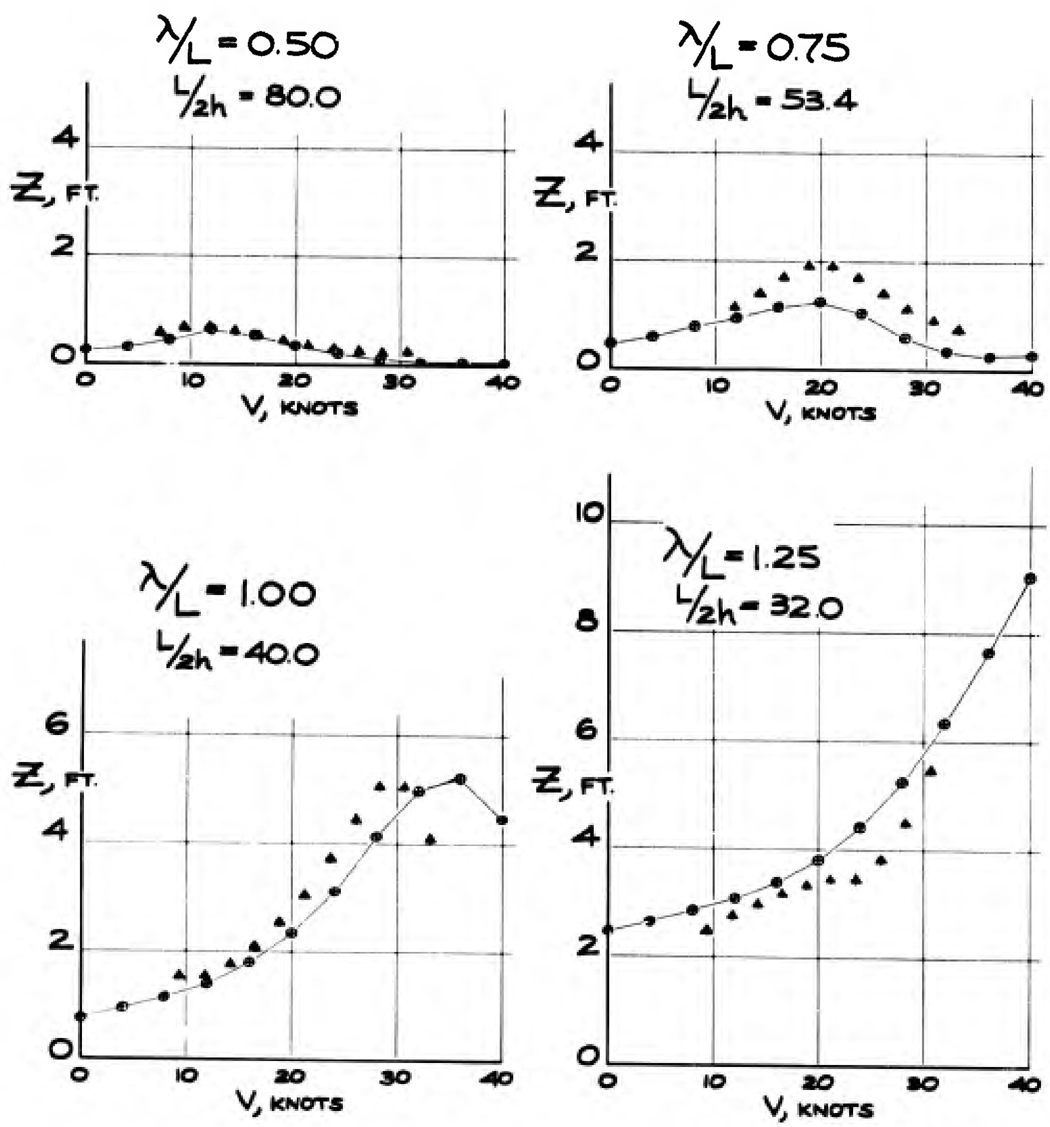

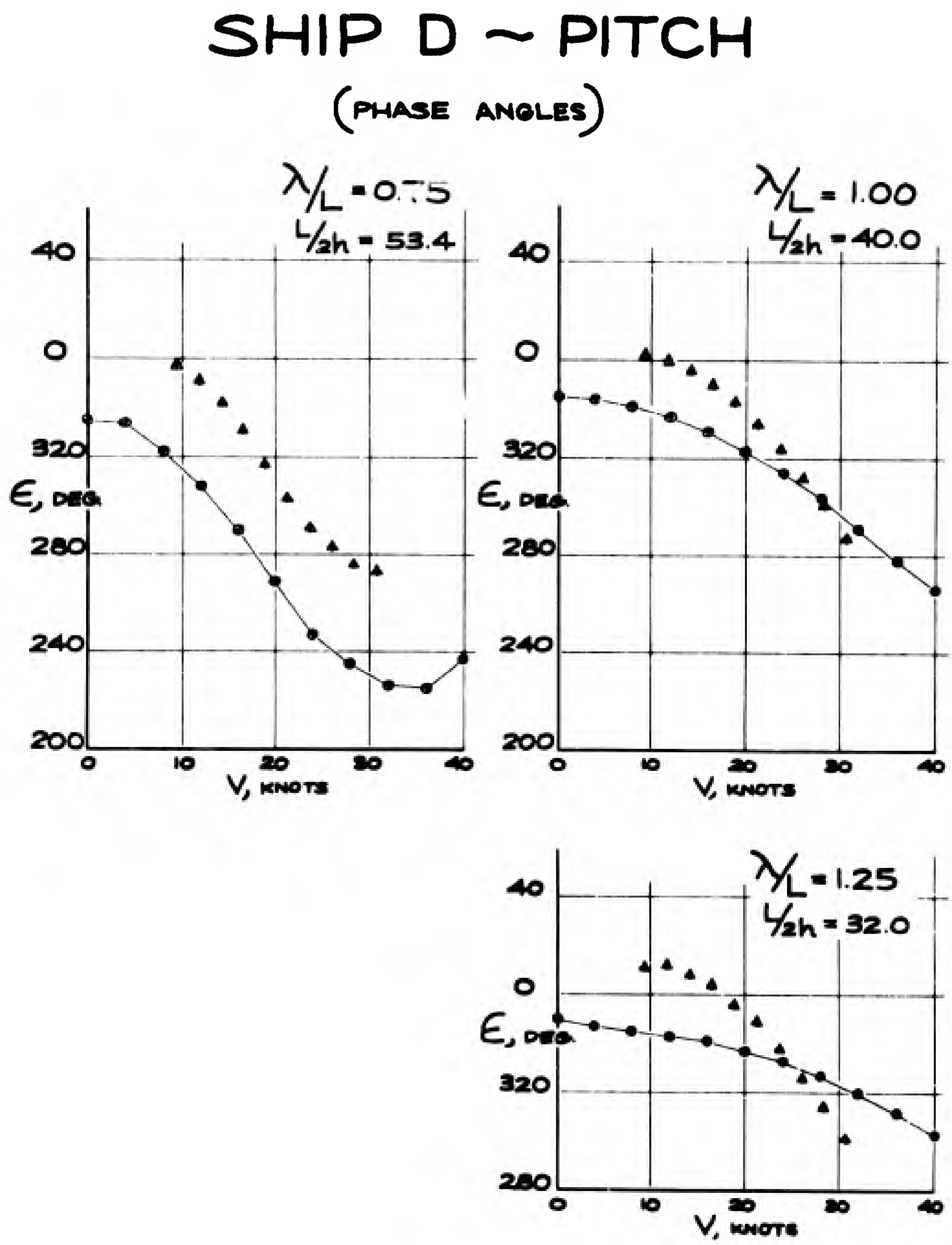
SHIP D ~ PITCH
(PHASE ANGLES)
λ/L = 0.75
L/2h = 53.4
λ/L = 1.00
L/2h = 40.0
λ/L = 1.25
L/2h = 32.0
ε, DEG.
V, KNOTS

SHIP D ~ HEAVE

(PHASE ANGLES)

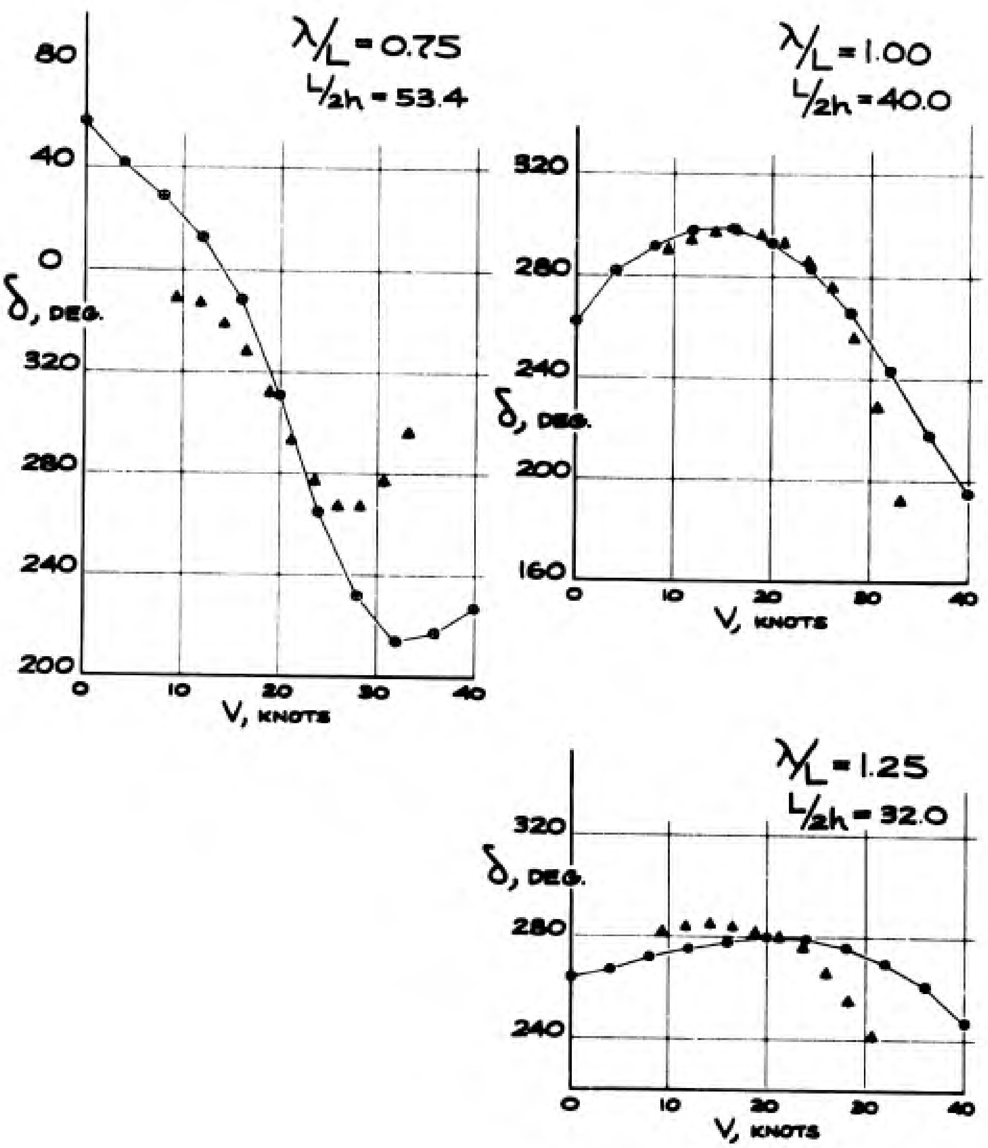

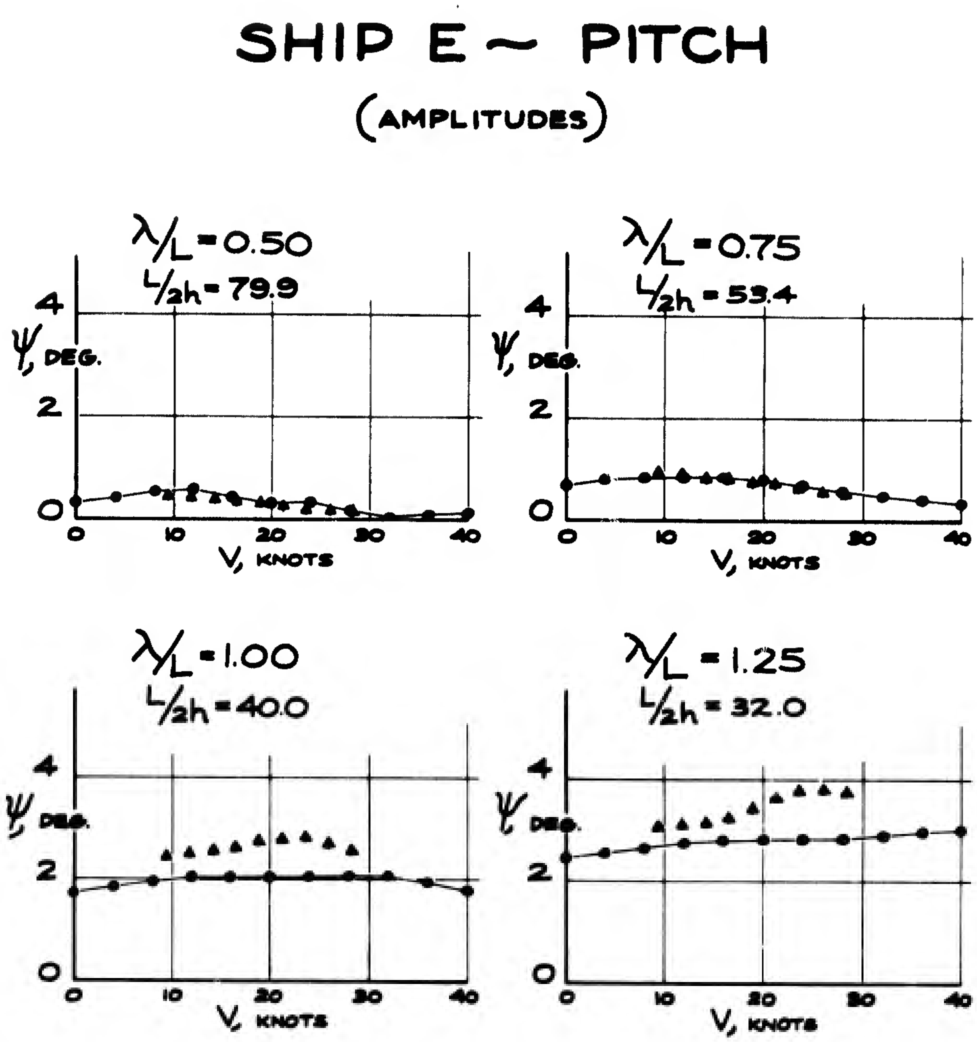
SHIP E ~ PITCH
(AMPLITUDES)
λ/L = 0.50
L/2h = 79.9
λ/L = 0.75
L/2h = 53.4
λ/L = 1.00
L/2h = 40.0
λ/L = 1.25
L/2h = 32.0
ψ, DEG.
V, KNOTS
0
2
4
10
20
30
40

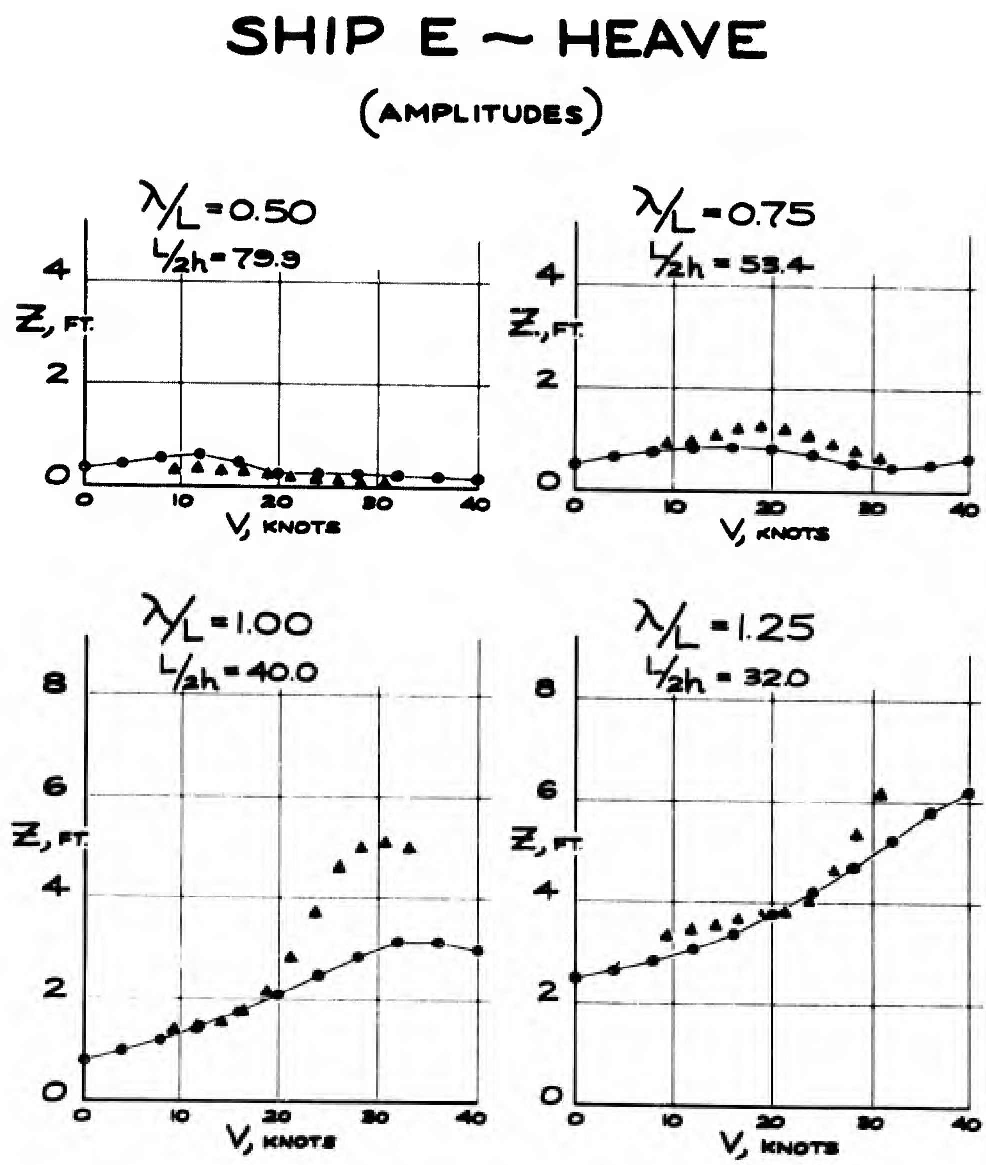
SHIP E ~ HEAVE
(AMPLITUDES)
λ/L = 0.50
L/2h = 79.9
λ/L = 0.75
L/2h = 53.4
λ/L = 1.00
L/2h = 40.0
λ/L = 1.25
L/2h = 32.0
Z, FT.
V, KNOTS
0
10
20
30
40
2
4
6
8

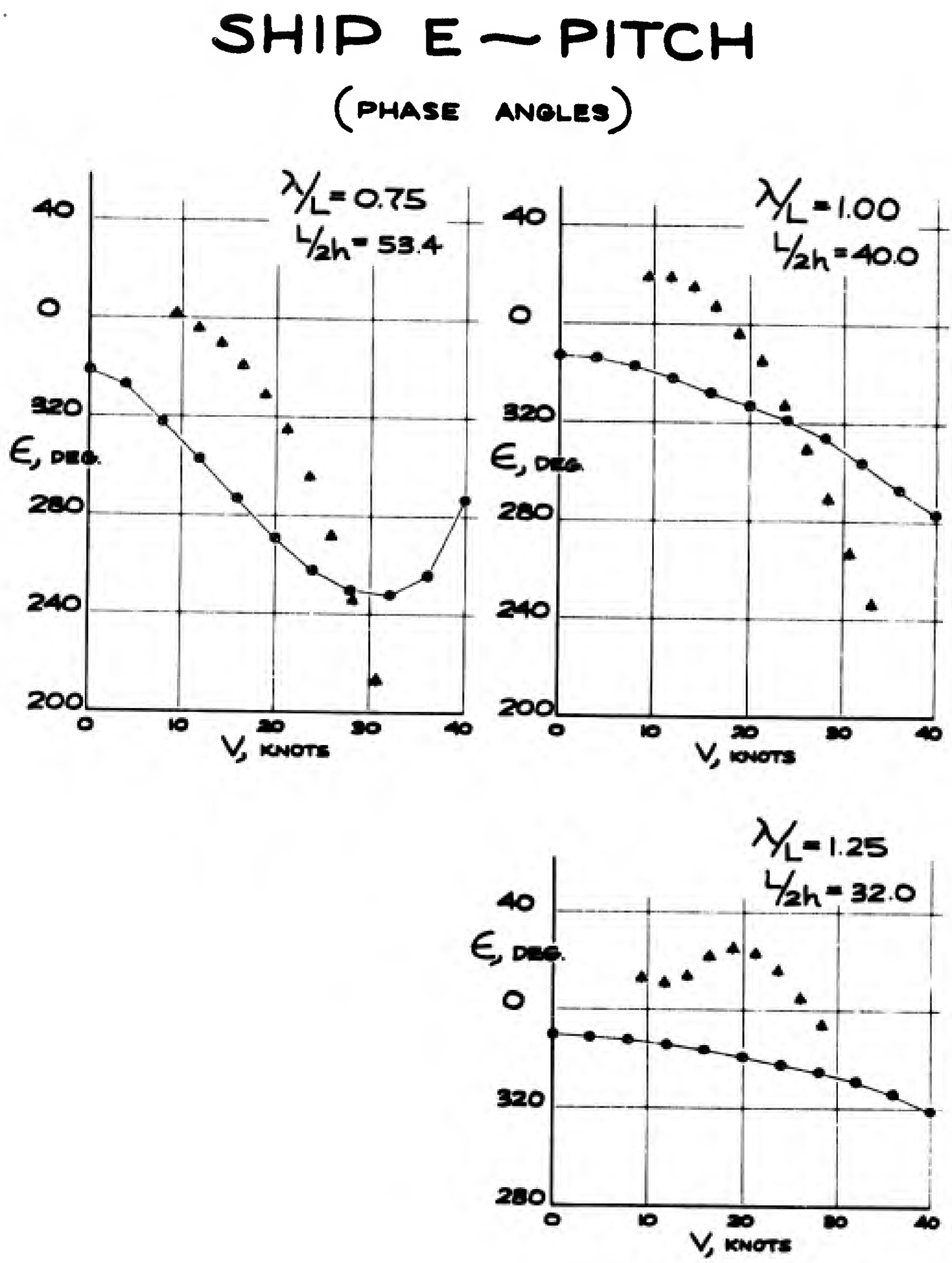
SHIP E — PITCH
(PHASE ANGLES)
λ/L = 0.75
L/2h = 53.4
λ/L = 1.00
L/2h = 40.0
λ/L = 1.25
L/2h = 32.0
ε, DEG.
V, KNOTS
40
0
320
280
240
200
0
10
20
30
40

SHIP E ~ HEAVE

(PHASE ANGLES)

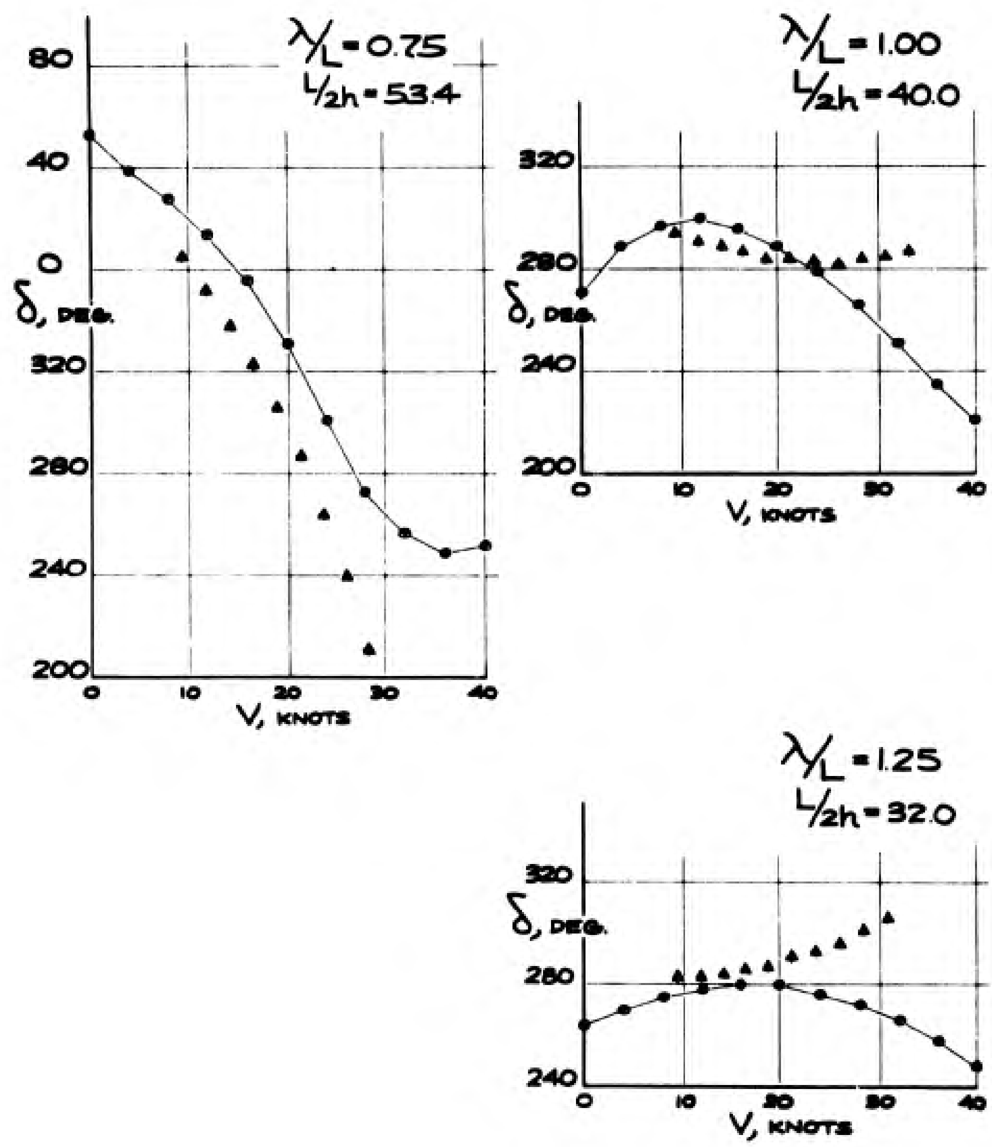

SHIP F – PITCH

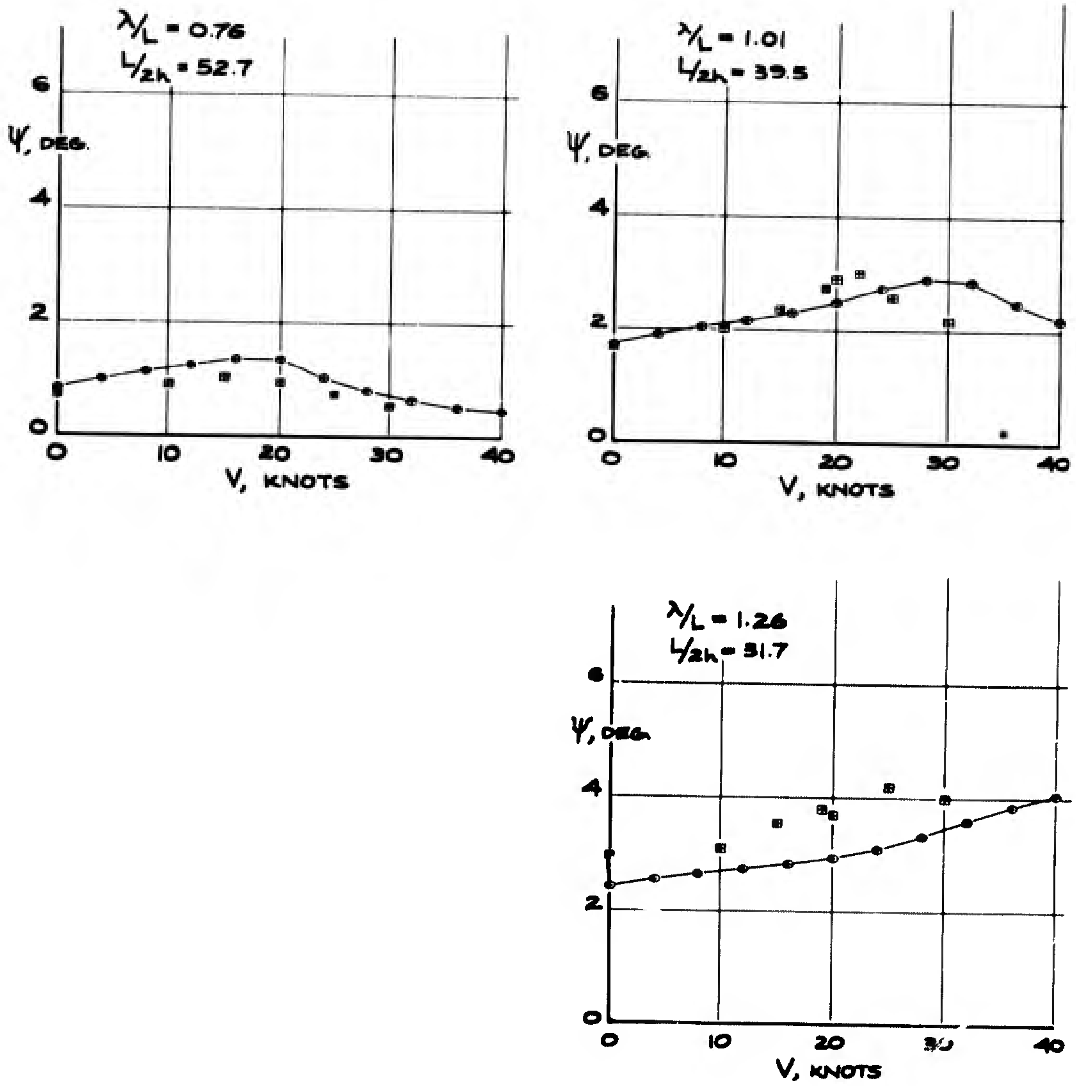
λ/L = 0.76
L/2h = 52.7
ψ, DEG.
V, KNOTS
λ/L = 1.01
L/2h = 39.5
ψ, DEG.
V, KNOTS
λ/L = 1.26
L/2h = 31.7
ψ, DEG.
V, KNOTS

SHIP F — HEAVE

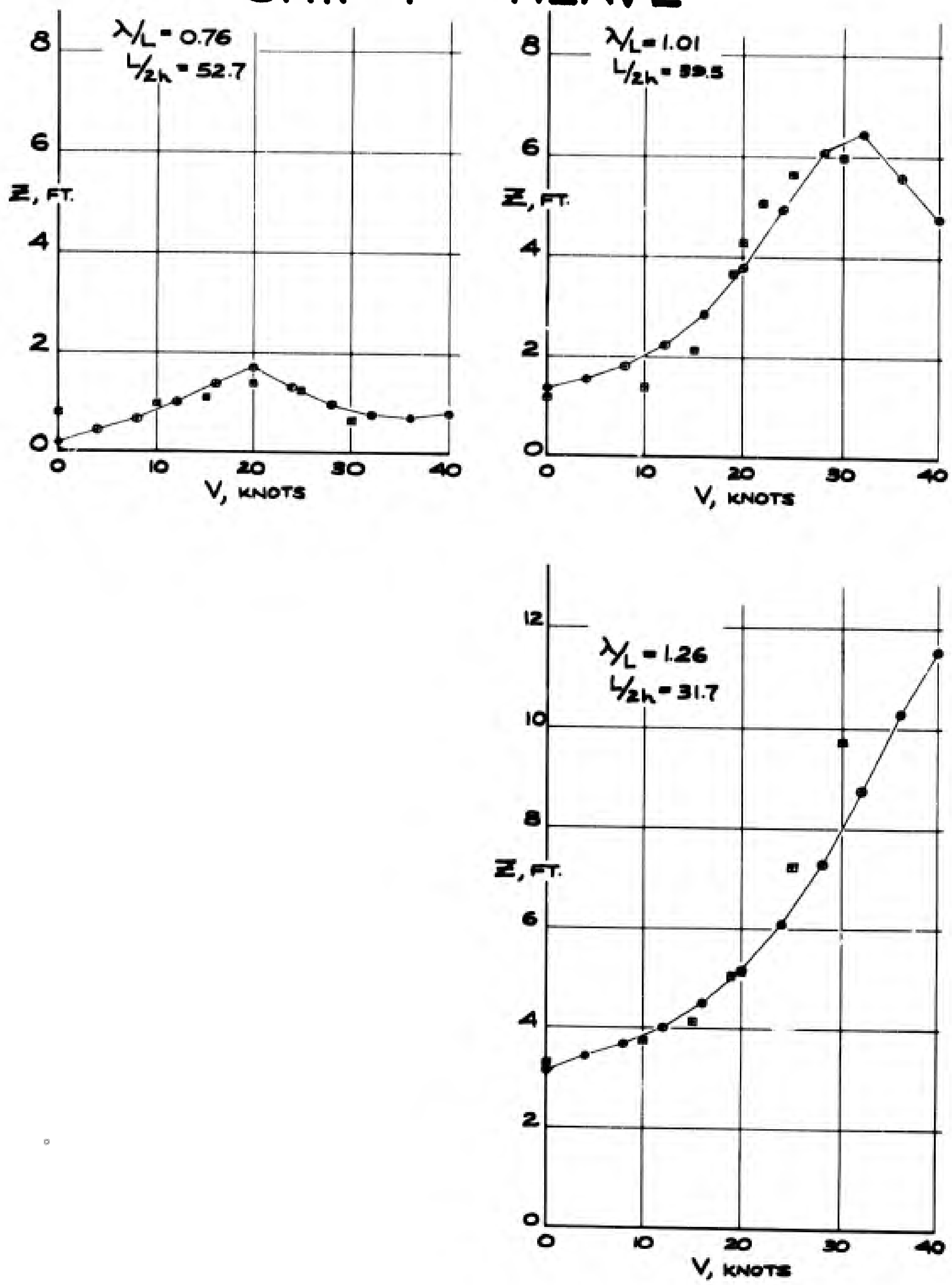
λ/L = 0.76
L/2h = 52.7
Z, FT.
V, KNOTS
λ/L = 1.01
L/2h = 39.5
Z, FT.
V, KNOTS
λ/L = 1.26
L/2h = 31.7
Z, FT.
V, KNOTS

SHIP G – PITCH

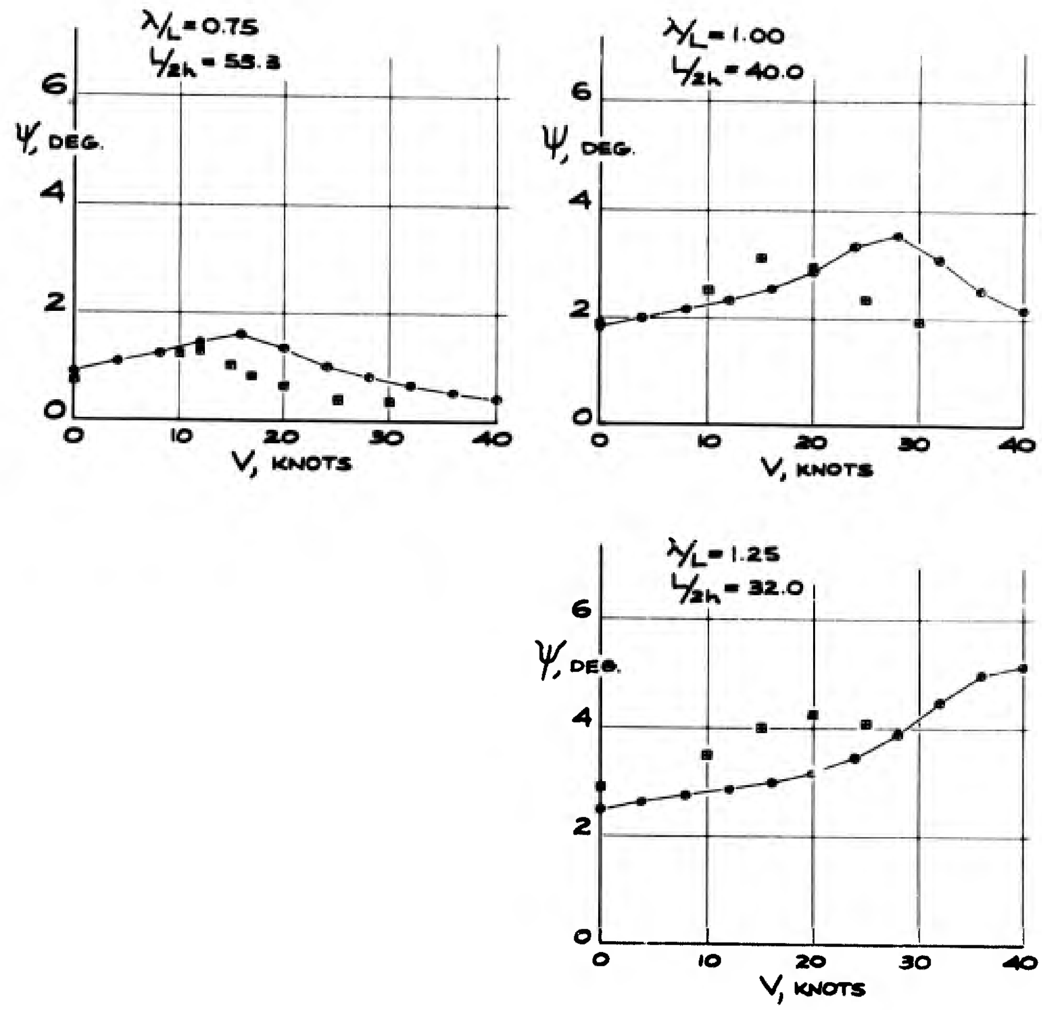
λ/L = 0.75
L/2h = 55.3
ψ, DEG.
V, KNOTS
λ/L = 1.00
L/2h = 40.0
ψ, DEG.
V, KNOTS
λ/L = 1.25
L/2h = 32.0
ψ, DEG.
V, KNOTS

SHIP G ~ HEAVE

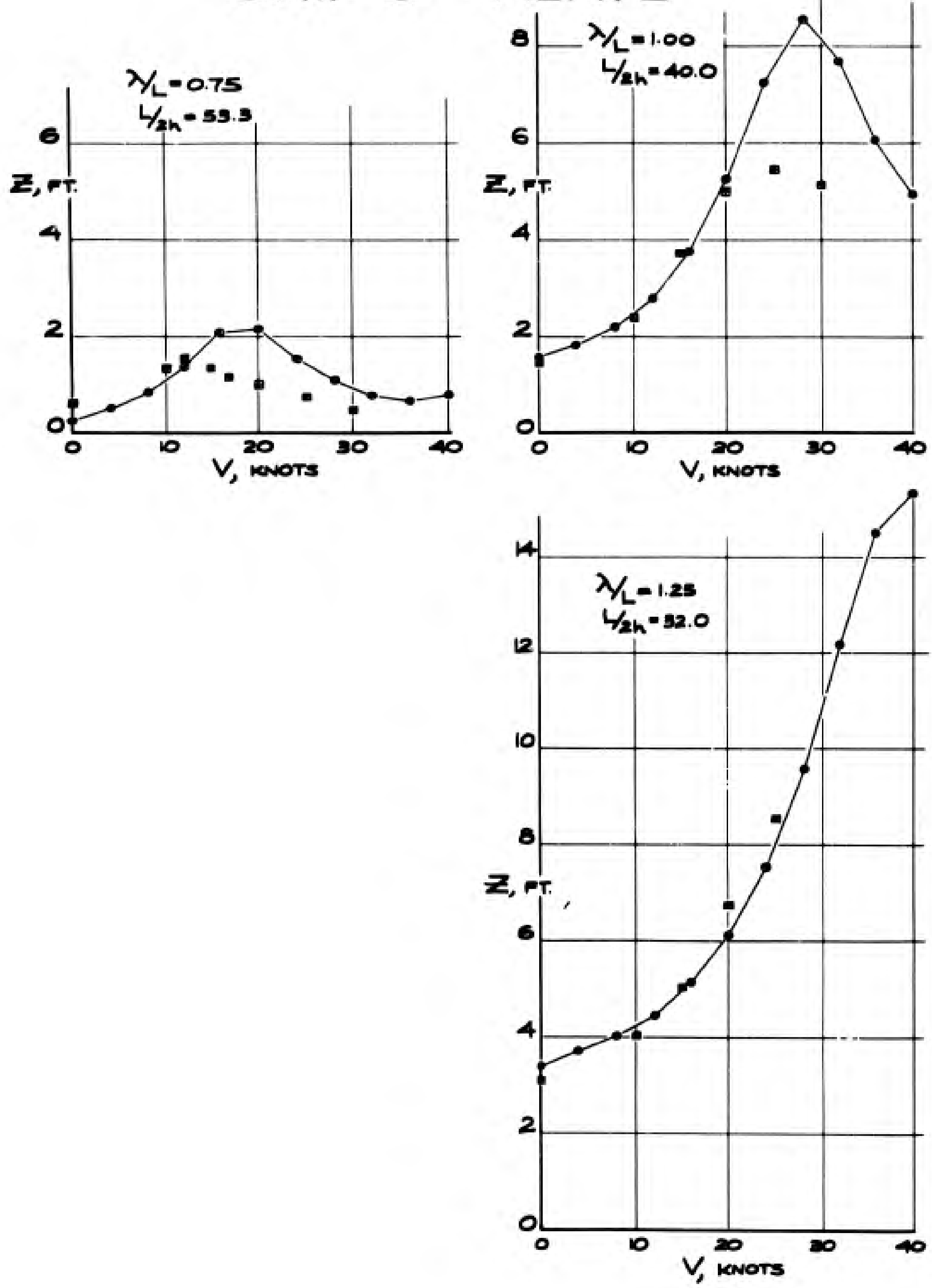
λ/L = 0.75
L/2h = 53.3
Z, FT.
0
2
4
6
0
10
20
30
40
V, KNOTS
λ/L = 1.00
L/2h = 40.0
Z, FT.
0
2
4
6
8
0
10
20
30
40
V, KNOTS
λ/L = 1.25
L/2h = 32.0
Z, FT.
0
2
4
6
8
10
12
14
0
10
20
30
40
V, KNOTS

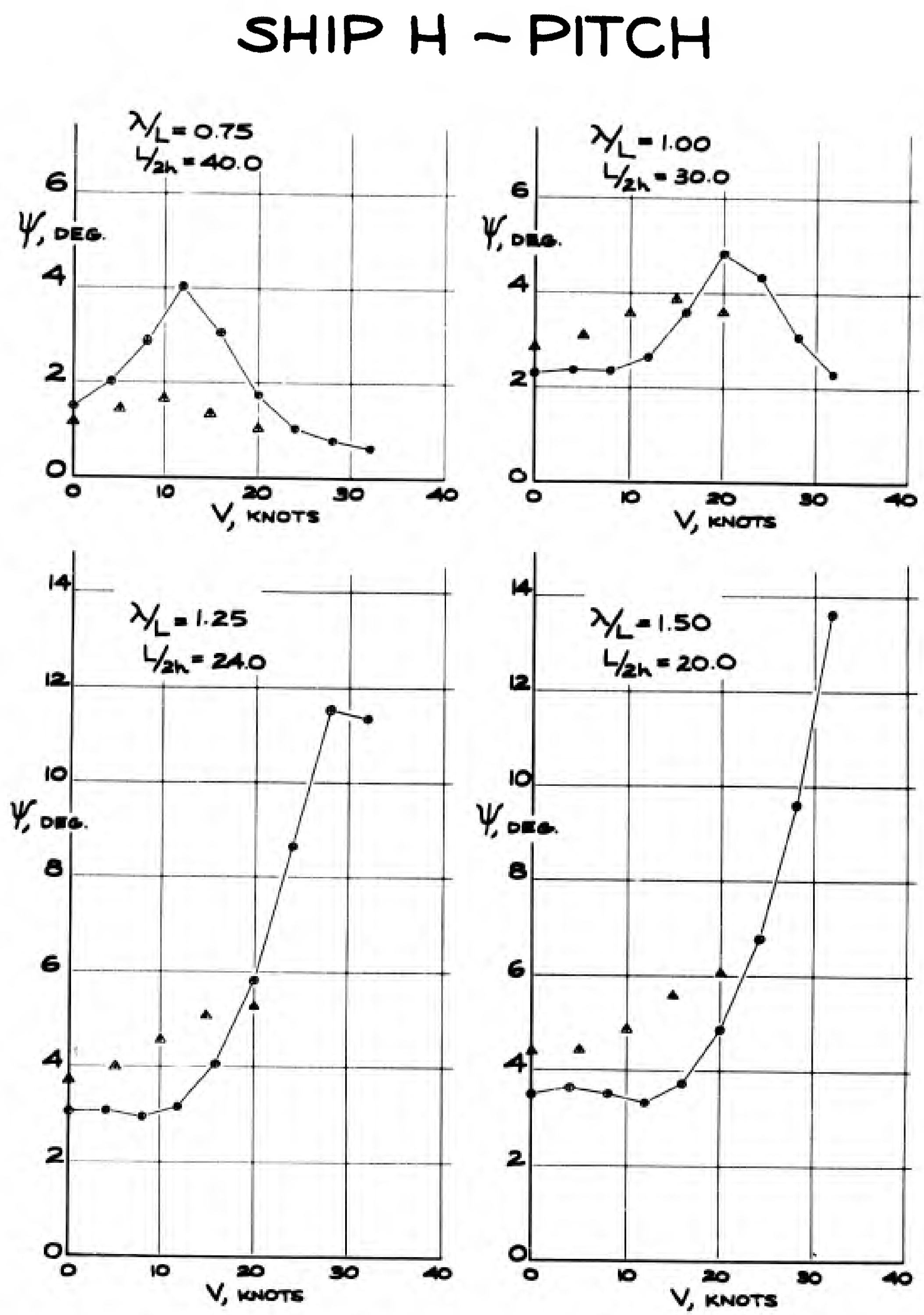
SHIP H ~ PITCH
λ/L = 0.75
L/2h = 40.0
ψ, DEG.
V, KNOTS
λ/L = 1.00
L/2h = 30.0
ψ, DEG.
V, KNOTS
λ/L = 1.25
L/2h = 24.0
ψ, DEG.
V, KNOTS
λ/L = 1.50
L/2h = 20.0
ψ, DEG.
V, KNOTS

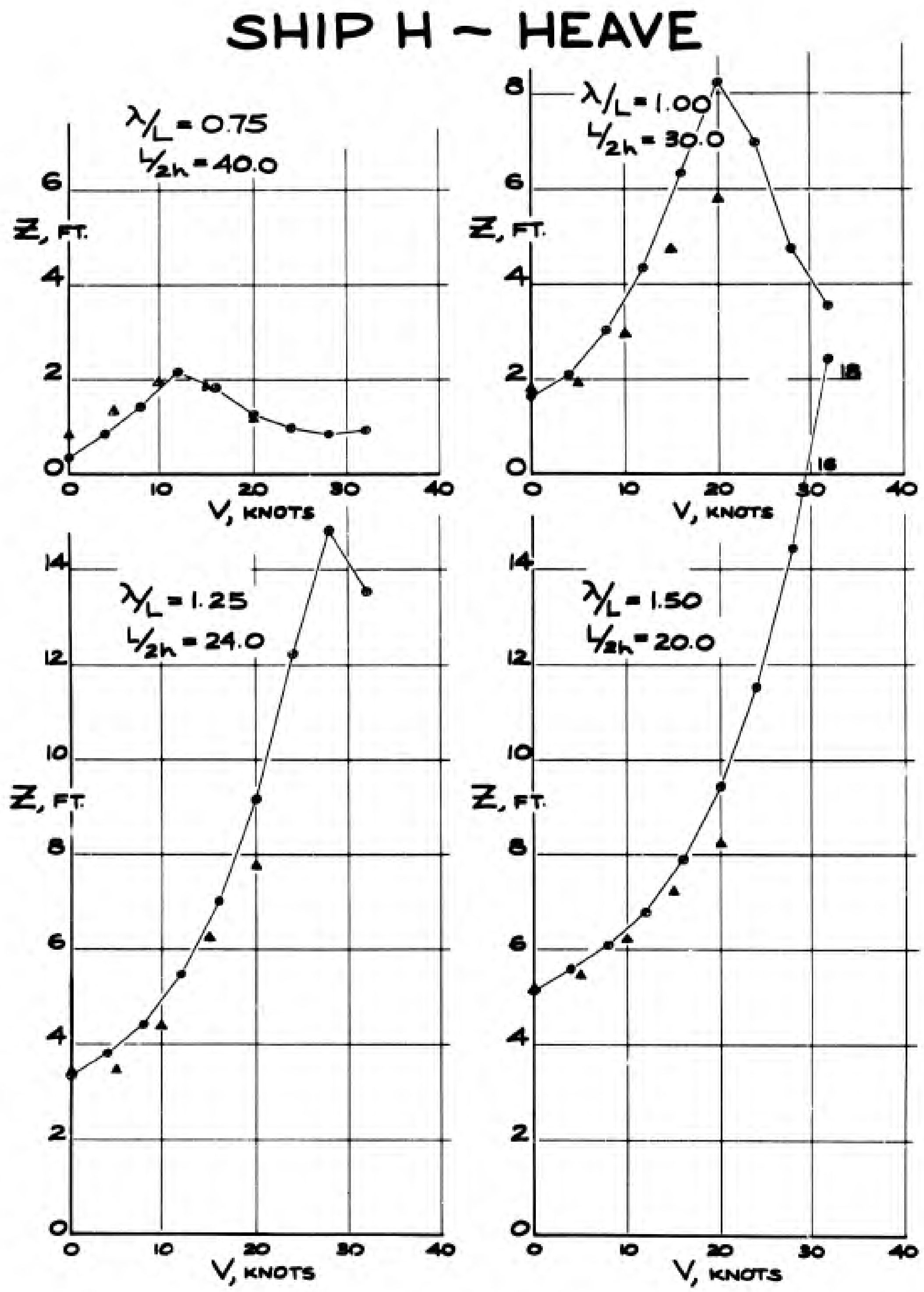
SHIP H ~ HEAVE
λ/L = 0.75
L/2h = 40.0
λ/L = 1.00
L/2h = 30.0
λ/L = 1.25
L/2h = 24.0
λ/L = 1.50
L/2h = 20.0
Z, FT.
V, KNOTS
18
16

SHIP J ~ PITCH

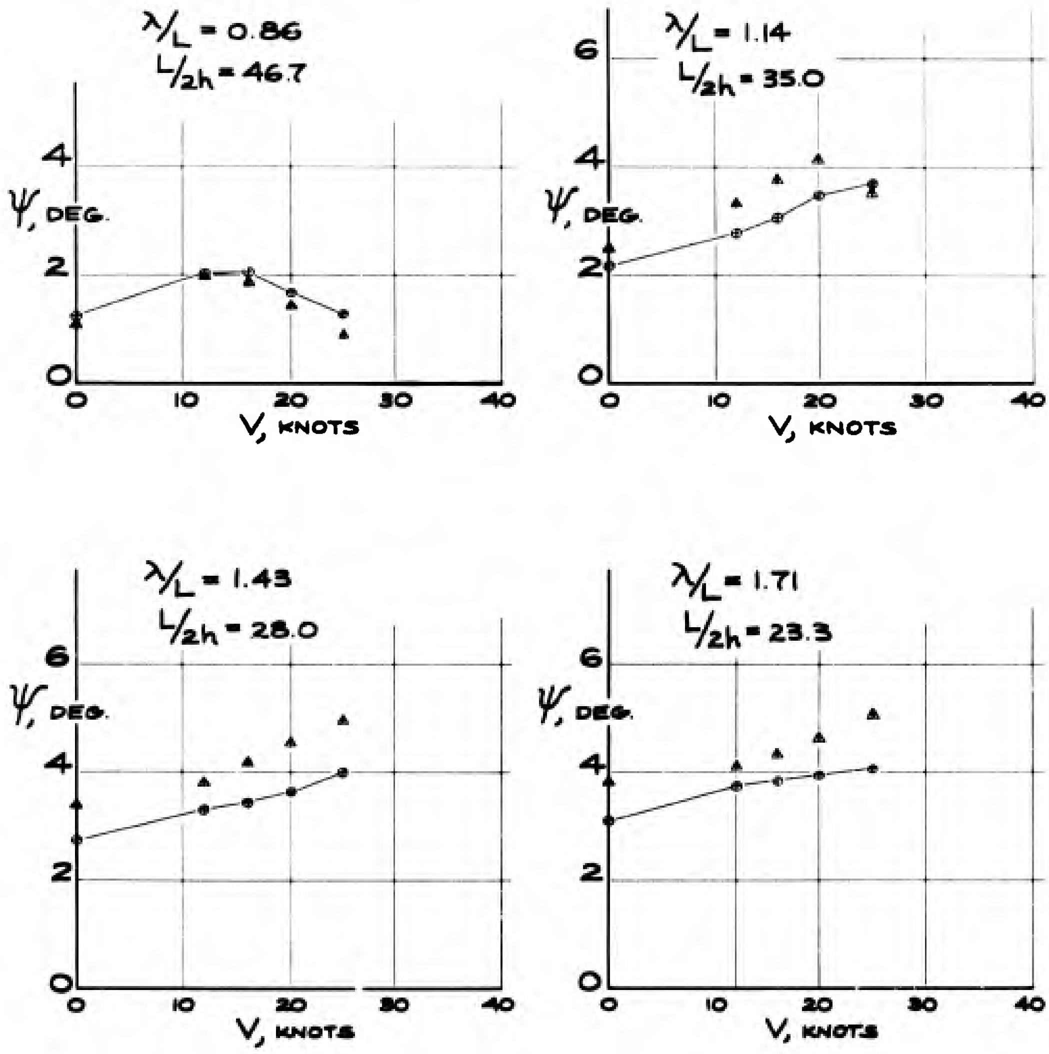
λ/L = 0.86
L/2h = 46.7
ψ, DEG.
V, KNOTS
λ/L = 1.14
L/2h = 35.0
ψ, DEG.
V, KNOTS
λ/L = 1.43
L/2h = 28.0
ψ, DEG.
V, KNOTS
λ/L = 1.71
L/2h = 23.3
ψ, DEG.
V, KNOTS

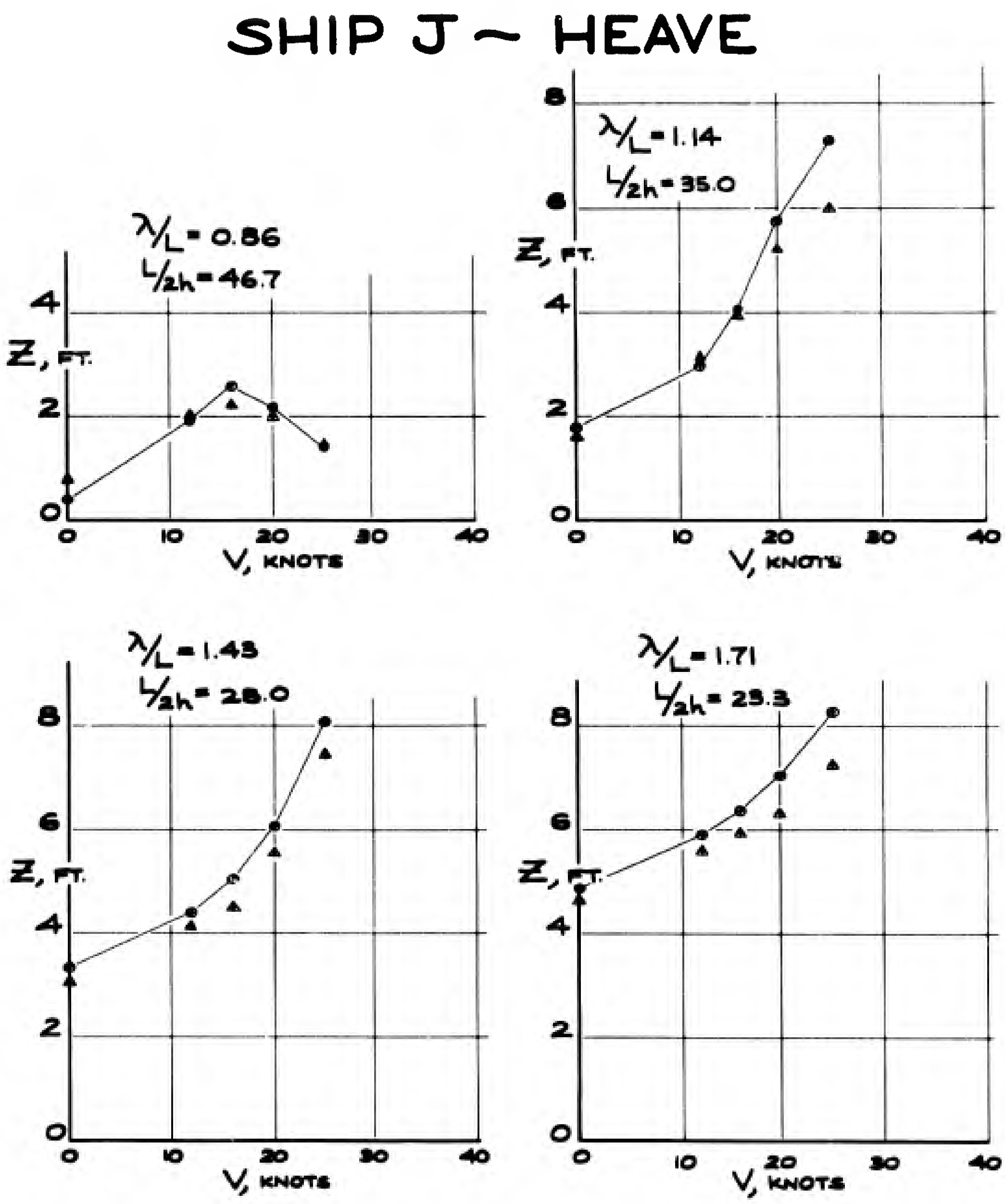
SHIP J ~ HEAVE
λ/L = 0.86
L/2h = 46.7
λ/L = 1.14
L/2h = 35.0
λ/L = 1.43
L/2h = 28.0
λ/L = 1.71
L/2h = 23.3
Z, FT.
V, KNOTS
0
2
4
6
8
10
20
30
40

SHIP K ~ PITCH

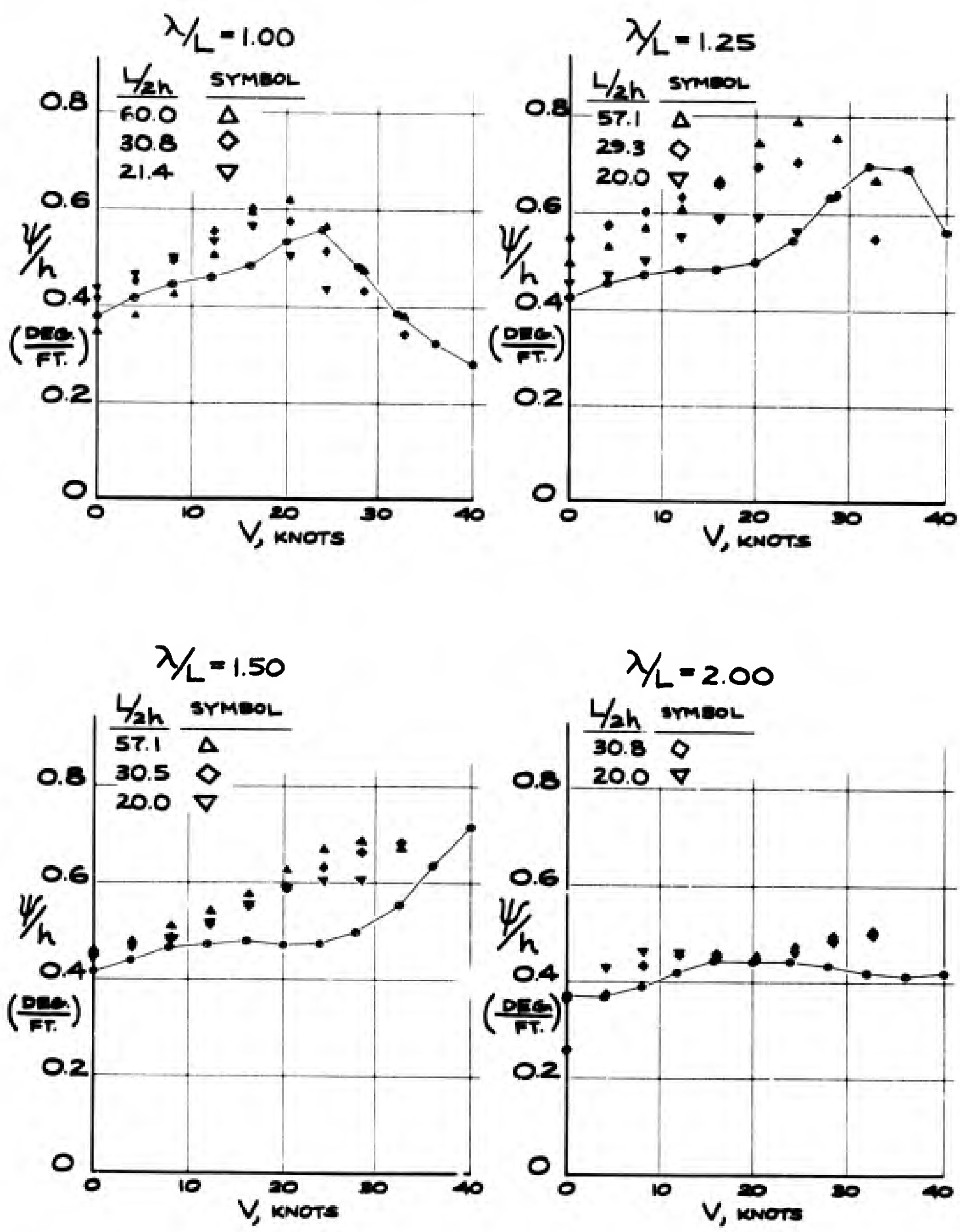

λ/L = 1.00
L/2h SYMBOL
60.0 △
30.8 ◇
21.4 ▽
λ/L = 1.25
L/2h SYMBOL
57.1 △
29.3 ◇
20.0 ▽
λ/L = 1.50
L/2h SYMBOL
57.1 △
30.5 ◇
20.0 ▽
λ/L = 2.00
L/2h SYMBOL
30.8 ◇
20.0 ▽
ψ/h (DEG./FT.)
V, KNOTS

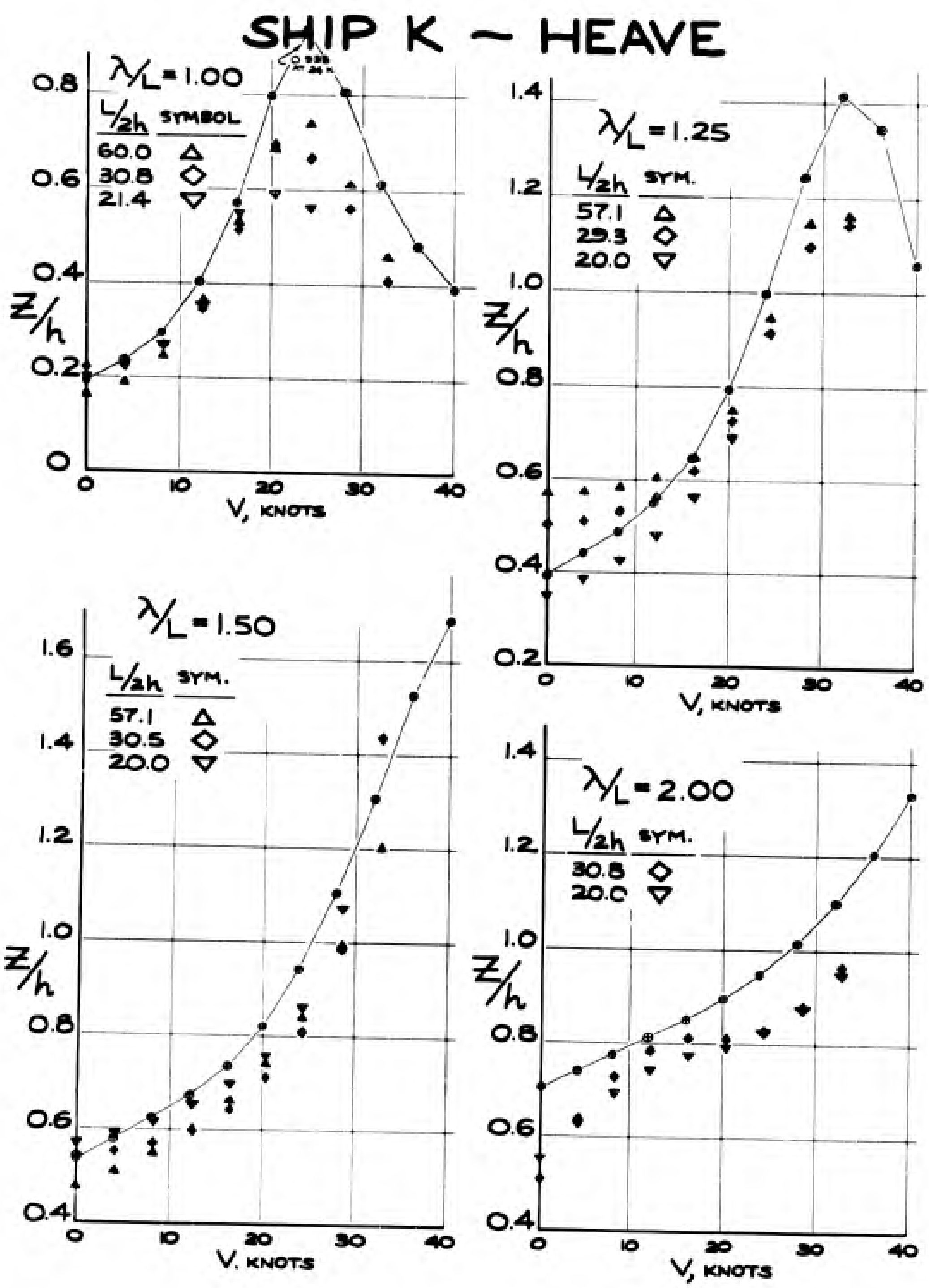
SHIP K ~ HEAVE
λ/L = 1.00
L/2h SYMBOL
60.0 △
30.8 ◇
21.4 ▽
Z/h
V, KNOTS
λ/L = 1.25
L/2h SYM.
57.1 △
29.3 ◇
20.0 ▽
Z/h
V, KNOTS
λ/L = 1.50
L/2h SYM.
57.1 △
30.5 ◇
20.0 ▽
Z/h
V, KNOTS
λ/L = 2.00
L/2h SYM.
30.8 ◇
20.0 ▽
Z/h
V, KNOTS

REPLY TO THE DISCUSSION

L. Vassilopoulos and P. Mandel
Massachusetts Institute of Technology
Cambridge, Massachusetts

*Professor Grim has pointed out that the algorithm we have been using was originally intended to be valid only for the frequency range of waves which severely excites pitching and heaving. The new information which he has supplied to us privately has been used by Professor Porter to make the comparisons shown in his discussion, which for normal type ship sections show excellent agreement. There are two main reasons for pursuing comparisons between Professor Grim's work and that of Professor Porter. First, there is the natural urge to make a comparison between two well-founded theoretical approaches to a question; especially in view of the fact that the first section of the paper still showed disagreement between theory and experiment for resonant conditions. In this regard Professor Porter's program does indicate higher damping in heave than the 1959 Grim data which was used in the first part of this paper. This would tend to reduce the gap between theory and experiment shown there. Secondly, Professor Porter's approach allows for the effect of changes in ship section shape which is important for sections found at the ends of the ship, whose contribution to pitch damping should be significant. Whether this refinement is of importance in the final answer as far as motion amplitudes are concerned we do not yet know. At the moment we would point out that Professor Grim's subroutine is very much faster than that of Professor Porter, but the latter program has not as yet been optimized with respect to time consumed in the machine.

Mr. Gale's contribution supplements the objectives of the first part of the paper. His correlations are related to a family of destroyer forms and hence agreement appears better than in our results because of the wallsidedness of the ship sections in the vicinity of the designed waterline. In the M.I.T. program, a ship can be defined by any number of sections up to and including 20; nevertheless, it appears that computations using 10 sections yield approximately similar results. With respect to added mass computation, we prefer either the Grim or the Porter data to the Ursell-Prohaska data even though the differences according to Mr. Gale's calculations do not seem to be large.

The comments of Professor Abkowitz are particularly welcome because he is an acknowledged leader and teacher in the United States in this field. A point on semantics was mentioned by Professor Abkowitz. The differences between the approach of this paper and that of Korvin indicate that the newer approach may be regarded as a "pure strip" theory, whereas the Korvin approach should properly be referred to as a "modified-slender body" theory. The first part of the paper demonstrates the practical utility of the Korvin-Kroukovsky and Jacobs theory. Indeed, this was our primary objective. The fact that we

*See comments by Dyer on paper by Gerritsma and Beukelman.

attempted to reinterprete the above theory in the second part was solely due to the difficulties explained in the previous paragraph. To Dr. Kaplan who has, we believe, in the past, offered explanations for the "erroneous time differentiation," the situation is very clear; to an outsider who attempts to trace back and forth the use of Galilean and non-Galilean coordinate systems in the derivation of the coefficients, the situation is not that clear. With the assistance of Professor Abkowitz, we developed the new approach with the hope that it would yield identical results to the Korvin approach. We did not get identical results, but we did clarify several of the coefficients. With the additional corrections and explanations offered by Professor Abkowitz, the situation may be summarized as follows:

If the added mass distribution for a given ship form is zero at the ends, then the new and Korvin-Kroukovsky approaches differ in two coefficients only, C and E. If the above assumption is not fulfilled, then they differ in four coefficients, namely, e, B, C, and E. We would point out that for several kinds of ships the added mass at the stern is not zero, for example, destroyers, the latest aircraft carriers or even trawlers. Hence, added mass end-effects may be responsible for discrepancies between theory and experiment for these kinds of ships. Furthermore, the new approach as extended by Professor Abkowitz always satisfied the equalities indicated by the more sophisticated hydrodynamic analyses of Newman-Timman, whereas the Korvin-Kroukovsky approach does not. Finally, we believe that the new excitation term will be numerically as adequate as the Jacobs one, due to the small speed dependency.

The authors wish to express their sincere thanks to all discussers. In this case it is not a cliché to say that each and every one of them made a significant contribution to the content of this paper.

* * *

SOME TOPICS IN THE THEORY OF COUPLED SHIP MOTIONS

J. Kotik and J. Lurye
TRG Incorporated
Melville, New York

1. INTRODUCTION

In this paper we present several different results in the theory of ship motions. Some of the results express certain physical quantities in terms of other such quantities, while the remaining results are in the direction of computing physical quantities by solving boundary value problems. The following of our results are of the first type:

Kramers-Kronig relations with forward speed and cross-coupling.

Impulse response in terms of force coefficient for simple harmonic motion.

As work of the second type we present a numerical approach which seeks simplicity by avoiding integrations over curved surfaces and approximations to or representations of curved surfaces. These results already obtained are only a beginning, since they assume zero forward speed, but they are sufficiently promising to encourage us to extend them to include forward speed.

2. KRAMERS-KRONIG RELATIONS FOR HYDRODYNAMIC CROSS-COUPLING COEFFICIENTS AT FORWARD SPEED

In this section we sketch the proof that the real and imaginary parts of the complex hydrodynamic cross-coupling coefficients are connected by the Kramers-Kronig relations* in the case of a submerged body having forward speed. We begin by defining these coefficients.

Let the aforementioned body at first be at rest in a steady flow which (1) satisfies the usual normal velocity condition on the body surface, (2) satisfies the linearized free surface condition, and (3) becomes uniform with velocity $-c\hat{x}$ as $x \to \pm\infty$. (Here $\hat{x}$ is a unit vector in the direction of the positive x axis.) This flow evidently represents forward motion of the body at speed c in the positive x direction. (The x and y axes are horizontal, the z axis is positive upwards, and the origin of the x, y, z coordinate system is at the center of gravity of the

*See footnote after Eq. (2.2).

body when at rest.) Now suppose the body executes a small time-harmonic motion of angular frequency σ in one of the six modes: surge, sway, heave, roll, pitch, or yaw. These modes are denoted respectively by the index $i = 1, 2, \ldots 6$ with $i = 1, 2, 3$ representing translations parallel to the x, y, z axes respectively and $i = 4, 5, 6$ representing rotations about those axes. If $F_{ij} e^{-i\sigma t}$ is the complex hydrodynamic force or moment exerted by the fluid on the body in the jth mode when the body has a complex linear or angular velocity $e^{-i\sigma t}$ in the ith mode with all other velocities zero, then the complex hydrodynamic cross-coupling coefficient H_{ij} is defined by

$$H_{ij}(\sigma) = -F_{ij}(\sigma) \tag{2.1}$$

where the dependence on frequency has been indicated.

It is a familiar fact that a knowledge of the H_{ij} together with the inertial and hydrostatic properties of the body suffices to determine the steady state response of the body to an arbitrary time-harmonic set of exciting forces or moments applied simultaneously in all six modes.

Writing

$$H_{ij}(\sigma) = H^{R}_{ij}(\sigma) + H^{I}_{ij}(\sigma) \tag{2.2}$$

we now outline the proof that H^{R}_{ij} and H^{I}_{ij} satisfy the Kramers-Kronig relations.*

General Equations for Transient Problem

Consider the transient disturbance that results when the body, initially at rest in the steady flow, is given at $t = 0$ a small displacement which is an arbitrary function of time in the ith mode. We characterize this displacement by a vector function of position and time $\vec{\eta}_i(x, y, z, t)$ defined only on the undisplaced body surface (call it S_0), such that $\vec{\eta}_i(x, y, z, t)$ is the displacement at time t in the ith mode of a body surface point whose coordinates were (x, y, z) at $t = 0$. Let $\hat{\mu}_1, \hat{\mu}_2, \hat{\mu}_3$ be unit vectors in the $x, y,$ and z directions respectively, $x_1(t), x_2(t), x_3(t)$ the instantaneous magnitudes of the translational displacements in the first three modes, and $x_4(t), x_5(t), x_6(t)$ the instantaneous magnitudes of the angular displacements in the last three modes.

Then

$$\vec{\eta}_i(t) = x_i(t)\,\hat{\mu}_i \qquad i = 1, 2, 3 \tag{2.3}$$

$$\vec{\eta}_i(x, y, z, t) = x_i(t)\,\hat{\mu}_{i-3} \times \vec{r} \qquad i = 4, 5, 6 \tag{2.4}$$

---

*Strictly, only after certain terms have been subtracted from the H_{ij}, do the real and imaginary parts of the remainder satisfy the Kramers-Kronig relations. See Eqs. (2.24) ff.

where

$$\bar{r} = x\hat{\mu}_1 + y\hat{\mu}_2 + z\hat{\mu}_3 . \tag{2.5}$$

Note that as indicated, $\bar{\alpha}_i$ is independent of x, y, z for $i = 1, 2, 3$. Note also that Eq. (2.4) is valid only for small x_i $(i = 4, 5, 6)$.

Now let $\psi_i(x, y, z, t)$ be the disturbance potential associated with the small displacement $x_i(t)$ in the ith mode only, where $x_i(t) = 0$ for $t < 0$. Then in addition to being a solution of Laplace's equation, ψ_i also satisfies the following conditions:

$$\frac{\partial \psi_i}{\partial z} + \frac{1}{g}\frac{\partial^2 \psi_i}{\partial t^2} - 2\frac{c}{g}\frac{\partial^2 \psi_i}{\partial x \partial t} + \frac{c^2}{g}\frac{\partial^2 \psi_i}{\partial x^2} = 0 \quad (z = 0,\ t > 0) \tag{2.6}$$

$$\frac{\partial \psi_i}{\partial n} = -\left[\frac{\partial \bar{\alpha}_i}{\partial t} + \nabla \times (\bar{\alpha}_i \times \bar{V}_o)\right] \cdot \hat{n} \quad (x, y, z) \text{ on } S_o,\ t > 0. \tag{2.7}$$

In Eq. (2.7) [1], $\hat{n}$ is the unit normal to S_o pointing into the fluid, $\partial/\partial n$ is differentiation in the direction of $\hat{n}$, and $\bar{V}_o(x, y, z)$ is the velocity at (x, y, z) of the steady flow generated by the body at rest in the uniform stream.

The two initial conditions on ψ_i, applied at $t = 0+$ on the undisturbed free surface, are

$$\psi_i(x, y, 0, 0+) = 0 \tag{2.8}$$

$$\frac{\partial}{\partial t}\psi_i(x, y, 0, t)_{t=0+} = 0 . \tag{2.9}$$

In case $\dot{x}_i(0+) = 0$, Eq. (2.8) follows from the fact that ψ_i vanishes not only on $z = 0$ at $t = 0+$, but throughout the fluid. Equation (2.9) is then a consequence of Eq. (2.8) combined with the fact that the free surface elevation due to the body motion is zero at $t = 0+$.

In case the body suddenly acquires a finite velocity at $t = 0+$, i.e., $\dot{x}_i(0+) \neq 0$, then ψ_i vanishes on $z = 0$ at $t = 0+$, though not in general vanishing throughout the fluid. This follows from the equations of impulsively generated motion [2] combined with the fact that the pressure is zero on the free surface. Equation (2.9) then follows as before.

Now by modifying a procedure used by Cummins [3] we can write the following representation for the potential $\psi_i(x, y, z, t)$:

$$\psi_i(x, y, z, t) = \dot{x}_i(t)\,\phi_i(x, y, z) + \int_{-\infty}^{t} \dot{x}_i(\tau)\,\psi_{1i}(x, y, z, t-\tau)\,d\tau . \tag{2.10}$$

Here $\phi_i(x, y, z)$ is a time-independent potential function satisfying the free surface condition

$$\phi_i(x, y, 0) = 0 \tag{2.11}$$

and the boundary condition

$$\frac{\partial \phi_i}{\partial n} = -\hat{\mu}_i \cdot \hat{n} \quad \text{on } S_o, \quad i = 1, 2, 3 \tag{2.12a}$$

$$\frac{\partial \phi_i}{\partial n} = -(\hat{\mu}_{i-3} \times \bar{r}) \cdot \hat{n} \quad \text{on } S_o, \quad i = 4, 5, 6. \tag{2.12b}$$

$\psi_{1i}(x, y, z, t)$ is a potential function that satisfies the free surface condition, Eq. (2.6), for $t > 0$, and the boundary condition

$$\frac{\partial \psi_{1i}}{\partial n} = -\nabla \times (\hat{\mu}_i \times \bar{V}_o) \cdot \hat{n} \quad \text{on } S_o, \quad i = 1, 2, 3 \tag{2.13a}$$

$$\frac{\partial \psi_{1i}}{\partial n} = -\nabla \times \left[(\hat{\mu}_{i-3} \times \bar{r}) \times \bar{V}_o\right] \cdot \hat{n} \quad \text{on } S_o, \quad i = 4, 5, 6 \tag{2.13b}$$

for $t > 0$.*

The initial conditions on ψ_{1i} are

$$\psi_{1i}(x, y, 0, 0+) = 0 \tag{2.14}$$

and

$$\frac{\partial}{\partial t} \psi_{1i}(x, y, 0, t)_{t=0+} = -g \frac{\partial}{\partial z} \phi_i(x, y, z)_{z=0}. \tag{2.15}$$

It can be verified by direct substitution that the function $\psi_i(x, y, z, t)$ defined by Eq. (2.10) does indeed satisfy Eqs. (2.6), (2.7), (2.8), and (2.9) when the functions $\phi_i(x, y, z)$ and $\psi_{1i}(x, y, z, t)$ satisfy Eqs. (2.11) through (2.15). We recall that $\bar{\alpha}_i$ appearing in Eq. (2.7) is given by Eq. (2.3) or (2.4).

Duhamel's Principle

We now suppose the body, initially at rest in the stream, to be given (at $t = 0$) a unit displacement in the ith mode. The fact that such a displacement is not small is irrelevant. Let the potential corresponding to the unit displacement be $\hat{\psi}_i(x, y, z, t)$. Since in this case $\dot{x}_i(t) = \delta(t)$, it follows from Eq. (2.10) that

*Note that ϕ_i has the dimensions of potential/velocity when $i = 1, 2, 3$ and potential $\times$ time when $i = 4, 5, 6$. ψ_{1i} has the dimensions potential/length when $i = 1, 2, 3$ and potential/angle = potential when $i = 4, 5, 6$.

$$\Phi_i(x,y,z,t) = \delta(t)\,\psi_i(x,y,z) + H(t)\,\chi_i(x,y,z,t) \tag{2.16}$$

where $\delta(t)$ is the Dirac delta function and $H(t)$ the Heaviside unit function. Note that $\delta(t)$ has the dimension $1/T$.

Denote by $p_i(x,y,z,t)$ the linearized pressure arising from the unit displacement, the pressure being evaluated on the displaced surface of the body but expressed in terms of coordinates on the undisplaced surface S_o. Then from the linearized form of Bernoulli's principle, we have

$$p_i(x,y,z,t) = -\rho\left[\frac{\partial\Phi_i}{\partial t} + \vec{V}_0(x,y,z)\cdot\nabla\Phi_i - \frac{1}{2}\,\vec{\alpha}_i(x,y,z,t)\cdot\nabla\left(V_0^2(x,y,z)\right)\right]$$

$$(x,y,z) \text{ on } S_o . \tag{2.17}$$

In Eq. (2.17), the last term on the right corrects for the fact that coordinates on the undisplaces surface are used in expressing the pressure on the displaced surface. In that term $\vec{\alpha}_i$ has the forms of Eq. (2.3) or (2.4) with $x_i(t) = H(t)$, the Heaviside unit function.

Let $f_{ij}(t)$ be the hydrodynamic force or moment on the body in the jth mode arising from the unit displacement applied at $t = 0$ to the body in the ith mode. Then

$$f_{ij}(t) = -\iint_{S_o} p_i(x,y,z,t)\,\hat{n}\cdot\hat{\mu}_j\,dS \qquad \begin{array}{l} i = 1,\ldots 6 \\ j = 1,2,3 \end{array} \tag{2.18}$$

$$f_{ij}(t) = -\iint_{S_o} p_i(x,y,z,t)\,\vec{r}\times\hat{n}\cdot\hat{\mu}_{j-3}\,dS \qquad \begin{array}{l} i = 1,\ldots 6 \\ j = 4,5,6 . \end{array} \tag{2.19}$$

In Laplace's equation and in the Eqs. (2.6) through (2.9) satisfied by ψ_i, the coefficients of χ_i are independent of time. From this it follows that if the unit displacement is applied at $t = \tau$ instead of $t = 0$, the resulting force or moment will be $f_{ij}(t-\tau)$. Moreover, all the equations are linear. Thus we may invoke Duhamel's principle and write that $f_i^j(t)$, the force or moment in the jth mode corresponding to the velocity $\dot{x}_i(t)$ in the ith mode, is given by

$$f_i^j(t) = \int_{-\infty}^{t} f_{ij}(t-\tau)\,\dot{x}_i(\tau)\,d\tau . \tag{2.20}$$

In particular, when $\dot{x}_i(t) = H(t)\,e^{-i\sigma t}$,

$$f_i^j(t) = \int_0^t f_{ij}(t-\tau)\,e^{-i\sigma\tau}\,d\tau$$

$$= e^{-i\sigma t}\int_0^t f_{ij}(\tau')\,e^{i\sigma\tau'}\,d\tau' . \tag{2.21}$$

From Eq. (2.21), we see that if $F_{ij}e^{-i\sigma t}$ is the complex steady state hydrodynamic force or moment on the body in the jth mode corresponding to the steady state velocity $e^{-i\sigma t}$ in the ith mode, then

$$F_{ij} = \int_0^\infty f_{ij}(\tau')\,e^{i\sigma\tau'}\,d\tau' = -H_{ij} \tag{2.22}$$

where $f_{ij}(t)$ is given by Eqs. (2.18) and (2.19) and the second equality in (2.22) comes from Eq. (2.1).

Kramers-Kronig Relations

If the integral in (2.22) converged suitably for all real σ, then it would be an analytic function of σ in the half plane $\operatorname{Im}\sigma > 0$, vanishing as $\sigma \to \infty$, whence it would follow that H^R_{ij} and H^I_{ij} satisfy the Kramers-Kronig relations. Now, construction of $f_{ij}(\tau)$ from Eqs. (2.16) through (2.19) reveals that in fact, H_{ij} is the sum of two types of functions of σ, such that the real and imaginary parts of the first type satisfy the Kramers-Kronig relations, while the functions of the second type are too singular either at $\sigma = 0$ or $\sigma = \infty$ for the Kramers-Kronig relations to hold. On the other hand, the functions of the second type depend only on infinite frequency potentials and on the steady flow in the absence of oscillations, and may therefore be regarded as easier to calculate. Thus it is the less-known part of H_{ij} that satisfies the Kramers-Kronig relations.

Specifically, when $i, j = 1, 2, 3$ we find by substituting from Eqs. (2.16), (2.17), and (2.18), into Eq. (2.22):

$$\begin{aligned}
\frac{1}{\rho} H_{ij}(\sigma) = {} & \int_0^\infty h'(\tau)\,e^{i\sigma\tau}\,d\tau \iint_{S_o} \phi_i\ \hat{n}\cdot\hat{\mu}_j\,dS \\
& + \int_0^\infty h(\tau)\,e^{i\sigma\tau}\,d\tau \iint_{S_o} \overline{V}_o\cdot\nabla\phi_i\ \hat{n}\cdot\hat{\mu}_j\,dS \\
& - \frac{1}{2}\int_0^\infty e^{i\sigma\tau}\,d\tau \iint_{S_o} \left[\hat{\mu}_i\cdot\nabla(V_o^2)\right]\ \hat{n}\cdot\hat{\mu}_j\,dS \\
& + \int_0^\infty h(\tau)\ \psi_{1i}(x,y,z,\tau)\,e^{i\sigma\tau}\,d\tau \iint_{S_o} \hat{n}\cdot\hat{\mu}_j\,dS \\
& + \int_0^\infty \frac{\partial}{\partial\tau}\psi_{1i}(x,y,z,\tau)\,e^{i\sigma\tau}\,d\tau \iint_{S_o} \hat{n}\cdot\hat{\mu}_j\,dS \\
& + \int_0^\infty \overline{V}_o\cdot\nabla\psi_{1i}(x,y,z,\tau)\,e^{i\sigma\tau}\,d\tau \iint_{S_o} \hat{n}\cdot\hat{\mu}_j\,dS \qquad \begin{array}{l} i = 1, 2, 3 \\ j = 1, 2, 3\,. \end{array}
\end{aligned} \tag{2.23}$$

After some manipulation this reduces to

$$
\begin{aligned}
H_{ij}(\sigma) = \hat{H}_{ij}(\sigma) &- i\sigma\rho \iint_{S_o} \phi_i \, \hat{n}\cdot\hat{\mu}_j \, dS \\
&+ \rho \iint_{S_o} \bar{V}_o \cdot \nabla\phi_i \, \hat{n}\cdot\hat{\mu}_j \, dS + \rho \iint_{S_o} g_i \, \hat{n}\cdot\hat{\mu}_j \, dS \\
&+ \frac{\rho}{i\sigma} \iint_{S_o} \left[\hat{\mu}_i \cdot \nabla(V_o^2)\right] \hat{n}\cdot\hat{\mu}_j \, dS \qquad \begin{matrix} i = 1, 2, 3 \\ j = 1, 2, 3 \, . \end{matrix}
\end{aligned}
\tag{2.24}
$$

Although details are omitted, we have assumed in deriving Eq. (2.24) that the

$$\lim_{t\to\infty} \psi_{1i}(x, y, z, t)$$

exists and is equal to the incremental steady flow associated with the body in its displaced position.

In Eq. (2.24), the potential $g_i(x, y, z)$ is defined as

$$\lim_{t\to 0} \psi_{1i}(x, y, z, t)$$

and is therefore the infinite frequency potential satisfying the boundary condition in Eq. (2.13) on S_o.

The real and imaginary parts of H_{ij} satisfy the Kramers-Kronig relations:

$$\hat{H}^R_{ij}(\sigma) = \frac{1}{\pi} \fint_{-\infty}^{\infty} \frac{\hat{H}^I_{ij}(\sigma')}{\sigma' - \sigma} \, d\sigma' \tag{2.25}$$

$$\hat{H}^I_{ij}(\sigma) = -\frac{1}{\pi} \fint_{-\infty}^{\infty} \frac{\hat{H}^R_{ij}(\sigma')}{\sigma' - \sigma} \, d\sigma' \tag{2.26}$$

where the bar on the integral indicates the Cauchy principal value.

Thus from a knowledge of either $\hat{H}^R_{ij}$ or $\hat{H}^I_{ij}$, the other can be inferred, while as already mentioned, the remaining terms in Eq. (2.24) may be regarded as comparatively easy to calculate.

For completeness, we include the expressions for H_{ij}, analogous to Eq. (2.24), for the remaining mode pairs. We have

$$H_{ij}(\sigma) = \hat{H}_{ij}(\sigma) - i\sigma\rho \iint_{S_o} \phi_i\, \hat{n}\cdot\hat{\mu}_j\, dS + \rho \iint_{S_o} \bar{V}_o \cdot \nabla\phi_i\, \hat{n}\cdot\hat{\mu}_j\, dS + \rho \iint_{S_o} g_i\, \hat{n}\cdot\hat{\mu}_j\, dS$$

$$+ \frac{\rho}{i\sigma} \iint_{S_o} \left[\hat{\mu}_{i-3}\times\bar{r}\cdot\nabla(V_o^2)\right] \hat{n}\cdot\hat{\mu}_j\, dS \qquad \begin{matrix} i = 4, 5, 6 \\ j = 1, 2, 3 \end{matrix} \tag{2.27}$$

$$H_{ij}(\sigma) = \hat{H}_{ij}(\sigma) - i\sigma\rho \iint_{S_o} \phi_i\, \bar{r}\times\hat{n}\cdot\hat{\mu}_{j-3}\, dS$$

$$+ \rho \iint_{S_o} (\bar{V}_o\cdot\nabla\phi_i)\, \bar{r}\times\hat{n}\cdot\hat{\mu}_{j-3}\, dS + \rho \iint_{S_o} g_i\, \bar{r}\times\hat{n}\cdot\hat{\mu}_{j-3}\, dS$$

$$+ \frac{\rho}{i\sigma} \iint_{S_o} \left[\hat{\mu}_i\cdot\nabla(V_o^2)\right] \bar{r}\times\hat{n}\cdot\hat{\mu}_{j-3}\, dS \qquad \begin{matrix} i = 1, 2, 3 \\ j = 4, 5, 6 \end{matrix} \tag{2.28}$$

$$H_{ij}(\sigma) = \hat{H}_{ij}(\sigma) - i\sigma\rho \iint_{S_o} \phi_i\, \bar{r}\times\hat{n}\cdot\hat{\mu}_{j-3}\, dS$$

$$+ \rho \iint_{S_o} (\bar{V}_o\cdot\nabla\phi_i)\, \bar{r}\times\hat{n}\cdot\hat{\mu}_{j-3}\, dS + \rho \iint_{S_o} g_i\, \bar{r}\times\hat{n}\cdot\hat{\mu}_{j-3}\, dS$$

$$+ \frac{\rho}{i\sigma} \iint_{S_o} \left[\hat{\mu}_{i-3}\times\bar{r}\cdot\nabla(V_o^2)\right] \bar{r}\times\hat{n}\cdot\hat{\mu}_{j-3}\, dS \qquad \begin{matrix} i = 4, 5, 6 \\ j = 4, 5, 6\,. \end{matrix} \tag{2.29}$$

In all of these, the real and imaginary parts of $\hat{H}_{ij}(\sigma)$ satisfy Eqs. (2.25) and (2.26).

We conclude with the following remarks:

1. The Kramers-Kronig relations imply that any symmetry property in i and j possessed by the element $\hat{H}^R_{ij}$ is shared by $\hat{H}^I_{ij}$ and vice-versa. Thus one need only establish such a property for the real or imaginary part alone.

2. It is known [4] that a submerged body oscillating in a stream can for certain modes, frequency ranges, and speeds acquire energy from the stream as a result of the oscillation (negative damping). The question then naturally arises whether the Kramers-Kronig relations can still hold if over some part of the frequency range negative damping occurs. Highly tentative considerations indicate that there is at least a possibility of deriving a modified form of the Kramers-Kronig relations in the case of negative damping; however, no firm conclusions have been reached as yet.

3. EXPRESSION OF THE IMPULSE RESPONSE IN TERMS OF ADDED-MASS AND DAMPING PARAMETERS

In [5] it was pointed out that $F(t)$, the hydrodynamic force exerted by the body when the body acceleration is $\delta(t)$, can be calculated from either the damping or added-mass parameter (for simple-harmonic oscillation) via the Kramers-Kronig relations followed by a Fourier transformation. We will now discuss this point further, including some observations on a later publication [6] which also treats transients and their relations to force parameters.

Let us recall that according to Eq. (A-5) of [5] we have

$$\int_0^\infty F(\tau')\, e^{i\sigma\tau'}\, d\tau' = \tau\rho\, p'(\sigma) = \tau\rho\left[p_m'(\sigma) + i p_d'(\sigma)\right] \tag{3.1}$$

where

$F(t)$ = hydrodynamic heave force exerted by the body on the fluid, per unit step heave velocity of the body at $t = 0$, $F(t) = 0$ for $t < 0$;

$p'(\sigma)$ = force parameter = $p_m' + i p_d'$;

$p_m'(\sigma)$ = added-mass parameter;

$p_d'(\sigma)$ = damping parameter;

σ = radian frequency of oscillation;

τ = submerged (or any other) volume of the body for three-dimensional problems, and volume/unit length for two-dimensional problems.

It follows that

$$F(t) = \frac{\tau\rho}{2\pi}\int_{-\infty}^{\infty} p'(\sigma)\, e^{-i\sigma t}\, d\sigma$$

$$= \frac{\tau\rho}{\pi}\int_0^\infty \left[p_m'(\sigma)\cos\sigma t + p_d'(\sigma)\sin\sigma t\right] d\sigma$$

$$= \frac{\tau\rho}{\pi}\left\{p_m'(\infty)\,\pi\delta(t) + \int_0^\infty \left[\Delta p_m'(\sigma)\cos\sigma t + p_d'(\sigma)\sin\sigma t\right] d\sigma\right\}, \tag{3.2}$$

where

$$\Delta p_m'(\sigma) = p_m'(\sigma) - p_m'(\infty).$$

However, it is sufficient to know either $p_m'(\sigma)$ or $p_d'(\sigma)$, due to the Kramers-Kronig relations, and in fact those relations imply the following:

$$F(t) = V\rho p_m'(\infty)\,\delta(t) + \frac{2}{\pi} V\rho \int_0^\infty p_d'(\sigma)\sin\sigma t\,d\sigma \tag{3.3}$$

$$F(t) = V\rho p_m'(\infty)\,\delta(t) + \frac{2}{\pi} V\rho \int_0^\infty \left[\Delta p_m'(\sigma)\right]\cos\sigma t\,d\sigma \tag{3.4}$$

($\delta(t)$ has dimensions T^{-1}). Note that the δ-function acceleration of the body produces a δ-function hydrodynamic force having strength proportional to the added-mass parameter at infinite frequency. Heave at infinite frequency is uniform translation of the double body in an infinite fluid. Note also that the two integrals in (3.3) and (3.4) are equal. This implies that

$$\int_0^\infty \Delta p_m'(\sigma)\,d\sigma = 0\,, \tag{3.5}$$

a useful fact which does not seem to have been observed previously.

The relations Eqs. (3.2) - (3.4) are useful for direct calculation, when $p_m'(\sigma)$ and/or $p_d'(\sigma)$ are known, exactly or approximately, and for finding asymptotic expansions as $t \to 0, \infty$. For example, to find $F(t)$ as $t \to \infty$, we first write

$$\int_0^\infty p_d'(\sigma)\sin\sigma t\,d\sigma = -\,p_d'(\sigma)\frac{\cos\sigma t}{t}\Bigg|_0^\infty + \int_0^\infty \frac{\cos\sigma t}{t}\frac{\partial}{\partial\sigma}\left[p_d'(\sigma)\right]d\sigma$$

$$= \frac{p_d'(0)}{t} + o(1)\,. \tag{3.6}$$

Now as stated in [5], for the heaving motion of a cylinder of arbitrary section,

$$p_d'(0) = (2a)^2/V\,, \tag{3.7}$$

where $2a$ = width at the free surface and V is the submerged volume per unit length, so that for such a cylinder, we have from Eq. (3.3)

$$F(t) \sim \frac{2}{\pi} V\rho\,\frac{(2a)^2}{Vt} = \frac{8a^2\rho}{\pi t} \quad \text{as} \quad t \to \infty\,. \tag{3.8}$$

This hydrodynamic force per unit length exerted by the body on the fluid is downward if the δ-function acceleration is downward.

For an arbitrary heaving three-dimensional body we have, as noted in [5],

$$p_d'(\sigma) = p_d(Ka) = b_1 Ka + o(Ka)\,, \tag{3.9}$$

as $Ka \to 0$, with

$$b_1 = \frac{\pi^2}{2\pi} a^3, \qquad a = \sqrt{A_c/\pi} \tag{3.10}$$

where A_c is the area in which the body intersects the free surface. Hence, at least formally,

$$\begin{aligned} p_d'(\sigma) &\sim b_1 a \frac{\sigma^2}{g} \\ \frac{\partial}{\partial\sigma} p_d'(\sigma) &\sim (2b_1 a\sigma/g) \\ \frac{\partial^2}{\partial\sigma^2} p_d'(\sigma) &\sim 2b_1 a/g, \end{aligned} \tag{3.11}$$

all as $\sigma \to 0$.

After integrating by parts several times, we may write

$$\begin{aligned} \int_0^\infty p_d'(\sigma) \sin \sigma t \, d\sigma &= -\frac{1}{t^3}(2b_1 a/g) - \int_0^\infty \frac{\cos \sigma t}{t^3} \frac{\partial^3}{\partial\sigma^3} p_d'(\sigma)\, d\sigma \\ &= -\frac{1}{t^3} \cdot \frac{2}{g} \frac{A_c^2}{2\pi} + o(1/t^3) \\ &= -\frac{A_c^2}{g\pi} \cdot \frac{1}{t^3} + o(1/t^3) \end{aligned} \tag{3.12}$$

as $t \to \infty$. Therefore, from Eq. (3.6) the heave force exerted by an arbitrary body is

$$F(t) \sim \frac{2}{\pi}\rho\left(-\frac{A_c^2}{g}\frac{1}{t^3}\right) = -\frac{2\rho A_c^2}{\pi g t^3} \tag{3.13}$$

as $t \to \infty$. We see that this force exerted by the body on the fluid is upward if the δ-function acceleration is downward.

We will now find the heave displacement, for large time, of a body released at zero velocity from hydrostatic disequilibrium. The equation of motion, for an arbitrary surface-piercing body, is

$$M\ddot{y}_0(t) = -\rho g A_c y_0(t) - \int_0^t F(t-\tau)\, \ddot{y}_0(\tau)\, d\tau \tag{3.14}$$

where $y_o(t)$ is the heave displacement measured with respect to the position of buoyant equilibrium. For three-dimensional bodies, M is the mass of the body, and A_c its cross-section area in the free surface, while for two-dimensional bodies M is the mass per unit length of the body and A_c its width in the free surface.

Taking the Laplace transform of Eq. (3.14), introducing the initial conditions that $y_o(t) = y_o(0)$ at $t = 0$, $\dot{y}_o(0) = 0$, and converting Fourier transforms, we find for $Y_o(\omega)$, the Fourier transform of $y_o(t)$,

$$Y_o(\omega) = \frac{-iy_o(0)\,\omega[\pi\rho\,p'(\omega)+M]}{\rho g A_c - \omega^2[\pi\rho\,p'(\omega)+M]} \tag{3.15}$$

Separating real and imaginary parts, we can write Eq. (3.15) in the form

$$Y_o(\omega) = -iy_o(0)\left[Y_o'^R(\omega) + iY_o'^I(\omega)\right] \tag{3.16}$$

where the primes mean that $-iy_o(0)$ has been factored out as shown. $Y_o'^R$ and $Y_o'^I$ have the following forms:

$$Y_o'^R(\omega) = \frac{\omega(\pi\rho\,p_m'+M)\left[\rho g A_c - \omega^2(\pi\rho\,p_m'+M)\right] - \omega^3\pi^2\rho^2 p_d'^2}{\left[\rho g A_c - \omega^2(\pi\rho\,p_m'+M)^2\right]^2 + \omega^4\pi^2\rho^2 p_d'^2} \tag{3.17}$$

$$Y_o'^I(\omega) = \frac{\omega\pi\rho^2 p_d' g A_c}{\left[\rho g A_c - \omega^2(\pi\rho\,p_m'+M)^2\right]^2 + \omega^4\pi^2\rho^2 p_d'^2} \tag{3.18}$$

Since $p_m'(\omega)$ is an even function and $p_d'(\omega)$ an odd function of ω, one sees from Eqs. (3.17) and (3.18) that $Y_o'^R$ is odd and $Y_o'^I$ is even in ω. It follows that upon taking the inverse Fourier transform of Eq. (3.15) we can write

$$y_o(t) = \frac{y_o(0)}{\pi}\int_0^\infty \left(Y_o'^I(\omega)\cos\omega t - Y_o'^R(\omega)\sin\omega t\right) d\omega . \tag{3.19}$$

We now use Eq. (3.19) together with Eqs. (3.17) and (3.18) to infer the asymptotic form of $y_o(t)$ as $t \to \infty$. This form depends on the behaviour of $Y_o'^I(\omega)$ and $Y_o'^R(\omega)$ in the neighborhood of $\omega = 0$. We treat the cases of two- and three-dimensional bodies separately.

Two-Dimensional Bodies

In this case [5]

$$p_m'(\omega) \doteq -\frac{2A_c^2}{\pi}\log\omega , \qquad \omega \to 0 \tag{3.20}$$

$$p_d'(0) \approx \frac{A_c^2}{g} . \tag{3.21}$$

From these equations combined with Eqs. (3.17) and (3.18) we infer that

$$Y_o'^R(\sigma) \approx -\frac{2}{\pi}\frac{A_c}{g}\,\sigma\log\sigma , \qquad \sigma \to 0 \tag{3.22}$$

$$Y_o'^I(\sigma) \approx \frac{A_c}{g}\,\sigma , \qquad \sigma \to 0 . \tag{3.23}$$

Incorporating these results into the integral of Eq. (3.19) we find, through integrating by parts, the following leading terms at large t:

$$\int_0^\infty Y_o'^I(\sigma)\cos\sigma t\,d\sigma \approx -\frac{A_c}{gt^2} , \qquad t \to \infty \tag{3.24}$$

$$\int_0^\infty Y_o'^R(\sigma)\sin\sigma t\,d\sigma \approx -\frac{A_c}{gt^2} , \qquad t \to \infty \tag{3.25}$$

whence

$$y_o(t) \approx -\frac{2}{\pi}\,y_o(0)\,\frac{A_c}{gt^2} = -\frac{4}{\pi}\,y_o(0)\,\frac{a}{gt^2} , \qquad t \to \infty \tag{3.26}$$

where $a = A_c/2$ is the half-width of the cylindrical body in the free surface.

Equation (3.26) gives the large time behaviour of the heave displacement of a cylindrical body released at zero velocity from a position of hydrostatic disequilibrium. The expression on the far right of this equation agrees with that obtained by Ursell [6] for a half-submerged circular cylinder of radius a. However we now see that this expression is valid for cylinders of arbitrary cross section having a width $2a$ in the free surface.

Three-Dimensional Bodies

For three-dimensional bodies, we have [5]

$$p_m'(\sigma) \approx p_m'(0) - \frac{1}{\pi}\frac{A_c^2}{\pi g}\sigma^2\log\sigma \qquad \sigma \to 0 \tag{3.27}$$

$$p_d'(\sigma) \approx \frac{A_c^2}{2\pi g}\sigma^2 \qquad \sigma \to 0 . \tag{3.28}$$

Incorporating these results into Eqs. (3.17) through (3.19), we find after a number of integrations by parts in (3.19)

$$y_0(t) \sim -\frac{6}{\pi} y_0(0) \frac{A_c}{g^2 t^4} \qquad t \to \infty . \tag{3.29}$$

A comparison of this expression with the corresponding one for cylindrical bodies, Eq. (3.26), shows that:

1. the approach to buoyant equilibrium in three dimensions is asymptotically faster than in two dimensions by a factor proportional to $1/t^2$, and

2. the approach to equilibrium in three dimensions is asymptotically from the side of the equilibrium position defined by the initial displacement; in two dimensions the approach is from the side opposite the initial displacement.

It is our intention to present, in a future publication, calculations of transient forces and displacements using Hi-Fi approximations* to $p_d'(\cdot)$.

4. NUMERICAL DETERMINATION OF HYDRODYNAMIC COUPLING COEFFICIENTS FROM VOLUMETRIC SINGULARITY DISTRIBUTIONS

In this section we outline briefly a numerical scheme for calculating the hydrodynamic coupling coefficients H_{ij} (already defined in Sections 2, 3, and 4) for a fully or partially submerged body engaging in small time harmonic oscillations. Our computer program so far covers only the zero speed case, but its extension to forward speed should present no difficulty in principle; the chief additional complication would center on the calculation of the time-harmonic Green's function for a point source in a steady stream below a free surface.

The idea of the method is to approximate the velocity potential exterior to the oscillating body by the potential of a time-harmonic finite set of singularities contained in the interior of the body surface. These singularities will usually be either sources or dipoles although higher order multipoles can also be used. The strengths of the singularities are determined by the requirement that the normal velocity they induce on the submerged portion of the undisplaced body surface, S_o, should best approximate the actual normal velocity of S_o in a certain mean square sense.† Specifically, let $P_m (m = 1, \dots M)$ be the points where the M singularities of complex strength q_m are located interior to S_o, and let $P^n (n = 1, \dots N)$ be a set of points on S_o with $N > M$. Let a_{mn} be the complex normal velocity at P^n due to a singularity of unit strength at P_m, the singularity potential satisfying the linearized free surface condition. Finally let V^n by the actual complex normal velocity of S_o at P^n due to the oscillation. Then we seek to determine the q_m so as to minimize the mean square expression

$$J = \frac{1}{N} \sum_{n=1}^{N} \left| V^n - \sum_{m=1}^{M} a_{mn} q_m \right|^2 . \tag{4.1}$$

*Examples are given in [5].

†However, we plan to consider other types of approximation as well.

Note that the value of J when the q_m have their minimizing values, serves as a measure of the closeness with which the exact potential exterior to S_o has been approximated.

It is easily shown that the minimizing q_m satisfy the following set of linear algebraic equations:

$$\sum_{m=1}^{M} b_{km} q_m = c_k \qquad k = 1, \ldots M \tag{4.2}$$

where

$$b_{km} = \sum_{n=1}^{N} a_{kn}^{*} a_{mn} \tag{4.3}$$

$$c_k = \sum_{n=1}^{N} a_{kn}^{*} V^{n} . \tag{4.4}$$

where the asterisk denotes complex conjugate.

Once the q_m are determined by solving Eq. (4.2), several methods are available for calculating the hydrodynamic forces and moments on the body and thereby the hydrodynamic coupling coefficients.

Lagally's Method

Cummins [7] has derived an extension of Lagally's theorem to time-dependent flows, which can be used to obtain the oscillatory hydrodynamic forces acting on the body. The calculation is exceedingly simple, requiring (for the linearized force in the case of small oscillations) a knowledge of the singularity strengths and locations and nothing else. (A simple summation over the singularities must be performed.) However, this method suffers from two limitations. One, it is applicable only to fully submerged bodies since the extension of Lagally's theorem to bodies that pierce the free surface does not yet seem to have been accomplished. Two, even for fully submerged bodies, Cummins' method gives only the forces and not the moments.

Energy Method

By considering the rate at which energy is radiated out to infinity, one can express the real parts of the complex cross-coupling coefficients for time-harmonic motions as a sum over the singularities. The terms in the sum involve the singularity strengths and certain potentials or potential gradients evaluated at the singularity locations. With this technique, the real parts of the coupling coefficients corresponding to both forces and moments can be obtained. Moreover the body need not be fully submerged. Finally, once the real parts of the coupling coefficients are determined as a function of the frequency, the imaginary parts can be calculated from the Kramers-Kronig relations.

We quote the result for a distribution of sources:

$$H_{ij}^{R} = -2\pi\rho\omega \, \mathrm{Im} \sum_{m=1}^{N_i} \sum_{k=1}^{N_j} (q_{im} q_{jk}^{*} + q_{im}^{*} q_{jk}) \, \psi^{*}(P_{im}, P_{jk}) . \tag{4.5}$$

Here the $q_{im}(m = 1, \ldots N_i)$ are the strengths of the sources at the points P_{im}, these sources generating the approximate motion in the ith mode, while the $q_{jk}(j = 1, \ldots N_j)$ have the same significance for the jth mode. Some of the points P_{im} and P_{jk} may coincide. The function of position $\psi(P_{im}, P_{jk})$ is the regular part of the Green's function $G(P_{im}, P_{jk})$ satisfying the free surface condition. Finally, ρ is the fluid density and ω the angular frequency of the oscillation.

Pressure Integrals

The most obvious way to arrive at the forces and moments on the body is to use the singularity strengths to obtain the pressure distribution on the submerged body surface and then form the appropriate pressure integrals over that surface. From a computational standpoint, it is extremely important to note that the integrations need not be carried out over the actual surface of the body. Rather, one can express each component of force or moment as an integral or combination of integrals over the plane domains defined by projecting the submerged part of the body surface onto each of the three coordinate planes. Thus only ordinary double integrals over plane regions need be computed.

We conclude with the results of a preliminary numerical test. These results were obtained by applying our procedure to the case of a prolate spheroid in an infinite fluid. The assumed motion of the spheroid was a small time-harmonic translation in the direction of its axis (surge). The thickness-to-length ratio was 1/8. For the singularity distribution, we chose a set of 45 axially directed dipoles located on the axis of the spheroid. Having determined the dipole strengths in the manner already described, we then calculated the amplitude of the linearized time-harmonic pressure on the surface of the spheroid.

Our results are shown in Figs. 1 and 2. Figure 1 is a plot of the normalized real amplitude of the time-harmonic dipole moment vs normalized axial distance. The normalized real amplitude is defined as μ/μ_0, where μ is the real amplitude of the unnormalized dipole moment, and μ_0 is the amplitude of the dipole moment at the center of the spheroid. The normalized axial distance is x/a, where x is the distance from the center of the spheroid measured along its axis and a is the half-length of the spheroid. The solid curve represents the exact continuous distribution of dipole strength — this is known to be parabolic for surge in an infinite fluid — while the two broken curves represent approximations computed by our procedure. In both of the latter, a discrete distribution of 45 equally spaced axial dipoles was assumed to lie between the foci. The two approximations differ in that the mean-square boundary condition involved 48 points on the spheroid surface in the one case and 96 points in the

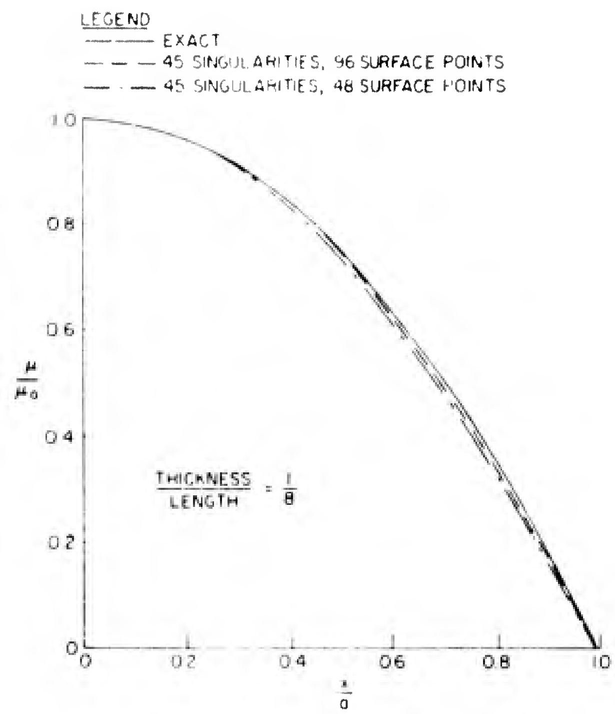

Fig. 1 - Normalized amplitude of dipole moment for surging prolate spheroid

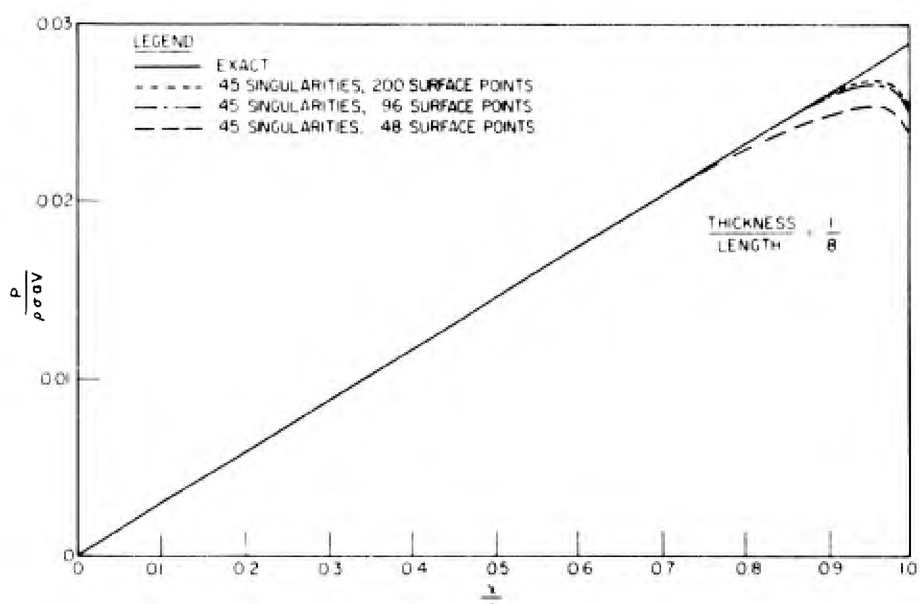

Fig. 2 - Normalized amplitude of time-harmonic pressure on surface of surging prolate spheroid

other. As one might have expected, the second approximation is somewhat better; however both are very close to the exact distribution.

In Fig. 2 we have plotted the normalized real amplitude of the time-harmonic pressure on the surface of the spheroid vs normalized axial distance. (From symmetry, the pressure is obviously a function of the axial coordinate only.) The normalized real amplitude is defined as $P/\rho\omega aV$, where P is the real amplitude of the unnormalized pressure, and V is the real amplitude of the spheroid velocity. The solid curve represents the exact pressure distribution, which in the case of surge in an infinite fluid, is known to be a linear function of the axial distance. As can be seen from their labels, two of the broken curves were calculated from the approximate dipole distributions of Fig. 1. The third pressure curve was obtained from a discrete distribution of 45 dipoles whose strengths were computed by applying the mean square boundary condition to a set of 200 points on the spheroid surface. Evidently it is only near the nose that the approximate pressures depart sensibly from the exact one, and even there the relative error is less than 15%.

It is worth noting that neither the computation of the dipole strengths nor the subsequent pressure calculations exceeded 0.01 hr of IBM 7094 machine time for any one case.

REFERENCES

1. R. Timman and J. N. Newman, "The Coupled Damping Coefficients of a Symmetric Ship," Journal of Ship Research 5, pp. 1-7, March 1962.

2. H. Lamb, Hydrodynamics, 6th ed., Dover Publications, New York, pp. 10-11 (1945).

3. W. E. Cummins, The Impulse Response Function and Ship Motions, David Taylor Model Basin Report presented at the Symposium on Ship Theory, Institut für Schiffbau der Universität Hamburg, 25-27, January 1962.

4. J. N. Newman, "The Damping of an Oscillating Ellipsoid Near a Free Surface," Journal of Ship Research 5, pp. 44-58, December 1961.

5. J. Kotik and V. Mangulis, "On the Kramers-Kronig Relations for Ship Motions," International Shipbuilding Progress 9, pp. 361-367, September 1962.

6. F. Ursell, "The Decay of the Free Motion of a Floating Body," Journal of Fluid Mechanics 19, Part 2, pp. 305-319, June 1964.

7. W. E. Cummins, "The Force and Moment on a Body in a Time-Varying Potential Flow," Journal of Ship Research 1, pp. 7-18, April 1957.

* * *

KNOWN AND UNKNOWN PROPERTIES OF THE TWO-DIMENSIONAL WAVE SPECTRUM AND ATTEMPTS TO FORECAST THE TWO-DIMENSIONAL WAVE SPECTRUM FOR THE NORTH ATLANTIC OCEAN

Willard J. Pierson, Jr.
New York University
New York, New York

ABSTRACT

The two-dimensional wave spectrum has been estimated once by stereo photogrammetric techniques, and a number of times by buoys developed by the National Institute of Oceanography. The results obtained do not contradict each other. Some questions have recently been resolved and one remains unresolved. There do not appear to be spectral components in a pure wind sea traveling in a direction opposed to the wind. The theory relating wave number to frequency from linear considerations can be applied. Whether or not the spectrum is bi-modal as a function of direction for certain frequencies is not yet decided. A form for the directional spectrum of a fully developed wind sea is proposed.

Under certain assumptions about the generation of wind seas attempts to forecast the two-dimensional spectrum at 519 points on the North Atlantic have been made. Verification of the forecasts against observed two-dimensional spectra are not possible. However, they verify fairly well in terms of significant height and against the observed frequency spectra and in terms of swell and wave decay. It appears that the forecasting procedure is fairly close to being correct.

INTRODUCTION

Nearly all of the papers at this symposium are concerned with the deterministic mathematics applicable to the analysis of the classical hydrodynamic problems that are concerns of the naval hydrodynamicist. However, one of the inputs to the problem of understanding the motions of marine craft at sea is essentially probabilistic in nature. The actual sequence of waves that will be met on a given cruise can never be predicted before the fact. To predict certain features of the behavior of such a craft on a certain cruise for, say, the next 6 hours or, perhaps, even the next 24 hours, one must give up the deterministic world and predict the probabilities of certain events and statistics derivable from them.

Such predictions can be quite refined statements, given sufficient knowledge and understanding of a number of factors. For example, it may be possible some day to make statements of the following kind:

1. Merchant ship design A is superior to merchant ship design B for cruises between New York and the English Channel because (1) if each ship were to follow the least time track route on each cruise for five years, merchant ship A would average five days two hours per crossing as opposed to six days one hour for ship B, (2) the bow of ship A would ship water 560 (±20) times (with a probability of 0.99) during the five year period and ship B would ship water 650 (±3) times (with the same probability) and (3) ship A would slam only 6 (±3) times (with a probability of 0.99) whereas B would slam 50 (±5) times.

2. Of five ships available for a rescue mission at a certain point, this particular ship should move as quickly as possible to that point. It will arrive two hours (±20 minutes) sooner than the earliest of the other four ships. The second ship to send is such and such a ship as a safety factor or as a standby reserve.

3. All ships in a certain part of the North Pacific will encounter seas in excess of the highest measured for the past decade beginning 18 hours from now and ending 30 hours from now. All possible safety precautions should be taken immediately. Predicted conditions for specific points in this area follow.

Statements such as these will be possible when it is possible to describe the directional spectrum of the waves at every point on the ocean as a function of the winds over the ocean. The first statement can be made on the basis of the historical files of weather data. The second and third require the wind field to be forecasted a day or so into the future.

It is therefore necessary to describe this directional spectrum in its infinite variety and to predict its form at future times. Strangely enough, this problem is, to a large extent, deterministic. As an analogy, to predict the variance of a sample to be drawn from a normal population is not the same as to predict the actual values that would be drawn at random from a normal population with a known variance. In this particular problem, to predict the features of the directional spectrum that will be estimated from observations of waves in a particular area is not the same thing as to predict the exact form of the waves that will be observed in a particular area. The predicted spectrum in turn permits the determination of many wave and ship motion parameters such as the significant wave height, the average pitch motion, the number of slams and so on. One then assumes that the predicted parameters are those that will be the population parameters at the point of interest for the event of interest. These parameters are then estimated directly from observation, if possible, and compared with the prediction. The attempt is successful if the predicted and estimated values agree within the sampling variability of the estimate.

The purpose of this paper is to summarize what we now think we know about the directional spectrum of waves at sea and to discuss how we are trying to predict this directional spectrum at 519 points in the North Atlantic Ocean.

FULLY DEVELOPED WIND SEAS

If the wind blows with constant speed and direction for a long enough time over an initially calm ocean area, if this ocean area is big enough, if no waves propagate into this area from outside it, and if the turbulent features of the wind do not change, then a fully developed wind sea should be observed over part of this area, and wave observations made in this fully developed wind sea should all be samples that have come from the same population. The spectral estimates, $\hat{S}(\omega,\theta)$, made from these observations should display sampling variability in terms of departures from some unknown population spectrum $S(\omega,\theta)$.

There are only a few available estimates of $\hat{S}(\omega,\theta)$. There are, however, now available in useful form about 500 estimates of $\hat{S}(\omega)$ that were obtained from the analysis of waves recorded at a fixed point as a function of time. These estimates are given by Moskowitz, Pierson, and Mehr (1962,1963) and by Pickett (1962).

Of these 500 spectral estimates, $\hat{S}(\omega)$, about 40 were found by Moskowitz (1964) to correspond to fully developed seas for winds from 20 to 40 knots. All of the others could not be simply defined by the wind speed measured at the time the wave record was made. As one example for winds near 20 knots, the waves are usually higher than those expected for a fully developed sea because components left over from previously higher winds and components from swell are present.

Given some form for $S(\omega,\theta)$ to describe the spectra of fully developed wind seas, one is therefore a long way from describing the spectrum that will be estimated at a particular point at sea because the wind will not have been constant in speed and direction and waves from a distance may have propagated into the area. The spectrum for a fully developed wind sea is however a fundamental building block in attempts to describe the spectra that will occur in more complex situations.

KNOWN PROPERTIES OF THE SPECTRUM

Directional Spectra and Frequency Spectra

The directional spectrum of waves can be thought of as being written in the form

$$S(\omega,\theta) = S(\omega)\ [f(\omega,\theta)] \tag{1}$$

where $f(\omega,\theta)$ in turn can be written as

$$f(\omega,\theta) = \frac{1}{2\pi} + \sum_{n=1}^{\infty} \left[a_n(\omega) \cos n\theta + b_n(\omega) \sin n\theta\right] . \tag{2}$$

It then follows that

$$\int_{-\pi}^{\pi} S(\omega,\theta)\, d\theta = S(\omega) \tag{3}$$

and that

$$\int_{-\pi}^{\pi} f(\omega,\theta)\, d\theta = 1 . \tag{4}$$

An attempt to describe $S(\omega,\theta)$ correctly therefore implies that $S(\omega)$ is correct. If spectra estimated from a time history at a point are not correctly described then surely directional spectra estimated from more complete data will not be correctly described.

The Frequency Spectrum

The book, Ocean Wave Spectra, describes a wide variety of proposed forms for $S(\omega)$ as reviewed and summarized at the Easton Conference on Waves held in 1961. Based on an application of a theory given by Kitaigorodskii (1961), and by means of the results of Moskowitz (1964), Pierson and Moskowitz (1964) have proposed a new form for $S(\omega)$. It is given by Eq. (5).

$$S(\omega) = \frac{\alpha g^2}{\omega^5} e^{-\beta(\omega_o/\omega)^4} , \tag{5}$$

where $\alpha = 8.10\times 10^{-3}$, $\beta = 0.74$ and $\omega_o = g/U$. Here U is the wind speed measured at 19.5 meters above the sea surface. The anemometer that measured U was at this elevation on the ship.

This spectrum has many features that agree with other proposed spectra and an analysis of the effect of the variation of wind with height has reconciled many of the apparent discrepancies pointed out so strongly at the Easton conference.

[I might add parenthetically that the spectrum proposed by my colleague, Dr. Neumann, is remarkably close to this one for winds near 30 knots. It is, however, seriously off for higher winds, and any design considerations based on the spectrum due to Neumann for high winds should be re-evaluated (see Pierson, 1964).]

As the group to which this paper is addressed does not consist of those working on the problem of forecasting ocean waves, it is important to remark that the above spectral form represents the writer's opinion as to the best presently available description of the frequency spectrum of a fully developed wind sea. If one becomes seriously interested in using this spectrum for applications in naval hydrodynamics, he should check the opinions of those workers in this field who may not agree with this belief.

Known Properties of $S(\omega, \theta)$

With a handful of directional spectrum estimates available, it is not surprising that not much is known about $S(\omega, \theta)$. The available estimates have been given by Cote et al (1960), Longuet-Higgins et al (1963) (and in other publications describing the same data), Cartwright (1963), and Cartwright and Smith (1964). It was assumed in Cote et al that $S(\omega, \theta)$ was zero outside of the range $-\pi/2 < \theta < \pi/2$ where $\theta = 0$ is the direction toward which the wind was blowing. There were good reasons for this assumption and the data bore them out, but it could not be proved that $S(\omega, \theta)$ was zero outside the above range.

Analyses by Longuet-Higgins et al (1963) were able to obtain the first five values in Eq. (2), that is $1/2\,a_0$, $a_1(\omega)$, $b_1(\omega)$, $a_2(\omega)$, and $b_2(\omega)$. The results suggested that $S(\omega, \theta)$ was not zero for spectral components traveling opposite to the wind. However, a new device, called a cloverleaf buoy, developed at the National Institute of Oceanography now yields $a_3(\omega)$ and $b_3(\omega)$. Indeed, that part of $S(\omega, \theta)$ outside of $-\pi/2 < \theta < \pi/2$ is small. The preponderance of the available evidence now is that little or no spectral energy in a fully developed wind sea will be associated with spectral components traveling opposite to the wind.

All of the available directional spectrum estimates also indicate that $S(\omega, \theta)$ is more strongly peaked for low frequencies and that it broadens with increasing frequency. One possible explanation for this effect is contained in the theories of Phillips (1957), which suggest that $S(\omega, \theta)$ should have two peaks that move further apart with increasing frequency. None of the presently available directional spectrum estimates have the resolution and the degrees of freedom necessary to resolve the question of whether or not this bi-modal form occurs. An experiment could be designed to resolve this question by the combined use of both stereo-photogrammetric techniques and the latest buoy developed at the National Institute of Oceanography.

For some applications of the power spectrum, it is desirable to be able to describe the sea surface as a function of distance instead of as a function of time at a point. This involves the transformation from an ω, θ representation to an ℓ, m representation where $\ell^2 + m^2 = k^2$, $k = \omega^2/g$, $\ell = \omega^2 \cos\theta/g$ and $m = \omega^2 \sin\theta/g$. A discussion in <u>Ocean Wave Spectra</u> suggested that k did not seem to be given by ω^2/g, but since then Mr. Cartwright of the National Institute of Oceanography has informed me that subsequent analyses all verify this linear representation between wave number and frequency to within the present accuracy of the available data. This result does not eliminate the problem completely as nonlinear effects of a more subtle nature are present. It will be a long time before these nonlinear effects are completely understood.

For information purposes, in our attempts to forecast waves for the North Atlantic, the form given by Cote et al (1960) has been used. In the notation of this paper the function S(,) is given by Eq. (6) for $- \; 2 \quad \quad 2$ and by zero otherwise.

$$f(\;,\;)\quad \frac{1}{\;}\left[1 + \left(0.50 + 0.82\, e^{-(\quad _0)^4 \; 4}\right)\cos 2 \; + 0.032\, e^{-(\quad _0)^4 \; 4}\cos 4\;\right]. \tag{6}$$

One should note that the Fourier series representation of S(,) as in Eq. (2) would require many more terms to fulfill the zero otherwise condition that was assumed in the above expression.

FORECASTING DIRECTIONAL WAVE SPECTRA

At present, my colleagues and I are attempting to predict the directional wave spectrum, S(,), given the winds over the North Atlantic Ocean. If S(,) is the directional wave spectrum, if one has the directions, 0, 6, 3, 2, 2 3, 5 6, , and so on to 2 with respect to north as zero, and if one has certain frequencies, $f_1, f_2, \ldots, f_{16}$, then our forecasting scheme attempts to predict 180 numbers, one of which would be, for example,

$$\int_{f_3}^{f_4}\left[\int_{-\;12}^{\;12} S(\;,\;)\, d\;\right] df\,. \tag{7}$$

Stated another way, the directional spectrum is described by the variance contributions to fifteen frequency ranges for each of twelve direction intervals at each point.

Based on some theory, and some empiricism — considerations too numerous to detail here* — we have started with observed winds over the North Atlantic ocean for December 9 to 17, 1955, December 11 to 27, 1959, and November 17 to 30, 1961. These winds have been described at each grid point of interest in the problem every six hours for each of the above periods. The winds are then used to predict these 180 numbers to define the directional spectrum at each grid point. No adjustments are made in the wave spectra and in the forecasting procedure for the entire period of the forecast.

The output consists of numbers that describe the directional spectrum as defined above at each grid point. From them, we can get the frequency spectrum by summing over direction and the significant height by summing these sums over frequency, taking the square root of the sum and multiplying it by 4. (The spectra discussed above are all in terms of variance, and the total volume under S(,) equals the variance of the wave motion.)

The first indication of a good forecast is in the verification of the significant height. It tells one that the area under S( ) as predicted agrees favorably with the estimate of this area as obtained from an ocean wave record obtained as a time history at a point.

*See, for example, Pierson and Tick (1964).

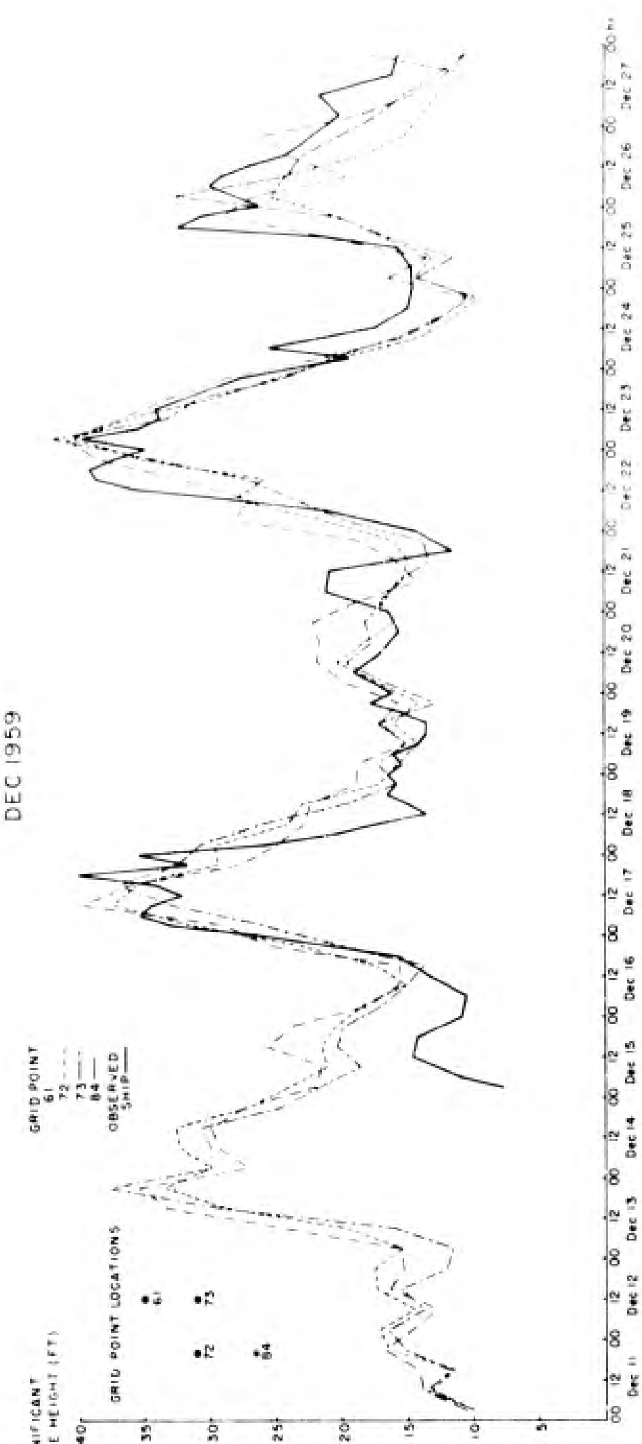

Fig. 1 - Preliminary results on forecasts for the significant height as a function of time at weather ship J in the North Atlantic

For December 1955 and December 1959 these results were verified by the data provided by the British weather ships that are equipped with the Tucker shipborne wave recorder. For November 1961 verification is against the wave records obtained at Argus Island by the U.S. Naval Oceanographic Office.

Figure 1 shows the significant wave height predicted at four points surrounding the British weather ship in December 1959 and the significant wave height obtained from the records obtained by the British weather ship. Four major cyclonic storms passed the weather ship during this period. The waves reached significant heights of 40 feet and decreased after each storm to significant heights near 15 feet. The predictions are quite good and although not shown the frequency spectra check quite well most of the time.

Our other results are equally encouraging. The November forecasts were verified in a completely different oceanic area by means of records obtained by a different wave recording system. The data for the November forecasts were not used in developing the procedure, and, although again not shown here, the results are quite good.

The 180 numbers that describe the directional spectrum show a wide variation of odd forms such as one would expect from sea plus swell, crossed seas, and swell. Most spectra cover a range of directions in excess of 180 degrees. Directional spectra cannot be verified as no data were taken to estimate them. However, the directional spectra cannot be too far off because it would be virtually impossible to obtain the good results that have been obtained for the significant height and the frequency spectra if the directional spectra were wrong.

If a fully developed sea should occur at a particular point, the numbers predicted would be obtained by substituting Eqs. (5) and (6) into (7).

Presently we are developing ways to process 300,000 ship reports so as to produce wind fields for fifteen months of weather data. Forecasts of the directional spectra for these fifteen months will then be prepared. These results will be verified against frequency spectra already tabulated by Moskowitz, Pierson and Mehr. At that time, some statements can be made concerning the overall accuracy of our procedures.

REFERENCES

Cartwright, D. E. (1963): The use of directional spectra in studying the output of a wave recorder on a moving ship. Ocean Wave Spectra, Prentice-Hall, Inc.

Cartwright, D. E., and N. D. Smith (1964): Buoy techniques for obtaining directional wave spectra. Trans. 1964 Buoy Technology Symposium, Marine Technology Soc., Washington, D.C.

Cote et al (1960): The directional spectrum of a wind generated sea as determined from data obtained by the Stereo Wave Observation Project. Meteor. Papers, vol. 2, no. 6, New York University.

Longuet-Higgins, M. S., D. E. Cartwright, and N. D. Smith (1963): Observations of the directional spectrum of sea waves using the motions of a floating buoy. Ocean Wave Spectra, Prentice Hall, Inc.

Moskowitz, L. (1964): Estimates of the power spectra for fully developed seas for wind speeds of 20 to 40 knots. Journal of Geophysical Research, vol. 69, no. 24, pp. 5161-5180.

Moskowitz, L., W. J. Pierson, and E. Mehr (1962, 1963): Wave spectra estimated from wave records obtained by the OWS Weather Explorer and the OWS Weather Reporter. (I) and (II). Technical report prepared for U.S. Naval Oceanographic Office under contract N62306-1042, New York University, Research Division, School of Engineering and Science.

Ocean Wave Spectra (1963): Proceedings of a conference at Easton, Maryland. Prentice Hall, Inc.

Phillips, O. M. (1957): On the generation of waves by turbulent wind. J. Fluid Mech., 2, 417 445.

Pickett, R. L. (1962): A series of wave power spectra. (Informal Manuscript Report No. 0-65-62.) U.S. Naval Oceanographic Office.

Pierson, W. J. (1964): The interpretation of wave spectra in terms of the wind profile instead of the wind measured at a constant height. Jour. Geophys. Res., vol. 69, no. 24, pp. 5191-5204.

Pierson, W. J., and L. Moskowitz (1964): A proposed spectral form for fully developed wind seas based on the similarity theory of S. A. Kitaigorodskii. Jour. Geophys. Res., vol. 69, no. 24, pp. 5181-5190.

Pierson, W. J., and L. J. Tick (1964): Wave spectra hindcasts and forecasts and their potential uses in military oceanography. First U.S. Navy Symposium on Military Oceanography, June 1964.

* * *

DISCUSSION

A. Silverleaf
National Physical Laboratory
Teddington, England

Professor Pierson's application of mathematical technique to sea state studies has long been of the greatest value to those of us in Britain concerned with the performance of ships in waves. I am sure that most of us will agree that the two-dimensional or unidirectional wave spectrum is a "fundamental building block" which will aid further developments. However, in Britain we do not all agree with Professor Pierson's suggestion that the formula in (5) is the best for naval architecture purposes at the present time. An independent analysis by Scott (Ref. A) on behalf of the British Towing Tank Panel suggests that it is not the best or even the most appropriate fit to the Moskowitz data. For example, Professor Pierson's relation between the frequency of the spectrum peak f_o and the average wave period T_V is

$$f_o = 0.77 \, T_V$$

while that recommended by the B.T.T.P. is

$$f_o = 0.501 \, T_V + 1.43 \, T_V^2 .$$

Consequently, an alternative formula has been proposed for use by the British towing tanks which are now carrying out experiments on models in irregular waves much more frequently than in the past, so that it has become urgently necessary to formulate a standard of sea spectra for such experiments.

In his introduction Professor Pierson mentions three possible types of prediction of seakeeping performance. I suggest that only the first of these represents the purpose of seakeeping research from the point of view of the ship designer and operator, who is primarily interested in knowing whether or not ship A will perform better than ship B for a particular purpose on a specified route. Professor Pierson suggests that the data necessary to make this type of prediction can be obtained from historical records and some current work in Britain is being devoted to just this approach. Statistical information about wind and wave conditions in the principal areas where ships operate is being analysed and processed using data collected from voluntary observing ships and recorded on punched cards at the Meteorological Office. At present data from 125 Marsden squares have been grouped into 52 areas defining most of the principal shipping routes to give a detailed account of the likely sea conditions during all seasons of the year. A first report on this scheme has recently been issued (Ref. B) and it is intended to publish a complete compendium on ocean wave statistics within the next year or so.

REFERENCES

A. Scott, J. R., A Darbyshire Type Spectrum Suitable as a Standard for Model Tests and as a Basis for Long Term Ship Prediction.

B. Hogben, N., Lumb, F. E. and Cartwright, D. E., The Presentation of Wave Data from Voluntary Observing Ships. Ship Report 49, July 1964.

* * *

REPLY TO THE DISCUSSION

W. J. Pierson, Jr.
New York University
New York, New York

Mr. Silverleaf states that the formula I gave in my paper may not be the best and proposes an alternate on the basis of work by Scott. It would be interesting to see if the subsets obtained by Scott would pass the test applied by Mr. Moskowitz to his data. On the other hand, it may be the best. For example, the ITTC has adopted a form quite similar to the form we have obtained at N.Y.U. It must be emphasized that the formula represents only fully developed wind seas as a function of the wind velocity. The documentation for our results is substantial and it forms a convincing total picture. Recent work of Kraus (1965) provides added support.

Partially developed seas, dead seas, and swell all have spectra that differ from the form I gave. Whether meaningful averages of such spectra can be obtained is questionable, and I have expressed certain doubts in this connection in correspondence with Mr. Hogben.

I believe that all of the examples given in my paper come within the domain of the naval architect. It is his responsibility to see that the ships he builds are so thoroughly understood that their performance in any given situation can be correctly described. Other inputs are needed from meteorology and oceanography, but in principle the problems posed differ only in degree and not in kind. Although not stated explicitly in my paper, each ship captain who receives such a warning should be thoroughly acquainted with the expected behavior of his vessel for the predicted extreme condition.

Our work on waves would never have reached its present stage without the foresight of the National Institute of Oceanography in Great Britain. The routine collection of wave data by means of British weather ships and the Tucker shipborne wave recorder has been the cornerstone of our work.

REFERENCE

Kraus, E. B. (1965): The Influence of the oceans on atmospheric disturbances and circulations. Woods Hole Oceanographic Contribution No. 1576.

* * *

Friday, September 11, 1964

Morning Session

SHIP MOTIONS

Chairman: F. H. Todd

David Taylor Model Basin
Washington, D.C.

FORCE PULSE TESTING OF SHIP MODELS

W. E. Smith and W. E. Cummins
David Taylor Model Basin
Washington, D.C.

INTRODUCTION

In a recent paper [1] one of the authors proposed that a useful and revealing way of treating oscillatory motions of a ship was to relate them to the transient response to an impulse. The response to an arbitrary excitation would be exhibited as a convolution integral over the past history of the excitation. The idea was hardly original, as this device is widely used in the discussion of linear systems. However, there seemed to be some reluctance by those working in the field to treat the ship response in this fashion. Most writers preferred to restrict their attention to the frequency response function.

There have been some exceptions to this trend, notably Fuchs and MacCamy in the discussion of the motions of a floating block [2], Dalzell in the treatment of destroyer motions in severe sea states [3], and the paper by Davis and Zarnick for the present symposium [4]. However, all of these are concerned with responses to wave pulses or hypothetical wave impulses, and not the response to a force or moment impulse. The present paper is concerned with this latter problem. As a matter of fact, the solutions to the two problems, the response to the wave pulse or impulse and the response to a force or moment excitation, complement each other very effectively. The first solution characterizes the total wave-ship system, while the second enables us to construct the equations of motion and thus separate the effects of damping, added mass, coupling, and hydrodynamic memory. When both solutions are known, the wave excitation can be determined, and one is then in a position to say not only what the ship does but why it does it. The designer then has clues as to how to make changes in the design in order to improve seakeeping qualities.

One can discuss and even use the impulse response function without directly measuring it, as it is simply the Fourier transform of the frequency response function. If the latter is known for all frequencies, the impulse response function can be computed. But to directly determine the frequency response function, one must measure the response to a set of frequencies at suitably close intervals over the whole frequency range in which there is significant response. The alternative approach is most attractive. That is, apply a known impulse or equivalent excitation to the model and observe the response. The frequency response function can then be computed, and we have replaced a time consuming and expensive test program requiring many runs with a single run. This paper is concerned with such measurements.

In principle, the experiment is beautifully simple. In practice, there are a number of difficulties to overcome. First and most obviously, we are dealing with a system with six degrees of freedom, and there is strong coupling among some of the modes of oscillation. A much more serious and subtle problem arises from the fact that we obtain the response of the ship for all frequencies from a small set of relatively short records. Thus, the desired information is highly compressed in the time scale. The resolution of this information requires records of very high quality and an analysis procedure which degrades the data as little as possible.

Prior to the presentation of Ref. 1, experiments were performed to test this procedure as a practical tool. Declining oscillations were used instead of impulsive excitation, but most of the troubles encountered would be even more characteristic of the latter type of test. The measurement system was somewhat superior to those typical of seakeeping work at that time. In the process of analysis it became quite clear that major improvements were necessary in order for the technique to be other than a curiosity.

There were several sources of difficulty, and as the method of overcoming these are key factors in the present paper, they will be mentioned here. First is the question of accuracy. It is clear that when desired data is superimposed, the accuracy to which it can be separated is certainly no higher than the net accuracy of the system. The original system had an accuracy of perhaps 5 percent and this was not good enough. The second major difficulty was noise, as it is evident that the real objective is a high signal to noise ratio. By noise we mean here all unwanted disturbances such as wall reflections and true electrical noise. The input for the declining oscillation experiment is a step function, which is completely suitable theoretically, but has undesirable qualities practically. These arise from the fact that the step function has harmonic content at all frequencies, all the way to infinity, and such an excitation not only causes the model to oscillate, but in addition it vibrates as a beam at its natural frequency. Further, all instruments, attachments, etc., are excited in their various natural frequencies. In consequence, the signal to noise ratio was well below that which is necessary.

As the potential value of the transient experiment is great, much effort has been devoted to upgrading our measurement and analysis system since these early tests. The present paper is a progress report on the present state of this program. The details will be discussed in the subsequent sections, but the most significant accomplishments will be mentioned here.

The first is a technique of towing the model, rather than self propelling it. This is contrary to the current trend toward powered models for seakeeping work. However, we feel that this technique offers real advantages. Specifically, we measure <u>all</u> restraints on the model imposed by the towing, guidance, and excitation system. The sum of these is the net input to the model. Thus, towing gear inertias and frictions are of no concern, as their effects are included in the measured input.

The second achievement is the use of an excitation pulse of controlled harmonic content. The technique is an analog of that used by Davis and Zarnick for generating wave pulses. An oscillatory excitation is imposed on the model by means of a variable speed drive which sweeps from the highest frequency desired down to the lowest frequencies which can be treated in our basin. Because of the method of generation, the very high frequency content of the step or impulse response is avoided. Because of the shape of the pulse, the separation into the various frequencies is achieved with good accuracy. And because of the length of the pulse, the intense concentration of the information is eased.

The third achievement is a system of significantly improved absolute accuracy, about two percent. The present limiting factor is the use of magnetic tape in the data handling path. It is possible that the use of tape can be avoided, with a further significant improvement.

The last major advance has been the use of a new system for converting data from analog to digital form. This system has the capability of converting as many as 6,000 data spots per second, distributed among the various channels of data. It has been possible to sample the data at a rate of 30 spots per cycle of the highest frequency investigated.

The net result of all these improvements has been a very high signal to noise ratio. In the range of greatest interest, the noise is 45 db below the signal level. As a result, we have been able to characterize the model from frequencies so low that shallow water and wall effects become significant (in a basin 240 ft × 360 ft × 20 ft deep!) up to higher frequencies than any previously investigated. And this entire range was covered in a pair of runs lasting perhaps 50 seconds.

The system has been in use only a short time, and we have much more to learn about it. The earlier, unreported tests produced a vast amount of information about how not to run the experiment. This time we have been more successful, but we have discovered a number of additional refinements which will be necessary before we can do all that we wish with the system. These proposed changes will be discussed in a later section.

THE EXPERIMENT

This initial experiment was primarily designed to provide an evaluation of pulse techniques as a method of obtaining the frequency response relationship between exciting forces and the motions of a ship. A Series 60 Block 0.60 ship form was oscillated in pitch and heave. All forces and responses were measured and the damping and added mass terms in pitch and heave were computed. This permits a direct comparison with the results obtained by Gerritsma [5] for a similar form.

Experimental Details

As the effect of surge upon heave and pitch is generally considered to be small, it was decided to restrict the analysis to these latter two modes only.

However, the towing system allowed small oscillations in surge, and it is planned to undertake a three-mode analysis at a later date.

The towing system is as shown in Figs. 1 and 2. Such an arrangement permits the application of tow forces at the model center of gravity while permitting responses in all six degrees of freedom. Restoring forces in the surge and sway modes are provided by springs K_1 and K_2. External forces in the heave, surge and sway modes are measured, using variable reluctance force gauges. The motions in the six degrees of freedom are measured by film type potentiometers mounted as indicated on the tow strut and excitation forces by force gauges mounted in the model.

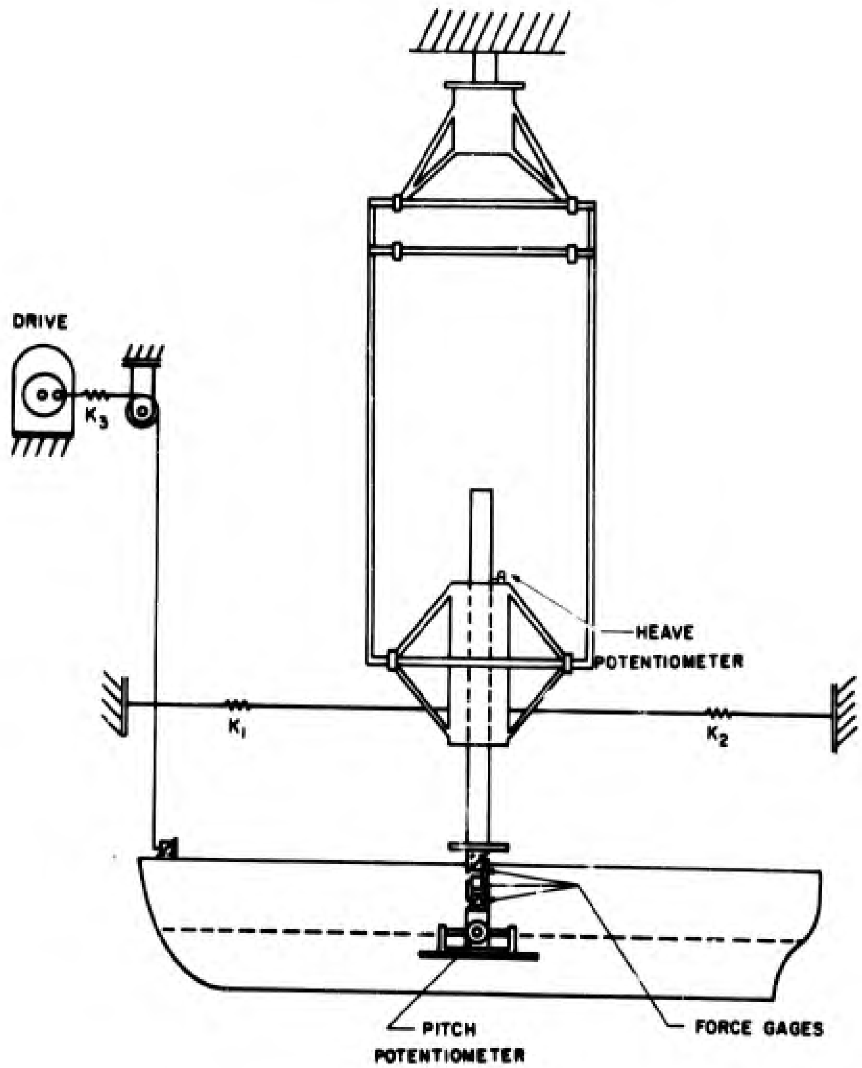

Fig. 1 - Pitch and heave experiment

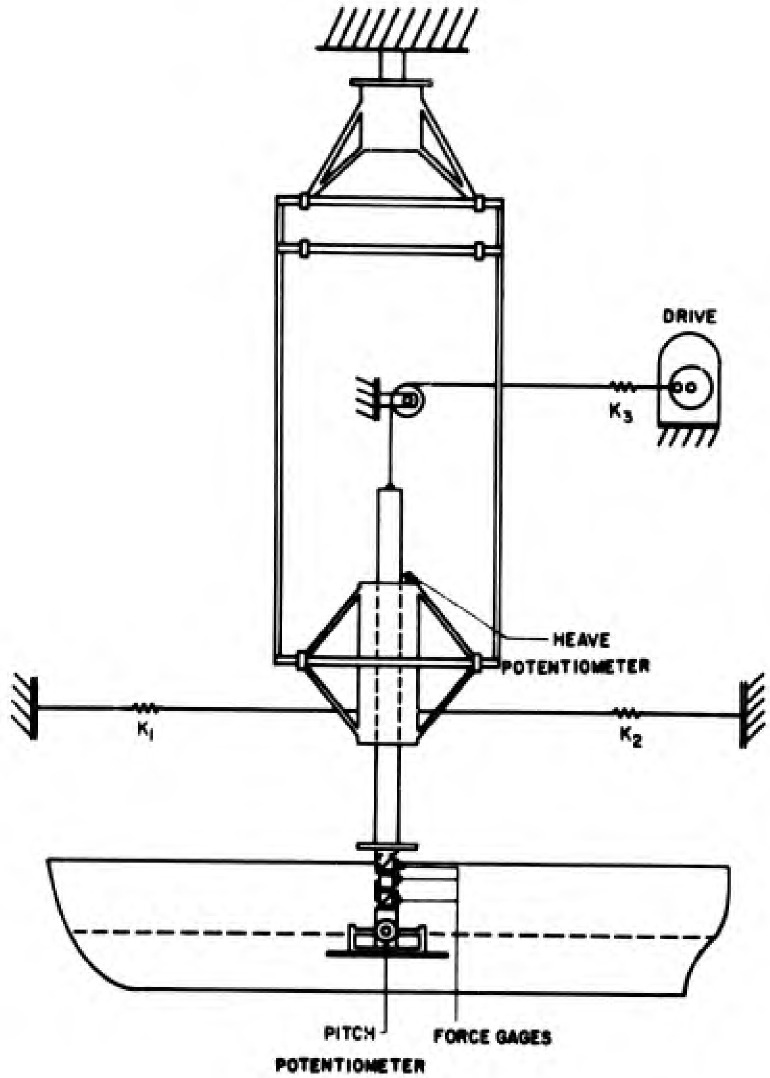

Fig. 2 - Heave experiment

Excitation is provided by an electric motor — variable speed drive arrangement, with the forces transmitted to the model via a spring and cable. (Tests were conducted at speeds of Fr. = 0, 0.025, 0.05, 0.075, 0.10, 0.15, 0.20, 0.25, 0.30, 0.35). Two series of tests were conducted: In one the model was excited in the heave mode only, and in the second the model was excited simultaneously in pitch and heave. In the heave test the excitor cable was attached to the heave staff as shown in Fig. 2. The six motions as well as forces along the heave, surge and sway axis were measured. In the pitch heave experiment, as shown in Fig. 1, an excitation cable was attached to the bow of the model through a fourth (excitation) force gauge. Measurements were the same as in the heave experiment, except for the addition of the excitation force gauge. For each test condition, the frequency of the excitation force was varied manually, adjusting the speed of the drive system from 0 to 3.5 cycles per second. The amplitude of the excitation eccentric was fixed at one inch. The frequency spectrum of the excitation signal is shown in Fig. 3.

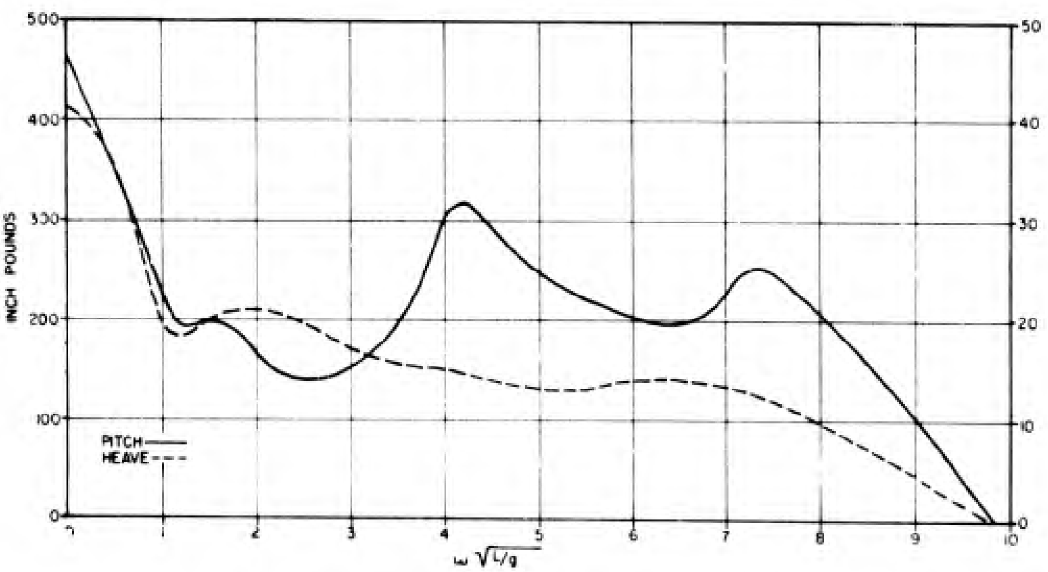

Fig. 3 - Excitation force spectrum

The measurement system was as shown in Fig. 4. DTMB block gauges were used to measure forces and moments. High resolution film type potentiometers were used to measure the motion. All data was recorded simultaneously on Sanborn strip chart recorders and FM analog magnetic tape. The instrumentation system, exclusive of recorders, has an accuracy of 0.2 percent, a dynamic range of 60 db, and a frequency response which is essentially flat from 0 to 100 cycles. Phase shift between any two channels was held to less than one part in 10,000. The tape recorder, however, the system's weakest link, is accurate to only 1-1/2 to 2 percent, and its dynamic range is limited to 38 to 42 db.

Test Procedures

As previously mentioned, tests were conducted over a range of Froude numbers, from 0 to 0.4. For each test condition, the model and carriage were accelerated to the appropriate speed with the oscillator turned off. Care was taken to ensure that the model had reached a steady state condition and that all energy in the model-free surface memory had dissipated. When steady state conditions were established, the recorders were turned on and allowed to run 3 to 5 seconds before the excitation. Excitation was started with an initial frequency setting of 3.5 cycles per second, and was swept from 3.5 cps to 0 in

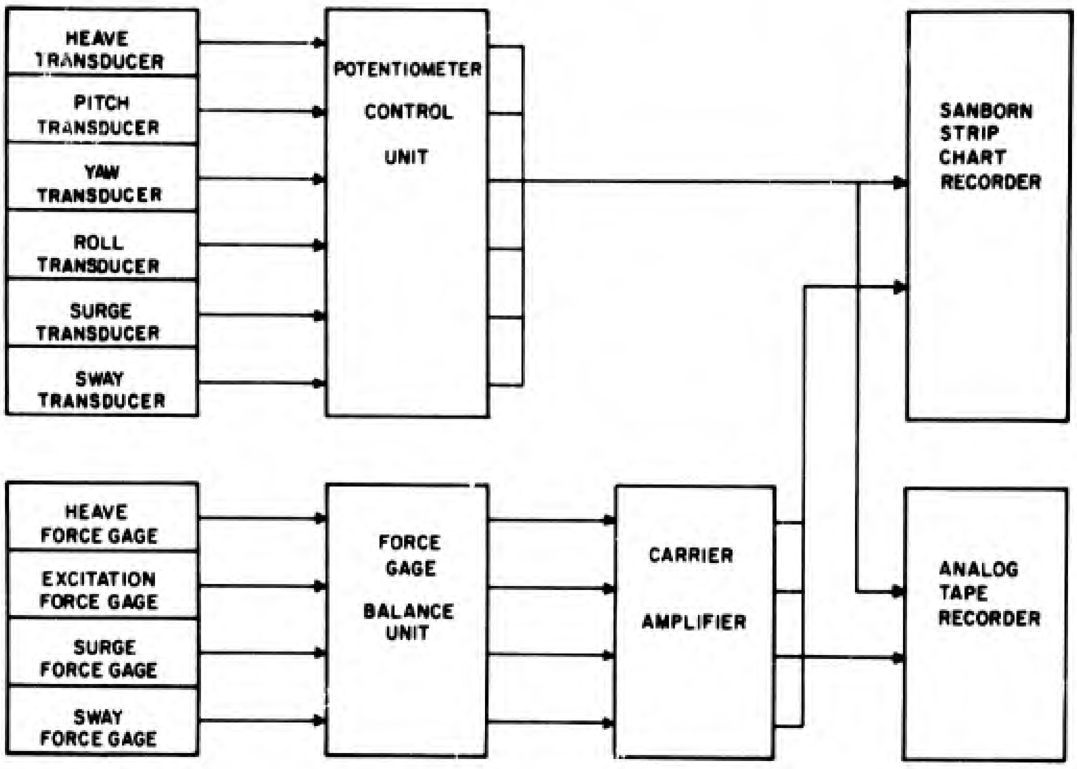

Fig. 4 - Analog measurement system

about 20 seconds, care being taken to see that the excitor was stopped at zero amplitude. Recording continued until any remaining motions had ceased. Typical recording time ranged from 28 to 48 seconds, depending on carriage speed. Test results were as shown in Fig. 5. It should be recognized that the towing structure, and thus the towing carriage, was used as a reference for all measurements.

When the model was excited by a force restricted in bandwidth, with negligible energy above 5 cycles per second, the measured signals were excellent, with a dynamic range and accuracy limited only by the 40 db range of the analog tape recorder. However, when a relatively broadband signal was used, such as an impulse or step function, the model, strut and carriage structure were excited at their own natural frequencies and produced oscillations which almost completely masked the motion responses of the model.

DATA ANALYSIS

One of the inherent disadvantages of a digital record is that it provides information about the corresponding time function at the sampled instants only. Discrete samples completely define a continuous function, $f(t)$, only if the function is absolutely band-limited, and then only if the sampling frequency is at

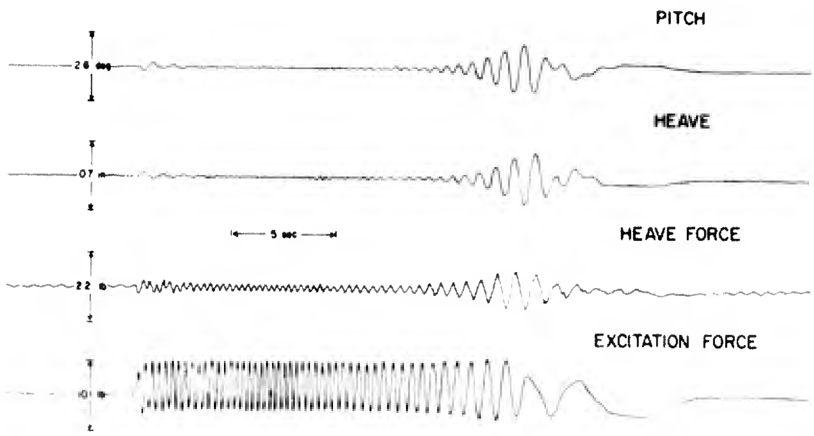

Fig. 5 - Test record from pitch experiment

least twice the highest frequency, F, in the signal [6]. Further, the recovery of the original signal from the digital data is predicated on the use of an ideal filter.

When dealing with empirical data and actual filters, this sampling theorem is of little use, as there is rarely an absolute limiting frequency, F, and filters cannot be built which are capable of cutting off perfectly above any assigned F. It is certain that data collected from a vibrating towing-carriage does not meet this condition.

As in a practical case there are many additional considerations, such as the effects of filtering on the desired signal, aliasing, interpolation methods used for signal recovery, and limited availability of computer time, the selection of a sampling rate required to provide 1 percent accuracy is anything but clear-cut. A more rigorous method of using the sampling theorem has long been needed but the mathematics for anything other than the ideal case is quite complex. Likewise, the obvious solution of increasing the sampling rate by orders of magnitude, while within the capabilities of the analog-digital converter, quickly becomes impractical from the standpoint of the increasing computer time necessary for each analysis.

In order to select the proper sampling rate, an experiment was run in which typical samples of analog data were first digitized at 6,000 samples per channel per second. A harmonic analysis was performed and the complex spectra so obtained were used as analysis accuracy standards. The same data was then sampled and analyzed at successfully lower sampling rates until a difference approaching 1 percent was observed in the spectra. The sampling rate finally selected was 125 samples per channel per second. This sampling rate, coupled with an average run length of 48 seconds, produces approximately 6,000 data points per channel per test condition, or approximately 60,000 data points per test run.

In performing the actual Fourier transformation to obtain the complex frequency response function, an additional problem must be considered. When model tests are conducted at forward speeds, quantities such as pitch, heave, and surge force are in general not zero, even in a steady state translation. The actual records of a transient pulse test, as analyzed, are necessarily truncated, and thus have the form of an oscillatory pulse superimposed upon a rectangular pulse of length equal to the record. See Fig. 6. The recorded signal can be considered as part of function,

$$f(t) = f_0 + f_1(t) \qquad -\infty < t < +\infty$$

where f_0 is a constant and $f_1(t)$ is the pulse excitation or response. The function $f(t)$ has no Fourier transform unless f_0 is zero, but our only interest is the transform of $f_1(t)$. The truncated signal, $f^T(A)$, which is the one actually treated, can be written

$$\begin{aligned} f^T(t) &= f_0 + f_1(t) \qquad & 0 < t < T \\ &= 0 & \text{elsewhere} . \end{aligned}$$

This function does have a Fourier transform. If $f_1(t)$ is zero outside the interval $(0,T)$ the transform of $f^T(t)$ will be equal to the transform of $f_1(t)$ plus the transform of a rectangular pulse of height f_0 and length T. However, the

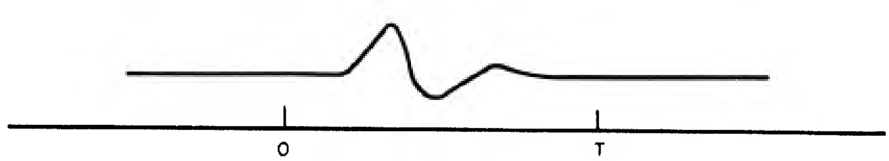

Fig. 6a - The recorded signal $f(t)$

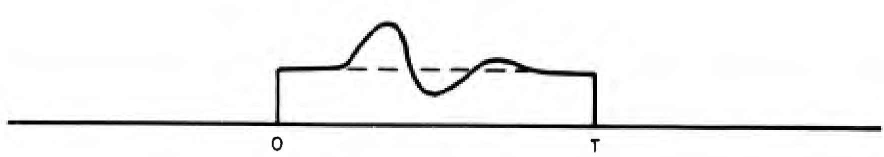

Fig. 6b - The analyzed signal $f^T(t)$

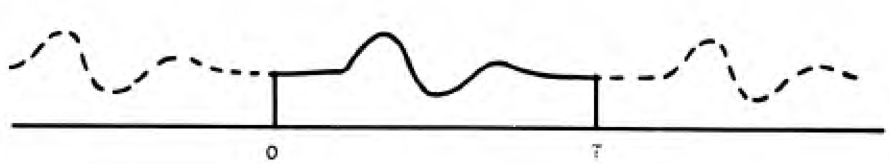

Fig. 6c - The analyzed signal imbedded in a periodic function

Fourier transform of the rectangular pulse will be zero for the frequencies $\Delta\omega$, $2\Delta\omega$, $3\Delta\omega$, ... where $\Delta\omega = 2\pi/T$. At these frequencies, the transform of $f^T(t)$ will have the same value as the transform of $f_1(t)$. Therefore, if we restrict our calculations to this set of frequencies, we need not concern ourselves with estimating f_0.

Another way of treating the same problem is to consider $f^T(t)$ to be one cycle of a periodic signal. This periodic signal would be the response to a periodic sequence of pulses with period T. Such an analysis is permissible because the memory of model is less than T, and the effect of all previous pulses will have dissipated before the start of a new pulse in the sequence. This periodic signal can be analyzed in a Fourier series. The effect of f_0 will appear in the constant term but in none of the others. Thus, the Fourier coefficients corresponding to the frequencies $\Delta\omega$, $2\Delta\omega$, $3\Delta\omega$, ... completely define the function, where $\Delta\omega$ has the same meaning as before. But these Fourier series coefficients are identical with the values of the Fourier integral transforms of $f^T(t)$ and $f_1(t)$ at the same set of frequencies, and we arrive at the same conclusion as in the analysis of a single pulse.

This periodic type analysis was used for all test data in order to eliminate any dc components. The basic assumption, which is inherent in any truncation process, is that the transient has completely decayed before the instant of truncation. This assumption will never be strictly correct, and the degree to which it is not fulfilled may be an important source of error.

It should be noted that the phases obtained from this periodic type analysis are referred to the arbitrary starting instant and are therefore meaningless in terms of the physical test. If, however, only the phase difference between data channels are considered, the results immediately become physically meaningful.

The data analysis sequence is as shown in Fig. 7. Suitable computer programs were written to analyze the data, to invert the resulting matrix of coefficients (see following section), and to compute the damping and added mass terms for each of the harmonics considered. Also, a computer was programmed to plot the resulting a's and b's versus the nondimensional frequency, $\omega\sqrt{L/g}$.

Equations of Motion

The relation between the excitations and responses of a ship, under the assumption of linearity, can be written in various ways. In terms of the impulse response functions [1] we have

$$x_j(t) = \sum_{i=1}^{6} \int_0^{\infty} R_{ij}(\tau)\, f_i(t-\tau)\, d\tau \qquad j = 1,2,\ldots,6 \tag{1}$$

where $R_{ij}(t)$ is the response in the jth mode to a unit impulse at $t = 0$ in the ith mode. The matrix of functions $R_{ij}(t)$ thus completely characterizes the response of a ship to an arbitrary set of excitations. In the following discussion we adopt the convention:

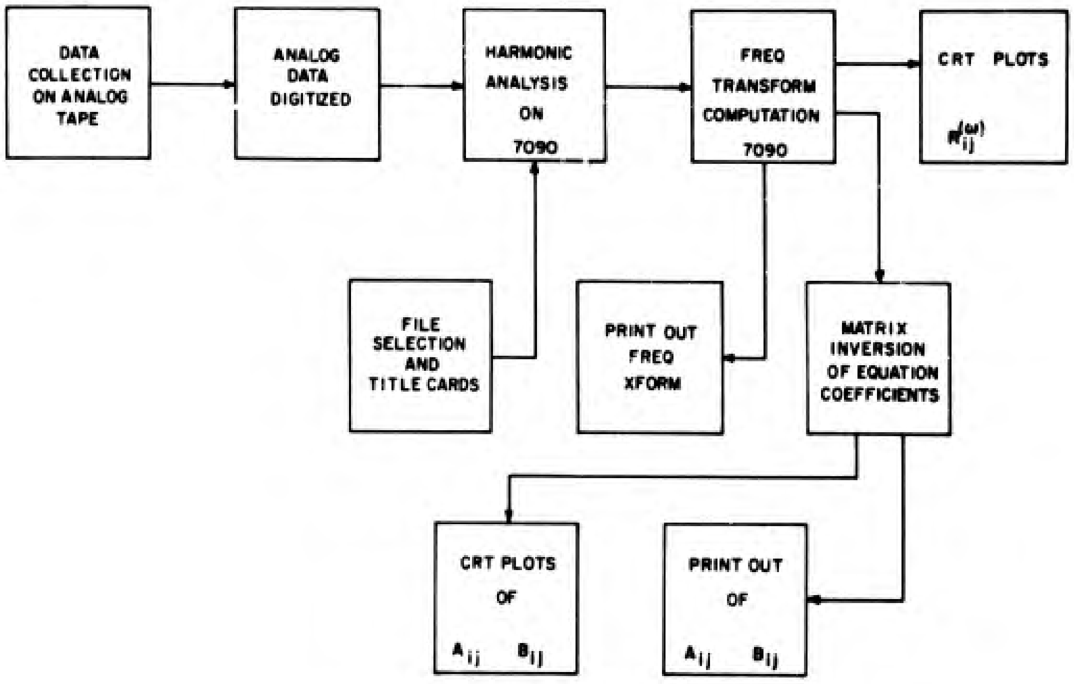

Fig. 7 - Digital analysis system

x_1 = surge (positive forward),

x_2 = sway (positive to port),

x_3 = heave (positive upward),

x_4 = roll (positive deck to starboard),

x_5 = pitch (positive bow downward),

x_6 = yaw (positive bow to port).

If the excitations are sinusoidal with frequency ω, we can write

$$f_i(t) = F_i \cos(\omega t + \epsilon_i)$$

and Eq. (1) reduces to

$$x_j(t) = \sum_{i=1}^{6} F_i \left[(R_{ij}^c)^2 + (R_{ij}^s)^2\right]^{1/2} \cos(\omega t + \epsilon_i - \epsilon_{ij}) \tag{2}$$

where

$$\tan \epsilon_{ij} = R^{s}_{ij}(\omega)/R^{c}_{ij}(\omega) ,$$

$$R^{c}_{ij}(\omega) = \int_0^\infty R_{ij}(\tau) \cos \omega\tau \, d\tau ,$$

$$R^{s}_{ij}(\omega) = \int_0^\infty R_{ij}(\tau) \sin \omega\tau \, d\tau .$$

We will make use of the complex function

$$R^{*}_{ij}(\omega) = R^{c}_{ij}(\omega) + iR^{s}_{ij}(\omega) .$$

The frequency dependent functions, R^{c}_{ij} and R^{s}_{ij}, are the in-phase and out-of-phase responses in the jth mode to a sinusoidal excitation in the ith mode.

The conventional manner of writing the system of coupled equations of motion is

$$\sum_{j=1}^{6} (a_{jk}\ddot{x}_j + b_{jk}\dot{x}_j + c_{jk}x_j) = F_k \cos(\omega t + \epsilon_k) , \qquad k = 1,2,\ldots,6 . \tag{3}$$

Using Eqs. (2) and (3), it is possible to develop a system of equations between the coefficients a_{ij}, b_{ij} and the functions R^{c}_{ij}, R^{s}_{ij}. The c_{jk} are assumed to be determined from static tests. Thus, from the matrix $[R^{*}_{ij}(\omega)]$ we can determine the matrices $[a_{ij}]$ and $[b_{ij}]$.

Experimentally, enough information can be obtained from a series of six tests in which the six sets of excitations are linearly independent to determine $[R^{*}_{ij}]$ and subsequently the coefficients.

As we stated above, we have restricted ourselves to the two modes of heave and pitch. The model was free to respond in all six modes, and all restraints were measured, but in the analysis it was assumed that the coupling between these two modes and the remaining modes was negligible.

Experiment I

The model was excited in heave and pitch by imposing a pulse $f(t)$ at the bow (see Fig. 1). The excitations were $f_3(t) = f(t) + g(t)$ and $f_5(t) = -\ell \cdot f(t)$, where ℓ is the distance of application of $f(t)$ from the center of gravity and $g(t)$ is any constraining force in heave. (There is no constraining moment in pitch.) The responses were $x_3(t)$ and $x_5(t)$. As discussed above, the excitations and responses were resolved into Fourier series:

$$
\begin{aligned}
f_3(t) &= \sum_{n=1}^{\infty} F_3(\omega_n)\, e^{i\omega_n t} \\
f_5(t) &= \sum_{n=1}^{\infty} F_5(\omega_n)\, e^{i\omega_n t} \\
x_3(t) &= \sum_{n=1}^{\infty} x_3(\omega_n)\, e^{i\omega_n t} \\
x_5(t) &= \sum_{n=1}^{\infty} x_5(\omega_n)\, e^{i\omega_n t}
\end{aligned} \tag{4}
$$

where F_3, F_5, x_3, and x_5 are complex valued coefficients.

For a linear system, the components of the response for a given frequency ω are due only to the excitations at that frequency. Thus, we have

$$
\begin{aligned}
x_{3\,I}(\omega) &= F_{3\,I}(\omega)\, R^*_{33}(\omega) + F_{5\,I}(\omega)\, R^*_{53}(\omega) \\
x_{5\,I}(\omega) &= F_{3\,I}(\omega)\, R^*_{35}(\omega) + F_{5\,I}(\omega)\, R^*_{55}(\omega) .
\end{aligned} \tag{5}
$$

Experiment II

The model was excited in heave only. The analysis is identical with the above, except that the excitations $F_{5\,II}$ are zero. We have the equations

$$
\begin{aligned}
x_{3\,II} &= F_{3\,II}\, R^*_{33} \\
x_{5\,II} &= F_{3\,II}\, R^*_{35} .
\end{aligned} \tag{6}
$$

From Eqs. (5) and (6), we obtain

$$
\begin{aligned}
R^*_{33} &= \frac{x_{3\,II}}{F_{3\,II}} \\
R^*_{35} &= \frac{x_{5\,II}}{F_{3\,II}} \\
R^*_{53} &= \frac{x_{3\,I}}{F_{5\,I}} - \frac{F_{3\,I}\, x_{3\,II}}{F_{5\,I}\, F_{3\,II}} \\
R^*_{55} &= \frac{x_{5\,I}}{F_{5\,I}} - \frac{F_{3\,I}\, x_{5\,II}}{F_{5\,I}\, F_{5\,II}} .
\end{aligned} \tag{7}
$$

Determination of the Coefficients

As R^*_{ij} is the response in the jth mode to the excitation $e^{i\omega t}$ in the ith mode, substitution in the equations of motion yields the following relations:

$$\begin{aligned}
-a_{33}\omega^2 R^*_{33} + i b_{33}\omega R^*_{33} + c_{33}R^*_{33} - a_{53}\omega^2 R^*_{35} + i b_{53}\omega R^*_{35} + c_{53}R^*_{35} &= 1 \\
-a_{35}\omega^2 R^*_{33} + i b_{35}\omega R^*_{33} + c_{35}R^*_{33} - a_{55}\omega^2 R^*_{35} + i b_{55}\omega R^*_{35} + c_{55}R^*_{35} &= 0 \\
-a_{33}\omega^2 R^*_{53} + i b_{33}\omega R^*_{53} + c_{33}R^*_{53} - a_{53}\omega^2 R^*_{55} + i b_{53}\omega R^*_{55} + c_{53}R^*_{55} &= 0 \\
-a_{35}\omega^2 R^*_{53} + i b_{35}\omega R^*_{53} + c_{35}R^*_{53} - a_{55}\omega^2 R^*_{55} + i b_{55}\omega R^*_{55} + c_{55}R^*_{55} &= 1 .
\end{aligned} \tag{8}$$

Separating the real and imaginary parts of the equations, we obtain the eight equations:

$$\begin{aligned}
(c_{33} - \omega^2 a_{33})\, R^c_{33} - \omega b_{33} R^s_{33} + (c_{53} - \omega^2 a_{53})\, R^c_{35} - \omega b_{53} R^s_{35} &= 1 \\
(c_{33} - \omega^2 a_{33})\, R^s_{33} + \omega b_{33} R^c_{33} + (c_{53} - \omega^2 a_{53})\, R^s_{35} + \omega b_{53} R^c_{35} &= 0 \\
(c_{33} - \omega^2 a_{33})\, R^c_{53} - \omega b_{33} R^s_{53} + (c_{53} - \omega^2 a_{53})\, R^c_{55} - \omega b_{53} R^s_{55} &= 0 \\
(c_{33} - \omega^2 a_{33})\, R^s_{53} + \omega b_{33} R^c_{53} + (c_{53} - \omega^2 a_{53})\, R^s_{55} + \omega b_{53} R^c_{55} &= 0 \\
(c_{35} - \omega^2 a_{35})\, R^c_{33} - \omega b_{35} R^s_{33} + (c_{55} - \omega^2 a_{55})\, R^c_{35} - \omega b_{55} R^s_{35} &= 0 \\
(c_{35} - \omega^2 a_{35})\, R^s_{33} + \omega b_{35} R^c_{33} + (c_{55} - \omega^2 a_{55})\, R^s_{35} + \omega b_{55} R^c_{35} &= 0 \\
(c_{35} - \omega^2 a_{35})\, R^c_{53} - \omega b_{35} R^s_{53} + (c_{55} - \omega^2 a_{55})\, R^c_{55} - \omega b_{55} R^s_{55} &= 1 \\
(c_{35} - \omega^2 a_{35})\, R^s_{53} + \omega b_{35} R^c_{53} + (c_{55} - \omega^2 a_{55})\, R^s_{55} + \omega b_{55} R^c_{55} &= 0 .
\end{aligned} \tag{9}$$

Let

$$\mathbf{R} = \begin{bmatrix} R^c_{33} & -R^s_{33} & R^c_{35} & -R^s_{35} \\ R^s_{33} & R^c_{33} & R^s_{35} & R^c_{35} \\ R^c_{53} & -R^s_{53} & R^c_{55} & -R^s_{55} \\ R^s_{53} & R^c_{53} & R^s_{55} & R^c_{55} \end{bmatrix} \tag{10}$$

$$\mathbf{K} = \begin{bmatrix} c_{33} - \omega^2 a_{33} & c_{35} - \omega^2 a_{35} \\ \omega b_{33} & \omega b_{35} \\ c_{53} - \omega^2 a_{53} & c_{55} - \omega^2 a_{55} \\ \omega b_{53} & \omega b_{55} \end{bmatrix} \tag{11}$$

Then the above system of equations can be written

$$\mathbf{R} \cdot \mathbf{K} = \begin{bmatrix} 1 & 0 \\ 0 & 0 \\ 0 & 1 \\ 0 & 0 \end{bmatrix} \tag{12}$$

By inverting the matrix R, we can directly obtain the matrix by

$$\mathbf{K} = \mathbf{R}^{-1} \begin{bmatrix} 1 & 0 \\ 0 & 0 \\ 0 & 1 \\ 0 & 0 \end{bmatrix} \tag{13}$$

and the coefficients in the two coupled equations of motion may be computed.

TEST RESULTS

As previously mentioned testing was done at a range of Froude numbers from Fr. = 0 to 0.35. However, due to a time limitation, only the cases for Fr. = 0, 0.15, and 0.30 are presented in this progress report. The results at Fr. = 0.15 and 0.30 are of course directly comparable with those obtained by Gerritsma.

The responses obtained at zero speed were particularly good. In the non-dimensional frequency range $1 < \omega\sqrt{L/g} < 6$ there was very little scatter and the results were similar to those obtained by Gerritsma. Wall effects were significant only below $\omega\sqrt{L/g} = 1.0$ and then only at clearly defined multiples of tank width. Considerable scatter in the data did occur above 6.0 which can be traced to the dynamic range limitations inherent in an analog tape recorder. The principal damping and added mass terms obtained from this experiment are shown in Figs. 8 and 9.

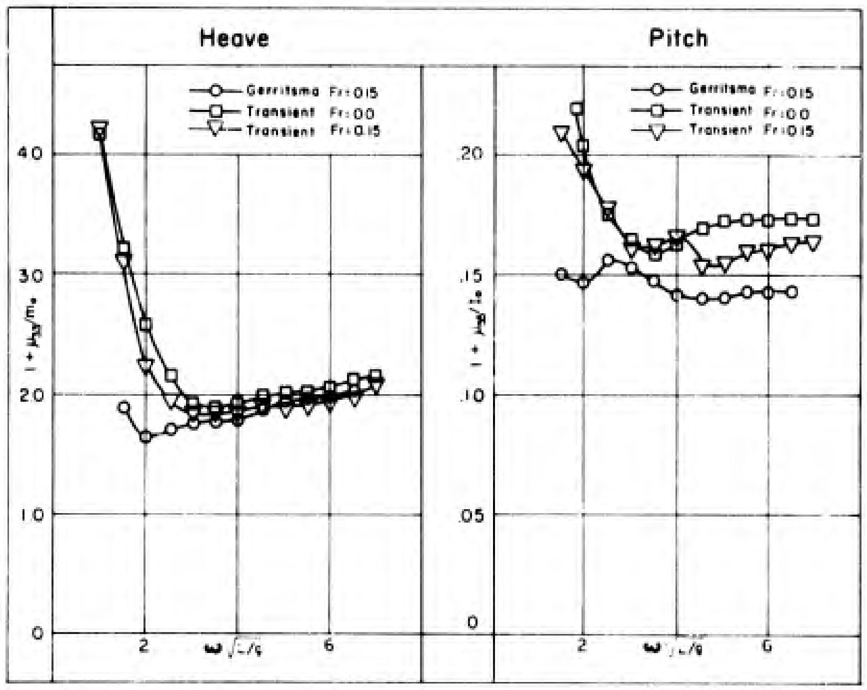

Fig. 8a - Added mass

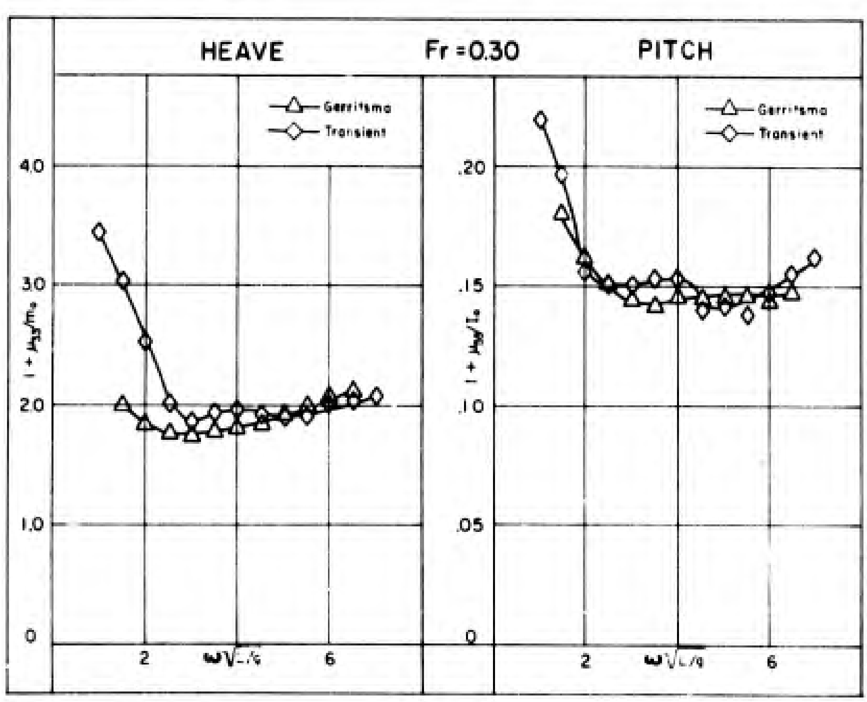

Fig. 8b - Added mass

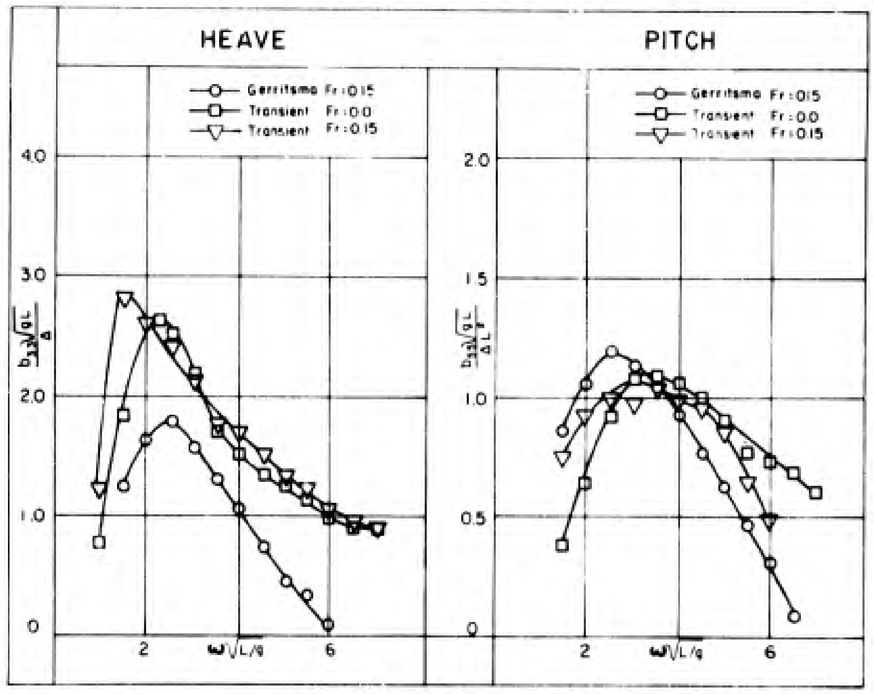

Fig. 9a - Damping

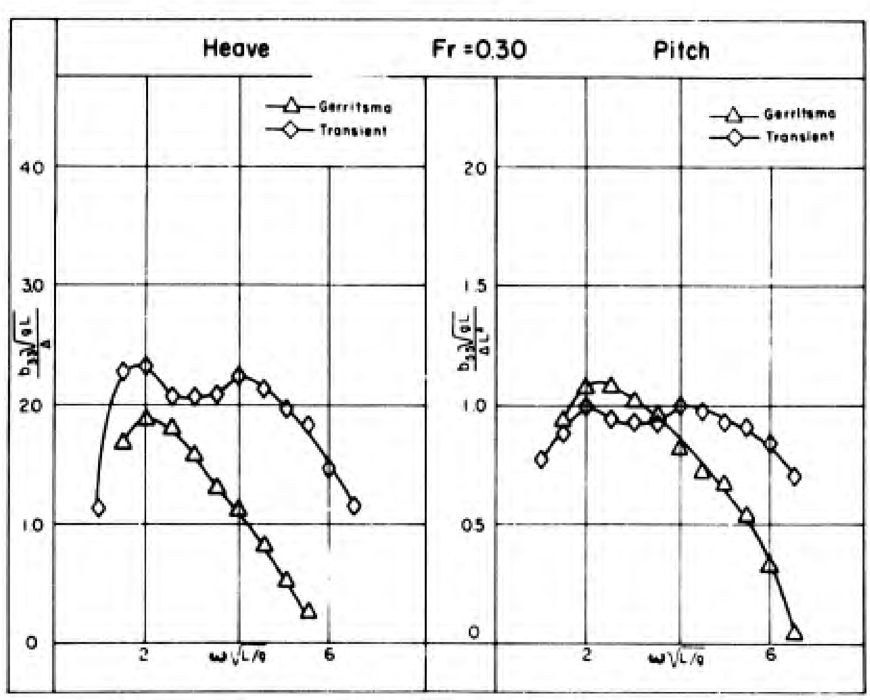

Fig. 9b - Damping

Similarly the forward speed cases were good over the same frequency range. There was, however, some evidence that coupling of surge into heave and pitch was significant at forward speeds and indicates the desirability of a three mode (pitch, heave and surge) analysis. The damping and added mass terms are shown along with those reported by Gerritsma.

CONCLUSIONS

It is apparent from the preliminary results that good perimental results can be obtained even at zero speed in a 240 by 360 ft tank. While wall effects do occur, they appear only as one or two sharply defined discontinuities in the response data. The results also indicate that, while a two mode pitch and heave test can be conducted, a further increase in accuracy should be obtained by an extension to the three mode analysis. While there is much to be done, especially in such areas as increasing the dynamic range of the instrumentation system and an extension to a 3 or 4 mode analysis, it is felt that these preliminary results demonstrate not only the validity of the pulse testing technique but further show that satisfactory results are within the capability of modern instrumentation and measurement systems.

MODEL DETAILS

Series 60 Parent Form

L	Length between perpendiculars	10.0 ft
B	Beam	1.35 ft
H	Draft	0.53 ft
Δ	Displacement	239.3 lb
C_b	Block coefficient	0.60
A	Area of waterline plane	9.39 ft^2
C_{wl}	Waterline coefficient	0.71
I_o	Mass moment of inertia for pitch (in air)	557.89 lb in./sec^2
r_o	Radius of gyration	0.25L
m_o	Mass of model	7.439 slugs

REFERENCES

1. Cummins, W. E., "The Impulse Response Function and Ship Motions," Presented at Symposium on Ship Theory at Institut für Schiffbau der Universität Hamburg, 25-27 Jan. 1962, Schiffstechnik H. 47 B. 9 (June 1962).

2. Fuchs, R. A. and MacCamy, R. C., "Linear Theory of Ship Motion in Irregular Waves," Institute of Engineering Research, Wave Research Laboratory T.R. Series 61, Issue 2, University of California, Berkeley, California (July 1953).

3. Dalzell, J. F., "Cross-Spectral Analysis of Ship-Model Motions: A Destroyer Model in Irregular Long-Crested Head Seas," Davidson Laboratory, Stevens Institute of Technology, Report 810 (Apr. 1962).

4. Davis, M. C., Cdr. USN and Zarnick, E. E., "Testing Ship Models in Transient Waves," To be presented at the Fifth Symposium on Naval Hydrodynamics, 10-12 Sept. 1964.

5. Gerritsma, J., "Shipmotions in Longitudinal Waves," International Shipbuilding Progress, Vol. 7 (1960).

6. Hamming, R. W., "Numerical Methods for Scientists and Engineers," McGraw-Hill, New York (1962).

* * *

DISCUSSION OF FOUR PAPERS

Leo Joseph Tick
New York University
University Heights, Bronx, New York

Since the papers by Smith and Cummins; Breslin, Savitsky and Tsakonas; and Davis and Zarnick, concern themselves with testing, I will first combine my comments to these papers.* These papers and the oral discussion which followed devoted some time to the pros and cons of various methods for determining the defining properties of systems (mostly linear). Unfortunately, the lack of a careful description of the logic of test procedures has served to add considerable confusion. With a hope (?) of providing some clarification, I start with brief discussions of "test functions." The test situation consists, as I see it, of some system, device, etc., whose input-output characteristics one wishes to determine. A test procedure is to be used to make the determination as distinct from an analytical one.

To make the discussion simpler, suppose we restrict ourselves to linear systems. In this case the system is usually characterized by the transfer

*pp. 439, 461, 507.

function or the impulse response; these being Fourier transforms of each other. The testing procedure then consists of driving the system with some function and measuring both the input and output and performing relevant calculations. The minimum requirement of a good test function is that it should be rich in the frequencies of interest.

It will usually be the case that the calculations will involve some sort of division. If the numerator has an error component which is fairly uniform over the entire frequency range, then the ratio will be of lower quality for those values at which the denominator is smallest. Since the denominator will consist of some characteristic of the input function, it is best that the denominator be fairly constant. With these characteristics in mind, let us now look at three possible classes of input functions: (1) sine waves; (2) deterministic functions like the ramp, or pulse, or step, and (3) stationary random input. The sine wave is of course the worst as far as frequency content is concerned since it has only one frequency. As a compensatory feature, the transfer function at this frequency is estimated by a very simple operation on the output and it can be estimated quite accurately since all we have to extract from the continuous record is just the amplitude and the phase angle. The effect of noise in the measuring system should be quite small. We also have a measure of linearity of the system from visual inspection of the output.

This is a very expensive way to proceed since it requires a very large number of sine wave tests to complete the analysis of the entire frequency band.

The pulse test function is a very convenient one because all frequencies are present in an equal amount. The calculations to be performed on the output are quite simple. To estimate the transfer function, one merely takes the Fourier transform of the response.* The drawback to this test function is that it may be difficult to generate as the Davis, etc., paper indicates.

Now no system is exactly linear, but this observation should bother no one since it is sufficient for dealing with problems of nature that the systems are enough so for the purposes of its use. Therefore, one should try to test under conditions which are representative of the conditions of use. One would not test in very high waves. Similarly the fast rise time of a good pulse may activate nonlinear modes of response.

Finally, the stationary random test function is in some way a mixture of the previous two. There is some sort of repetition, albeit, an average one, and a "pulsiness." We may make the function broadband in frequencies (in an average sense), and its spectrum as flat as our generating methods will allow. As pointed out by Davis, the system will have to be brought into a steady state before the relevant arithmetic may be performed on the output, and in case of

*If I seem casual about this operation, I am just reflecting the speakers. Let me assure you though that this is a numerical operation fraught with error especially at the higher frequencies as we will then be taking differences of a large number of numbers of approximately equal magnitude. Since experimental data usually has low significance (numerically speaking) this is a real problem.

model testing this may use up a significant proportion of the available test time. The amount of usable test time may give rise to estimates having large sampling variability. The arithmetic processes involved here, though lengthy, are well understood and present no difficulty.

One of the most important contributions of statistics to experimentation is the formalization of the notion and the provision of methodologies for having an experiment provide its own measure of its errors. This is done by setting the problem in a probabilistic framework by either assuming it into existence of manufacturing it by so-called "randomization" operations.

Those of you who have read books or attended lectures on experimental design, that branch of statistics concerned with these problems, will recall these points. This attribute of an experiment does not come free. The price for putting it into this framework is to blunt the precision of the results.

All of these attributes and philosophy of statistical experimental design have their analogs in random test functions. If one uses a deterministic test function, a transfer function can be calculated whether it exists or the calculated one has any relationship to the true one. Verification is required from some other source, e.g., previous experiments, etc., before one can have confidence in the calculations.

If these verifications are available, the experiment can be economic and precise.

On the other hand, if the test function is embedded in a family of test functions in such a way as to make the statistical manipulation allowable, the experiment itself will provide a measure of its own error; and that will be the coherency function. It seems to me that this is worth something and, as mentioned above, it does cost.

What all this comes down to is simply that the choice of a test function is not a simple or clear one.

A point which seems to have been neglected in Dr. Ochi's paper and the discussion following is why such a simple procedure works at all. After all, slamming is a very complicated process and yet the simplest of models appear to be producing excellent answers. Being the original instigator of this approach, I think I can throw some light on this problem.

Way back (I guess it is more than 7 years ago by now) when I was wondering if some model could not be constructed for slamming predictions, I was looking at some destroyer data. I do not quite remember who was with me at the time although I think it was Martin Bates, then of the then Bell Aircraft, who commented that if you put the data through a low-pass filter you could hardly tell from the resulting record that a slam had occurred. This indicated to me that slamming did not change the gross aspects of the motion and that a simple model, based on the occurrence of conditions which induce slamming, might serve to make an average occurrence prediction. This observation appears to have been justified.

* * *

DETERMINISTIC EVALUATION OF MOTIONS OF MARINE CRAFT IN IRREGULAR SEAS

John P. Breslin, Daniel Savitsky, and Stavros Tsakonas
Stevens Institute of Technology
Hoboken, New Jersey

ABSTRACT

The concepts of linear system analysis are applied to the coupled motion of marine craft to illustrate in greater detail than previously provided the procedures for obtaining their instantaneous response in arbitrary irregular long-crested waves. The solutions of the coupled equations of motion for heave and pitch in long-crested regular seas are examined to show how the ship-sea transfer function can be identified when the wave is regarded as the input rather than the actual forces and moments. The theoretical expressions for the response to arbitrary forcing functions are next examined and shown to involve the inverse Fourier transform of the ship-sea transfer function and this is identified as the system impulsive response function. This function is convoluted with the given surface wave record to provide the instantaneous response. The characteristics of these impulsive response functions are discussed in some detail and means for their determination from theory and experiments are outlined.

Application of the procedures are made to exhibit the high accuracy of deterministically calculated motions derived from models of a destroyer, underwater body, and hydrofoil craft. Results of calculation of the bending moment of a surface ship model are also exhibited. It is concluded that the method can be applied to all features of marine craft responses attending irregular wave motion which satisfy the requirements of linear systems.

INTRODUCTION

Operation of marine vehicles in irregular seas is a problem of serious concern to the naval architect. It is important that reliable analytical methods be available to predict the motions, acceleration, degree of deck wetting, etc., of these craft before they are constructed and put to sea.

In 1953, two important papers on ship motions in irregular seas were published. St. Denis and Pierson [1] considered the statistical aspects of ship motion and presented methods for determining the probabilistic behavior of a ship in a random sea. A second method of analysis, which is complementary to that of St. Denis and Pierson, was introduced by Fuchs and MacCamy [2]. This later method is not statistical, but deterministic; it is based, therefore, not on the knowledge of the statistical properties of the sea, but on that of the actual time history record of the sea surface.

The statistical approach makes use of spectral analysis techniques and the characteristics of the ship response to random wave excitation are defined in terms of an energy spectrum based on frequency of wave encounter. This is the so-called transfer function method whose application has been successfully demonstrated by many researchers over the past years for a variety of marine craft, i.e., St. Denis and Pierson [1] and Dalzell [3] in the case of motion of displacement ships; Dalzell [4] for the case of ship bending moment; Savitsky [5] for submerged bodies in irregular waves; and Bernicker [6,7] for the case of fully wetted and super-ventilated surface piercing hydrofoil systems.

The deterministic approach employs the concept of the impulsive response function, as given in linear analysis, to define the time history of ship motion in terms of the actual time history of the surface wave profile of the irregular sea. As the name implies, the impulsive response function describes the time history of the response of a given system when acted upon by an input consisting of a unit impulse at zero time. Superposition of these unit impulses to represent the actual wave excitation yields the total response of the system. Fuchs and MacCamy [2,8] first applied this technique for simple bodies in a random head sea. In recent years, the Davidson Laboratory, Stevens Institute of Technology, has investigated the application of this deterministic technique to predicting the random motions of a variety of marine vehicles, including displacement ships, hydrofoil craft, and submerged bodies in irregular waves. It is the purpose of this paper to present a review of the deterministic technique, to discuss its limitations, and to compare the results of the analytical studies conducted at Davidson Laboratory with experimental data. Some of these results have already appeared in the published Davidson Laboratory reports, but will be summarized herein in an attempt to form a unified presentation.

This work was sponsored by several bureaus of the U.S. Navy, including the Bureau of Ships, Bureau of Naval Weapons, and Office of Naval Research. The preparation of this paper was sponsored by the Davidson Laboratory, Stevens Institute of Technology.

THEORETICAL FOUNDATIONS

The linear theory of the motions of bodies in waves has been the subject of many papers and presentations in the past. As a result, there are several clear analyses of bodies in both regular and irregular waves, the latter case having been dealt with by spectral procedures. However, the deterministic or instantaneous response of bodies in a given, nonuniform, temporally varying wave has not been given an entirely clear analysis beginning with the equations of motion. The procedures used thus far have treated the motion as the output of a linear system due to a wave input. This involves the identification of (for systems with several degrees of freedom) what might be termed a "lumped" transfer function (or response to waves of discrete frequencies) and from this to calculate formally a correspondingly lumped impulsive response function which, when convoluted with the given wave record, yields the instantaneous motion. Although this procedure has been shown to work exceedingly well (see section on applications) questions arise as to the character of these impulsive response functions primarily because the analysis has not been sufficiently lucid. At the risk of appearing pedantic, the elementary theory is reexamined in the following pages in the hope of providing a firmer foundation for the more-or-less mechanical procedures used in arriving at the instantaneous response of a hull within, or upon, the surface of a long-crested sea which is arbitrarily specified.*

Heaving and Pitching In or Under Regular Waves

Korvin-Kroukovsky [9] (1955) was quick to realize that the combined heaving and pitching of responses of a ship are the solutions to a coupled pair of ordinary second-order, linear differential equations with coefficients which vary with imposed frequency. Following his notation, the differential equations of motion are, for the case of simple harmonic forcing functions:

$$a\ddot{z} + b\dot{z} + cz + d \cdot \ddot{\theta} + e\dot{\theta} + g\theta = F_o e^{i\omega t} \tag{1}$$

$$A\ddot{\theta} + B\dot{\theta} + C\theta + D \cdot \ddot{z} + E\dot{z} + Gz = M_o e^{i\omega t} \tag{2}$$

where

- z is the heave displacement from equilibrium,
- θ is the pitch displacement from equilibrium,
- a, b, c are the virtual mass, damping and spring coefficients for pure heaving,
- d, e, f are corresponding cross coupling coefficients due to pitch,
- A, B, C are the virtual mass moment of inertia, damping and spring coefficients for pure pitching,
- D, E, G are corresponding cross coupling coefficients due to heave,
- F_o and M_o are the complex force and moment excitations for a regular wave of amplitude $|\eta_o|$ with the understanding that only the real parts of the right-hand sides of (1) and (2) are to be ultimately retained.

(The dot notation is used to represent a total derivative with respect to time.)

*The severity of the given wave trace (as a function of time) must be such as to permit application of linear system analysis.

The solutions of this pair of equations are written (again in Korvin-Kroukovsky's notation) in the compact complex variable form:

$$z = \left(\frac{F_o S - M_o Q}{PS - QR}\right) e^{i\omega t} \tag{3}$$

$$\theta = \left(\frac{M_o P - F_o R}{PS - QR}\right) e^{i\omega t} \tag{4}$$

where

$$\begin{aligned} P(\omega) &= -2\omega^2 + ib\omega + c \\ Q(\omega) &= -d \cdot \omega^2 + ie\omega + g \\ R(\omega) &= -D \cdot \omega^2 + iE\omega + G \\ S(\omega) &= -A\omega^2 + iB\omega + c\,. \end{aligned} \tag{5}$$

Inspection of (3) and (4) shows that the response in heave and pitch are both linear combinations of the forces and moments and response or transfer functions of the body. Consider only the response in heave (pitch follows in complete analogy) which may be written

$$z(t) = z_f + z_m \tag{6}$$

where

$$z_f = F_o \left(\frac{S}{PS - QR}\right) e^{i\omega t} = F_o\, \Phi_f(\omega)\, e^{i\omega t} \tag{7}$$

and

$$z_m = -M_o \left(\frac{Q}{PS - QR}\right) e^{i\omega t} = -M_o\, \Phi_m(\omega)\, e^{i\omega t}. \tag{8}$$

The complex functions Φ_f and Φ_m are called frequency response or transfer functions in heave per unit applied force and moment and are evaluated in terms of an amplitude and phase angle in the form:

$$\Phi_f = A_f(\omega)\, e^{-i\epsilon(\omega)}; \qquad \Phi_m = A_m(\omega)\, e^{-i\delta(\omega)} \tag{9}$$

where

$$A_f(\omega) = \left|\frac{S(\omega)}{T(\omega)}\right|; \qquad A_m(\omega) = \left|\frac{Q(\omega)}{T(\omega)}\right| \tag{10}$$

and, for brevity $T(\omega) = PS - QR$.

As is well known, these unit response functions depend only on the body coefficients themselves and not on the forcing functions. In what follows, it will be necessary to consider the forcing functions characteristics in some detail.

The forcing functions F_o and M_o for the case of bodies in regular waves are in general complicated functions of incident wave frequency. Conceptually they are secured by considering the in- and out-of-phase pressure distributions developed on the body when restrained from moving in the wave system. Thus, in general, they take the form

$$F_o e^{i\omega t} = a'(\omega) \frac{\partial^2 \eta}{\partial t^2} + ib'(\omega) \frac{\partial \eta}{\partial t} + c'\eta \tag{11}$$

$$M_o e^{i\omega t} = A'(\omega) \frac{\partial^2 \eta}{\partial t^2} + iB'(\omega) \frac{\partial \eta}{\partial t} + C'\eta \tag{12}$$

where η is the wave or vertical fluid displacement at the body (which may be submerged) referenced to some arbitrary point on the body (often to the center of mass or amidships as a convention). For any regular progressive wave the vertical motion at any point ζ is

$$\begin{aligned} \eta(\xi, \zeta, t) &= |\eta_o| e^{+\frac{i\omega|\omega|\xi}{g} - \frac{\omega^2 \zeta}{g}} e^{i\omega t} \\ &= |\eta_o| g(\omega, \xi, \zeta) e^{i\omega t} \end{aligned} \tag{13}$$

where $|\eta_o|$ is the amplitude of the wave at the surface and

$$g(\omega, \xi, \zeta) = e^{\frac{i\omega|\omega|\xi}{g} - \frac{\omega^2 \zeta}{g}} . \tag{14}$$

The complex exciting force and moment (11) and (12) become, after use of (13),

$$\begin{aligned} F_o(\omega, \xi, \zeta) &= (-\omega^2 a'(\omega) + i\omega b'(\omega) + c') |\eta_o| g(\omega, \xi, \zeta) \\ M_o(\omega, \xi, \zeta) &= (-\omega^2 A'(\omega) + i\omega B'(\omega) + c') |\eta_o| g(\omega, \xi, \zeta) . \end{aligned} \tag{15}$$

Thus it is seen that the force and moment acting on a body are both proportional to the wave amplitude on the surface and are arbitrarily phased to the body through the coordinates ξ, ζ. For sake of brevity let the force and moment per unit of wave amplitude be written

$$\frac{F_o}{|\eta_o|} = f'(\omega) \; g(\omega, \xi, \zeta) \tag{16}$$

and

$$\frac{M_o}{|\eta_o|} = m'(\omega) \; g(\omega, \xi, \zeta) \tag{17}$$

where f' and m' are the complex polynomials

$$\begin{aligned} f'(\omega) &= -\omega^2 a'(\omega) + i\omega b'(\omega) + c' \\ m'(\omega) &= -\omega^2 A'(\omega) + i\omega B'(\omega) + C'. \end{aligned} \tag{18}$$

Equations (15) and (16) now allow one to express the response of the coupled system in terms of wave amplitude by inserting them in (7) and (8) and summing to yield

$$\begin{aligned} \frac{z(t)}{|\eta_o|} &= \left[\Phi_f(\omega)\ f'(\omega) - \Phi_m(\omega)\ m'(\omega)\right] g(\omega,\xi,\zeta)\ e^{i\omega t} \\ &= \left(\frac{S(\omega)\ f'(\omega) - Q(\omega)\ m'(\omega)}{T(\omega)}\right) g(\omega,\xi,\zeta)\ e^{i\omega t}. \end{aligned} \tag{19}$$

Thus one may recognize a lumped or effective frequency response function for heave (with freedom in pitch) for the ship-sea system per unit of wave amplitude as

$$\Phi_{z\theta}(\omega,\xi,\zeta) = \left(\frac{S(\omega)\ f'(\omega) - Q(\omega)\ m'(\omega)}{T(\omega)}\right) g(\omega,\xi,\zeta). \tag{20}$$

This can be reduced to an amplitude function which depends on ω and ζ and a phase angle which depends upon ω and ξ (or x); thus

$$\Phi_{z\theta}(\omega,\xi,\zeta) = A(\omega,\zeta)\ e^{-i\sigma(\omega,\xi)} \tag{21}$$

and this is what is determined from either theory or from recorded responses of a model in regular waves. It is important to note that an arbitrariness is introduced into the phase by the reference system used or, what is the same thing, by the arbitrary definition of phase.

Instantaneous Motion in Arbitrary Time-Varying Waves

The equations for heave and pitch motion are the same as (1) and (2) for regular onset waves, but now the right-hand sides are functions of time explicitly and are not functions of discrete frequencies. Thus $F_o e^{i\omega t}$ and $M_o e^{i\omega t}$ are replaced in Eqs. (1) and (2) by $F(t)$ and $M(t)$. The common procedure in solving the equations in this case is to employ Fourier integral transforms which may be defined as follows:

If $\hat{z}$ is the Fourier time transform of $z(t)$, then

$$\hat{z}(\omega) = \int_{-\infty}^{\infty} z(t)\, e^{-i\omega t}\, dt \tag{22}$$

and the inverse transform is

$$z(t) = \frac{1}{2\pi} \int_{-\infty}^{\infty} \hat{z}(\omega) e^{i\omega t} d\omega . \tag{23}$$

One then multiplies Eqs. (1) and (2) through by $e^{-i\omega t}$ and integrates over all time from $-\infty$ to $+\infty$ under the assumption of vanishing z, $\dot{z}$, θ and $\dot{\theta}$ at $\pm\infty$ and the satisfaction of integrability conditions by $F(t)$ and $M(t)$. The solution for heave is, as an example, given by

$$z = z_f + z_m = \frac{1}{2\pi} \int_{-\infty}^{\infty} \frac{S(\omega)}{T(\omega)} \hat{F}(\omega) e^{i\omega t} d\omega - \frac{1}{2\pi} \int_{-\infty}^{\infty} \frac{Q(\omega)}{T(\omega)} \hat{M}(\omega) e^{-i\omega t} d\omega \tag{24}$$

where one next replaces the transforms $\hat{F}$ and $\hat{M}$ by

$$\left.\begin{matrix} \hat{F} \\ \hat{M} \end{matrix}\right\} = \int_{-\infty}^{\infty} \left.\begin{matrix} F(\tau) \\ M(\tau) \end{matrix}\right\} e^{-i\omega\tau} d\tau \tag{25}$$

and, upon interchange of the orders of integration, obtains the familiar result

$$z = z_f + z_m = \frac{1}{2\pi} \int_{-\infty}^{\infty} F(\tau) \int_{-\infty}^{\infty} \frac{S(\omega)}{T(\omega)} e^{i(t-\tau)\omega} d\omega - \frac{1}{2\pi} \int_{-\infty}^{\infty} M(\tau) \int_{-\infty}^{\infty} \frac{Q(\omega)}{T(\omega)} e^{i(t-\tau)\omega} d\omega \tag{26}$$

which leads to the definition of the kernel functions

$$K_f(u) = \frac{1}{2\pi} \int_{-\infty}^{\infty} \frac{S(\omega)}{T(\omega)} e^{iu\omega} d\omega \tag{27}$$

$$K_m(u) = \frac{1}{2\pi} \int_{-\infty}^{\infty} \frac{Q(\omega)}{T(\omega)} e^{iu\omega} d\omega . \tag{28}$$

These are defined as the impulsive response function for the body in the fluid. It is to be noted that they are dependent only on the body coefficients obtained from either the impulsive response in calm water or from the response of the body to regular waves. The final expression for the heave is then

$$z = z_f + z_m \tag{29}$$

with

$$z_f = \int_{-\infty}^{\infty} F(\tau) K_f(t-\tau) d\tau \tag{30}$$

$$z_m = -\int_{-\infty}^{\infty} M(\tau) K_m(t-\tau) d\tau \tag{31}$$

which simply states that the total heave response is the algebraic sum of two convolutions of the force and moment time histories with the appropriate impulsive response functions.

However, one does not have at his disposal the force and moment time histories, but rather only the wave input time history. It is, therefore, necessary to eliminate the explicit dependence of the result on F and M and to determine how one operates on the known (or given) wave record to determine the motions. For simplicity, the following development is applied only to part of the response z_f to illustrate the procedure.

It is noted from (16) that the normalized force at any discrete frequency is known and hence one can express the force as a function of time and the instantaneous surface wave $\eta_0(\tau)$ by convoluting the wave with the force transfer function, or

$$F(t) = \frac{1}{2\pi} \int_{-\infty}^{\infty} \eta_0(\tau';\xi) \int_{-\infty}^{\infty} f'(\omega') \, g(\omega', \xi, \zeta) \, e^{i\omega'(t-\tau')} \, d\omega' d\tau' . \tag{32}$$

Upon insertion of this into (30) and through the use of (27), one finds that this part of the response takes the form:

$$z_f = \frac{1}{(2\pi)^2} \int_{\tau=-\infty}^{\infty} \left\{ \int_{-\infty}^{\infty} \eta_0(\tau';\xi) \int_{-\infty}^{\infty} f' g \, e^{i\omega'(\tau-\tau')} \, d\omega' \right\} \int_{-\infty}^{\infty} \frac{S(\omega)}{T(\omega)} \, e^{i\omega(t-\tau)} \, d\omega \, d\tau .$$

Interchanging the order of integration and noting that the τ-integral is simply

$$\int_{-\infty}^{\infty} e^{i(\omega'-\omega)\tau} \, d\tau = 2\pi\delta(\omega'-\omega)$$

where δ is the Dirac delta function, yields

$$z_f = \frac{1}{2\pi} \int_{\tau'=-\infty}^{\infty} \eta_0(\tau,\xi) \int_{\omega=-\infty}^{\infty} \frac{S(\omega)}{T(\omega)} \, e^{i\omega t} \int_{\omega'=-\infty}^{\infty} f'(\omega') \, g(\omega') \, e^{-i\tau'\omega'} \, \delta(\omega'-\omega) \, d\omega' d\omega \, d\tau'$$

and, because of the delta function property the ω'-integral produces $f'(\omega) g(\omega) e^{i\tau'\omega}$ to give

$$z_f = \frac{1}{2\pi} \int_{\tau'=-\infty}^{\infty} \eta_0(\tau',\xi) \int_{-\infty}^{\infty} \frac{f'(\omega) \, g(\omega,\xi,\zeta) \, S(\omega)}{T(\omega)} \, e^{i\omega(t-\tau')} \, d\omega \, d\tau' \tag{33}$$

a completely similar result would be secured for the motion constituent z_m so the total motion can be written

$$z(t) = \frac{1}{2\pi}\int_{-\infty}^{\infty} \eta_0(\tau',\xi)\int_{-\infty}^{\infty}\left(\frac{f'(\omega)\,S(\omega) - m'(\omega)\,Q(\omega)}{T(\omega)}\right) g(\omega,\xi,\zeta)\, e^{i\omega(t-\tau')}\, d\omega\, d\tau' \,. \tag{34}$$

The integrand is immediately recognized as the effective or lumped frequency response function for the ship-sea system defined by Eq. (20). Hence the ω-integral is the effective impulsive heave response function for the ship-sea system:

$$K_{z\theta}(u;\xi,\zeta) = \frac{1}{2\pi}\int_{-\infty}^{\infty}\left(\frac{f'(\omega)\;S(\omega) - m'(\omega)\;Q(\omega)}{T(\omega)}\right) g(\omega,\xi,\zeta)\; e^{iu\omega}\, d\omega$$

$$= \frac{1}{2\pi}\int_{-\infty}^{\infty} \Phi_{z\theta}(\omega)\; e^{iu\omega}\, d\omega \tag{35}$$

so that for both heave and pitch

$$\left.\begin{matrix} z(t;\xi,\zeta) \\ \theta(t;\xi,\zeta) \end{matrix}\right\} = \int_{\tau'=-\infty}^{\infty} \eta_0(\tau',\xi) \left\{\begin{matrix} K_{z\theta}(t-\tau';\xi,\zeta) \\ K_{\theta z}(t-\tau';\xi,\zeta) \end{matrix}\right\} d\tau' \tag{36}$$

where $K_{\theta z}$ is the impulsive response of the ship-sea system in pitch with freedom in heave present.

It is of interest to note that the same result for the response can be obtained by normalizing the forcing functions with respect to the vertical fluid displacement at depth. To illustrate this, consider the forcing function $F(t)$ in this light and one can write

$$F(t) = \frac{1}{2\pi}\int_{-\infty}^{\infty} \eta(\tau',\xi,\zeta)\int_{-\infty}^{\infty} f'(\omega')\; e^{\frac{i\omega'|\omega'|\xi}{g}}\; e^{i\omega'(t-\tau')}\, d\omega' d\tau' \tag{37}$$

where it is to be noted that $e^{-\omega^2\zeta/g}$ has been suppressed and the motion at depth $\eta(\tau,\xi,\zeta)$ is used. Then the component response in heave is

$$z_f(t;\xi,\zeta) = \frac{1}{2\pi}\int_{-\infty}^{\infty} F(\tau)\int_{-\infty}^{\infty}\frac{S(\omega)}{T(\omega)}\, e^{i\omega(t-\tau)}\, d\omega\, d\tau$$

$$= \frac{1}{(2\pi)^2}\int_{-\infty}^{\infty}\int_{-\infty}^{\infty} \eta(\tau',\xi,\zeta)\int_{-\infty}^{\infty} f'(\omega')\; e^{\frac{i\omega'|\omega'|\xi}{g}}\; e^{i\omega'(\tau-\tau')}\, d\omega' d\tau'$$

$$\times \int_{-\infty}^{\infty}\frac{S(\omega)}{T(\omega)}\, e^{i\omega(t-\tau)}\, d\omega\, d\tau$$

and again

$$\int_{-\infty}^{\infty} e^{i(\omega' - \omega)\tau}\, d\tau = 2\pi\delta(\omega' - \omega)$$

and

$$2\pi \int_{\omega'=-\infty}^{\infty} f'(\omega')\, e^{\frac{i\omega'|\omega'|\zeta}{g}}\, e^{-i\omega'\tau'}\delta(\omega' - \omega)\, d\omega' = 2\pi f'(\omega)\, e^{\frac{i\omega|\omega|\zeta}{g}}\, e^{-i\omega\tau'} .$$

Then

$$z_f(t;\xi,\zeta) = \frac{1}{2\pi}\int_{-\infty}^{\infty} \eta(\tau';\xi,\zeta) \int_{-\infty}^{\infty} \frac{S(\omega)\, f'(\omega)}{T(\omega)}\, e^{\frac{i\omega|\omega|\zeta}{g}}\, e^{i\omega(t-\tau')}\, d\omega\, d\tau' . \quad (38)$$

Now if one wishes to refer this to the wave at the surface

$$\eta(\tau';\xi,\zeta) = \frac{1}{2\pi}\int_{-\infty}^{\infty} \eta(\tau'';\xi,0) \int_{-\infty}^{\infty} e^{-\frac{\omega'^2\zeta}{g}}\, e^{i\omega'(\tau'-\tau'')}\, d\omega'\, d\tau'' . \quad (39)$$

The same integration procedure applies and the previous result is obtained, namely,

$$z_f(t;\xi,\zeta) = \frac{1}{2\pi}\int_{-\infty}^{\infty} \eta(\tau;\xi,0) \int_{-\infty}^{\infty} \frac{S(\omega)\, f'(\omega)}{T(\omega)}\, e^{-\frac{\omega^2\zeta}{g} + \frac{i\omega|\omega|\zeta}{g}}\, e^{i\omega(t-\tau)}\, d\omega\, d\tau . \quad (40)$$

Thus it is seen that the response calculated in terms of the subsurface motions as given by (38) is the same as that given by (40) when the subsurface motion is referred to that on the surface by Eq. (39).

Evaluation of the Impulsive Response Function for Ships

It is clear from Eq. (35) that the impulsive response function for coupled motion depends upon a knowledge of the response of the system to normalized forces and moments at discrete frequencies, i.e., one must know the frequency response operators, or what is called the transfer function. One may seek to evaluate $\Phi_{z\eta}(\omega)$ and $\Phi_{\theta z}(\omega)$ from theory alone or from experimental records of model responses in either regular or irregular waves.

At present one may calculate the transfer functions from theory by using Grim's [10] methods for estimation of the body coefficients, eight of which are frequency dependent. Gerritsma's [11] recently completed work on determination of the body coefficients has given strong support to the procedures used by Korvin-Kroukovsky and Jacobs [12] for ship motion calculations. It is to be noted that, in dealing with a "lumped" heave-pitch and pitch-heave response operators, it is also necessary to specify the normalized excitations as functions of incident frequency. Integration required to obtain the impulsive response functions would undoubtedly have to be done by computer since the transfer functions with frequency-dependent coefficients are very complicated.

An attractive alternative to theory is the use of experimentally determined responses of a model of the vessel to either regular or irregular waves. It is now a routine procedure to obtain from towing tank tests the amplitude response operators and their respective phases at selected values of frequency. In such tests the motions are related to wave measurements made by wave wire or other devices placed ahead of the model or abeam in time with amidships. It can, therefore, be appreciated that these transfer functions (obtained by graphing amplitude and phase response against incident frequency) are indeed dependent upon the location of the wave wire. It is often found that the impulsive response function derived from such data exhibits values other than zero for negative values of time t in distinction to completely mechanical or electrical systems for which it is known that $K(t) = 0$ for $t < 0$. It is intuitively clear from physical concepts that the ship (or model) will respond to a wave before the crest (say) reaches the bow because of the spatial distribution of both the ship and the pressure field of the wave. It will be shown in the following section how the extent of the part of $K(t)$ for negative t can be reduced by judicious positioning of the wave measurement with respect to the model. In any event, it will be necessary to have some "future" information of the wave in order to compute the present time motion for all cases in which the vessel is of length comparable to the exciting waves.

For those interested in applying this technique, it is appropriate to indicate in some detail how the impulsive response function for any mode of motion may be obtained from data obtained from a model in (a) regular waves and (b) irregular waves.

$K(t)$ from Regular Wave Tests

If one regards the regular sea motion (in a towing tank experiment) as the input

$$\eta_o = |\eta_o| \sin \omega t$$

and one records the output of any mode of the model motion as

$$x(t) = |\eta_o| A(\omega) \sin [\omega t - \varphi(\omega)]$$

where $\varphi(\omega)$ is the phase angle referenced to the wave and $A(\omega)$ is the amplitude response of the model in a particular mode, then the transfer function or complex response function per unit amplitude of input is identified as

$$\Phi(\omega) = A(\omega)\, e^{-i\varphi(\omega)}. \tag{41}$$

Upon completion of a plot of $A(\omega)$ and $\varphi(\omega)$ for enough discrete values of ω so that smooth curves may be drawn to define both $A(\omega)$ and $\varphi(\omega)$, one may then find the impulsive response function by applying the operation

$$K(t) = \frac{1}{2\pi}\int_{-\infty}^{\infty} \Phi(\omega)\, e^{i\omega t}\, d\omega = \frac{1}{2\pi}\int_{-\infty}^{\infty} A(\omega)\, e^{i[\omega t - \varphi(\omega)]}\, d\omega$$

$$= \frac{1}{2\pi}\int_{-\infty}^{\infty} A(\omega)\cos\left[\omega t - \varphi(\omega)\right] d\omega + \frac{1}{2\pi}\int_{-\infty}^{\infty} A(\omega)\sin\left[\omega t - \varphi(\omega)\right] d\omega .$$

Since $K(t)$ must be a real function, the last integral must vanish identically for all values of t. This requires that $\varphi(\omega)$ be an odd function of ω (and if it is not then something is in error in its determination!). Since $A(\omega)$ must be an even function of ω, then calculate $K(t)$ from

$$K(t) = \frac{1}{\pi}\int_{0}^{\infty} A(\omega)\cos\left[\omega t - \varphi(\omega)\right] d\omega . \tag{42}$$

It must be realized that by referencing the force and moment functions to the wave, an arbitrary phase angle is introduced or simply that the phase of the frequency response function is tied to the location of the wave measurement relative to the body. To clarify this, suppose that the heave and pitch of a surface model is recorded at the center of mass and the wave is measured abreast of the center of mass. Then the derived impulsive response function will exhibit features peculiar to this reference point. It will, for example, have values different from zero for negative time which then requires that the wave motion forward of amidships be known or, in effect, "future waves" are required in order to compute the response at the present time. If it is desired to reduce the extent of the negative time for which the empirically derived impulsive response function has nonzero values by, say, referring the motion to waves measured forward of the bow, it is necessary to shift the phase of the transfer function by the angle $i(\omega|\omega|x/g)$ where x is the amount of the horizontal shift (taking care to regard x as positive or negative) so that the modified transfer function becomes

$$\Phi(\omega, x) = A(\omega)\, e^{-i\left[\varphi(\omega) + \frac{\omega|\omega|x}{g}\right]} \tag{43}$$

and the modified impulsive response function is

$$K(t, x) = \frac{1}{\pi}\int_{0}^{\infty} A(\omega)\cos\left(\omega t - \varphi(\omega) - \frac{\omega|\omega|x}{g}\right) d\omega . \tag{44}$$

In addition, it will be necessary to convolute this shifted function $K(x, t)$ with the wave record at the new point so that the η and the K are consistently referenced to the same point of measurement. If only the wave record abeam of the center of mass is available, this can also be shifted to the same point as is discussed in a later section.

$K(t)$ from Irregular Wave Tests

One method of obtaining the impulsive response function from motion records is to first calculate the frequency response function from the relation

$$\hat{\eta}\,\Phi(\omega) = \hat{z}(\omega)$$

or

$$\Phi(\omega) = \frac{\int_{-\infty}^{\infty} z(t)\, e^{-i\omega t}\, dt}{\int_{-\infty}^{\infty} \eta(t)\, e^{-i\omega t}\, dt} \tag{45}$$

and then to proceed to $K(t)$ as indicated above.

Another procedure is to use spectral analysis techniques which have been applied to the statistical analysis of ship motions. The spectrum of the model motion is given by the calculation

$$|X(\omega_e)|^2 = \frac{1}{2\pi}\int_{-\infty}^{\infty}\left[\lim_{T\to\infty}\frac{1}{T}\int_{-T/2}^{T/2} X(t)\, X(t-\tau)\, dt\right] e^{-i\omega_e\tau}\, d\tau \tag{46}$$

and the wave height spectrum is similarly provided by

$$E = |\eta(\omega_e)|^2 = \frac{1}{2\pi}\int_{-\infty}^{\infty}\left[\lim_{T\to\infty}\frac{1}{T}\int_{-T/2}^{T/2} \eta(t)\, \eta(t-\tau)\, dt\right] e^{-i\omega_e\tau}\, d\tau\,. \tag{47}$$

The amplitude of the frequency response function is related to the motion and wave spectra by

$$|\Phi(\omega)|^2 = \frac{|X(\omega_e)|^2}{E} \tag{48}$$

and the phase φ is calculated from

$$\varphi(\omega_e) = \tan^{-1}\left[\frac{\operatorname{Im}\psi(\omega_e)}{\operatorname{Re}\psi(\omega_e)}\right] \tag{49}$$

where ψ is the cross-spectrum defined by

$$\psi(\omega_e) = \frac{1}{2\pi}\int_{-\infty}^{\infty}\left[\lim_{T\to\infty}\frac{1}{T}\int_{-T/2}^{T/2} \eta(t)\, X(t-\tau)\, dt\right] e^{-i\omega_e\tau}\, d\tau\,. \tag{50}$$

The Effect of Shift of Wave Measurement on Reference Points

Suppose that a wave system is moving from left to right in the direction of positive x or ξ and one has by measurement a knowledge of the waves as a function of time at $x = \xi_0$ and $z = 0$ and asks what the fluid motion is at some point $x = \xi$ and $z = -\zeta$ "downwind" so $\xi > \xi_0$. The answer can be secured by regarding the fluid as one following the linear system concept that at any discrete frequency:

output = input $\times$ unit frequency response function

and thence to deduce an impulsive response function which is then convoluted with the known wave record.

However, a much more direct approach is to utilize the foregoing formulas for heave response by regarding the body to be shrunk to a point and thus indistinguishable from a fluid element. The heave frequency response function of the ship-sea system contracts to

$$\Phi_z = e^{\frac{i\omega|\omega|(\xi-\xi_0)}{g} - \frac{\omega^2\zeta}{g}} \tag{51}$$

and the vertical fluid motion at ξ, ζ in terms of the surface motion $\eta(t;\xi_0,0)$ is

$$z_w(t;\xi,\zeta) = \int_{-\infty}^{\infty} \eta(\tau;\xi_0,0)\,K_w(t-\tau;\xi-\xi_0,\zeta)\,d\tau \tag{52}$$

where the wave-induced impulsive response function is given by

$$K_w(u;\xi-\xi_0,\zeta) = \frac{1}{2\pi}\int_{-\infty}^{\infty} e^{\frac{i\omega|\omega|(\xi-\xi_0)}{g} - \frac{\omega^2\zeta}{g}}\, e^{i\omega u}\,d\omega . \tag{53}$$

This integral can be expressed (as shown in Appendix A) by

$$K_w = \frac{1}{2\sqrt{\pi}} R_e \left\{\sqrt{\frac{g}{Z}} \exp\left(\frac{gu^2}{4Z}\right) \mathrm{Erfc}\left(\pm\frac{iu}{2}\sqrt{\frac{g}{Z}}\right)\right\} \tag{54}$$

where

R_e indicates that only the real part is to be retained,

$Z = \zeta - i(\xi - \xi_0)$,

Erfc is the complementary error function (which is tabulated for complex arguments).

(The plus sign is applied for positive time u and the minus for negative u.)

Some reflection on the parametric dependence of K_w on ζ and ξ imbedded in (54) will reveal that the action of the fluid between the two points is to filter the wave-induced motion as an inverse function of the complex "distance" z which means that the filtering effect depends on $(\xi^2 + \zeta^2)^{1/2}$ and the "aspect" of the point defined by the angle $\tan^{-1}(\xi/\zeta)$.

Evaluation for $\zeta = 0$ yields the same result as given by Davis and Zarnick [14], viz.,

$$K_w(t; \xi - \xi_o, 0) = \alpha \left\{ \cos\left(\frac{\pi}{2}(\alpha t)^2\right)\left[\frac{1}{2} + C(\alpha t)\right] + \sin\left(\frac{\pi}{2}(\alpha t)^2\right)\left[\frac{1}{2} + S(\alpha t)\right]\right\} \tag{55}$$

where

$$\alpha = \sqrt{\frac{g}{2\pi(\xi - \xi_o)}} ; \qquad C(\alpha t) = \int_0^{\alpha t} \cos\left(\frac{\pi}{2}\mu^2\right) d\mu ; \qquad S(\alpha t) = \int_0^{\alpha t} \sin\frac{\pi}{2}\mu^2 \, d\mu .$$

The functions C and S are Fresnel integrals which are tabulated.

Curves of K_w/α for $\zeta = 0$ and $\zeta = 50$ feet are shown in Fig. 1. It is seen that the amount of future time wave record needed at $\xi_o, 0$ to compute the present time disturbance at ξ, ζ increases as one moves downward into the fluid. As ξ is made large with respect to ξ_o, less and less future time record is required as would be expected. For $\zeta = 0$ and large α or $\xi \to \xi_o$

$$K_w(u; \xi - \xi_o, 0) \to \frac{1}{\sqrt{2}} \alpha \cos\left(\frac{\pi}{4} - \frac{\pi}{2}(\alpha u)^2\right)$$

which, being even in t, shows that both future and past information are equally weighted at ξ.

The function K_w as given by (54) collapses to the known, very simple, result when one moves the point ξ, ζ under the point $\xi_o, 0$. Then the argument of the complementary error function becomes a pure imaginary and its value is then unity leaving

$$K_w(u; 0, \zeta) = \frac{1}{\sqrt{2}}\sqrt{\frac{g}{2\pi\zeta}}\, e^{-\frac{gu^2}{4\zeta}} = \frac{\beta}{\sqrt{2}} e^{-\pi(\beta u)^2} . \tag{56}$$

A universal curve of K_w/β is plotted against βu (or βt) in Fig. 2. It is seen that this function is symmetric, indicating that the motion at depth requires equal knowledge of future and past waves.

These results allow one to handle the following problem. Suppose one has a system $K(t)$ for a particular mode of motion which has been derived from data in which the wave information was secured at $\xi, 0$ and then one wishes to calculate the motions of a ship using wave records secured or assumed at some point ξ_1. One may then do either of two operations:

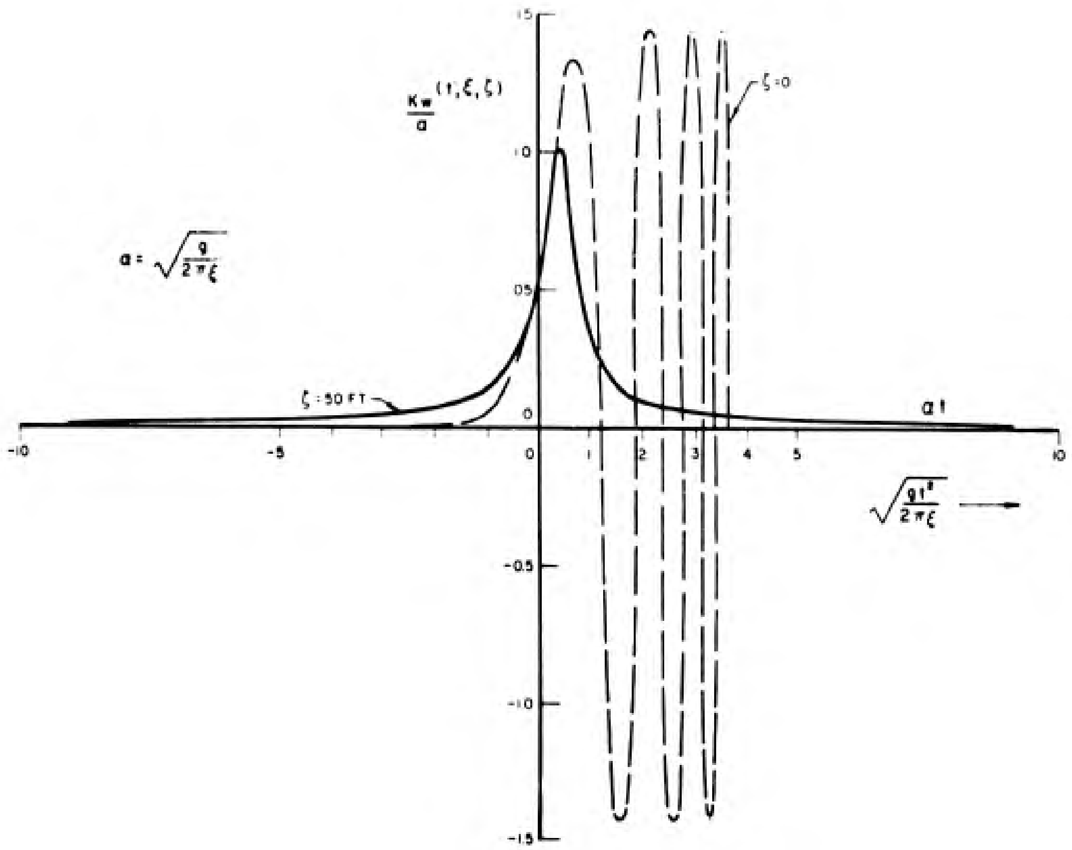

Fig. 1 - The impulsive response function for wave-induced fluid motion as a function of horizontal separation ξ and for vertical distances ζ = 0, 50 ft

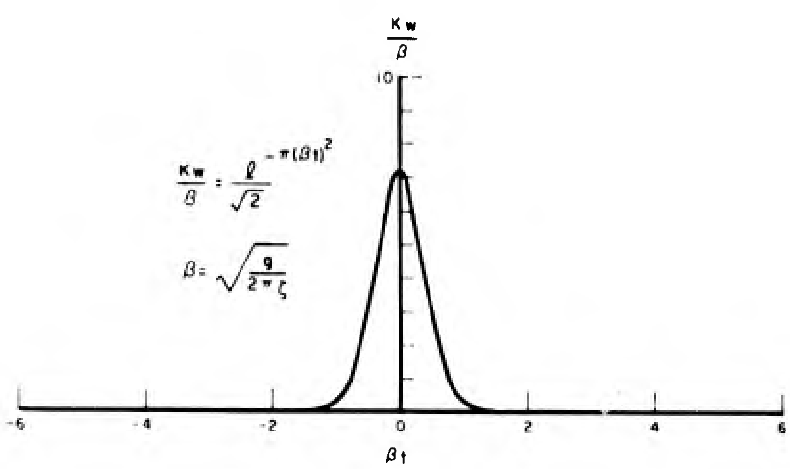

Fig. 2 - Heave impulsive response function for destroyer in head seas

(a) "Shift" the wave input from ξ_1 to ξ_0 so that it may then be convoluted with the $K(t)$ determined for waves measured at ξ_0; or

(b) "Shift" the $K(t)$ from ξ_0 to ξ_1.

Step (a) is accomplished by convoluting the given wave record with K_w given by (55) and then convolve that result with the system $K(t)$ to obtain the response. Step (b) is accomplished by modifying the transfer function from which $K(t)$ is computed by the factor

$$e^{\pm \frac{i\omega|\omega|}{g}|\xi_0 - \xi_1|}$$

(taking care to apply the correct sign to the exponent!) and thence to compute a new $K(t)$ which can be convoluted with the given wave record.

APPLICATIONS OF IMPULSIVE RESPONSE TECHNIQUE TO PREDICT SHIP MOTIONS IN IRREGULAR SEAS

The previous sections of this paper have discussed the significance of the impulsive response function and have described its application in determining the time history of ship motions in irregular seas. During the past several years, the Davidson Laboratory has employed this technique to evaluate the motions of a variety of marine craft operating in random seas. The results of these applications will be summarized and discussed.

Displacement Ship in Head Seas

In 1961, Fancev [13] used the impulsive response technique to determine the time history of heave and pitch motion of a destroyer model in irregular long-crested head seas. The model used in the experiments was the DD692 Class Destroyer (long hull). The full-scale ship is 392 ft long, has a beam of 40.83 ft and has a displacement of 3471 long tons in salt water. The model was tested in moderately high, irregular, long-crested head waves that had a broad energy spectrum. The average height of the waves was about 1/60 of the model length. Measurements were made of the wave elevation (at a constant distance forward of the model LCG), pitch angle, heave at the LCG and bending moment amidship. Dalzell [3] reported the results of these tests and, by the method of cross-spectral analysis, derived the transfer function of the destroyer for a wide range of speeds. It will be recalled from Eq. (21) that the transfer function $\Phi(\omega)$ is written:

$$\Phi(\omega) = A(\omega)\, e^{-i\phi(\omega)} = P(\omega) + iQ(\omega)$$

where

$$\begin{aligned} P(\omega) &= A(\omega)\cos[\phi(\omega)] \\ Q(\omega) &= -A(\omega)\sin[\phi(\omega)] \end{aligned} \qquad (57)$$

and where $A(\omega)$ is the amplitude function relating the wave amplitude to amplitude of ship motion for regular waves of a given frequency ω. $\phi(\omega)$ is the phase angle between the crest of a regular surface wave and the peak of the corresponding sinusoidal motion of the ship. Dalzell found that the transfer functions obtained in the cross-spectral analysis agreed very well with those obtained from tests of the DD692 in regular waves over a range of speed-length ratios from 0 to 1.25. The experimental values of the transfer function ($A(\omega)$ and $\phi(\omega)$) for pitch and heave are summarized in Figs. 1 and 2 of Dalzell's paper.

Fancev used the transfer function obtained by Dalzell to develop the impulsive response function $K(t)$ relating the motion of the destroyer at the LCG to the instantaneous wave profile recorded by the wave wire located ahead of the test model. As developed in a preceding section of this paper (Eq. (42), expanded):

$$K(t) = \frac{1}{\pi}\int_0^{\infty} \left[P(\omega)\cos\omega t - Q(\omega)\sin\omega t\right] d\omega .$$

Fancev performed this integration by a graphic numerical method and his results are plotted in Figs. 3 and 4 of this paper showing the heave and pitch impulsive response functions of the destroyer at a Froude number of 0.187. It is

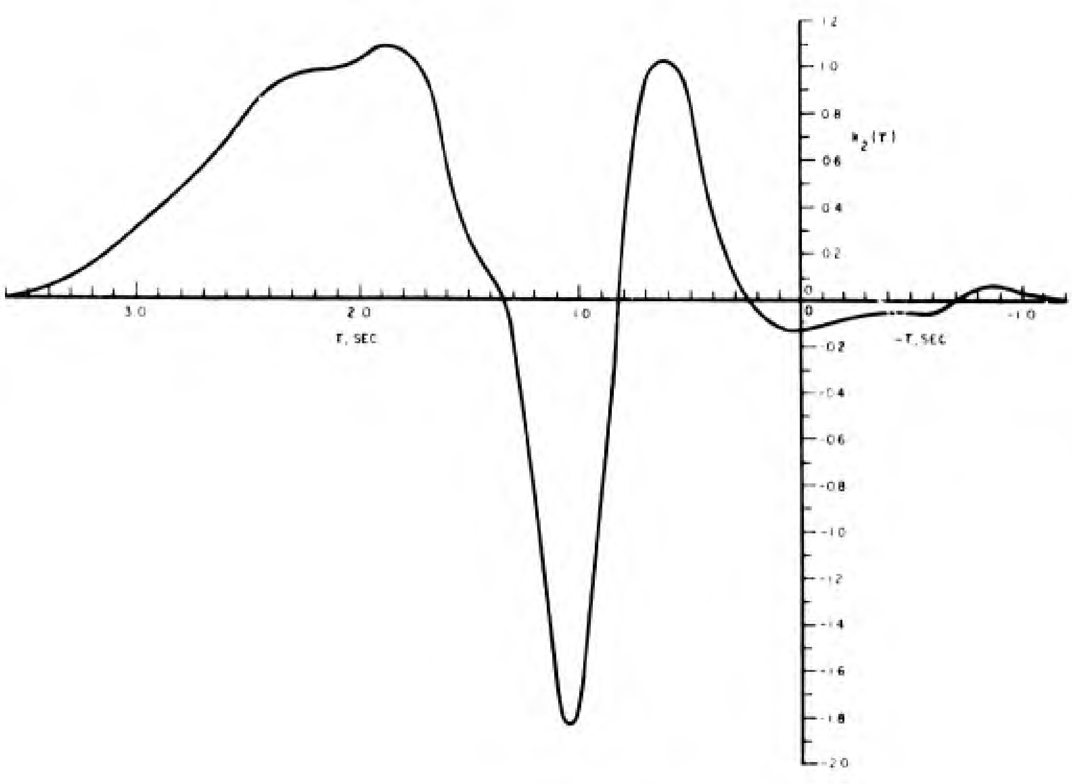

Fig. 3 - Pitch impulsive response function for destroyer in head seas

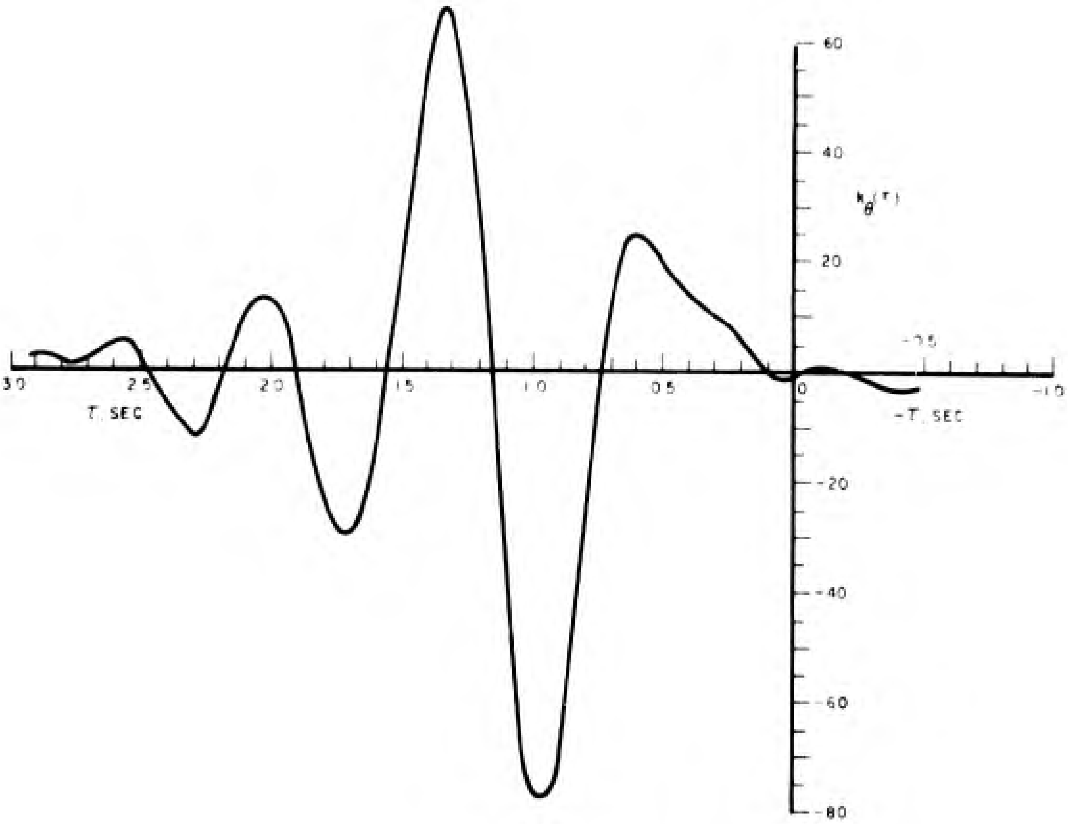

Fig. 4 - Pitch and heave motions for destroyer in head seas predicted by impulsive response technique

seen that the response functions are physically realizable, i.e., $K(t) = 0$ for $t < 0$. If the surface wave probe were located at the LCG of the model, Fancev shows that the resultant response function would have values for $t < 0$ and hence be classified as physically nonrealizable. The physical explanation for this is that when the ship is long, relative to the wave length, the ship responds to the wave crest even before it reaches the bow and before this wave is recorded by a wave probe located at the LCG; hence, in this case, the ship motion would always precede the arrival of the wave crest at the LCG.

The heave and pitch time histories were computed on an IBM 1620 by evaluating the convolution integrals [Eq. (36)],

$$X(t) = \int_{-\infty}^{\infty} K_z(\tau)\, \eta(t-\tau)\, d\tau$$

$$\theta(t) = \int_{-\infty}^{\infty} K_\theta(\tau)\, \eta(t-\tau)\, d\tau$$

where $\eta(t)$ is the time history of surface wave profile measured by the wave probe forward of the model. Figure 5 shows the results of the prediction of heave and pitch response to irregular seas. The continuous lines are tracings of the oscillograph records of heave motion and pitch motion obtained from the tests in Ref. 3. The circled points represent the results of convolving the impulsive responses of Figs. 3 and 4 with the surface wave time history. On the whole agreement between observed and predicted responses is considered excellent, hence validating the accuracy of the impulsive response technique in obtaining deterministic solutions.

Submerged Bodies in Beam Seas

The Davidson Laboratory has conducted an extensive series of model tests to determine the motions of a submerged, asymmetrically finned body at zero velocity when acted upon by regular and irregular long-crested waves approaching the body from various directions. In these tests, the motions of the submerged body were recorded in terms of the surface wave profile directly above the body. Response operators for heave, roll, and pitch motion in beam seas and head seas have been developed from these data by Savitsky and Lueders [5]. The response operators obtained from irregular wave tests were found to be in agreement with those obtained from tests in regular waves. The general conclusion of this study was that, in regular beam seas, the heave and sway motions are those of a water particle at the center of gravity of the body. Also, in beam seas, the hydrodynamic roll moment is proportional to the wave slope at depth, (or equivalently to the inertia forces which vary as ω^2) and the roll motions are determined by using this wave slope, the natural roll frequency and damping of the body, and the usual dynamical equations of motion of a linear, single degree of freedom oscillator.

Dalzell used the results of Ref. 5 to determine the impulsive response function of the submerged body and to calculate the time history of heave and roll motions in irregular beam seas. Dalzell's results are rederived below following the theoretical procedures described in the previous section of this paper. It will be recalled that, in the present theoretical development, the kernel function of the wave system (due to shift of wave reference points) was separately developed and then combined with the kernel function of the mechanical system to derive a so-called "system" impulsive response function.

Since the test body was submerged, the wave characteristics at depth of submergence (ζ), will be used as the input to the system. (It has been shown in the theoretical section that it is equivalent to referencing the output to the wave on the surface.) The relation between the measured regular surface wave profile and the orbital motions at depth exhibits a zero phase shift and an attenuation in amplitude of orbital motion given by the relation $e^{-\omega^2\zeta/g}$. The kernel function relating surface wave profile to wave profile at depth is given in Eq. (56) which is reproduced below:

$$K_w(t;0,\zeta) = \frac{1}{2}\sqrt{\frac{g}{\pi\zeta}}\, e^{-\frac{gt^2}{4\zeta}}. \tag{58}$$

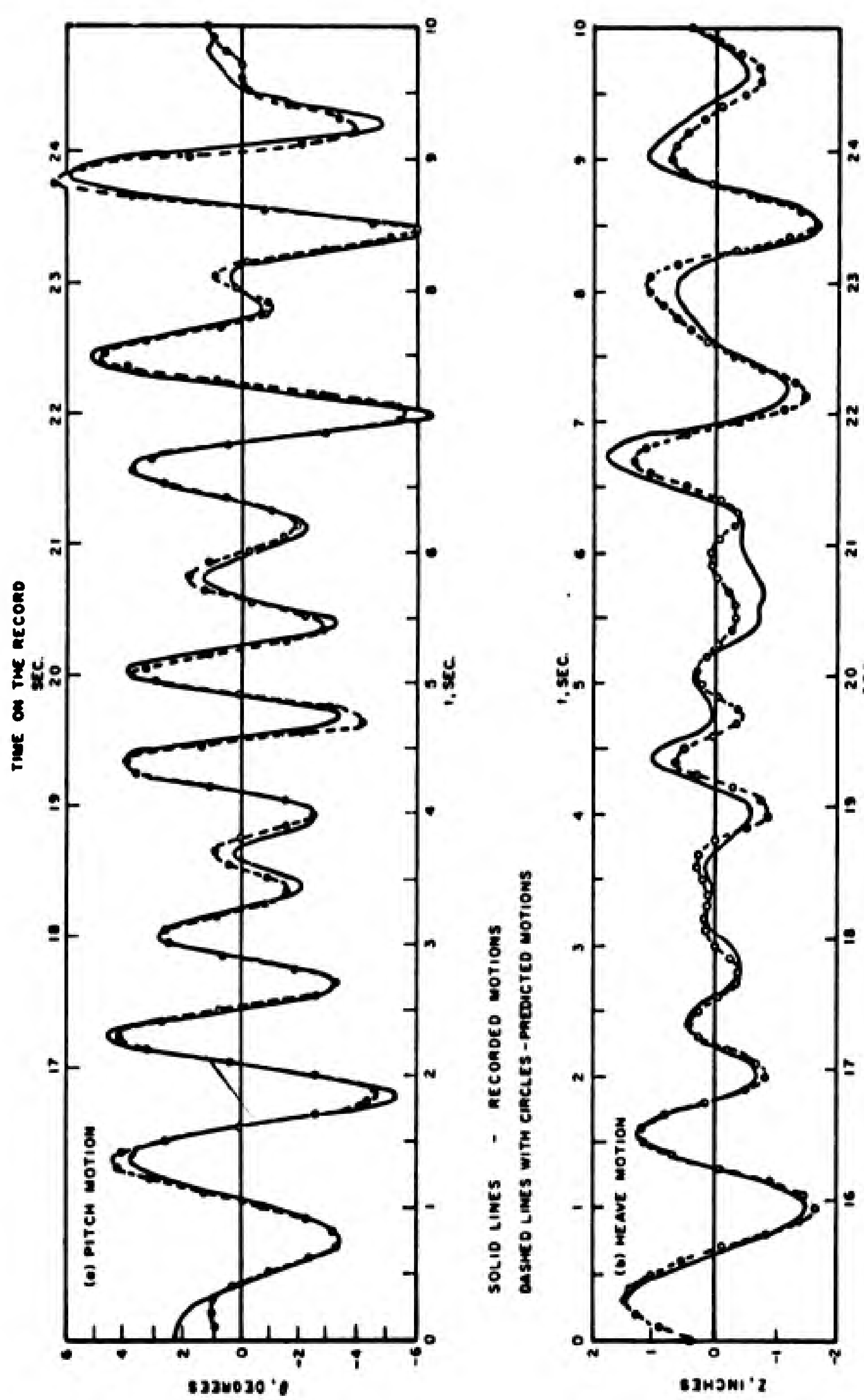

Fig. 5 - Impulsive response function for wave-induced fluid motion as a function of depth ζ at $\xi = 0$

This function (plotted in Fig. 2) is seen to be a symmetrical function of time and hence requires some future time knowledge of surface wave profile in order to predict the wave profile at depth. Using the above kernel in a convolution integral will provide a time history of the orbital motions at depth $\eta(t)$ in terms of the time history of the irregular surface wave profile, $\eta_o(t)$ immediately above the test point.

$$\eta(t) = \int_{-\infty}^{\infty} \eta_o(\tau) \frac{1}{2} \sqrt{\frac{g}{\pi \zeta}}\, e^{-\frac{g(t-\tau)^2}{4\zeta}}\, d\tau . \tag{59}$$

Predicted Heave Time Histories

Considering the heave motion of the neutrally buoyant submerged body, it was shown in Ref. 5 that the body behaves in heave and sway like a water particle at depth, i.e., it has identical amplitude $A(\omega) = 1$ and zero phase $\varphi(\omega) = 0$, relative to a submerged wave particle. The heave transfer function of the submerged body (relative to water motion at depth) is then

$$\Phi(\omega) = A(\omega)\, e^{-i\varphi(\omega)} = (1)\, e^{-0} = 1 . \tag{60}$$

The impulsive response function of this mechanical system is then written

$$K(t)_M = \frac{1}{2\pi} \int_{-\infty}^{\infty} \Phi(\omega)\, e^{i\omega t}\, d\omega = \frac{1}{2\pi} \int_{-\infty}^{\infty} e^{i\omega t}\, d\omega = \delta(t) \tag{61}$$

where δ is the Dirac delta function. Operating with the delta function on a bounded and continuous function $f(t)$, it can be shown that

$$\int_{-\infty}^{\infty} f(t)\, \delta(t-t_o)\, dt = f(t_o) . \tag{62}$$

Thus, convolving the body heave impulsive response function [Eq. (61)] with the wave motion at depth, Eq. (59), gives the time history of heave motion $z(t)$ of the submerged body in terms of the surface wave profile (η_o) to be

$$z(t) = \int_{-\infty}^{\infty} \int_{-\infty}^{\infty} \eta_o(\tau') \frac{1}{2} \sqrt{\frac{g}{\pi \zeta}}\, e^{-\frac{g(\tau-\tau')^2}{4\zeta}}\, d\tau'\, \delta(t-\tau)\, d\tau$$

so that

$$z(t) = \int_{-\infty}^{\infty} \eta_o(\tau') \frac{1}{2} \sqrt{\frac{g}{\pi \zeta}}\, e^{-\frac{g(t-\tau')^2}{4\zeta}}\, d\tau' . \tag{63}$$

The above integral was evaluated by Dalzell and resulted in a computed heave time history of submerged body. The analytical results are compared

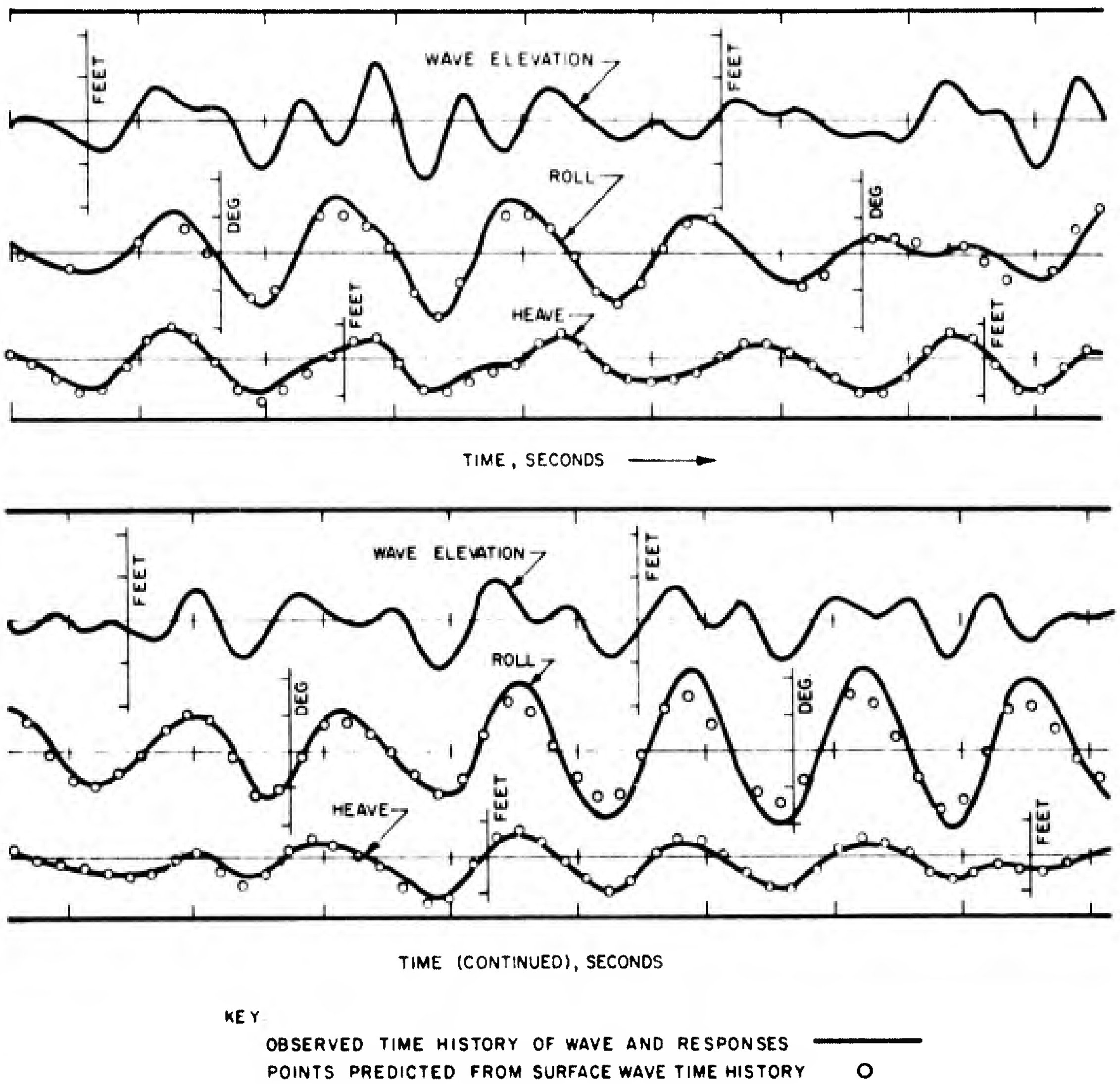

Fig. 6 - Deterministic prediction of roll and heave response for submerged body in irregular beam seas

with experimental values in Fig. 6. It is seen that there is excellent agreement between computed and measured values of heave. Also included in Fig. 6 is the time history of the irregular surface wave profile.

Predicted Roll Time Histories

As shown in Ref. 5, the roll motions of a submerged body in regular beam seas are derivable from the equations of motion of a damped, linear, single degree of freedom oscillating system and are expressed by the following equation:

$$\Theta = \frac{\omega^2}{g}\,\eta_o\, e^{-\frac{\omega^2 h}{g}} \left\{ \frac{1}{\left\{\left[1 - \left[\frac{\omega}{\omega_n}\right]^2\right]^2 + \left[2\zeta'\left[\frac{\omega}{\omega_n}\right]\right]^2\right\}^{1/2}} \right\} \tag{64}$$

where

Θ = maximum roll amplitude,

ω_n = natural roll frequency of submerged body,

ω = wave frequency,

η_o = surface wave amplitude,

h = depth to center of vertical fin on submerged body, and

ζ' = damping ratio in roll.

Since the wave orbital motion at depth h has an amplitude equal to

$$\eta_o\, e^{-\frac{\omega^2 h}{g}},$$

then the response amplitude, $A(\omega)_h$, defined as the ratio of maximum roll amplitude to wave amplitude at depth is equal to:

$$A(\omega)_h = \frac{\omega^2}{g} \left\{ \frac{1}{\left\{\left[1 - \left(\frac{\omega}{\omega_n}\right)^2\right]^2 + \left[2\zeta'\frac{\omega}{\omega_n}\right]^2\right\}^{1/2}} \right\}. \tag{65}$$

The phase angle, φ, between passage of the wave crest over the submerged body and maximum roll amplitude of the submerged body can be derived from Ref. 5 to be:

$$\varphi(\omega) = \arctan\left[\frac{2\zeta'\frac{\omega}{\omega_n}}{1 - \left(\frac{\omega}{\omega_n}\right)^2}\right] - \frac{\pi}{2}. \tag{66}$$

The transfer function for the submerged body in roll is thus known (Fig. 7).

$$\Phi(\omega)_h = A(\omega)_h\, e^{i\varphi(\omega)} = P(\omega) + iQ(\omega)$$

where $A(\omega)$ and $\varphi(\omega)$ are given by Eqs. (65) and (66) above.

Evaluating the real and imaginary parts of the transfer function results in the following:

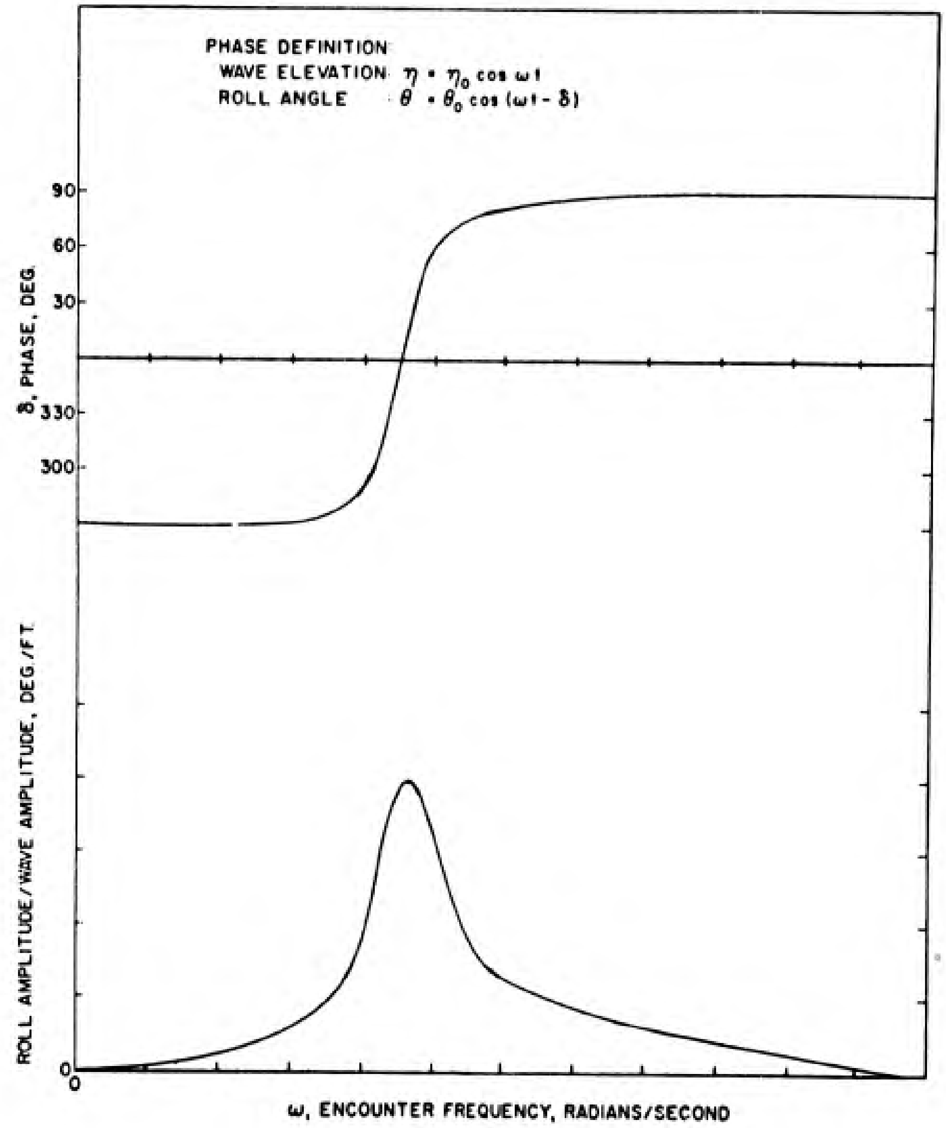

Fig. 7 - Roll transfer function for submerged body in beam seas

$$P(\omega) = A(\omega)_n \cos [\varphi(\omega)]$$

$$= \frac{\omega^2}{g} \left\{ \frac{1}{\left[1 - \left(\frac{\omega}{\omega_n}\right)^2\right]^2 + \left[2\zeta' \frac{\omega}{\omega_n}\right]^2} \right\} \cos \left\{ \tan^{-1} \left[\frac{2\zeta' \frac{\omega}{\omega_n}}{1 - \left(\frac{\omega}{\omega_n}\right)^2} \right] - \frac{\pi}{2} \right\} \quad (67)$$

and

$$Q(\omega) = -A(\omega)_n \sin[\epsilon(\omega)]$$

$$= -\frac{\omega^2}{g}\left\{\frac{1}{\left[1-\left(\frac{\omega}{\omega_n}\right)^2\right]^2 + \left[2\zeta\frac{\omega}{\omega_n}\right]^2}\right\} \sin\left\{\tan^{-1}\left[\frac{2\zeta\frac{\omega}{\omega_n}}{1-\left(\frac{\omega}{\omega_n}\right)^2}\right] - \frac{\pi}{2}\right\}. \tag{68}$$

Hence the impulsive response function for the submerged body in roll relative to the wave orbital motions at depth is evaluated by the following equation derived from the Fourier integral

$$K_\theta(t) = \frac{1}{\pi}\int_0^\infty [P(\omega)\cos\omega t + Q(\omega)\sin\omega t]\, d\omega \tag{69}$$

where $P(\omega)$ and $Q(\omega)$ are given by Eqs. (67) and (68). It is interesting to note that $K(t)$ given in Eq. (69) is independent of submergence. This is to be expected so long as the submerged body motions are related to wave orbital velocities at body depth.

Since the desired deterministic solution involves relating the time history of the surface wave profile to the time history of the roll motions of the submerged body, it is necessary to first know the wave motion at depth in terms of the wave motion at the surface. Equation (59) shows this relation to be:

$$\eta_h(t) = \int_{-\infty}^{\infty} \eta_o(\tau)\,\frac{1}{2}\sqrt{\frac{g}{\pi h}}\, e^{-\frac{g(t-\tau)^2}{4h}}\, d\tau$$

where

$\eta_o(t)$ = time history of surface wave profile,

$\eta_h(t)$ = time history of orbital motion at depth h, and

h = depth of submergence to center of vertical fin.

The time history of roll motion in terms of the surface wave profile can now be obtained by use of the convolution integral:

$$\theta(t) = \int_{-\infty}^{\infty} K_\theta(\tau')\,\eta_h(t-\tau')\, d\tau' \tag{70}$$

where $K_\theta(\tau')$ is given by Eq. (69) and $\eta_h(t)$ is given by Eq. (59) in terms of the surface wave elevation $\eta_o(t)$. The expression for $\theta(t)$ can be rewritten as:

$$\phi(t) = \int_{-T}^{T} K'_{\phi}(\tau)\, \eta_o(t-\tau)\, d\tau \tag{71}$$

where $K'_{\phi}(\tau)$ represents the so-called "system" impulsive response function which combines the vertical shift in wave axis system [Eq. (59)] with the transfer function of the submerged body in roll [Eq. (69)]. In effect, this system response function directly relates the surface wave profile, η_o, with the motion of the submerged body. This is the impulsive response function determined experimentally by Dalzell and reproduced in Fig. 8 of this report. The apparent period of oscillation in Fig. 8 was equal to the natural roll frequency of the submerged body which is as it should be. The logarithmic decrement of the oscillation of the roll impulsive response function was calculated and found to agree closely with the logarithmic decrement found from experimental roll decay curves. The reason for the existence of $K(t)$ for negative time (as shown in Fig. 8) is that in the subject experiment the only available input time history was that of the surface wave elevation directly over the body. Dalzell indicated that the use of either the wave slope at depth or the hydrodynamic rolling moment as inputs would have led to only phase lags in the system (rather than lead and lag angles as given in Eq. (66) and hence result in a so-called physically realizable impulsive response function where $K(t) = 0$ for $t < 0$.

Using the convolution integral in Eq. (71), the time history of roll motions was computed by Dalzell and the results are reproduced in Fig. 6 of this paper. As in the case of heave, it is seen that there is excellent agreement between computed and experimental time histories.

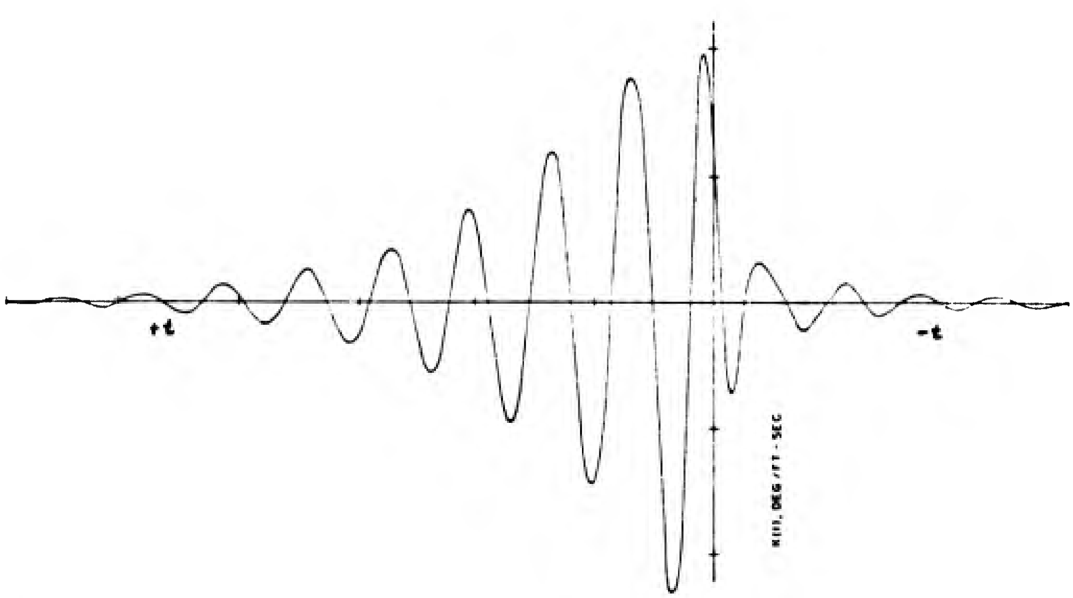

Fig. 8 - Roll impulsive response for submerged body (derived from transfer function in Fig. 7)

Surface Piercing Hydrofoil Craft in Head Seas

The impulsive response technique was also applied by Bernicker to compute the heave and pitch time histories of a fully wetted surface-piercing dihedral hydrofoil craft in irregular waves. The test model was a simulated hydrcfoil craft with twin surface-piercing dihedral foils placed symmetrically fore and aft of the center of gravity. The surface wave profile was measured by a probe located at 82 percent of the foil spacing ahead of the center of gravity. Pitch and heave motions were measured about the center of gravity.

The transfer functions for both heave and pitch were determined by Bernicker from cross-spectrum analysis of tests in irregular seas. The complex transfer function for heave and pitch, for a particular test speed, are reproduced in Figs. 9 and 10 respectively. The $P(\omega)$ and $Q(\omega)$ functions plotted thereon are used to calculate the impulsive response function [Eq. (42)]. Since both $P(\omega)$ and $Q(\omega)$ are given in graphical form, an IBM 1620 program was used to evaluate this integral numerically. The results of these integrations are given in Figs. 11 and 12 which plot the impulsive response function in heave and pitch, respectively. It will be noted from these plots that $K(t)$ does not vanish for negative values of time and hence some future time of the surface wave input is required to evaluate the convolution integral. Bernicker attributes the requirement of input for negative or future time to the particular longitudinal location of the surface wave probe used in these tests. Since the longitudinal position of the wave probe affects only the phase component of the transfer function of the hydrofoil craft, it is clear that the "system" impulsive response function is dependent upon the position of the wave probe and, hence, is not unique to the craft characteristics. As can be ascertained from Eq. (52) of this report, there is some optimum spacing between the wave probe and test model which will result in an impulsive response function that exists only for positive values of time. This optimum spacing was not determined in Bernicker's paper.

Figure 13 shows the results of evaluating the time history of hydrofoil heave and pitch motion using the impulsive response functions of Figs. 11 and 12 in the convolution integral together with the surface wave time history $\eta_o(t)$. The solid lines are the original time history as taken in experiment, and the discrete points are from the computer calculation. It is seen that the comparison, for the most part, is quite good.

Bending Moment Time Histories

In addition to computing motion time histories by the method of the impulsive response function, Dalzell also computed time histories of midship bending moments on a destroyer in irregular, long-crested head seas. The analytical procedure was identical to that previously discussed and the results are given in Fig. 14. Once again the agreement between computed and experimental results is excellent.

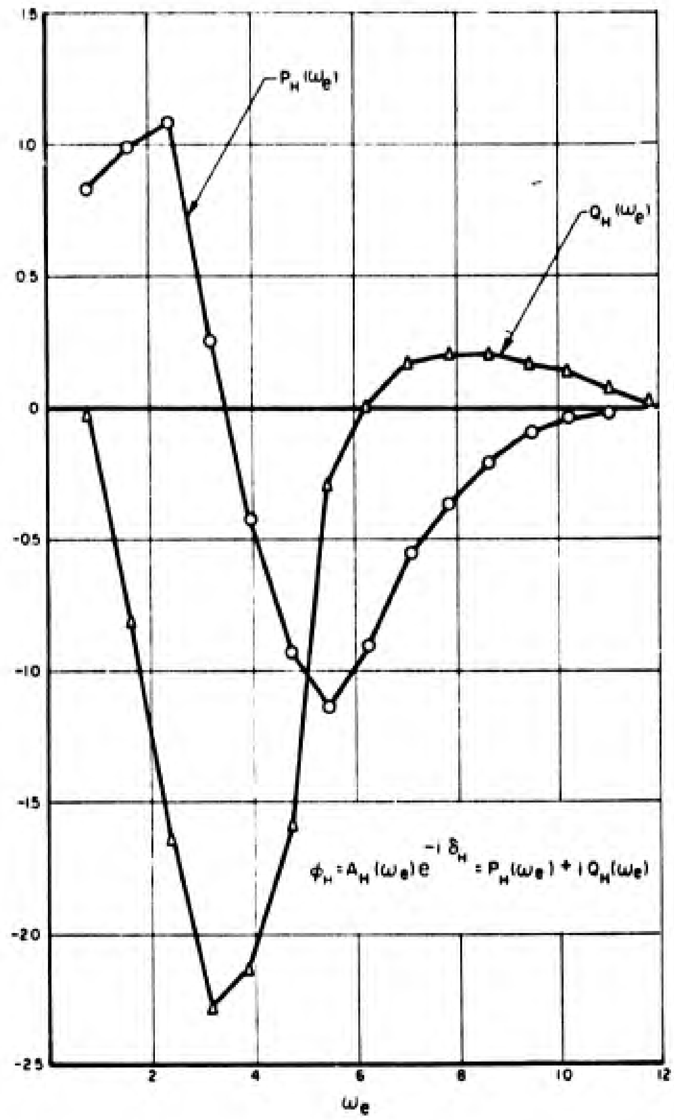

Fig. 9 - Complex transfer function for heave motion of hydrofoil craft in irregular head seas

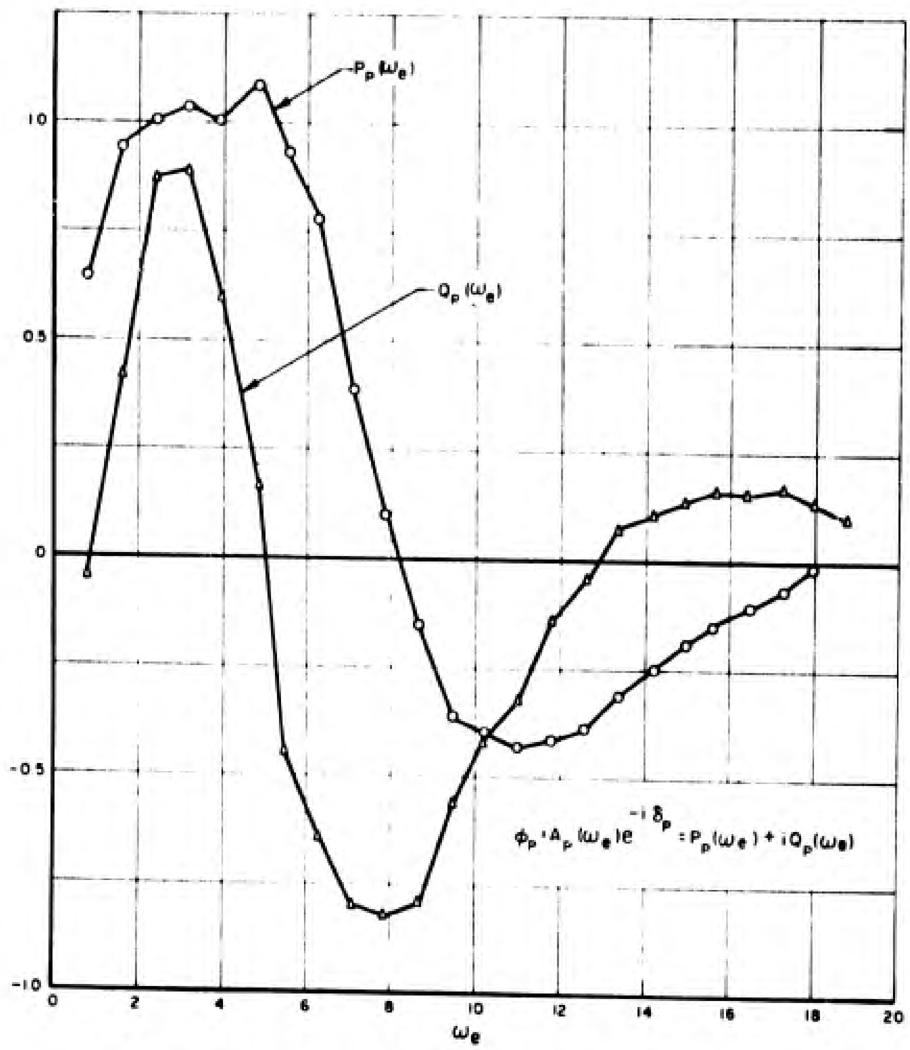

Fig. 10 - Complex transfer function for pitch motion of hydrofoil craft in irregular head seas

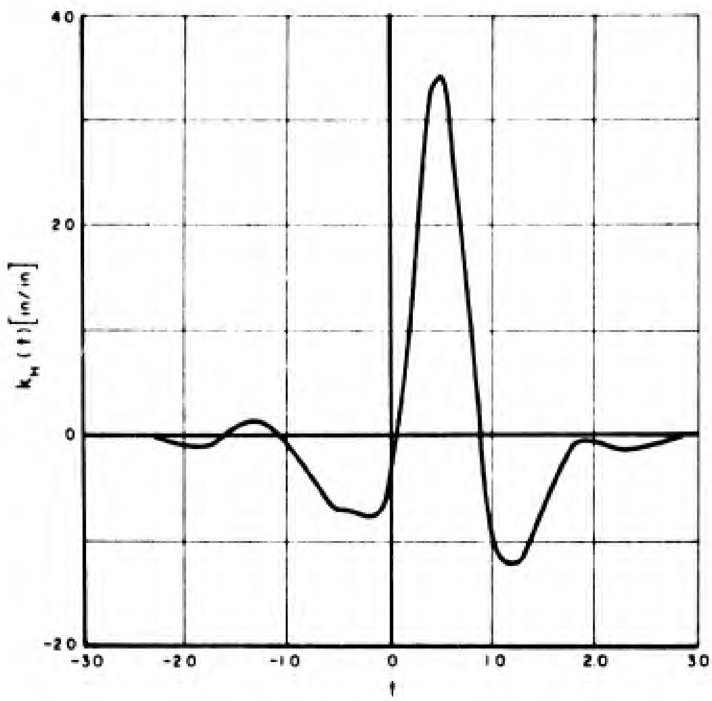

Fig. 11 - Impulsive response function for heave motion of hydrofoil craft in head seas

CONCLUSIONS

Time histories of the motions of marine vehicles in irregular seas can be reliably calculated by employing the technique of the impulsive response function.

The impulsive response functions of hydrodynamic systems depend on both wave input exciting forces, which are frequency dependent, and upon the calm water frequency characteristics of the marine craft. In addition, the wave surface profile is commonly used as a representation of the exciting forces and the length of the vehicle is usually large relative to discrete wave lengths. Consequently, the impulsive response properties of these hydrodynamic systems are distinct from the usual electrical or mechanical systems.

Theory provides a method for shifting either the system impulsive response function or the irregular wave record from one spatial reference point to another. This shifting can lead either to increasing or decreasing the amount of wave information required in future time.

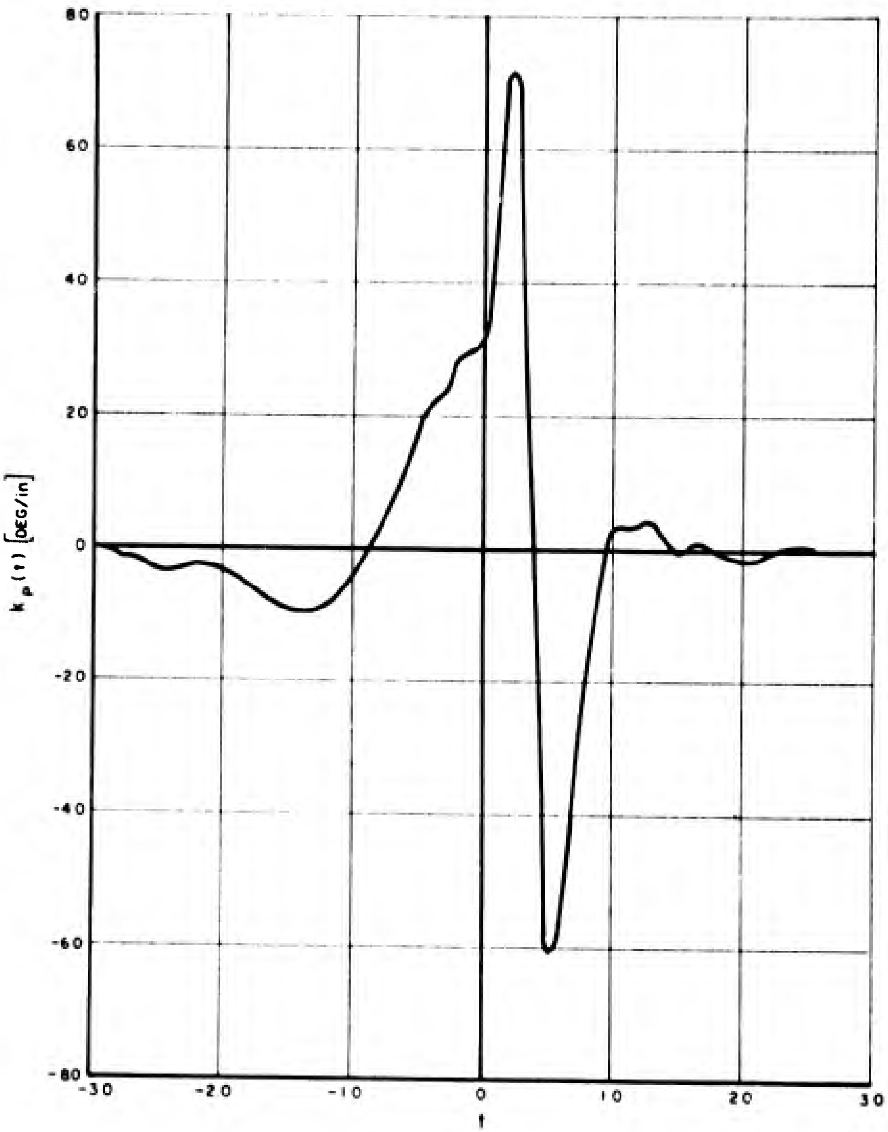

Fig. 12 - Impulse response function for pitch motion of hydrofoil craft in head seas

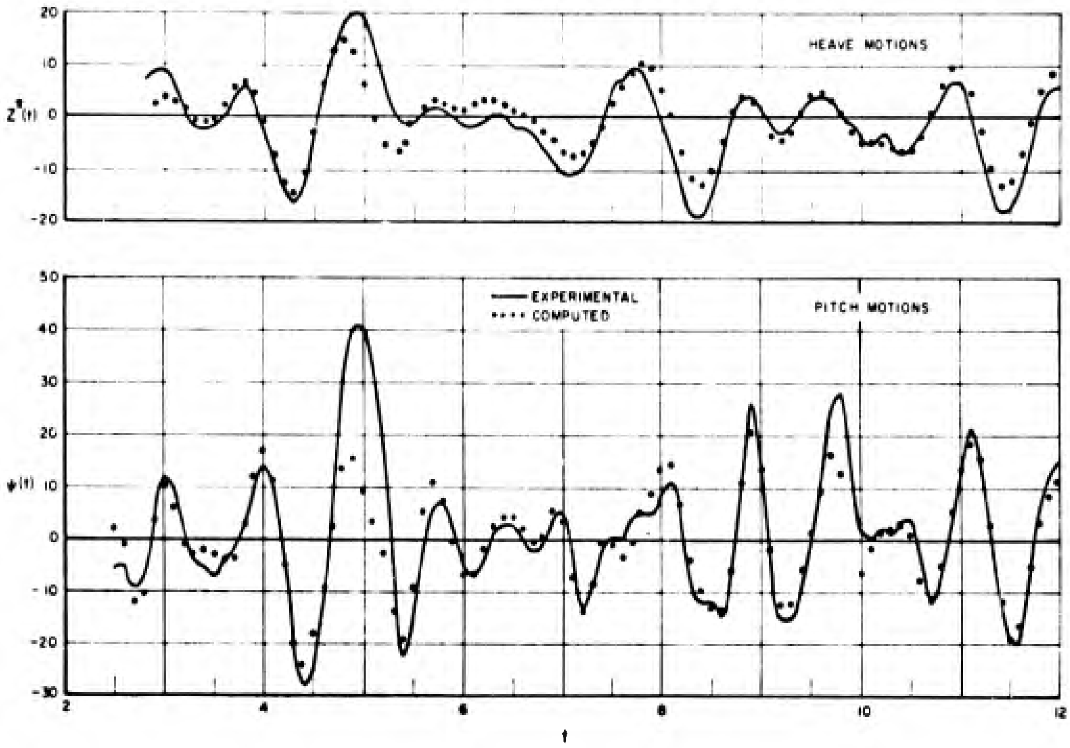

Fig. 13 - Deterministic solution of heave and pitch motions of hydrofoil craft in irregular head seas

The procedures provided in this paper have been shown to be successful in predicting the motions and bending moments of surface ship models, and the motions of hydrofoil craft and submerged bodies in irregular long-crested waves. Hence the technique is also expected to be directly applicable to other features attending the operation of marine craft in a seaway, i.e., deck wetting, bow slamming, acceleration, etc.

ACKNOWLEDGMENT

The authors would like to acknowledge the contributions made to the present subject by Mr. John F. Dalzell during his employment at the Davidson Laboratory, Stevens Institute of Technology. Miss W. Jacobs has contributed valuable assistance in resolving certain of the details of the mathematical analysis.

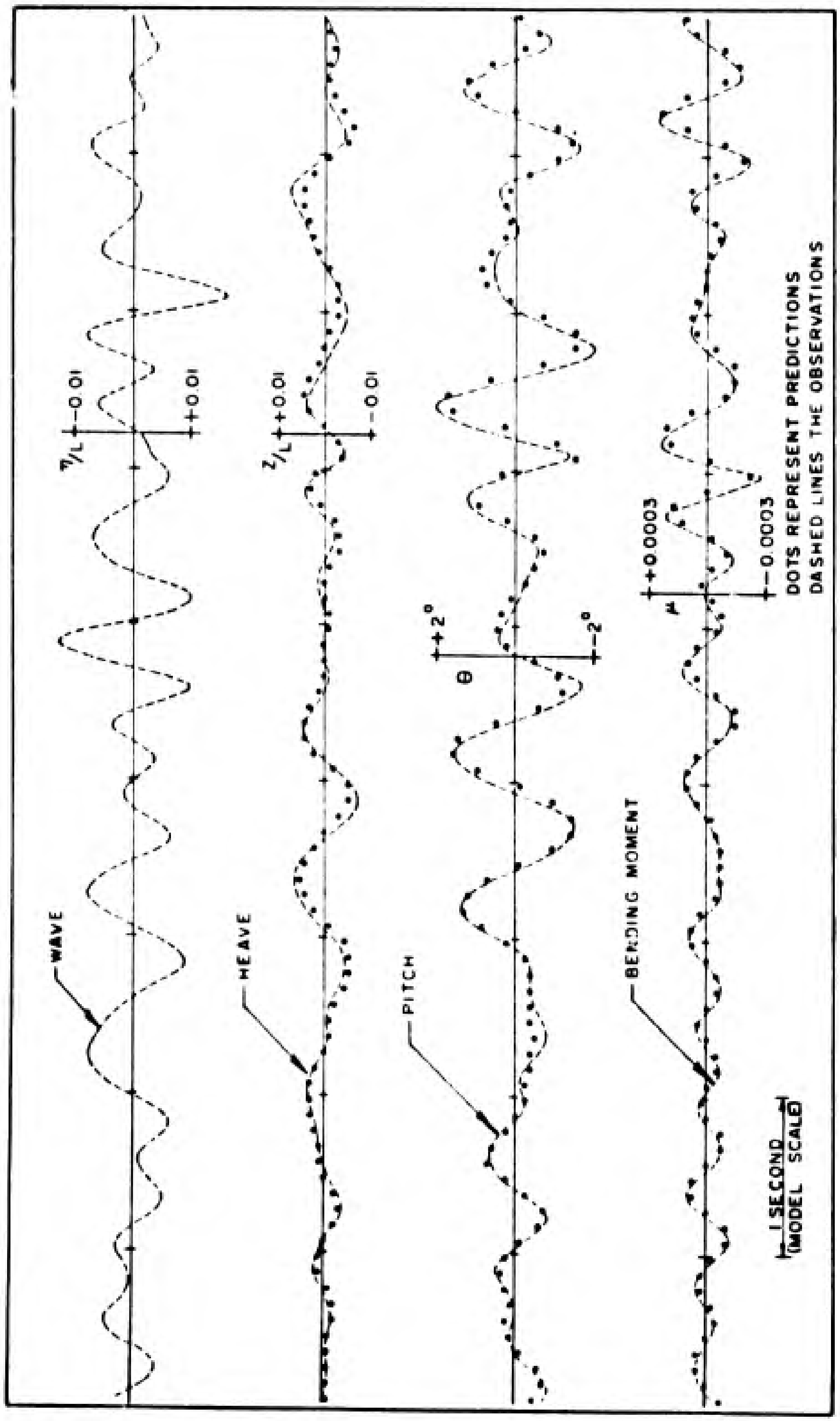

Fig. 14 - Deterministic predictions of pitch, heave and bending moment time histories for destroyer in irregular head seas

NOMENCLATURE

$A(\omega)$	modulus of transfer function
$\varphi(\omega)$	phase angle of transfer function
$\Phi(\omega)$	complex transfer function
$P(\omega)$	real part of complex transfer function
$Q(\omega)$	imaginary part of complex transfer function
t	real time
τ, τ'	dummy time variable
ω	circular frequency of wave, radius/sec
ω_n	natural frequency of physical system, radius/sec
ξ	distance in horizontal direction
ζ	distance in vertical direction
ζ'	damping ratio of oscillating system
η_o	surface wave amplitude
η	amplitude of wave orbital motion at depth
h	depth to center of vertical fin on submerged body
$\delta(\tau)$	Dirac delta function
Θ	amplitude of roll motion, radians
$z(t)$	time history of vertical motions
$\theta(t)$	time history of angular motions

REFERENCES

1. St. Denis, M. and Pierson, W. J., "On the Motions of Ships in Confused Seas," The Society of Naval Architects and Marine Engineers, Vol. 61, 1953.

2. Fuchs, R. A. and MacCamy, R. C., "A Linear Theory of Ship Motion in Irregular Waves," Institute of Engineering Research, Wave Research Laboratory T.R. Series 61, Issue 2, University of California, Berkley, California, July 1953.

3. Dalzell, John F., "Cross-Spectral Analysis of Ship-Model Motions: A Destroyer Model in Irregular Long-Crested Head Seas," Davidson Laboratory, Stevens Institute of Technology, Report 810, April 1962.

4. Dalzell, John F., "Some Further Experiments on the Application of Linear Superposition Techniques to Responses of a Destroyer Model in Extreme Irregular Head Seas," Davidson Laboratory, Stevens Institute of Technology, Report 918, September 1962.

5. Savitsky, Daniel and Lueders, Dennis, "Motion of Submerged Bodies in Regular and Irregular Waves," Schiffstecknik Bd. 9-1962-Heft 47.

6. Bernicker, Richard P., "Hydrofoil Motions in Irregular Seas," Davidson Laboratory, Stevens Institute of Technology, Report 909, November 1962.

7. Bernicker, Richard P., "Heaving and Pitching Motions of Superventilated Hydrofoil Craft in Irregular Seas," Davidson Laboratory, Stevens Institute of Technology, Report 958, June 1963.

8. Fuchs, R. A., "Prediction of Linear Effects from Instrument Records of Wave Motion," Institute of Engineering Research, Waves Research Laboratory T.R. Series 3, Issue 337, University of California, Berkley, California, June 1952.

9. Korvin-Kroukovsky, B. V., "Investigation of Ship Motions in Regular Waves," SNAME Vol. 63, 1955, pp. 386-435.

10. Grim, O., "Die Schwingungen von schwimmenden, zweidimensionalen Korpern," Hamburgische Schiffbau-Versuchsanstalt Gesellschaft Report No. 1171, September 1959.

11. Gerritsma, J. and Benkelman, W., "The Distribution of the Hydrodynamic Forces on a Heaving and Pitching Ship Model in Still Water," Publication No. 22, Shipbuilding Laboratory Technological University, Delft, Holland, June 1964.

12. Korvin-Kroukovsky, B. V. and Jacobs, W. R., "Pitching and Heaving Motions of a Ship in Regular Waves," SNAME Transactions 1957.

13. Fancev, Mladen, "A Check on the Linearity of a Ship Motion System," Davidson Laboratory, Stevens Institute of Technology TM-126, November 1961.

14. Davis, M. C., Lt. Cdr. USN and Zarnick, Ernest E., "Testing Ship Models in Transient Waves," Paper prepared for Fifth Symposium on Naval Hydrodynamics, Bergen, Norway, September 1964.

15. Dalzell, John F., "A Note on the Deterministic Calculation of Roll and Heave Response of a Submerged Body in Irregular Seas," Davidson Laboratory, Stevens Institute of Technology, TN 713, February 1964.

16. Bernicker, R. P., "Deterministic Predictions of the Motions of a Hydrofoil Craft in Irregular Seas," Davidson Laboratory, Stevens Institute of Technology, Report 1003, January 1964.

Appendix A

The wave-induced impulsive response function for a fluid, viz.,

$$K_w = \frac{1}{2\pi} \int_{-\infty}^{\infty} e^{\frac{\omega|\omega|}{g}(-\zeta + i\xi)} e^{i\omega u} d\omega$$

can be reduced to

$$K_w = \frac{R_e}{\pi} \int_0^{\infty} e^{-\frac{\omega^2 Z}{g}} e^{-i\omega u} d\omega$$

where $Z = \zeta - i\xi$.

Now let

$$\lambda = \frac{\omega^2 Z}{g}$$

and then the integral is converted to a Laplace transform type:

$$K_w = \pm \frac{1}{2\pi} R_e \sqrt{\frac{g}{Z}} \int_0^{\infty} \frac{\exp}{\sqrt{\lambda}} \left(\mp u \sqrt{\frac{\lambda g}{Z}} \right) e^{-\lambda} d\lambda$$

and this can be found (see, for example, Tables of Integral Transforms, Vol. 1, McGraw Hill, 1954) to be expressed in terms of the complementary error function Erfc:

$$K_w(u; Z) = \frac{1}{2\sqrt{\pi}} R_e \sqrt{\frac{g}{Z}} e^{-\frac{gu^2}{4Z}} \operatorname{Erfc} \left(\pm \frac{iu}{2} \sqrt{\frac{g}{Z}} \right).$$

* * *

DISCUSSION

John F. Dalzell
Southwest Research Institute
San Antonio, Texas

Since this discussor was associated with the initial work on the techniques discussed in the paper he cannot take serious technical exceptions, and must admit responsibility for the lack of initial lucidity referred to in the Introduction. "Translations" from the mathematical developments of other branches of technology, which the theoretical part of this paper is in large part, are made necessary by the bewildering array of names for the same thing so often found in the literature. The initial development of the techniques described in the paper was characterized by expediency rather than elegance and consequently the quite general notions of the impulsive response and the convolution integral combined with a digital computer yielded plenty of numbers but no equations.

The writer should comment that practical computer evaluation of the Fourier transform and the convolution integral is dependent on the integrands going to zero within practical ranges of ω or τ. Fortunately, this almost happens in all the modes of motion discussed in the paper and the errors incurred by integration over less than an infinite interval are not serious. One would have quite a difficult time using the kernel function for wave motion "induced" by horizontal separation (Fig. 1) unless the frequency content of the wave record was known in advance (the highest wave frequency containing appreciable energy dictates how many of the oscillations toward positive τ must be retained).

The attitude of some of those committed to the statistical approach is that deterministic calculations of random phenomena can only ultimately result in a set of statistics which are easier obtained by power spectrum (frequency domain) calculations. This is probably true. On the other hand, there were those 5 years ago who said that the power spectrum methods were all well and good but that they did not take account of the occasional motion extremes observed in most samples except for very low sea states, and that marine vehicle motions became nonlinear in the mathematical sense very soon after wave heights reached visible proportions. The present gambit was initiated as an aid in the investigation of how far linear systems concepts could apply in severe seas. It was intended as a complementing demonstration of how adequate or inadequate linear systems concepts were. Figure 14 of the paper is the least significant of the 3 similar plots from Ref. 4. Figure 14 of Ref. 4 shows almost as good agreement between time domain predictions and observations for a wave whose significant height was 4 times greater than that shown in Fig. 14 of the paper, a result indicated by frequency domain analysis.

The foregoing remarks were offered to illustrate that the methods discussed in the paper were originally intended as, and used for, investigations complementary to frequency domain analyses. It is the writer's opinion that the particular analysis technique discussed in the paper may be viewed as a useful special purpose tool which can be very beneficial but which may not necessarily yield directly usable information.

DISCUSSION

M. Fancev
Institut Za Brodska Hidrodinamika
Zagreb, Yugoslavia

In dealing with any real problem of the ship motion stabilization one receives little help from a statistical treatment of sea and motion properties, but rather has to look for a deterministic way of analysis. During my stay at Davidson Laboratory in 1961, I tried first the Fourier Series synthesis with known transfer functions and wave time history [13]. Although the results were good, the impulsive response technique appeared more practical and simple in application, and motion predictions (reproduced here in Fig. 4) proved to be reliable. Further extensive work at the Davidson Laboratory on this subject, as may be seen from the paper, confirmed the validity and practibility of the impulsive response technique.

The authors are to be congratulated on the pedantic and precise development of the theory for the covered modes of oscillations leaving so little to the intuitive way of reasoning.

Wasn't this pedantry a little vague in the section following Eq. (42), as regards the oddness and evenness of phase angle and amplitude of response, respectively? These conclusions follow from a pure mathematical expression, but a physical interpretation introducing negative frequencies could be easier followed.

The chapter on the shift of wave measurements cleared entirely the conception of physical realizability, which has to be understood in this specific application of impulsive response technique.

In the motion stabilization application some "free" future time will have to be on disposal for the selection of proper orders for the control system of stabilizers. One way to get this time "fund" is the measurement of waves well off the ship, but this could be either impractical or unreliable. Practically, the bow, the stern, and the sides of the ship are mostly too remote from C.G. to be used for wave measurements. In such a case impulsive response will exhibit values other than zero for "future" time, but because of the loss of the precision of prediction, one could cut off a piece of the impulsive response to get the required "future" time. Here again the statistics could enter and make this truncation in a proper way thereby giving the limitations and expectations of such a procedure.

Such a truncation of impulsive response (without any special statistical treatment) I did in Ref. 13 and I succeeded in forecasting the pitch and heave 3.6 seconds in advance (full scale) with quite the same degree of precision as without truncation (Figs. 14 and 15 of Ref. 13). It has to be emphasized that irregular waves, in this case, were measured at the wave probe a half model length ahead of the model.

DISCUSSION

G. J. Goodrich
National Physical Laboratory
Teddington, England

The collection of statistical full scale ship motion data is a long tedious job taking at least a year for a good sample but it would seem that it is now feasible to reduce this to a computer technique.

Large quantities of recorded sea data are available from weather ships fitted with wave recorders which make regular measurements throughout the year. These data could be fed as input to the computer and the resulting ship motions obtained by the methods suggested by Dr. Breslin.

The results of the calculations could be sampled statistically in an extremely short time and in this way vast quantities of statistical data could be obtained.

* * *

DISCUSSION

Samuel M. Y. Lum
Bureau of Ships
Washington, D.C.

Aside from minor typographical errors and inadvertent omissions in some of the equations scattered throughout the text, I would like to raise some questions on four issues stimulated by this interesting paper.

The first involves what appears to be an apparent mathematical oversight. The question concerns the derivation of the wave-induced impulsive response function presented in the appendix. As it presently stands, this will affect some of the other equations and the final result. This oversight will detract from the overall generality and limit the application. I refer in particular to the failure to distinguish between ω, the wave frequency, and ω_e, the system frequency of encounter. The former is strictly a characteristic of the wave as determined by a wave probe geographically fixed without bringing the craft into the picture. The latter, ω_e, is related to the frequency of encounter as seen by a wave probe fixed to a moving reference having the same speed of advance as the craft. This inconsistency or error of omission can readily be detected by going back to the equation of a simple harmonic, two-dimensional progressive wave as seen by a fixed wave probe,

$$\eta = |\eta_0| \cos\left(\frac{2\pi}{\lambda}\xi + \omega t\right) .$$

Let us now make a coordinate transformation to a moving (x, z) reference frame, free to translate with forward speed U of the body but constrained in pitch, heave, and surge.

$$\xi = Ut + x$$

$$\zeta = z .$$

Suppose we locate a wave probe at some prescribed distance x_0 with respect to an origin corresponding to the midship station of the moving reference. Furthermore, if the particle displacement at some reference depth z_0 below the calm water datum is required, then an attenuation factor $e^{-(2\pi/\lambda)z_0}$ must be applied to the surface wave. The resulting equation for the wave encountered by a point on the body at depth z_0 can be obtained as

$$\eta(x_0, z_0, t) = |\eta_0| e^{-\frac{2\pi}{\lambda}(z_0 - i x_0)} e^{i\omega_e t} .$$

The real part notation has been left out temporarily without obscuring the issue. Making use of two well-known wave relations

$$c = \sqrt{\frac{g\lambda}{2\pi}} = \frac{\omega\lambda}{2\pi}$$

and

$$\omega_e = \frac{2\pi}{T_e} = \frac{2\pi}{\lambda}(c - U\cos\chi) = \omega \pm \frac{\omega^2}{g} U$$

where χ is the heading angle. Then restricting this to head (+) and following (-) seas in the $\pm$ designation, the wave number may be expressed as

$$\frac{2\pi}{\lambda} = \frac{\omega^2}{g} = \frac{\omega_e}{c \pm U} .$$

Substituting this back in the equation for η,

$$\eta(x_0, z_0, t) = |\eta_0| e^{\frac{i\omega^2}{g}(x_0 + i z_0)} e^{i\omega_e t} .$$

When compared to the above equation, the authors' corresponding version of the wave as denoted by their Eq. (13), lacks the subscript e in the driving frequency for the general case. Hence, the results can only be valid for the special case of beam seas or for zero speed-of-advance. This omission was evident in many of the ensuing equations. The error can be easily remedied by inserting the subscript e for all frequencies identified with the system frequency-of-encounter. On the other hand, the ω without subscript e will be retained for those equations involving the function

$$g(\omega, \xi, \zeta) = e^{\frac{i\omega^2}{g}(\xi + i\zeta)}$$

as given in Eq. (14).

Without this correction, the wave-height information as seen by the body is implied to be the same as that picked up by the stationary probe. This is tantamount to a wave excitation on a body essentially hove-to or a body running in cross-seas. If we assume the latter to be the case, then the significance of this error implies the loss of a cross-product term $U\varphi_{wx}$ in the linearized pressure integral. This can be shown by examining the Bernoulli equation. For the case of a body advancing with forward speed U, the pressure terms after linearization can be written

$$\frac{\Delta p}{\rho} \approx U(\varphi_{1x} + \varphi_{2x}) + g\zeta + \varphi_{1t} + \varphi_{2t} \, .$$

Subscripts 1 and 2 are used here to denote quantities related to calm-water and wave respectively. Then φ_{1x} is the longitudinal perturbation velocity in calm water, φ_{2x} (or φ_{wx}) is the corresponding contribution in waves. φ_{1t} and φ_{2t} are the unsteady contributions to the pressure in calm-water and waves respectively.

On the other hand, the linearized pressure due to the body running with forward speed U in calm water conditions is

$$\frac{\Delta p_1}{\rho} \approx U\varphi_{1x} + g\zeta + \varphi_{1t} \, .$$

Adding this to the contribution due to the seaway but with the body held fixed,

$$\frac{\Delta p_2}{\rho} = \varphi_{2t}$$

gives

$$\frac{\Delta p_1 + \Delta p_2}{\rho} = U\varphi_{1x} + g\zeta + \varphi_{1t} + \varphi_{2t} \, .$$

Comparing the above pressure equation to that of the previous case where the total pressure was obtained with body translating with speed in waves shows a loss of the $U\varphi_{2x}$ contribution.

The second issue is the age-old question of the extent of the validity of the somewhat heuristic development of the mathematical model adopted. These refer to the forcing functions employed in Eqs. (11) and (12). Basically, it assumes a lumped mass, dashpot, spring system. It utilizes the wave information at the wave probe station and transfers the fluid particle effects to the center of mass by means of proper geometric phase shift. The total excitation force induced by the wave was then obtained by computing the kinematic acceleration, velocity and displacement of the fluid particle at the mass center of the body and then multiplying by suitable coefficients determined post-priori. Is it correct for us to assume that the crux of the whole approach lies in the adjustment of the coefficients a', b', c' and A', B', C' appearing in the forcing functions specified so as to be compatible with the measured response data?

It is observed that the wave height information or fluid particle displacement is strictly a point function at a given instant of time as measured by the wave probe. Its subsequent introduction into the forcing functions specified by Eqs. (11) and (12) leaves one with some apprehension as to how the total flow field and hence total force over the entire body is generated. What is needed is some spatial integration of the total field effects of each individual particle action over the entire body surface. It is only for very long-crested waves in comparison to body length or beam seas encounter that the approximation will meet with success.

The third issue is perhaps more philosophical in nature. While the surge degree-of-freedom in the system equations has generally been neglected in practice, there are evidence that indicate that such a neglect may not be justified. This happens especially in certain following-seas condition where the craft may be running in a "surfboarding" condition. In severe instances, this can lead to broaching. With the modern computers available today, computational drudgery should pose no problem. Has there been any attempts to try a similar three degree-of-freedom (with and without coupling) response problem to justify the neglect of surge or to define the bounds for its neglect because of second-order effects?

Finally, I would like to state a dream for the future to come in the ship motion studies. While the major brunt of the work so far has been concentrated in the realm of analysis, i.e., to predict the motion given the ship and the seaway, the naval architect in the design office is still looking for a rational approach to design his ships for seaworthiness and minimum motion. It is opportune for someone to undertake the problem of synthesis and the ultimate optimization problem. This undertaking implies an understanding of pole-zero synthesis, defining a meaningful criterion for optimization, plus an identification of the parameters of ship form, loading, hydrodynamic characterization, and seastate environment so as to tie in the relation to the poles and zeroes of the transfer function. Such poles and zeroes, if properly characterized, serve to define the behavior of the ship. At this stage, it is not important to get unnecessarily involved into fine details and accuracy but to look at the broad approach and to arrive at definitive concepts and trends. Such an approach is still awaiting as the eventual goal of ship motion studies to tie in with a rational design practice. This is useful even if only to improve our present go, no-go methods.

* * *

REPLY TO THE DISCUSSION

J. P. Breslin, D. Savitsky, and S. Tsakonas
Stevens Institute of Technology
Hoboken, New Jersey

It is a rather difficult task to try to answer all the discussers of our paper due to the variety of aspects tackled by the discussers and due to the extent to which some of them went. Some of the facts brought up by Dr. Yamanouchi and Dr. Pierson should be considered as complete and independent studies and deserve better classification than being characterized as discussions.*

The estimation of impulse response function by statistical methods as suggested by Dr. Yamanouchi is interesting and useful since it incorporates better the statistical properties of the medium. But the evaluation of the impulse function through a large number of algebraic equations makes the method somehow cumbersome and of questionable stability. His comments on the effect of nonlinear damping on the calculation are very interesting but not directly related to the linear problem which is under consideration.

Dr. Pierson's remarks on the subjects (a) ship in short-crested waves and (b) coherency and resolvability of spectral and cross-spectral shapes and (c) the solution of specific problems which are nonlinear, are interesting and applicable to the problem of ship motion in short-crested waves, where the nonlinear characteristics are dominant.

As for Mr. Lum's remark about some "mathematical oversight" by the authors, we would like to emphasize the fact that the primary objective of this present paper is to demonstrate the method of evaluating the impulse response function of a marine craft running in arbitrary irregular long-crested waves, and bring up the most pertinent characteristic of the approach. Thus an idealized situation was selected such as to exhibit the main feature of the approach. Equations (11) and (12) do not imply the corresponding system to be one of "lumped parameters" since the coefficients are frequency dependent. We should further keep in mind that this study is based on a linearized version of the coupling ship motion in heave and pitch and the results are applicable only for long-crested waves. His burning desire to reach the stage of issuing criteria and formulae useful for the design of a ship for seaworthiness and minimum motion can only be achieved after a rigorous and more realistic study of the hydrodynamic aspects of the problem. The fulfillment of this long range objective should wait until this part of the problem is clarified and, in the meantime, the fragmentary information should be properly utilized.

*See discussions by Pierson and Yamanouchi on the paper by Ogilvie and discussion by Tick on the paper by Cummins and Smith.

Mr. M. Fancev's kind words are appreciated and we would like to take this opportunity to thank him and Mr. J. Dalzell for their pioneering work which has been useful and inspiring to the authors.

We do share the same opinion with Mr. G. Goodrich about the usefulness of this method to classify existing data and utilized their statistical properties to examine the long-time exposure to rough seas by relatively short-time computer runs.

We would like to thank all discussers for their stimulating contributions.

* * *

TESTING SHIP MODELS IN TRANSIENT WAVES

Lt. Cdr. M. C. Davis, USN and Ernest E. Zarnick
David Taylor Model Basin
Washington, D.C.

ABSTRACT

The seaworthiness characteristics of a ship design are often determined by a series of model tests in regular waves. This report describes a new model test procedure which makes use of a transient wave disturbance having energy distributed over all wave lengths of interest. With the use of this transient wave technique, the testing time required to characterize a model is reduced by an order of magnitude. In this report, the basic behavior of a unidirectional transient wave is discussed, and a simple Fourier transformation is developed in order to link wave height records measured at any two separated points along the path of such a wave. A particular form of transient wave, which is approximately sinusoidal with linearly varying frequency, has been used to test successfully a number of ship models. The results of these tests are presented and the practical problems in generating, measuring, and analyzing transient wave tests are discussed.

INTRODUCTION

The linear theory of ship motion in a random seaway has become generally accepted as a useful approximation to the actual nonlinear phenomena involved in ship-wave interaction. As outlined in the pioneering work of St. Denis and Pierson [1] the random sea surface can be visualized as a superposition of two-dimensional sinusoidal waves continuously distributed in amplitude, wave length, and direction. The total ship response in any degree of freedom is found from a summation of the responses to each individual wave component.

The primary role of a ship model testing facility, in providing information for quantitative full-scale motion prediction using this theory, is to measure the response of a model to sinusoidal waves of unit amplitude over the entire range of ship speed, wave length, and direction of encounter. The Harold E. Saunders Maneuvering and Seakeeping Facility, located at the David Taylor Model Basin, is admirably suited to conduct such an investigation in head and oblique waves.

The scope of a complete model measurement program is without parallel in other engineering fields which perform frequency response testing of dynamic systems. A numerical example will illustrate the large number of tests which are required to characterize a model in regular waves. Assuming that the functions involved can be suitably approximated by tests at 10 wave lengths, 30-degree increments in direction from ahead to astern, and 5 speeds, 350 separate model tests are required, with measurement and analysis of a number of dynamic variables on each test. A program such as this requires a major investment of time and money, and any techniques which can be developed to abbreviate the test time without technical compromise will reap high dividends.

It is clear that relative wave direction and model speed must remain fixed for any one test. However, under these constant conditions, a series of experiments in varying wave lengths is nothing more than a frequency response determination of a linear dynamic system, a common experiment in systems investigations for many engineering disciplines.

The frequency response characteristics of linear systems may be measured in three fundamental ways, that is, using sinusoidal, random, or transient excitations. The first two techniques are commonly employed in testing ship models. The latter technique, using a transient water wave, is the subject of this report.

A transient wave will contain energy which, in general, is distributed over a range of wave lengths. Thus, a single motion test can yield information about the response of the ship at all wave lengths of interest. In the representative example just quoted, the number of tests required to characterize a ship design can be reduced from 350 to 35.

In the following sections, the theoretical and practical aspects of transient wave testing are presented. First, the basic mathematics of linear systems analysis are outlined. Then, the analytic peculiarities of the ship-wave system are discussed, stressing the fact that a wave is not properly an "input" as the term is usually understood. Next, the complex subject of unidirectional water-wave transients is treated in a simplified fashion by developing an expression which relates various wave height time histories that might be recorded at various points along the path of the wave.

A particular wave which arises quite naturally from this analysis is the one which would, in theory, produce an impulse of infinite height and zero duration at some measurement point. An approximation to this theoretical waveform is quite easy to generate in a seakeeping facility; it has been extensively used at DTMB for model testing because of its several attractive analytical properties.

Three sets of model tests are reported herein to support the theory and to illustrate some of the practical problems, especially associated with the measurement of wave height, that can be anticipated in using transient waves to excite ship motion.

PRELIMINARY THEORY

Mathematics of Transient Testing

Suppose that a linear dynamic system (such as shown in Fig. 1) is under investigation, with an "input" $x(t)$ as the independent excitation, and an "output"

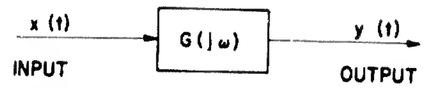

Fig. 1 - General linear system representation

$y(t)$ as the dependent or forced variable. If $x(t)$ is a sinusoidal signal at a particular frequency, then, in general, $y(t)$ will asymptotically approach a steady-state sinusoidal response at the frequency. The ratio of the output amplitude to the input amplitude and the phase difference between output and input for all frequencies define the frequency response of this system, represented by the complex transfer function $G(j\omega)$, where ω is the frequency in radians per second.

When the system $G(j\omega)$ is at rest and a sudden transient $x(t)$ is applied at $t = 0$, then some response $y(t)$ will be measured, usually involving decaying transients. It is well known that a transient signal can be decomposed into a continuous distribution of infinitesimal sinusoidal components with the aid of the Fourier transform. For example, the Fourier transform $X(j\omega)$ of a particular input signal $x(t)$ is given by the complex quantity

$$X(j\omega) = \int_{-\infty}^{\infty} dt \; x(t) \; e^{-j\omega t} \tag{1}$$

which represents the amplitude and phase of the incremental components at frequency ω. Considering the output to be a summation of the response to each of the input frequencies, the well-known relation

$$Y(j\omega) = X(j\omega) \; G(j\omega) \tag{2}$$

gives a proper amplification and phase change to each of these components.

To summarize, the frequency response of a system $G(j\omega)$ can be found from a single transient experiment with input and output transforms $X(j\omega)$ and $Y(j\omega)$, respectively, with the relation

$$G(j\omega) = \frac{Y(j\omega)}{X(j\omega)} \; . \tag{3}$$

In the transient testing of ship models, the input $x(t)$ is arbitrarily defined as the instantaneous amplitude of the undisturbed two-dimensional wave surface which would pass through the center of gravity of the model; see Fig. 2. The output $y(t)$ is the time history of any one of the pertinent response variables, such as roll, pitch, or heave.

The use of a water wave input is the key distinction between transient tests of ship models and those conducted, for example, in control systems analysis where often a voltage is available for easy introduction of input transients.

Visualization of the Ship-Wave System

The fact that the wave height referenced to the center of gravity of the model is defined as the input can lead to great mathematical difficulties. For

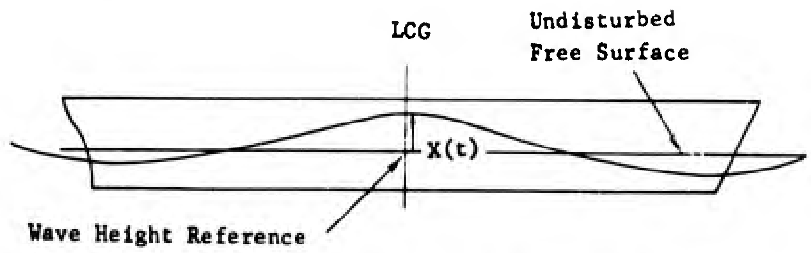

Fig. 2 - Wave height defined as an input signal

example, in defining a linear system in the time domain it is conventional to use a unit impulse as a standard input, which causes an "impulse response" whose Fourier transform is identical to the frequency response function. This is seen from Eq. (2), where

$$Y(j\omega) = G(j\omega) \tag{4}$$

because the transform $X(j\omega)$ of a unit impulse is unity.

Since it is impossible for a physical system to look into the future, to "laugh before it's tickled," the impulse response must be zero prior to $t = 0$ (when the impulse arrives). However, in the ship motion problem there is no reason to believe that the inverse transform of an experimental frequency response will exist only in positive time. In fact, as will be shown later in this report, an "impulse" of wave height observed at $t = 0$ at the center of gravity of the model would be caused by the contraction of a wave train, which had previously passed along the forward part of the ship, producing force on the hull and resultant motion in negative time. Thus, a more accurate description of the phenomena involved would be the very general configuration pictured in Fig. 3, where unidirectional wave height and ship motion are both viewed as responses to some undefined initial excitation, the mechanism which produces the waves. However, since wave height and ship motion are completely related in the sense that they respond to the single cause, it is proper to consider that ship motion can be related to wave height by the frequency relation

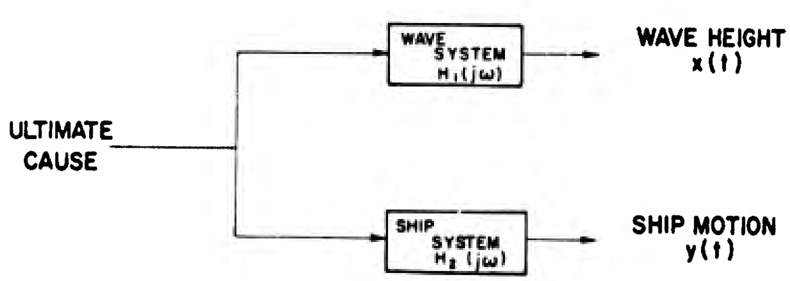

Fig. 3 - Representation of wave height and ship motion as "effects" rather than "cause" and "effect"

$$Y(j\omega) = X(j\omega)\left\{\frac{H_2(j\omega)}{H_1(j\omega)} = G(j\omega)\right\} \tag{5}$$

where $G(j\omega)$ is not properly the response of a physical system but the ratio of the frequency response of two physical systems.

With this philosophical restriction in mind, we will continue to call wave height an input and ship motion an output, but at no time will the intervening system be required to have the characteristics of a real physical system.

Wave Transients

The study of transient waves on a free surface is an advanced top in hydrodynamic theory, but it is amenable to the "systems" approach if linear wave behavior is assumed. Consider first that all waves are traveling in the same direction on a surface of infinite extent and in a fluid of infinite depth. Suppose further that a wave disturbance of finite energy per unit crest length has been traveling for all time and is observed at a single stationary point x_1. The wave height $\eta(x_1, t)$ may be expressed in terms of its Fourier transform by the relation:

$$\eta(x_1, t) = \frac{1}{2\pi}\int_{-\infty}^{\infty} d\omega\, N(x_1, \omega)\, e^{j\omega t}. \tag{6}$$

Following the technique of Stoker [2], the complex quantity $N(x_1, \omega)$ is visualized as the infinitesimal wave component with frequency $+\omega$. This wave at any instant of time extends over the entire plane and at any one point persists for all time. At another point x_2, which is a distance x along the direction of wave travel from x_1, this same infinitesimal wave is observed but with a phase lag of $\omega^2 x/g$ radians, according to linearized wave theory. That is, the time history at x_2 is given by

$$\eta(x_2, t) = \frac{1}{2\pi}\int_{-\infty}^{\infty} d\omega\, N(x_1, \omega)\, e^{-j\omega|\omega|x/g}\, e^{j\omega t} \tag{7}$$

where the absolute value of ω is used in the phase operator to ensure that the quantity

$$N(x_2, \omega) = N(x_1, \omega)\, e^{-j\omega|\omega|x/g} \tag{8}$$

is conjugate with $N(x_2, -\omega)$. This property is necessary in order that a Fourier transform represent a real function of time.

The operator $e^{-j\omega|\omega|x/g}$ can thus be viewed as the "transfer function" of water, or the frequency response function which relates wave heights measured at two points separated by a distance x in the direction of travel.

To illustrate this result, suppose that

$$\eta(x_1, t) = \cos \omega_0 t . \tag{9}$$

The Fourier transform of this wave height is given by

$$N(x_1, \omega) = \pi\left[\mu_0(\omega - \omega_0) + \mu_0(\omega + \omega_0)\right] \tag{10}$$

where $\mu_0(\cdot)$ represents the unit impulse. The transform of $\eta(x_2, t)$ is given by

$$N(x_2, \omega) = \pi\left[\mu_0(\omega - \omega_0) + \mu_0(\omega + \omega_0)\right] e^{-j\omega|\omega|x/g} . \tag{11}$$

We have for $\eta(x_2, t)$, then, the relation

$$\eta(x_2, t) = \frac{1}{2\pi}\int_{-\infty}^{\infty} d\omega\, \pi\left[\mu_0(\omega - \omega_0) + \mu_0(\omega + \omega_0)\right] e^{-j\omega|\omega|x/g}\, e^{j\omega t}$$

$$= \frac{1}{2}\left(e^{-j\omega_0^2 x/g}\, e^{j\omega_0 t} + e^{j\omega_0^2 x/g}\, e^{-j\omega_0 t}\right)$$

$$= \cos\left(\omega_0 t - \omega_0^2 x/g\right) \tag{12}$$

which is a well-known result from linear wave theory.

The remarks of the previous section apply to wave height pairs in the sense that the latter are both "effects" rather than "cause" and "effect." However, with knowledge of wave height at one point, the corresponding time history at another point can be determined by convolving the first wave height with the inverse transform of $e^{-j\omega|\omega|x/g}$ as is well known from linear systems analysis. This inverse transform is computed in the Appendix and yields the "weighting function" or "impulse response" of water

$$w(\tau) = a \cos \frac{\pi}{2} a^2 \tau^2 \left[\frac{1}{2} + \frac{\tau}{|\tau|} C(a\tau)\right] + a \sin \frac{\pi}{2} a^2 \tau^2 \left[\frac{1}{2} + \frac{\tau}{|\tau|} S(a\tau)\right] \tag{13}$$

where

$$a \triangleq \left(\frac{g}{2\pi x}\right)^{1/2} \tag{14}$$

and

$$C(a\tau) = \int_0^{a\tau} dm \cos \frac{\pi}{2} m^2 , \qquad S(a\tau) = \int_0^{a\tau} dm \sin \frac{\pi}{2} m^2 . \tag{15}$$

This weighting function is shown in Fig. 4, where

$$w(\tau) \approx \sqrt{g/\pi x}\,\cos\left(\frac{g\tau^2}{4x} - \frac{\pi}{4}\right) \tag{16}$$

as $a\tau$ becomes large. This function can be heuristically interpreted as a linear frequency sweep which looks back into the past of the wave height signal being processed and detects those frequency components that have gone by at a past time which would influence present wave height at a distance x in the direction of the wave. This is motivated by the convolution integral

$$\eta(x_2, t) = \int_{-\infty}^{\infty} d\tau \; w(\tau)\; \eta(x_1, t - \tau) \tag{17}$$

which is the time domain equivalent of

$$N(x_2, \omega) = N(x_1, \omega)\, e^{-j\omega|\omega|x/g}. \tag{18}$$

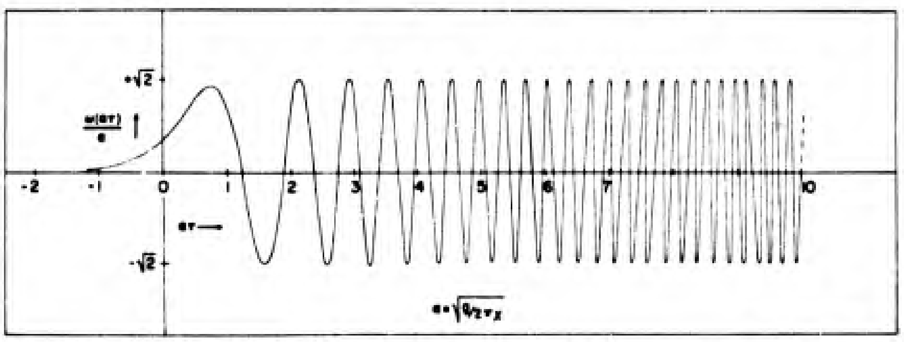

Fig. 4 - Weighting function of unidirectional waves in water

Suppose we ask the physically ridiculous but mathematically interesting question: "What signal would be observed at x_1 if a unit "impulse" of wave height were recorded at x_2?" A unit impulse is described as a signal which is zero except at an instant in time where it has infinite amplitude, such that the integral over this point has a value of unity. The Fourier transform of a unit impulse is 1.0.

Solving Eq. (18), we find that

$$N(x_1, \omega) = e^{j\omega|\omega|x/g}. \tag{19}$$

This can be readily shown to have an inverse transform which is equivalent to that shown in Fig. 4 except for a reversal of the time variable.

Thus, if we observe a transient wave in the water which initially has a very high frequency (associated with slow velocity) and if this frequency linearly decreases toward zero with constant amplitude and tapers off as in Fig. 4 with time reversed, then at some point in space and time a very large wave would be created for a brief instant, assuming that linear wave theory holds. This phenomenon can be viewed as the simultaneous meeting of a large number of wave components whose individual speeds and starting times were properly adjusted so that the faster traveling waves were behind but catching up with the slower ones.

For the purposes of wave generation in a model-testing facility, it is manifestly impossible to provide a sinusoidal wave at infinite frequency. However, it is certainly possible to generate a wave train which has a frequency varying linearly from the highest desired value toward zero. Such waves have been the backbone of the Model Basin transient studies and will be described more fully along with experimental results in the following sections. Briefly, the linear theory appears to hold quite well, and in the early exploratory studies very large peaked waves — approximating the impulse — were formed, although they were limited by cresting and other nonlinear mechanisms.

An important property associated with a transient water wave is that the magnitude of the Fourier transform remain constant regardless of where it is observed and when the origin in time is fixed; i.e., the water transfer function is solely a phase operator. For a pair of moving probes separated by a fixed distance x, the same frequency response relation is applicable. However, transforms of wave height measured at nonzero speed are computed using the frequency-of-encounter time scale, where each wave length component corresponding to a stationary frequency ω is measured at the frequency

$$\omega_e = \omega + \omega^2 \frac{v}{g} \tag{20}$$

where v is the speed of the wave probes against the direction of wave travel. If a Fourier transform of a transient is computed for one wave height measurement, the companion wave measurement in the direction of wave travel will have the same magnitude at each frequency but the phase will be shifted by $e^{-j\omega|\omega|x/g}$ where ω is the stationary frequency of the wave component concerned. For waves traveling in the same direction as the wave probes, ambiguities exist, and special techniques, which are beyond the scope of this report, must be employed.

The preceding treatment of transient water waves does not follow a conventional path in that spatial effects are suppressed and initial conditions or exciting forces on the water are not considered. If an instrument measures unidirectional wave height at some point for all time, then the time history at any other point is readily estimated through transform techniques. Even though a wavemaker may be generating the transient wave in the testing basin, the height-measuring probe and the ship model considered the wave to be one that has been traveling forever on an infinite surface.

TEST TECHNIQUES

Outline of Model Testing Technique Using Transient Waves

Transient testing with a model in ahead waves is accomplished quite easily. As currently conducted, the first waves to be generated are slowly progressing high-frequency waves. When these first waves have traversed a portion of the test basin, the model is brought up to speed in calm water and measurement of all dynamic variables is commenced. The wave train passes, induces motion, and then the water and model return to the quiescent condition where recording is stopped.

Each time-record is used to compute a Fourier transform from a common time base. The wave height transform must be corrected to the location of the model center of gravity by the transfer function $e^{-j\omega|\omega|x/g}$, where x is the distance to the ahead wave probe and ω is the wave frequency. The ratio of motion transform to corrected wave height transform defines the transfer function, amplitude and phase for that motion.

Programming for Transient Wave Generation

The wavemaking system in the Harold E. Saunders Maneuvering and Seakeeping Facility, described recently by Brownell [3], is quite well suited for the generation of transient waves. Eight electrohydraulic servo systems can be used to control the flow of air to and from domes along the shorter side of the basin, thus imparting energy to the water which travels away in the form of waves. These servo systems can be driven in unison by an electrical signal from either a low-frequency sine wave generator or a tape recorder.

The actuator servo system has proved to be a considerable improvement over the previous electromechanical arrangement for wave generation, which provided a constant-amplitude variable-frequency, sinusoidal excitation to the water. The actuator system can allow independent control of both amplitude and frequency, or it can introduce transient or random disturbances of more general form. Random wave generation has been described recently in Ref. 4.

The transient waveform which has been used to date is characterized by a linearly decreasing frequency, starting at the highest frequency of interest for model testing — nominally 1.0 cps. The electrical signal that produces these waves is recorded on magnetic tape by the crude but effective procedure of linearly decreasing the frequency of a low-frequency sinusoidal source.

The frequency response characteristics of the basin, relating wave height to actuator motion, are such that frequency components near 0.4 to 0.5 cps are greatly amplified. Two modes of transient waves have been used — one has the program amplitudes weighted so as to counteract this frequency behavior; the other has a constant amplitude with varying frequency.

Fourier Analysis of Recorded Transients

The Fourier transform of a transient record is defined by the mathematical relation

$$F(j\omega) = \int_{-\infty}^{\infty} dt\ f(t) \cos \omega t - j \int_{-\infty}^{\infty} dt\ f(t) \sin \omega t \tag{21}$$

and is readily accomplished by digital computation or by special-purpose devices designed for this application.

For this exploratory investigation, it was decided to use a particular analog computer configuration which has interesting properties. A single channel is shown in Fig. 5 where conventional analog computer symbols are used. As described in Ref. 5, this undamped resonant circuit is driven by a transient input and oscillates as $t \to \infty$ at an amplitude corresponding to the magnitude of the transform of the input transient at the particular frequency ω and with a phase corresponding to the phase of the transform. A number of similar computer configurations all adjusted to the same frequency, were driven simultaneously by the tape-recorded transients resulting from a particular experiment in order to maintain a common time base for phase measurements.

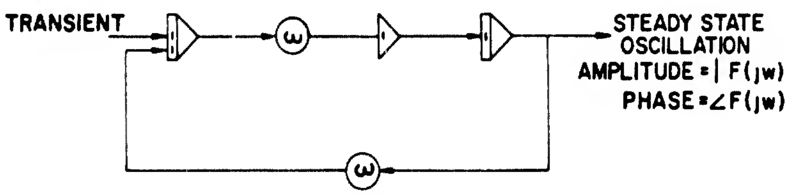

Fig. 5 - Transient analyzer configuration on analog computer

The use of this scheme for transient analysis was motivated by considerations of accessibility and operator control of the computations. However, for mass handling of transient records on an assembly-line basis, other techniques will be employed.

TEST RESULTS

Tests of three different models are described in this report. Emphasis is placed on a correlation of transient wave results with regular wave results rather than on a complete description of the characteristics of any particular hull form. A chronological description is used to indicate the problems encountered and the progress obtained to date.

Test Series 1

The first transient tests were conducted in December 1962 using Model 4941, a 13-ft model of a C4-S-A3 Mariner hull which had been previously tested in regular waves. Pitch and heave in ahead waves were measured as well as wave height with a sonic wave probe mounted approximately 12 ft abeam of the center of gravity of the model.

The philosophy of wave generation during this series of tests was to create a wave which would contract and "peak," as described in an earlier section, at a point somewhere near the model. Figure 6 shows the records taken during a

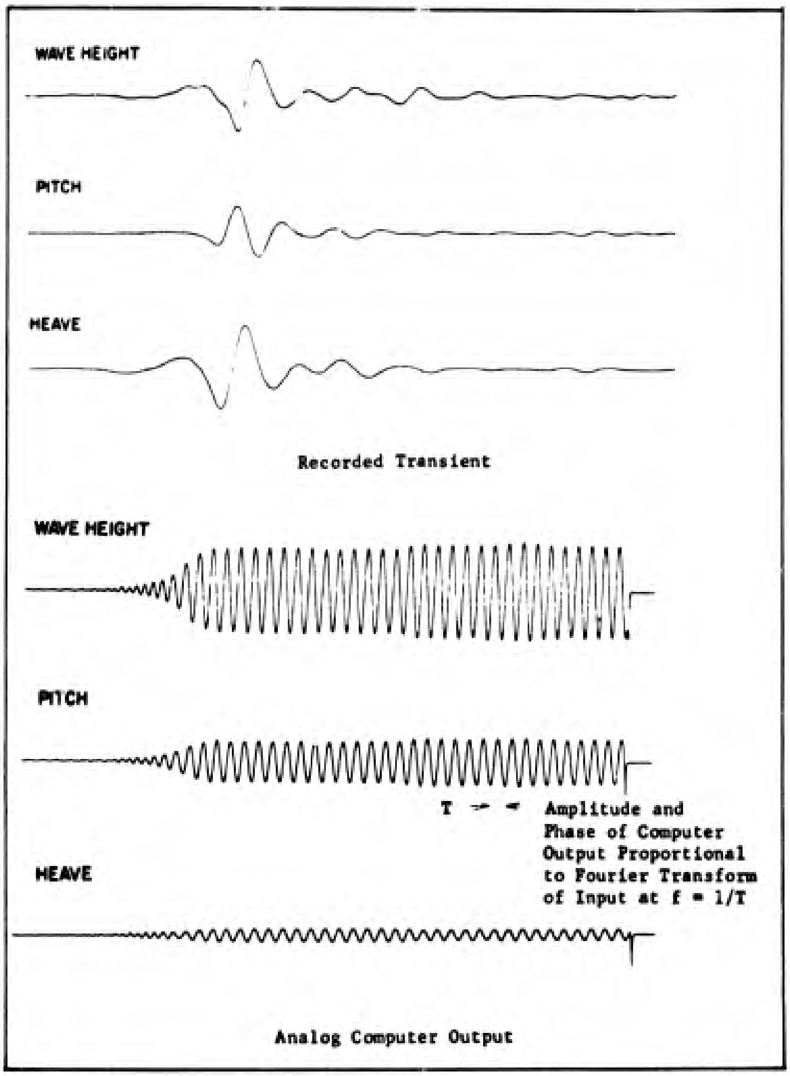

Fig. 6 - Measured transients for Model 4949 and typical analog computer frequency response measurement

typical test where the wave transient reached a peak height at the location of the stationary model. Along with these signals, the outputs of the analog computer circuitry (described in the previous section) are displayed for a particular frequency of analysis.

These sinusoidal outputs have magnitudes which are essentially equal to the magnitudes of the Fourier transforms of the respective signals up to that point. Although the variation of these amplitudes at the end of the transient has been a vexing problem with this method of transient analysis, sources of test error have been uncovered such as waves reflected from the sloping beach.

Another practical difficulty encountered is also seen in the transient wave height record where the energy in the water does not decay rapidly after passage of the main signal. Fortunately, much of this disturbance is above the frequency range of interest.

A zero-speed transient test was analyzed at many different frequencies using the relative lull at the end of the passage of the main wave as the defined end of the transient. Figures 7 and 8 display the resulting heave and pitch frequency responses; they show good agreement with those of the regular wave

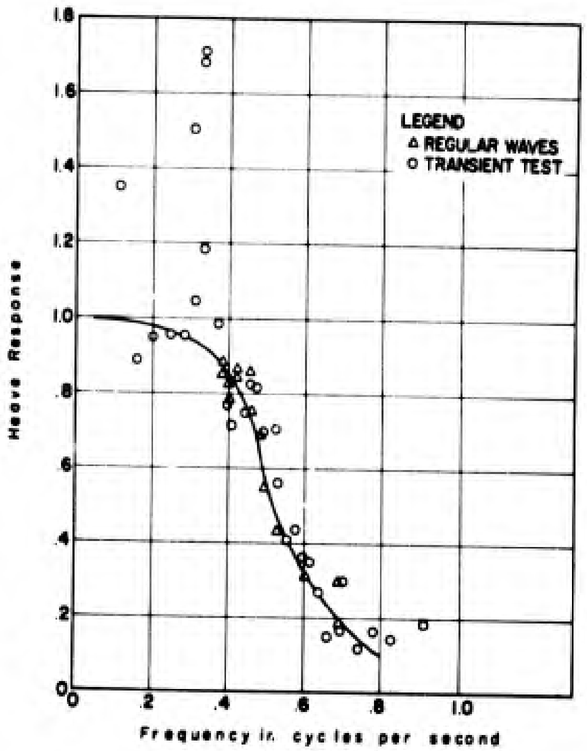

Fig. 7 - Heave response for Model 4941 at zero speed in head waves; transient test compared with regular wave test results

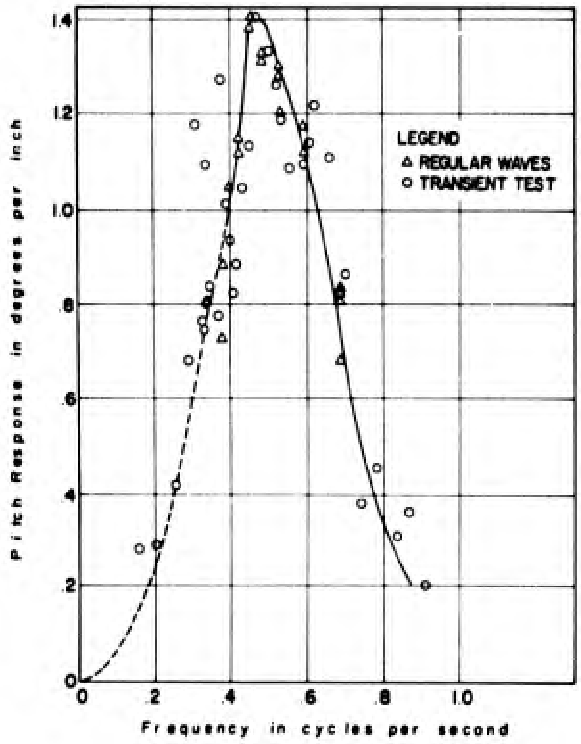

Fig. 8 - Pitch response for Model 4941 at zero speed in head waves; transient test compared with regular wave test results

tests. The only severe deviation is a sharp peak near 0.35 cps in both responses; it was caused by an unexplained sharp null in the measured wave height transform.

In Fig. 9 the heave/pitch ratio is plotted for the zero-speed case. Although heave/pitch ratio plays no part in prediction of motion, it is a ratio which has as much significance as any other in the isolated transient experiment, since all three dynamic quantities are "effects," as previously discussed. This ratio has the virtue of being independent of errors in wave height measurement, and has provided a useful index of the accuracy of the motion measurements throughout the series of transient tests.

A forward speed transient test was conducted at a speed corresponding to a Froude number of 0.09. Unfortunately, heave calibration was lost and only pitch results are valid, as given in Fig. 10. These results show a moderate agreement with the regular wave pitch response.

In analyzing the results of these initial tests, it was felt that the transient technique had demonstrated considerable promise but that there were many possibilities for improvement in testing techniques.

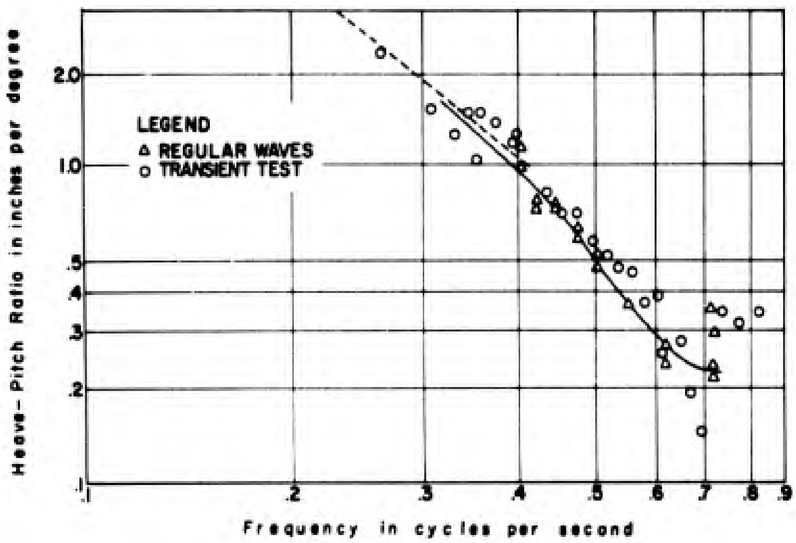

Fig. 9 - Heave/pitch ratio for Model 4941 at zero speed in head waves; transient test compared with regular wave test results

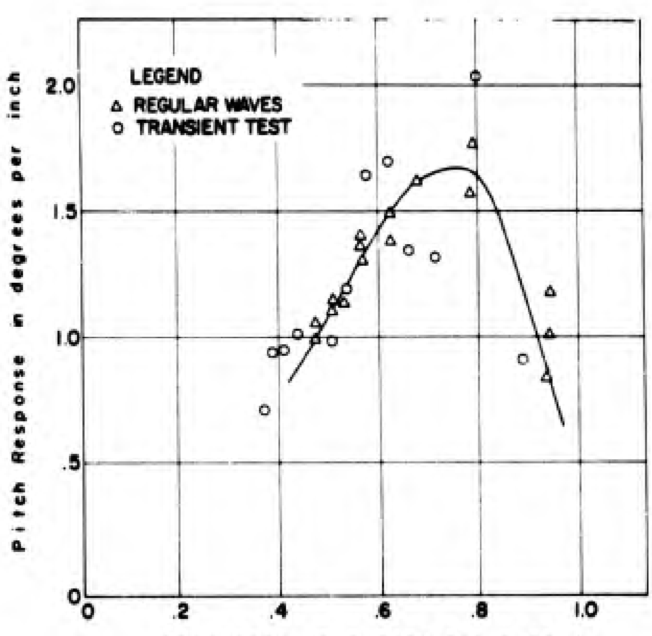

Fig. 10 - Pitch response for Model 4941 in heave waves at a Froude number of 0.09; transient test compared with regular wave test results

First of all, it was recognized that there is no particular virtue in having a model at the point of contraction of the wave transient, since the amplitude of an ideal wave transform is invariant with position. In fact, there is a strong possibility that nonlinear water or model behavior would be accentuated near the point of highest wave amplitude and that surge modulation effects would be significant. In addition, passing through a longer program before it coalesced would mean that more controlled energy could be imparted to the wave excitation, which, other things being equal, would lessen the effects of extraneous noise. And finally, the practical virtue of not having to conduct a precisely timed meeting of model and wave is still another motivation for altering and extending the duration of the wave transient.

A second major source of error was believed to be in the wave height measurement. Besides the previously mentioned wave reflections from the beach, there was a considerable possibility that waves generated by the model were being picked up by the side wave probe. Although there are some advantages in measuring a wave signal at its geometric reference point, they seem to be outweighed by the readily demonstrated fact that waves are generated much more efficiently by the model in the abeam direction rather than in the ahead direction.

Test Series 2

A second series of transient tests was conducted during January 1963; in these tests an attempt was made to profit from the lessons learned in the initial tests. The model selected was a Series 60, Block 0.60 hull form, Model 4606. Heave and pitch were measured in ahead waves. Attention was focused on the zero-speed case in order to minimize the number of factors affecting the experiment.

During these tests, wave height was measured with two sonic probes. One was placed in the same location as in the previous tests, approximately 12 ft abeam of the model center of gravity, and the other was located 19 ft 2 in. ahead of the center of gravity.

The wave program employed was considerably longer than that used in the previous test series. The excitation signals from both Series 1 and 2 are displayed for comparison in Fig. 11, which shows that the duration of the control voltage for the second test was doubled, that is, raised from 40 to 80 seconds.

A typical transient test recording of this series is shown in Fig. 12. The wave height and motions are seen to be of a form considerably different from that observed during the first tests; they resemble the varying frequency and amplitude characteristics that would be predicted by theory. One immediately obvious result is that the side wave measurement contains a peculiar null in its envelope which is not present in the ahead wave measurement, an anomaly which is most likely due to model-created waves generated to the side.

In Figs. 13 and 14, respectively, frequency response operators obtained from four transient tests in heave and pitch are compared with regular wave measurements made during the same series of tests. Agreement seems to be

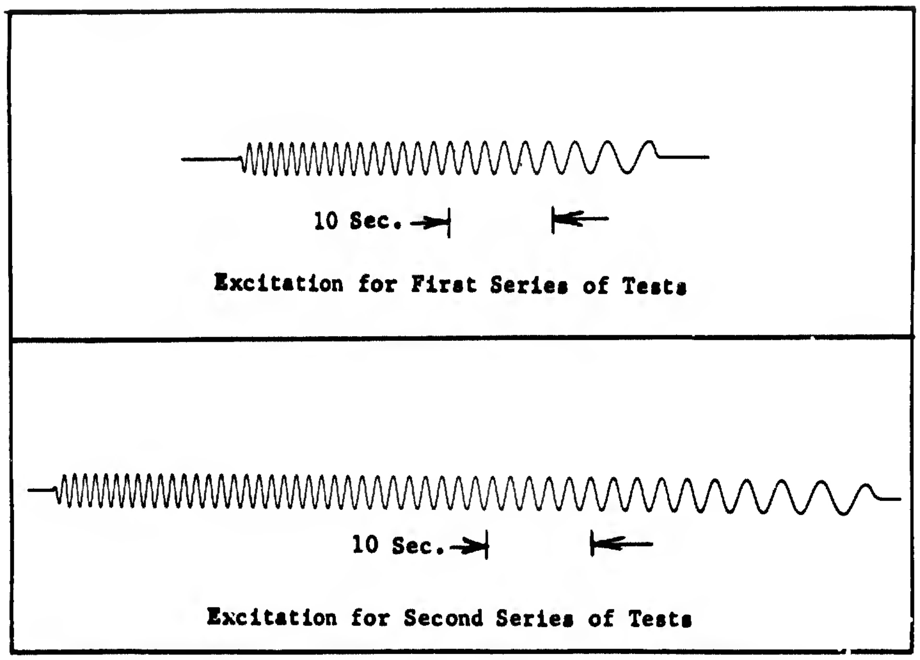

Fig. 11 - Transient voltage excitation to wavemaking system during first and second series of model tests

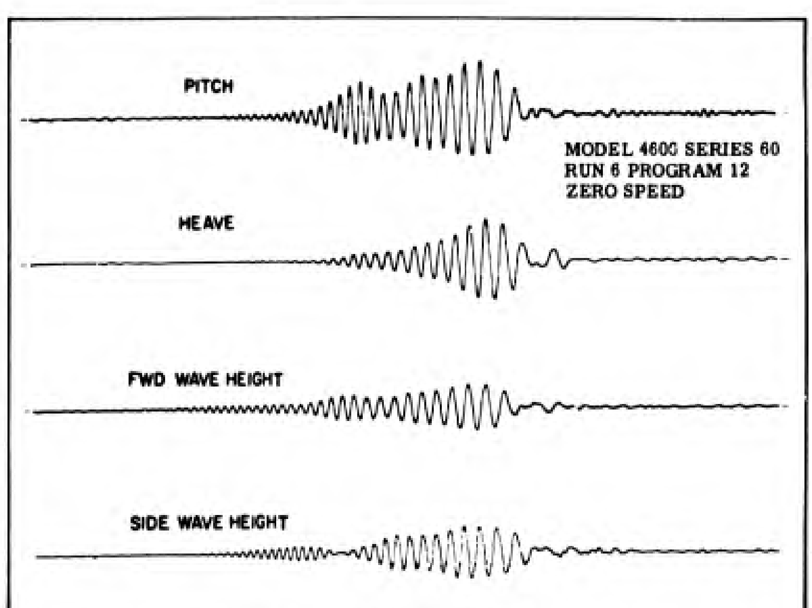

Fig. 12 - Typical transient recording taken during second series of model tests

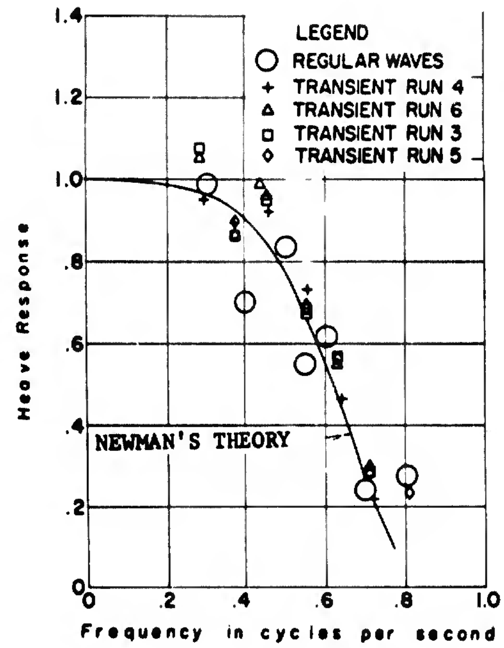

Fig. 13 - Heave response for Model 4606 at zero speed in head waves; transient test compared with regular wave test results

quite good over most of the frequency range. The solid curves, which are also shown on these plots, were computed on the basis of slender-body hydrodynamic theory by Newman [6] for a roughly similar hull, Series 60, Block 0.70.

The Newman computation neglects everything but buoyancy. For many models tested at the David Taylor Model Basin, the resonant frequencies of heave and pitch are sufficiently high so that in a zero speed test, the wave length components that produce significant pitch and heave motions act at frequencies which are considerably below resonance. The resulting motions are essentially a wave force measurement or the response of the ship without ship dynamics. The comparison between computed and measured zero speed response is very impressive.

A detailed frequency analysis was conducted for one test shown in Figs. 13 and 14, and wave height transform amplitudes were computed for the same wave program measured without the model in the water. This was done in order to remove the hypothesized effect of model generated waves. A comparison of analyzed wave heights measured under these various conditions is presented in Fig. 15 which shows a large percentage variation in the high frequency range.

The heave/pitch ratio for these tests is shown in Fig. 16. The ratio demonstrates a considerable consistency except for some of the regular wave values. These deviations, together with Fig. 13, lead to a strong suspicion that the heave measurements during the regular wave tests at 0.4 and 0.55 cps were low.

The results of this second series of transient tests added further experimental support for the utility of transient waves in ship model testing. In most cases, frequency response functions could be estimated with about 10 percent

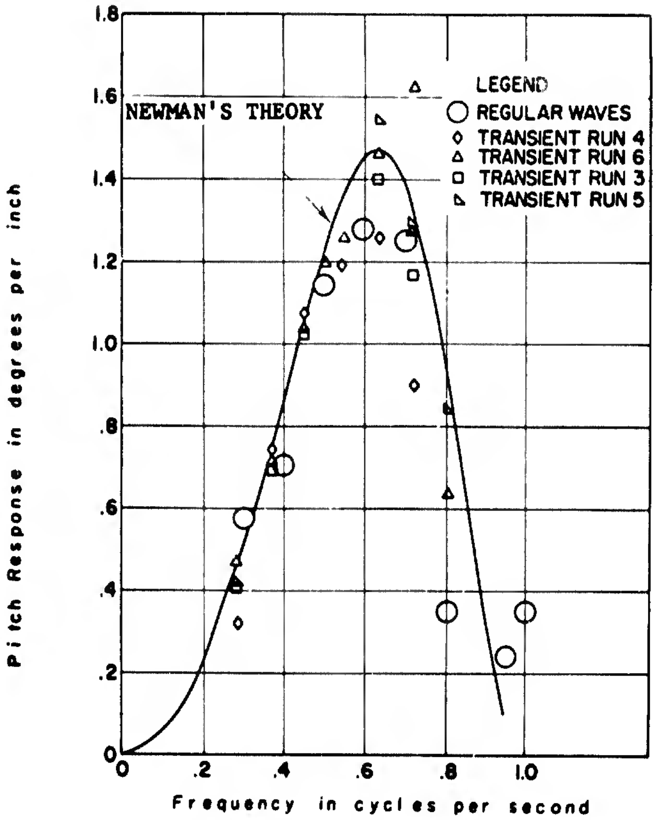

Fig. 14 - Pitch response for Model 4606 at zero speed in head waves; transient test compared with regular wave test results

accuracy. By far the major source of error concerned the measurement of wave height, either through the corruption of the incoming wave with model-generated waves or through some nonlinear mechanism associated with water dynamics or wave measurement.

Several further improvements in test technique appeared feasible as a result of this second series. First, the use of an excitation voltage with varying frequency and constant amplitude resulted in a water wave having essentially the same frequency but an amplitude which reflected the sensitivity of the wave-making system to certain frequencies. This type of excitation influences the magnitude of the wave height transform; see Fig. 15 which shows these large variations over the frequency range. It was felt that preliminary amplitude weighting of the control voltage would counteract the known frequency characteristics of the basin and produce a wave with more uniform distribution of energy over the frequency interval used in testing. The result would be that (1) extraneous "noise" in wave measurement would be overridden by significant amplitude

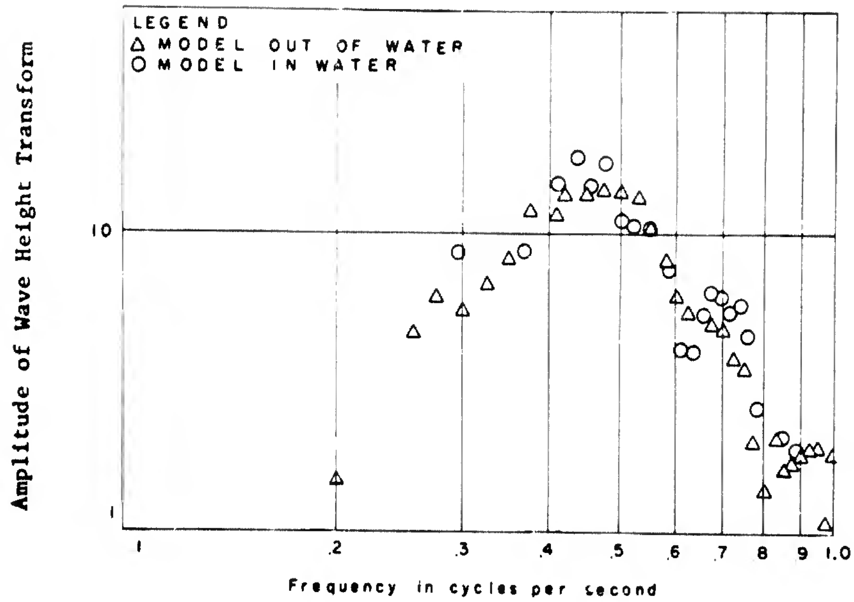

Fig. 15 - Comparison of wave height measurements made with two probes with and without model in water

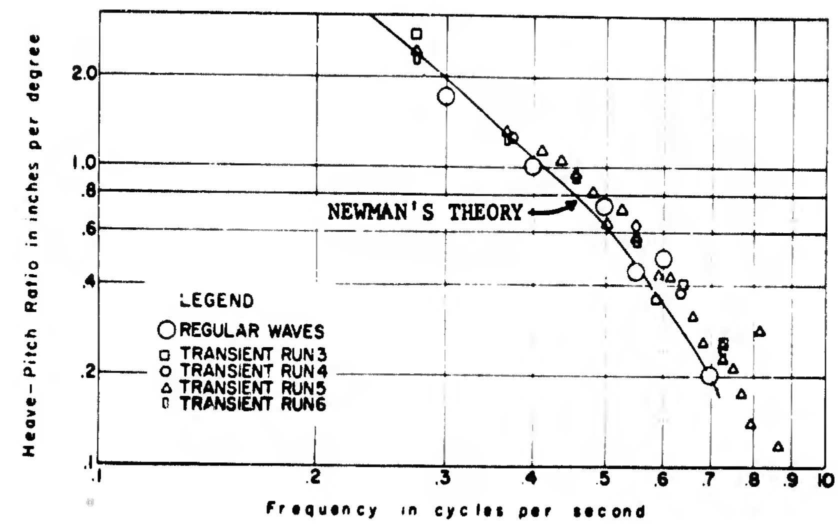

Fig. 16 - Heave/pitch ratio for Model 4606 at zero speed in head waves; transient test compared with regular wave test results

of the exciting wave and (2) transfer function computation would not involve the ratio of two rapidly varying transform amplitudes.

Another desirable feature of an adequate comparison between transient and regular wave testing was highlighted by the variations in heave transfer function measurement using regular waves (as observed in Fig. 13). To minimize questions as to the accuracy of tests in regular waves, a large number of tests should be conducted throughout the frequency range — many more than are usually called for in routine testing.

Test Series 3

The third and final series of transient tests to be presented in this report was conducted in April 1963, using Model 4889. Heave and pitch were again measured in ahead waves, and wave height was provided by two sonic probes mounted 12 and 20 ft ahead of the model center of gravity.

The program used in this series is shown in Fig. 17. Based on the observed frequency behavior of previous transient tests, both amplitude and frequency sweep rate were varied so as to yield the proper cancellation of basin frequency response.

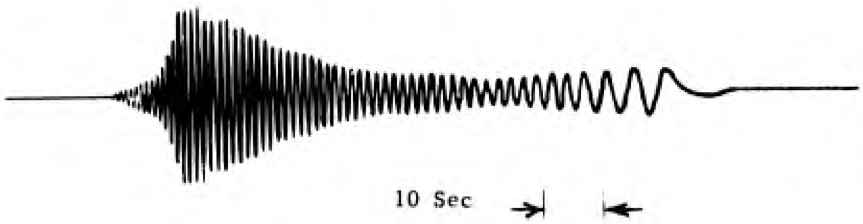

Fig. 17 - Excitation voltage program for third series of transient tests

Regular and transient tests were conducted at zero speed and at a model speed corresponding to a Froude number of 0.14. The transfer function plots — heave, pitch, and heave/pitch — are presented in Figs. 18, 19, and 20, respectively, for zero speed. The corresponding phase data are presented in Fig. 21. The agreement between the regular wave tests and the transient tests is impressive. Of special interest is the heave/pitch ratio, which, of course, is independent of wave-height measurement error. The agreement between regular and transient wave tests shown in these figures presents the strongest indication of the potential accuracy of the transient technique, and incidentally, of the linearity of motion response of a ship in waves. Note also that the pitch transfer function in Fig. 19 demonstrates, convincingly through a close-spaced series of regular wave tests, the lack of smoothness of pitch response when examined in detail.

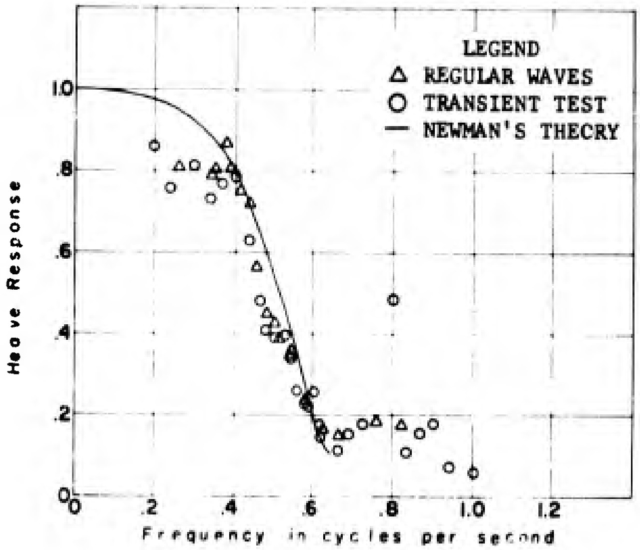

Fig. 18 - Heave response for Model 4889 at zero speed in head waves; transient test compared with regular wave test results

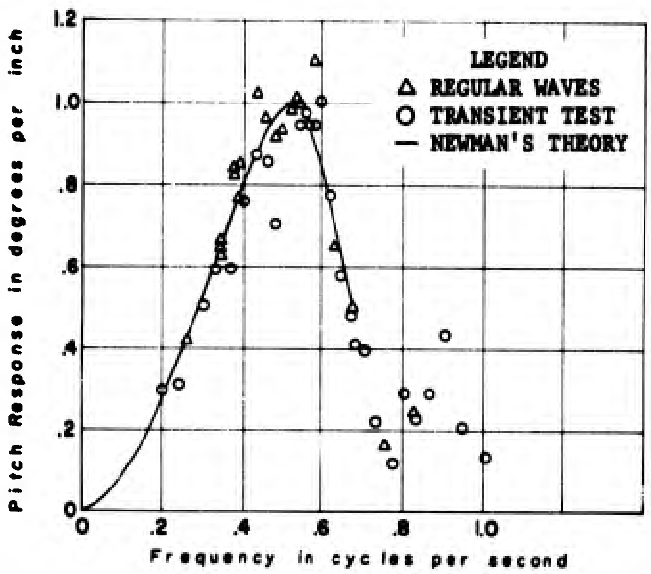

Fig. 19 - Pitch response for Model 4889 at zero speed in head waves; transient test compared with regular wave test results

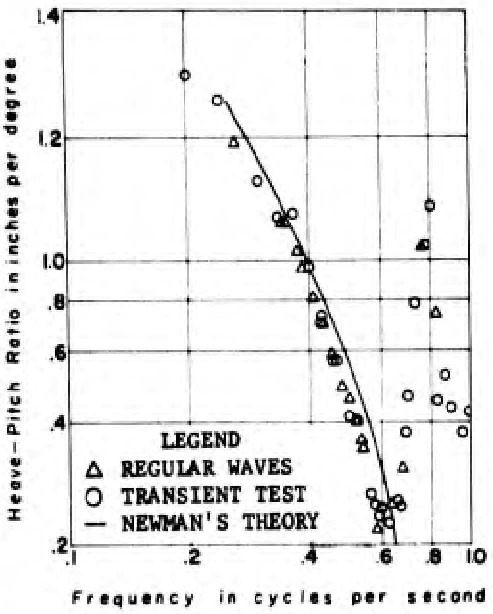

Fig. 20 - Heave/pitch ratio for Model 4889 at zero speed in head waves; transient test compared with regular wave test results

The ahead speed results are presented in Figs. 22, 23, 24, and 25 where again good correlation is noted.

The appearance of transient wave records taken during this series is somewhat different from that of earlier test records. Figure 26 shows the zero-speed test with a wave height record which appears to be distorted in contrast with the smooth quasi-sinusoidal wave behavior presented earlier in Fig. 12. This is a result of one of the techniques which was used to vary the transform amplitude of the input voltage to the wavemakers, a varying frequency sweep rate which caused a nonuniform deformation of the wave shape.

The progressive transformation of this wave shape is shown in Fig. 27, which presents measurements taken on the program at three locations. For contrast, similar measurements for the transient of the second series of tests are given in Fig. 28, where the contraction of the shape is much more orderly. In both figures, waves were measured without a model in the water.

Another interesting test performed during this series employed a human transient generator. To investigate the degree of corruption of wave height recording by model-generated waves, the model was made to oscillate in pitch by manually forcing the bow over a range of frequencies. Generated waves were measured by the two forward wave probes and analyzed for their Fourier content, along with the motion record. The transfer functions, wave height/pitch motion, are given in Fig. 29, where for the nearer probe an average wave height of 1 in. results for a pitch motion of 5 deg over the high-frequency band. The effect of heave is neglected.

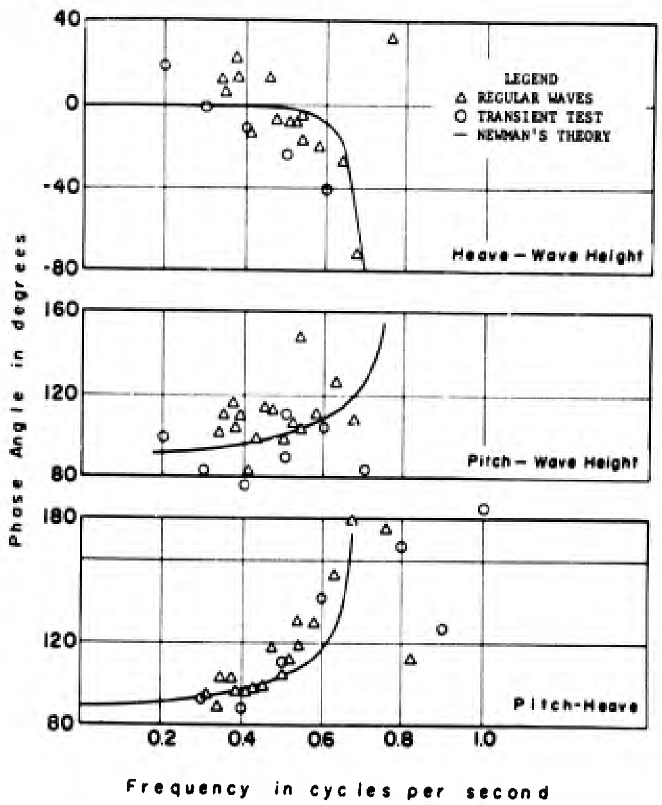

Fig. 21 - Phase angle between pitch-wave height, heave-wave height, and pitch-heave at zero speed; transient test compared with regular wave test results

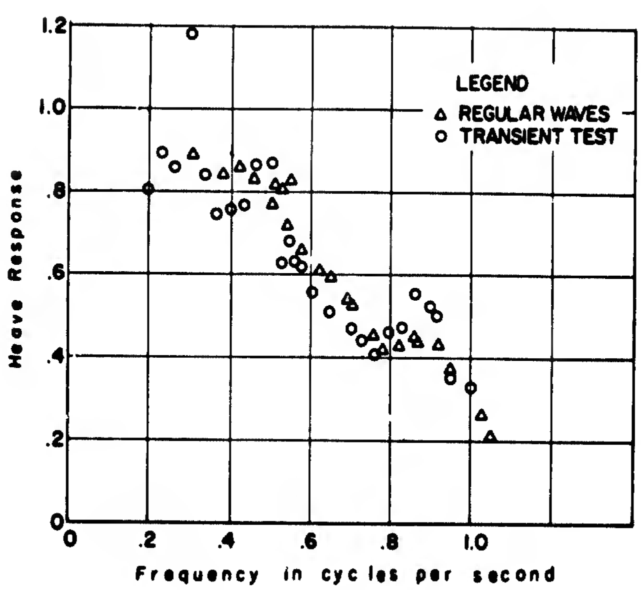

Fig. 22 - Heave response for Model 4889 in head waves at a Froude number of 0.14; transient test compared with regular wave test results

221-249 O - 66 - 35

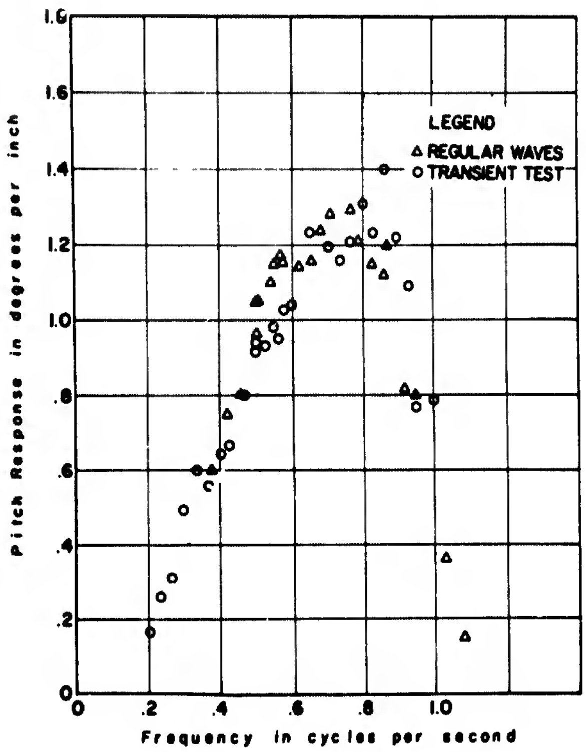

Fig. 23 - Pitch response for Model 4889 in head waves at a Froude number of 0.14; transient test compared with regular wave test results

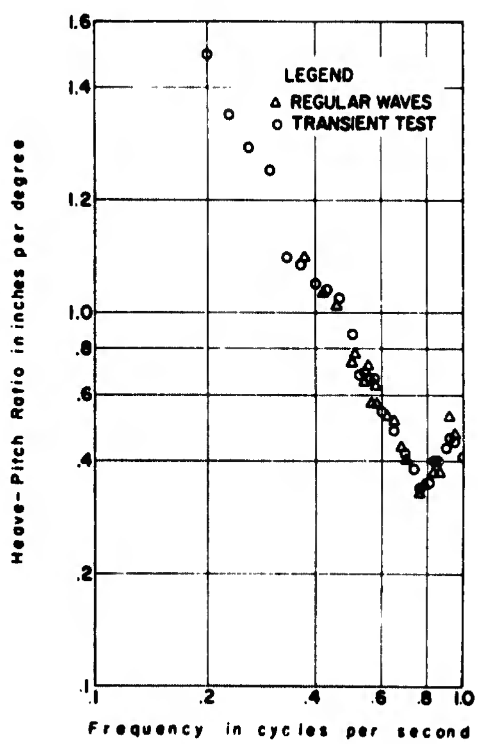

Fig. 24 - Heave/pitch ratio for Model 4889 in head waves at a Froude number of 0.14; transient test compared with regular wave test results

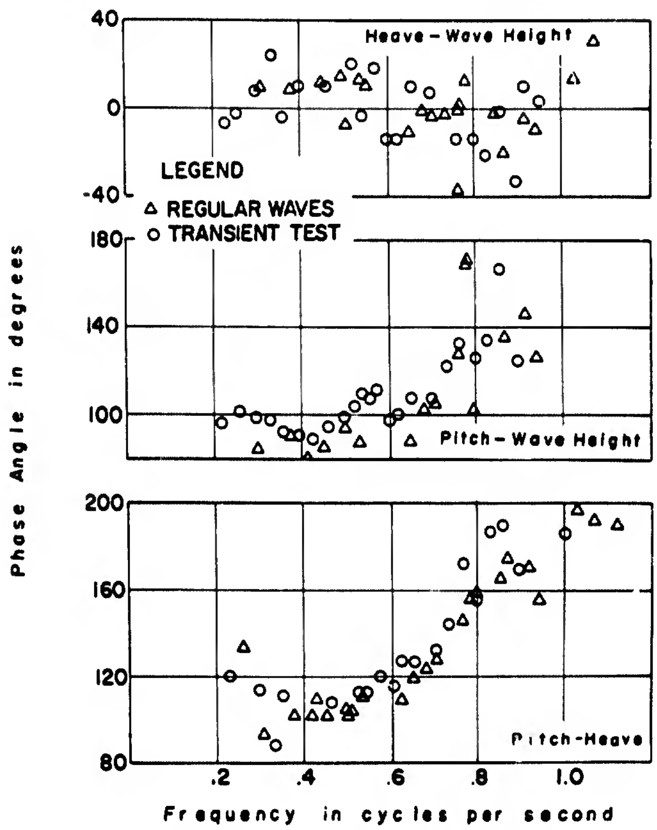

Fig. 25 - Phase angle between pitch-wave height, heave-wave height and pitch-heave at a Froude number of 0.14; transient test compared with regular wave test results

The results of this final series of tests show clearly that the transient technique is a usable tool for the investigation of ship response to waves; however, further improvement is possible. When considering (1) the very close agreement between transient and regular heave/pitch ratios observed in Figs. 20 and 24 and (2) the variation in the other frequency response estimates that is due solely to choice of forward or after wave height probe, an unwavering finger of suspicion points to the measurement of the dynamic wave disturbance.

Figure 30 compares the wave height transform of the zero-speed transient, with that of the forward speed run properly transferred to the frequency scale of the stationary measurement. The general agreement is quite good, but the difference resulting from measurements made only 8 ft apart on the same wave — with forward and after probes — is puzzling.

To weigh the possibility of this difference being associated with model-generated waves, Fig. 31 displays the same wave height transform at zero speed compared with that of a similar measurement made under identical conditions except that the model was not in the water. The agreement is not impressive,

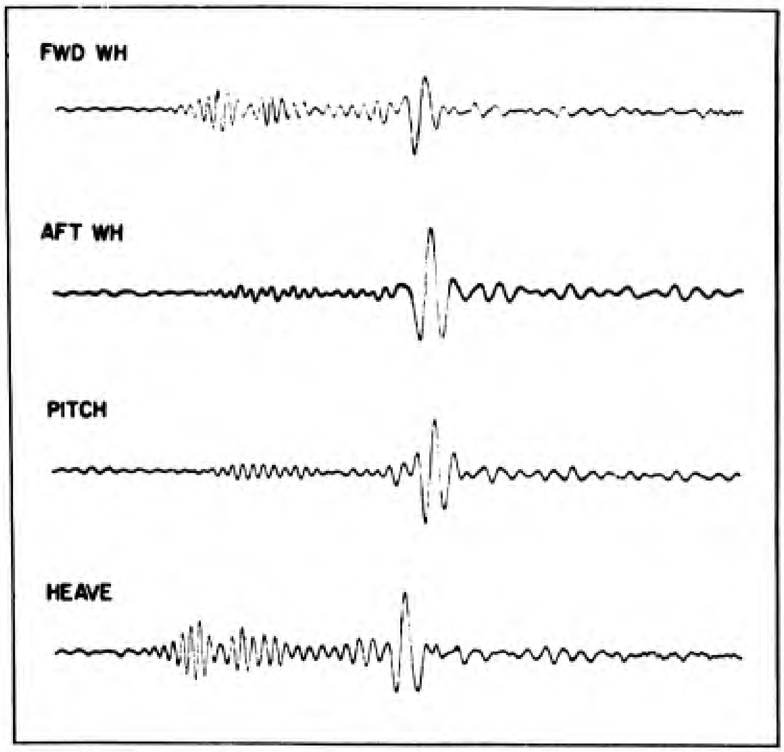

Fig. 26 - Record of transient test conducted with Model 4889 at zero speed in head waves

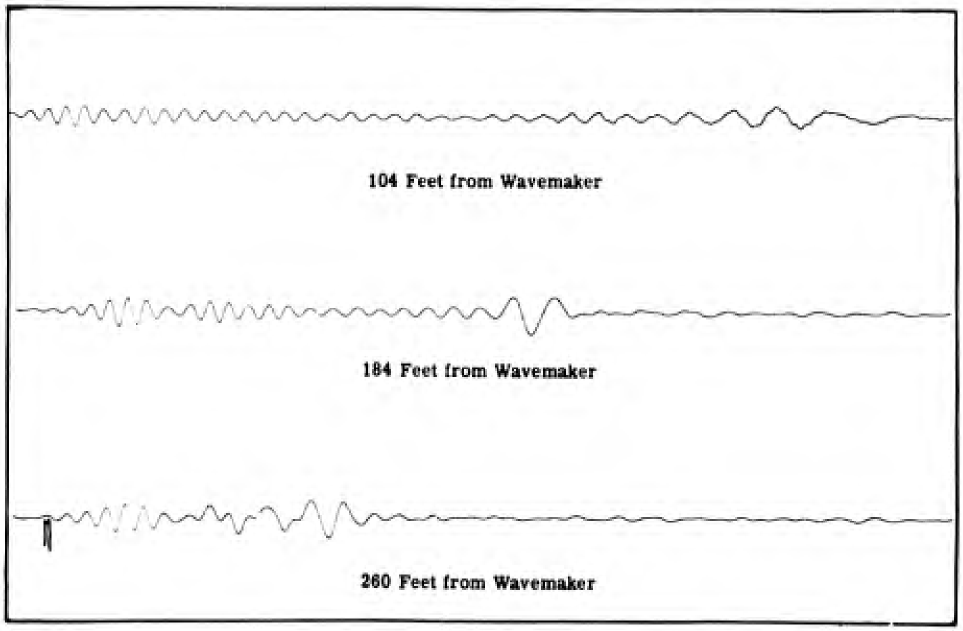

Fig. 27 - Transient waveform measured at various locations in basin; program used in third series of test

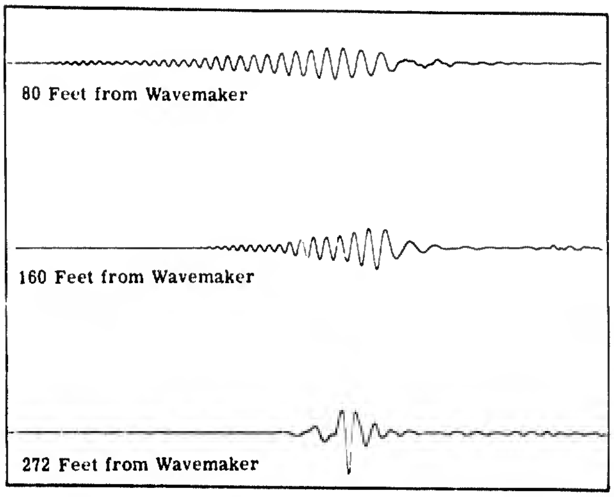

Fig. 28 - Transient waveform measured at various locations in basin; program used in second series of test

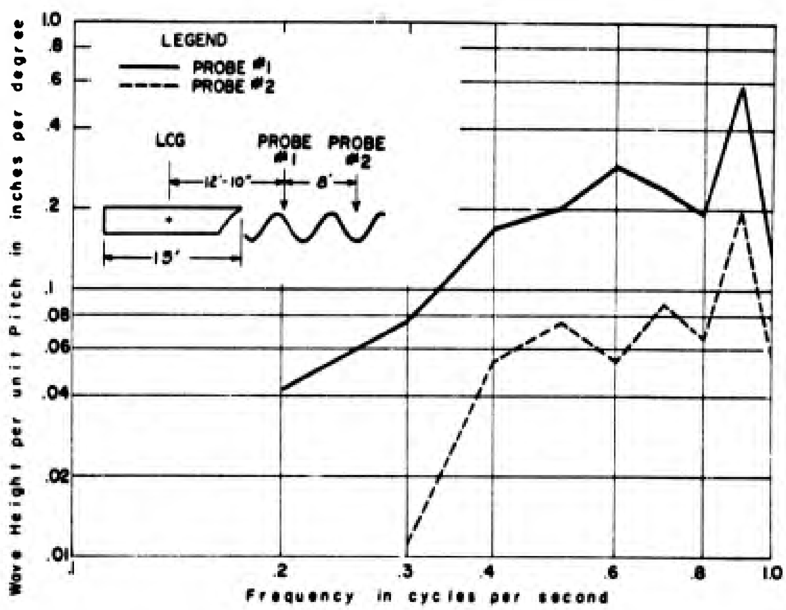

Fig. 29 - Model generated wave height/forced ratio; effect of motion generated waves on forward wave height measurement

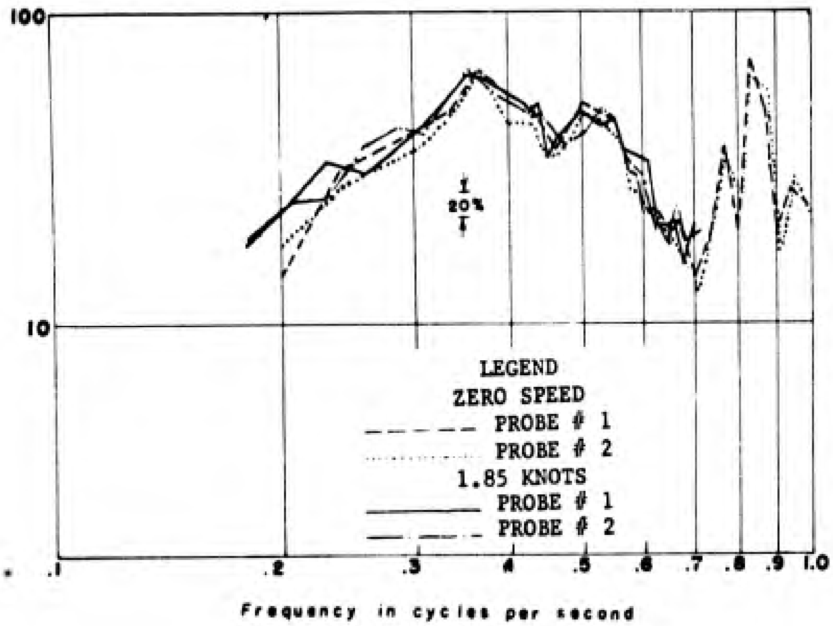

Fig. 30 - Comparison of transient wave height spectra measured during zero and forward speed runs with Model 4889

and the wave transforms of the latter measurement do not correlate well, forward probe with after probe. The remaining sources of error in the wave height transform estimate have obviously not been isolated by these tests.

AREAS OF CONTINUING DEVELOPMENT EFFORT

General

The understanding and counteracting of the various factors leading to an inaccurate wave height measurement will be undertaken as the major effort in developing further the capability of the transient wave test. A series of tests in waves, with and without a model, is planned in order to investigate the error contributions from (1) nonlinear water dynamics, (2) nonlinear measurement by the wave height probe, (3) spatial variations in basin waves, (4) side or end reflections, (5) residual waves after passage of the main wave, (6) faulty Fourier analysis, (7) electronic interaction between adjacent wave probes, and (8) model-generated waves.

A second major goal will be the development of a program for a transient wave with linear sweep rate, constant amplitude over the frequency range of interest, and smooth starting and ending, so as to minimize initial and terminal transients and the extraneous "noise" at the end of the wave train.

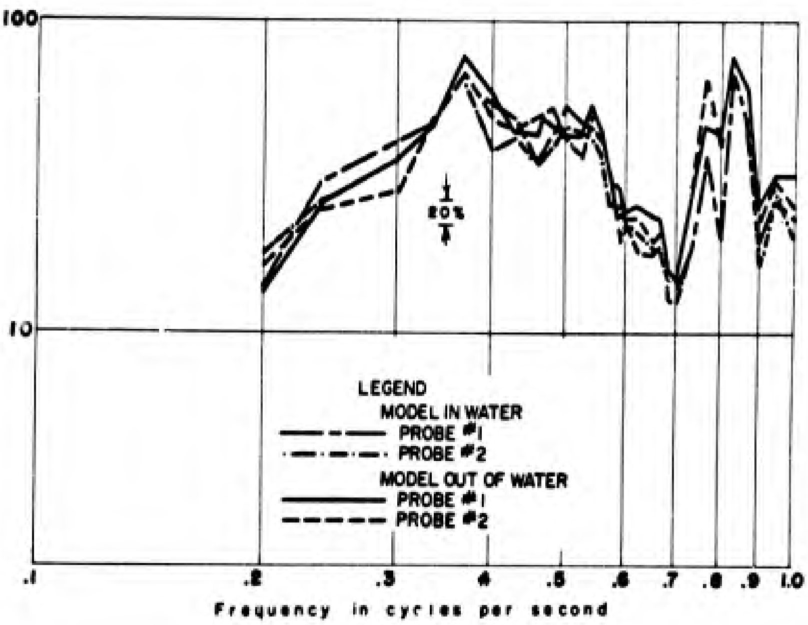

Fig. 31 - Comparison of transient wave height spectra measured with and without model in water at zero speed

To assist in these investigations and to speed up data analysis, digital computer programs are being written for Fourier transform computations. An important part of these programs will be the "smoothing" of the transient records prior to transformation, or the multiplication of all time histories by a quantity which is unity over the duration of the test and eases to zero at the beginning and end of the test. This smoothing, standard in spectral analysis, will considerably reduce the effect of residual noise in the water near the end of a run.

After more experience has been gained in forward speed runs, a critical analysis must be made to determine the effect of surge variations in transient analysis. This very knotty theoretical problem might require conducting wave transient tests at reduced wave height levels in order to avoid the time distortion of motion records.

The particular problems associated with tests in astern waves must be resolved. Unfortunately, a given frequency measured in the water with respect to the moving model can originate from astern waves at three different wave lengths. This ambiguity may force the use of transient waves with energy in more limited frequency bands, the use of multiple wave probes to make use of phase information, or both.

Special Use of the Transient Testing Technique

In one interesting use of a transient test, the variance of all motions in a given unidirectional random seaway can be found directly without need for frequency analysis. To show how this can be done, consider the equation which relates mean square motion $\overline{m^2}$ to the wave power spectral density at the frequency of encounter $\Phi(\omega)$ and to the applicable transfer function $G(\omega)$:

$$\overline{m^2} = \frac{1}{2\pi} \int_{-\infty}^{\infty} d\omega \; \Phi(\omega) \; |G(\omega)|^2 . \tag{22}$$

In a transient test, the integral square motion is given by

$$\int_{-\infty}^{\infty} dt \; m^2(t) = \frac{1}{2\pi} \int_{-\infty}^{\infty} d\omega \; |N(\omega)|^2 \; |G(\omega)|^2 \tag{23}$$

where $N(\omega)$ is the Fourier transform of the measured wave height, using a well-known relation from linear systems theory. Thus, if $N(\omega)^2$ is programmed to be equal to the wave height spectrum $\Phi(\omega)$, we have

$$\underbrace{\overline{m^2}}_{\text{Random}} = \underbrace{\int_{-\infty}^{\infty} dt \; m^2(t)}_{\text{Transient}} . \tag{24}$$

Simple analog data processing, conducted during the model test, would square and integrate the motions of interest and yield, at the end of the run, voltages proportional to motion variances in the defined random seaway.

Although such a simplified scheme of data processing would not extract much of the significant information available from a transient test, it is conceivable that there might be occasions when a very fast answer to the seaworthiness characteristics of a ship form in a given seaway would be required. One example would be a search for the worst combination of speed and heading.

GENERAL APPLICATIONS OF THE TRANSIENT TECHNIQUE

The method for producing a transient water wave described in this report was developed in order to take account of the behavior of waves on a free surface. The form of this wave, however, would appear to have considerable promise for applications in many linear systems investigations.

Conventionally, a pulse-like transient is used for system excitation. The frequency range of the excitation is determined primarily by the concentration of the transient about a single point in time, and the amount of signal needed to produce measurable response is a function of the amplitude levels of the pulse. As a consequence, to faithfully reproduce a rapidly changing signal, measurement requirements are severe and the probability of nonlinear behavior of the system under test is high because of the large inputs often required to override the effects of measurement noise in the recorded output signal.

The use of a signal with linearly varying frequency and constant amplitude as an input signal removes these strong drawbacks to the pulse technique, however. Since it has constant amplitude, the input can be constrained to lie within the linear range. With proper choice of sweep rate and starting frequency, the controlled signals can have any desired energy level in each frequency band and thus defeat to a great extent the effects of random measurement noise.

Another strong advantage in the use of transients with a linear sweep rate is that in many cases the entire transfer function of a system can be obtained by cursory analysis of the transient records alone. If the rate of change of frequency and amplitude is slow enough, the signals involved behave very much like sinusoidal waves. From the integration method of stationary phase [2], it can be shown that the amplitude of the transform at frequency ω of such a signal is equal to one-half of the single amplitude of the signal at the apparent local frequency ω divided by the square root of the rate of frequency change (in cps/sec). Such a computation was performed for the transient test shown in Fig. 13 for the heave measurement. The results of this computation for the heave transfer function are shown in Fig. 32. This figure compares the measurement and calculation techniques and shows that there is good agreement among them.

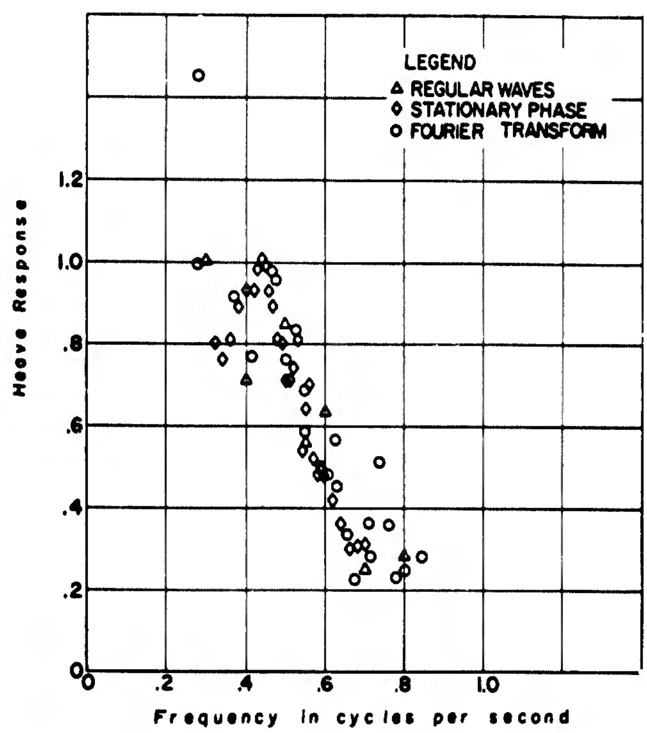

Fig. 32 - Comparison of methods of analysis of heave response operators

SUMMARY AND CONCLUSIONS

The complete determination of the response of a ship in regular waves involves a large and expensive testing program. When the transient wave technique is used properly, the total testing time can be reduced by an order of magnitude.

In a theoretical discussion of ship dynamics, it has been stated that the usual systems representation of ship motion as an "output" and wave height as an "input" is a misconception; both dynamic quantities are "output." Water wave transients traveling in a single direction can be readily analyzed with the use of Fourier transforms; the transforms of two measurements on a single wave transient are related by the so-called "transfer function" of water, $e^{-j\omega|\omega|x/g}$, where x is the distance separating the measurement points in the direction of wave travel.

The wave used at the Model Basin for transient testing has a continuously increasing wave length which results in an intense concentration of wave energy for a short period of its travel. Model transient tests are commenced in calm water, then passed through a wave having energy in all frequencies of interest, and eventually returned to the smooth water condition. The transfer function for a particular motion variable is found for all frequencies by dividing the Fourier transform of the motion transient by that of the wave height record, referenced to the model center of gravity. With a suitably tailored wave transient, mean square motion levels in a particular random seaway can be found immediately by squaring and integrating the motions during a transient test.

Transient tests conducted on three models in ahead waves have verified the theory presented. Close agreement between transient and regular wave tests has been obtained for heave and pitch motions at zero and forward speed. The major difficulty encountered has been in the generation and measurement of waves, where further refinements and research are proposed. Digital programs are being written for the bulk processing of transient records.

Finally, the technique of using a transient excitation which is a linear frequency sweep is an original contribution to general linear systems analysis; it has virtues of linearity and noise-immunity, the capability of determining frequency response of a system by visual inspection of the transient records.

Appendix

WEIGHTING FUNCTION OR IMPULSE RESPONSE OF WATER

It has been shown in this report that the operator $e^{-j\omega|\omega|x/g}$ is the frequency response function that relates wave height measured at two points separated by a distance x in the direction of travel. The weighting function $w(\tau)$ can be determined by taking the inverse Fourier transform of the frequency response function:

$$w(\tau) = \frac{1}{2\pi}\int_{-\infty}^{+\infty} e^{-j\omega|\omega|x/g}\, e^{j\omega\tau}\, d\omega . \tag{A-1}$$

Expanding into trigonometric terms and noting the symmetrical properties of the function, we have after simplification

$$w(\tau) = \frac{1}{\pi}\int_0^{\infty} \cos\,(-\omega^2\, x/g + \omega\tau)\, d\omega = \frac{1}{\pi}\int_0^{\infty} \cos\,(\omega^2\, x/g - \omega\tau)\, d\omega . \tag{A-2}$$

Employing the technique used by Lamb [7] we let

$$\zeta = \frac{x^{1/2}}{g^{1/2}}\left(\omega - \frac{g\tau}{2x}\right)$$

and

$$\sigma = \frac{g^{1/2}\tau}{2x^{1/2}} .$$

These terms are substituted into Eq. (A-2), yielding

$$w = \frac{1}{\pi}\,\frac{g^{1/2}}{x^{1/2}}\int_{-\sigma}^{\infty} \cos\,(\zeta^2 - \sigma^2)\, d\zeta$$

$$= \frac{1}{\pi}\,\frac{g^{1/2}}{x^{1/2}}\left[\int_{-\sigma}^{0} \cos\,(\zeta^2 - \sigma^2)\, d\zeta + \int_0^{\infty} \cos\,(\zeta^2 - \sigma^2)\, d\zeta\right]$$

$$= \frac{1}{\pi}\,\frac{g^{1/2}}{x^{1/2}}\left\{\cos\sigma^2\left[\int_{-\sigma}^{0} \cos\,\zeta^2\, d\zeta + \int_0^{\infty} \cos\,\zeta^2\, d\zeta\right]\right.$$

$$\left. + \sin\sigma^2\left[\int_{-\sigma}^{0} \sin\,\zeta^2\, d\zeta + \int_0^{\infty} \sin\,\zeta^2\, d\zeta\right]\right\} . \tag{A-3}$$

We can make the following identification:

$$\int_{-\sigma}^{0} \cos\,\zeta^2\, d\zeta = \int_0^{\sigma} \cos\,\zeta^2\, d\zeta = \frac{\sigma}{|\sigma|}\sqrt{\pi/2}\;\; C(\mu) ;$$

$$\int_{-\sigma}^{0} \sin\,\zeta^2\, d\zeta = \int_0^{\sigma} \sin\,\zeta^2\, d\zeta = \frac{\sigma}{|\sigma|}\sqrt{\pi/2}\;\; C(\mu) ;$$

$$\int_0^{\infty} \sin \zeta^2 \, d\zeta = \int_0^{\infty} \cos \zeta^2 \, d\zeta = \frac{1}{2}\sqrt{\pi/2}$$

where

$$C(\mu) \triangleq \int_0^{\mu} \cos\left(\frac{1}{2}\pi\mu^2\right) d\mu \, ; \qquad S(\mu) \triangleq \int_0^{\mu} \sin\left(\frac{1}{2}\pi\mu^2\right) d\mu \, .$$

Substituting the above into Eq. (A-3), yields

$$w = \left(\frac{g}{2\pi x}\right)^{1/2} \left\{ [\cos \sigma^2] \left[\frac{1}{2} + \frac{\sigma}{|\sigma|} C\left(\sqrt{2/\pi} \times \sigma\right)\right] + [\sin \sigma^2] \left[\frac{1}{2} + \frac{\sigma}{|\sigma|} S\left(\sqrt{2/\pi} \times \sigma\right)\right]\right\} .$$

For simplification, let

$$a = \left(\frac{g}{2\pi x}\right)^{1/2} .$$

Then

$$\sigma = \sqrt{\pi/2} \times a\tau$$

and

$$w(a\tau) = a \left\{ \left[\cos \frac{\pi}{2} a^2 \tau^2\right] \left[\frac{1}{2} + \frac{\tau}{|\tau|} C(a\tau)\right] + \left[\sin \frac{\pi}{2} a^2 \tau^2\right] \left[\frac{1}{2} + \frac{\tau}{|\tau|} S(a\tau)\right]\right\} . \qquad \text{(A-4)}$$

For large values of a or τ, going back to Eq. (A-3), we find that

$$w(a\tau) \approx a \left\{\left[\cos \frac{\pi}{2} a^2 \tau^2 + \sin \frac{\pi}{2} a^2 \tau^2\right]\right\}$$

$$= \sqrt{2} \, a \cos\left(\frac{\pi}{2} a^2 \tau^2 - \frac{\pi}{4}\right)$$

$$= \sqrt{\frac{g}{\pi x}} \cos\left(\frac{g\tau^2}{4x} - \frac{\pi}{4}\right) \qquad \tau >> 0 \, . \qquad \text{(A-5)}$$

REFERENCES

1. St. Denis, M. and Pierson, W. J., "On the Motions of Ships in Confused Seas," Transactions, The Society of Naval Architects and Marine Engineers, Vol. 61 (1953).

2. Stoker, J. J., "Water Waves," Interscience Publishers, Inc., New York (1957).

3. Brownell, W. F., "Two New Hydromechanics Research Facilities at the David Taylor Model Basin," Presented before Chesapeake Section, The Society of Naval Architects and Marine Engineers (Dec 1962). Also David Taylor Model Basin Report 1690 (Dec 1962).

4. Davis, M. C., "Simulation of a Long Crested Gaussian Seaway," David Taylor Model Basin Report 1755 (Mar 1963).

5. Huskey, H. D., et al., "Computation of Fourier Integrals without Analog Multipliers," Computer Handbook, McGraw Hill Book Co., Inc., New York (1962).

6. Newman, J. N., "A Slender Body Theory for Ship Oscillations in Waves," In Preparation for Journal of Fluid Mechanics.

7. Lamb, H., "Hydrodynamics," Sixth Edition, Dover Publications (1945).

* * *

DISCUSSION

E. V. Laitone
University of California
Berkeley, California

Since the linearized equations of motion for either the pitch or the roll of a ship in regular waves can be written as

$$\ddot{\theta} + b\dot{\theta} + k\theta = A_0 \; I_m \; e^{i\omega t}; \tag{1}$$

therefore there is a distinct advantage in running a series of model tests in regular waves. This advantage over the pulse or transient-type wave test occurs because Eq. (1) represents a circle in the velocity amplitude and phase plane as shown in Fig. 1

$$|\dot{\theta}| = \frac{A_0}{b} \cos \phi_{\dot{\theta}} \; . \tag{2}$$

Consequently the departure of the experimental points from a perfect circle for varying values of the regular wave frequency (ω) directly indicates either the nonlinear effects, or the dependence of b or k upon ω, for constant values of A_0. Similarly varying A_0 and repeating the tests for different values of ω illustrates the nonlinear dependence of b or k upon the amplitude (A_0) of the regular wave. A transient wave test could not so easily pin-point the wave frequencies or amplitudes that correspond to a breakdown of the assumed linearity which results in Eq. (1).

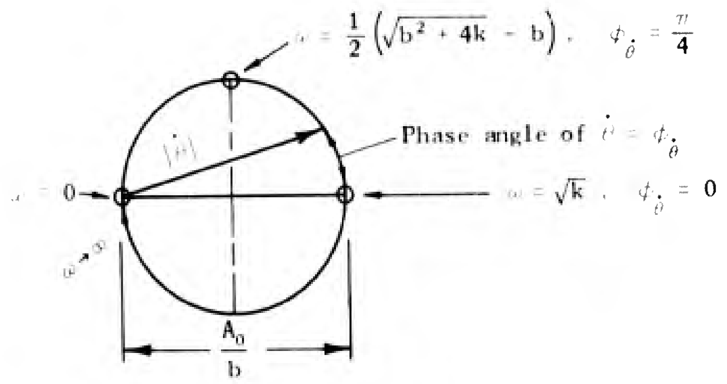

Figure 1

In addition various other simple relations can be derived for determining b or k quickly. For example when the phase angle of the response $\dot{\theta}$ is exactly 90° with respect to the regular wave at frequency ω, then

$$\omega = \sqrt{k}, \qquad |\theta| = \frac{A_0}{b\omega} = \frac{A_0}{b\sqrt{k}}. \tag{3}$$

Similarly if the phase angle of $\dot{\theta}$ is exactly 45° then

$$|\theta| = \frac{A_0}{\sqrt{2}\,(k - \omega^2)} = \frac{A_0}{\sqrt{2}\,(b\omega)}. \tag{4}$$

* * *

REPLY TO THE DISCUSSION

M. C. Davis and E. E. Zarnick
David Taylor Model Basin
Washington, D.C.

Mr. E. V. Laitone is apparently unaware of some of the more recent developments in the area of ship motions. It has been known for some time that second-order differential equations do not properly describe ship motions, particularly in the pitch and heave modes which we have concerned ourselves with in our paper. This problem has been glossed over in the past by the use of frequency dependent coefficients. The tests in waves are further complicated by the fact that the wave height (referenced at the center of gravity) is defined as the input to the system which results in a particular amplitude phase relationship exclusive of any dynamics effects. Consequently, these data would not be expected to describe a circle if plotted in the velocity phase plane as suggested by Mr. Laitone, and furthermore, the departure from such a circle would shed no light as to the nature of the problem. A better understanding of the problem can be obtained by separating the effects of added mass, damping, cross coupling and hydrodynamic memory by use of the integro-differential equations of motion developed by Dr. Cummins. This information, along with knowledge of the wave excitation, should provide us with information as to why a ship performs the way it does as well as possible changes in design to improve her seakeeping qualities.

We would like to apologize to Dr. Leo Tick* if we have in any way contributed to his confusion. We are also very grateful for his pedagogical dissertation on the basic philosophy of testing. Of special note is his recollection of profound personal conversations (with someone whose name he can't quite remember). Apparently the choice of a suitable test function is not clear to him. This is understandable. The choice of a test function or procedure depends upon many factors. We may be less philosophical and more pragmatic; this choice in the final analysis depends upon whether or not it serves the purpose intended, i.e., to provide an efficient and economical means of obtaining a reliable measurement of the transfer functions. We believe that the transient test technique meets these objectives. We have provided both theoretical and experimental evidence to support our claims. It is anyone's prerogative to accept or reject them.

* * *

*See discussion by Tick (p. 457) on paper by Smith and Cummins.

PREDICTION OF OCCURRENCE AND SEVERITY OF SHIP SLAMMING AT SEA

Michel K. Ochi
David Taylor Model Basin
Washington, D.C.

ABSTRACT

Basic properties which govern ship slamming in rough seas are discussed from theoretical consideration. Specifically, the probability of occurrence of slamming, magnitude of impact pressure associated with slamming, and time interval between successive slams are studied from a statistical approach, and formulae are derived for the prediction of these events. The prediction method is also applied to the problem of deck wetness caused by shipping of green water at sea. Theoretical results are compared with those obtained in experiments conducted on a MARINER model in rough seas.

INTRODUCTION

When a ship navigates at certain speeds in rough seas she frequently experiences slamming at which time the forward bottom sustains large forces resulting from the impact.

Slamming occurs at random at sea. The severity of slamming and time interval between two successive slams are also at random. Sometimes a ship may slam successively with varying intensity; while again no slamming may occur for a relatively long period of time and then suddenly a severe slam occurs. In statistical terms slamming is a random phenomenon, and the severity and time interval between successive slams are random variables. For this random phenomenon, only one study has appeared in the literature as of this date. This study made by Tick concerns the prediction of the rate of occurrence of slamming at sea [1].

The purpose of the present paper is to develop a method for predicting the probability of occurrence and severity of slamming, and the time interval between successive slams in rough seas. Specifically, it is the intent of this paper to predict the following:

(a) Probability of occurrence of slamming for given conditions, such as for a given sea state, course angle, loading condition, etc.

(b) Probability distribution of impact pressure associated with slamming, and magnitudes of the average one-third and one-tenth highest impact pressures.

(c) Probability distribution of the time interval between successive slams and between two severe slams. Probability that a time, τ (or more), elapses between severe slams.

(d) Probability of occurrence and severity of deck wetness caused by shipping of green water, i.e., application of the theory to the deck wetness problem.

The above subjects are evaluated theoretically, and the results are compared with statistically analyzed experimental results obtained in tests conducted on a 13-ft MARINER model.

PREDICTION OF OCCURRENCE OF SLAMMING

Basic Concept

Prediction of the occurrence of slamming is made from two viewpoints: one being the prediction of slamming occurrence per cycle of wave encounter, the other being that per unit time. The question pertaining to how many times a ship will slam during a certain period of time belongs to the latter prediction. The basic concepts used for development of the theory for these two predictions are, however, essentially the same.

First, the conditions leading to slamming will be discussed. Szebehely has shown that three conditions should exist for slamming to occur [2]. They are: (a) bow (forefoot) emergence, (b) certain magnitude of vertical relative velocity between ship bow and wave, and (c) unfavorable phase between bow motion and wave motion. The present author has also arrived at the same conclusion through his tests [3]. Tick considered three conditions in the development of his theory for predicting the number of slams per unit time. These are: (a) bow emergence, (b) relative velocity, and (c) angle between keel line and wave surface at the instant of impact [1].

All of the above conditions were inferred from results of model experiments conducted in regular waves. The question then arises as to whether or not these are necessary and sufficient conditions leading to slamming in rough seas also. To answer this question, data obtained from slamming tests conducted in irregular waves were carefully analyzed, and two conditions leading to slamming in rough seas were obtained. They are: (a) bow (forefoot) emergence, and (b) a certain magnitude of relative velocity between wave and ship bow. In other words, the probability of occurrence of slamming is the joint probability that the bow emerges and that the relative velocity exceeds a certain magnitude at the instant of reentry.

Bow emergence is prerequisite for slamming. Results of the tests revealed that slamming never occurred without bow emergence. This was found to be true irrespective of sea state, ship speed, course angle or loading condition [4]. However, bow emergence is not a sufficient condition for slamming. There

were many cases during the tests in which no appreciable impact pressure was imparted to the ship bottom even though the forefoot emerged from the water surface. It was found that a certain magnitude of relative velocity between wave and ship bow (hereafter referred to as the threshold velocity) was required to induce slamming.

The threshold velocity is a critical relative velocity between ship bow and waves below which slamming does not occur. Although little information is available concerning the magnitude of the threshold velocity associated with slamming, the magnitude was evaluated from various available sources [3-5], and the results are tabulated in Table 1. For convenience, the values have been converted to those for a 520-ft ship for comparison with the MARINER. As can be seen in the table, the values have been obtained for various test conditions. Nevertheless, the magnitudes of the threshold velocity are nearly constant with an average of 12 ft/sec. To determine the threshold velocity for the cargo vessels (U- and V-Form) listed in Table 1, ship speed was increased until the ship started to slam in the given regular waves ($\lambda/L = 1$, $h/\lambda = 1/30$). The speeds for which slamming first appeared were 10.4 and 11.9 knots for the U- and V-Form, respectively. The relative velocities evaluated for these speeds were taken as the threshold velocities. For higher ship speeds slamming was severe, and hence the relative velocities between wave and the ship bow for these speeds could not be considered as the threshold velocity. Note that the threshold velocity is the minimum velocity which causes slamming.

In regular wave tests conducted on a high speed craft listed in the table, an immersion sensing element was fixed to the model at Station 2. Hence, the relative motion between wave and the bow was directly measured, and the relative velocity was obtained by differentiation.

It is of great interest to mention that the magnitude of the threshold velocity evaluated from the MARINER tests in irregular waves is very close to that evaluated for other types of vessels tested in regular waves. For evaluation of the threshold velocity for the MARINER the data obtained in a severe Sea State 7 at a ship speed of 10 knots were analyzed [4]. Since the wave measuring device was located 9.83 feet (410 feet full scale) ahead of the model in these tests, one assumption was introduced in the analysis. That is, waves measured at the location of the wave probe would maintain their form until they reached the ship bow. With this assumption, the magnitude of relative velocity at the instant the ship slammed was evaluated from simultaneous records of pressure, ship motion, bow vertical acceleration and wave. Figure 1 shows the relationship between relative velocity and impact pressure measured at 0.10 L aft of the forward perpendicular. As can be seen in the figure, no impact pressure is observed for a relative velocity less than 12 ft/sec. On the basis of the above finding, it is considered appropriate to take 12 ft/sec as the threshold velocity associated with slamming for a 520-ft ship. The reader's attention is called to the fact that this magnitude of threshold velocity cannot be used universally. For a ship of different length, the above given value should be modified according to the Froude scaling law.

Table 1
Threshold Velocity for Various Types of Ships
(Values are Converted to Those for a 520-ft Vessel)

Type of Ship	Cargo (U-Form)	Cargo (V-Form)	LIBERTY	MARINER	High Speed Craft (V-Form)
Block coefficient	0.741	0.741	0.733	0.624	0.479
Draft	Light	Light	Light	Light	Design
Waves	Regular	Regular	Regular	Irregular	Regular
λ/L	1.00	1.00	0.91	Severe Sea State 7	1.50
h/λ	1/30	1/30	1/16.7		1/34
Ship speed (knots)	10.4	11.9	10 (Estimated)	10.0	18.4
Location where the threshold velocity is evaluated	0.053 L aft of FP	0.093 L aft of FP	FP	0.10 L aft of FP	0.1 L aft of FP
Threshold velocity (ft/sec)	14.0	11.9	10 to 14.3	12.0	11.8
Reference	[3]	[3]	[5]	[4]	Unpublished

In connection with other proposed conditions leading to slamming (such as unfavorable phase between bow and wave motion and angle between keel and wave), it is mentioned that these are included in the two required conditions found from the present tests. For example, the phase changes from time to time in irregular waves, and it is apparent that the largest relative velocities are associated with the out of phase motions. Thus, it may be concluded that bow emergence and threshold velocity are the only conditions prerequisite to ship slamming.

It is noted here that the occurrence of impact pressure at Station 2 (0.1 L aft of the forward perpendicular) was used as a criterion for slamming. The justification of this statement is given in Ref. 4.

Probability of Occurrence of Slamming per Cycle of Wave Encounter

Let w be the wave displacement and b the bow (forefoot) displacement from their respective at rest (zero) positions (see Fig. 2). Upward displacement is

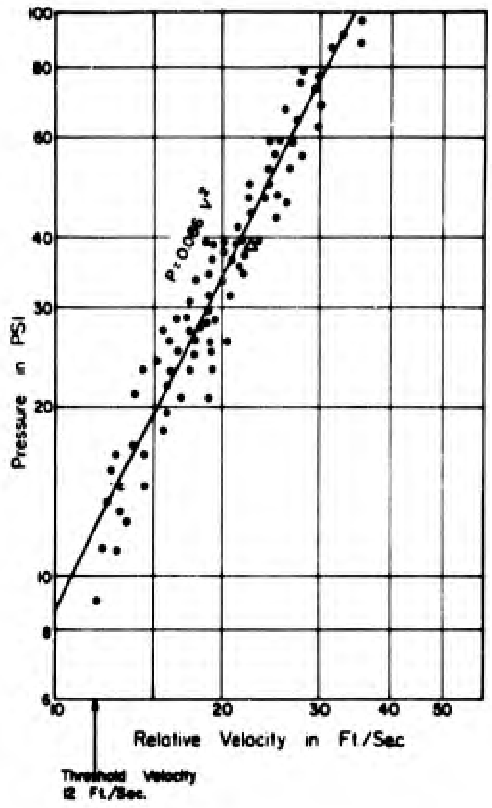

Fig. 1 - Pressure on the keel plate as a function of impact velocity (MARINER, Station 2, light draft, ship speed 10 knots, moderate Sea State 7)

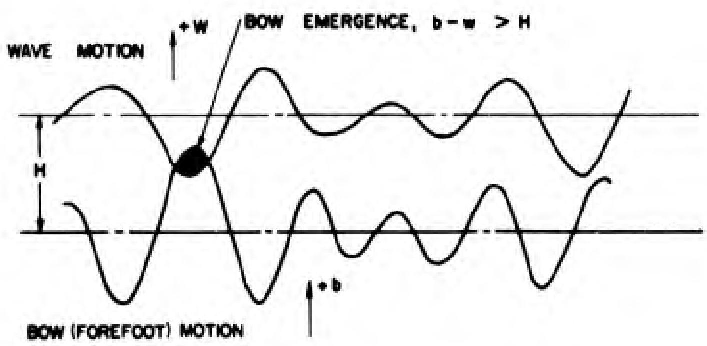

Fig. 2 - Explanatory sketch of bow emergence

taken as positive. The distance between these two zero-lines is equal to the ship draft, H, at a specific location, x (in this example, Station 2), for which the probability of slamming is evaluated. Note that this draft is not necessarily the design draft. Next, let $r = b - w$; then the relative motion, r, must always be positive and greater than H when bow emergence occurs.

For a better understanding of the relationship between slamming and relative motion, Fig. 3 was prepared. Figure 3(a) is an explanatory figure showing time history of relative motion. At the instant of a slam as the bow re-enters the water, the relative motion $r(t)$ must be positive and equal to H. The relative velocity $\dot{r}(t)$ at this instant is negative and its absolute value must be greater than the threshold velocity, $\dot{r}_*$. The above condition is given on the phase-plane diagram shown in Fig. 3(b).

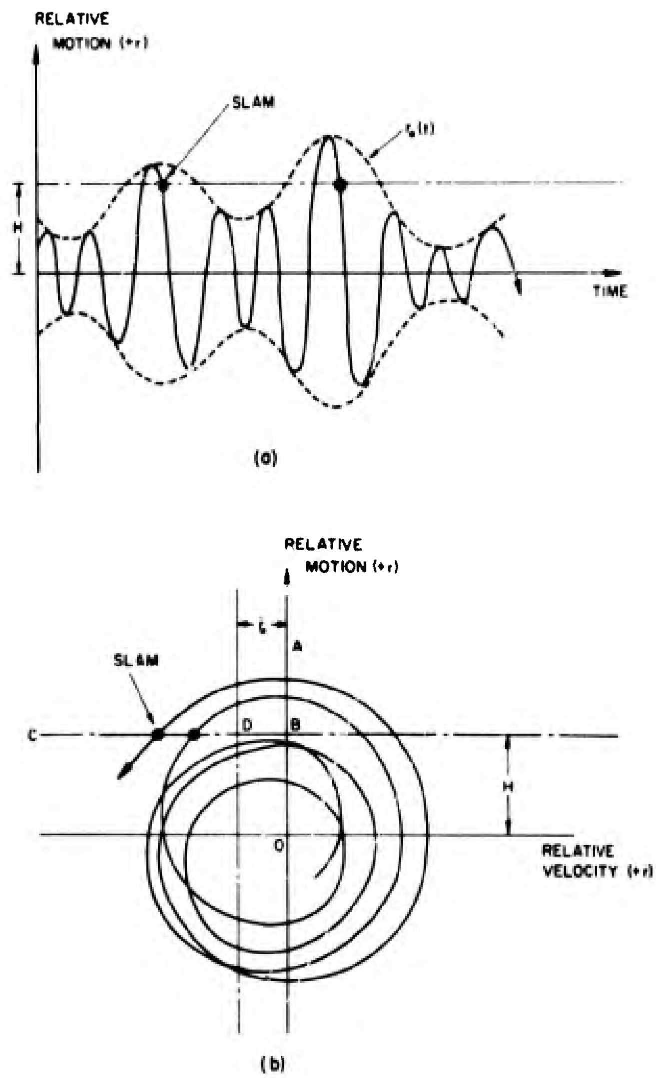

Fig. 3 - Explanatory sketch of time history of relative motion and phase-plane diagram

The relative motion is considered as a random variable having a narrow-band normal distribution with zero mean, since the relative motion is a combination of pitch, heave, and wave motions, all of which have narrow-band normal distribution with zero mean. The relative motion is expressed by the following formula

$$r(t) = r_o(t) \cos \{\omega_o t + \epsilon_o(t)\} \tag{1}$$

where

$r_o(t)$ = amplitude of the envelope of the relative motion,

ω_o = expected frequency = $\sigma_{\dot{r}}/\sigma_r$,

ϵ_o = slowly varying phase angle,

σ_r^2 = variance of relative motion,

$\sigma_{\dot{r}}^2$ = variance of relative velocity.

It is noted that the relation $\omega_o = \sigma_{\dot{r}}/\sigma_r$ holds since a narrow-band normal process with zero mean is considered. Assuming that $\dot{r}_o$ and $\dot{\epsilon}_o$ are small for a narrow-band normal process, the following equation is derived from Eq. (1).

$$r_o^2 = r^2 + \frac{\dot{r}^2}{\omega_o^2} . \tag{2}$$

Now, the probability density function of $r_o(t)$ is a Rayleigh distribution. Since slamming occurs only when the relative motion is positive, the probability density function of the positive $r_o(t)$ can be written by

$$f(r_o) = \frac{2r_o}{R_r'} e^{-\frac{r_o^2}{R_r'}} , \qquad r_o \geq 0 . \tag{3}$$

Note that Eq. (3) represents the probability density function of the cross points on the OA-line in Fig. 3(b), and that the parameter, R_r', involved in the equation is not eight times but is twice the variance of the relative motion. Hence R_r' is equal to the cumulative energy density, i.e., the area under the energy spectrum, E, using the St. Denis-Pierson definition of the spectrum. From Eqs. (2) and (3),

$$f(r_o) = \frac{2\sqrt{r^2 + \frac{\dot{r}^2}{\omega_o^2}}}{R_r'} e^{-\left(\frac{r^2 + \frac{\dot{r}^2}{\omega_o^2}}{R_r'}\right)} . \tag{4}$$

As was mentioned earlier, slamming occurs when the relative velocity exceeds the threshold velocity at the instant of reentry, i.e., $r = H$, and $\dot{r} \geq \dot{r}_*$.

In the phase-plane diagram shown in Fig. 3(b), slamming occurs whenever the circle crosses the line DC. Thus, the probability of occurrence of slamming is given by

$$
\begin{aligned}
\text{Prob}\,\{\text{Slam}\} &= \text{Prob}\,\{r = H,\ \dot{r} \geq \dot{r}_*\} \\
&= \left[-e^{-\left(\frac{r^2 + \frac{\dot{r}^2}{\omega_o^2}}{R_r'}\right)} \right]_{|\dot{r}| = |\dot{r}_*|,\ r = H}^{\infty} \\
&= e^{-\frac{1}{R_r'}\left(H^2 + \frac{\dot{r}_*^2}{\omega_o^2}\right)} \\
&= e^{-\left(\frac{H^2}{R_r'} + \frac{\dot{r}_*^2}{R_{\dot{r}}'}\right)}
\end{aligned}
\tag{5}
$$

where

H = draft at the ship bow,

$\dot{r}_*$ = threshold relative velocity,

R_r' = twice the variance of relative motion,

$R_{\dot{r}}'$ = twice the variance of relative velocity = $R_r' \omega_o^2$.

As can be seen in Eq. (5), it is necessary to evaluate the variances of relative motion and velocity for estimation of the probability. The application of the superposition principle by using the response amplitude operators may be valid to evaluate the variances even for conditions severe enough to induce slamming. The justification of this statement will be given in the next section in which a comparison between the predicted and measured probability of occurrence of slamming are shown.

The variances of relative motion and velocity at an arbitrary point along the ship length can be approximately estimated from irregular wave tests also. The method for evaluating the variances for this case is discussed in Appendix 1.

Number of Slams per Unit Time

The number of slamming occurrences per unit time is essentially an application of the problem of the expected number of zero crossings per unit time. The theory on the zero-crossing problem was first developed by Rice [6], and later applied to ship slamming by Tick [1]. Therefore, the development of the theory will not be described here, but the formula which meets our requirements ($r = H$, $|\dot{r}| \geq \dot{r}_*$) is given instead.

The number of slams per unit time, N_s is given by

$$N_s = \frac{1}{2\pi}\sqrt{\frac{R'_{\dot{r}}}{R'_r}}\, e^{-\left(\frac{H^2}{R'_r} + \frac{\dot{r}_*^2}{R'_{\dot{r}}}\right)} . \tag{6}$$

The definitions of R'_r, $R'_{\dot{r}}$, H, and $\dot{r}_*$ are the same as those used in Eq. (5). It is noted that Eqs. (5) and (6) are related by the formula for the expected period, T_o, for a narrow-band random variable having a normal distribution with zero mean.

$$T_o = \frac{1}{2\pi}\sqrt{\frac{R'_r}{R'_{\dot{r}}}} . \tag{7}$$

Table 2 shows the predicted probability of occurrence of slamming per cycle of wave encounter and the number of slams in a 30-minute operation of the MARINER for various conditions. Included also in the table are the experimental values observed in tests conducted on a 13-ft model [4]. To evaluate the predicted values, the response amplitude operators of the relative motion at Station 2 were obtained for various course angles and ship drafts by conducting tests in regular waves, and the superposition technique was used for estimating the variance of the relative motion. The variances of relative velocity were obtained from the energy spectra of the relative motion [7]. Examples of the response amplitude operators of the relative motion and the computed energy spectra of relative motion and velocity are shown in Fig. 4.

As can be seen in Table 2, the predicted values show satisfactory agreement with the observed values; there being approximately a 10 to 15 percent discrepancy, except for moderate and full draft conditions. For the deep draft condition, however, the discrepancy of 25 percent is not surprising since the probability is small. Thus, the application of superposition principle for evaluation of relative motion and velocity appears to be adequate to obtain realistic engineering estimates of the probability of occurrence of ship slamming at sea.

It is of interest to discuss the effects of course angle and loading condition on the probability of occurrence of slamming. It was found experimentally that the probability decreases with increase of course angle and with increase of loading. In other words, the probability of slamming is highest when a ship navigates in head seas at light draft condition [4]. The occurrence of slamming becomes less with increasing course angle because both the relative motion and velocity between wave and ship bow significantly decrease as can be seen in Table 2. For example, the computed R'_r and $R'_{\dot{r}}$ (twice the variances of relative motion and velocity, respectively) for a 45 degree course angle both decrease to 60 percent of their values in head seas. On the other hand, the occurrence of slamming becomes less with increase of loading primarily because ship draft deepens and thereby bow emergence is less frequent. As can be seen in Table 2,

Table 2
Comparison of Predicted and Observed Probability and Number of Slams (MARINER)

Sea state	Mild 7	←		Moderate 7		→	Severe 7
Wind velocity (knots)	35	←		39		→	41
Wind duration (hours)	23.5	←		27.5		→	32.5
Significant wave height (ft)	23.4	←		31.2		→	35.0
Course angle (degrees)	0	0	25	45	0	0	0
Ship speed (knots)	←			10			→
Loading condition	Light	Light	Light	Light	Moderate	Full	Light
Draft at Station 2 (ft)	17.1	17.7	17.1	17.1	23.7	29.8	17.1
R'_r (ft^2)	276	505	439	314	492	463	605
$R'_{\dot{r}}$ (ft^2/sec^2)	145	238	207	145	208	181	305
Probability of slams per cycle of wave encounter							
Predicted	0.128	0.306	0.256	0.146	0.160	0.06	0.385
Observed	0.135	0.333	0.298	0.152	0.198	0.082	0.414
Number of slams in a 30 minute operation							
Predicted	27	60	50	29	30	12	78
Observed	28	66	57	29	40	16	84

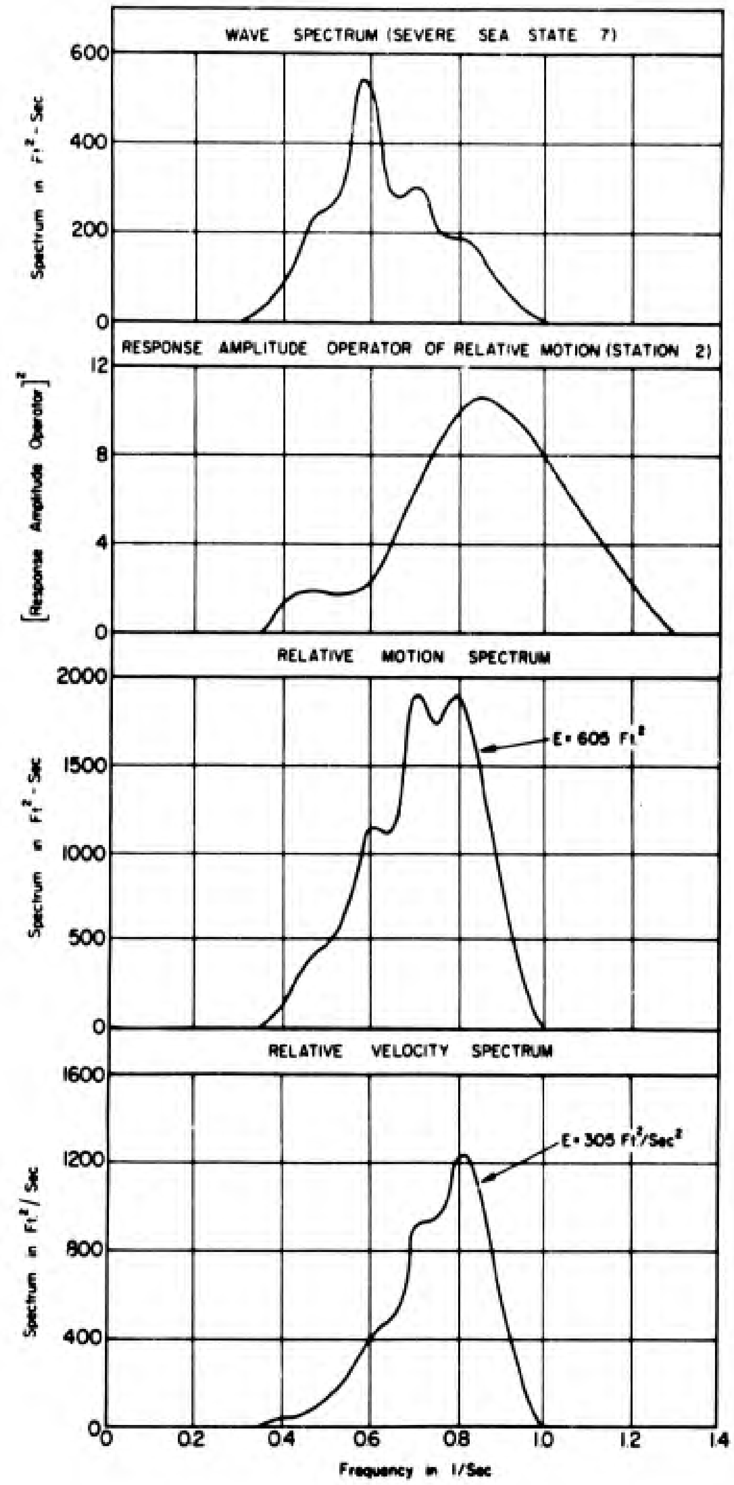

Fig. 4 - Energy spectra of relative motion and relative velocity by applying the superposition technique (MARINER, light draft, severe Sea State 7, head seas)

the computed R_r' decreases only slightly with increase of loading. However, the probability of bow emergence is an exponential function of the square of the draft at the bow [Eq. (5)], and thereby the probability decreases drastically with increase of the draft.

For a better understanding of the above statement, Fig. 5 was prepared to show the computed probability of slamming as well as the probability of bow emergence and the probability that the relative velocity exceeds the threshold velocity for the MARINER in head seas of a moderate Sea State 7 at a ship speed of 10 knots. The probability of occurrence of slamming, is, of course, the product of the other two probabilities. It is clear in the figure that the probability of bow emergence, Prob $[r > H]$, is responsible for the rapid decrease in the probability of slamming.

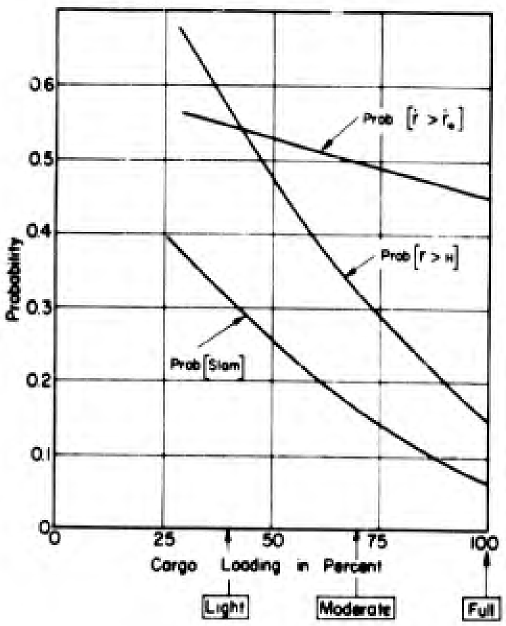

Fig. 5 - Probabilities of occurrence of slamming and bow emergence, and probability that the relative velocity exceeds the threshold velocity

PREDICTION OF SEVERITY OF SLAMMING

Ship slamming is always accompanied by an impact pressure on the flat bottom, and the magnitude of the pressure is indicative of the severity of slamming. The impact pressure is approximately proportional to the square of the magnitude of relative velocity at the instant of impact as was shown in Fig. 1. The same conclusion was obtained from results of tests conducted in regular waves [3]. Hence, this basic relation of the impact pressure and relative velocity will be considered in the development of the theory. Prior to a discussion on the prediction of slamming severity, a statistical consideration of the magnitude of relative velocity will be given.

Prediction of the Magnitude of Relative Velocity Between Wave and Ship Bow

In order to predict the magnitude of relative velocity between wave and the ship bow, the probability density function of the relative velocity associated with slamming must be established. In other words, the probability density function of the cross points on the DC-line shown in Fig. 3(b) should be obtained. Although the relative velocity associated with slamming was defined as negative, the sign will be changed hereafter for convenience.

Since slamming occurs when the relative motion is equal to H, let $r = H$ in Eq. (2). Then,

$$r_o^2 = H^2 + \frac{\dot{r}^2}{\omega_o^2} . \tag{8}$$

Consider the probability density function of r_o when r_o is greater than H; namely, consider the probability density function of the cross points on the BA-line shown in Fig. 3(b). The result is

$$f(r_o) = \frac{2r_o}{R_r'} e^{-\frac{1}{R_r'}(r_o^2 - H^2)} , \qquad r_o \geqq H . \tag{9}$$

From Eqs. (8) and (9),

$$f(\dot{r}) = \frac{2\dot{r}}{R_{\dot{r}}'} e^{-\frac{\dot{r}^2}{R_{\dot{r}}'}} , \qquad \dot{r} \geq 0 . \tag{10}$$

Thus, the probability density function of the cross points on the BC-line in Fig. 3(b), neglecting the sign of the relative velocity, is the Rayleigh distribution.

Next consider the probability density function of the cross points on the DC-line in the figure, since it is necessary to consider the threshold velocity, $\dot{r}_*$, for slamming. Then, the probability density function of the relative velocity for slamming is given by

$$f(\dot{r}) = \frac{2\dot{r}}{R_{\dot{r}}'} e^{-\frac{1}{R_{\dot{r}}'}(\dot{r}^2 - \dot{r}_*^2)} , \qquad \dot{r} \geqq \dot{r}_* . \tag{11}$$

where

$R_{\dot{r}}'$ = twice the variance of relative velocity,

$\dot{r}_*$ = threshold velocity.

Thus, the probability density function of the relative velocity associated with slamming is a truncated Rayleigh distribution. The truncation should be made at the threshold velocity, $\dot{r}_*$, which is a function of a ship length as was mentioned earlier.

From the probability density function given in Eq. (11), the average of one-third highest (significant), $\tilde{\dot{r}}_{1/3}$, and one-tenth highest, $\tilde{\dot{r}}_{1/10}$, values of the relative velocity can be obtained as follows:

$$\tilde{\dot{r}}_{1/3} = 3\, e^{\frac{\dot{r}_*^2}{R_r'}} \left[\dot{r}_{1/3}\, e^{-\frac{(\dot{r}_{1/3})^2}{R_r'}} + \sqrt{\pi R_r'} \left\{ 1 - \Phi\left(\sqrt{\frac{2}{R_r'}}\, \dot{r}_{1/3} \right) \right\} \right] \tag{12}$$

where

$$\dot{r}_{1/3} = \sqrt{\dot{r}_*^2 - R_r' \log \frac{1}{3}}$$

$$\Phi(u) = \frac{1}{\sqrt{2\pi}} \int_{-\infty}^{u} e^{-\frac{t^2}{2}}\, dt$$

$$\tilde{\dot{r}}_{1/10} = 10\, e^{\frac{\dot{r}_*^2}{R_r'}} \left[\dot{r}_{1/10}\, e^{-\frac{(\dot{r}_{1/10})^2}{R_r'}} + \sqrt{\pi R_r'} \left\{ 1 - \Phi\left(\sqrt{\frac{2}{R_r'}}\, \dot{r}_{1/10} \right) \right\} \right] \tag{13}$$

where

$$\dot{r}_{1/10} = \sqrt{\dot{r}_*^2 - R_r' \log \frac{1}{10}} .$$

The derivation of these formulae is given in Appendix 2.

A comparison between theoretical probability density function and the histogram of the relative velocity obtained from tests conducted on a MARINER model is shown in Fig. 6 (values are converted to those for full scale). The example shown in the figure is for tests conducted in a severe Sea State 7 at a 10-knot ship speed, the same condition as was shown in Fig. 1. As can be seen in Fig. 6, the prediction curve agrees well with the observed histogram. Also, the average of the one-third and one-tenth highest values calculated by Eqs. (12) and (13), respectively, agree well with the measured values.

Prediction of the Magnitude of Impact Pressure Associated with Slamming

It was shown earlier that the impact pressure associated with slamming is approximately proportional to the square of the relative velocity and that the

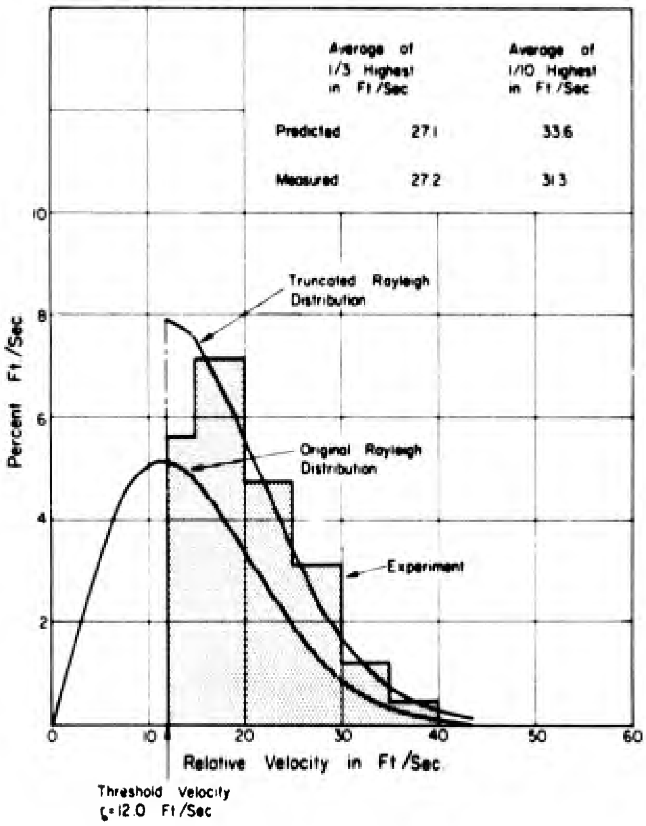

Fig. 6 - Comparison between sample histogram and the truncated Rayleigh distribution for relative velocity (severe Sea State 7, ship speed 10 knots, light draft)

probability distribution of the relative velocity follows a truncated Rayleigh distribution. From these two conditions, the probability density function of the impact pressure can be derived.

Let the impact pressure associated with slamming, p, be expressed by

$$p = 2C\dot{r}^2 \tag{14}$$

where

C = constant dependent upon the ship section shape,

$\dot{r}$ = relative velocity.

From Eqs. (11) and (14) and with the aid of the transformation theorem on random variables, the following truncated exponential probability density function can be derived for the impact pressure associated with slamming

$$f(p) = \frac{1}{2CR_{\dot{r}}^2} e^{-\frac{1}{2CR_{\dot{r}}^2}(p-p_*)}, \qquad p \geq p_* \tag{15}$$

where

p = impact pressure = $2C\dot{r}^2$,

p_* = threshold pressure = $2C\dot{r}_*^2$.

The probability that an impact pressure exceeds a certain magnitude, p_o, per cycle of wave encounter can be obtained

$$\text{Prob}\,\{p \geq p_o\} = \int_{p_o}^{\infty} f(p)\,dp = e^{-\frac{1}{2CR_{\dot{r}}^2}(p_o-p_*)}, \qquad p_o \geq p_* . \tag{16}$$

It is of importance to note here that Eq. (16) is a conditional probability; namely, it represents the probability that an impact pressure exceeds a certain magnitude given that a slam occurred. Hence, the probability that an impact pressure exceeds a certain magnitude in a given sea state and at a given ship speed is the product of the two probabilities given by Eqs. (5) and (16). Also, the problem concerning how many times an impact pressure exceeds a certain magnitude in a prescribed ship operation time can be obtained by multiplying the operation time by the product of Eqs. (6) and (16).

The averages of one-third highest, $\bar{p}_{1/3}$ and one-tenth highest, $\bar{p}_{1/10}$ pressures are given by the following formulae:

$$\bar{p}_{1/3} = \left(2C\ \dot{r}_*^2 + 2.10\ R_{\dot{r}}^2\right) \tag{17}$$

$$\bar{p}_{1/10} = \left(2C\ \dot{r}_*^2 + 3.30\ R_{\dot{r}}^2\right) . \tag{18}$$

Derivation of Eqs. (17) and (18) are given in Appendix 2.

Figure 7 shows a comparison between the theoretical probability density function and the histogram of impact pressure obtained at 0.1 L aft of the forward perpendicular of the MARINER in a severe Sea State 7 at a 10-knot ship speed. The value $2C = 0.086$, determined from Fig. 1, was used in the calculation. Included in the figure are the predicted average of the one-third and one-tenth highest pressures calculated by Eqs. (17) and (18) as well as the observed values. As can be seen in the figure, the theoretical density function is truncated at 12.4 psi due to the threshold relative velocity. Although pressures lower than 12.4 psi were actually observed a few times during the tests, reasonable agreement between theoretical and experimental results can be seen in the figure. The discrepancy is of the order of 10 percent for the average of the one-third highest, and 20 percent for the average of the one-tenth highest values.

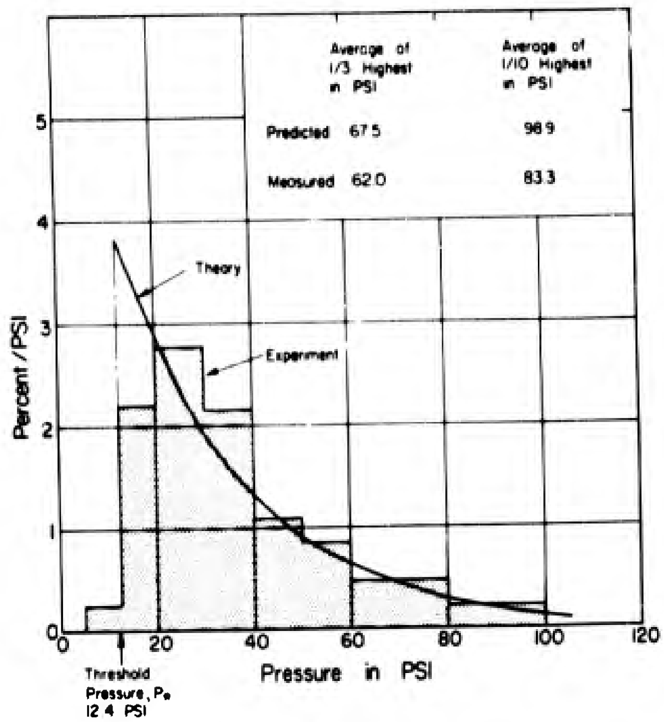

Fig. 7 - Comparison between experimentally obtained histogram of slamming pressure and predicted probability density function (severe Sea State 7, ship speed 10 knots, light draft)

Comparison between theory and experiment were made for two additional cases; namely for moderate and mild Sea State 7, at a 10-knot ship speed. The results are shown in Figs. 8 and 9, respectively. Two histograms are shown in Fig. 9; one obtained from a 30-minute observation in a mild Sea State 7, while the other was obtained from a 70-minute observation in the same sea state. Although some discrepancy between the experimental histogram and the theoretical probability density function can be seen in Figs. 8 and 9, good agreement was obtained between the predicted and observed averages of one-third and one-tenth highest values in these two cases.

It is noted here that a discrepancy between the experimental histogram and the theoretical probability density function is noticeable in the neighborhood of the threshold pressure. The discrepancy for these marginal conditions might be attributed to the actual angle between wave and keel. For higher relative velocity, however, the angle would not be expected to have a strong influence upon the magnitude of impact pressure.

It is of interest to mention that the probability density function of the impact pressure given by Eq. (15) can also be applied for any course angle or loading condition. Figure 10 shows a comparison between the experimental

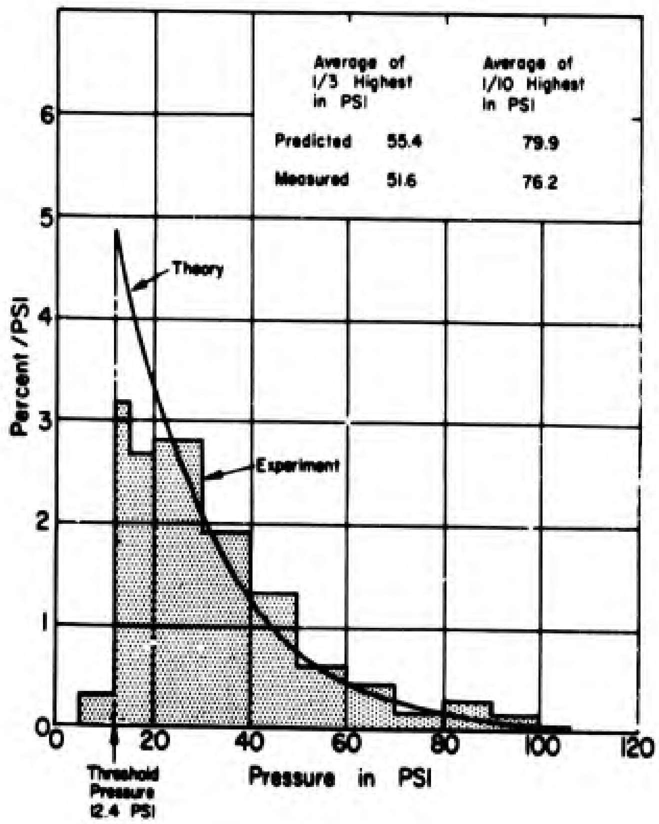

Fig. 8 - Comparison between experimentally obtained histogram of slamming pressure and predicted probability density function (moderate Sea State 7, ship speed 10 knots, light draft)

histograms and the predicted probability density functions for various course angles in a moderate Sea State 7, at a 10-knot ship speed. Figure 11 shows a similar comparison for various loading conditions. The prediction curves were established by using the values listed in Table 2, and a threshold velocity of 12 ft/sec. Satisfactory agreement between the prediction curve and the experimental histogram can be seen in these figures. Based on these results, it is concluded that the impact pressure associated with slamming follows a truncated exponential probability law.

PREDICTION OF THE TIME INTERVAL BETWEEN SLAMS

Prediction of the Time Interval Between Successive Slams

For prediction of the time interval between successive slams, the following question must first be answered: is the slamming phenomenon a sequence of events occurring in time according to the Poisson process? If the occurrence

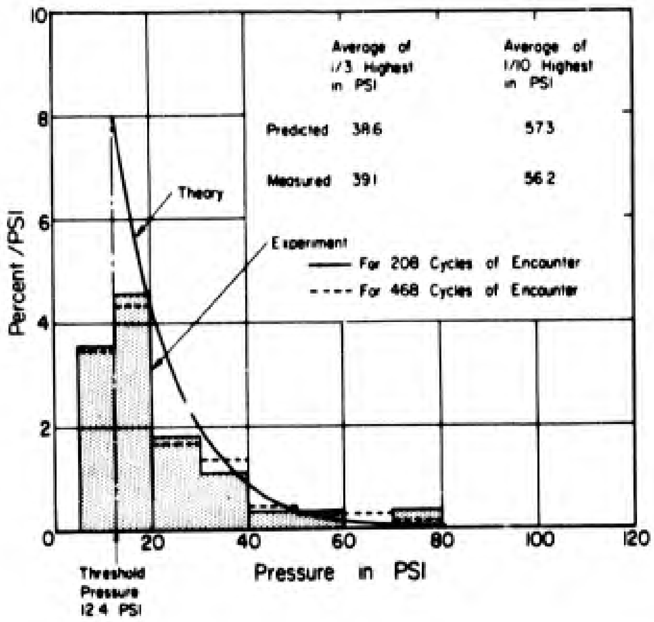

Fig. 9 - Comparison between experimentally obtained histogram of slamming pressure and predicted probability density function (mild Sea State 7, ship speed 10 knots, light draft)

of slamming is considered as a Poisson process, then the time interval between successive slams is a random variable which must follow an exponential probability law theoretically [8].

In order to obtain an answer to the above question and thereby to determine the probability density function for the time interval between successive slams, a sample of the time history of slamming obtained in tests conducted on a MARINER model will be shown.

Figure 12 shows the time history of slamming pressure (converted to full scale) measured at 0.1 L aft of the forward perpendicular in a severe Sea State 7 at a 10-knot ship speed [4]. The ship was in light draft condition; specifically, 40 percent of cargo loading. A total of 84 slams were observed during 203 cycles of wave encounter in a 31 min-7 sec observation. It is noted that the sample shown in the figure is the composite of four records taken in the tests. Hence, there exists three points of discontinuity as marked in the figure. Although the tests were carefully conducted, there is a possibility that several wave encounters and a small amount of time were lost at these discontinuities. The vertical line marked in the figure indicates a slam whose pressure magnitude is proportional to the height of the line. The black circles indicate wave encounters without slamming.

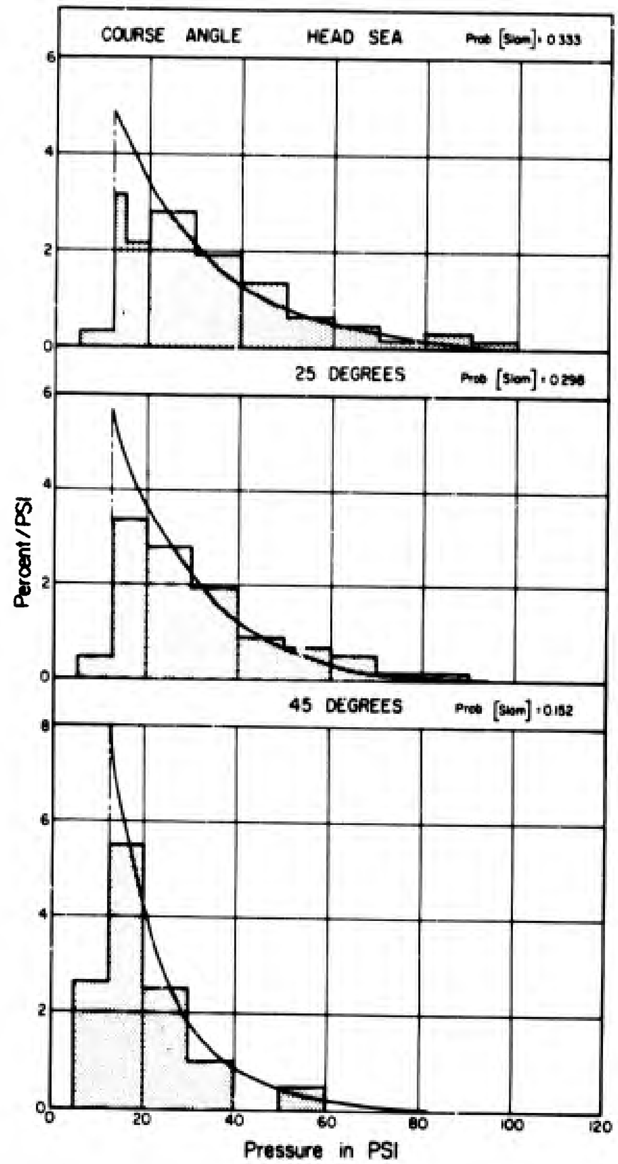

Fig. 10 - Sample histograms and the predicted probability density functions for impact pressure observed at 0.10 L aft of FP for various course angles (moderate Sea State 7, ship speed 10 knots, light draft)

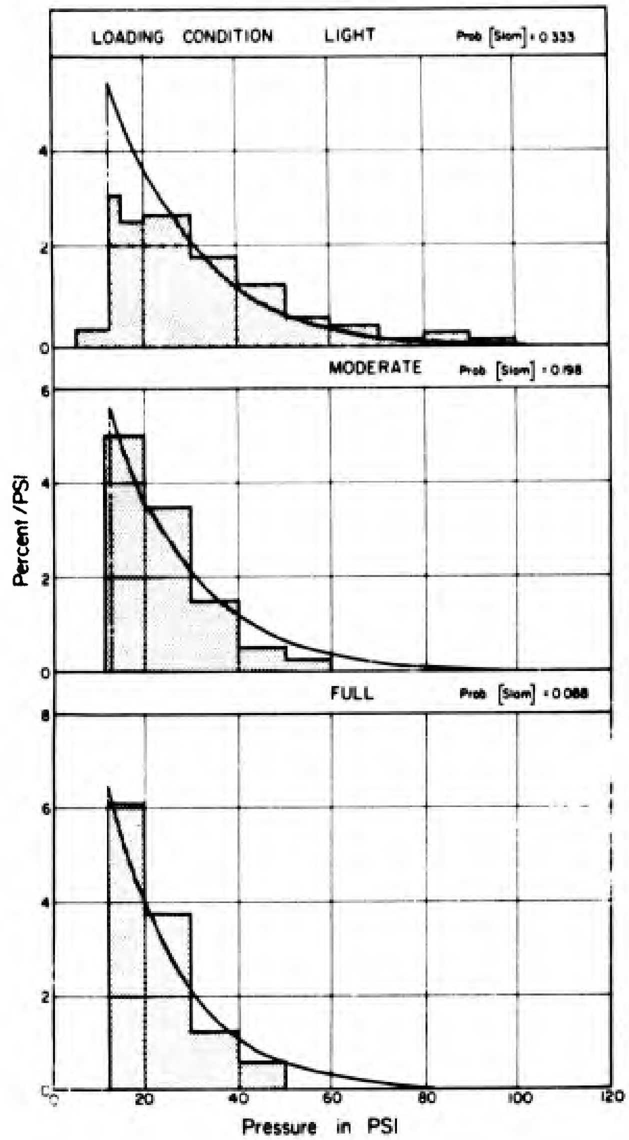

Fig. 11 - Sample histograms and the predicted probability density functions of impact pressure observed at 0.10 L aft of FP for various loading conditions (moderate Sea State 7, ship speed 10 knots, head seas)

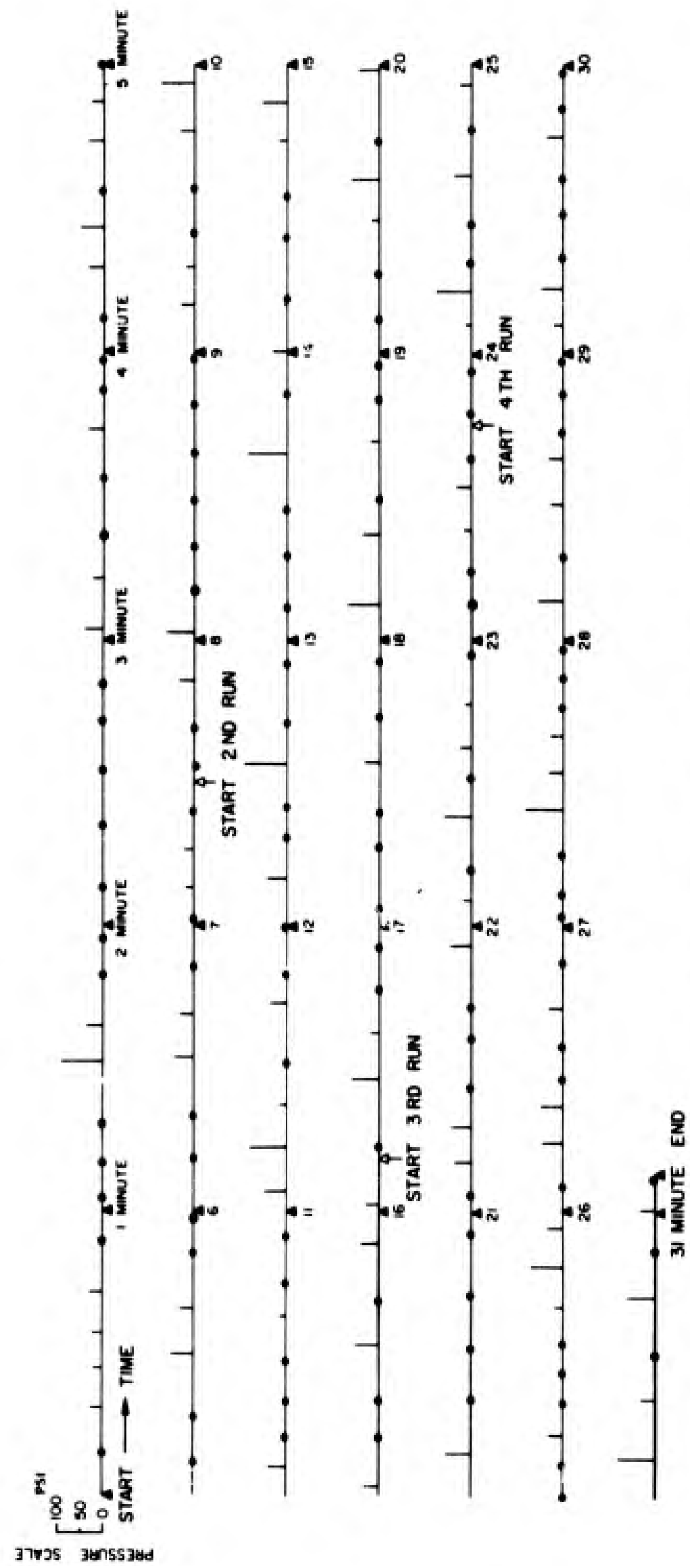

Fig. 12 - Time history of slamming (light draft, ship speed 10 knots, severe Sea State 7)

As can be seen in the figure, the shortest time interval between two successive slams is 7.7 sec, a value very close to the natural pitching period of 7.6 sec. Although periods shorter than the natural pitching period were observed between two wave encounters, no slamming was observed for these cases. Hence, it may safely be assumed that the natural pitching period is the minimum time interval between two successive slams.

Figure 13 was prepared to verify that slamming is a sequence of events occurring in time following a Poisson process. In preparation of this figure, the number of slams occurring during 20 sec intervals was counted from the time history (Fig. 12), and the experimental frequency for each number was obtained. To determine the Poisson distribution curve, the expected value (mean) of slams for every 20 sec was computed from the frequency. By using this value (0.89), the Poisson distribution was obtained by the following formula:

$$P(X = r) = \frac{\lambda^r}{r!} e^{-\lambda} \tag{19}$$

where

λ = expected value,

r = integer.

The result is included in Fig. 13. From evidence shown in the figure, slamming may be considered as a sequence of events occurring in time following a Poisson process for at least a size of sample (93 observations) shown in the figure.

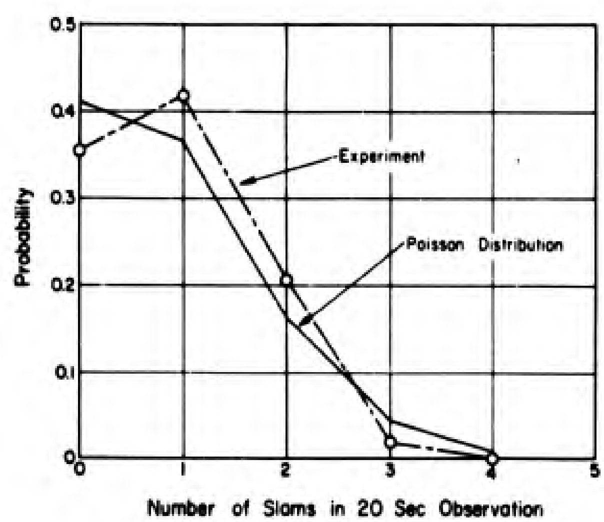

Fig. 13 - Comparison between the probability density for number of slams in 20 sec observation and Poisson distribution

On the basis of the above discussion, it is expected theoretically that the time interval between two successive slams follows an exponential probability law. However, one condition must be considered for the present problem. That is, the shortest time interval between successive slams is very close to the natural pitching period as was mentioned earlier. With this modification, a truncated probability density function is derived for the time interval between successive slams as follows:

$$f(t) = N_s e^{-N_s(t-t_*)}, \qquad t \geq t_* \tag{20}$$

where

N_s = number of slams per unit time,

t_* = minimum time interval between two successive slams (natural pitching period).

Results of numerical calculations using Eq. (20) are shown in Fig. 14 along with the histogram obtained in the experiment.

A further comparison between theory and experiment was made for the time interval between successive slams in bi-directional waves. The bi-directional

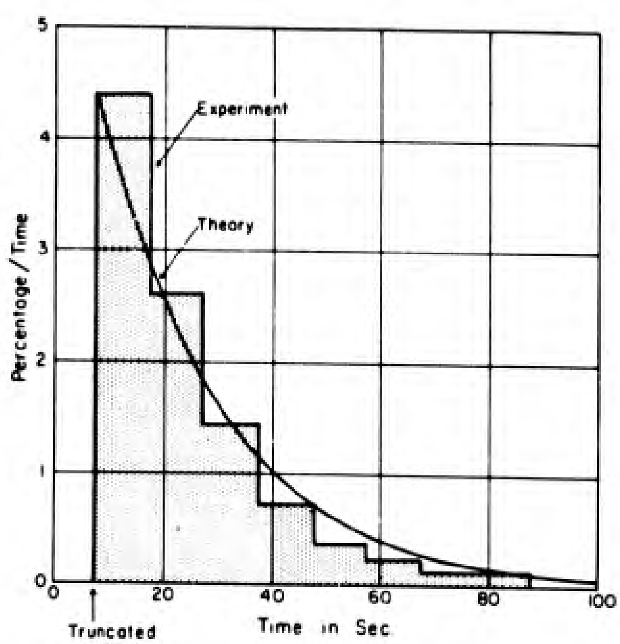

Fig. 14 - Sample histogram and the predicted probability density function for time interval between successive slams (severe Sea State 7, ship speed 10 knots, light draft, head seas)

waves were composed of two wave systems corresponding to a moderate Sea State 7 and Sea State 5 coming from directions at 90 degrees to each other. In this case, the frequency of occurrence of slamming is higher than that in the long-crested waves (moderate Sea State 7 alone); however, the severity of the slams for the former is considerably less than that for the latter [4]. A total of 164 slams were observed in a 57.7 minute observation, hence N_s in Eq. (20) is equal to 0.0475 per sec. By using this value, the predicted curves shown in Fig. 15 were obtained. The actually observed minimum time interval between successive slams was 6.2 sec in this case, a value somewhat lower than the natural pitching period. Nevertheless, good agreement can be seen between the predicted probability density function and the experimental histogram. Thus, it may be concluded that the time interval between successive slams follows a truncated exponential probability law.

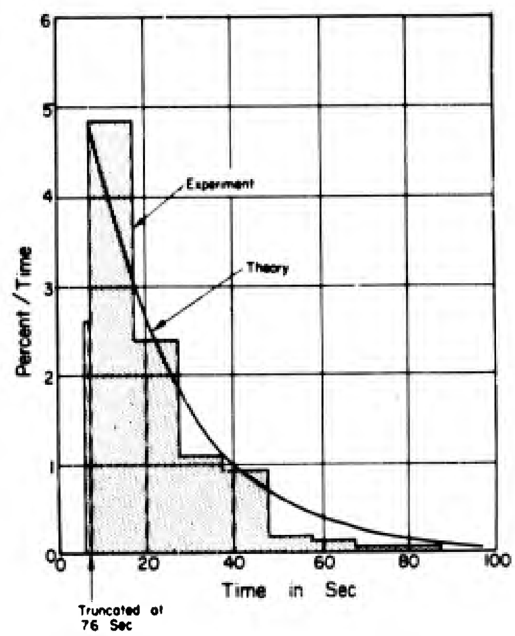

Fig. 15 - Sample histogram and the predicted probability density function for time interval between successive slams (bi-directional waves, ship speed 10 knots, light draft)

Prediction of the Time Interval Between Two Severe Slams

In the foregoing discussion, the severity of slamming was not introduced. Here, the discussion will be expanded to include the probability problem of time interval between two severe slams. In other words, the time interval between two slams, both of which cause an impact pressure of magnitude greater than a certain value will be considered. The method of approach is as follows: Eq. (20) is the probability density function of the time interval between two successive slams. We may now evaluate the time interval between m slams considering that every mth time the slam is severe, and that the magnitudes of impact pressure for these slams exceed a certain value. Here, m can be determined by taking the inverse value of the probability given by Eq. (16) since that equation gives the probability that an impact pressure exceeds a certain magnitude per cycle of wave encounter. That is

$$m = \frac{1}{\int_{p_o}^{\infty} f(p)\, dp} = e^{\frac{1}{2CR_r'}(p-p_*)} . \tag{21}$$

It is known in general that the waiting time to observe the mth occurrence of an event when a sequence of events is occurring in time following the Poisson process obeys the gamma probability law given by the following equation [8]

$$g(t) = \frac{N_s^m}{\Gamma(m)} t^{m-1} e^{-N_s t} , \qquad t > 0 . \tag{22}$$

For the present problem, however, the probability density function must be truncated at mt_* (where, t_* is the natural pitching period). Then, by using the condition that the probability between mt_* and ∞ for the truncated probability function must be equal to one, the following truncated gamma probability density function is derived:

$$g(t) = \frac{\frac{N_s^m}{\Gamma(m)} t^{m-1} e^{-N_s t}}{\int_{mt_*}^{\infty} \frac{N_s^m}{\Gamma(m)} t^{m-1} e^{-N_s t} dt} , \qquad t \geq mt_* . \tag{23}$$

The constant m in the above equation was given in Eq. (21), and m is not always an integer. Hence, the denominator in Eq. (23) cannot be expressed by a practically usable formula. However, the integration can be evaluated as follows: Let $N_s t = Z/2$, and obtain the probability density function of a random variable Z. Then, the denominator of Eq. (23) is equivalent to

$$\int_{mZ_*}^{\infty} \frac{1}{2^m} \frac{1}{\Gamma(m)} Z^{m-1} e^{-\frac{Z}{2}} dZ , \qquad Z \geq mZ_* \tag{24}$$

where $mZ_* = 2mN_s t_*$.

The above integral is the probability integral of the incomplete gamma function and a table is available for this integration [9]. The integral values for various m, N_s, and t_* appropriate for full scale ships were taken from Ref. 9, and are shown in Fig. 16(a).

The probability that a time T, or more, elapses before the next severe slam occurs can readily be obtained from Eq. (23). That is,

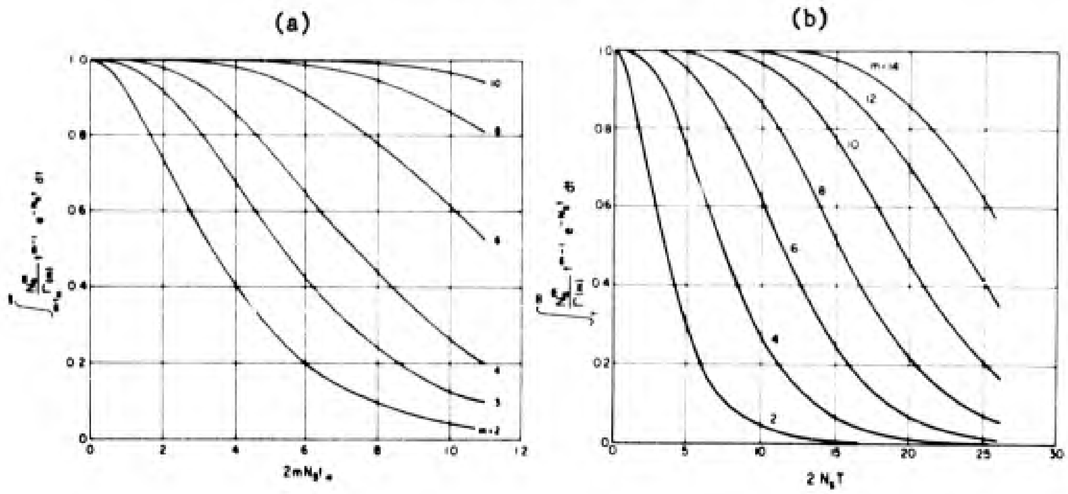

Fig. 16 - The probability integral of the incomplete gamma function, Ref. 9

$$\text{Prob}\,\{t \geq T\} = \frac{\displaystyle\int_T^{\infty} \frac{N_s^m}{\Gamma(m)}\, t^{m-1}\, e^{-N_s t}\, dt}{\displaystyle\int_{mt_*}^{\infty} \frac{N_s^m}{\Gamma(m)}\, t^{m-1}\, e^{-N_s t}\, dt}\,. \tag{25}$$

The integral value of the numerator in the above equation for various m, N_s, and T, appropriate for full scale ships are given in Fig. 16(b).

A numerical example of Eq. (23) will be given as follows: Consider the MARINER to be operating at light draft condition (40 percent of cargo loading) at a 10-knot speed in a severe Sea State 7. We will evaluate the probability density of the time interval between two severe slams for which an impact pressure of 50 psi or greater will be applied at the location 0.10 L aft of the forward perpendicular. In this case, we have

$$2C = 0.086 \text{ psi-sec}^2/\text{ft}^2,$$

$$p_o = 50 \text{ psi},$$

$$p_* = 2C\dot{r}_*^2 = 12.4 \text{ psi},$$

$$R_r' = 605 \text{ ft}^2 \text{ (see Table 2)},$$

$$R_{\dot{r}}' = 305 \text{ ft}^2/\text{sec}^2 \text{ (see Table 2)},$$

$$N_s = 0.0435 \text{ 1/sec [by Eq. (6)]},$$

$$t_* = 7.6 \text{ sec},$$

$$m = 4.19 \text{ [by Eq. (21)]}.$$

By using these values and Eq. (23) the time interval between two severe slams was evaluated, and the results are shown in Fig. 17. Included also in the figure is the experimentally obtained histogram. On the basis of the agreement between experimental and theoretical results, it is concluded that the time interval between two severe slams follows a truncated gamma probability law.

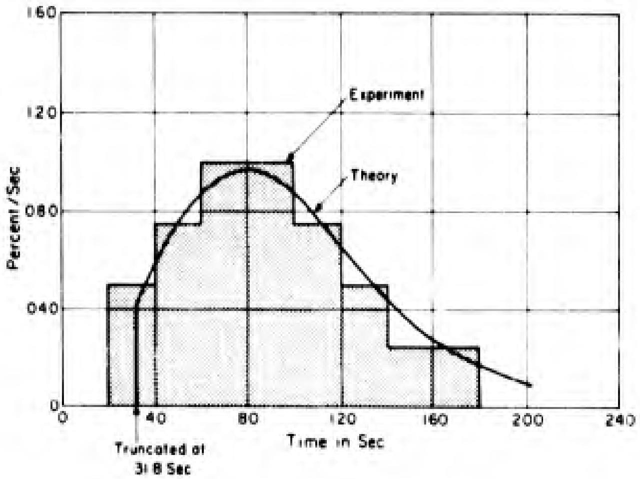

Fig. 17 - Sample histogram and the predicted probability density function for time interval between two severe slams (severe Sea State 7, ship speed 10 knots, light draft)

APPLICATION OF THE PREDICTION METHOD TO THE DECK WETNESS PROBLEM

Prediction of Probability of Occurrence of Deck Wetness

The problem of probability of occurrence of deck wetness due to shipping of green water can be treated in a manner similar to that for slamming. However, two differences in the treatment of these phenomena must be considered. These are: (1) The bow emergence and threshold velocity are the required conditions leading to slamming, while the bow submergence is the condition leading to deck wetness. (2) The reference location along the ship length for which the probability should be considered is 0.1 L aft of the forward perpendicular for slamming, and the forward perpendicular for deck wetness. Since deck wetness is caused by the green water flowing over the deck from the top of the stem, it is proper to consider the forward perpendicular as a reference point. Justification for selection of the reference point of 0.1 L aft of the forward perpendicular for slamming is given in Ref. 4. With the above two considerations, the probability of occurrence of deck wetness can be obtained from Eq. (5), by substituting D (freeboard at the forward perpendicular) for H (draft at Station 2), and by letting $\dot{r}_* = 0$. That is,

$$\text{Prob (Deck Wetness)} = \text{Prob } (r > D) = e^{-\frac{D^2}{R'_r}} \tag{26}$$

where

D = freeboard at FP,

R'_r = twice the variance of relative motion at FP.

It is noted that R'_r in the above equation has a different value from that in Eq. (5), since the relative motion between wave and ship bow at the forward perpendicular is considered for this case.

The number of occurrences of deck wetness per unit time, N_w, is given by

$$N_w = \frac{1}{2\pi}\sqrt{\frac{R''_r}{R'_r}}\, e^{-\frac{D^2}{R'_r}} . \tag{27}$$

Table 3 shows comparisons between predicted and observed probability of occurrence of deck wetness per cycle of wave encounter and number of deck wetnesses in a 30-minute operation of the MARINER in a moderate Sea State 7 at a 10-knot speed. Variance of the relative motion at the forward perpendicular used in the computation of the probability was evaluated by the method given in Appendix 1. Although satisfactory agreement between the predicted and observed values can be seen in Table 3 for full loading condition, agreement for moderate and light loading conditions is poor. However, this is not surprising since only 12 occurrences were observed for the moderate and 4 occurrences for the light load condition as compared to 34 occurrences for full draft condition. It is noted that a comparison of the predicted value with the observed value which was obtained from a small number of samples is not statistically proper. However, the comparison is included in the table to provide some indication of how significantly the probability decreases with decrease of loading condition.

It is of interest to discuss the effect of freeboard forward on the probability of occurrence of deck wetness. Newton, based on his experimental study on a destroyer-type vessel, concluded that the freeboard forward had a most important influence on the degree of wetness [10]. Newton's conclusion derived from tests in regular waves is valid in irregular waves also since the probability of occurrence of deck wetness decreases significantly with increase of freeboard forward [see Eq. (26)] and since the severity of wetness also decreases as will be seen later in Eq. (30).

As a practical example of the effect of freeboard forward on the probability of occurrence of deck wetness per cycle of wave encounter, Fig. 18 was prepared. The figure shows the probability of deck wetness of the MARINER for various heights of freeboard forward. The probability was computed for a 10-knot speed in a moderate Sea State 7 for full load condition. The actual height of the freeboard forward on the MARINER is 36.7 feet. As can be seen in Fig. 18, if the freeboard were increased by 10 percent, the probability of deck wetness would decrease by 32 percent. Conversely, if the freeboard were decreased by 10 percent, the probability would increase by 42 percent.

Table 3
Comparison of Predicted and Observed Probability and Number of Deck Wetnesses (MARINER)

Sea state	← Moderate 7 →		
Wind velocity (knots)	← 39 →		
Wind duration (hours)	← 27.5 →		
Significant wave height (ft)	← 31.2 →		
Course angle	← 0 →		
Ship speed (knots)	← 10 →		
Loading condition	Full	Moderate	Light
Freeboard forward (at FP) (ft)	36.7	43.1	50.2
R_r' at FP (ft^2)	733	778	799
$\dot{R}_r'$ at FP (ft^2/sec^2)	298	329	364
Probability of deck wetness per cycle of wave encounter			
Predicted	0.159	0.092	0.043
Observed	0.175	0.060	0.020
Number of deck wetnesses in a 30-minute operation			
Predicted	29	17	8
Observed	34	12	4

Prediction of Severity of Deck Wetness

As was mentioned earlier, the pressure associated with slamming is of the impact type and is proportional to the square of the relative velocity between wave and ship bow at the instant of impact. The pressure associated with deck wetness, on the other hand, is not an impact type and approximately corresponds to a static pressure due to the head of water flowing over the deck. Thus in the

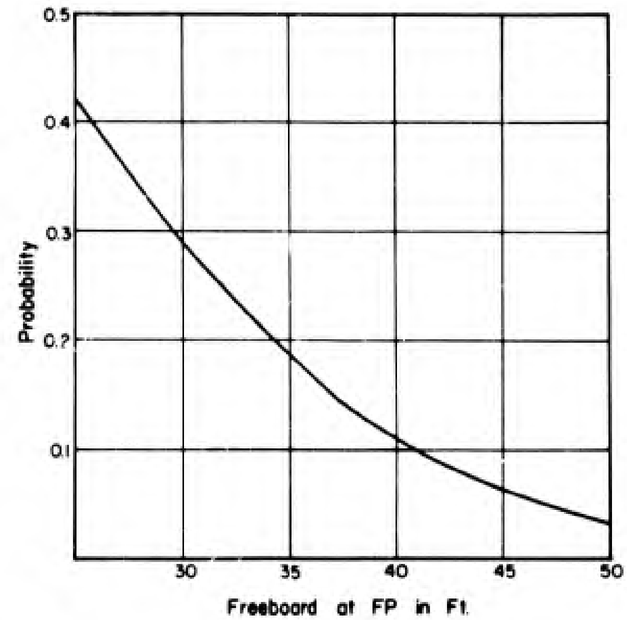

Fig. 18 - Effect of freeboard forward on the probability of occurrence of deck wetness (moderate Sea State 7, ship speed 10 knots, full draft)

derivation of the probability density function for the pressure due to green water, the following conditions will be considered. These are: (1) magnitude of relative motion is greater than the freeboard forward (bow submergence condition) and (2) magnitude of peak pressure during one cycle of deck wetness is equal to the static water-head corresponding to the difference between the maximum value of relative motion and the freeboard forward.

Now, the double amplitude distribution of the relative motion follows the Rayleigh probability law. Since deck wetness occurs only when the bow is submerging, the relative motion in one direction is taken instead of the peak-to-peak value. Then, analogous to Eq. (9), the probability density function of the amplitude of the relative motion r_o, when r_o is greater than the freeboard forward, D, is given by

$$f(r_o) = \frac{2r_o}{R'_r} e^{-\frac{1}{R'_r}(r_o^2 - D^2)} , \qquad r_o \geqq D . \tag{28}$$

It is convenient to express the above formula in terms of pressure units (psi). For this, let $q_o = r_o/a$ and $q_* = D/a$. Here, $a = 2.32$ ft/psi if r_o and D are expressed in the foot-unit. Then, the probability density function given in Eq. (28) becomes

$$f(q_o) = \frac{2a^2}{R_r'} q_o e^{-\frac{a^2}{R_r'}(q_o^2 - q_*^2)}, \qquad q_o \geq q_* . \tag{29}$$

Since q_o in the above equation is the pressure corresponding to the peak of the relative motion, and q_* is that corresponding to the freeboard forward, the pressure due to the green water on the deck q, is the difference between them. Thus, the probability density function of the pressure due to green water can be derived from Eq. (29):

$$f(q) = \frac{2a^2}{R_r'} (q + q_*) e^{-\frac{a^2}{R_r'}((q+q_*)^2 - q_*^2)}, \qquad q > 0 \tag{30}$$

where

q = pressure due to green water on the deck (psi),

R_r' = twice the variance of relative motion between wave and ship bow (ft^2),

q_* = D/a (psi),

D = freeboard at the ship bow (ft),

a = constant = 2.32 (ft/psi).

Equation (30) is essentially a truncated Rayleigh distribution. However the base line is shifted, so it may be considered as a modified Rayleigh distribution.

The average of the one-third highest (significant), $\tilde{q}_{1/3}$, and one-tenth highest $q_{1/10}$ pressures are given by the following formulae respectively:

$$\tilde{q}_{1/3} = 3\left[q_{1/3} e^{-\frac{a^2}{R_r'}((q_{1/3}+q_*)^2 - q_*^2)} + \sqrt{\pi}\sqrt{\frac{R_r'}{a^2}}\, e^{\frac{a^2}{R_r'}q_*^2} \left(1 - \Phi\left\{\sqrt{\frac{2a^2}{R_r'}}(q_{1/3} + q_*)\right\}\right)\right] \tag{31}$$

where

$$q_{1/3} = \sqrt{q_*^2 - \left(\frac{R_r'}{a^2}\right)\left(\log \frac{1}{3}\right)} - q_*$$

$$\Phi(u) = \frac{1}{\sqrt{2\pi}} \int_{-\infty}^{u} e^{-\frac{t^2}{2}}\, dt$$

$$\overline{q}_{1/10} = 10\left[q_{1/10}\, e^{-\frac{a^2}{R'_r}\left\{(q_{1/10}+q_*)^2 - q_*^2\right\}} + \sqrt{\pi}\sqrt{\frac{R'_r}{a^2}}\, e^{\frac{a^2}{R'_r} q_*^2}\left(1 - \Phi\left\{\frac{2a^2}{R'_r}\,(q_{1/10}+q_*)\right\}\right)\right] \tag{32}$$

where

$$q_{1/10} = \sqrt{q_*^2 - \left(\frac{R'_r}{a^2}\right)\log\left(\frac{1}{10}\right)} - q_* .$$

The derivation of the above formulae is the same as that for the average of the one-third highest and one-tenth highest slamming pressures.

Figure 19 shows a comparison of the theoretical probability density function of pressure experienced on deck due to green water with an experimental histogram. The experimental histogram was obtained from tests on the MARINER operating at a 10-knot speed in a moderate Sea State 7. Included also in the figure are the averages of the one-third and one-tenth highest pressures.

Another comparison between theory and experiment was made for a high speed research ship form and the result is shown in Fig. 20. This form is one of the Series 64 family having a block coefficient of 0.45. The freeboard at the

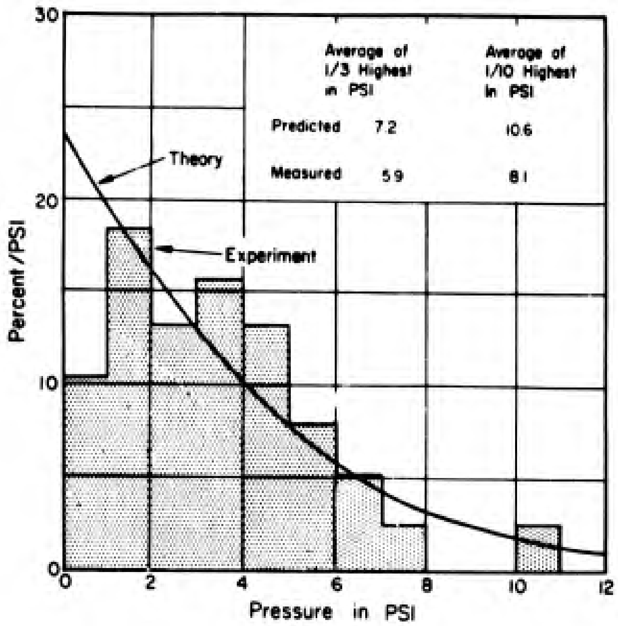

Fig. 19 - Histogram of pressure experienced on the deck due to green water (MARINER, moderate Sea State 7, ship speed 10 knots, full draft)

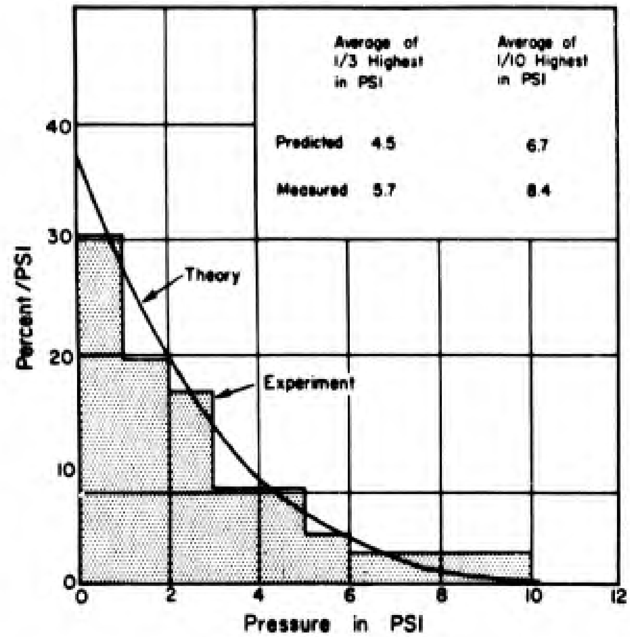

Fig. 20 - Histogram of pressure experienced on deck due to green water (high speed research ship, Sea State 6, ship speed 20 knots, design draft)

forward perpendicular is 23.7 ft. Tests were made in a head Sea State 6, at 20-knot ship speed [11]. (All values have been converted to those for a 400-ft ship.) In these tests, 36 deck wetnesses were observed in 236 wave encounters, hence the probability of deck wetness per cycle of wave encounter was 0.153. For computing the pressures by Eqs. (30) through (32), the variance of the relative motion was estimated from Eq. (26) by using the above probability.

On the basis of the reasonable agreement between theory and experiment shown in Figs. 19 and 20, it may be concluded that the pressure associated with green water on the deck follows a modified Rayleigh probability law.

CONCLUSIONS

A theoretical study was made to predict the probability of occurrence and severity of ship slamming, and the time interval between successive slams in rough seas. The theory was also applied to the deck wetness problem. The theoretical results were compared with experimental results obtained from tests conducted on a 13-ft MARINER model. On the basis of the results of this study, the following conclusions are drawn:

1. The linear theory of superposition of ship motion in waves may be used to obtain realistic engineering estimates of frequency and intensity of slamming

and green water. For the MARINER, the predictions are valid at least up to a severe Sea State 7, ship speed 10 knots.

2. The conditions leading to ship slamming in rough seas are bow emergence and a certain magnitude of relative velocity between wave and ship bow (threshold velocity). It is considered appropriate to take 12 ft/sec as the threshold velocity for a 520-ft ship. For a ship of different length, the above given value should be modified according to the Froude scaling law.

3. Probability of occurrence of slamming decreases with increase of course angle from head seas because both the relative motion and relative velocity decrease with increasing course angle. The probability of occurrence of slamming decreases with increase of loading condition primarily because the probability of bow emergence significantly decreases with increasing draft.

4. Relative velocity between wave and ship bow at the instant of slamming follows a truncated Rayleigh probability law. Truncation should be made at the threshold velocity.

5. Impact pressure applied to a ship's forward bottom when slamming occurs follows a truncated exponential probability law. Truncation should be made for the pressure induced by the threshold velocity. The law appears to be valid for any course angle and loading condition.

6. Time interval between successive slams follows a truncated exponential probability law. Truncation should be made at the natural pitching period of the ship.

7. The time interval between two severe slams follows a truncated gamma probability law.

8. The probability of occurrence of deck wetness is simply the probability of bow submergence. It is an exponential function of relative motion between wave and ship bow and the freeboard forward. The probability decreases significantly with increase of freeboard forward.

9. Pressure associated with deck wetness follows a modified Rayleigh probability law.

ACKNOWLEDGMENTS

The author wishes to express his appreciation to Dr. W. E. Cummins for the valuable discussions and his encouragement received during the course of this project. Thanks are also due to Lt. Cdr. M. C. Davis (USN) for his technical advice.

The assistance of Mrs. S. R. Zoomstein and Mr. J. A. Kallio in carrying out the numerical calculations is gratefully acknowledged.

REFERENCES

1. Tick, L. J., "Certain Probabilities Associated with Bow Submergence and Ship Slamming in Irregular Seas," Journal of Ship Research, Vol. 2, No. 1 (1958)

2. Szebehely, V. G. and Todd, M. A., "Ship Slamming in Head Seas," David Taylor Model Basin Report 913 (1955)

3. Ochi, K., "Model Experiments on Ship Strength and Slamming in Regular Waves," Transactions, Society of Naval Architects and Marine Engineers, Vol. 66 (1958)

4. Ochi, M. K., "Extreme Behavior of a Ship in Rough Seas — Slamming and Shipping of Green Water," Paper to be presented before the Annual Meeting of the Society of Naval Architects and Marine Engineers (1964)

5. Szebehely, V. G. and Lum, S. M., "Model Experiments on Slamming of a Liberty Ship in Head Seas," David Taylor Model Basin Report 914 (1955)

6. Rice, S. O., "Mathematical Analysis of Random Noise," Bell System Tech. Journal, Vol. 23 (1944) and Vol. 24 (1945)

7. Cartwright, D. E., "On the Vertical Motions of a Ship in Sea Waves," International Shipbuilding Progress, Vol. 5, No. 52 (1958)

8. Parzen, E., "Stochastic Processes," Holden-Day, Inc., San Francisco, U.S.A.

9. National Bureau of Standards, "Handbook of Mathematical Functions," Applied Mathematics Series 55, U.S. Department of Commerce (1964)

10. Newton, R. N., "Wetness Related to Freeboard and Flare," Transactions, Royal Institution of Naval Architects, Vol. 101 (1959)

11. Sheehan, J. M., "Model Tests of a Series 64 Hull Form in Regular, Irregular, and Transient Waves," David Taylor Model Basin Report (In preparation)

Appendix 1

METHOD OF EVALUATION OF VARIANCES OF RELATIVE MOTION AND VELOCITY BETWEEN WAVE AND SHIP BOW

The relative motion and velocity between wave and ship bow at a specific location along the ship length can be obtained from model experiments if an immersion sensing element is fixed to the model at the longitudinal position of interest. By this method, tests in regular waves provide the response amplitude operator of relative motion at this location. Then, by applying the superposition principle, the energy spectra of the relative motion and the velocity and thereby the variances for a given sea state can be obtained. That is

$$\sigma_r^2 = \frac{E_r}{8} = \frac{1}{8}\int \Phi_r(\omega_e)\, d\omega_e$$
$$\sigma_{\dot r}^2 = \frac{1}{8}\int \omega_e^2\, \Phi_r(\omega_e)\, d\omega_e \qquad \text{(A.1)}$$

where

σ_r^2 = variance of relative motion,

$\sigma_{\dot r}^2$ = variance of relative velocity,

E_r = cumulative energy density of relative motion, i.e., the area under the relative motion spectrum,

$\Phi_r(\omega_e)$ = energy density of relative motion,

ω_e = frequency.

For a constant speed test it is possible to obtain the response amplitude operator of the relative motion by installation of an accelerometer in the model at the location of interest, and a wave-height probe on the carriage so that it is in line with the accelerometer. The above two methods are the direct methods for obtaining the relative motion and velocity at a specific location.

It is necessary in practice, however, to evaluate the variances of relative motion and velocity at arbitrary points along the ship length for a given sea. For this, the response amplitude operators of relative motion at the points of interest may be evaluated from the pitch, heave, and wave motions including their respective phases. Another approximate method to estimate the variances of relative motion and velocity at arbitrary points is to use the correlation coefficients if the variances of vertical motion and/or acceleration are known at two points along the ship length. The method is as follows:

The variance of the relative motion at an arbitrary point along the ship length is given by

$$\sigma_r^2 = \sigma_w^2 + \sigma_x^2 - 2\rho_{wx}\sigma_w\sigma_x \qquad \text{(A.2)}$$

where

σ_r^2 = variance of relative motion between wave and ship bow at point x,

σ_w^2 = variance of wave motion,

σ_x^2 = variance of vertical motion at point x,

ρ_{wx} = correlation coefficient between wave and vertical motion at point x.

The variance of wave motion, σ_w^2, is simply determined from the energy spectrum for a given sea state. Variance of vertical motion at an arbitrary point, X, can be evaluated by the following formulae if the variances of motion at two different points along the ship length, σ_a^2 and σ_b^2 are known.

$$\sigma_x^2 = \left(\frac{x-b}{a-b}\right)^2 \sigma_a^2 + 2\rho_{ab}\left(\frac{x-b}{a-b}\right)\left(\frac{a-x}{a-b}\right)\sigma_a\sigma_b + \left(\frac{a-x}{a-b}\right)^2 \sigma_b^2 \tag{A.3}$$

where

x, a, b = distances between points X, A, and B from the aft perpendicular (see Fig. 21),

σ_a^2 = variance of vertical motion at point A,

σ_b^2 = variance of vertical motion at point B,

ρ_{ab} = correlation coefficient of vertical motion at two different points, A and B.

Thus, the relative motion at arbitrary point along ship length can be obtained from Eqs. (A.2) and (A.3). However, two correlation coefficients, ρ_{ab} and ρ_{wx}, involved in these equations must be determined experimentally.

The correlation coefficient, ρ_{ab}, can be obtained by the following formula with the aid of auto and cross-spectral analysis of the vertical motions at points A and B.

$$\rho_{ab} = \frac{\mathrm{Cov}_{ab}}{\sigma_a \sigma_b} = \sqrt{\frac{\left(\int C_{ab}(\omega_e)\, d\omega_e\right)^2 + \left(\int Q_{ab}(\omega_e)\, d\omega_e\right)^2}{\int \Phi_{aa}(\omega_e)\, d\omega_e \int \Phi_{bb}(\omega_e)\, d\omega_e}} \tag{A.4}$$

where

$C_{ab}(\omega_e)$ = energy density of cospectrum, i.e., energy density of the real part of the cross-spectrum of vertical motions at points A and B,

$Q_{ab}(\omega_e)$ = energy density of quadrature spectrum, i.e., energy density of the imaginary part of the cross-spectrum of vertical motions at points A and B,

$\Phi_{aa}(\omega_e)$ = energy density of the auto-spectrum of vertical motion at point A,

$\Phi_{bb}(\omega_e)$ = energy density of the auto-spectrum of vertical motion at point B.

In the above formula, the definition of the variance and covariance given by St. Denis and Pierson was used. If the acceleration is measured instead of the vertical motion at one point (say, point A), Eq. (A.3) is still valid, since the acceleration spectrum can easily be converted to the motion spectrum. The following relations are used in Eq. (A.4) in this case.

$$C_{ab}(\omega_e) = -\frac{1}{\omega_e^2} C_{\ddot{a}b}(\omega_e)$$

$$Q_{ab}(\omega_e) = -\frac{1}{\omega_e^2} Q_{\ddot{a}b}(\omega_e) \tag{A.5}$$

$$\Phi_{aa}(\omega_e) = \frac{1}{\omega_e^4} \Phi_{\ddot{a}\ddot{a}}(\omega_e) .$$

The value of the correlation coefficient, ρ_{ab}, depends on the relative position of the two points A and B. As will be shown later in Table 4, if point A is located near the ship bow and point B is located near the midship, the correlation coefficient is very small for conditions severe for slamming. This means that the motions at these points (ship bow and midship) are statistically almost uncorrelated, and thereby the second term of Eq. (A.3) can be neglected practically.

The correlation coefficient, ρ_{wx}, can be obtained by a formula similar to that for the coefficient ρ_{ab}. That is,

$$\rho_{wx} = \frac{Cov_{wx}}{\sigma_w \sigma_x} = \sqrt{\frac{(\int C_{wx}(\omega_e)\, d\omega_e)^2 + (\int Q_{wx}(\omega_e)\, d\omega_e)^2}{\int \Phi_{ww}(\omega_e)\, d\omega_e \int \Phi_{xx}(\omega_e)\, d\omega_e}} \tag{A.6}$$

where

$C_{wx}(\omega_e)$ = energy density of cospectrum, i.e., energy density of the real part of the cross-spectrum of wave and vertical ship motion,

$Q_{wx}(\omega_e)$ = energy density of quadrature spectrum, i.e., energy density of the imaginary part of the cross-spectrum of wave and vertical ship motion,

$\Phi_{ww}(\omega_e)$ = energy density of the auto-spectrum of wave,

$\Phi_{xx}(\omega_e)$ = energy density of the auto-spectrum of motion.

If the wave is measured not at the same location at which the bow motion is measured but at a certain distance ahead of the model (as is illustrated in Fig. 21), then the following phase correction due to the distance between wave probe and point X is required in the evaluation of the cross-spectrum

$$\Phi_{wx}(\omega_e) = \Phi_{\bar{w}x}\, e^{-\frac{i\omega^2 s}{g}} \tag{A.7}$$

where

$\Phi_{wx}(\omega_e)$ = cross spectrum between wave and vertical ship motion at point X,

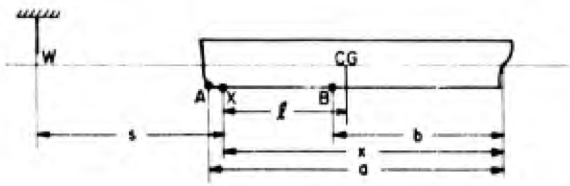

Fig. 21 - Explanatory sketch of distances a, b, x, etc.

$\Phi_{\bar{w}x}(\omega_e)$ = cross spectrum between wave and vertical ship motion measured at two different points, W and X, respectively,

S = distance between points W and X.

If this correction is included, the correlation coefficient between wave and ship motion at points X becomes:

$$\rho_{wx} = \sqrt{\frac{\left(\int |\Phi_{\bar{w}x}(\omega_e)| \cos(\epsilon - \theta)\, d\omega_e\right)^2 + \left(\int |\Phi_{\bar{w}x}(\omega_e)| \sin(\epsilon - \theta)\, d\omega_e\right)^2}{\int \Phi_{\bar{w}\bar{w}}(\omega_e)\, d\omega_e \int \Phi_{xx}(\omega_e)\, d\omega_e}} \tag{A.8}$$

where

$$|\Phi_{\bar{w}x}(\omega_e)| = \sqrt{\left\{C_{\bar{w}x}(\omega_e)\right\}^2 + \left\{Q_{\bar{w}x}(\omega_e)\right\}^2},$$

$C_{\bar{w}x}(\omega_e)$ = energy density of cospectrum between wave and vertical ship motion measured at two different points, W and X,

$Q_{\bar{w}x}(\omega_e)$ = energy density of quadrature spectrum between wave and vertical ship motion measured at two different points W and X,

$\epsilon(\omega_e)$ = $\tan^{-1}\left\{Q_{\bar{w}x}(\omega_e) / C_{\bar{w}x}(\omega_e)\right\}$,

$\Phi_{\bar{w}\bar{w}}(\omega_e)$ = energy density of auto-spectrum of wave measured at point W,

$\Phi_{xx}(\omega_e)$ = energy density of auto-spectrum of vertical ship motion measured at point X,

θ = $\omega^2 S/g$,

ω_e = encounter period with wave = $\omega + (V/g)\omega^2$,

ω = wave period,

V = ship speed.

Table 4
Values of Correlation Coefficients (MARINER, Light Draft)

Sea state	Mild 7	Moderate 7	← Severe 7 →	
Ship speed (knots)	10	10	10	15
Correlation coefficient of vertical motion, ρ_{ab}				
Between 0.034 L aft of FP and CG	0.04	0.06	0.06	0.05
Between 0.1 L aft of FP and CG	–	0.12	–	–
Correlation coefficient of vertical velocity, $\rho_{\dot{a}\dot{b}}$				
Between 0.034 L aft of FP and CG	0.03	0.05	0.02	0.04
Between 0.1 L aft of FP and CG	–	0.08	–	–
Correlation coefficient of relative motion between wave and ship, ρ_{wx}				
At 0.034 L aft of FP	0.48	0.40	0.41	0.33
At 0.10 L aft of FP	(0.53)	0.45 (0.46)	(0.46)	(0.39)
At CG	0.84	0.86	0.83	0.77
Correlation coefficient of relative velocity between wave and ship, $\rho_{\dot{w}\dot{x}}$				
At 0.034 L aft of FP	0.36	0.30	0.34	0.31
At 0.1 L aft of FP	(0.42)	0.36 (0.37)	(0.40)	(0.37)
At CG	0.80	0.83	0.79	0.74

Note: Values in parentheses are those estimated by the interpolation.

In the case when acceleration is measured instead of vertical ship motion, a modification similar to that given in Eq. (A.5) is required. That is,

$$\Phi_{\bar{w}x}(\omega_e) = -\frac{1}{\omega_e^2}\,\Phi_{\bar{w}\ddot{x}}(\omega_e) \qquad \text{(A.9)}$$

where

$\Phi_{\bar{w}x}(\omega_e)$ = energy density of cross-spectrum between wave and vertical ship motion,

$\Phi_{\bar{w}\ddot{x}}(\omega_e)$ = energy density of cross-spectrum between wave and vertical acceleration.

The variance of relative velocity between wave and ship bow can be obtained by the same procedure as that for the relative motion.

Numerical examples of the evaluated correlation coefficients, ρ_{ab}, ρ_{wx} (for relative motion) and $\rho_{\dot{a}\dot{b}}$, $\rho_{\dot{w}\dot{x}}$ (for relative velocity) are tabulated in Table 4. These were evaluated from experimental results obtained on MARINER in Sea State 7. As can be seen in Table 4, the correlation coefficients ρ_{ab} and $\rho_{\dot{a}\dot{b}}$ are very small in this case, since point A is located near the forward perpendicular and point B is located at the center of gravity.

From this table, the coefficients required for evaluating the relative motion and velocity at an arbitrary point along the ship length can be estimated by either interpolation or extrapolation.

Appendix 2

DERIVATION OF THE AVERAGE OF THE HIGHEST ONE-THIRD AND HIGHEST ONE-TENTH VALUES FOR THE TRUNCATED RAYLEIGH AND EXPONENTIAL PROBABILITY DENSITY FUNCTIONS

(A) TRUNCATED RAYLEIGH PROBABILITY DENSITY FUNCTION

It was mentioned in the text that the probability of the relative velocity between wave and ship bow follows a truncated Rayleigh probability law. The probability density function in this case is given by Eq. (11) in the text. That is,

$$f(\dot{r}) = \frac{2\dot{r}}{R_r'} e^{-\frac{1}{R_r'}(\dot{r}^2 - \dot{r}_*^2)} , \qquad \dot{r} \geq \dot{r}_* . \tag{A.10}$$

The average of the one-third highest values for this probability density function is evaluated as follows: Let $\dot{r}_{1/3}$ be the lower limit of the one-third highest values of relative velocity. Then

$$\text{Prob}\left\{\dot{r} > \dot{r}_{1/3}\right\} = \int_{\dot{r}_{1/3}}^{\infty} f(\dot{r})\, d\dot{r} = \frac{1}{3} . \tag{A.11}$$

From Eqs. (A.10) and (A.11)

$$\dot{r}_{1/3} = \sqrt{\dot{r}_*^2 - R_r' \log \frac{1}{3}} \; . \tag{A.12}$$

Next, let the average of the one-third highest values be $\tilde{\dot{r}}_{1/3}$, and consider their moment about the origin of the probability density function. Then

$$\frac{1}{3}\tilde{\dot{r}}_{1/3} = \int_{\dot{r}_{1/3}}^{\infty} \dot{r}\, f(\dot{r})\, d\dot{r} = \frac{2}{R_r'} e^{\frac{\dot{r}_*^2}{R_r'}} \int_{\dot{r}_{1/3}}^{\infty} \dot{r}^2 e^{-\frac{\dot{r}^2}{R_r'}} d\dot{r}$$

$$= e^{\frac{\dot{r}_*^2}{R_r'}} \left[\dot{r}_{1/3} e^{-\frac{(\dot{r}_{1/3})^2}{R_r'}} + \sqrt{\pi R_r'} \left\{ 1 - \Phi\left(\sqrt{\frac{2}{R_r'}}\, \dot{r}_{1/3} \right) \right\} \right] \tag{A.13}$$

where

$$\Phi(u) = \frac{1}{\sqrt{2\pi}} \int_{-\infty}^{u} e^{-\frac{t^2}{2}} dt \; . \tag{A.14}$$

Thus

$$\tilde{\dot{r}}_{1/3} = 3\, e^{\frac{\dot{r}_*^2}{R_r'}} \left[\dot{r}_{1/3} e^{-\frac{(\dot{r}_{1/3})^2}{R_r'}} + \sqrt{\pi R_r'} \left\{ 1 - \Phi\left(\sqrt{\frac{2}{R_r'}}\, \dot{r}_{1/3} \right) \right\} \right] \tag{A.15}$$

where $\dot{r}_{1/3}$ is given in Eq. (A.12).

The above equation gives the average of the one-third highest values of the relative velocity for the truncated Rayleigh distribution.

Similarly, the average of the one-tenth highest of the relative velocity for the truncated Rayleigh distribution is given by

$$\tilde{\dot{r}}_{1/10} = 10\, e^{\frac{\dot{r}_*^2}{R_r'}} \left[\dot{r}_{1/10} e^{-\frac{(\dot{r}_{1/10})^2}{R_r'}} + \sqrt{\pi R_r'} \left\{ 1 - \Phi\left(\sqrt{\frac{2}{R_r'}}\, \dot{r}_{1/10} \right) \right\} \right] \tag{A.16}$$

where

$$\dot{r}_{1/10} = \sqrt{\dot{r}_*^2 - R_r' \left(\log \frac{1}{10}\right)} \; . \tag{A.17}$$

Suppose that the distribution is not truncated and that the double amplitude is considered instead of the single amplitude; then, $\dot{r}_* = 0$ and $R'_{\dot{r}} = 4E_{\dot{r}}$ (where $E_{\dot{r}}$ = area under the spectrum for the relative velocity). In this case, we have from Eqs. (A.15) and (A.16)

$$\tilde{\dot{r}}_{1/3} = 2.83\sqrt{E_{\dot{r}}}$$
$$\dot{r}_{1/10} = 3.60\sqrt{E_{\dot{r}}} \,. \tag{A.18}$$

These are well known formulae for the averages of the one-third highest and one-tenth highest double amplitudes of the ordinary Rayleigh distribution.

(B) TRUNCATED EXPONENTIAL PROBABILITY DENSITY FUNCTION

As was given by Eq. (15) in the text, the truncated exponential probability density function may be expressed as

$$f(p) = \frac{1}{2CR'_{\dot{r}}}\, e^{-\frac{1}{2CR'_{\dot{r}}}(p-p_*)}\,, \qquad p \geq p_* \tag{A.19}$$

where

p = pressure = $2C\dot{r}^2$,

p_* = truncated pressure = $2C\dot{r}_*^2$,

$R'_{\dot{r}} = 2\sigma_{\dot{r}}^2$,

C = constant.

Then, the lower limit of the one-third highest values, $p_{1/3}$, can be obtained from the following relation:

$$\text{Prob}\ \ p > p_{1/3} = \int_{p_{1/3}}^{\infty} f(p)\, dp = \frac{1}{3}\,. \tag{A.20}$$

Hence

$$p_{1/3} = p_* - 2CR'_{\dot{r}}\left(\log\frac{1}{3}\right). \tag{A.21}$$

Next, let the average of the one-third highest pressures be $\tilde{p}_{1/3}$, and take the moment about the origin of the density function. That is,

$$\frac{1}{3}\tilde{p}_{1/3} = \int_{p_{1/3}}^{\infty} p\ f(p)\ dp\ . \tag{A.22}$$

From Eqs. (A.19), (A.21) and (A.22) the average of the highest one-third values becomes

$$\tilde{p}_{1/3} = p_* + 2CR'_{\dot{r}}\left(1 - \log\frac{1}{3}\right)$$

$$= 2C\left(\dot{r}_*^2 + 2.10\ R'_{\dot{r}}\right)\ . \tag{A.23}$$

Similarly, the average of the highest one-tenth values is

$$\tilde{p}_{1/10} = p_* + 2CR'_{\dot{r}}\left(1 - \log\frac{1}{10}\right)$$

$$= 2C\left(\dot{r}_*^2 + 3.30\ R'_{\dot{r}}\right)\ . \tag{A.24}$$

* * *

DISCUSSION

G. Aertssen
University of Gent
Gent, Belgium

The first look at this paper gives the impression that it is a remarkable example of the truncated exponential probability law applied to the study of slamming and deck wetness from model results. Were it not that there is much more in it for the naval architect it would not have deserved much attention.

There is a difficulty in carrying out slamming experiments on models because the rigidity of the model cannot be easily scaled up to the rigidity of the ship. Giving the relation impact pressure, relative velocity, the author however gives — I think for the first time — the means to correlate his model results with full scale. His threshold velocity is 12 ft/sec and if I modify this value, according to the Froude scaling law, to a cargo ship of 480 ft I obtain a threshold velocity of 11.5 ft/sec which according to the author's relation transforms to our impact pressure of 11 psi. I am interested in this cargo ship of 480 ft because last winter I made a westbound crossing of the North Atlantic in very severe weather on board such a ship which was instrumented by the Centre Belge de Recherches Navales. There were on board a shipborne wave recorder, strain gages, ship motion recorders, 2 pressure transducers in the keelplate, etc. When weather was worsening, shocks were felt but the impacts on the forebody did not induce any reaction among ship's officers until at a certain moment they mentioned in the log book: "le navire travaille et fatigue," the ship works and there is fatigue. At this moment the whipping stresses in the main deck stringerplate amidships were 0.5 t per sq in. and the impact pressure on the pressure transducer located at 0.15 Lpp from FP was about 10 psi. The ship was in nearly full-loaded condition and the location of the pressure transducer was not exactly the same as the location 0.1 Lpp indicated by Dr. Ochi. Unfortunately I have no impact data of this ship in light-loaded condition hitherto, but the nice agreement between the threshold of whipping stresses and impact pressure established on our cargo ship in nearly full-loaded condition and the threshold of velocity established by Dr. Ochi is certainly an encouragement to believe in his prediction of slamming from model results.

This prediction of slamming is very well presented in Table 2 for a Mariner ship. Looking at the number of slams in a 30 minute operation there are in a moderate Sea State 7 only 12 slams in full-loaded against 60 in light-loaded condition in head waves and they are again reduced when the captain changes course 45 degrees. This might indeed give the picture of what happens on the bottom at the forebody and the danger of damage there. But modern cargo liners are longitudinally framed and often reinforced in the forebody beyond classification requirements, so today bottom damage is more seldom stated after a crossing in severe weather condition. Whipping stresses however are excited in the main girder and they might increase to a certain extent the longitudinal bending stresses and be a source of fatigue. Therefore I think that perhaps more than the number of slams these whipping stresses ought to be considered. At each slam there is a vibration in the ship main girder and an initial whipping stress. Summing up these initial whipping stresses for let us say again a 30 minute operation and dividing by the number of low cycle stress oscillations a slam number is obtained which might as well give the intensity of the effect of slamming on the hull girder. Establishing this slam number, whipping stresses less than 0.4 t per sq in. were ignored. I had these whipping stresses measured in a sea state about the mild 7 Beaufort of Dr. Ochi's paper, once in light-loaded condition on a cargo ship of 446 ft in waves $\bar{H}_{1/10}$ = 27 ft at 12.5 knots, on another occasion in nearly full-loaded condition on a cargo ship of 480 ft in waves $\bar{H}_{1/10}$ = 33 ft at 9 knots, and in this nearly full-loaded condition the whipping stresses and the slam number representing their intensity were larger than in light-loaded condition. In light-loaded condition the severe slams are heard like a gun shot whereas in full-loaded condition they are more like far-off thunder. In light-loaded condition the slams are more conspicuous and captains are keen to reduce speed. That is perhaps one of the reasons why the slam number is not larger in light-loaded than in full-loaded condition. As long as not too much green water is shipped the captain of a full-loaded cargo ship goes ahead in high waves and modern cargo ships with a long forecastle and a fair fore freeboard maintain a good speed in these high waves.

And here I should like to ask Dr. Ochi why he has taken the same speed of 10 knots for his comparison light-loaded and full-loaded? Has he any information as to what extent captains of Mariners accept 60 slams, i.e., 2 slams every minute, in light-loaded condition in waves of 31 ft significant height? As a rule captains of cargo ships of 10,000 tons deadweight and 16 knots service speed do not accept these waves at a speed of 10 knots, when in light-loaded condition.

DISCUSSION

E. V. Lewis
Webb Institute of Naval Architecture
Glen Cove, Long Island, New York

This paper is of particular significance because it attempts to establish criteria for the occurrence of slamming. Such criteria have been badly needed in connection with the calculation of ship performance in irregular seas by the method of superposition. The criteria will make possible, for example, the determination of the speed at which slamming would become serious — or the prediction of comparative slamming characteristics of alternative ship designs.

It is hoped that for completeness the work will be continued to allow for the effect of section shape on the critical vertical velocity for slamming — and also to allow for the effect of form and fullness on the fore and aft location of the critical section.

The equations for various probabilities in evaluating performance in irregular seas will be very useful. It should be pointed out that the probabilities are based on assumed stationary conditions — constant ship speed and heading, as well as steady sea conditions. Hence, the equations must be used with caution. For in the case of the full-scale ship at sea, the shipmaster is certain to change course or speed if slamming becomes serious, so that conditions would not remain stationary.

Another point is in regard to the assumption in the paper that the pressure of water on deck is purely static. It would be expected that there would be considerable dynamic effect associated with the aftward velocity of the water.

* * *

DISCUSSION

W. A. Swaan
Netherlands Ship Model Basin
Wageningen, Netherlands

In the course of the last 10 years the possibilities of applying the superposition theory or the problem of ship motions in irregular seas have covered an increasing range of phenomena. At first only ship motions were considered, subsequently the superposition methods for resistance and power were evaluated and checked by experiments. The results presented in this paper here cover the final gap, that is the relative motions at the bow with the associated problems of slamming and wetness. The test results leave no doubt about the possibility to apply these methods to ship predictions from now on with full confidence.

In his explanation about the basic concept the author distinguished two problems; that is the prediction of the probability of slamming per cycle and the prediction of the number of cycles per unit time. I would like to make a minor remark on both points.

In Appendix 1 it is mentioned that it is possible to determine the relative motion at the bow using an accelerometer on the model and a wave probe in front of it. This seems to be a method containing some uncertainties. In the first place it will be necessary to know the smooth water level at the station which is considered critical for slamming.

In Eq. (5) of the paper this is assumed to be equivalent to the draft. This may be true for a vessel like the "Mariner" at a speed of only 10 knots but at higher Froude numbers a significant difference may be found because of the smooth water bow wave system of the ship. The bow wave of a ship usually decreases the probability of slamming and increases the wetness. The second objection against the use of a wave height transducer in front of the model is that the bow of a pitching and heaving ship creates an oscillating bow wave which will affect the variance of the relative motions. This will be somewhat less important for fine ships than for full ships. It is therefore concluded that the only reliable way to measure the relative motion is to do so at the critical station which is used for the determination of the probability of slamming per cycle.

The second remark concerns the use of the second moment of the spectrum in order to obtain the expected number of zero upcrossings. Our experience indicates that the quotient of the spectrum area and the first moment gives a better approximation to the number of zero upcrossings. This is only of importance when the spectrum is not narrow because otherwise the two methods yield the same result. The sea spectrum, however, is not always narrow, for instance when it is desired to simulate a Neumann spectrum which has a width of ϵ = 0.815. Using the first moment of the spectrum will result in the prediction of less slams per unit time as is shown in the Table 1 where results are shown from some relative bow motion and wave height measurements.

The width of the spectrum was estimated with the quotient of the number of maxima and the number of zero upcrossings. According to the results in Table 1, Eq. (7) from the paper is more accurate in predicting the number of maxima than in predicting the number of zero upcrossings.

Table 1

Test No.	Zero Up-Crossings per Unit Time (%)	Maxima per Unit Time (%)	$\frac{1}{2\pi}\sqrt{\frac{M_1}{M_0}}$ (%)	$\frac{1}{2\pi}\sqrt{\frac{M_2}{M_0}}$ (%)	ϵ
		Waves			
1	100	111	104	110	0.43
2	100	110	104	110	0.42
3	100	112	105	111	0.45
4	100	113	105	111	0.47
		Relative Motion			
1	92	103	95	100	0.45
2	94	105	97	102	0.45
3	91	102	94	100	0.45
4	92	101	93	99	0.43

* * *

DISCUSSION

L. Vassilopoulos
Massachusetts Institute of Technology
Cambridge, Massachusetts

For those involved in seakeeping research the present paper is a very welcome contribution for it deals with the two most important phenomena that dictate the speed which a high-powered fine ship can sustain in rough water operation, namely slamming and wetness occurrence. At the same time the probabilistic methods presented and verified in Dr. Ochi's paper provide further useful tools for a realistic evaluation of the importance of seaworthiness in ship design.

Although the author's analysis and verification was performed only for a Mariner model at moderate speeds, there is no reason to believe that a similar approach would be invalid for other conventional ship forms and at slightly more severe conditions. Of particular interest are the conclusions with regard to the actual mechanisms of slamming and wetness phenomena and the necessary and sufficient conditions which must prevail for their occurrence. It is particularly encouraging that in the case of slamming the number of critical factors has been reduced from three in regular seas to two in irregular seas. This favorable result overcomes otherwise unsurmountable calculation difficulties.

The formula that Dr. Ochi has developed for the probability of slamming rests on the assumption that the relative motion of an arbitrary ship point is a narrow-band Gaussian process. Although the satisfactory correlation of measured and predicted results which Dr. Ochi shows suggests that this appears to be the case, it must be stressed that one cannot a priori assume that the relative motion will indeed be a narrow-band process because the wave motion is not always a narrow-band process, except perhaps for severe sea conditions. Further, the sum of two narrow-band processes need not necessarily be a narrow-band process itself. Any absolute ship response, however, such as bow motion for example, can safely be regarded as a narrow-band process since the wave motion is mostly wide-band and the ship-system is strongly resonant.

The next step in Dr. Ochi's analysis follows the approach employed in other engineering fields in that attention is focused on the envelope of the time function rather than its amplitude. In this connection I would like to point out that Eq. (2) can indeed be regarded as the definition of the envelope and which, stated otherwise, essentially regards $|r_0(t)|$ as the instantaneous radius of the image point on the phase plane diagram of Fig. 3(b). Dealing with the envelope rather than with the actual amplitude turns out to be very convenient for we can immediately obtain a closed form expression for the probability of slamming, such as Eq. (5). I cannot precisely follow the steps leading to (5), but I assume that Dr. Ochi multiplies the integrated Rayleigh probability density functions for the relative motion and the relative velocity. This is, of course, permissible since both processes are Gaussian and hence linearly as well as statistically independent.

The author employs the nomenclature "probability of slamming per cycle of wave encounter." For a narrow-band process one may perhaps speak of cycles in an extended sense and even then the precise meaning of cycle is not very clear. But for a wide-band process, like the wave motion record, is it really possible to identify a cycle of wave encounter? Also, Fig. 3 seems to indicate that slamming only occurs when $r = H$ and $\dot{r} \geq \dot{r}^*$. Is it not more correct to say that slamming can occur as long as $r \geq H$ and provided that the relative velocity has assumed at least its threshold value?

The paper deals with the wetness problem in a similar and more simplified way and thus provides prediction methods for the propeller emergence problem also. The author has obtained a fascinating result with regard to the distribution of slamming occurrences. It seems to me that utilization of the exponential distribution of the time intervals between slams together with the expected number of slams per unit time as developed by Tick can be used to provide an answer in a statistical sense of the average sustained speed for a given ship. Has the author perhaps examined whether the wetness phenomenon is also a sequence of events which are Poisson distributed?

In conclusion, I would like to raise one further point which was so strongly mentioned by Professor Weinblum in his paper presented during the First

Symposium on Naval Hydrodynamics ten years ago: Is it not true that the time has come for a scientific evaluation of the freeboard problem of a ship on the basis of wetness considerations? It would seem that Dr. Ochi's paper as well as that of Mr. Goodrich in this Symposium both provide essential evidence that we are properly equipped to undertake such an investigation.

* * *

REPLY TO THE DISCUSSION

Michel K. Ochi
David Taylor Model Basin
Washington, D.C.

Professor Lewis mentioned that the probabilities presented in this paper are based on assumed stationary conditions, i.e., ship speed, heading as well as sea conditions are constant. The assumption of stationary conditions, however, is considered to be a proper approach in the analysis. Since voluntary reduction of speed or change of course angle are entirely dependent on the personal judgment of ship operators, it is appropriate not to include human elements in establishing the statistical rules.

He also discussed that the aftward velocity of the green water would have a considerable dynamic effect on the pressure on the deck. The pressure on the deck reported in this paper is the vertical component of green water flowing over the deck from the top of the stem. Pressure records obtained in the experiments have shown that pressure normal to the deck is not an impact type and that the pressure magnitude approximately corresponds to the static water head experienced at the stem. Judging from these results there is no reason to believe that consideration of the dynamic effect of the aftward velocity is necessary for the vertical pressure on the deck. This consideration is of course necessary for the horizontal component (aftward direction) of pressure on the deck, since the green water would crash at the front face of the deck superstructure with considerable velocity.

Mr. Swaan remarked that the bow wave of a ship usually decreases the probability of slamming and increases the wetness. For this reason, he said most reliable way to obtain the relative motion is to measure it at the location considered. Consideration will be given to his remarks in future experiments by the author.

Professor Aertssen asked why the same speed of 10 knots was used for comparison of frequency of occurrence of slamming for light and full draft

*See discussion by Pierson to paper by Ogilvie and discussion by Tick to paper by Cummins and Smith.

conditions. This is due to the following reason: that is, if different speeds are used for comparison, two factors (speed and loading condition) both of which significantly affect the frequency of occurrence of slamming are involved in the results, and hence we cannot identify which factor had the greatest effect on the frequency. For example, the result of full scale trials introduced by Professor Aertssen shows that the slam number for full loading condition is higher than that for light loading condition. However, we cannot conclude from this result that full loading is more severe than the light loading, since the speed was higher for the full load than for the light load condition. It is also noted that the slam number as defined by Professor Aertssen is expressed in terms of whipping stress. This automatically includes the ship mass effect. In other words, even if the ship motions are the same for two different drafts, whipping stresses are quite different since the dynamic characteristics are entirely different. Thus, we cannot identify which factor increased the slam number for full loading. Thus, in order to obtain the effect of loading condition the same speed was used for evaluating the frequency of occurrence of slamming for light and full draft so that the difference in slamming rate could be attributed to the difference of ship motion characteristics.

Mr. Vassilopoulos questioned whether or not the relative motion between wave and ship bow is a narrow-band Gaussian process. It cannot be said, of course, that the relative motion is a sharp narrow-band Gaussian process as is frequently observed in strongly resonant vibratory systems. However, the following table may provide some information on this subject.

Sea State	Expected Frequency for Narrow-Band Gaussian Process, $\sqrt{R'_r\, R'_r}$	Domain of Significant Energy in the Observed Spectrum of Relative Motion
Severe 7	0.71	0.68 to 0.78
Moderate 7	0.69	0.65 to 0.75
Mild 7	0.72	0.68 to 0.75

The above table pertains to a ship speed of 10 knots and light draft condition. Since the expected frequencies lie in the domains of significant energy in the observed spectra, it may be said that the relative motion can be treated as a narrow-band Gaussian process.

Mr. Vassilopoulos pointed out that the condition $r \geq H$ be used instead of $r = H$ in Eq. (5) of the paper. Although the final result is the same for both conditions, $r \geq H$ is the correct expression.

The author agrees with Mr. Vassilopoulos' opinion that the deck wetness condition should be considered in the freeboard requirement. The author would like to continue further studies of the effect of section shape on the magnitude of threshold velocity as was suggested by Professor Lewis, although the values obtained on five different ships have shown fairly consistent values.

THE INFLUENCE OF FREEBOARD ON WETNESS

G. J. Goodrich
National Physical Laboratory
Teddington, England

ABSTRACT

Model experiments in regular waves and probability theory have been used to predict the probability of occurrence of wetness at the fore-end of a ship of given type. Calculations made for ships of different fullness have suggested that the frequency of occurrence of wetness varies with block coefficient as well as with length for a given free-board ratio.

INTRODUCTION

The prediction of the probability of occurrence of wetness from model experiments in regular waves has been attempted by Newton [1] using statistical sea data to represent full scale conditions. Newton's work suggested that for a given freeboard ratio a 200 ft ship would be drier than say a 400 ft ship under North Atlantic conditions. This general conclusion seemed contrary to what would be expected and consideration was given to the possibility of using model data and probability theory to predict the probability of occurrence of wetness for ships of different fullness and length.

The intention of the present paper is not to provide detailed design information but to indicate a method of analysis which could be used for specific design studies and to show the trend of the variation of wetness with ship length and block coefficient.

WETNESS DEFINITION

When considering the prediction of the probability of occurrence of wetness it is sufficient to say that if the motion of the bow relative to the water surface is such that the water rises above the deck level at the fore end, then the probability of wetness exists. No attempt is made to say how wet the deck will be, nor to what height the water will rise above the deck.

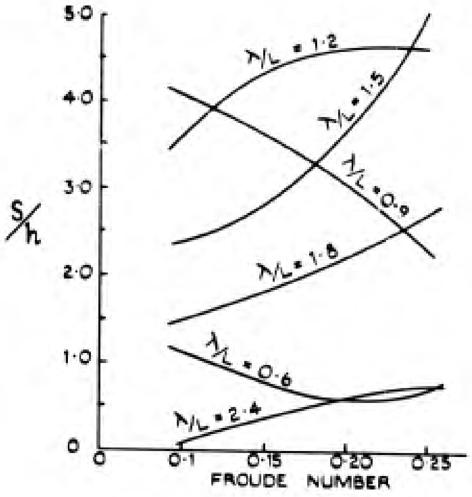

Fig. 1a - Response curves for constant λ/L 0.70 C_B

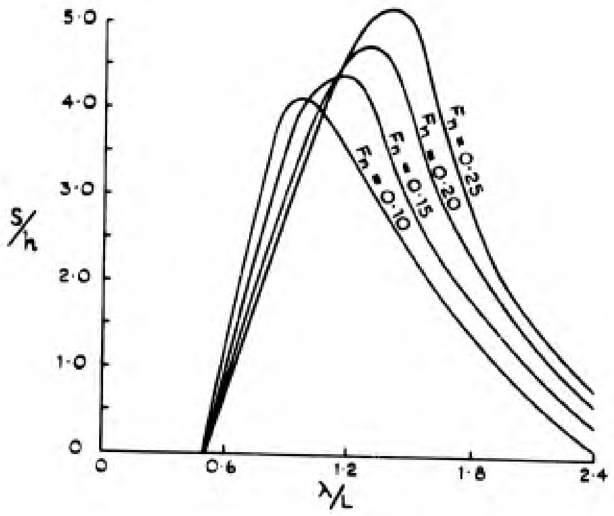

Fig. 1b - Response curves for constant speed 0.70 C_B

MODEL DATA

The most systematic model data available at present are those of Vossers and Swaan [2] and these have been used in the present analysis. Measurements were made of the relative bow motions of a series of models and the response curves presented as the ratio of the relative bow motion to wave height on a base of block coefficient and for a range of speeds. Cross curves have been derived of the relative bow motion to wave height ratio for constant wave lengths to a base of Froude Number. Some account has been taken of the loss in speed due to wave action by assuming a loss in speed curve for each model. The responses have then been obtained from the cross curves for the speed corresponding to the particular Beaufort scale being considered. Typical response curves are given in Figs. 1a and 1b for the 0.70 C_B form.

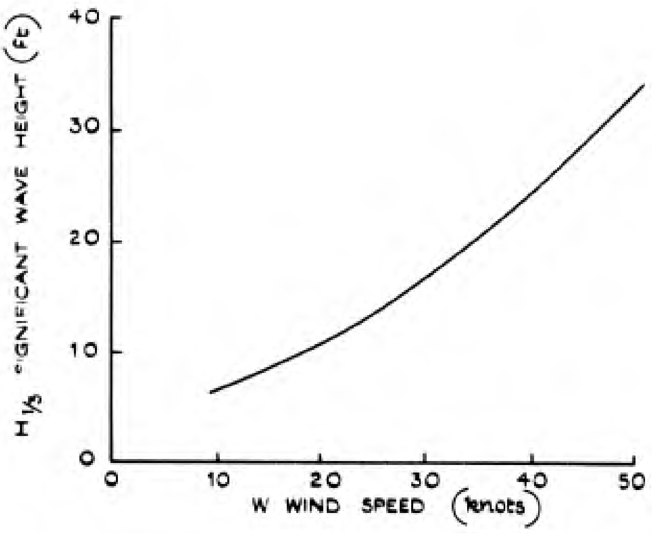

Fig. 2 - Significant wave height vs wind speed

REPRESENTATION OF THE SEA

Sea spectra are needed in the analysis in order to obtain motion response spectra and a modified form of the Darbyshire formulation has been used. The curve of significant wave height against wind speed shown in Fig. 2 was used and the three Darbyshire spectra are shown in Fig. 3.

The equation of the Darbyshire spectrum is

$$\left(\frac{H_f}{H}\right)^2 df = 23.9 \exp - \left(\frac{(f - f_o)^2}{0.00847\ [(f - f_o) + 0.042]}\right)^{1/2} df$$

where

$H^2 = \Sigma H_f^2$,

H_f^2 = spectral ordinate,

f = frequency,

f_o = frequency of the peak value of the spectrum,

$H_{1/3}$ = 1.65H.

This latter value of $H_{1/3}$ is that derived by Darbyshire from his analysis. The spectrum in this form cannot be combined directly with response operators which are expressed in terms of wave length to ship length ratios, nor in frequencies of encounter. If the response curves for one ship speed and for varying

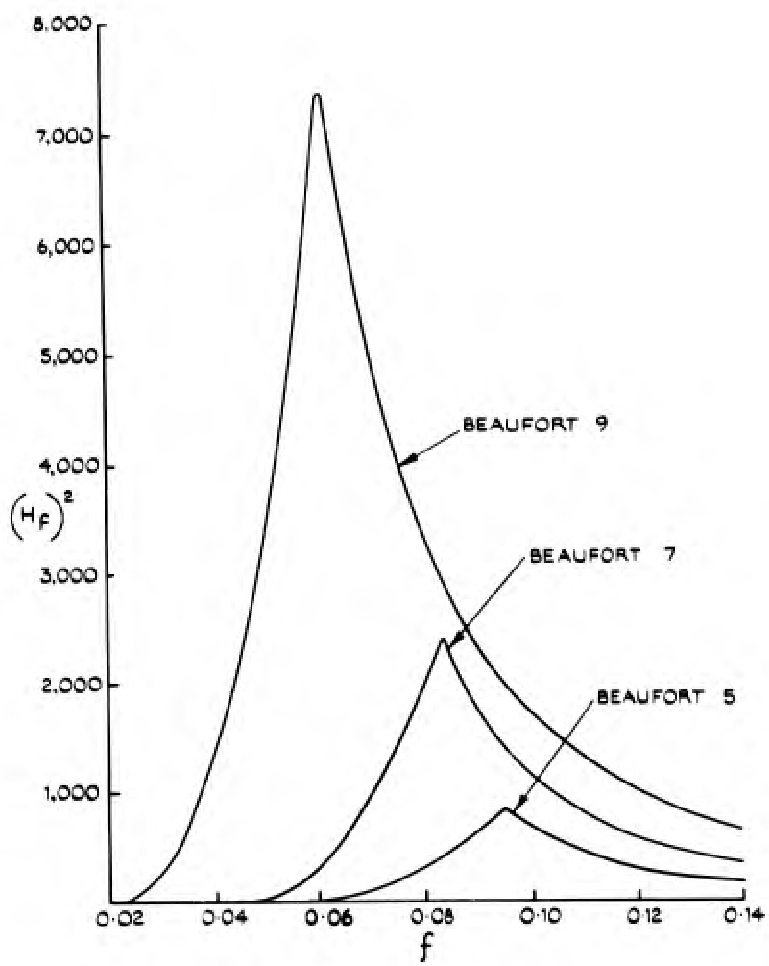

Fig. 3 - Sea spectra used in the analysis

wave length are used they can be combined with a spectrum transformed from the frequency base to a wave length base. The transformation is:

$$[r(\lambda)]^2 = \frac{H^2}{4} \times \frac{1}{2}\sqrt{\frac{g}{2\pi}} \times \lambda^{-3/2} \frac{d\lambda}{df}\left(\frac{H_f}{H}\right)^2 df$$

and includes the change from the energy expressed in terms of wave height, to the energy in terms of wave amplitude.

It must be appreciated that although a unique curve of significant wave height versus wind speed has been used, wide variations of wave height exist in practice for a given wind speed. It is assumed that using this "mean curve" and deriving the resulting response spectra results in mean values of the root mean square response for a given wind speed or Beaufort Number.

METHOD OF ANALYSIS

A number of gross assumptions have been made in the analysis as follows:

(a) It has been assumed that for the extreme motions the conditions remain linear. The model experiments were carried out for a constant height-ship length ratio of 1/50.

(b) It has been assumed that the motion is regular about the mean still water draught of the ship.

(c) The head sea case only has been considered with no spreading of the wave spectra.

(d) For comparative purposes it has been assumed that the ships are in the head sea condition 100% of the time.

Other assumptions made in the analysis will be stated later.

By combining the response curves such as in Fig. 1 with the sea spectra given in Fig. 3, the response spectra are obtained and by integration of these spectra, the mean square response is derived

$$s_m^2 = \sum \left(\frac{s}{h}\right)^2 [r(\lambda)]^2 .$$

The derived curves of root mean square response amplitude s_m for a range of Beaufort numbers are shown in Fig. 4 for 0.70 C_B ships of 200, 400 and 600 ft lengths.

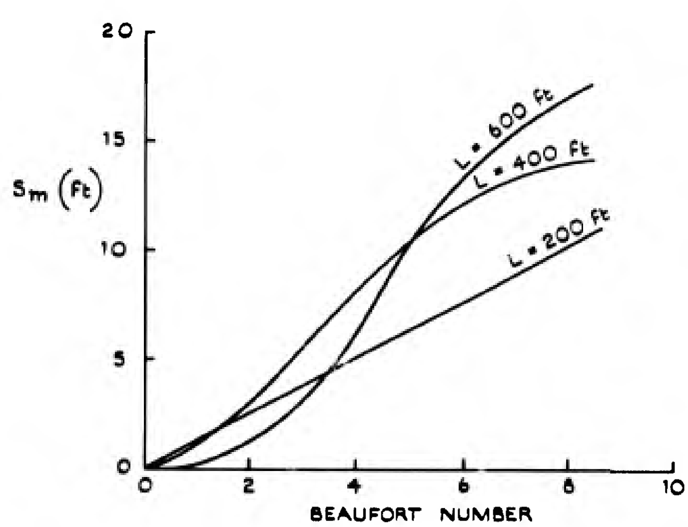

Fig. 4 - Root mean square response for constant ship lengths 0.70 C_B

It has been assumed that the short term distribution of the variation of relative vertical motion of the bow will have a Rayleigh distribution. With this distribution the probability of exceeding a specific value of relative bow motion S_i is

$$e^{-S_i^2/S_m^2}.$$

In order to obtain the long-term distribution of S, a weighting factor for weather distribution must be included. As was stated earlier no weighting factor has been included in this analysis to take account of variations in the sea direction. The probability of exceeding a specific value of S_i is therefore:

$$Q_i = \sum_j e^{-(S_i/S_m)^2} \times P_j$$

where P_j is the weighting factor for the general weather probability distribution. The weather distribution used is given below over the range of weather groups 1 to 5.

Group	Beaufort Number	Distribution %
1	0-3	52.0
2	4-5	29.0
3	6-7	15.0
4	8-9	3.5
5	10-11	0.5

The mean value of S_m for each group has been used in the calculation of Q_i, with values of S_i of 10, 20 and 30 ft for all lengths of ships. From the calculated values of Q_i for specific values of S_i probability curves can be drawn such as in Fig. 5. If freeboard at the fore perpendicular is substituted for S_i then these curves show the probability of the water rising above the freeboard. A non-dimensional freeboard ratio can be used, (defined as the ratio of the freeboard at the fore perpendicular to the ship length) rather than absolute freeboard and the results for the 0.60, 0.70 and 0.80 C_B ships are given in terms of this ratio in Figs. 6, 7 and 8. The curves for the 0.80 C_B ships include lengths of up to 1000 ft since there is a growing interest in the behaviour of bulk cargo carriers of such lengths.

Figures 9, 10 and 11 show the freeboard ratio required for various ship lengths for equal probability of wetness.

DISCUSSION OF RESULTS

The results show that for equal probability of occurrence the freeboard ratio decreases with increasing ship length. The results for the 0.60 and 0.80 C_B ships are similar but the analysis shows that the 0.70 C_B ships require a greater freeboard. This result is a direct consequence of the higher responses obtained for

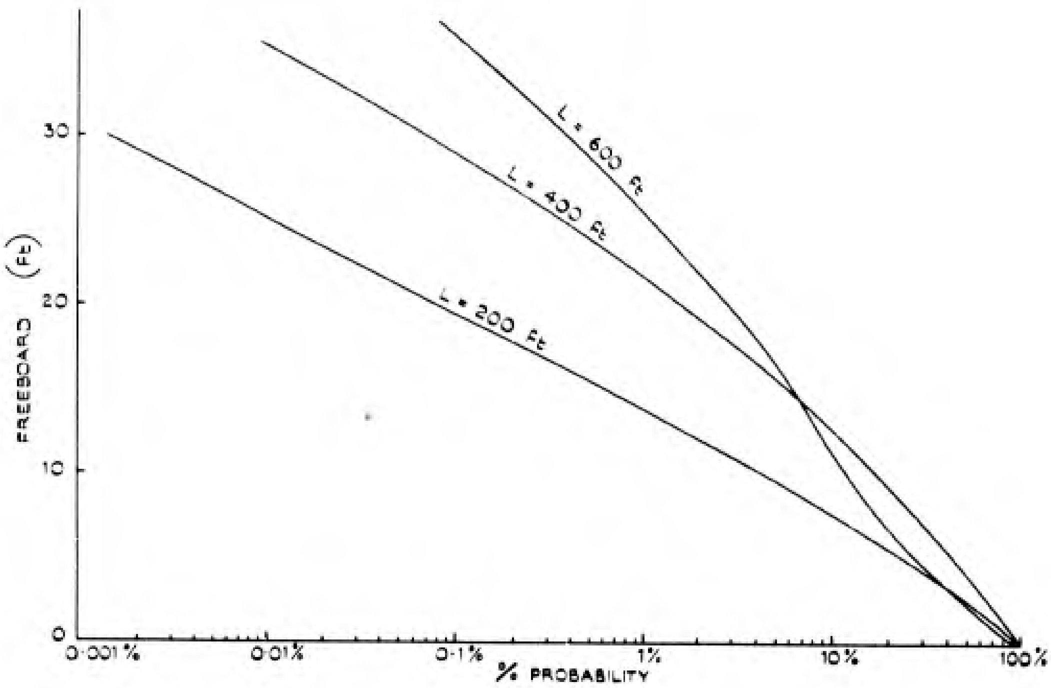

Fig. 5 - Freeboard vs probability of wetness for constant ship lengths 0.70 C_B

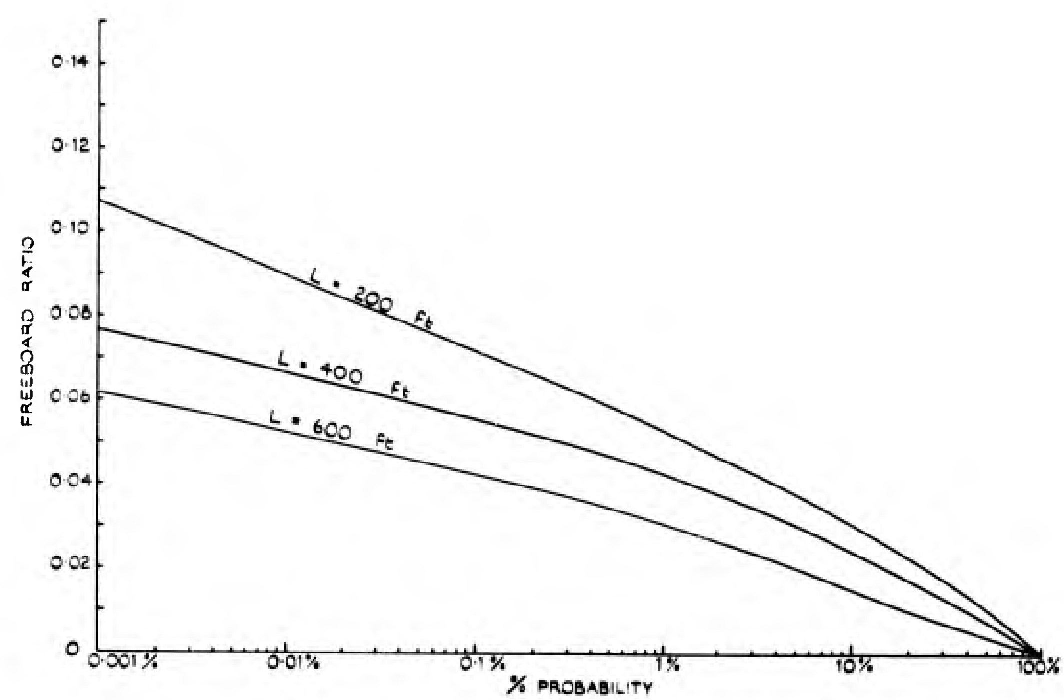

Fig. 6 - Freeboard ratio vs probability of wetness for constant ship lengths 0.60 C_B

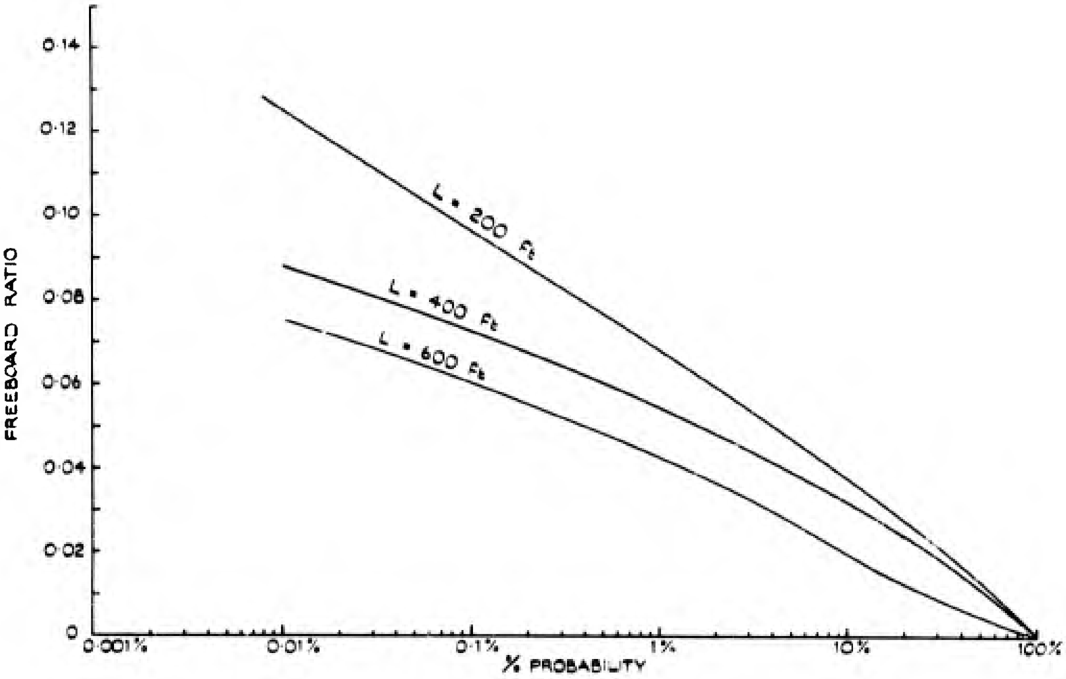

Fig. 7 - Freeboard ratio vs probability of wetness for constant ship lengths 0.70 C_B

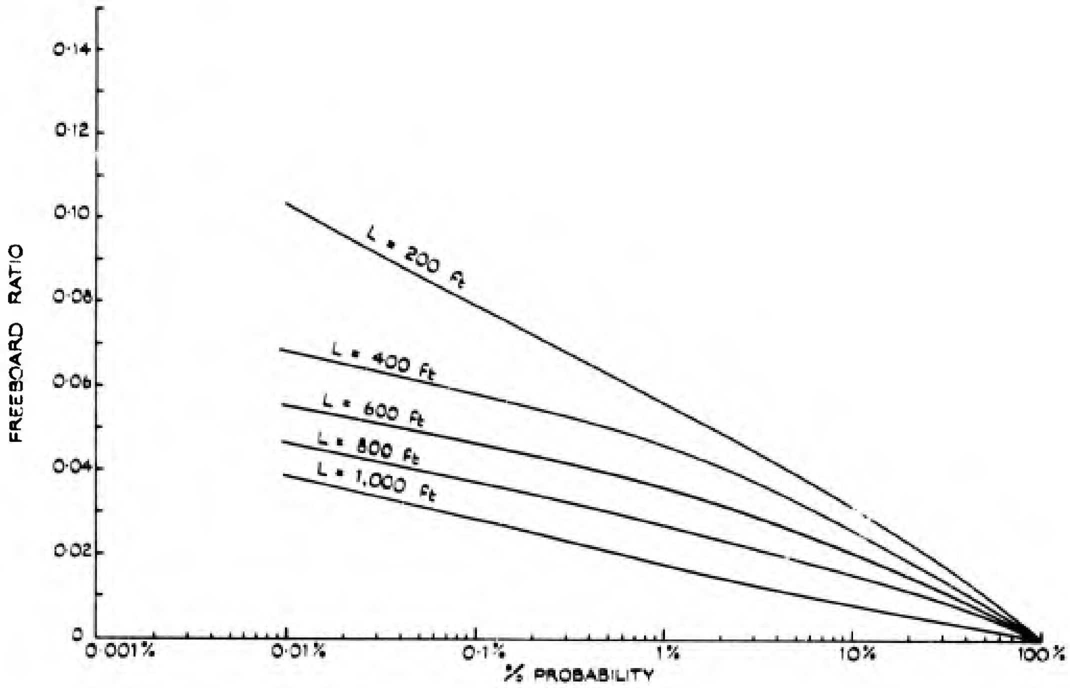

Fig. 8 - Freeboard ratio vs probability of wetness for constant ship lengths 0.80 C_B

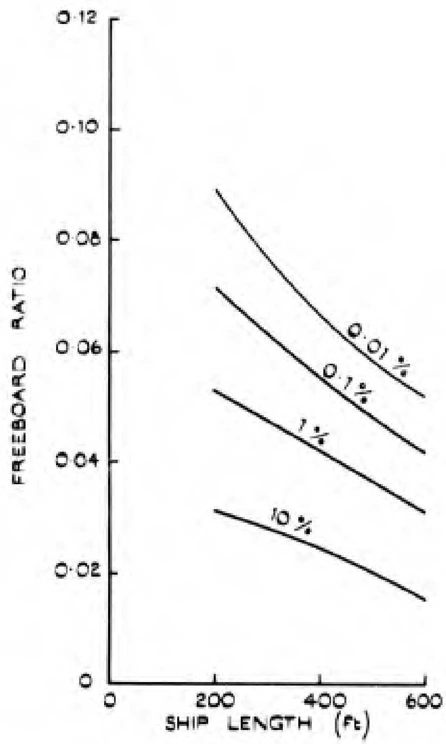

Fig. 9 - Curves of freeboard ratio for constant probability of wetness 0.60 C_B

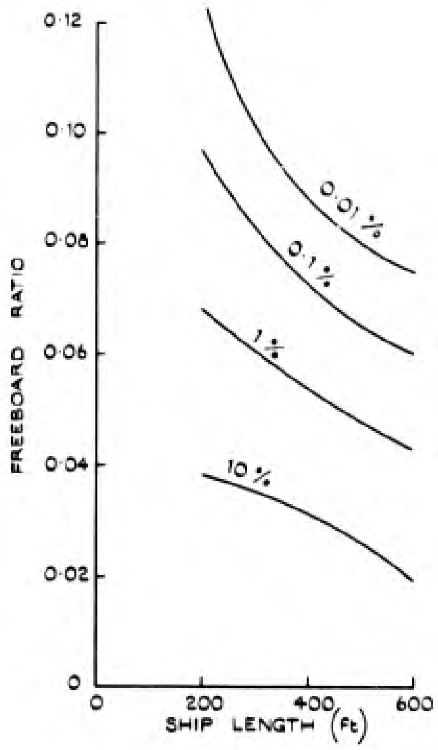

Fig. 10 - Curves of freeboard ratio for constant probability of wetness 0.70 C_B

the 0.70 C_B model tests. In Fig. 11, the slope of the lines of freeboard ratio for constant probability of occurrence of wetness indicate that for ship lengths in excess of 600 ft a constant freeboard gives equal probability.

The question arises as to what is an acceptable level of probability of wetness. At this stage it is difficult to say what is acceptable but ships which are known to be good sea ships could be plotted in the diagrams in order to see what level of probability would be expected for them.

It is the intention to run models of the 0.60, 0.70 and 0.80 block coefficient in irregular wave systems to check the number of times wetness occurs in a given train of waves. The system of generating irregular waves in the Ship Division's No. 3 Tank is such that the scale of the spectrum is easily modified. A constant length model can therefore be used with varying scale of spectrum to simulate different ship lengths.

ACKNOWLEDGMENT

This work has been carried out as part of the research programme of the National Physical Laboratory, and the paper is published by permission of the Director of the Laboratory.

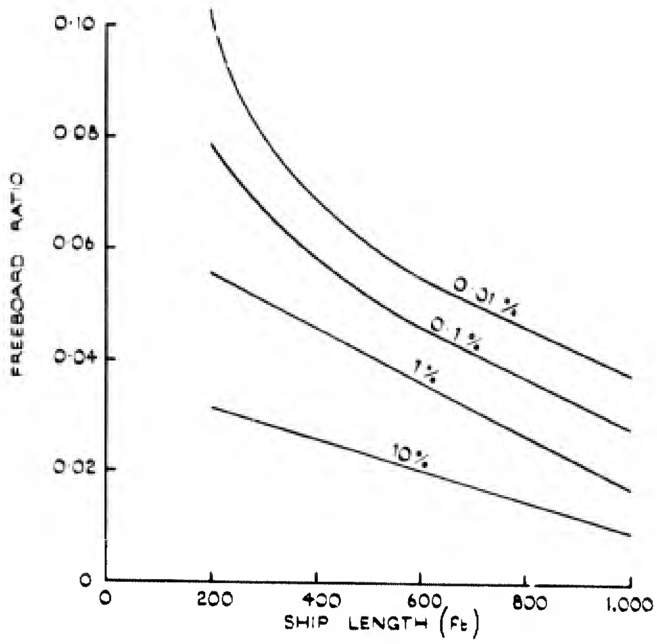

Fig. 11 - Curves of freeboard ratio for constant probability of wetness 0.80 C_B

REFERENCES

1. Newton, R. N., "Wetness Related to Freeboard and Flare," Royal Institution of Naval Architects, Vol. 102, 1960.

2. Vossers, G., Swaan, W. A., and Rijken, H., "Experiments with Series 60 Models in Waves," Society of Naval Architects & Marine Engineers, Vol. 68, 1960.

DISCUSSION

E. V. Lewis
Webb Institute of Naval Architecture
Glen Cove, Long Island, New York

This paper shows how available techniques for predicting ship behavior in any particular sea condition—as described in my own paper—can be significantly extended by considering representative sea spectra of different levels of severity. Then, with the help of probability theory, long-term predictions can be made of quantities such as frequency of deck immersion forward. This approach provides a rational basis for establishing standards of bow freeboard.

One question arises regarding ship speeds in the calculations. It would be of interest to know what speeds were assumed for each ship and each sea spectrum, since the wetness certainly depends on speed.

* * *

DISCUSSION

R. F. Lofft
Admiralty Experimental Works
Gasport, England

As one who was concerned with Newton's original paper on wetness, I am pleased to see this work being developed and extended in Goodrich's paper. Both papers point to the need for more wave data, and the need for caution in interpreting results based on present sparse data.

In Newton's paper, the wave information was taken from Darbyshire's tables of frequency of occurrence of waves of given length and height, published in 1955. These were the dominant waves, and shorter or longer waves which were present simultaneously were ignored. This may account for some emphasis on waves around 500-700 ft long, and so to an underestimate of wetness of smaller ships, in particular.

On the other hand, the Darbyshire spectra on which Goodrich's work is based, relates specifically to local wind-generated seas, and excludes swell waves, which may affect larger ships. This paper therefore may give a somewhat optimistic picture of the wetness of the longer ships, as in Fig. 11. Clearly we cannot obtain reliable estimates of wetness until more complete and reliable data are available on sea spectra and their frequency of occurrence.

It should be pointed out that the "wetness" derived by Goodrich corresponds approximately to the very wet condition as defined by Newton. It is not uncommon for ships to be under spray, i.e., Newton's wet condition, without the bow becoming immersed.

Finally, plottings of the form of Figs. 9-11 are purely comparative. It means nothing to the mariner, or to the designer, to be told that a particular ship has a probability of wetness of 0.01%. Studies of this nature must be associated closely with sea experience to be meaningful. If plottings of this type were prepared for existing ships of known good or bad reputations for wetness, as advocated by Newton, then perhaps an equivalence could be established between the estimated probability of wetness and a degree of wetness which could be regarded as acceptable in practice.

* * *

Friday, September 11, 1964

Afternoon Session

SHIP MOTIONS

Chairman: C. Falkemo

Chalmers Tekniska Hogskola
Goteborg, Sweden

HYDROFOIL MOTIONS IN A RANDOM SEAWAY

B. V. Davis and G. L. Oates
De Havilland Aircraft of Canada, Limited
Downsview, Ontario, Canada

INTRODUCTION

This paper outlines the analog simulations and the complementary model test programmes conducted by De Havilland (Canada) during the design of the 200 ton FHE-400 Hydrofoil Ship for the Royal Canadian Navy.

The equations of motion required to describe the motions of the hydrofoil are discussed in detail, together with the simulation of the equations and the seaway forcing functions. The model trials are also discussed and it is demonstrated that good correlation has been achieved between predicted and actual behaviour of a 1/4 scale model of the FHE-400 and between simulated and actual seaways.

The achievement of satisfactory dynamic stability requires an iterative design procedure similar to that followed in aircraft design, first to establish steady-state requirements and then to examine the dynamic behaviour. When examining the hydrofoil system in a seaway, it is necessary to consider hydrodynamic and structural requirements in order to develop a balanced and practical design. This is illustrated in Fig. 1.

Initial studies can be carried out using simplified equations with calculated derivatives, as only "broad" outlines are required. Subsequent studies have to be performed in greater detail as more accurate information becomes available from calculations and model trials data. The initial studies should show up any major shortcomings in the design. Some modifications are likely to result from the initial simulations. Once a reasonable foil configuration has been derived, then extensive model trials should be conducted and the results used for further and more accurate dynamic stability studies. Sophisticated equations are then required to take account of all significant nonlinearities.

Because of the complex nature of both the ship and random seaway simulation, model trials are necessary to verify theoretical predictions. While towing tank trials of foil units are necessary to measure resistance and to provide foil derivatives, it is even more important to evaluate "seagoing" models, preferably manned, in order to measure response in a scale seaway. By comparing measured response with the mathematical model, the validity of the simulation can be established.

HISTORICAL NOTE

The design study and stability analysis reviewed in this paper commenced in October 1960 and has led to the current contract to design and build a 200 ton development prototype ship known as the FHE-400, for the Royal Canadian Navy.

The initiative came from the Canadian Defence Research Board, following many years of surface piercing foil system development at the Naval Research Establishment, Halifax, Nova Scotia.

In 1959 N.R.E. published a report which considered the feasibility of a 200 ton ship based upon a canard arrangement, of fixed surface piercing foils. N.R.E. recognized the advantages of a canard arrangement in reducing head sea accelerations and improving stability in following seas. In addition, they foresaw the need to develop a foil design method to provide optimum foil angle of attack range in high sea states. Further, N.R.E. emphasized the value of designing a foil system to provide maximum damping in the hullborne mode of operation which is particularly important in a military search mode.

Encouraged by the technical interest of other NATO navies, the Canadian Government agreed with N.R.E.'s contention that a thorough design study should be made and awarded a contract to De Havilland (Canada) in 1960.

The work statement drawn up by the Defence Research Board in consultation with the R.C.N., laid down the parameters to be considered. These included the development of design methods for foils, response characteristics in random seas and the performance to be achieved. N.R.E. supported the programme with their 3-1/2 ton experimental test craft and an experienced trials team to conduct sea trials of the foil system developed by De Havilland. The trials conducted from 1961 to date have substantiated the predictions made by N.R.E. in 1959.

This paper discusses the design and stability studies and the supporting N.R.E. trials of the RX craft fitted with a representative foil system, 1/4 scale full size.

DESIGN METHOD

As there are many factors to be considered in relation to the dynamic stability it is helpful to have a clear picture of the relation of this study to the other design parameters.

Once the basic role has been decided upon, the required performance, range, load carrying capacity and approximate craft size can be determined; the latter of course, will be dictated to some extent by the sea state in which the craft will have to operate, as the hull will have to clear all but the larger waves. Parametric studies have to be carried out to determine the optimum configuration and size to meet the design requirements. These parameters then dictate the foil areas that are necessary to support the craft throughout the required foilborne speed range. Foil section thicknesses and section types are dictated by the maximum design speed and by structural stiffness. In this respect there is some conflict between hydrodynamic requirements for the thinnest possible foil section, to avoid cavitation, and structural requirements for the thickest possible section to avoid divergence and flutter. In some instances the maximum speed may well be decided by stiffness of the foil elements, as sections below a certain thickness may suffer from hydroelastic problems. This minimum thickness may not be sufficiently low to allow cavitation free operation at the maximum design speed and a physical limit will be placed on the maximum attainable speed. Stability is also adversely affected by cavitation. Foil loads, however, are effectively limited by cavitation, which is beneficial in this respect.

When the hydrodynamics, hydrostatics, hydroelastics, structural integrity, power and machinery requirement, operational roles, accommodation spaces, etc., have been considered then the initial stages in the design of a practical hydrofoil craft will have been completed. At this stage the dynamic stability and the operational environment of the craft have to be considered in some detail. Foilborne seakeeping in rough water is of paramount importance since the craft must be stable under all sea conditions and must have acceptable response characteristics from the standpoint of human tolerance to motion. Some factors influencing craft motions are foil taper ratios (for surface piercing foils), rate of change of lift with angle of attack and rate of change of lift with immersion depth. The foil system should be insensitive to angle of attack changes (i.e., low C_{L_α}) to reduce the effect of wave orbital velocities but should be relatively sensitive to changes in immersion depth (C_{L_h}) to control foil broaching and hull slamming. The ideal response would be with the craft platforming all waves below those which would cause broaching or slamming and contouring all larger waves. In practice this ideal is not attainable and the craft motions are between platforming and contouring for all significant waves.

To obtain the above characteristics some compromise is necessary. A low C_{L_α} usually implies a low aspect ratio (Fig. 2) and this yields a low lift-drag ratio which is detrimental to performance. For maximum performance the foil system should have the highest possible L/D ratio. A good compromise in this respect can be achieved with a canard system, in which 80-90% of the total lift is provided by the main foil. The bow foil supplies only 10-20% of the total lift; therefore its L/D ratio can be relatively low without contributing an unacceptably high drag to the total. Thus the bow foil can be optimised to produce minimum motions resulting in relatively small angle of attack excursions at the main foil. The main foil can then be designed to have a high aspect ratio (low drag) without incurring unacceptably high accelerations at the craft c.g. In practice the main foil $\partial C_L/\partial\alpha$ and $\partial C_L/\partial h$ lift-curve slopes have to be optimised to produce satisfactory performance in both head and following seas. However, the values so obtained do not differ greatly from those desirable for best performance. The bow foil unit is optimised to produce minimum motions in a seaway and to a large extent, controls the natural frequency of the craft in pitch and gives adequate separation between the craft natural frequency and the dominant frequencies of encounter in head seas which produce significant inputs of energy to the craft (Figs. 3, 4, 19 and 20). It is considered that fully cavitating bow foil sections are necessary to provide the required characteristics in a surface piercing system. These sections give low-lift curve slopes and are not subject to large lift changes due to changing from fully wetted to fully or partially cavitating flow. The bow foil system can be designed to provide a low $\partial C_L/\partial\alpha$ and the optimum $\partial C_L/\partial h$.

Some of the interrelated problems to be examined and solved are listed below:

1. Hydrodynamics — (Foil section design, cavitation suppression, ventilation effects, hydrodynamic loads, performance predictions, etc.)

2. Hydrostatics

3. Hydroelastics — (To date there is no accurate and proven method for predicting flutter speeds of surface piercing or cavitating foils and much research still needs to be done.)

4. Dynamic Stability — (The stability equations had to be developed together with a method for simulating the random seaway.)

5. Structural Integrity — (Lightweight structures of adequate stiffness are difficult to design and required sophisticated analysis.)

6. Materials — (High strength materials had to be found for the foils and random fatigue studies conducted. Coatings had to be developed to help guard against corrosion and erosion.)

7. Transmission Design — (As with many other hydrofoil problems this is practically at the current limit of the "state of the art" in gear technology because of the high torque and low weight requirement.)

THEORETICAL EQUATIONS OF MOTION

Hydrofoil Ship Simulation

Two methods of simulating the motions of a surface piercing hydrofoil in a random seaway have been derived and both methods were used in the design of the hydrofoil under consideration.

The first method is based on the normal aircraft equations, in which sets of partial derivatives representing the sum of various force or moment contributions are used to simulate the craft dynamics. The second method differs from the first in that the various forces at the craft centre of gravity are obtained by summing the forces developed by each foil element. Moments at the c.g. are the product of these elemental forces and their respective moment arms about the c.g.

The first series of studies to broadly define the hydrofoil was carried out in calm water using linear equations of the aircraft type suitably modified to account for free surface effects. Small perturbations were assumed and a series of partial derivatives was calculated for the complete hydrofoil. These equations were sufficiently accurate for the initial studies, but proved to be inadequate when more detailed information became available and a more accurate simulation was required. Varying coefficients had to be introduced. All of the derivatives are functions of immersion depth and second order derivatives had to be introduced to account for some of the more nonlinear functions. This results in a set of complicated equations. In fact, each variable has to be written in the form of a Taylor series and linearisation of even the second order terms can lead to significant errors, particularly in the roll derivatives.

These equations became very cumbersome, difficult to mechanize on the computer and still had significant inaccuracies in the roll terms. Because of the complex analog computer set-up required and the inaccuracies that were still present in the nonlinear "Taylor Series" equations, the so-called "explicit variable" method of simulation was developed, in order to simplify the computation and to achieve greater coherence in the derivation of the longitudinal and lateral equations for the surface piercing hydrofoil. Each derivative is a function of immersion depth, which in turn is a function of heave, pitch and wave effects, all of which are derived from the longitudinal equations. In the explicit variable simulation, this coherence can be achieved because all forces are derived from two parameters; the lift-curve slope for a given foil element, and the total angle of attack on that element due to all motions about the craft centre of gravity.

The development of these equations from Euler's basic equations of motion is outlined below for the axis convention of Fig. (i).

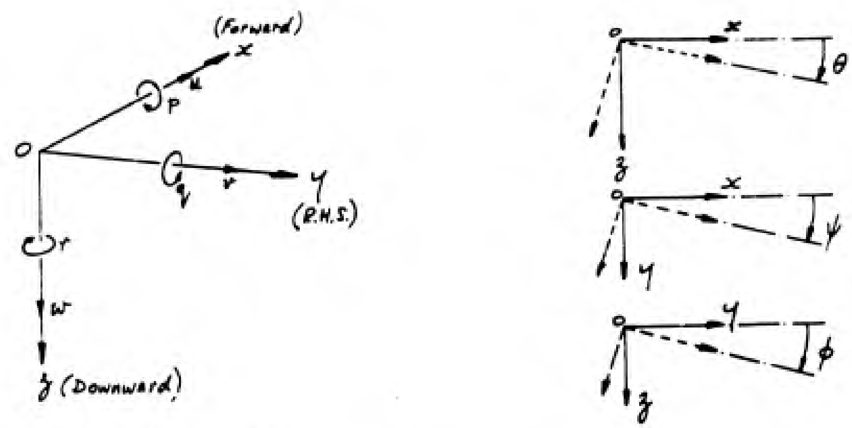

Assume a rigid body with Oxz as a plane of symmetry.

Figure (i)

Assume a rigid body with Oxz as a plane of symmetry. Euler's equations are:

Linear Motions and Forces

$$m(\dot{U} + QW - RV) = X - mg \sin \Theta \qquad (1)$$

$$m(\dot{V} + RU - PW) = Y + mg \cos \Theta \sin \Phi \tag{2}$$

$$m(\dot{W} + PV - QU) = Z + mg \cos \Theta \cos \Phi \tag{3}$$

Angular Motions and Moments

$$A\dot{P} - E\dot{R} + QR(C - B) - EPQ = L \tag{4}$$

$$B\dot{Q} + RP(A - C) + P^2 - R^2 = M \tag{5}$$

$$E\dot{P} + C\dot{R} + PQ(B - A) + EQR = N \tag{6}$$

Velocities Along Space Axes

$$\dot{x}_s = U \cos \Theta \cos \Psi + V(\sin \Phi \sin \Theta \cos \Psi - \cos \Phi \sin \Psi) + W(\cos \Phi \sin \Theta \sin \Psi - \sin \Phi \cos \Psi) \tag{7}$$

$$\dot{y}_s = U \cos \Theta \sin \Psi + V(\sin \Phi \sin \Theta \sin \Psi + \cos \Phi \cos \Psi) + W(\cos \Phi \sin \Theta \sin \Psi + \sin \Phi \cos \Psi) \tag{8}$$

$$\dot{z}_s = -U \sin \Theta + V \sin \Phi \cos \Theta + W \cos \Phi \cos \Theta \tag{9}$$

Relations between Angular Velocities

$$P = \dot{\Phi} - \dot{\Psi} \sin \Theta \tag{10}$$

$$Q = \dot{\Theta} \cos \Phi + \dot{\Psi} \cos \Theta \sin \Phi \tag{11}$$

$$R = \dot{\Psi} \cos \Theta \cos \Phi - \dot{\Theta} \sin \Phi \tag{12}$$

$$\dot{\Theta} = Q \cos \Phi - R \sin \Phi \tag{13}$$

$$\dot{\Phi} = P + Q \sin \Phi \tan \Theta + R \cos \Phi \tan \Theta \tag{14}$$

$$\dot{\Psi} = (Q \sin \Phi + R \cos \Phi) \sec \Theta . \tag{15}$$

All of the dynamic relationships that are necessary to investigate the motions of a body in response to impressed forces and moments are given in the above equations. These equations are general and are accurate for motions of any magnitude. The hydrofoil motions, however, are relatively limited, in which case small angle approximations can be made for this craft without any significant loss of accuracy, thus the equation can be simplified. This simplification can be accomplished by writing all of the equations in terms of their deviations from a fixed or reference condition with the exception of the craft forward speed (u) and heading angle (ψ), which are subject to large changes. Small approximations cannot be applied to them. The parameters in the deviation equations will be denoted by lower case letters. Reference values will be denoted by the suffix zero. Thus (U, V, W) (P, Q, R) (Θ, Φ, Ψ) are redefined as

$$U = (u_o + u)$$

$$P = (p_o + p)$$

$$\Theta = (\theta_o + \theta),$$

etc. The hydrofoil reference condition will be with the axes of the craft horizontal and with the craft travelling symmetrically in the Ox direction. Thus

$$v_o = w_o = p_o = q_o = r_o = \theta_o = \phi_o = 0 .$$

ψ_o is usually put equal to 0. However, any arbitrary value may be assigned without affecting the equations of motion.

Making small angle approximations and substituting the perturbation variables in the foregoing equations we have Euler's equations for small perturbations.

Linear Motions and Forces

$$m\dot{u} = X - mg\,\theta \tag{16}$$

$$m\,[\dot{v} + (u_o + u)\,r] = Y + mg\,\phi \tag{17}$$

$$m\,[\dot{w} - (u_o + u)\,q] = Z + mg \tag{18}$$

Angular Motions and Moments

$$A\dot{p} - E\dot{r} = L \tag{19}$$

$$B\dot{q} = M \tag{20}$$

$$C\dot{r} - E\dot{p} = N \tag{21}$$

Velocities Along Space Axes

$$\dot{x}_s = (u_o + u)\cos\psi - v\sin\psi \tag{22}$$

$$\dot{y}_s = (u_o + u)\sin\psi + v\cos\psi \tag{23}$$

$$\dot{z}_s = -(u_o + u)\,\theta + w \tag{24}$$

Relations between Angular Velocities

$$p = \dot{\phi} \tag{25}$$

$$q = \dot{\theta} \tag{26}$$

$$r = \dot{\psi} . \tag{27}$$

The above equations could be simplified further if the reference forces and moments were to be subtracted from the basic equation. However, hydrodynamic forces and moments are more readily derived in terms of their full values rather than in changes from the reference condition. It is more convenient, therefore, to leave the equations in this form.

Since the full values for the forces and moments have been left in the equations the craft probably will not be in a trimmed condition at the reference condition but will stabilize out at some other attitude.

Some caution is necessary when considering craft centre of gravity height above the sea surface. It is necessary to translate velocities into space axes before integrating to derive position. For example $\dot{w}$ may be integrated directly to give w the velocity of the craft along the instantaneous, or current direction of the craft Oz axis, but to find the c.g. height, velocities must be converted to space axes. $\dot{z}_s$ is the parameter that is to be integrated in this case.

Consider the craft to be moving in the $x_B z_B$ plane with a constant velocity V directed along $O_B x_B$ away from a set of space fixed axes $O_s x_s y_s z_s$ which was coincident with the moving axis system $O_B x_B y_B z_B$ at time $t = 0$. At time t, let $O_B x_B$ make an angle θ with $O_s x_s$ [Fig. (ii)]

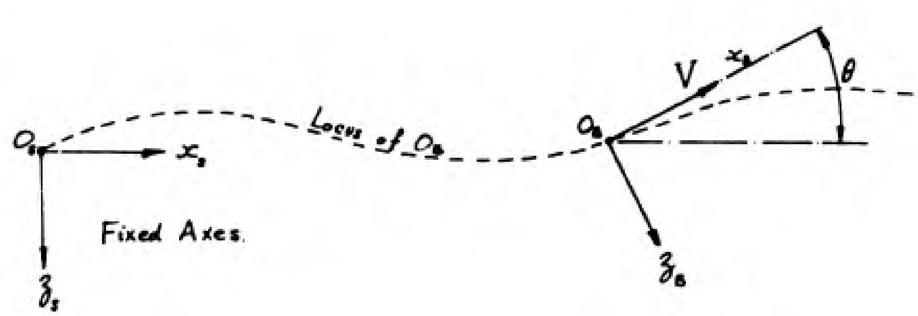

Figure (ii)

The components of O_B relative to O_s are

$$\dot{x}_s = V \cos\theta \tag{28}$$

$$\dot{z}_s = -\dot{V} \sin\theta . \tag{29}$$

The acceleration in the z_s direction is obtained by differentiating $\dot{z}_s$ thus

$$\ddot{z}_s = -V \sin\theta - V \cos\theta\dot{\theta} ; \tag{30}$$

however, $\dot{V} = 0$ as V is stated to be constant. Therefore

$$\ddot{z}_s \quad - V \cos \quad . \tag{31}$$

Consider now a point where the velocity of O_B is parallel to $O_s x_s$ then $\quad 0$ and $\ddot{z}_s \quad - V$. Thus the body possesses an acceleration in the $O_s z_s$ direction (centrifugal force) due to an impressed force, however, no acceleration is evident in the body axis component $\ddot{z}_B$. In the moving axis system (by definition) there is never any component of velocity (V) along $O_B z_B$ that is $\dot{z}_B \quad 0$, hence $\ddot{z}_B \quad 0$.

Note that no definition of displacement of O_B is given with respect to its own axis. Distances quoted in body axes merely serve to locate parts of the body with respect to O_B. To obtain displacements, velocity components in space fixed axes must be integrated.

Euler's equations take all of the above effects into account, but to ensure that the results are interpreted correctly, it is recommended that the results be transformed into components with respect to space fixed axes. The reverse also applies and care must be taken when applying external forces to the craft. These have to be correctly resolved into craft axes before substitution into the equation of motion.

The Normalised Equations

In order to compare craft of various sizes it is convenient to normalise the various parameters in the equations of motion. If this is not done, then for two craft which were similar in design but different in scale size, a different transformation law would exist between most of the sets of equivalent parameters relating to the two craft. This comparison of results obtained for the two craft would require recognition of how each variable should scale in relation to changes in craft scale size. Scaling for the analog computer is also complicated if the equations are not normalised. Computers operate within rather a limited voltage range so that changing the scale size of the simulated craft would involve changing the voltage scaling levels within the computer for most of the problem parameters. It is convenient, therefore, to make the parameters more or less independent of scale size.

Satisfactory normalising can be accomplished by dividing each parameter by a reference value of that parameter to produce a set of nondimensional variables, the reference values being selected according to the scale size or performance of the craft. Because differentiation in the equations is with respect to time, it is necessary also to scale the time variable.

Four reference parameters are required for the hydrofoil equations representing combinations of length, mass and time. They are:

$\quad$ = fluid mass density (slugs/cu ft),

s = reference length (usually semi-span of selected foil in feet),

S_o = reference area (usually the area of the selected foil in sq ft),

V_o = reference velocity (ft/sec).

The specific parameters required representing mass, time, and force are obtained from products or divisions of the four standard parameters.

All inertias

$$i_{xx} = \frac{I_{xx}}{\frac{1}{2}\rho S_o s^3} = \frac{A}{\frac{1}{2}\rho S_o s^3}.$$

Development of the Normalised Equations

As stated earlier the forces and moments impressed on the craft are non-linear functions of craft position and motion. Expressions for these forces and moments in terms of hydrodynamic derivatives are subject to significant errors unless high order derivatives are used. Therefore all forces are derived for each foil element as functions of angle of attack and immersion depth. These are the simplest functions which can describe adequately the forces developed by each foil. Thus for example, the foil lift C_L at a depth $\hat{h}$ is $C_{L,(\hat{h})}\alpha$, where α is the total angle of attack on the foil element due to all motions. That is

$$\alpha_{total} = (\alpha_o + \alpha_d) \text{ radians}$$

where

α_o = the reference angle of attack for a given foil in calm water,

α_d = the "dynamic" contribution to angle of attack and represents the angle between the longitudinal axis and the free stream direction, and

$\hat{h}$ = the foil element normalised immersion depth.

$\hat{h}$ and α are derived as follows. Consider a foil element at a longitudinal distance $\hat{x}$ and lateral distance $\hat{y}$ from the craft c.g. Then it can be shown that

$$\hat{h}_{foil} = (\hat{h}_o + \Delta\hat{h}_{c.g.} - \hat{x}\hat{\theta} + \hat{y}\hat{\phi} - \hat{h}_w)\cos\phi$$

$$= \hat{h}_o + \Delta\hat{h}_{c.g.} - \hat{x}\hat{\theta} + \hat{y}\hat{\phi} - \hat{h}_w \qquad (42)$$

(assuming $\cos\phi \approx 1.0$), where

$\hat{h}_{foil}$ = the reference immersion depth of the foil [Fig. No. (iii)],

$\Delta\hat{h}_{c.g.}$ = the perturbation about the reference height due to heave of the complete craft,

$$\Delta \hat{h}_{c.g.} = \int \left[\hat{w} - \hat{\theta}(1 + \hat{u})\right] d\hat{t} . \tag{43}$$

$\hat{h}_w$ = the change in water height from datum at the foil (Note: $\hat{h}_w$ is given in space coordinates and has to be resolved into craft coordinates),

$\hat{\theta}$ = pitch angle of the boat, and

$\hat{\phi}$ = roll angle of the boat.

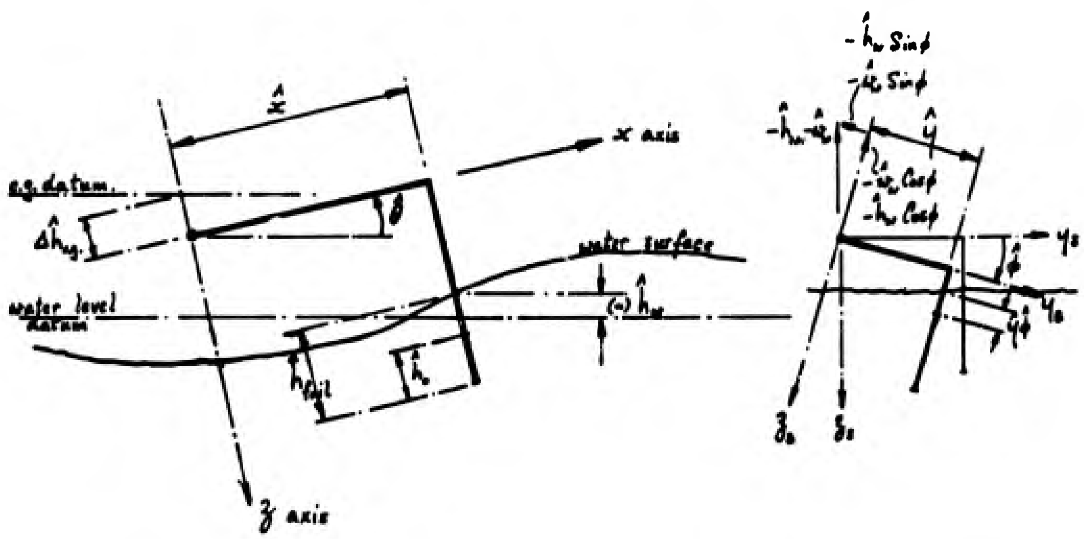

Note: for small angles the following assumptions can be made

Sin $\phi \approx \phi$ radians

Cos $\phi \approx 1.0$

Figure (iii)

The expression for angle of attack is basically the differential of the above equation.

$$\alpha = \alpha_o + (\hat{w}_{c.g.} - \hat{x}\dot{\hat{\theta}} + \hat{y}\dot{\hat{\phi}} - \hat{w}_w \cos \hat{\phi})$$

$$= \alpha_o + (\hat{w} - \hat{x}\dot{\hat{\theta}} + \hat{y}\dot{\hat{\phi}} - \hat{w}_w)$$

$$= \alpha_o + \alpha_d \tag{44}$$

for fixed forward velocity.

For a varying forward velocity

$$\alpha = \alpha_o[1 + 2(\hat{u} - \hat{u}_w)] + \alpha_d(1 + \hat{u} - \hat{u}_w) \tag{45}$$

this expression is derived as follows. Consider the instantaneous velocity

$$V_i = u_o + u - u_w$$

where

u_o = reference or steady-state velocity,

u = the perturbation of craft velocity, and

u_w = the horizontal component of wave orbital velocity.

Now

$$\frac{V_i}{u_o} = (1 + \hat{u} - \hat{u}_w)$$

where

$$\hat{u} = \frac{u}{u_o}$$

$$\hat{u}_w = \frac{u_w}{u_o}$$

(the normalised velocity perturbation).

Thus

$$\alpha = \alpha_o + \frac{u_o}{V_i}(\hat{w} - \hat{x}\dot{\hat{\theta}} + \hat{y}\dot{\hat{\phi}} - \hat{w}_w)$$

$$= \alpha_o + \frac{(\hat{w} - \hat{x}\dot{\hat{\theta}} + \hat{y}\dot{\hat{\phi}} - \hat{w}_w)}{1 + \hat{u} - \hat{u}_w}$$

$$= \alpha_o + \frac{\alpha_d}{(1 + \hat{u} - \hat{u}_w)} . \tag{46}$$

Now steady lift $L = 1/2\,\rho U_o^2 S_o \times f(\alpha, \hat{h})$ and unsteady lift $= 1/2\,\rho(U_o + u)^2 S \times f(\alpha, \hat{h})$.

Normalising is based on U_o the steady-state reference velocity thus C_{L_α} is normalised with respect to $1/2\,\rho U_o^2 S$ and $\alpha = w/(U_o + u)$. Therefore we have to consider the variation in the product $V_i^2 \alpha$:

$$V_i^2 \alpha = U_o^2 (1 + \hat{u} - \hat{u}_w)^2 \left[\alpha_o + \frac{\alpha_d}{(1 + \hat{u} - \hat{u}_w)} \right]$$

$$= U_o^2 \alpha_o (1 + \hat{u} - \hat{u}_w)^2 + U_o^2 \alpha_d (1 + \hat{u} - \hat{u}_w) . \tag{47}$$

For small perturbations in $\hat{u}$ and $\hat{u}_w$ the u^2 terms can be neglected thus

$$V_i^2 \alpha = U_o^2 \alpha_o \left[1 + 2 (\hat{u} - \hat{u}_w) \right] + U_o^2 \alpha_d (1 + \hat{u} - \hat{u}_w) \tag{48}$$

Thus

$$\alpha = \alpha_o \left[1 + 2 (\hat{u} - \hat{u}_w) \right] + \alpha_d (1 + \hat{u} - \hat{u}_w) . \tag{49}$$

In the drag terms there is the expression $V_i^2 \alpha^2$. This becomes

$$V_i^2 \alpha^2 = U_o^2 (1 + \hat{u} - \hat{u}_w)^2 \left[\alpha_o + \frac{\alpha_d}{(1 + \hat{u} - \hat{u}_w)} \right]^2$$

$$= U_o^2 \left[\alpha_o (1 + \hat{u} - \hat{u}_w) + \alpha_d \right]^2 .$$

Sideslip angles are obtained in a similar manner to give

$$\beta_d = \left[\hat{v} + \hat{x} \dot{\hat{\psi}} - \hat{z} \dot{\hat{\phi}} - \hat{v}_w - \hat{w}_w \hat{\phi} \right] \tag{50}$$

for fixed speed and

$$\beta_{total} = \beta_d (1 + \hat{u} - \hat{u}_w)$$

for varying speed.

Only the expression for thrust remains to be derived before the final equations can be written. Two effects need to be considered: (1) the effect of changes in throttle setting and (2) the effect of changes in water velocity at the propeller.

Let k be the increment of thrust horsepower available for a given change in throttle setting, then the effect of a change in throttle setting can be expressed as

$$T = T_o (1 + k) . \tag{51}$$

If thrust is assumed to be a function of local water velocity at the propeller when the throttle setting is constant, then an expression of the following form is derived.

$$T = T_o \left(\frac{V}{V_i}\right)^n = \frac{T_o}{(1 + \hat{u} - \hat{u}_w)^n} . \tag{52}$$

Combining the above effects we have

$$T = (1 + k) \frac{T_o}{(1 + \hat{u} - \hat{u}_w)^n} = T_o \left[\frac{(1 + k)}{(1 + \hat{u} - \hat{u}_w)^n}\right] . \tag{53}$$

If we assume small perturbations (the above expressions will not hold for large speed fluctuations) expand the R.H.S. of the equation and neglect all but the first term in the binomial expansion

$$(1 + \hat{u})^n = (1 + n\hat{u}) + \frac{n(n-1)\hat{u}^2}{2!} + \ldots .$$

We have

$$T = T_o(1 + k)[1 - n(\hat{u} - \hat{u}_w)] \tag{54}$$

and

$$\frac{T}{\frac{1}{2}\rho V_o^2 S_o} = C_T(1 + k)[1 - n(\hat{u} - \hat{u}_w)] . \tag{55}$$

The complete set of equations may now be written in the following normalised form:

Normalised Euler Equations for Small Perturbations

Linear Motions and Forces

$$2\mu\dot{\hat{u}} = \frac{\text{Thrust} - \text{Drag}}{\frac{1}{2}\rho V_o^2 S_o} - C_{L_o}\hat{\theta} \tag{56}$$

$$2\mu[\dot{\hat{v}} + \hat{r}(1 + \hat{u})] = \frac{\text{Side force}}{\frac{1}{2}\rho V_o^2 S_o} + C_{L_o}\hat{\phi} \tag{57}$$

$$2\mu[\dot{\hat{w}} - \hat{q}(1 + \hat{u})] = -\frac{\text{Lift force}}{\frac{1}{2}\rho V_o^2 S_o} - C_{L_o} . \tag{58}$$

Angular Motions and Moments

$$i_{xx}\ddot{\hat{\phi}} - i_{zx}\ddot{\hat{\psi}} = \frac{\text{Rolling moment}}{\frac{1}{2}\rho V_o^2 S_o s} \tag{59}$$

$$i_{yy}\ddot{\theta} = \frac{\text{Pitching moment}}{\frac{1}{2}\rho V_o^2 S_o s} \tag{60}$$

$$i_{zz}\ddot{\psi} - i_{zx}\ddot{\phi} = \frac{\text{Yawing moment}}{\frac{1}{2}\rho V_o^2 S_o s} . \tag{61}$$

Velocities Along Space Axes

$$\dot{\hat{x}}_s = (1 + \hat{u}) \cos \psi - \hat{v} \sin \psi \tag{62}$$

$$\dot{\hat{y}}_s = (1 + \hat{u}) \sin \psi + \hat{v} \cos \psi \tag{63}$$

$$\dot{\hat{z}}_s = - (1 + \hat{u})\hat{\theta} + \hat{w} . \tag{64}$$

Equations (56) to (61) are required for the six degrees of freedom of the craft. Equations (62) to (64) are the relations between craft and space axes and are required for relating sea motion to craft motion.

Hydrofoil Equations

Basic Equations

Heave

$$2\mu[\dot{\hat{w}} - \dot{\hat{\theta}}(1 + \hat{u})] = - C_{L_o} - C_L \tag{65}$$

Surge

$$2\mu\dot{\hat{u}} + \hat{\theta} C_{L_o} = C_{T_o} - [C_D + C_{D_o}] \tag{66}$$

Pitch

$$i_{yy}\ddot{\theta} = C_m + C_{m_o} + (i_{zz} - i_{xx}) \dot{\hat{\phi}}\dot{\hat{\psi}} \tag{67}$$

Sideforce

$$2\mu[\dot{\hat{v}} + \dot{\hat{\psi}}(1 + \hat{u})] = C_y + C_{L_o}\hat{\phi} \tag{68}$$

Roll

$$i_{xx}\ddot{\phi} = C_l + i_{xz}\ddot{\psi} + (i_{yy} - i_{zz}) \dot{\hat{\theta}}\dot{\hat{\psi}} \tag{69}$$

Yaw

$$i_{zz}\ddot{\psi} = C_n + i_{xz}\ddot{\phi} + (i_{xx} - i_{yy}) \dot{\hat{\phi}}\dot{\hat{\theta}} . \tag{70}$$

Expanded Equations

The expanded equations, including the expressions for the basic forces and variations due to speed perturbations are as follows:

Heave

$$2\mu[\dot{\hat{w}} - \dot{\theta}(1+\hat{u})] = -C_{L_{\alpha(F)}}(\hat{h}_F)\alpha_{(F)} \cdot K_{\alpha} - C_{L_{\alpha(c)}}(\hat{h}_{(c)})\alpha_{(c)}$$

$$-\left[C'_{L_{\alpha(L)}}(\hat{h}_L)\alpha_{(L)}\right]\cos\phi_{(L)} - \left[C'_{L_{\alpha(R)}}(\hat{h}_R)\alpha_{(R)}\right]\cos\phi_{(R)} - C_{L_0}. \quad \textbf{(71)}$$

Surge

$$2\mu\dot{\hat{u}} \cdot \theta C_{L_0} = C_{T_0}(1+k)\left[1 - n(\hat{u} - \hat{u}_w)\right]$$

$$- C_{D(F)}(\hat{h}_F)\left[1 + 2(\hat{u} - \hat{u}_{w(F)})\right] - K_{D_{i(F)}}(\hat{h}_F)\left[\alpha_{o(F)}(1 + \hat{u} - \hat{u}_{w(F)}) + \alpha_{d(F)}\right]^2$$

$$- C_{D(c)}(\hat{h}_c)\left[1 + 2(\hat{u} - \hat{u}_{w(c)})\right] - K_{D_{i(c)}}(\hat{h}_c)\left[\alpha_{o(c)}(1 + \hat{u} - \hat{u}_{w(c)}) + \alpha_{d(c)}\right]^2$$

$$- C_{D(L)}(\hat{h}_L)\left[1 + 2(\hat{u} - \hat{u}_{w(L)})\right] - K_{D_{i(L)}}(\hat{h}_{(L)})\left[\alpha_{o(L)}(1 + \hat{u} - \hat{u}_{w(L)}) + \alpha_{d(L)}\right]^2$$

$$- C_{D(R)}(\hat{h}_R)\left[1 + 2(\hat{u} - \hat{u}_{w(R)})\right] - K_{D_{i(R)}}(\hat{h}_{(R)})\left[\alpha_{o(R)}(1 + \hat{u} - \hat{u}_{w(R)}) + \alpha_{d(R)}\right]^2$$

$$- C_{D_{\gamma}}\hat{v} . \quad \textbf{(72)}$$

Pitch

$$i_{yy}\ddot{\theta} = \hat{x}_{(F)}\left[C_{L_{\alpha(F)}}(\hat{h}_F)\alpha_{(F)}k_{\alpha}\right] + \hat{x}_{(c)}\left[C_{L_{\alpha(c)}}(\hat{h}_c)\alpha_{(c)}\right]$$

$$- \hat{x}_{(L)}\left[C'_{L_{\alpha(L)}}(\hat{h}_L)\alpha_{(L)}\right]\cos\phi_{(L)} + \hat{x}_{(R)}\left[C'_{L_{\alpha(R)}}(\hat{h}_R)\alpha_{(R)}\right]\cos\phi_{(R)}$$

$$+ C_{T_0}(1+k)\left[1 - n(\hat{u} - \hat{u}_{w(c)})\right]\hat{z}_{(T)} - C_{D_{(M)(total)}}(\hat{h}_{(c)})\hat{z}_{(M)(drag)}$$

$$- C_{D_{(F)(total)}}(h_F)\hat{z}_{(F)(drag)} + C_{m_0}(\hat{h}) + C_{m_{\alpha}}(\hat{h}_{(c)})\alpha + (i_{zz} - i_{xx})\dot{\phi}\dot{\psi}. \quad \textbf{(73)}$$

Sideslip

$$2\mu\left[\dot{\hat{v}} + \dot{\hat{\psi}}(1+\hat{u})\right] = C_{y_{\beta(F)}}(\hat{h}_F)\beta_{(F)} + C_{y_{\beta(c)}}(\hat{h}_c)\beta_{(c)}$$

$$- \left[C'_{L_{\alpha(L)}}(\hat{h}_L)\alpha_{(L)}\right]\sin\Gamma_{(L)} + \left[C'_{L_{\alpha(R)}}(\hat{h}_R)\alpha_{(R)}\right]\sin\Gamma_{(R)}$$

$$+ C_{L_0}\hat{\phi} . \qquad (74)$$

Roll

$$i_{xx}\ddot{\hat{\phi}} = -\hat{z}_{(F)}\left[C_{y_{\beta(F)}}(\hat{h}_F)\beta_{(F)}\right] - \hat{z}_{(c)}\left[C_{y_{\beta(c)}}(\hat{h}_{(c)})\beta_{(c)}\right]$$

$$- \hat{y}_{(L)}\left[C'_{L_{\alpha(L)}}(\hat{h}_L)\alpha_{(L)}\right] - \hat{y}'_{(R)}\left[C'_{L_{\alpha(R)}}(\hat{h}_{(R)})\alpha_{(R)}\right]$$

$$+ \left[C_{\ell_{\alpha(L)}}\left(\hat{h}_{L_{D.P.}}\right)\alpha_{(L)(D.P.)}\right] + \left[C_{\ell_{\alpha(R)}}(\hat{h}_{(R)(D.P.)})\alpha_{(R)(D.P.)}\right]$$

$$+ i_{xz}\ddot{\hat{\psi}} + (i_{yy} - i_{zz})\dot{\hat{\theta}}\dot{\hat{\psi}} . \qquad (75)$$

Yaw

$$i_{zz}\ddot{\hat{\psi}} = \hat{x}_{(F)}\left[C_{y_{\beta(F)}}(\hat{h}_F)\beta_{(F)}\right] + \hat{x}_{(c)}\left[C_{y_{\beta(c)}}(\hat{h}_c)\beta_{(c)}\right]$$

$$- \hat{x}_{(L)}\left[C'_{L_{\alpha(L)}}(\hat{h}_L)\alpha_{(L)}\right]\sin\Gamma_{(L)} + \hat{x}_{(R)}\left[C'_{L_{\alpha(R)}}(\hat{h}_R)\alpha_{(R)}\right]\sin\Gamma_{(R)}$$

$$+ C_{D_{(L)(total)}}\hat{y}_{(L)} + C_{D_{(R)(total)}}\hat{y}_{(R)} + (i_{xx} - i_{yy})\dot{\hat{\phi}}\dot{\hat{\theta}} . \qquad (76)$$

Care must be exercised when applying these equations to a particular hydrofoil as it is possible to overestimate some effects such as damping in roll. If side forces, for example, are assumed to be derived from equivalent vertical struts which in fact have an appreciable dihedral angle then the roll damping may be overestimated. In some instances due to foil geometry the local velocity vector $\dot{\phi}\hat{z}$ may be along the foil element and not normal to the foil as is implied in the above equations.

Forces and Moments

In the case of the hydrofoil craft, if the foil system is considered as a whole, then the foil derivatives are usually functions of more than two dependent variables. However, if the foil system is divided into a number of elements, then for a particular foil element the lift, drag and side forces are a function of two variables only, the immersion depth and the angle of attack. These variables can be obtained at any instant, for a given foil element, and the forces along the three body axes continuously computed. The moments about the craft c.g. are then given by the product of these forces and their moment arms about the c.g., the net forces and moments at the craft c.g. being obtained by a summation of the forces acting on the individual foil elements. These net forces and moments when divided by the appropriate inertia coefficients then produce the linear and angular accelerations that are required in the basic Euler equations of motion.

Derivation of Forces

The basis for computation of the forces acting on a given foil or strut element is the lift-curve slope (C_{L_α}) together with the angle of attack on that element. The lift coefficient (C_L) developed being a product of C_{L_α} and α. The lift-curve slope is a function of immersion depth (h) and aspect ratio (A) which also is a function of immersion depth when the foil element is surface piercing and is readily obtainable from Refs. 12, 17, 18, 19, 20 and 21. The angle of attack experienced by a foil is due to pitch and roll, yaw and heave rates together with wave orbital velocities, the actual angle of attack at any instant being dependent upon the free stream velocity and the respective distances from the craft c.g. in the x, y and z directions.

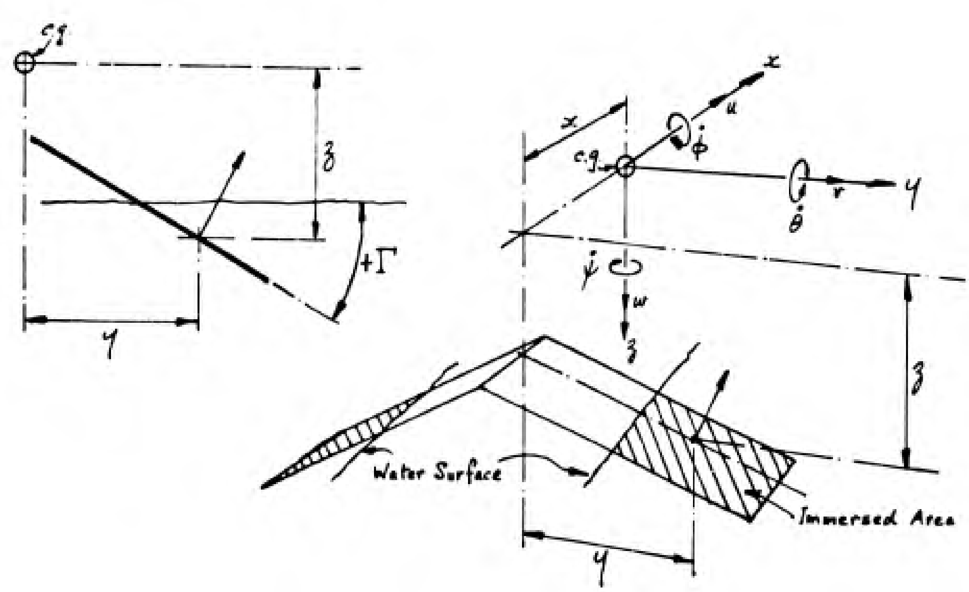

Figure (iv)

For example consider a point on a surface piercing foil element as shown in Fig. (iv). The velocity normal to the foil element is

$$v_{\perp} = \pm\left[-(v + x\dot{\psi} - z\dot{\phi} - v_{w_i}\cos\phi - w_{w_i}\sin\phi)\sin\Gamma\right.$$

$$\left. + (w - x\dot{\theta} - v_{w_i}\sin\phi - w_{w_i}\cos\phi)\cos\Gamma\right] \text{ (ft/sec)}. \tag{77}$$

The angle of attack is

$$\alpha = \frac{v_{\perp}}{U_i}.$$

The sideslip angle is

$$\beta = \frac{v}{U_i}.$$

$$\alpha_{foil} = \alpha_o$$

$$\pm\left[\frac{-(v + x\dot{\psi} - z\dot{\phi} - v_{w_i}\cos\phi - w_{w_i}\sin\phi)\sin\Gamma + (w - x\dot{\theta} + y\dot{\phi} + v_{w_i}\sin\phi - w_{w_i}\cos\phi)\cos\Gamma}{U_i}\right] \tag{78}$$

for small perturbations $\sin\phi \approx 0$ and $\cos\phi \approx 1.0$, $U_i \approx U_o$. Therefore

$$\alpha_{foil} = \alpha_o \pm \left[-\left(\frac{v}{U_o} + \frac{x}{U_o}\dot{\psi} - \frac{z}{U_o}\dot{\phi} - \frac{v_w}{U_o}\right)\sin\Gamma + \left(\frac{w}{U_o} - \frac{x}{U_o}\dot{\theta} + \frac{y}{U_o}\dot{\phi} - \frac{w_w}{U_o}\right)\cos\Gamma\right],$$

$$\hat{v} = \frac{v}{U_o} = \beta, \quad \phi = \hat{\phi}, \quad \hat{w} = \frac{w}{U_o}, \quad \hat{x} = \frac{x}{s},$$

and

$$\hat{x}\dot{\hat{\psi}} = \frac{x}{s}\left(\frac{s}{V}\times\dot{\psi}\right) = \frac{x}{V}\dot{\psi};$$

but $U_o = V$, therefore

$$\hat{x}\dot{\hat{\psi}} = \frac{x}{U_o}\times\dot{\psi}.$$

Therefore

$$\alpha_{foil} = \alpha_o \pm \left[-(\hat{v} + \hat{x}\dot{\hat{\psi}} - \hat{z}\dot{\hat{\phi}} - v_w)\sin\Gamma + (\hat{w} - \hat{x}\dot{\hat{\theta}} + \hat{y}\dot{\hat{\phi}} - \hat{w}_w)\cos\Gamma\right]. \tag{79}$$

Thus for left- and right-hand foil elements

$$\alpha_{(L)} = \alpha_{o_{(L)}} + \left(\hat{v} + \hat{x}_{(L)}\dot{\hat{\psi}} - \hat{z}_{(L)}\dot{\hat{\phi}} - \hat{v}_{w_{(L)}}\right)\sin\Gamma_{(L)} - \left(\hat{w} - \hat{x}_{(L)}\dot{\hat{\theta}} + \hat{y}_{(L)}\dot{\hat{\phi}} - \hat{w}_{w_{(L)}}\right)\cos\Gamma_{(L)} \tag{80}$$

$$\alpha_{(R)} = \alpha_{o_{(R)}} - \left(\hat{v} + \hat{x}_{(R)}\dot{\hat{\psi}} - \hat{z}_{(R)}\dot{\hat{\phi}} - \hat{v}_{w_{(R)}}\right)\sin\Gamma_{(R)} + \left(\hat{w} - \hat{x}_{(R)}\dot{\hat{\theta}} + \hat{y}_{(R)}\dot{\hat{\phi}} - \hat{w}_{w_{(R)}}\right)\cos\Gamma_{(R)} \tag{81}$$

It will be seen from the foregoing that it is convenient to produce the net angle of attack normal to the foil element. C_{L_α} can be obtained for vertical forces or for forces normal to the foil. It is logical therefore to derive the lift normal to an element and to then resolve this into vertical and horizontal components to produce the lift and side forces respectively. In this manner any dihedral angle (Γ) and roll angle (ϕ) can be taken into account in the computation of forces

Derivation of Moments

The moments about the craft centre of gravity are dependent upon the foil element loading distribution and thus the centre of pressure location relative to the c.g. For a surface piercing foil the loading varies with immersion depth and therefore spanwise c.p. has to be derived as a function of the foil immersion depth (h). A linear variation with h is usually sufficiently accurate. Chordwise c.p. movement is usually a negligible percentage of the distance from the foil element c.p. to the craft c.g. and can be assumed fixed at say the foil quarter chord position.

REGULAR AND RANDOM SEAWAY CALCULATIONS

Regular Seas

Simulated regular seas are an important aid to hydrofoil craft design. They are easy to produce and much useful data can be obtained. For example, magnification factors can be determined for a realistic range of amplitude for each significant frequency as shown in Figs. 3 to 6.

The regular seas to be simulated are usually decided by the frequency of encounter range which gives a significant energy input to the craft (Figs. 9 and 11). Once the frequency of encounter is known then it is a simple process to derive the other parameters that are necessary for the sinusoidal wave simulation. The pertinent expressions for gravity waves are as given below.

Frequency of Encounter

$$\omega' = 2\pi f' \quad (\text{rad/sec}) \tag{1}$$

$$\omega' = \omega + \frac{V}{g}\omega^2 \quad (\text{rad/sec}). \tag{2}$$

Wave Frequency

$$\omega = 2\pi f \qquad (\mathrm{rad/sec}). \tag{3}$$

Wave Length

$$\lambda = \frac{2\pi g}{\omega^2} \qquad (\mathrm{ft}). \tag{4}$$

Wave Orbital Velocity

$$\begin{aligned} w_w &= 2\pi Z_o f \\ &= Z_o \omega \qquad (\mathrm{ft/sec}). \end{aligned} \tag{5}$$

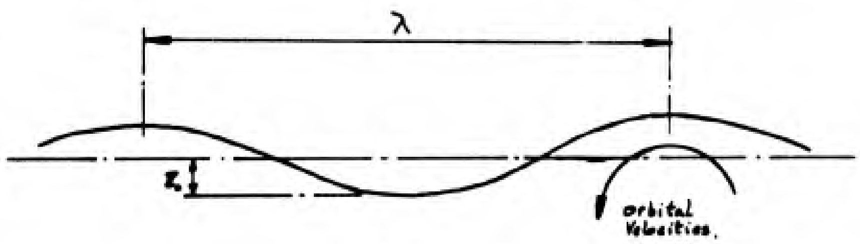

Figure (v)

Sinusoidal waves can be simulated by a second order system

$$-\ddot{Z}_o = +\omega^2 Z_o \tag{6}$$

such that

$$Z_i = +Z_o \cos \omega t \tag{7}$$

where t = time in seconds.

The horizontal and vertical components of the orbital velocities with these waves are given by the following expressions:

Vertical Component

$$w_w = -\omega Z_o \sin \omega t . \tag{8}$$

Horizontal Component

$$u_w = +\omega Z_o \cos \omega t . \tag{9}$$

The vertical component w_w has a phase angle $\Phi_w = 90^\circ$ relative to the wave amplitude; the horizontal component u_w has a phase angle $\Phi_u = 0^\circ$ and is in phase with the waves.

When there is more than one foil then there will be a phase lag between the forward and rear foil units. If we denote the forward and rear foils by the subscripts (F) and (R) respectively and the phase lag is Φ then we have the general expression based on

$$\Phi = \frac{2\pi L}{\lambda} \text{ radians} .$$

where L = distance between front and rear foils (feet),

$$\cos(\omega t - \Phi) = \cos \omega t \cos \Phi + \sin \omega t \sin \Phi \tag{10}$$

$$\omega \sin(\omega t - \Phi) = \omega \sin \omega t \cos \Phi - \omega \cos \omega t \sin \Phi . \tag{11}$$

The equations for the wave and the orbital velocity components at the front and rear foils can now be written, viz:

Wave Amplitude

$$Z_{(F)} = Z_o \cos \omega t \tag{22}$$

$$Z_{(R)} = Z_o \cos(\omega t - \Phi_{(R)}) = Z_o \cos \omega t \cos \Phi_{(R)} + Z_o \sin \omega t \sin \Phi_{(R)} . \tag{23}$$

Vertical Component of Orbital Velocity

$$w_{w(F)} = -\omega Z_o \sin \omega t \tag{24}$$

$$-w_{w(R)} = +\omega Z_o \sin(\omega t - \Phi_{(R)}) = +\omega(Z_o \sin \omega t \cos \Phi_{(R)} - Z_o \cos \omega t \sin \Phi_{(R)}) . \tag{25}$$

Horizontal Component of Orbital Velocity

$$u_{w(F)} = +\omega Z_o \cos \omega t \tag{26}$$

$$u_{w(R)} = \omega Z_o \cos(\omega t - \Phi_{(R)}) = \omega(Z_o \cos \omega t \cos \Phi_{(R)} + Z_o \sin \omega t \sin \Phi_{(R)}) . \tag{27}$$

The computer block diagram for simulating the above seaway is given in Fig. 7 for a front foil and a main foil, with the main foil split into three elements, left foil, centre foil, and right foil, denoted by the subscripts (L), (C), and (R) respectively.

Random Seas

At the beginning of the hydrofoil stability study, it was recognized that exclusive use of regular sinusoidal seas as forcing functions might be misleading, since they are hardly representative of actual seaway conditions. It was decided, therefore, to simulate a random seaway based on a mathematical model which is used successfully for wave forecasting purposes.

The following subsections are contributed by E. R. Case (De Havilland Staff Engineer) who was responsible for the original analysis and simulation of the random seaway for the hydrofoil study, and the subsequent spectral and statistical analysis of the computer and trials results.

The random seaway

The most obvious feature of a seaway is the almost complete lack of any consistent order or pattern to the wave motion, an observation which led to consideration of the seaway as a random process. By assuming further that the process was Gaussian, Pierson [23,24] derived a mathematical model based on a Fourier representation of random noise due to Rice [26], and the propagation properties of deep-water gravity waves. About the same time, Longuet-Higgins [22], using the Gaussian assumption, and the results of Rice's paper, derived the statistical distribution of wave heights for wave forecasting purposes. The remaining quantity required to complete the description of the seaway as a random process was the power spectrum, which was supplied by Neumann [27] on the assumption that the wave energy varied as the fifth power of the generating wind velocity. These results were successfully incorporated in a book published by the United States Navy [23] on practical methods of wave forecasting.

On the basis of the above, the Pierson representation and the Neumann spectrum were assumed to characterize a seaway with sufficient accuracy for the purposes of the stability study. It was assumed further that a Neumann wind speed of 22 knots corresponds to a Sea State Five.

A typical estimate of a seaway surface elevation probability distribution function is shown in Fig. 8. The linearity indicates normality out to over four standard deviations, which validates the Gaussian assumption for engineering purposes.

Attention was restricted to the consideration of "sea" waves, which, as distinct from "swell" waves, exist within a storm generating area due to the action of the local winds. Attention was further restricted to a seaway which had reached the fully-developed state, where a state of equilibrium exists in the interchange of energy between the waves and the wind. The fully-developed sea state is reached only when the generating wind has blown over a sufficient fetch and time duration [23], and can be considered a stationary, ergodic random process.

The Neumann spectrum applies only to the fully-developed seaway [28], and takes the form in the one-dimensional case, for $f \geq 0$

$$\Phi_z(f) = \frac{c_1}{f^6} e^{-c_2/v^2 f^2} (ft)^2 \text{ cps} \tag{28}$$

where f is the wave frequency in cycles per second, v is the generating wind speed in knots, and c_1 and c_2 are constants. A typical wave elevation spectrum is shown in Fig. 9.

Implicit in the description of the seaway as a stationary Gaussian random process is the assumption that the instantaneous surface elevation at any point results from the superposition of an infinite number of small sinusoidal components of different frequency, phase and direction of propagation. Analytically, the wave elevation can be expressed as a stochastic integral of the form

$$Z(t) = \int_0^\infty \cos\left[\omega t - \phi(\omega)\right] \sqrt{2\Phi_z(f)\,df} \tag{29}$$

where $\omega = 2\pi f$ and $\Phi(\omega)$ is a randomly chosen phase angle uniformly distributed in the range $(0, 2\pi)$. While this is not integrable in the ordinary sense, it can be expressed in the form of a Fourier sum (see St. Denis and Pierson).

This representation can be extended to include the effects of distance by using the wave equation for transverse wave motion for each sinusoidal component.

Thus, if x is the distance measured in the direction of the wind from a fixed point on the earth, the wave elevation can be expressed by

$$Z(t, x) = \int_0^\infty \cos(\omega t - \Omega x - \phi) \sqrt{2\Phi_z(f)\,df} \tag{30}$$

where

Ω = wavenumber = $\omega/c = 2\pi/\lambda$,

λ = wavelength in feet, and

c = crest speed (wave celerity) in knots.

If each of the small sinusoidal components is assumed to propagate as a gravity wave, then, in addition,

$$\Omega = \frac{\omega^2}{g} = \frac{g}{c^2} .$$

The validity of this assumption has been confirmed by the general success of the wave forecasting methods based on Pierson's theory. The wave elevation can then be expressed by

$$Z(t,x) = \int_0^{\infty} \cos\left(\omega t - \frac{\omega^2}{g} x - \phi\right) \sqrt{2\Phi_z(f)\, df} \,. \tag{31}$$

Equation (31) can be differentiated to give what can be assumed to represent the vertical component of the water particle orbital velocity. Thus,

$$w(t,x) = \dot{Z}(t,x) = -\int_0^{\infty} \sin\left(\omega t - \frac{\omega^2}{g} x - \phi\right) \sqrt{2\Phi_w(f)\, df} \tag{32}$$

where the spectral density for the vertical velocity is given by

$$\Phi_w(f) = (2\pi f)^2\, \Phi_z(f) \,.$$

The hydrofoil ship in the random seaway

The random seaway can be considered as a disturbance input to the hydrofoil craft. These inputs induce motions, which are not present in calm water, and which result from a combination of wave elevation, orbital velocities and the forward velocity of the craft. If the reference coordinate system is chosen fixed to the hydrofoil ship, then the effects of the seaway and craft velocities can be combined together to produce wave elevation and orbital velocity forcing functions which are functions of craft speed. This is accomplished by transforming the original seaway spectra by a change of variable to produce new spectra which are functions of frequency of encounter.

To illustrate briefly, consider the coordinate systems as illustrated in Fig. 10. The moving coordinate system is designated by primes. The coordinate transformation is then given by

$$x = x' + Vt \quad \text{and} \quad Z = Z' \tag{33}$$

where V, the ship speed, is defined to be negative in head seas.

Substituting Eq. (33) in Eq. (31) gives

$$Z(t,x') = \int_0^{\infty} \cos\left(\omega' t - \frac{\omega^2}{g} x' - \phi\right) \sqrt{2\Phi_z'(f')\, df'} \tag{34}$$

where the frequency of encounter ω' is given by

$$\omega' = \omega - \frac{V}{g}\omega^2 = 2\pi f' \tag{35}$$

and the "transformed" wave elevation spectrum by

$$\Phi_z'(f') = \frac{\Phi_z(f)}{1 - \frac{2V}{g}\omega} \,, \tag{36}$$

an expression which is easily derived from the fact that the mean square wave elevation is unchanged by the coordinate transformation. The orbital velocity expressions are transformed in a similar fashion, and, along with Eq. (34), formed the basis for the simulation. An example of the effect of the transformation on wave elevation spectra is given in Fig. 11.

Simulation of the random seaway

The basic method used for simulating the random seaway is common in analogue computer practice, and involves the use of suitable linear filters to shape the output of a random noise generator to obtain signals with the desired power spectra. The simulation was done entirely in moving coordinates, and thus all spectra were functions of frequency of encounter. In addition, the simulation was done for constant craft velocity only, since varying velocity would require filters with changing characteristic frequencies and consequent extravagant use of analogue computer components. Head, following and beam seas were simulated for both the quarter and full scale hydrofoil craft for speeds of 25 and 50 knots, respectively.

The starting point for the simulation was the vertical velocity spectrum since, in sea coordinates at least, wave elevation is obtained therefrom by an integration rather than a differentiation. In moving coordinates, wave elevation is obtained from vertical velocity by a "transformed" integration, the characteristics of which can be derived by considering the frequency response function of an integrator as a function of frequency of encounter. The frequency response of an integrator in sea or fixed coordinates is

$$I(j\omega) = \frac{1}{j\tau\omega} \tag{37}$$

where ω is the sea frequency. Using (35), the frequency transformation given in terms of frequency of encounter is

$$\omega = \frac{1 \pm \sqrt{1 - \frac{4V}{g} \times \omega'}}{2V/g} . \tag{38}$$

Substituting (38) in (37) will give the frequency response of a "transformed" integrator, thus

$$I'(j\omega') = \frac{2V/g}{j\tau\left[1 \pm \sqrt{1 - (4V/g)\,\omega'}\right]} . \tag{39}$$

It can be seen that $I'(j\omega')$ has the same 90° phase lag for all frequencies as the ordinary integrator, but that the magnitude is quite complicated. While (39) is obviously non-realizable in the strict sense, it can be approximated over a range of frequencies by a combination of minimum and non-minimum phase networks. The procedure was to first approximate the magnitude without regard to phase with a combination of first and second order filters, and then correct the overall phase to approximate 90° over the frequency range by all-pass networks. Typical head and following sea transformed integrator frequency response characteristics are shown in Fig. 12.

A block diagram of the head sea simulation is shown in Fig. 13. Notice that the transformed integration involved two all-pass filters, the difference in phase between them being such that the phase angle between w' and z' is 90°.

Figure 14 shows the filter arrangement for following seas. Following seas present special problems since the transformed wave elevation spectrum can contain both following and head components for certain craft velocities; and indeed also a steady value for that component whose crest velocity is equal to the craft velocity. Simulation for such a condition is clearly impossible, since the transformed integrator and foil separation filters would have to be approximated over an infinite number of decades in frequency. When the craft velocity is high enough, however, all significant frequencies become head components and a simulation is feasible. The simulation is similar to that of the head sea except for the all-pass filters which are required to supply the constant component of foil separation phase shift required.

It should be noted that simulation of the effect of the separation between the foils cannot be accomplished by a Padé approximation to a pure delay. The delay is distributed, and has a phase characteristic proportional to the square of the frequency. The foil separation filter required two second order all-pass filters to approximate the transformed phase shift over the significant frequency range of the vertical velocity spectrum.

A second method of simulation, using a number of superimposed sinusoids of appropriate amplitude and frequency, was used for simulating following seas at the lower ship speed. The method was unsuitable for the other cases, however, because of excessive demands on computing equipment to give a sufficient number of components to approximate a normal distribution.

ANALOG COMPUTER SIMULATION TECHNIQUES

Analog Simulation of the Equations of Motion

As mentioned previously the lift-curve slope is the basis for computation of all lift forces active on the foils. This is simulated on a function generator in the analog computer. The diode function generator creates a sequence of straight lines that are connected together to form the desired function. Obviously if a large number of segments are used then the function will be generated more accurately than if just a few points are selected. In practice about 8 or 9 "break points" will simulate most lift curves with sufficient accuracy. For example consider the following lift curve [Fig. (vi)]:

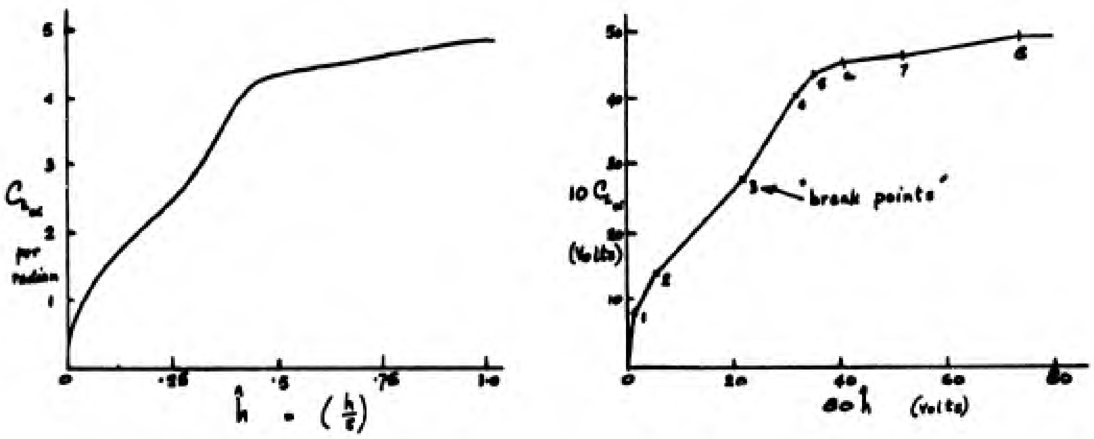

(a) (b)

Figure (vi)

An arbitrary voltage scaling of 80 volts/per unit $\hat{h}$ and 10 volts per unit C_{L_α} is assumed. The input to the function generator will be 80 $\hat{h}$ volts which gives an output of 10 C_{L_α} volts. This voltage is then fed into one channel of an electronic multiplier and multiplied by $(\alpha_0 + \alpha_d)$ to give C_L as a voltage. C_L is then subsequently summed with other voltage variables in the dynamic equations. If C_L is equal to the weight of the craft (C_{L_0}) then the heave equation for example will be in balance and the output of the vertical acceleration integrator will be zero. This is of course an oversimplified example, but it does illustrate the basic procedure on the computer. A simplified circuit for the heave equation is shown in Fig. 15.

Cavitation

Cavitation and its effect on the craft dynamics is very important and must be simulated if a realistic representation of the hydrofoil motions is to be obtained from the computer. Cavitation gives rise to nonlinearities in the lift-curve for a given foil element. A typical example is shown in Fig. (vii). The angles of attack at which partial cavitation and eventually full cavitation occurs are a function of cavitation number and thus speed. The step in the curve and the C_L at which the slope changes are a function of the lift-curve slope (C_{L_α}) which in turn is a function of immersion depth. The lift on a cavitating hydrofoil is obviously a complicated function to simulate. However, a reasonable approximation can be made by simulating the lift as shown in Fig. 16 to produce the curve of Fig. (vii) b.

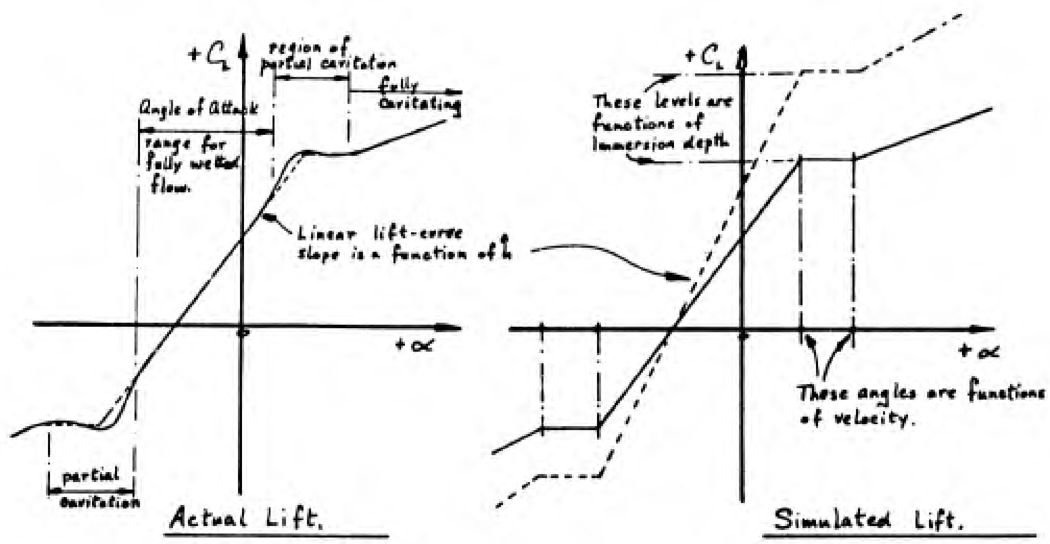

(a) (b)

Figure (vii)

Ventilation

Cavitation is unlikely to occur on foil elements at the slower foilborne speeds unless the foil angle of attack is very large ($>10^\circ$). However, ventilation, which has a similar effect, can occur at any speed when a foil is surface piercing or is close to the surface.

The effects of ventilation have been simulated on the analog computer, but this proved to be an extremely complex problem requiring a large number of computing elements.

The criterion for ventilation of a given foil element may be either the angle of attack (α) or the lift coefficient (C_L). α was used in our simulation. In terms of α, at a given speed it was assumed that there exists a fixed value of α, (α_v, say) for which ventilation must occur if $\alpha > \alpha_v$. Similarly, there exists an α stop (α_s), for which ventilation, if occurring, will stop when $\alpha < \alpha_s$. It was also assumed that if ventilation does occur, it will occur down to the first fully submerged fence, also, if $\alpha_s < \alpha < \alpha_v$ and if ventilation is occurring, it will cease if a fence goes through the water surface, either coming in or going out. The amount of lift (or rolling moment) lost due to ventilation is a fixed, but controllable fraction of the lift due to the affected portion of the foil which would have been calculated if no ventilation were assumed.

α is continuously available in the simulation, therefore, it is possible to produce a circuit to subtract the correct amount of lift from the total for the given foil element. This, however, is not straightforward, as a function of the following form is required [Fig. (viii)]:

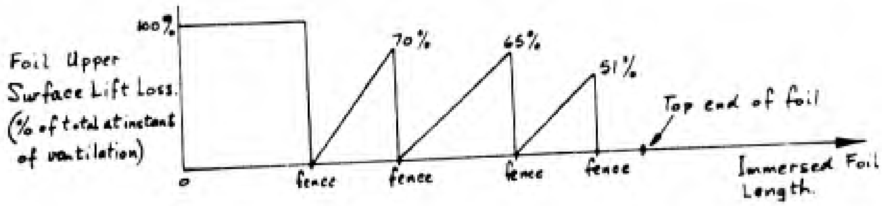

Figure (viii)

This function cannot be produced on a standard diode function generator because of the sudden changes in slope, therefore, an "X-Y" variplotter has to be used with a conducting stylus replacing the pen and a sheet of resistance material (carbon) cut at the fence positions and fed with voltages at each end of each section to produce voltage as a function of position. These voltages are then picked off by the stylus and fed into the equations through the necessary circuitry.

Simulation of ventilation has shown that ventilation has only minor effects on stability if the stability margins are adequate without ventilation. However, if stability is marginal without ventilation then the addition of these effects will cause instability.

Unsteadiness Effects

Circulation Delay

When the angle of attack on a foil surface is suddenly changed the pressure distribution on that surface does not adjust itself instantaneously to the new conditions. It responds in a transient manner and approaches the eventual steady-state value asymptotically as shown in Fig. 17.

This delay is due mainly to the relatively slow change of lift due to circulation, and to a lesser extent, the lift response associated with accelerating a certain mass of fluid due to instantaneous reaction of that fluid against the foil section.

The circulation lift change is usually given in terms of indicial functions, i.e., curves of lift change versus time after a "step" change in angle of attack. These indicial functions for low aspect ratio wings start at or above the eventual steady-state level and drop initially for about 1 chord length of travel to meet a rising exponential which yields approximately half the lift change in about 4 chord lengths. Ninety-eight percent of the steady-state lift is achieved after approximately 6 chord lengths of travel.

Two exponentials of the form shown in Fig. 17 were superimposed to produce an approximation to the curves of Ref. 16. Ideally for a surface piercing hydrofoil we should consider a varying aspect ratio, but for practical purposes it is quite adequate to consider a fixed mean aspect ratio with the changes in circulation being considered as being subject to the same delay whatever the cause of change in circulation delay.

Circulation delay effects become more marked at the higher aspect ratios, therefore, an aspect ratio value biased toward the high side was chosen so that the simulated effects would be more severe than in practice. An aspect ratio of 6 was assumed using the data from Ref. 16.

The results of response studies on a hydrofoil craft using the exponentials of Fig. 17 are given in Fig. 18. It can be seen that the effect of lift delay has a minor effect on the overall hydrofoil craft motions.

Virtual Inertia (Added Mass Effects)

Virtual inertia is usually considered as the inertia of the body of water that can be thought of as moving with the foils and which adds to the craft inertia when the foils are imparting an acceleration to the surrounding water. There are some instances, however, when the fluid mass opposes the craft inertia such as in a seaway when the body of water surrounding the foils may be imparting a disturbing acceleration to the craft.

Some studies of this effect were carried out but the indications were that the effect on the craft motions was small, producing only minor changes in peak accelerations for the shortest and steepest seas (Fig. 18).

As a result of these studies virtual inertia effects were neglected in all subsequent simulations.

MODEL TRIALS

General

Predicted hydrofoil ship characteristics require verification by model trials, in a similar manner to the experiments usually conducted on conventional ship and aircraft models.

For the hydrofoil ship, stability in a seaway is the major consideration, the measurement of model resistance and lift characteristics being important secondary problems.

For a new vehicle concept, it is essential to verify scaling laws and provide experimental proof of theoretical performance and stability predictions.

The hydrodynamic design of the FHE-400 is supported by the results of a series of model trials, mainly carried out at the National Physical Laboratory and the Admiralty Research Laboratory in London, and at the Canadian Naval Research Establishment, Halifax, and the National Research Council in Ottawa. Initial trials to determine resistance and seakeeping were conducted by the Davidson Laboratory, S.I.T. in Hoboken, New Jersey. The model programme consisted of a series of fourteen models of eight different sizes, ranging from 1/25 scale to 1/4 scale. The model trials are listed in Table 1 together with a brief description of each model, its size and purpose, trials dates, and test facilities used.

The model trials which have provided a direct input to the stability and control study are described below in greater detail.

Table 1
List of FHE-400 Model Trials

Froude Scale Model Description	Trials Dates	Measurements and Observations	Facility
1/25 Scale Hydrofoil Ship	Oct. 61	Displacement Performance Displacement and Foilborne Seakeeping. Hove-To Sea-keeping.	S.I.T. New Jersey
1/25 Scale Hydrofoil Ship Free Powered Model	Sept. 62 May 63	Foilborne Seakeeping on all headings	D.H. Ontario
1/16 Scale Hydrofoil Ship	Apr. 63 Aug. 63	Displacement Performance Displacement and Foilborne Seakeeping. Hove-To Sea-keeping.	N.P.L. N.P.L. N.P.L. London
	Dec. 63 Jan. 64	Displacement Performance in Calm Water only	N.R.C. Ottawa
1/8 Scale Main Foil	Nov. 62 May 63 Mar. 64 Aug. 64	Foil and Pod Pressure Distribution. Resistance, Lift, Yawing, Rolling and Pitching Moments.	N.P.L.
1/8 Scale Bow Foils Subcavitating and Superventilating Models	Nov. 62	Resistance, Lift, Yawing, Rolling and Pitching Moments.	N.P.L.
1/8 Scale Coupled Model. Hull beam carrying main foil and bow foil	Nov. 62	Foilborne Stability in Calm and Rough Water.	N.P.L.

Table 1 (Continued)
List of FHE-400 Model Trials

Froude Scale Model Description	Trials Dates	Measurements and Observations	Facility
1/4 Scale RX Craft	Oct.-Nov. 61 Dec. 61 to Apr. 62 May-June 62 Aug.-Oct. 62 Dec. 62 Jan. 63 Mar.-Oct. 63 May-Aug. 64	Foilborne Stability, Control and Seakeeping in Calm and Rough Water	N.R.E.
1/4 Scale Bow Foil for RX Craft	Mar. 63	Resistance, Lift, Yawing, Rolling and Pitching Moments	N.P.L. & N.R.E. Halifax
1/12 Scale Main Foil 2D Cavitation Model	Dec. 63 Projected Sept. 64	Lift, Resistance and Pitching Moment for attached and separated flow.	A.R.L. London
1/12 Scale Bow Foil 2D Cavitation Model	Dec. 63 Projected Sept. 64		A.R.L.
1/6 Scale Bow Foil Flutter Model	Projected Sept. 64	Hydroelastic Characteristics	N.P.L.
1/2 Scale 2D Main Foil Model	Apr. 64 Projected Oct. 64	Wind Tunnel check of foil hydrodynamic characteristics	N.R.C.
1/16 Scale Power Pod Model	Sept. 63	Pod Pressure Distribution	N.R.C.

1/16 Scale Hydrofoil Ship Model

The model was tested at N.P.L. to establish resistance at hullborne speeds through the takeoff regime, in calm water and head and following seas. In addition hove-to behaviour was investigated and measurements made at various speeds of heave acceleration and pitching rates, in various seas and gross weight conditions.

1/8 Scale Foil Models

Bow and main foil models have been tested in the N.P.L. towing tanks at Feltham. Using special dynamometers provided by N.P.L., trials data included foil unit lift, drag, sideforce, pitching moment, yawing moment, and rolling moment over a range of Froude speeds and depths of immersion. Both subcavitating and supercavitating bow foil models were evaluated. The effect of bow foil downwash on the main foil was measured and found to be small. The main foil model was fitted with pressure taps at the centre section and power pod to obtain foil and foil to pod interference pressure distributions to verify theoretical predictions. N.P.L. developed a scanning valve to read up to 90 taps.

Finally, the bow and main foil model were coupled to a beam representing the hull, free to heave and trim. The results of towing trials in calm and rough water were scaled up to 1/4 size and are shown in Figs. 5 and 6 in comparison with the predicted response of the 1/4 scale RX craft in sinusoidal seas.

1/4 Scale Fully Cavitating Bow Foil Model

The 1/4 scale bow foil was built for the RX manned model. The size of the N.P.L. towing tank and dynamometer provided the opportunity to compare the data from tank trials with the simulation and with the measured response of the RX test craft.

1/4 Scale RX Craft

The craft is owned and operated by the Naval Research Establishment of the Canadian Defence Research Board. The RX equipped with the 1/4 scale foil system designed and built by De Havilland weighs about 3-1/2 tons. The hull and forward boom are not representative of the FHE-400; neither is the propulsion system, consisting of a gasoline engine 'Vee' drive and single propeller. Because of the 'Vee' drive the hull clearance is only 2/3 of the FHE-400 design clearance.

In addition to providing the craft and test crew, N.R.E. have fitted instrumentation to record the following data:

(a) Linear acceleration angles and angular rates at the C.G., vertical acceleration at the bow foil.

(b) Main foil lift, drag and sideforce and bow foil lift.

(c) Main and bow foil element stresses through strain gauges.

(d) Bow foil steering loads and helm angles.

(e) Velocity, engine RPM and propeller thrust.

A 14 channel oscillograph paper recorder is used except when acquiring data for spectral analysis of response in a random seaway. This work requires a 7 channel FM tape recorder for craft motions and seaway characteristics, the latter measured separately at a moored wave pole.

1/12 Scale Cavitation Models

Two dimensional models of the main foil subcavitating section and the fully cavitating bow foil sections were tested at speeds up to 50 knots in the A.R.L. whirling arm facility. The lift, drag, and pitching moment data was obtained which verified the predicted cavitation limits for the subcavitating foil and the nonlinear characteristics of the supercavitating section.

POWER SPECTRAL ANALYSIS

It is necessary to use statistical methods in order to compare predicted and measured hydrofoil response in a random seaway.

One suitable method is to compare the power spectral densities of the predicted and measured data. This approach gives R.M.S. values and a measure of how closely the random motions approach a Rayleigh distribution.

If Rayleigh statistics are assumed, then all the statistical characteristics are defined as shown in Table 2.

Table 2
Rayleigh Probability Distribution

Peak amplitudes may be obtained using the following constants:

The most frequent amplitude	= 1.41 × R.M.S. value
The average amplitude	= 1.77 × R.M.S. value
Average of highest 1/3	= 2.83 × R.M.S. value
Average of highest 1/10	= 3.60 × R.M.S. value

Strictly speaking, the Rayleigh probability distribution only applies when the spectrum is narrow.

Results from simulated and measured hydrofoil ship response in a random seaway indicate that most of the response variables have sufficiently narrow spectra so that their peak distributions are predominantly Rayleigh. For design purposes, such as defining the foil system fatigue environment, the assumption of Rayleigh statistics is considered adequate.

Power spectral analysis has been used extensively in the FHE-400 design, for stress and fatigue life predictions, habitability requirements and equipment installation design.

The predicted and measured response of the 1/4 scale manned RX craft was used to verify the FHE-400 foil system design method. The motions of the RX craft in a 1/4 scale random seaway were recorded on magnetic tape which was then processed at the National Research Council Statistical Analysis Facility in Ottawa. Power spectral densities of vertical acceleration at the centre of gravity, pitch angle, main foil lift and the seaway amplitude were obtained, the last measured at a separate moored wave pole.

The theoretical dynamic stability simulation results were recorded on magnetic tape and similarly processed at N.R.C. to obtain predicted power spectral densities. The correlation between predictions and measurement is presented in Figs. 19 to 25.

Only head seas data is presented since following and beam sea motions are of lesser magnitude and low frequency, making them less suitable for statistical analysis and easier to compare visually. It has been found that sinusoidal analysis is adequate for the study of motions in beam and following seas.

HYDROFOIL SHIP STABILITY CHARACTERISTICS

This paper summarizes the methods developed for the design of the 200 ton FHE-400 hydrofoil ship for the R.C.N. Since surface piercing hydrofoils are usually required to be inherently stable, some comments on particular problems are given. Longitudinal stability in pitch and heave is relatively easy to achieve, provided that lift discontinuities due to ventilation or cavitation can be avoided or minimised. Foil unit lift slope and heave stiffness can be optimized for head and following sea response. Following sea "takeoff" is not a problem with the canard arrangement discussed. Greater heave stiffness is required in following seas and some compromise between pitch and heave motions and accelerations is necessary.

Open ocean operation requires a high ships' centre of gravity which compounds the problem of achieving inherent lateral stability. The six degree of freedom simulation revealed the need for roll stability augmentation of the FHE-400 at low foilborne speeds. This is achieved by rotating the main foil anhedral tips as "ailerons." At intermediate and high foilborne speeds, the anhedral tips are fixed since they provide adequate restoring forces without change of incidence. The steerable bow foil gives positive directional control at all operational speeds, both hullborne and foilborne. While the ship can be steered "manually" at high speeds the simulation showed the need for a yaw damper to prevent heading drift.

The relationship between full size FHE-400 motions and the motions of the 1/4 scale RX craft are given in Table 3.

Analog computer predictions of FHE-400 response in a random seaway are given in Figs. 26 to 33.

Figure 34 shows the plan and profile views of the FHE-400 prototype ship; the bow foil and main foil units are illustrated in Figs. 35 and 36.

Table 3
Relationship Between Model and Full Scale Response

If R_s is the ratio between the craft reference lengths and R_v is the ratio between the reference velocities, then $R_s = R_v^2$ (Froude scaling). Thus when model response is shown in a particular seaway then the full scale motions relative to the model, in an equivalent seaway, are as follows:

1. FHE-400 will experience linear motions R_s times those of the model.
2. FHE-400 linear velocities will be $\sqrt{R_s}$ times those of the model.
3. FHE-400 linear accelerations will be identical with those of the model.
4. FHE-400 angular excursions will be identical with those of the model.
5. FHE-400 angular velocities will be $1/\sqrt{R_s}$ times those of the model.
6. FHE-400 angular accelerations will be $1/R_s$ times those of the model.
7. Events will happen $1/\sqrt{R_s}$ times as fast for FHE-400 than for the model.

Further studies are continuing on detail stability and control characteristics, including hydroelastic effects, stability augmentation system response, and towed body effects. A control console has been installed with the analog computer equipment and allows "manual" operation of steering, roll and throttle controls for realistic simulation of rough water operation, takeoff and landing and turning maneuvers.

While it is hoped that the depth of the programme described will have encompassed most of the problem areas, final proof will rest with sea trials of the prototype ship.

SYMBOLS

A = rolling inertia (slugs, ft^2)

B = pitch inertia (slugs, ft^2)

b = foil immersed span (ft)

c = foil chord (ft)

C = yaw inertia (slugs, ft)

D = operator d/dt

D = product of inertia (slugs, ft^2)

E = product of inertia (slugs, ft^2)

F = product of inertia (slugs, ft^2)

f = wave frequency (cycles/sec)

f' = frequency of encounter (cycles/sec)

g = acceleration due to gravity (ft/sec^2)

h = immersion depth (ft)

I = integral operator

$I(j\omega)$ = frequency response of integrator

I_{xx} = rolling inertia (slugs, ft^2)

I_{yy} = pitching inertia (slugs, ft^2)

I_{zz} = yawing inertia (slugs, ft^2)

I_{xz} = product of inertia (slugs, ft^2)

i_{xx} = normalized moment of inertia $(I_{xx}/\rho S_s^3)$

i_{yy} = normalized moment of inertia $(I_{yy}/\rho S_s^3)$

i_{zz} = normalized moment of inertia $(I_{zz}/\rho S_s^3)$

i_{zx} = normalized product of inertia $(I_{zx}/\rho S_s^3)$

$j = \sqrt{-1}$

k = fractional increment of thrust horsepower

K_{D_i} = induced drag curve slope $dC_{D_i}/d\alpha^2$

L = rolling moment (lb-ft)

M = pitching moment (lb-ft)

m = mass = (W/g) (slugs)

N = yawing moment (lb-ft)

O = origin

P = rate of rotation about x axis (rads/sec)

p = rolling velocity (rads/sec)

Q = rate of rotation about y axis (rads/sec)

q = pitching velocity (rads/sec)

q = dynamic pressure = $1/2\,\rho V^2$ (lb/sq ft)

R = rate of rotation about z axis (rads/sec)

r = yawing velocity (rads/sec)

S = foil immersed area (sq ft)

S_o = reference area (sq ft)

s = semi-span = $(b/2)$ (ft)

t = time (sec)

t^* = $b/2V$ = s/V = ratio of ref. distance to ref. velocity

$\hat{t}$ = t/t^* = normalized time

U = velocity along x axis (ft/sec)

u_o = steady-state or reference velocity (ft/sec)

u = perturbation in velocity along x axis (ft/sec)

u_w = horizontal component of wave orbital velocity (ft/sec)

$u(t,x)$ = horizontal component of wave orbital velocity (ft/sec)

V = free stream velocity (ft/sec)

V_o = reference velocity (ft/sec)

v = velocity along y axis (ft/sec)

v_w = horizontal component of wave orbital velocity (ft/sec)

W = weight (lb)

w = velocity along z axis (ft/sec)

w_w = vertical component of wave orbital velocity (ft/sec)

$w(t,x)$ = vertical component of wave orbital velocity (ft/sec)

X = longitudinal forces (along x axis) (lb)

x = horizontal distance in sea coordinates (random seaway)

x = longitudinal axis

Y = sideforce (along y axis) (lb)

y = lateral axis

Z = vertical forces (along z axis) (lb)

z = vertical axis

$z(t, z)$ = instantaneous sea surface elevation

z_w, z_L, z_R, z_F = wave amplitudes (ft)

α = angle of attack

α_o = steady-state angle of attack

α_d = dynamic angle of attack

β = sideslip angle

Γ = dihedral angle (degrees)

Φ = roll angle in Euler equation

Φ = phase angle (regular seas) (radians)

$\Phi(f, x)$ = spectral density of wave surface elevation (ft^2/cycle/sec)

$\Phi_z(f)$ = Neumann power spectral density function (random seas) (ft^2/cycle/sec)

ϕ = randomly chosen phase angle (random seas) (radians)

ϕ = roll angle (radians)

$\dot{\phi}$ = rolling velocity $(d\phi/dt)$ (radians/sec)

$\ddot{\phi}$ = rolling acceleration $(d^2\phi/dt^2)$ (radians/sec)

λ = wave length (ft)

μ = nondimensional relative density parameter $m/\rho S_o s$

ρ = fluid mass density (slugs/cu ft)

τ = integrator time constant

ψ = yaw angle (radians)

ω = angular rate (rads/sec)

ω = wave frequency (rads/sec)

ω' = frequency of encounter (rads/sec)

Coefficients

C_D = drag coefficient = Drag/qS_o

C_L = lift coefficient = Lift/qS

C_{L_α} = lift-curve slope = $dC_L/d\alpha$

C_{L_h} = lift-curve slope = dC_L/dh

C_ℓ = rolling moment coefficient = L/qSb

C_m = pitching moment coefficient = M/qSb

C_n = yawing moment coefficient = N/qSb

Subscripts

$(\ )_o$ = steady-state or reference condition

$(\ )_F$ denotes front foil

$(\ )_M$ denotes main foil

$(\ )_L$ denotes left-hand side of main foil

$(\ )_R$ denotes right-hand side of main foil

$(\ )_w$ denotes wave

ACKNOWLEDGMENTS

The authors wish to thank the Royal Canadian Navy for permission to use much of the information presented in this paper. We gratefully acknowledge the advice and assistance of R. W. Becker, E. R. Case, P. A. Maritan and A. C. Stonell.

Thanks are also due to E. Ball, F. Miller, Mrs. N. Iles and Miss L. Wilkinson for the preparation of the manuscript.

REFERENCES

1. Etkin, B.: Dynamics of Flight. John Wiley and Sons, Inc., New York 1959.

2. Duncan, W. J.: Control and Stability of Aircraft. Cambridge University Press, Cambridge 1952.

3. Perkins and Hage: Airplane Performance Stability and Control.

4. Gibbs and Cox: Hydrofoil Handbook.

5. Glauert: Aerofoil and Airscrew Theory.

6. Silverstein and Katzoff: Design Charts for Predicting Downwash Angles and Wake Characteristics Behind Plain and Flapped Wings. NACA TR 648. 1940.

7. Ribner: Notes on the Propeller and Slipstream in Relation to Stability. NACA ARR L41 12a. (WR L-25) 1944.

8. Michael, W. H., Jr.: Analysis of the Effects of Wing Interference on the Tail Contributions to the Rolling Derivatives. NACA TN 2332 (also TR 1086) 1951.

9. Campbell and McKinney: Summary of the Methods for Calculating Dynamic Lateral Stability and Response and for Estimating Lateral Stability Derivatives. NACA TR 968. 1950.

10. Toll and Quijo: Approximate Relations and Charts for Low Speed Stability Derivatives of Swept Wings. NACA TN 1581. 1948.

11. Imlay: Theoretical Motions of Hydrofoil Systems. 1948. NACA TR 918.

12. DeYoung and Harper: Theoretical Symmetric Span Loading at Subsonic Speeds for Wings Having Arbitrary Plan Form. NACA TR 921.

13. DeYoung: Theoretical Antisymmetric Span Loading at Subsonic Speeds for Wings Having Arbitrary Plan Form. NACA TR 1056. 1951.

14. Jones, R. T.: The Unsteady Lift of a Wing of Finite Aspect Ratio. NACA R 681.

15. Tobak, M.: On the Use of the Indicial Function Concept in the Analysis of Unsteady Motion of Wings and Wing-Tail Combinations. NACA R 1188. 1954.

16. Drischler, J. A.: Approximate Indicial Lift Functions for Several Wings of Finite Span in Incompressible Flow as obtained from Oscillatory Lift Coefficients. NACA TN 3639. 1936.

17. Wadlin, K. L., Shufford, C. L., McGehee, J. R.: A Theoretical and Experimental Investigation of the Lift and Drag Characteristics of a Hydrofoil at Sub-Critical and Super-Critical Speed. NACA TR 1232. 1955.

18. Brown, P. W.: Force Characteristics of Surface Piercing Fully Ventilated Dihedral Hydrofoils. S.I.T. Report No. 698. Oct. 1958.

19. Brown, P. W.: A Generalized Theory of the Impact Characteristics of Surface Piercing, Fully Ventilated Dihedral Hydrofoils. S.I.T. Report No. 731. July 1959.

20. Fridsma, G.: Force and Moment Characteristics of a Surface Piercing Fully Ventilated Dihedral Hydrofoil. S.I.T. Report No. 795. Nov. 1960.

21. Johnson, V. E., Jr.: Theoretical and Experimental Investigation of Supercavitating Hydrofoils Operating Near the Free Water Surface. NASA Tech. Report R-93. 1961.

22. Longuet-Higgins, M. S.: On the Statistical Distribution of the Heights of Sea Waves. Journal Marine Research II, pp. 245-6. 1952.

23. Pierson, Neumann and James: H. O. Pub. 603, Hydrog. Office, U.S.N. Practical Methods for Observing and Forecasting Ocean Waves by Means of Wave Spectra and Statistics.

24. Pierson, W. J., Jr.: A Unified Mathematical Theory for the Analysis, Propagation and Refraction of Storm Generated Ocean Surface Waves. Part I and II, 1952. Research Division, College of Engineering, New York University.

25. Pierson, W. J., Jr.: An Interpretation of the Observable Properties of Sea Waves in Terms of the Power Spectrum of the Gaussian Record. Trans. Am. Geophysical Union, Vol. 35, No. 5. 1954.

26. Rice, S. O.: Mathematical Analysis of Random Noise, B.S.T.J. Vols. 23 and 24. 1944-5.

27. Neumann, G.: An Ocean Wave Spectra and a New Method of Forecasting Wind Generated Sea. B.E.B. Tech. Memo 43, 1953.

28. St. Denis and Pierson: On the Motions of Ships on Confused Seas. Trans. SNAME, Vol. 61. 1953.

29. Jasper, N. H.: Statistical Distribution Patterns of Ocean Waves and of Wave-Induced Ship Stresses and Motions with Engineering Applications. Trans. SNAME Vol. 64. 1956.

30. Cartwright and Longuet-Higgins: The Statistical Distribution of the Maxima of a Random Junction. Proc. Royal Soc. London. Series A, Vol. 237, p. 212. 1956.

31. Korvin-Kroukovsky, B. V. and Lewis, E. V.: Ship Motions in Regular and Irregular Seas. S.I.T. Technical Memorandum N 106. July 1954.

32. Weaver, D. K.: Design of R.C. Wide-Band 90 Degree Phase Difference Network. Proc. I.R.E. April 1954.

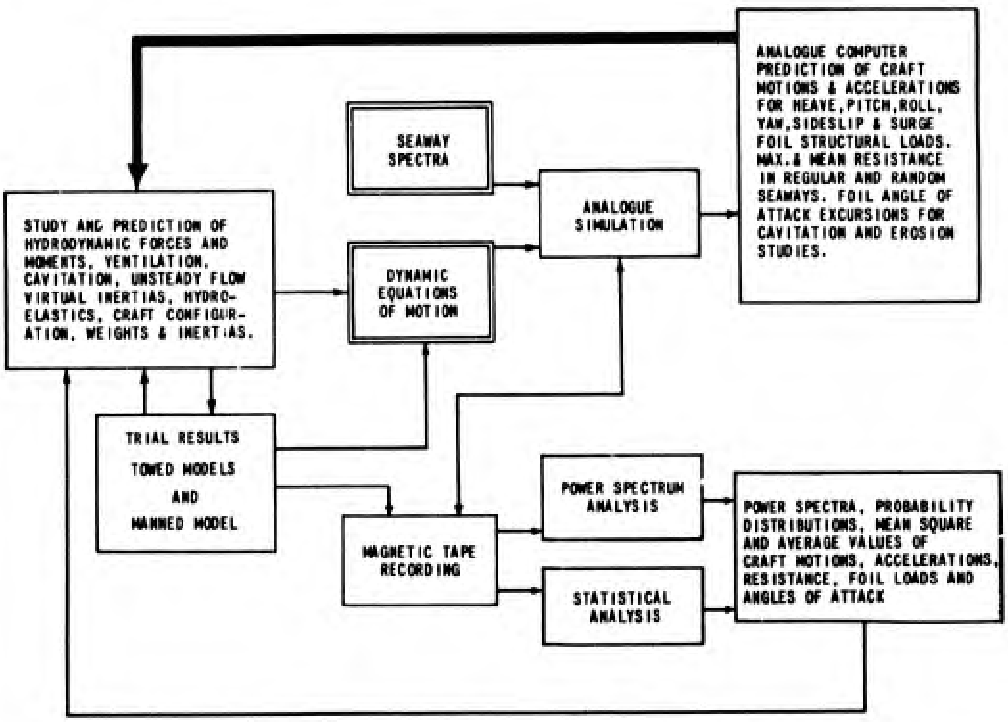

Fig. 1 - Hydrofoil dynamic stability study simplified iterative design procedure

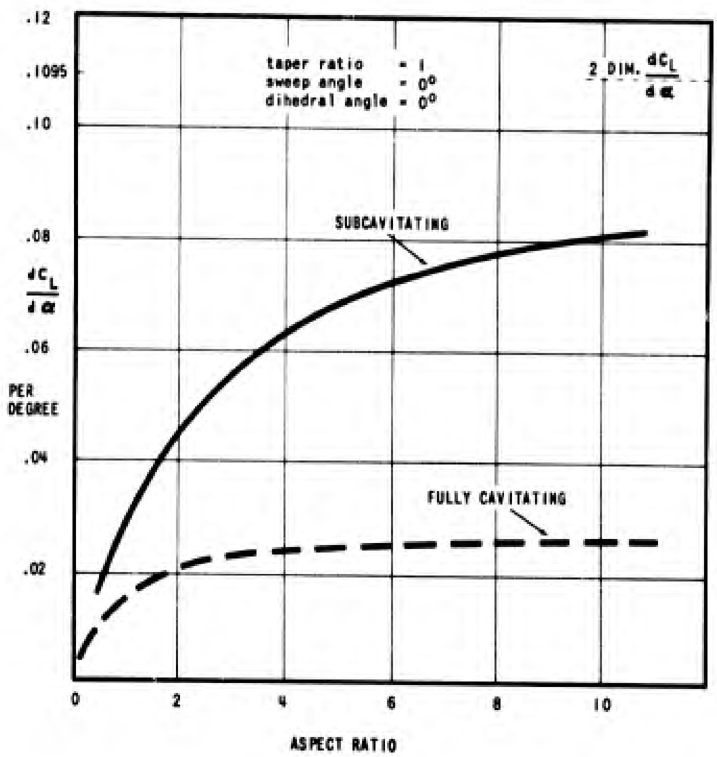

Fig. 2 - Variation of lift curve slope with aspect ratio

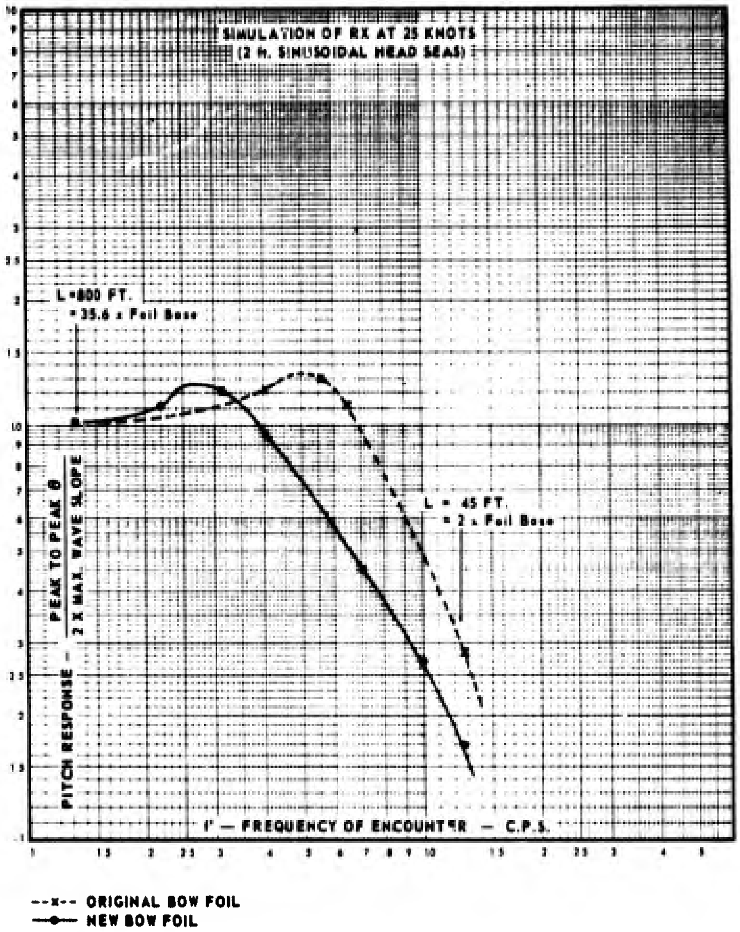

Fig. 3 - Pitch response

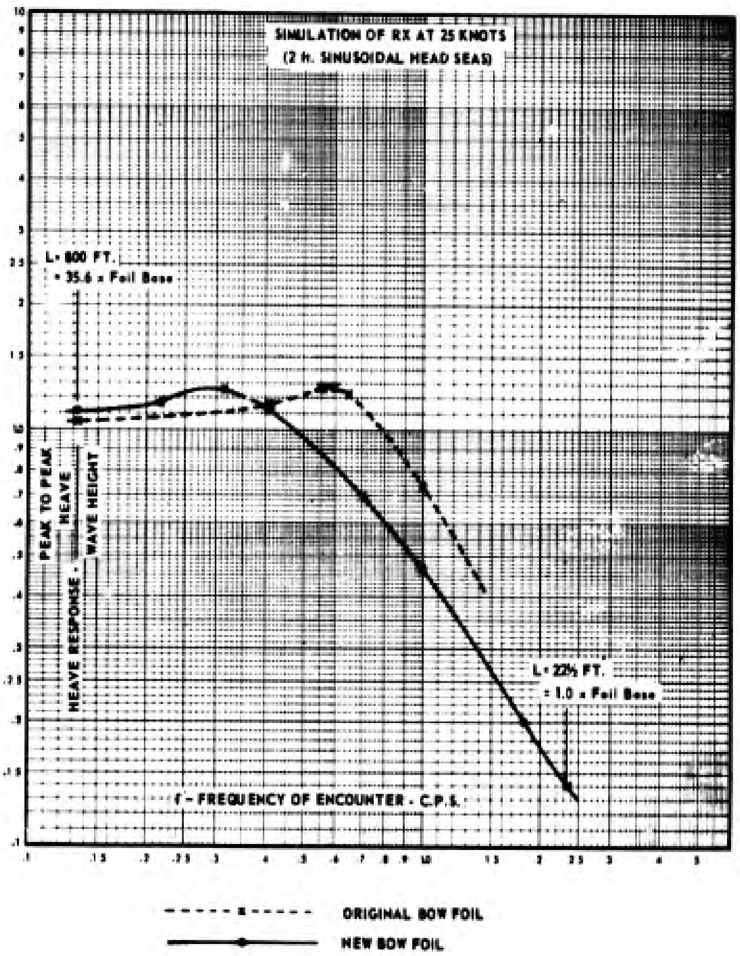

Fig. 4 - Heave response

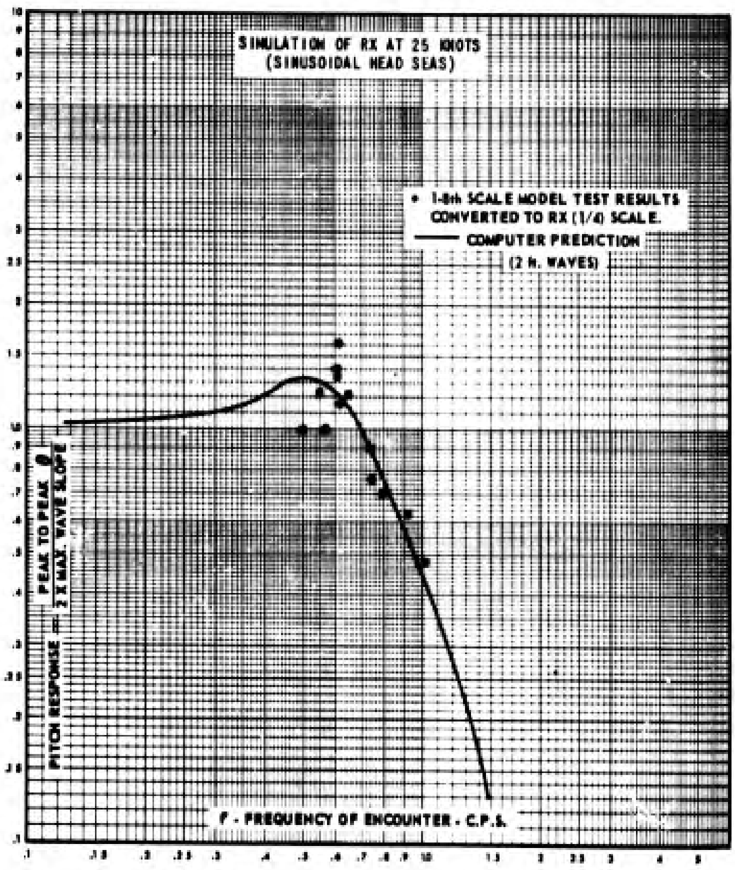

Fig. 5 - Pitch response

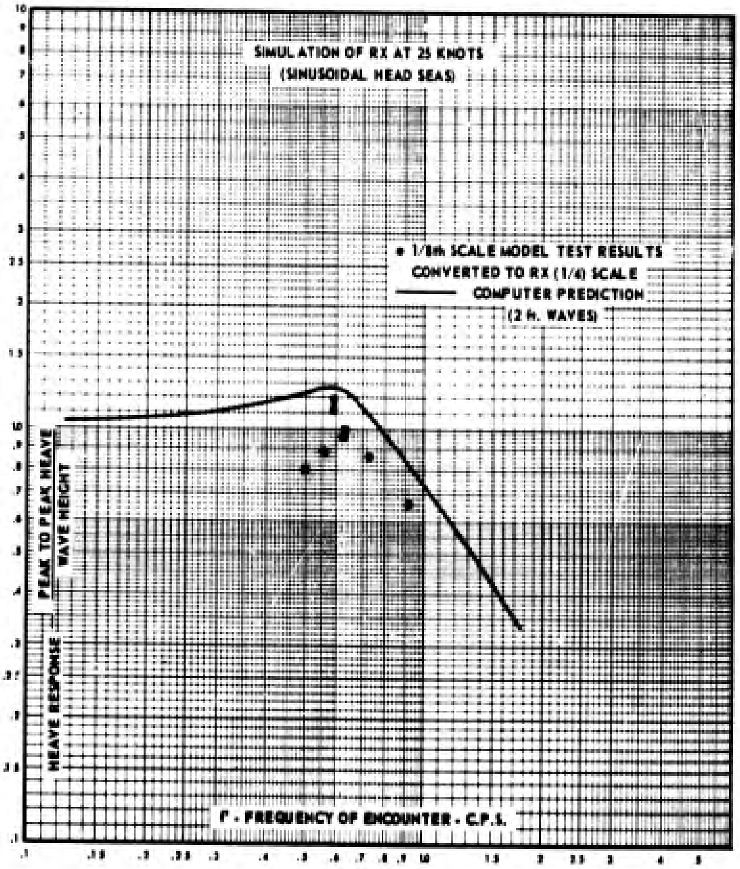

Fig. 6 - Heave response

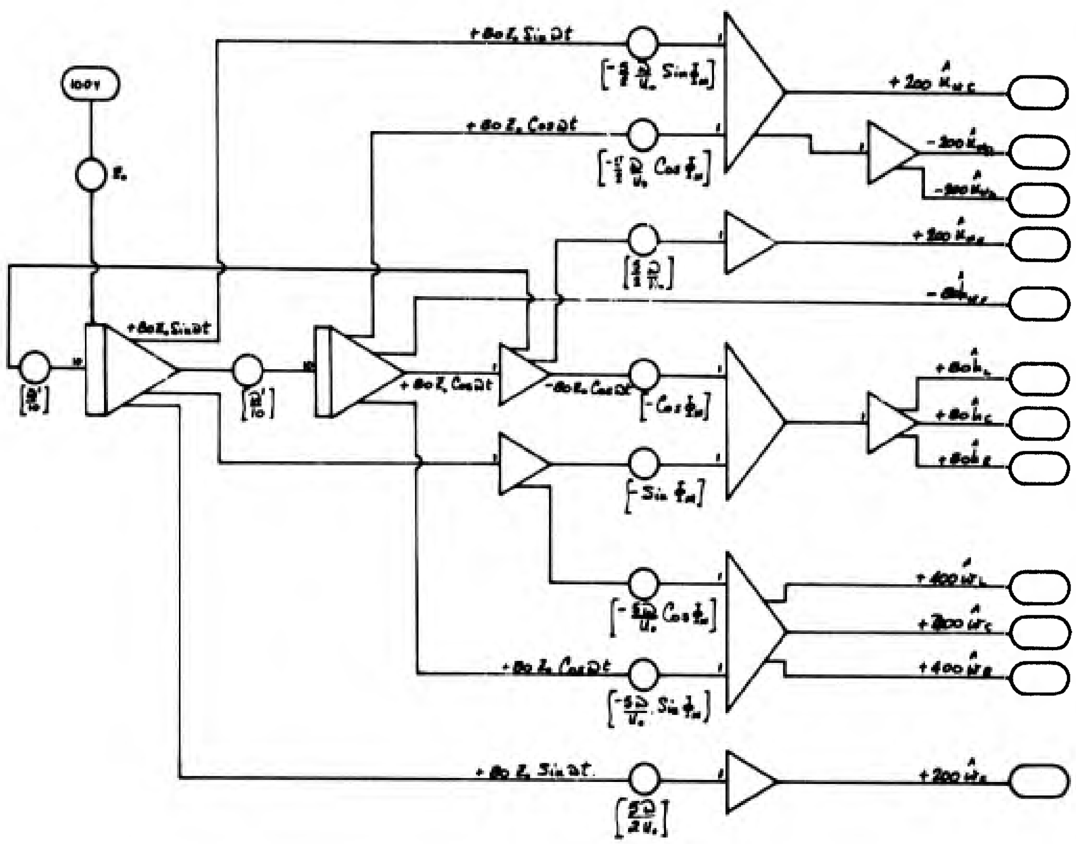

Fig. 7 - Typical sine wave generator circuit

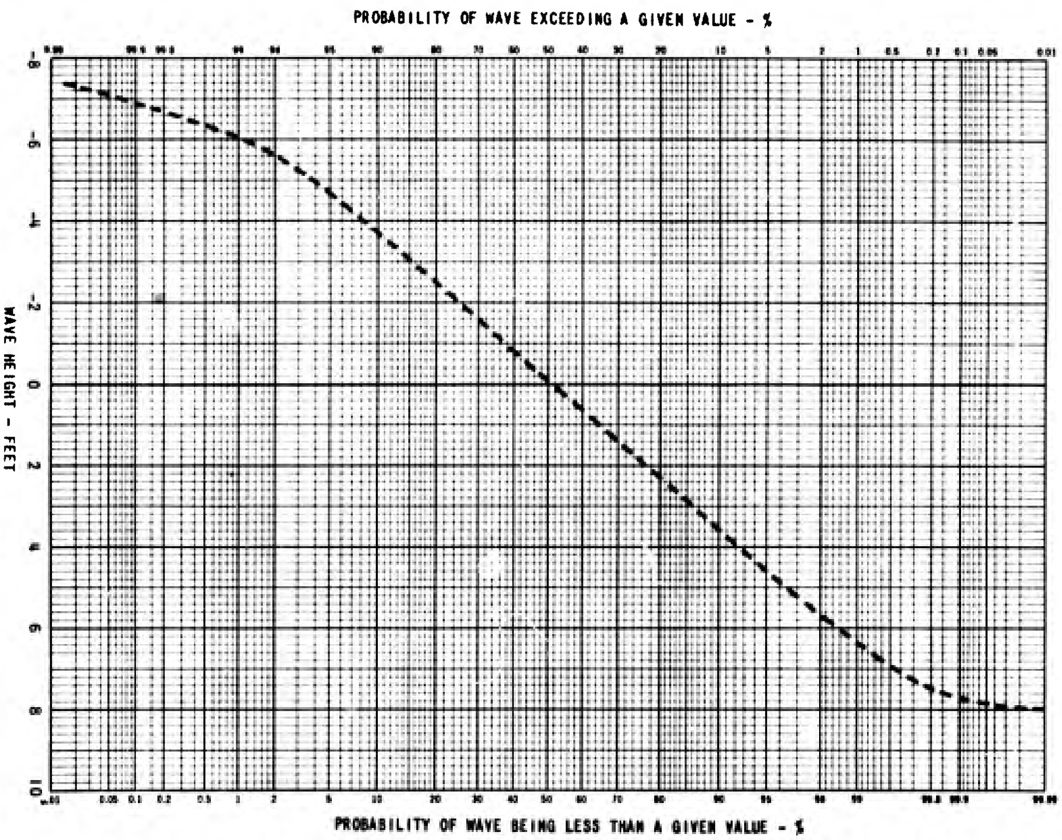

Fig. 8 - Probability distribution function -- Sea State 5

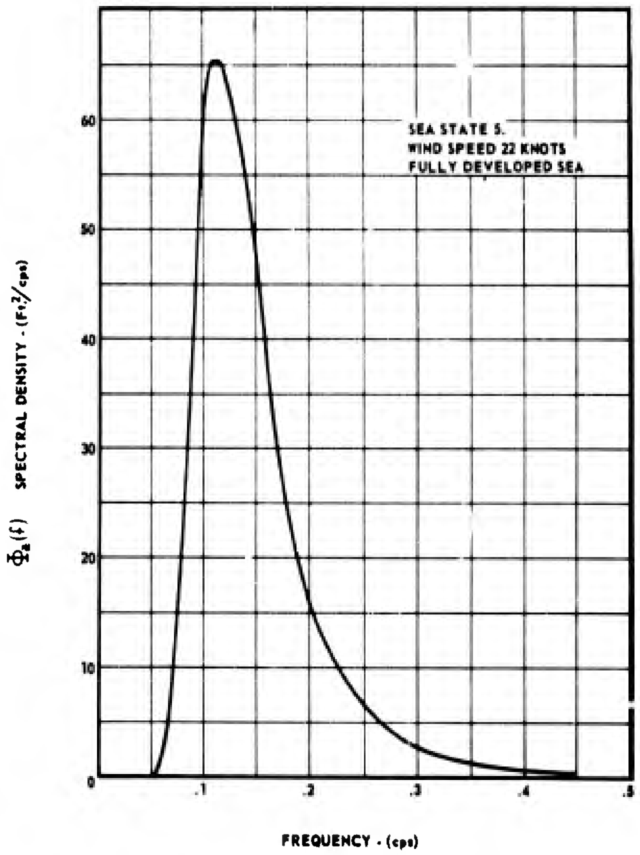

Fig. 9 - Wave elevation spectrum

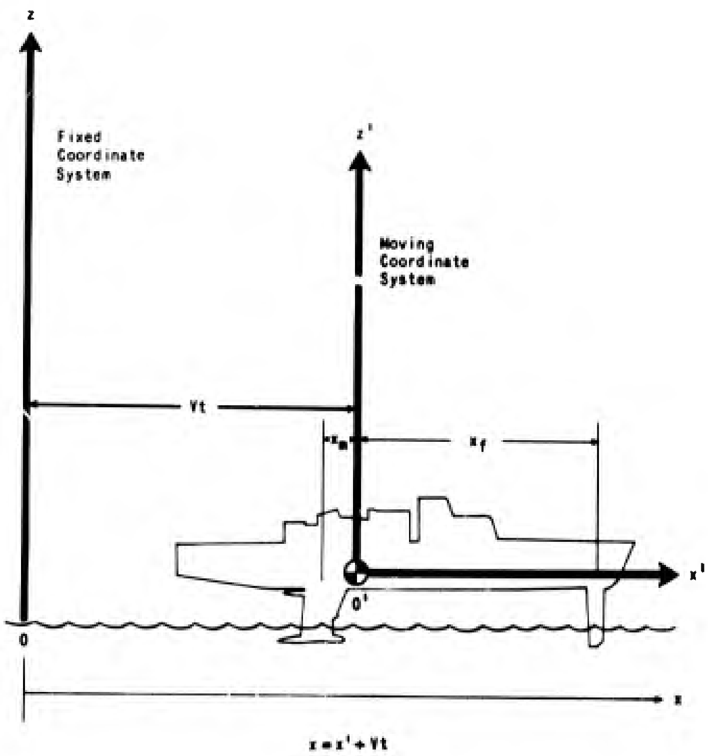

Fig. 10 - Coordinate transformation

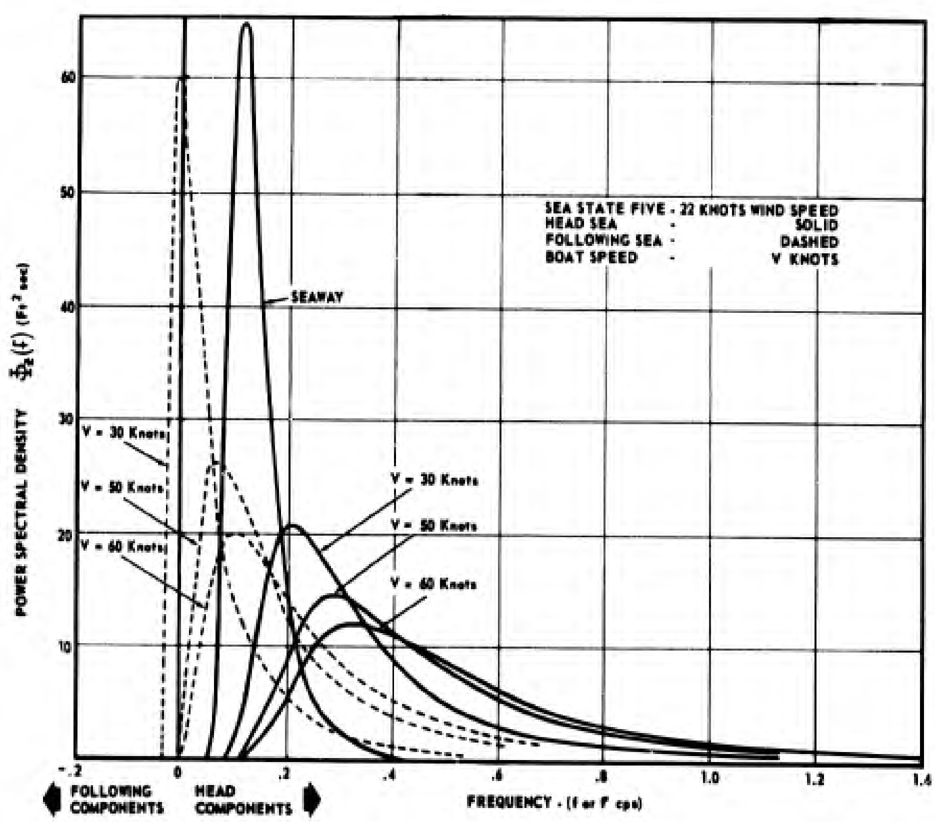

Fig. 11 - Transformed wave elevation spectra

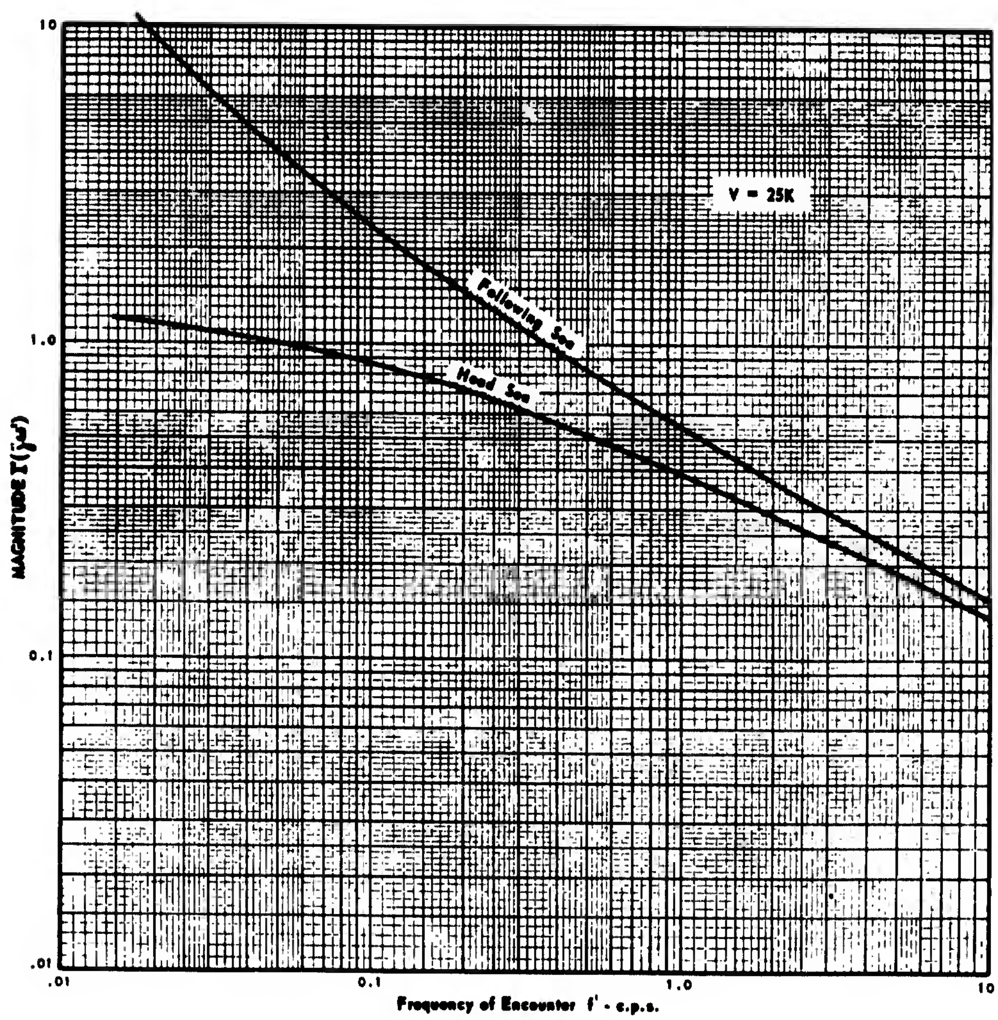

Fig. 12 - Typical transformed integrator frequency response

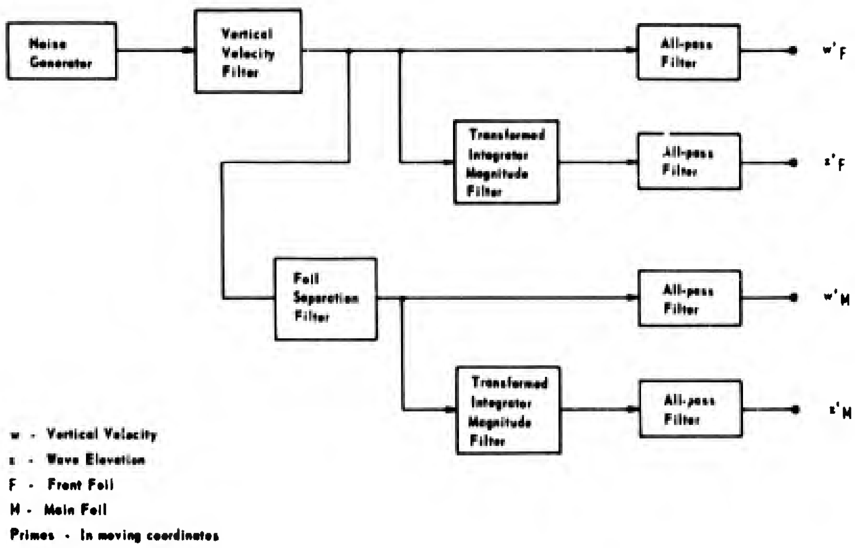

Fig. 13 - Head sea simulation

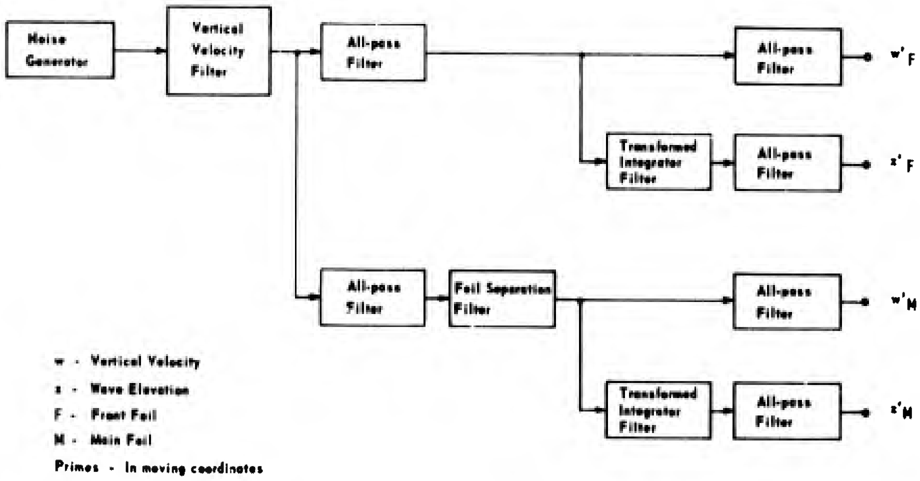

Fig. 14 - Following sea simulation

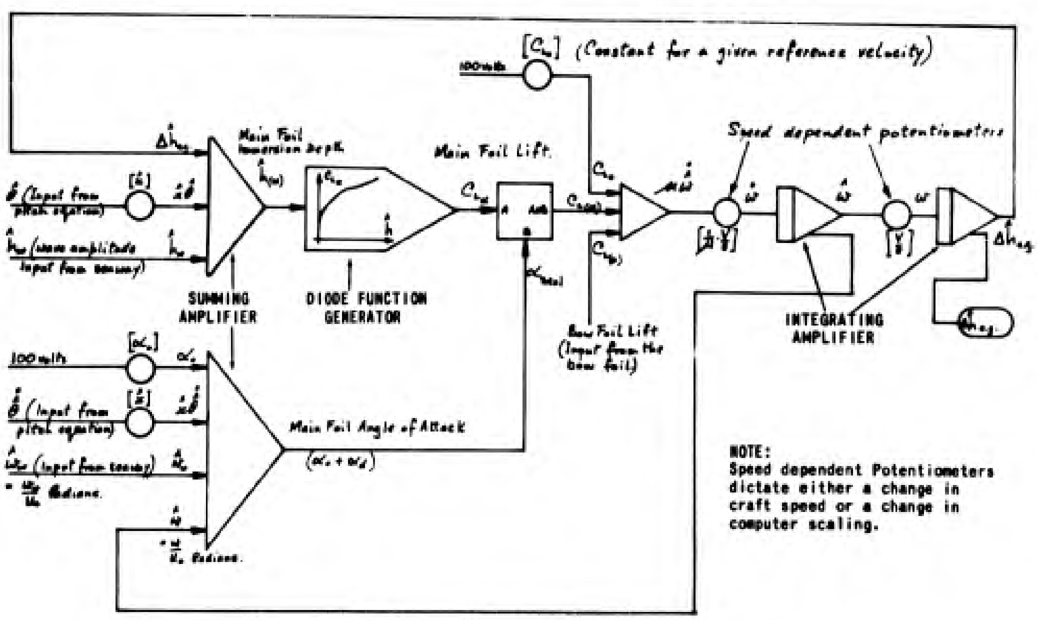

All of the equations are built up in this manner with the various inputs feeding into the summing amplifiers and integrators etc..

Fig. 15 - Simplified block diagram of heave equation

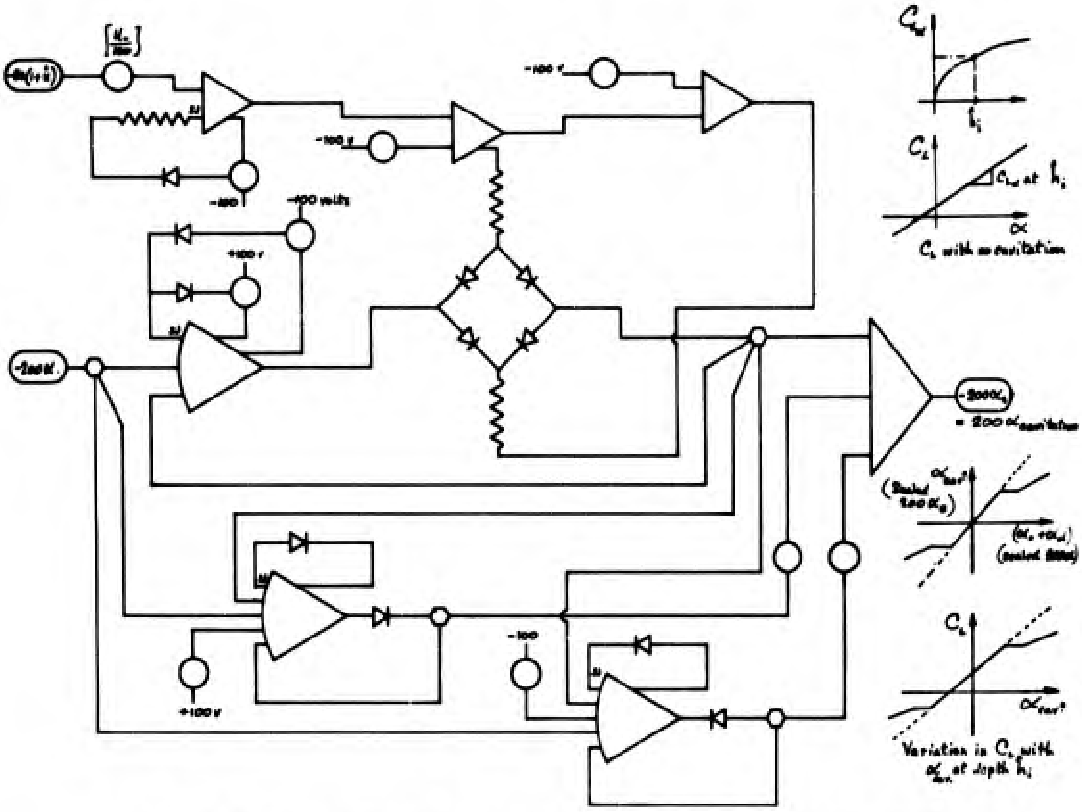

Fig. 16 - Typical circuit to simulate cavitation on a foil element

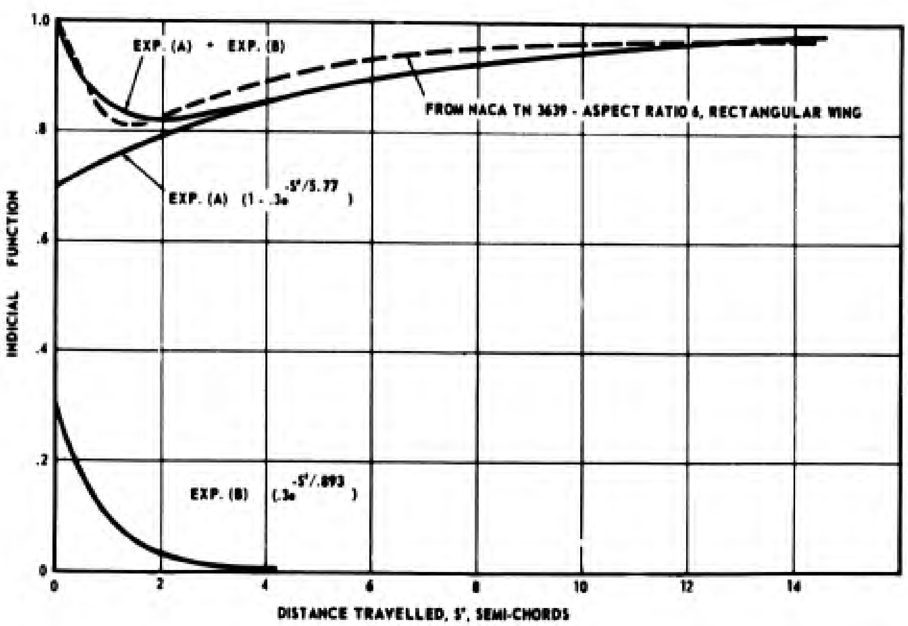

Fig. 17 - Exponential approximation to indicial function

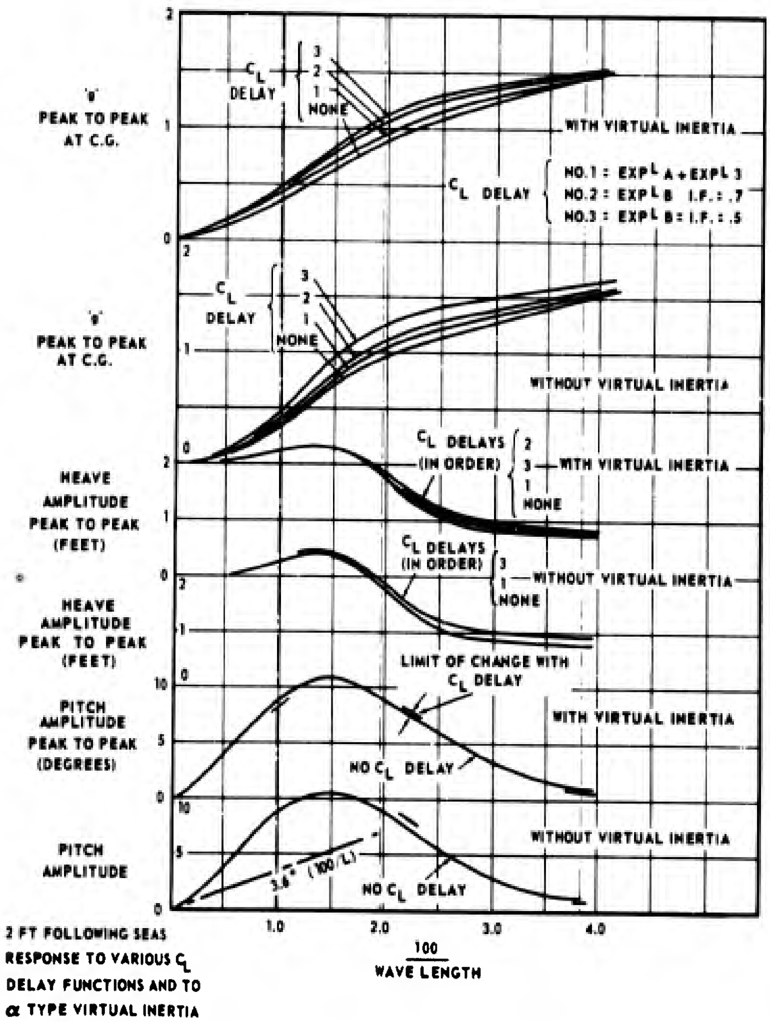

Fig. 18 - RX craft -- longitudinal heave/pitch only

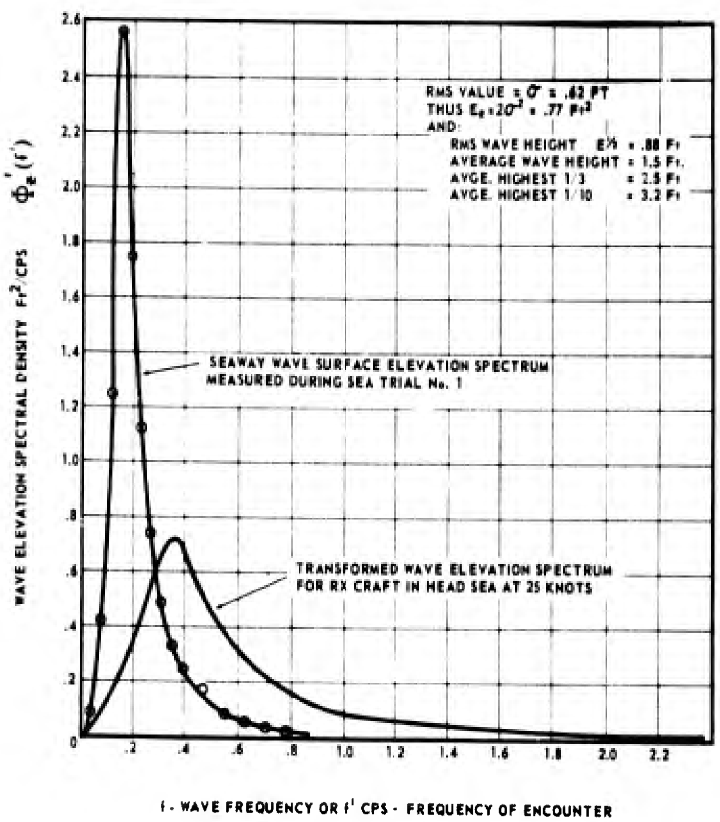

Fig. 19 - RX sea trial No. 1
wave elevation spectra

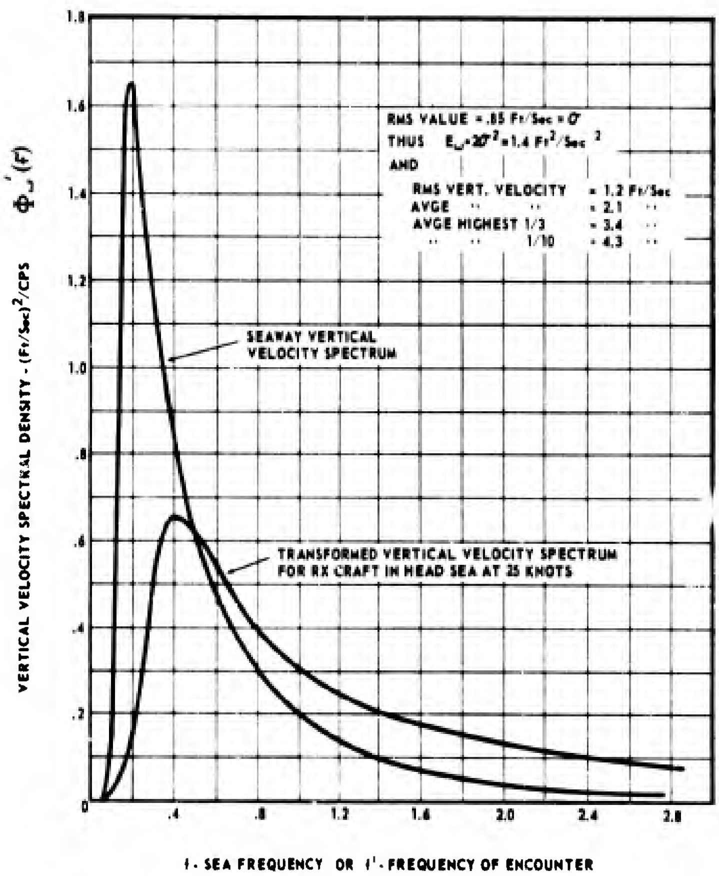

Fig. 20 - RX sea trial No. 1 vertical velocity spectra as derived from measured wave elevation spectrum

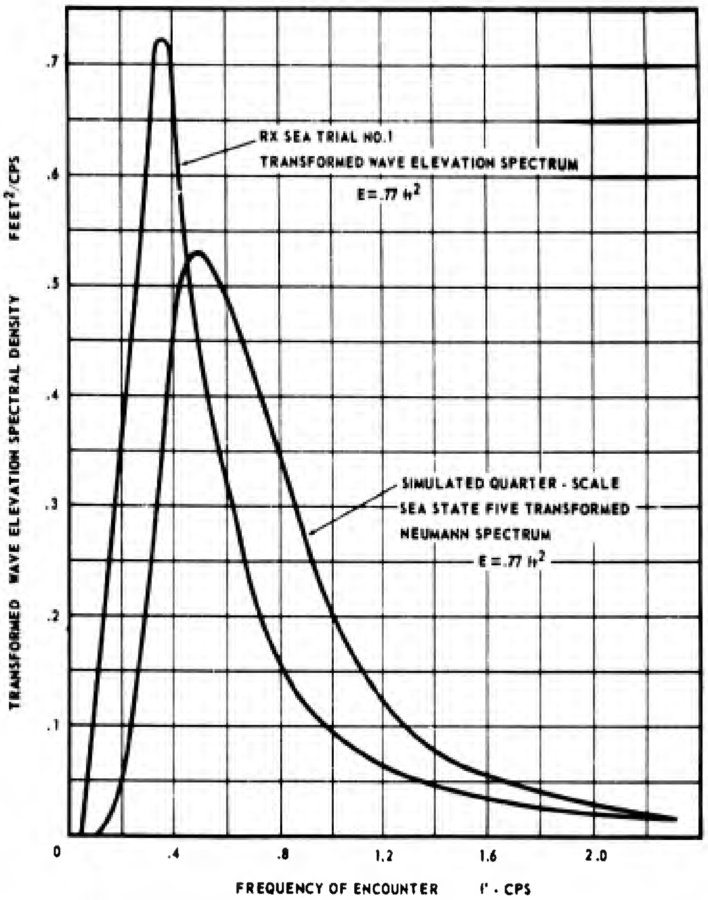

Fig. 21 - Comparison of transformed wave elevation spectra

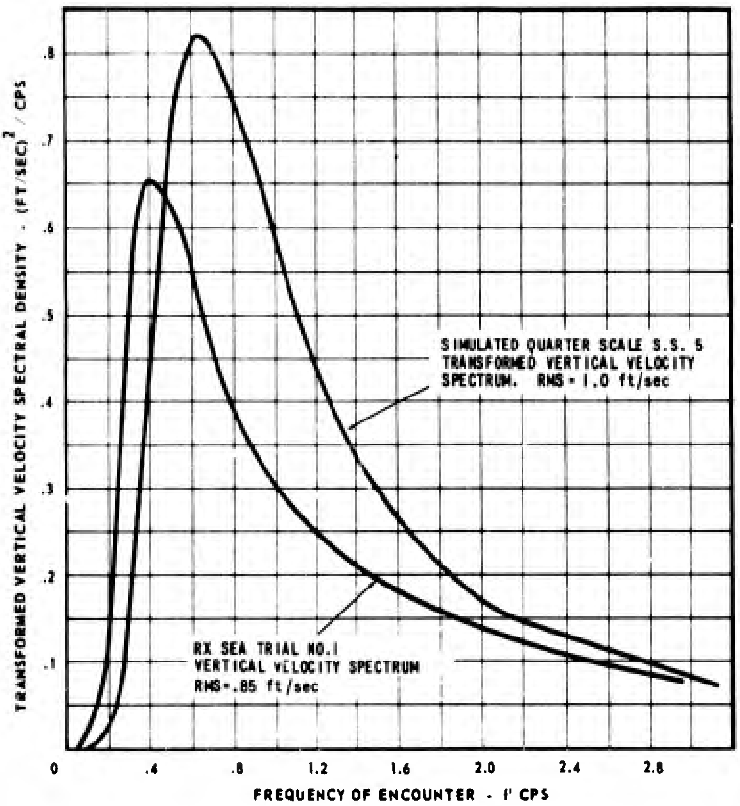

Fig. 22 - Comparison of transformed vertical velocity spectra

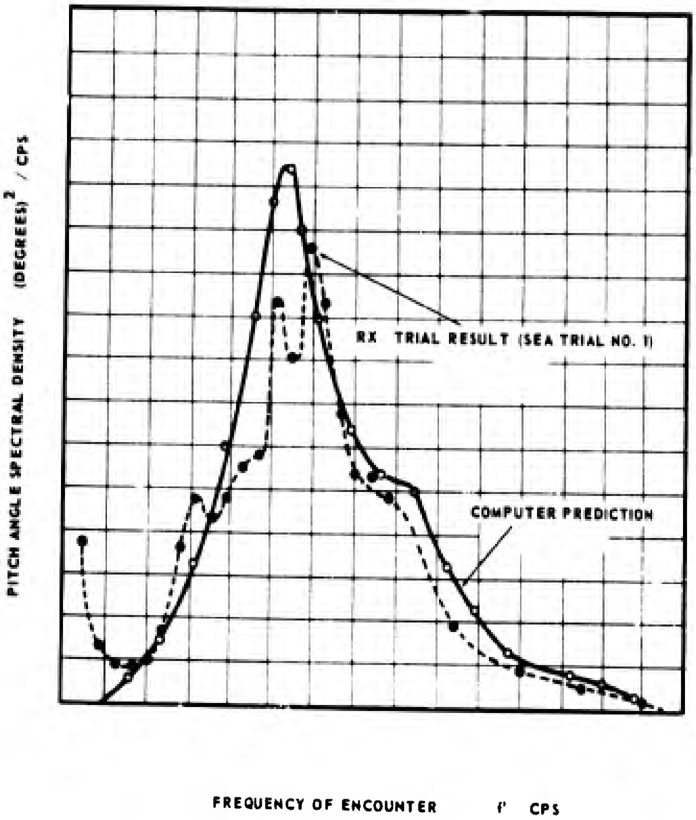

Fig. 23 - Comparison of pitch angle spectra

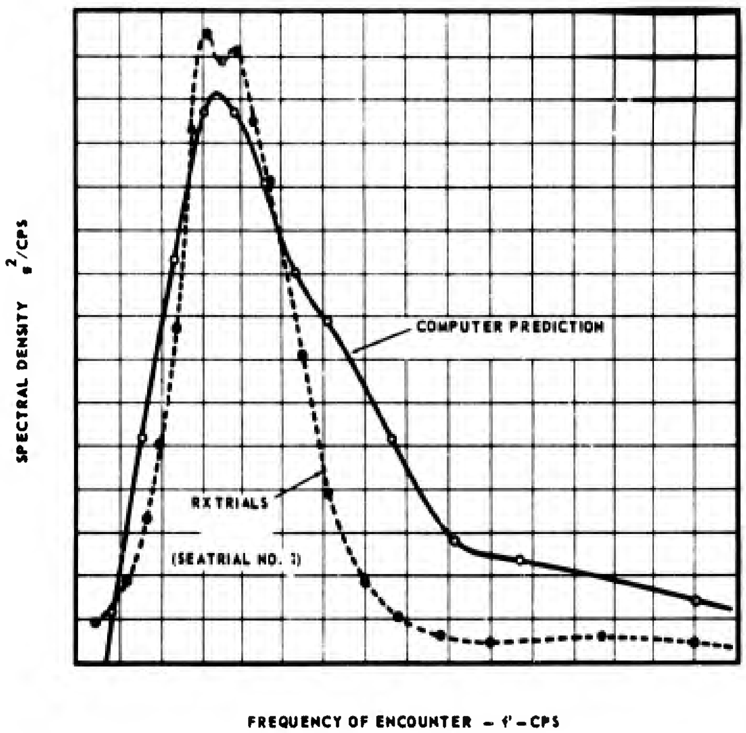

Fig. 24 - Comparison of center of gravity vertical acceleration spectra

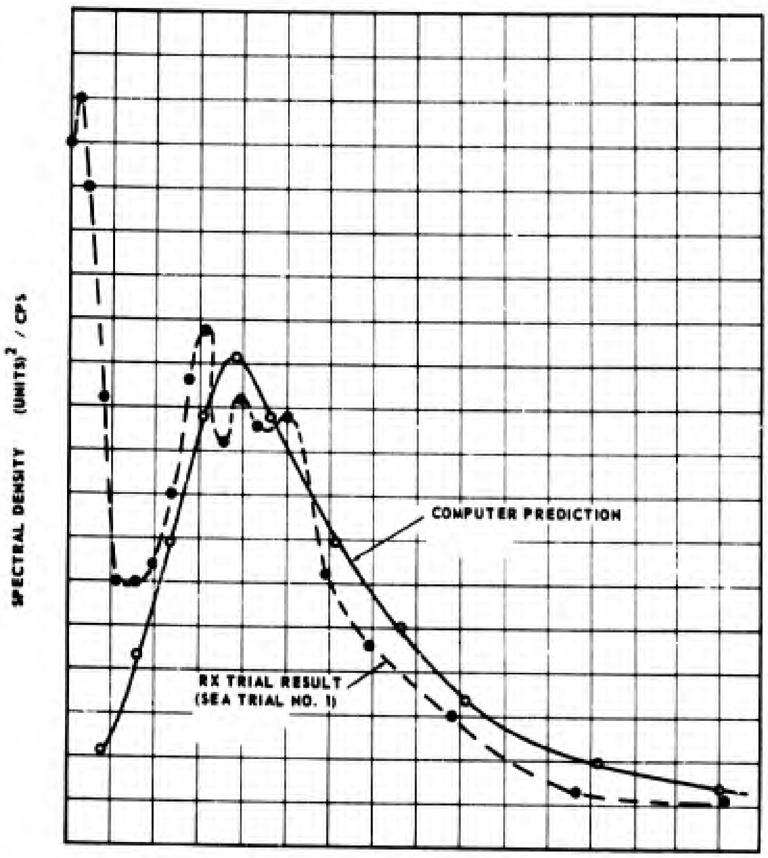

Fig. 25 - Comparison of main foil lift coefficient spectra

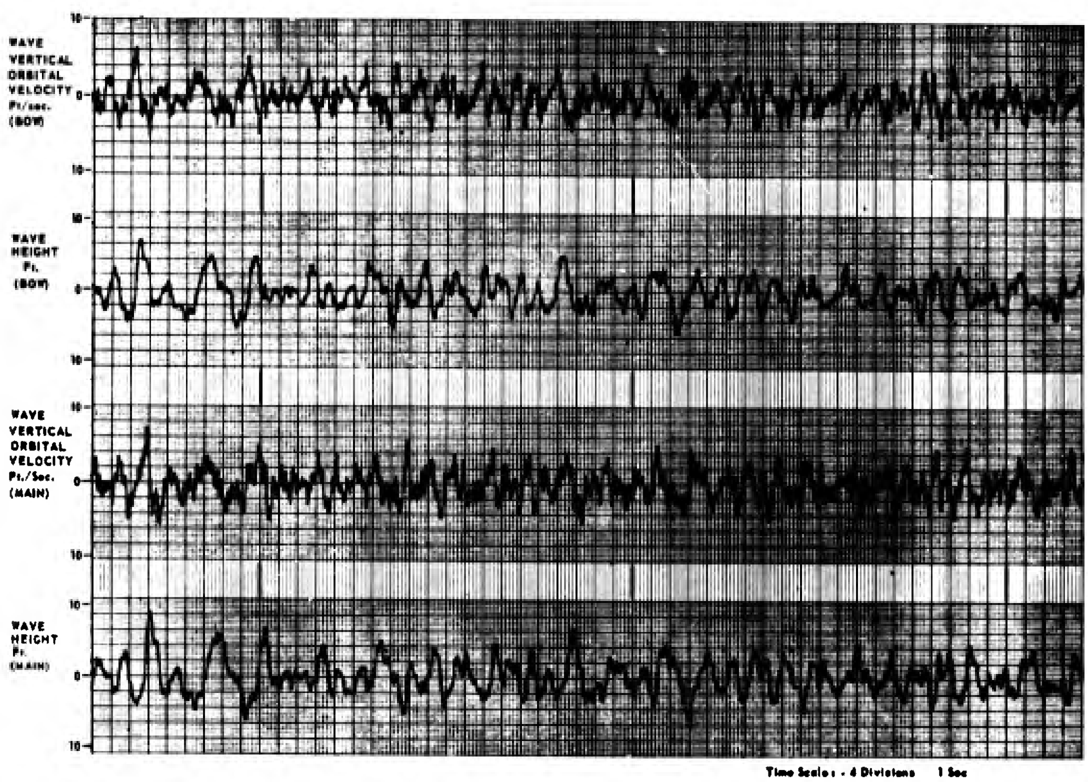

Fig. 26 - Sample computer traces: R200 at 50 knots head sea wave traces -- State 5 random sea forcing functions

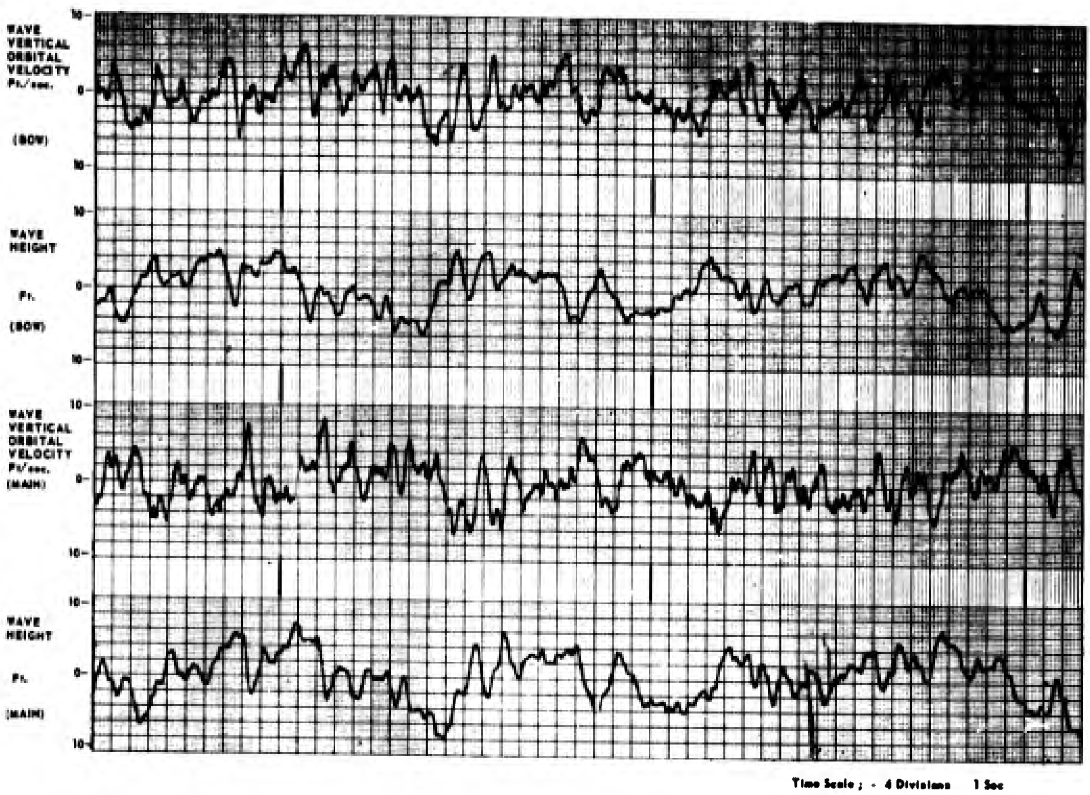

Fig. 27 - Sample computer traces: R200 at 50 knots following sea wave traces -- State 5 random sea forcing functions

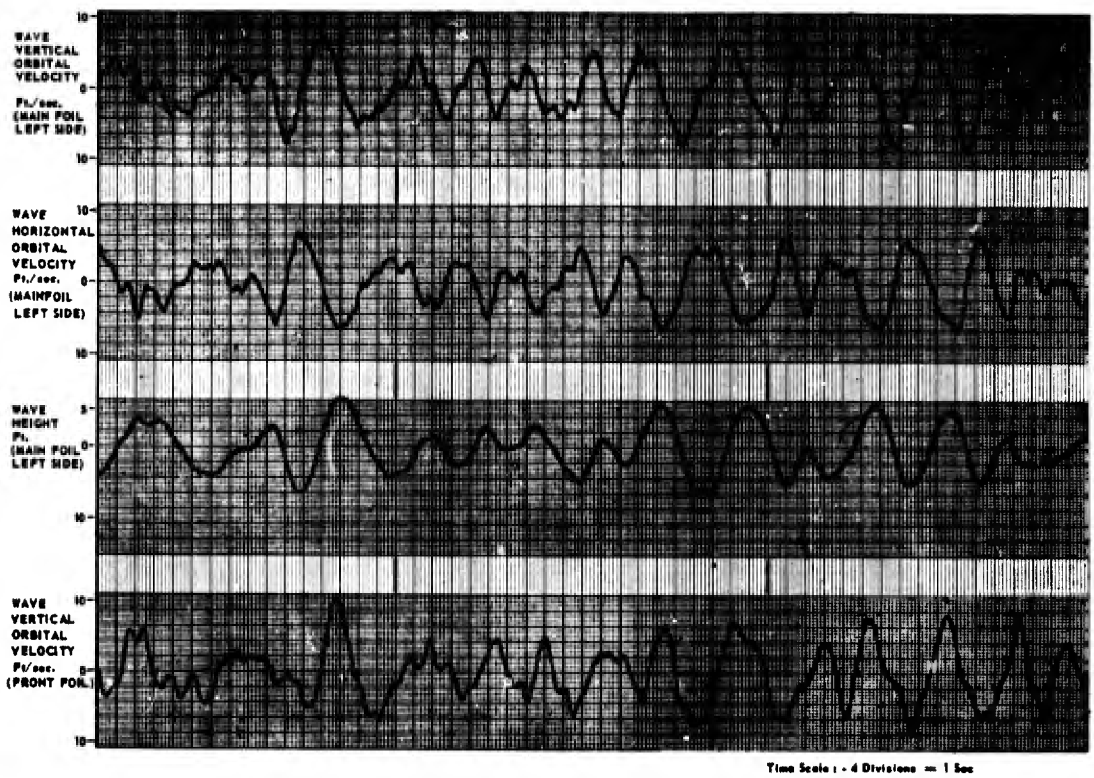

Fig. 28 - Sample computer traces: R200 at 50 knots beam sea wave traces -- State 5 random sea forcing functions

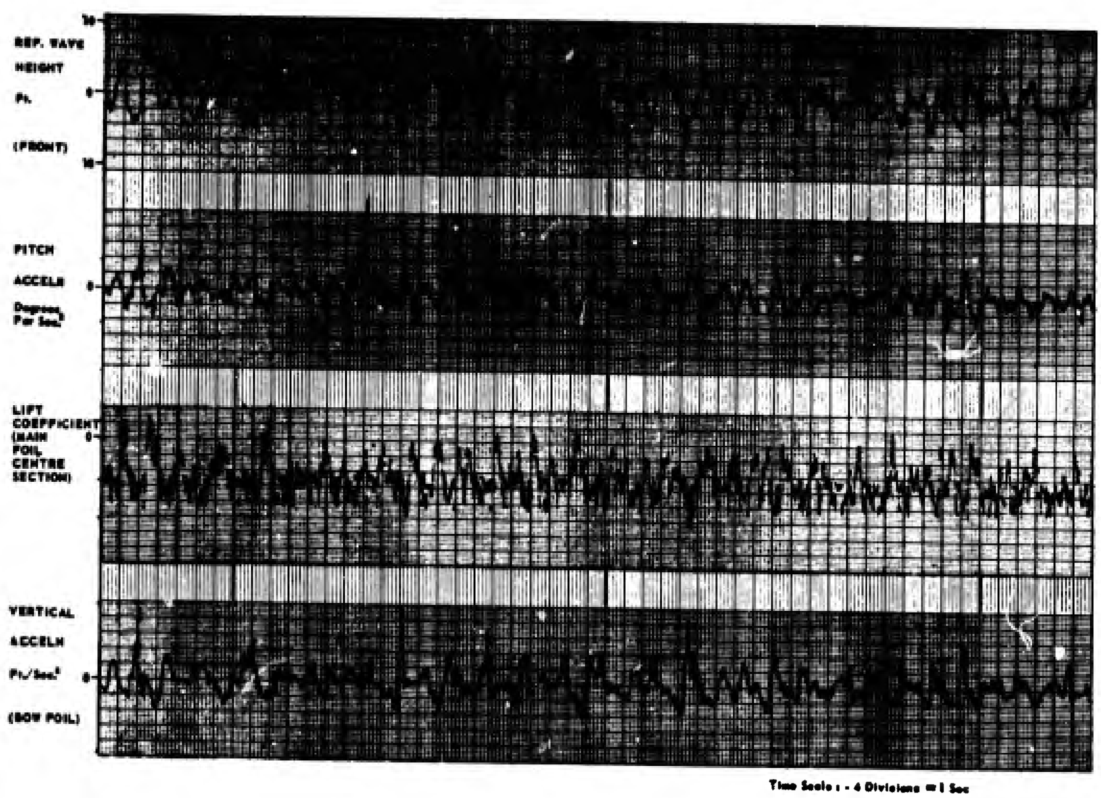

Fig. 29 - Sample computer traces: head sea — R200 response at 50 knots to a State 5 random sea

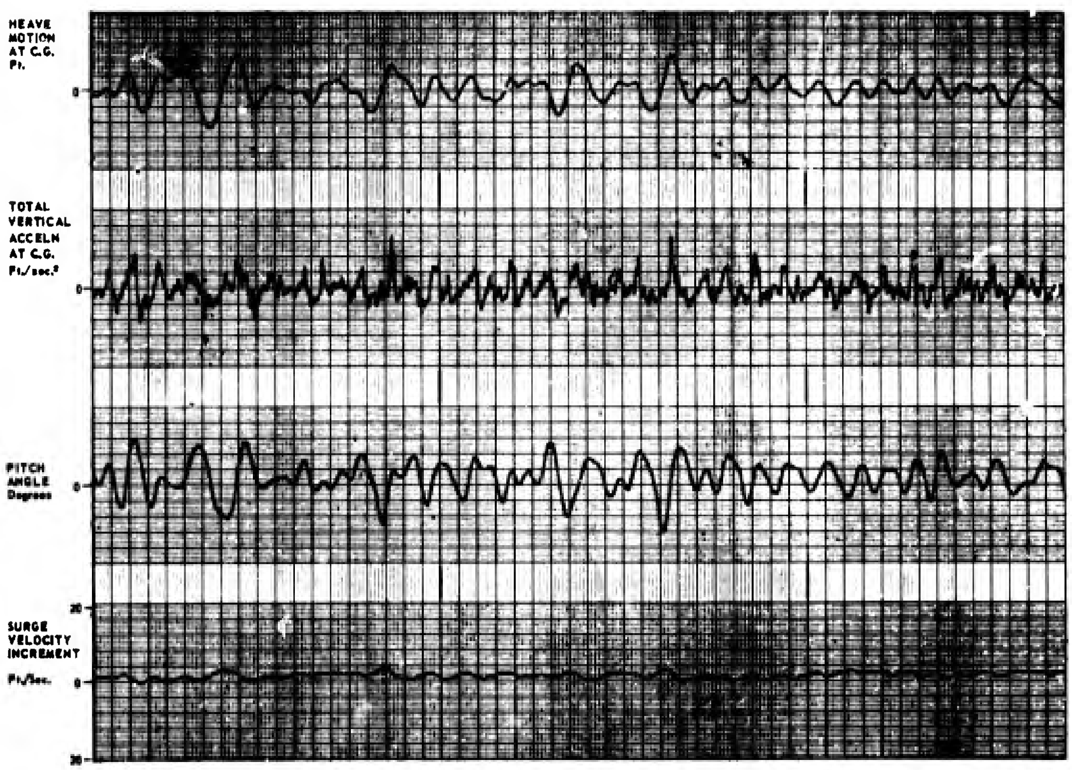

Fig. 30 - Sample computer traces: head sea -- R200 response at 50 knots to a State 5 random sea

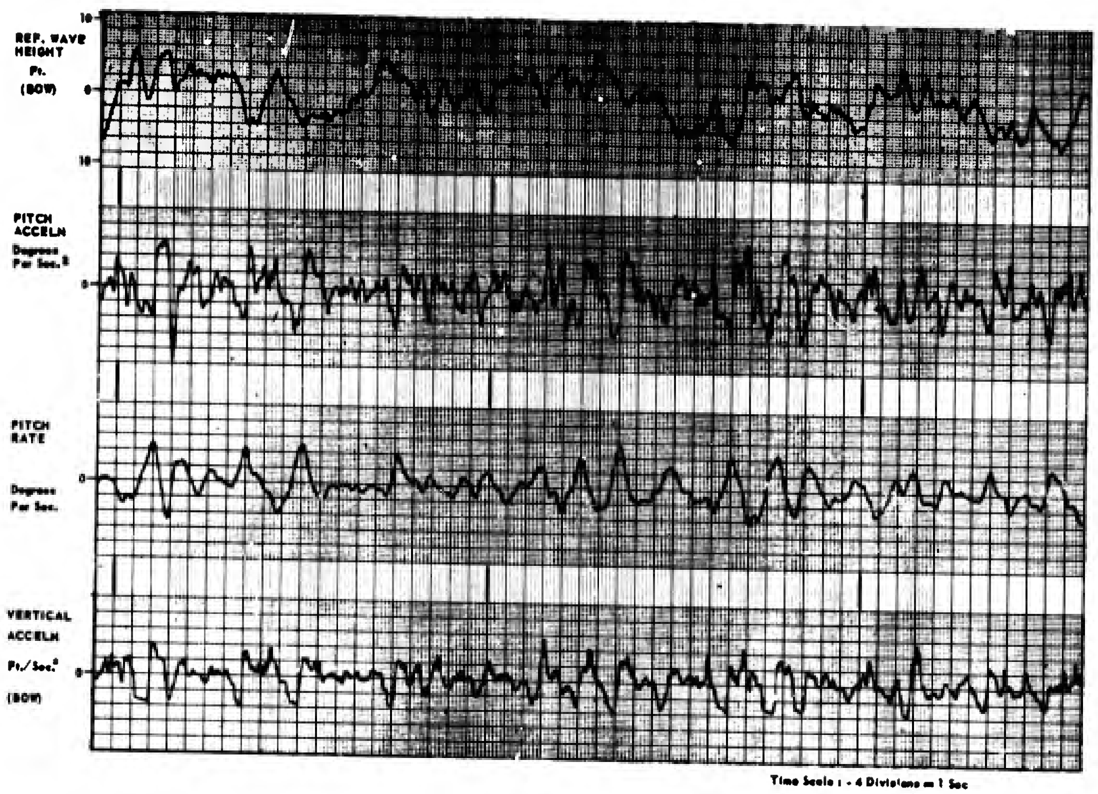

Fig. 31 - Sample computer traces: following sea -- R200 response at 50 knots to a State 5 random sea

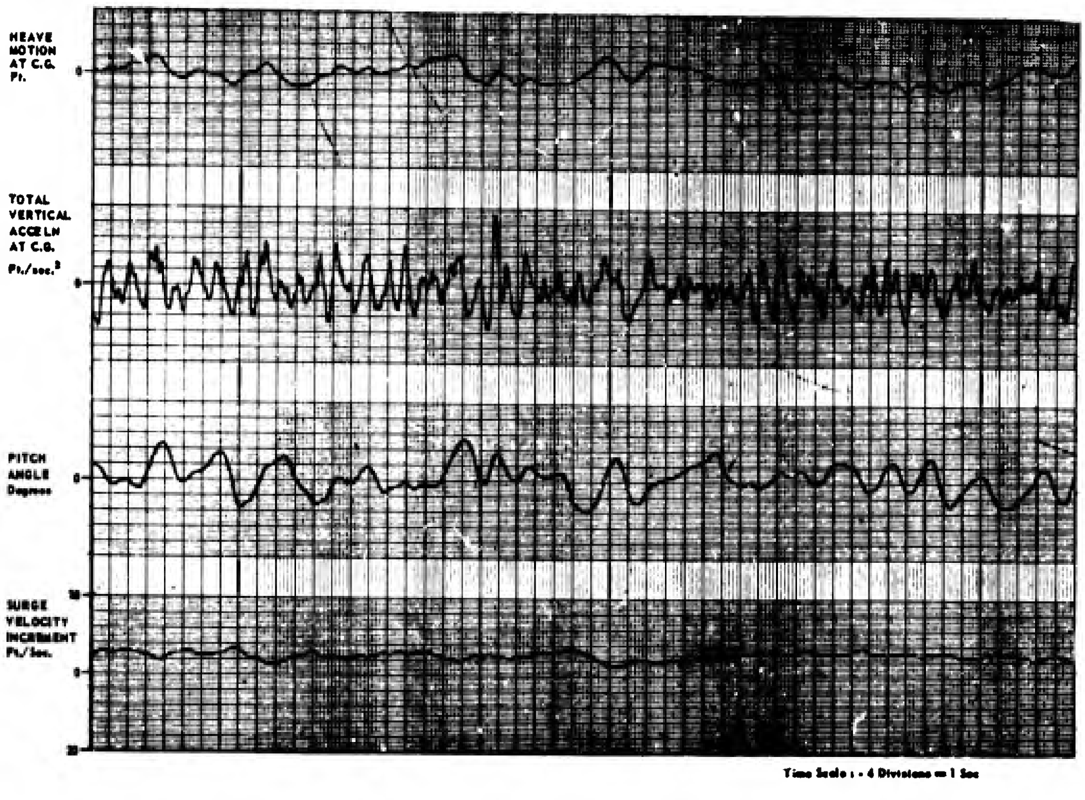

Fig. 32 - Sample computer traces: following sea -- R200 response at 50 knots to a State 5 random sea

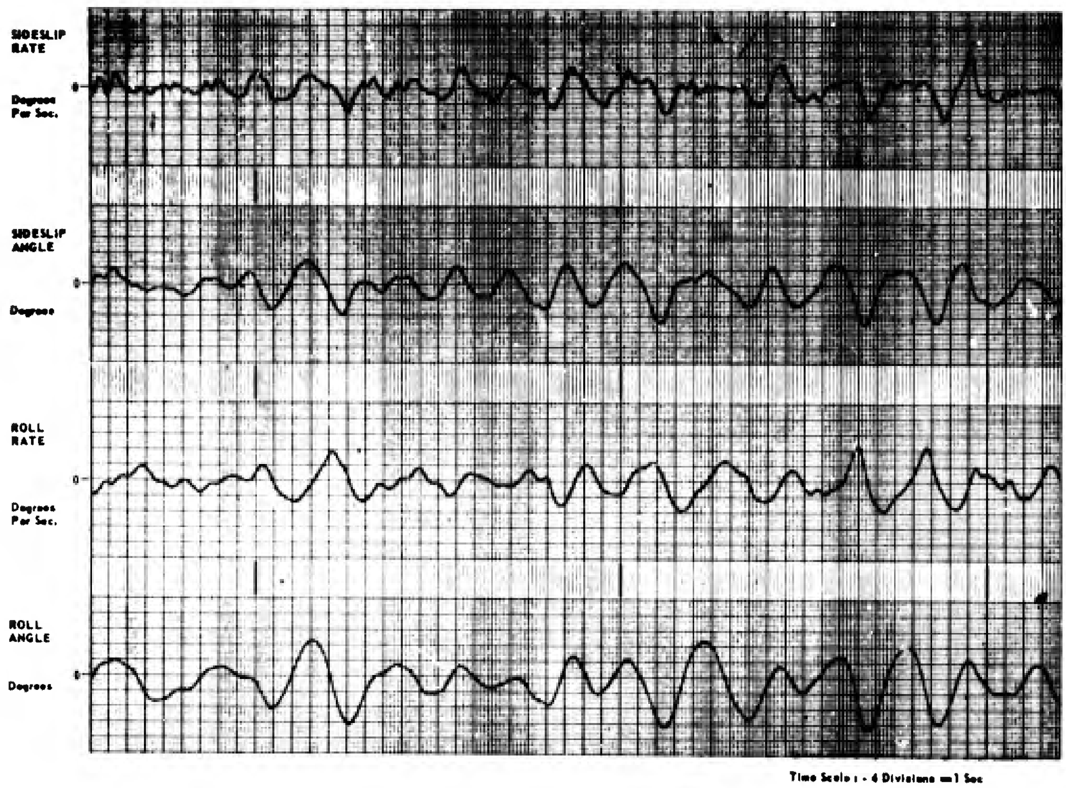

Fig. 33 - Sample computer traces: beam sea — R200 response at 50 knots to a State 5 random sea

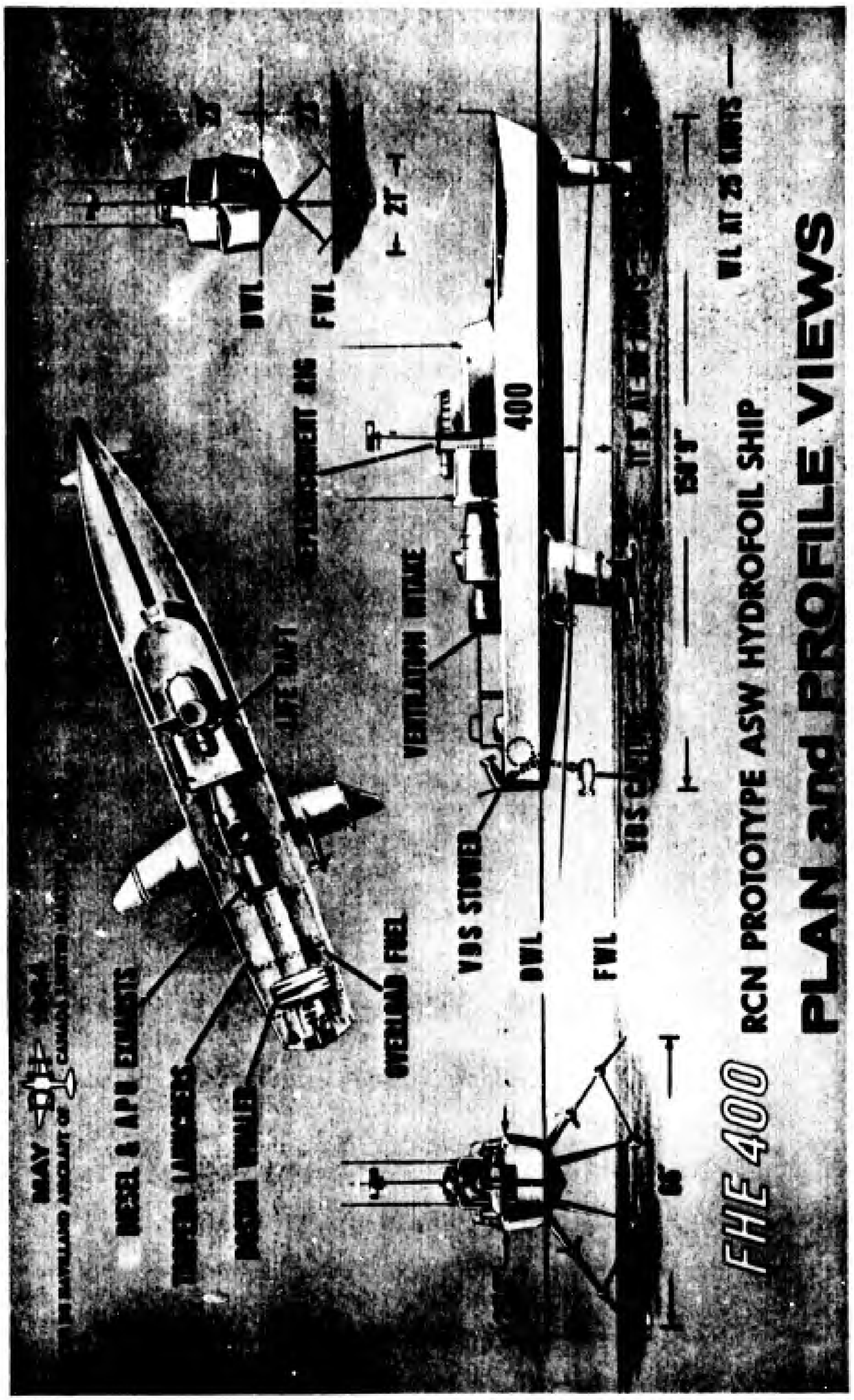

Fig. 34 - Plan and profile views

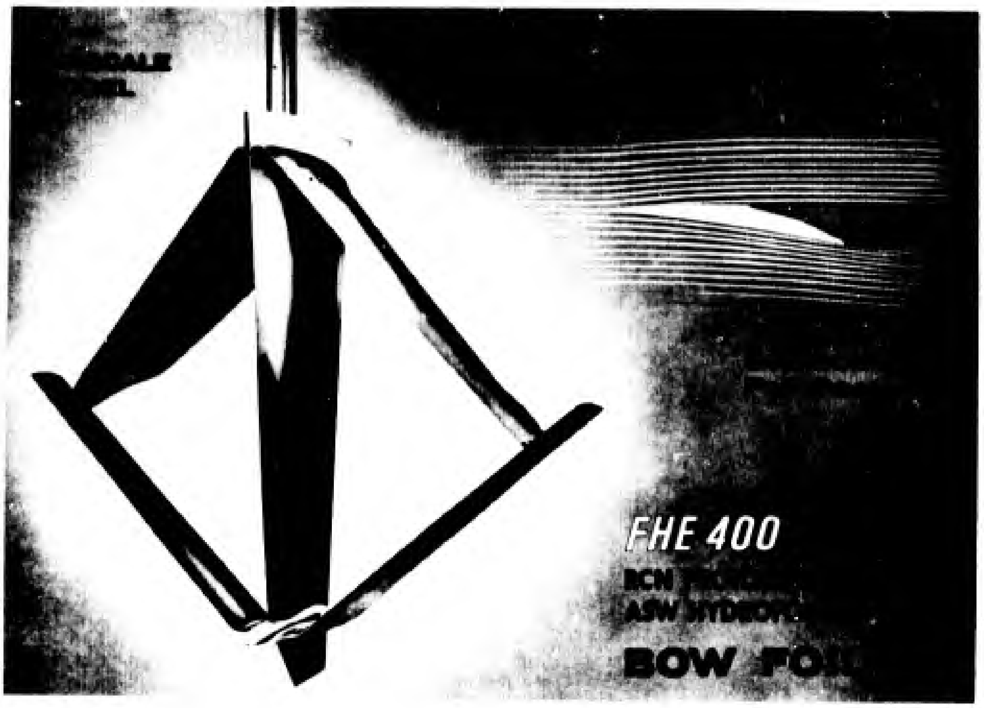

Figure 35

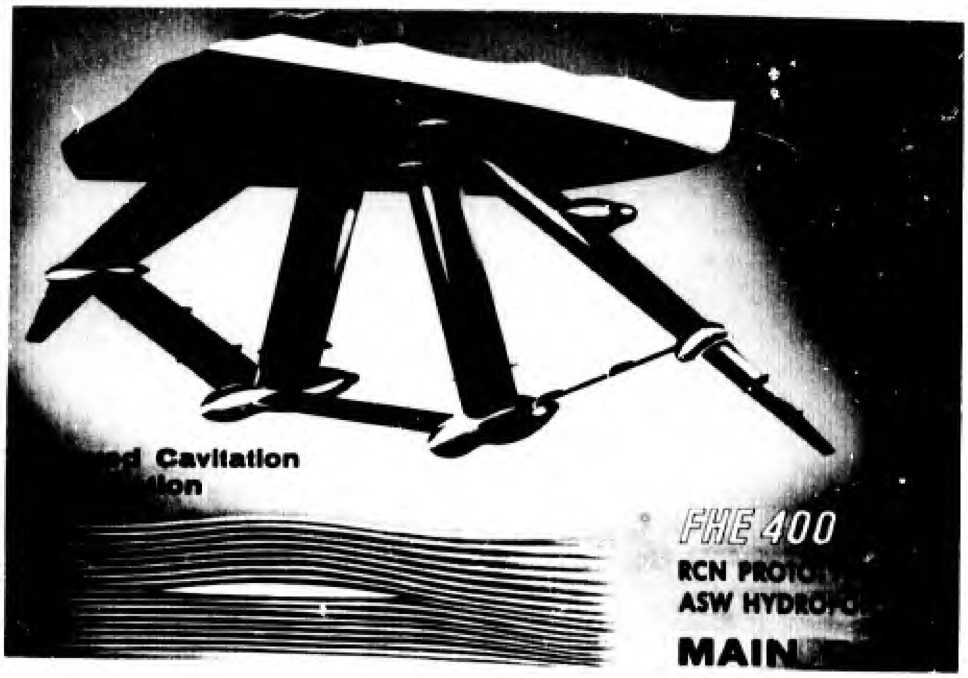

Figure 36

*   *   *

DISCUSSION

H. D. Ranzenhofer
Grumman Aircraft Engineering Corporation
Bethpage, Long Island, New York

Generally, the paper is excellent, in that it presents a full and detailed picture of De Havilland's work on the FHE-400 hydrofoil ship, in terms of the approaches used and the results obtained. The thoroughness of the work is attested to, in part, by the extensive use of both fixed and free models in the development.

The analysis in some respects, parallels that used at the Grumman Aircraft Engineering Corporation in our work in the hydrofoil field.

It is interesting to note that the authors' conclusions as to the complexity of the craft equations of motion when using the method of small perturbations are identical to ours.

Another item of significance is the use of the surge degree of freedom in the analog computer program. From the results obtained, it may be inferred that, for the foilborne cruising conditions, craft forward velocity can be assumed constant, thus eliminating the surge equation. For our work in the design and development of hydrofoil autopilots, this assumption was made. However, the surge equation is useful in studying takeoff and landing performance if hull lift and drag terms are included. A possible limiting factor here is the amount of analog equipment available; it was found in our work that the addition of the surge equation and associated terms required a 50% increase in a five degree of freedom analog program.

A point of criticism is the omission of the lift and drag equations from the discussion of the approach using forces and moments. These forces comprise the major portions of the total force and moment terms, X, Y, Z, L, M, and N in Eqs. (1) through (6) and in our opinion would be of interest to others in this area.

The frequency response charts form a valuable basis for performance comparisons with other hydrofoil craft, but only if identical wave length-to-height ratios are used for all craft, or if wave lengths are normalized to foil base or another suitable craft parameter.

* * *

DISCUSSION

A. Silverleaf
National Physics Laboratory
Teddington, England

This paper is probably the most thorough account yet available of the overall development of the design of a seagoing hydrofoil ship of unorthodox and advanced foil configuration. Among the many significant points which it raises is the clear indication that fixed surface-piercing foils may yet have an important and useful role to play in such craft in spite of many recent statements to the contrary. The authors have naturally emphasised the value of analogue computer studies in investigating the motions in a seaway of a craft of this kind. It is, of course, important to simulate correctly the performance characteristics of ventilated foils in such analogue calculations, particularly if the motions of the craft may cause ventilation to be intermittent, alternating with short periods during which the foils are either fully or partly wetted, in which case their force characteristics will be very different.

Some of the early experiments at N.P.L. with a 1/8 scale skeleton model of the complete craft, free to heave and pitch, showed that intermittent ventilation of the bow foil unit could occur in certain sea conditions. In these circumstances there were disturbing differences between the analogue computer calculations of the craft motions and those measured on the large model in the high speed towing tank at Feltham. However, when steps were taken by the authors to ensure that ventilation was continuous, the motions of the model were very considerably improved and there was then good agreement with the calculated values. This episode well illustrates the need to simulate the correct physical conditions in any computer calculations; if the hydrodynamics are incorrectly reproduced it is unlikely that useful conclusions will be obtained.

The authors have pointed out that many of the model experiments have been carried out at N.P.L.; as mentioned in Table 1 these include not only measurements to determine hydrodynamic performance but some very unusual experiments to investigate hydroelastic characteristics. All these experiments have been and are being made as one aspect of a most interesting three-part approach; analogue computer studies in Toronto, trials with a manned craft in Halifax, and model experiments at Feltham have proceeded simultaneously and in parallel. It is I think fair to say that, particularly during the early development stages, each of these three approaches identified and resolved problems which at first sight appeared more than daunting. This comprehensive and thorough attack emphasises the need for such procedures if advanced high speed marine craft are to be successfully developed.

* * *

THE BEHAVIOUR OF A GROUND EFFECT MACHINE OVER SMOOTH WATER AND OVER WAVES

W. A. Swaan and R. Wahab
Netherlands Ship Model Basin
Wageningen, Netherlands

ABSTRACT

The results of tests on the over water behaviour of a flying model of a Ground Effect Machine are given and discussed. Over smooth water the effect of a variation in water depth was investigated. Over waves the variables were the wave length, height and direction, and the rise height. The effect of side wind was also considered.

INTRODUCTION

The information presently available on the behaviour of ground effect machines over water is rather limited. See Refs. [1] through [8]. It is based on the experience gained with a few man-carrying prototypes and a number of model tests. The model experiments were in general conducted with a fixed model with the object to determine the static forces and the effect of the air cushion on the water surface.

Additional information has been obtained now with a dynamically scaled free model of the SKMR-I "Hydroskimmer" in a model basin where various wave patterns were simulated. In order to avoid telemetering problems and energy storage in the model a towing carriage was used. The maximum carriage speed in the seakeeping basin of the N.S.M.B. is about 15 ft sec^{-1}. The service speed and size of the SKMR-I is such that a very small model would be required to use this carriage for the whole prototype speed range. In view of these problems it was decided to construct a 5 ft long model of the SKMR-I with a weight of about 22 lbs. Equivalent speeds up to 35 knots could be attained with a model of this size.

The N.S.M.B. was only concerned with the model tests, which have been reported in Refs. [9] and [10], and not with the design of SKMR-I itself. In this paper some of the most characteristic data are discussed.

GENERAL CONSIDERATIONS

The model of the G.E.M. was tested in the Seakeeping Laboratory and in the Shallow Water Laboratory of the N.S.M.B.

It would have been desirable to use a model with six degrees of freedom but that requires an autopilot in order to keep the model in its track. Because of weight considerations it was decided to be content with only three degrees of freedom for the model. In terms normally used in naval architecture they are: heave, pitch and roll. This restriction is only of importance for the behaviour of the model in oblique seas.

In order to compensate for the lack of information caused by restricting some of the motions the exciting forces were measured for surge and sway together with the yawing moment.

The vehicle considered here proceeds over a free water surface, therefore the Froude number ($V/\sqrt{gL}$) must be the same for model and prototype in order to equalize the scale factors for inertia forces and gravity forces. The same rule must be applied in order to simulate the dynamic properties of the air cushion as shown by Tulin [4].

The Reynolds number is of importance in order to take into account the effect of viscosity. This has some effect on the flow around the vehicle in forward flight and for the behaviour of the jets.

The fact that this Reynolds number is different for model and prototype will not be of importance for the frictional resistance because this will be small in comparison with the total drag.

The jet flow will be highly turbulent in the actual vehicle. Because the Reynolds number of the model jets exceeds the theoretical critical value of 5500 it is justified to assume the model jets to be turbulent as well. It is therefore expected that the flow around the model will be to a large extent similar to that around the prototype.

Another aspect which had to be considered is the effect of surface tension which was clearly visible in the amount of spray generated by the jets. The surface tension will be primarily of importance for the energy needed for maintaining height. This aspect was not included in the program and therefore it is considered to be of minor importance that the Weber number necessary to ensure similarity with respect to surface tension, is not the same for model and prototype.

DESCRIPTION OF THE MODEL

The 1/14 scale model of the SKMR-I "Hydroskimmer" was made of plywood, aluminum and plastic foam in order to provide for sufficient stiffness and strength combined with light weight. A general arrangement plan of the model is given in Fig. 1.

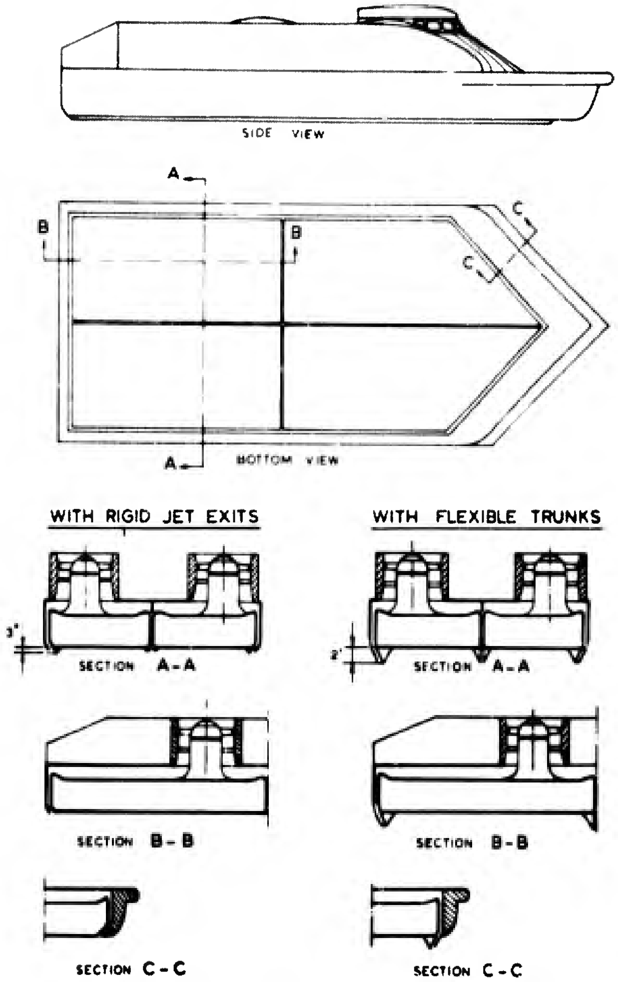

Fig. 1 - General arrangement

Table I gives some of the principal characteristics of the "SKMR-I." It was equipped with four independently controlled cushion fans, driven by synchronous electric motors. The number of revolutions of the cushion fans could be adjusted by changing the frequency of the alternating current supplied to the motors.

The cushion fans of the model were designed independently of the fans in the actual G.E.M. Therefore there is no relation at all between the numbers of revolution per unit time mentioned in this paper and the values for the actual vehicle. They should be considered as a parameter representing the power absorption.

The model was tested with two different bottom configurations. The first one had rigid jet exits, in the second one the jet exits consisted of flexible trunks. Both are illustrated in Fig. 1. The flexible trunks were manufactured of a plastic covered fabric. The shape was maintained by means of air pressure provided by the jets. Propulsion screws, nozzles and control devices were not

Table 1

	Model with Rigid Jet Exits	Model with Flexible Trunks
Length, over all	65.3 ft	65.3 ft
Length, air cushion	57.15 ft	57.15 ft
Beam	26.8 ft	26.8 ft
Air cushion area	108.7 ft	108.7 ft
Total weight	58490 lbs	62500 lbs
Centre of gravity		
above flat bottom	5.08 ft	5.50 ft
forward of centre nozzle intersection	0.53 ft	0.53 ft
Longitudinal radius of gyration	16.19 ft	17.11 ft
Longitudinal mass moment of inertia	476400	659300 ft lbs sec^2
Transverse radius of gyration	876 ft	8.92 ft
Transverse mass moment of inertia	139500 ft lbs sec^2	154600 ft lbs sec^2

simulated. The forward speed of the model was provided by the towing carriage. The connection between the model and the towing carriage consisted of an apparatus which left the model free to heave, pitch and roll. It enabled the measurement of these motions by means of potentiometers. The resistance, lateral force and yawing moment were determined by means of strain gauge balances. Model and towing apparatus are shown in Figs. 2 and 3.

During the tests the weight distribution corresponded with the conditions of the actual which is shown in Table 1.

THE TEST PROGRAM

The purpose of the investigations was to get an insight into the behaviour and the forces working on the vehicle when proceeding over smooth water of various depths and over waves. The tests conducted may be divided into the following categories.

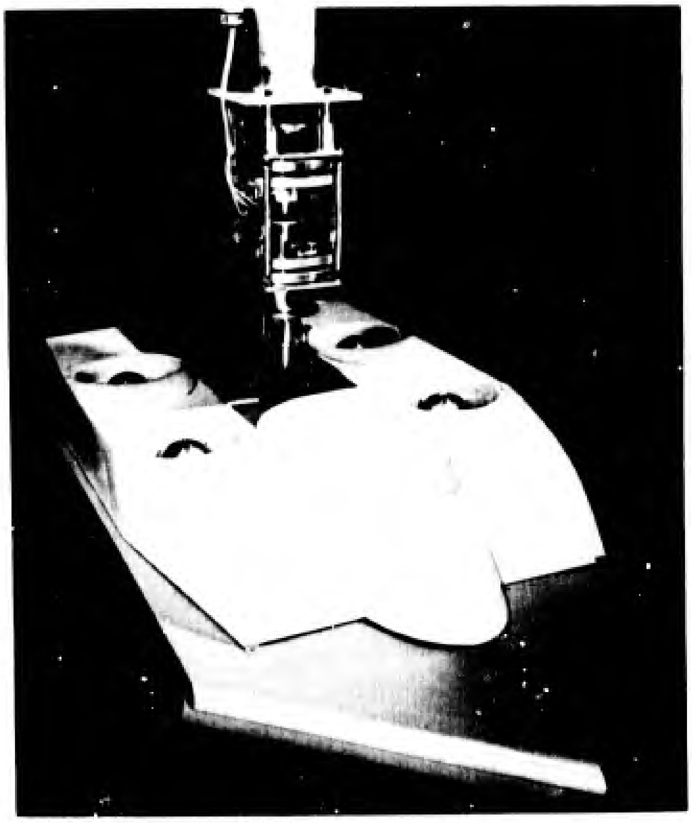

Fig. 2 - Model and towing apparatus

In the first instance the static and dynamic properties were investigated on the model hovering over smooth water and over land. For this purpose the static stability, the reactions of the model to an impulse and the relation between the rise height and the number of revolutions of the cushion fans were determined. These tests were performed both on the model with flexible trunks and with rigid jet exits. Over the water the model appeared to be liable to self-induced roll pitch and heave oscillations when fitted with rigid jet exits.

It was felt that the tendency to self-induced rolling would be inconvenient in an operational GEM.

Moreover this phenomenon could obscure the effect of oblique waves on the motions. Therefore it was tried to improve the over water hovering behaviour of the model with rigid jet exits by minor structural changes in the bottom configuration by modifying the central jet effectiveness and the directions of the side jets. The model was tested also with varied radii of gyration. None of these modifications improved the roll behaviour very much. The increment of the radius of gyration, needed for a substantial reduction of the roll amplitude, was beyond the possibilities of practical application.

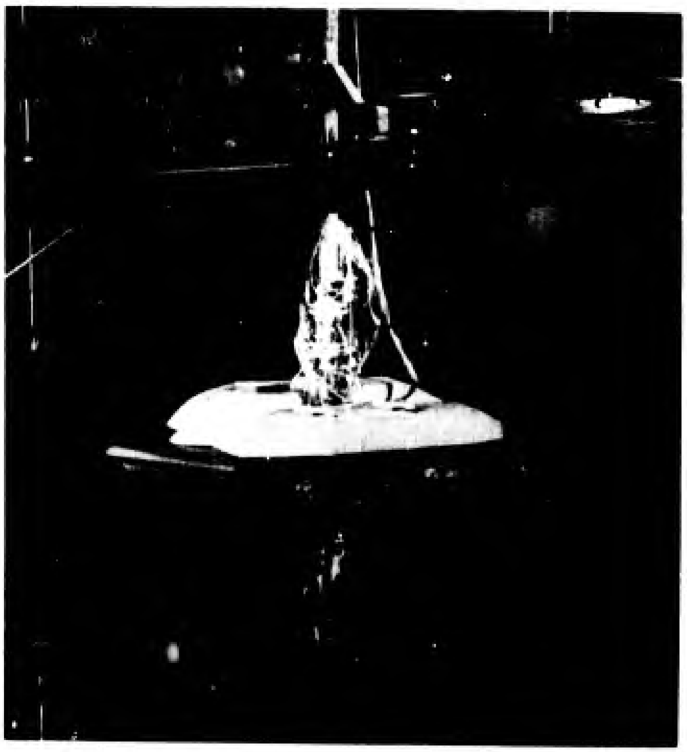

Fig. 3 - Model flying over shallow water

The tests with the model flying over smooth water were conducted with the rigid jet exits of original shape.

The model fitted with flexible trunks was liable to self-induced roll oscillations only and the amplitudes were smaller compared with the model fitted with rigid jet exits. For this reason the tests in waves were executed with flexible trunks only.

Flying over smooth water the resistance and the motions of the model were investigated as a function of the water depth.

The behaviour of the vehicle proceeding over waves was investigated on the model flying in several directions over regular deep water waves of various lengths and one height. The effect of variations in the wave height, rise height and trim was investigated for wave directions and wave lengths which appeared to be the worst for the model.

Most of the tests were conducted on the model having zero trim at zero speed, with the four cushion fans adjusted as to keep the differences between the numbers of revolutions of the fans as small as possible. In the trimmed condition the numbers of revolutions of the fore and aft cushion fans differed in order to give 1 ft difference in height between the bow and stern. The numbers of revolutions given in the diagrams are average values of the four motors, scaled up for the actual vehicle.

Finally the model was tested flying over beam seas with a 15 knots wind coming from the same direction as the waves. This wind was generated by some fans mounted on the towing carriage. The number of revolutions and the direction of these fans were adjusted in such a way that at 28 knots the resultant wind speed and direction had the correct values.

The speed range in which the vehicle was investigated was limited by the maximum speed of the towing carriages of the Seakeeping Laboratory and of the Shallow Water Laboratory. They enabled measurements up to speeds corresponding to 35 and 22 knots respectively. Unfortunately these are considerably lower than the maximum speed of the actual vehicle.

THE RECORDED DATA

The Figs. 4 through 14 are graphical representations of the most characteristic data recorded. The given values apply to the actual vehicle.

Motions, forces and moments are in general characterized by a mean value and a periodic oscillation round that mean. The periodic oscillations are shown as double amplitudes. The mean values are given as the difference with respect to the stationary condition with the cushion fans off.

In Fig. 5 the number of points determined during the hovering tests did not justify the fairing of curves. Therefore the actual test results are indicated. The curves in the other figures are the result of fairing or cross fairing. The number of points available for fairing depended on the investigated speed range. Over a speed range from 0 to 35 knots generally about 12 runs at various speeds were made. For a speed range from 20 to 35 knots about 6 points were considered to be sufficient.

In general the test results appeared to be reproducible in a satisfactory manner. However, the lateral force and yawing moment showed a rather large scatter. This was caused by torsional vibration in the towing apparatus. The natural frequencies of this instrument combined with the model were in effect not high enough for the wave experiments, especially at higher speeds.

The vertical motion of the centre of gravity is designated as heave. The mean value (rise height) over land is the distance between the ground and the flat bottom. Over water it is just the difference in height with respect to the floating condition in still water.

The mean pitch angle (trim) is considered positive with the bow down. Roll is positive when starboard side is down.

The wave direction was defined as the angle between the velocity vectors of the vehicle and the waves, positive when counterclockwise.

The motions are shown in degrees and inches. The forces are given in metric tons (2205 lbs) which are about equal to long tons (2240 lbs).

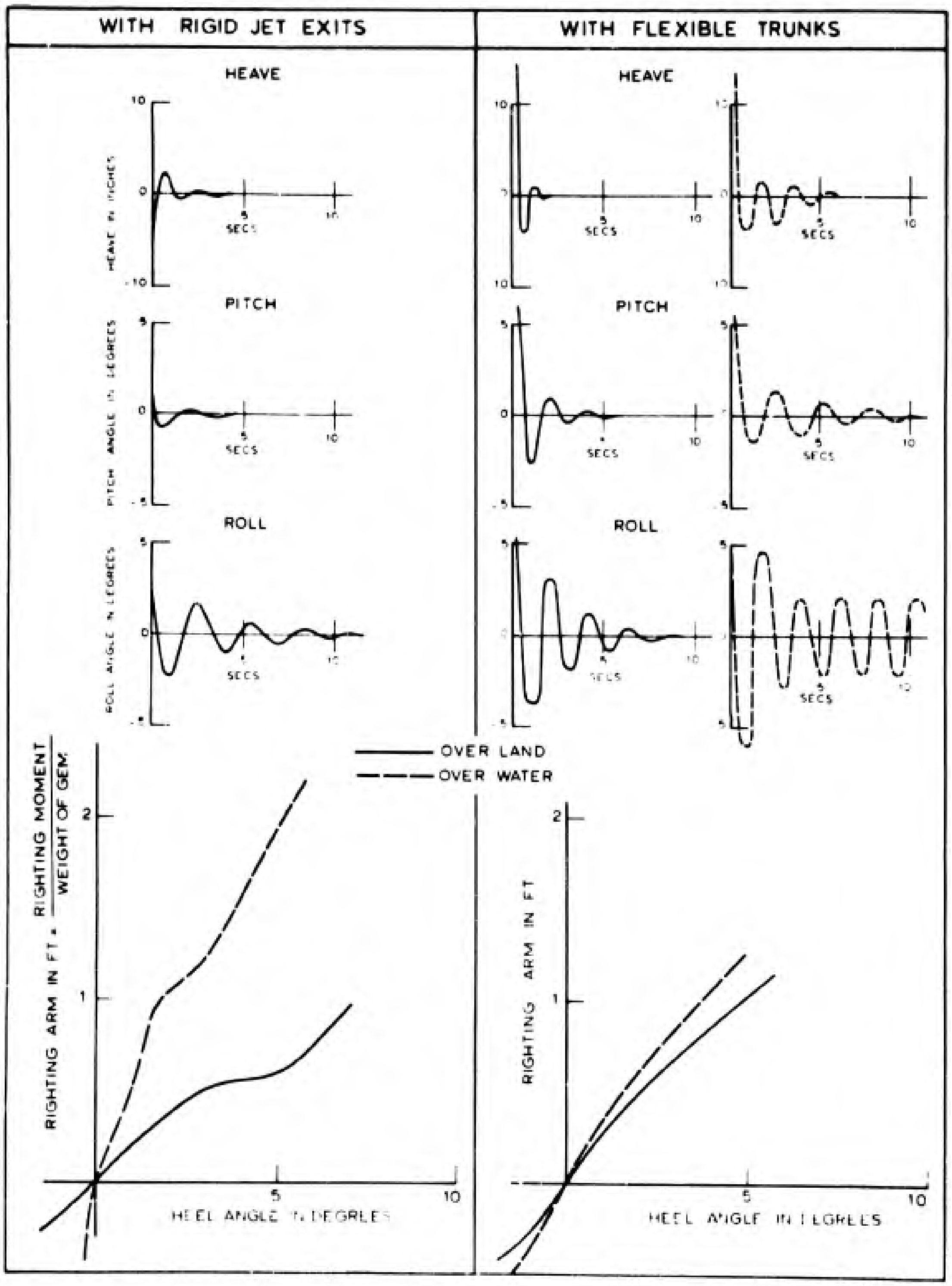

Fig. 4. Motion extinction and transverse stability curves, 2580 fan revolutions per minute

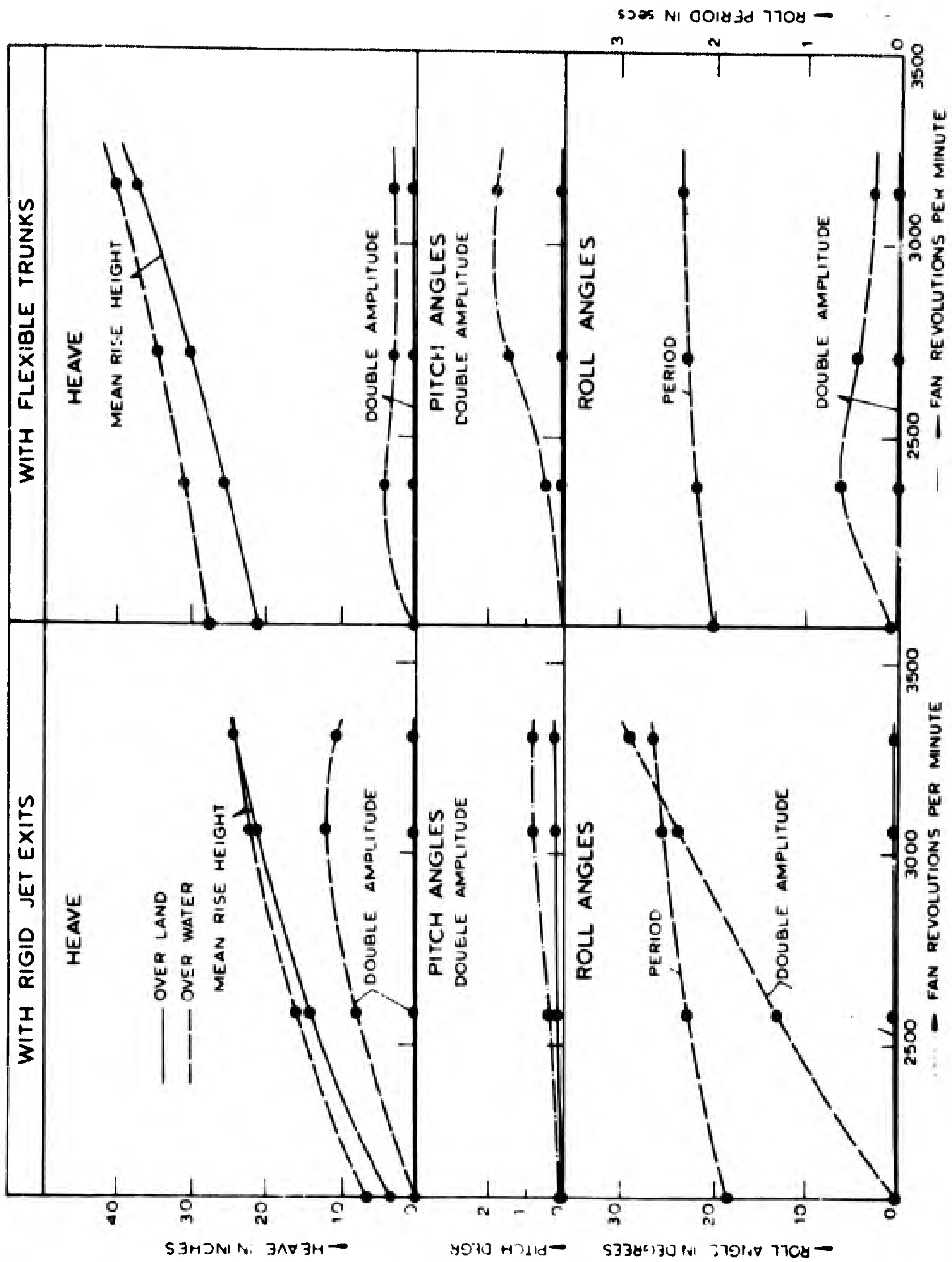

Fig. 5 - Behaviour at zero speed

Accelerations are given with the acceleration due to gravity (32.18 ft/sec^2) as unit. They were measured at the bow and stern of the model, in the longitudinal plane of symmetry.

The resistance over waves was only determined as an average value.

HOVERING PERFORMANCE

When hovering over land the model provided with flexible trunks or rigid jet exits was stable in pitch, roll and heave. The motion extinction curves are given in Fig. 4. Because of the rapid extinction it is difficult to draw definite conclusions. However, the results indicate that the heave and pitch motions were well damped. The roll damping may be qualified as fair.

Over water, the hovering behaviour of the model provided with rigid jet exits was characterized by a sustained roll and heave oscillation, apparently caused by a dynamic unstability. The rolling developed fairly slowly. It took about two cycles to double the amplitude. The model appeared also to be dynamically unstable in pitch, but to a less degree than in roll.

The most remarkable phenomenon found during the tests was that the model with rigid jet exits had two modes of motion, one of which always prevailed. Which of the two dominated during a test depended partly on the initial disturbances to which the model was subjected. The model might roll considerably while pitching slightly or it might pitch considerably while rolling was only moderate. At the lower hovering heights the model showed a preference for the mode of motion in which rolling was dominant. The Figures refer to this condition. The behaviour described here is illustrated in Fig. 5.

It was found that if the centre of gravity of the model was fixed at the same mean rise height which the model had when it was free to heave, the roll motion remained. This gave rise to the supposition that the origin of the roll motion could be explained by considering the uncoupled equation of motion. When the roll angle is indicated by φ, this equation is:

$$M\ddot{\varphi} + N\dot{\varphi} + B\varphi = 0 .$$

Because the roll damping was not too large, the roll period may be approximated by $2\pi\sqrt{M\ B}$.

The coefficient B is a measure for the static stability. The measurements indicate that the value of B is larger for the vehicle hovering over water than over land. This is in contradiction with the experiences of Kuhn, Carter and Schade [5]. The natural roll periods over land and over water were almost equal. This leads to the conclusion that the virtual moment of inertia if the model hovering over water was larger than hovering over land, which is acceptable.

The origin of the roll motion could possibly be explained by a non-linearity in the damping coefficient N, caused by the presence of the free water surface under the air cushion. A complete investigation into the cause of the dynamical unstability would require the execution of forced roll and heave experiments over a range of frequencies and using various base pressures. Such an investigation was not included in the present research.

When fitted with flexible trunks the model in the over water hovering condition only suffered from self-induced roll oscillations, with amplitudes smaller than when the jet exits were rigid. The heave and pitch damping seem to have increased also, in spite of the enlargement of the air cushion by means of flexible trunks.

Comparison of the extinction curves over land and over water learns that the heave and pitch damping is larger over land than over water. The natural periods of these motions were smaller over land.

FLYING BEHAVIOUR OVER SMOOTH WATER AND OVER LAND

The behaviour of the model with both rigid jet exits and flexible trunks was quite satisfactory over land. It was dynamically stable in roll, pitch and heave. It skimmed smoothly over the ground with no appreciable change of trim at speeds up to 20 knots.

Flying over smooth deep water, rolling decayed with increasing speed. The motion returned above the hump speed and it decayed again with further increase of the forward speed. In shallow water the picture was the same. This behaviour is shown in the Figs. 6 through 9.

The resistance curves had their highest hump at speeds between 10 and 12 knots, corresponding with Froude numbers between 0.40 and 0.45. These are speeds for which also the highest specific wave resistances of ship hulls are found. Apparently the water depth did not largely affect the speed where the resistance showed the highest hump. It affected primarily only the height of the hump.

BEHAVIOUR OF THE MODEL PROCEEDING OVER REGULAR WAVES

The natural periods of the pitch, heave and roll motions at zero speed lie between 1.8 and 2.5 seconds. It is reasonable to assume that these quantities do not change much with increasing speed. So the speed range and simulated wavelengths assure that in many cases the period of encounter was equal to the natural period.

Figure 10 shows only slight humps in the curves of the pitch and heave amplitudes. This indicates that these motions were well damped. The curves of the roll amplitude have a hump at the speed for which the period of encounter is expected to be about equal to the natural period. This picture of the dynamic properties is in accordance with that obtained from the motion extinction curves of the model hovering over smooth water. In these conditions the motions are

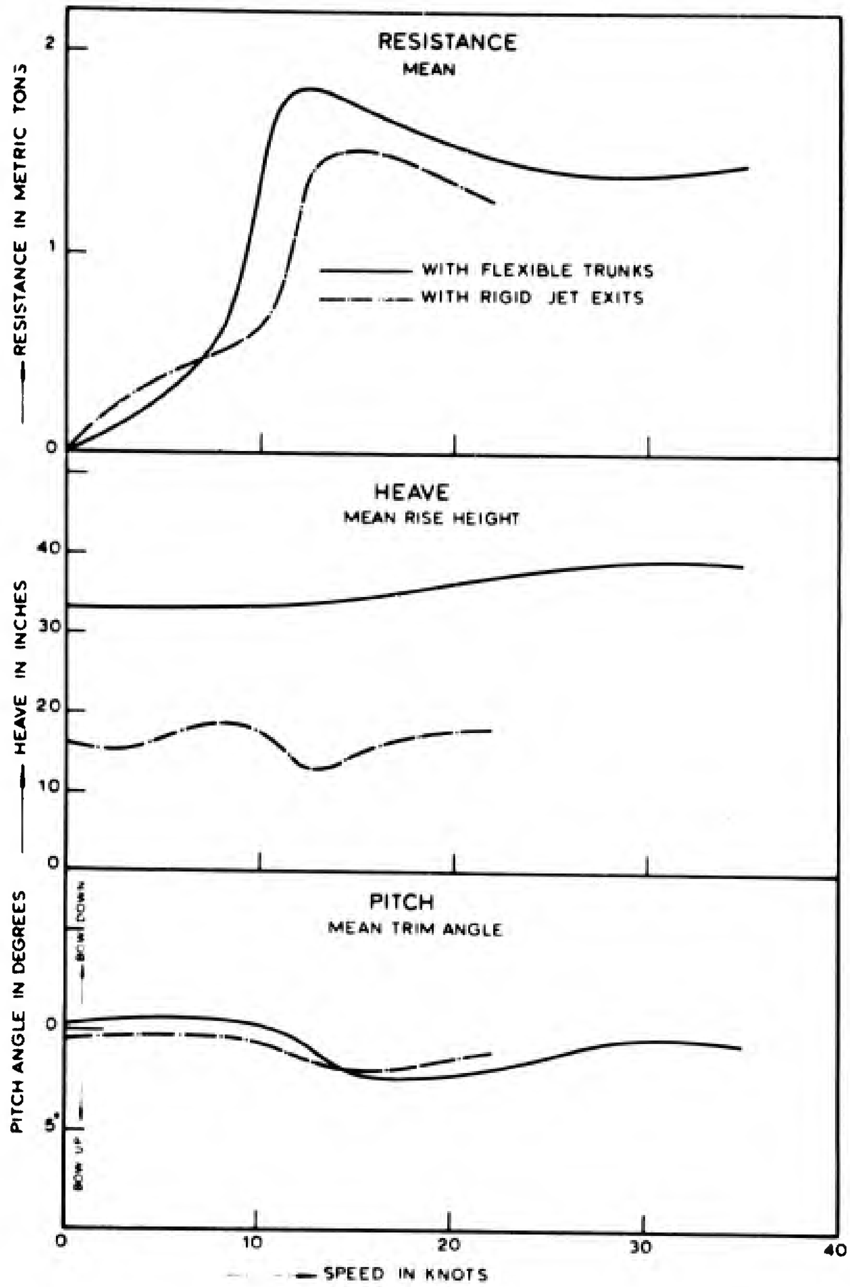

Fig. 6 - Flying behaviour in smooth deep water, 2580 fan revolutions per minute

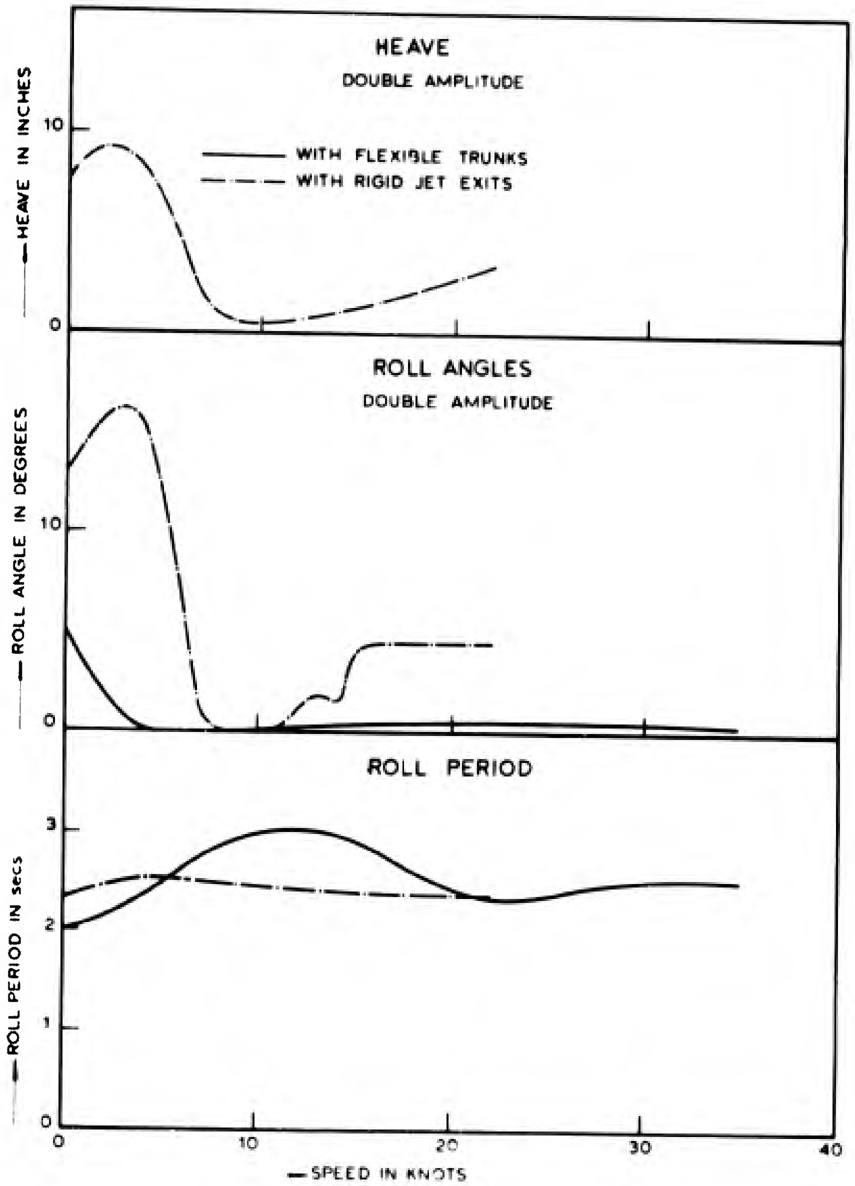

Fig. 7 - Flying behaviour in smooth deep water, 2580 fan revolutions per minute

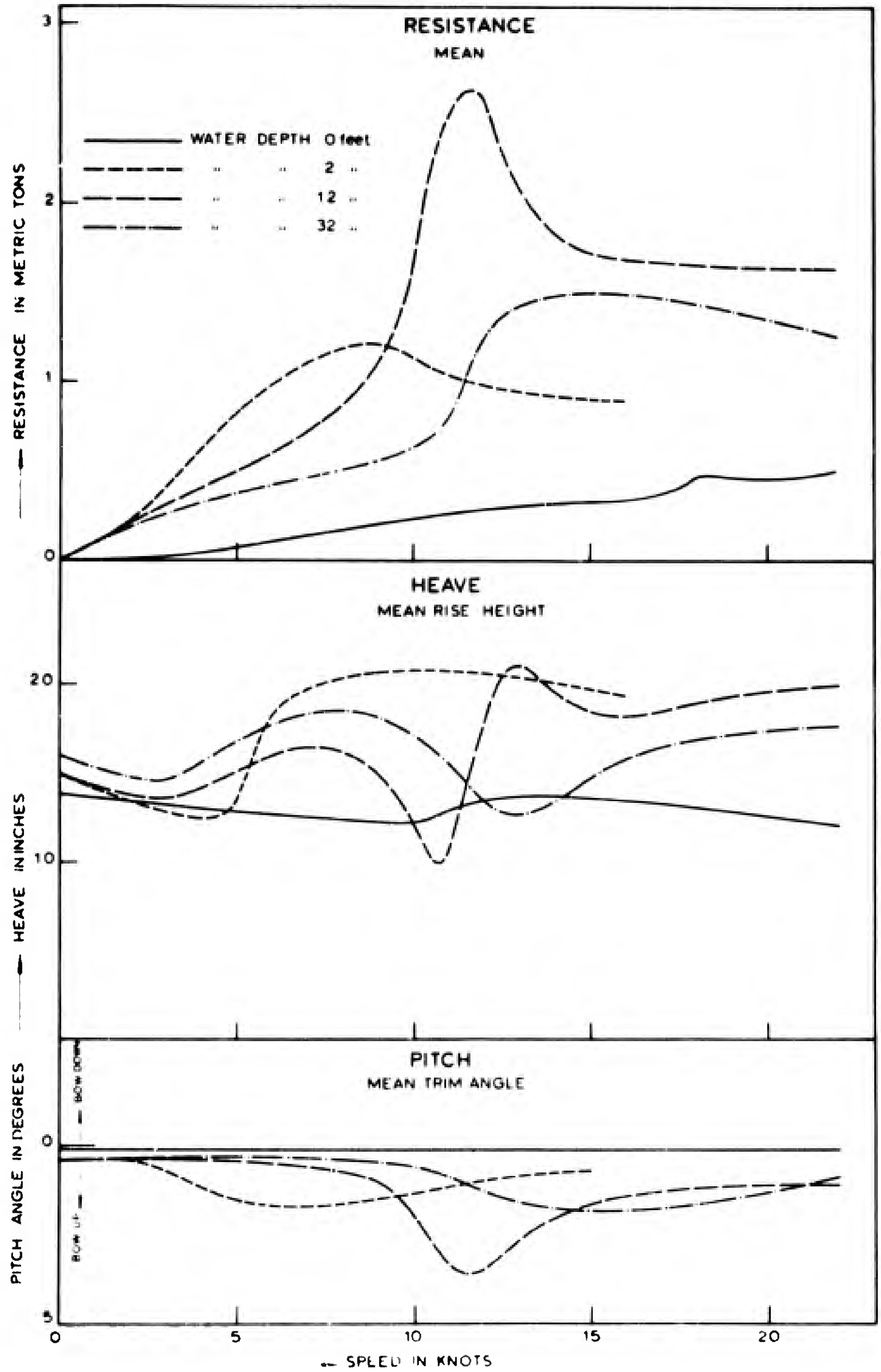

Fig. 8 - Flying behaviour over land and in smooth shallow water, 2580 fan revolutions per minute

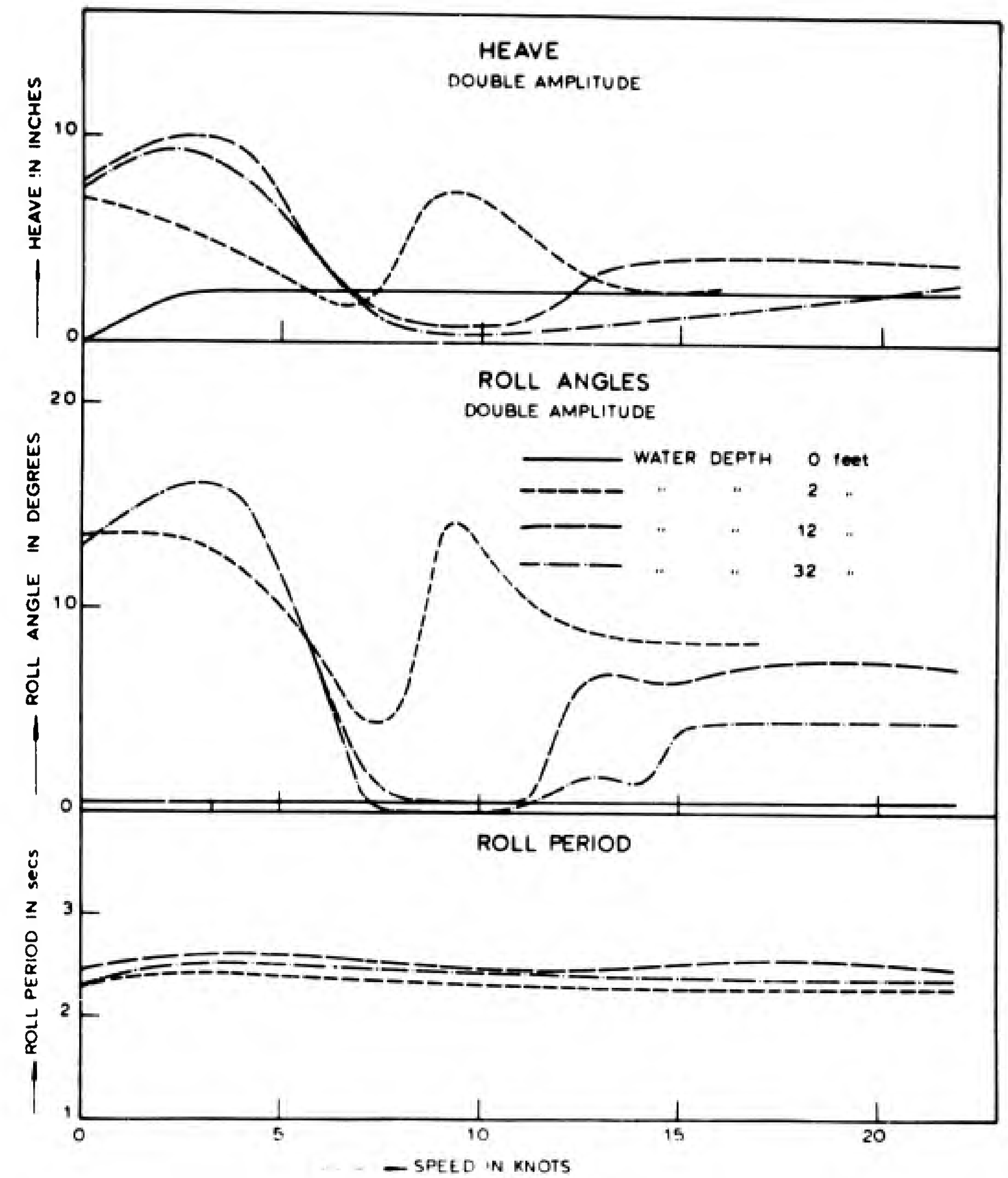

Fig. 9 - Flying behaviour over land and in smooth shallow water, 2580 fan revolutions per minute

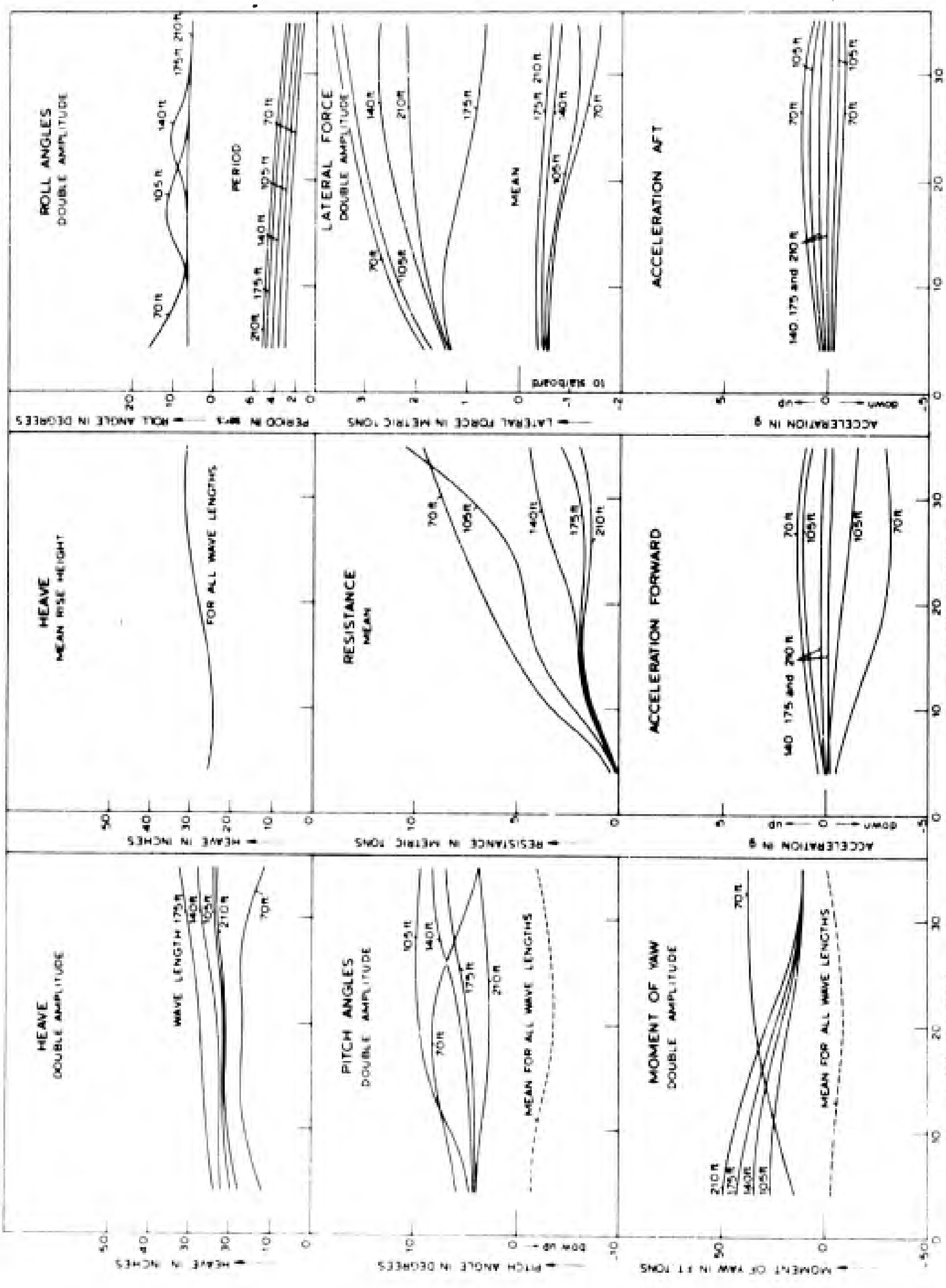

Fig. 10 - Behaviour in regular waves, wave direction 135° (bow sea), wave height 2 feet, 2580 fan revolutions per minute

to a large extent proportional to the exciting force and moment for heave and pitch respectively. So the largest pitch amplitudes were expected in waves of about the air cushion length. The experiments showed that the largest amplitudes occurred when the waves were slightly longer.

With regard to the wave direction, it was found that pitch, resistance and accelerations were the largest in head seas as appears from Fig. 11. Conceivably, the roll motion, lateral force and yawing moment were maximum in beam seas. The worst condition for the model appeared therefore to be a bow sea

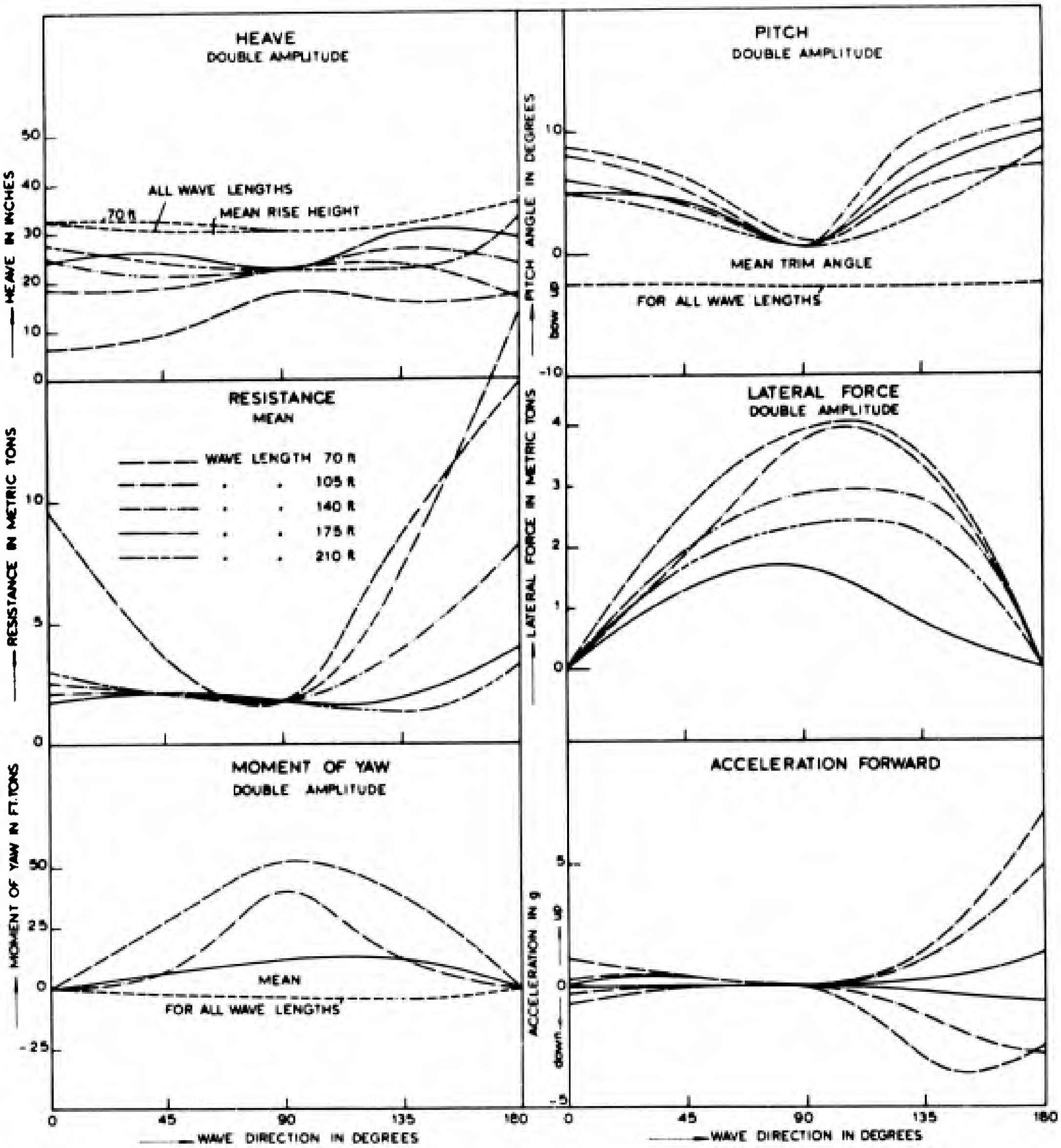

Fig. 11 - Effect of wave direction at 30 knots, wave height 2 feet, 2580 fan revolutions per minute

because the resistance and vertical motions were still considerable while combined with the lateral force and yawing moment occurring in oblique seas.

The effect of a variation in wave height is shown in Fig. 12. It indicates that an increment of the wave height increased the motion amplitudes and resistance about proportionally. At higher speeds, however, the amplitudes of the lateral force, yawing moment and accelerations forward increased more than proportionally. The accelerations aft were hardly affected by the wave height. The effect of the wave height on the mean values of the lateral force and yawing moment was small in comparison with that on the amplitudes. For small differences the rise height increased with increasing wave height. If the increments exceeded a certain value the rise height remained constant.

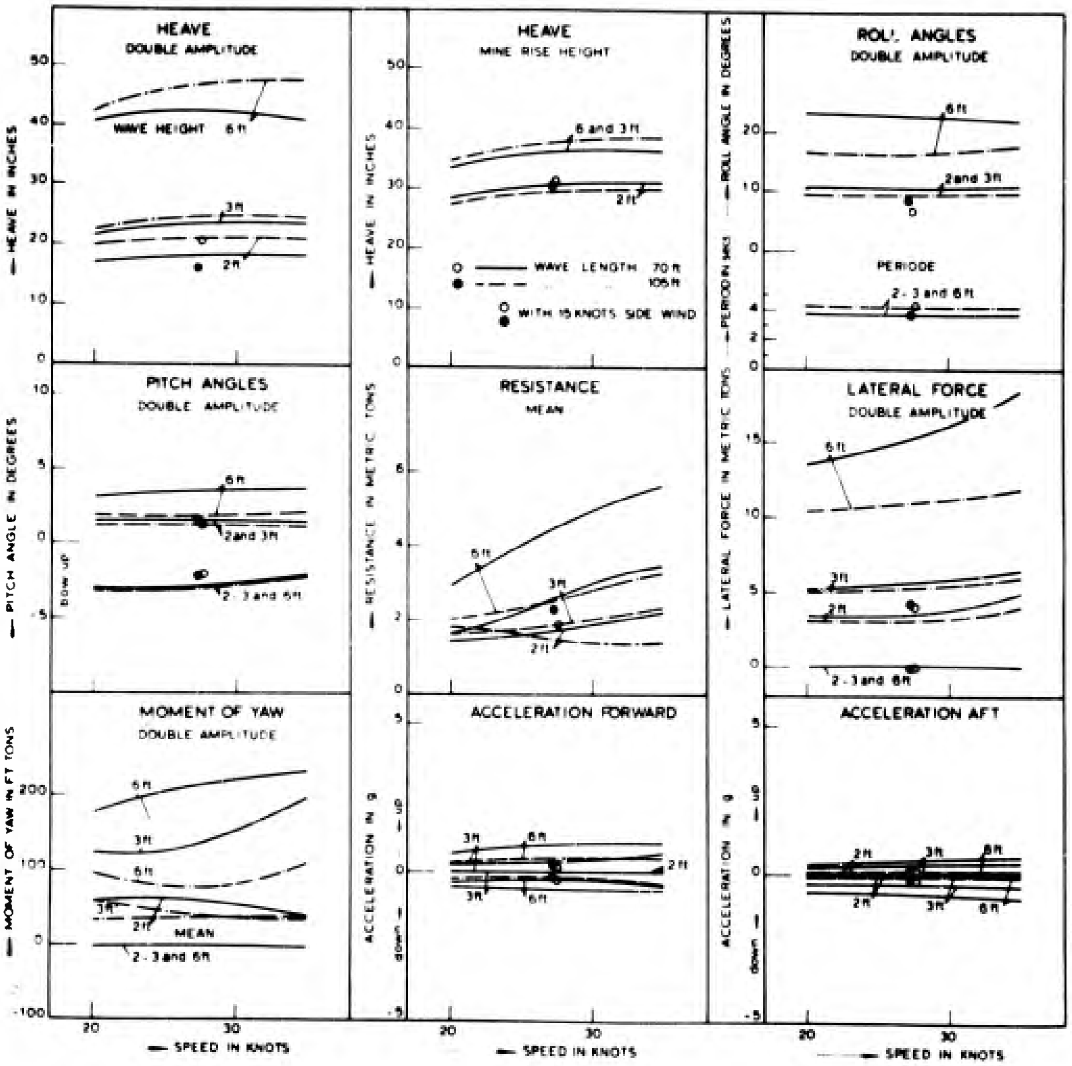

Fig. 12 - Effect of wave height and side wind, wave direction 90° (beam sea), 2580 fan revolutions per minute

Figure 13 learns that the resistance, the pitch and heave amplitudes decreased when the rise height was increased by means of higher fan revolutions. The accelerations were therefore expected to be lower at larger flying heights. This appeared to be true except for the accelerations forward in bow seas.

When the cushion fans were adjusted in such a way that at zero speed the vehicle was trimmed by head or by stern, the character of the behaviour did not change very much.

Comparison of Fig. 14 with Fig. 10 shows that heave and pitch amplitudes are lower in both trimmed conditions than at even keel. At speeds over 30 knots the resistance increased with trim by the head and decreased when the vehicle was trimmed by the stern. At lower speeds this was reversed.

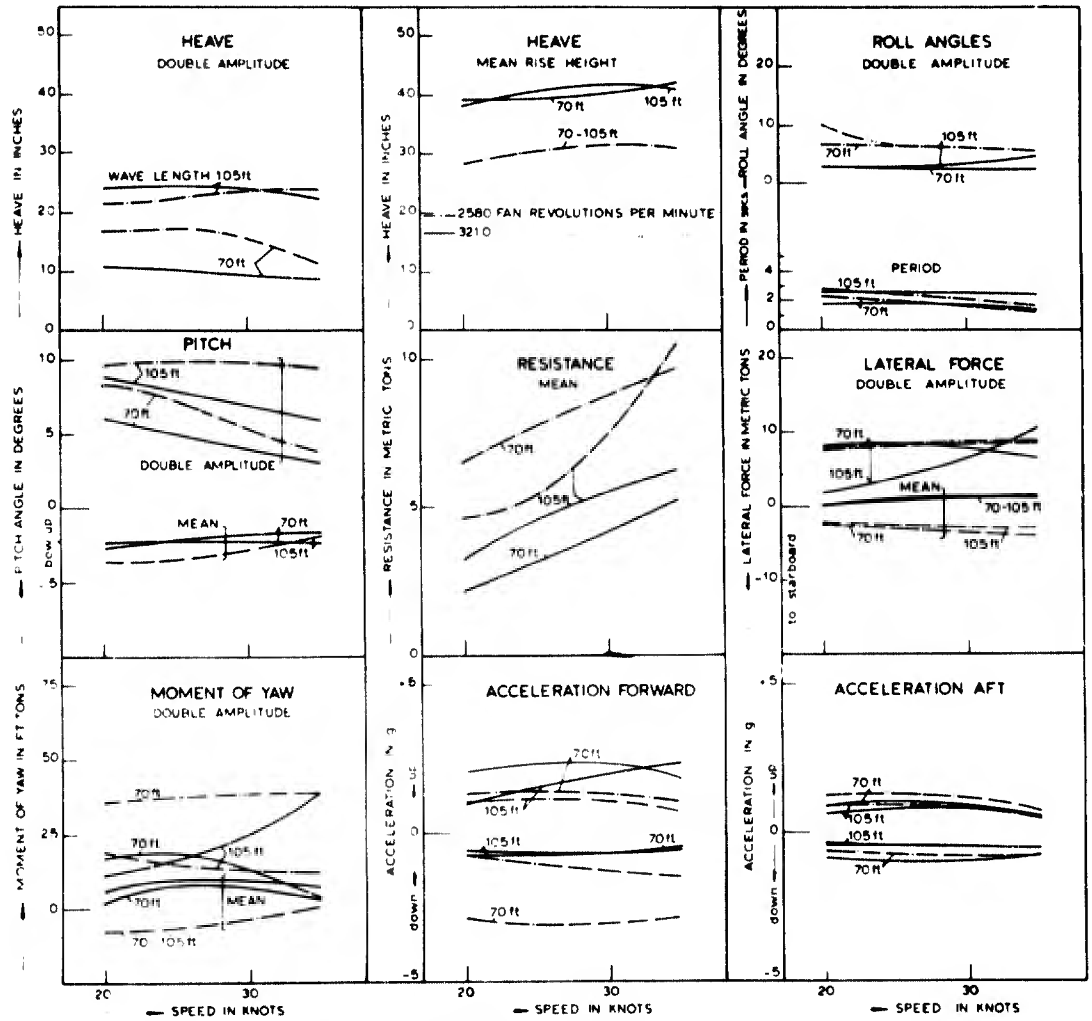

Fig. 13 - Effect of rise height. Wave direction 135° (bow sea), wave height 2 feet.

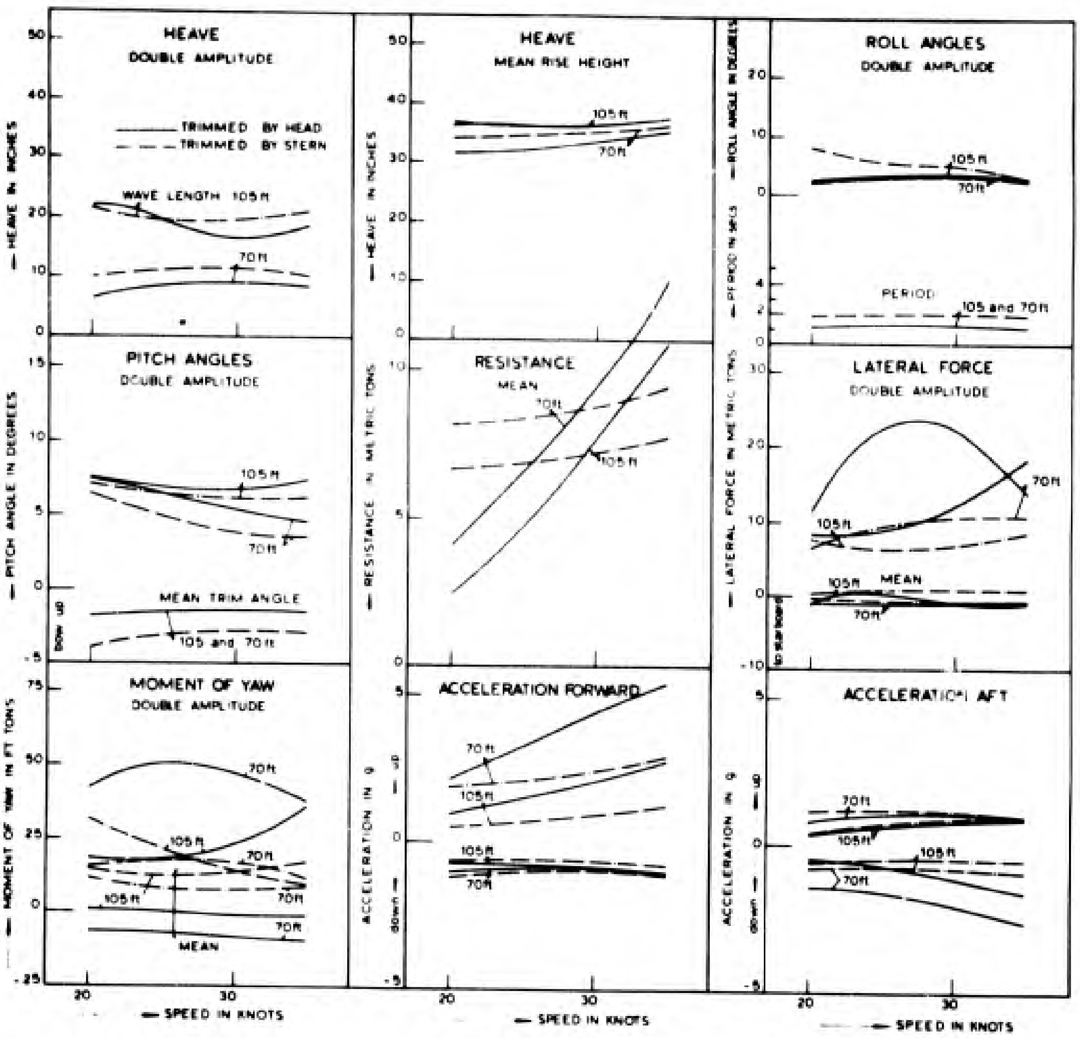

Fig. 14 - Effect of trim on the behaviour in waves. Wave direction 135° (bow sea), wave height 2 feet, 2580 fan revolutions per minute

The effect of a beam sea combined with a side wind was investigated for a speed of 28 knots only. The measured data are given in Fig. 13. It shows that the effect of a side wind was very small.

CONCLUSION

With regard to the behaviour of the vehicle the following general conclusions may be drawn.

The design with rigid jet exits proved to be dynamically unstable over water especially in regard to rolling. Minor changes in the jet exit arrangement could not remove this difficulty. The installation of flexible trunks, however, improved the behaviour considerably. Although it is expected that the dynamical unstability is caused by non-linear damping this could not be established with certainty. The weight of the model was such that the base pressure during the experiments was higher than in the actual design condition.

The resistance over smooth water showed a maximum in the speed range between 9 and 14 knots depending on the water depth. The highest resistance hump in shallow water was about 50% higher than on deep water.

The pitch and heave motions of the model proceeding in regular waves showed the character of well damped systems. The behaviour was apparently worst in bow seas of about vehicle length or somewhat longer.

With increased cushion power and resulting larger rise heights the motions and resistance showed a tendency to decrease.

At high speeds the resistance could be reduced considerably by trimming the vehicle by stern. In this condition the motions decreased as well. A side wind seemed to have only a minor effect on the behaviour of the vehicle.

The measured data did not show many unexplainable trends and in general the results could be reproduced within reasonable limits. An exception must be made for the yawing moment and sway amplitudes which records were rather blurred by high frequency noise.

REFERENCES

1. Fuller, F. L., "Gravity Wave Drag Theory for the Waterborne Ground Effect Vehicle," Grumman Aircraft Engineering Corp., Research Note RN-111, June 1959.

2. Hirsch, A. E., "The Hovering Performance of a Two Dimensional Ground Effect Machine Over Water," Symposium on Ground Effect Phenomena, Princeton University, Princeton, 1959.

3. Mack, L. R., "Theoretical and Experimental Research on Annular Jets Over Land and Over Water," Symposium on Ground Effect Phenomena, Princeton University, Princeton, 1959.

4. Tulin, M. P., "On the Vertical Motions of Edge Jet Vehicles," Symposium on Ground Effect Phenomena, Princeton University, Princeton, 1959.

5. Kuhn, R. E., Carter, A. W. and Schade, R. O., "Over Water Aspects of Ground Effect Vehicles," Institute of Aeronautical Sciences, paper no. 60-14, New York, 1960.

6. Lin, J. D., "Dynamic Behaviour of Ground Effect Machines Over Waves," Journal of Ship Research, Vol. 6, number 4, April 1963.

7. Wiegel, R. L., c.s., "Research on Annular Nozzle Type Ground Effect Machine Operating Over Water"; "Operation Over Waves," Hydraulic Engineering Laboratory, University of California, Berkeley, 1963.

8. Cumming, J. D., "Research in Annular Nozzle Type Ground Effect Machine Operating Over Water"; "Water Surface Configuration," Hydraulic Engineering Laboratory, University of California, Berkeley, 1963.

9. "Tests with a Flying Model of a Ground Effect Machine SKMR-I 'Hydroskimmer'," Seakeeping Test Report no. 121, Netherlands Ship Model Basin, August 1963.

10. "Tests with a Model of a Ground Effect Machine SKMR I 'Hydroskimmer' Flying Over Regular Waves," Seakeeping Test Report no. 157. Netherlands Ship Model Basin, July 1964.

* * *

DISCUSSION

W. A. Cragg
Saunders-Roe Division of Westland Aircraft Limited
Wight, England

For reasons of commercial security it is relatively rare for practical data obtained on models of full scale hovercraft to be published and I personally would like to say that I was, therefore, very pleased to see this excellent paper by Mr. W. A. Swaan and Mr. R. Wahab.

This is all the more interesting to me because in the Saunders-Roe Tanks we spend a fair proportion of our time testing hovercraft.

We now have full scale area model test results for the N1, N2, N3 and 5 full scale variants of the N5 (these are craft ranging in weight from 7 to 37 tons) and, with this background, I can confirm that the type of test reported in Mr. Swaan's paper, using dynamically scaled free models, can give results which correlate acceptably well with data obtained in the full scale regime, although as a result of our experience we would prefer not to use a model quite so small as the N.S.M.B. Hydroskimmer because of scale effects in the jets.

The N.S.M.B. model test philosophy, in which the propulsion propellers are not represented is, I feel, acceptable except in cases where the propellers can affect the flow into the fan intakes. The way in which the fan intake flow is represented is important because the intake flow geometry determines the moment arm at which the momentum drag acts. This moment affects the crafts running trim and this in turn affects the drag. Correct representation of the intake flow is thus essential.

Mr. Swaan's paper presents results obtained in regular seas. We have found tests in such an environment of only limited usefulness and it is now our practice to run all hovercraft tests whether for ourselves or customers in irregular seas having energy spectra based on a Darbyshire formulation modified to make it represent the coastal and local conditions with which we have to deal in our full scale trials.

We have found good agreement between the derived amplitude response operators and the accelerations obtained from irregular sea tests and regular sea tests up to sea conditions associated with a wind of Beaufort force 5 but beyond this, I feel that irregular sea testing is essential because of the nonlinearity of response.

A further point which is perhaps worth mentioning is that we have used motion extinction curves similar to those given in Mr. Swaan's paper, together with the static characteristics and a fairly simple wave impact theory as inputs to an analogue computer. In this work we have found that we can predict the model motion and accelerations and the effect of pitch control systems, steering system failures, etc., to a very acceptable degree of accuracy at least in regular waves and irregular waves up to a Beaufort force 5 wind.

(This work has been published by my colleague, Mr. J. Stafford, as a paper read before the British Society of Instrument Technology in June, 1963 and appears in their transactions).

The Wageningen data shows that the value of $V/\sqrt{gL}$ at which the hump pitching attitude occurs decreases as water depth decreases. The way in which it does this agrees precisely with our own findings and the way in which the corresponding resistance varies is also generally similar.

In connection with the presentation of the data, I would like to see values given for the momentum drag. This would facilitate analysis and comparison with other data.

In closing I would like to make a further small criticism. It is a pity the test points have not been shown in Figs. 6 to 9. I feel the curves have been over-smoothed and that there should be almost a discontinuity for example in the heave curves at Froude numbers between 0.3 and 0.6 depending on water depth.

* * *

DISCUSSION

R. F. Lofft
Admiralty Experimental Works
Gasport, England

This paper represents a useful addition to the published literature on the behaviour of hovercraft over water. It illustrates the difficulty of testing models of such light, high-speed craft in normal ship model tanks. It is generally impossible to fit equipment in the model to measure all the motions of interest, and the arrangement adopted by the authors to permit heave, pitch and roll, and to restrain the model in yaw, sway and surge seems a reasonable compromise.

Turning now to several points of detail:

(1) The two diagrams at the bottom of Fig. 4 show that, with rigid jets, the righting arm is much greater over water than over land, while with flexible jets, the difference is much less. No reason can be seen for this and it would be interesting to have the authors' comments.

(2) The results of the shallow water tests in Fig. 8 show a marked peak in the resistance curve at 12 ft depth. It is interesting to note that this occurs at the critical speed for this depth, viz. 11.7 knots. The same does not appear to be true for the other two depths tested, at which the critical speeds are 4.7 knots for 2 ft depth and 19 knots for 32 ft.

(3) Figure 10 gives the results of tests in waves with flexible trunks, in which the mean rise height is given as 25-30 inches. This is nearly 10 inches less than the corresponding figures for still water, from Fig. 6. This is somewhat surprising, since the wave tests show the mean rise height to be independent of wave length, and one would therefore expect it to be about the same as in still water.

(4) The authors suggest that the maximum pitch amplitude would be expected to occur in waves of about air cushion length. This is true of normal ship speeds; but at higher speeds, e.g., in model tests of fast planing craft, it has been found that maximum pitching generally occurs in waves of 2 - 2-1/2 times model length. This is consistent with the results in Figures 10 and 11 in which the greatest pitch occurred in waves 105 ft long - nearly twice the air cushion length.

* * *

REPLY TO THE DISCUSSION

W. A. Swaan and R. Wahab
Netherlands Ship Model Basin
Wageningen, Netherlands

It is gratifying to have Mr. Crago's comment on the test results because of his experience both with models and actual hovercrafts. The small size of the model was necessary because of the maximum available carriage speed otherwise it would certainly have been desirable to use a bigger model. The use of regular waves was selected in order to obtain an impression about the transfer functions. Moreover the wave generator in the Seakeeping Laboratory is not suitable for the generation of irregular long crested oblique waves. It is true however that the use of irregular waves is to be preferred in many respects when predictions have to be made for the performance in a given area where the sea conditions are known. Because the air flow for the jet system was not measured the momentum drag can not be determined from the experiments. However Fig. 8 gives the total resistance when flying over concrete. Because of the negligible trim, resistance must be mainly momentum drag.

In regard to Mr. Lofft's question about the effect of the flexible trunks on the difference between the stability over land and over water it must be remarked that the cause of this phenomenon can only be found when measurements are taken of both pressure and water surface shape under the vehicle. The energy loss caused by the smooth water surface waves is not only compensated by the resistance of the GEM but also by the air cushion. This can be shown by the fact that no "wave resistance" will be found notwithstanding the visibility of surface waves if the GEM is kept horizontal, provided that the air flow is kept constant. Therefore it is the opinion of the authors that coincidence of maximum resistance with the critical speed is not physically necessary.

In the conclusions it is mentioned that pitch angles are the largest with waves of about vehicle length or somewhat larger while Mr. Lofft notices that the diagrams show a maximum at about double the air cushion length. However, if the system had no damping, the maximum pitch angles would occur at resonance; that is a wave length of 175 ft at the speed of 30 knots in bow seas.

Because the maximum under these conditions occurs in much shorter waves it is clear that damping is rather large. Therefore the pitch angles are much more determined by the wave moment than by the frequency of encounter. The remark about the effect of wave length or pitch must be considered in this light, although it is admitted that the expression "about air cushion length" was stretched somewhat too far.

* * *

BEHAVIOR OF UNUSUAL SHIP FORMS

E. M. Uram and E. Numata
Stevens Institute of Technology
Hoboken, New Jersey

INTRODUCTION

Four years ago, almost to the exact date, the Third Naval Hydrodynamics Symposium, constituted and attended by many of the gentlemen participating in this symposium was held at Scheveningen in the Netherlands; a short skip, gurgle, or flight from here, depending upon which unusual high performance ship one chose to use. Almost the entire symposium was devoted to discussions on the nature and problems associated with high performance ships. The papers of Mr. Owen Oakley [1] of the United States Navy Bureau of Ships, Dr. Van Manen [1] of the Netherlands Ship Model Basin, and Dr. Breslin and Professor Lewis [1] of our own laboratory, at that time pointed out many of the design and operational problems attendent with the unusual ships shown in Fig. 1. Their relative power and seakeeping behavior were discussed based upon reasonable analytical estimates, or very limited experiments. A substantial number of the other papers presented at that symposium and at other subsequent meetings offered information concerning the performance and limitations of hydrofoil craft, planing craft, and GEM's. We will not reiterate these arguments at this time, but just point out that the prime objective is the attainment of high speeds in rough seas while maintaining reasonable horsepower requirements and reducing the well known severity of motions in seas at high speeds.

We will be concerned in this discussion primarily with unusual surface or sub-surface vessels in the 3,000 ton displacement class at speeds in the vicinity of 40 to 50 knots, although we will discuss the behavior of these ships over the entire speed range. The design philosophy of unusual form surface ships such as the Large Bulb Ship (Escort Research Vessel) and the Semi-Submerged Ship (Decks Awash Ship) is such as to change the pitching and heaving periods so that the ship will operate in sub-critical or super-critical zones of operation as defined by Professors Lewis [2] and Mandel [3]; operation conditions in which the ship is not in resonance with the encountered wave system. The shallow running submersibles like the Shark Form and Semi-Submarine take advantage of the attenuation with depth of wave system effects. However, the single surface piercing strut of these ships makes them unacceptable from a stability and control point of view. The Hydrofoil Semi-Submarine, Fig. 2, is a design conceived by the senior author [4] affording inherent stability in this ship type. The stability referred to is defined as the ability of the vessel with controls fixed to seek and return to its initial trim, depth, and course after being disturbed from these conditions.

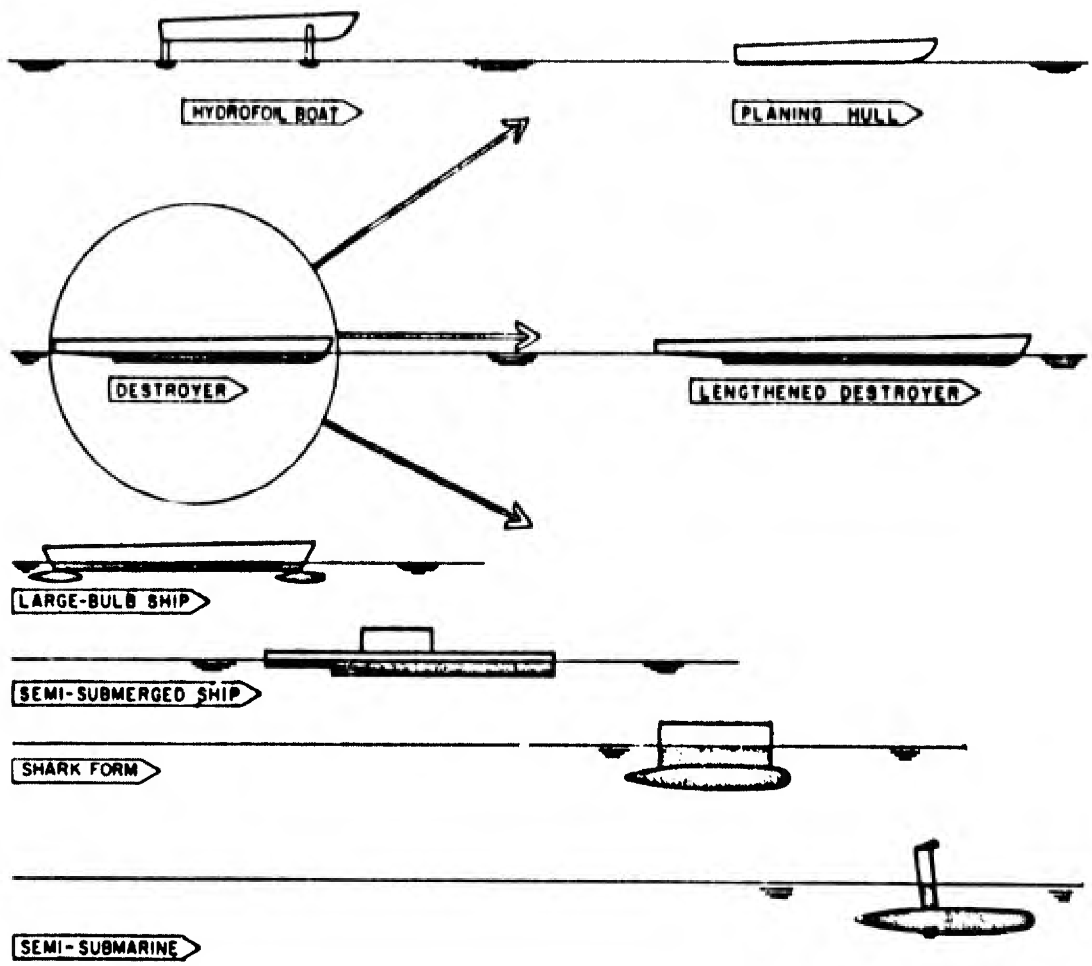

Fig. 1 - Ship forms for high speed at sea

The Third Symposium was a major impetus which propagated substantial investigative work into the performance of these unusual ship forms. The Bureau of Ships and the Office of Naval Research supported an extensive program to obtain information concerning the performance of these unusual ship forms. A substantial investigation of the characteristics of the Shark Form was conducted at the Massachusetts Institute of Technology by Professor Mandel [5] and his associates in a relatively low speed range. It gives us pleasure to say that a substantial amount of work was done at our own Davidson Laboratory on the Semi-Submerged Ship [6], the Large Bulb Ship [7] and the Hydrofoil Semi-Submarine [8]. Professor Mandel [9], acting as a consultant and member of the Panel on Naval Vehicles of the National Academy of Sciences' Committee on Undersea Warfare, published a primarily analytical, exhaustive comparative study of novel ship types from which we will draw from time to time. It is of general interest to note at this point that Professor Mandel's study of endurance and pay load indicates that the pay loads for all of the ship types that we will

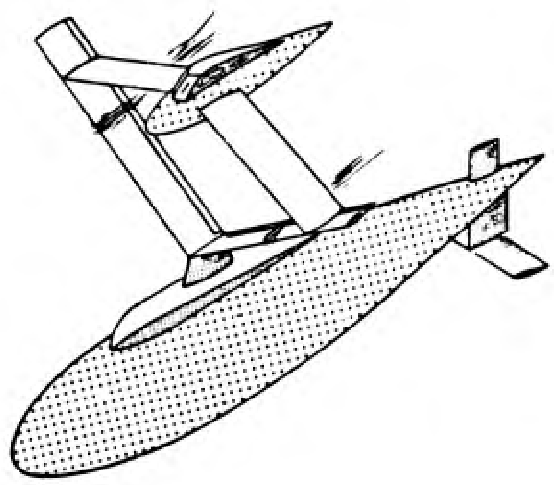

Fig. 2 - Hydrofoil semi-submarine

discuss today in the 3,000 ton class are very much competitive in the 2,000 mile endurance range at a cruise speed of 20 knots.

It is mainly our purpose in this paper to present comparisons of the several unusual form ships based upon experimental information accumulated to date. First we will take up the powering characteristics of these ships in both calm and regular sea conditions and then go on to the motion characteristics under these same conditions. It is of interest to point out that most of the results we will present on the Hydrofoil Semi-Submarine and Large Bulb Ship are relatively new and have not been discussed widely. Therefore, we will dwell in some detail on some of the characteristics of these two particular ships.

SPEED AND POWER BEHAVIOR

The resistance characteristics of the Large Bulb Ship with the forward bulb in various positions was investigated in the course of the study. As shown in Fig. 3, the results for residual resistance are given for the various bulb positions, as well as for the bare hull, and it is seen that the most forward bulb position results in substantial residual resistance reductions from the bare hull as well as the other bulb positions over the speed range. It was this forward bulb position that was used during the remainder of the study on ship motions.

In order to establish the existence of an optimum form for the semi-submarine hull, a study was made of streamlined body of revolution characteristics in which it was discovered that in the high speed range, Froude number in the vicinity of unity, the residual resistance coefficient of such bodies running near the surface can be considered to be approximately 25% of the deeply submerged frictional resistance coefficient. Therefore, it was necessary only

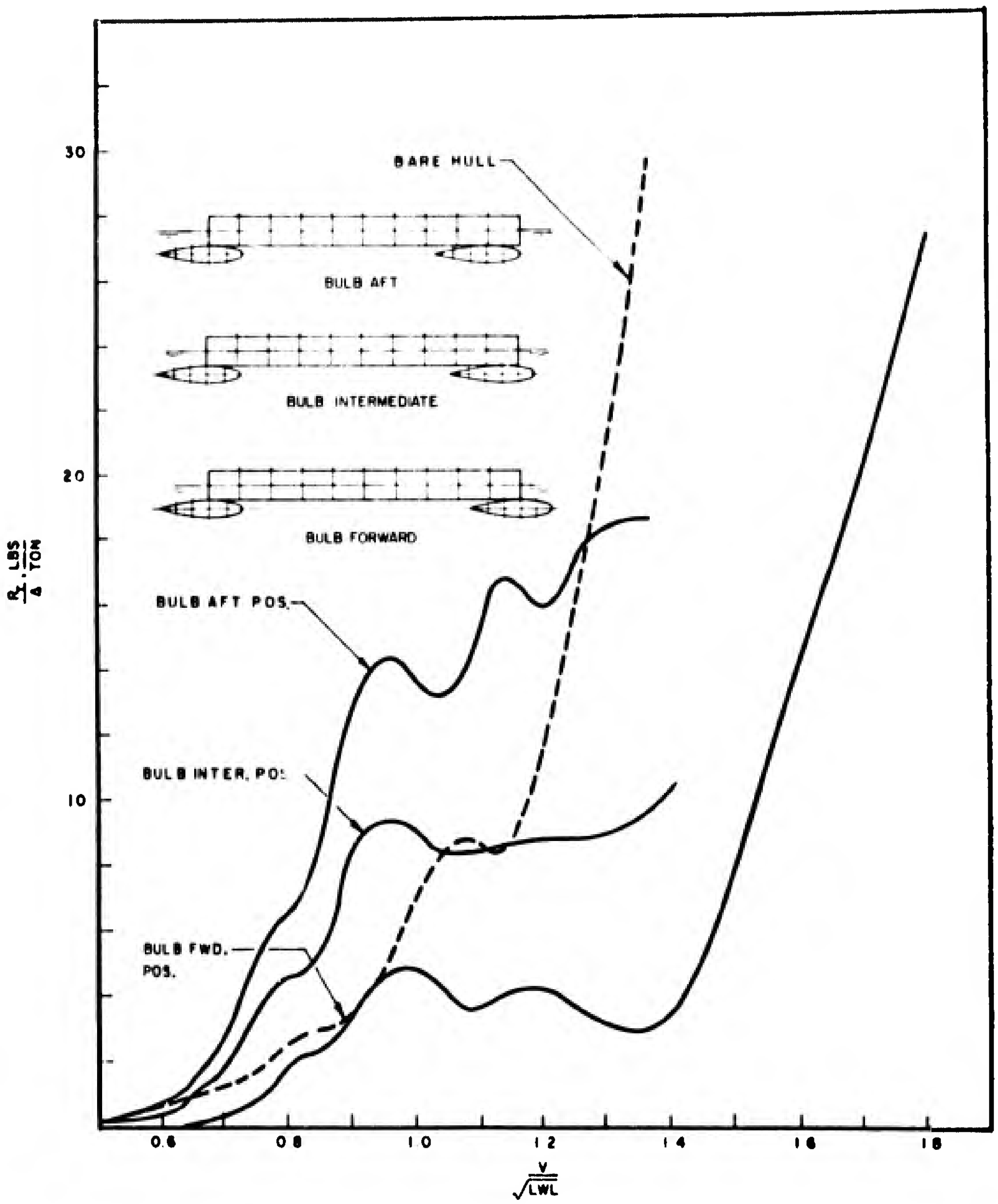

Fig. 3 - Residual resistance comparison for various large bulb ship configurations

to study the deep submergence frictional characteristics in order to determine whether there indeed exists an optimum form in the design Froude number range. Figure 4 indicates for such bodies the specific horsepower (EHP per ton of displacement) as a function of speed, fineness ratio and body length. Since for each set of fineness ratio curves the velocity is constant and the abcissa used is body length, it is possible to associate a Froude number with that velocity and body length. Therefore, a Froude number scale is superimposed on the abcissa of the figure. We see from Fig. 4 that there does indeed exist for, say, a 3,000 ton vessel an optimum fineness ratio of 5. This was used in the design of the Hydrofoil Semi-Submarine.

We will dwell a little further on the Hydrofoil Semi-Submarine in order to acquire a proper interpretation of the information to be presented subsequently for comparison with the other ships. A substantial part of the tests performed

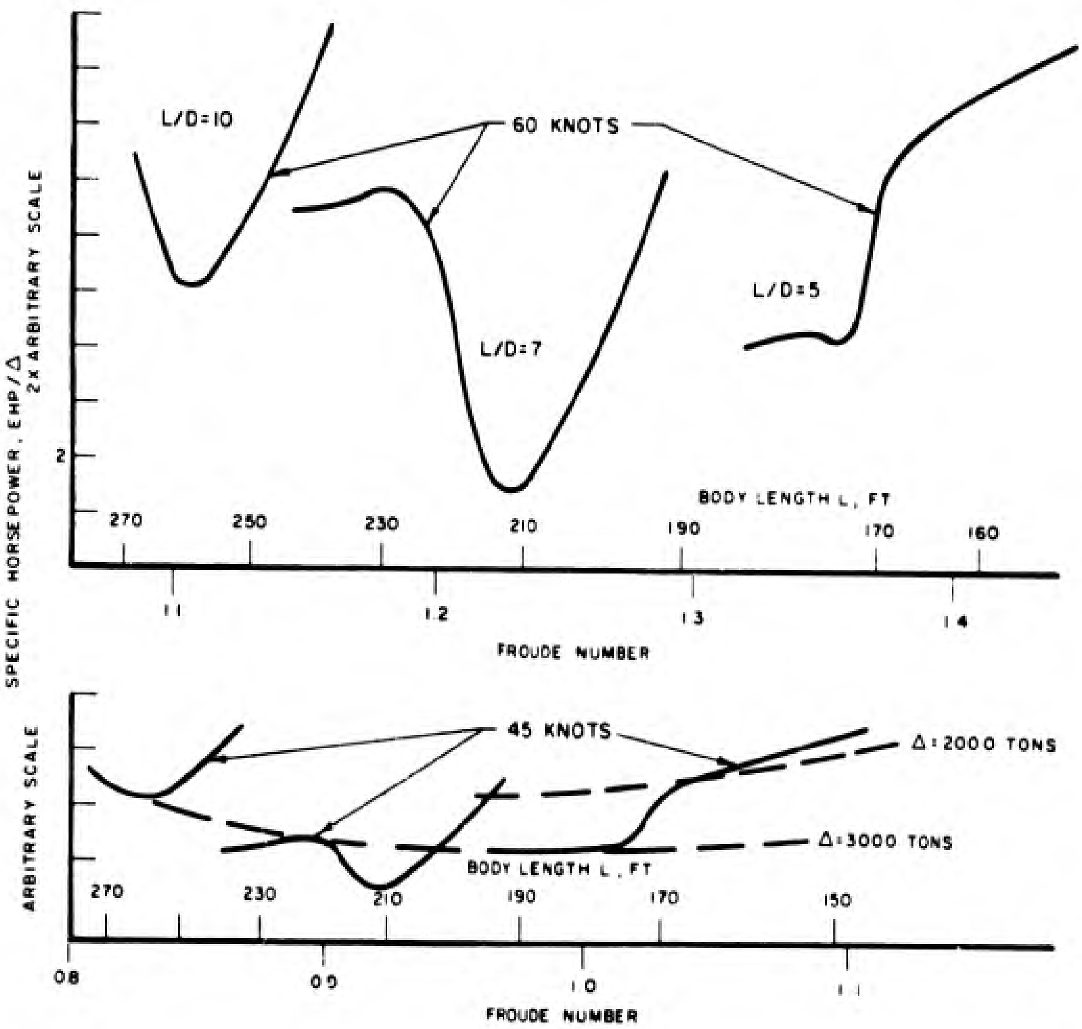

Fig. 4 - Specific horsepower (streamline bodies of revolution at deep submergence)

on the Hydrofoil Semi-Submarine were such that the ship was free to surge, pitch and heave; the variable ballast, hydrofoil flap and stem plane angles being set for an equilibrium ship trim attitude at the design depth and run speed. During the runs the model exhibited excellent stability and sought its own running equilibrium trim condition for the speed of the run. Therefore, the ship depth and trim attitude, in many cases was different from design conditions or from those used in the tests conducted under restrained motion conditions. Figure 5 shows the pitch and heave equilibrium attitudes of the Hydrofoil Semi-Submarine in calm water and we see that the assumed trim angle of the vessel varied around the design equilibrium trim angle of zero degrees. We see, also, that the submergence depth of the vessel varied around the design depth of approximately 1.5 diameters below the surface. Figure 6 shows the corresponding calm water total resistance coefficient as a function of Froude number. Also shown for comparison are results obtained from the restricted motion tests at the design depth for various trim angles. The calm water resistance coefficient plot is, therefore, quite realistic; representing what might actually be encountered under operational conditions while the other curves give much lower resistance coefficients under absolutely ideal conditions. The calm water resistance coefficient was used in the calculations of horsepower requirements.

Figure 7 depicts the mean equilibrium attitudes of the Hydrofoil Semi-Submarine in regular waves. Not all of the data are presented here, but enough are presented to give an idea of the range of conditions encountered. Figure 8 and Fig. 9 show the total resistance coefficient as a function of Froud number for this ship under regular following waves. We see that there apparently is no discernible difference in the drag coefficient with respect to the height of the wave system in 1.0 L waves, whereas in wave lengths twice the ship length a substantial difference exists between the resistance coefficients for different wave heights. Further, spotted onto these figures is the calm water resistance curve. In both figures we see that the resistance coefficient in regular following waves is higher than the calm water resistance, particularly for the wave height to ship length ratio of 1/22.5.

These resistance coefficients and resistance coefficients taken from Van-Mater's [7] data for the Large Bulb Ship, Lewis' and Odenbrett's [6] for the Semi-Submerged Ship and Davidson Laboratory data for a conventional destroyer were used to calculate the horsepower requirements for the calm water and various regular sea conditions. The standard calculation method for EHP was employed with the exception that a 30% increase in the Schoenherr skin friction coefficient was applied to the Hydrofoil Semi-Submarine to account for the skin friction contribution of the main hydrofoil system and stern planes. This is reasonable and in keeping with knowledge of the additional frictional resistance experienced in normal submarines due to the sail, fair water, and stern planes. Figure 10 gives an EHP comparison of the various unusual form ships and the conventional destroyer in calm water. We see that up to 30 knots the power of the Hydrofoil Semi-Submarine is substantially higher than the other three ships, whose powers are comparable, because the Semi-Submarine experiences its maximum wavemaking resistance in this speed range. Between 30 and 40 knots all three unusual ship forms are better than the conventional destroyer. At 40 knots and above the Hydrofoil Semi-Submarine is substantially better than the

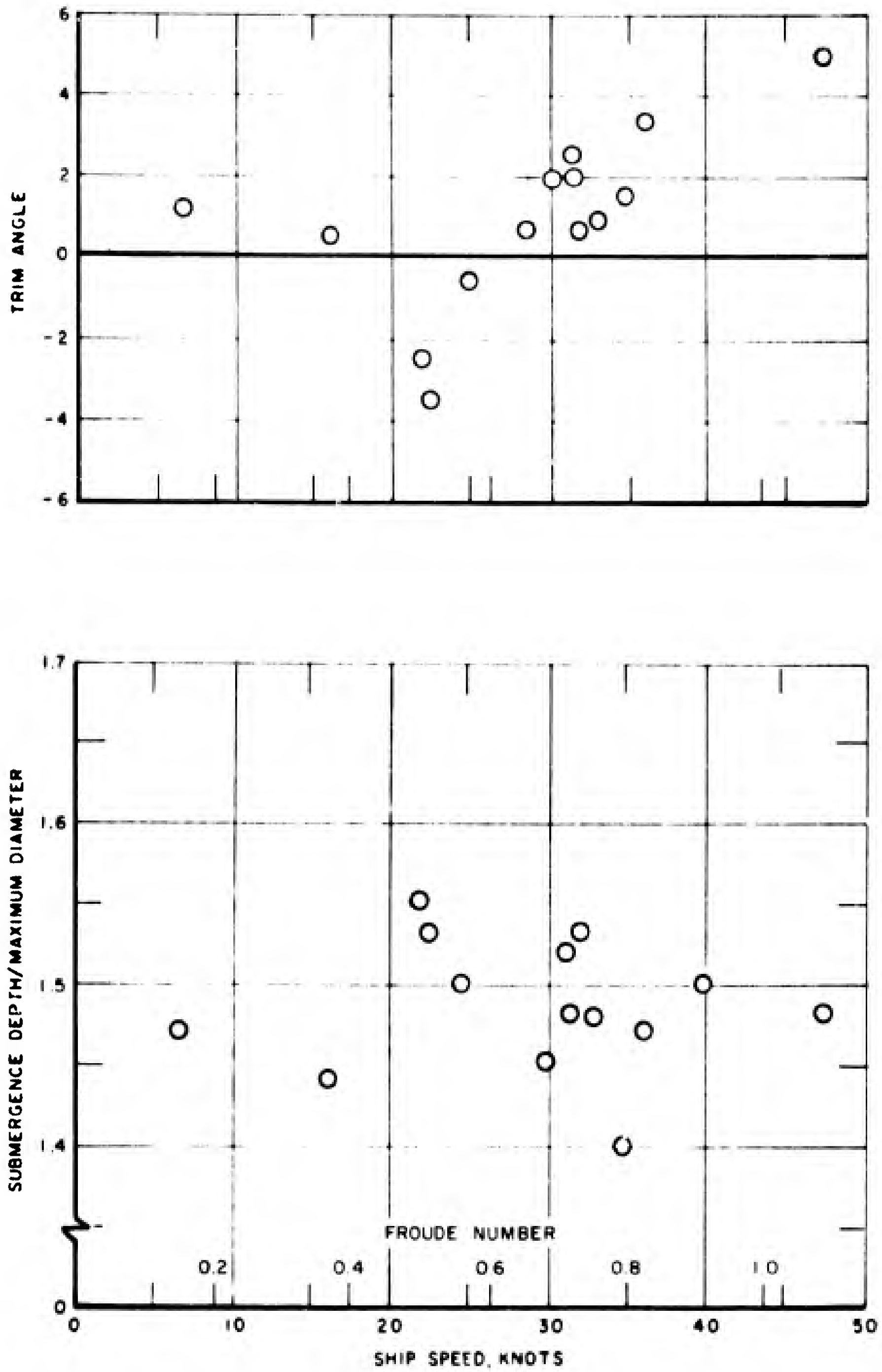

Fig. 5 - Pitch and heave equilibrium attitudes calm water (hydrofoil semi-submarine)

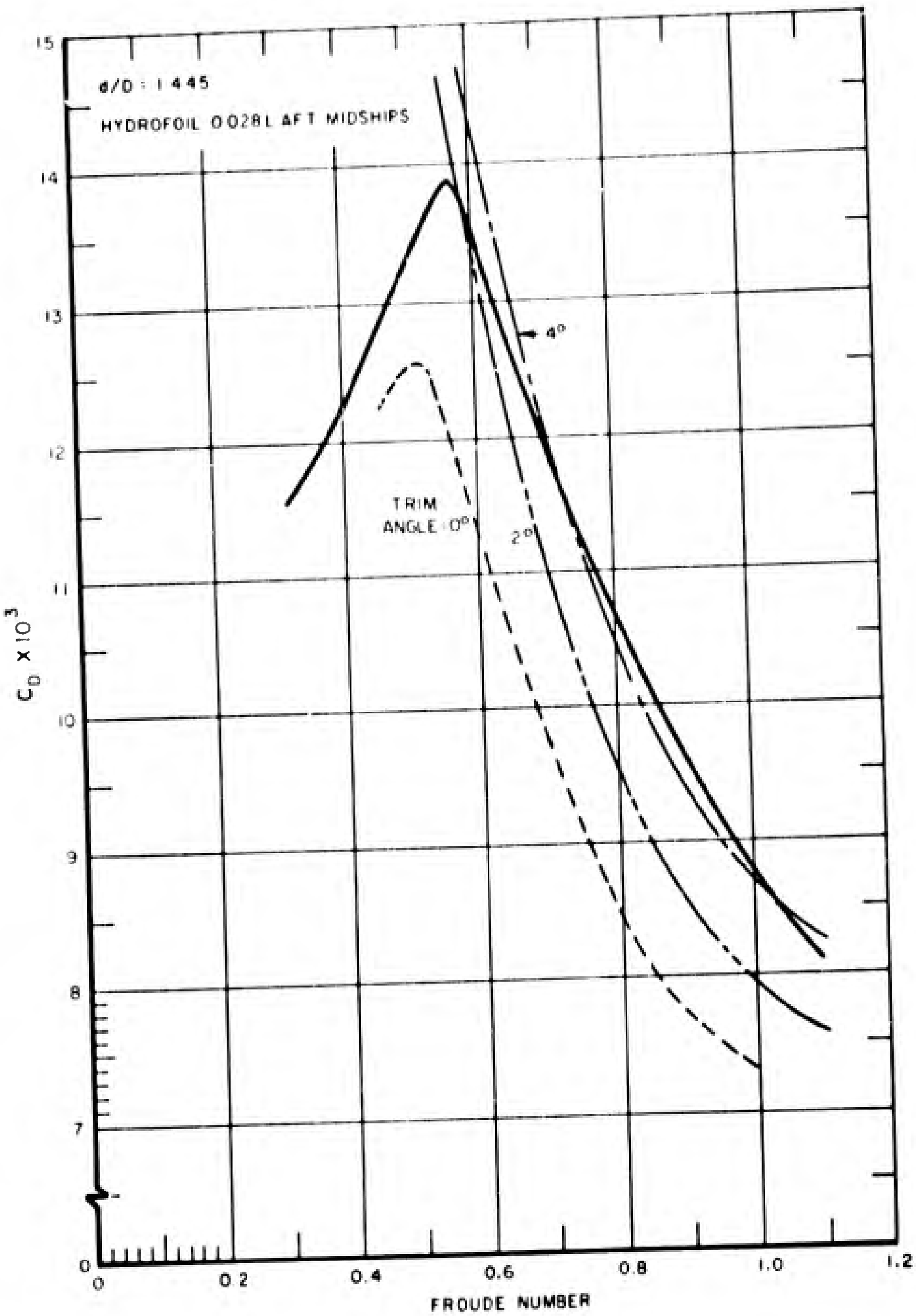

Fig. 6 - C_D vs Froude number motion tests in calm water (hydrofoil semi-submarine)

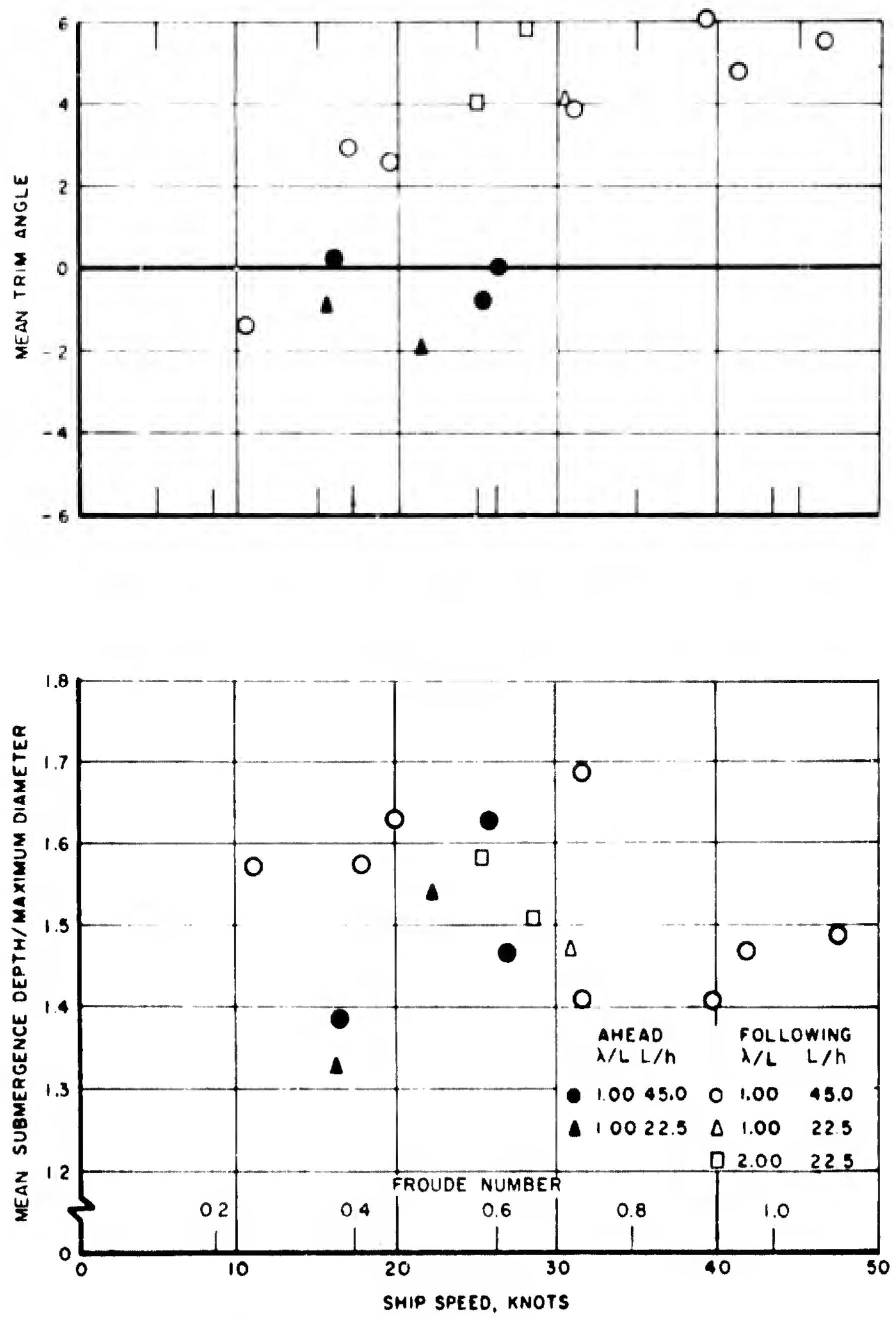

Fig. 7 - Mean pitch and heave attitudes regular waves
(hydrofoil semi-submarine)

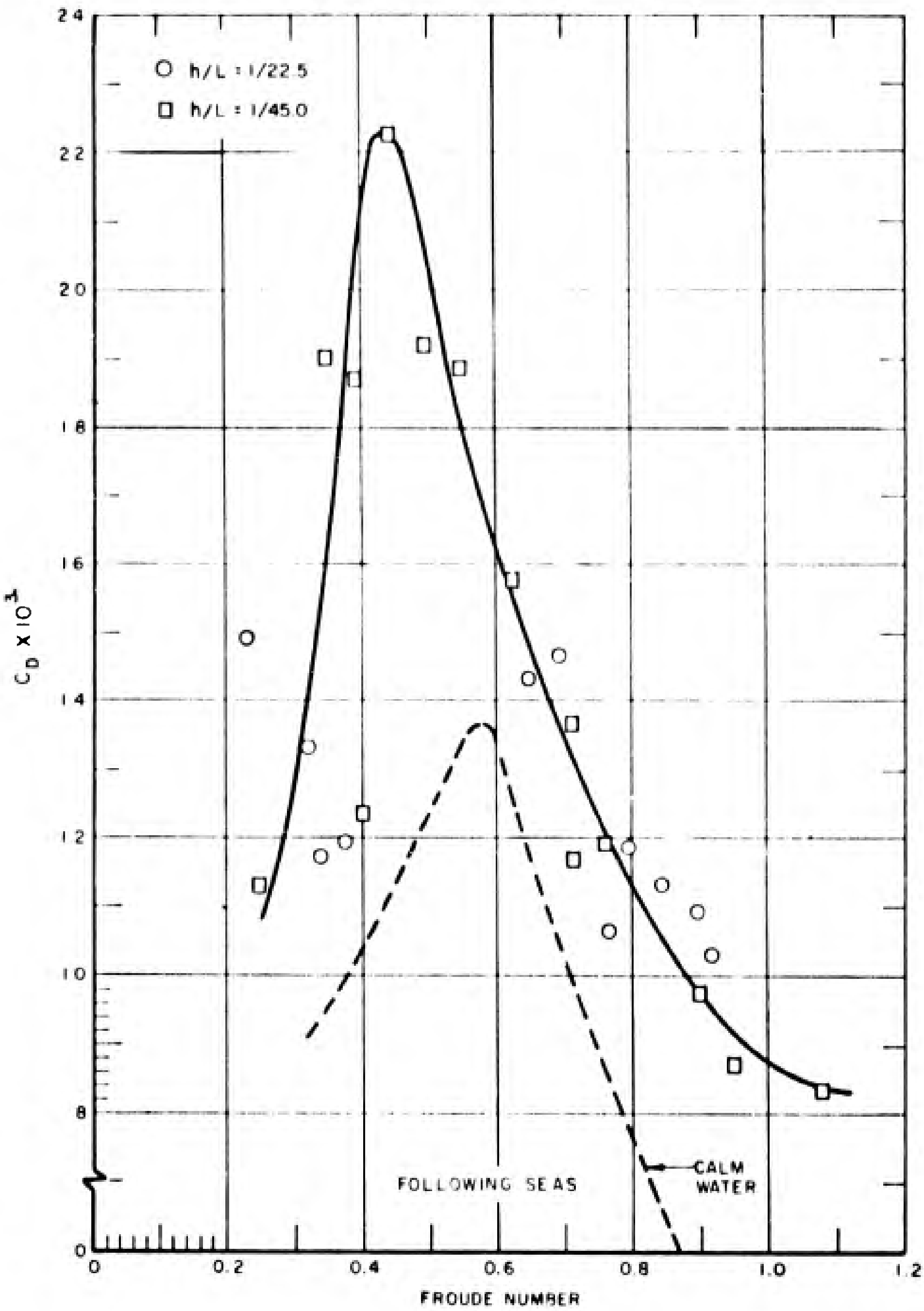

Fig. 8 - C_D vs Froude number regular 1.0 L waves (hydrofoil semi-submarine)

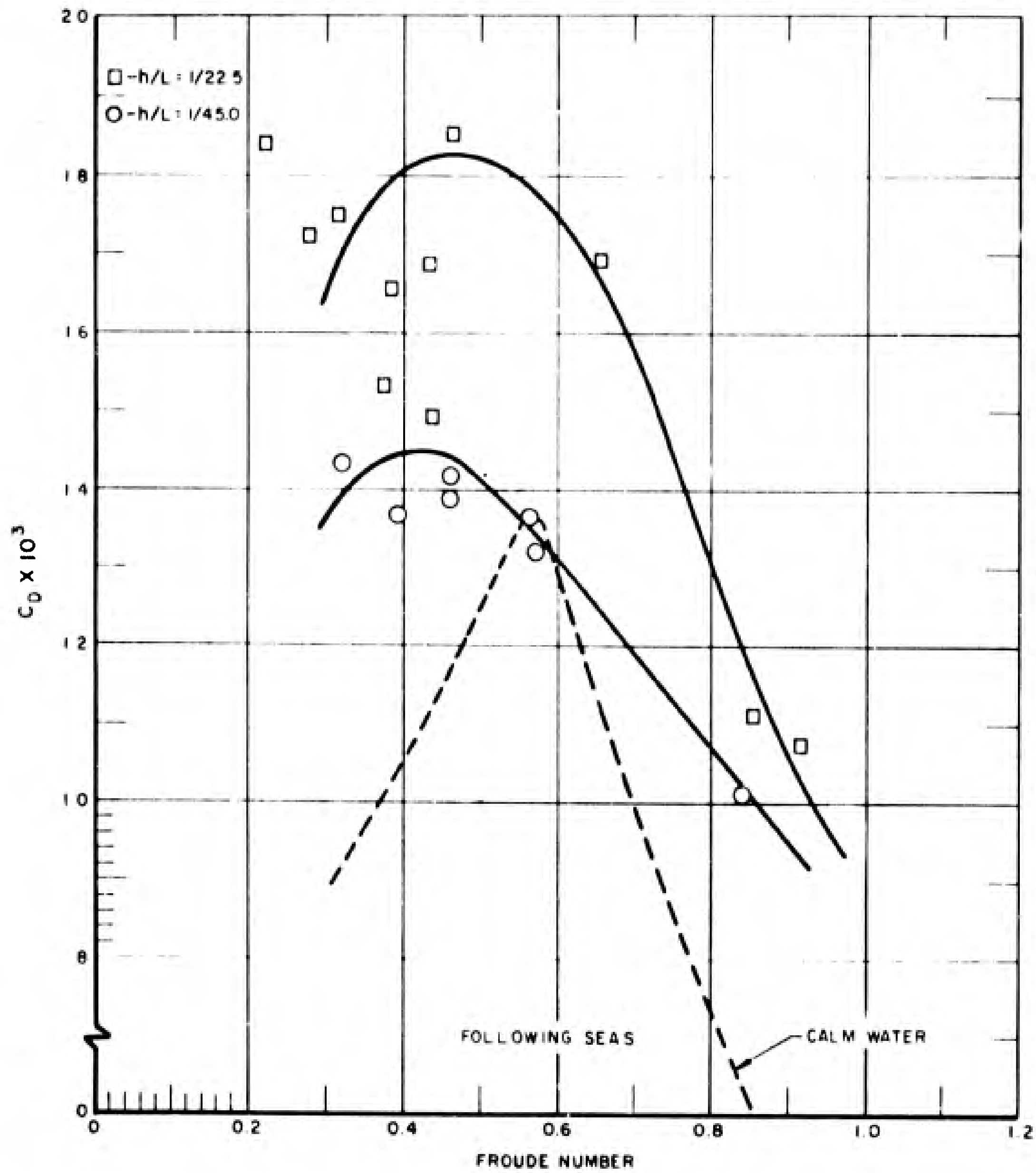

Fig. 9 - C_D vs Froude number regular 2.0 L waves (hydrofoil semi-submarine)

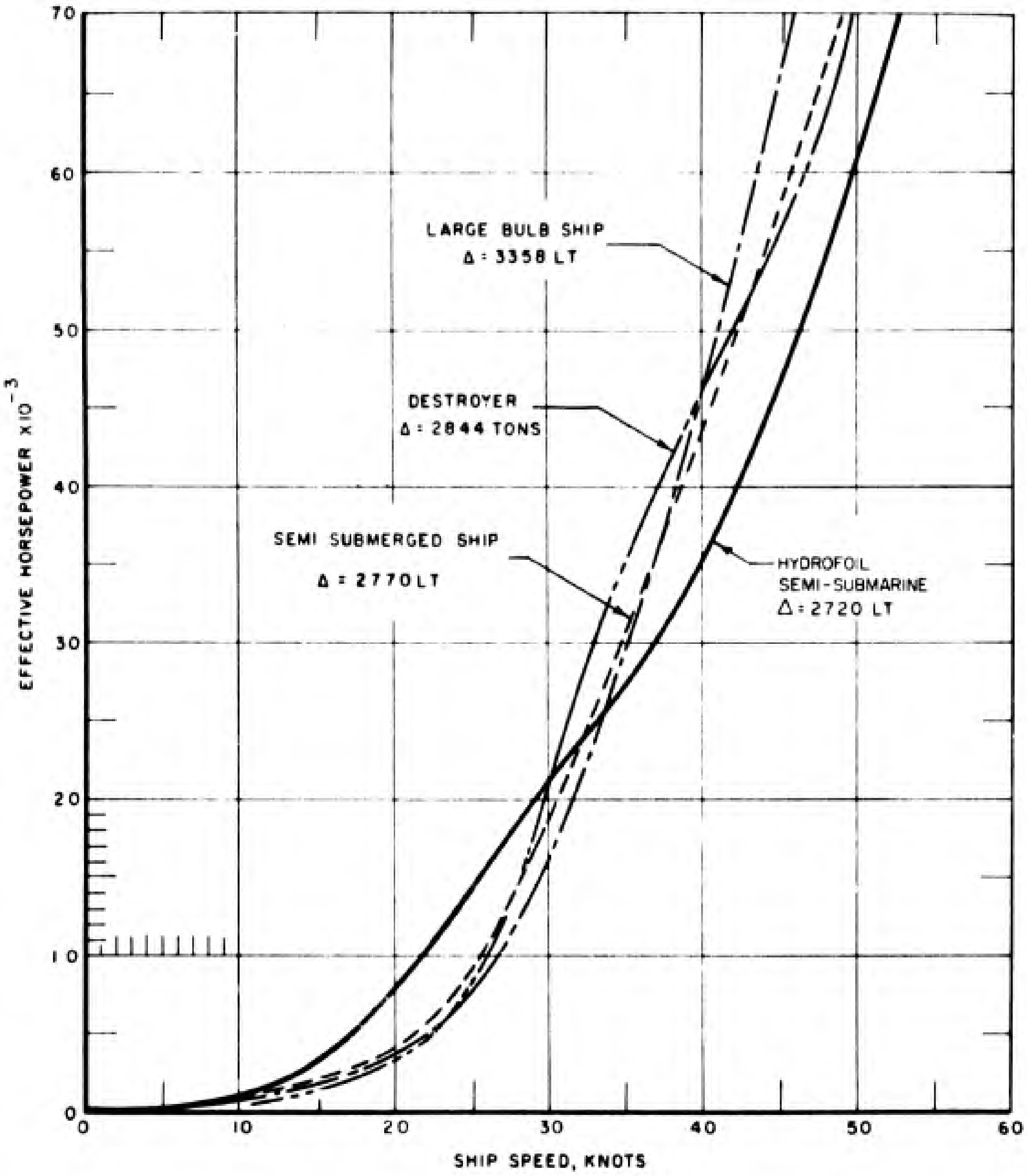

Fig. 10 - Effective horsepower comparison calm water

other ships; the conventional destroyer is next best, followed by the Semi-Submerged Ship and the Large Bulb Ship, in that order. The Shark Form would be higher than all of the ships over the entire speed range.

Figures 11 and 12 present an EHP comparison in regular waves. As in calm water, the Hydrofoil Semi-Submarine shows to best advantage at speeds

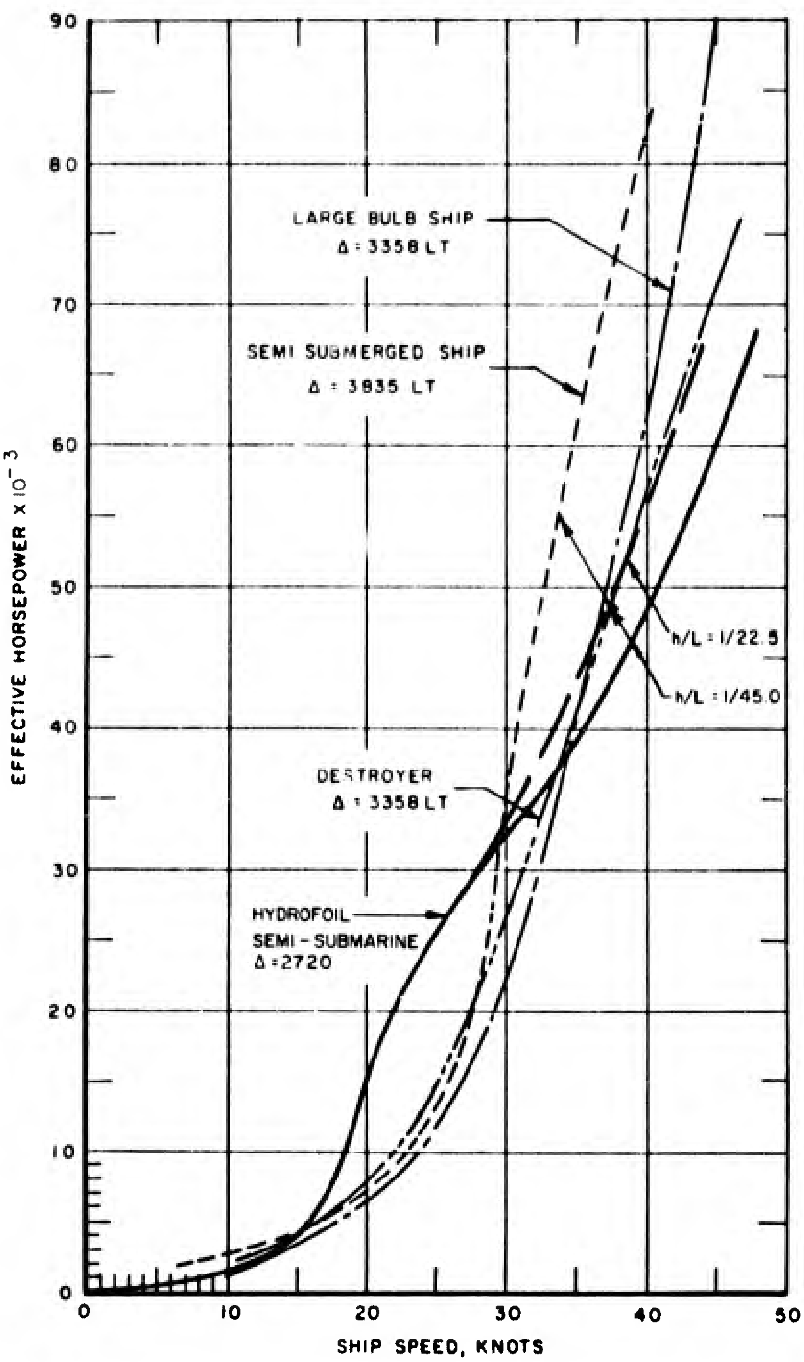

Fig. 11 - Effective horsepower comparison
regular 1.0 L waves

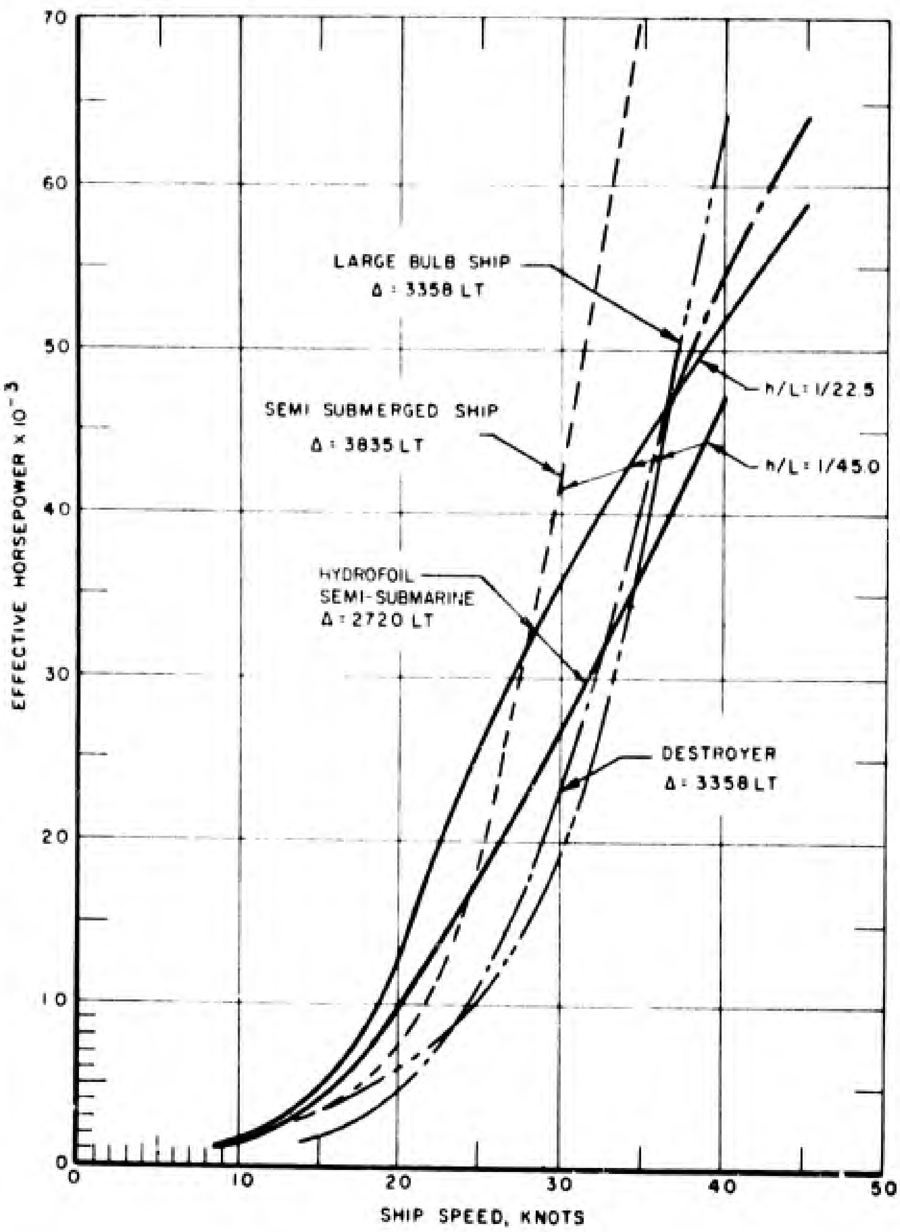

Fig. 12 - Effective horsepower comparison regular 2.0 L waves

above 35 knots, while the Large Bulb Ship generally has an advantage at speeds up to 35 knots.

MOTIONS BEHAVIOR

Professor Mandel's calculations [9] on the critical speed zones of operation for various sea states having a Neumann spectra are reproduced, in part, in

Figure 13; critical speed zones correspond to severe motions, wet decks, and slamming while sub and supercritical zones correspond to very moderate motions and intermediate zones to motions intermediate between the two extreme conditions. A complete analysis of this figure is given in Mandel's paper. It is of interest for our purposes to examine the major differences in zone extent predicted for these unusual ships and, further, to remark that these results of an idealized analysis are supported to a large extent by the available regular sea data. The destroyer is seen to be sub or supercritical in all following seas, while the Semi-Submarine enjoys these conditions for all ahead seas and following

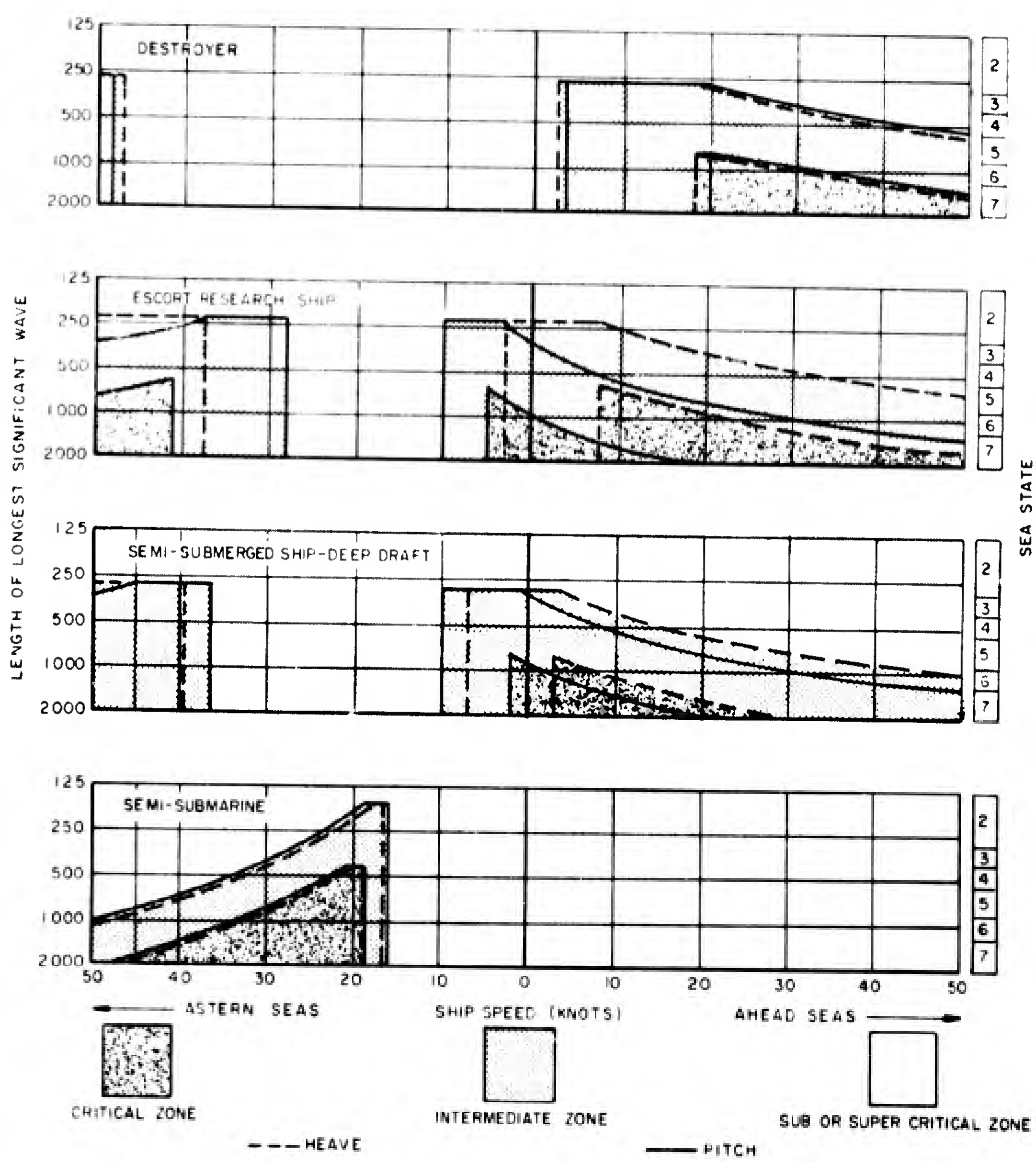

Fig. 13 - Operation zones in rough seas for several unusual ships

seas up to about 15 knots. It is interesting that the analysis correctly infers increased heave activity for the Large Bulb Ship. The figure indicates that reduced motions at high speed can be expected from all the unusual ship forms.

For particular speed ranges, Mandel investigated the extent of each zone area relative to the entire plot area for a given speed range. Figure 14 was so constructed and gives a more direct comparison of the various ships although the probability of a sea state occurrence is not included. It is seen that the Semi-Submarine is superior in the narrow, low and high speed ranges of 0-20 knots and 40 to 50 knots as well as over the entire speed range, 0-50 knots.

Motions data, mostly in regular seas, for these ships, the pertinent dimensions of which are given in Tables 1, 2 and 3, have been obtained at the Davidson Laboratory. Figure 15 shows results for regular 1.0 L head waves. Substantial pitch reductions are realized with both the Large Bulb and Semi-Submerged ships above 10 knots and heave reductions realized above 20 knots. The detuning transfers the severe motions to the low speeds, as predicted. Figure 16 shows that in 2.0 L waves pitch reductions are obtained above 20 knots but both surface type unusual ship forms encounter more severe heave motions over the speed range than does the destroyer. Results in irregular seas for the Large Bulb Ship, Figure 17, show pitch reductions at high speed but substantial heave increases are incurred.

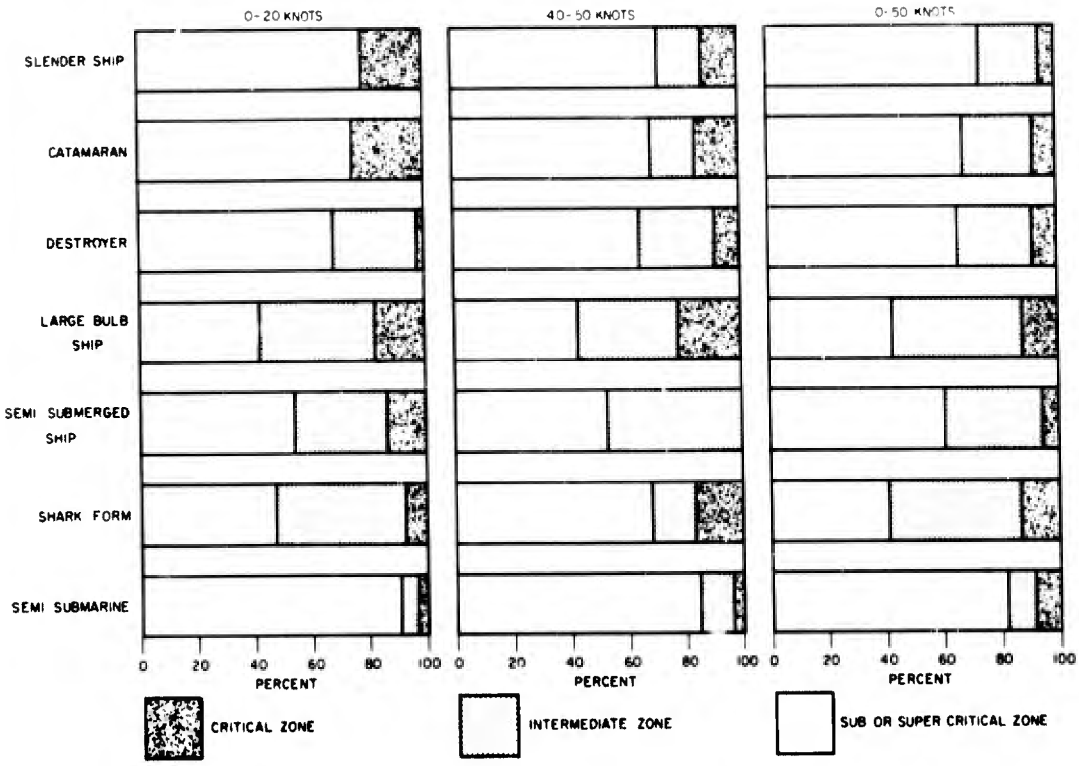

Fig. 14 - Extent of operation zones relative to entire operation range, operation range: State 2 to 7 head and following seas, 0 to 50 knots

Table 1
Hydrofoil Semi-Submarine Principal Data

		Ship	←(λ = 45)→	Model
Length		168.75		3.75
Maximum Diameter, ft.		33.75		0.75
Displacement		2,720 tons		65.3 lbs.
L.C.B. (fwd of midship), ft.		7.8		0.1733 in.
V.C.B. (above body axis), in.		9.45		0.21
V.C.G. (above body axis), in.		3.6		0.08
G.B., in.		5.85		0.13
Radius of Gyration (Long.)		0.22 L		0.22 L
Surface Area, sq. ft.		13,000		6.55
Hydrofoil (NACA 16-009)				
Chord, ft.		15	(20% flap)	0.33
Span (wetted @ d/D = 1.5), ft.		79.0		1.755
Aspect Ratio (planform)		5.26		5.26
Dihedral Angle, degrees		35		35
Area (wetted), sq. ft.		~2,760		~1.38
Horizontal Stern Plane (NACA 16-009)				
Chord Ft.		15		0.333
Span, ft.		33.75		0.75
Aspect Ratio		2.25		2.25
Area (wetted), sq. ft.		22.5		0.50
Vertical Stern Planes (NACA 16-009)				
Chord, ft.	Top	10.75		0.239
	Bottom	15.0		0.333
Midspan, ft.	Top	11.25		0.25
	Bottom	10.60		0.236
Area (wetted),	Top	120		0.060
	Bottom	157		0.0785
Aspect Ratio	Top	1.045		1.045
	Bottom	0.707		0.707

Table 2

Characteristic	Model Data	Full-Scale Data		
	Large-Bulb Model	Large-Bulb Ship	Semi-Submerged Ship	Destroyer
LOA, ft.	7.93	440.7	383.0	391.0
LWL, ft.	6.22	345.7	383.0	383.6
Length of each bulb, ft.	1.704	94.7		
Diam. of each bulb, ft.	0.341	18.9		
Beam, ft.	0.618	34.4	36.4	40.8
Draft, ft.				
Hull, normal displacement	0.309	17.2	13.0	14.1
Bottom of bulb, normal displacement	0.647	36		
Deep displacement			17.0	
Displacement				
Hull, normal	31.50 lb.	2480 LT	2770 LT	3471 LT
Bulbs, normal	12.60 lb.	991 LT		
Total, normal	44.10 lb.	3471 LT	2770 LT	3471 LT
Deep			3835 LT	
$\Delta/(LWL/100)^3$	84	84	68*	62
Water-plane coefficient	0.637	0.637	.57*	.77
Wetted-area coefficient, $WA/\nabla^{2/3}$	9.83	9.83	7.57*	8.07
Longitudinal radius of gyration	.30 LWL	.30 LWL	.27 LWL*	.24 LWL
Natural pitching period, T_p, sec.	1.20	8.9	7.9*	4.9
Period-length ratio $T_p/\sqrt{LWL}$	.48	.48	.40*	.25
Natural heave period, sec.	.84	6.3	6.5*	5.1
Scale ratio	1	55.6		

*At deep draft, achieved by flooding bow and stern peak tanks

Table 3
Shark Form Principal Data

	Ship	Model
Length, ft.	225	4.0
Maximum Diameter, ft.	32	0.571
Displacement (Total)	3,000 tons	56.6 lbs.
Radius of Gyration (Long.)	0.17 L	0.17 L
Wetted Surface (Total) sq. ft.	26,000	8.21
Pitch Period, sec.	21.3	2.5
Heave Period, sec.	13.4	2.0
Strut Length, ft.	14.05	2.5
Strut Maximum Beam, ft.	1.405	0.25
Hull Prismatic Coefficient	0.60	0.60
Strut Prismatic Coefficient	0.60	0.60
Hull and Strut Offsets	see reference 5	

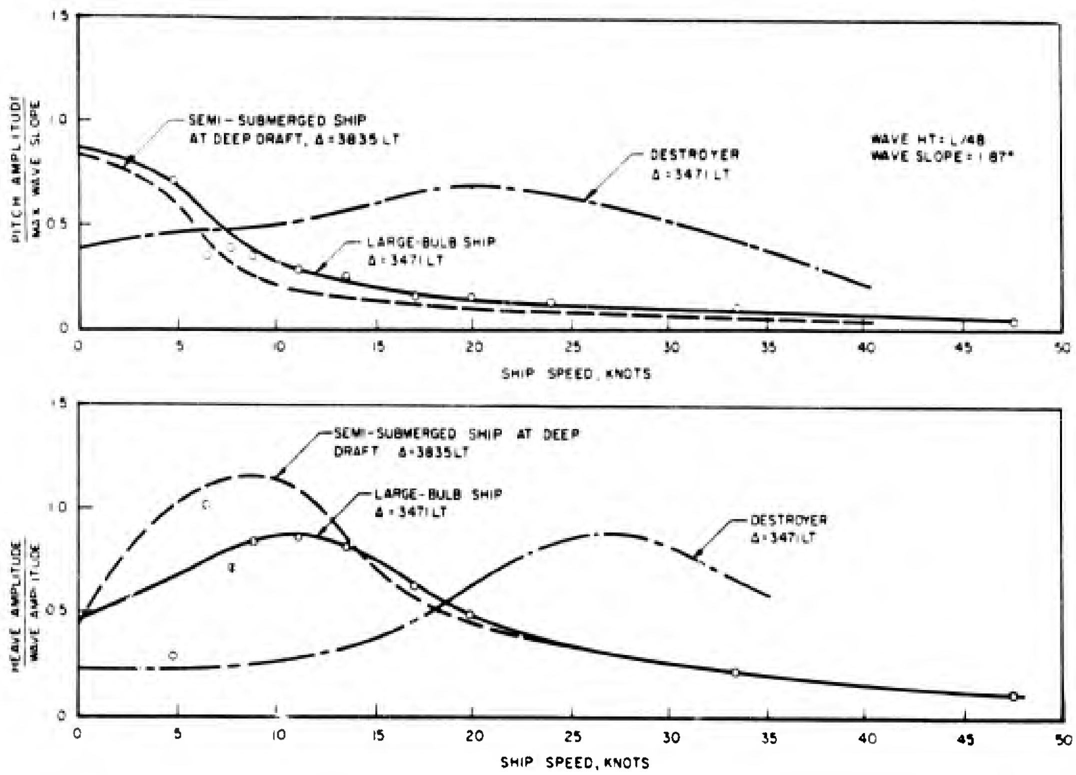

Fig. 15 - Pitching and heaving motions in regular 1.0 L waves

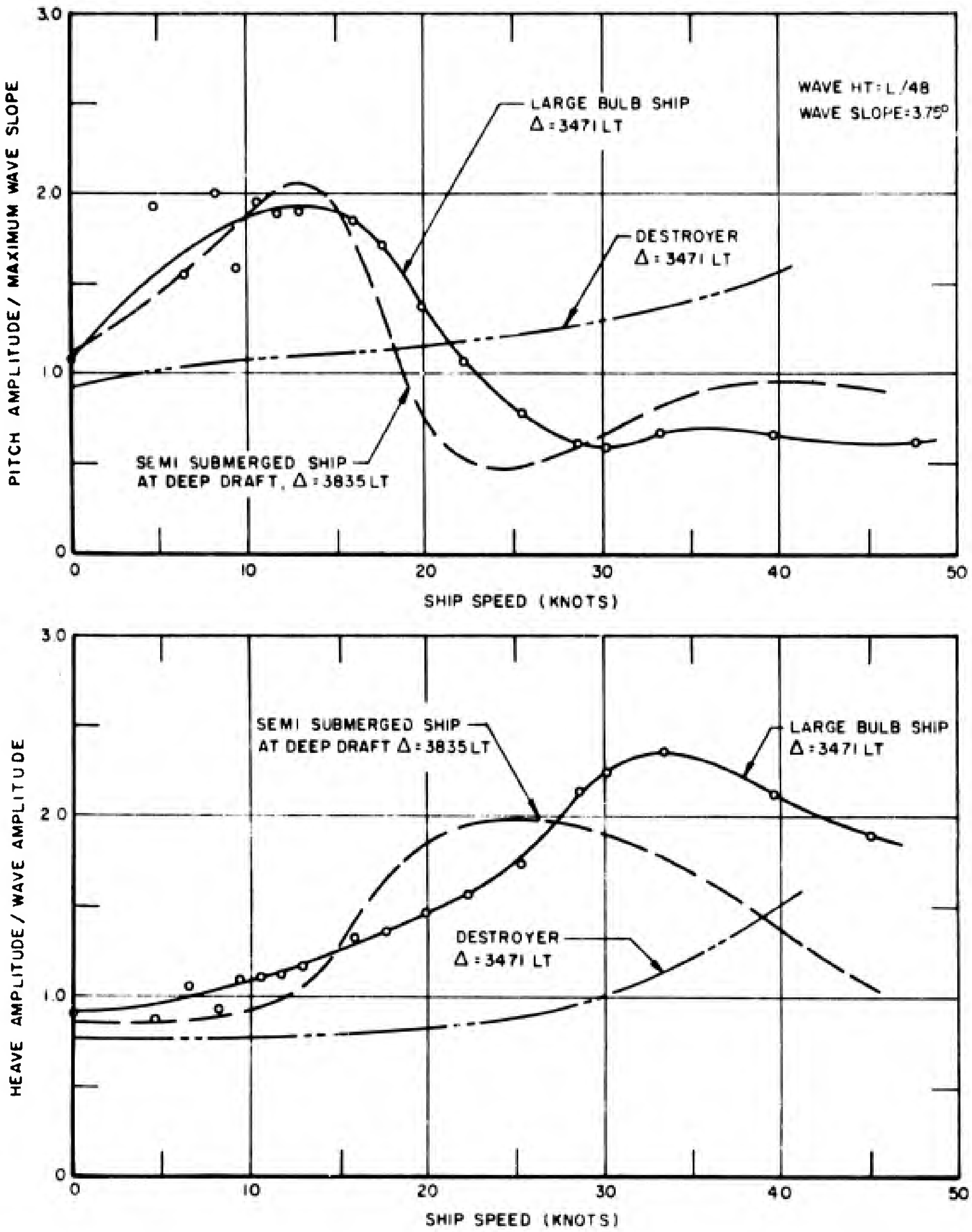

Fig. 16 - Pitching and heaving motions in regular 2.0 L waves

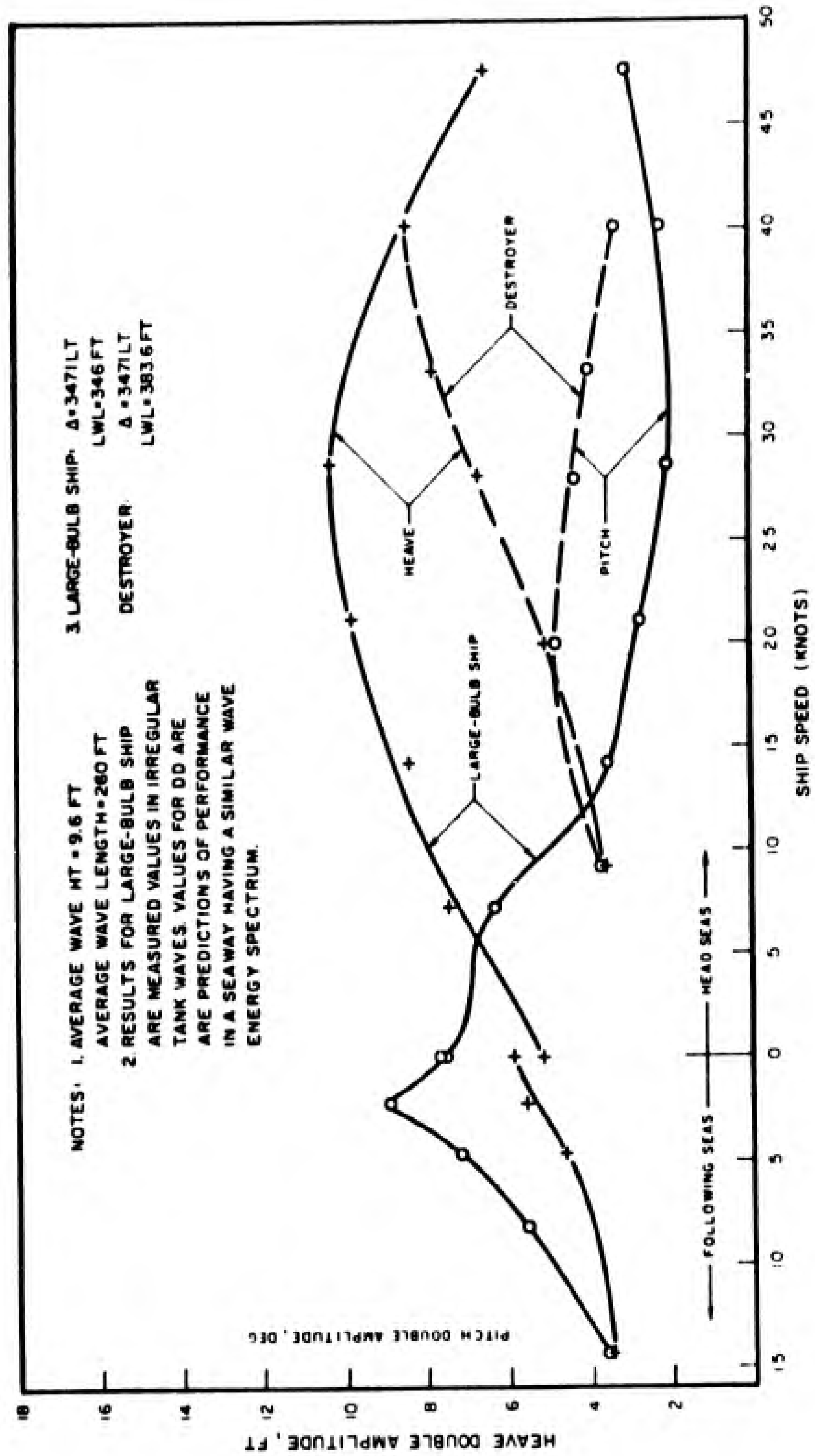

Fig. 17 - Average pitching and heaving motions of L.B.S. in irregular seas

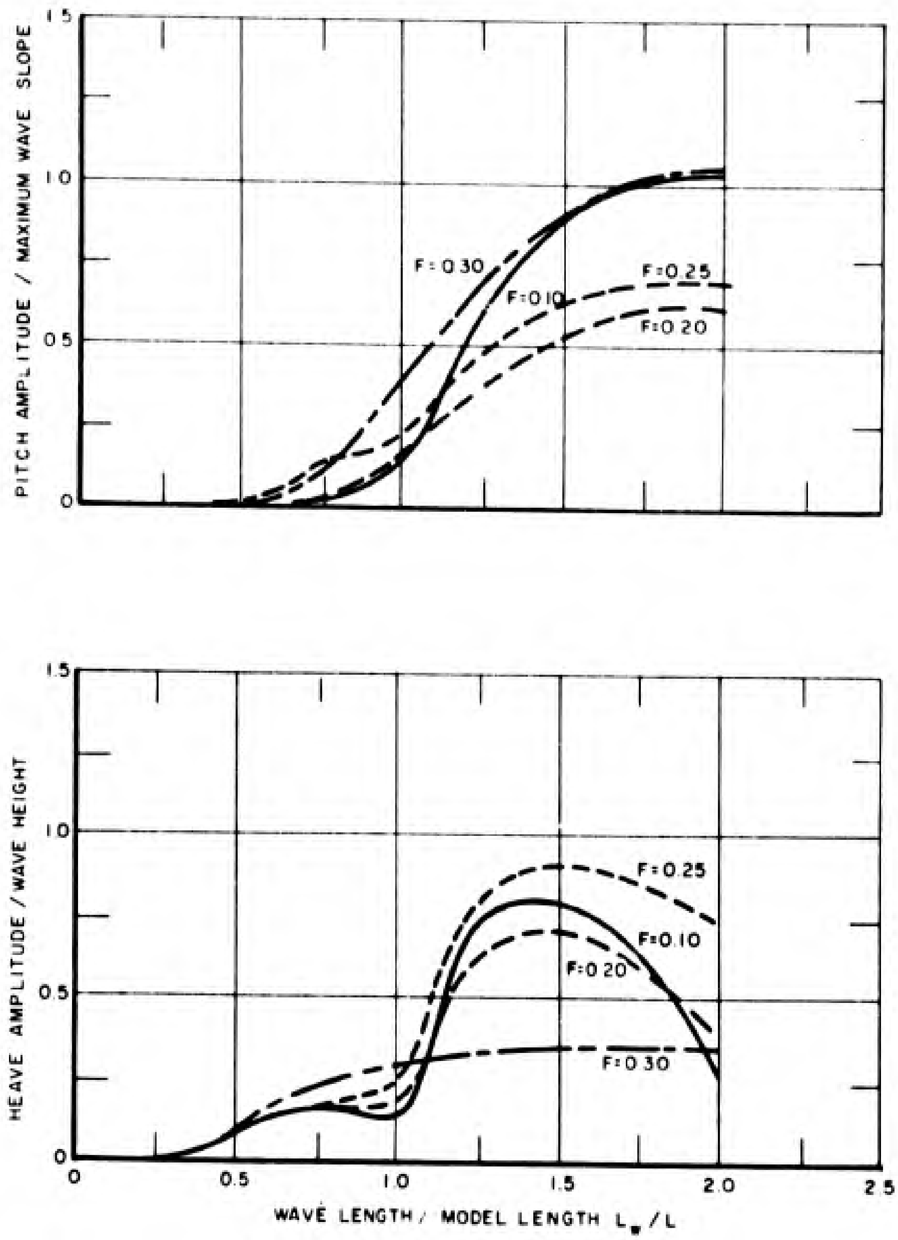

Fig. 18 - Shark form motions

Shark Form motion behavior with varying wave length in following regular seas, obtained at Massachusetts Institute of Technology, over a very limited speed range, 0 to about 10 knots (F = 0.30) is given in Fig. 18. Although, as Mandel points out, the behavior for F = 0.1 is suspect, the behavior at the other Froude numbers gives insight as to influence of wave length on the motions for a given operating speed.

The pitch response of the Hydrofoil Semi-Submarine in 1.0 L and 2.0 L regular waves is presented in Figs. 19 and 20, while the heave response is given in

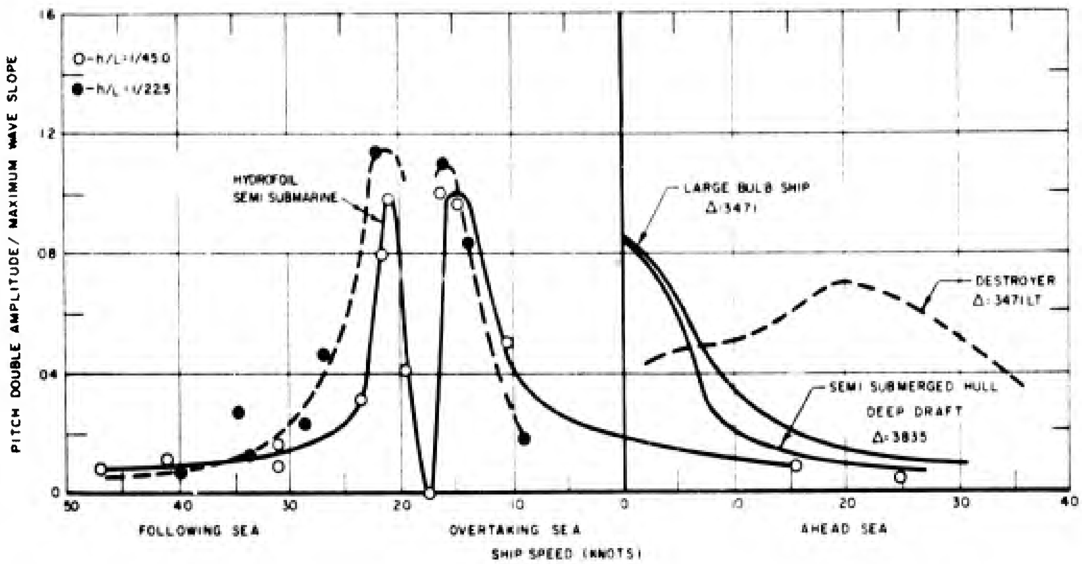

Fig. 19 - Pitching motion in regular 1.0 L waves

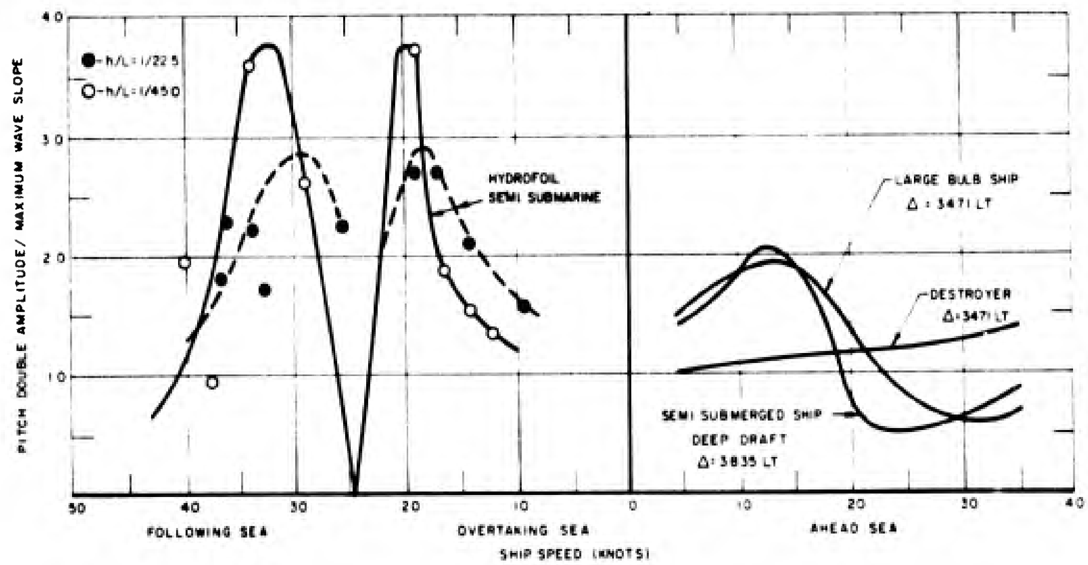

Fig. 20 - Pitching motion in regular 2.0 L waves

Figs. 21 and 22 for 1.0 L and 2.0 L waves, respectively. An interesting comment is in order here concerning the nature of the response. As will be noted, the response data in ahead seas of the other three ships also shown on the figures for comparison, have similar characteristics in that the response reaches a peak under critical conditions and then falls off. However, the response of the Hydrofoil Semi-Submarine contains two peaks instead of one. It was found that for the condition where the ship speed exactly equalled the wave celerity in overtaking

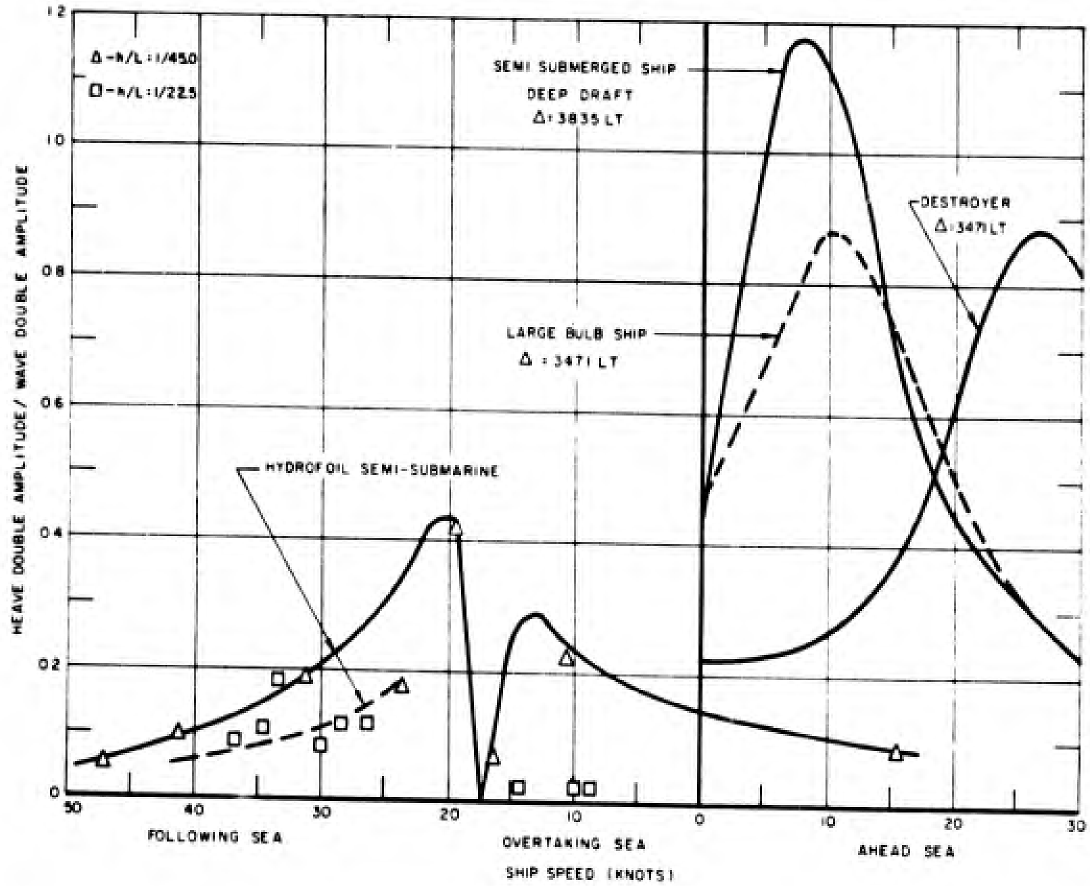

Fig. 21 - Heaving motion in regular 1.0 L waves

seas, the ship "locked in" with the wave pattern and experienced no pitch or heaving motions. It is unfortunate, or fortunate, depending upon how one views the situation, that the model natural frequency and wave-exciting frequency, as well as the model speed and wave celerity correspondence occurred roughly at the same operating condition. In irregular seas, this condition can be expected to occur, but would be of importance only if the wave with celerity correspondence is that wave having a major contribution to the ship excitation.

Figures 19 and 20 indicate that the pitch response of the Hydrofoil Semi-Submarine is indeed critical, as theory predicts, in following seas in the velocity range between 10 and 25 knots. The pitch amplitude response is somewhat larger than the destroyer, but only slightly larger than the Large Bulb Ship and the Semi-Submerged Ship in their respective critical ranges. In 2.0 L waves, the Hydrofoil Semi-Submarine in its critical region has a substantially higher pitch response to the wave system than any of the other three ships. However, it must be pointed out that, whereas in surface vessels very little can be done to control or alleviate the situation because of their inherent very large longitudinal metacentric height and large wave exciting moments, such is not the case for the Hydrofoil Semi-Submarine. The very small longitudinal metacentric height and exciting moments of this type ship afford a great advantage. It would be no problem, with a relatively simple control system, to activate the main foil flaps or the stern plane to counter these motions. Quite possibly, control by manual adjustments of the control surfaces may only be required as the motion picture records indicate the pitch frequency to be quite low.

Figures 21 and 22 present the heave response for 1.0 L and 2.0 L regular waves. Beyond doubt, it is seen that the heave characteristics of the Hydrofoil Semi-Submarine are far superior to any of the ships with which it is compared. Since this ship has an extremely small water plane area, its natural frequency in heave relative to the excitation from the wave system would be very near zero (practically that of a submarine). The heave characteristics, therefore, are more dictated by the hydrodynamic forces resulting from the pitch variations of the ship, its change in proximity to the free surface and the effect of the wave system on vertical force and pitching moment induced upon the ship due to its proximity to the surface, as forcing functions. As indicated, through prudent design this ship concept can be made quite stable relative to the hydrodynamic forces and moments on the ship and large heave motions can be avoided.

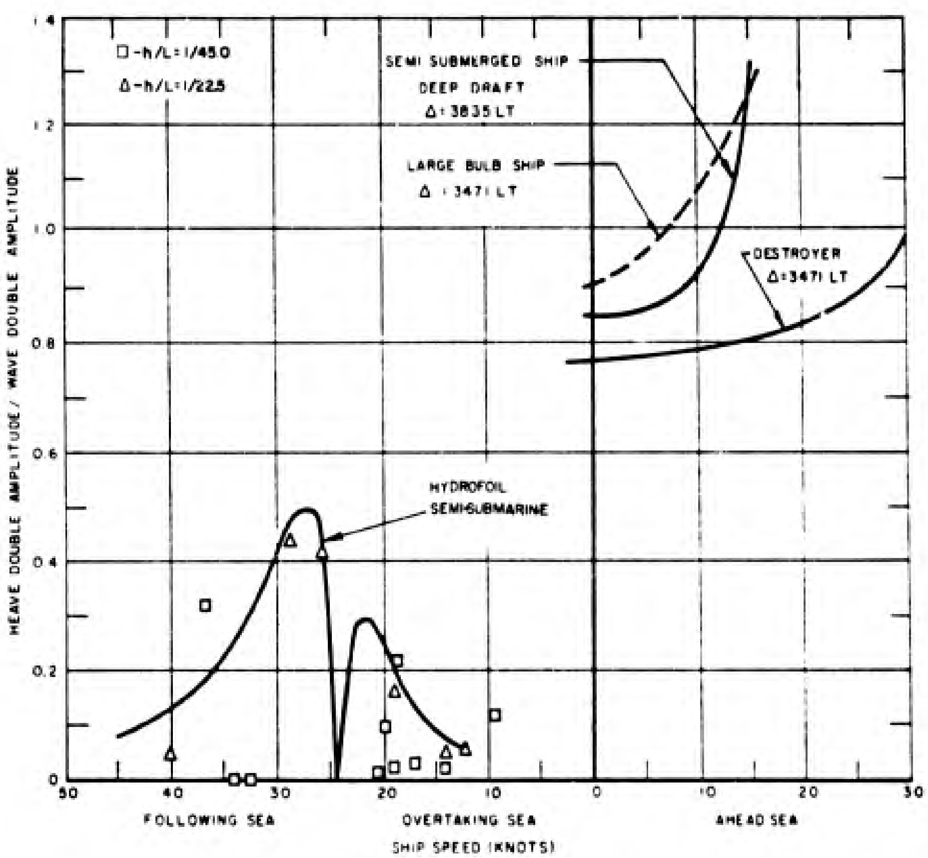

Fig. 22 - Heaving motion in regular 2.0 L waves

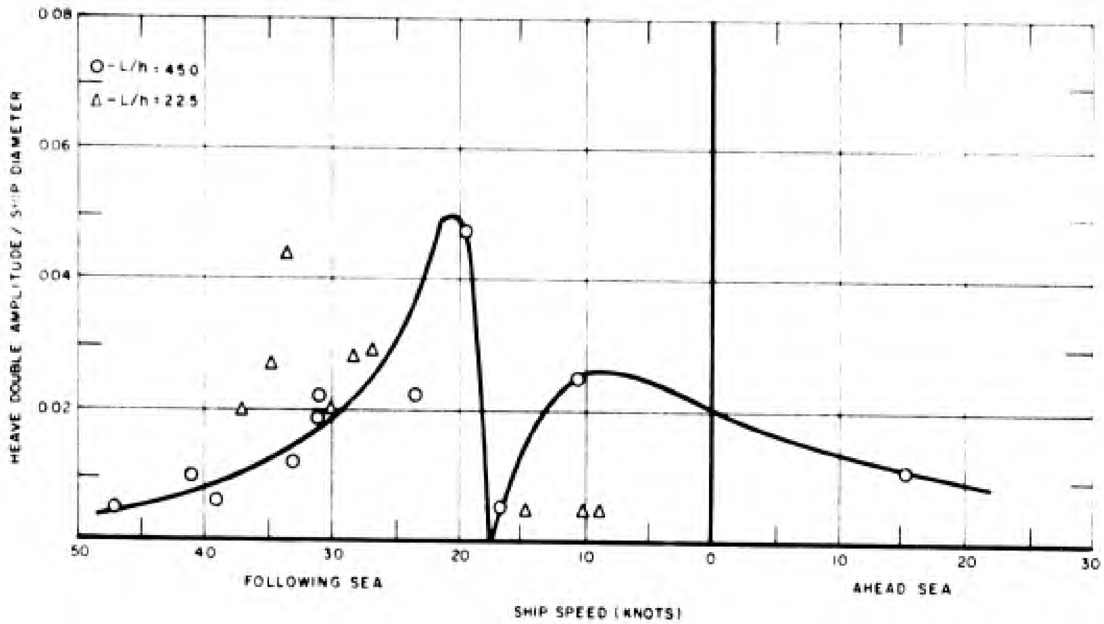

Fig. 23 - Heave double amplitude/ship diameter in 1.0 L waves (hydrofoil semi-submarine)

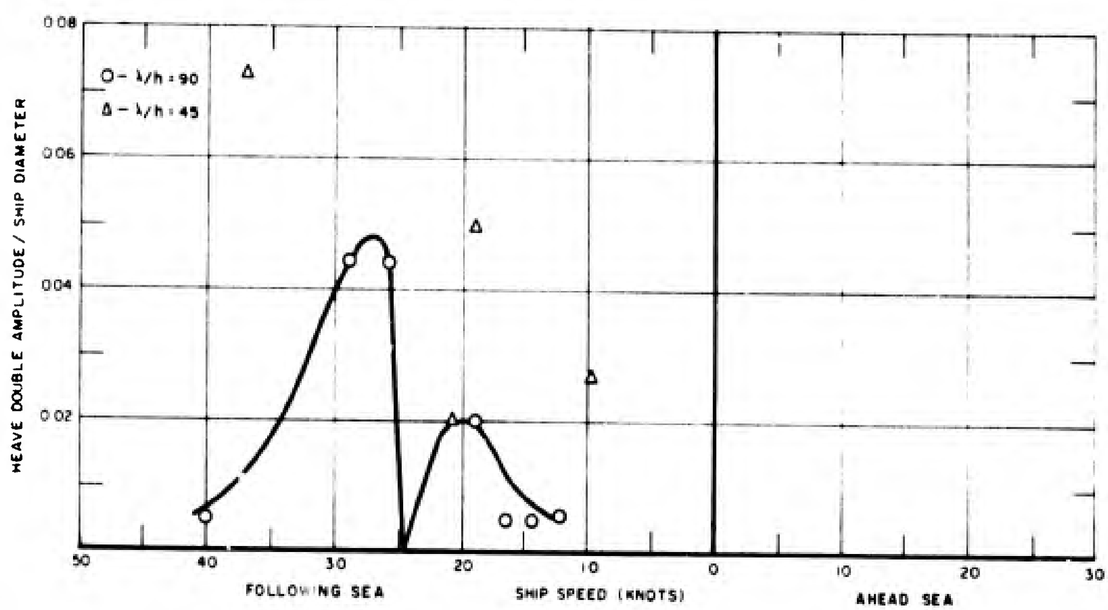

Fig. 24 - Heave double amplitude/ship diameter in 2.0 L waves (hydrofoil semi-submarine)

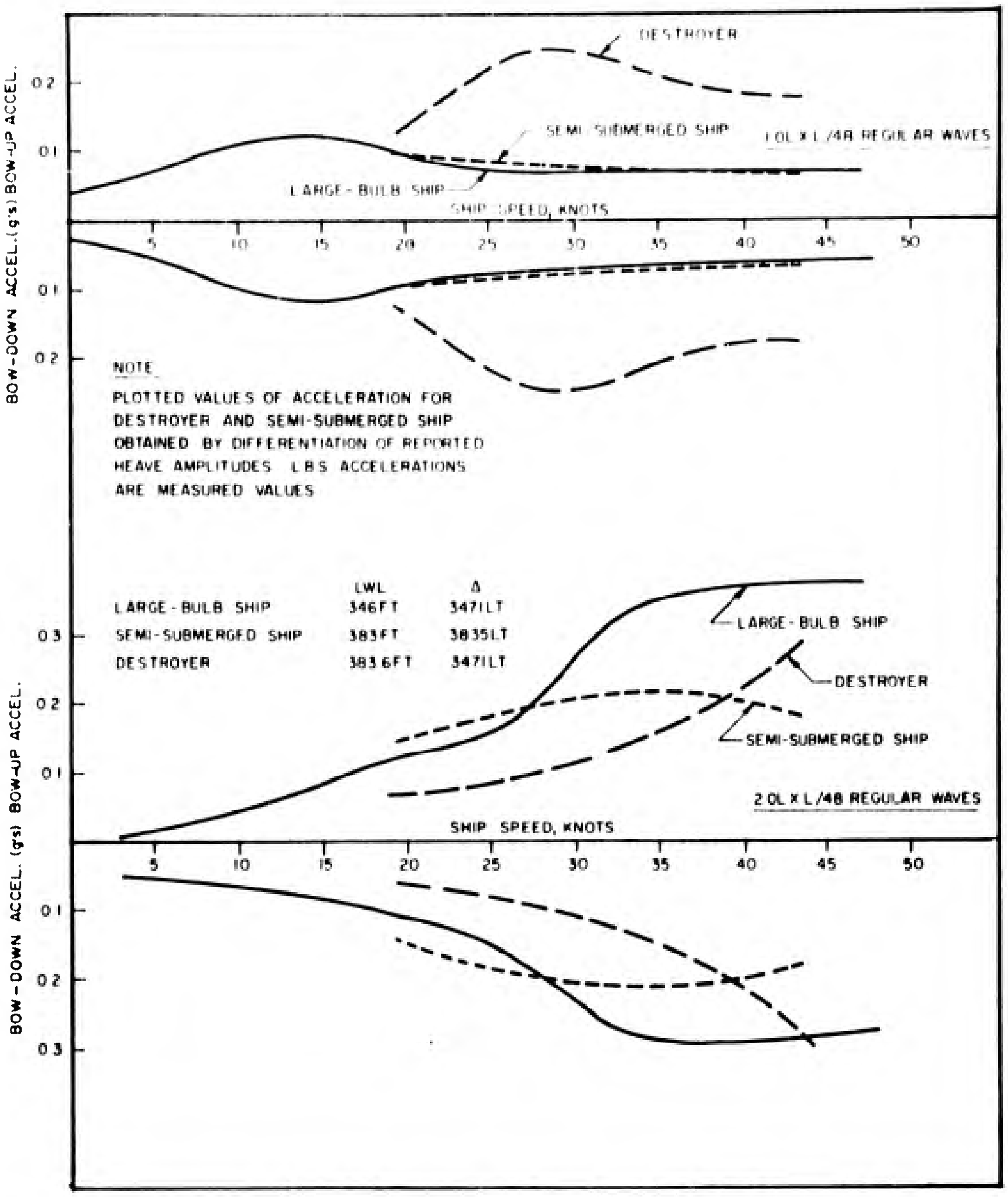

Fig. 25 - Comparison of heave (C.G.) accelerations in regular waves

Finally, in Figs. 23 and 24, it is of interest to show the heave amplitude relationship to the ship diameter for the Hydrofoil Semi-Submarine since it is of importance that this ship traverse a limited corridor in the vertical plane. These figures show that for either wave condition and for various wave heights the ship rarely can be expected to traverse, above or below its equilibrium running depth, distances greater than 3% of the ship's diameter.

Part of the acceleration data obtained by VanMater [7] is shown in Fig. 25. It is seen that in 1.0 L regular waves the unusual surface ship forms are superior to the destroyer, while in 2.0 L regular waves they offer greater accelerations. No acceleration data was obtained for the Hydrofoil Semi-Submarine, but, as we will see, a study of the motion picture records indicates the pitching motions are of low frequency, resulting in relatively low pitch accelerations.

It has been our pleasant task to attempt to collect and summarize the work done on unusual ship forms and realizing the inadequacy imposed by space and time limitations, we hope we have furnished an up-to-date balance sheet to aid those interested in possible application of the unusual ship form concepts.

REFERENCES

1. Third Symposium on Naval Hydrodynamics, Office of Naval Research ACR-65, September 1960

2. Lewis, E. V., "Ship Speeds in Irregular Seas," SNAME Volume 63, 1955, pp. 134-174

3. Mandel, P., "Subcritical and Supercritical Operation of Ships in Waves," SNAME Journal of Ship Research, Volume 4, No. 1, June 1960

4. Uram, E. M., "Research on High Speed Ship Forms," 4th Seminar on Ship Behavior at Sea, June 1962, Davidson Laboratory TM 136, January 1963

5. Mandel, P., "The Potential of Semi-Submerged Ships in Rough Water Operation," New England Section SNAME March 1960. (See also Sahlgren, J. A., "The Performance of a High Speed Displacement Ship in Critical and Supercritical Operation", SM Thesis, MIT, 1959)

6. Lewis, E. V. and Odenbrett, C., "Preliminary Evaluation of a Semi-Submerged Ship for High Speed Operation in Rough Seas," SNAME Journal of Ship Research, Volume 3, No. 4, March 1960

7. VanMater, P. R., "Preliminary Evaluation of a Large-Bulb Ship for High Speed Operation in Smooth Water and Rough Seas," Davidson Laboratory Report 834, May 1964

8. Uram, E. M., "Study of the Design and Behavior of a Hydrofoil Semi-Submarine," Davidson Laboratory Report 1023, August 1964

9. Mandel, P., "A Comparative Evaluation of Novel Ship Types," SNAME Trans. Volume 70, 1962

* * *

DISCUSSION

E. V. Lewis
Webb Institute of Naval Architecture
Glen Cove, Long Island, New York

This paper presents results of an interesting and important investigation into a possible means of obtaining higher speed in an air-breathing near-surface ship. This ship shows superior resistance characteristics in comparison with other ships at speeds above 35 knots, in both smooth and rough water. The ingenious hydrofoil strut design provides an excellent solution to the problem of stability in a vertical plane, enabling the craft to maintain constant depth below the surface.

An interesting feature of this hydrofoil semi-submarine is its motions in waves. Its long natural periods of heaving and pitching result in "supercritical" conditions of operation for all head seas. It is only in astern seas that large motions are experienced, and since the periods of encounter are very long, accelerations must be low. It thus appears clear that such a craft would be an excellent complement to a more conventional type of surface craft: the former would be able to make high speed in head seas and the latter in astern seas. Operational studies should be made to evaluate the effectiveness of pairs of such ships working together in A.S.W. and other naval missions.

A SURVEY OF SHIP MOTION STABILIZATION

Alfred J. Giddings
Bureau of Ships
Washington, D.C.

and

Raymond Wermter
David Taylor Model Basin
Washington, D.C.

ABSTRACT

A brief historical review of significant developments in stabilization is presented. Some recent investigations in roll are discussed followed by a survey of the progress and potentialities of pitch stabilization. The important differences between pitch and roll stabilization are examined, and the reasons for the greater difficulty of the former are discussed. Since pitching, relative to rolling is not a sharply tuned resonant phenomenon, large magnitude moments are needed to develop appreciable effects. Model test results are presented to indicate the degree of stabilization possible and the vibration problem associated with bow fin installations is examined. The effects of configuration, platform area and aspect ratio are also mentioned.

INTRODUCTION

Stabilization of ship motions can be considered in a very broad sense, or in a narrow sense. In the broadest sense, consideration should be given to static stability, motion amplitude and controllability in each of the six degrees of freedom of rigid body ship motions. A more narrow view might consider only the limiting or prevention of one of the motions. It is the aim of this paper to strike a middle ground, recognizing that there are significant and undesirable motions in all six degrees of freedom, but expanding only on those of particular interest.

It is advisable to define what is meant by "stabilization" in this paper. By this is meant the deliberate limiting of a ship motion caused by waves, which motion is otherwise stable. With this definition, automatic steering of a directionally unstable ship, or of a stable ship in calm waters are only of passing interest while the more obvious cases of pitch and roll "stabilization" in a seaway are of definite interest.

A cursory examination of the literature on ship motions and stabilization reveals some interesting trends. The principal interest of those writing on prediction of ship motions has been in the longitudinal plane, while in contrast, the writers on motion stabilization have been more interested in the lateral motions. This may well be due to the almost linear and seemingly manageable nature of pitch and heave motions which attracts theorists away from nonlinear rolling and turning problems, while the highly commercial nature of roll and course stabilization has attracted inventors and engineers.

The paper will provide a brief survey of the state of the art in stabilizing the motions of translation, course keeping, roll stabilization and pitch stabilization. The latter of these is to be the subject of a more elaborate discussion.

SURVEY OF THE ART

Translatory Motion Stabilization

The deliberate stabilization of translatory motions of conventional ships has very little technology or theory to survey. While it could be said that mooring problems are problems of stabilization and control of lateral translation, the process of mooring is more an art in the classical sense than in the scientific sense.

Shipboard devices which affect lateral motion directly include bow thrusters, vertical axis propellers and right angle drives. The application of these devices to conventional ships has been for purposes other than "stabilization," as defined in this paper.

In the case of submarines, hydrofoils, and ground effect machines, the control of vertical translation has received a great deal of attention, but this subject would warrant an extensive survey of itself, beyond the scope of the paper.

It should be recognized that the physics of ships is such that pitch and heave, yaw and sway, and roll and sway are so strongly coupled that control or stabilization of the angular partner of each couple inevitably affects the other. The effect on translatory motion is a by-product of the angular stabilization, rather than a deliberately sought objective.

Translatory accelerations on the order of one-tenth of gravity are not unusual. In order to have significant direct effects on such motions, control forces on the order of 5 to 10 percent of the ship weight would be needed. Generation of such forces by direct means is impracticable.

Yaw Stabilization

Stabilization or control of yaw is the most ancient of stabilization problems. It is actually not vital that a ship be stable in yaw, but it is vital that it be controllable. Provision of adequate stability and controllability for ships is such an obvious necessity, that years of tradition and experience provide useful design rules. References 1 and 2 provide useful information on the selection and design of rudders. The many Naval Architecture text books also offer practical methods leading to design of directionally stable and controllable ships.

There have been analyses of the forces and moments in yaw exerted by a seaway, especially Refs. 3, 4, 5, and 6. The inherent stability on course of ships is discussed in Ref. 7, and the automatic control of directionally unstable ships is treated in Ref. 8. The general subject of automatic steering control is treated in Refs. 9 and 10. Additional references on the subject are [11] and [12].

In general, yaw stabilization or course-keeping has been in the province of commercial developments. The devices and methods used are largely proprietary, and their success is evident from their widespread use. Even without automatic systems, the control of a well designed ship in a seaway is well within the capabilities of skilled men.

Roll Stabilization

General Discussion

All ships are stable in roll in that a properly loaded intact ship will not capsize, so that roll stabilization is really roll angle limitation. In contrast to the yaw case, as long as rolling is a stable motion, it need not be "controllable." There is an extensive background of experience on the control of roll in a seaway. The subject has fascinated inventors since steamships were invented, and the general subject is dominated by inventions. A glance through the patent office files on roll stabilization reveals not only the bad drafting favored by patent attorneys, but evidence of the highly imaginative approaches generated by the problem.

The roll stabilizers can be divided into two major groups, internal to the ship and external. Each of these can be further divided into active and passive types. Table 1 categorizes stabilizers from a mechanical point of view. Chadwick [13] offered a more elegant and complete categorization based on the dynamics involved.

Bilge Keels

The earliest deliberate roll damping devices were bilge keels, fitted to steamships to make up for the roll damping lost when the sails were removed. References 1 and 14 present curves of bilge keel size as a function of ship size, based upon experience with ships in the past. References 15 and 16 present experimental results on the forces acting on bilge-keel-like plates oscillating in water. It is rare that an occasion requiring more than rule of thumb design of bilge keels will arise, but when such a case is at hand, analysis of bilge keel forces can be carried out using simple concepts and data such as that cited.

Bilge keels can be counted on to increase hull damping in roll by 50 to 100 percent. This will result in 25 to 50 percent reduction in roll. It must be remembered however, that the principal advantage of bilge keels is found at low speeds. As ship speed is increased the hull damping increases proportionately

Table 1
Classification of Anti-Roll Devices

	Internal	Percent of Ship Weight	External	Percent of Ship Weight
Active, up to 85 percent average stabilization	Active Tanks	1/2 to 1	Fins, Flapped and Plain	1/4 to 1
	"Sperry" Gyroscopes	2 to 3		
	Moving Weights	1 to 2		
Passive, about 50 percent average stabilization	Frahm Tanks	1/2 to 1-1/2	Bilge Keels	1/2 to 1
	Free Surface Tanks	1/2 to 1-1/2	"Fishermans" Keels	1
	"Schlick" Gyroscopes	5	Fin Keels	1
			Staysails	1/2 to 1

more than the bilge keel damping. There is a small increase in hull inertia due to bilge keels, but the principal effect is increased hull damping. Historically, bilge keels have been discussed in the literature by White [17] and Spear [18], followed by many individual model test reports on specific designs, too numerous to mention.

Certain fishing craft are reported to use a technique for roll reduction while adrift. Booms are rigged out over each side, and lines carrying weighted drogues are lowered into the water. As the boat is rolled, it tends to pull up one of the drogues which provides damping, while the other drogue sinks. The ubiquitous staysail is also used for roll damping by boats throughout the world. There may well be other unique and homely devices used on boats in specific instances.

Anti-Rolling Fins

Anti-rolling fins have had a relatively long history. References 59 and 60 are among the earliest references to this form of roll stabilization. Chadwick [13] gives a good historical view of fin stabilization, and Bell [21] discusses the history of fin controls. In general, progress in fin stabilization has been characterized by a series of inventions, each limited more by the state of the art in automatic controls rather than in hydrodynamics or mechanical engineering. Only within the past fifteen to twenty years has it been possible to design and analyze fully automatic controllers through straightforward engineering, rather than through inventive inspiration and insight.

The current state of the art in fin stabilizers is shown by Chadwick [13], DuCane [22] and Flipse [23]. The latter commendably frank reference, along with Ref. 24 discuss actual performance at sea of specific installations, while Chadwick, Bell, and DuCane deal with control theory and design.

Various types of fins are used by the different manufacturers. There are articulated-flap fins and simple fins, both tapered and untapered. The range of aspect ratios selected depends on the method of retraction, or lack of retraction. The hydrodynamic design of fins [25] is influenced strongly by maximum lift coefficient as limited by cavitation and the free surface, while lift curve slope and low drag considerations are not very important. Unsteady effects on lift slope are not significant, even considering the high tilt rates required. There is evidence [26] that the maximum lift coefficient is augmented by unsteady effects, but use of this phenomenon in design is not widespread. Unsteady effects must be included in the computation of tilting torque. The torque loads proportional to acceleration and velocity are significant, and if not allowed for, the slow response of the fins to control system orders could be embarrassing.

In those cases where flapped fins have been specified by designers, cavitation must have been a principal consideration. For merchant ships, wherein cruising speed and full speed are nearly the same, the design speed for the fins is relatively high. To economize on fin size, the desired stabilization capacity is provided with the fins producing nearly their maximum lift coefficient. Under these conditions, the more uniform pressure distribution on flapped fins is beneficial. For warships, or ships having a cruising speed much less than maximum, the design condition for the fins is not as severe. Large lift coefficients are required only at cruising speed, and the fin angle is limited at higher speeds to maintain the stress level in the stock. At speeds where cavitation would be a concern, only small lift coefficients are required. For this reason, plain fins may be used. The elimination of the flap actuator and flap hinge structure may in turn save enough weight to compensate for the increased area of a plain fin.

Stabilizer fins are usually located in pairs, port and starboard. If more than one pair is to be installed, the downwash effects of the forward fins upon the flow to the after fins must be considered.

Most modern roll control systems use combinations of roll angle, roll velocity and roll acceleration to generate ordered fin angles. The "Denny Brown" types order fin angle [21] while the Sperry type orders fin lift [13,23] using a deflection gage within the fin to feedback the lift. Earlier control systems used much simpler concepts, having been analyzed and designed to deal with regular waves. As experience with real seas and the ability to analyze random seas has accumulated, more sophisticated controls have been adopted [21].

It is possible to design control systems to minimize any of several parameters of the motion. The most common index of performance is roll angle reduction, although roll velocity or acceleration could be the factor of most interest. References 27 and 28 are two of many papers in the control system literature which discuss designing to minimize various energy criteria. Minimum energy demand on the stabilizer, or minimum energy of residual motions are but two of the possibilities. How much benefit such refined techniques might give to ship motion reduction remains to be seen.

Model tests of anti-rolling fins, either alone or on ship models, have not been reported in the open literature. As more and more model tanks develop the ability to generate random model seas, perhaps greater use of ship model testing to prove out design concepts will result. Factors such as the interaction of bilge keels and stabilizer fins, yaw-heel, and the interaction of a passive tank stabilizer with active fin stabilizers could be examined on model scale. Even without wavemakers, model tests using rotating eccentric weights or other roll moment devices can be of use in examining the hydrodynamics of stabilizers.

Stabilizing Tanks

Anti-rolling tanks have had a checkered history. Since Froude's first speculations [29] a great variety of tank installations have been tried, with different degrees of success. Until recent times, the most successful of these were Frahm tanks [30] either cross-connected within the ship, or with port and starboard tanks open to the sea. More recently, passive tanks with free-surfaced cross connections have been successful [31]. Active tank stabilizers have not had a successful past, but the future looks brighter.

A series of reports by Chadwick [20,32] analyze the dynamics of both active and passive anti-roll tanks. This analysis for passive tanks was extended slightly in Ref. 31. Blagoveschensky [33] presents a simplified analysis for passive tanks open to the sea. Hydronautics, Inc. under the sponsorship of the Bureau of Ships is currently conducting a theoretical study of active anti-roll tanks. This study will once again reanalyze the equations of roll motion as presented by Chadwick to insure that all significant nonlinear terms are properly included. Pumping rate specifications and tank design criteria will be established and it is hoped that sufficient information will be generated to permit a successful design.

The recent success of the free surface type passive tanks compared to the narrow acceptance of Frahm tanks is due to several factors. The high internal damping due to wavemaking in free surface tanks makes precision of design less demanding than for Frahm tanks. The tank response curves are flatter, and highly nonlinear in a fashion kind to the designer. The recent trend for ship design to be controlled more by volume than weight has also made it easier for the owner to accept the weight of tank stabilizers.

Application of theory to describe the action of Frahm tanks was shown to be fairly successful (Chadwick [20]) in that assumption of linear damping within the tank gave fair approximations to the model test results. Little agreement has been found for free surface tanks. The theory developed in Ref. 31 included a provision for equivalent nonlinear tank damping evident from model test results. In addition, the U-tube analogy for computation of the natural frequency of free surface tanks has been shown to be somewhat inaccurate. Reference 58 presents some corrections, based upon basic shallow water wave theory compared with experimental results.

An additional comparison is presented here. As derived in Refs. 30 and 31, the natural frequency of oscillation of the fluid in a U-tube can be found from

$$\omega_u = \sqrt{\frac{2g}{S}} \tag{1}$$

where

ω_u = tank frequency, by U-tube analogy, and

S = effective length of the U-tube.

$$S = \int_0^L \frac{A_o}{A}\, ds \tag{2}$$

where

A_o is the area (constant) of free surface in one "wing tank" of the U-tube,

A is the cross section area of the U-tube normal to the U-tube centerline,

s is the girth-like coordinate along the centerline, and

L is the total "girth length" of the centerline.

In the case of a free surface tank, the U-tube analogy is applied by assuming that the U-tube centerline is as shown in Fig. 1a.

Reference 34 presents an approximate solution for the natural frequency of a tank of the configuration shown in Fig. 1b,

$$\omega_L = \sqrt{\frac{\pi g}{S'} \tanh \frac{\pi h}{S'}} \tag{3}$$

where

ω_L = tank frequency, by "exact" theory,

S' = "effective beam of tank," and

h = fluid depth.

The effective beam of the given tank configuration is shown by Lamb to be

$$S' = B + \frac{2\pi r^2}{\ell_t} . \tag{4}$$

Relating the two methods of calculating frequency;

$$\frac{\omega_u}{\omega_L} = \sqrt{\frac{2(1+S)\coth\left(\frac{\pi a}{1+\frac{2}{S}}\right)}{\pi a}} \tag{5}$$

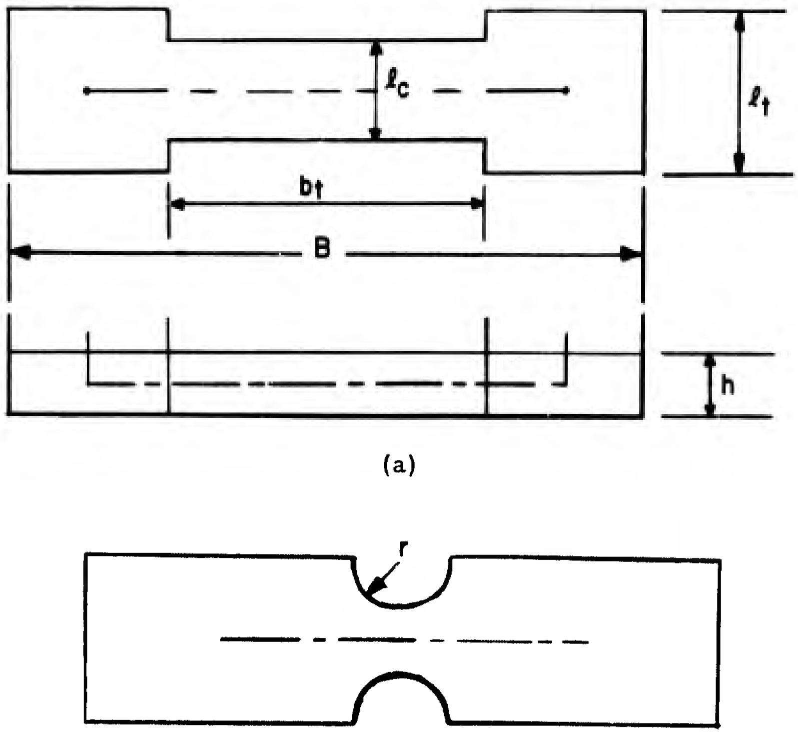

(a)

(b)

Fig. 1 - Typical tank configuration

where

$$\xi = \frac{2\pi r^2}{B\ell_t}$$

$$a = h/B$$

$$\tau = S/B .$$

Applying Eq. (2) to the computation of τ for the configuration shown yields:

$$\tau = a + \frac{\left(\frac{1}{2} - \frac{r}{B}\right)^2}{a} + \frac{\left(\frac{1}{2} - \frac{r}{B}\right)}{a} \frac{\ell_t}{B} \left[-\frac{\pi}{2} + \frac{\ell_t}{r\sqrt{\frac{\ell_t^2}{4r^2} - 1}} \tan^{-1} \sqrt{\frac{\frac{\ell_t}{2r} + 1}{\frac{\ell_t}{2r} - 1}} \right] . \qquad (6)$$

Table 2 indicates that the U-tube analogy can be used, with appropriate care, as an approximation to a more precise theory, at least for this particular family of tank geometrics.

Table 2
Comparison of a U-Tube Analogy with Theory

r/B	0	.04	.06	.08	.09	1.0
$\frac{\omega(\text{U-tube})}{\omega(\text{Lamb})}$	.90	.916	.916	.861	.762	0

Active Internal Systems

This paper will not elaborate on moving weight or gyroscope systems. It can be said that moving weights have an attraction due to the possible high density of such an installation. It may be that the effective density of a moving weight system, after including the volume needed for the operating machinery, necessary to move the weights and safety devices, would be about the same as that for a tank system. The additional property of a solid weight system that there is no loss in hydrostatic stability when at rest is also attractive. However, there is no active research or development known to the authors in this field. Reference 35, besides being interesting reading, contains a good discussion of the first successful moving weight installation.

Gyroscopes, both passive and active have been installed in many ships in the past. References 36 and 37 discuss early installations. The dynamics of both types of gyroscopes are analyzed by Diemel [38]. Their great weight and the engineering difficulties of highly loaded bearings have limited their acceptance. The most recent installations of gyrostabilizers was in POLARIS submarines, where they performed well enough, but changes in operational concepts caused their removal.

Recent Applications

A limited number of naval installations have been completed or studied since the recent paper by Vasta, et al. [31]. These have usually all been in an area requiring stabilized gun, launching, or search platforms. Oceanographic research ships have all been considered for the installation of passive tank systems in recent years.

The recent studies conducted on passive anti-roll tanks and active anti-roll fins will be discussed. The results of full scale trials and/or model tests will be presented.

Interpretation of full scale tests requires care. To quote Pierson [39], "The surface of the sea is a mess." This complicates the roll records. It is rare that the statistical properties of the sea remain static long enough to complete the schedule of trials necessary for a good evaluation. The trial analysis therefore demands a good deal of judgment on the part of both the analyzers and the readers, especially without good measurements of sea conditions.

USNS ELTANIN — Passive Tanks. The USNS ELTANIN (TAK 270) was converted from a cargo ship to a scientific research ship of 3330 tons displacement.

Anti-roll tanks were installed in late 1961 and full scale sea trials were conducted by the David Taylor Model Basin in December 1961 [40]. Figure 2 shows a photograph of the ship and indicates the general tank location while Fig. 3 presents a schematic sketch of the tanks. These tanks displace 75 tons when filled with 6.5 feet of water. The trials were conducted over a three-day period and Figs. 4 and 5 show the measured sea spectra.

(a) External view of tanks from starboard side

(b) External view of tanks looking forward from bridge

Fig. 2 - Location of tanks on the ship

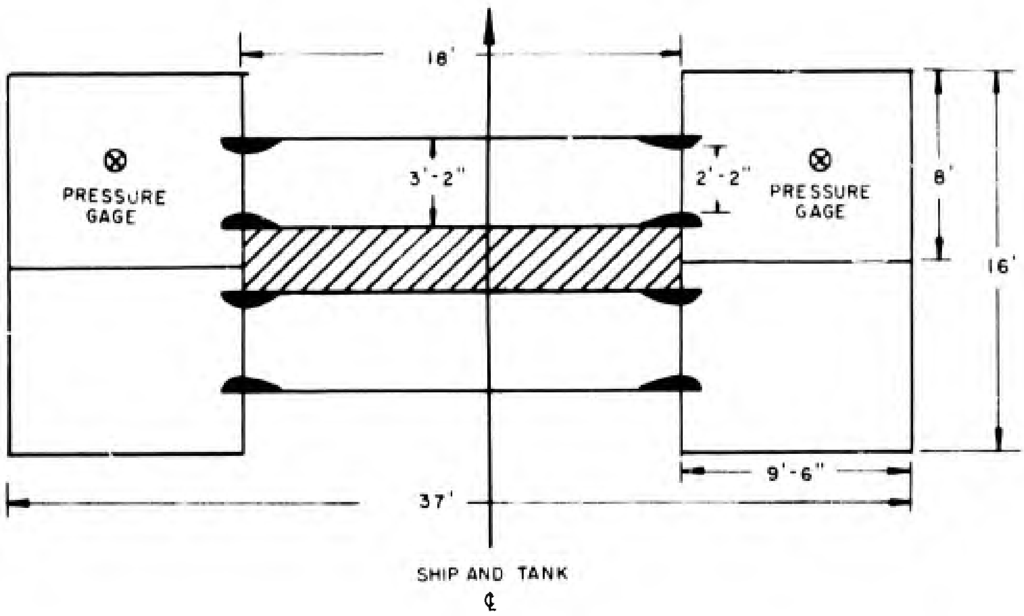

(a) Top view

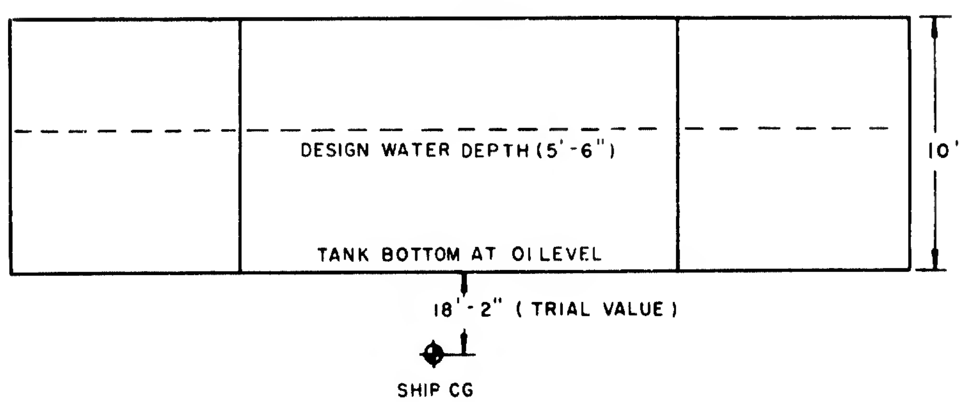

(b) Side view

Fig. 3 - Sketch of principal dimensions of tank system

Tank tuning experiments were conducted over the three-day period in the several seas encountered and while the results of these experiments as plotted in Fig. 6 indicate that an optimum water depth had not been achieved, it would appear that 6.5 feet of water yields a reasonable operating condition. Figure 7 presents the effect of sea angle encounter. The sea spectra curves presented in Fig. 5 indicate extreme variations in sea conditions and consequently, the test results presented by Fig. 7 cannot be interpreted as indicative of representative trends without extensive interpolation between sea spectra.

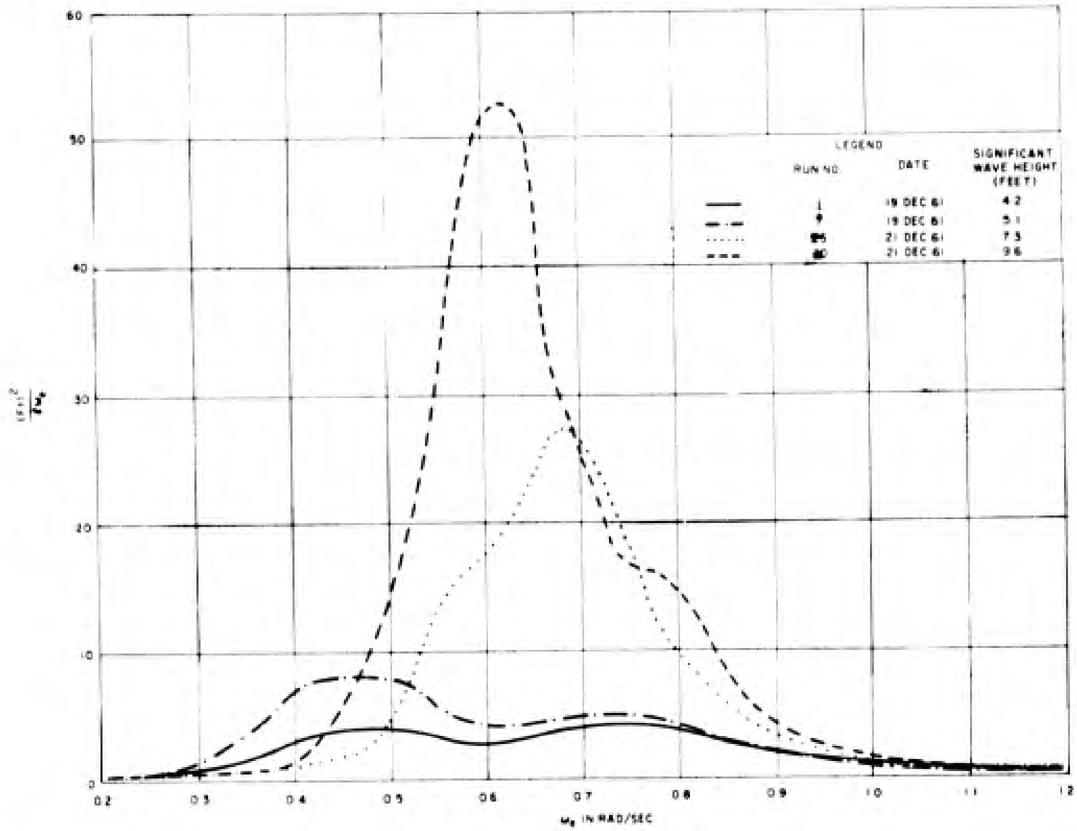

Fig. 4 - Sea spectra as measured (ing trials of first and third days

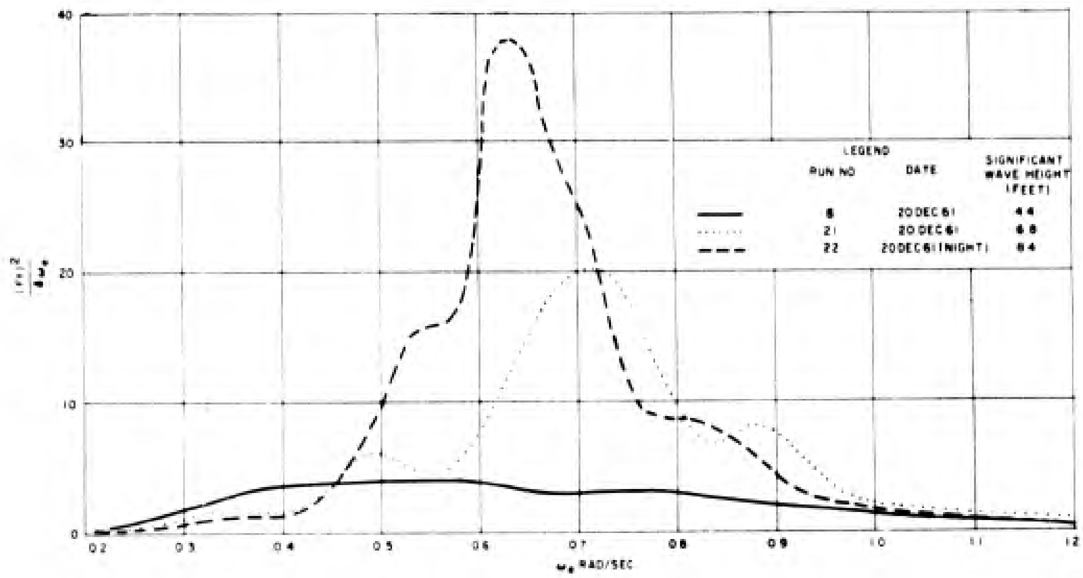

Fig. 5 - Sea spectra as measured during trials of second day

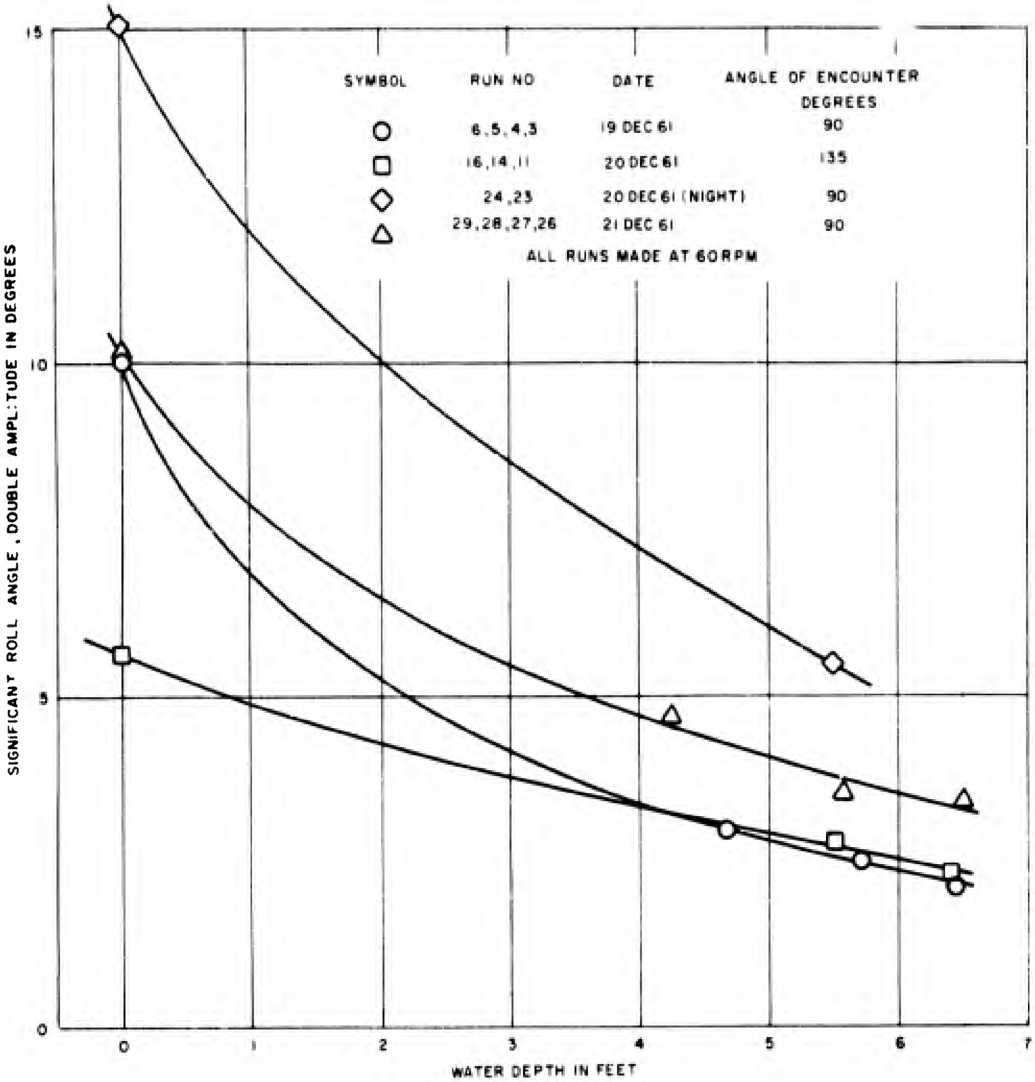

Fig. 6 - Effect of various water levels on tank effectiveness

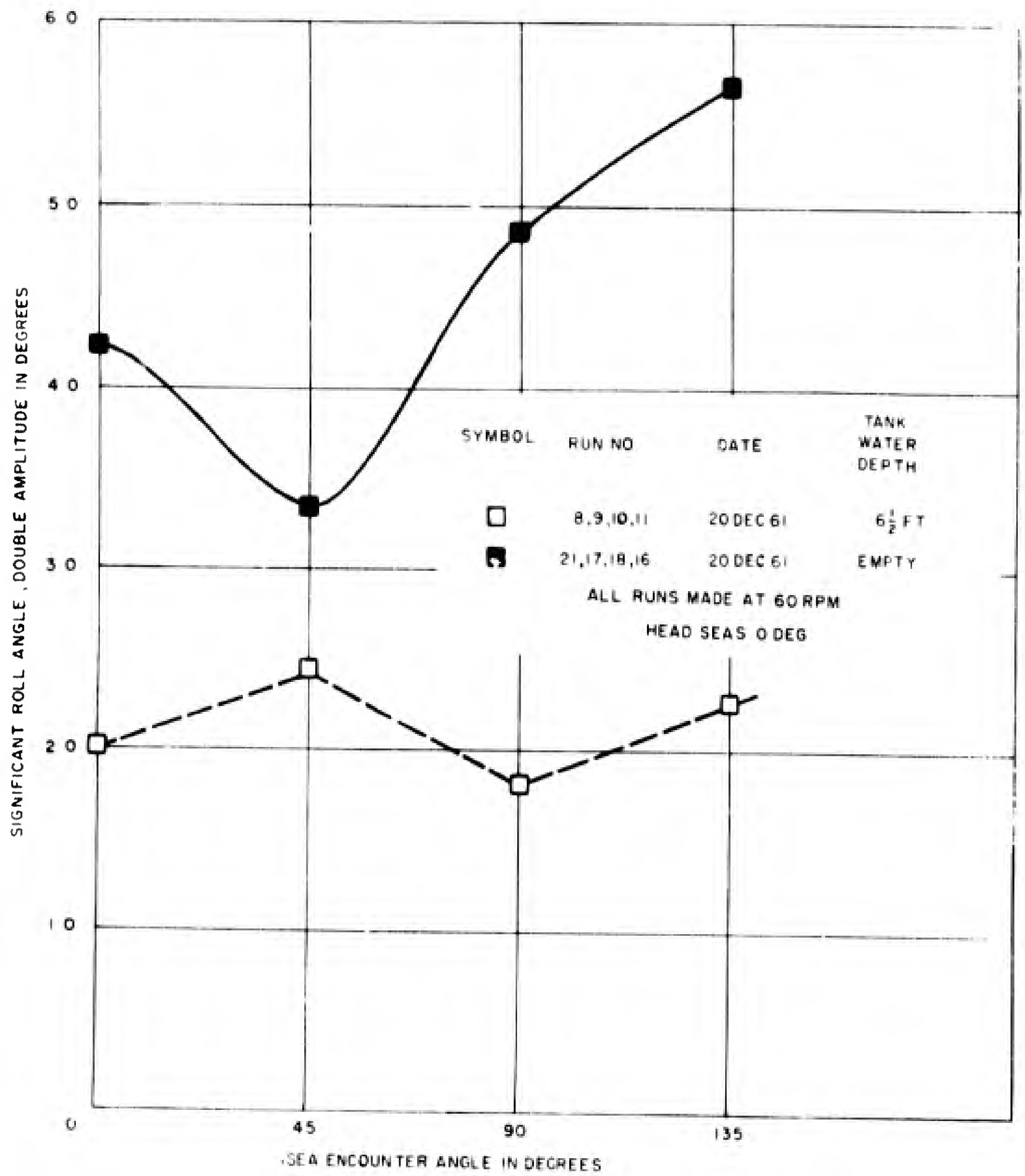

Fig. 7 - Effect of sea encounter angle on tank effectiveness

Finally, Fig. 8 indicates the effect of speed on roll stabilization. An interesting and contrary effect is the increased roll amplitude with increase in percentage roll stabilization with increased speed. One would expect the natural hull damping to increase in the unstabilized condition and the percentage of roll stabilization to decrease with increased speed. The changing sea environment

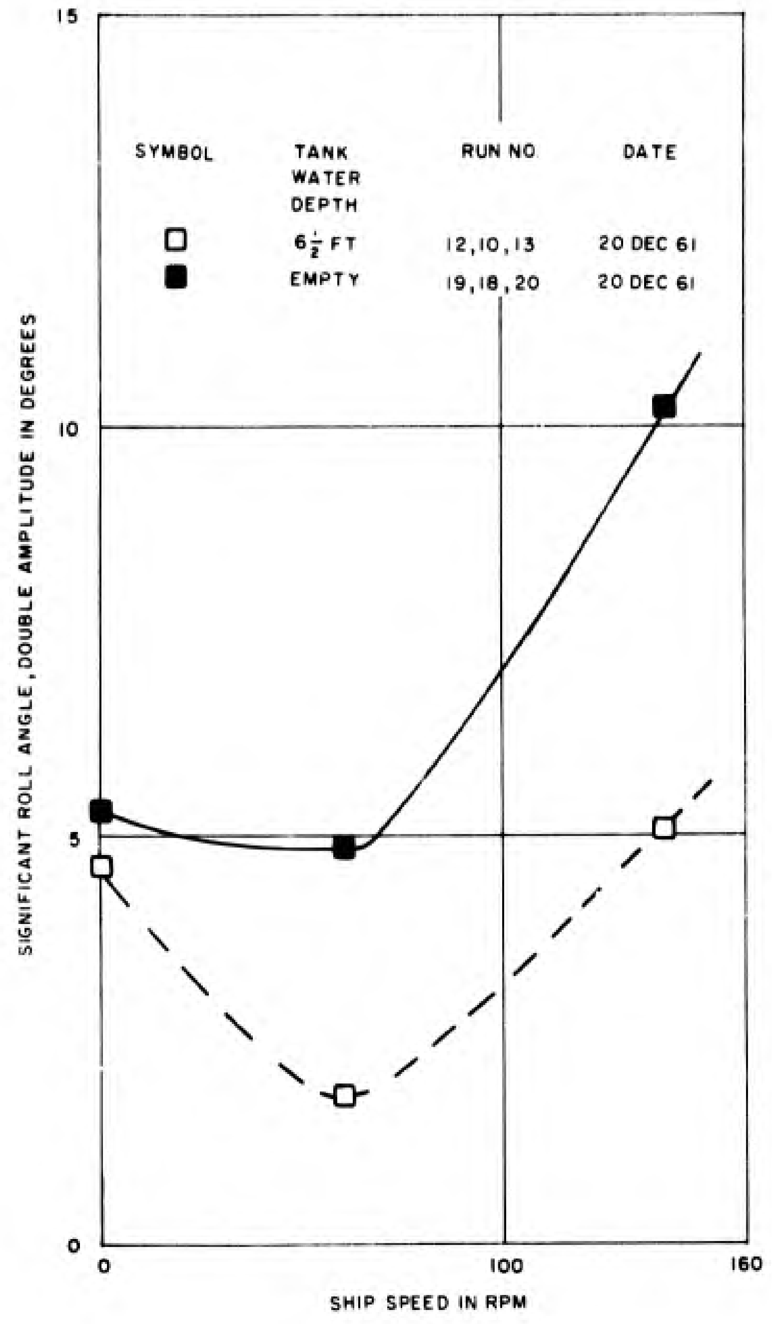

Fig. 8 - Effect of ship speed on tank effectiveness

must again be suspected. Foster [40] continues to explain that a considerable directional spectra must have existed in the confused beam sea and as speed increased the frequency of encounter with these directional components approached the natural roll period, resulting in increased roll response.

USNS GILLISS — Passive Tanks. The USNS GILLISS is a 209-foot, 1200-ton oceanographic research ship and is one of a large class of such ships. The design specifications of the ship limited the displacement to the stated value. Maximum length was maintained consistent with the displacement to provide as much work space as possible. The ship was fitted with anti-roll tanks consisting of two wing tanks with an open channel crossover and fixed entrance nozzles.

Full scale sea trials were conducted by the David Taylor Model Basin in December 1963. Figure 9 presents the results of the tank tuning experiments. These tests were conducted on two separate days in both beam and quartering seas. These curves indicate a very well defined trend toward an optimum water depth of 3.5 feet. It should be noted that the tank effectiveness can be decreased by the addition of too much water. Whether this is due to poor tuning or the limiting of tank fluid transfer due to overhead clearance is not clear.

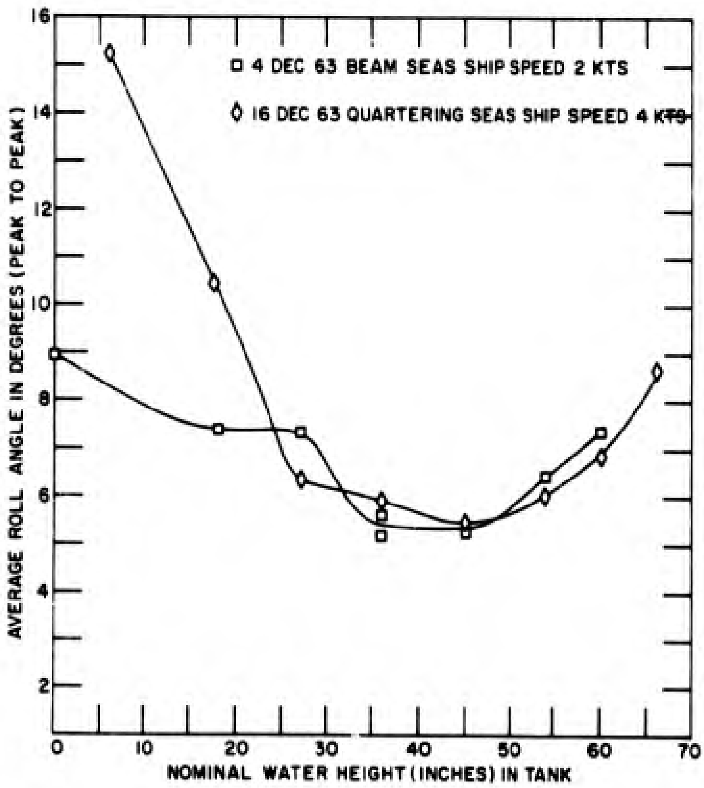

Fig. 9 - Effect of various water levels on passive anti-roll tank effectiveness

Figure 10 shows the effect over various angles of encounter with the seaway, in both the stabilized and unstabilized condition. While these curves again indicate the general effectiveness of the tanks, they also indicate that the changing environment makes it impossible to draw definitive design conclusions.

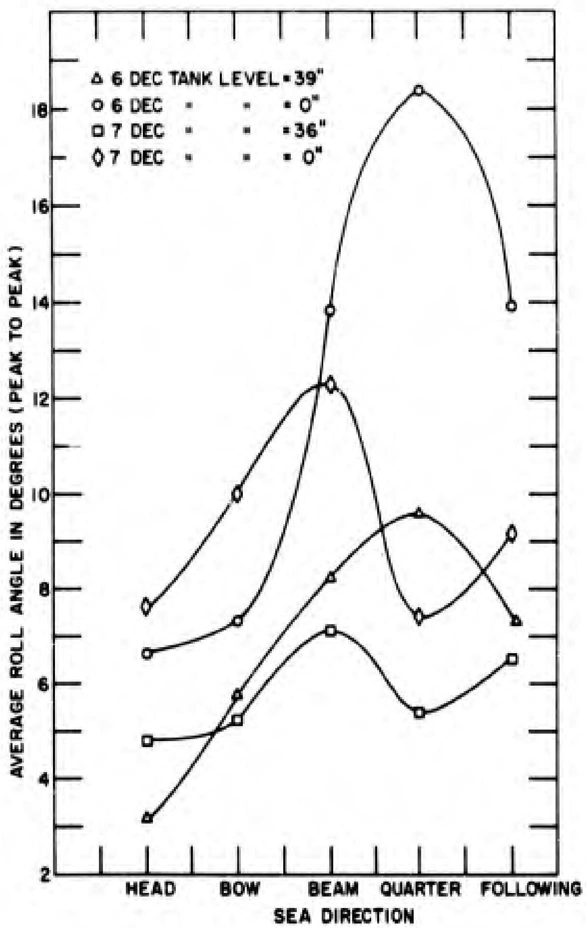

Fig. 10 - Effect of sea direction on passive anti-roll tank effectiveness

Bench tank tests and model tests conducted in irregular seas at the Davidson Laboratory [41] showed that significant stabilization was possible, as much as 90 percent at resonance. Figure 11 shows the roll amplitude operator indicating this result. It is further concluded that once tanks are tuned to damp out the narrow frequency band of roll response, rolling at resonance is limited to amplitudes approximately equal to the maximum surface wave slope. Finally, as might be expected, bilge keels had small effect in further reducing the roll of a ship already stabilized by a passive tank system.

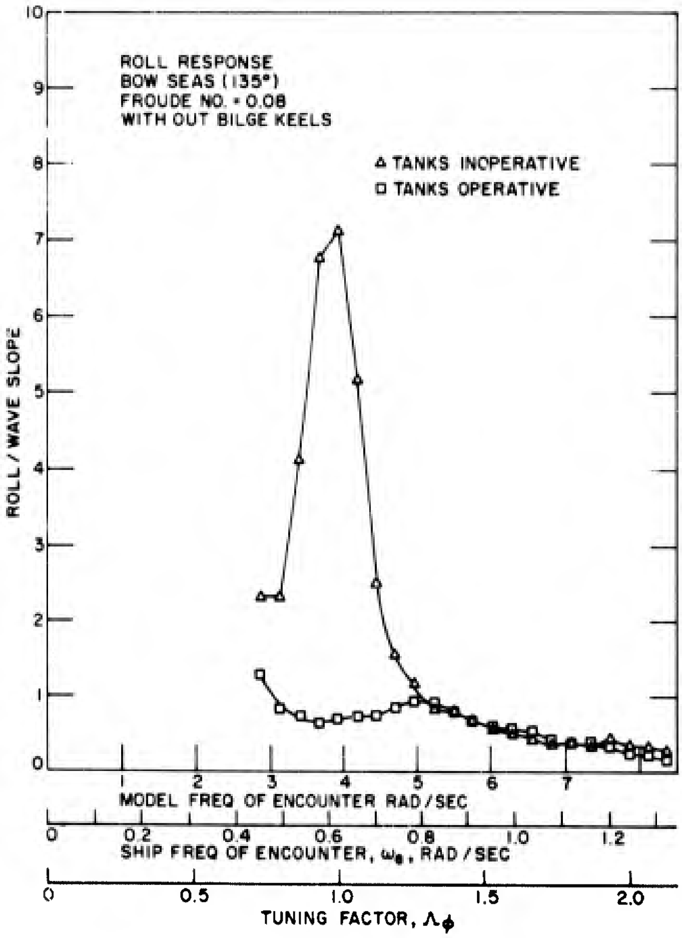

Fig. 11 - Effectiveness of passive anti-rolling tanks

In continuing the model study on the AGOR class of ship, the Davidson Laboratory conducted experiments in regular waves to determine speed and wave height effects [42]. This study concluded that an increase in the height of regular beam waves decreases the effectiveness of the tank system and the peak of the unstabilized roll response moves to a slightly lower frequency. Figure 12 shows a comparison of the various roll responses derived from experiments conducted by Refs. 41 and 42.

The speed study indicated the obvious result of an increase in roll damping with increased speed for the unstabilized ship condition and an increase in the stabilized roll amplitudes (decreasing tank effectiveness with increased speed).

ARIS-3 Passive Tanks. The ARIS-3 is a design for a 496-foot Advanced Range Instrumentation Ship of 13,600 tons displacement. Bench tests were conducted at the David Taylor Model Basin on a 1/20-scale model passive tank. In addition to determining the depth of water required for properly tuned operation,

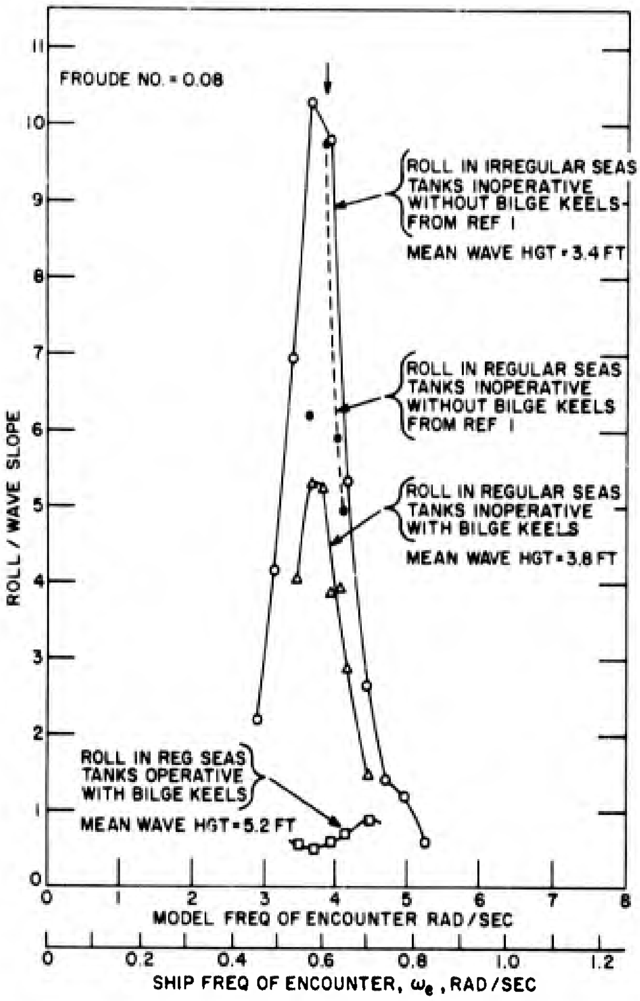

Fig. 12 - Roll response of AGOR in irregular and regular beam seas with different types of stabilization

3 different nozzle shapes were investigated to determine damping effects. Figure 13 indicates the general tank arrangement while Fig. 14 shows the various nozzle configurations.

The results of these experiments, Fig. 15, indicated that nozzle configuration "A" gave the most favorable dynamic characteristics based on the more desirable moment produced. Figure 16 shows the variation of phase angle between moment and roll angle with roll frequency and indicates no appreciable advantage between nozzles.

The effect of water depth is shown in Figs. 17 and 18. Generally speaking, low water depth would be more advantageous at low frequencies, higher water levels at the midfrequency range with no appreciable effect for either water depth at high frequencies.

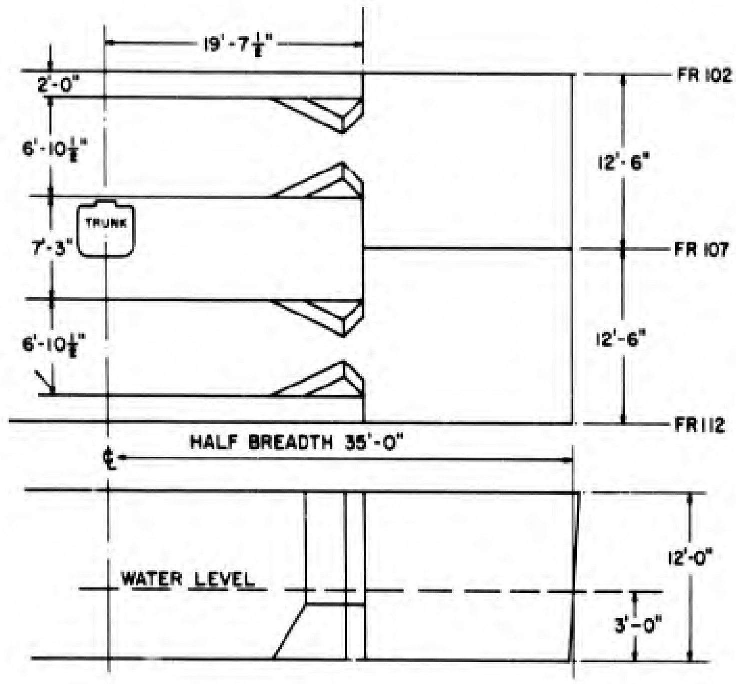

Fig. 13 - ARIS-3 anti-roll tank configuration

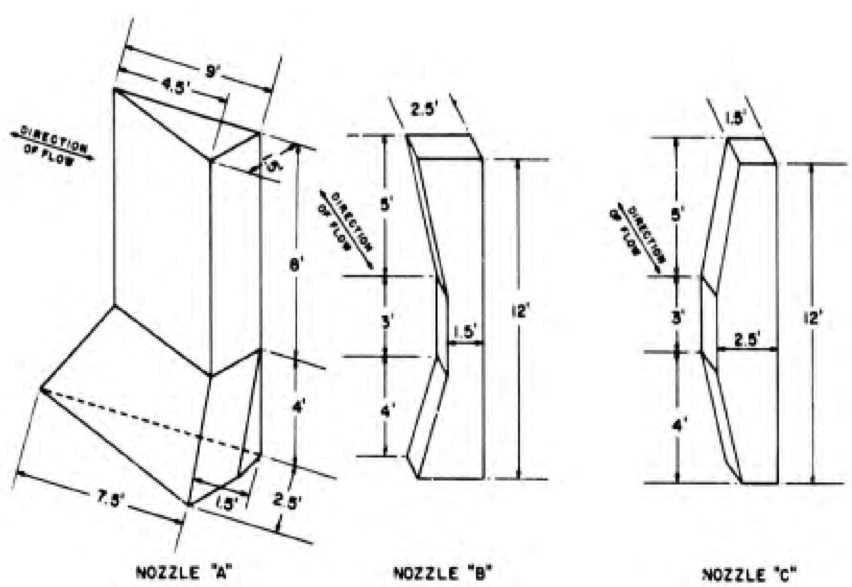

Fig. 14 - Various nozzle configurations tested with ARIS-3 anti-roll tank

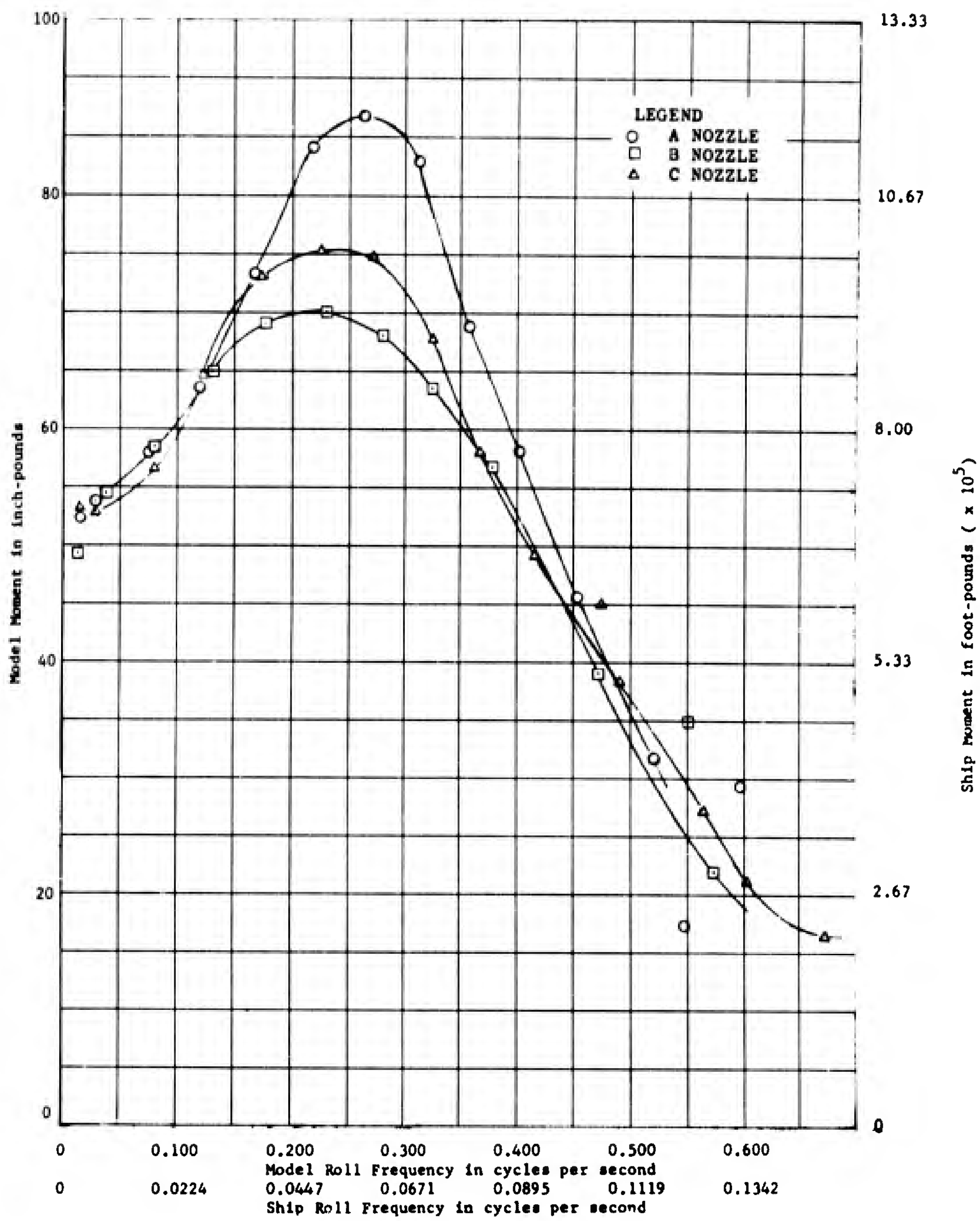

Fig. 15 - Variation of tank moment with roll frequency for three different nozzles

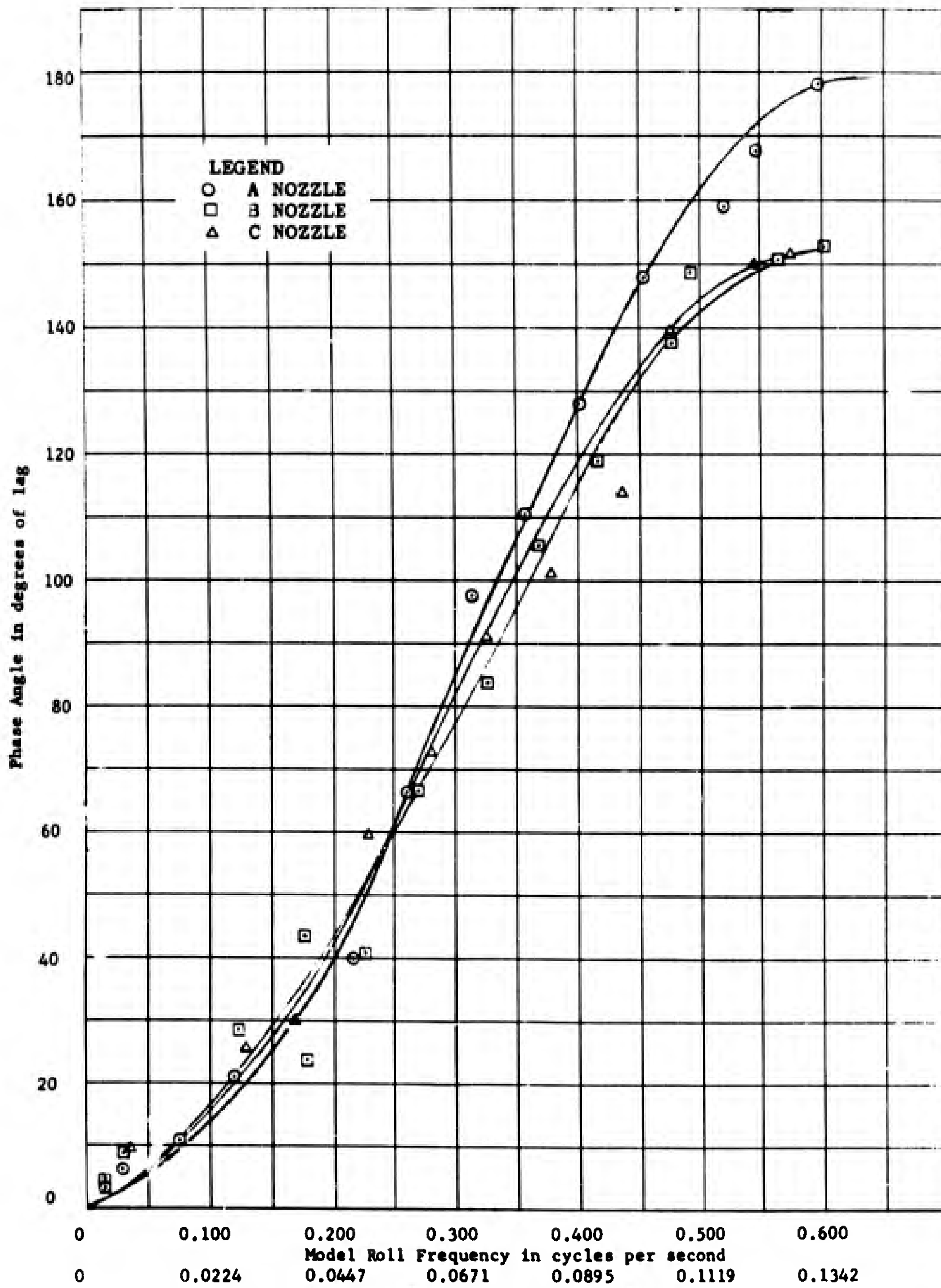

Fig. 16 - Variation of phase angle between moment and roll angle with roll frequency for three different nozzles

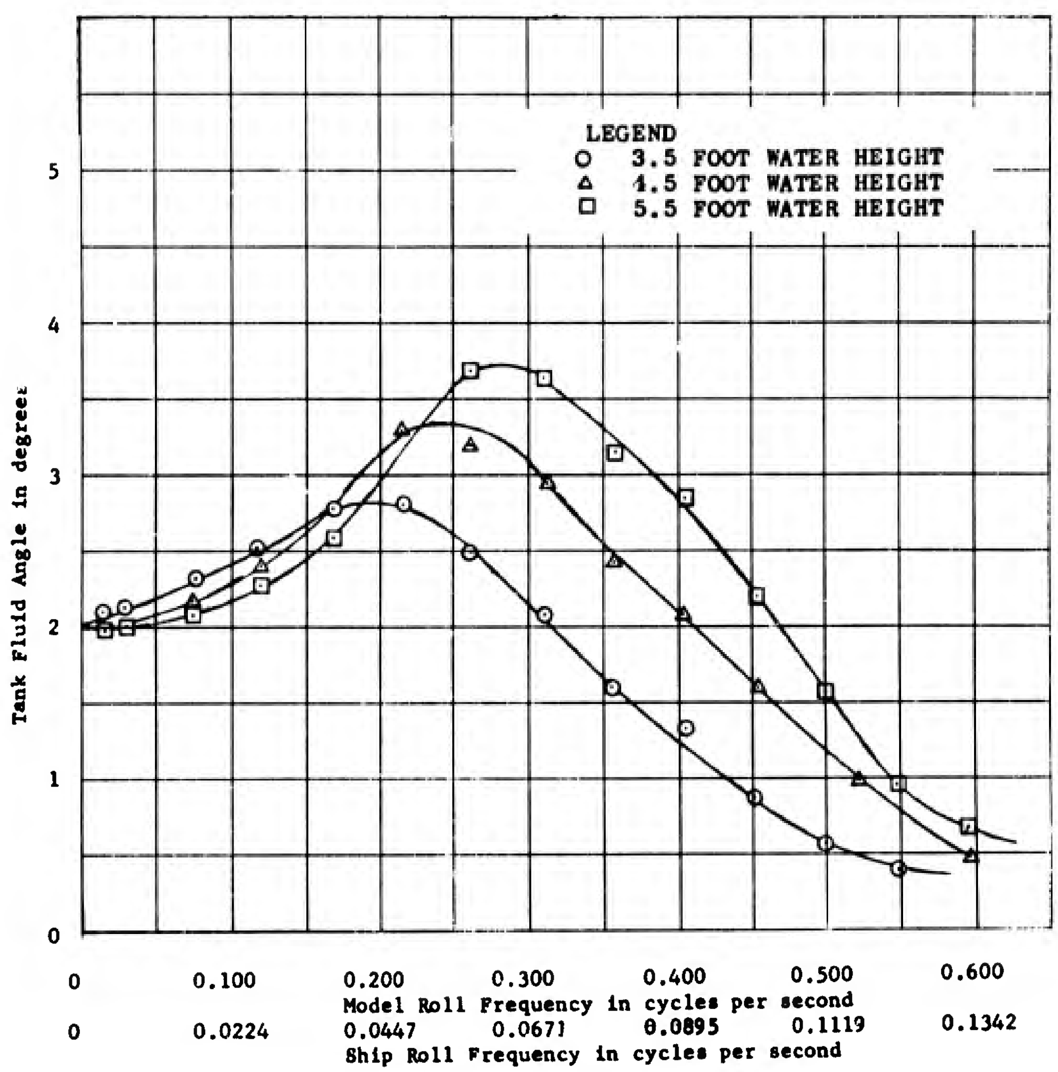

Fig. 17 - Variation of tank moment with roll frequency for three different water depths

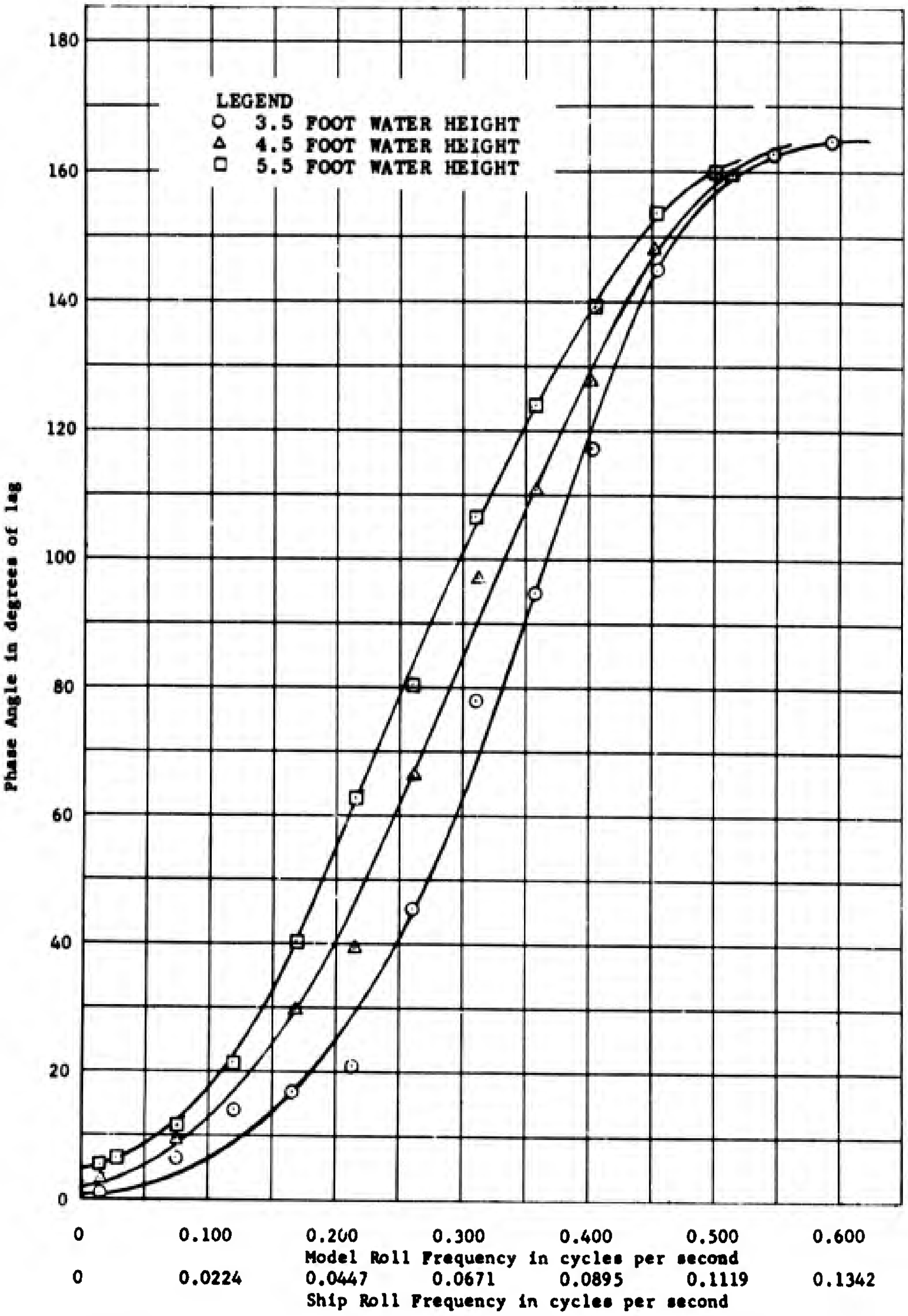

Fig. 18 - Variation of phase angle between moment and roll angle with roll frequency for three different water depths

This study further attempted to compute damping assuming that the tank-ship system could be described by a second order differ tial equation with either linear or quadratic damping terms. It was indicated that while the quadratic damping might be a reasonable representation in the vicinity of tank resonance, damping was shown to be a much more complicated phenomenon that can be treated with present knowledge.

The results of the above as yet unpublished work of Finkel led to the design of a tank system which was installed in a 1/38.15-scale model. Tests were conducted in regular waves and indicated that roll would be reduced by as much as 55 percent in a beam sea at a speed of 7 knots, Fig. 19. These predictions could not be extended to the irregular sea condition because of the nonlinearities involved in the roll phenomenon.

AVT-7 — Passive Tank. The AVT-7 is a planned conversion from the CVL 48 and is a 683 foot hull of 18,760 tons. Model tests were again conducted on a 1/19 scale model tank. This tank was installed below the roll axis of the ship. The tank was again oscillated over the frequency range with various water depths; the tank configuration is shown in Fig. 20. Tank moment versus frequency is

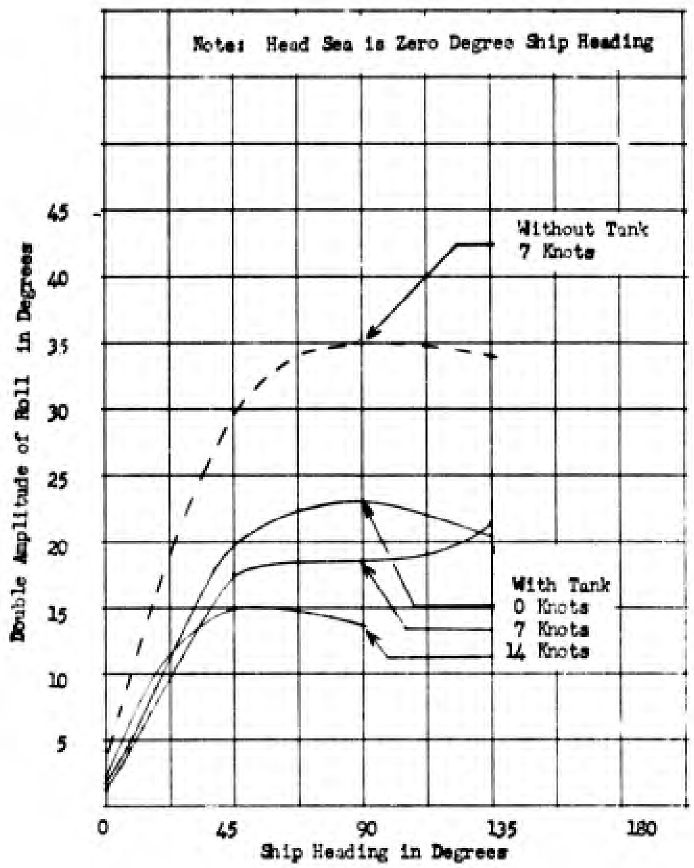

Fig. 19 - Variation of maximum roll angle with ship heading for a wave steepness of 1/50

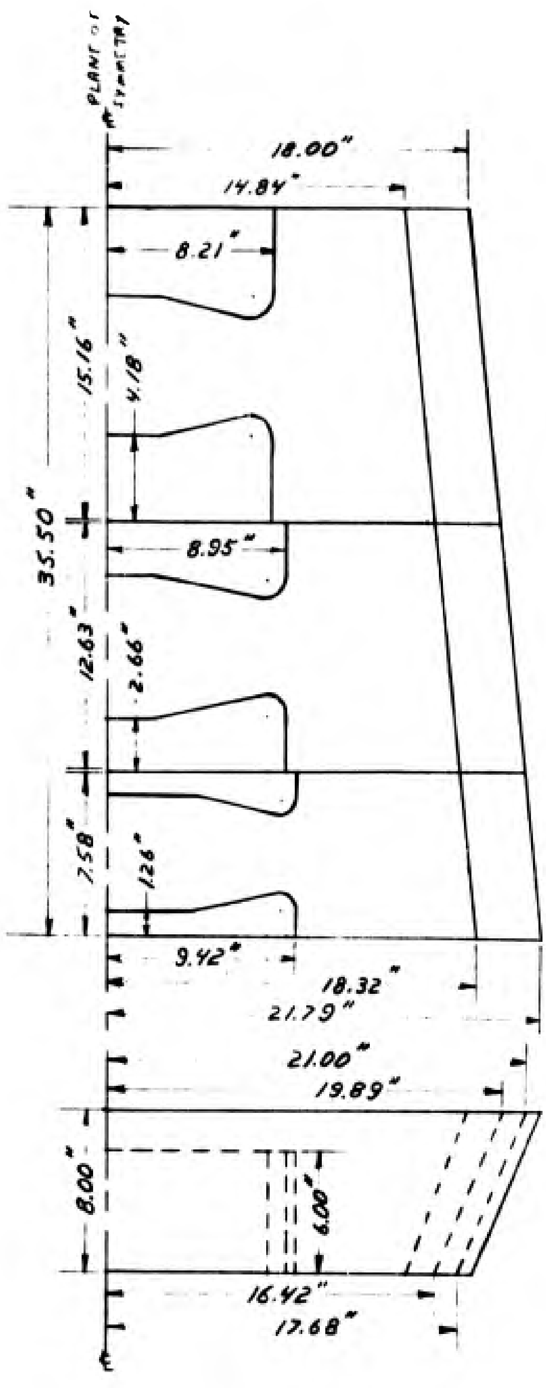

Fig. 20 - Symmetrical plan view of 1/19 scale model tank

shown in Fig. 21 while the variation of phase angle between moment and roll is shown in Fig. 22. The general conclusions arrived at from these experiments are in agreement with those reached in previous tests. There appears to be no unexpected adverse effect from putting the tanks below the roll axis.

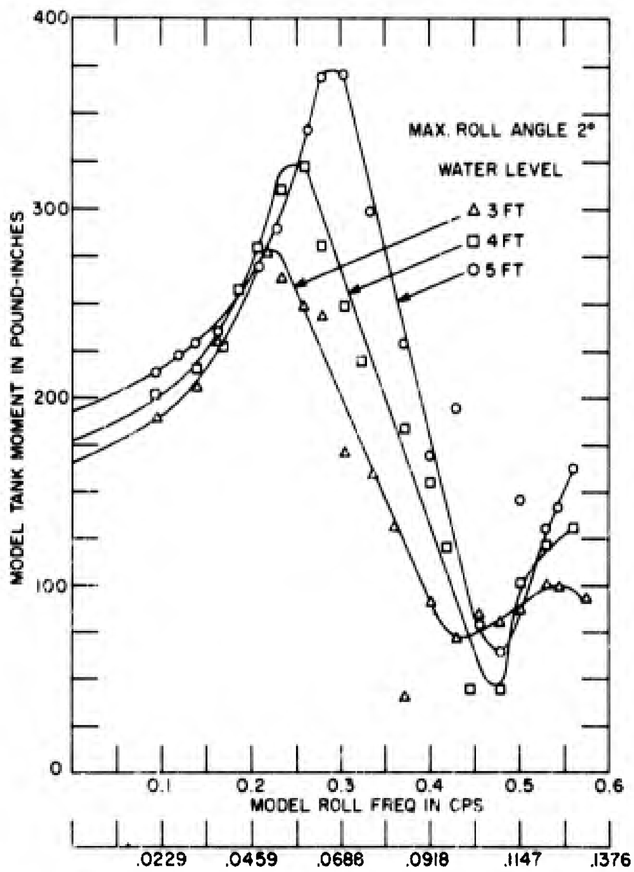

Fig. 21 - Tank moment as a function of roll frequency 3, 4, and 5 foot water levels at 2 degrees roll amplitude

USS BRONSTEIN — Active Fins. The USS BRONSTEIN (DE 1037) is a 350-foot ASW vessel of 2500 tons displacement. This ship is fitted with active anti-rolling fins that are fixed in the out-rigged position. In other respects this installation is similar to that of the USS GYATT [43].

Forced roll experiments were performed on this ship during the sea trials conducted early in 1964. Figure 23 shows the comparison of the stabilized and unstabilized roll quenching capability. Figure 24 compares the roll angle envelopes for the stabilized and unstabilized conditions and it may be seen that the damping of the stabilized curve is approximately 3 times that of the unstabilized curve.

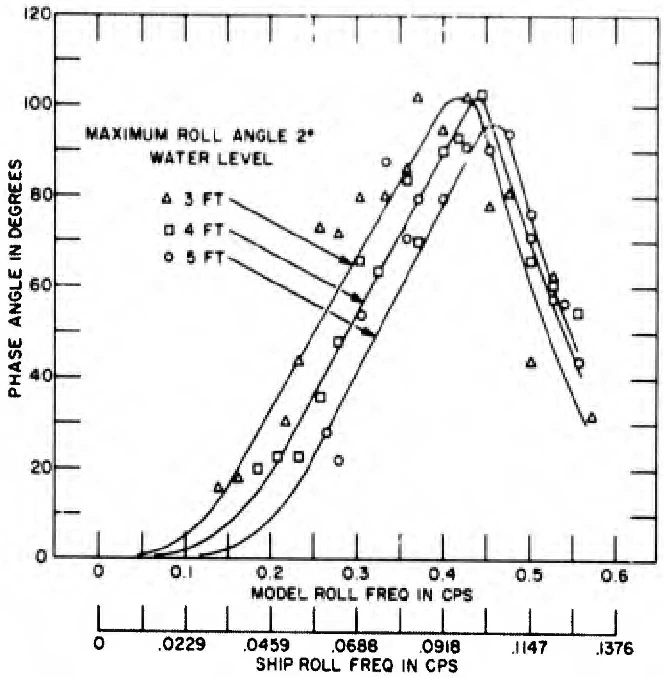

Fig. 22 - Phase lag of tank moment relative to roll for 3, 4, and 5 foot water levels at 2 degrees roll amplitude

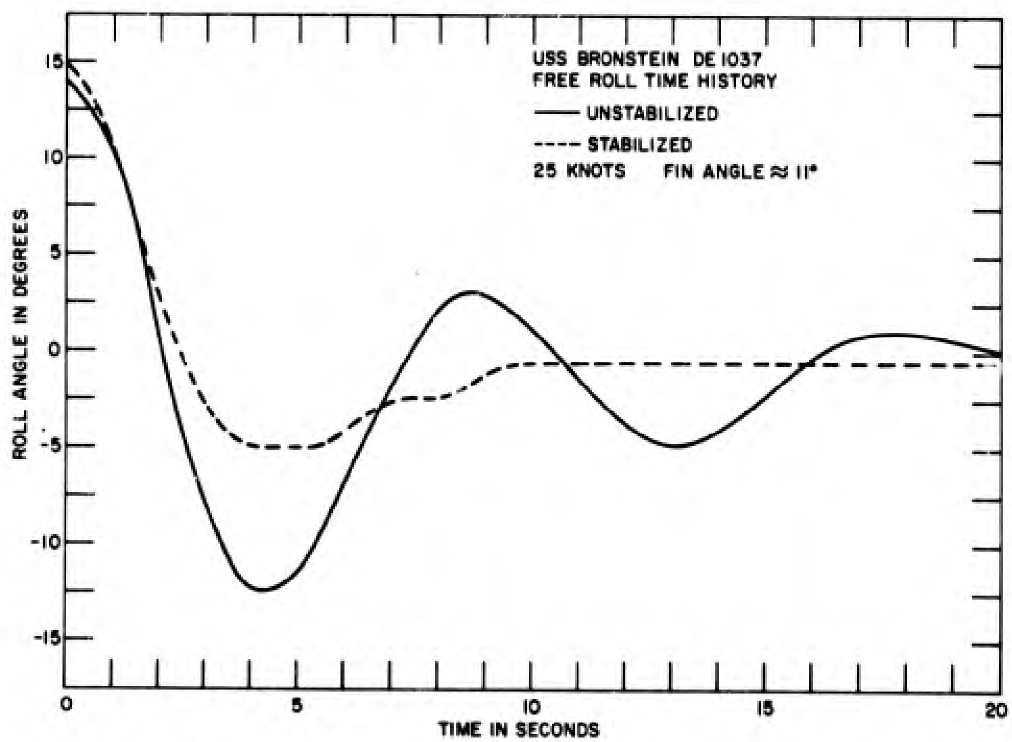

Fig. 23 - Comparison of stabilized and unstabilized roll

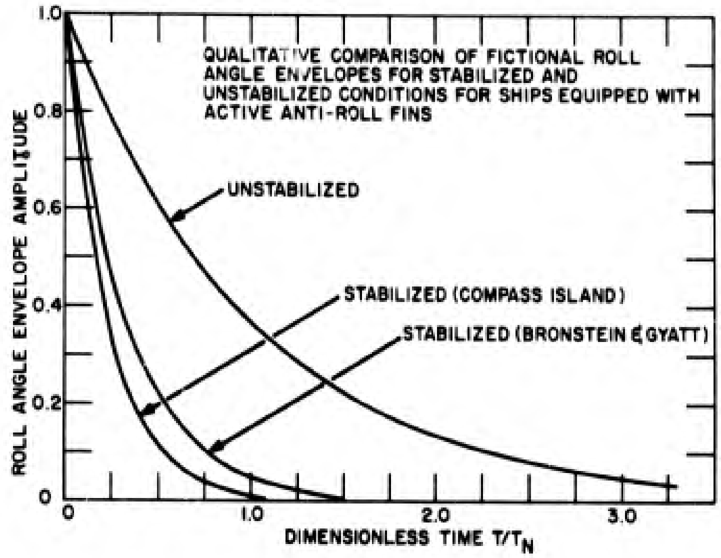

Fig. 24 - Comparison of roll angle envelopes

The application of stabilizer fins to this class of ship is the first since those previously reported on GYATT, COMPASS ISLAND and OBSERVATION ISLAND [31]. The apparent success of all installations would seem to indicate that more attention should be given to this area of stabilization. It should be mentioned that the tests presently under discussion were conducted at a ship speed of above 20 knots. There appears to be an obvious advantage to using active fin roll stabilizers on high speed ships.

Current Studies. Under sponsorship of the David Taylor Model Basin, the Southwest Research Institute is conducting a continuing study of ship roll stabilization tanks [44,45]. This program provides for four related studies: (a) Theoretical tank damping characteristics; (b) experimental tank damping characteristics; (c) extended theory of ship-tank systems; and (d) application to design.

After progressing in phase (a) and (b) for a period of time it became apparent that the study was hampered by a lack of a physical understanding of the tank fluid behavior. Finkel also discovered this in his work on ARIS-3 as did Motora and Lalangas [41]. To illustrate the point, Fig. 25 shows comparisons of several experimental approaches. The lack of agreement is startling. Additional experimentation is indicated and a nonlinear model must be discovered.

Pitch Stabilization

Pitch stabilization has received a moderate degree of attention in recent years in both theoretical and experimental studies but as yet these studies have not resulted in a successful full scale installation. The problems of reducing pitch are quite different from those of roll stabilization. Pitch is already considerably dampened by the ship's hull. This of course means that large forces

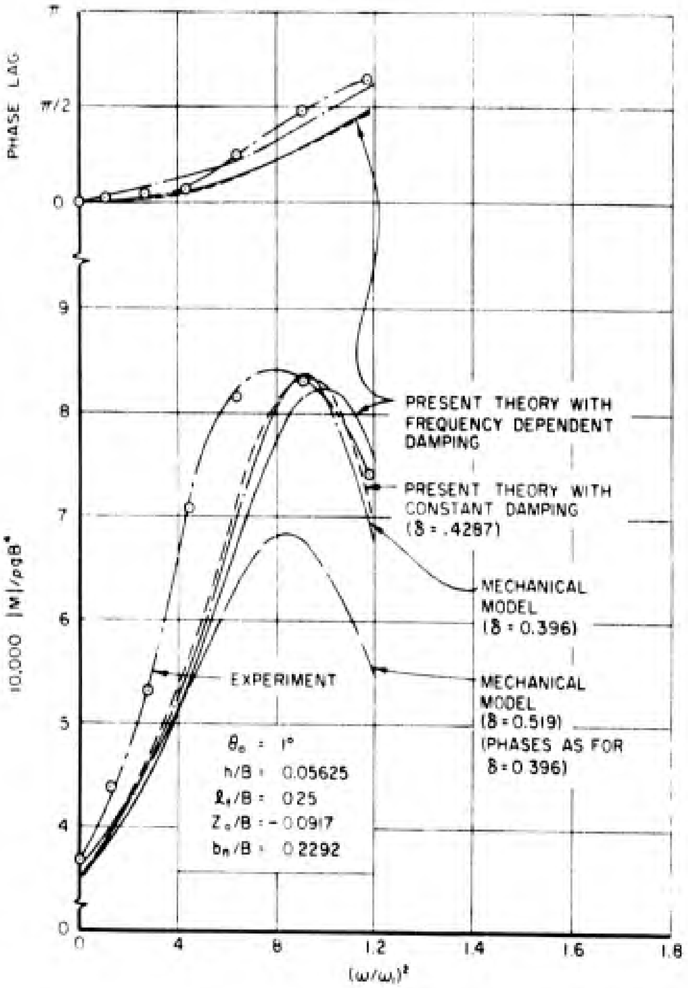

Fig. 25 - Comparison of various mathematical models with experiment

must be involved in any further magnification of this damping. It is quite impractical to generate these large forces by means of internal devices generally associated with roll stabilization, i.e., tanks, gyros, moving weights. To further complicate the problem, the pitch phenomenon is not resonance dominated as is roll, that is to say, the roll spectrum is sharply tuned while pitch responds to a broad range of frequencies.

Thus, all attempts at pitch stabilization have been through the use of external devices, capable of sustaining the large forces involved. These devices have been fixed bow fins, moveable stern fins and to a lesser degree moveable bow fins and fixed stern fins. Only the fixed bow fins have been installed on ships, these installations being made on the RYNDAM of the Holland-American Line and the American ship COMPASS ISLAND. While considerable pitch reduction was achieved in both cases, a severe horizontal bow vibration associated with the fin installation caused their removal. This vibration problem has been the subject of much of the investigation conducted on bow fins in recent years; it has also caused the virtual abandonment of these devices as pitch stabilizers.

The highlights of the work conducted in this area will be the subject of this section. Mention will also be made of some recent experiments not as yet reported in the literature.

Fixed Bow Fins

In 1956, Pournaras [46] fitted a set of fins to a Series 60, Block 60 model. The fins were flat plates with a planform area 2.5 percent of the load waterplane area. The leading edge was swept back to reduce tip load and thereby decrease the root-bending moment. The fins were also fitted with tip fences. From the limited tests conducted it was observed that pitching motion was considerably reduced, the speed range was extended, much less green water was shipped over the bow, and forefoot emergence was eliminated. Of most significance, however, Pournaras noted that on the downward stroke, sheets of water were forced around the leading and trailing edge of the fins, closed in over the upper surface and formed a whirl near the water surface as the two sheets met. Removal of the tip fence caused the formation of a third sheet and added to the problem.

In a subsequent study, Pournaras [47] tested four different fin configurations on a model of a MARINER class ship. In addition to varying planform, some of the fins were slotted and others had through holes in an attempt to destroy the sheet vorteces. Figure 26 shows these various fin arrangements. All configurations were fitted with fences with the exception of fin 3.

Figure 27 shows a summary of test results obtained and indicates that while substantial pitch reductions were obtained, configuration variation had very little effect. The major conclusions of this study are summarized as follows:

1. Fins operate most effectively near the synchronous range and have little effect at higher or lower frequencies.

2. Fins have little effect on the phase lag of heave and pitch but it should be remembered that a slight change in phase could have a marked effect on relative motions.

3. Area of fin planform has little effect on motions.

4. The loadings caused by the vorticity effect can be lessened by deeper submergence, greater fin span, tip fences and relief mechanisms such as slots and holes.

Next, Abkowitz [48] conducted a comprehensive study on the effect of bow anti-pitching fins on ship motions. This study included a discussion on the nature of pitch damping in addition to presenting some experimental results of tests conducted on a Series 60 Block 60 model, an aircraft carrier model and a destroyer model. All indicated good pitch reduction trends and good agreement with theoretical calculations. It was again concluded that the major effect was produced at resonance.

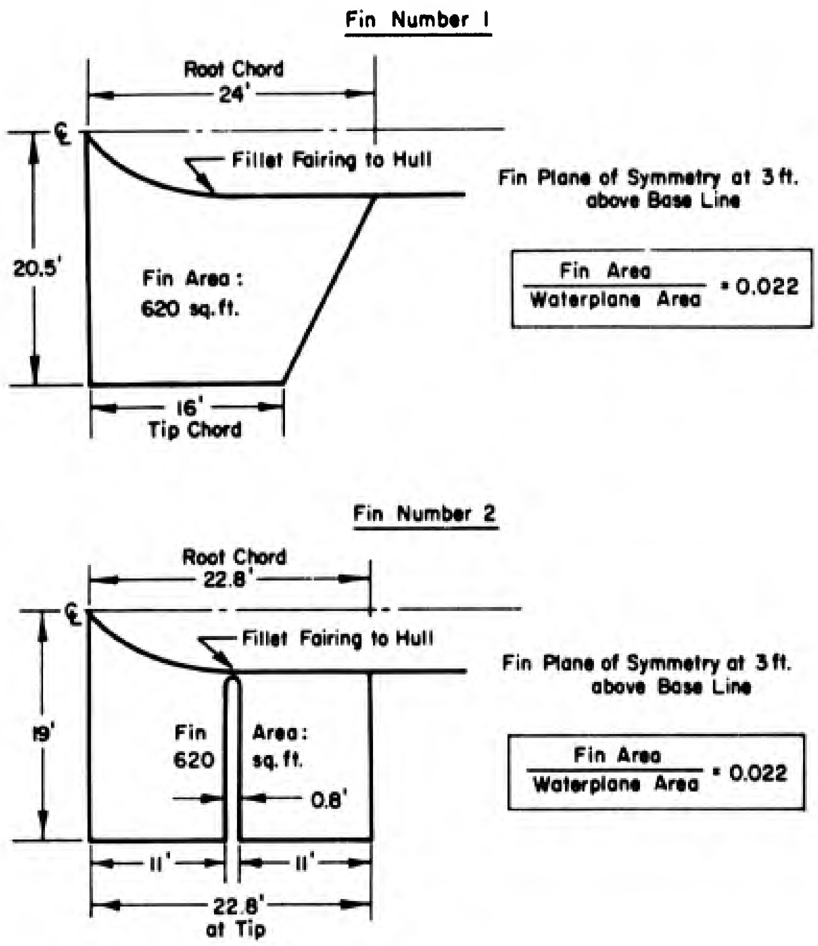

Fin Number 2s – Obtained from Fin Number 2, by cutting 5 ft. off each tip, P & S.

Tips off Centerline : 14 ft.
Fin Area : 400 sq. ft.

$$\frac{\text{Fin Area}}{\text{Waterplane Area}} = 0.014$$

Fin Number 2h – Obtained from Fin Number 2s, by drilling two 1½ ft. diameter holes 2 ft. aft of leading edge of fwd fin and two 1½ ft. diameter holes 2 ft. fwd of trailing edge of aft fin. Area and span of fins not changed.

Fig. 26a - Plan views of anti-pitching fins 1 and 2

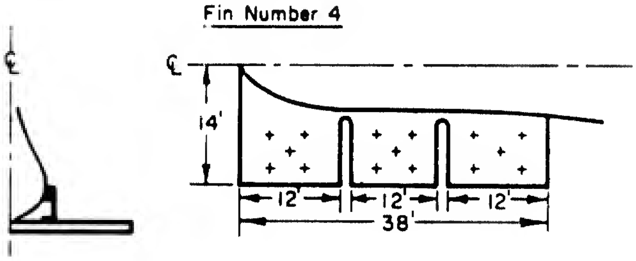

Fins separated by 1 ft.

Upper surface of fin tangent to baseline.

Fin Area: 640 sq ft.

$$\frac{\textbf{Fin Area}}{\textbf{Waterplane Area}} = 0.023$$

Fin Number 4h

Obtained from Fin Number 4, by drilling five 1-ft diameter holes on each fin as indicated in sketch.

Fin 3 – Same as Fin Number 1 with 30° dihedral angle.

Fig. 26b - Views of anti-pitching fin 4 and description of anti-pitching fin 3

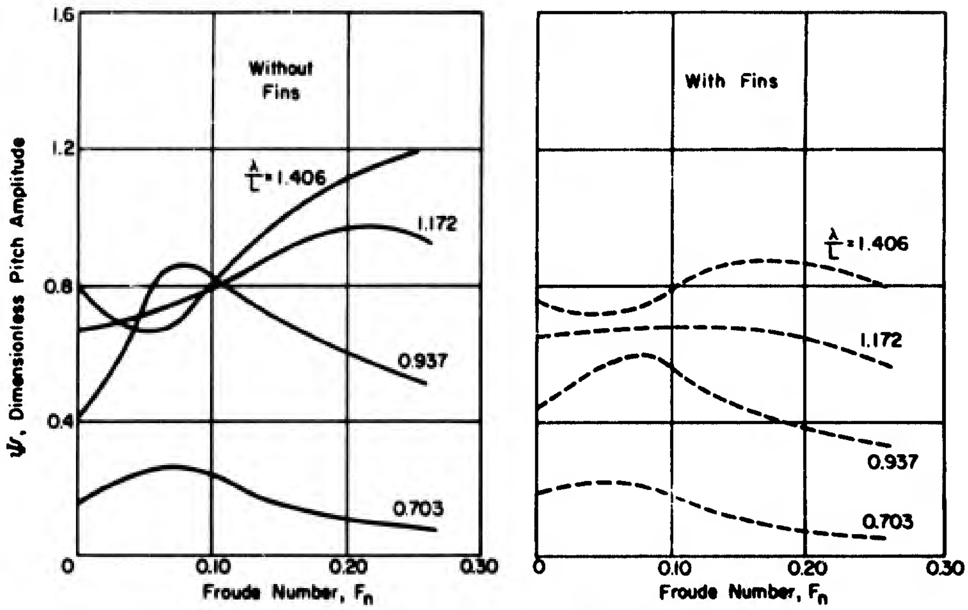

Fig. 27a - Dimensionless pitch amplitudes

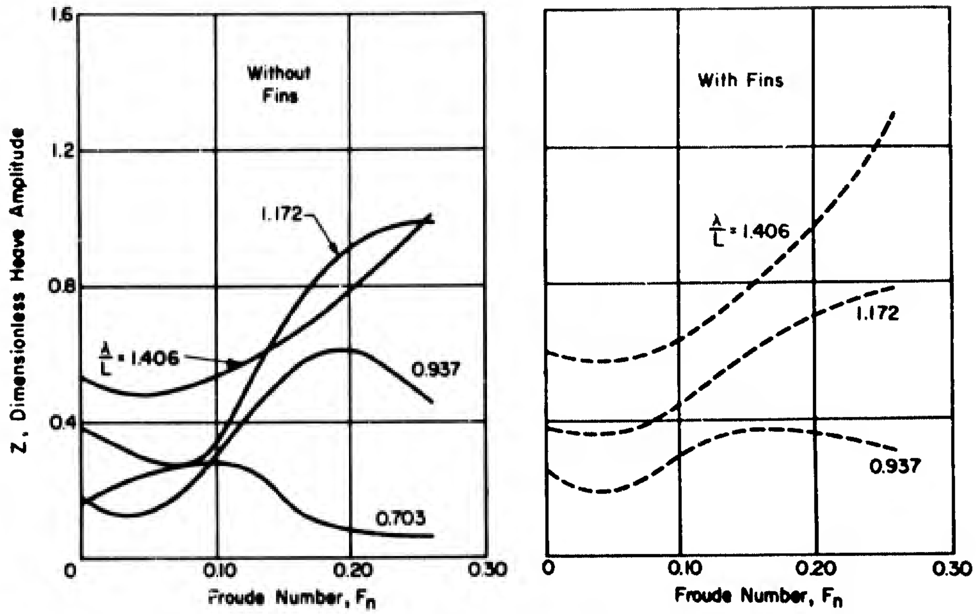

Fig. 27b - Dimensionless heave amplitudes

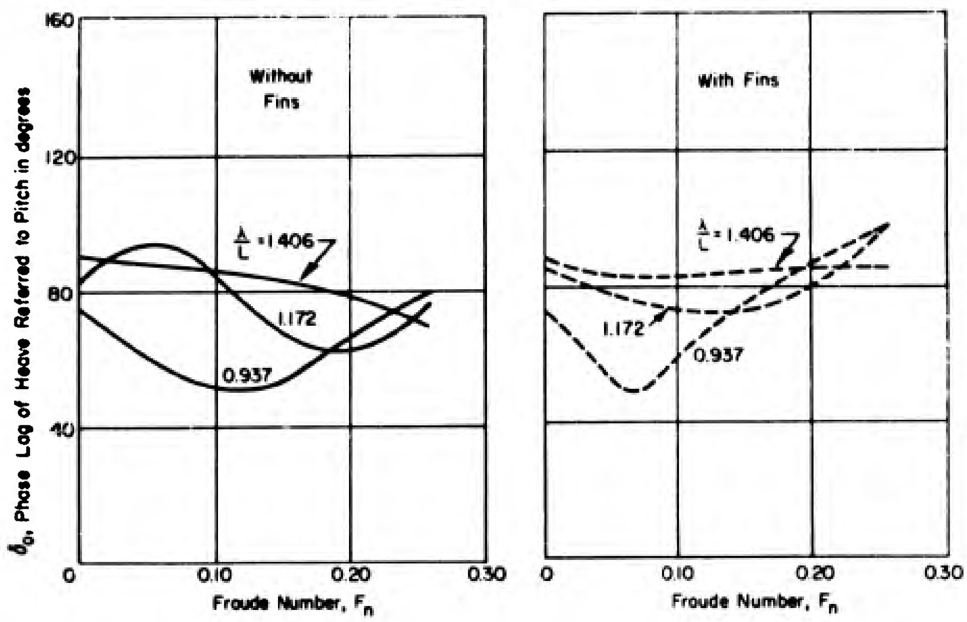

Fig. 27c - Phase lag of heave referred to pitch

Abkowitz concluded that the horizontal vibration at the bow was due to the large angle of attack on the fin during the downward motion giving rise to a low pressure on the upper-fin surface. Just before the downward stroke begins (fin near surface) the fin is near the surface and the low pressure area causes a suction and possible ventilation. As the fin goes deeper, the bubble collapses causing a large pressure impact. He further concludes that since port and starboard fins do not ventilate uniformly, a differential pressure impact situation is created. He is at variance with the conclusions of Pournaras in that tip fences will be harmful rather than beneficial since they increase aspect ratio which in turn will increase the low pressure on the upper surface and lower the angle of attack at which the breakdown occurs.

Abkowitz further conducted some comparative experiments between trumpet shaped fins and hydrofoil fins located at the keel and concluded that hydrofoil fins would produce less horizontal vibration and when separation did occur, only small horizontal vibrations were produced.

In 1959, Becker and Duffy [49] presented the results of full scale sea trials conducted on the COMPASS ISLAND. It was concluded in this study that pitch was reduced but the magnitude of reduction could not be properly established because of lack of an exact "without fin" correlation condition. Vertical and transverse vibrations were excited in the ship, very seriously in heavy seas. While it was possible to calculate the fundamental mode of the vertical hull stresses (±11,000 psi) the transverse vibration was not measured. This was unfortunate since it was apparent that the transverse mode was excited at a more moderate sea state than the vertical, and all previous studies have indicated the transverse mode to be the probable problem area.

Stefun [50] continued the effort by conducting an interesting experimental study investigating the effect of planform area and aspect ratio. Table 3 presents a summary of the various fin configurations. This study again reaches the general conclusion that fins are effective mostly at near synchronous condition and again significant pitch reductions were achieved. Aspect ratio is indicated to be a significant parameter. Pitch reduction is 30 percent less for a fin with an aspect ratio of 0.5 compared to a fin with an aspect ratio of 2.0. It was further indicated that while an increase in planform area was helpful in achieving increased pitch reduction this increase was not in direct proportion to the increase in this area. The fins decreased ship resistance in waves of between 75 and 120 percent of the ship length. Heave was increased in long waves while in intermediate waves, heave was increased at low speed and decreased at high speed.

Finally, this study indicated that the use of tip fences reduced pitch by an additional 5 percent. This is the result of apparent increased aspect ratio due to the addition of tip fences. It should be noted that this particular study used tip fences for the reasons stated by Pournaras [10,11].

Table 3
Fin Particulars

Fin No.	Plan Area (A_w = waterplane area)	Aspect Ratio	Tip Fences (length, width)
1	$0.02\,A_w$	2.0	None
2	$0.02\,A_w$	0.5	None
3	$0.01\,A_w$	1.5	2.1, 0.6
4	$0.02\,A_w$	1.5	3.0, 1.25
4(a)	$0.02\,A_w$	1.5	None
5	$0.04\,A_w$	1.5	4.25, 1.5

In 1962, Stefun and Schwartz [51] presented the results of a study conducted to determine the effects of various bow fin configurations on hull vibrations. These tests were conducted on an aircraft carrier model using 16 different fin configurations as shown in Fig. 28. All tests were conducted at one wavelength (λ/h = 40, 30, and 24). The results of this study are presented in Fig. 29 as a figure of merit. This figure is defined to mean that for any fin, N

$$\frac{\text{Pitch Reduction (Fin N)/Pitch Reduction (Fin 1)}}{\text{Vibration Level (Fin N)/Vibration Level (Fin 1)}} = \text{Figure of Merit.}$$

While none of the fins completely eliminated transverse hull vibrations, considerable improvement was indicated by several configurations. Aspect ratio, tip fences or increased depth of submergence showed improvements. Holes, dihedral angle and swept edges showed less improvement and while annular fins indicated promise, the test results showed much more research would be required before their entire nature would be understood.

In 1961, Ochi [52] conducted a very complete hydroelastic study on a ship equipped with an anti-pitching fin. In addition to forwarding an explanation as to the mechanism of the induced vibration the study also discussed the effect of the fin location, size and configuration.

While there is general agreement that the induced vibration is caused by a cavity collapse (or cavity collapse plus fin slam in the case of shallow draft), the study differs as to the cause of the mechanism inducing the vibration. The premise forwarded here is that rather than the vibration being purely horizontal in nature, it is initially a torsional vibration. If the natural frequencies of both the torsional and horizontal modes correspond, the vibration is severe.

Fin	Plan View	End View	Particulars
1	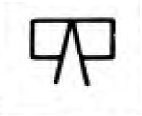	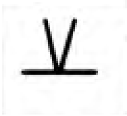	Span - 6.8 in., Chord - 3.4 in. Area - 4.4 percent of waterplane area Aspect Ratio - 2.0
1(a)	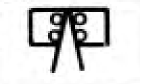	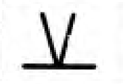	Same as Fin 1 except for four 1.0-in.-diameter holes.
1(b)	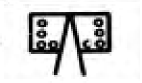	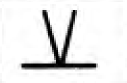	Same as Fin 1 except for eight 0.5-in.-diameter holes.
1(c)	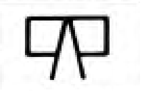	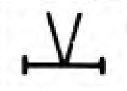	Fin 1 with tip fences. Fence height - 1.0 in.
1(d)	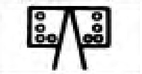	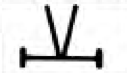	Fin 1(b) with tip fences.
1(e)	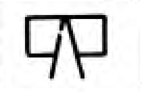		Fin 1 with strut to increase depth of submergence by 50 percent.
1(f)	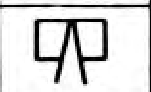		Fin 1 with 25-deg positive dihedral.
1(g)	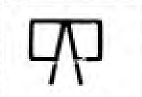		Fin 1 with 25-deg negative dihedral.

Fin	Plan View	End View	Particulars
2	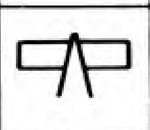	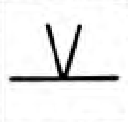	Span - 9.6 in., Chord - 2.4 in. Area - 4.4 percent of waterplane area Aspect Ratio - 4.0
2(a)		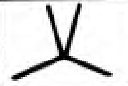	Fin 2 with 25-deg negative dihedral.
3		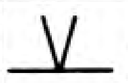	Fin 2 with 25-deg sweep-back.
3(a)	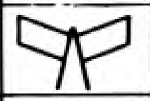	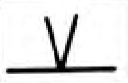	Fin 2 with 25-deg sweep-forward. (Fin 3 reversed)
4	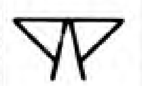	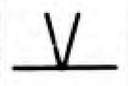	Maximum Span - 9.6 in. Maximum Chord - 4.8 in. Area - 4.4 percent of waterplane area
4(a)	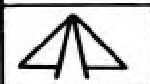	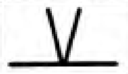	Fin 4 reversed
5	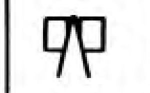		Circular Cylinders: Diameter - 2.0 in. Length - 3.0 in.
5(a)	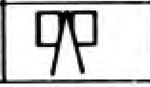	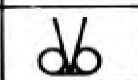	Fin 5 mounted above keel line.

Fig. 28 - Various anti-pitching fin configurations

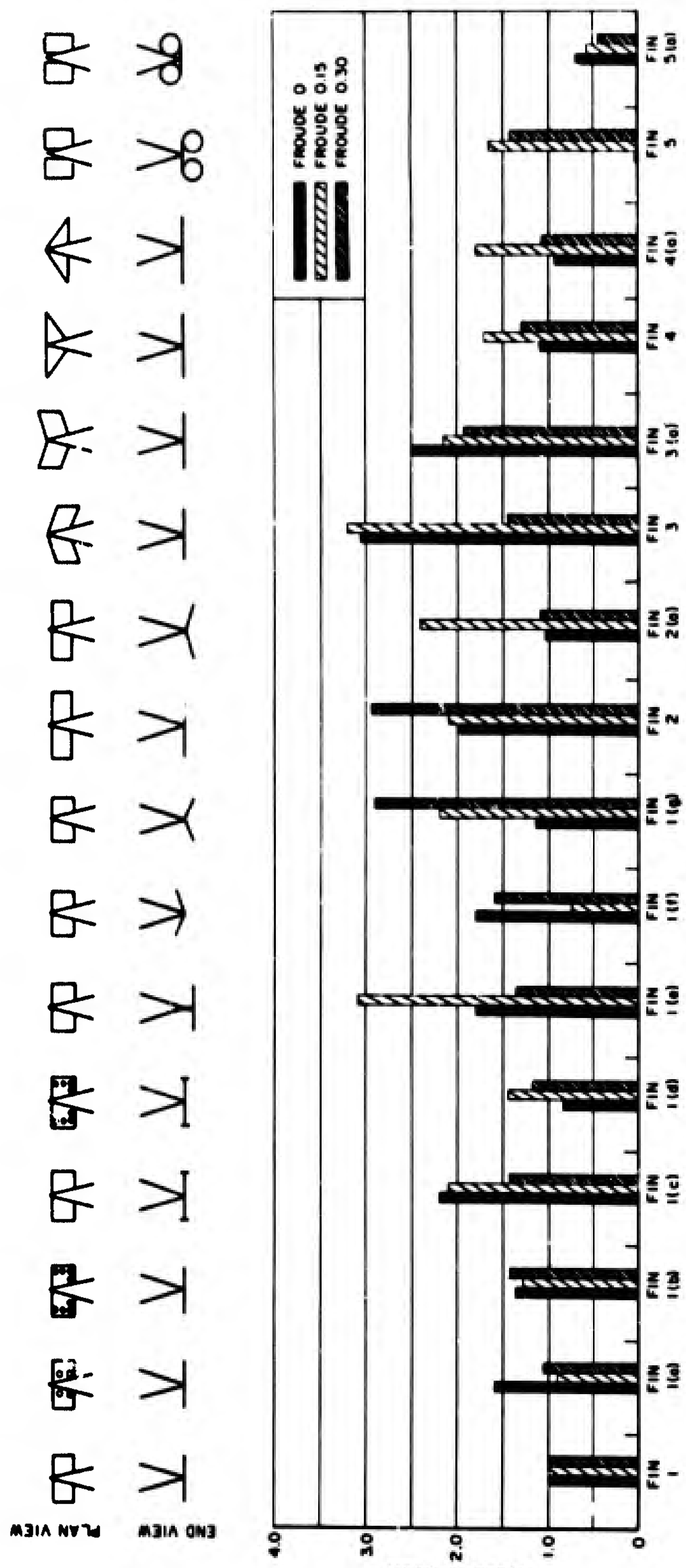

Fig. 29 - Qualitative evaluation of fin performance

Many other investigators have also made the point that the time differential of port and starboard collapse also add to the severity of the vibration. Ochi goes further and states that if this time differential is the same as the loading time, the vibration will be magnified It is further stated that if the fins remain below the water surface within some limit (8 feet for the MARINER), the cavity will not form and thus vibration will not occur.

Some other general conclusions are as follows:

1. Maximum pitch reduction is achieved by fins located in the forward 10 percent of the ship.

2. More severe vibration is induced by fins in these forward locations.

3. Planform area and pitch reduction are linearly proportional for the MARINER hull.

4. Vibration increases with fin area and with violence of pitching.

5. Fins with properly designed holes can be as effective as solid fins in reducing pitch and are superior in reducing vibration.

In selecting an optimum fin location, Ochi presents an interesting comparison of parameters which is reproduced here as Table 4. The values underlined with the double line are considered to be acceptable design values and of course only the location with all parameters underlined will be optimum.

Table 4
Optimum Fin Location for Various Parameters at a 15-Knot Ship Speed

	Location of Fin Aft of FP				
	FP	0.05 L	0.10 L	0.15 L	0.20 L
	Increase (%)				
Resistance	0	1.9	9.2	16.0	
	Reduction (%)				
Pitching	22.8	21.9	18.5	21.4	
Heave	31.5	20.7	12.9	8.0	
Bow Vertical Acceleration	24.5	19.0	15.5	11.8	
Slamming	85.0	85.0	81.8	67.7	
	Intensity				
Induced Vibration	1	0.66	0.35	0.10	0.02

Fixed Fins — Partially Activated

Brief mention will be made here of various suggestions and/or studies that have been forwarded to retard flow separation over a fixed bow fin. They are termed partially activated because some means of flap or flow control would have to be provided for their proper operation.

In his paper, Abkowitz [48] mentions a study conducted at MIT wherein boundary layer suction was used to control the pressure on the suction side of the fin. While the angle at which breakdown occurred was increased it was not prevented at large pitch angles.

Stefun and Schwartz [51] recommend further study in the use of moveable trailing edge flaps as devices to retard the onset of stale. Along this same general line, Goodman and Kaplan [53] have recently proposed the use of a jet-flapped hydrofoil as an anti-pitching fin. This device would take advantage of the existence of two pressure peaks (leading and trailing edge) causing the forward peak to be smaller than for a conventional foil for the same loading. This initial theoretical study indicated the foil did not separate. It was concluded therefore that the jet-flapped foil would be cavitation limited and for reasons of the lower initial pressure peak considerably more lift would be produced before cavitation occurred. The authors of this preliminary work plan additional efforts in this area.

Activated Bow Fins

The authors were unable to find any experimental work dealing with activated bow fins. Abkowitz [48] discusses this type of fin from the point of view of automatic control. With pitching motions as the control the fin angle would be additionally increased over an already large angle caused by the large amplitude of pitch. This method of control would therefore hasten the onset of ventilation. This leads to the concept of negative control, that is when the pressure on the foil reached a certain point, the foil angle would be decreased and thereby retard the onset of ventilation. The results of a computer study at MIT comparing this type of activated bow fin with a fixed fin indicated no difference in either method. Abkowitz concludes that there is little to recommend the use of an active bow fin.

Fixed Stern Fins

Abkowitz [48] makes mention of the use of fixed stern fins and concludes that they would be much less effective than bow fins. In addition to the obvious disadvantages of operating in the ship's boundary layer, the stern fin would probably increase the excitation due to waves and the pitch damping effect would also be reduced. The force applied to a stern fin would also produce less moment than a bow fin since the apparent pitch axis is generally aft of amidships.

In his experiments, Ochi [52] fitted a stern fin of equal area to the bow fin to the MARINER model. It was also found that the stern fin was much less effective than the bow fin in reducing pitch. Vibration was not a problem although maximum vibration still occurred at the bow. A combination of fixed stern fin and bow fin was also much less effective than a properly designed bow fin.

Activated Stern Fins

Spens [54,55] conducted model experiments on a MARINER class ship fitted with activated stern fins and tested these fins operating singly and in combination with fixed bow fins. The stern fins were NACA 0012 airfoil section of 22 foot span and 14.75 foot chord. These fins were fitted forward of the propeller as shown in Fig. 30. The fixed bow fins were similar to those fitted to the COMPASS ISLAND and are shown in Fig. 31.

After first conducting forced oscillation tests in calm water to determine basic fin characteristics, controlled tests were conducted in both regular and irregular waves. Table 5 presents the results of the regular wave tests while Table 6 shows those test results obtained in irregular seas (fully developed Newmann spectrum for 26 knot wind). These results indicate that the oscillating stern fins alone perform as effectively as fixed bow fins alone. There further appeared to be an additive benefit to using both sets of fins. It can also be seen

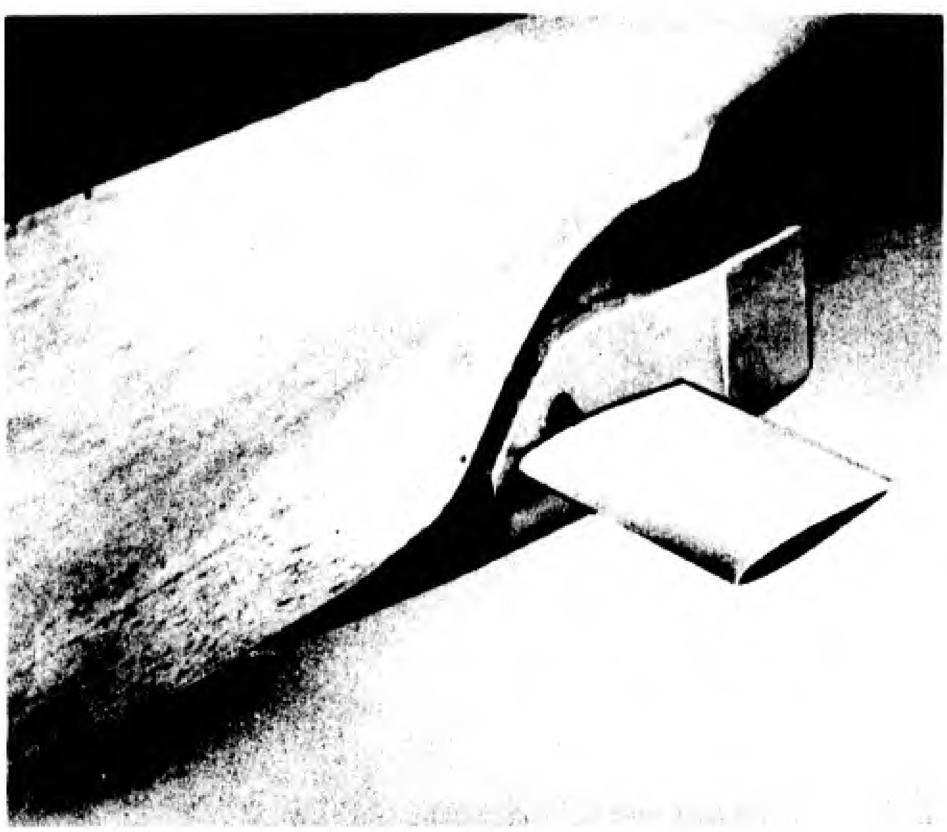

(a) Model as towed

Fig. 30 - Stern fins (Continued)

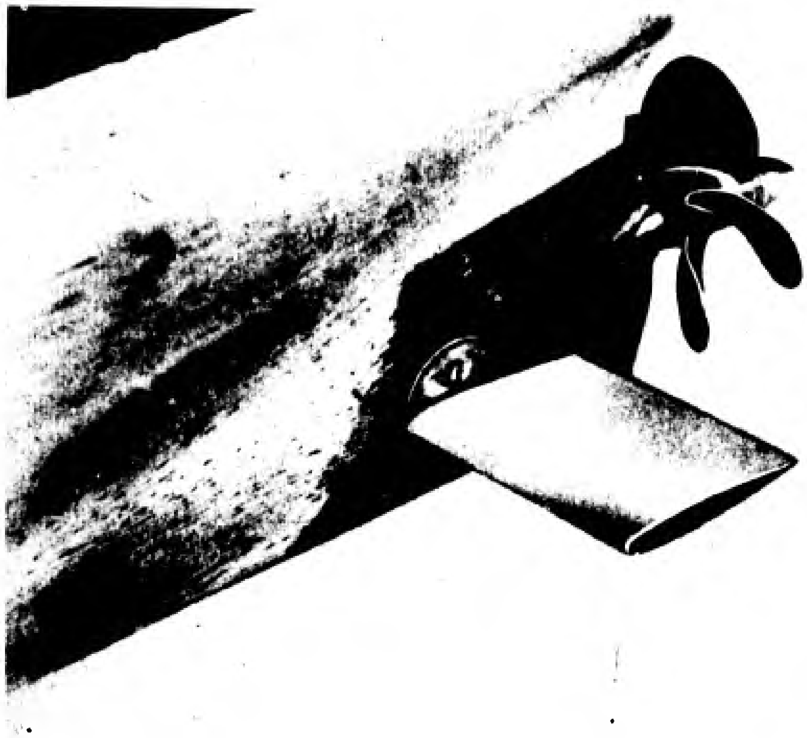

(b) Model equipped for self-propulsion

Fig. 30 - Stern fins

that while the bow fins increase in effectiveness with increased wave height (or increased angle of attack before the breakdown), stern fins produce a rather constant result irrespective of wave height.

Table 5
Effect of Oscillating Stern Fins With and Without Fixed Bow Fins in Regular Waves

Wavelength	1.0 L	1.3 L		1.5 L
Wave height	L/80	L/80	L/40	L/80
Pitch without fins, deg (double amplitude)	2.8	4.0	7.6	3.24
Pitch reduction by stern fins oscillating $\pm 25°$	1.45	1.7	1.5	1.1
Pitch reduction by oscillating stern fins together with fixed bow fins, deg	1.8	2.2	2.8	1.4

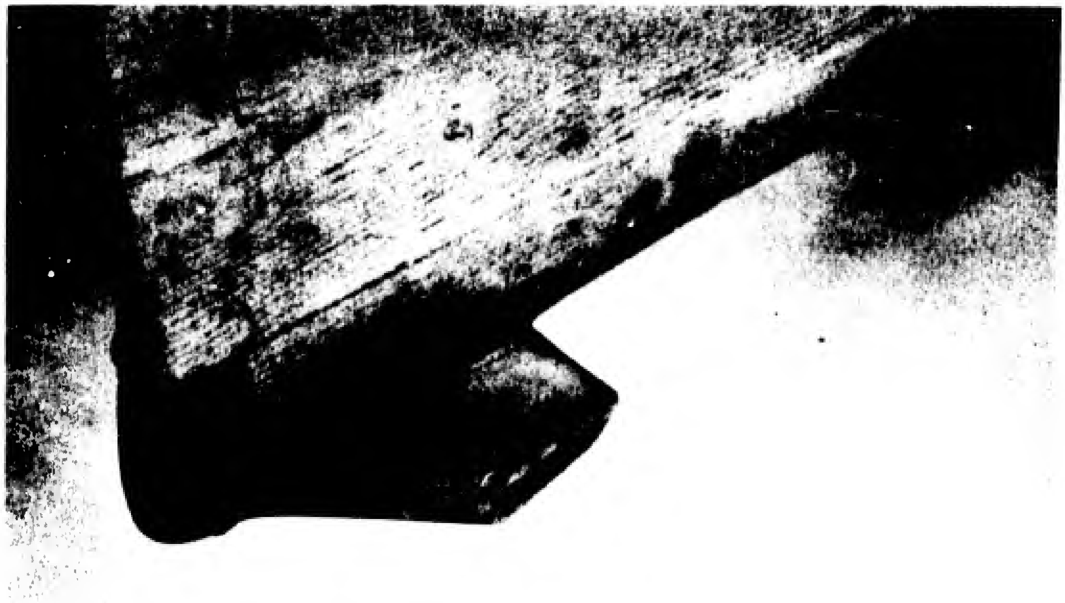

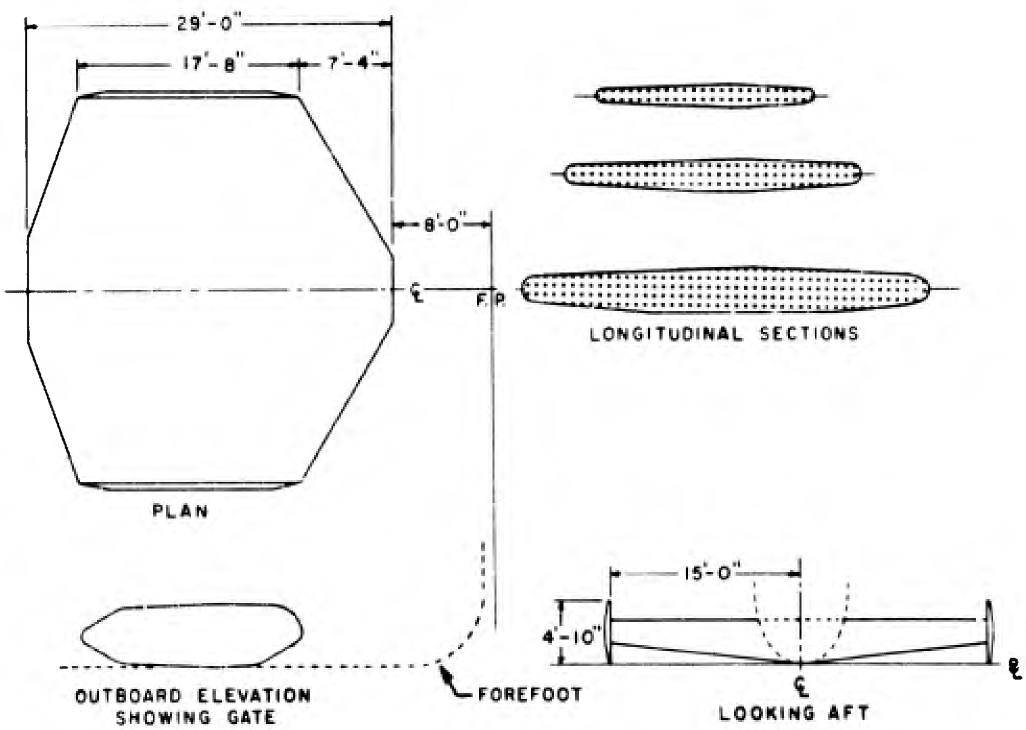

Fig. 31 - Bow fins

Table 6
Effect of Fins in Irregular Waves

	No Fins	Stern Fins Oscil-lating ±25°	Fixed Bow Fins	Bow and Stern Fins Together
Average of 1/3 largest pitches = $P_{1/3}$, deg (double amplitude)	6.2	4.9	4.9	3.9
Reduction in $P_{1/3}$		1.3	1.3	2.3
Average pitch = P_{av}, deg (double amplitude)	3.9	3.2	3.1	2.4
Reduction in P_{av}		0.7	0.8	1.5

Gersten and Cox performed additional work with activated stern fins at the David Taylor Model Basin. The results of these experiments are as yet unpublished. The tests were conducted on a model of the DE 1040 fitted with a pumpjet. The aft end of the pumpjet was further fitted with an oscillating flap in addition to an upper and lower flap in the shroud. An automatic control loop using pitch and pitch rate as control parameters was incorporated in these tests.

Experiments were conducted in calm water to determine which of several flap configurations could produce the largest pitching moment. Comparative tests with and without a flap fitted to the pumpjet were further conducted in irregular seas. As might be expected the flap arrangement with the largest total area produced the greatest calm water pitching (41.2 sq ft of flaps in pumpjet shroud plus 95.6 sq ft of flap C fitted to stern of pumpjet). Table 7 shows the preliminary results of the tests conducted in irregular waves. The table indicates that some pitch reduction was achieved in each case. These test data are undergoing complete analysis and a report should be issued soon. The decrease in fin effectiveness for increased wave height is an unexpected result.

Miscellaneous

One other area appears worthy of mention although it does not fall within any of the above categories. This is a technique of effectively reducing waterplane area by the use of open tanks. Linearized equations of motion for such a system are given in the Appendix. Results of such tests will be reported by Gersten in a forthcoming Taylor Model Basin Report. The work was performed on an oddly formed special purpose type naval vessel. A stern tank with sides open to the sea was fitted to this ship which had unusually bad pitching characteristics. Results of these tests indicated that while maximum motions were not reduced through the use of the tank, these maximums were transferred to much lower speeds. This would permit the ship to operate effectively in the design speed range.

Table 7
Preliminary Results of Activated Stern Fin Tests

Sea State	Ship Speed (knots)	Flap Oscil-lating	Percent Pitch Reduction Based on Pitch (rms)
Middle 5	16.3	No	
Middle 5	16.3	Yes	18.4
Middle 5	22.1	No	
Middle 5	22.1	Yes	22.5
Middle 6	16.3	No	
Middle 6	16.3	Yes	9.0
Middle 6	22.1	No	
Middle 6	22.1	Yes	17.2

CONCLUSIONS AND RECOMMENDATIONS

It should be stated that a design capability exists to produce successful installations of roll stabilization devices in ships. In the case of passive tanks, however, much remains to be learned of the nonlinear behavior of the tank-ship system. It has been indicated that many experimenters have concluded that the basic lack of a physical understanding of the behavior of the tank fluid will prevent further progress in this field. The knowledge required will probably only be gained through the proper simulation of a nonlinear model. Southwest Research will continue their efforts in this area and additional work is planned at the Taylor Model Basin.

Model and full-scale experiments will continue to be important design tools in this area until more theory is understood, even though both methods also have limitations. The continually changing nature of a seaway makes the collection of definitive design information during full-scale sea trials an extremely difficult task. While the capability for measuring sea spectra is increasing, proper account cannot be taken of the directional components of their effects on frequencies of encounter. Since the roll phenomenon may be nonlinear it is additionally difficult to properly normalize test data collected in this changing environment. Extreme care must be exercised when design information is extracted from full scale experiments.

While the various forcing functions can be controlled to a high degree during model experiments, scale effects and nonlinearities continue to complicate this approach. However, there are a large number of projects currently in progress aimed at providing an understanding of these scale effects and an insight into the basic nature of ship roll. It is felt that as nonlinear model tank simulations are achieved and the model problem areas cited above are rationalized, the model experiment will provide the most definitive design information.

Model experiments should also be conducted to provide design information for active fins and to evaluate the performance of existing designs. The Taylor Model Basin is currently designing such an experiment to evaluate the fin performance on a new class of destroyer escort. The same control device previously used during the activated stern fin experiments will be adapted to these tests. Suitable control parameters of roll angle, roll velocity and/or roll acceleration will be selected.

Additional experiments should be conducted on pitch stabilizing devices. In at least two areas cited there is discrepancy as to the effect of aspect ratio. These discrepancies might more fully be understood if the nature of varying aspect ratio were more closely examined. Stefun [50] and Stefun and Schwartz [51] vary aspect ratio independent of area. In both cases, the fin with larger span (increased aspect ratio) perform more reasonably in reduction of both pitch and vibration. Abkowitz [48] contends, however, that increased aspect ratio will have the effect of increasing low pressure on the upper surface and enhances the onset of breakdown. Laminar separation on the model may be the cause of varying test results in this area.

It would appear that for many naval applications, the use of pitch stabilization devices would definitely be in order. In addition to the common arguments in favor of stabilizing pitch for reasons such as stable radar sonar, or fire control platforms, Spens [55] makes one other valid point. He relates a pitch reduction to a possible decrease in freeboard and/or forefoot depth. When one considers the design difficulty associated with increasing freeboard or draft of smaller vessels such as destroyers any freeboard decrease would be a decided design advantage.

Increased depth and proper configuration design are the most important parameters to consider in bow fin design. Since the maximum depth of fin is a parameter not easily changed, lift control devices would have important design application. Additional model tests should be conducted to find proper design criteria and to clarify the hydrodynamics of the phenomena. In this respect, the following areas should be investigated:

1. Moveable flaps and jet flaps.

2. Activated bow fins using the pressure on the suction face as a control parameter.

3. Additional boundary layer control studies.

4. Additional investigation on parameters effecting relative bow motions and the subsequent effect on performance of bow anti-pitching fins.

5. Additional investigation of activated stern fins. In addition to conventional devices already described, items such as ring control surfaces around the propeller might be investigated applicably.

6. Investigation of scale effect on model results such as Reynolds number, near surface effects, etc.

Appendix

EQUATIONS OF MOTION FOR ANTI-PITCHING TANK

With the recent interest in passive anti-roll tanks, it is of interest to speculate on anti-pitching tanks. If, for instance, the forepeak tank of a ship were somewhat enlarged and fitted with large openings at the bottom, the surging of water in and out as the ship and waves interact might reduce pitching. Reference 56 reports on one special case in this regard. The tank involved was in the stern of a slender double-ended ship form. Not enough data is presented to compare with and without tanks, but the influence of the size of the tank openings on the pitch period is presented.

Figure 32 shows, in schematic form, the geometry of a bow tank open to the sea at the bottom. The equations of motion, assuming uncoupled pitch and heave for the "unstabilized" ship, have been derived using the Lagrangian formulation. Linearizing assumptions include all the usual ones in regard to small motions and linear damping. The tank geometry is assumed to be such that the area of the tank free surface does not change as the tank water level changes. It is also assumed that added mass terms and other coefficients of the ship are constants.

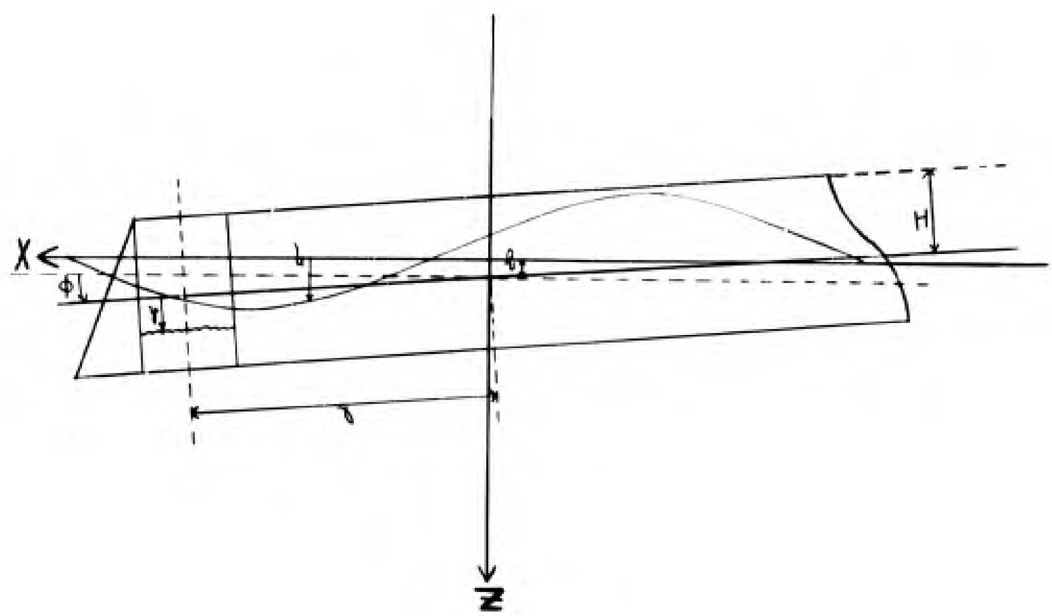

Fig. 32 - Sketch of coordinate system

The equations are:

$$I_{\phi\phi}\ddot{\phi} + B_{\phi}\dot{\phi} + k_{\phi\phi}\phi + I_{\phi h}\ddot{z} + I_{\phi h}\ddot{h} + k_{\phi h}h = ik_{\phi\phi}K_{\phi}\frac{2\pi\eta_o}{\lambda}e^{i\omega t}$$

$$I_{\phi h}\ddot{\phi} + I_{zz}\ddot{z} + B_z\dot{z} + k_{zz}z + I_{zh}\ddot{h} + k_t h = K_z k_{zz}\eta_o e^{i\omega t}$$

$$I_{\phi h}\ddot{\phi} + k_{\phi h}\phi + I_{zh}\ddot{z} + k_{tt}z + I_{th}\ddot{h} + B_t\dot{h} + k_t h = K_h k_t \eta_o e^{i\left(\omega t + \frac{2\pi l}{\lambda}\right)}$$

where

ϕ = pitch amplitude radians, positive bow up

z = heave amplitude feet, positive up

h = change in tank water level from equilibrium, feet, positive up

$I_{\phi\phi}$ = pitch inertia of ship, tank mass and "added mass"

I_{zz} = heave inertia of ship, tank mass and "added mass"

I_t = tank mass = $\rho A_o S$

A_o = area of tank free surface

$$S = \int_{-H}^{0} \frac{A_o}{A}\,ds$$

H = draft to bottom of tank

A = cross section (waterplane) area of tank at any vertical location

ρ = mass density of seawater

B_{ϕ}, B_z, B_t = linear damping coefficients in pitch, heave and of tank water motion

$k_{\phi\phi}, k_{zz}$ = pitch and heave "stiffnesses" excluding the tank free surface effect

k_t = $\rho g A_o$, "tank" stiffness

$I_{\phi h}$ = $\rho \ell \forall$

$\forall$ = tank volume

ℓ = distance of tank center of gravity from ship center of gravity, positive forward

$I_{zh} = \rho \forall$

$k_{\phi h} = \rho g \ell A_o$

K_ϕ = wave "effectiveness term" in pitch [57], the result of integrating the static wave profile over the hull length to determine pitching moment

K_z = wave "effectiveness" term in heave [57]

$K_h = e^{-2\pi H/\lambda}$, attenuation of wave height to keel

η_o = wave amplitude

ω = wave frequency.

The equations are symmetrical, and made somewhat more manageable in that several of the cross coupling terms are equal.

The equations can be rewritten by defining several natural frequencies and coupling coefficients. Dividing all equations by $k_{\phi\phi}$

$$\frac{\ddot{\phi}}{\omega_\phi^2} + \frac{b_\phi}{\omega_\phi}\dot{\phi} + \phi + \frac{\lambda_t}{\omega_{z\alpha}^2}\ddot{Z} + \frac{\lambda_t}{\omega_{z\alpha}^2}\ddot{\alpha} + \lambda_t \alpha = iK_\phi \left(\frac{\pi\ell}{\lambda}\right)\left(\frac{\eta_o}{\ell}\right) e^{i\omega t}$$

$$\frac{\lambda_t}{\omega_{z\alpha}^2}\ddot{\phi} + \frac{\lambda_{z\phi}}{\omega_z^2}\ddot{Z} + \frac{\lambda_{z\phi} b_\phi}{\omega_z}\dot{Z} + \lambda_{z\phi} Z + \frac{\lambda_t}{\omega_{z\alpha}^2}\ddot{\alpha} + \lambda_t \alpha = K_z \lambda_t \left(\frac{\eta_o}{\ell}\right) e^{i\omega t}$$

$$\frac{\lambda_t}{\omega_{z\alpha}^2}\ddot{\phi} + \lambda_t \phi + \frac{\lambda_t}{\omega_{z\alpha}^2}\ddot{Z} + \lambda_t Z + \frac{\lambda_t}{\omega_t^2}\ddot{\alpha} + \frac{\lambda_t b_t}{\omega_t}\dot{\alpha} + \lambda_t \alpha = K_h \lambda_t \left(\frac{\eta_o}{\ell}\right) e^{i\left(t + \frac{2\pi l}{\lambda}\right)}$$

where

$$Z = \frac{z}{\ell}, \qquad \alpha = \frac{h}{\ell},$$

$$\omega_\phi^2 = \frac{k_{\phi\phi}}{I_{\phi\phi}}, \qquad \omega_t^2 = \frac{k_t}{I_t},$$

$$\omega_z^2 = \frac{k_{zz}}{I_{zz}}, \qquad \omega_{z\alpha}^2 = \frac{k_t}{I_{hz}} = \frac{gA_o}{\forall},$$

$$b_\phi \equiv \frac{B_\phi}{\sqrt{k_{\phi\phi} I_{\phi\phi}}}, \qquad \lambda_t = \frac{\ell^2 k_t}{k_{\phi\phi}},$$

$$b_z \equiv \frac{B_z}{\sqrt{k_{zz} I_{zz}}}, \qquad \lambda_{z\phi} = \frac{\ell^2 k_{zz}}{k_{\phi\phi}}.$$

$$b_t \equiv \frac{B_t}{\sqrt{k_t I_t}},$$

When the tank parameters are set equal to zero, the equations reduce to the familiar simple equations for uncoupled pitch and heave.

To find a solution, assume that

$$\phi = \phi_o e^{i\omega t},$$

$$Z = Z_o e^{i\omega t},$$

$$\alpha = \alpha_o e^{i\omega t}.$$

Then,

$$\left(1 - \frac{\omega^2}{\omega_\phi^2} + i b_\phi \frac{\omega}{\omega_\phi}\right)\phi_o - \lambda_t \frac{\omega^2}{\omega_{z\alpha}^2} Z_o + \left(1 - \frac{\omega^2}{\omega_{z\alpha}^2}\right)\lambda_t \alpha_o = iK_\phi \left(\frac{2\pi\ell}{\lambda}\right)\left(\frac{\eta_o}{\ell}\right)$$

$$\frac{-\lambda_t \omega^2}{\omega_{z\alpha}^2}\phi_o + \left(1 - \frac{\omega^2}{\omega_z^2} + i b_z \frac{\omega}{\omega_z}\right)\lambda_{z\phi} Z_o + \left(1 - \frac{\omega^2}{\omega_{z\alpha}^2}\right)\lambda_t \alpha_o = K_z \lambda_t \left(\frac{\eta_o}{\ell}\right)$$

$$\left(1 - \frac{\omega^2}{\omega_{z\alpha}^2}\right)\phi_o + \left(1 - \frac{\omega^2}{\omega_{z\alpha}^2}\right) Z_o + \left(1 - \frac{\omega^2}{\omega_t^2} + i b_t \frac{\omega}{\omega_t}\right)\alpha_o = K_h \frac{\eta_o}{\ell}\left(\cos\frac{2\pi\ell}{\lambda} + i \sin\frac{2\pi\ell}{\lambda}\right)$$

In principle, given all the coefficients, these equations could be solved for pitch as a function of wave amplitude, and a response operator derived.

REFERENCES

1. Mandel, P., "Some Hydrodynamic Aspects of Appendage Design," Society of Naval Architects and Marine Engineers, Vol. 61, 1953

2. Taplin, A., "Notes on Rudder Design Practice," First Symposium on Ship Maneuverability, David Taylor Model Basin Report 1461, May 1960

3. Wahab, R. and Swaan, W. A., "Coursekeeping and Broaching of Ships in Following Seas," Journal of Ship Research, Vol. 7, No. 4, Apr 1964

4. Davidson, K. S. M., "The Steering of Ships in Following Seas," Stevens Institute of Technology, Experimental Towing Tank, TM 94, Apr 1960

5. DuCane, P. and Goodrich, G. J., "The Following Sea, Broaching and Surging," Royal Institute of Naval Architects, Vol. 104, No. 2, Apr 1962

6. Grim, O., "Surging Motion and Broaching Tendencies in a Severe Irregular Sea," Davidson Laboratory Report 929, Nov 1962

7. Dieudeonne, Jean, "Collected French Papers on the Stability of Route of Ships at Sea, 1949-1950," David Taylor Model Basin Translation 246, Jan 1953

8. Strandhagen, A. G., "Preliminary Analysis of Manual and Automatic Steering of a Directionally Unstable Model which Exhibits a Loop," David Taylor Model Basin Report 1280, Oct 1958

9. Schiff, L. and Gimprich, M., "Automatic Steering of Ships by Automatic Control," Society of Naval Architects and Marine Engineers, Vol. 57, 1959

10. Nomoto, Kensaku, "Directional Stability of Automatically Steered Ships with Particular Reference to Their Bad Performance in Rough Sea," First Symposium on Ship Maneuverability, David Taylor Model Basin Report 1461, May 1960

11. Sutherland, W. H. and Korvin-Kroukovsky, "Some Notes on the Directional Stability and Control of Ships in Rough Seas," Stevens Institute of Technology, Experimental Towing Tank, Note No. 91, Oct 1948

12. Davidson, K. S. M. and Schiff, L., "Turning and Course Keeping Qualities," Society of Naval Architects and Marine Engineers, Vol. 54, 1946

13. Chadwick, J. H., "On the Stabilization of Roll," Society of Naval Architects and Marine Engineers, Vol. 63 (1955)

14. Heller, S. R., Discussion of "Some Hydrodynamic Aspects of Appendage Design," Ref. 1

15. Martin, M., "Roll Damping Due to Bilge Keels," University of Iowa, Nov 1958

16. Keulegan, G. H. and Carpenter, L. H., "Forces on Cylinders and Plates in an Oscillating Fluid," Journal of Research, National Bureau of Standards, Vol. 60, No. 5, May 1958

17. White, W. H., "The Qualities and Performances of Recent First Class Battleships," Institute of Naval Architects

18. Spear, L., "Bilge Keels and Rolling Experiments USS OREGON," Society of Naval Architects and Marine Engineers, 1898

19. Minorsky, N., "Problems of Anti Rolling Stabilization of Ships by the Activated Tank Method," American Society of Naval Engineers, Vol. 47, 1935

20. Chadwick, J. H. and Klotter, K., "On the Dynamics of Anti-Rolling Tanks," Stanford University, Feb 1953 and Forshungshefte für Schiffstechnik, 1955

21. Bell, J., "Ship Stabilization, Controls and Computation," Institute of Naval Architects, 1957

22. DuCane, P. and Dadd, R. H., "Control of Roll-Damping System," First Symposium on Ship Maneuverability

23. Flipse, J. E., "Stabilizer Performance on the SS MARIPOSA and SS MONTEREY," Society of Naval Architects and Marine Engineers, Vol. 65, 1957

24. Wallace, W., "Experiences in the Stabilization of Ships," Institution of Engineers and Shipbuilders in Scotland, Vol. 98, 1955

25. Chadwick, J. H., "The Anti-Roll Stabilization of Ships by Means of Activated Fins," TR No. 2, Stanford University, Feb 1953

26. DuCane, P., Discussion on "Stabilizer Performance on the SS MARIPOSA and SS MONTEREY," Ref. 23

27. Avramescu, A., "A New Comprehensive Integral Criterion for Optimalization of Automatic Control Systems," from Rev. Elecltotechn. et Energ (RPR) Vol. A7, No. 1, 1962

28. Aref'ev, B. A., "Use of the Integral Criterion in Certain Control Problems," Isvestia Vysshikh Vchebnykh Zavedeniy Priborostroyeniye, Vol. 6, No. 1, 1963

29. Froude, W., "On the Rolling of Ships," Institute of Naval Architects, 1862

30. Frahm, H., "Results of Trials of the Anti-Rolling Tanks at Sea," Institute of Naval Architects, Vol. 53, 1911

31. Vasta, J., et al., "Roll Stabilization by Means of Passive Tanks," Society of Naval Architects and Marine Engineers, Vol. 69, 1961

32. Chadwick, J. H. and Morris, A. J., "The Anti Roll Stabilization of Ships by Means of Activated Tanks," Stanford University (in four parts) Dec 1950, Jan 1951, Jul 1951, Mar 1951

33. Blagoveshchensky, S. N., "Theory of Ship Motions," Dover Publications, New York, 1962

34. Lamb, H., "Hydrodynamics," Sixth Edition, Dover Publications, 1945

35. Thornycroft, J. I., "Steadying Vessels at Sea" (Moving Weight System), Institute of Naval Architects, 1892

36. Jackson, P. R., "The Stabilization of Ships by Means of Gyroscopes" (Sperry System), Institute of Naval Architects, 1920

37. White, W., "Experiments with Dr. Schlicks Gyroapparatus for Steadying Ships," Institute of Naval Architects, 1907

38. Deimel, R. F., "Mechanics of the Gyroscope," The MacMillan Co., 1929, Dover Publications, 1950

39. Pierson, Willard J., Jr., "Ocean Waves," International Science and Technology, No. 30, Jun 1964

40. Foster, John J., "Preliminary Evaluation of Passive Roll Stabilization Tanks Installed Aboard the USNS ELTANIN (TAK 270)," David Taylor Model Basin Report 1622, May 1962

41. Motora, Seiza and Lalangas, Petros A., "Experimental Study of a Passive Anti-Rolling Tank Installation in a Ship Model Running in Oblique Seas," Davidson Laboratory Report R-961, May 1963

42. Lalangas, Petros A., "Effect of Speed and Wave Height on the Rolling of a Ship Model with Passive Anti-Roll Tanks," Davidson Laboratory Report LR-1018, Mar 1964

43. Zarnick, E. E., "USS GYATT (DDG 712) Anti-Rolling Fin Evaluation in a State 4 Sea," David Taylor Model Basin Report 1182, Jan 1958

44. Dalzell, John F. and Wen-Hwa Chu, "Studies of Ship Roll Stabilization Tanks," Southwest Research Institute Quarterly Progress Report Project No. 55-1268-2, Sep 1963

45. Dalzell, John F., "Continuation of Studies of Ship Roll Stabilization Tanks," Southwest Research Institute Proposal 2-3175, Mar 1964

46. Pourmaras, Ulysses A., "Pitch Reduction with Fixed Bow Fins on a Model of the Series 60, 0.60 Block Coefficient," David Taylor Model Basin Report 1061, Oct 1956

47. Pourmaras, Ulysses A., "A Study of the Sea Behavior of a MARINER-Class Ship Equipped with Antipitching Bow Fins," David Taylor Model Basin Report 1084, Oct 1958

48. Abkowitz, Martin A., "The Effect of Antipitching Fins on Ship Motions," Transactions of the Society of Naval Architects and Marine Engineers, Vol. 67, 1959

49. Becker, Louis A. and Duffy, Donald J., "Strength of Antipitching Fins and Ship Motions Measured on USS COMPASS ISLAND (EAG 153)," David Taylor Model Basin Report 1282, Apr 1959

50. Stefun, George P., "Model Experiments with Fixed Bow Antipitching Fins," Journal of Ship Research, Vol. 3, No. 2, Oct 1959

51. Stefun, George P. and Schwartz, F. M., "Effect on Hull Vibrations of Various Bow Anti-Pitching Fin Configurations," David Taylor Model Basin Report 1659, Nov 1962

52. Ochi, Kazuo M., "Hydroelastic Study of a Ship Equipped with an Antipitching Fin," Transactions of the Society of Naval Architects and Marine Engineers, Vol. 69, 1961

53. Goodman, Theodore R. and Kaplan, Paul, "Feasibility of Employing Jet Flapped Hydrofoils as Ship Anti-Pitching Fins," Oceanics Inc. Report No. 63-08, Dec 1963

54. Spens, Paul G., "Research on the Reduction of Pitching Motion of Ships by Means of Controllable Fins," Davidson Laboratory Report No. 733, Dec 1958

55. Spens, Paul G., "Research on the Reduction of Pitching Motions of Ships by Controllable Fins," Davidson Laboratory Report No. 913, Nov 1962

56. Lalangas, P., Van Mater, P. R., and Marks, W., "Interim Report on Model Experiments on Escort Research Vessel in Waves," Stevens Institute of Technology Report 814, Nov 1960

57. Giddings, A. J., "Engineering Estimates of Ship Motions," Bureau of Ships Associate of Senior Engineers, 1964 (to be published by American Society of Naval Engineers)

58. Giddings, A. J., "Progress in Tank Stabilizers," Fourth Seminar on Ship Behavior at Sea, Stevens Institute, Jun 1962

59. Motora, S., "Steadying Device of the Rolling of Ships," U. S. Patent, 1925

60. Allan, J. F., "The Stabilization of Ships by Activated Fins," Institution of Naval Architects, Vol. 87, 1945

* * *

DISCUSSION

Peter DuCane
Vosper Limited
Portsmouth, England

The authors of this interesting paper mention that model tests of anti-rolling fins either alone or on ship models have not been reported. However, we at Vosper have, in fact, carried out quite a number with what we consider to be a useful degree of success so far as the actual results are concerned.

We claim that in the case of the nonretracting low aspect ratio fin we can produce a fin section which can be equally, or more, effective than the flapped fin for the same area.

Without entering unduly into details it could be mentioned that in many cases it is clear that the greatest percentage of roll reduction does not of necessity indicate the most comfortable condition so far as roll amplitude is concerned.

Quite small rolling amplitudes in certain complex wave patterns can give a most disappointing result on the basis of roll reduction with fins on against fins off. However, these cases do not really matter to the passenger and there is probably still quite a possibility of saving power in the operation of these fins by area reduction.

The fin sizes can be substantially reduced without much loss of effective performance in their true capacity as roll dampers if, instead of 3°-4° being aimed for, say 6°-7° double amplitude is aimed for under the same conditions — no passenger could reasonably complain at this.

At the same time I believe it is a short sighted policy to ignore the possibility of, and in fact reported occurrence of, quite large rolls in "stabilised" ships under certain circumstances.

The situation is, of course, that the activated fin is not in truth a stabiliser, or if it is ordered to act as one by an amplitude signal in the control system it is a very poor stabiliser. By far the most important function of an anti-rolling activated fin is to act as a damper controlled from a velocity signal.

As the fins are usually designed on an empirical basis to cause a heel of 5°-7° when at full incidence and full cruising speed it can well be understood that this means little in restoring effect when considering a roll induced by yaw at practically no frequency when leading up to conditions of broaching such as are met by even the largest liners in a quartering sea.

While acting as a damper a sluggish fin movement can cause an important phase lag leading towards the case where the fin is helping the roll. I do not say for one minute this is a normal state of affairs but in nearly all installations this can happen despite the fact that most of the time the fitting of anti-rolling fins is highly effective and universally popular. This is where the acceleration term can help by incorporating an element of phase advance and getting things moving in plenty of time.

Incidentally we as a firm always point out that good as they may be fins do not, of necessity, reduce the incidence of sea sickness and it is a somewhat dangerous policy to say they do because it is probably more the pitching accelerations which cause the trouble.

It is probably time that "stabilising" devices were offered subject to performance specifications as the present method of advertising the optimum reduction percentage under ideal conditions, or at least specially selected conditions is meaningless and misleading.

The difficulty here, of course, is in specifying, in a meaningful way, the seaway in which the performance specified should be achieved and furthermore in recording the nature of the actual sea in which the performance is achieved.

Though without first hand experience it must surely be a somewhat sobering thought that at the very low frequencies experienced in quartering seas in the Western Ocean there is quite a likelihood, if not certainty, that the water in any passive tank will provide an unstabilising moment just at the wrong time.

Again I thank the authors.

* * *

DISCUSSION

John F. Dalzell
Southwest Research Institute
San Antonio, Texas

The discussor would, in all sincerity, like to compliment the authors on one of the most straightforward and informative papers on the subject to come his way in some time. The authors' summary of the work on passive anti-roll tanks at Southwest Research Institute is adequate and exactly to the point. We have recently submitted a draft Technical Report* summarizing our efforts in this field which concludes, as did the authors, that a nonlinear model must be discovered before any significant gain over present design methods can be foreseen, and that experiments will continue to play a large part in passive anti-roll

*Studies of Ship Roll Stabilization Tanks, Technical Report No. 1, Contract NONR 3926(00), by John F. Dalzell, Wen-Hwa Chu, J. Everett Modisette, Southwest Research Institute, August 1964.

tank investigations. We feel that the tank scale effect problem must be further explored if passive anti-rolling tanks are to continue to be installed in seakeeping basin ship models. We have attained better agreement than that shown in Fig. 25 of the paper between our current weakly nonlinear theory and other experimental data. This better agreement is, however, not sufficiently good for practical use. One further remark is perhaps justified and that is that detailed space-time mappings of the free surface in a tank indicate that the fluid seldom behaves in a fashion similar to either that in a U-tube or to a first mode standing wave. Evidently, considerable additional effort on the fluid dynamics of the free-surface passive anti-rolling tank will be necessary.

* * *

DISCUSSION

S. Motora
University of Tokyo
Tokyo, Japan

I would like to make some short comments on the anti-pitching tank. As Mr. Giddings has mentioned, the idea is to put openings at the bottom of fore or aft peak tanks to let sea water come in and out in a 90 degree phase lag behind the pitching motion resulting in a reduction of pitching motion.

This problem was initiated by the Technical Research Laboratory of Hitachi Shipbuilding Co. and was published in the fall, last year. In that paper, movement of the water level in open tanks, installed at the bow and the stern, is analysed theoretically, and the pitching angle of a ship in regular waves, affected by such tanks, is calculated. A model experiment with a model of a passenger ship was conducted to check the calculation. Two tanks were installed; one at the bow and one at the stern. The total water plane area of the tanks was 25 percent of the ship's water plane area.

Results are as shown in Fig. 1, where a is the area of the openings at the bottom of the tanks and A is the waterplane area of the tanks. About 45 percent reduction at the maximum was attained.

I treated the same problem and dealt mainly with the fundamental characteristics of tanks with openings under the waterline.

At first, let us consider a tank with a vertical wall. In Fig. 2, suppose a tank has openings of area a. Free surface area of the tank is A, the depth of the openings is h_o, heaving of the tank is z, and elevation of tank water is ξ.

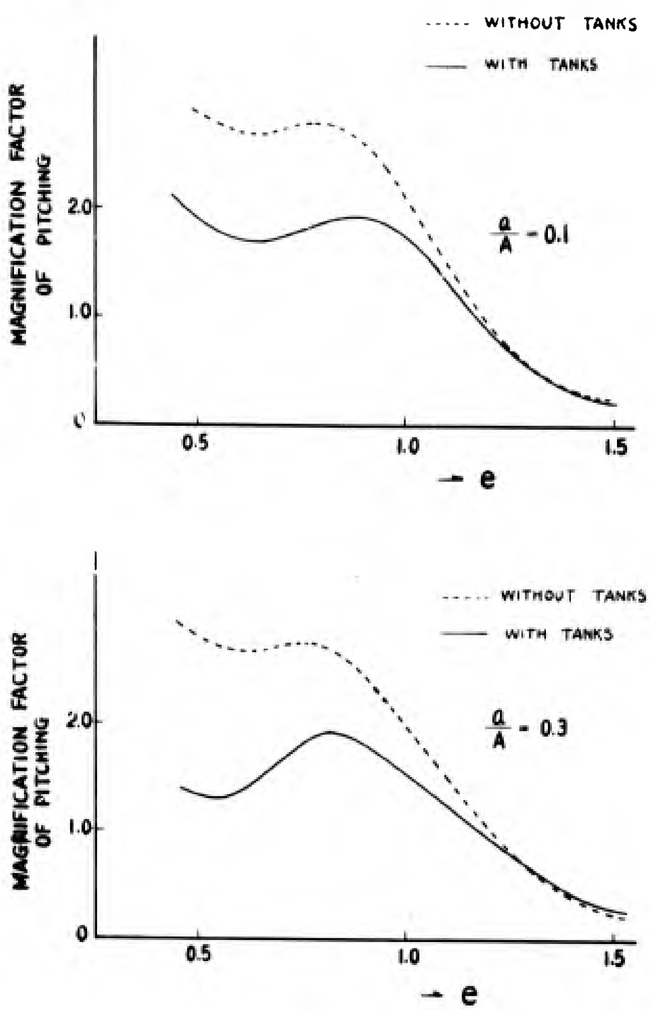

Figure 1

Then the equation of motion will be written as Eq. 1 in Fig. 1. It is noted that the excitation is modulated by a function which becomes zero when $\omega_o = \sqrt{g/h_o}$. It means that tank water does not move at all at this frequency regardless of amount of heave. Therefore, this frequency will be called as zero response frequency.

From this it can be seen that h_o should be chosen so that ω_o does not coincide with the natural frequency of pitching. Considering the average pitching period, it can be easily seen that h_o should not be too large.

On the other hand, the resonant frequency of the tank water level is also $\sqrt{h_o/g}$ which is the same as the zero-response frequency. Therefore, in this case of wall sided tanks, the response of tank water is very small and will not be effective.

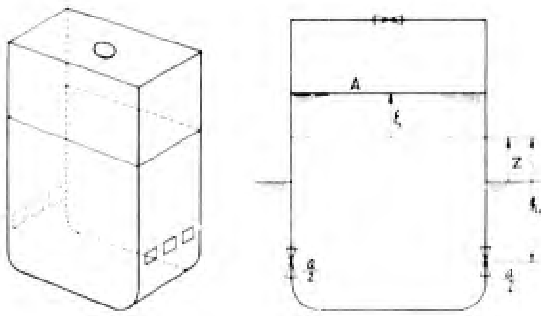

$$h_0\ddot{\zeta} + \frac{1}{2}\left(\frac{A}{a}\right)^2\dot{\zeta}^2 + g\zeta = \left[h_0\omega^2 - g\right]\bar{Z}e^{i\omega t} \quad ------(1)$$

$\omega_0 = \sqrt{\frac{g}{h_0}}$ ZERO RESPONSE FREQUENCY

$\omega_1 = \sqrt{\frac{g}{h_1}}$ NATURAL FREQUENCY OF TANK WATER LEVEL

Figure 2

In Fig. 3, the magnification factor of the response of the tank water level is plotted against the frequency. Two solid lines show the solution of the Eq. 1 for A/a = 4.17 and 6.52. It can be seen that the smaller the openings, the less response. Plots are made of the experimental values. There are some disagreements with the theory, but, if the damping coefficient is doubled, i.e., the effective area of the openings is reduced to 7/10, the theoretical values agree very well with the experimental data.

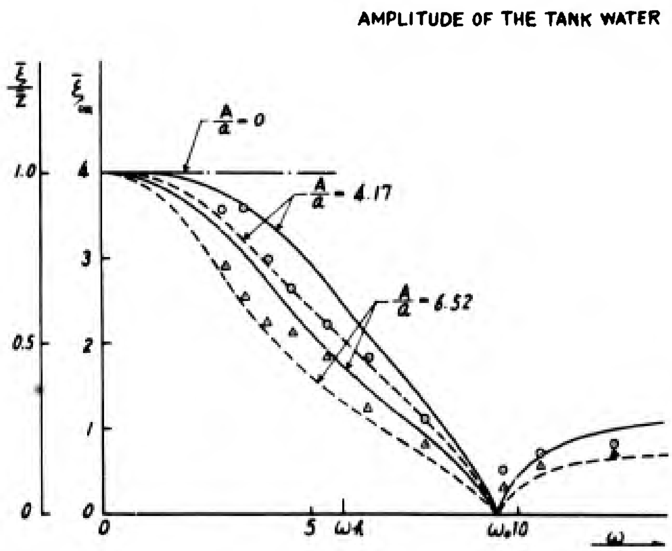

Figure 3

To avoid the defect that zero-response frequency coincides to the resonant frequency of the tank water, a flared tank was studied. In this case, as shown in Fig. 4, the inertia term changes somewhat and h_o becomes h_o' in this case. Since $h_o' > h_o$ for normal flare, resonant frequency does not coincide with the zero frequency and becomes nearer to the ship's natural pitching frequency. Therefore the effectiveness of the tank will be improved.

TANK WITH FLARED WALLS

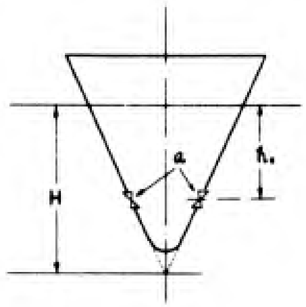

$$\underbrace{H \ln \frac{H}{H-h_o}}_{h_o'} \ddot{\zeta} + \frac{1}{2}\left(\frac{A}{a}\right)^2 \dot{\zeta}^2 + g\zeta = (h_o\omega^2 - g)\bar{Z}e^{i\omega t} \quad \text{-----}(2)$$

$$\omega_o = \sqrt{\frac{g}{h_o}}, \qquad \omega_s = \sqrt{\frac{g}{h_o'}}$$

Figure 4

However, the amount of the flare will not be chosen arbitrarily. If ducts of certain length l are attached to the openings, the equation of motion will be written as Eq. 3 in Fig. 5.

In general

$$h_o' = \int_0^{l} \left(\frac{A}{ax}\right) dx$$

is called hydraulic length. The longer and narrower the duct, the longer the hydraulic length and the smaller the resonant frequency.

Therefore it will be possible to bring the resonant frequency of tank water to equality with the pitching frequency, and to make it quite different from the zero-response frequency.

A 2m model of a catamaran was provided with fore open tank and tested in waves. The waterplane area of the tank is 5 percent of the total waterplane area.

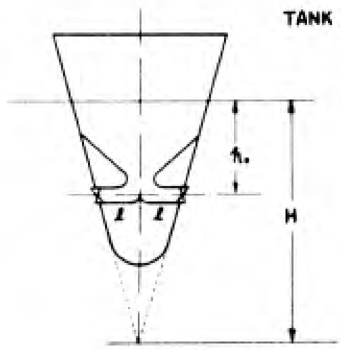

TANK WITH DUCTED HOLES.

$$\underbrace{\left(\frac{A}{a}l + H\ln\frac{H}{H-h_0}\right)}_{h_0'}\ddot{\xi} + \frac{1}{2}\left(\frac{A}{a}\right)^2 + g\xi = (h_0\omega^2 - g)\bar{Z}e^{i\omega t} \quad ------(3)$$

h_0' = HYDRAULIC LENGTH = $\int_0^l \frac{A}{ax}\,dx$

$\omega_0 = \sqrt{\frac{g}{h_0}}, \qquad \omega_s = \sqrt{\frac{g}{h_0'}}$

Figure 5

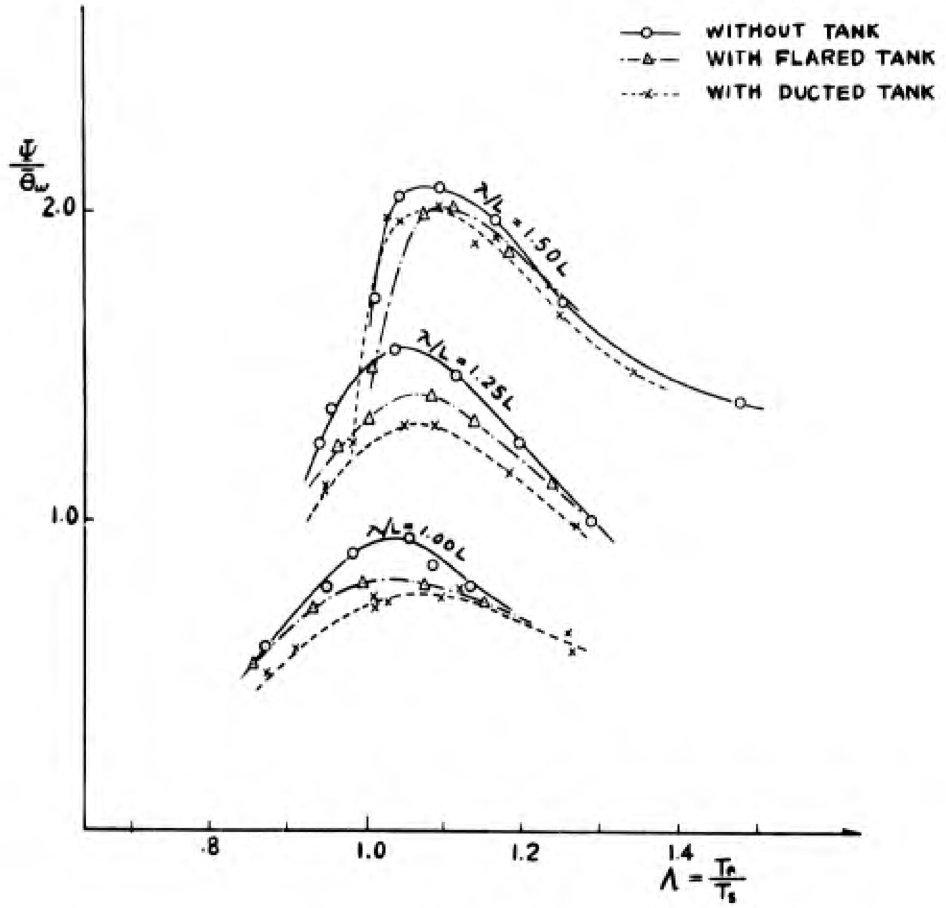

Figure 6

In Fig. 6, solid lines show the pitching magnification factor when the tank was blocked. Broken lines show the results with a flared tank and with simple holes.

Chain lines show the results with a flared tank and with ducted openings. About a 20 percent reduction at the maximum was attained with a ducted tank.

* * *

DISCUSSION

E. Numata
Stevens Institute of Technology
Hoboken, New Jersey

Davidson Laboratory is pleased to have been associated with the USN Bureau of Ships and DTMB in experimental model research on anti-pitching fins and passive anti-rolling tanks since 1956. One of the earliest, although subsidiary, investigations conducted at DL concerned the magnitude of the influence of fixed bow anti-pitching fins on the longitudinal midship bending moment of the COMPASS ISLAND. It was found that the fins had no adverse effect on hull bending moment.

In connection with stern anti-pitching fins, an analytical study for DTMB at Davidson Laboratory showed that in head seas at wave and ship speed conditions bracketing synchronous pitching motion, the hydrodynamic angle of attack of fixed stern fins is very small. Thus stern fins must be activated to be effective, producing a stabilizing moment and decrease in pitch angle which are proportional primarily to their amplitude of oscillation and relatively independent of the pitching amplitude. We found this to be true also in the case of oscillating fins astern of a pump jet propeller on a destroyer escort model tested for Eastern Research Group several years ago. This characteristic of a fixed number of degrees reduction may explain why in the author's Table 7 the percentage pitch reduction decreases as sea state and pitch angle increase.

In connection with full scale evaluation trials of passive anti-rolling tanks, it seems to me that instead of vainly hoping for ideal wave conditions of unvarying severity and direction, it might be better to conduct trials in the calm seas one usually finds when searching for rough water. Rolling excitation could be provided by some form of portable oscillating weight device. Since most naval and oceanographic vessels fitted with passive tanks are of modest size with reasonable metacentric heights, it should not be too great an engineering problem to design and assemble a device whose oscillation frequency can be varied while providing sufficient roll exciting moment to give a static heel of about 2°. Thus a frequency response could be obtained for the ship with and without the passive tanks operating. The omission of sway excitation would be a necessary but not totally undesirable condition.

* * *

DISCUSSION

K. C. Ripley
John J. McMullen Associates, Inc.
Washington, D.C.

I desire to comment on the figure of 90 percent as the reduction of roll at ships resonance, that was mentioned by Mr. Giddings in connection with one of the slides of his talk, namely, the slide showing Fig. 11 of the paper.

The design of passive tanks of the particular ship to which Fig. 11 refers is one with which I am familiar. Up until late 1960, I had been employed for 25 years with the U.S. Bureau of Ships, and during this time designed a number of passive anti-rolling tanks, one of which was for the Oceanographic Research Vessel, AGOR. This is the vessel that by model test in an irregular, bow sea showed the reduction of roll at ships resonance of the 90 percent.

It is my opinion that the foregoing, reported roll reduction is real, and can be accepted as representative of what would have been obtained by the same or similar test performed full-scale at sea. This opinion just expressed is based on personal experience obtained at sea with a merchant ship. This ship tested at sea was fitted with bilge keels, and was tested for the stabilizer tanks operative, and inoperative. The sea was a quartering sea. The reduction of roll at ships resonance was found to be 85 percent.

How is it possible for the reduction of roll at ships resonance to be as large as 85 to 90 percent when the test is conducted in an irregular sea, whether the sea be model-scale, or full-scale? When the reduction of roll is found for another condition of test, namely, for a bench model type of test, the reduction of roll is not as great. In this latter type of test, the roll response is that for pure, steady-state, forced roll. In the former type of test, nothing closely resembling steady roll is ever obtained, and what might appear to be forced roll is in reality an interaction between the instant to instant values of stored energy of roll of the ship, and the instant to instant values of input of energy of roll from the sea.

It is well known that ships at sea tend to roll at or near ships resonance almost irrespective of the frequencies of excitation existing in the sea. We all know that this is what actually happens in roll at sea, but then we are all prone to forget what the actual situation at sea is, in order that we may treat the instant to instant roll as representing steady-state forced roll. It is true that after a ship has been well stabilized against roll, the ship will behave more like one the roll of which is pure forced roll. Before the ship has been well stabilized against roll, however, the ship will be rolling more often at ships resonance than otherwise would be the case. It is clear that a roll reduction at ships resonance as great as 85 to 90 percent when the determination is by test at sea is both reasonable, and comprehensible. A part of the roll reduction is from having a less amount of energy tending to roll the ship at the ships natural frequency, and a part of the roll reduction is from allowing less forced roll of the ship when the roll can be treated as more nearly resembling pure, forced roll.

I want to compliment the authors for an interesting and informative paper. The paper by being a survey is a mine of information on a wide range of topics, having to do with ship motion stabilization.

* * *

DISCUSSION

A. Silverleaf
National Physical Laboratory
Teddington, England

This interesting survey is almost as surprising for its omissions as for the topics which it discusses at some length. For instance, it is more than surprising to find no reference to the paper by the late J. F. Allan, "The Stabilisation of Ships by Activated Fins," Transactions of the Institution of Naval Architects, 1945, Vol. 87, which was the first published account of the modern development of the type of roll stabiliser still that most commonly used and adopted. The authors' suggestion that the design of activated fin stabilisers has developed in an unscientific manner is completely contrary to the facts. Activated fin stabilisers of the type now known as the Denny-Brown-A.E.G. have been continuously developed for the past 25 years by a skillful and systematic combination of theory, model experiment and full scale practice. This applies not only to the activating and control mechanisms but also to the basic hydrodynamic design of the fins themselves, for which in 1942 I developed an inverse Theodersen procedure for designing foil shapes with delayed cavitation characteristics. Similar methods were being independently and simultaneously developed for aerofoil sections and have produced among other things the well known "flat top" sections. The authors' doubts about the value of roll stabilisers of this type were certainly not endorsed by the crews of the ships of the Royal Navy fitted with such stabilisers during the Second World War; in many cases they were the only ships able to offer any effective defence against air attack because they provided a reasonably stable firing platform.

The authors' discussion of roll stabilisers of the passive tank type is of great interest to us at N.P.L., where such stabilisers have been designed for some time. It is our growing opinion that a wide variety of shapes and configurations can be effectively used for this purpose, and indeed it is almost true to say that only a very good man can design a really bad system. Dr. Kaplan's reference to activated pitch stabilisers revives interesting memories for me. Almost seven years ago Mr. Goodrich and I took out a provisional patent for just such a stabiliser, incorporating a jet flap, but allowed it to lapse because we found great difficulty in producing a system of reasonable overall mechanical and hydrodynamic efficiency. Naturally we shall be most interested in this new attempt to exploit this attractive idea. However, I might venture a word of caution. While many devices, including bulbous bows and fins, show a reduction in pitch in regular waves, this improvement is often not shown in terms of significant motions in irregular waves. General experiments in regular waves are not carried out in long enough wave lengths in which these devices can show undesirable response characteristics; experiments in irregular wave systems include the responses to such wave lengths.

* * *

REPLY TO THE DISCUSSION

Alfred J. Giddings
Bureau of Ships
Washington, D.C.

and

Raymond Wermter
David Taylor Model Basin
Washington, D.C.

The authors' are pleased with the response to the paper. Mr. Ripley's remarks are appreciated, as coming from one who re-initiated the interest in passive tank stabilization.

The additional information on anti-pitching tanks presented by S. Motora is especially interesting. Continued work on this line may well lead to much improved seakeeping, at least for special ships.

Mr. Dalzell's recent work on the details of anti-roll tank dynamics is somewhat discouraging in that the nonlinearities inherent in the phenomenon are confirmed. The simplified analyses that have sufficed for design in the past, must be replaced by more elegant processes to realize the full potential of passive tanks.

The state of the art in fin stabilization as discussed by Commander DuCane continues to advance. The reduction of design fin capacity as advocated by the Commander, is not endorsed by the authors. There may be cases, for ships with very long roll periods, wherein the fin capacity is not so readily taxed, but for most ships, saturation would defeat the value of the fins. It is agreed that the circumstance associated with the occasional very large roll should be clarified.

Fin effectiveness in a following sea is reduced by the orbital velocity of the water, and by the difficulty of designing a control system to cope with low frequency disturbances as well as the more usual frequencies.

The literature having to do with seasickness substantiates Commander Du-Cane's statement as to the motion that is the principal cause. In addition to the literature, personal experience leads to this conclusion.

In regard to the specification of performance for fin stabilizers, it might be possible to test the performance of the control system by pre-programming the fins on one side of the ship to a certain time history of fin angle, and having the control system and the fins on the other side stabilize.

The authors' must apologize to Mr. Silverleaf for the apparent omission of reference to Mr. Allan's work. This reference was inadvertently omitted in the typing of the manuscript. An errata sheet was issued correcting this oversight prior to the meeting but was not available in time for distribution.

The authors' conclusions on the inventive approach to design of active anti-roll fins was based on published literature. It is apparent from Mr. Silverleaf's remarks that a great deal of unpublished scientific work has been performed in this area. The reference to additional model work in this design area was made specifically with respect to activating ship model fins, that is to say model investigations of the entire control loop. To the authors' knowledge, little work has been done in this area.

The authors agree with Mr. Silverleaf's views on the design of passive tanks.

The authors are grateful for Mr. Numata's interesting observations and supplemental comments. His proposal for inducing roll by a moveable weight system is an interesting one and is quite parallel to the present scheme of forcing roll with active fins and determining roll quenching ability. We would have to determine the amount of weight required for such a system and the required frequency responses of the control system before we could evaluate the practicality of applying such a scheme to practice.

* * *

A VORTEX THEORY FOR THE MANEUVERING SHIP

Roger Brard
Bassin d'Essais des Carenes de la Marine
Paris, France

FOREWORD

The present text differs on many points from the draft which was prepared for the 5th Symposium on Naval Hydrodynamics held at Bergen (10-12 September 1964). Firstly it appeared necessary to correct many misprints and also omissions which made the reading difficult. Moreover it was useful to explain with more details the theoretical views which lead to the introduction of a delayed circulation around a maneuvering submerged body.

The line of thought is unchanged, but some results are presented with a greater precision.

The new paragraph on some experimental results (par. 16) shows that some "apparent coefficients" may be found increasing and not decreasing when the reduced frequency increases. That seems to mean that the effects of the terms in $\partial/\partial t$ in the equations of the motion may be higher than in the case of a wing of infinite aspect ratio. The effects of the wake on the stern planes are confirmed to be very high.

INTRODUCTION

The work to be done in the naval hydrodynamic field in order to solve the problems related to the unsteady motion of the ship is often a very difficult one. A mathematical model of the physical phenomena has to be found. That requires various compromises. For, if the equations, which the mathematical model leads to, were too complicated in regard to the possibilities of an effective treatment, no real improvement would have been obtained.

That is undoubtedly why the equations of the classical ship hydrodynamics are differential and of the second order. Nevertheless, in some cases, such equations are not suitable at all, and the modern ship hydrodynamics must often consider other classes of equations. It is, for instance, admitted that the equations which govern the rolling, heaving and pitching motions of a surface ship on irregular waves are integro-differential equations of the Volterra's type [1]. That is already true even on regular seas, because the waves generated by the ship have to be added to the incident waves.

The problem which the present paper is devoted to is that of the maneuvering ship.

For this problem, a "classical" theory already exists. That is, the quasi-steady motion theory. It is admitted that, with the exception of the effects of the so-called "added masses," the hydrodynamic forces exerted on the maneuvering ship are identical to those found for a steady motion with the same angles of attack and the same linear and angular velocities.

That leads to a set of differential equations of the second order.

This set is rather complicated in the case of a submerged body in an infinite fluid because the number of the degrees of freedom is high. Moreover, the linear approximation is most often insufficient. Consequently, the equations contain many, many terms. As the theory is unable to yield them, it is necessary to resort to an empirical determination of their numerical values. When the equations are written, it is necessary to solve them by using analog computers. And the work is not finished by this time. The empirical determination of the coefficients of the equations would have been practically impossible if the motion had not been split in its components; then the results so obtained must be gathered. That is not so easy since the equations are not linear. Consequently a comparison between the calculated motion and the real motion of the model or of the full scale ship must be undertaken.

Finally, the precise study of the maneuvering qualities of a ship, especially of a submarine, requires a great deal of work.

Therefore, the idea that the quasi-steady motion theory might be too simple is attractive to very few. That is, however, the question about which the author of this paper has tried to make up his mind.

The starting point of the present investigation is that the hydrodynamic set of forces exerted on a maneuvering ship is partly due to some circulation around the ship. If so, this circulation around the body generates a vortex wake since the circulation along a closed fluid circuit is null. And the vortex wake is what prevents the equations to be purely differential. As in the Kármán-Sears theory of the unsteady motion on an airfoil of infinite aspect ratio [2], we shall expect to deal with Volterra's integro-differential equations. Consequently the forces in the real motion and those calculated by using the quasi-steady motion theory must differ from one another, no circulating being able to take instantaneously the value relating to the steady motion. This starting point needs some comments.

For the quasi-steady motion theory does not preclude some circulation. Indeed, this circulation cannot come from the set of forces deduced by Lagrange's method from the kinetic energy of the absolute motion of the fluid surrounding the body: it is assumed that this motion depends upon a velocity potential regular at the infinity. But, if some circulation exists in the steady motion, we shall find it in the equations expressing the quasi-steady motion theory.

That is the case, because the lift is not null. For instance, when the lift component on the z-axis is opposite to the direction of this axis, the mean pressure on the upperside of the body is smaller than on the lowerside; on the contrary, the mean velocity is greater on the upperside. And the circulation around the body along closed circuits parallel to the (x,y)-plane is necessarily non-null.

The same reasoning holds in the case of a maneuvering surface ship, the lift being now in a horizontal plane. In 1950, one of our assistants has calculated a distribution of free and bound vortices for a thin surface ship in a steady turning motion and obtained by this way some results which help understanding several phenomena unexplained to this time (see [3] and also [4]).

Some authors [5-7] probably have ideas quite similar to the one expressed above. But they are principally interested in the configuration of the vortex wake and in the mechanism of the transport into the wake of the vorticity which originates in the boundary layer. Such a line of thought is the best from a scientific point of view. Unfortunately, such a study is very difficult and will not lead rapidly to results that the naval architects may easily use. That is why we have chosen here another way.

A mathematical model of the vortex shedding has to be defined. Preferably it has to be flexible enough to be adaptable to the various hull forms we encountered in the practice. Consequently, this model is not made for giving all the means necessary for a complete calculation, in each case, of the hydrodynamic set of forces in steady and unsteady motions. In return, it has to yield the general form of the expression of this set, and also, to supply a criterion which permit to decide whether, according to the experimental results, the differences between the quasi-steady forces and the real forces are negligible or not.

The present paper gives a first answer to this problem.

Section I defines a mathematical model of the wake vortex and leads to the Volterra's integro-differential equations which govern, in an unsteady motion, the circulation and the forces exerted on the body. Attention is drawn — as in [8] — to the pressure distribution on the hull, and also to the effects on the stern planes and rudders of the wake generated by the submerged body itself.

Section II shows that in a harmonic forced motion, the forces differ from those given by the quasi-steady motion theory. Some experimental results show that there is a possibility to estimate the magnitude of the errors involved in the quasi-steady theory. Some of them are small. Others are significant.

Section III is devoted to possible further developments of our present views. It is shown that tests in various steady and harmonic forced motions are able to yield all the unknown coefficients and functions found in the so-called "true" equations of the free quasi-rectilinear motions. Unfortunately, other motions are of great interest too, those which require non-linear equations. In these cases, the technique of the steady and harmonic forced motions is unable, in its present state, to supply all the necessary information. Moreover, the "true" equations are more complicated than those of the quasi-steady theory and lead, not in principle, but in fact, to non-negligible difficulties even in the field where the equations are linear.

The first answer given here is therefore faulty. The conclusions of this paper will probably not satisfy fully the naval architects. It is hoped, however, that the ideas developed here may be of some practical interest.

I. THE FORCES EXERTED ON A SUBMERGED BODY MOVING IN AN INFINITE FLUID

1. Notations

Let $O'(x', y', z')$ be a dextrorsum set of fixed axis. The z'-axis is vertical and positive downwards.

We consider also a dextrorsum set of axis $O(x, y, z)$ attached to the submerged body.

When the body is in a normal position (that is, when the heel and trim are null), the z axis is vertical and positive downwards.

The x axis is going from the stern to the bow. O is in the middle transverse section. Generally, the body is symmetrical with respect to the (z, x) plane.

The coordinates of O referred to the fixed axis are ξ, η, ζ.

In order to define the position of the body we introduce firstly a set of axis $O(x_1, y_1, z_1)$ having its origin at O, but with the axis Ox_1, Oy_1, Oz_1 parallel to the axis $O'x', O'y', O'z'$ respectively. We consider three non-Eulerian angles ψ, θ, φ (Fig. 1).

ψ is the head angle. By a ψ-rotation about the z_1-axis, the x_1-axis comes in the (z, x) plane on an axis Ox_2; by this rotation, the y_1-axis comes on an axis Oy_2. The z_2-axis coincides with the z_1-axis.

θ is the trim angle. By a θ-rotation around the y_2-axis, the x_2-axis comes on the x_3-axis; by the same rotation, the y_2-axis and the z_2-axis come, respectively on axis Oy_3 and Oz_3. The x_3-axis coincides with the x-axis.

φ is the heel angle. By a φ-rotation about the x-axis, the y_3-axis and the z_3-axis come, respectively, on the y-axis and on the z-axis.

The absolute velocity of O is $\mathbf{V}_E$, of components $\dot\xi, \dot\eta, \dot\zeta$ on the fixed axis. The components of $\mathbf{V}_E$ on the x, y, z-axis are respectively u, v, w.

$\dot\zeta$ is the heaving velocity; the derivatives $\dot\psi, \dot\theta, \dot\varphi$ are, respectively, the heading velocity, the pitching velocity and the rolling velocity.

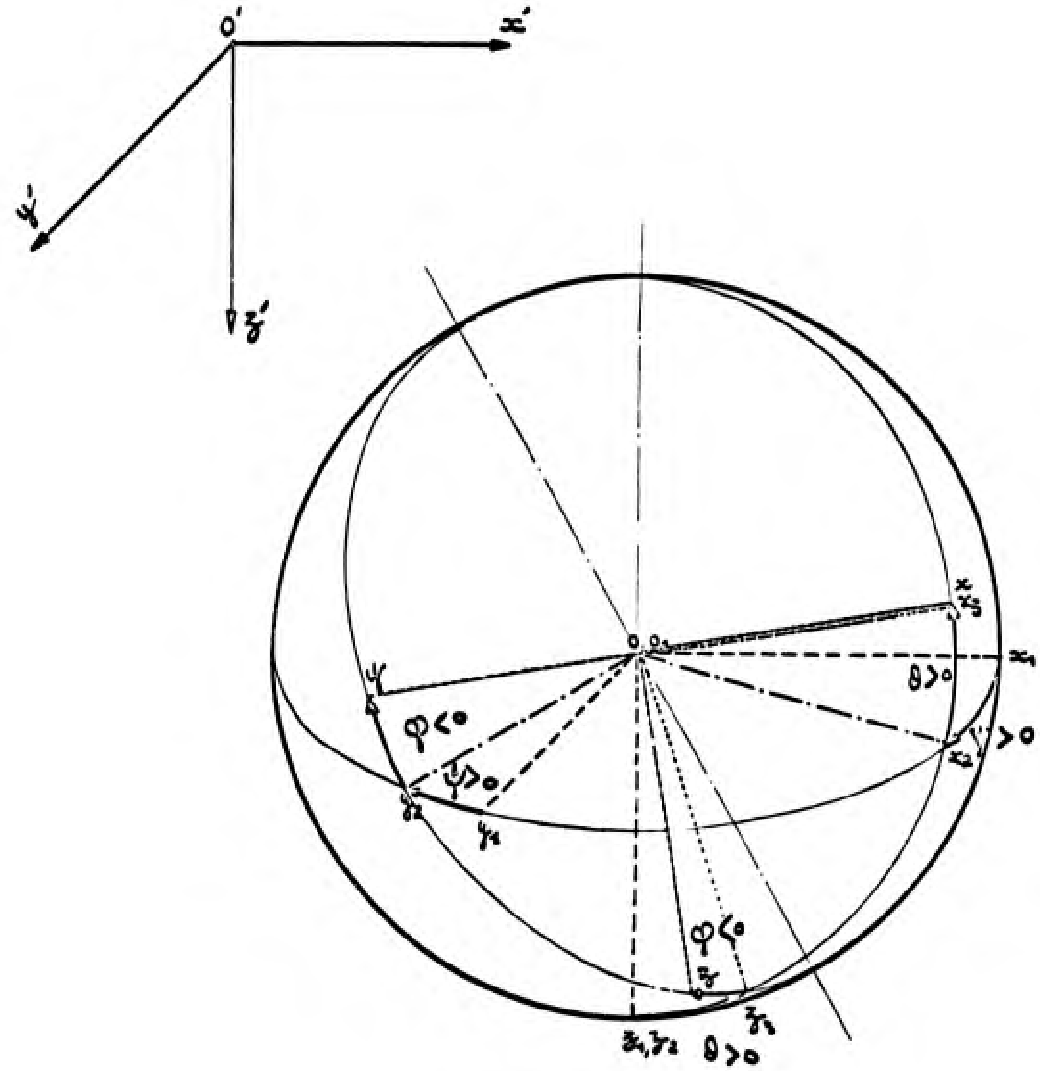

Figure 1

Between the unit vectors $\mathbf{i}_{x'}, \mathbf{i}_{y'}, \mathbf{i}_{z'}$ and the unit vectors $\mathbf{i}_x, \mathbf{i}_y, \mathbf{i}_z$ we have the relations deduced from the following table:

	$\mathbf{i}_x$	$\mathbf{i}_y$	$\mathbf{i}_z$
$\mathbf{i}_{x'}$	$\cos\psi\cos\theta$	$-\sin\psi\cos\phi+\cos\psi\sin\theta\sin\phi$	$\sin\psi\sin\phi+\cos\psi\sin\theta\cos\phi$
$\mathbf{i}_{y'}$	$\sin\psi\cos\theta$	$\cos\psi\cos\phi+\sin\psi\sin\theta\sin\phi$	$-\cos\psi\sin\phi+\sin\psi\sin\theta\cos\phi$
$\mathbf{i}_{z'}$	$-\sin\theta$	$\cos\theta\sin\phi$	$\cos\theta\cos\phi$

(1)

Moreover, the components p, q, r of the angular velocity of the body on the moving axis are

$$p = \dot{\phi} - \dot{\psi}\sin\theta, \qquad q = \dot{\theta}\cos\phi + \dot{\psi}\cos\theta\sin\phi, \qquad r = \dot{\psi}\cos\theta\cos\phi - \dot{\theta}\sin\phi. \tag{2}$$

Let G be the center of gravity of the body. Let δm be the mass of a small volume δW which coordinates with respect to axis parallel to the x, y, z-axis, but having their origin at G, are x'', y'', z''. When the body is symmetrical with respect to the (z, x)-plane, the moments of inertia of the body are

$$I_1 = \Sigma(y''^2 + z''^2)\delta m, \quad I_2 = \Sigma(z''^2 + x''^2)\delta m, \quad I_3 = \Sigma(x''^2 + y''^2)\delta m, \quad I_{13} = \Sigma(z''x'')\delta m. \tag{3}$$

Let ρ be the specific mass of the fluid, and μ the mean density of the body with respect to the fluid. We introduce dimensionless coefficients by the formulae:

$$I_1 = \rho W L^2 \mu x_1, \quad I_2 = \rho W L^2 \mu x_2, \quad I_3 = \rho W L^2 \mu x_3, \quad I_{13} = \rho W L^2 \mu x_{13}, \tag{4}$$

where L is the length of the body along the x-axis.

When G is not at 0, its coordinates are $L\xi_G, 0, L\zeta_G$. We assume that ξ_G, ζ_G have negligible squares and products. Otherwise, the moments of inertia of the body about the (x, y, z)-axis would be

$$I_1' = \rho W L^2 \mu (x_1 + \xi_G^2), \quad I_2' = \rho W L^2 \mu x_2, \quad I_3' = \rho W L^2 \mu (x_3 + \zeta_G^2), \quad I_{13}' = \rho W L^2 \mu (x_{13} + \zeta_G \xi_G). \tag{5}$$

The set of the absolute forces has a general resultant $\mathfrak{F}$ and a resultant moment $\mathbf{I}$ referred about the origin 0 of the axis attached to the body. One has:

$$\mathfrak{F} = X\mathbf{i}_x + Y\mathbf{i}_y + Z\mathbf{i}_z, \qquad \mathbf{I} = \mathfrak{L}\mathbf{i}_x + \mathfrak{M}\mathbf{i}_y + \mathfrak{N}\mathbf{i}_z. \tag{6}$$

In this paper, we don't consider the relative forces, that is the forces in the set of axis attached to the body.

2. Some Particular Motions

Motions Parallel to the (z, x)-Plane — The y-component $v + rx - pz$ of the absolute velocity of any point attached to the body is null. Consequently

$$v = 0, \quad r = 0, \quad p = 0. \tag{1}$$

Therefore

$$\dot{\phi} = \dot{\psi}\sin\theta = \dot{\theta}\,\mathrm{tg}\,\phi\,\mathrm{tg}\,\theta, \qquad q = \frac{\dot{\theta}}{\cos\phi}. \tag{2}$$

When $\varphi = 0$, one has $\dot{\varphi} = \dot{\psi} = \dot{\theta}\, \mathrm{tg}\, \varphi / \cos\theta = 0$, ψ = constant. The motion is also parallel to a vertical plane.

Motions Parallel to the (x, y)-Plane — The z-component $w + py - qx$ of the absolute velocity of any point attached to the body is null. Consequently

$$w = 0, \quad p = 0, \quad q = 0 .$$

Therefore

$$\dot{\varphi} = \dot{\psi} \sin\theta, \qquad \dot{\theta} = -\dot{\psi} \cos\theta \,\mathrm{tg}\, \varphi, \qquad r = \dot{\psi} \frac{\cos\theta}{\cos\varphi} . \tag{3}$$

This motion is parallel to the horizontal plane when φ and θ are simultaneously equal to zero.

Quasi-Rectilinear Motions Parallel to the x-Axis — In the case, we substitute $U + u$ for u.

One considers that

$$\frac{u}{U}, \quad \frac{v}{U}, \quad \frac{w}{U} \tag{4}$$

are small. B being the breadth of the body,

$$\frac{Bp}{U} = \frac{B}{L}, \quad \frac{Lp}{U}, \quad \frac{Lq}{U}, \quad \frac{Lr}{U} \tag{5}$$

are small too. The square and products of ratios (4) and (5) are negligible.

3. Vortices Attached to a Body on Steady Motion in its (z, x)-Plane

It is well known that a submerged body may be considered as equivalent to a distribution of bound vortices when no wake exists and to a distribution of free and bound vortices when a wake is shed. On the other hand, it is well known, too, that a closed filament vortex is equivalent to a distribution of doublets. To write the expressions of the forces generated by such a distribution of vortices or doublets, it is helpful to bear in mind the main aspects of the theory.

3.1. Bound Vortices are Equivalent to a Submerged Body in a Perfect Fluid

As a matter of fact, when the fluid is quite perfect, the absolute motion of the fluid may be considered as generated by a distribution of vortices located on the hull when the angular velocity Ω is equal to zero, on the hull and inside the body, when $\Omega \neq 0$.

This possibility comes from the property of the vector $\mathbf{W}(M)$, having its origin in M, and defined by the formula

$$\mathbf{W}(M) = \iiint_{\Omega} \frac{\mathbf{V}(\mu)}{\mu M}\, d\Omega(\mu),$$

where $\mathbf{V}(\mu)$, which has its origin in μ, is continuous with respect to the point μ which describes the volume Ω; its first derivatives also are assumed to be continuous; moreover

$$\operatorname{div} \mathbf{V}(\mu) = 0.$$

Taking for Ω the space Ω_e exterior to the body, and for $\mathbf{V}(\mu)$ the absolute velocity $\mathbf{V}_0 = -\mathbf{grad}\, \Phi_0$ of the fluid, then using the equation

$$\operatorname{curl} \operatorname{curl} \mathbf{W} = \mathbf{grad} \operatorname{div} \mathbf{W} - \nabla \mathbf{W}, \tag{1}$$

where

$$\nabla = \frac{\partial^2}{\partial x^2} + \frac{\partial^2}{\partial y^2} + \frac{\partial^2}{\partial z^2},$$

we obtain

$$\frac{1}{4\pi} \operatorname{curl} \left\{ \iint_S \frac{\mathbf{n} \wedge \mathbf{V}_0(\mu)}{\mu M}\, dS(\mu) \right\} - \frac{1}{4\pi}\, \mathbf{grad} \iint_S \frac{\mathbf{n}\mathbf{V}_0(\mu)}{\mu M}\, dS(\mu) = \begin{cases} \mathbf{V}_0(M), \text{ when } M \text{ is in } \Omega_e, \\ 0, \text{ when } M \text{ is in } \Omega_i, \end{cases}$$

Ω_i being the volume inside the body.

Taking now for Ω the volume Ω_i, and for $\mathbf{V}(\mu)$ the absolute velocity of μ considered as at rest with respect to the body, we have $\mathbf{V}(\mu) = \mathbf{V}_E(\mu)$ with

$$\mathbf{V}_E(\mu) = \mathbf{U} + \mathbf{Q} \wedge \mathbf{O}\boldsymbol{\mu}, \quad \operatorname{curl} \mathbf{V}_E = 2\mathbf{Q},$$

and

$$\frac{1}{4\pi} \operatorname{curl} \left\{ - \iint_S \frac{\mathbf{n} \wedge \mathbf{V}_E(\mu)}{\mu M}\, dS(\mu) + \iiint_{\Omega} \operatorname{curl} \mathbf{V}_E \frac{d\Omega_i(\mu_i)}{\mu_i M} \right\}$$

$$+ \frac{1}{4\pi}\, \mathbf{grad} \iint_S \frac{\mathbf{n}\mathbf{V}_E(\mu)}{\mu M}\, dS(\mu) = \begin{cases} 0 \text{ when } M \text{ is in } \Omega_e, \\ \mathbf{V}_E \text{ when } M \text{ is in } \Omega_i. \end{cases}$$

By addition, we find, with $\mathbf{V}_{r_o} = \mathbf{V}_o - \mathbf{V}_E =$ the relative velocity of the fluid,

$$\frac{1}{4\pi}\,\text{curl}\left[\left\{\iint_S \frac{\mathbf{n}\wedge\mathbf{V}_{r_o}}{\mu M}\,dS(\mu)\right\} + \left\{\iiint \frac{2\mathbf{Q}}{\mu_i M}\,d\Omega_i(\mu_i)\right\}\right] = \begin{cases}\mathbf{V}_o(M) \text{ when } M \text{ is in } \Omega_e\,, \\ \mathbf{V}_E(M) \text{ when } M \text{ is in } \Omega_i\,,\end{cases} \tag{2}$$

since $\mathbf{V}_E\mathbf{n} = \mathbf{V}_o\mathbf{n}$ on S.

Let us consider now the surface of the hull as covered by a very thin boundary layer (of thickness δ); we see that a vortex equal to $(1/\delta)\ \mathbf{n}\wedge\mathbf{V}_r$ on the mean surface $S(m)$ between the internal face S_i and the external face S_e of the boundary layer, and to $2\mathbf{Q}$ in Ω_i, generates an absolute fluid motion which has the following properties: outside the body, the motion is identical to that of the fluid; inside the body, the fluid is at rest with respect to the body.

3.2. A Distribution of Doublets is Equivalent to a Distribution of Bound Vortices When the Angular Velocity is Equal to Zero

When $\mathbf{Q} = 0$, we have a velocity potential in Ω_e and in Ω_i, which may be regarded as due to doublets normal to the hull:

$$\Phi_o = -\frac{1}{4\pi}\iint_{S(m)} \gamma_o(m) \times \frac{d}{dn_m}\frac{1}{mM} \times dS(m)\,, \quad \mathbf{V} = -\,\mathbf{grad}\ \Phi_o = \begin{cases}\mathbf{V}_o \text{ in } \Omega_e\,, \\ \mathbf{U} \text{ in } \Omega_i\,,\end{cases} \tag{3}$$

$\mathbf{n}$ being the unit vector normal to the hull and positive outwards.

Therefore, m_i and m_e being on the normal $\mathbf{n}(m)$ to $S(m)$, m_i on S_i, m_e on S_e, we have

$$\frac{1}{2}\,\gamma_o(m) - \frac{1}{4\pi}\iint_S \gamma_o(m')\,\frac{d}{dn_{m'}}\,\frac{1}{m'm}\,dS(m') = f(m) \tag{4}$$

with

$$f(m) = \mathbf{U}\left[\mathbf{i}_x x(m_i) + \mathbf{i}_y y(m_i) + \mathbf{i}_z z(m_i)\right] + \text{constant.} \tag{5}$$

Equation (5) is Fredholm's equation of the 2nd kind relative to an <u>interior</u> Dirichlet's Problem. For any value C of the constant in the right member of (5), the solution of (4) is unique. One has

$$\Phi_o(m_e) - \Phi_o(m_i) = -\,\gamma_o(m)\,.$$

Therefore when another constant C' is substituted for C, $\Phi_o(m_e)$ is changed in $\Phi_o(m_e) + C' - C$. Hence the motion of the fluid outside the body does not depend upon the value of the constant C.

Let us assume this constant chosen in such a way that $\gamma_o(m) = 0$ on the forebody. Let $C_o(m)$ be the rings normal to $\mathbf{V}_{r_o}(m)$, σ_o the arc of this ring, σ'_o the arc of their orthogonal trajectories $\mathcal{C}_o$ ($\sigma'_o = 0$ at the forebody, >0 behind), $\mathbf{i}_o, \mathbf{i}'_o$ the unit vectors tangent to C_o and to $\mathcal{C}_o$ respectively, the directions of these vectors being those of $d\sigma_o > 0$, $d\sigma'_o > 0$, and these directions themselves being chosen in such a way that $-\mathbf{n} = \mathbf{i}_o \wedge \mathbf{i}'_o$.

The flux of the vortex $T_0 = (1/\delta)\, n \wedge V_{r_0}$ inside the small area $\delta d\sigma'_0$ normal to C_0 is equal to $d\gamma_0$ and is constant between two rings C_0, C'_0 of abscissae σ'_0, $\sigma'_0 + d\sigma'_0$ on $\mathcal{C}_0$ (see Fig. 2).

The rings $C_0(m)$ are the curves $\gamma_0(m)$ = constant. Moreover, on S_e, $V_{r_0} d\sigma'_0 = d\gamma_0$. When $Q = 0$, $v = 0$, that is when we have a motion parallel to the (z, x)-plane with no angular velocity, it is convenient for what follows to write

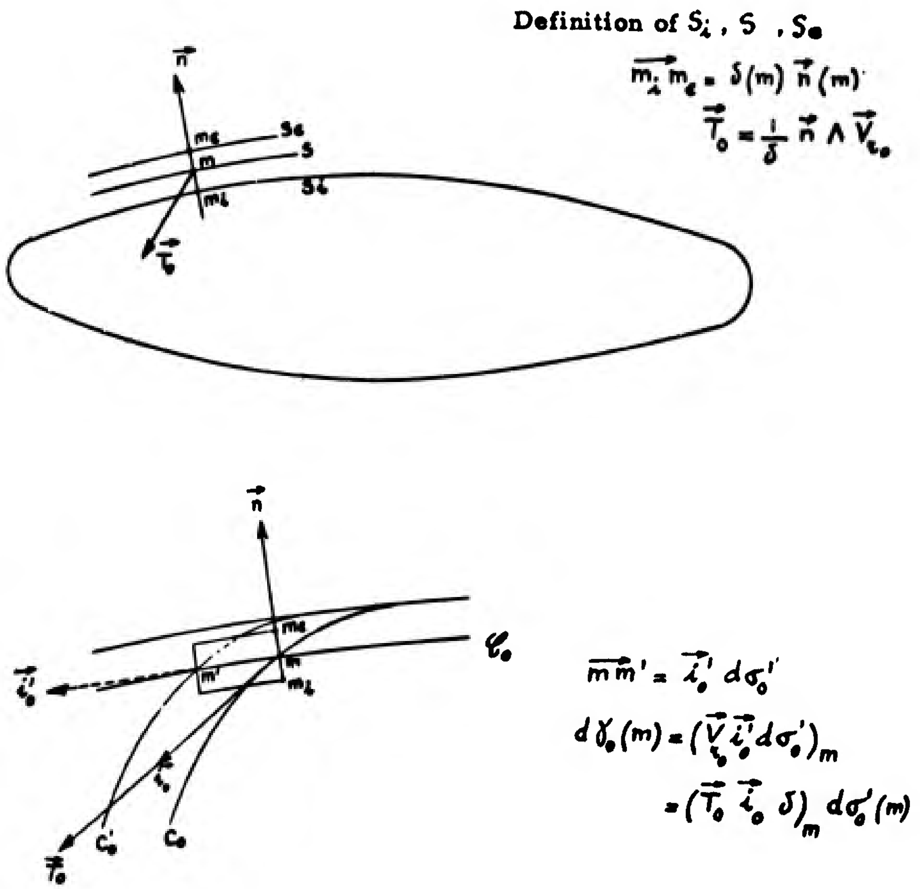

Definition of the bound vortex $\vec{T}_0$ (= const. along C_0).

and of the density $\gamma_0(m)$ of doublets normal to the hull

when :

1°) there is no wake,

2°) the angular velocity is null.

Figure 2

$$\Phi_0(M) = \Phi_{00}(M) + \Phi_{00}(M)\frac{u}{U} + \Phi_{01}(M)\frac{w}{U}, \tag{6}$$

with

$$\Phi_{00}(M) = -\frac{1}{4\pi}\iint_S \gamma_{00}(m)\frac{d}{dn_m}\frac{1}{mM}\,dS(m),$$

$$\Phi_{01}(M) = -\frac{1}{4\pi}\iint_S \gamma_{01}(m)\frac{d}{dn_m}\frac{1}{mM}\,dS(m). \tag{7}$$

Functions $\gamma_{00}(m)$ and $\gamma_{01}(m)$ are solutions of the same Fredholm's equation of the 2nd kind, with a right member equal to $Ux(m_i)+C_0$ for γ_{00}, and to $Uz(m_i)+C_1$ for γ_{01}.

The potentials Φ_{00}, Φ_{01} may be regarded as generated by bound vortices $\mathbf{t}_{00}$ and $\mathbf{t}_{01}$. The rings on which the vortices $\mathbf{t}_{00}$ are lying are the curves γ_{00} = constant. If $d\sigma'_{00}$ is the distance between two rings γ_{00} = constant, $d\sigma'_0$ being positive downstream, $\mathbf{i}'_{00}$ the unit vector tangent to S and normal to the ring, $\mathbf{i}_{00}$ the unit vector tangent to the ring, with $\mathbf{i}_{00} = \mathbf{n}\wedge\mathbf{i}'_{00}$, one has

$$\mathbf{t}_{00}\delta = \mathbf{n}\wedge\mathbf{i}'_{00}\frac{d\gamma_{00}}{d\sigma'_{00}}. \tag{8}$$

A similar formula gives the vortex $\mathbf{t}_{01}$.

3.3. Case When the Angular Velocity is not Equal to Zero (Fig. 3)

Let us assume now that $u/U = 0$, $w/U = 0$, $Lq/U \neq 0$.

The absolute velocity potential is

$$\Phi_0(M) = \Phi_{00}(M) + \Phi_{02}\frac{Lq}{U}, \quad \text{when M is in } \Omega_e. \tag{9}$$

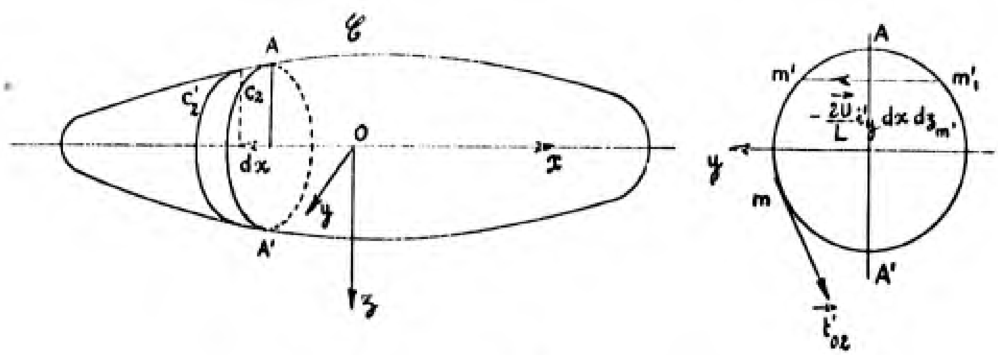

Figure 3

There is no velocity potential in Ω_i since $q \neq 0$, and curl $\mathbf{V}_0 = 2q\mathbf{i}_y$. But we may write:

$$-\mathbf{grad}\ \Phi_{0\,2}(M) = \frac{1}{4\pi}\ \mathrm{curl}\left\{\iint_S \frac{\delta\mathbf{t}_{0\,2}(m)}{mM}\, dS(m) + \frac{U}{L}\iiint_{\Omega_i} \frac{2\mathbf{i}_y}{\mu_i M}\, d\Omega_i(\mu_i)\right\},\quad M \text{ in } \Omega_e\,. \qquad (10)$$

We have to define $\mathbf{t}_{0\,2}(m)$ (Fig. 3).

In order to do that, let us consider on S the rings c_2 and c_2' located in the planes of abscissae x and $x + dx$, $(dx < 0)$. Let m', m_1' be two points on c_2, m' being on the starboard side, m_1' on the portside, with $z(m_1') = z(m')$. A, origin of the arc σ_2 on c_2, is chosen on the upper arc of the contour $\mathcal{C}$ along which the planes tangent to S are parallel to $\mathbf{i}_y$. A' being on c_2 and on the lower arc of $\mathcal{C}$, we consider a point m on the arc $m'A'm_1'$. Let $d\sigma_2'(m')$, $d\sigma_2'(m)$ be the distances measured on S, at m' and at m, respectively, between c_2 and c_2'. These distances are considered as positive. Moreover, $\mathbf{i}_2(m)$ is the unit vector tangent to c_2; $\mathbf{i}_2(m)$ is positive with respect to the x-axis. The arc $d\sigma_\ell > 0$ has a direction identical to this of $\mathbf{i}_2$.

Now we define at m an element of bound vortex $\mathbf{dt}_{0\,2}'(m) = \mathbf{i}_2(m)dt'(m)$ by the condition that

$$dt'(m)(\delta d\sigma_2')_m = +\frac{2U}{L}\ \mathbf{i}_y(\mathbf{n}\, d\sigma_2\, d\sigma_2')_{m'}\,.$$

Consequently, the filament vortex which intensity is equal to

$$-\frac{2U}{L}\ \mathbf{i}_y dx\, dz(m')$$

on the segment $m_1'm'$ and to $\mathbf{dt}_{0\,2}'(m)(\delta d\sigma_2')_m$ on the arc $m'A'm_1'$, is closed and this intensity is constant along the filament vortex. It is the flux cf the vortex $(2U/L)\mathbf{i}_y$ through the small area $(d\sigma_2 d\sigma_2')_m$, on S.

The total vortex at m has an intensity given by

$$\mathbf{t}_{0\,2}'(m)(\mathbf{i}_2\delta d\sigma_2')_m = \int_A^m \left[\frac{2U}{L}\ \mathbf{i}_y(m')\ \mathbf{n}(m')\ d\sigma_2'(m')\right] d\sigma_2(m')\,. \qquad (11)$$

This vortex is equal to zero at A.

It constitutes with the vortices $(2U/L)\mathbf{i}_y$ located in Ω_i, a family of closed filament vortices having a constant intensity along their length. Consequently, the vector

$$\mathbf{V}_{0\,2}'(M) = \frac{1}{4\pi}\ \mathrm{curl}\left\{\iint_S \frac{\delta\mathbf{t}_{0\,2}'(m)}{mM}\, dS(m) + \iiint_{\Omega_i} \frac{2U}{L}\ \mathbf{i}_y\ \frac{d\Omega_i(\mu_i)}{\mu_i M}\right\} \qquad (12)$$

satisfies the condition

$$\operatorname{curl} \mathbf{V}'_{0\,2}(M) = \begin{cases} 0 \text{ in } \Omega_e , \\ \dfrac{2U}{L}\, \mathbf{i}_y \text{ in } \Omega_i . \end{cases}$$

Consequently, $\mathbf{V}'_{0\,2}(M)$ depends in Ω_e upon a velocity potential. Let $\Phi'_{0\,2}(M)$ be this potential. One has

$$\mathbf{V}'_{0\,2}(M) = -\mathbf{grad}\, \Phi'_{0\,2}(M) \text{ in } \Omega_e .$$

In Ω_i, $\mathbf{V}'_{0\,2}$ does not depend on a velocity potential; but

$$\mathbf{V}'_{0\,2}(M) - \frac{U}{L}\, \mathbf{i}_y \wedge \mathbf{OM}$$

depends on a velocity potential ϕ:

$$-\mathbf{grad}\, \phi(M) + \mathbf{V}'_{0\,2}(M) = \frac{U}{L}\, \mathbf{i}_y \wedge \mathbf{OM} \text{ in } \Omega_i .$$

Let us now consider the velocity potential $\Phi''_{0\,2}(M)$ defined in Ω_i and in Ω_e by the distribution of doublets $\gamma'(m)$ on S so that

$$\Phi''_{0\,2}(M) = -\frac{1}{4\pi} \iint_S \gamma'(m) \frac{d}{dn_m} \frac{1}{mM}\, dS(m) , \tag{13}$$

with

$$\frac{1}{2}\gamma'(m) - \frac{1}{4\pi} \iint_S \gamma'(m') \frac{\delta}{dn_{m'}} \frac{1}{m'm}\, dS(m') = -\phi(m_i) + \text{constant} .$$

One has

$$\Phi''_{0\,2}(M) = \phi(M) + \text{constant in } \Omega_i .$$

Hence, one has

$$-\mathbf{grad}\, \Phi''_{0\,2}(M) = -\mathbf{grad}\, \phi(M) = -\mathbf{V}'_{0\,2}(M) + \frac{U}{L}\, \mathbf{i}_y \wedge \mathbf{OM} \text{ in } \Omega_i .$$

Therefore

$$-\mathbf{grad}\, \Phi''_{0\,2}(m_i) + \mathbf{V}'_{0\,2}(m_i) = \frac{U}{L}\, \mathbf{i}_y \wedge \mathbf{O}m_i \text{ on } S_i .$$

When M passes through the boundary layer, from m_i to m_e, the normal component of $\mathbf{grad}\, \Phi''_{0\,2}$ is continuous. The normal component of $\mathbf{V}'_{0\,2}$ is continuous, too. Consequently

$$-\mathbf{grad}\left[\Phi''_{0\,2}(m_e) + \Phi'_{0\,2}(m_e)\right] \mathbf{n}(m_e) = \left[-\mathbf{grad}\ \Phi''_{0\,2}(m_e) + \mathbf{V}'_{0\,2}(m_e)\right] \mathbf{n}(m_e)$$

$$= \frac{U}{L}\left[\mathbf{i}_y \wedge 0m_e\right] \mathbf{n}(m_e)\ . \tag{14}$$

Therefore $\Phi''_{0\,2} + \Phi'_{0\,2}$ fulfils on S_e the same condition as the wanted potential $\Phi_{0\,2}$. Because these two potentials are regular in Ω_e and at the infinity, one has

$$\Phi_{0\,2}(M) = \Phi''_{0\,2}(M) + \Phi'_{0\,2}(M) + \text{constant in } \Omega_e\ . \tag{15}$$

This equation defines $\mathbf{t}_{0\,2}(m)$; one has

$$\mathbf{t}_{0\,2}(m) = \frac{1}{\delta}\left\{-\mathbf{grad}\ \Phi_{0\,2}(m_e) - \mathbf{i}_y \wedge 0m_e\right\} \wedge \mathbf{n}(m_e)\ . \tag{16}$$

This solution does not depend upon the choice of the rings c_2 since the potential $\Phi_{0\,2}$ is perfectly defined (with the exception of an additive constant), by the condition on S_e.

3.4. The Vortex Distribution When the Fluid is not Quite Perfect

In this case a vortex wake exists. Let us assume firstly that

$$u = 0\ ,\quad q = 0\ ,\quad \frac{w}{U} \neq 0\ .$$

The total velocity potential may be written:

$$\phi_0 = \phi_{0\,0} + \phi_{0\,1}\,\frac{w}{U}\ , \tag{17}$$

where

$$\phi_{0\,0} = \Phi_{0\,0} + \Psi_{0\,0}\ ,\qquad \phi_{0\,1}\,\frac{w}{U} = \Phi_{0\,1}\,\frac{w}{U} + \Psi_{0\,1}\,\frac{w}{U}\ .$$

In these expressions $\Phi_{0\,0}$, and $\Phi_{0\,1}(w/U)$ are the solutions obtained in par. 3.2. The potential $\Psi_{0\,0}$ has to be added to $\Phi_{0\,0}$ when a wake already exists for $w/U = 0$; the potential $\Psi_{0\,1}(w/U)$ has to be added to $\Phi_{0\,1}(w/U)$ when a wake exists for $w/U \neq 0$.

Figure 4 suggests that the wake is made of free filament vortices shed along a not necessarily closed line $\mathfrak{C}_{0\,1}$. $\mathfrak{C}_{0\,1}$ is approximately in the (x,y)-plane.

For reasons of generality, we consider a closed line $\mathfrak{C}'_{0\,1}$ which contains the arc $\mathfrak{C}_{0\,1}$. On the arc $\mathfrak{C}'_{0\,1} - \mathfrak{C}_{0\,1}$ no vortex is shed.

It is possible to consider $\Psi = \Psi_{0\,0} + \Psi_{0\,1}(w/U)$ as generated by two families f'_0, f''_0 of free and bound vortices (Fig. 5).

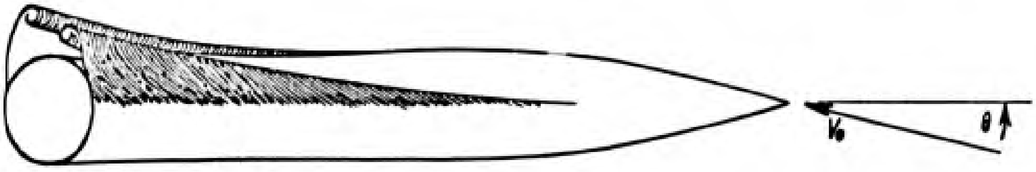

Figure 4

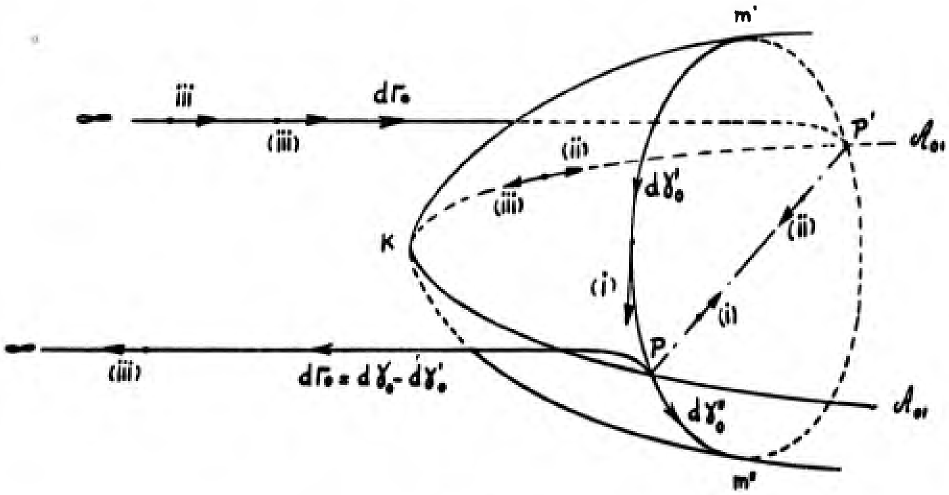

Figure 5

A vortex of the f_0'-family is lying on a closed contour made itself of two arcs; one is $P'm'P$ starting from P' on the port side of $\mathcal{A}_{01}$, and going to P, on the starboard side of $\mathcal{A}_{01}$. m' is on the upper side S' of S, the other arc is made of the streamline of the relative motion starting from P and going to the infinity downstream, and of the similar streamline starting from P', but described in the opposite direction. The intensity of the filament vortex above is $d\gamma_0'$.

A vortex of the f_0''-family is similar to the previous one; but the arc $Pm''P'$ has to be substituted for $P'm'P$, m'' being on the lower side S'' of S; moreover the streamlines starting from P and P' are described from P' to the infinity downstream, and from the infinity downstream to P. The intensity of the filament vortex is $d\gamma_0''$.

The intensity of the free vortex resulting from the addition $(f_0') + (f_0'')$ is

$$d\Gamma_0 = d\gamma_0' - d\gamma_0'' \text{ along } P \infty P' . \tag{18}$$

The arcs $P'm'P$ and $Pm''P'$ are orthogonal to the contribution of Ψ_0 in the total relative velocity on S_e.

It is possible also to consider a free vortex of the f_0'-family as made of three vortices of intensity $d\gamma_0'$: vortex (i) on the arc $P'm'P$ and the segment PP'; vortex (ii) on the arc PKP' of $\mathfrak{C}_{01}$ (K in the (z, x)-plane), and on the segment $P'P$; and vortex (iii) on the arc $P'KP$ of $\mathfrak{C}_{01}$, and on the stream lines of the relative motion starting from P and P' and leading to the infinite downstream.

Vortex (i) is equivalent to a distribution of normal doublets on the part $S'(P)$ of S' behind the arc $P'm'P$ and on the part $\Sigma_1(P)$ of the surface $\Sigma_1(P)$ generated by the segment PP' when P and P' describe $\mathfrak{C}_{01}$;

Vortex (ii) is equivalent to a distribution of normal doublets on the surface $\Sigma_1(P)$;

Vortex (iii) is equivalent to a distribution of doublets on the part $\Sigma(P)$ of the wake which edges are the arc $P'KP$, and the streamlines starting from P and from P'.

Because the distributions of doublets on $\Sigma_1(P)$ are equal and opposite, the contribution in Ψ_0 of the vortices (i), (ii), (iii) is due only to the doublets distributed on $S'(P)$ and on $\Sigma(P)$.

A similar reasoning may be repeated for a vortex of the f_0''-family.

Finally, the contribution in Ψ_0 of the vortices just considered is

$$d\Psi_0 = d\chi_0 + d\chi_0' , \tag{19}$$

with

$$\left.\begin{aligned} d\chi_0 &= -\frac{1}{4\pi}\iint_{\Sigma(P)} \frac{d}{dn_\mu}\frac{1}{\mu M}\, d\Sigma(\mu) \times d\Gamma_0(P) , \\ d\chi_0' &= \frac{1}{4\pi}\iint_{S'(P)} \frac{d}{dn_{m'}}\frac{1}{m'M}\, dS'(m') \times d\gamma_0' + \frac{1}{4\pi}\iint_{S''} \frac{d}{dn_{m''}}\frac{1}{m''M}\, dS''(m'') \times d\gamma_0'' . \end{aligned}\right\} \tag{19'}$$

In these formulae, the unit vector $\mathbf{n}_\mu$ is normal to Σ, and therefore, approximately identical to $\mathbf{i}_z$; the unit vectors $\mathbf{n}_{m'}, \mathbf{n}_{m''}$ are positive outwards.

The total potential χ_0 is therefore given by

$$\chi_0(M) = -\frac{1}{4\pi}\int_{\mathfrak{C}_{01}} \Gamma_0(P)dy_P \int_{-\infty}^{\lambda(y_P)} \frac{d}{dn_\mu}\frac{1}{\mu M}\, d\xi(\mu) , \tag{20}$$

where P describes the arc $P_1'K \cdot P_1$, P_1' and P_1 being the extremities of $\mathfrak{C}_{01}$, and $x(y_P)$ the abscissa of P on $\mathfrak{C}_{01}$. The coordinates of μ on Σ are ξ, y_P.

On the other hand, the total potential $\chi_0'(M)$, generated by doublets on S, may be written

$$\chi_0'(M) = -\frac{1}{4\pi}\iint_{S'+S''} \gamma_0'(m)\,\frac{d}{dn_m}\,\frac{1}{mM}\,dS(m). \tag{21}$$

Of course

$$\chi_0(M) = \chi_{00} + \chi_{01}\,\frac{w}{U},$$

χ_{00} being due to Γ_{00} and $\chi_{01}(w/U)$ to $\Gamma_{01}(w/U)$, and, similarly:

$$\chi_0'(M) = \chi_{00}' + \chi_{01}'\,\frac{w}{U}.$$

When u/U, $Lq/U \neq 0$, we have:

$$\left.\begin{aligned}
\chi_0(M) &= \chi_{00} + \chi_{00}\,\frac{u}{U} + \chi_{01}\,\frac{w}{U} + \chi_{02}\,\frac{Lq}{U},\\
\chi_0'(M) &= \chi_{00}' + \chi_{00}'\,\frac{u}{U} + \chi_{01}'\,\frac{w}{U} + \chi_{02}'\,\frac{Lq}{U},\\
\Psi_0(M) &= \Psi_{00}' + \Psi_{00}\,\frac{u}{U} + \Psi_{01}\,\frac{w}{U} + \Psi_{02}\,\frac{Lq}{U},
\end{aligned}\right\} \tag{22}$$

with

$$\Psi_{0i} = \chi_{0i} + \chi_{0i}', \qquad (i = 0, 1, 2). \tag{23}$$

Now let us assume that χ_{00} is known. Since Ψ_{00} must satisfy the condition $\Psi_{00}(M_i) =$ constant, when M_i is in Ω_i, the density $\gamma_{00}(m)$ on S is given by the Fredholm's equation of the 2nd kind:

$$\frac{1}{2}\,\gamma_{00}(m) - \frac{1}{4\pi}\iint_S \gamma_{00}(m')\,\frac{d}{dn_{m'}}\,\frac{1}{m'm}\,dS(m') = -\chi_{00}(m_i) = -\chi_{00}(m), \tag{24}$$

m_i and m being on the same normal to S and infinitely close to one another.

The solution of Eq. (24) is:

$$\gamma_{00}(m) = -2\chi_{00}(m) + \iint_S A(m, m_1)\,\chi_{00}(m_1)\,dS(m_1), \tag{25}$$

where $A(m,m_1)$ is the "solving nucleus" of the Fredholm's equation.

We observe that $\chi_{00}(m)$ is discontinuous when M is crossing through Σ; the discontinuity is:

$$\chi_{00}(M') - \chi_{00}(M'') = \Gamma_0(\mu), \qquad \text{with } \mathbf{M'M''} = \epsilon\mathbf{n}_\mu, \quad (\epsilon > 0).$$

But, when M is in the vicinity of P, as P is on an edge of Σ, the discontinuity is the half of the previous one. Consequently, Eq. (25) gives

$$\gamma_{00}(m') - \gamma_{00}(m'') = \Gamma_{00}(P), \qquad (m', m'' \text{ infinitely close to } P), \tag{26}$$

which was easy to foresee.

We have yet to determine $\Gamma_{00}(P)$.

In order to do that, we need to know a condition which must be satisfied on $\mathcal{C}_{01}$. Let us assume, as a first approximation, that Σ may be regarded as nearly parallel to the (x, y)-plane even in the vicinity of $\mathcal{C}_{01}$. In this case, the condition

$$\frac{d}{dn_\mu}\left[\chi_{00}(\mu) + \chi'_{00}(\mu)\right] = -\frac{d}{dn_\mu}\Phi_{00}(\mu), \qquad x(\mu) = x(P) - 0, \tag{27}$$

may be expressed rather easily. It is a singular Fredholm's equation of the first kind which yields the unknown function $\Gamma_{00}(P)$.

Similar reasonings may be repeated for Γ_{01} and Γ_{02}, and finally, the problem consisting in the determination of the wake is, in principle, solved, at least, under the condition that the $\mathcal{C}_{01}$-line is known. The latter problem, of course, depends upon the mechanism which governs the transport into the wake of the vorticity which originates in the boundary layer. For the present moment, if a complete, explicit solution had to be given, it would be necessary to consider the $\mathcal{C}_{01}$-line as supplied by the experiment.

In the considerations above, we don't take into account the tendency of the free vortices to wind around themselves and to form two vortices only at some distance from the body. This question would be of importance. But, on this paper, we mainly need to have an idea on the structure of the various potentials which sum gives the motions of the fluid outside the body.

We note finally that

$$\Psi_0(m_e) = -\left[\gamma_{00}(m_1) + \gamma_{00}(m_1)\frac{u}{U} + \gamma_{01}(m_1)\frac{w}{U} + \gamma_{02}(m)\frac{u}{U}\right]. \tag{28}$$

4. Case of an Unsteady Quasi-Rectilinear Motion Parallel to the (z, x)-Plane

Let $t' = Ut/L$ be the reduced time (L = length of the body).

We assume that the components of the absolute velocity of the origin of the axis attached to the body and the absolute angular velocity (of components p, q, r on these axis) satisfy the following conditions:

$$
\begin{aligned}
&v = p = r = 0\,, \quad \text{for } -\infty < t' < +\infty\,,\\
&\mathbf{V} = (U+u)\mathbf{i}_x + v\mathbf{i}_y + w\mathbf{i}_z\,,\\
&U \ \text{constant}\,, \quad \left(\frac{u}{U}\right)_{t'} = 0 \text{ for } t' < 0\,, \quad = f_{00}(t') \text{ for } t' > 0\,,\\
&\left(\frac{w}{U}\right)_{t'} = 0 \text{ for } t' < 0\,, \quad = f_{01}(t') \text{ for } t' > 0\,,\\
&\left(\frac{Lq}{U}\right)_{t'} = 0 \text{ for } t' < 0\,, \quad = f_{02}(t') \text{ for } t' > 0\,;
\end{aligned}
\tag{1}
$$

f_{00}, f_{01}, f_{02} are given functions of the reduced time t'; their squares and products are negligible.

The velocity potential of the absolute motion is:

$$\varphi(M,t') = \Phi_{00}(M) + \sum_{k=0}^{2} \Phi_{0k}(M)\, f_{0k}(t') + \left[\Psi_{00}(M) + \sum_{k=0}^{2} \Psi_k(M,t')\right]. \tag{2}$$

In order to study the structure of the wake, we assume firstly that

$$f_{00}(t') \equiv 0\,, \qquad f_{02}(t') \equiv 0 \text{ for } t' > 0\,.$$

Let us consider the bound and free vortices which generate $\Psi_1(M,t')$.

At time $t' > 0$, a vortex generated in a small interval $(\tau', \tau' + d\tau')$, with $0 < \tau' < \tau' + d\tau' < t'$, is for instance, made of two filament vortices: one of them is of intensity $d_P d_{\tau'} \Gamma_1'(P,\tau')$, and lies on a closed contour made of an arc $P'm_{\tau'}'P$ on S', and on a U-shaped arc $PP_{\tau'}P_{\tau'}'P'$, where $P_{\tau'}P_{\tau'}'$ is deduced from the segment PP' by a translation nearly equal to $-\mathbf{i}_x L(t'-\tau')$; the other one is of intensity $d_P d_{\tau'} \Gamma_1''(P,\tau')$, and lies on the arc $Pm_{\tau'}''P'$ on S'' and on the arc $P'P_{\tau'}'P_{\tau'}P$ defined above.

Consequently, the total intensity on the arc $PP_{\tau'}P_{\tau'}'P'$ is equal to

$$d_P d_{\tau'} \Gamma_1(P,\tau') = d_P d_{\tau'} [\Gamma_1'(P,\tau') - \Gamma_1''(P,\tau')]\,.$$

As explained on Fig. 6, the first filament vortex is equivalent to a set of three vortices (a), (b), (c) of the same intensity $d_P d_{\tau'} \Gamma_1'(P,\tau')$. Vortex (a) is lying on $P'm_{\tau'}'P$ and on the segment PP'; vortex (b) is lying on the arc PKP' and on the segment $P'P$; vortex (c) is lying on the arc $P'KP$ and on the arc $PP_{\tau'}P_{\tau'}'P'$.

Vortex (a) is equivalent to a distribution of normal doublets on the part $S'(P,\tau')$ of S' behind the arc $P'm_{\tau'}'P$, and on the part $\Sigma_1(P)$ behind the segment PP' of the surface Σ_1 generated by PP' when P and P' describe the $\mathcal{C}_{01}$-line. Vortex (b) is equivalent to a distribution of normal doublets on $\Sigma_1(P)$. Vortex

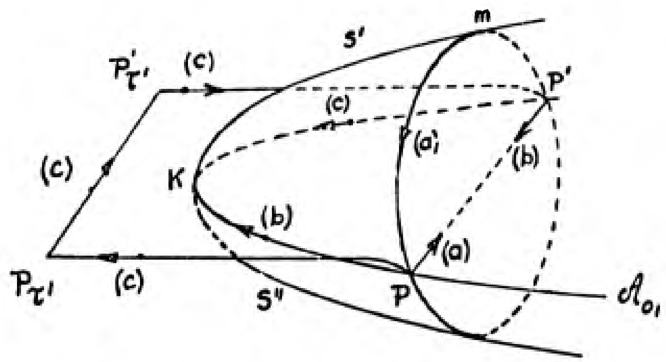

Figure 6

(c) is equivalent to a distribution of normal doublets on the part $\Sigma(P, t'-\tau')$ of the wake surface $\Sigma(t')$ between the arc $P'KP$ of $\mathcal{A}_{01}$, and the arc $PP_{\tau'}P'_{\tau'}P'$.

Obviously the two distributions on $\Sigma_1(P)$ are equal and opposite. Hence the vortex $d_P d_{\tau'} \Gamma'_1(P,\tau')$ lying at the time t' on the arc $P'm'_{\tau'}P$ and on the contour $PP_{\tau'}P'_{\tau'}P'$ is equivalent to the sum of the distributions of normal doublets on $S'(P,\tau')$ and on $\Sigma(P, t'-\tau')$.

An identical reasoning applied to vortex $d_P d_{\tau'} \Gamma''_1(P,\tau')$ lying, at the time t', on the arc $Pm''_{\tau'}P'$ and on the arc $P'P'_{\tau'}P_{\tau'}P$ shows finally that, we have to deal with two distributions of doublets, say on $S'(P,\tau')$ and $S''(P,\tau')$ and on $\Sigma(P, t'-\tau')$:

$$d_P d_{\tau'} \Psi_1(P,t') = d_P d_{\tau'} \chi_1(M,t') + d_P d_{\tau'} \chi'_1(P,t') . \tag{3}$$

with

$$\left.\begin{aligned} d_P d_{\tau'} \chi'_1(M,t') &= \frac{1}{4\pi} d_P d_{\tau'} \left[\iint_{S'(P,\tau')} \Gamma'_1(P,\tau') \frac{d}{dn_{m'}} \frac{1}{m'M} dS'(m') \right. \\ &\quad \left. + \iint_{S''(P,\tau')} \Gamma''_1(P,\tau') \frac{d}{dn_{m''}} \frac{1}{m''M} dS''(m'') \right] \\ d_P d_{\tau'} \chi_1(M,t') &= -\frac{1}{4\pi} d_P d_{\tau'} \Gamma_1(P,\tau') \iint_{\Sigma(P,t'-\tau')} \frac{d}{dn_\mu} \frac{1}{\mu M} d\Sigma(\mu) . \end{aligned}\right\} \tag{3'}$$

Now, let us consider at time t' the potential

$$\chi_1(M,t') = -\frac{1}{4\pi} \iint_{\Sigma(t')} \sigma_1(\mu) \frac{d}{dn_\mu} \frac{1}{\mu M} d\Sigma(\mu) . \tag{4}$$

Let ξ', η' be the absolute abscissa and ordinate of μ on $\Sigma(t')$. The density $\sigma_1(\mu)$ on the area $d\xi' d\eta'$ is the effect of the free vortices shed during the interval $(0, \tau')$ along the arcs PP_1 and $P'P'_1$, with $y'_P = \eta'$ (or $y'_{P'} = \eta'$ when $\eta' < y(K)$) and

$$\tau' = t' - \frac{X'(\mu) - \xi'}{L} ,$$

$X'(\mu)$ being the absolute abscissa of P (or P'). Consequently

$$\sigma_1(\mu) = \Gamma_1(\mu, \tau')$$

and we may write

$$\chi_1(M, t') = -\frac{1}{4\pi} \int_{y'(P'_1)}^{y'(P_1)} d\eta' \int_{X'(\eta') - Lt'}^{X'(\eta')} \Gamma_1\left(\mu, t' - \frac{X'(\mu) - \xi'}{L}\right) \frac{d}{dn_\mu} \frac{1}{\mu M} d\xi'(\mu), \quad \text{(4a)}$$

where $X'(\eta')$ is the absolute abscissa at t' of P (or P'), and $X(\eta') - Lt'$ its absolute abscissa at $t' = 0$ (see Fig. 7).

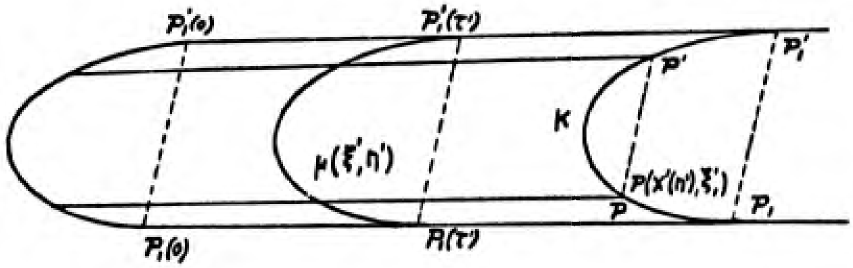

Figure 7

An equivalent for this expression is:

$$\chi_1(M, t') = -\frac{1}{4\pi} \int_{y_{P'}}^{y_{P'}} dy_P \int_0^{t'} \Gamma_1(y_P, \tau') \frac{d}{dn_\mu}$$

$$\times \left\{[x(M) - x(P) - L(t' - \tau')]^2 + [y(M) - y(P)]^2\right.$$

$$\left. + [z(M') - z(P)]^2\right\}^{-1/2} d\tau' . \quad \text{(4b)}$$

At time t', the potential $\chi'_1(M, t')$ due to the distribution of normal doublets on S' and S'' is:

$$\chi_1'(M,t') = -\frac{1}{4\pi}\left[\iint_{S'} \gamma_1'(m',t')\,\frac{d}{dn_{m'}}\,\frac{1}{m'M}\,dS'(m')\right.$$

$$\left. + \iint_{S''} \gamma_1''(m,t')\,\frac{d}{dn_{m''}}\,\frac{1}{m''M}\,dS(m'')\right], \tag{5}$$

and we have

$$\psi_1(M,t') = \chi_1(M,t') + \chi_1'(M,t'). \tag{6}$$

The density $\gamma_1'(m,t')$ is due to the sum of doublets $\Gamma_1'(P,t')$ on the part $S'(P,t')$ behind the arc $P'm_t',P$ which passes through m'; γ_1' depends upon t' because, firstly, $\Gamma_1'(P,t')$ depends also on the time, and secondly, because the arc $P'm_t',P$ just mentioned above depends not only on m', but also upon t' when m' is given. Consequently one has:

$$\gamma_1'(m',t') = \Gamma_1'[P(m',t'),t'], \qquad \gamma_1''(m'',t') = \Gamma_1''[P(m'',t'),t'],$$

where in the right members, P is a function of m' and of t'.

The potentials $\chi_1(M,t')$ and $\chi_1'(M,t')$ satisfy the condition

$$\chi_1(m_i,t') + \chi_1'(m_i,t') = \text{constant} \tag{7}$$

(with respect to m_i). Therefore, we have:

$$\left.\begin{matrix}\gamma_1'(m',t')\\ \\ \gamma_1''(m'',t')\end{matrix}\right\} = -2\chi_1(m_i,t') + \iint_S A(m,m_1)\,\chi_1(m_1,t')\,dS(m_1) \tag{8}$$

and

$$\gamma_1'(m',t') - \gamma_1''(m'',t') = \Gamma_1(y_P,t') \tag{9}$$

(m', m'' infinitely close to P).

Moreover, we have

$$\frac{d}{dn_\mu}\left[\chi_1(\mu,t') + \chi_1'(\mu,t')\right] = -\frac{d}{dn_\mu}\,\Phi_{01}(\mu)\left(\frac{w}{U}\right)_{t'}$$

$$= \frac{d}{dn_\mu}\,\Psi_{01}(\mu)\left(\frac{w}{U}\right)_{t'}, \quad x(\mu) = x(P) - 0. \tag{10}$$

Lastly, we observe that

$$\Psi_1(m_e,t') = -\gamma_1(m,t') + \text{constant}. \tag{11}$$

Let P_e be the point on S_e infinitely close to P. Putting

$$\frac{\partial}{\partial z} \Psi_{01}(P_c) = G(P) , \tag{12}$$

Eq. (10) gives:

$$\frac{\partial}{\partial z} \Psi_1(P_c, t') = G(P) \left(\frac{w}{U}\right)_{t'} . \tag{13}$$

Let "a_1" be the case when

$$\left(\frac{w}{U}\right)_{t'} = \left(\frac{w}{U}\right)_{0+} = \text{constant} \neq 0 \text{ for } t' > 0 .$$

In the case "a_1," one has:

$$\gamma_1(m, t') = \gamma_1^*(m, t') \left(\frac{w}{U}\right)_{0+} , \qquad \Gamma_1(\eta', t') = \Gamma_1^*(\eta', t') \left(\frac{w}{U}\right)_{0+} ,$$

and so on. Equation (13) yields

$$\int_{y_{P_1'}}^{y_{P_1}} d\eta' \int_{-\infty}^{X'(\eta')} \frac{\Gamma_1^*(\eta', \tau')}{\Gamma_{01}(\eta')} \frac{\partial^2}{\partial\xi'\partial\eta'} G(\eta_P')d\xi' = \int_{y_{P_1'}}^{y_{P_1}} d\eta' \int_{-\infty}^{X'(\eta')} \frac{\partial^2}{\partial\xi'\partial\eta'} G(\eta_P')d\xi', \tag{14}$$

where $\Gamma_1^*(\eta', \tau') = 0$ when $\xi' < X(\eta') - Lt'$, while

$$\frac{\partial^2}{\partial\xi'\partial\eta'} G(\eta_P')d\xi'$$

is the contribution in $G(P)$ of the area $d^2\Sigma = d\xi' d\eta'$ when the motion is steady, say when

$$t' = +\infty , \quad \Gamma_1^*(\eta', t') = \Gamma_1^*(\eta', +\infty) = \Gamma_{01}(\eta') .$$

Equation (14) takes into account the fact that χ_1 and consequently Ψ_1 are linear and homogeneous with respect to Γ_1.

Putting

$$\Gamma_1^*(\eta', t') = \Gamma_{01}(\eta') F^*(\eta', t') , \quad [F^*(\eta', t') = 0 \text{ for } t' < 0, \; F^*(\eta', +\infty) = 1] , \tag{15}$$

Eq. (14) becomes

$$\int_{y_{P_1'}}^{y_{P_1}} d\eta' \int_{X(\eta')-Lt'}^{X(\eta')} F^*(\eta', \tau') \frac{\partial^2}{\partial\xi'\partial\eta'} G(\eta_P')d\xi' = G(\eta_P') = \int_{y_{P_1'}}^{y_{P_1}} d\eta' \int_{-\infty}^{X(\eta')} \frac{\partial^2}{\partial\xi'\partial\eta'} G(\eta_P')d\xi',$$

or putting

$$\frac{\partial^2}{\partial\xi'\partial\eta'} G(\eta_P')d\xi' = J(\eta_P', \eta', t'-\tau')d\tau':$$

$$\int_{y_{P_1}'}^{y_{P_1}} d\eta' \int_0^{t'} F^*(\eta', \tau') J(\eta_P', \eta', t'-\tau')d\tau' = G(\eta_P')$$

$$= \int_{y_{P_1}'}^{y_{P_1}} d\eta' \int_{-\infty}^{t'} J(\eta_P', \eta', t'-\tau')d\tau'.$$

Using the Laplace transforms, and putting

$$j(\eta_P', \eta', s) = \int_0^\infty e^{-st'} J(\eta_P', \eta', t')dt',$$

$$f^*(\eta', s) = \int_0^\infty e^{-st'} F^*(\eta', t')dt',$$

and so on, we obtain

$$\int_{y_{P_1}'}^{y_{P_1}} f^*(\eta', s)\, j(\eta_P', \eta', s)d\eta' = \frac{1}{s}\int_{y_{P_1}'}^{y_{P_1}} j(\eta_P', \eta', o)d\eta'. \tag{16}$$

Let $u_q(\eta_P')$, $v_q(\eta')$ be the Schmidt's fundamental functions of the nucleus $j(\eta_P', \eta', o)$. One has

$$\int_{y_{P_1}'}^{y_{P_1}} u_q(\eta')\, u_r(\eta')d\eta' = 0, \text{ when } r \neq q, \quad = 1 \text{ when } r = q,$$

$$\int_{y_{P_1}'}^{y_{P_1}} v_q(\eta')\, v_r(\eta')d\eta' = 0, \text{ when } r \neq q, \quad = 1 \text{ when } r = q.$$

Therefore, we may write:

$$j(\eta_P', \eta', o) = \sum_p a_p u_p(\eta_P') v_p(\eta'),$$

$$j(\eta_P', \eta', s) = \sum_n \lambda_n(s)\, k_n(\eta_P', \eta') = \sum_n \lambda_n(s) \sum_r b_{np}\, u_p(\eta_P')\, v_p(\eta'),$$

$$f^*(\eta', s) = \sum_r f_r^*(s)\, v_r(\eta').$$

Substituting in Eq. (16), we get:

$$\int_{y_{P_1'}}^{y_{P_1}} \left[\sum_r f_r^*(s)\, v_r(\eta')\right] \left[\sum_n \lambda_n(s) \left\{\sum_p b_{np}\, u_p(\eta_P')\, v_p(\eta')\right\}\right] d\eta'$$

$$= \frac{1}{s} \int_{y_{P_1'}}^{y_{P_1}} \left[\sum_p a_p\, u_p(\eta_P')\, v_p(\eta')\right] d\eta' .$$

Putting

$$c_p = a_p \int_{y_{P_1'}}^{y_{P_1}} v_p(\eta')\, d\eta' ,$$

we obtain

$$\sum_p u_p(\eta_P') \left[\sum_n \lambda_n(s)\, b_{np}\right] f_p^*(s) = \frac{1}{s} \sum_p c_p\, u_p(\eta_P') ,$$

or

$$f_p^*(s) = c_p \frac{1}{s \sum_n \lambda_n(s)\, b_{np}} .$$

Therefore

$$F^*(\eta', t') = \sum_p v_p(\eta')\, F_p^*(t')$$

is known.

Of course, for $t' = +\infty$, the motion is steady, and consequently

$$1 = F^*(\eta', +\infty) = \sum_p v_p(\eta') .$$

This equation must hold for any value of η' in the range $\eta_{P_1'}' < \eta' < \eta_{P_1}'$.

Obviously there is a contradiction unless $F^*(\eta', t')$ is independent of η'. That leads to

$$\Gamma_1^*(\eta', t') = \Gamma_{01}(\eta')\, F^*(t') .$$

Then, Eq. (16) gives

$$\int_0^{t'} \frac{d}{d\tau'} F^*(\tau') \, J'(\eta'_P, \eta', t'-\tau')d\tau' = G(\eta'_P) = J'(\eta'_P, +\infty)$$

where

$$\frac{\partial}{\partial\tau'} J'(\eta'_P, t'-\tau') = -\frac{\partial}{\partial\tau'} J'(\eta'_P, t'-\tau')$$

$$= \int_{y_{P'_1}}^{y_{P_1}} J(\eta'_P, \eta', t'-\tau')d\eta', \quad \text{with } J'(\eta'_P, 0) = 0 .$$

Using again the Laplace transform, we obtain:

$$s f^*(s) \, j'(\eta'_P, s) = \frac{1}{s} G(\eta'_P) = \frac{1}{s} J'(\eta'_P, +\infty) .$$

Consequently, we may introduce a function $h(s)$ and write:

$$j'(\eta'_P, s) = G(\eta'_P) \, h(s) .$$

Expression

$$\frac{\partial}{\partial\tau'} H(t'-\tau')d\tau' . \, G(\eta'_P)$$

is the contribution in $G(\eta'_P)$, when the motion is steady, of the area $d\Sigma$ between the two arcs deduced from C_{01} by the translations $-i_x L(t'-\tau')$ and $-i_x L(t'-\tau'-d\tau')$ and the two streamlines of the relative motion coming from P and P'.

Function $\dot{F}^*(t')$ is the solution of a singular Volterra's equation of the first kind

$$\int_0^{t'} \dot{F}^*(\tau') \, H(t'-\tau')d\tau' = 1 .$$

Putting $\tau' = \lambda t'$, $t'-\tau' = (1-\lambda)t'$, this equation becomes:

$$t' \int_0^1 \dot{F}^*[\lambda t'] \, H[(1-\lambda)t']d\lambda = 1 ,$$

what implies

$$\dot{F}^*[\lambda t'] \, H[(1-\lambda)t'] = O\{t'^{-1}\} \tag{21}$$

for t' very small.

So Eq. (20) is quite analogous to the equation which yields the circulation around an airfoil of infinite span in case "a_1."

Equation (20) is not convenient for numerical calculations. But, if the nucleus $H(t')$ was really known, as in the case of the airfoil of infinite aspect ratio, it would be possible to solve it after some transformations. Equation (20) is equivalent to

$$\int_0^{t'} A(t'-\theta)d\theta \int_0^{\theta} \dot{F}^*(\tau')\, H(\theta-\tau')d\tau' = \int_0^{t'} A(t'-\theta)d\theta = \int_0^{t'} A(\tau')d\tau' .$$

or to

$$\int_0^{t'} \dot{F}^*(\tau') \left[\int_{\tau'}^{t'} A(t'-\theta)\, H(\theta-\tau')d\theta\right] d\tau' = \int_0^{t'} A(\tau')d\tau' .$$

The nucleus in the brackets is

$$(t'-\tau') \int_0^1 A[(1-\lambda)(t'-\tau')]\, H[\lambda(t'-\tau')]d\lambda = K(t'-\tau') . \tag{22}$$

If we choose $A(t')$ in such a way that $K(0) = 1$, what implies only

$$A(t') = 0\{\dot{F}^*(t')\} \tag{23}$$

for t' small, we obtain, deriving with respect to t':

$$\dot{F}^*(t') + \int_0^{t'} \dot{F}^*(\tau')\, K(t'-\tau')d\tau' = A(t') , \tag{24}$$

what is the wanted form of (20).

Now consider the density $\gamma_1^*(m,t')$ of the distribution of doublets on the hull. Since

$$\frac{\partial}{\partial z}\gamma_1^*(m,t') = \frac{\partial}{\partial z}\Phi_{01}(m) ,$$

when t' is small, and m close to $\mathfrak{C}_{01}$, one has

$$\gamma_1^*(m,0+) = 0(1) . \tag{25}$$

This result is compatible with the conditions

$$\Gamma_1^*(y_P, t') = \gamma_1^*(m', t') - \gamma_1^*(m'', t') ,$$

$$\Gamma_1^*(y_P, 0+) = 0 ,$$

(m', m'' infinitely close to P), which lead to

$$\gamma_1^*(m', 0+) - \gamma_1^*(m'', 0+) = 0 .$$

We set

$$\gamma_1^*(m, t') = \gamma_1^*(m, 0+) + \delta\gamma_1^*(m, t') \tag{26}$$

with

$$\delta\gamma_1^*(m, 0+) = 0 , \qquad \frac{\partial}{\partial t'} \delta\gamma_1^*(m, 0+) = 0(1) . \tag{27}$$

The variation of $\delta\gamma_1^*(m, t')$ between $(0, t')$ is partly due to the fact that $\gamma_1^*(m, t')$ depends upon the distribution of the arcs $P'm'_t, P$, $P'm''_t, P$ on the hull, distribution which is variable with t'. For $t' = 0+$, these arcs are concentrated in the vicinity of $\mathcal{C}_{01}$.

Now, consider the case "b_1," when $(w/U)_{t'}$ is, for $t' > 0$, an arbitrarily given function.

For (20), we have to substitute:

$$\int_0^{t'} \dot{F}_1(t' - \tau') \, H(t' - \tau') d\tau' = \left(\frac{w}{U}\right)_{t'} , \tag{28}$$

the general solution of which is:

$$F_1(t') = \left(\frac{w}{U}\right)_{0+} F^*(t') + \int_0^{t'} \frac{d}{d\tau'} \left(\frac{w}{U}\right)_{t'} F^*(t' - \tau') d\tau' \tag{29}$$

when $(w/U)_{t'}$ is continuous for $t' > 0$. One has

$$\Gamma_1(\eta', t') = \Gamma_{01}(\eta') \, F_1(t') . \tag{30}$$

Because of (8) the density $\gamma_1(m, t')$ of the distribution of doublets on the hull is:

$$\gamma_1(m, t') = \int_0^{t'} F_1(t') \, H_{01}(m, t' - \tau') d\tau' . \tag{31}$$

That gives, in the case "a_1," the expression already written above:

$$\gamma_1^*(m, t') \left(\frac{w}{U}\right)_{0+} = \left(\frac{w}{U}\right)_{0+} \int_0^{t'} F_1^*(\tau') \, H_{01}(m, t'-\tau') d\tau'$$

$$= \left(\frac{w}{U}\right)_{0+} \left[\gamma_1^*(m, 0) + \delta\gamma_1^*(m, t')\right] . \tag{32}$$

and, in the case "b_1":

$$\gamma_1(m, t') = \left(\frac{w}{U}\right)_{0+} \left[\gamma_1^*(m, 0+) + \delta\gamma_1^*(m, t')\right]$$

$$+ \int_0^{t'} \frac{d}{d\tau'} \left(\frac{w}{U}\right)_{t'} \left[\gamma_1^*(m, 0) + \delta\gamma_1^*(m, t'-\tau')\right] d\tau'$$

$$= \left(\frac{w}{U}\right)_{t'} \gamma_1^*(m, 0+) + \left(\frac{w}{U}\right)_{0+} \delta\gamma_1^*(m, t')$$

$$+ \int_0^{t'} \frac{d}{d\tau'} \left(\frac{w}{U}\right)_{t'} \delta\gamma_1^*(m, t'-\tau') d\tau' , \tag{33}$$

when $(w/U)_{t'}$ is continuous for $t' > 0$.

If $(w/U)_{t'}$ has discontinuities of the first kind for $t' > 0$, one has the general formulae:

$$F_1(t') = \int_0^{t'} \left(\frac{w}{U}\right)_{t'} \frac{\partial}{\partial t'} F^*(t'-\tau') d\tau' , \tag{29'}$$

and

$$\gamma_1(m, t') = \left(\frac{w}{U}\right)_{t'} \gamma_1^*(m, 0+) + \int_0^{t'} \left(\frac{w}{U}\right)_{t'} \frac{\partial}{\partial t'} \delta\gamma_1^*(m, t'-\tau') d\tau' . \tag{33'}$$

In the case of the quasi-steady motion, we would have a circulation

$$\left(\frac{w}{U}\right)_{t'} \Gamma_{01}(\eta') \, F^*(+\infty) = \Gamma_{01}(\eta') \left(\frac{w}{U}\right)_{t'}$$

and a density of doublets

$$\left(\frac{w}{U}\right)_{t'} \gamma_{01}(m) = \left(\frac{w}{U}\right)_{t'} \left[\gamma_1^*(m, 0+) + \delta\gamma_1^*(m, +\infty)\right] .$$

That leads in the case "a_1," to the deficiencies

$$\left(\frac{w}{U}\right)_{0+} \Delta\Gamma_1^*(m, t') = \left(\frac{w}{U}\right)_{0+} \Gamma_{01}(\eta')\,[1 - F^*(t')]$$

$$= \left(\frac{w}{U}\right)_{0+} \Gamma_{01}(\eta') \int_0^{t'} \dot{F}^*(\tau')\,[H(t' - \tau') - 1]\,d\tau' ,$$

and

$$\left(\frac{w}{U}\right)_{0+} \Delta\gamma_1^*(m, t') = \left(\frac{w}{U}\right)_{0+} \left[\delta\gamma_1^*(m, +\infty) - \delta\gamma_1^*(m, t')\right] .$$

When $(w/U)_{t'}$ is arbitrarily given, the differences are:

$$\left.\begin{aligned} \Delta\Gamma_1(\eta', t') &= \Gamma_{01}(\eta') \left[\left(\frac{w}{U}\right)_{t'} - \int_0^{t'} \left(\frac{w}{U}\right)_{t'} \frac{\partial}{\partial t'} F^*(t' - \tau')d\tau'\right] , \\ \Delta\gamma_1(m, t') &= \left(\frac{w}{U}\right)_{t'} \delta\gamma_1^*(m, +\infty) - \int_0^{t'} \left(\frac{w}{U}\right)_{t'} \frac{\partial}{\partial t'} \delta\gamma_1^*(m, t' - \tau')d\tau' . \end{aligned}\right\} \quad (34)$$

In the cases "b_0," when $(w/U)_{t'} = 0$, $(Lq/U)_{t'} = 0$, $(u/U)_{t'} = f_{00}(t')$ for $t' > 0$, and in the case "b_2," when $(u/U)_{t'} = 0$, $(w/U)_{t'} = 0$ and $(Lq/U)_{t'} = f_{02}(t')$, we have similar formulae.

In the general case, $f_{00}(t')$, $f_{01}(t')$, $f_{02}(t')$ being arbitrarily given for $t' > 0$, we get:

$$\left.\begin{aligned} \Gamma(\eta', t') &= \sum_{i=0}^{2} \Gamma_{0i}(\eta') \int_0^{t'} f_{0i}(\tau') \frac{\partial}{\partial t'} F^*(t' - \tau')d\tau' , \\ \gamma(m, t') &= \sum_{i=0}^{2} \left\{ f_{0i}(t')\, \gamma_i(m, 0+) + \int_0^{t'} f_{0i}(\tau') \frac{\partial}{\partial t'} \delta\gamma_i(m, t' - \tau')d\tau' . \right. \end{aligned}\right\} \quad (35)$$

5. Hydrodynamic Forces Due to the Velocity Potential (case of par. 4)

5.1. Definition of the Hydrodynamic Forces

When w/U and Lq/U are small, there are no strong eddies due to separation. Therefore the set of forces acting on the body is purely the sum of the following sets:

(i) $(\mathcal{F}_S)$ due to gravity (weight of the body, hydrostatic pressures),

(ii) $(\mathcal{F}_c)$ due to the inertia of the body,

(iii) $(\mathcal{F}_{\nu})$ due to viscosity (friction or, more exactly, viscous drag),

(iv) $(\mathcal{F}_{\phi})$ due to the velocity potential of the absolute motion,

(v) $(\mathcal{F}_T)$ due to the propeller, and

(vi) forces due to the system — if any — which reduces the freedom of the body or generates its forced motion.

The set of hydrodynamic forces is $\mathcal{F}_{\phi}$. We assume here that the body is not fitted with planes and fins (see par. 6).

For what follows, it is helpful to separate the set of forces $(\mathcal{F}_{\phi})$ into two additive parts, $\mathcal{F}_i$ and $\mathcal{F}'$, $(\mathcal{F}_i)$ existing alone when there is no wake, while $(\mathcal{F}')$ is the contribution of the wake.

It is possible to obtain rigorously this result by starting from the contribution in the absolute momentum of the fluid of each part of ϕ (see par. 5.3). However, we will firstly proceed using an approximate expression of the hydrodynamic pressure $p(m_e, t')$ on S_e.

The velocity potential $\phi(M, t')$ is, at time $t' + dt'$, when M is at rest with respect to the fixed axis:

$$\phi(M, t' + dt') = \phi'(x', y', z', t' + dt') = \phi(x - u_E dt', y - v_E dt', z - w_E dt', t' + dt') , \quad (1)$$

where u_E, v_E, w_E are the components of the absolute velocity $\mathbf{V}_E(M, t')$ of the point attached to the body which, at t', coincides with M. Consequently:

$$\frac{\partial \phi'}{\partial t}(M, t') = \frac{\partial \phi}{\partial t}(M, t') - \mathbf{V}_E(M, t') \ \mathbf{grad} \ \phi(M, t') . \quad (2)$$

The hydrodynamic pressure is given by:

$$\frac{1}{\rho}\left[p(M, t') - p_\infty\right] = \frac{\partial \phi'}{\partial t}(M, t') - \frac{1}{2} V^2(M, t') , \quad (3)$$

where $\mathbf{V}(M, t')$ is the absolute velocity of the fluid at M. $\mathbf{V}_r$ being its relative velocity at the same point, one has

$$\frac{1}{\rho}\left[p(M, t') - p_\infty\right] = \frac{\partial \phi}{\partial t}(M, t') + (\mathbf{V}_E \mathbf{V})_{M, t'} - \frac{1}{2} V^2(M, t') \quad (4)$$

$$\frac{1}{\rho}\left[p(M, t') - p_\infty\right] = \frac{\partial \phi}{\partial t}(M, t') + \frac{1}{2} V_E^2(M, t') - \frac{1}{2} V_r^2(M, t') . \quad (4')$$

Since $|V \, V_E|$ is generally small, we could neglect the last term in the right member of (4) and write

$$\frac{1}{\rho} p(m_e, t') = \frac{1}{\rho} p_\infty + \left[\frac{\partial \phi}{\partial t} - \mathbf{V}_E \ \mathbf{grad} \ \phi\right]_{m_e, t'}$$

This expression being linear with respect to ϕ, we would obtain

$$\frac{1}{\rho} p(m_e, t') = \frac{1}{\rho} p_\infty + \frac{1}{\rho} p_i(m_e, t') + \frac{1}{\rho} p'(m_e, t') \tag{5}$$

with

$$\left.\begin{aligned} \frac{1}{\rho} p_i(m_e, t') &= \left[\frac{\partial}{\partial t} - \mathbf{V}_E \ \mathbf{grad}\right]\left[\Phi_{00}(m_e) + \sum_{k=0}^{2} \Phi_{0k}(m_e)\ f_{0k}(t')\right], \\ \frac{1}{\rho} p'(m_e, t') &= \left[\frac{\partial}{\partial t} - \mathbf{V}_E \ \mathbf{grad}\right]\left[\Psi_{00}(m_e) + \sum_{k=0}^{2} \Psi_k(m_e, t')\right]. \end{aligned}\right\} \tag{6}$$

$p_i(m_e, t')$ generates the set of forces $(\mathcal{F}_i)$ when the fluid is quite perfect, say when there is no wake; $p'(m_e, t')$ gives the contribution of the wake in the hydrodynamic forces.

In order to use the density of the distribution of normal doublets on S and the equation

$$\Psi_k(m_e, t') = -\gamma_k(m, t'),$$

it is, however, easier to consider the streamlines $\mathcal{C}$ of the relative motion on S_e. These streamlines are the orthogonal trajectories of the curves γ = constant, where γ is the total density of the normal doublets on S. Because all the components of γ are small with respect to γ_{00}, that is, with respect to the density of normal doublets which generate Φ_{00}, we may consider that the unit vector $\mathbf{i}'_\sigma$ tangent at m_e to the streamline $\mathcal{C}$ passing through m_e at t' is practically independent of t'. We choose $\mathbf{i}'_\sigma$ positive downstream and also the element of arc $d\sigma'$ on $\mathcal{C}$. Consequently, the relative velocity $\mathbf{V}_r(m_e, t')$ is approximately given by

$$\begin{aligned} \mathbf{V}_r(m_e, t') &= V_r(m_e, t')\ \mathbf{i}'_\sigma(m_e) \\ &= -\frac{\partial}{\partial\sigma'}\left[\Phi_{00}(m_e) + \sum_{k=0}^{2} \Phi_{0k}(m_e)\ f_{0k}(t')\right] - \left[\mathbf{V}_E \mathbf{i}'_\sigma\right]_{m_e, t'} \\ &\quad - \frac{\partial}{\partial\sigma'}\left[\Psi_{00}(m_e) + \sum_{k=0}^{2} \Psi_k(m_e, t')\right]. \end{aligned}$$

Hence,

$$-\frac{1}{2} V_r^2(m_e, t')$$

is the sum of the three following terms:

$$\left.\begin{aligned}
-\frac{1}{2}V_{r_i}^2 &= -\frac{1}{2}\left\{\frac{\partial}{\partial\sigma'}\left[\Phi_{00}(m_e)+\sum_{k=0}^{2}\Phi_{0k}(m_e)\,f_{0k}(t')\right]+\left[\mathbf{V}_E\mathbf{i}'_\sigma\right]_{m_e,t'}\right\}^2 ,\\
(t) &= -\frac{1}{2}\left\{\frac{\partial}{\partial\sigma'}\left[\Psi_{00}(m_e)+\sum_{k=0}^{2}\Psi_k(m_e,t')\right]\right\}^2\\
&\quad -\left[\frac{\partial}{\partial\sigma'}\sum_{k=0}^{2}\Phi_{0k}(m_e)\,f_{0k}(t')\right]\times\frac{\partial}{\partial\sigma'}\left[\Psi_{00}(m_e)+\sum_{k=0}^{2}\Psi_k(m_e,t')\right],\\
-\frac{1}{2}V_{r'}^2 &= -\left[\frac{\partial}{\partial\sigma'}\Phi_{00}(m_e)+\mathbf{V}_E\mathbf{i}'_\sigma\right]\times\frac{\partial}{\partial\sigma'}\left[\Psi_{00}(m_e)+\sum_{k=0}^{2}\Psi_k(m_e,t')\right].
\end{aligned}\right\}\quad(7)$$

Since (b) is negligible, we obtain

$$\left.\begin{aligned}
\frac{1}{\rho}p_i(m_e,t') &= \frac{\partial}{\partial t}\left[\sum_{k=0}^{2}\Phi_{0k}(m_e)\,f_{0k}(t')\right]+\frac{1}{2}V_E^2(m_e,t')-\frac{1}{2}V_{r_i}^2(m_e,t'),\\
\frac{1}{\rho}p'(m'_e,t') &= \left\{\frac{\partial}{\partial t}-\left[\frac{\partial}{\partial\sigma'}\Phi_{00}(m_e)+\mathbf{V}_E(m_e,t')\,\mathbf{i}'_\sigma(m_e)\right]\frac{\partial}{\partial\sigma'}\right\}\\
&\qquad\times\left\{\Psi_{00}(m_e)+\sum_{k=0}^{2}\Psi_k(m_e,t')\right\}.
\end{aligned}\right\}\quad(8)$$

In par. 5.4, we give the expression of the set of forces $(\mathcal{F}_i)$ due to p_i. Now we consider the set of forces $\mathcal{F}'$ due to $p'(m_e,t')$.

5.2. The Set of Absolute Forces Due to the Wake

Let us assume, for instance, that we are in the case "b_1" of par. 4, when $(u/U)_{t'}$, $(Lq/U)_{t'}$ are identically null, while $(w/U)_{t'}$ is, for $t'>0$, an arbitrarily given function of t'.

According to a result of par. 4, the density of the normal doublets on S due to $\Psi_1(m_e,t')$ is:

$$\gamma_1(m,t') = \left(\frac{w}{U}\right)_{t'}\gamma_1^*(m,0+)+\left(\frac{w}{U}\right)_{0+}\gamma_1^*(m,t')+\int_0^{t'}\frac{d}{d\tau'}\left(\frac{w}{U}\right)_{\tau'}\gamma_1^*(m,t'-\tau')\,d\tau' \quad (9)$$

when $(w/U)_{t'}$ is continuous for $t'>0$.

The pressure $p'_1(m_e,t')$ due to $\Psi_1(m_e,t')=-\gamma_1(m,t')$ is given by

$$\frac{1}{\rho}\,p_1'(m_e,t') = -\frac{U}{L}\,\frac{\partial}{\partial t'}\,\gamma_1(m,t') + \left[\mathbf{V}_E(m_e,t')\;\mathbf{i}_\sigma'(m_e) + \frac{\partial}{\partial\sigma'}\,\Psi_{00}(m_e)\right]\frac{\partial}{\partial\sigma'}\,\gamma_1(m,t')$$

or by

$$\frac{1}{\rho}\,p_1'(m_e,t') = -\frac{U}{L}\Bigg[\gamma_1^*(m,0+)\,\frac{d}{dt'}\left(\frac{w}{U}\right)_{t'} + \left(\frac{w}{U}\right)_{0+}\frac{\partial}{\partial t'}\,\delta\gamma_1^*(m,t')$$

$$+\int_0^{t'}\frac{d}{d\tau'}\left(\frac{w}{U}\right)_{\tau'}\frac{\partial}{\partial t'}\,\delta\gamma_1^*(m,\,t'-\tau')\,d\tau'\Bigg]$$

$$+\left[\mathbf{V}_E\mathbf{i}_\sigma' + \frac{\partial}{\partial\sigma'}\,\Phi_{00}\right]\frac{\partial}{\partial\sigma'}\Bigg[\left(\frac{w}{U}\right)_{t'}\gamma_1^*(m,0+) + \left(\frac{w}{U}\right)_{0+}\delta\gamma_1^*(m,t')$$

$$+\int_0^{t'}\frac{d}{d\tau'}\left(\frac{w}{U}\right)_{\tau'}\delta\gamma_1^*(m,t'-\tau')\,d\tau'\Bigg]. \qquad (10)$$

Let us consider firstly the particular case "a_1," when

$$\left(\frac{w}{U}\right)_{t'} = \left(\frac{w}{U}\right)_{0+} \neq 0$$

for $t' > 0$. Let

$$p_1'^*(m_e,t')\left(\frac{w}{U}\right)_{0+}$$

be the expression of $p_1'(m_e,t')$ in this case. Equation (10) gives:

$$\frac{1}{\rho}\,p_1'^*(m_e,t') = -\frac{U}{L}\,\frac{\partial}{\partial t'}\,\delta\gamma_1^*(m,t') + \left[\mathbf{V}_E\mathbf{i}_\sigma' + \frac{\partial}{\partial\sigma'}\,\Phi_{00}\right]\times\frac{\partial}{\partial\sigma'}\left[\gamma_1^*(m,0+) + \delta\gamma_1^*(m,t')\right].$$

Therefore, one has

$$\frac{1}{\rho}\,p_{01}(m_e) = \frac{1}{\rho}\,p_1'^*(m_e,+\infty) = \left[\mathbf{V}_E\mathbf{i}_\sigma' + \frac{\partial}{\partial\sigma'}\,\Phi_{00}\right]\frac{\partial}{\partial\sigma'}\left[\gamma_1^*(m,0+) + \delta\gamma_1^*(m,+\infty)\right]. \qquad (11)$$

Now consider the difference in the case "b_1," when $(w/U)_{t'}$ is an arbitrarily given function, between the pressure $p_{01}(m_e)(w/U)_{t'}$ in the quasi-steady motion and the pressure $p_1'(m_e,t')$ in the real motion. Assuming that $(w/U)_{t'}$ is continuous for $t' > 0$, we have:

$$\frac{1}{\rho}\,p_{01}(m_e)\left(\frac{w}{U}\right)_{t'} - \frac{1}{\rho}\,p_1'(m_e,t') = \frac{1}{\rho}\,\Delta p_1'(m_e,t'), \qquad (12)$$

where

$$\frac{1}{\rho}\,\Delta p_1'(m_e,t') = \frac{1}{\rho}\,p_1'^{(i)}(m_e,t') + \frac{1}{\rho}\,\Delta' p_1'(m_e,t'). \qquad (12')$$

with

$$-\frac{1}{\rho}\,p_1'^{(i)}(m_e,t') = \frac{U}{L}\,\gamma_1^*(m,0+)\,\frac{d}{dt'}\left(\frac{w}{U}\right)_{t'}\,. \tag{13}$$

and

$$\frac{1}{\rho}\,\Delta' p_1'(m_e,t') = \left[\mathbf{V}_E\mathbf{i}_\sigma' + \frac{\partial}{\partial\sigma'}\,\Phi_{00}\right] \times \frac{\partial}{\partial\sigma'}\left\{\delta\gamma_1^*(m,+\infty)\left(\frac{w}{U}\right)_{t'} - \left(\frac{w}{U}\right)_{0+}\delta\gamma_1^*(m,t')\right.$$
$$\left. - \int_0^{t'}\frac{d}{d\tau'}\left(\frac{w}{U}\right)_{\tau'}\,\delta\gamma_1^*(m,\,t'-\tau')d\tau'\right\}$$
$$+\frac{U}{L}\left\{\left(\frac{w}{U}\right)_{0+}\frac{\partial}{\partial t'}\,\delta\gamma_1^*(m,t') + \int_0^{t'}\frac{d}{d\tau'}\left(\frac{w}{U}\right)_{\tau'}\,\delta\gamma_1^*(m,\,t'-\tau')d\tau'\right\}. \tag{14}$$

Integrating by parts the integrals in the right member of (14), we get:

$$\frac{1}{\rho}\,\Delta' p_1'(m_e,t') = \left(\frac{w}{U}\right)_{t'}\left\{\left[\mathbf{V}_E\mathbf{i}_\sigma' + \frac{\partial}{\partial\sigma'}\,\Phi_{00}\right]\frac{\partial}{\partial\sigma'}\,\delta\gamma_1^*(m,+\infty) + \frac{U}{L}\frac{\partial}{\partial t'}\,\delta\gamma_1^*(m,0+)\right\}$$
$$-\int_0^{t'}\left(\frac{w}{U}\right)_{\tau'}\left\{\left[\mathbf{V}_E\mathbf{i}_\sigma' + \frac{\partial}{\partial\sigma'}\,\Phi_{00}\right]\frac{\partial}{\partial\sigma'} - \frac{U}{L}\frac{\partial}{\partial t'}\right\}\frac{\partial}{\partial t'}\,\delta\gamma_1^*(m,\,t'-\tau')d\tau'\,. \tag{14'}$$

This equation holds when $(w/U)_{t'}$ has jumps for $t'>0$.

Let us introduce now the difference

$$\Delta'\delta\gamma_1^*(m,t') = \delta\gamma_1^*(m,+\infty) - \delta\gamma_1^*(m,t')\,. \tag{15}$$

We set

$$R(m,t') = \left[\left(\mathbf{V}_E\mathbf{i}_\sigma' + \frac{\partial}{\partial\sigma'}\,\Phi_{00}\right)\frac{\partial}{\partial\sigma'} - \frac{U}{L}\frac{\partial}{\partial t'}\right]\Delta'\delta\gamma_1^*(m,t')\,. \tag{16}$$

We obtain

$$R(m,0) = \left(\mathbf{V}_E\mathbf{i}_\sigma' + \frac{\partial}{\partial\sigma'}\,\Phi_{00}\right)\frac{\partial}{\partial\sigma'}\,\delta\gamma_1^*(m,+\infty) + \frac{U}{L}\frac{\partial}{\partial t'}\,\delta\gamma_1^*(m,0)\,,$$

$$R(m,+\infty) = 0\,.$$

So Eqs. (14') and (14) give respectively:

$$\frac{1}{\rho}\,\Delta' p_1'(m_e,t') = \left(\frac{w}{U}\right)_{t'} R(m,0) + \int_0^{t'}\left(\frac{w}{U}\right)_{\tau'}\frac{\partial}{\partial t'}\,R(m,\,t'-\tau')d\tau'\,, \tag{17'}$$

$$\frac{1}{\rho}\Delta' p_1'(m_e, t') = \left(\frac{w}{U}\right)_{0+} R(m, t') + \int_0^{t'} \frac{d}{d\tau'}\left(\frac{w}{U}\right)_{\tau'} R(m, t'-\tau')d\tau' . \tag{17}$$

We note that the first term in $R(m,0)$ comes from the fact that the circulation around the body is null at $t' = 0+$. It leads to a deficiency of the pressure. But the second term acts in the opposite direction.

In the quasi-steady motion, the resultant force and the resultant moment referred about the origin of the moving axis are respectively

$$\mathcal{F}_{01}\left(\frac{w}{U}\right)_{t'} = -\left(\frac{w}{U}\right)_{t'} \iint_S p_{01}(m_e)\, \mathbf{n}(m_e)\, dS(m_e) , \tag{18}$$

$$\mathbf{I}_{01}\left(\frac{w}{U}\right)_{t'} = -\left(\frac{w}{U}\right)_{t'} \iint_S p_{01}(m_e)\, \mathbf{Om}_e \wedge \mathbf{n}(m_e)\, dS(m_e) . \tag{19}$$

In the real motion, the resultant force and the resultant moment are, respectively,

$$\mathcal{F}_1'(t') = \mathcal{F}_{01}\left(\frac{w}{U}\right)_{t'} + \mathcal{F}_1'^{(i)}(t') - \Delta'\mathcal{F}_1'(t') , \tag{20}$$

$$\mathbf{I}_1'(t') = \mathbf{I}_{01}\left(\frac{w}{U}\right)_{t'} + \mathbf{I}_1'^{(i)}(t') - \Delta'\mathbf{I}_1'(t') , \tag{21}$$

with, for instance:

$$\left.\begin{aligned}
\mathcal{F}_1'^{(i)}(t') &= \rho \frac{U}{L} \frac{d}{dt'}\left(\frac{w}{U}\right)_{t'} \iint_S \gamma_1(m, 0+)\, \mathbf{n}(m_e)\, dS(m_e) , \\
\Delta'\mathcal{F}_1'(t') &= -\rho \iint_S dS(m)\, \mathbf{n}(m) \left[\left(\frac{w}{U}\right)_{t'} R(m,0) \right. \\
&\quad \left. + \int_0^{t'} \left(\frac{w}{U}\right)_{\tau'} \frac{\partial}{\partial t'} R(m, t'-\tau')d\tau' \right] .
\end{aligned}\right\} \tag{22}$$

The force $\mathcal{F}_1'^{(i)}(t')$ and the moment $\mathbf{I}_1'^{(i)}(t')$ act in order to increase the apparent inertia of the body and will be included in the final formulae in the set of forces $\mathcal{F}_i$ (see par. 5.4). They do not exist in the theory of the thin airfoil of infinite aspect ratio. On the contrary, the force $\Delta'\mathcal{F}_1'(t')$ and the moment $\Delta'\mathbf{I}_1(t')$ are quite analogous with those found in this theory.

Similar formulae can be obtained when $(u/U)_{t'} \neq 0$, $(w/U)_{t'} = 0$, $(Lq/U)_{t'} = 0$ for $t' > 0$ (case "b_0") or when $u/U(t') = 0$, $(w/U)_{t'} = 0$, $(Lq/U)_{t'} \neq 0$ (case "b_2"). The total set of forces due to the wake in the most general case is the sum of those found in the three cases "b_0," "b_1" and "b_2."

5.3. Another Expression of the Set of Forces Due to the Velocity Potential Ψ

The absolute momentum due to the distribution of normal doublets

$$\frac{1}{4\pi} d\Sigma(\mu) \frac{d}{dn_\mu} \frac{1}{\mu M}$$

on a small surface $d\Sigma(\mu)$ is

$$\rho \, d\Sigma(\mu) \, \mathbf{n}(\mu) ,$$

it acts through point μ.

Consequently, the total set of hydrodynamic forces exerted on the body may be obtained by starting from the variations during the interval $(t', t' + dt')$ of the absolute momentum due to the distributions of normal doublets on S and on the wake surface. These momentums are additive. Consequently, the set of forces $(\mathcal{F}_i)$ comes from the velocity potential:

$$\Phi = \Phi_{00}(m_e) + \sum_{k=0}^{2} \Phi_{0k}(m_e) \, f_{0k}(t') ,$$

while the set of forces $(\mathcal{F}')$ comes from the velocity potential:

$$\Psi = \Psi_{00}(m_e) + \sum_{k=0}^{2} \Psi_{0k}(m_e, t') .$$

Here, we deal only with the set of forces $(\mathcal{F}')$. The set $(\mathcal{F}_i)$ will be obtained in par. 5.4 by another way using the absolute kinetic energy due to Φ.

Let us consider the case "b_1."

At time t' the absolute momentum of the fluid is

$$Q_1(t') = Q_1'(t') + Q_1''(t') .$$

$Q_1'(t')$ is due to the doublets distributed on the wake and $Q_1''(t')$ to those distributed on S.

The general resultant of the hydrodynamic forces due to Ψ_1 is

$$\mathcal{F}_1'(t') = -\frac{U}{L} \frac{d}{dt'} (Q_1' + Q_1'') .$$

One has

$$Q_1'(t') = \rho\, \mathbf{n}_\mu \int_{\mathcal{C}_{01}} \Gamma_{01}(\eta')d\eta' \int_{X'(\eta',t')-Lt}^{X'(\eta',t')} F_1(\mu)d\xi'$$

$$= \rho\, \mathbf{i}_z L \int_{\mathcal{C}_{01}} \Gamma_{01}(\eta')d\eta' \int_{0+}^{t'} F_1(\tau')d\tau'$$

with

$$F_1(t') = \left(\frac{w}{U}\right)_{0+} F^*(t') + \int_0^{t'} \frac{d}{d\tau'}\left(\frac{w}{U}\right)_{\tau'} F^*(t'-\tau')d\tau',$$

when $(w/U)_{t'}$ is continuous for $t'>0$.

Similarly,

$$Q_1''(t') = \rho \iint_S \gamma_1(m,t')\, \mathbf{n}(m)\, dS(m)$$

with

$$\gamma_1(m,t') = \left(\frac{w}{U}\right)_{t'} \gamma_1^*(m,0+) + \left(\frac{w}{U}\right)_{0+} \delta\gamma_1^*(m,t') + \int_0^{t'} \frac{d}{d\tau'}\left(\frac{w}{U}\right)_{\tau'} \delta\gamma_1^*(m,\, t'-\tau')d\tau'.$$

Hence:

$$\mathcal{F}_1'(t') = -\rho \frac{U}{L}\frac{d}{dt'}\left(\frac{w}{U}\right)_{t'} \iint_S \gamma_1^*(m,0+)\, \mathbf{n}(m)\, dS(m)$$

$$-\rho\, \mathbf{i}_z U \int_{\mathcal{C}_{01}} \Gamma_{01}(\eta')d\eta' \left[\left(\frac{w}{U}\right)_{0+} F^*(t') + \int_0^{t'} \frac{d}{d\tau'}\left(\frac{w}{U}\right)_{\tau'} F^*(t'-\tau')d\tau'\right]$$

$$-\rho \left(\frac{w}{U}\right)_{0+} \frac{U}{L}\frac{\partial}{\partial t'} \iint_S \delta\gamma_1^*(m,t')\, \mathbf{n}(m)\, dS(m)$$

$$-\rho\, \frac{U}{L}\int_0^{t'} \frac{d}{d\tau'}\left(\frac{w}{U}\right)_{\tau'} d\tau' \iint_S \frac{\partial}{\partial t'}\delta\gamma_1^*(m,\, t'-\tau')\, \mathbf{n}(m)\, dS(m)\, .$$

In the case "a_1," when $(w/U)_{t'} = (w/U)_{0+} \neq 0$ for $t'>0$, one has, at $t'>0$, a general resultant

$$\mathfrak{F}_1'^*(t')\left(\frac{w}{U}\right)_{0+} = \left(\frac{w}{U}\right)_{0+}\left\{-\rho\,\mathbf{i}_z U\int_{\mathcal{C}_{01}}\Gamma_{01}(\eta')d\eta' \times \mathbf{F}^*(t')\right.$$

$$\left.-\rho\frac{U}{L}\iint_S \frac{\partial}{\partial t'}\,\delta\gamma_1^*(m,t')\;\mathbf{n}(m)\;dS(m)\right\}.$$

Consequently, in the quasi-steady motion, we have a general resultant:

$$\mathfrak{F}_{01}'(t') = \left(\frac{w}{U}\right)_{t'}\left[-\rho\,\mathbf{i}_z U\int_{\mathcal{C}_{01}}\Gamma_{01}(\eta')d\eta'\right]. \tag{23}$$

The difference between this resultant and the resultant in the real motion is

$$\Delta\mathfrak{F}_1'(t') = \mathfrak{F}_{01}'\left(\frac{w}{U}\right)_{t'} - \mathfrak{F}_1'(t').$$

One has

$$\Delta\mathfrak{F}_1'(t') = -\mathfrak{F}_1'^{(i)}(t') + \Delta'\mathfrak{F}_1'(t')$$

where

$$\mathfrak{F}_1'^{(i)}(t') = -\rho\frac{U}{L}\frac{d}{dt'}\left(\frac{w}{U}\right)_{t'}\iint_S \gamma_1^*(m,0+)\;\mathbf{n}(m)\;dS(m).$$

Moreover:

$$\Delta'\mathfrak{F}_1'(t') = -\rho\,\mathbf{i}_z U\int_{\mathcal{C}_{01}}\Gamma_{01}(\eta')d\eta'\left[\left(\frac{w}{U}\right)_{t'} - \left(\frac{w}{U}\right)_{0+}\mathbf{F}^*(t')\right.$$

$$\left.-\int_0^{t'}\frac{d}{d\tau'}\left(\frac{w}{U}\right)_{\tau'}\mathbf{F}^*(t'-\tau')d\tau'\right]$$

$$+\rho\frac{U}{L}\left[\left(\frac{w}{U}\right)_{0+}\iint_S\frac{\partial}{\partial t'}\,\delta\gamma_1^*(m,t')\;\mathbf{n}(m')\;dS(m)\right.$$

$$\left.+\int_0^{t'}\frac{d}{d\tau'}\left(\frac{w}{U}\right)_{\tau'}d\tau'\iint_S\frac{\partial}{\partial t'}\,\delta\gamma_1^*(m,t'-\tau')\;\mathbf{n}(m)\;dS(m)\right].$$

Let $Z_1'(t')$, $Z_{01}'(w/U)_{t'}$ be the components on the z-axis of the forces above. We put:

$$Z_{01}'\left(\frac{w}{U}\right)_{t'} = -\frac{1}{2}\rho AU^2 a_1\left(\frac{w}{U}\right)_{t'} \tag{24}$$

where A is the projected area of the body on the (x, y)-plane.

The first bracket in the expression of $\Delta'\mathcal{F}_1'(t')$ is

$$\left(\frac{w}{U}\right)_{0+}[1-F^*(t')] + \int_{0+}^{t'} \frac{d}{d\tau'}\left(\frac{w}{U}\right)_{\tau'}[1 - F^*(t'-\tau')]\, d\tau'$$

$$= \left(\frac{w}{U}\right)_{t'}[1 - F^*(0)] + \int_0^{t'} \left(\frac{w}{U}\right)_{\tau'} \frac{\partial}{\partial t'}[1 - F^*(t'-\tau')]\, d\tau' .$$

The second bracket is

$$\left(\frac{w}{U}\right)_{t'} \iint_S \frac{\partial}{\partial t'} \varphi_1^*(m,0)\, \mathbf{n}(m)\, dS(m) + \int_0^{t'} \left(\frac{w}{U}\right)_{\tau'} d\tau' \iint_S \frac{\partial^2}{\partial t'^2} \varphi_1^*(m, t'-\tau')d\tau' .$$

The new expressions hold even when $(w/U)_{t'}$ is not continuous for $t' > 0$.

Hence, putting

$$\zeta(t') = 1 - F^*(t') - \frac{2}{ALUa_1} \iint_S \frac{\partial}{\partial t'} \varphi_1^*(m, t')\, \mathbf{n}(m)\, \mathbf{i}_z dS(m') , \tag{25}$$

we have

$$\Delta Z_1'(t') = Z_{01}'\left(\frac{w}{U}\right)_{t'} - Z_1'(t') = -Z_1'^{(i)}(t') + \Delta' Z_1'(t') , \tag{26}$$

with

$$Z_1'^{(i)}(t') = -\rho \frac{U}{L} \frac{d}{dt'}\left(\frac{w}{U}\right)_{t'} \iint_S \varphi_1^*(m, 0+)\, \mathbf{n}(m)\, \mathbf{i}_z\, dS(m) , \tag{27}$$

and

$$\Delta' Z_1'(t') = -\frac{1}{2}\rho A U^2 a_1 \left\{ \left(\frac{w}{U}\right)_{t'} \zeta(0) + \int_0^{t'} \left(\frac{w}{U}\right)_{\tau'} \frac{\partial}{\partial t'} \zeta(t'-\tau')\, d\tau' \right\} . \tag{28}$$

In the last formula

$$\zeta(0) = 1 - \frac{2}{ALUa_1} \iint_S \frac{\partial}{\partial t'} \varphi_1^*(m,0)\, \mathbf{n}(m)\, \mathbf{i}_z\, dS(m) < 1 ,$$

$$\zeta(+\infty) = 0 . \tag{25'}$$

In the quasi-steady motion, the component on the x-axis of the resultant force is null, but not in the real motion. One has

$$\Delta X_1'(t') = -X_1'^{(i)}(t') + \Delta' X_1'(t') \tag{29}$$

with

$$X_1'^{(i)}(t') = -\rho \frac{U}{L} \frac{d}{dt'} \left(\frac{w}{U}\right)_{t'} \iint_S \gamma_1^*(m, 0+)\, \mathbf{n}(m)\, \mathbf{i}_x\, dS(m)\,, \tag{30}$$

and

$$\Delta' X_1'(t') = -\rho \frac{U}{L} \left[\left(\frac{w}{U}\right)_{0+} \iint_S \frac{\partial}{\partial t'} \delta\gamma_1^*(m, t')\, \mathbf{n}(m)\, \mathbf{i}_x\, dS(m) \right.$$

$$\left. + \int_0^{t'} \frac{d}{d\tau'} \left(\frac{w}{U}\right)_{\tau'} d\tau' \iint_S \frac{\partial}{\partial t'} \delta\gamma_1^*(m, t'-\tau')\, \mathbf{n}(m)\, \mathbf{i}_x(m)\, dS(m) \right].$$

This expression may be written:

$$\Delta' X_1'(t') = \frac{1}{2} \rho A U^2 a_1 \left\{ \left(\frac{w}{U}\right)_{t'} \psi(0) + \int_0^{t'} \left(\frac{w}{U}\right)_{\tau'} \frac{\partial}{\partial t'} \psi(t'-\tau') d\tau' \right\}. \tag{31}$$

with

$$\psi(t') = \frac{2}{ALUa_1} \iint_S \frac{\partial}{\partial t'} \delta\gamma_1^*(m, t')\, \mathbf{n}(m)\, \mathbf{i}_x\, dS(m)\,. \tag{32}$$

The first formula (25') shows that, at $t' = 0+$, the deficiency is, in case "a_1," less than 1.

We have, moreover, components $Z_1'^{(i)}(t')$, $X_1'^{(i)}(t')$ and $-\Delta' Z_1'(t')$, $\Delta' X_1'(t')$.

Although $\gamma_1^*(m, 0+) = 0(1)$, the component $Z_1'^{(i)}(0+)$ is small, because firstly, $\gamma_1^*(m, 0+)$ has significant values only when m is close to $\mathcal{C}_{01}$, and secondly, in this case, $\mathbf{n}(m)$ is nearly normal to $\mathbf{i}_z$. The components $X_1'^{(i)}(t')$ and $-\Delta' X_1'(t')$ are small too, for the first of the previous reasons, and also because the projected area of the body on the (y, z)-plane is small with respect to A.

Now, let us consider the moment of the momentum. It is

$$\mathbf{W}_1(t') = \mathbf{W}_1'(t') + \mathbf{W}_1''(t')\,,$$

with

$$\mathbf{W}_1'(t') = -\rho\, \mathbf{i}_y L \int_{\mathcal{C}_{01}} \Gamma_{01}(\eta')\, d\eta' \int_0^{t'} \xi'(\mu)\, \mathbf{F}_1(\tau')\, d\tau' .$$

$$\mathbf{W}_1''(t') = \rho \iint_S \left[\left(\frac{w}{U}\right)_{t'} \gamma_1^*(m, 0+) + \left(\frac{w}{U}\right)_{0+} \delta\gamma_1^*(m, t') \right.$$

$$\left. + \int_0^{t'} \frac{d}{d\tau'} \left(\frac{w}{U}\right)_{\tau'} \delta\gamma_1^*(m, t'-\tau')\, d\tau' \right] \mathbf{O}'m \wedge \mathbf{n}(m)\, dS(m) .$$

The resulting moment is

$$\mathbf{I}_1'(t') = \mathbf{i}_y \mathfrak{M}_1'(t') = -\frac{U}{L} \frac{d}{dt'} \left[\mathbf{W}_1'(t') + \mathbf{W}_1''(t') \right] .$$

Because $\xi'(\mu)$ is independent of t', we have

$$\mathfrak{M}_1'(t') = \rho U \int_{\mathcal{C}_{01}} \Gamma_{01}(\eta') \times \mathbf{x}(\eta') \times d\eta' \left[\left(\frac{w}{U}\right)_{0+} \mathbf{F}^*(t') + \int_{0+}^{t'} \frac{d}{d\tau'} \left(\frac{w}{U}\right)_{\tau'} \mathbf{F}^*(t'-\tau')\, d\tau' \right]$$

$$-\rho \frac{U}{L} \frac{d}{dt'} \left(\frac{w}{U}\right)_{t'} \iint_S \gamma_1^*(m, 0+) \left[z(m)\, \mathbf{n}(m) \mathbf{i}_x - x(m)\, \mathbf{n}(m) \mathbf{i}_z \right] dS(m)$$

$$-\rho \frac{U}{L} \left(\frac{w}{U}\right)_{0+} \iint_S \frac{\partial}{\partial t'} \delta\gamma_1^*(m, t') \left[z(m)\, \mathbf{n}(m) \mathbf{i}_x - x(m)\, \mathbf{n}(m) \mathbf{i}_z \right] dS(m)$$

$$-\rho \frac{U}{L} \int_{0+}^{t'} \frac{d}{d\tau'} \left(\frac{w}{U}\right)_{\tau'} d\tau' \iint_S \frac{\partial}{\partial t'} \delta\gamma_1^*(m, t'-\tau') \left[z(m)\, \mathbf{n}(m) \mathbf{i}_x - x(m)\, \mathbf{n}(m) \mathbf{i}_z \right] dS(m)$$

$$+\rho U \iint_S \left[\left(\frac{w}{U}\right)_{t'} \gamma_1^*(m, 0+) + \left(\frac{w}{U}\right)_{0+} \delta\gamma_1^*(m, t') \right.$$

$$\left. + \int_0^{t'} \frac{d}{d\tau'} \left(\frac{w}{U}\right)_{\tau'} \delta\gamma_1^*(m, t'-\tau')\, d\tau' \right] \mathbf{i}_z \mathbf{n}(m)\, dS(m) .$$

It is assumed here that the moving axis coincide at time t' with the fixed axis, and the moment is referred about the latter. The last term comes from the derivative

$$\frac{d}{dt}\, \mathbf{a}'\mathbf{m} \wedge \mathbf{n}(m) .$$

In the quasi-steady motion, the moment is

$$\mathfrak{M}_{01}\left(\frac{w}{U}\right)_{t'} = \left\{\rho U \int_{\mathcal{L}_{01}} \Gamma_{01}(\eta') \cdot \mathbf{x}(\eta') \times d\eta' \right.$$

$$\left. + \rho U \iint_S \left[\gamma_1^*(m, 0+) + \delta\gamma_1^*(m, +\infty)\right] \mathbf{i}_z\, \mathbf{n}(m)\, dS(m)\right\} \left(\frac{w}{U}\right)_{t'} . \tag{33}$$

The difference between the two moments is

$$\Delta\mathfrak{M}_1'(t') = \mathfrak{M}_{01}\left(\frac{w}{U}\right)_{t'} - \mathfrak{M}_1'^{(i)}(t') + \Delta'\mathfrak{M}_1'(t') \tag{34}$$

with

$$\mathfrak{M}_1'^{(i)}(t') = -\rho \frac{U}{L} \frac{d}{dt'} \left(\frac{w}{U}\right)_{t'} \iint_S \gamma_1^*(m, 0+) \left[z(m)\, \mathbf{n}(m)\, \mathbf{i}_z - x(m)\, \mathbf{n}(m)\, \mathbf{i}_z\right] dS(m) . \tag{35}$$

In order to get $\Delta'\mathfrak{M}_1'(t')$, we will reason as above.

The contributions of the first terms in $\mathfrak{M}_1'(t')$ and in $\mathfrak{M}_{01}(w/U)_{t'}$ lead to

$$\rho U \int_{\mathcal{L}_{01}} \Gamma_{01}(\eta') \times \mathbf{x}(\eta') \times d\eta' \left\{\left(\frac{w}{U}\right)_{0+} [1 - F^*(t')] + \int_{0+}^{t'} \frac{d}{d\tau'} \left(\frac{w}{U}\right)_{\tau'} [1 - F^*(t' - \tau')]\, d\tau'\right\} .$$

The second term in $\mathfrak{M}_{01}(w/U)_{t'}$, and the last term in $\mathfrak{M}_1'(t')$ give:

$$\rho U \iint_S \left\{\left(\frac{w}{U}\right)_{0+} \left[\delta\gamma_1^*(m, +\infty) - \delta\gamma_1^*(m, t')\right]\right.$$

$$\left. + \int_{0+}^{t'} \frac{d}{d\tau'} \left(\frac{w}{U}\right)_{\tau'} \left[\delta\gamma_1^*(m, +\infty) - \delta\gamma_1^*(m, t' - \tau')\right] d\tau'\right\} \mathbf{i}_z\, \mathbf{n}(m)\, dS(m) .$$

Lastly, the terms in the 3rd and 4th lines in the expression of $\mathfrak{M}_1'(t')$ give the contribution:

$$\rho \frac{U}{L} \iint_S \left\{\left(\frac{w}{U}\right)_{0+} \frac{\partial}{\partial t'} \delta\gamma_1^*(m, t') + \int_0^{t'} \frac{d}{d\tau'} \left(\frac{w}{U}\right)_{\tau'} \left[\frac{\partial}{\partial t'} \delta\gamma_1^*(m, t' - \tau')\right] d\tau'\right\}$$

$$\times \left\{z(m)\, \mathbf{n}(m)\, \mathbf{i}_x - x(m)\, \mathbf{n}(m)\, \mathbf{i}_z\right\} dS(m) .$$

Integrating by parts, we obtain

$$\Delta'\mathfrak{M}_1'(t') = \rho U \int_{\mathcal{C}_{01}} \Gamma_{01}(\eta')\ x(\eta') d\eta' \left\{ \left(\frac{w}{U}\right)_{t'} [1 - F^*(0)] + \int_0^{t'} \left(\frac{w}{U}\right)_{\tau'} \frac{\partial}{\partial t'} [1 - F^*(t' - \tau')]\, d\tau' \right\}$$

$$+ \rho U \iint_S \mathbf{n}(m)\mathbf{i}_z\ dS(m) \left\{ \left(\frac{w}{U}\right)_{t'} [\delta\gamma_1^*(m, +\infty) - \delta\gamma_1^*(m, 0)] + \int_0^{t'} \left(\frac{w}{U}\right)_{\tau'} \frac{\partial}{\partial t'} [\delta\gamma_1^*(m, +\infty) - \delta\gamma_1^*(m, t' - \tau')]\, d\tau' \right\}$$

$$+ \rho \frac{U}{L} \iint_S [z(m)\ \mathbf{n}(m)\mathbf{i}_x - x(m)\ \mathbf{n}(m)\mathbf{i}_z] S(m) \left\{ \left(\frac{w}{U}\right)_{t'} \frac{\delta}{\delta t'} \delta\gamma_1^*(m, 0) + \int_0^{t'} \left(\frac{w}{U}\right)_{\tau'} \frac{\partial^2}{\partial t'^2} \delta\gamma_1^*(m, t' - \tau')\, d\tau' \right\}.$$

Let

$$\mathfrak{M}_{01} \left(\frac{w}{U}\right)_{t'} = \frac{1}{2} \rho A L U^2 a_1' \left(\frac{w}{U}\right)_{t'} \tag{36}$$

be the moment in the quasi-steady motion. We have

$$a_1' = \frac{2}{ALU} \left\{ \int_{\mathcal{C}_{01}} \Gamma_{01}(\eta')\ x(\eta') d\eta' + \iint_S [\gamma_1^*(m, 0+) + \delta\gamma_1^*(m, +\infty)]\ \mathbf{i}_z \mathbf{n}(m)\ dS(m) \right\}. \tag{37}$$

Then, putting

$$\alpha'(t') = \frac{2}{ALUa_1'} \left\{ \int_{\mathcal{C}_{01}} \Gamma_{01}(\eta')\ x(\eta') d\eta' [1 - F^*(t')] + \iint_S [\delta\gamma_1^*(m, +\infty) - \delta\gamma_1^*(m, t')]\ \mathbf{n}(m)\ \mathbf{i}_z\ dS(m) + \iint_S \frac{\partial}{\partial t'} \delta\gamma_1^*(m, t')\ [z(m)\ \mathbf{n}(m)\mathbf{i}_x - x(m)\ \mathbf{n}(m)\mathbf{i}_z]\ dS(m) \right\}. \tag{38}$$

we have

$$\left.\begin{aligned}\phi'(0) &= \frac{2}{ALUa_1'}\left\{\int_{a_{01}} \Gamma_{01}(\eta')\, x(\eta')d\eta' + \iint_S \delta\gamma_1^*(m,+\alpha)\ \mathbf{n}(m)\mathbf{i}_z\ dS(m)\right. \\ &\left. + \iint_S \frac{\partial}{\partial t'}\gamma_1^*(m,0)\ \left[z(m)\ \mathbf{n}(m)\mathbf{i}_x - x(m)\ \mathbf{n}(m)\mathbf{i}_z\right] dS(m)\right\}, \\ \phi'(+\infty) &= 0,\end{aligned}\right\} \quad (38')$$

and

$$\Delta'\mathfrak{M}_1'(t') = \frac{1}{2}\rho ALU^2 a_1'\left[\left(\frac{w}{U}\right)_{t'}\phi'(0) + \int_0^{t'}\left(\frac{w}{U}\right)_{\tau'}\frac{\partial}{\partial t'}\phi'(t'-\tau')d\tau'\right] \quad (39)$$

This last formulae holds even when $(w/U)_{t'}$ is discontinuous for $t'>0$.

The expression of the deficiency $\Delta'\mathfrak{M}_1'(t')$ and the expression of $\mathfrak{M}_1'^{(i)}(t')$ could be subject to comments similar to those made above about $\Delta'Z_1'(t')$, $\Delta'X_1'(t')$ and $Z_1'^{(i)}(t')$, $X_1'^{(i)}(t')$.

In the following paragraphs, the effects of $Z_1'^{(i)}(t')$, $X_1'^{(i)}(t')$ and $\mathfrak{M}_1''^{(i)}(t')$ will be included in the contributions of the accelerations in the set of forces due to the pressure p_i.

In the first draft of this paper, we gave an affirmative answer to the following question: is the deficiency $\Delta'\mathcal{F}_1'$ fixed with respect to the body? But in fact the proof given was not valid.

In the case of an airfoil of infinite aspect ratio, it is possible to show starting either from the momentum of the fluid Q or from the pressure $p'(m_e, t')$, that the deficiency of the lift and its moment are actually proportional to one another, the ratio being independent of the time.* We think that it is true also in the present case. But the proof would require a finer analysis that the one given above, although the latter is sufficient in order to yield the structure of the main formulae.

In return, however, we have, in cases "b_0" and "b_2,"

$$\gamma_0^*(m,t') = \mathcal{G}\{\Gamma_{00}(\eta')\ F^*(t')|m\}, \quad \gamma_2^*(m,t') = \mathcal{G}\{\Gamma_{02}(\eta')\ F^*(t')|m\}, \quad (40)$$

$\mathcal{G}$ being the linear and homogeneous functional defined by

$$\gamma_1^*(m,t') = \mathcal{G}\{\Gamma_{01}(\eta')\ F^*(t')|m\}.$$

For this reason, it seems that the three functions ϕ, ψ, ϕ' introduced here are suitable also in the cases "b_0" and "b_2" as in the case "b_1." We will admit this fact, at least for the sake of simplifying the writing. For instance, we will have:

*See, respectively, (2) and (8).

$$\left.\begin{aligned} Z_0'(t') &= -\frac{1}{2}\,\rho AU^2 a_0 \left\{\left(\frac{u}{U}\right)_{t'}\,\phi(0) + \int_0^{t'} \left(\frac{u}{U}\right)_{\tau'} \frac{\partial}{\partial t'}\,\phi(t'-\tau')d\tau'\right\}, \\ Z_2'(t') &= -\frac{1}{2}\,\rho AU^2 a_2 \left\{\left(\frac{Lq}{U}\right)_{t'}\,\phi(0) + \int_0^{t'} \left(\frac{Lq}{U}\right)_{\tau'} \frac{\partial}{\partial t'}\,\phi(t'-\tau')d\tau'\right\}, \end{aligned}\right\} \quad (41)$$

and so on.

In par. 8, the notations used here will be slightly modified. We will use a, a' instead of a_1, a_1' and b, b' instead of a_2, a_2'.

5.4. Set of Hydrodynamic Forces Due to p_i and $p'^{(i)}$

When the body is symmetrical with respect to the (z, x)-plane, the kinetic energy of the fluid in the absolute motion due to the potential

$$\Phi_{00} + \Phi_{00}\left(\frac{u}{U}\right)_{t'} + \Phi_{01}\left(\frac{w}{U}\right)_{t'} + \Phi_{02}\left(\frac{Lq}{U}\right)_{t'} + \Phi_{03}\left(\frac{v}{U}\right)_{t'} + \Phi_{04}\left(\frac{Lr}{U}\right)_{t'} + \Phi_{05}\left(\frac{Lp}{U}\right)_{t'}$$

is

$$\begin{aligned} 2T = \rho W\{&\mu_1(U+u)^2 + \mu_2 v^2 + \mu_3 w^2 + 2\mu_{13}(U+u)w \\ &- 2L\,[\nu_{35}wq + \nu_{15}(U+u)q + \nu_{24}vp + \nu_{26}vr] \\ &+ L^2\,[\lambda_1 p^2 + \lambda_2 q^2 + \lambda_3 r^2 - 2\lambda_{13}pr]\}\,, \end{aligned}$$

where W is the volume of the body.

The components of the set of forces X_i, Y_i, Z_i, $\mathfrak{L}_i$, $\mathfrak{M}_i$, $\mathfrak{N}_i$ are given by the Lagrangian expressions:

$$X_i = -\frac{d}{dt}\,\frac{\partial T}{\partial(U+u)} - \left(q\,\frac{\partial T}{\partial w} - r\,\frac{\partial T}{\partial v}\right), \;\ldots\ldots\;\ldots\ldots$$

$$\mathfrak{L}_i = -\frac{d}{dt}\,\frac{\partial T}{\partial p} - \left(v\,\frac{\partial T}{\partial w} - w\,\frac{\partial T}{\partial v}\right) - \left(q\,\frac{\partial T}{\partial r} - r\,\frac{\partial T}{\partial q}\right), \;\ldots\ldots\;\ldots$$

Writing before the accelerations $\mu_1', \ldots$ for $\mu_1, \ldots$, in order to take into account the forces due to the pressures $p'^{(i)}$, and assuming that u/U, w/U, Lq/U are of negligible squares and products, we get, in the case of a motion parallel to the (z, x)-plane: (with

$$Z_i' = \sum_{k=0}^{2} Z_k'^{(i)}\,,$$

and so on):

$$\left.\begin{aligned}
Z_i + Z_i' &= \frac{1}{2}\rho A U^2 \frac{2W}{AL}\left\{\mu_1 \frac{Lq}{U} - \mu_3' \frac{L\dot{w}}{U^2} - \mu_{13}' \frac{L\dot{u}}{U^2} + \nu_{35}' \frac{L^2\dot{q}}{U^2}\right\}, \\
X_i + X_i' &= \frac{1}{2}\rho A U^2 \frac{2W}{AL}\left\{-\mu_{13} \frac{Lq}{U} - \mu_{13}' \frac{L\dot{w}}{U^2} - \mu_{13}' \frac{L\dot{u}}{U^2} + \nu_{15}' \frac{L^2\dot{q}}{U^2}\right\}, \\
\mathfrak{M}_i + \mathfrak{M}_i' &= \frac{1}{2}\rho A L U^2 \frac{2W}{AL}\left\{\mu_{13} + 2\mu_{13} \frac{u}{U} + (\mu_3 - \mu_1) \frac{w}{U} + \nu_{35}' \frac{L\dot{w}}{U^2} + \nu_{15}' \frac{L\dot{u}}{U^2} - \lambda^2 \frac{L^2\dot{q}}{U^2}\right\}.
\end{aligned}\right\} \quad (42)$$

As is well known, the force is null in a steady motion, when $Lq/U = 0$, but not the moment if the body is not symmetrical with respect to the (x, y)-plane $(\mu_{13} \neq 0)$. When $q \neq 0$, the force and the moment are not null, even when the motion is steady.

6. Sets of Fo[illegible]es on the Diving Planes and Fins, Effect of the Wake

The diving planes and fins contribute to the forces $\mathcal{F}_i$ (par. 5.4) and $\mathcal{F}_c$ (par. 7). We assume here that the expressions of these forces take into account the effect of the diving planes and fins.

But we have yet to introduce the effects of the lift, moment and drag due to the diving planes and fins. We neglect here the history of their motion because the length of their chord is small with respect to the length of the body itself.

Let $L\xi_B, 0, L\zeta_B$ the coordinates of the axis O_B of a diving plane B, $L\eta_B$ the ordinate of the center of the lifting surface, and σ_B its area. In η_B and σ_B, the fin associated with the plane is assumed to be included.

When the motion is steady and parallel to the x-axis $(w = 0,\ q = 0)$, the wake may induce on the plane a velocity which component on the z-axis is $w_{0B} = a_{0B}U$. The components of the relative incident velocity are

$$-U,\ 0,\ a_{0B}U .$$

Let β be the angle of the plane. $\beta = 0$ when the lift due to the previous incident velocity is null; $\beta > 0$, when the lift generated by the plane has a negative component on the z-axis.

In the most general quasi-steady motion, the relative incident velocity is

$$-U\left[1 + \left(\frac{u}{U}\right)_{t'} + \left(\frac{Lq}{U}\right)_{t'} \zeta_B\right],\ 0,$$

$$-U\left[\left(\frac{w}{U}\right)_{t'} - \left(\frac{Lq}{U}\right)_{t'} \xi_B - a_{0B} - a_{0B}\left(\frac{u}{U}\right)_{t'} - a_{1B}\left(\frac{w}{U}\right)_{t'} - a_{2B}\left(\frac{Lq}{U}\right)_{t'}\right].$$

The four last terms in the z-component are due to the velocities induced by the wake on the plane; a_{1B} and a_{2B} are positive dimensionless coefficients. Consequently, in such a quasi-steady motion; the effective angle of attack is

$$\beta_e = \beta + \left(\frac{w}{U}\right)_{t'} - \left(\frac{Lq}{U}\right)_{t'} \xi_B - a_{0B}\left(\frac{u}{U}\right)_{t'} - a_{1B}\left(\frac{w}{U}\right)_{t'} - a_{2B}\left(\frac{Lq}{U}\right)_{t'} .$$

Let us assume that we are in the case "a_1":

$$\left(\frac{u}{U}\right)_{t'} = 0 , \quad \left(\frac{Lq}{U}\right)_{t'} = 0 \text{ for } -\infty < t' < +\infty ;$$

$$\left(\frac{w}{U}\right)_{t'} = 0 \text{ for } t' < 0, \quad = \left(\frac{w}{U}\right)_{0+} \neq 0 \text{ for } t' > 0.$$

At $t' = 0+$, the velocity induced by the wake is null; at $t' = +\infty$, it is $a_{1B}(w/U)_{0+}$. At $t' > 0$, it is

$$a_{1B}\left(\frac{w}{U}\right)_{0+} \phi_{1B}(t') ,$$

where ϕ_{1B} is an increasing function equal to zero at $t' = 0+$, and to 1 at $t' = +\infty$. In the general case, when $(w/U)_{t'}$ is a given function $f_{01}(t')$, the velocity induced by the wake generated by $f_{01}(t')$ is

$$\left(\frac{w}{U}\right)_{0+} \phi_{1B}(t') + \int_{0+}^{t'} \frac{d}{d\tau'}\left(\frac{w}{U}\right)_{\tau'} \phi_{1B}(t'-\tau')d\tau' = \int_0^{t'} f_{01}(\tau') \frac{\partial}{\partial t'} \phi_{1B}(t'-\tau')d\tau'$$

$$= \int_0^{t'} f_{01}(\tau') \dot{\phi}_{1B}(t'-\tau')d\tau' .$$

Finally, when

$$\left(\frac{u}{U}\right)_{t'} = f_{00}(t') , \quad \left(\frac{w}{U}\right)_{t'} = f_{01}(t') , \quad \left(\frac{Lq}{U}\right)_{t'} = f_{02}(t') ,$$

the effective angle of attack becomes

$$\beta_e' = \beta + \left(\frac{w}{U}\right)_{t'} - \left(\frac{Lq}{U}\right)_{t'} \xi_B - \int_0^{t'} \sum_{k=0}^{2} a_{kB}\, f_{0k}(\tau') \times \dot{\phi}_{kB}(t'-\tau')d\tau' . \qquad (1)$$

The square of the incident velocity is

$$U^2\left\{1 + 2\left(\frac{u}{U}\right)_{t'} + 2\left(\frac{Lq}{U}\right)_{t'} \zeta_B\right\} . \qquad (2)$$

Let c_{x_B}, c_{L_B} and c_{m_B} be the characteristic coefficients of the plane fitted to the body.

The absolute set of forces due to the plane, referred to the axis attached to the body, is

$$X_B = -\frac{1}{2}\,\rho S_B U^2 \left\{1 + 2\left(\frac{u}{U}\right)_{t'} + 2\left(\frac{Lq}{U}\right)_{t'} \xi_B\right\} c_{x_B}(1 + \ldots)\,.$$

$$Y_B = 0\,,$$

$$Z_B = -\frac{1}{2}\,\rho S_B U^2 \left\{1 + 2\left(\frac{u}{U}\right)_{t'} + 2\left(\frac{Lq}{U}\right)_{t'} \xi_B\right\} c_{L_B}\,\alpha_e\,.$$

$$\mathfrak{L}_B = \frac{1}{2}\,\rho S_B L U^2 \left\{1 + 2\left(\frac{u}{U}\right)_{t'} + 2\left(\frac{Lq}{U}\right)_{t'} \xi_B\right\} \left[-\eta_B c_{L_B}\,\alpha_e\right]\,,$$

$$\mathfrak{M}_B = \frac{1}{2}\,\rho S_B L U^2 \left\{1 + 2\left(\frac{u}{U}\right)_{t'} + 2\left(\frac{Lq}{U}\right)_{t'} \xi_B\right\} \left[-\zeta_B c_{x_B} + \left(\xi_B c_{L_B} - c_{m_B}\right)\alpha_e\right],$$

$$\mathfrak{N}_B = \frac{1}{2}\,\rho S_B L U^2 \left\{1 + 2\left(\frac{u}{U}\right)_{t'} + 2\left(\frac{Lq}{U}\right)_{t'} \xi_B\right\} \left[\eta_B c_{x_B}\right].$$

But a set of diving plane is generally made of two parts, symmetrical with respect to the (z, x)-plane. Consequently, $\mathfrak{L}_B$ and $\mathfrak{N}_B$ are null. The non-null components of the set of forces are

$$\left.\begin{aligned}
X_B &= -\frac{1}{2}\,\rho S_B U^2 c_{x_B}\left[1 + 2\left(\frac{u}{U}\right)_{t'} + 2\left(\frac{Lq}{U}\right)_{t'} \xi_B\right],\\
Z_B &= -\frac{1}{2}\,\rho S_B U^2 c_{L_B}\left\{\beta\left[1 + 2\left(\frac{u}{U}\right)_{t'} + 2\left(\frac{Lq}{U}\right)_{t'} \xi_B\right]\right.\\
&\qquad \left. + \left[\left(\frac{w}{U}\right)_{t'} - \left(\frac{Lq}{U}\right)_{t'} \xi_B\right] - \sum_{k=0}^{2} a_{0k}\, f_{0k}(t')\right\} - \Delta Z_B\,.\\
\mathfrak{M}_B &= \frac{1}{2}\,\rho S_B L U^2 \left\{\left[-\zeta_B c_{x_B} + \left(\xi_B c_{L_B} - c_{m_B}\right)\beta\right]\left[1 + 2\left(\frac{u}{U}\right)_{t'} + 2\left(\frac{Lq}{U}\right)_{t'} \xi_B\right]\right.\\
&\qquad + \left[\xi_B c_{L_B} - c_{m_B}\right]\left[\left(\frac{w}{U}\right)_{t'} - \left(\frac{Lq}{U}\right)_{t'} \xi_B\right]\\
&\qquad \left. - \left[\xi_B c_{L_B} - c_{m_B}\right]\left[\sum_{k=0}^{2} a_{0k}\, f_{0k}(t')\right]\right\} - \Delta\mathfrak{M}_B\,.
\end{aligned}\right\} \quad (3)$$

with

$$\left.\begin{aligned}
\Delta Z_B &= \frac{1}{2}\rho\sigma_B U^2 c_{L_B}\left[\sum_{k=0}^{2} a_{0k}\left\{f_{0k}(t') - \int_0^{t'} f_{0l}(\tau')\,\dot{\phi}_{kB}(t'-\tau')\,d\tau'\right\}\right],\\
\Delta\mathfrak{M}_B &= -\frac{1}{2}\rho\sigma_B LU^2\,(\xi_B c_{L_B} - c_{m_B})\\
&\quad\times\left[\sum_{k=0}^{2} a_{0k}\left\{f_{0k}(t') - \int_0^{t'} f_{0k}(\tau')\,\dot{\phi}_{kB}(t'-\tau')\,d\tau'\right\}\right].
\end{aligned}\right\}\quad (4)$$

Obviously, the delayed circulation around the body gives $-\Delta Z_1^{\bullet}(0+) < 0$, $-\Delta Z_{2B}^{\bullet}(0+) < 0$, $-\Delta\mathfrak{M}_{1B}^{\bullet}(0+) < 0$, $-\Delta\mathfrak{M}_{2B}(0+) < 0$, and leads to an increase of the efficiency of the plane. Because c_{L_B} is great with respect to a_1 (see par. 5), the effect of a diving plane located near the stern of the body may be very important and shall not be neglected.

7. Other Sets of Forces Exerted on the Body (case of Par. 4)

The constituents of the total set of forces were encountered at the beginning of par. 5. In par. 5 and 6, we studied the forces due to the velocity potential of the absolute motion. Let us now consider the other constituents.

7.1. Forces Due to Gravity

Let $L\xi_B, 0, L\zeta_B$ be the coordinates of the center of gravity of the body, $L\xi_c, 0, L\zeta_c$ those of the center of the volume, μ the density of the body with respect to the fluid.

We assume that the square of the angle of trim θ is negligible.

The components on the axis attached to the body of the forces and moment due to gravity are

$$\left.\begin{aligned}
&X_g = -\rho g\,W(\mu-1)\,\theta\,, \quad Y_g = 0\,, \quad Z_g = \rho g\,W(\mu-1)\,,\\
&\mathfrak{L}_c = 0\,, \quad \mathfrak{M}_c = \rho g\,WL\left[-(\mu\zeta_G - \zeta_c)\theta + (\mu\xi_G - \xi_c)\right], \quad \mathfrak{N}_c = 0\,.
\end{aligned}\right\}\quad (1)$$

7.2. Forces of Inertia for the Body

Let $\rho WL^2\mu\chi_1$, $\rho WL^2\mu\chi_2$, $\rho WL^2\mu\chi_3$ be the moments of inertia of the body with respect to axis acting through G and parallel to the axis $O(x,y,z)$. Let $\rho WL^2\mu\chi_{13}$ be the rectangular moment of inertia due to the product zx.

Assuming that u/U, v/U, w/L, Lp/U, Lq/U, Lr/U have negligible squares and products and the same for ξ_G, ζ_G, the general expression of the set of forces of inertia is:

$$
\left.
\begin{aligned}
X_c &= \frac{1}{2}\rho AU^2 \frac{2W}{AL}\mu \left[-\frac{L\dot{u}}{U^2} - \frac{L^2\dot{q}}{U^2}\zeta_G + \frac{L^2\dot{r}}{U^2}\xi_G\right], \\
Y_c &= \frac{1}{2}\rho AU^2 \frac{2W}{AL}\mu \left[-\frac{Lr}{U} - \frac{L\dot{v}}{U^2} - \frac{L^2\dot{r}}{U^2}\xi_G + \frac{L^2\dot{p}}{U^2}\zeta_G\right], \\
Z_c &= \frac{1}{2}\rho AU^2 \frac{2W}{AL}\mu \left[\frac{Lq}{U} - \frac{L\dot{w}}{U^2} + \frac{L^2\dot{q}}{U^2}\xi_G\right], \\
\mathfrak{L}_c &= \frac{1}{2}\rho ALU^2 \frac{2W}{AL}\mu \left[\frac{Lr}{U}\zeta_G + \frac{L\dot{v}}{U^2}\zeta_G - \chi_1\frac{L^2\dot{p}}{U^2} + \chi_{13}\frac{L^2\dot{r}}{U^2}\right], \\
\mathfrak{M}_c &= \frac{1}{2}\rho ALU^2 \frac{2W}{AL}\mu \left[-\frac{L\dot{u}}{U^2}\zeta_G + \frac{L\dot{w}}{U^2}\xi_G - \chi_2\frac{L^2\dot{q}}{U^2}\right], \\
\mathfrak{N}_c &= \frac{1}{2}\rho ALU^2 \frac{2W}{AL}\mu \left[-\frac{Lp}{U}\zeta_G - \frac{L\dot{v}}{U^2}\xi_G - \chi_3\frac{L^2\dot{r}}{U^2} + \chi_{13}\frac{L^2\dot{p}}{U^2}\right].
\end{aligned}
\right\} \quad (2)
$$

In the present case, the motion is parallel to the (z, x)-plane. Then, taking into account the formulae (42), par. 5.4, we have:

$$
\left.
\begin{aligned}
Z_c + Z_i &= \frac{1}{2}\rho AU^2 \frac{2W}{AL}\left[(\mu+\mu_1)\frac{Lq}{U} - (\mu+\mu_3')\frac{L\dot{w}}{U^2} - \mu_{13}'\frac{L\dot{u}}{U^2} + (\nu_{35}'+\mu\xi_G)\frac{L^2\dot{q}}{U^2}\right], \\
X_c + X_i &= \frac{1}{2}\rho AU^2 \frac{2W}{AL}\left[-\mu_{13}\frac{Lq}{U} - \mu_{13}'\frac{L\dot{w}}{U^2} - (\mu+\mu_1')\frac{L\dot{u}}{U^2} + (\nu_{15}'-\mu\zeta_G)\frac{L^2\dot{q}}{U^2}\right], \\
\mathfrak{M}_c + \mathfrak{M}_i &= \frac{1}{2}\rho ALU^2 \frac{2W}{AL}\left[\mu_{13} + 2\mu_{13}\frac{u}{U} + (\mu_3-\mu_1)\frac{w}{U} + (\nu_{35}'+\mu\xi_G)\frac{L\dot{w}}{U^2}\right. \\
&\qquad \left. + (\nu_{15}'-\mu\xi_G)\frac{L\dot{u}}{U^2} - (\lambda_2'+\mu\chi_2)\frac{L^2\dot{q}}{U^2}\right].
\end{aligned}
\right\} \quad (3)
$$

7.3. Viscous Drag and Propeller

We assume, for simplification, that the viscous drag may be expressed by a c_x and a c_m-coefficient. On the other hand, we assume that the thrust of the propeller is T, the suction coefficient t, we neglect the torque due to the propeller.

Finally, when the motion is parallel to the (z, x)-plane, we have a set of forces

$$\left.\begin{array}{ll} \text{on } Oz: & \left\{ \frac{1}{2} \, A U^2 \left[\left(C_x + \sum \frac{B}{A} c_{x_B}\right) \cdot (1 - t)\right] \right\} \cdot \left(\frac{T}{\frac{1}{2} \, A U^2} \right) \\ \text{on } Ox: & - \frac{1}{2} \, A U^2 \left[\left(C_x + \sum \frac{B}{A} c_{x_B}\right) \cdot (1 - t)\right] \end{array}\right\} \quad (4a)$$

The moment about the y-axis is

$$- \frac{1}{2} \, A L U^2 \left[\left(C_m + \sum \frac{B}{A} c_{x_B} \, B\right) + \cdots \right] . \qquad (4b)$$

In these formulae, symbol $\sum$ indicates that we may have to deal with several sets of planes.

8. Final Formulae (case of par. 4: quasi-rectilinear motion parallel to the (z, x)-plane)

Nature of the Forces	$Z/\left(\frac{1}{2} AU^2\right)$	$X/\left(\frac{1}{2} AU^2\right)$	$\mathfrak{M}/\left(\frac{1}{2} ALU^2\right)$
	Quasi Steady Motion - Classical Forces of Inertia		
Gravity	$\frac{2W}{AL} \frac{gL}{U^2}$ [illegible]	$\frac{2W}{AL} \frac{gL}{U^2}$ [illegible]	$\frac{2W}{AL} \frac{gL}{U^2}$ [illegible]
Propeller friction (diving planes included)	$\left[C_x + \sum \frac{B}{A} c_{x_B} \cdot (1 - t)\right]$	$\left[C_x + \sum \frac{B}{A} c_{x_B} \cdot (1 - t)\right]$	$\left[C_m + \sum \frac{B}{A} c_{x_B} B\right]$
$\mathfrak{F}_c + \mathfrak{F}_i + \mathfrak{F}$ (diving planes included)	$\frac{2W}{AL} \left[\cdots \left(\frac{Lq}{U}\right)_t \cdots \left(\frac{L\dot{w}}{U^2}\right)_t \cdots \left(\frac{L\dot{u}}{U^2}\right)_t \cdots G \left(\frac{L^2\dot{q}}{U^2}\right)_t \right]$	$\frac{2W}{AL} \left\{ \cdots \frac{Lq}{U} \cdots \frac{L\dot{w}}{U^2} \cdots \frac{L\dot{u}}{U^2} \cdots G \frac{L^2\dot{q}}{U^2} \right\}$	$\frac{2W}{AL} \left\{ \cdots 2 \cdots \left(\frac{u}{U}\right)_t \cdots \left(\frac{w}{U}\right)_t \cdots G \left(\frac{L\dot{w}}{U^2}\right)_t \cdots G \left(\frac{L\dot{u}}{U^2}\right)_t \cdots X_2 \left(\frac{L^2\dot{q}}{U^2}\right)_t \right\}$
Circulation around the body (diving planes included)	$a_0 \left(\frac{u}{U}\right)_t \cdots a \left(\frac{w}{U}\right)_t \cdots b \left(\frac{Lq}{U}\right)_t$	0	$a_0 \left(\frac{u}{U}\right)_t \cdots a \left(\frac{w}{U}\right)_t \cdots b \left(\frac{Lq}{U}\right)_t$
Diving planes (effect of the wake generated by the body not included)	$\sum \frac{B}{A} c_{L_B} \left\{ \left[1 + 2 \left(\frac{u}{U}\right)_t + 2 \left(\frac{Lq}{U}\right)_t \cdots B\right] + \left[\left(\frac{w}{U}\right)_t \cdots \left(\frac{Lq}{U}\right)_t \cdots B\right] \right\}$	0	$\sum \frac{B}{A} \left(B c_{L_B} \cdots c_{m_B} \right) \left\{ \left[1 + 2 \left(\frac{u}{U}\right)_t + 2 \left(\frac{Lq}{U}\right)_t \cdots B\right] + \left[\left(\frac{w}{U}\right)_t \cdots \left(\frac{Lq}{U}\right)_t \cdots B\right] \right\}$
Diving planes (effect of the wake due to the body)	$\sum \frac{B}{A} c_{L_B} \left[a_{0B} \left(\frac{u}{U}\right)_t + a_{1B} \left(\frac{w}{U}\right)_t + a_{2B} \left(\frac{Lq}{U}\right)_t\right]$	0	$\sum \frac{B}{A} \left(B c_{L_B} \cdots c_{m_B} \right) \left[a_{0B} \left(\frac{u}{U}\right)_t + a_{1B} \left(\frac{w}{U}\right)_t + a_{2B} \left(\frac{Lq}{U}\right)_t\right]$

(Continued)

Nature of the Forces	$Z/\left(\frac{1}{2}\rho A U^2\right)$	$X/\left(\frac{1}{2}\rho A U^2\right)$	$M/\left(\frac{1}{2}\rho A L U^2\right)$
		Effect of the Delayed Circulation	
Circulation around the body	$a_0\left[\left(\frac{u}{U}\right)_t \zeta(0) + \int_0^{t'} \left(\frac{u}{U}\right)_{\tau} \zeta(t'-\tau)\,d\tau\right]$	$a_0\left[\left(\frac{u}{U}\right)_t \zeta(0) + \int_0^{t'} \left(\frac{u}{U}\right)_{\tau} \zeta(t'-\tau)\,d\tau\right]$	$a_0\left[\left(\frac{u}{U}\right)_t \zeta(0) + \int_0^{t'} \left(\frac{u}{U}\right)_{\tau} \zeta(t'-\tau)\,d\tau\right]$
	$+a\left[\left(\frac{w}{U}\right)_t \zeta(0) + \int_0^{t'} \left(\frac{w}{U}\right)_{\tau} \zeta(t'-\tau)\,d\tau\right]$	$a\left[\left(\frac{w}{U}\right)_t \zeta(0) + \int_0^{t'} \left(\frac{w}{U}\right)_{\tau} \zeta(t'-\tau)\,d\tau\right]$	$a\left[\left(\frac{w}{U}\right)_t \zeta(0) + \int_0^{t'} \left(\frac{w}{U}\right)_{\tau} \zeta(t'-\tau)\,d\tau\right]$
	$+b\left[\left(\frac{Lq}{U}\right)_t \zeta(0) + \int_0^{t'} \left(\frac{Lq}{U}\right)_{\tau} \zeta(t'-\tau)\,d\tau\right]$	$b\left[\left(\frac{Lq}{U}\right)_t \zeta(0) + \int_0^{t'} \left(\frac{Lq}{U}\right)_{\tau} \zeta(t'-\tau)\,d\tau\right]$	$b\left[\left(\frac{Lq}{U}\right)_t \zeta(0) + \int_0^{t'} \left(\frac{Lq}{U}\right)_{\tau} \zeta(t'-\tau)\,d\tau\right]$
Diving planes	$\frac{B}{A} C_{L_B}\left[a_{oB}\left(\frac{u}{U}\right)_t + a_{1B}\left(\frac{w}{U}\right)_t\right.$		$\frac{B}{A}\left(\ell_B C_{L_B} \pm C_{m_B}\right)\left[a_{oB}\left(\frac{u}{U}\right)_t\right.$
	$\left.+ a_{2B}\left(\frac{Lq}{U}\right)_t\right]$		$\left.+ a_{1B}\left(\frac{w}{U}\right)_t + a_{2B}\left(\frac{Lq}{U}\right)_t\right]$
	$+ \frac{B}{A} C_{L_B}\left[a_{oB}\int_0^{t'} \left(\frac{u}{U}\right)_{\tau} \zeta_{oB}(t'-\tau)\,d\tau\right.$	0	$+\frac{B}{A}\left(\ell_B C_{L_B} \pm C_{m_B}\right)$
	$+ a_{1B}\int_0^{t'} \left(\frac{w}{U}\right)_{\tau} \zeta_{1B}(t'-\tau)\,d\tau$		$\left[a_{oB}\int_0^{t'} \left(\frac{u}{U}\right)_{\tau} \zeta_{oB}(t'-\tau)\,d\tau\right.$
	$\left.+ a_{2B}\int_0^{t'} \left(\frac{Lq}{U}\right)_{\tau} \zeta_{2B}(t'-\tau)\,d\tau\right]$		$+ a_{1B}\int_0^{t'} \left(\frac{w}{U}\right)_{\tau} \zeta_{1B}(t'-\tau)\,d\tau$
			$\left.+ a_{2B}\int_0^{t'} \left(\frac{Lq}{U}\right)_{\tau} \zeta_{2B}(t'-\tau)\,d\tau\right]$

9. More General Quasi-Rectilinear Motions

One of the reasons why we are interested in the motions parallel to the (z,x)-plane of symmetry of the hull, is that they are also parallel to the vertical plane. As a consequence, if we know which forces are exerted on the body in forced motions parallel to the (z,x)-plane, we are able to determine the free, natural motions in the vertical plane.

Motions parallel to the horizontal plane are also of a great importance. But their approach is much more complicated.

Let us consider the equations:

$$\dot{\zeta} = -(U+a)\theta + v\phi + w, \quad p = \dot{\phi}, \quad q = \dot{\theta} + \dot{\psi}\phi, \quad r = \dot{\psi} - \dot{\theta}\phi .$$

When the motion is parallel to the horizontal plane, $\dot{\zeta} = 0$. But the components normal to the (z,x)-plane of the hydrodynamic force and of the force of inertia of the body do not act through the same point. Consequently, they generate a X-component for the resulting moment; p and ϕ cannot keep null values. Even if $\theta \equiv 0$, the final motion is not parallel to the (x,y)-plane, since w and q are different from zero.

A motion parallel to the horizontal plane is generally impossible when the diving planes are at a zero angle. For instance, the steady motions are, in this case, helicoidal motions around a vertical axis.

Let us assume that u, w, q are null.

The arc C' along which the free vortices are shed depends upon the form of the hull.

1°) We consider firstly the case when there are, in the (z, x)-plane, no singularities, appendages and so on, which constrain this arc to be located in this plane.

a) $p = 0$. Because of the symmetry of the hull with respect to the (z, x)-plane, the arc C' is in the (z, x)-plane, or in a plane parallel to it. Consequently, when the motion is quasi-rectilinear and parallel to the x-axis, the wake surface is approximately parallel to the (z, x)-plane. The previous reasonings for the motions parallel to the (z, x)-plane hold in the present case, provided v/U and Lr/U are respectively substituted for w/U and Lq/U.

b) $p \neq 0$. It is possible that an U-shaped free vortex shed during the small interval $(\tau', \tau' + d\tau')$ have, at t', an orientation with respect to the axis attached to the body different from the orientation at $\tau' + d\tau'$. In this case the summation at t' of the effects of the free vortices shed during the intervals $(\tau', \tau' + d\tau')$ cannot be carried out on the same manner as in the case of a motion parallel to the (z, x)-plane. This case occurs, for instance, for a body of revolution with respect to the x-axis.

2°) Let us assume that there are in the (z, x)-plane singularities so that the arc C' is in this plane.

a) $p = 0$. This case is quite similar to this of par. 1°) a). It is the simplest from the point of view considered in this paper.

b) $p \neq 0$. In this case, if $|p|$ is relatively great, the wake surface is not a plane; it is more or less helicoidal. The nuclei found in the integrals which yield the effect of the wake depend not only upon $t' - \tau'$, but also on τ', and the expression of the hydrodynamic forces due to the wake is much more complicated than in the case when the motion is parallel to the (z, x)-plane.

3°) It occurs very often that the singularities mentioned above (par. 2°) exist only on the upperside of the body, and not on the lower side, or inversely. In this case, when $p = 0$, the wake surface is inclined with respect to the (z, x)-plane. Consequently, the velocities induced by the wake on the body itself and on the rudder and planes generate necessarily forces which components on the z-axis are not null (see Fig. 8).

If, for instance, $Lr/U = 0$, $v/U > 0$, and if, moreover, the upper arc of C' is located in the (z, x)-plane, because of the singularities of the hull, but not its lower arc, this latter is located on the portside of the hull; the wake surface induces on the body and on the diving planes located on the stern velocities

Figure 8

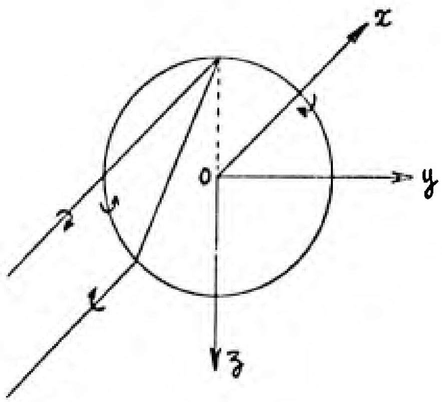

which components on the z-axis are 0. Consequently, the variation of Z and of $\mathfrak{M}$ are both 0. This effect is independent of the sign of v U. It leads to a perturbation of the motion in the vertical plane even when the angle of heel is null.

4°) When the six parameters u U, w U, Lq U, v U, Lr U, Lp U depend upon the time, is it possible to add the effect of the wake due to the three first of them and the effects of the wake due to the three others? The velocities due to one of the wakes may act on the configuration of the other wake. Nevertheless, when the dissymmetry of the body with respect to the (x, y)-plane is not too strong, and, when, moreover, we are in the case of par. 2°) with moderate angles of heel, the velocities due to the wake parallel to the (x, y)-plane are nearly parallel to the wake due to the variations of v U and Lr U and inversely. So it is possible, in a first approximation, to obtain the set of hydrodynamic forces exerted on the body in a quasi-rectilinear motion parallel to the x-axis by adding the sets of forces separately found for motions parallel to the (z, x)-plane and for motions parallel to the (x, y)-plane.

In paragraphs 10, 11, 12, we restrict our analysis, for reason of simplicity, to the cases when such an addition is allowed (however, in par. 12.4, we will consider a more general case).

We set

$$\left(\frac{u}{U}\right)_{t'} \quad f_{00}(t'), \quad \left(\frac{w}{U}\right)_{t'} \quad f_{01}(t'), \quad \left(\frac{Lq}{U}\right)_{t'} \quad f_{02}(t'),$$

$$\left(\frac{v}{U}\right)_{t'} \quad f_{03}(t'), \quad \left(\frac{Lr}{U}\right)_{t'} \quad f_{04}(t'), \quad \frac{B}{L}\left(\frac{Lp}{U}\right)_{t'} \quad \frac{B}{L}\, f_{05}(t').$$

and assume, in par. 10, 11, 12, that these functions have negligible squares and products.

10. The Absolute Forces Due to the Velocity Potential (case of par. 9)

The velocity potential in the absolute motion is

$$\varphi(M,t') = \Phi_{00}(M) + \sum_{k=0}^{5} \Phi_{0k}(M)\ f_{0k}(t') + \sum_{k=0}^{5} \Psi_k(M,t') .$$

Potentials Φ are those which are found alone when the fluid is quite perfect. Potentials Ψ_k yield the effect of the wake. This formula involves the hypothesis at the end of par. 9. However, in the present paragraph, we don't consider the effects of the wake on the appendages (see par. 11).

10.1 Effects on the Wake on the Body Itself

The contribution of $f_{05}(t')$ in $\mathbf{V}_E(M)$ is

$$\mathbf{V}_{SE}(M,t') = -\mathbf{i}_y pz(M) + \mathbf{i}_z py(M) .$$

$(\mathbf{V}_E\mathbf{n})_m$ is generally very small when m is on S. For this reason, we neglect here the contribution of f_{05}.

As seen in par. 5.3, the wake has an effect on the apparent forces of inertia. This effect will be taken into account in par. 10.2.

For reasons of simplicity, we will change slightly the notations of par. 5.3. We use here the following symbols: a for the lift due to w/U; b for the lift due to Lq/U; a' for the moment due to w/U; b' for the moment due to Lq/U; (a_1, a_1') and (b_1, b_1'), are substituted respectively for (a, a') and (b, b') in the terms coming either from v/U or from Lr/U.

Moreover, we assume, as in par. 5, that a set of three functions φ, ψ, φ' is sufficient for yielding all the effects of the delayed circulation when f_{03}, f_{04} are null; and in the same way that a similar set $\varphi_1, \psi_1, \varphi_1'$ gives this effect when f_{00}, f_{01}, f_{02} are null.

Lastly, we admit that the $\mathcal{P}$-component of the moment, when f_{03}, f_{04} are different from zero, may be expressed by means of two coefficients m, m'.

Finally, that leads, for quasi-steady motions, to the set of forces

$$\left.\begin{aligned}
X_{\Phi_0} &= 0 ,\\
Y_{\Phi_0} &= -\frac{1}{2}\rho AU^2 \left[a_1 \left(\frac{v}{U}\right)_{t'} + b_1 \left(\frac{Lr}{U}\right)_{t'}\right] ,\\
Z_{\Phi_0} &= -\frac{1}{2}\rho AU^2 \left[a_0 + a_0 \left(\frac{u}{U}\right)_{t'} + a \left(\frac{w}{U}\right)_{t'} + b \left(\frac{Lq}{U}\right)_{t'}\right] .
\end{aligned}\right\} \quad \begin{matrix}(1)\\ \text{(Cont.)}\end{matrix}$$

$$\left.\begin{aligned}
\mathcal{K}_{\varphi_0} &= \frac{1}{2}\rho ALU^2\left[ma_1\left(\frac{v}{U}\right)_{t'} + m'b_1\left(\frac{Lr}{U}\right)_{t'}\right],\\
\mathcal{M}_{\varphi_0} &= \frac{1}{2}\rho ALU^2\left[a_0' + a_0'\left(\frac{u}{U}\right)_{t'} + a'\left(\frac{w}{U}\right)_{t'} + b'\left(\frac{Lq}{U}\right)_{t'}\right],\\
\mathcal{N}_{\varphi_0} &= \frac{1}{2}\rho ALU^2\left[a_1'\left(\frac{v}{U}\right)_{t'} + b_1'\left(\frac{Lr}{U}\right)_{t'}\right].
\end{aligned}\right\} \qquad (1)$$

The effect of the delayed circulation gives a system of forces

$$X = X_{\varphi_0} - \Delta X, \ \ldots,\ \ldots,\ \ldots,\ \ldots,\ \ldots \qquad (2)$$

where

$$\left.\begin{aligned}
\Delta X &= \frac{1}{2}\rho AU^2\left\{\sum_{k=0}^{k}\left[f_{0k}(t')\,\psi(0) + \int_0^{t'} f_{0k}(\tau')\,\dot\psi(t'-\tau')\,d\tau'\right]\right.\\
&\qquad\left. + \sum_{k=3}^{4}\left[f_{0k}(t')\,\psi_1(0) + \int_0^{t'} f_{0k}(\tau')\,\dot\psi_1(t'-\tau')\,d\tau'\right]\right\},\\
\Delta Y &= -\frac{1}{2}\rho AU^2\left\{a_1\left[\left(\frac{v}{U}\right)_{t'}\varphi_1(0) + \int_0^{t'}\left(\frac{v}{U}\right)_{\tau'}\dot\varphi_1(t'-\tau')\,d\tau'\right]\right.\\
&\qquad\left. + b_1\left[\left(\frac{Lr}{U}\right)_{t'}\varphi_1(0) + \int_0^{t'}\left(\frac{Lr}{U}\right)_{\tau'}\dot\varphi_1(t'-\tau')\,d\tau'\right]\right\},\\
\Delta Z &= -\frac{1}{2}\rho AU^2\left\{a\left[\left(\frac{w}{U}\right)_{t'}\varphi(0) + \int_0^{t'}\left(\frac{w}{U}\right)_{\tau'}\dot\varphi(t'-\tau')\,d\tau'\right]\right.\\
&\qquad\left. + b\left[\left(\frac{Lq}{U}\right)_{t'}\varphi(0) + \int_0^{t'}\left(\frac{Lq}{U}\right)_{\tau'}\dot\varphi(t'-\tau')\,d\tau'\right]\right\},\\
\Delta\mathcal{K} &= \frac{1}{2}\rho ALU^2\left\{ma_1\left[\left(\frac{v}{U}\right)_{t'}\varphi_1(0) + \int_0^{t'}\left(\frac{v}{U}\right)_{\tau'}\dot\varphi_1(t'-\tau')\,d\tau'\right]\right.\\
&\qquad\left. + m'b_1\left[\left(\frac{Lr}{U}\right)_{t'}\varphi_1(0) + \int_0^{t'}\left(\frac{Lr}{U}\right)_{\tau'}\dot\varphi_1(t'-\tau')\,d\tau'\right]\right\},
\end{aligned}\right\} \qquad \begin{matrix}(3)\\ \text{(Cont.)}\end{matrix}$$

$$
\left.
\begin{aligned}
\mathcal{Z}_i &= \frac{1}{2}\,\rho ALU^2 \Bigg\{ a' \left[\left(\frac{w}{U}\right)_{t'} \zeta'(0) + \int_0^{t'} \left(\frac{w}{U}\right)_{\tau'} \dot{\zeta}'(t'-\tau')\, d\tau' \right] \\
&\qquad + b' \left[\left(\frac{Lq}{U}\right)_{t'} \zeta'(0) + \int_0^{t'} \left(\frac{Lq}{U}\right)_{\tau'} \dot{\zeta}'(t'-\tau')\, d\tau' \right] \Bigg\}, \\
\mathcal{Y}_i &= \frac{1}{2}\,\rho ALU^2 \Bigg\{ a_1' \left[\left(\frac{v}{U}\right)_{t'} \zeta_1'(0) + \int_0^{t'} \left(\frac{v}{U}\right)_{\tau'} \dot{\zeta}_1'(t'-\tau')\, d\tau' \right] \\
&\qquad + b_1' \left[\left(\frac{Lr}{U}\right)_{t'} \zeta_1'(0) + \int_0^{t'} \left(\frac{Lr}{U}\right)_{\tau'} \dot{\zeta}_1'(t'-\tau')\, d\tau' \right] \Bigg\}.
\end{aligned}
\right\} \qquad (3)
$$

10.2. Effects of Potentials Φ

These effects give a system of forces $(X_i, Y_i, \ldots)$ which expression will be added to the expression of the forces of inertia of the body in par. 12.

11. Forces Due to the Appendages (case of par. 9)

We assume here that the contribution of the appendages in the forces $\mathcal{F}_c$ and $\mathcal{F}_i$ will be included in the expressions of the latter (see par. 12). We consider now the effects of the various lifts generated by appendages as diving planes and fins, rudder and aileron, sail.

11.1. Diving Planes and Fins

The set of forces on diving planes and fins was studied in par. 6, but with the restriction that

$$f_{03} = 0, \quad f_{04} = 0, \quad f_{05} = 0.$$

The absolute velocity of the axis O_B of a diving plane B is

$$\mathbf{V}_E(O_B) = \mathbf{i}_x\,[U + u + Lq\,\zeta_B] + \mathbf{i}_y\,[v + Lr\,\xi_B - Lp\,\zeta_B] + \mathbf{i}_z\,[w - Lq\,\xi_B].$$

The absolute velocity of the center of the lifting surface is

$$\mathbf{V}_{E_B} = \mathbf{i}_x\,[U + u + Lq\,\zeta_B - Lr\,\eta_B] + \mathbf{i}_y\,[v + Lr\,\xi_B - Lp\,\zeta_B] + \mathbf{i}_z\,[w + Lp\,\eta_B - Lq\,\xi_B].$$

In order to obtain simpler formulae, we will assume that the effect of the component of $\mathbf{V}_B$ parallel to the span is negligible (in fact, some corrections would be necessary; the lift decreases, particularly on the part of the plane which is in the hydrodynamical shadow of the hull). According to this hypothesis, the velocity induced by the wake due to f_{03}, f_{04}, f_{05} has no effect on the diving plane. The square of the effective velocity is consequently

$$U^2 \left[1 + 2\left(\frac{u}{U}\right)_{t'} + 2\left(\frac{Lq}{U}\right)_{t'} \zeta_B - 2\left(\frac{Lr}{U}\right)_{t'} \eta_B\right].$$

The component on the z-axis of the effective incident velocity is, in the quasi-steady motion:

$$-U\left\{\left(\frac{w}{U}\right)_{t'} - f_{02}(t')\xi_B + f_{05}(t')\eta_B - a_{0B} - a_{0B} f_{00}(t') - a_{1B} f_{01}(t') - a_{2B} f_{02}(t')\right\}.$$

The plane is at a zero angle β when the lift generated is null, the motion being parallel to the x-axis. Consequently, in the quasi-steady motion, the effective angle β_e is

$$\beta_e = \beta + \left[f_{01}(t') - f_{02}(t')\xi_B + f_{05}(t')\eta_B\right] - \sum_{k=0}^{2} a_{kB} f_{0k}(t').$$

In the real motion, the velocity induced by the wake is

$$\sum_{k=0}^{2} a_{kB}\left[f_{0k}(0+)\,\phi_{kB}(t') + \int_0^{t'} \frac{d}{d\tau'} f_{0k}(\tau')\,\phi_{kB}(t'-\tau')\,d\tau'\right]$$

$$= \sum_{k=0}^{2} a_{kB} \int_0^{t'} f_{0k}(\tau')\,\dot{\phi}_{kB}(t'-\tau')\,d\tau',$$

and the effective angle of attack is $\beta_e' = \beta_e - \Delta\beta_e$, with

$$\Delta\beta_e = -\sum_{k=0}^{2} a_{kB}\left[f_{0k}(t') - \int_0^{t'} f_{0k}(\tau')\,\dot{\phi}_{kB}(t'-\tau')\,d\tau'\right].$$

Consequently, the set of hydrodynamic forces acting on the diving plane and fin B is:

$$X_B = -\frac{1}{2}\rho\sigma_B U^2 c_{x_B}\left[1 + 2f_{00} + 2f_{02}\zeta_B - 2f_{04}\eta_B\right],$$

$$Y_B = 0,$$

$$Z_B = -\frac{1}{2}\rho\sigma_B U^2 c_{L_B}\left[1 + 2f_{00} + 2f_{02}\zeta_B - 2f_{04}\eta_B\right]$$

$$\times\left[\beta + (f_{01} - f_{02}\xi_B) + f_{05}\eta_B - \sum_{k=0}^{2} a_{kB} f_{0k} - \Delta\beta_e\right],$$

$$\mathcal{L}_B = -\frac{1}{2}\rho\sigma_B L U^2 c_{L_B}\left[1 + 2f_{00} + 2f_{02}\zeta_B - 2f_{04}\eta_B\right]\eta_B$$

$$\times\left[\beta + (f_{01} - f_{02}\xi_B) + f_{05}\eta_B - \sum_{k=0}^{2} a_{kB} f_{0k} - \Delta\beta_e\right],$$

$$\mathcal{M}_B = -\frac{1}{2}\rho\sigma_B L U^2 \zeta_B c_{x_B}\left[1 + 2f_{00} + 2f_{02}\zeta_B - 2f_{04}\eta_B\right]$$

$$+\frac{1}{2}\rho\sigma_B L U^2\left[\xi_B c_{L_B} - c_{m_B}\right]\left[1 + 2f_{00} + 2f_{02}\zeta_B - 2f_{04}\eta_B\right]$$

$$\times\left[\beta + (f_{01} - f_{02}\xi_B) + f_{05}\eta_B - \sum_{k=0}^{2} a_{kB} f_{0k} - \Delta\beta_e\right],$$

$$\mathcal{N}_B = \frac{1}{2}\rho\sigma_B L U^2 c_{x_B}\left[1 + 2f_{00} + 2f_{02}\zeta_B - 2f_{04}\eta_B\right]\eta_B.$$

Taking into account the fact that a diving plane is made of two parts symmetrical with respect to the (z,x)-plane, and neglecting the squares and products of the functions f_{0k}, we get:

$$\left.\begin{aligned}
X_B &= -\frac{1}{2}\rho\sigma_B U^2 c_{x_B}\left[1 + 2\left(\frac{u}{U}\right)_{t'} + 2\left(\frac{Lq}{U}\right)_{t'}\zeta_B\right],\\
Y_B &= 0,\\
Z_B &= -\frac{1}{2}\rho\sigma_B U^2 c_{L_B}\left\{\beta\left[1 + 2\left(\frac{u}{U}\right)_{t'} + 2\left(\frac{Lq}{U}\right)_{t'}\zeta_B\right]\right.\\
&\quad\left.+\left[\left(\frac{w}{U}\right)_{t'} - \left(\frac{Lq}{U}\right)_{t'}\xi_B\right] - \sum_{k=0}^{2} a_{kB} f_{0k}(t')\right\} - \Delta Z_B,\\
\mathcal{L}_B &= -\frac{1}{2}\rho\sigma_B L U^2 c_{L_B}\left\{-2\left(\frac{Lr}{U}\right)_{t'}\beta + \left(\frac{Lp}{U}\right)_{t'}\right\}\eta_B^2,\\
\mathcal{M}_B &= -\frac{1}{2}\rho\sigma_B L U^2\zeta_B c_{x_B}\left[1 + 2\left(\frac{u}{U}\right)_{t'} + 2\left(\frac{Lq}{U}\right)_{t'}\zeta_B\right]\\
&\quad+\frac{1}{2}\rho\sigma_B L U^2\left[\xi_B c_{L_B} - c_{m_B}\right]\left\{\beta\left[1 + 2\left(\frac{u}{U}\right)_{t'} + 2\left(\frac{Lq}{U}\right)_{t'}\zeta_B\right]\right.\\
&\quad\left.+\left[\left(\frac{w}{U}\right)_{t'} - \left(\frac{Lq}{U}\right)_{t'}\xi_B\right] - \sum_{k=0}^{2} a_{kB} f_{0k}(t')\right\} - \Delta\mathcal{M}_B,\\
\mathcal{N}_B &= -\frac{1}{2}\rho\sigma_B L U^2 c_{x_B}\times 2\left(\frac{Lr}{U}\right)_{t'}\eta_B^2.
\end{aligned}\right\}\qquad (1)$$

where

$$\left.\begin{aligned} Z_B &= \frac{1}{2}\rho\sigma_B U^2 c_{L_B} \sum_{k=0}^{2} a_{kB}\left[f_{0k}(t') - \int_0^{t'} f_{0k}(\tau')\,\dot{\gamma}_{kB}(t'-\tau')\,d\tau'\right], \\ M_B &= -\frac{1}{2}\rho\sigma_B L U^2 (\xi_B c_{L_B} - c_{m_B}) \sum_{k=0}^{2} a_{kB}\left[f_{0k}(t') - \int_0^{t'} f_{0k}(\tau')\,\dot{\gamma}_{kB}(t'-\tau')\,d\tau'\right]. \end{aligned}\right\} \quad (2)$$

11.2. Rudders, Ailerons, and Other Appendages Located in the (z,x)-Plane

Let $L\xi_A, 0, 0$, be the coordinates of the axis O_A of a rudder A; $L\xi_A, 0, L\zeta_A$ those of the center of the lifting surface, which area (aileron included) is σ_A.

The absolute velocity of the center of the lifting surface is

$$\mathbf{V}_{E_A} = \mathbf{i}_x\left[(U+u) + Lq\zeta_A\right] + \mathbf{i}_y\left[v + Lr\xi_A - Lp\zeta_A\right] + \mathbf{i}_z\left[w - Lq\xi_A\right].$$

We assume that the components of the incident velocity parallel to the span (hence, to $\mathbf{i}_z$) have no effect (this assumption is similar to the hypothesis already made about the diving planes and motivates similar comments).

According to this assumption, the velocity induced by the wake generated by $f_{00}(t')$, $f_{01}(t')$ and $f_{02}(t')$ has no effect on the rudder. The square of the effective velocity is

$$U^2\left[1 + 2\left(\frac{u}{U}\right)_{t'} + 2\left(\frac{Lq}{U}\right)_{t'}\zeta_A\right].$$

The component on the y-axis of the effective incident velocity is, in the quasi-steady motion:

$$-U\left\{\left(\frac{v}{U}\right)_{t'} + f_{04}(t')\xi_A - f_{05}(t')\zeta_A - a_{3A}f_{03}(t') - a_{4A}f_{04}(t')\right\}.$$

The rudder is at a zero angle α when the rudder is in the (z,x)-plane; α is >0 when the lift has on the y-axis a negative component. In the quasi-steady motion, the effective angle of attack is

$$\alpha_e = \alpha + \left[f_{03}(t') + f_{04}(t')\xi_A - f_{05}(t')\zeta_A\right] - \sum_{k=3}^{4} a_{kA}f_{0k}(t').$$

In the real motion, the velocity induced by the wake has on the y-axis a component

$$\sum_{k=3}^{4} a_{kA}\left[f_{0k}(0+)\,\phi_{kA}(t') + \int_0^{t'} \frac{d}{d\tau'}\, f_{0k}(\tau')\,\phi_{kA}(t'-\tau')\,d\tau'\right]$$

$$= \sum_{k=3}^{4} a_{kA}\int_0^{t'} f_{0k}(\tau')\,\dot{\phi}_{kA}(t'-\tau')\,d\tau' ,$$

and the effective angle is $\alpha_e' = \alpha_e - \Delta\alpha_e$, with

$$\Delta\alpha_e = -\sum_{k=3}^{4} a_{kA}\left[f_{0k}(t') - \int_0^{t'} f_{0k}(\tau')\,\dot{\phi}_{kA}(t'-\tau')\,d\tau'\right].$$

One has

$$\phi_{kA}(0) = 0\,,\quad \phi_{kA}(+\infty) = 1\,;$$

$\phi_{kA}(t')$ is monotonic.

The set of hydrodynamic forces due to the rudder (and aileron) is:

$$X_A = -\frac{1}{2}\rho\sigma_A U^2 c_{x_A}\left[1 + 2\left(\frac{u}{U}\right)_{t'} + 2\left(\frac{Lq}{U}\right)_{t'}\zeta_A\right][1+\ldots]\,,$$

$$Y_A = -\frac{1}{2}\rho\sigma_A U^2 c_{L_A}\left[1 + 2\left(\frac{u}{U}\right)_{t'} + 2\left(\frac{Lq}{U}\right)_{t'}\zeta_A\right]$$

$$\times\left[\alpha + (f_{03} + f_{04}\xi_A - f_{05}\zeta_A) - \sum_{k=3}^{4} a_{kA}\,f_{0k} - \Delta\alpha_e\right],$$

$$Z_A = 0\,,$$

$$\mathfrak{L}_A = \frac{1}{2}\rho\sigma_A LU^2 c_{L_A}\zeta_A\left[1 + 2\left(\frac{u}{U}\right)_{t'} + 2\left(\frac{Lq}{U}\right)_{t'}\zeta_A\right]$$

$$\times\left[\alpha + (f_{03} + f_{04}\xi_A - f_{05}\zeta_A) - \sum_{k=3}^{4} a_{kA}\,f_{0k} - \Delta\alpha_e\right],$$

$$\mathfrak{M}_A = \frac{1}{2}\rho\sigma_A LU^2 c_{x_A}\zeta_A\left[1 + 2\left(\frac{u}{U}\right)_{t'} + 2\left(\frac{Lq}{U}\right)_{t'}\zeta_A\right],$$

$$\mathfrak{N}_A = -\frac{1}{2}\rho\sigma_A LU^2\left(\xi_A c_{L_A} - c_{m_A}\right)\left[1 + 2\left(\frac{u}{U}\right)_{t'} + 2\left(\frac{Lq}{U}\right)_{t'}\zeta_A\right]$$

$$\times\left[\alpha + (f_{03} + f_{04}\xi_A - f_{05}\zeta_A) - \sum_{k=3}^{4} a_{ka}\,f_{0k} - \Delta\alpha_e\right].$$

In these formulae, c_{L_A}, c_{x_A} and c_{m_A} are the characteristic coefficients of the rudder (and aileron, if any) or of the sail.

Finally, one has:

$$\left.\begin{aligned}
X_A &= -\frac{1}{2}\rho\sigma_A U^2 c_{x_A}\left[1+2\left(\frac{u}{U}\right)_{t'}+2\left(\frac{Lq}{U}\right)_{t'}\zeta_A\right],\\
Y_A &= -\frac{1}{2}\rho\sigma_A U^2 c_{L_A}\left\{\alpha\left[1+2\left(\frac{u}{U}\right)_{t'}+2\left(\frac{Lq}{U}\right)_{t'}\zeta_A\right]\right.\\
&\quad\left.+\left[\left(\frac{v}{U}\right)_{t'}+\left(\frac{Lr}{U}\right)_{t'}\xi_A-\left(\frac{Lp}{U}\right)_{t'}\zeta_A\right]-\sum_{k=3}^{4}a_{kA}\,f_{0k}(t')\right\}-\Delta Y_A,\\
Z_A &= 0,\\
\mathfrak{L}_A &= \frac{1}{2}\rho\sigma_A LU^2 c_{L_A}\zeta_A\left\{\alpha\left[1+2\left(\frac{u}{U}\right)_{t'}+2\left(\frac{Lq}{U}\right)_{t'}\zeta_A\right]\right.\\
&\quad\left.+\left[\left(\frac{v}{U}\right)_{t'}+\left(\frac{Lr}{U}\right)_{t'}\xi_A-\left(\frac{Lp}{U}\right)_{t'}\zeta_A\right]-\sum_{k=3}^{4}a_{kA}\,f_{0k}(t')\right\}-\Delta\mathfrak{L}_A,\\
\mathfrak{M}_A &= \frac{1}{2}\rho\sigma_A LU^2 c_{x_A}\zeta_A\left[1+2\left(\frac{u}{U}\right)_{t'}+2\left(\frac{Lq}{U}\right)_{t'}\zeta_A\right],\\
\mathfrak{N}_A &= -\frac{1}{2}\rho\sigma_A LU^2\left[\xi_A c_{L_A}-c_{m_A}\right]\left\{\alpha\left[1+2\left(\frac{u}{U}\right)_{t'}+2\left(\frac{Lq}{U}\right)_{t'}\zeta_A\right]\right.\\
&\quad\left.+\left[\left(\frac{v}{U}\right)_{t'}+\left(\frac{Lr}{U}\right)_{t'}\xi_A-\left(\frac{Lp}{U}\right)_{t'}\zeta_A\right]-\sum_{k=3}^{4}a_{kA}\,f_{0k}(t')\right\}-\Delta\mathfrak{N}_A,
\end{aligned}\right\}\quad(3)$$

with

$$\left.\begin{aligned}
\Delta Y_A &= \frac{1}{2}\rho\sigma_A U^2 c_{L_A}\sum_{k=3}^{4}a_{kA}\left[f_{0k}(t')-\int_0^{t'}f_{0k}(\tau')\,\dot{\phi}_{kA}(t'-\tau')\,d\tau'\right],\\
\Delta\mathfrak{L}_A &= \frac{1}{2}\rho\sigma_A LU^2 c_{L_A}\zeta_A\sum_{k=3}^{4}a_{kA}\left[f_{0k}(t')-\int_0^{t'}f_{0k}(\tau')\,\dot{\phi}_{kA}(t'-\tau')\,d\tau'\right],\\
\Delta\mathfrak{N}_A &= \frac{1}{2}\rho\sigma_A LU^2\left[\xi_A c_{L_A}-c_{m_A}\right]\sum_{k=3}^{4}a_{kA}\left[f_{0k}(t')-\int_0^{t'}f_{0k}(\tau')\,\dot{\phi}_{kA}(t'-\tau')\,d\tau'\right].
\end{aligned}\right\}\quad(4)$$

When the rudder is made of two parts symmetrical with respect to the (x, y)-planes, the term in ζ_A are vanishing, but not those in ζ_A^2. In this case, one has:

$$
\left.
\begin{aligned}
X_A &= -\frac{1}{2}\rho_A U^2 c_{x_A}\left[1+2\left(\frac{u}{U}\right)_{t'}\right],\\
Y_A &= -\frac{1}{2}\rho_A U^2 c_{L_A}\left\{\iota\left[1+2\left(\frac{u}{U}\right)_{t'}\right]+\left[\left(\frac{v}{U}\right)_{t'}+\left(\frac{Lr}{U}\right)_{t'}\xi_A\right]-\sum_{k=3}^{4} a_{kA}\, f_{0k}(t')\right\}-\Delta Y_A,\\
Z_A &= 0,\\
\mathfrak{L}_A &= \frac{1}{2}\rho_A L U^2 c_{L_A}\left\{\iota\left[1+2\left(\frac{u}{U}\right)_{t'}\right]+\left[\left(\frac{v}{U}\right)_{t'}+\left(\frac{Lr}{U}\right)_{t'}\xi_A\right]-\sum_{k=3}^{4} a_{kA}\, f_{0k}(t')\right\}-\Delta\mathfrak{L}_A,\\
\mathfrak{M}_A &= \frac{1}{2}\rho_A L U^2 c_{x_A}\times 2\left(\frac{Lq}{U}\right)_{t'}\times\zeta_A^2,\\
\mathfrak{N}_A &= -\frac{1}{2}\rho_A L U^2\left[\xi_A c_{L_A}-c_{m_A}\right]\\
&\quad\cdot\left\{\iota\left[1+2\left(\frac{u}{U}\right)_{t'}\right]+\left[\left(\frac{v}{U}\right)_{t'}+\left(\frac{Lr}{U}\right)_{t'}\xi_A\right]-\sum_{k=3}^{4} a_{kA}\, f_{0k}(t')\right\}-\Delta\mathfrak{N}_A;
\end{aligned}
\right\}\quad(3')
$$

$$
\left.
\begin{aligned}
\Delta Y_A &= \text{as above},\\
\Delta\mathfrak{L}_A &= 0,\\
\Delta\mathfrak{N}_A &= \text{as above}.
\end{aligned}
\right\}\quad(4')
$$

Of course, this simplification is impossible in the case of such appendages as sails.

11.3. Some Comments About the Previous Formulae

1°) At the beginning of a maneuvering, the delay in the growth of the circulation around the body increases the efficiency of the rudder and diving planes.

2°) c_{m_A} and c_{m_B} have been taken >0 when, in a steady motion, the torque about the axis tends to bring back the rudder or the diving plane to zero angle.

12. Other Sets of Forces Acting on the Body (case of par. 9)

12.1. Gravity

The set of forces is

$$
\left.
\begin{aligned}
X_S &= \frac{1}{2}\rho AU^2 \frac{2W}{AL}\frac{gL}{U^2}\left[-(\mu-1)\theta\right] , \\
Y_S &= \frac{1}{2}\rho AU^2 \frac{2W}{AL}\frac{gL}{U^2}\left[(\mu-1)\phi\right] , \\
Z_S &= \frac{1}{2}\rho AU^2 \frac{2W}{AL}\frac{gL}{U^2}\left[\mu-1\right] , \\
\mathfrak{L}_S &= \frac{1}{2}\rho ALU^2 \frac{2W}{AL}\frac{gL}{U^2}\left[(-\mu\zeta_G-\zeta_c)\phi\right] , \\
\mathfrak{M}_S &= \frac{1}{2}\rho ALU^2 \frac{2W}{AL}\frac{gL}{U^2}\left[-(\mu\zeta_G-\zeta_c)\theta-(\mu\xi_G-\xi_c)\right] , \\
\mathfrak{N}_S &= \frac{1}{2}\rho ALU^2 \frac{2W}{AL}\frac{gL}{U^2}\left[(\mu\xi_G-\xi_c)\phi\right] .
\end{aligned}
\right\} \quad (1)
$$

12.2. Friction, Propeller

Here the thrust T of the propeller $(1/2)\rho AU^2\tau$ and the moment about the y-axis is $(1/2)\rho ALU^2\lambda\tau$. t is the suction coefficient. One has

$$
\left.
\begin{aligned}
X_{f+T} &= \frac{1}{2}\rho AU^2\left[-C_x+\tau(1-t)\right] , \\
Y_{f+T} &= 0 , \\
Z_{f+T} &= \frac{1}{2}\rho AU^2\left[-C_x+\tau(1-t)\right]\theta , \\
\mathfrak{L}_{f+T} &= \frac{1}{2}\rho ALU^2\lambda_Q , \\
\mathfrak{M}_{f+T} &= \frac{1}{2}\rho ALU^2\left[-C_m+\lambda\tau\right] , \\
\mathfrak{N}_{f+T} &= 0 .
\end{aligned}
\right\} \quad (2)
$$

12.3. Forces of Inertia $\mathfrak{F}_c$ for the Body, Forces Due to Potentials Φ and to Pressures $p'^{(i)}$

The components of the general resultant on the (x, y, z)-axis are:

$$\left.\begin{aligned}
X_c + X_i + X_i' &= \frac{1}{2}\rho AU^2 \frac{2W}{AL}\left\{-\mu_{13}\frac{Lq}{U} - (\mu+\mu_1')\frac{L\dot{u}}{U^2} - \mu_{13}'\frac{L\dot{w}}{U^2}\right.\\
&\qquad \left. + (\nu_{15}' - \mu\zeta_G)\frac{L^2\dot{q}}{U^2} + \mu\xi_G\frac{L^2\dot{r}}{U^2}\right\},\\
Y_c + Y_i + Y_i' &= \frac{1}{2}\rho AU^2 \frac{2W}{AL}\left\{\mu_{13}\frac{Lp}{U} - (\mu+\mu_1)\frac{Lr}{U} - (\mu+\mu_2')\frac{L\dot{v}}{U^2}\right.\\
&\qquad \left. + (\nu_{24}' + \mu\zeta_G)\frac{L^2\dot{p}}{U^2} + (\nu_{26}' - \mu\xi_G)\frac{L^2\dot{r}}{U^2}\right\},\\
Z_c + Z_i + Z_i' &= \frac{1}{2}\rho AU^2 \frac{2W}{AL}\left\{(\mu+\mu_1)\frac{Lq}{U} - \mu_{13}'\frac{L\dot{u}}{U^2} - (\mu+\mu_3')\frac{L\dot{w}}{U^2} + (\nu_{35}' + \nu\xi_G)\frac{L^2\dot{q}}{U^2}\right\}.
\end{aligned}\right\} \quad (3)$$

In these formulae the squares and product of ζ_G, ξ_G are neglected. Lastly, the components of the resultant moment are:

$$\left.\begin{aligned}
\mathfrak{L}_c + \mathfrak{L}_i + \mathfrak{L}_i' &= \frac{1}{2}\rho ALU^2 \frac{2W}{AL}\left\{-\mu_{13}\frac{v}{U} - (\nu_{15} - \mu\zeta_G)\frac{Lr}{U}\right.\\
&\qquad \left. + (\nu_{24}' + \mu\zeta_G)\frac{L\dot{v}}{U^2} - (\lambda_1' + \mu\chi_1)\frac{L^2\dot{p}}{U^2} + (\lambda_{13}' + \mu\chi_{13})\frac{L^2\dot{r}}{U^2}\right\},\\
\mathfrak{M}_c + \mathfrak{M}_i + \mathfrak{M}_i' &= \frac{1}{2}\rho ALU^2 \frac{2W}{AL}\left\{\mu_{13} + 2\mu_{13}\frac{u}{U} + (\mu_3 - \mu_1)\frac{w}{U}\right.\\
&\qquad \left. + (\nu_{15}' - \mu\zeta_G)\frac{L\dot{u}}{U^2} + (\nu_{35}' + \mu\xi_G)\frac{L\dot{w}}{U^2} - (\lambda_2' + \mu\chi_2)\frac{L^2\dot{q}}{U^2}\right\},\\
\mathfrak{N}_c + \mathfrak{N}_i + \mathfrak{N}_i' &= \frac{1}{2}\rho ALU^2 \frac{2W}{AL}\left\{-(\mu_2 - \mu_1)\frac{v}{U} + (\nu_{24} + \nu_{15} - \mu\zeta_G)\frac{Lp}{U} + \nu_{26}\frac{Lr}{U}\right.\\
&\qquad \left. + (\nu_{26}' - \mu\xi_G)\frac{L\dot{v}}{U^2} + (\lambda_{13}' + \mu\chi_{13})\frac{L^2\dot{p}}{U^2} - (\lambda_3' + \mu\chi_3)\frac{L^2\dot{r}}{U^2}\right\}.
\end{aligned}\right\} \quad (4)$$

12.4. Case When the Wake Generated in a Motion Parallel to the (x, y)-Plane is not Parallel to the (z, x)-Plane

We assume that, because of singularities, appendages, and so on, on the upperside of the hull, one of the two arcs which constitute the arc $\mathfrak{C}'$ along which the free vortices are shed is in the (z, x)-plane, is on the upperside of the hull. The other arc of $\mathfrak{C}'$ is on the portside when

$$\frac{v}{U} + \frac{rx}{U} > 0$$

for the values of x inferior to the abscissa of the axis of the gyration here considered (this abscissa is normally positive for the natural gyrations, and, consequently, for the forced gyrations which are not too different from the natural ones).

The component on the z-axis of the velocity induced by the wake is always positive, whatever the sign of $v/U + rx/U$ may be. It seems that it is a quadratic form of the arguments v/U and rx/U, or more exactly of the arguments:

$$\int_0^{t'} \frac{d}{d\tau'}\left(\frac{v}{U}\right)_{\tau'} \phi_3(x, t'-\tau')\, d\tau', \qquad -\int_0^{t'} \frac{d}{d\tau'}\left(\frac{Lr}{U}\right)_{\tau'} \phi_4(x, t'-\tau')\, d\tau',$$

when $(v/U)_{t'}$ and $(Lr/U)_{t'}$ are continuous for $t'>0$. Functions $\phi_3(x,t'), \phi_4(x,t')$ are null for $t'=0$, and their limits, for $t'=+\infty$, are finite and positive.

This assumption leads to introduce new functions $\phi_3(t')$, $\phi_4(t')$, $\phi_3'(t')$, $\phi_4'(t')$ null for $t'=0$, equal to 1 for $t'=+\infty$, and to add to the previous components of the hydrodynamic forces exerted on the body itself, the components

$$\left.\begin{aligned} -Z &= \frac{1}{2}\,\rho A U^2 \left| c_3 \int_0^{t'} \left(\frac{v}{U}\right)_{\tau'} \dot\phi_3(t'-\tau')\, d\tau' - c_4 \int_0^{t'} \left(\frac{Lr}{U}\right)_{\tau'} \dot\phi_4(t'-\tau')\, d\tau' \right| > 0, \\ -M &= \frac{1}{2}\,\rho A L U^2 \left| c_3' \int_0^{t'} \left(\frac{v}{U}\right)_{\tau'} \dot\phi_3'(t'-\tau')\, d\tau' - c_4' \int_0^{t'} \left(\frac{Lr}{U}\right)_{\tau'} \dot\phi_4'(t'-\tau')\, d\tau' \right| > 0, \end{aligned}\right\} \quad (5)$$

where c_3, c_3', c_4, c_4' are positive dimensionless coefficients.

There is also an effect on the diving planes located at the stern. The effective angle of attack $\beta_e' = \beta_e - \Delta\beta_e$ (cf. par. 11) becomes

$$\beta_e' = \beta_e - \Delta\beta_e - \delta\beta_e, \text{ with } \delta\beta_e = -\left| a_{3B} \int_0^{t'} \left(\frac{v}{U}\right)_{t'} \dot\phi_3''(t'-\tau')\, d\tau' - a_{4B} \int_0^{\tau'} \left(\frac{Lr}{U}\right)_{\tau'} \dot\phi_4''(t'-\tau')\, d\tau' \right|. \quad (6)$$

In this formula, a_{3B} and a_{4B} are positive dimensionless coefficients, and $\phi_3''(t')$, $\phi_4''(t')$ are null for $t'=0$ and equal to 1 for $t'=+\infty$.

13. Other Motions of Practical Interest

Previously we restricted our analysis to the "quasi-rectilinear" motions. But there are other motions of great interest, and particularly, the change of depth and the change of head.

In many circumstances, the angles β and α are not small. Consequently, the variations of u/U, w/U, Lq/U, v/U, Lr/U and Lp/U may be great.

In such circumstances, the equations of the "quasi-steady motions" are the same as above, at least when the steady effects of the wake are neglected. However, many coefficients which are found in the set of forces $(\mathcal{F}_i)$ are unknown. Generally, the theory is unable to yield them. It is necessary to resort to experiments. But tests on models themselves require special and complicated instrumentation because of the high number of degrees of freedom and, consequently, because of the number of the coefficients which are to be determined.

If we now consider the effects of the wake, we encounter difficulties which we partly emphasized in par. 9. When the nuclei found in the integral equations of the motions are functions of $t'-\tau'$ only, they can be deduced, as we will see in Section II of this paper, from measurements made with small harmonic forced motions. But, when these nuclei are functions not only of $t'-\tau'$, but also of τ', the problem is much more intricate.

The main difficulties are of two types.

The first is due to the fact that, for certain forms of hull, there is no reason why the free vortices should be shed along lines attached to the body (for instance, that is the case of a submerged body of revolution, the complication, in this case, being due to the fact that the axis of revolution is not always of revolution for the distribution of the masses inside the body).

The second is due to the curvature of the trajectory described by the origin of the axis attached to the body, and also, to the roll motion. Obviously, the velocities induced by the wake are no more given by the formulae above.

That does not mean that there are no possibilities to investigate this problem with some chance of success, but, before undertaking such a research, it is desirable to check whether the effects of the wake are or not of importance.

That is why, in the next section, we study the effects of the wake in harmonic forced motions in the (z, x)-plane. We will see that these effects are not negligible, at least for some coefficients. That will give a lead for fruitful researches.

II. STEADY AND HARMONIC FORCED MOTIONS PARALLEL TO THE (z, x)-PLANE

14. Definition of These Motions — Set of Forces Acting on the Body

14.1. Steady Motions, Purely Heaving Motions, Purely Pitching Motions

The fixed axis $O'z'$, $O'x'$ are in the (z, x)-plane. The z'-axis is vertical and positive downwards. The x'-axis is horizontal. The absolute coordinates of the origin O of the axis attached to the body are ζ, ξ.

We assume here that

$$\frac{d\xi}{dt} = \text{constant} .$$

The angle of trim is $\theta = (O'x', Ox)$. θ^2 is assumed to be negligible. The absolute velocity of O is

$$\mathbf{V}(O) = \mathbf{i}_{z'} \frac{d\zeta}{dt} + \mathbf{i}_{x'} \frac{d\xi}{dt} = \mathbf{i}_z w + \mathbf{i}_x (U + u) .$$

One has

$$w = \frac{d\zeta}{dt} \cos\theta + \frac{d\xi}{dt} \sin\theta \cong \frac{d\zeta}{dt} + \frac{d\xi}{dt}\theta, \quad U + u = -\frac{d\zeta}{dt}\sin\theta + \frac{d\xi}{dt}\cos\theta \cong \frac{d\zeta}{dt}\theta + \frac{d\xi}{dt} .$$

Therefore

$$w \cong \frac{d\zeta}{dt} + U\theta , \qquad U \cong \frac{d\xi}{dt} , \qquad u \cong 0 . \tag{1}$$

The drift angle is

$$\epsilon = (\mathbf{V}(O), Ox) \cong \frac{w}{U} = \theta + \frac{1}{U}\frac{d\zeta}{dt} . \tag{2}$$

The angular velocity is

$$\mathbf{i}_y q = \mathbf{i}_y \frac{d\theta}{dt} .$$

$(w/U)^2$, $(Lq/U)^2$ and $|(w/U)(Lq/U)|$ are assumed to be negligible.

A. Steady motions

The steady motions here considered are defined by the conditions:

$$\theta = \text{constant} , \qquad \frac{d\zeta}{dt} = 0 .$$

Consequently, we have:

$$\epsilon \cong \frac{w}{U} = \overline{\theta} , \qquad \frac{Lq}{U} = 0 , \qquad (\overline{\theta} = \text{constant} = \theta) . \tag{3}$$

The set of forces have the components on the axis attached to the body:

$$\overline{Z}, \ \overline{X}, \ \overline{\mathfrak{M}} .$$

B. Purely heaving motions

In these motions θ = constant.

Let $O'z'_1, O'x'_1$ be fixed axis respectively directed as the z-axis and the x-axis.

Let ζ'_1, ξ'_1 be the coordinates of O in the new set of axis. We have

$$\zeta'_1 = \xi\theta + \zeta, \qquad \xi'_1 = \xi - \zeta\theta .$$

In the purely heaving motions here considered, one has:

$$\frac{1}{L}\,\zeta\theta = O(\epsilon^2) ;$$

this product is therefore negligible. Moreover

$$\frac{w}{U} = \theta + \frac{1}{U}\frac{d\zeta}{dt}$$

is a sinusoidal function of the time. Therefore, we set:

$$\zeta'_1 = \zeta(0) + U\,t + \bar{z} + z_0 \cos \omega t \quad (\bar{z} = \text{constant},\ z_0 > 0,\ \theta = \text{constant} = \bar{\theta}) ,$$

and obtain

$$\frac{w}{U} = \bar{\theta} + \frac{z_0}{L}\,\frac{\omega L}{U}\,\cos\left(\omega t + \frac{\pi}{2}\right), \qquad \frac{L\dot{w}}{U^2} = -\frac{z_0}{L}\left(\frac{\omega L}{U}\right)^2 \cos \omega t . \tag{4}$$

In these motions, the components of the set of forces are:

$$\left.\begin{aligned} Z &= \bar{Z} + Z_{h_1} \cos \omega t + Z_{h_2} \cos\left(\omega t + \frac{\pi}{2}\right) , \\ X &= \bar{X} + X_{h_1} \cos \omega t + X_{h_2} \cos\left(\omega t + \frac{\pi}{2}\right) , \\ \mathfrak{M} &= \bar{\mathfrak{M}} + \mathfrak{M}_{h_1} \cos \omega t + \mathfrak{M}_{h_2} \cos\left(\omega t + \frac{\pi}{2}\right) . \end{aligned}\right\} \tag{5}$$

The subscript 1 is relative to the components in phase with the motion; the subscript 2 is relative to those which are out of phase with the motion.

C. Purely pitching motions

In these motions θ is a sinusoidal function of the time: $\theta = \bar{\theta} + \theta_0 \cos \omega t$, ($\bar{\theta}$ constant, $\theta_0 > 0$); moreover, $O'z'_1, O'x'_1$ being fixed axis, with $(z', z'_1) = \bar{\theta}$; the ordinate $\zeta'_1 = \bar{\zeta} + \zeta$ is also a sinusoidal function of the time chosen in such a way that the angle of drift be a constant. Consequently, the purely pitching motions here considered are defined by the conditions

$$\left.\begin{aligned}
&\theta = \bar{\theta} + \theta_0 \cos \omega t\,, \quad (\theta_0 > 0)\,, \quad \frac{w}{U} = \bar{\theta}\,, \quad \zeta = \bar{\zeta} - \frac{U\theta_0}{\omega} \cos\left(\omega t - \frac{\pi}{2}\right)\,,\\
&\frac{L\dot{w}}{U^2} = 0\,, \quad \frac{Lq}{U} = \theta_0 \frac{\omega L}{U} \cos\left(\omega t + \frac{\pi}{2}\right)\,, \quad \frac{L^2\dot{q}}{U^2} = \frac{d}{dt'}\,\frac{Lq}{U} = -\theta_0 \left(\frac{\omega L}{U}\right)^2 \cos \omega t\,.
\end{aligned}\right\} \quad (6)$$

The set of forces has the components:

$$\left.\begin{aligned}
Z &= \bar{Z} + Z_{p_1} \cos \omega t + Z_{p_2} \cos\left(\omega t + \frac{\pi}{2}\right)\,,\\
X &= \bar{X} + X_{p_1} \cos \omega t + X_{p_2} \cos\left(\omega t + \frac{\pi}{2}\right)\,,\\
\mathfrak{M} &= \bar{\mathfrak{M}} + \mathfrak{M}_{p_1} \cos \omega t + \mathfrak{M}_{p_2} \cos\left(\omega t + \frac{\pi}{2}\right)\,.
\end{aligned}\right\} \quad (7)$$

14.2. The Set of Forces in a Steady Motion

Using results of par. 8, and substituting $\bar{\theta}$ for w/U, we get:

$$\left.\begin{aligned}
\bar{Z} = \frac{1}{2}\rho A U^2 \Bigg\{ &\frac{2W}{AL}\frac{gL}{U^2}(\mu - 1) + \left[-\left(c_x + \Sigma \frac{\sigma_B}{A} c_{x_B} + \Sigma \frac{\sigma_A}{A} c_{x_A}\right) + \tau(1 - t)\right]\bar{\theta}\\
&- a_0 - a\bar{\theta} - \Sigma \frac{\sigma_B}{A} c_{L_B}(1 - a_{1B})\bar{\theta} - \Sigma \frac{\sigma_B}{A} c_{L_B}\beta \Bigg\}\,,\\
\bar{X} = \frac{1}{2}\rho A U^2 \Bigg\{ &\frac{2W}{AL}\frac{gL}{U^2}\left[-(\mu - 1)\bar{\theta}\right] + \left[-\left(c_x + \Sigma \frac{\sigma_B}{A} c_{x_B} + \Sigma \frac{\sigma_A}{A} c_{x_A}\right) + \tau(1 - t)\right]\Bigg\}\,,\\
\bar{\mathfrak{M}} = \frac{1}{2}\rho A L U^2 \Bigg\{ &\frac{2W}{AL}\frac{gL}{U^2}\left[(\mu\xi_G - \xi_c) - (\mu\zeta_G - \zeta_c)\bar{\theta}\right]\\
&+ \left[-\left(c_m + \Sigma \frac{\sigma_B}{A} c_{x_B}\zeta_B + \Sigma \frac{\sigma_A}{A} c_{x_A}\zeta_A\right) + \lambda\tau\right]\\
&+ a_0' + \frac{2W}{AL}\left[\mu_{13} + (\mu_3 - \mu_1)\bar{\theta}\right] + a'\bar{\theta} + \Sigma \frac{\sigma_B}{A}\left(\xi_B c_{L_B} - c_{m_B}\right)(1 - a_{1B})\bar{\theta}\\
&+ \Sigma \frac{\sigma_B}{A}\left(\xi_B c_{L_B} - c_{m_B}\right)\beta \Bigg\}\,.
\end{aligned}\right\} \quad (8)$$

14.3. The Set of Forces in a Purely Heaving Motion

We have to substitute $\bar{\theta}$ for θ,

$$U\dot{\gamma} + \frac{z_0}{L}\,\frac{\omega L}{U}\cos\left(\omega t + \frac{\pi}{2}\right)$$

for $w\,U$, and

$$-\frac{z_0}{L}\left(\frac{\omega L}{U}\right)^2 \cos \omega t$$

for $L\dot{w}\,U^2$ in formulae of par. 8.

We obtain, for instance: (given by the first formula 8)

$$Z = \bar{Z} + \frac{1}{2}\rho A U^2 \left\{ \frac{2W}{AL}(\mu + \mu_3)\left(\frac{\omega L}{U}\right)^2 \cos\omega t - \left[a + \Sigma\,\frac{B}{A}\,c_{L_B}(1 - a_{1B})\right]\frac{\omega L}{U}\cos\left(\omega t + \frac{\pi}{2}\right)\right\}\frac{z_0}{L}$$

(which comes also from the contribution of the quasi-steady motion);

$$Z = \bar{Z} + \frac{1}{2}\rho A U^2 a\left\{\gamma(0)\,\frac{\omega L}{U}\cos\left(\omega t + \frac{\pi}{2}\right) + \frac{\omega L}{U}\int_0^{t'}\cos\left(\frac{\omega L}{U}\,t' + \frac{\pi}{2}\right)\dot{\gamma}(t' - \tau')\,d\tau'\right\}\frac{z_0}{L}$$

(which gives the effect on the body itself of the delayed circulation around the body);

$$Z = \bar{Z} + \frac{1}{2}\rho A U^2 \left\{ -\Sigma\,\frac{B}{A}\,c_{L_B} a_{1B}\,\frac{\omega L}{U}\cos\left(\omega t + \frac{\pi}{2}\right)\right.$$

$$\left. + \Sigma\,\frac{B}{A}\,c_{L_B} a_{1B}\,\frac{\omega L}{U}\int_0^{t'}\cos\left(\frac{\omega L}{U}\,\tau' + \frac{\pi}{2}\right)\dot{\gamma}_{1B}(t' - \tau')\,d\tau'\right\}\frac{z_0}{L}$$

(which gives the effect on the diving planes and fins of the delayed circulation around the body).

Because the harmonic motion is assumed to be perfectly established the interval $(0, t')$ is infinitely wide, and consequently, the lower limits in the integrals above must be taken equal to $-\infty$. But we have

$$\int_{-\infty}^{t'}\cos\left(\frac{\omega L}{U}\,\tau' + \frac{\pi}{2}\right)\dot{\gamma}(t' - \tau')\,d\tau' = \int_0^{\infty}\cos\left[\frac{\omega L}{U}(t' - \tau') + \frac{\pi}{2}\right]\dot{\gamma}(\tau')\,d\tau'$$

$$= \cos\omega t \times g\left(\frac{\omega L}{U}\right) + \cos\left(\omega t + \frac{\pi}{2}\right) f\left(\frac{\omega L}{U}\right), \tag{9}$$

where

$$f\left(\frac{\omega L}{U}\right) = \int_0^{\infty}\dot{\gamma}(\tau')\cos\left(\frac{\omega L}{U}\,\tau'\right)d\tau', \quad g\left(\frac{\omega L}{U}\right) = \int_0^{\infty}\dot{\gamma}(\tau')\sin\left(\frac{\omega L}{U}\,\tau'\right)d\tau' \tag{10}$$

are the cosine and sine Fourier transforms of the derivative $\dot{\gamma}(t')$.

Finally, we obtain

$$\left.\begin{aligned}
Z_{h_1}\cos\omega t &= \frac{1}{2}\rho A U^2\left\{\frac{2W}{AL}(\mu+\mu_3) + a\,\frac{g\left(\frac{\omega L}{U}\right)}{\frac{\omega L}{U}}\right. \\
&\qquad \left. + \sum\frac{\sigma_B}{A}c_{L_B}a_{1B}\,\frac{g_{1B}\left(\frac{\omega L}{U}\right)}{\frac{\omega L}{U}}\right\}\left(\frac{\omega L}{U}\right)^2\frac{z_0}{L}\cos\omega t\,, \\
Z_{h_2}\cos\left(\omega t+\frac{\pi}{2}\right) &= \frac{1}{2}\rho A U^2\left\{-a\left[1-\gamma(0)-f\left(\frac{\omega L}{U}\right)\right]\right. \\
&\qquad \left. -\sum\frac{\sigma_B}{A}c_{L_B}\left[1-a_{1B}f_{1B}\left(\frac{\omega L}{U}\right)\right]\right\}\frac{\omega L}{U}\frac{z_0}{L}\cos\left(\omega t+\frac{\pi}{2}\right)\,,
\end{aligned}\right\} \tag{11}$$

where

$$f_{1B}\left(\frac{\omega L}{U}\right) = \int_0^\infty \dot{\gamma}_{1B}(\tau')\cos\left(\frac{\omega L}{U}\tau'\right)d\tau',\qquad g_{1B}\left(\frac{\omega L}{U}\right) = \int_0^\infty \dot{\gamma}_{1B}(\tau')\sin\left(\frac{\omega L}{U}\tau'\right)d\tau' \tag{12}$$

are the cosine and sine Fourier transforms of the derivative $\dot{\gamma}_{1B}(t')$.

A quite similar reasoning leads to:

$$\left.\begin{aligned}
X_{h_1}\cos\omega t &= \frac{1}{2}\rho A U^2\left\{\frac{2W}{AL}\mu'_{13} - a\,\frac{g'_1\left(\frac{\omega L}{U}\right)}{\frac{\omega L}{U}}\right\}\left(\frac{\omega L}{U}\right)^2\frac{z_0}{L}\cos\omega t\,, \\
X_{h_2}\cos\left(\omega t+\frac{\pi}{2}\right) &= \frac{1}{2}\rho A U^2\left\{-a\left[\psi(0)+f'_1\left(\frac{\omega L}{U}\right)\right]\right\}\frac{\omega L}{U}\frac{z_0}{L}\cos\left(\omega t+\frac{\pi}{2}\right)\,,
\end{aligned}\right\} \tag{13}$$

where

$$f'_1\left(\frac{\omega L}{U}\right) = \int_0^\infty \dot{\psi}(\tau')\cos\left(\frac{\omega L}{U}\tau'\right)d\tau',\qquad g'_1\left(\frac{\omega L}{U}\right) = \int_0^\infty \dot{\psi}(\tau')\sin\left(\frac{\omega L}{U}\tau'\right)d\tau'. \tag{14}$$

Similarly, we obtain

$$\begin{aligned}
\mathfrak{M}_{h_1}\cos\omega t &= \frac{1}{2}\rho A L U^2\left\{\frac{2W}{AL}(\mu'_{35}+\mu\xi_G) - a'\,\frac{g'(\omega L/U)}{\omega L/U}\right. \\
&\qquad \left. -\sum\frac{\sigma_B}{A}(\xi_B c_{L_B}-c_{m_B})\,a_{1B}\,\frac{g_{1B}(\omega L/U)}{\omega L/U}\right\}\left(\frac{\omega L}{U}\right)^2\frac{z_0}{L}\cos\omega t.
\end{aligned} \tag{15}$$

(Cont.)

$$\mathfrak{M}_{h_2} \cos\left(\alpha t + \frac{\pi}{2}\right) = \frac{1}{2}\rho ALU^2 \left\{ \frac{2W}{AL}(\mu_3 - \mu_1) + a'\left[1 - \phi'(0) - f'\left(\frac{\alpha L}{U}\right)\right]\right.$$

$$\left. + \Sigma \frac{\sigma_B}{A}(\xi_B c_{L_B} - c_{m_B})\left[1 - a_{1B} f_1\left(\frac{\alpha L}{U}\right)\right]\right\} \frac{\alpha L}{U}\frac{z_0}{L}\cos\left(\alpha t + \frac{\pi}{2}\right), \qquad (15)$$

with

$$f'\left(\frac{\alpha L}{U}\right) = \int_0^\infty \dot{\phi}'(\tau')\cos\left(\frac{\alpha L}{U}\tau'\right)d\tau', \qquad g'\left(\frac{\alpha L}{U}\right) = \int_0^\infty \dot{\phi}(\tau')\sin\left(\frac{\alpha L}{U}\tau'\right)d\tau'. \qquad (16)$$

14.4. The Set of Forces in a Purely Pitching Motion

In formulae of par. 8, we have to substitute:

$$\bar{\theta} + \theta_0 \cos\alpha t \text{ for } \theta, \quad \bar{\theta} \text{ for } \frac{w}{U}, \quad \theta_0 \frac{\alpha L}{U}\cos\left(\alpha t + \frac{\pi}{2}\right) \text{ for } \frac{Lq}{U},$$

$$-\theta_0\left(\frac{\alpha L}{U}\right)^2 \cos\alpha t \text{ for } \frac{L^2\dot{q}}{U^2}.$$

That gives: $[\bar{Z}$ = expression given by (8)],

$$\left.\begin{aligned}
Z_{p_1}\cos\alpha t &= \frac{1}{2}\rho AU^2\left\{-\frac{1}{\left(\frac{\alpha L}{U}\right)^2}\left[C_x + \Sigma\frac{\sigma_B}{A}c_{x_B} + \Sigma\frac{\sigma_B}{A}c_{x_A} + \tau(1-t)\right]\right. \\
&\quad - \frac{2W}{AL}(\nu'_{35} + \mu\xi_G) + b\, g\left(\frac{\alpha L}{U}\right)\Big/\left(\frac{\alpha L}{U}\right) \\
&\quad \left. + \Sigma\frac{\sigma_B}{A}c_{L_B} a_{2B} g_{2B}\left(\frac{\alpha L}{U}\right)\Big/\left(\frac{\alpha L}{U}\right)\right\}\left(\frac{\alpha L}{U}\right)^2 \theta_0 \cos\alpha t. \\
Z_{p_2}\cos\left(\alpha t + \frac{\pi}{2}\right) &= \frac{1}{2}\rho AU^2\left\{\frac{2W}{AL}(\mu + \mu_1) - b\left[1 - \phi(0) - f\left(\frac{\alpha L}{U}\right)\right] - \Sigma\frac{\sigma_B}{A}c_{L_B}\times 2\beta\zeta_B\right. \\
&\quad \left. + \Sigma\frac{\sigma_B}{A}c_{L_B}\left[\xi_B + a_{2B} f_{2B}\left(\frac{\alpha L}{U}\right)\right]\right\}\frac{\alpha L}{U}\theta_0\cos\left(\alpha t + \frac{\pi}{2}\right),
\end{aligned}\right\} \qquad (17)$$

where

$$f_{2B}\left(\frac{\alpha L}{U}\right) = \int_0^\infty \dot{\phi}_{2B}(\tau')\cos\left(\frac{\alpha L}{U}\tau'\right)d\tau', \qquad g_{2B}\left(\frac{\alpha L}{U}\right) = \int_0^\infty \dot{\phi}_{2B}\left(\frac{\alpha L}{U}\right)\sin\left(\frac{\alpha L}{U}\tau'\right)d\tau'.$$

Similarly, we obtain: $[\bar{X}$ = expression given by (8)],

$$\left.\begin{aligned} X_{p_1} \cos \omega t &= \frac{1}{2}\rho AU^2 \left\{ -\frac{2W}{AL}\frac{gL}{U^2}(\mu - 1)\Big/\left(\frac{\omega L}{U}\right)^2 \right. \\ &\qquad \left. - \frac{2W}{AL}(\nu'_{15} - \mu\zeta_G) - b\, g'_1\left(\frac{\omega L}{U}\right)\Big/\left(\frac{\omega L}{U}\right) \right\} \left(\frac{\omega L}{U}\right)^2 \theta_0 \cos \omega t\,, \\ X_{p_2} \cos\left(\omega t + \frac{\pi}{2}\right) &= \frac{1}{2}\rho AU^2 \left\{ -\frac{2W}{AL}\mu_{13} \right. \\ &\qquad \left. - a\left[\varphi(0) + f'_1\left(\frac{\omega L}{U}\right)\right]\right\} \frac{\omega L}{U}\theta_0 \cos\left(\omega t + \frac{\pi}{2}\right). \end{aligned}\right\} \quad (18)$$

Lastly, we get: [$\mathfrak{M}$ = expression given by (8)],

$$\left.\begin{aligned} \mathfrak{M}_{p_1} \cos \omega t &= \frac{1}{2}\rho ALU^2 \left\{ -\frac{2W}{AL}\frac{gL}{U^2}(\mu\zeta_G - \zeta_C)\Big/\left(\frac{\omega L}{U}\right)^2 + \frac{2W}{AL}(\lambda'_2 + \mu\chi) \right. \\ &\qquad \left. + b'g'\left(\frac{\omega L}{U}\right)\Big/\left(\frac{\omega L}{U}\right) - \Sigma\frac{\sigma_B}{A}(\xi_B c_{L_B} - c_{m_B})\, a_{2B}\, g_2\left(\frac{\omega L}{U}\right)\Big/\left(\frac{\omega L}{U}\right)\right\} \\ &\qquad \times \left(\frac{\omega L}{U}\right)^2 \theta_0 \cos \omega t\,, \\ \mathfrak{M}_{p_2} \cos\left(\omega t + \frac{\pi}{2}\right) &= \frac{1}{2}\rho ALU^2 \left\{ b'\left[1 - \varphi'(0) - f'\left(\frac{\omega L}{U}\right)\right] + \Sigma\frac{\sigma_B}{A}(\xi_B c_{L_B} - c_{m_B})\, 2\beta\zeta_B \right. \\ &\qquad \left. - \Sigma\frac{\sigma_B}{A}(\xi_B c_{L_B} - c_{m_B})\left[\xi_B + a_{2B}\, f_{2B}\left(\frac{\omega L}{U}\right)\right]\right\} \\ &\qquad \times \frac{\omega L}{U}\theta_0 \cos\left(\omega t + \frac{\pi}{2}\right). \end{aligned}\right\} \quad (19)$$

15. Interpretation of Experiment Results (Steady and Harmonic Forced Motions)

15.1. Steady Forced Motions

By testing a submerged body in various steady motions — without and with diving planes, without and with propeller — it is possible [see par. 14.2, Eq. (8)] to get the numerical values of the following coefficients:

$$\left.\begin{aligned} &C_x,\ c_{x_B},\ c_{x_A},\ C_m, \\ &a,\ a',\ \frac{\sigma_B}{A}c_{L_B},\ \frac{\sigma_B}{A}c_{L_B}(1 - a_{1B}),\ \frac{\sigma_B}{A}\left(\xi_B c_{L_B} - c_{m_B}\right),\ \frac{\sigma_B}{A}\left(\xi_B c_{L_B} - c_{m_B}\right)(1 - a_{1B}), \\ &\mu_{13},\ \mu_3 - \mu_1\,. \end{aligned}\right\} \quad (1)$$

15.2. "True" and "Apparent" Coefficients

Now, let us consider the expressions of the forces in harmonic forced motions.

We define the "apparent" coefficients of the motion by the following formulae:

a) **From par. 14, Eq. (1'), we deduce:**

$$\frac{2W}{AL}(\mu + \mu_{3_{app}}) = \frac{2W}{AL}(\mu + \mu_3') + a\,\frac{g\left(\frac{\omega L}{U}\right)}{\omega L\ U} \quad \text{(without planes)},$$

$$\frac{2W}{AL}(\mu + \mu_{3_{app}}) = \frac{2W}{AL}(\mu + \mu_3') + a\,\frac{g\left(\frac{\omega L}{U}\right)}{\omega L\ U} + \Sigma\,\frac{S_B}{A}\,c_{L_B} a_{1B}\,\frac{g_{1B}\left(\frac{\omega L}{U}\right)}{\omega L\ U} \quad \text{(with planes)},$$

$$a_{app} = a\left[1 - \zeta(0) - f\left(\frac{\omega L}{U}\right)\right] \quad \text{(without planes)},$$

$$a_{app} = a\left[1 - \zeta(0) - f\left(\frac{\omega L}{U}\right)\right] + \Sigma\,\frac{S_B}{A}\left[c_{L_B}\ 1 - a_{1B}\,f_{1B}\left(\frac{\omega L}{U}\right)\right] \quad \text{(with planes)}. \tag{2}$$

b) **The first equation of Eq. (13), par. 14, gives:**

$$\frac{2W}{AL}\,\mu_{13_{app}} = \frac{2W}{AL}\,\mu_{13}' - a\,\frac{g_1'\left(\frac{\omega L}{U}\right)}{\omega L\ U}\,. \tag{3}$$

c) **From par. 14, Eq. (15), it follows:**

$$\frac{2W}{AL}(\mu_{35_{app}} + \mu\xi_G) = \frac{2W}{AL}(\mu_{35}' + \mu\xi_G) + a'\,g'\left(\frac{\omega L}{U}\right)\Big/\left(\frac{\omega L}{U}\right) \quad \text{(without planes)},$$

$$\frac{2W}{AL}(\mu_{35_{app}} + \mu\xi_5) = \frac{2W}{AL}(\mu_{35}' + \mu\xi_G) + a'\,g'\left(\frac{\omega L}{U}\right)\Big/\left(\frac{\omega L}{U}\right)$$

$$+ \Sigma\,\frac{S_B}{A}\left(\xi_B c_{L_B} - c_{m_B}\right) a_{1B}\,g_{1B}\left(\frac{\omega L}{U}\right)\Big/\left(\frac{\omega L}{U}\right) \quad \text{(with planes)},$$

$$\frac{2W}{AL}(\mu_3 - \mu_1) + a_{app}' = \frac{2W}{AL}(\mu_3 - \mu_1) + a'\left[1 - \zeta'(0) - f'\left(\frac{\omega L}{U}\right)\right] \quad \text{(without planes)},$$

$$\frac{2W}{AL}(\mu_3 - \mu_1) + a_{app}' = \frac{2W}{AL}(\mu_3 - \mu_1) + a'\left[1 - \zeta'(0) - f'\left(\frac{\omega L}{U}\right)\right]$$

$$+ \Sigma\,\frac{S_B}{A}\left(\xi_B c_{L_B} - c_{m_B}\right)\left[1 + a_{1B}\,f_{1B}\left(\frac{\omega L}{U}\right)\right] \quad \text{(with planes)}. \tag{4}$$

d) **From par. 14, Eq. (17), we get:**

$$\left.\begin{aligned}
&\frac{2W}{AL}\left(\nu_{35_{app}}+\mu\xi_G\right)=\frac{2W}{AL}\left(\nu'_{35}+\mu\xi_G\right)-b\,g\left(\frac{\omega L}{U}\right)\Big/\left(\frac{\omega L}{U}\right)\quad\text{(without planes)},\\
&\frac{2W}{AL}\left(\nu_{35_{app}}+\mu\xi_G\right)=\frac{2W}{AL}\left(\nu'_{35}+\mu\xi_G\right)-b\,g\left(\frac{\omega L}{U}\right)\Big/\left(\frac{\omega L}{U}\right)\\
&\qquad\qquad-\Sigma\,\frac{\sigma_B}{A}\,c_{L_B}\,a_{2B}\,g_{2B}\left(\frac{\omega L}{U}\right)\Big/\left(\frac{\omega L}{U}\right)\quad\text{(with planes)},\\
&\frac{2W}{AL}\left(\mu+\mu_1\right)-b_{app}=\frac{2W}{AL}\left(\mu+\mu_1\right)-b\left[1-\zeta(0)-f\left(\frac{\omega L}{U}\right)\right]\quad\text{(without planes)},\\
&\frac{2W}{AL}\left(\mu+\mu_1\right)-b_{app}=\frac{2W}{AL}\left(\mu+\mu_1\right)-b\left[1-\zeta(0)-f\left(\frac{\omega L}{U}\right)\right]\\
&\qquad\qquad+\Sigma\,\frac{\sigma_B}{A}\,c_{L_B}\,\xi_B+a_{2B}\,f_2\left(\frac{\omega L}{U}\right)\quad\text{(with planes)}.
\end{aligned}\right\}\quad(5)$$

e) **The first equation of Eq. (18) gives:**

$$\frac{2W}{AL}\left(\nu_{15}-\mu\zeta_G\right)=\frac{2W}{AL}\left(\nu'_{15}-\mu\zeta_G\right)+b\,g'_1\left(\frac{\omega L}{U}\right)\Big/\left(\frac{\omega L}{U}\right).\qquad(6)$$

f) **Lastly, Eqs. (19), par. 14, yield:**

$$\left.\begin{aligned}
&\frac{2W}{AL}\left(\lambda_{2_{app}}+\mu\lambda_2\right)=\frac{2W}{AL}\left(\lambda'_2+\mu\lambda_2\right)+b'\,\frac{g\left(\frac{\omega L}{U}\right)}{\omega L\;U}\quad\text{(without planes)},\\
&\frac{2W}{AL}\left(\lambda_{2_{app}}+\mu\lambda_2\right)=\frac{2W}{AL}\left(\lambda'_2+\mu\lambda_2\right)+b'\,\frac{g\left(\frac{\omega L}{U}\right)}{\omega L\;U}\\
&\qquad\qquad-\Sigma\,\frac{\sigma_B}{A}\left(\xi_B c_{L_B}-c_{m_B}\right)a_{2B}\,\frac{g_{2B}\left(\frac{\omega L}{U}\right)}{\omega L\;U}\quad\text{(with planes)},\\
&b'_{app}=b'\left[1-\zeta'(0)-f'\left(\frac{\omega L}{U}\right)\right]\quad\text{(without planes)},\\
&b'_{app}=b'\left[1-\zeta'(0)-f'\left(\frac{\omega L}{U}\right)\right]\\
&\qquad\qquad-\Sigma\,\frac{\sigma_B}{A}\left(\xi_B c_{L_B}-c_{m_B}\right)\left[\xi_B+a_{2B}\,f_2\left(\frac{\omega L}{U}\right)\right]\quad\text{(with planes)}.
\end{aligned}\right\}\quad(7)$$

Equations (2) to (7) show that the "apparent" coefficients are constant if, and only if, the effects of the wake are negligible. When this is not the case, they depend upon the "reduced frequency."

According to the quasi-steady theory, the harmonic forced motions should yield the coefficients which are found in the $(\mathcal{F}_i)$-set of forces. In fact, they may yield the effects of the wake and allow to check whether these effects shall be taken into account for practical purposes.

15.3. The Behaviour of the "Apparent Coefficients"

Let us consider again the functions f, f', f_1, f_{1B}, g, g', g_1, g_B.

We have admitted (par. 5) that an unique set of functions φ, ψ, φ' is sufficient in order to define the wake due to the body. We admit, here, for the same reason, that the functions φ_{1B}, φ_{2B} (and φ_{0B}) are identical.

Such an assumption is presently not essential, since, in principle, the interest of tests on a body in harmonic forced motions is to supply these functions. But, the discussion which follows will be easier.

Firstly, we may observe that, for instance:

$$f(0) = \int_0^{\infty} \dot{\varphi}(\tau')d\tau' = \varphi(\infty) - \varphi(0) = -\varphi(0) .$$

Consequently, any "apparent" coefficient involved in an "out phase" force or moment has, when $\omega L/U \rightarrow 0$, a limit equal to its "true" value. For instance [see (2)]:

$$\lim_{\omega L/U \rightarrow 0} a_{app} = a ,$$

and so on. On the contrary:

$$g(0) = 0 , \quad \frac{g\left(\frac{\omega L}{U}\right)}{\omega L/U} \neq 0 \text{ for } \frac{\omega L}{U} = 0 .$$

Therefore, when $\omega L/U$ is small, if we neglect the wake effects, we have a small error about the apparent coefficients involved in the out phase force and moment; on the contrary, the error may be great if we deal with those involved in the in-phase force and moment. When $\omega L/U$ is great, the errors concerning this second family of coefficients are small (provided the reduced frequency is not high enough to change the nature of the flow around the body).

Because φ_B is increasing from zero to 1, $\dot{\varphi}$ is decreasing from a positive value to zero, and

$$f_B = \int_0^\tau \varphi_B(\tau') \cos\left(\frac{\omega L}{U} \tau'\right) d\tau'$$

is positive and decreasing with a limit equal to zero. Hence

$$a_{1B}\left[1 - f_{1B}\left(\frac{\omega L}{U}\right)\right]$$

is increasing. Therefore, the apparent efficiency of the planes must increase with $\omega L/U$ (see Fig. 9a).

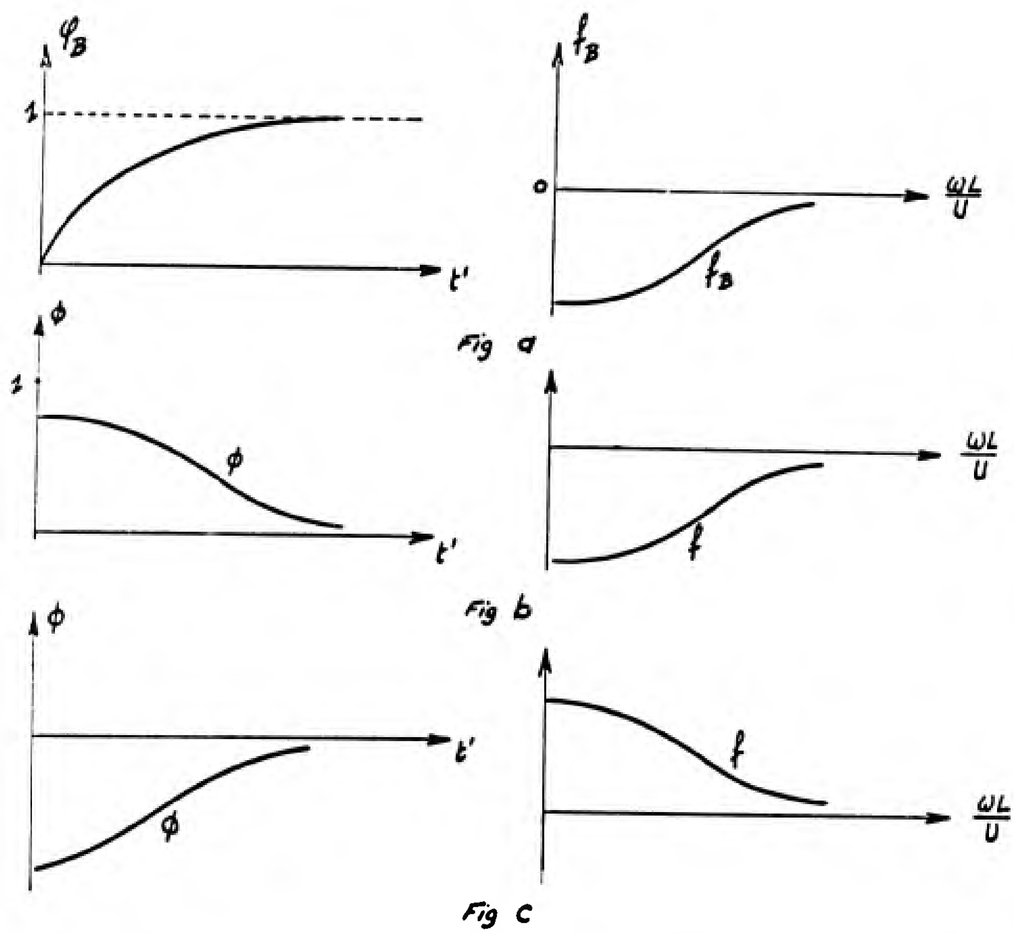

Figure 9

Let us consider again f, f', f_1. We know that $\varphi(0) < 1$. In the case of an airfoil of infinite span, $\varphi(0) = 1/2$. If, here, we have also $0 < \varphi(0) < 1$, φ is decreasing and probably f increases. Therefore a_{app} decreases when $\omega L/U$ increases (Fig. 9b). If, on the contrary, $\varphi(0) < 0$, φ is increasing, f decreasing and a_{app} is increasing (Fig. 9c).

We note that functions f and f_B are not necessarily monotonic. In its present state, the theory yields only the general behaviour of these functions. The real behaviour should be supplied by experiments. Nevertheless, on Fig. 9a, b, c, f and f_B are assumed to be monotonic.

Functions g are null when $\omega L/U = 0$, and when $\omega L/U = \infty$; but

$$g\left(\frac{\omega L}{U}\right)\Big/\frac{\omega L}{U}$$

may be monotonic. We may consider that probably the general behaviour of

$$g\left(\frac{\omega L}{U}\right)\Big/\left(\frac{\omega L}{U}\right)$$

is rather similar to that of $f(\omega L/U)$. However, the possibility for one or several functions $g/(\omega L/U)$ to be increasing at first, and then decreasing, or vice-versa cannot be excluded a priori.

Lastly we will observe that, in certain terms, the variations of the apparent coefficient may be damped because they are the sums of a constant term of a great value and of a variable term. That is, for instance, the case for $a_{3_{app}}$, a'_{app}, b_{app}, $\lambda_{2_{app}}$ but not for a_{app}. Moreover, some terms are probably small (a_{35}, b') and their variations are probably of a little importance.

15.4. Calculation of $\varphi, \psi, \varphi', \varphi$

From the considerations above, it results that, when an "apparent" coefficient varies in a wide range, that is due mainly to a function f. Consequently, it is necessary to take into account the variation of the functions φ, ψ, φ' or φ related to this coefficient when writing and solving the equation of the free quasi-rectilinear motion.

In principle, such a function φ may be obtained by starting from the experimental values of f or g. However, it is easily seen that the f-functions are known with a better accuracy than the g-functions (except when the variation of the coefficient are small, but, in this case, the knowledge of the φ-function involved is of no practical interest).

Finally, we consider that φ must be given by

$$\varphi(t') = \frac{2}{\pi}\int_0^{\infty} f\left(\frac{\omega L}{U}\right)\cos\left(\frac{\omega L}{U}t'\right)d\left(\frac{\omega L}{U}\right).$$

Because $q(\infty) = 0$, one has:

$$q(t') = \int_{\infty}^{t'} \dot{q}(\tau')\, d\tau'.$$

16. Some Experimental Results

We included in the draft of this paper, and we reproduce here four sheets (Nos. I to IV) which show the behaviour of some apparent coefficients related to Z and $\mathfrak{M}$ for a model of about 3 m in length, fitted with planes

$$\left(\Sigma \frac{\sigma_B}{A} = 0{,}0239\right).$$

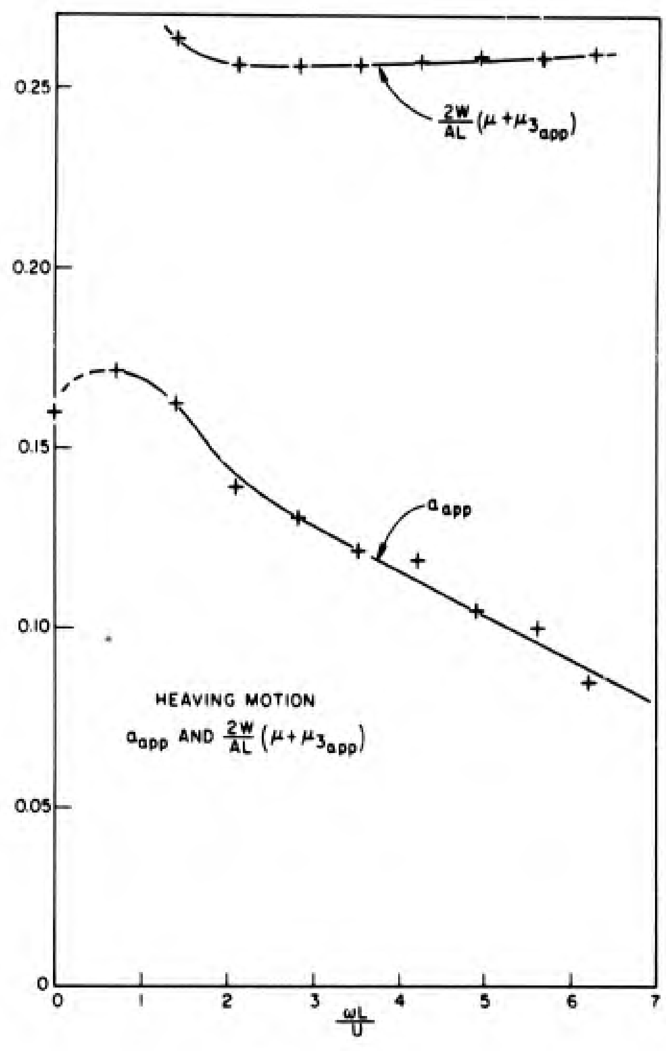

Figure I

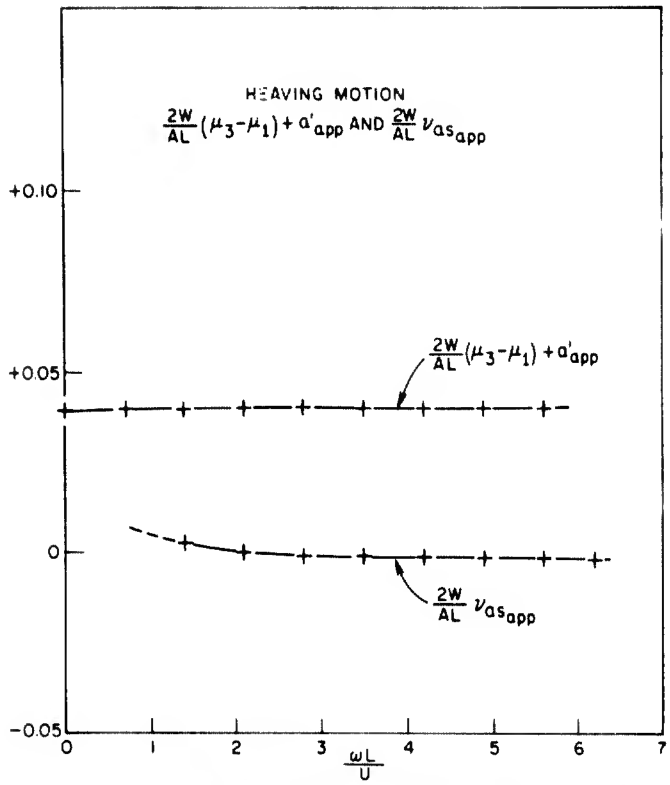

Figure II

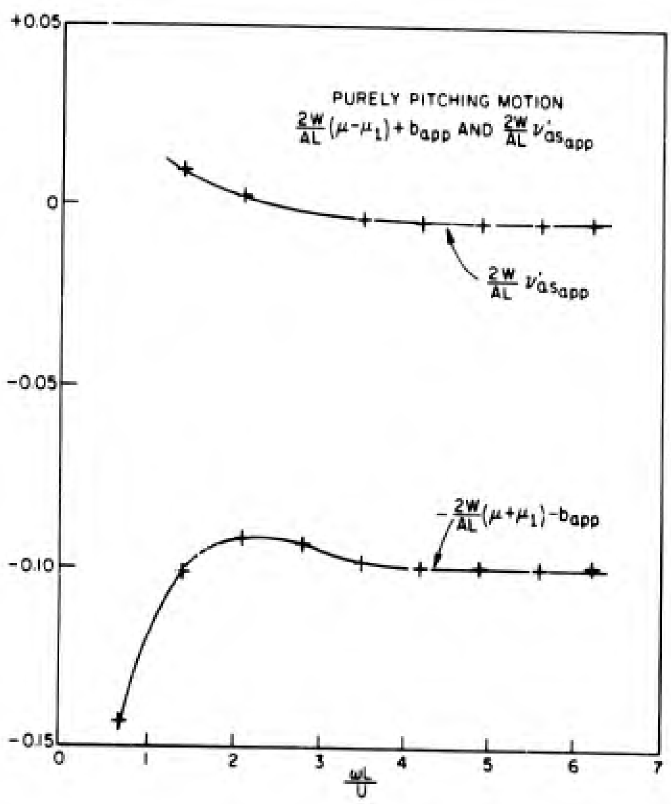

Figure III

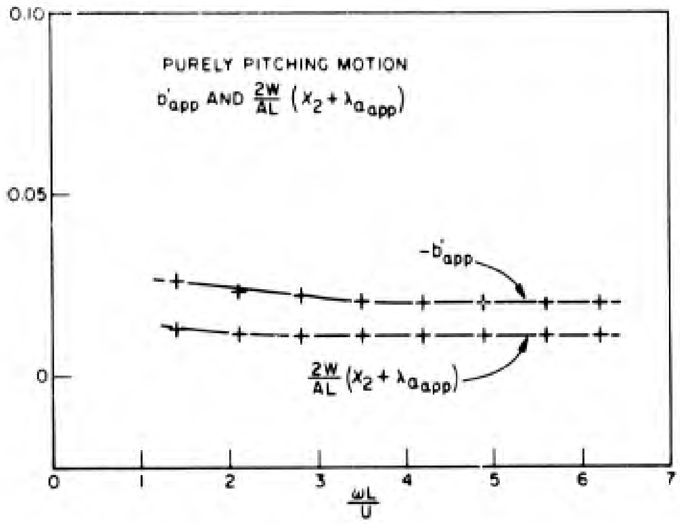

Figure IV

These planes were located near the stern (at about 0, 12 the total length of the model).

The sheets show that the variations of some apparent coefficients may be great, particularly those of a_{app}.

These variations have been explained not only by the influence of the wake on the body, but also by its influence on the planes. It was thought that $0 < f(0) < 1$, and, consequently, that the wake acts in opposite directions on the body and on the planes.

At the time, we considered as certain that ϕ and ϕ' were identical; and found that the lift acts through a point behind the middle section in the case when $Lq/U = 0$, and also in the case when $w/U = 0$.

Later on, other tests were carried out by using our Planar Motions Mechanism. They showed that it is possible that $\phi < 0$, and consequently, that the wake already acts on the body itself in such a way that a_{app}, without planes, is increasing function of $\omega L/U$. In this case, the total variation of a_{app} with planes may be very large; the limit seems to be obtained for $\omega L/U = 10$ or 12, and to be about three times higher than the value for $\omega L/U = 0$.

In spite of these new experiments, we do not deem to be able presently to formulate general conclusions about the effects of the wake on the body itself. In return, we think that the effect of the wake on rudders or stern planes is really of a great importance. A closer analysis of this phenomena would require the study of the blockage effect, of the waves generated by the moving body and also of the influence on the lift of the Reynold's number which is already great during steady forced motions.

III. POSSIBLE FURTHER DEVELOPMENTS – GENERAL CONCLUSIONS

The purpose of the present section is to examine to what extent the ideas outlined above, may influence some problems of importance from a practical point of view.

17. Stability of the Steady Motions

Two cases should be studied. In the first case, one assumes that the control devices are "OFF." In the second case, the control devices are "ON" and act so as to keep constant the characteristics of the steady motion; the pilot system is included in the chain and the loop is closed.

Let λ_i be the parameters which define the motion, α_j the parameters which define the action of the control devices. Let λ_i^o, α_j^o, the values of λ_i, α_j in the steady motion. The method generally used to study the stability consists in the research of solutions of the form

$$\delta\lambda_i = \lambda_i - \lambda_i^o = \ell_i e^{st}, \qquad \delta\alpha_j = \alpha_j - \alpha_j^o = a_j e^{st}.$$

By substituting in the equations of the motion, one obtains an "equation in s"; the steady motion is stable when all the roots of this equation are negative or have a negative real part.

When the equation of the motion contains terms of the form

$$\int_{-\infty}^{t'} \lambda_i(\tau') \dot{\phi}(t'-\tau') d\tau',$$

the substitution leads to terms

$$\mathfrak{L}(\dot{\phi}) = \int_0^{\infty} e^{-s\tau'} \dot{\phi}(\tau') d\tau',$$

which are the Laplace Transforms of the derivatives $\dot{\phi}, \dot{\psi}, \dot{\phi}', \dot{\Phi}$ introduced in pars. 5 and 12.

The "equation in s" so obtained is no more algebraic and its study is more difficult. But of course, it is not impossible.

The stability of the steady motions gives rise to various comments:

1°) The steady motions in the vertical plane are necessarily rectilinear. The problem may be completely solved by measurements of the forces in steady and harmonic forced motions in the (z, x)-plane. But it is possible also to use other ways (at the French Navy Tank, we generally carry out tests on a semi-model with its (z, x)-plane on the free surface of the tank).

2°) The problem connected with the stability of course of a submerged body in the horizontal plane are more complicated than those related to the surface ship because of the particular influence of the heel.

3°) We have not studied the stability of the steady motions in the case when the history of the previous motions is not negligible. That should be done; perhaps the effective stability is not so high as predicted by the quasi-steady motion approximation.

18. The Response to the Control Devices

This problem is difficult because of the effect of the wake generated by the body itself on the rudders and planes.

We showed that at the beginning of a maneuver, the efficiency of a rudder or of a diving stern plane is higher than that deduced from tests in a steady motion. That comes from the fact that, at the beginning of the maneuver, the wake which should reduce the effective angle of attack on the rudder, is not fully developed.

Moreover, when, for one or several functions φ, one has $\varphi(0) \neq 0$, the effect of pressures p_i' is so high that the lift (or the moment) following immediately a perturbation is greater than at $t' = +\infty$. Consequently, it may happen that the response of the body is quite different from that suggested by the word "deficiency." This point shall be emphasized, because the set of forces $\mathfrak{F}$ in the quasi-steady motion and the real set of forces $\mathfrak{F} - \Delta\mathfrak{F}$ don't act along a same line. For instance, at the beginning of a gyration, the heel could be greater than in the steady turning motion, even when the rudders are located so as to avoid an $\mathfrak{L}$-moment of their lifts in a steady turning motion.

19. The "True" Equations of the Motion

19.1. <u>Motions in the (z, x)-Plane</u>

The question examined here is as follows: In the case of a planar motion in the (z, x)-plane, how is it possible to deduce the "true" equations of the free motions from the forces and moment measured in a harmonic forced motion?

These "true" equations are those we have to substitute for the equations of the quasi-steady motions.

When they are reduced to the linear terms, the three equations of the motion are obtained by writing that

$$Z = 0, \quad X = 0, \quad \mathfrak{M} = 0,$$

$Z, X, \mathfrak{M}$ being the forces and moment given in par. 8.

As explained in par. 15.1, tests carried out in steady forced motions give the numerical values of

$$\left.\begin{array}{l} C_x, \quad \Sigma \dfrac{\sigma_B}{A} c_{x_B}, \quad \Sigma \dfrac{\sigma_B}{A} c_{x_A}, \quad C_m, \\[2ex] a, \quad \dfrac{\sigma_B}{A} c_{L_B}, \quad \dfrac{\sigma_B}{A} \left(\xi_B c_{L_B} - c_{m_B}\right); \quad a_{1B}, \\[2ex] \mu_{13}, \quad a' + \dfrac{2W}{AL} (\mu_3 - \mu_1) . \end{array}\right\} \tag{1}$$

We need to know also:

$$\left.\begin{array}{c} \dfrac{2W}{AL} (\mu + \mu_1), \quad \dfrac{2W}{AL} (\mu + \mu'_3), \quad \mu'_{13}, \quad \nu'_{35} + \mu\xi_G, \quad \tau'_{15} - \mu\zeta_G, \quad \lambda'_2 + \mu\lambda_2, \\[2ex] a_0, \quad a'_0, \quad a_{0B}; \quad b, \quad b', \quad a_{2B}; \\[2ex] \varphi, \ \psi, \ \varphi'; \\[2ex] \varphi_B . \end{array}\right\} \tag{2}$$

Let us operate, for instance, without planes. We obtain the numerical values of the apparent coefficients linked with the out-phase forces and moment:

$$a_{app} = a \left[1 - \varphi(0) - f\left(\frac{\omega L}{U}\right)\right] , \tag{3}$$

$$\frac{2W}{AL} (\mu_3 - \mu_1) + a'_{app} = \frac{2W}{AL} (\mu_3 - \mu_1) + a' \left[1 - \varphi'(0) - f'\left(\frac{\omega L}{U}\right)\right] , \tag{4}$$

$$\frac{2W}{AL} (\mu + \mu_1) - b_{app} = \frac{2W}{AL} (\mu + \mu_1) - b \left[1 - \varphi(0) - f\left(\frac{\omega L}{U}\right)\right] , \tag{5}$$

$$b'_{app} = b' \left[1 - \varphi'(0) - f'\left(\frac{\omega L}{U}\right)\right] . \tag{6}$$

$$-\frac{2W}{AL} \mu_{13} - a \left[\psi(0) + f'_1\left(\frac{\omega L}{U}\right)\right] . \tag{7}$$

Consequently, from (3), we deduce the expressions of the function f. Equation (5) gives b_{app} (and b) and also f'; Eq. (4) gives a second time the same function f', and also

$$a' + \frac{2W}{AL} (\mu_3 - \mu_1) .$$

Lastly Eq. (7) gives f'_1.

By inversion of the Fourier integrals, we obtained φ, ψ, φ' and also their sine Fourier Transforms g. Going to the apparent coefficients linked with the in-phase forces and moment, we get

$$\frac{2W}{AL}(\mu + \mu_3'), \quad \mu_{13}', \quad \mu_{35}' + \mu^2 G', \quad \mu_{15}' - \mu^2 G', \quad \mu_2' + \mu\lambda_2 .$$

In many cases, these five coefficients will be either nearly constant or small, and the calculation of the g-functions will be perhaps without practical interest.

Similar reasoning based on the results of the harmonic tests with planes would show the possibility to obtain φ.

Practically all the unknown coefficients and functions may be determined, except those which are connected with the variations of u U. In its present state, our Planar Motion Mechanism is unable to yield them, because no sinusoidal motion parallel to the x-axis is possible. But it is to see that the system could be modified for that purpose, if necessary.

19.2. Motions in the (x, y)-Plane

From pars. 10-12, we could deduce, for this family of motions, formulae similar to those of par. 8, and we could show, in the same manner as in 19.1, that harmonic forced motions in the (x, y)-plane give also the numerical values of the coefficients and functions which are needed to write the equations of the motion in the (x, y)-plane, or more generally, of any motion, provided the expressions of the forces are additive.

20. Effects of the Non-Linearity and Other Sources of Errors

20.1. Non-Linearity

The so-called "true" equations are true only in the linear field. The non-linearity may affect many points of the semi-theoretical views explained in this paper. Some of them are related to the part of the quasi-steady motions theory which we use in our formulae. Some others concern specifically the structure of the wake and the method used for taking its effects into account.

1°) Because submerged bodies are generally very poor lifting surfaces, the coefficients a, b, a', b', for the motions in the (z, x)-planes, a_1, b_1, a_1', b_1', for the motions in the (x, y)-plane, are not really constant. A question would be to know whether it is possible to substitute for their expressions versus the drift angles ε or δ such expression as $a^{\circ}\delta$ for $a\delta + \alpha\delta|\delta|$ or for $a\delta + \alpha\delta^3$.

We have also to observe that our integrals

$$a\int_0^{t'} \left(\frac{w}{U}\right)_{\tau'} \dot{\varepsilon}(t' - \tau')\, d\tau' , \ldots .$$

become

$$\int_0^{t'} \left[a\left(\frac{w}{U}\right)_{\tau'} + \alpha\left(\frac{w}{U}\right)_{\tau'}\left|\frac{w}{U}\right|_{\tau'}\right]\dot{\phi}(t'-\tau')\,d\tau', \ldots .$$

2°) The non-linearity is also to be taken into account when the motions are not really quasi-rectilinear. From a practical point of view, this is very serious since, in many cases, the trajectory of the origin O of the moving axis is not a straight line. In such a case, the nuclei depend upon τ' and $t'-\tau'$, and not upon $t'-\tau'$ only. Consequently, we encounter here a new problem, which consists in the empirical determination of the new function $\phi(\tau', t'-\tau')$ which have to be substituted for $\phi(t'-\tau')$.

A similar circumstance happens when the heel becomes great even if the trajectory of O is nearly a straight line, for, in this case, the wake cannot be considered as a plane surface but is an helicoidal surface. The first phase in a change of heading would be different and the wake due to a gyration in the vertical plane could have a severe effect on the trim.

3°) The non-linearity may affect also the scale effect since the coefficients a, b, ..., depend upon the Reynolds' number. This cause of error exists also in the quasi-static theory, but it has no effect on the functions $\phi_1, \ldots, \phi_1'$.

20.2. Other Causes of Errors

They are the effects of the free surface and those of the walls and of the bottom of the tank.

In order to get accurate measurements of the sets of forces, it is necessary to operate at a sufficiently high speed. But U becomes great and the range of values of $\omega L/U$ which is accessible becomes narrow. In order to increase this range, one may be obliged to operate sometimes beyond the critical speed $U/\sqrt{gH}$, where H is the depth of the tank, and sometimes below. On the other hand, the coefficient $V/\sqrt{g\zeta}$, where ζ is the depth of O may be great and consequently, the waves generated by the model may be not negligible at all. Lastly because the range of values of ω is not very wide (from 1.1 to 3.27) it may be necessary to work at various values of $\omega L/U \cdot U^2/gL$ in order to keep constant the values of $\omega L/U$ and, consequently, the changes of the wave patterns which results from that, may lead to errors about the true effect of the reduced frequency.

That means that experiments conceived in order to determine the functions $\phi_1, \ldots, \phi_1'$ require a very caution approach.

21. The Solving of the True Equations

Generally, one admits that, when the forces acting on the model are known, the equations of the maneuvering ship may be solved by analog computers.

Such computers are most often fitted with curve-plotters, and it is possible to get the curves which give the motion of the body following a given maneuver as a function of time.

However, if we deal with integral equations, the conventional analog computers are no more sufficient. Bigger computers, analog, digital, or hybrid, are in fact necessary and the work to be undertaken to study all the possible interesting cases becomes really huge . . .

22. General Conclusions

22.1. As already stated in the Introduction, this paper is devoted to the effects of the circulation around a ship on the set of hydrodynamic forces exerted on her.

As a matter of fact, the subject is restricted to the case of a submerged body in an infinite fluid. But the case of a surface ship is similar, apart of the fact that the free surface effects have to be taken into account.

22.2. Our mathematical model is defined in Section I, pars. 3 and 4.

We start from the possibility to substitute for a submerged body moving in a perfect fluid an equivalent distribution of bound vortices on its hull (and inside the volume interior to the body when the angular velocity is not identically null). Consequently, a motion is defined in the whole space; the fluid interior to the body is at rest with respect to the latter. Then we introduce a new family of bound and free vortices in order to get a wake. This new family has to be added to the first.

We consider firstly the case of a <u>small</u> motion with one degree of freedom around an <u>uniform</u> motion of velocity U parallel to the x-axis. This small motion is assumed to be parallel to the (z, x)-plane of symmetry. Neglecting the deflection of the fluid due to the reaction of the body on the fluid or, which is equivalent, to the velocities induced by the vortices on themselves, we admit that the free vortices are at rest with respect to the fixed axis. They are lying on U-shaped arcs which are nearly located on planes parallel to the (x, y)-plane; because the angle of attack (or the reduced angular velocity) is small, these arcs are approximately located on a wake surface attached to the body along a line which is assumed to be known (given by experience for each body), and which acts as the trailing edge of a lifting surface. The bound vortices associated to these free vortices are distributed on the hull. The total distribution fulfils the condition that the circulation around a closed fluid arc is equal to zero. The total potential equivalent to the free and bound vortices of the second family induces a velocity which is null inside the body and which, outside the body, is tangent to the external face of the hull and to the surface of the wake. It is shown that these conditions lead, when the motion is unsteady, to a formula which gives the circulation in term of the circulation in the quasi-steady motion. This expression is a convolution function

$$\Gamma(t') = \int_0^{t'} \Gamma_0(\tau') \frac{\partial k}{\partial t'} (t' - \tau') \, d\tau' ,$$

where t' is the reduced time $t' = Ut/L$, L being the length of the body, and $t' = 0$ the time at the beginning of the unsteady motion.

Then we have to add the effects of a motion with three degrees of freedom u/U, w/U, Lq/U, the total motion being still parallel to the (z,x)-plane. In order to do that, we admit that these three parameters have negligible squares and products, and, consequently, that the wake surface is practically the same as in the previous case.

22.3. In par. 5, we introduce the hydrodynamic forces due to the total velocity potential of the absolute motion of the fluid. For the sake of simplification, we assume here that the body is not fitted with planes or fins. We consider firstly the distribution of the pressure on the hull. It is shown that it is the sum of three terms. One is due to the velocity potential when the fluid is quite perfect, that is, when the wake is not taken into account. The two other terms are due to the wake. The first of them is generated by a local Kutta-Joukowsky or gyroscopic effect; the second is due to the partial derivative with respect to the time. A second method, more rapid, gives the total force and moment starting from the absolute momentum of the fluid and from its moment with respect to the fixed axis. In order to do that, we substitute to the vortices a distribution of doublets normal to the hull and to the wake. We show that it is possible to express the difference between the set of forces yielded by the quasi-steady motion theory and the real set of forces in terms of convolution functions:

$$\sum_k \int_0^{t'} f_{0k}(\tau')\, \dot{\lambda}(t' - \tau')\, d\tau'$$

for the lift,

$$\sum_k \int_0^{t'} f_{0k}(\tau')\, \dot{\mu}(t' - \tau')\, d\tau'$$

for the drag,

$$\sum_k \int_0^{t'} f_{0k}(\tau')\, \dot{\nu}'(t' - \tau')\, d\tau'$$

for the moment; $f_{0k}(t')$, $k = 0, 1, 2$, are the arbitrarily given functions

$$\left(\frac{u}{U}\right)_{t'}, \quad \left(\frac{w}{U}\right)_{t'}, \quad \left(\frac{Lq}{U}\right)_{t'}.$$

We call "deficiencies" these differences. In fact, each deficiency is made of two terms, one of them is really a deficiency, because it is due to the fact that the circulation is unable to take instantaneously the value relating to the quasi-steady motion; but the second one which is due to the partial derivative $\partial/\partial t$, acts in the opposite sense. The three functions $\lambda, \ldots, \nu'$ are probably the same whatever k may be; but we did not prove that rigorously. Moreover we cannot prove that they are proportional to one another (which is the case for an airfoil of infinite aspect ratio). From a theoretical point of view, something is lacking there but, from a practical point of view, that is without great importance, because these functions may be obtained through experiments.

In par. 6, we consider the forces acting on the planes and fins. We neglect the effect of the history of their own motion. But we take into account the effect of the velocity due to the wake generated by the body itself and show that it acts so as to increase the efficiency of these appendages at the beginning of a maneuver.

Paragraph 7 is devoted to the other set of forces acting on the body (friction, gravity, inertia, ...), and par. 8 gives the total expression of the forces when the motion is parallel to the (z,x)-plane.

22.4. Paragraphs 9-12 are devoted to motions not parallel to the (x,y)-plane. In par. 9, we explain the difficulties we have encountered in this task. They are partly due to the fact that in the most general case, the field of vortices may be different from the sum of those which we deal with when the number of degrees of freedom is smaller. For instance, at a given instant t', perhaps the free vortices are generally shed along a line only and not, simultaneously, along the two lines which are respectively related to the components of the motion parallel to the (z,x)-plane, and to its components parallel to the (x,y)-plane. Nevertheless, after a discussion, we admit that such an addition is possible in some cases of great importance from a practical point of view, when the perturbations are small. Consequently, we obtain final formula similar to those of par. 8. But it is necessary to consider, that in some cases, particularly when the angle of heel is great, or when the body turns with a small radius of gyration, the nuclei found in the integral expressions of the forces and moments depend not only upon the difference $t' - \tau'$, but also upon τ' (see par. 13).

22.5. In Section II (pars. 14-16), we examine the case of steady and harmonic forced motions in the (z,x)-plane. Such a study leads to consider the differences between the case of the quasi-steady motion theory and the theory developed in the previous paragraphs.

In both cases, it is possible to express the lift, the drag and the moment in phase with the motion in terms which are proportional to the square of the reduced frequency $\omega L/U$, and the lift, the drag and the moment outphase with respect to the motion, in terms which are proportional to the reduced frequency itself. But, if we use the quasi-steady motion theory, we find that the coefficients before $(\omega L/U)^2$ or $\omega L/U$ are constants; on the contrary, if we take into account the delayed circulation, they depend upon the reduced frequency.

That leads to define "apparent" coefficients. Those related to the outphase forces and moments, have their limits, for $\omega L/U \to 0$, equal to the "true" coefficients; the other are equal to their true values only for large values of $\omega L/U$.

Consequently, tests carried out in harmonic forced motions give the possibility to decide whether the effects of the wake are of importance, or may be neglected. Experiments showed that some of the apparent coefficients, those which are not mixed with terms of inertia of the body or with term coming from the rotation of the axis attached to the body, have important relative variations. Experiments show also that the effects of the wake on the stern diving planes and fins are very high.

22.6. In Section III, pars. 17-21, we examine some possible further developments.

The equations of motions nearly parallel to the x-axis involve unknown coefficients and functions. The unknown coefficients are those we find in the steady forced motions, the "added masses" and the terms which come from the rotation of the axis attached to the body. The unknown functions are due to the wake; they are the Fourier transforms of the part of the apparent coefficients which depend upon the reduced frequency in the harmonic forced motions. Consequently tests in steady and in harmonic forced motion yield, in principle, all the unknown coefficients and functions which are necessary for writing the equations of such motions, although these motions are not harmonic.

The equations so obtained are not differential, but integro-differential. Consequently, they are more complicated than the differential equations introduced by using the classical static derivatives, that is, the theory of the quasi-steady motions. For the naval architects, this new aspect of the problem is somewhat unpleasant and it would be of interest to check whether the errors from the classical treatment of the problem are great or not. Probably they are not negligible in the transient motions. But, until now, we have had no possibility to compare the two families of solutions. Moreover, some people may consider as negligible differences which are important to the eyes of some others. In any case, we think that the views developed in this paper may explain some interesting particularities of the transient motions, because they call the attention to phenomena which prediction would be impossible according to the classical equations. Even if it is finally found that the differences between the solutions of the classical equations and those of the integro-differential equations are not very high, it is of interest to discern why. From this point of view, we think that harmonic forced motion tests are useful, because the results so obtained lead to understand better how the term coming from the partial derivative may partially cancel those coming from the delayed circulation or inversely.

Some points are yet to be emphasized. Firstly, tests in steady and harmonic forced motions require much care, because of the possible free surface effect in an ordinary tank. Moreover, it is possible that the planar motion mechanisms are not perfectly adapted for systematic research about such motions. For instance, the range of the possible amplitudes and frequencies is probably too narrow. For a point of importance would be to study the limits of the linear field.

That means that the planar motion mechanisms, which interest has been many times emphasized, do not enable us to solve all the problems involved in the maneuvering qualities of a submerged body. Tests in a steering tank with a rotating arm are certainly necessary in order to explore motions of great amplitude and gyrations at a very large angle of rudder, as was previously the case for researches about the maneuverability of the surface ships. The planar motion mechanisms give new means; but the latter do not replace the previous facilities. It is even allowed to deem that it is necessary to explore the maneuvering qualities of submerged bodies by using free models as it is already done in the case of surface ships.

22.7. Now we come back to the mathematical model which has been the starting point of the present paper. Obviously such a model could give too many remarks and criticisms. For instance, we consider as a fact that a wake exists, but the real structure of the wake is in connection with the mechanism of the transport into this wake of the vorticity which originates in the boundary layer. Certainly the approximation of the quasi-perfect fluid is not a refined one. The present theory does not stand on the same refined level as the theory of the wings of finite span. Many improvements would be desirable from a scientific point of view. But, for practical purposes, we have for the time being to admit semi-empirical theories. The quasi-steady motion theory which until now has been the only one practically used, is also a semi-empirical theory. The most important point in this paper is the following: In practice, have we or have we not to take into consideration the facts disclosed by harmonic forced motions tests?

We don't answer this question. But we sincerely hope that it is worth putting.

REFERENCES

1. W. E. Cummins, "The Impulse Response Function and Ship Motions, D.T.M.B. Report 1661, Oct. 1962.

2. Th. von Kármán and W. R. Sears, "Airfoil Theory for Non-Uniform Motions," Journal of the Aeronautical Sciences, Vol. 5, No. 10, Aug. 1938.

3. P. Casal, "Sur les Qualités Évolutives des Navires" (Thesis, 1950).

4. R. Brard, "Maneuvering of Ships in Deep Water in Shallow Water and in Canals," SNAME, Vol. 59, pp. 229-257, 1951.

5. S. B. Spangler, A. H. Sacks, J. N. Nielsen, "The Effect of Flow Separation from the Hull on the Stability of a High-Speed Submarine," Vidya Report No. 107, Aug. 1963, for O.N.R. and D.T.M.B.

6. E. J. Rodgers, "Vorticity Generation of a Body of Revolution at an Angle of Attack," Paper No. 64-FE.S (read before the American Society of Mechanical Engineers), Philadelphia, May 1964.

7. M. Sevik, "Lift on an Oscillating Body of Revolution," Am. Inst. of Aeron. and Astronautics Journal, pp. 302-306, Feb. 1964.

8. R. Brard, "Mouvements Plans Non Permanents d'un Profil Déformable," Bulletin de l'Association Technique Maritime et Aéronautique, Paris, 1963.

* * *

DISCUSSION

Nils H. Norrbin
Swedish State Shipbuilding Experimental Tank
Goteborg, Sweden

Admiral Brard has presented a fine piece of work on the mathematics of a changing system of lifting vortices on bodies in transient and periodic motions, accepting the physical picture of a flow separating along lines more or less parallel to the body axis and producing a downwash over almost the full length and width of the after body.

When the body changes its attitude the interference between the vortex wake and after body, and fins, does also change, and this interference must be dependent on the time history of the motion. The physical picture also brings with it the concept of a certain time required before a change of boundary flow conditions develops into a change of separation and vortex wake, thus complicating the dependence of the history of a transient motion, or of the frequency of a periodic one. The present speaker fails to see to which extent the results of the oscillator experiments quoted by the author are in any quantitative support of this theory.

To the speaker again, the flow separation parallel to the axis as mentioned is more associated either with surface ship forms with spontaneous separation, or with bodies of revolution at angles of attack no longer small. For the body of revolution at a small angle of attack, on the contrary, the Nonweiler theory suggests separation to occur much further aft and along the contour of a plane almost at right angles to the axis. The vortex wake then covers a narrow region of the after body only, and the circumferential flow will also be more rapidly adjusted to the boundary conditions, thus extending the domain of practically frequency independent derivatives. This might explain why ordinary differential equations with constant coefficients are seemingly sufficient to predict the normal motion of a fair shaped submarine, but it would be interesting to hear of the authors experience of such predictions.

* * *

DISCUSSION

A. J. Vosper
Admiralty Experimental Works
Gasport, England

The mathematical presentation in Admiral Brard's paper is welcomed as a laudable attempt to calculate the forces on a submerged body. This is a problem which has defeated many people in the past, so that the outcome of the author's work is awaited with interest.

I imagine that few will quarrel with the general principle expressed in the paper, that the motion of a ship or submarine depends on the past history of its motion. However, because of the insuperable difficulties involved in any other approach, the use of quasi-static derivatives has been widely accepted as a suitable approximation, since they were first introduced by G. H. Bryan in 1911. Professor W. J. Duncan later attempted to justify the use of quasi-static derivatives, and concluded that for the kinds of motion occurring in stability investigations of aircraft flight, the use of constant derivatives was justified. However, he admitted that the influence of the frequency parameter had been neglected, apart from its consideration in the studies of flutter of control surfaces.

It is not therefore surprising that in the submarine field, for which the theories from the aircraft world were adapted, a quasi-static approach has been used to consider motions well beyond the range of the small deviations for which it was derived. However, one cannot ignore the not inconsiderable argument that in submerged body work good correlation has been achieved between theory and practice. To this extent one can reasonably claim that the end has justified the means.

From this point of view, which is all-important to the practising naval architect, the introduction of a considerably more complex representation of the problem seems unnecessary. However, the case of a surface ship in a disturbed sea is entirely different and there may here be greater justification for the author's approach.

Comparison of data obtained by rotating arm and planar motion mechanism will undoubtedly help to throw light on this problem, and the I.T.T.C. Maneuverability Committee by sponsoring a series of international cooperative tests using the "Mariner" Class form, will eventually obtain data which may help to answer Admiral Brard's question.

Finally, I must admit to some lingering doubts about the basic concept of the planar motion mechanism. If Admiral Brard will permit, I would like to rephrase Question 1 on page 29: "Is it possible to deduce from the forces and moments measured in a harmonic forced motion, the true forces and moments experienced by a ship or submarine in a motion which is rarely harmonic?"

REFERENCES

1. G. H. Bryan, "Stability in Aviation," MacMillan, 1911.
2. W. J. Duncan, "Some Notes on Aerodynamic Derivatives," R. & M. 2115 (1945).
3. W. J. Duncan, "Control and Stability of Aircraft," C.U.P. (1952).

* * *

REPLY TO THE DISCUSSION BY NORRBIN

Roger Brard
Bassin d'Essais des Carenes de la Marine
Paris, France

Dr. Norrbin has drawn the attention to the mathematical model which I choose as a starting point. I agree that the choice is a difficult one and, indeed, I have hesitated for a fairly long time before deciding. That is why I wrote that the NACA model only "suggests" the physical picture of a surface wake limited by lines more or less parallel to the x-axis. As a matter of fact, the length and the shape of the arc along which the separation occurs depends strongly upon the hull form. For instance, for a thin surface ship, this arc is practically the keel line and the maximum of the density of the free and bound vortices is located near the bow. For a body of revolution, the arc depends also upon the angle of attack. But it does not seem to me that the final structure of the formulae giving the expression of the forces exerted on the ship or on the submerged body in an unsteady motion strongly depends upon these circumstances. I hope that, in the field of linearity, at least when the body is moving in its centerplane, the forces are always given by convolution functions. The behaviour of these functions may differ when the form of the hull changes, and their calculation should be very intricate. My purpose was only to give means in order to get these functions starting from experimental results and not through mathematical calculations.

When the motion is not parallel to the centerplane of the body, the form of the hull is of still greater importance. It is my intention to insist on this question in the final text of the paper. For instance, in the case of a nonsymmetric body with respect to the (x, y)-plane, strong forces along the z-direction and moment about the x-axis may appear. The intensity of these force and moment strongly depends on the form.

Presently, the theory does not permit to predict which hydrodynamic forces are exerted on the body whatever its form may be. But it leads to a method for deducing these forces from these measured in particular motions, the steady and harmonic forced motions. The theory also indicated that the wake has a great influence on the forces acting on the stern planes and fins.

Dr. Norrbin said that the surface of the body on which the wake acts is of small area when the body is of revolution and when the angle of attack is small. He expressed the opinion that it might explain why ordinary differential equations with constant coefficients are seemingly sufficient. I have indicated in the paper that, from my point of view, this question is presently not solved. It is quite evident that the coefficients which depend upon the added masses or which contain terms due to the rotation of the axis are much less sensitive to the history of the motion than the others. For this reason the history of the motion should act mainly on the lift coefficient due to the angle of drift.

* * *

REPLY TO THE DISCUSSION BY VOSPER

Roger Brard
Bassin d'Essais des Carenes de la Marine
Paris, France

From a practical point of view, the use of quasi-static derivatives is probably justified for solving the problems concerning the stability of steady motions. Of course, as indicated in Section 5.2 of the paper, the "equation in s" is different, at least in principle, whether the history of the past motion is taken into account or not. But the stability of the motion depends mainly upon the signs of the real parts of the roots of the equation which are in the vicinity of zero, and the signs seem to be very little affected by the history of the motion.

In some cases, it is possible to observe motions of surface ships, such as harmonic variation of the heading, the rudder angle being constant and equal to zero, for which complete explanation seemingly requires consideration of the history of the past motion.

In the case of a surface ship, I believe that we generally do not need a very accurate theory to predict the motion of the ship, and, therefore, to introduce in the calculation the effects of the history of the motion. But, I am not sure that these effects are not of importance in the case of a submerged body. You state that in submerged body work a good correlation has been achieved between practice and theory (that is the classical theory, without correction for taking into account the vortex wake generated by the body). I personally have no knowledge of results of comparisons between theory and experiments on models or on full-scale submerged bodies, which permit to conclude in a way or in the other. That is why I should be very grateful to you if you could give me more precise informations about this point.

I was surprised to find that our experiments carried out with the Planar Motion Mechanism show a great influence of the reduced frequency. Before getting these results, I considered the phenomenon as possible, but I did not believe that it could be of such great importance. However, I should like to remind you of the fact that the coefficients are not equally affected. It would be interesting to compare calculated motions with constant coefficients and with variable coefficients. But I have had no time to do it yet.

I have also some doubts about the possibility to deduce the time forces and moments acting on a ship or on a submarine from the forces measured in harmonic motion by use of a planar motion mechanism. But, perhaps the reasons behind our lines of thought are not identical. You seem to consider that your doubts are justified by the fact that the actual motion of a surface ship or a submarine is seldom harmonic; I rather consider that the actual motions of a ship or a submarine are often outside the linear field, and therefore, that the inversion of the Fourier integral becomes either impossible or meaningless.

* * *

Saturday, September 12, 1964

Morning Session

DRAG REDUCTION

Chairman: C. Prohaska

Hydro-Og Aerodynamisk Laboratorium
Lyngby, Denmark

221-249 O - 66 - 59

THE REDUCTION OF SKIN FRICTION DRAG

J. L. Lumley
The Pennsylvania State University
University Park, Pennsylvania

ABSTRACT

A survey and analysis is presented of the various principles which have been suggested to reduce the skin friction drag; a description of some of the techniques for the application of these principles and experimental results are given.

INTRODUCTION

The majority of the drag of a properly streamlined underwater vehicle is skin friction drag resulting from the excessive momentum transport of the turbulent boundary layer. All techniques which have been suggested for the reduction of skin friction drag act to reduce this transport by altering, or preventing the formation of, the turbulent boundary layer. Few of the techniques which we will describe are supported by complimentary experimental and theoretical information; for some, only theory exists; for others only experiment; for a few, there is both, but in conflict. I will try to present here the principles so far as they are known, the results where they are available, and attempt to explain the discrepancies.

CONVENTIONAL TECHNIQUES

General Considerations

Most of the drag reduction techniques which have been suggested involve the stabilization of the laminar boundary layer, and these will be referred to as conventional techniques. The boundary layers in question are always thin relative to some relevant length, and are usually considered, for an examination of stability, as plane parallel flows without inflection points.

In the discussion of the various stabilization techniques which follows, several things must be borne in mind. First, from the work of Klebanoff, Tidstrom and Sargent (1962) it is clear that transition can be caused in a laminar boundary layer at <u>any</u> Reynolds number by a sufficiently violent disturbance—of the order of ten percent of the free stream velocity. It must be anticipated that a laminar boundary layer can be successfully stabilized only in the absence of large disturbances, since once transition has occurred, few stabilization techniques could be expected to have the capacity to reestablish laminar flow downstream of a disturbance.* Disturbances appear either at the boundary, or in the free stream; consequently, great care must usually be exercised to make both as free of disturbances as possible. The only kind of stabilization that appears to be possible, then, is stabilization to small disturbances; that is, the preventing of small disturbances from growing to be big ones. This is what is customarily meant by stabilization.

There are, generally, two types of small disturbances to which laminar boundary layers are unstable. One consists of progressive waves; these are known as Tollmien-Schlichting waves (Lin (1955)). The other consists of streamwise standing vortices; these are known as Taylor-Goertler vortices (see Lin (1955), p. 96). The Taylor-Goertler type of instability only appears where there is concave curvature in the streamwise direction or where a surface is heated with a liquid flow above it in a gravitational field (Goertler (1959)). However, the condition on the curvature in order to assure the appearance of Tollmien-Schlichting waves before Taylor-Goertler ones is quite stringent, and probably few supposedly flat plates satisfy it. Practically without exception, the analyses which indicate a possibility of stabilization have reference only to Tollmien-Schlichting waves. In addition, most of these analyses have reference only to progressive waves in the streamwise direction. While for the ordinary boundary layer Squire's theorem (Lin 1955)) assures us that such waves become unstable first, in some of the situations under discussion, we may not have such assurance. While nearly all of the suggested techniques attempt to control the growth rate of the streamwise progressive waves, at least one (Kramer (1962a)) attempts to prevent the development of three-dimensionality, which appears to be (Klebanoff, Tidstrom & Sargent (1962)) a necessary prelude to transition, while another (Kramer (1962b)) attempts to control what appears to be a secondary instability associated with the developing three-dimensionality (Klebanoff, Tidstrom & Sargent (1962)).

There are distinct differences between discussions of stability on two dimensional bodies and on bodies of revolution. If the diameter of the body is increasing, two conflicting effects are felt. In the first, an increase in diameter means that the boundary layer must be spread over an ever widening area, promoting thinning and altering the profile (much as suction does). It might be expected that this would delay instability beyond the point to which it is already delayed by the favorable pressure gradient usually present on the forward part of a body of revolution. In the second, cross-stream vorticity is being stretched, which, due to the associated increase in intensity, should result in an earlier occurrence of Tollmien-Schlichting instability. There is evidence (Groth (1957)) to indicate that the stretching dominates. The picture is complicated further, however, by the possibility of Taylor-Goertler instabilities in the concave flow near the stagnation point (Goertler (1955), Goertler-Witting (1958)), and by the stretching (and intensification) of vorticity which may be present in the free stream.

*Although probably most will reestablish laminar flow if the disturbance is removed.

Finally, it should be mentioned that, even if the boundary layer can be stabilized in the absence of large disturbances, the wake cannot. The turbulent wake is known (Townsend (1956)) to be subject to large-scale, unsteady organized motions of the character of instabilities, which on a sphere interact strongly with the boundary layer and are responsible for the wandering of a rising free balloon of small size (Scoggins-private communication). It is possible that these motions, which are present in the wake of a streamlined body also, can disturb the supposedly stabilized boundary layer there.

Change of Profile

Of the various stabilization techniques* (see Fig. 1), the first method we will discuss is the alteration of the velocity profile to a more stable one. Roughly speaking, the stability of a profile is increased by an increase of the curvature of the profile, since the lower critical Reynolds number above which small disturbances will grow is monotonic with curvature of the profile at the critical layer. The critical layer is that layer at which the wave velocity and fluid velocities are equal (Lin (1955)). A more exact way of correlating this change in profile is through a shape parameter.

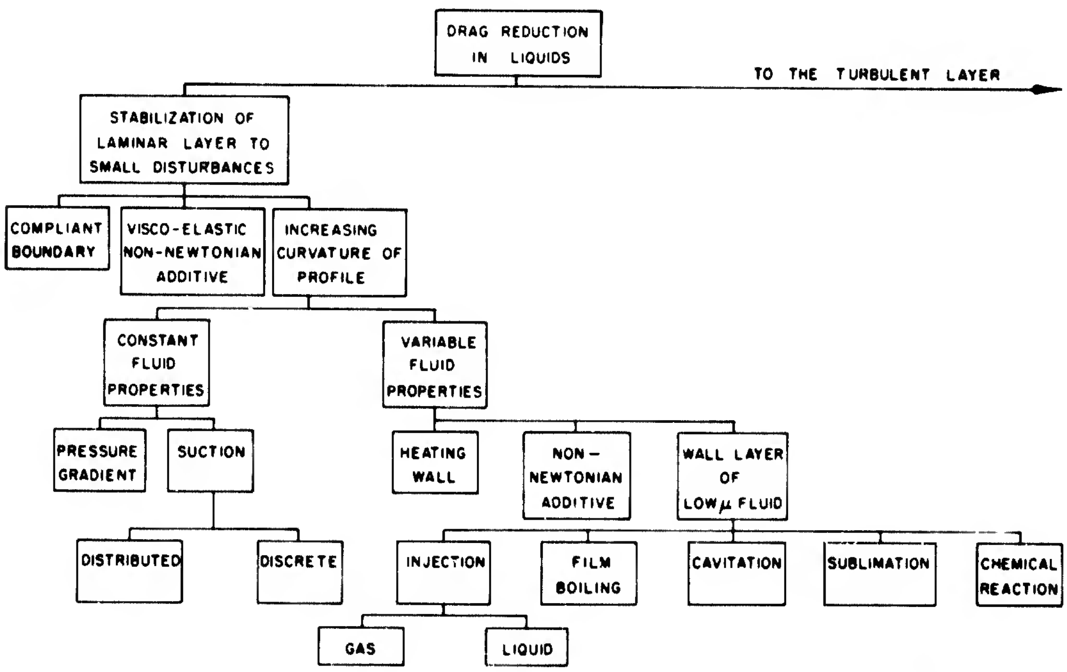

Fig. 1 - Techniques for the stabilization of the laminar layer to small disturbances

*Specific citations will not in general be given; reference should be made to the appropriate section of the bibliography.

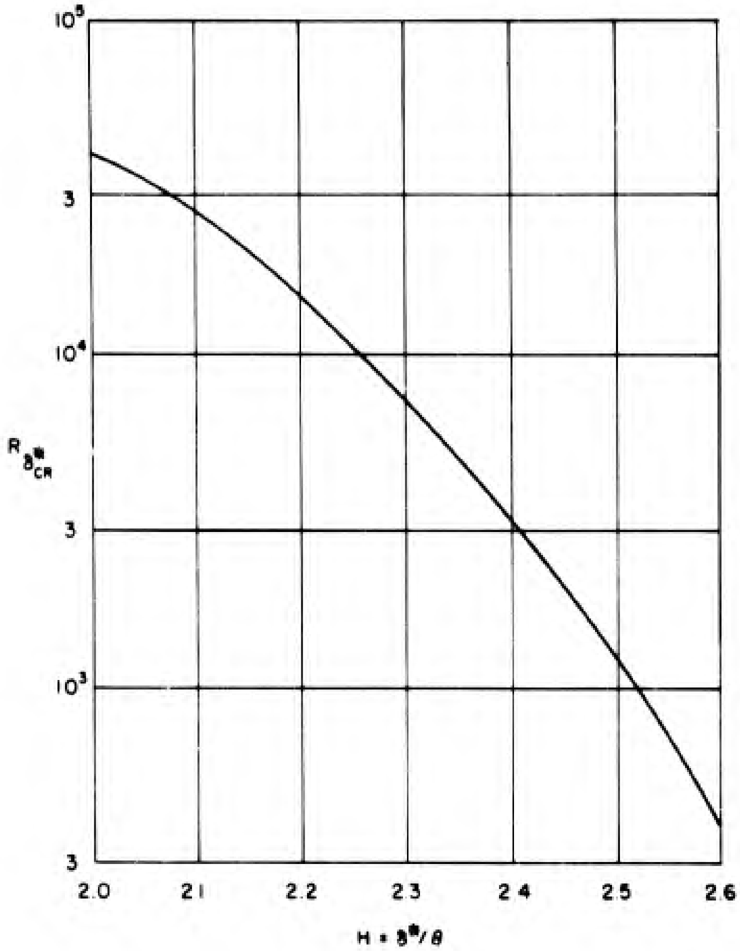

Fig. 2 - Effect of profile change expressed in terms of the ratio of displacement thickness to momentum thickness. (from Lin (1955)).

Figure 2 shows the lower critical Reynolds number versus a shape parameter, the ratio of displacement to momentum thickness. This parameter assumes the value unity for a "square" profile, and increases as the rise to free stream velocity becomes more gentle, reaching a value of roughly 3.5 at separation. While the curve in Fig. 2 was computed specifically for profiles in the presence of pressure gradients and heat transfer at the surface, it is only a slight generalization to speculate that the same curve will describe, at least qualitatively, the effect of other conditions which work principally through a change in profile.

In describing these stabilization methods, it should be remembered that some of them, especially suction, in addition to changing the profile (in a direction to increase the lower critical Reynolds number) may also prevent boundary layer growth, if applied with sufficient intensity. Thus a boundary layer permitted to grow will eventually reach its critical Reynolds number (based on thickness) no matter how delayed by a change in shape. A boundary layer whose growth is prevented may never reach its critical Reynolds number.

The ways in which the profile can be altered can be placed in two categories, depending on whether constant or variable fluid properties are necessary. Under the heading of methods which work with constant fluid properties we can include pressure gradients and suction. The suction may be either distributed, or it may be through discrete slots (see particularly the work of Pfenninger et. al.). Discrete slots are satisfactory so long as the boundary layer is caught by the next downstream slot before disturbances have time to grow to a significant extent. Among the methods that involve variable fluid properties, most are dependent on a variation of the ordinary viscosity μ. An increase of μ with distance from the wall increases the curvature. The viscosity μ can be varied in several ways: in water it can be changed by heating the wall, a film of a different fluid can be placed next to the wall, such as a gas film or a liquid with a lower μ—such a film being produced by injection, film boiling, cavitation, sublimation or chemical reaction. Finally, an additive could be placed in the boundary layer so that the fluid becomes non-Newtonian, in particular "shear-thinning"; then the high shear near the wall will mean a lower μ there and the μ will increase with distance from the wall. It should be mentioned that there is some disagreement as to whether the low μ fluid film should be considered primarily as a stabilization technique; this seems to be largely a matter of taste, and I have taken the position that if it did not stabilize, it would not work, since the low μ fluid would be mixed with the high.

Flexible Boundary

To the best of my knowledge there are only two methods that do not depend on changing the profile; the first of these is the stabilization of the laminar boundary layer by a compliant boundary. This does not damp the disturbances; as a matter of fact, it is a result of the theory (Betchov (1959), Benjamin (1960) Boggs & Tokita (1960), Landahl (1962)) that damping in the wall is in general destabilizing. Rather, the compliant boundary acts to change the phase relations between the pressure and the velocity in the neighborhood of the wall, resulting in an alteration of the Reynolds stresses there, and changing the energy budget of a disturbance. While a passive wall in general changes the lower critical Reynolds number, Betchov (1958) has shown that an active wall may be expected to eliminate it entirely. In a tenuously related investigation Wu (1959), has shown that a suitable active wall can propel.

In Fig. 3 are shown the phase relations induced at the surface by a visco-elastic material, together with the phase relations corresponding to a small disturbance in the region between the inner viscous layer and the critical layer of the laminar boundary layer over a rigid surface. If the former are added to the latter as a first order approximation, the influence on the disturbance Reynolds stress may be seen.

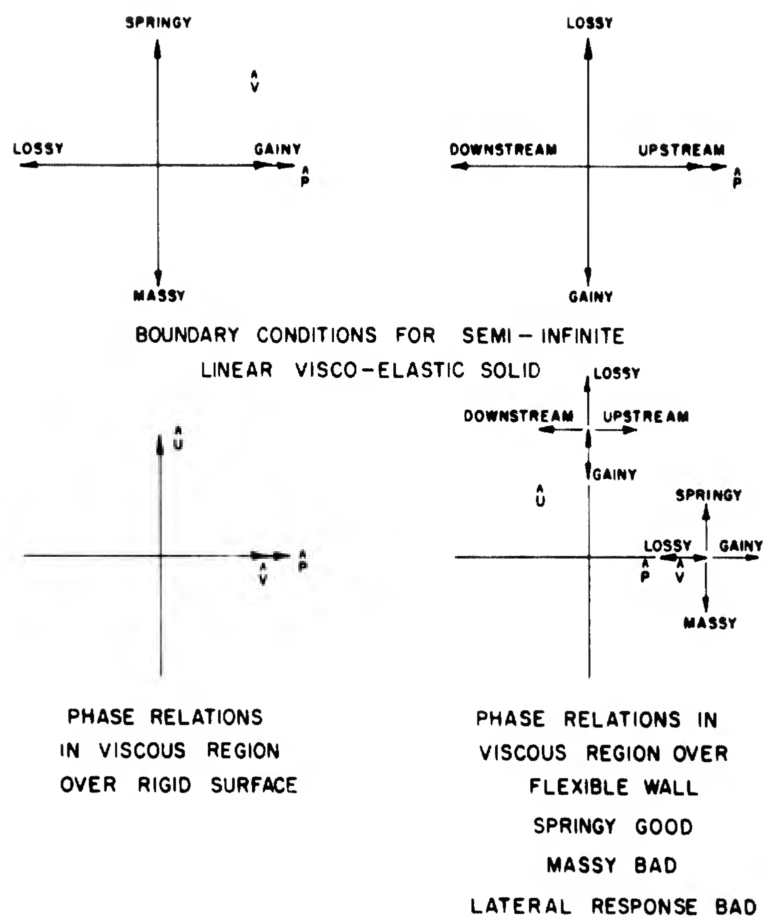

Fig. 3 - Small disturbance phase relations in the laminar boundary layer between the critical layer and the inner viscous layer: first order modification by flexible wall.

Non-Newtonian Additive

The second method not dependent on a change of profile (Giles 1964) depends on the use of a non-Newtonian additive of viscoelastic character. One may expect that if the apparent viscosity to a temporally sinusoidal simple shear increases with frequency, then the flow would be more stable to progressive waves, since the history of a material point involved in such a wave is unsteady. The opposite case is of greater interest for real fluids, and a recent analysis (Wen (1963)) indicates a destabilizing effect, but that may be because a model was used that is not materially objective.

Drawbacks of the Conventional Techniques

Most of these techniques are, or have been, under experimental investigation by various groups and individuals and show some prospects of success, but in most there are difficulties. Many of these difficulties are related to kinds of instability other than those considered in the analysis which suggested the experiment. For instance, with a gas film one has an interfacial instability of the Kelvin-Helmholtz (Lamb (1945)) type. With a heated wall one has a gravitational instability due to the density differences, which can be shown to be analogous to the instability on a wall concave in the streamwise direction (Goertler (1959), Kirchgaessner (1962)). The boundary layer over a flexible surface is subject to two types of instability not present in the boundary layer over a rigid surface (Benjamin (1963)). Furthermore, the difficulties mentioned earlier relative to freedom from disturbances, both at the surface and in the free stream, are not easily overcome. It should be remembered that natural transition due to the growth of small disturbances seldom occurs earlier than a length Reynolds number of 10^5. Simply by removing all the disturbances this figure can be increased by a factor of about twenty-five, but a limit is reached in this direction. It has been suggested by Betchov (1960) that this limit is due to amplified molecular agitation. To achieve a substantial reduction in drag, the length Reynolds number must be increased at least an order of magnitude beyond this. Furthermore, at these high Reynolds numbers the laminar boundary layer is very thin. The requirements on smoothness and in general the tolerances on construction of the surface are proportional to the inverse of the "Reynolds number per foot," and are extremely stringent. If all other disturbances are removed, the velocity field associated with a sound field can disturb the boundary layer, particularly in a gas-liquid combination. This velocity field in a liquid is ordinarily much smaller for a given sound pressure level than in a gas (by the ratio of the values of the product of density and speed of sound), but if there is a gas-liquid interface this does not appear to be true. Considered from all points of view it seems desirable to examine the possibility of altering a turbulent boundary layer so as to reduce the drag. If this can be done then all the difficulties mentioned above are eliminated.

NONCONVENTIONAL TECHNIQUES

General Considerations

Several approaches have been suggested by means of which the turbulent boundary layer may be altered. In order to understand how these may work, it is necessary to recall to mind the physical principles which govern the normal turbulent boundary layer. For simplicity, let us consider the boundary layer with zero pressure gradient. These principles are (cf, Townsend (1956)):

1. Reynolds number similarity: that the turbulence, once fully established, is predominantly inertial in the energy containing range (that part of the spectrum responsible for drag and heat transfer); <u>i.e.</u>,—that the structure of these eddies is essentially independent of viscosity.

2. The "Law of the Wall"—that there is a layer of turbulent fluid near the wall that has no characteristic length scale other than distance to the wall, and that this layer has a single characteristic velocity, and therefore a universal structure. By the first principle, this layer is independent of viscosity, so that the Reynolds stress is constant. Defining the characteristic velocity μ^* as the

root of the kinematic Reynolds stress, and noting that mean velocity differences in the layer also must scale with μ^*, we have $y\bar{\mu}'/\mu^* = 1/K$ a universal constant, which gives immediately the familiar logarithmic law $\bar{\mu}/\mu^* = 1/K \ln y/y_o$, where y_o is a constant yet to be determined.

3. The viscous sublayer—that there is a layer of fluid next to the wall in which dissipation is dominant, in the sense that no disturbance can be in equilibrium there without energy transfer into the layer. The profile of mean velocity there is nearly linear, since the stress is constant, and production of turbulent energy is not important. Phenomena seem superposable in this region (Sternberg (1961)) since the nonlinear convective-production terms are not significant. The thickness of the layer is fixed by the Reynolds number based on thickness. If we set $R = y^*\mu^*/\nu$ as the Reynolds number based on thickness where the sublayer profile, $\bar{\mu}/\mu^* = y\mu^*/\nu$, meets the logarithmic profile (roughly 12.6 in a normal boundary layer) then we can write

$$\bar{\mu}/\mu^* = \left[R - \frac{1}{K}\ln R\right] + \frac{1}{K}\ln\frac{y\mu^*}{\nu}$$

which fixes the value of the constant.

4. "Law of the Wake"—in the outer part of the layer, it is assumed that the profile is similar when referred to local length and velocity scales—$(\bar{\mu} - \bar{U})/\mu^* = f(y/\delta)$ which of course also involves Reynolds number similarity. If it is assumed that there is a region of overlap with the law of the wall, then we obtain the familiar drag law

$$\frac{\bar{U}}{\mu^*} = \left[R - \frac{1}{K}\ln R\right] + \frac{1}{K}\ln\frac{\delta\mu^*}{\nu}$$

This is the relationship which must be changed if the effect on drag of the turbulent boundary layer is to be changed.

Change of Viscosity

Let us now consider ways in which the familiar drag relationship can be changed (see Fig. 4). The simplest which comes to mind is a change of viscosity. This will not change the structure outside the viscous sublayer, since that was dominated by inertia. Therefore it does not matter whether the change in viscosity extends to the fluid outside the sublayer. A change in viscosity will not change the value of R so long as the change is uniform in the sublayer. Hence, any mechanism which changes the viscosity in the viscous sublayer will produce a turbulent boundary layer indistinguishable from a normal turbulent boundary layer at a different length Reynolds number. Since drag is only a weak function of length Reynolds number, this is not a particularly effective way to change drag. The viscosity in the viscous sublayer might be reduced by heating the wall (in a liquid).

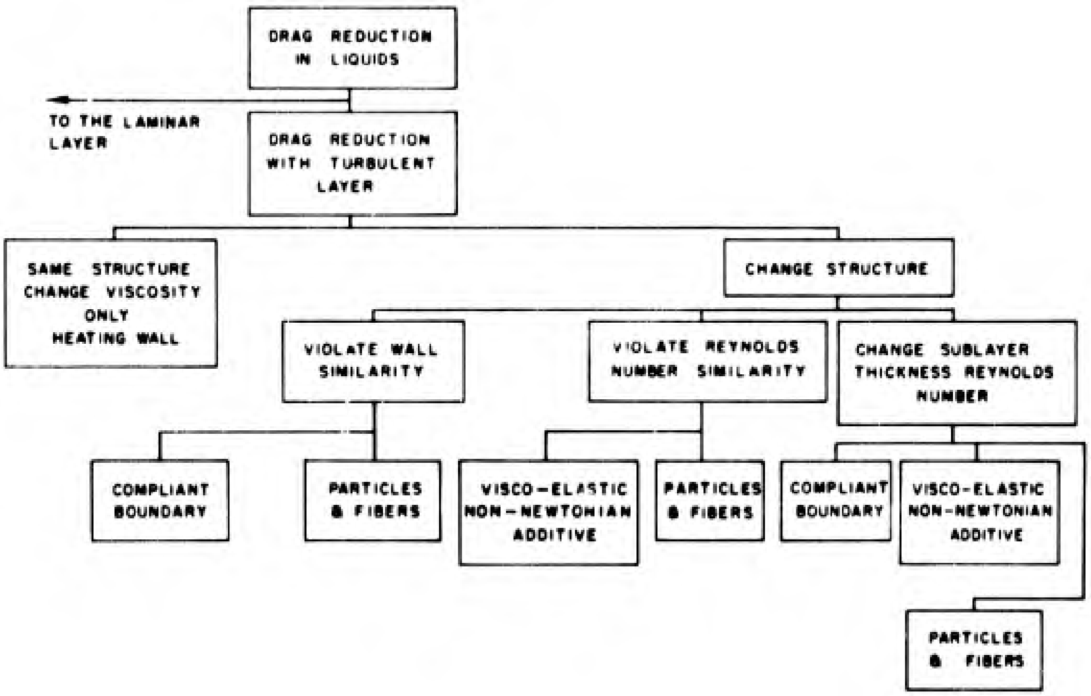

Fig. 4 - Techniques to alter the structure of the turbulent boundary layer

The Nonuniform Sublayer

Some question may be raised about the possibility of having a nonuniform value of ν through the sublayer; it is not difficult to show that for a non-Newtonian fluid of arbitrary constitutive equation in a zero-pressure gradient boundary-layer the viscous shear stress near the wall is constant to terms of third degree in distance from the wall, so that there will be a region of uniform strain rate and hence uniform viscosity. Relations will, of course, not be simple at the outer edge of the sublayer, but it seems unlikely that the picture developed above, which ignores this transition region between sublayer and inertial region (on the grounds that the transition is in a thin layer (Townsend (1956)) can be far wrong.

A hot wall (in a liquid) can produce a temperature (and hence viscosity) variation in the sublayer, if the heat flux is large enough, and a mechanism by which this could reduce drag has been suggested by G. B. Schubauer (private communication). The ratio of the temperature drop in the sublayer to that through the boundary layer is given to first order by (using a two-layer model)

$$\frac{(\Delta T)_{\text{sublayer}}}{(\Delta T)_{\text{boundary layer}}} = \frac{\sigma R_\Delta^* \bar{U}}{1 + R_\Delta^*(\sigma - 1)\,\bar{U}} .$$

At moderate Reynolds numbers (in liquids), most of this drop takes place in the sublayer, and we may take the temperature (and hence the viscosity) at the outer edge of the sublayer as being essentially the free stream value. Then the shear at the outer edge will be nearly that without heating at the same wall stress. If we take the thickness Reynolds number as being determined largely by the shear at the outer edge, then this will be essentially the same (although it may increase somewhat due to the favorable curvature of the profile) so that the thickness will be essentially the same. Thus the whole effect will appear from outside the sublayer as a slip at the wall of value (to first order)

$$\bar{\ }_{s} \quad \frac{R\,{}^{*}}{2}\,\frac{\ }{\ }.$$

Assuming self-preservation, negligible laminar length, and large Reynolds number, we may obtain the effect on * of a change in by this mechanism:

$$\frac{\ }{{}^{*}}\,\frac{d\ {}^{*}}{d} \quad \frac{{}^{*}R}{2U}$$

which is of the order of 1/4 at moderate Reynolds number. The sensitivity of viscosity to temperature in liquids suggests that (at ordinary pressures) changes in * by 20% may be possible before boiling occurs.

It should be mentioned in passing that surface heating in a gravitational field may produce secondary motions which will only increase the momentum transport and the drag.

Change in the Wall Layer

A slightly more sophisticated way in which the principles outlined above could be violated is by a change in the "law of the wall." This could be done by the introduction either of a length scale or of a velocity scale. These are essentially equivalent, since a height can be defined at which the mean velocity equals the velocity scale selected. Thus a new parameter is introduced, say the ratio of * to the new velocity scale. A simple way in which this can be done is by coating the wall with a nonrigid material having a Rayleigh wave speed below the free-stream speed. Then convected fluctuating pressure fields can exchange energy with the wall in the same manner as described by Phillips (1955) for the generation of ocean surface waves by turbulent wind. It is not obvious a priori why such an interchange should necessarily result in a reduction of drag. The random wave motion of the surface would necessarily be associated with dissipation of energy in the surface so that the simple existence of such an interaction would only increase the total dissipation, if it did not drastically alter the structure of the boundary layer so as to reduce the dissipation in the fluid. Again, we have, as before for the laminar layer, that damping in the wall material is probably detrimental, and it seems likely that we will not achieve favorable effects unless the damping in the surface material is considerably smaller than that in the fluid. This is the case for an air boundary layer over water, and P. A. Shepphard (private communication) has observed drag reduction in such boundary layers. Unfortunately, it is more difficult to find wall materials of viscosity lower than water.

Reynolds Number Similarity

Another way in which the boundary layer may be attacked is through the principle of "Reynolds number similarity." Violating this principle is not a straight-forward matter. For instance, if the fluid viscosity is increased, there will be no important change (other than the slow increase in drag associated with the weak dependence on length Reynolds number) until the dissipative and energy-containing scales are nearly equal, at which point the turbulence can no longer extract energy from the mean motion at a sufficient rate to maintain itself, and the flow will become laminar. This would, of course, result in a drag reduction, but falls more properly in the realm of stabilization. One might suggest using a non-Newtonian medium which is shear-thinning. If indeed it behaved as though it had a simple shear-dependent viscosity (Lumley (1964)) it would change nothing. In the high-shear viscous sublayer, its viscosity might be expected to be nearly the value of the solvent; in any event, R would remain unchanged. If the flow outside the sublayer were turbulent, then it would be inertia dominated, and nothing would be changed. Only by increasing the effective viscosity outside the sublayer until the layer became laminar could a change be made, and again this falls more properly under the heading of stabilization. Evidently, in order to influence Reynolds number similarity, it is necessary to have a material whose constitutive equation is such that terms in the energy equation, arising from that part of the stress which is not a pressure, are appreciable in the energy containing range of wave numbers, without being dissipative in character, so as not to turn the turbulence off. That is, they must be non-negligible in the energy containing range of wave numbers without being viscous in character. There is both theoretical (Lumley (1964)) and experimental (see particularly Fabula (1963)) support for the conclusion that only a material having viscoelastic properties can behave in this manner, although the exact mechanism is not understood.

Particles and Fibers

There has been reliable observation of drag reduction in flows containing particles and fibers. Although this effect is described as "damping" the turbulence, the intensities are observed to increase (Elata, Ippen (1961)). From the principle of Reynolds number similarity, we know that a simple change in the mechanism of dissipation, so long as the flow remained turbulent, would be unlikely to change the turbulent structure, since this is determined by inertia. There is a known interaction of suspended particles with the viscous sublayer, which will be described below, but if the observed drag reduction does not arise from this source, then it seems likely that it is due to a violation of Reynolds number similarity by the introduction of other length and time scales. Depending on the ratios of these scales to others in the flow, this may also be regarded as a violation of the law of the wall, of course, since particles having relatively small length or time scales may leave the outer part of the flow unaffected, beginning to exert an influence only as the scales of the energy containing eddies shrink to corresponding size as the wall is approached. Length scales may be introduced in a very direct way by long fibers, while velocity scales may be introduced by the settling velocity (in a gravitational field), and time scales by the characteristic time of the particles (the response time to a step function in relative velocity). The mechanism associated with this latter may be similar to viscoelasticity, since a particle of long characteristic time in a flow of short time scale will tend to remain motionless as the flow sloshes past it. Thus an unsteady fluid motion will be more dissipative than a steady one, as in a viscoelastic fluid having an effective viscosity increasing with the frequency of a temporally sinusoidal simple shear.* The particles will tend to store energy associated with steady, organized motions (steady from a Lagrangian viewpoint) and to oppose unsteady motion. This was probably first mentioned by Saffman (1962). See also Hino (1963).

The presence of particles, or colloidal suspensions, can of course, be even more effective if the suspended material tends to combine with itself to form elastic structures capable of resisting small shear. This is possible with Bentonite, and may explain observations in flocculated thoria (Eissenberg and Bogue (1963)) and in flows of fine aqueous suspensions of wax-laden oil droplets. The suspended material then behaves somewhat as a Bingham-Plastic and need not depend on a long time constant to make unsteady motions of the fluid more dissipative than steady ones at low shear.

Changing the Sublayer

Finally, we may change the boundary layer by changing R. The effect of a small change in R at constant $\bar{U}x/\nu$ is given by

$$\frac{R}{u_*}\frac{du_*}{dR} = \frac{u_*}{\bar{U}}\left(\frac{1}{\kappa} - R\right)$$

obtained by differentiating the expression for drag, assuming self-preservation, negligible laminar length, and indefinitely large Reynolds number. At the value of R associated with the normal turbulent boundary layer, this is negative, and of the order of one half.

R may be changed in a number of ways. If a viscoelastic medium is used, the effective viscosity of which in a temporally sinusoidal simple shear increases with frequency, we may expect that a disturbance which is unsteady (from the Lagrangian viewpoint) will be more dissipative than would be indicated by the viscosity at the steady shear rate. Since R (based on the steady state viscosity) is determined by that thickness below which all disturbances must import energy, we may expect R to be increased.* In a similar way, particles may be introduced in the sublayer. If their time scale is large they also will make unsteady motions more dissipative and thus increase R. If they can form elastic structures, like flocculated thoria, (Eissenberg & Bogue (1963)), the effect is even more pronounced. If the time and length scales are such that the energy containing eddies in the turbulent flow outside the sublayer are unaffected, then the familiar "law of the wall" will remain, κ will be unaffected, but the logarithmic part of the profile will be displaced upward. This effect is illustrated by Fig. 5, the mean velocity profile in a flow containing a low concentration of flocculated thoria, reproduced from Eissenberg and Bogue (1963).

*But real viscoelastic media appear to display the opposite behavior.

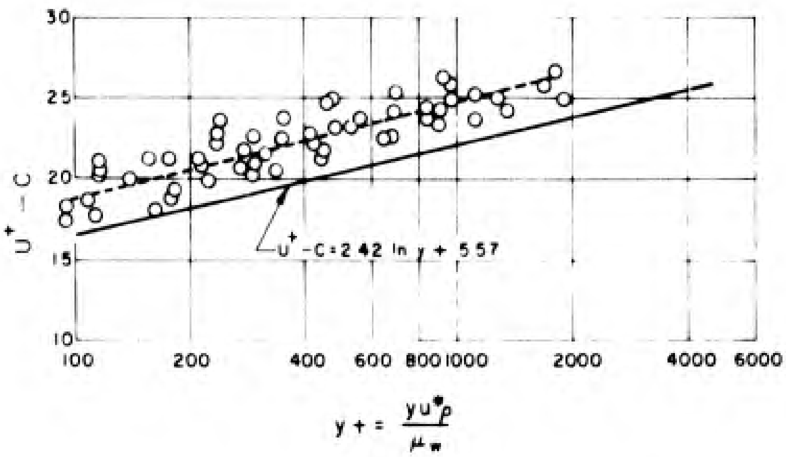

Fig. 5 - Velocity profile in the wall layer in flow of flocculated thoria, from Eissenberg and Bogue (1963). Nondimensionalization by shear velocity with small empirical correction c. Solid line is Newtonian profile.

Another method of changing R, suggested by G. F. Wislicenus (private communication) is to change the boundary condition, by making the surface flexible. Again, the action of such a surface depends in a detailed way on changing the phase relationships, and thus the Reynolds stress. To make this distinct from the violation of the law of the wall mentioned above, we must have the wave speed in the wall well above the free-stream speed. A detailed analysis based on energy considerations (Lumley and McMahon (1964)) shows that the situation is rather complicated, due to the fact that, although over a rigid wall no small disturbance can extract energy from a linear profile fast enough to maintain itself, while some large ones can, this is no longer true over certain flexible walls. Thus, while the wall changes the energy budget of large disturbances, it also provides a mechanism* by which small disturbances can extract energy. In Fig. 6 are shown the phase relationships calculated for small disturbances. It can be seen that, for this wall material, there is always a wave whose speed is such that it can extract energy. Evidently only a wall which is prevented from moving laterally is worth examining.

Conclusions

This outline has surely not exhausted the possibilities of changing (or eliminating) momentum transport in a turbulent boundary layer. For example, we have not discussed the possibility of influencing transition by oscillations of the

*Similar to Rayleigh wave propagation in the wall--the class B waves of Benjamin (1963).

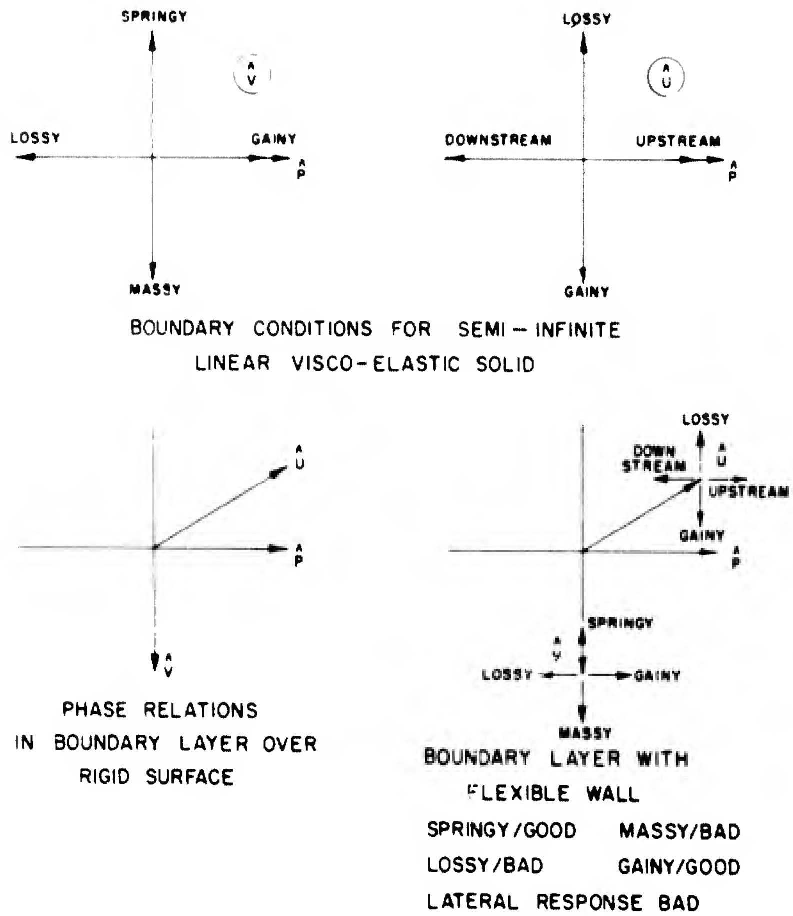

Fig. 5 - Small disturbance phase relations in a viscous region near the wall: first-order modification by flexible wall.

surface (Miller) & Fejer (1964)).* Detailed, qualitative experimental data on any technique is relatively sparse, as sparse, say, as equally detailed theory. Probably most is known about and greatest success has been achieved with suction through slots and the Toms phenomenon. The mechanism of the former is clear, though the mechanism of the latter is far from being so. If another speculation may be added to a growing list, it seems quite possible that we may learn more about the ordinary turbulent boundary layer by examining the effects of various changes; it is at least clear that there are interesting areas here for investigation.

*Nor have we discussed blowing, and other means of artifically thickening the turbulent boundary layer, since it does not seem obvious that one can recover the work done to thicken the layer.

ACKNOWLEDGMENTS

Many of the ideas embodied in this paper have grown from, and benefitted by, discussions with workers in the field; it is a pleasure to acknowledge this necessarily rather diffuse debt, although I take full responsibility for the form of the ideas as presented here. I am particularly grateful to my colleagues Drs. Hoult and Margolis for numerous comments and suggestions. The bibliography is not intended to be exhaustive, and represents a very personal selection from among those papers of which I was aware, and those which were brought to my attention by workers in this area; for this latter I am grateful. I am grateful to the author involved and to the Cambridge University Press and the American Institute of Chemical Engineers for permission to reproduce figures two and six respectively.

REFERENCES

1. General

Betchov, R. B. (1959), "Simplified Analysis of Boundary Layer Oscillation," Rept. No. E529174, Douglas Aircraft Co.

Betchov, R. B. (1960), "Thermal Agitation in Turbulence," STL/TR-60-0000 AE 279, Physical Research Lab., Space Technology Lab., Inc.

Brown, W. B. (1955), "Extension of the Exact Solution of the Orr-Sommerfeld Stability Equation to Reynolds Numbers of 4000," Northrop Corp., Norair Div., R NAI-58-73 (BLC-78).

Brown, W. B. (1959), "Numerical Calculation of the Stability of Cross-Flow Profiles in Laminar Boundary Layers on a Rotating Disc and on a Sweptback Wing and an Exact Calculation of the Stability of the Blasius Profile," Northrop Corp., Norair Div., R NAI-59-5 (BLC-117).

Granville, P. S. (1963), "Effect of Fluid Injection on Drag of Flat Plates at High Reynolds Number," Inst. Shipbldg. Progress, V. 10, No. 101, p. 30-33, Jan. 1963.

Gray, W. E. and Rullam, P. (1950), "Comparison of Flight and Tunnel Measurements of Transition on a Highly Finished Wing (King Cobra) RAE TN 2383."

Goertler, H. (1955), "Dreidimensionale Instabilitant der ebenen Staupunktstroemung gegenueber wirbelartigen Stoerungen, 50 Jahre Grenzschichtforschung," (H. Goertler, W. Tollmien, ed.) Vieweg, Braunschweig. p. 304.

Goertler, H. and Witting, H. (1958), "Theorie der sekundaeren instabilitaet der laminaren Grenzschichten, Boundary Layer Research," (H. Goertler, ed.) Springer-Verlag, Berlin, p. 77.

Goertler, H. (1959), "Ueber eine Analogie zwischen der Instabilitaeten laminarer Grenzschicht-Stroemungen an konkoven Waenden und an erwarmten Waenden," Ingeneur - Archiv 28 (Grammel Anniversary Issue) p. 71.

Groth, E. E. (1957), "Boundary Layer Transition on Bodies of Revolution," Northrop Corp., Norair Div., R NAI-57-1162 (BLC-100).

Klebanoff, P. S., Tidstrom, K. D. and Sargent, L. M. (1961), The Three-Dimensional Nature of Boundary Layer Instability," J. Fluid Mech. 12.

Kirchgaessner, K. (1962), "Einige Beispiele Zur Stabilitaets Theorie von Stroemungen an konkoven und erwarmten waender," Ingenienr-Archiv 31, p. 115.

Kuethe, A. M. (1957), "On the Stability of Flow in the Boundary Layer Near the Nose of a Blunt Body," Rand Corp., R. RM-1972.

Kulin, G. and Pao, Y. H. (1961), "Boundary Layer Stability on Blunt Nosed Bodies of Revolution," TR007-1, Hydronautics, Inc.

Lamb, H. (1945), "Hydrodynamics," Dover Publications, New York.

Lin, C. C. (1955), "The Theory of Hydrodynamic Stability," Cambridge, The University Press.

Miller, J. A. and Fejer, A. A. (1964), "Transition Phenomena In Oscillating Boundary Layer Flows," Journal of Fluid Mechanics, 18, p. 438-448.

Raetz, G. S. (1957), "A Method of Calculating Three-Dimensional Laminar Boundary Layers of Steady Compressible Flows," Northrop Corp., Norair Div., R. NAI-58-73 (BLC-114).

Siegel, R. and Shapiro, A. H. (1953), "The Effect of Heating on Boundary Layer Transition for Liquid Flow in a Tube," ASME Paper No. 53-A-178.

Sternberg, J. (1962), "A Theory for the Viscous Sublayer of a Turbulent Flow," J. Fluid Mech., 13, p. 241.

Townsend, A. A. (1956), "The Structure of Turbulent Shear Flow," Cambridge, The University Press.

2. Suction

Anon (1952), "Experiments on Distributed Suction Through a Rough Porous Surface," Cambridge Aero. Lab., Aero. Res. Council, C. P. 84.

Bacon, J. W., Jr., et. al. (1959), "Experiments on a 30° Swept 12% Thick Symmetrical Laminar Suction Wing in the 5 ft. by 7 ft. University of Michigan Tunnel," Northrop Corp., Norair Div., R. NOR-59-328 (BLC-119).

Braslow, Burrows, Tetervin, Visconti (1951), "Studies of Area Suction for the Control of the Laminar Boundary Layer on an NACA G4A010 Airfoil," NACA R 1025.

Burrows, D. L. and Schwartzberg, M. A. (1952), "Experimental Investigation of an NACA G4A010 Airfoil Section with 46 Suction Slots on Each Surface for Control of Laminar Boundary Layer," NACA TN 2644.

Carmichael, B. et. al. (1957), "Low Drag Boundary Layer Suction Experiments in Flight on the Wing Glove of an F-94A Airplane. Phase IV - Suction Through 81 Slots Between 8% and 95% Chord," Northrop Corp., Norair Div., R. NAI-57-1025 (BLC-102).

Dannenberg, R. E. and Wesberg, J. A. (1952), "Section Characteristics of a 10.5% Thick Airfoil With Area Suction as Affected by Chordwise Distribution of Permeability," NACA TN E847.

Gault, S. E. (1958), "An Experimental Investigation of Boundary Layer Control for Drag Reduction of a Swept Wing Section at Low Speed and High Reynolds Number," NASA TN D-320.

Goldsmith, J. (1956), "Investigation of the Flow in a Tube with Laminar Suction Through 80 Rows of Closely Spaced Holes," Northrop Corp., Norair Div., R. NAI-56-293 (BLC-86).

Goldsmith, J. (1958), "Preliminary Experiments on the Maintenance of Laminar Flow by Means of Suction in the Region of a Wing Leading Edge and Fuselage Juncture," Northrop Corp., Norair Div., R. NAI-58-249 (BLC-106).

Goldsmith, J. (1959), "Experiments with Laminar Flow Near the Juncture of a Fuselage and Wing Trailing Edge," Northrop Corp., Norair Div., R. NOR-59-306, (BLC-120).

Gross, L. W. (1962), "Investigation of a Peichardt Body of Revolution with Low Drag Suction in the Norair 7 × 10 ft. Wind Tunnel," Northrop Corp., Norair Div., R. NOR-62-126 (BLC-143).

Groth, E. E. et. al. (1957), "Low Drag Boundary Layer Suction Experiments in Flight on the Wing Glove of an F-94A Airplane, Phase II - Suction Through 69 Slots," Northrop Corp., Norair Div., R. NAI-57-318 (BLC-94).

Groth, E. E. (1958), "Low Speed Wing Tunnel Experiments on a Body of Revolution with Low Drag Boundary Layer Suction," Northrop Corp., Norair Div., R. NAI-58-335 (BLC-107).

Jones, and Head, (1951), "The Reduction of Drag by Distributed Suction," Proc. 3rd Anglo-American Aeronautical Conf. Brighton.

Lang, T. G., and Brooks, J. D., (1959), "Control of Torpedo Boundary Layers by Suction," U.S.N.O.T.S. NAVORD 6536.

Libby, P. A., Kaufman, L. and Harrington, R. P. (1952), "An Experimental Investigation of the Isothermal Laminar Boundary Layer on a Porous Flat Plate," J. Aero. Sci., 19, p. 127.

Loftin, L. K. and Horton, E. A. (1952), "Experimental Investigation of Boundary Layer Suction Through Slots to Obtain Extensive Laminar Boundary Layers on a 15% Thick Airfoil Section," NACA RM L52D02.

Parkhurst, R. C. (1955), "Recent British Work on Methods of Boundary Layer Control," Proc. Symp. "Boundary Layer Effects in Aerodynamics," Nat. Phys. Lab., Teddington.

Pfenninger, W. (1953), "Experiments with a 15% Thick Slotted Laminar-Suction Wing Model in the TDT Tunnel at NACA Langley Field," AFTR 59082 WADC.

Pfenninger, W. et. al. (1954), "Investigation of Laminar Flow in a Tube at High Reynolds Numbers and Low Turbulence With Boundary Layer Suction Through 80 Slots," Northrop Corp., Norair Div., R BLC-53.

Pfenninger, W. et. al. (1957), "Experiments on a 30° Swept 12% Thick Symmetrical Laminar Suction Wing in the 5 ft. by 7 ft. Michigan Tunnel," Northrop Corp., Norair Div., R. NAI-57-317 (BLC-93).

Raetz, G. S. (1953), "The Incompressible Laminar Boundary Layer on an Infinitely Long Swept Suction Wing with a Few Different Pressure and Suction Distribution," Northrop Corp., Norair Div., R. (BLC-14).

Raetz, G. S. (1953), "The Incompressible Laminar Boundary Layer on an Infinitely Long Swept Wing with Continuous Suction from the 0.37 Chord Line to the Trailing Edge," Northrop Corp. Norair Div., R. (BLC-25).

Raetz, G. S. (1953), "A Method of Calculating the Incompressible Laminar Boundary Layer on Infinitely Long Swept Suction Wings Adaptable to Small-Capacity Automatic Digital Computers," Northrop Corp., Norair Div., R. (BLC-11).

Raetz, G. S. (1954), "The Incompressible Laminar Boundary Layer on a Typical Tapered Swept Suction Wing," Northrop Corp., Norair Div., R. (BLC-21).

Schlichting, H. (1949), "An Approximate Method for Calculation of the Laminar Boundary Layer with Suction for Bodies of Arbitrary Shape," NACA TN 1216.

von Doenhoff, A. E. and Loftin, L. K., Jr. (1949), "Present Status of Research on Boundary Layer Control," J. Aero. Sci., 16, p. 729.

3. Gas Films

Afify, E. (1960). "On the Hydrodynamic Stability of a Gas-Water Interface," TRW ST M 142, Thompson-Ramo-Woolridge, Inc.

Aifify, E. (1959), "The Closed Analytic Solution of the Water Boundary Layer with a Gas Film on a Flat Plate," TRW-STM-83, Thompson, Ramo-Wooldridge, Inc.

Bradfield, W. S., Barkdoll, R. O. and Byrne, J. T. (1962), "Some Effects of Boiling on Hydrodynamic Drag," International Journal of Heat and Mass Transfer 5, 615.

Bullock, R. D. (1962), "An Experimental Investigation of the Use of Air to Reduce the Viscous Drag of a Flat Plate in Water," B. M. E. Thesis, University of Delaware.

Cess, R. D., Sparrow, E. M. (1961a), "Film Boiling in a Forced Convection Boundary Layer Flow," J. of Heat Transfer, 83, p. 370.

Cess, R. D., Sparrow, E. M. (1961b), "Subcooled Forced-Convection Film Boiling on a Flat Plate," J. of Heat Transfer, 83, p. 377.

Eichenberger, H. P. and Offutt, J. D. (1961), "About Gas Film Drag Reduction," ASME Paper 61-WA-218.

Johnson, V. E. and Ramick, T. A. (1961), "Drag Coefficients of Parabolic Bodies of Revolution Operating at Zero Cavitation Number and Zero Angle of Yaw," NASA TR R-86.

Krasnoff, E. (1962), "Equilibrium Gas-Water Boundary Layers," TRW ER 5101 Thompson-Ramo-Wooldridge, Inc.

Krasnoff, E. (1959), "Momentum Integral Approximation of a Gas-Water Boundary Layer on a Flat Plate," TRW STM-78 Thompson-Ramo-Wooldridge, Inc.

Krasnoff, E., et. al. (1961), "Preliminary Investigations of a Gas Film Hydrofoil," TRW ER 4317 Thompson-Ramo-Wooldridge, Inc.

Maeder, P. and Krosnoff, E. (1959), "Preliminary Study of Water Boundary Layer Stabilization by Gas Injection" TRW-STM-47, Thompson-Ramo-Wooldridge, Inc.

Offutt, J. D. (1962), "Gas Film Boundary Layer Stabilization Feasibility Demonstration," Final Report, ER-5110, Thompson-Ramo-Wooldridge, Inc.

Offutt, J. (1959), "Gas Film Distribution on a Torpedo Body with No Suction TRW STM-128." Thompson-Ramo-Wooldridge, Inc.

Pao, Y. H. (1961), "Viscous Flow Along a Surface with Gas Lubrication," TR-007-2, Hydronautics, Inc.

Sparrow, E. M., et. al. (1962), "A Two Phase Boundary Layer and its Drag Reduction Characteristics," TR ASME, J. Appl. Mech., p. 408.

Stefan, H. G. and Anderson, A. G. (1964), "Cavity Formation and Associated Drag in Supercavitating Flow Over Wedges in a Boundary Layer," Rept. No. 69, U. of Minnesota, St. Anthony Falls Hydraulic Lab.

Stoller, H. M. (1963), "Experimental Investigation of Gas Lubricated Water Boundary Layers," TR-007-3, Hydronautics, Inc.

Wilson, M. B. (1964), "An Experimental Study of a Cavity-Running Body," TR-007-4, Hydronautics, Inc.

4. Flexible Surfaces

Becker, E. ( ), "The Laminar Incompressible Boundary Layer Over a Plane Wall Deformed by Traveling Waves," Deutsche Versuchsanstalt fur Luftfahrt, Muelheim on der Ruhr.

Benjamin, T. B. (1963), "The Threefold Classification of Unstable Disturbances in Flexible Surfaces Bounding Inviscid Flows," J. of Fluid Mechanics, 16. p. 436.

Benjamin, T. B. (1960), "Effects of a Flexible Boundary on Hydrodynamic Stability," J. of Fluid Mechanics, 9, 513.

Boggs, F. W. and Frey, H. R. (1961)," The Effect of a Lamiflo Coating on a Small Planning Hull having Zero Dead Rise," U. S. Rubber Co. Res. & Dev. Rep.

Boggs, F. W., Frey, H. R. and Hahn, E. R. (1962), "Construction and Testing of Coatings for Drag Reduction," U. S. Rubber Co.

Boggs, F. W. and Tokita, N. (1960), "A Theory of the Stability of Laminar Flow Along Compliant Plates," Proc. 3rd Symp. Naval Hydrodynamics.

Galway, R. D. (1963), "An Investigation into the Possibility of Laminar Boundary Layer Stabilization Using Flexible Surfaces," M. Sc. Thesis, Queen's Univ., Belfast, Ireland.

Gregory, N. (1960), "The Present Position of Research on the Maintenance of Laminar Flow Over Flexible Surfaces," ARC. 22, 293-F.M. 3014-Perf. 1939.

Gregory, N. and Love, E. M. (1961), "Progress Report on an Experiment on the Effect of Surface Flexibility on the Stability of Laminar Flow," ARC Rept. 23314, F. M. 31136, Pef. 3053.

Harris, F. D. and Price, J. F. (1962), "Effect of a Flexible Wall on the Stability of a Poiseuille Flow," Physics of Fluids 5, p. 365.

Haines, F. D. and Price, J. F. ( ), "Stability of Plane Poiseuille Flow Between Flexible Walls," Proc. 4th U. S. National Congress Appl. Mech.

Kane, J. (1963), "The Propagation of Rayleigh Waves Past a Fluid Loaded Boundary," J. Math. Phys. 41, p. 179.

Karplus, H. B. (1963), "Turbulent Flow Transition Near Solid and Flexible Boundaries," Ill. Inst. Tech. Rept. No. IITRI 1205-4.

Kramer, M. O. (1962), "Boundary Layer Stabilization by Distributed Damping," Naval Engineers Journal, 74, p. 341-8.

Kramer, M. O. (1962), "Material Requirements for Boundary Layer Stabilizing Coatings—Water Application," Rand Corp. Memo., No. RM-3018-PR.

Kramer, M. O. (1961), "Dolphin's Secret," J. Am. Soc. Naval Eng's. 73, p. 103.

Kramer, M. O. (1962b), "Speculative Consideration on High-Frequency Instability of the Laminar Boundary Layer and its Effect on the Design of Stabilizing Coatings," Memo. RM-3284-PR, Rand Corp.

Kramer, M. O. (1960), "Boundary Layer Stabilization by Distributed Damping," J. Am. Soc. Naval Eng's. 72.

Kramer, M. O. (1957), "Boundary Layer Stabilization by Distributed Damping," J. Aer. Sci. 24.

Landahl, M. T. (1962), "On the Stability of a Laminar Incompressible Boundary Layer over a Flexible Surface," J. F. Mech. 13, p. 608.

Lang, T. G. (1963), "Porpoises, Whales and Fish: Comparison of Predicted and Observed Speeds," Nav. Eng'rs. J. 75.

Lang, T. G., Daybell, D. (1963), "Porpoise Performance Tests Conducted in a Seawater Tank," U.S.N.O.T.S. NAVWEPS 8060.

Laufer, J. and Maestrello, T. (1963), "The Turbulent Boundary Layer Over a Flexible Surface," Document D6-9708 Boeing Co.

Lumley, J. L. and McMahon, J. F. (1964), "Stability of Plane Couette Flow Over an Admissive Boundary." In preparation.

Mercer, A. G. (1962), "Turbulent Boundary Layer Flow Over a Flat Plate Vibrating with Transverse Standing Waves," U. Minn., St. Anthony Falls Hydr. Lab. Tech. Paper 41, Ser. B.

Nonweiler, T. R. F. (1961), "Qualitative Solutions of the Stability Equation for a Boundary Layer in Contact with Various Forms of Flexible Surface," ARC. 22, 670-FM3071.

Phillips, O. M. (1957), "On the Generation of Waves by Turbulent Wind," J. Fluid Mech. 2, p. 417.

Rae, W. J. and Moore, F. K. (1960), "On the Inviscid Stability of the Boundary Layer on a Flexible Wall," Cornell Aero Lab. Rep. No. AF-1285-A-5.

Ritter, H., Messum, T. T. (1964), "Water Tunnel Measurement of Turbulent Skin Friction on Six Different Compliant Surfaces of 1 ft. length," ARL/G/N9, Admiralty Res. Lab.

Ritter, H. and Porteous, J. S. (1963), "Water Tunnel Measurements of Skin Friction on a Compliant Coating," ARL/G/N8, Admiralty Res. Lab.

Smith, L. L. (1963), "An Experiment on Turbulent Flow in a Pipe with a Flexible Wall," Masters Thesis, U. of Wash., Seattle, College of Engineering.

Williams, J. E. Ffowcs (1964), "Reynold Stress Near a Flexible Surface Responding to Unsteady Air Flow," Bolt, Beranek & Newman, Report No. 1138.

Wu, T. Y. (1961), "Swimming of a Waving Plate," J. of Fluid Mech. 10. p. 321-345.

5. Non-Newtonian Fluids

Anon (1963), "The Effects of One Non-Newtonian Additive on the Speed of a MSB Minesweeper," Westco Research, Dallas, Texas.

Bayless, L. E. (1960), "The Anomalous Viscosity of Blood. Flow Properties of Blood," ed. Copley and Stainsby, Pergamon, p. 29.

Crawford, H. R., Pruitt, G. T. (1962), "Rheology and Drag Reduction of Some Dilute Polymer Solutions," U.S.N.O.T.S. Rept. N60530-6898.

Davies, C. N. (1949), "Discussion of Papers by Oldroyd and Toms," Proc. Int'l. Cong. Rheo. III. p. 47.

Dever, C. D., Harbour, R. J. and Seifert, W. F. (Assignors to Dow Chemical Co.) (1962), "Method of Decreasing Friction Loss in Flowing Fluids," U.S. Patent No. 3,023,760.

Dodge, D. W. and Metzner, A. B. (1960), "Turbulent Flow of Non-Newtonian Systems," Am. Inst. Chem. Eng. 5. p. 189.

Eisenberg, D. M. and Bogue, D. C. (1963), "Velocity Profiles of Thoria Suspensions in Turbulent Pipe Flow," A.I.Ch.E. Reprint, Symposium on Non-Newtonian Fluid Mechanics I.

Fabula, A. G. (1963), "The Toms Phenomenon in the Turbulent Flow of Very Dilute Polymer Solutions," Proc. 4th Int. Cong. Rheo. Brown.

Fabula, A. G., Hoyt, J. W. and Crawford, H. R. (1963), "Turbulent-Flow Characteristics of Dilute Aqueous Solutions of High Polymers," Bull. Amer. Phys. Soc. 8. p. 430.

Fabula, A. G., Hoyt, J. W. and Green, J. H. (1964), "Drag Reduction Through the Use of Additive Fluds," U.S.N.O.T.S., NAVWEPS 8434.

Gadd, G. E. (1963), "The Effect on the Turbulent Boundary Layer of Adding Guar Gum to the Water in Which a Disk Rotates," Ship T.M., 42 National Physical Lab., Ship Div.

Giles, W. B. (1964), "Laminar Viscoelastic Boundary Layers with Roughness," G. E. Advanced Technology Labs., Rept. No. 64GL51.

Granville, P. S. (1962), "The Frictional Resistance and Boundary Layer of Flat Plates in Non-Newtonian Fluids," J. Ship Res., 6, p. 43.

Hamill, P. A. (1964), "A Preliminary Experiment on the Effect of Additives on Hydrodynamic Drag," National Research Council of Canada, Div. of Mech. Eng'g., Ship Sect. Lab. Memo MTB65.

Hanks, R. W. (1963), "Laminar-Turbulent Transition for Fluids with Yield Stress," A.I.Ch.E.J. V. 9, No. 3, p. 306-309.

Hoyt, T. W. and Fabula, A. G. (1963), "Frictional Resistance in Towing Tanks," Proc. 10th International Towing Tank Conf.

Lindgren, E. Rune (1959), "Liquid Flow in Tubes III: Characteristic Data of the Transition Process," Arkivför Fysik 16, p. 101.

Lumley, J. L. (1964), "Turbulence in Non-Newtonian Fluids," Phys. of Fluids, 7, p. 335.

Lummus, J. L., Randall, B. V. (1964), "Development of Drilling Fluid Friction Additives for Project Mohole," Pan American Petroleum Corporation, Research Department, F64-P-54/295-3(4) Job #3918.

Merrill, E.W., Mickley, H. S. and Ram, A. (1962), "Degradation of Polymers in Solution Induced by Turbulence and Droplet Formation," J. Polymer Sci. 62. S109.

Oldroyd, J. G. (1948), "A Suggested Method for Detecting Wall-Effects in Turbulent Flow Through Tubes," Proc. Int'l. Cong. Rheo. II. p. 130.

Pruitt, G. T., Crawford, H. R. (1963), "Drag Reduction Rheology and Capillary End Effects of Some Dilute Polymer Solutions," U.S.N.O.T.S. Rept. 60530-8250.

Ripken, J. F. and Pilch, M. (1963), "Studies of the Reduction of Pipe Friction with the Non-Newtonian Additive CMC," Univ. of Minnesota, St. Anthony Falls Hydraulic Res. Lab. Tech. Rep. #42, Series B.

Savins, J. G. (1963), "Drag Reduction Characteristics of Solutions of Macromolecules in Turbulent Pipe Flow," A.I.Ch.E. Preprint, Symposium on Non-Newtonian Fluid Mechanics I, Houston, Texas.

Shaver, R. G. and Merrill, E. W. (1959), "Turbulent Flow of Pseudoplastic Polymer Solutions in Straight Cylindrical Tubes," A.I.Ch.E. Journal 5, p. 181.

Thurston, S. and Jones, R. D. (1964), "Experimental Model Studies of Non-Newtonian Soluble Coatings for Drag Reduction," AIAA Bulletin 1 (May), p. 225 (abstract only).

Toms, B. A. (1949)," Some Observations on the Flow of Linear Polymer Solutions Through Straight Tubes at Large Reynolds Numbers," Proc. Int'l Cong. Rheo. II, p. 135.

Wen, K. S. (1963), "On the Stability of a Laminar Boundary Layer for a Maxwellian Fluid," General Electric Space Sciences Laboratory Tech. Inf. Series R63SD102.

6. Particles and Fibers

Anon (1963), "Effect of Stationary Fibers on Drag Reduction," Westco Research.

Bugliarello, G. and Daily, J. W. (1961).

Tech. Assoc. Pul. Paper, Ind. 44 p. 881.

Chien, N. (1956), "The Present Status of Research on Sediment Transport," Transactions ASCE, 121, p. 883.

Daily, J. W. and Chu, T. K. (1961), 'Rigid Particle Suspensions in Turbulent Shear Flow: Some Concentration Effects," Tech. Rept. No. 48, MIT Hydro. Lab.

Einstein, H. A. and Chien, N. (1952), "Second Approximation of the Suspended Load Theory," 47, 2, Univ. of Calif.

Elata, C. and Ippen, A. T. (1961), "The Dynamics of Open Channel Flow with Suspensions of Neutrally Buoyant Particles," MFT Hydro. Lab. Tech. Rep. 45.

Hino, M. (1963), "Turbulent Flow with Suspended Particles," J. Hydraulics Div. ASCE 89, p. 161.

Ismail, H. M. (1952), "Turbulent Transfer Mechanism and Suspended Sediment in Closed Channel," Transactions, ASCE, 117, p. 409.

Murota, A. (1953), "On the Relation Between the Concentration of Suspended Sediment and the Velocity Distribution of Water Flow," J. Japan Soc. Civil Engineers, 38, p. 8.

Nino, M. (1962), "Changes in Turbulent Structures of Flow with Suspension of Solid Particles," Proceedings, 7th Conf. on Hydr. Res., Hydr. Committee, Japan Soc. Civil Engrs., p. 49.

Saffman, P. G. (1962), "Flow of a Dusty Gas Between Rotating Cylinders," Nature, 193, p. 463.

Shimura, H. (1957), "On the Characters of the Water Flow Containing Suspended Sediment," Transactions, J. Soc. Civil Engineers 46.

Sproull, W. T. (1961), "Viscosity of Dusty Gasses," Nature, 190, p. 976.

Tsubaki, T. (1955), "On the Effects of Suspended Sediment on Flow Characteristics," J. Japan Soc. Civil Eng's. 40.

Vanoni, V. A. (1946), "Transportation of Suspended Sediment by Water," Transactions, ASCE, 111, p. 67.

Vanoni, V. A. and Nomicos, G. N. (1961), "Resistance Properties of Sediment Laden Streams," Transactions, ASCE, 126, p. 1140.

* * *

DISCUSSION

S. K. F. Karlsson
Brown University
Providence, Rhode Island

The following comments refer to the effects on a fluid flow by a non-Newtonian additive, which have been discussed to some extent by Professor Lumley and which appear to offer possibilities for considerable reduction in skin friction in turbulent boundary layers.

For a visco-inelastic, shear thinning (Reiner-Rivlin) fluid, Lumley concluded (Phys. Fluids, Vol. 7, No. 3, March 1964) that turbulent transport effects in an existing turbulent flow would be no different from that in Newtonian fluids. However, it seems that this does not exclude the possibility that even in such a simple non-Newtonian fluid the development of instabilities both in the laminar and turbulent boundary layers may well be substantially altered, resulting in considerable changes of the overall boundary layer skin friction.

We have started some laminar stability experiments with such a non-Newtonian fluid in rotating Couette motion at Brown University recently, and although our geometry is different from that of the boundary layer, the results may still be of some interest here. Our fluid is a suspension of Milling Yellow, a dye stuff, in distilled water. Peebles and co-workers at the University of Tennessee have studied its properties extensively (e.g., A. E. Hirsch and F. N.

Peebles, The Flow of a Non-Newtonian Fluid in a Diverging Duct, experimental; Department of Engineering Mechanics Report, August 1964, University of Tennessee, Knoxville, Tennessee) and they found it to be a shear-thinning, visco-inelastic fluid.

Figure 1 shows the viscosity variation with shear rate of a particular sample of Milling Yellow as computed from data obtained with a capillary viscometer.

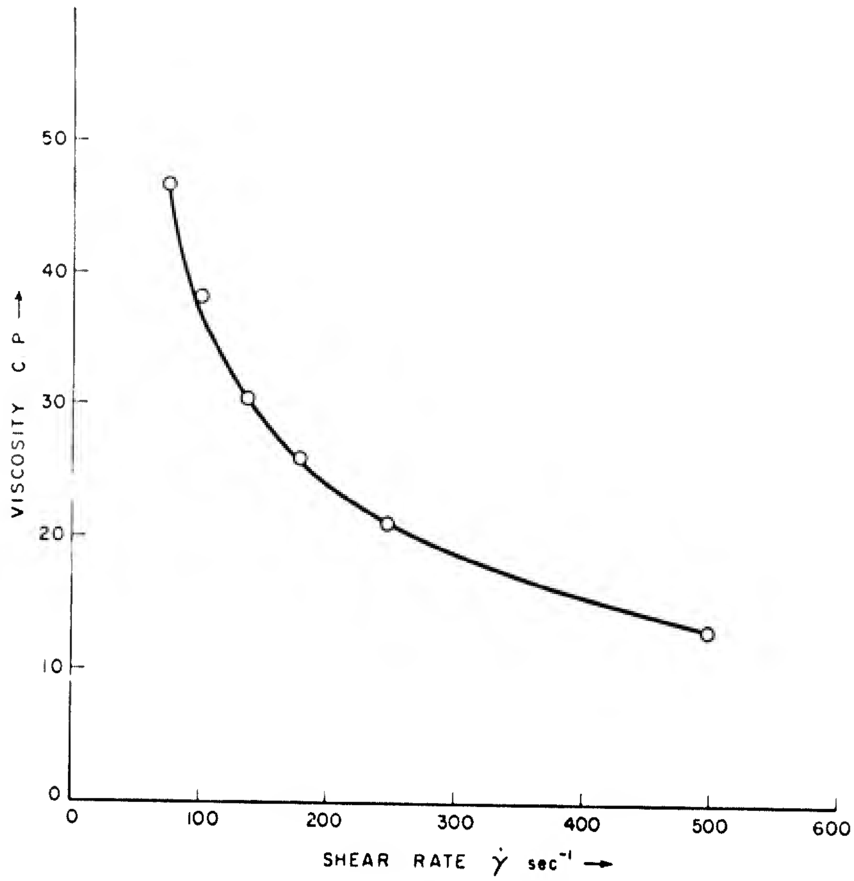

Fig. 1 - Rheological data for milling yellow: 1.608% concentration

The stability experiment performed is the well-known Taylor experiment in which one studies the motion of the fluid in the gap between two concentric cylinders rotating at different speeds. In our experiment the outer cylinder is stationary and only the inner one rotates. Because of the shear rate dependence of the viscosity the tangential velocity profile in the gap is different from that of a Newtonian fluid. Figure 2 shows a comparison between the two for identical boundary conditions at the inner (R = 3.14 cm) and the outer cylinder (R = 3.49), obtained by computation using the experimentally determined viscosity.

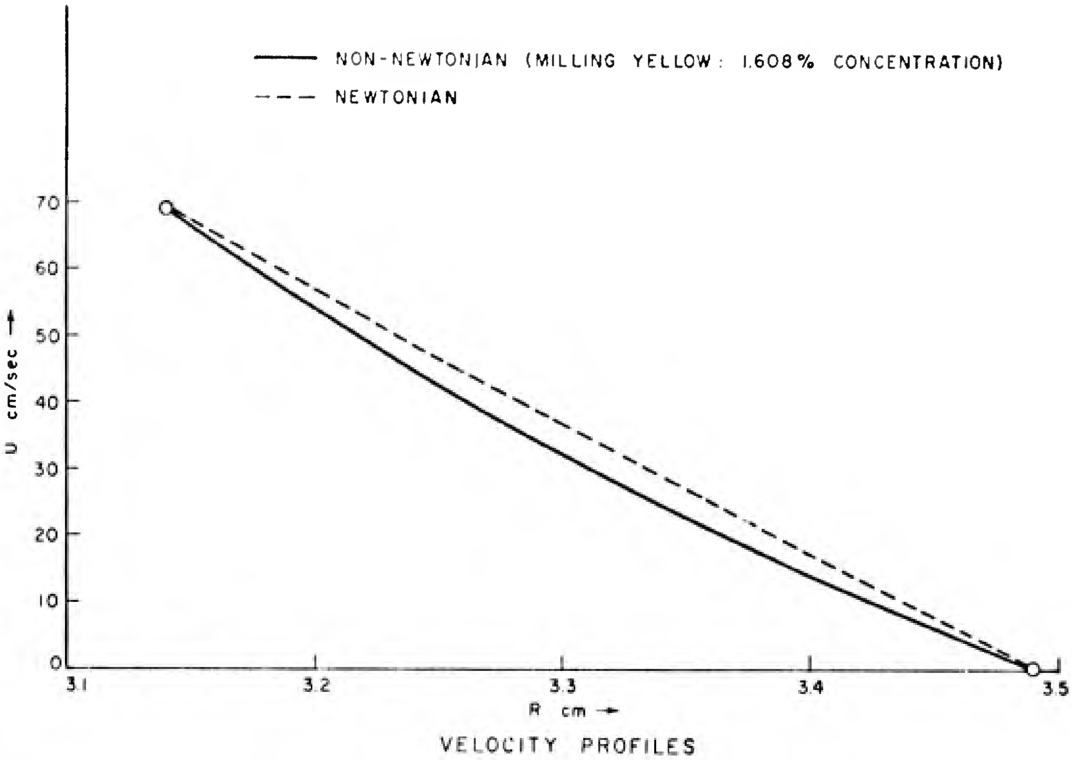

Fig. 2 - Velocity profiles

In our experiments we have made use of the fact that Milling Yellow suspensions are doubly refractive when subjected to a shearing motion. Thus, the flow field has been observed using standard birefringence techniques.

So far we have measured three different quantities as functions of concentration of the additive:

1. "critical" or "neutral stability" speed for the primary (Couette) motion, i.e., the rotation rate at which Taylor cells first appear;

2. the rotation rate when the Taylor cells first become unstable. This instability consists of a sinusoidal deformation of the cells, making the heretofore steady flow time dependent;

3. cell width of the primary cells, thus obtaining the wave number of the perturbation that is most unstable.

The results from these measurements appear in Figs. 3, 4 and 5. The critical velocity is given in terms of the Taylor number which is the significant non-dimensional quantity for this problem:

$$T = \frac{2\,{}^{2}}{1-{}^{2}}\, d^{4}\, \frac{{}^{2}}{{}^{2}}\,,$$

where

$$= \frac{R_1}{R_2} \text{ and } d = R_2 - R_1 .$$

In computing T we have used the value of viscosity, , which corresponds to the average shear stress in the gap. With this, somewhat arbitrary, choice of the viscosity the primary motion of the non-Newtonian fluid appears less stable than its Newtonian counterpart. (Fig. 3.)

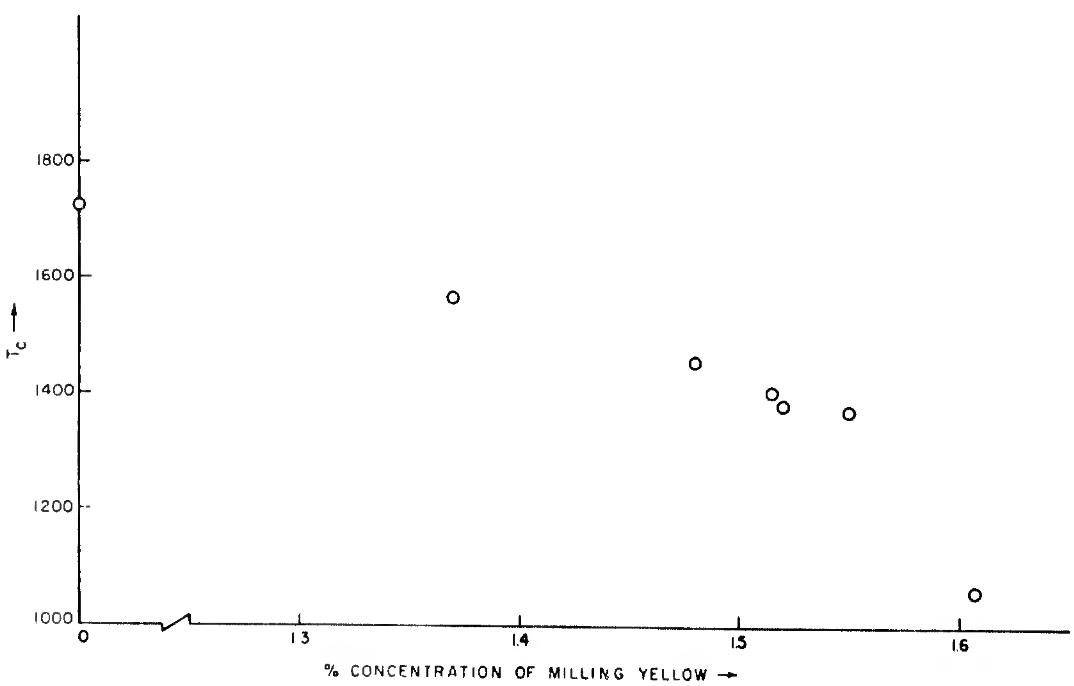

Figure 3

With respect to the second time dependent mode of instability, however, the non-Newtonian fluid is relatively more stable as can be seen in Fig. 4, showing the ratio between rotation rates for the appearance of the secondary and primary (Taylor) instabilities. Thus we have the seemingly somewhat contradictory result that the primary motion is less stable in the non-Newtonian fluid, whereas once the instability has occurred the resulting motion is relatively more stable, when compared to a Newtonian fluid.

Finally, Fig. 5 shows the variation with concentration of the Taylor cell width, normalized with the gap width between the cylinders. This plot is

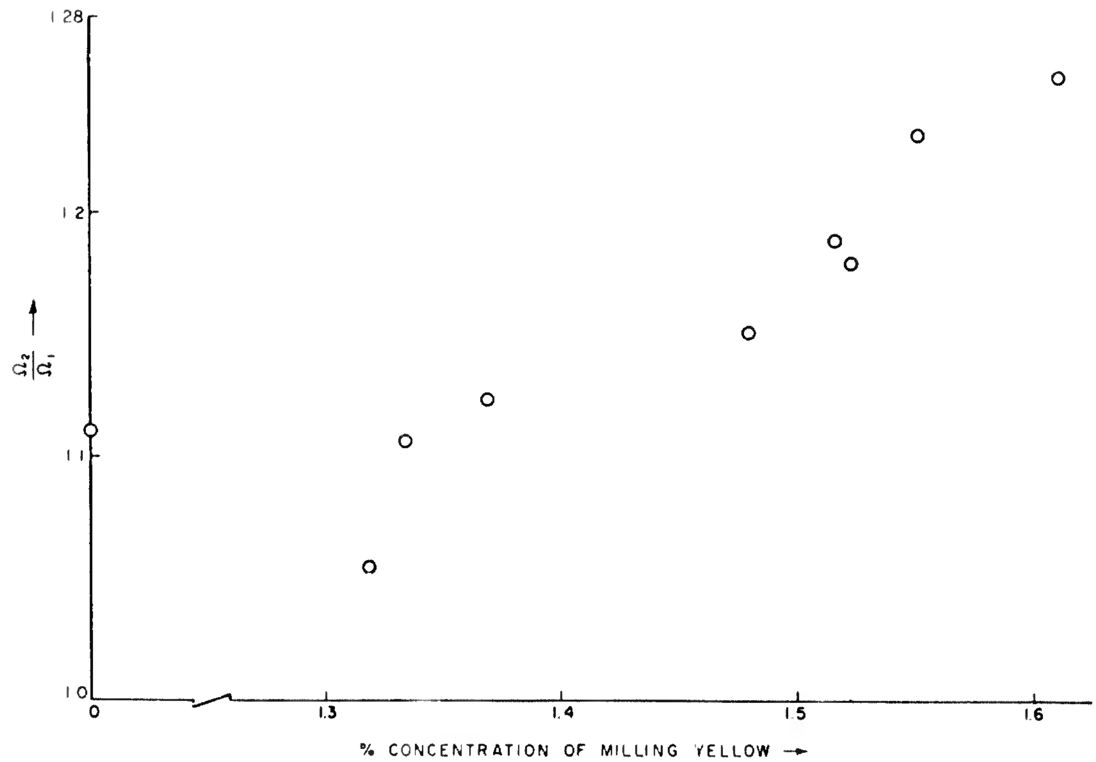

Figure 4

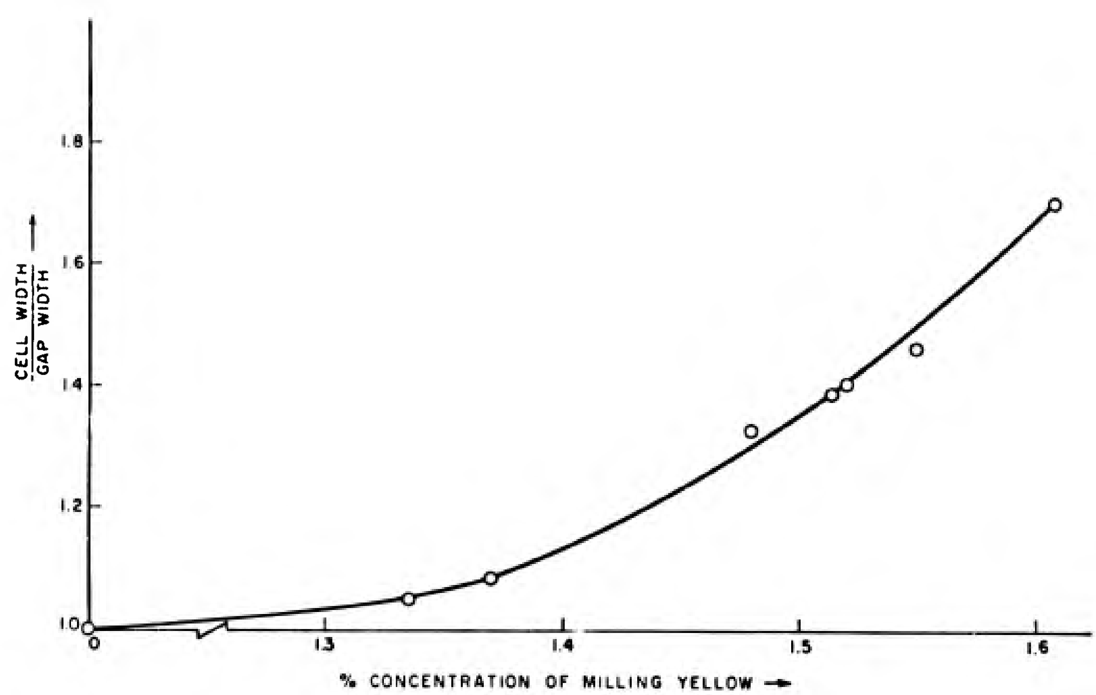

Figure 5

particularly interesting because it does not depend on our choice of viscosity. It exhibits a distinct and consistent variation of this parameter with concentration.

Hence it is clear that the non-Newtonian character of this fluid has a direct effect on the stability of its motion. Possibly this effect is a result of shear-induced normal stresses or anisotropy in the relation between stress and rate of strain, which is implied by the fact that the fluid is birefringent under shear.

* * *

DISCUSSION

A BASIC THEORY THAT COULD EXPLAIN DRAG REDUCTION IN A FLOW CARRYING ADDITIVES

A. Cemal Eringen
Purdue University
Lafayette, Indiana

Lumley [1], Hoyt and Fabula [2], and Vogel and Patterson [3] gave excellent experimental demonstrations of the phenomena of drag reduction by minute amount of additives to fluid surrounding a moving object. We do not possess as yet a theory explaining this phenomena. Classical Stokesian fluids do not contain a mechanism which could provide the desired mathematical treatment. In fact, I do not believe that even the modern theories of visco-elastic fluids [4] can throw light into this phenomena. Quite by accident, a new theory, "Simple Micro-fluids," introduced by Eringen [5], in a different context, seems to have just the proper mechanism for this purpose.

The theory of simple micro-fluids requires that we determine nineteen unknowns ρ, $i_{km} = i_{mk}$, ν_{kl} and v_k by solving nineteen partial differential equations given in [5] subject to appropriate boundary and initial conditions. Here ρ, i_{km}, ν_{kl} and v_k are respectively the mass density, the micro-inertia, the gyration tensor and the velocity vector. The micro-inertia i_{km} provides a mechanism for the inertial anisotropy. Roughly speaking, it is similar to the inertia tensor of rigid dynamics. The gyration tensor provides a mechanism for the local micromotions and small vortices.

The present theory is shown [5], [6] to contain the celebrated Navier-Stokes Theory of fluid dynamics and the theory of anisotropic fluids. A theory of turbulence based on this theory is as yet lacking.

Some sample calculations made are indicative of the above mentioned drag reductions. However, presently this work is too naive for publication and the possible application of the theory of simple micro-fluids to the problem of drag reduction by additives is brought to your attention as a conjecture.

REFERENCES

1. "The Reduction of Skin Friction Drag"

2. "The Effect of Additives on Fluid Friction"

3. "An Experimental Investigation of the Effect of Additives Injected into the Boundary Layer of Underwater Bodies"

4. A. C. Eringen, Nonlinear Theory of Continuous Media, McGraw-Hill, New York, 1962.

5. "Simple Micro-fluids," International Journal of Engineering Science, Vol. 2, No. 2, 1964.

6. A. C. Eringen, "Mechanics of Micromorphic Materials," ONR Technical Report No. 26, April 1964, presented at the XIth International Congress of Applied Mechanics, Munich, Germany, and scheduled for publication in the Proceedings.

* * *

DISCUSSION

Alan Kistler
Yale University
New Haven, Connecticut

Professor Lumley has given an apt summary of the various proposals for reducing the skin friction on objects moving through a liquid. Since the motivation for studying these methods is to find a way to reduce the total drag of an object, a few words about the rest of the drag problem for a submerged object might be appropriate. The neglected component (pressure drag) is associated with separation of the boundary layer. A technique that either increases or decreases the friction drag could have the opposite effect on the pressure drag. The change of sphere drag with transition is the best known example. All of the suggestions for affecting the friction could affect the separation either by changing the rate of momentum transport across the free shear layer or by changing the location of the separation point. Sufficiently detailed measurements of the pressure distribution about realistic shapes should be taken in order to evaluate and understand what is occurring when a particular drag reduction technique is being tested.

Aeronautical experience has shown that most drag reduction schemes that depend on the delay of transition, with the possible exception of boundary layer suction, do not work well outside of the wind tunnel. Surface roughness, wake interaction, and cross flow all work against laminar flow. For this reason, it appears likely that the techniques that change the structure of the turbulent boundary layer offer the most promise. The limits of what can be done with these techniques have still to be determined, however.

* * *

REPLY TO THE DISCUSSION

J. L. Lumley
The Pennsylvania State University
University Park, Pennsylvania

I wish to thank Professors Karlsson, Kistler and Eringen for their helpful comments. I feel that in particular the preliminary data presented by Karlsson indicates the caution with which one must use one's intuition in this very difficult problem. The contribution by Eringen will be somewhat more difficult to assess until turbulence dynamics have been worked out using the constitutive relations he suggests. Since the turbulence dynamics of non-Newtonian media in general are not understood, it is difficult to say whether constitutive relations fitting within the framework of the simple fluid of Noll* are adequate, or whether a locally orientable medium such as that proposed is required. The comments of Kistler seem particularly germane to the paper of Vogel and Patterson and suggest caution in the interpretation of their measurements in the near wake.

* * *

*Noll. W., Archiv. Rat. Mech. Anal. 2, (1958), 197.

THE EFFECT OF ADDITIVES ON FLUID FRICTION

J. W. Hoyt and A. G. Fabula
U. S. Naval Ordnance Test Station
Pasadena, California

INTRODUCTION

It is now well established that very small concentrations of many natural and synthetic high-polymer substances have the property of reducing the turbulent friction drag of the liquid in which they are suspended or dissolved. Because of the many immediate possible applications of such an effect, current interest is high.

The earliest published data showing turbulent-flow friction reductions in dilute polymer solutions appear to be those of B. A. Toms [1] who studied polymethylmethacrylate in chlorobenzene. Flow of "thickened gasoline" was the subject of a U.S. Patent in 1949 [2]. Work with aqueous solutions of polymers was reported simultaneously by Shaver & Merrill [3] and Dodge & Metzner [4] both of whom used sodium carboxymethylcellulose as the friction-reducing material. The technique has found commercial use in oil-field applications [5, 6].

Because the earlier workers in the field attributed the friction-reduction phenomenon to "non-Newtonian" fluid properties, the term has become synonymous with the effect. However, one purpose of this paper is to show that the turbulent-friction reduction effect can be observed (indeed, becomes most prominent) at polymer concentrations at which the solutions are Newtonian by conventional viscometry. Further, it will be shown that polymer additives can be effective in reducing the turbulent friction in concentrations of as little as a few weight parts per million (wppm).

Although the exact mechanism of the effect is not shown, general rules as to the type of material likely to be effective can be developed, and predictions can be made of the maximum polymer effectiveness in several simple flow situations. It is believed that the generalizations formulated here apply to all solvent fluids, but the experimental work has concentrated on aqueous solutions.

EXPERIMENTS WITH ROTATING DISKS

Simply because the apparatus happened to be on hand, early work in Pasadena was performed on a large-scale rotating disk facility. This equipment (Fig. 1) consists of a 3785 liter water tank in which a 45.7 cm diameter risk is rotated by a d-c electricmotor at such a speed that turbulent flow extends over a major portion of the disk. Disk speed and torque are measured using various concentrations of polymer additives in the tank. It can be reasoned that most of the torque is developed near the outer disk edge, so that torque reduction is essentially equivalent to friction reduction. Thus these terms are used interchangeably hereafter.

An example of the type of data obtained using this apparatus is given in Fig. 2. The polymer additive used here is guar gum, the refined endosperm of Cyamopsis tetragonolobus, a plant grown commercially in India, Pakistan, and the United States for food and industrial purposes.[1] At constant rotative speed, addition of the polymer produces immediate lowering of the torque until at concentrations of 300-400 wppm the torque has been reduced to between 30 and 40 percent of its pure water value. As the concentration is further increased, the torque is increased somewhat, which can be attributed to the increased viscosity of the solution.

Much more striking results can be obtained using the synthetic polymer poly(ethylene oxide) which is commercially available in four different molecular weight distributions.[2] Figure 3 shows data taken with the 45.7 cm diameter disk at 40 rev/sec for the four molecular weights of the same chemical. As molecular weight is increased, the material becomes more effective, and Fig. 3 shows that 70% torque or friction reduction may be obtained with less than 100 wppm of additive, using the highest molecular weight material.

Similar tests have been made using a wide variety of natural and synthetic polymers, with the results shown on Table I, where the weight parts per million to achieve a friction reduction of 35% (half way between no effect and the maximum of about 70% observed on this facility at 40 rev/sec) are listed together with the molecular weight of the polymer.

From the table, it appears that at least three significant parameters affect the ability of a polymer to lower the turbulent frictional resistance of the fluid in which it is dissolved: linearity, molecular weight, and solubility.

Linearity

The striking thing about the most effective polymers is that they are "long-chain" materials having an essentially unbranched structure. The chemical formulas of guar and poly(ethylene oxide) (Fig. 4) indicate this characteristic, and a photograph of a model of a segment of the poly(ethylene oxide) molecule further illustrates the thread-like appearance of the material.

While the exact configuration of these molecules in solution is poorly understood, calculations indicate approximate length-to-diameter ratios of from 350 to 500 for guar, and from 22,000 to 165,000 for poly(ethylene oxide) of 6 million molecular weight depending on the helix model selected, if we ignore, for the

[1] The guar gum used in these experiments was "Westco J-2 FP" supplied by the Western Company, Research Division, 1171 Empire Central, Dallas, Texas.
[2] Supplied by Union Carbide Corp., 270 Park Ave., New York, New York.

Table 1
Comparative Friction-Reduction Effectiveness of Water-Soluble Polymer Additives Measured With the Rotating-Disk Facility

Additive	C_R [a]	$M \times 10^{-6}$ [b]	Notable Characteristics
Guar gum, w, s (J-2FP)[c]	60	0.2	Straight chain molecule with single-membered side branches
Locust bean gum, m	260 (260)[d]	0.31	Similar to guar but with fewer side branches, causing reduced solubility and less hydrogen bonding
Carrageenan or Irish moss, M (Stamere NK)	650 (420)	0.1 - 0.8	Strongly charged anionic polyelectrolyte
Gum Karaya, m	780	9.5	Highly branched molecule; relatively insoluble; acidic
Gum Arabic, b	Ineff.	0.24 - 1	Highly branched molecule
Amylose, s (Superlose)	Ineff.	>0.15	Linear chain molecule; retrogrades rapidly
Amylopectin, s (Ramalin G)	Ineff.	1.2	Highly branched molecule
Hydroxyethyl cellulose, u			Nonionic; formed by addition of ethylene oxide to cellulose; has side branches of various lengths
(Cellosize QP-15000)	220	...	
(Cellosize QP-30000)	220	...	
(Cellosize QP-50000)	160	...	
Sodium Carboxymethylcellulose, h (CMC 7HSP)	400	0.2 - 0.7	.....
Poly(ethylene oxide), u			Very water soluble; no biological oxygen demand; apparently an unbranched molecule with unusual affinity for water
(Polyox WSR-35)	70	0.2	
(Polyox WSR-205)	44	0.6	
(Polyox WSR-301)	17	4	
(Polyox Coagulant)	12	>5	
Polyacrylamide, d			
(Separan NP10)	26	1	Nonionic
(Separan NP20)	25	2	Nonionic
(Separan AP30)	29	2-3	Anionic
Polyhall-27, s	130	...	.....

Table 1 (Continued)

Additive	C_R [a]	$M \times 10^{-6}$ [b]	Notable Characteristics
Polyvinylpyrrolidone, f			
(K30)	Ineff.	0.04	.....
(K90)	2900	0.36	.....
Polyvinyl alcohol, e			
(Elvanol 51-05)	Ineff.	0.032	.....
(Elvanol 72-60)	Ineff.	0.17 - 0.22	.....
Silicone, u (L-531)	Ineff.	...	.....
Polyacrylic acid, g			
(Goodrite 773x020 B-3)	Ineff.	0.006	.....
(Goodrite K-702)	Ineff.	0.090	.....
(Goodrite K-714)	Ineff.	0.2 - 0.25	.....
Carboxy vinyl polymer, g (Carbopol (941)	Ineff.	...	Inconclusive test due to precipitation upon dilution

[a] C_R = concentration required (in weight parts per million) for 35% disk-torque reduction at 40 rev/sec with lake water as the solvent.
[b] M = approximate molecular weight of the polymer according to the literature.
[c] The source of each polymer for this work is indicated by the letter after its name: b = Braun Div., Van Waters and Rogers, Inc.; d = Dow Chemical Co.; e = E. I. Dupont; f = General Aniline and Film Corp.; g = B. F. Goodrich Chemical Co.; h = Hercules Powder Co.; m = Meer Corp.; s = Stein, Hall and Co.; u = Union Carbide Chemicals Co.; w = Westco Research.
[d] C_R values in parenthesis are for solutions given heat treatment to increase polymer solubility.

moment, the molecular chain flexibility which will produce a Gaussian-coil configuration for such long molecules. Thus the linearity of the molecule appears to play an important role in the drag-reducing effect.

Molecular Weight

Accompanying the linearity is a corresponding increase in molecular weight. However, from the experiments with Gum Karaya (Table 1) it appears that high molecular weight in itself is not as effective as the linearity. The poly(ethylene oxide) is some 65 times more effective than the heavier Gum Karaya molecule, on a weight basis.

The effect of molecular weight (or linearity) can be demonstrated by replotting the disk data of Fig. 3 taken at a constant rotative speed of 40 rev/sec for poly(ethylene oxide) to give the logarithmic presentation of Fig. 5. In addition to showing the dependence of friction-reduction on molecular weight, Fig. 5 also indicates that substantial increases in molecular weight (degree of polymerization) would be required to achieve better friction-reduction performance by, say, an order of magnitude, with this particular chemical. Such unusually large macromolecules would suggest the possibility of finite particles also producing the friction reduction effect. Experiments with wood-pulp [7] show that this is indeed the case, but friction reductions were much lower than those reported here. This is possibly because of the third requirement for maximum effectiveness, solubility.

Solubility

Referring again to Table 1, tests with Carrageenan indicate the greater the solubility the more the friction reduction effect. Further, molecules which otherwise would be expected to be effective, such as Amylose, do not show up well, probably because of poor solubility.

FURTHER WORK WITH ROTATING DISKS

Because the large-scale rotating disk apparatus described in the previous section required large amounts of experimental solutions, a smaller apparatus was developed consisting of a 7.6 cm diameter disk rotating in two liters of solution. Figure 6 shows experimental data obtained with this equipment using guar gum. The maximum torque reduction obtained was on the order of 40%. Similar data are shown in Fig. 7 for solutions of poly(ethylene oxide). The values of the torque reduction which were obtained on this apparatus as compared with the large-scale equipment, together with the variation of torque reduction with rotative speed, suggest plotting these data as a function of Reynolds number.

Such a comparison is shown in Fig. 8 where data from the 7.6 cm, the 45.7 cm, and also a 76.2 cm disk are shown. The resultant envelope of maximum torque reduction obtained in this way seems surprisingly similar for many polymers, that is, the same maximum torque reduction at any given Reynolds number can be obtained with any of the "effective" polymers, with only the concentration required to obtain this reduction varying from polymer to polymer. The Reynolds number used in this plot is based on water viscosity without considering any viscosity increase due to the polymer. As some typical data for the maximum torque reduction curve of Fig. 8, Table 2 gives concentrations of various materials required to attain 70% reduction at a Reynolds number of 1.3 million with the 45.7 cm disk facility.

Effect of Sea Water

The work presented so far has been based entirely on tap water or water drawn directly from a fresh water lake. Additional tests were made with the 45.7 cm rotating disk to show the effect of sea water on the performance of polymer additives. As shown in Fig. 9, friction reduction data taken in simulated sea water agree closely with those obtained on fresh water for guar. The tests shown are at three different temperatures, ranging from 13°C to 27°C. Poly(ethylene oxide) is even less affected by presence of sea water salts.

Table 2
Concentrations (wppm) to Achieve 70% Torque Reduction at a Rotating Disk Re = 1,300,000

Guar gum (J-2FP)	500
Locust bean gum	1700
Gum Karaya	2700
Polyhall-27	850
Polyox-WSR 205	250
Separan AP 30	100

(The source and molecular weight of the above materials is given in Table 1)

Rheological Studies

Since high concentrations (above 1000 wppm) of these polymers are known to be shear-thinning, early explanations of the friction reduction were based on the "non-Newtonian" (i.e., variable) viscosity with rate of shear. Considerable effort was thus placed upon the rheology of these substances and how their shear-thinning behavior could explain drag reduction.

It was quickly realized, when rheograms were available, that at the concentrations where maximum friction reductions were obtained, these solutions were not "non-Newtonian," but of essentially constant viscosity, greater than that of the solvent. It was only at higher concentrations that departures from constant viscosity were evident. For example, Fig. 10 shows a rheogram for guar, and Fig. 11 for poly(ethylene oxide) of 4 million molecular weight.[3] At the concentrations of most interest (under 500 wppm for guar and under 100 wppm for poly(ethylene oxide) it is difficult, from these data, to ascribe a variable viscosity with shear to these solutions. The constant viscosity extends to very low shear as shown in Fig. 12.[4] Thus the term "non-Newtonian" is inappropriate for these fluids, unless one allows the possibility that non-steady measurements will show that these solutions display shear rigidities at high frequencies which ideal "Newtonian" fluids would not. J. L. Lumley [8] has recently argued that friction reductions should not be expected from the purely viscous, non-Newtonian class of fluids. Since many of the effective additives produce highly viscoelastic solutions in higher concentrations, it is possible that the drag reduction phenomenon is related to viscoelasticity. However, viscoelastic solutions are not necessarily effective drag reducers: e.g., Carbopol (Table 1).

[3] These data were obtained under U. S. Navy contract by the Western Company, Research Division, using Fann and Burrel-Severs viscometers.
[4] These data were obtained by J. M. Caraher of the Naval Ordnance Test Station, using a new type, helical-coil viscometer of his design.

Furthermore, additional experiments have shown that the effect is not enhanced by increasing the viscosity of solution of guar by "complexing" with sodium borate [9]. Increasing the viscosity in this way resulted in lowering the drag-reduction effect based upon the weight of guar in solution. In a typical test the viscosity was increased by a factor of 22 over the guar solution alone, by addition of sodium borate, and the drag reduction than obtained was only 70% of that which would have occurred using guar only.

However the friction reduction is produced, it seems clear that the action involved is suppression of turbulence intensity. Figure 13 shows test data from the 45.7 cm diameter disk for guar, correlated with disk Reynolds numbers based on water. At concentrations of guar up to 311 wppm, the slopes of the test curves are roughly parallel to, but lower than the turbulent flow water data. For 621 wppm and above, the slopes are roughly parallel to, but higher than, the laminar water flow case. From Fig. 10 it can be seen that no significant changes in Fig. 13 would result from use of Reynolds numbers based on the measured viscosities of the solutions for under 500 wppm.

PIPE FLOW EXPERIMENTS

The friction reducing effect of polymer solutions can be easily studied by measuring the pressure drop occurring in a given length of pipe in which the polymer solution flows. Many experimental facilities of this type have been constructed, and in general they are similar to that shown schematically in Fig. 14, except for the use of air-pressure pumping to minimize degradation of test solutions [10]. Pre-mixed polymer solution contained in tanks is forced through the pipe test section where the static-pressure gradient is measured. Flow rates can be determined by weighing the amount of polymer solution discharged in a given time. Discharged solution is discarded to minimize bias due to shear degradation which occurs very rapidly for many of the solutions. By comparison of similar data taken using pure water as the flowing medium, drag reduction may be calculated.

Typical data using poly(ethylene oxide) of 4 million molecular weight are shown in Fig. 15. Drag reduction of well over 75% is easily obtained. Similar data using the same polymer in sea water, but in a different apparatus,[5] are given in Fig. 16.

Another pipe flow apparatus, which is essentially a turbulent flow rheometer, has recently been constructed according to the sketch of Fig. 17. The piston of the cylinder is moved upward at 1.245 cm per second, forcing fluid through the small diameter pipe. The entire apparatus is mounted vertically to allow entrapped air to escape.

Some representative data from this instrument, taken at a constant flow velocity of 12.65 meters/sec (Reynolds number based upon water at 21.1°C of approximately 14,000) are given in Fig. 18.

[5]Data taken by the Western Co. under U. S. Navy contract.

Reynolds Number Correlation

Data from poly(ethylene oxide) of 4 million molecular weight has been correlated on a pipe flow Reynolds number basis using the viscosity of pure water. At a concentration of 100 wppm, drag reduction reaches a maximum of 78 - 79% at a Reynolds number of about 10.[5] At a lower concentration (30 wppm) the effect falls off at higher Reynolds numbers. A possible explanation for the fall-off is rapid shear degradation of the polymer at the higher flow velocities.

The envelope of maximum drag reduction shown on Fig. 19 is the maximum effect obtained for any polymer in pipe flow as a function of Reynolds number. Thus it is an empirical relationship for pipe flow corresponding to that given for rotating disks in Fig. 8. These pipe flow data are consistent in general with those reported in Ref. 11.

To further demonstrate the validity of Fig. 8, Table 3 gives some concentrations of materials required to attain the maximum drag reduction of 67% at a pipe flow Reynolds number of 14,000.

Table 3
Concentrations (wppm) of Material Required to Achieve 67% Drag Reduction in Pipe Flow at Re = 14,000

Guar (J-2FP)	400
Colloid HV-6* (refined Guar)	375
Polyox WSR-301	30
Colloid HV-2* (refined Guar)	500

*Source of polymer: Stein, Hall and Co.
Source of other materials listed in Table 1.

OTHER EXPERIMENTS

The drag reduction phenomena has been suggested [12] as a possible explanation of certain erratic fluctuations of measured resistance in some towing tanks.[6] Frictional drag measurements on the same model in the same towing tank are known to be subject in some tanks to considerable variation, always down from the "standard," and as much as 14%, with no other complete explanation than a "change in resistance characteristics of the water." Since it is known that many algae and marine organisms secrete mucous or slime, it is conceivable that these may act in the same manner as the compounds studied above.

[5] Data taken by the Western Co. under U. S. Navy contract.
[6] It appears that these fluctuations are reduced in tanks where the water is chemically purified.

The experiments shown in Table 4 were not intended to be rigorous, or even very quantitative, but simply tests to show the possibility that organic materials similar to those which might be present in towing tanks or other hydrodynamic facilities would affect the measured drag.

Table 4
Drag Reduction of Living Materials

Material	Observed Drag Reduction	Apparatus
Algae from fresh water aquarium (principally Ankistodesmus falcatus)	3.37%	7.6 cm disk
Same with green cells centrifuged out	3.38%	7.6 cm disk
Green cells resuspended in tap water	0.45%	7.6 cm disk
Bacteria-free culture of sea diatom Chaetoceros	1.5%	.109 cm pipe
Same concentrated to 1/6 volume	14.5%	.109 cm pipe
Slime from sea snail in sea water	9.1%	.109 cm pipe
Same concentrated to 1/3 volume	12.0%	.109 cm pipe
Scraped slime from sea fish in sea water	1.5%	.109 cm pipe
Same concentrated to 1/6 volume	14.5%	.109 cm pipe

The experiments shown in Table 4 were not intended to be rigorous, or even very quantitative, but simply tests to show the possibility that organic materials similar to those which might be present in towing tanks or other hydrodynamic facilities would affect the measured drag.

From Table 4 it is seen that sizeable reductions in drag can be obtained from a variety of natural substances. While concentrations required for significant effect were high enough that the contamination was apparent in these tests, it is conceivable that other, more effective natural contaminants may occur which approach the synthetic polymers in effectiveness at very low concentrations. The search for such contaminants in tank water at the time of such a drag reduction excursion must be directed at concentrations of a few parts per million, since 40% friction reduction or more for 2 wppm of high molecular weight polymer is demonstrated in Fig. 15.

It is interesting to speculate on the idea that some marine animals might have evolved the release of friction reducing agents into their boundary layer. This appears to be a possible area for further research.

APPLICATIONS

The only known present application of these materials as friction-reducing agents is in oil-field pumping operations. However, the attractive power reductions which seem attainable should promote extensive interest in the further use of these polymers.

In considering applications, however, careful thought must be given to practical matters such as surface roughness, mechanical polymer degradation, and economic feasibility.

Surface Roughness

A preliminary check on the effect of roughness was made with the large-scale rotating disk facility. The data shown in Figs. 2, 3, and 5, and Table 1 were obtained with a smooth, polished disk. Another disk with about 100 micro-inch rms machine-turned roughness was also tested, but showed no change in torque required for either water or guar solutions. A rough surface was then produced by means of wrinkle-finish paint. In water tests, the torque for a given speed was increased about 35% due to the roughness. Figure 20 shows that two or three times the concentration of guar gum was required to achieve a given torque reduction with the rough disk. Also, effects of rotative speed appear at low guar concentrations in contrast to the smooth disk data. Nevertheless it seems clear that the additive can be effective on practical structures.

Mechanical Degradation

The polymer molecules are subject to mechanical degradation as the friction-reduction process continues. For example, concentrations of 15 wppm of poly (ethylene oxide) of 4 million molecular weight were repeatedly tested in the large disk apparatus, with the results shown on Fig. 21. Each test was about 15 seconds in duration, repeated at intervals of 3 minutes or 10 minutes. Each test run with this polymer evidently contributed to the mechanical degradation. A similar test with guar gum did not show this effect, and this is the main reason for continued interest in this less effective, but apparently very sturdy polymer.

Economic Feasibility

The additive concentrations used in oil-field applications are about 1000 wppm and up [6]. Such concentrations, if assumed across the full turbulent boundary layer thickness are out of the question for boundary-layer applications.

This difference in feasible concentrations is simply because the unit of additive in pipe flow is used over and over again, until the end of the pipe, while in a vehicle boundary layer, the unit of additive is effective only on a certain wetted surface area for a certain time, before it is discarded into the wake.

This key difference can be seen more clearly by comparing fully established pipe flow and high Reynolds number flat-plate boundary-layer flow. A useful measure of performance is

$$\text{Additive Effectiveness (A.E.)} = \frac{\text{Power Saved}}{\text{Additive Weight Flow Rate}}$$

with units of hp - hr/kg.

In the following it is assumed that speeds are kept fixed and that only pipe length and plate length are varied.

For pipe flow, assume that an additive weight concentration per unit volume, C, produces a percent pressure-drop or friction reduction, R, for fully established turbulent flow in a pipe of diameter, D, for a throughput of Q with the mean flow velocity $U = 4Q/\pi D^2$. The pumping power saved is RP_o where P_o is the power required for $C = 0$. Thus

$$\text{A.E.} = \frac{RL(P_o/L)}{CQ} = \frac{RL}{C} \cdot \text{const.}$$

where P_o/L is the pumping power per unit length for $C = 0$. Thus if polymer degradation is negligible, A.E. will increase indefinitely with L.

For boundary-layer flow, one can assume for a first approximation that the local percent skin friction reduction will require about the same mean concentration across the turbulent boundary layer thickness, δ, as in pipe flow for $\delta = D/2$ and freestream speed $U_\infty = U$. The friction reduction factor, R, will be assumed to be determined by C as in the typical pipe flow results given earlier.

Because the additive concentration in the turbulent boundary layer will be continually reduced by mixing as the boundary layer thickens, more additive will have to be injected at intervals along the plate length, or else the concentration will have to be very large near the leading edge. In either case, the total additive supply rate per unit width will be $C(\delta - \delta^*) U_\infty$, where δ^* is the boundary-layer displacement thickness. If θ_o is the momentum thickness for $C = 0$, then the thrust power saved per unit width is

$$R\theta_o(\rho/2) U_\infty^3 .$$

Thus for a flat plate

$$\text{Additive Effectiveness} = \frac{R\theta_o(\rho/2) U_\infty^3}{C(\delta - \delta^*) U_\infty} .$$

For high Reynolds numbers, reasonable approximations are

$$\delta - \delta^* = k\delta = k'\theta$$

where k and k' are constants as L is varied. Thus

$$A.E. = \frac{R\theta_o}{C\theta} \times \text{const.}$$

and since $\theta/\theta_o = 1 - R$,

$$A.E. = \frac{R}{C(1-R)} \cdot \text{const.}$$

Thus in boundary-layer applications the additive effectiveness is helped by the reduced boundary-layer throughput as R is increased, but the increase with L is lost.

Since a concentration of a few wppm is 2 to 3 orders of magnitude smaller than used in the pipe-line applications, the newly discovered effectiveness at such concentration of the extremely high molecular weight, linear, soluble polymers now makes the situation more hopeful for boundary-layer applications. (Fortunately, for such applications, the extreme sensitivity of the same polymers to mechanical degradation may not be a major problem since the use-time of the polymer is short.) However, calculations indicate that even the increase in the factor $1/C$ by about 1000 still leaves the technique of reducing ship friction by boundary-layer additives economically uncompetitive.

Hence until additive costs can be brought considerably lower, this method of drag reduction appears to be reserved for applications where an emergency speed increase would be required. Of course, in an application where a large proportion of the total drag is frictional, such as a slow speed ship, the technique may look economic.

In any event, the applications of the rather basic experiments presented here are difficult to foresee. Certainly the possibilities of achieving substantial drag reductions with relatively small amounts of additive are attractive enough to warrant intensive further effort.

REFERENCES

1. Toms, B. A., "Some Observations on the Flow of Linear Polymer Solutions Through Straight Tubes at Large Reynolds Numbers," Proceedings of the International Rheological Congress, Scheveningen, Holland, 1948, pp. II-135-41.
2. Mysels, K. J., "Flow of Thickened Fluids," U.S. Patent 2,492,173, December 27, 1949.
3. Shaver, R. G., and E. W. Merrill, "Turbulent Flow of Pseudoplastic Polymer Solutions in Straight Cylindrical Tubes," AM INST CHEM ENGR, J, Vol. 5, No. 2 (1959), p. 181.

4. Dodge, D. W., and A. B. Metzner, "Turbulent Flow of Non-Newtonian Systems," AM INST CHEM ENGR, J, Vol. 5, No. 2 (1959), p. 189.

5. Dever, C. D., R. J. Harbour, and W. F. Seifert, "Method of Decreasing Friction Loss in Flowing Fluids," U.S. Patent 3,023,760, 6 March 1962.

6. Melton, L. L., and W. T. Malone, "Fluid Mechanics Research and Engineering Application in Non-Newtonian Fluid Systems," SOC PETR ENGR, J, March 1964, p. 56.

7. Massachusetts Institute of Technology. The Effects of Fibers on Velocity Distribution, Turbulence and Flow Resistance of Dilute Suspensions, by J. W. Daily and G. Bugliarello. Cambridge, Mass., MIT, October 1958. (Hydrodynamics Laboratory Technical Report No. 30.)

8. Lumley, J. L., "Turbulence in Non-Newtonian Fluids," PHYSICS OF FLUIDS, Vol. 7, No. 3 (March 1964).

9. Whistler, R. L., and J. N. BeMiller, Eds., "Industrial Gums" Academic Press, New York, 1959.

10. Fabula, A. G., "The Toms Phenomenon in the Turbulent Flow of Very Dilute Polymer Solutions," Fourth International Congress on Rheology, Brown University, August 1963. Interscience Div., John Wiley (In press).

11. Ripken, J. F., and M. Pilch, "Studies of the Reduction of Pipe Friction with the Non-Newtonian Additive CMC," St. Anthony Falls Hydraulic Laboratory Technical Paper 42, Series B, April 1963.

12. Hoyt, J. W., and A. G. Fabula, "Frictional Resistance in Towing Tanks," Tenth International Towing Tank Conference, London, September 1963.

* * *

DISCUSSION

H. Schwanecke
Hamburg Model Basin
Hamburg, Germany

At Hamburg Model Basin experiments are performed concerning the effect of polymer solutions on the viscous drag of the model of a surface ship. Additives of several molecular weights are used. The main problem is to distribute the polymer solutions all over the wetted surface as a film of sufficient concentration. May I ask Dr. Hoyt, if he has done any experiments in that way or if he knows about such experiments having been performed elsewhere? May I ask

Dr. Hoyt further, if there is any upper limit with respect to the molecular weight of the additives beyond which a film of a polymer solution is no longer obtained?

* * *

DISCUSSION

Marshall P. Tulin
Hydronautics, Incorporated
Laurel, Maryland

The authors are very much to be congratulated for their fine experimental studies. Their data should tend enormously toward a better understanding of the unexpected and puzzling effects which small concentrations of macromolecules seem to have on turbulence.

Our own experiments on a flat plate with leading edge injection confirm that a maximum drag reduction results when as little as 10 parts per million of Polyox WSR 301 is present in the boundary layer at the trailing edge. Unlike the flows in pipes and on rotating plates, however, a rather rapid decrease in effectiveness of the additive occurs when the concentration is increased only slightly beyond its optimum value. Perhaps this has to do with the special circumstances which accompany injection of the fluid containing additive.

We were curious whether macromolecules would affect "free" decaying turbulence as distinct from maintained turbulence in a shear flow in close proximity to a wall. Therefore we have studied the decay of a cylindrical cloud of turbulence. Rather, we have measured the diffusive spread of the cloud. These experiments show that additives do affect free turbulence and tend to increase the rate at which it decays.

I have been doing some theory on the effect on turbulence of weak solutions of macromolecules. It seems to me that the shear stiffness of the resulting viscoelastic solution is the crucial characteristic and that the generation of elastic shear waves by turbulence offers a mechanism for significant "damping" of turbulent motions. Figure 5 contains very clear evidence that the elastic shear stiffness controls the turbulence damping effect; it may be shown using certain results of the molecular theory for weak polymer solutions that this stiffness is virtually constant on the lines of constant torque ratio in this Figure.

* * *

REPLY TO THE DISCUSSION

J. W. Hoyt and A. G. Fabula
U. S. Naval Ordnance Test Station
Pasadena, California

The authors would like to thank the several discussors for their comments regarding this interesting new field in fluid dynamics.* It is to be hoped that theoretical attacks on the mechanism of drag reduction through the use of high-polymer solutions will soon give the firm foundation needed for further advances in the application of the method. Perhaps the approaches of Prof. Eringen and Mr. Tulin will provide the keys to this understanding. With regard to Dr. Schwanecke's questions, the only published data now available on the ejection of additives over a body seems to be the Vogel and Patterson paper in this Symposium. Our experience with various molecular weight additives seems to indicate that the higher the better, if the molecule is also fairly linear.

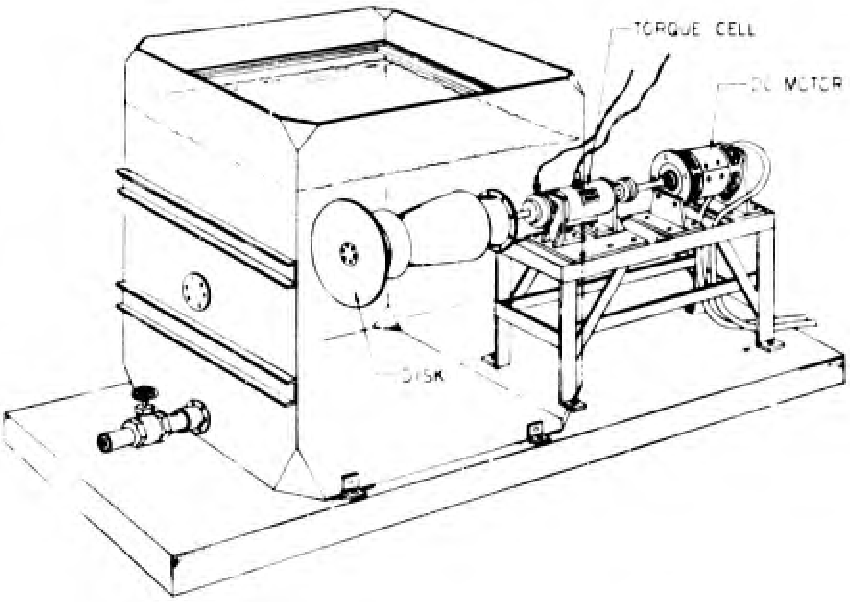

Fig. 1 - Large rotating-disk apparatus

*See contribution by Eringen to the paper by Lumley.

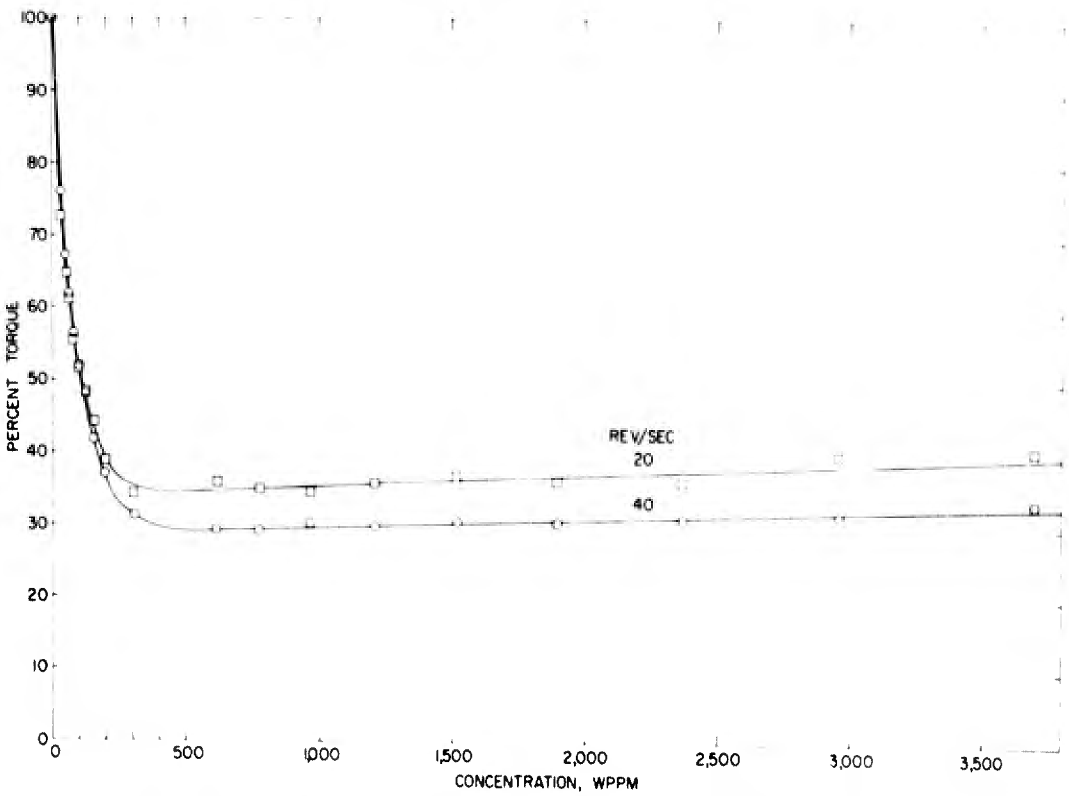

Fig. 2 - Rotating-disk torque curves for guar additive

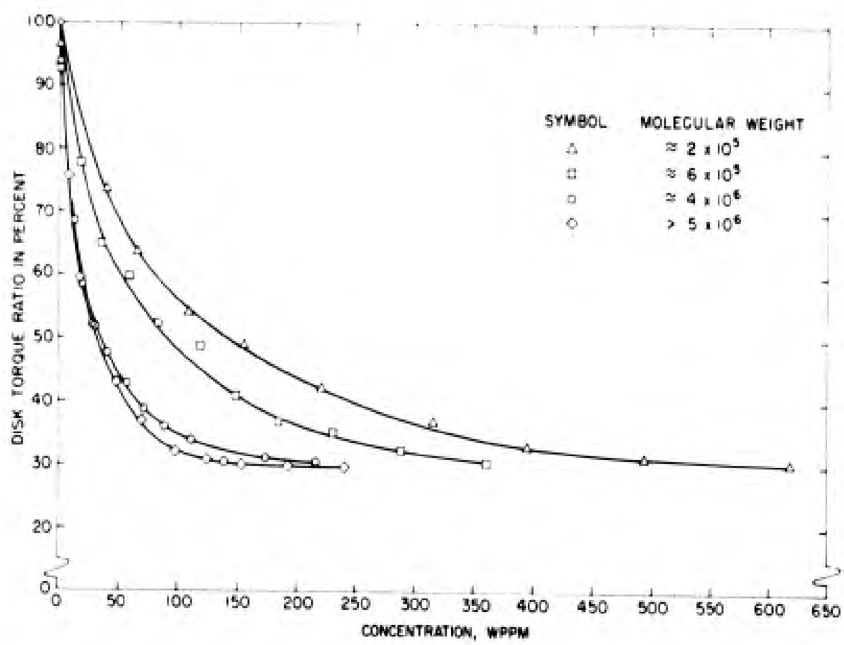

Fig. 3 - Rotating disk-torque curves for poly(ethylene oxide) additives

$$-O-CH_2-CH_2-O\left[CH_2-CH_2-O\right]_n CH_2-CH_2-$$

Poly(Ethylene Oxide)

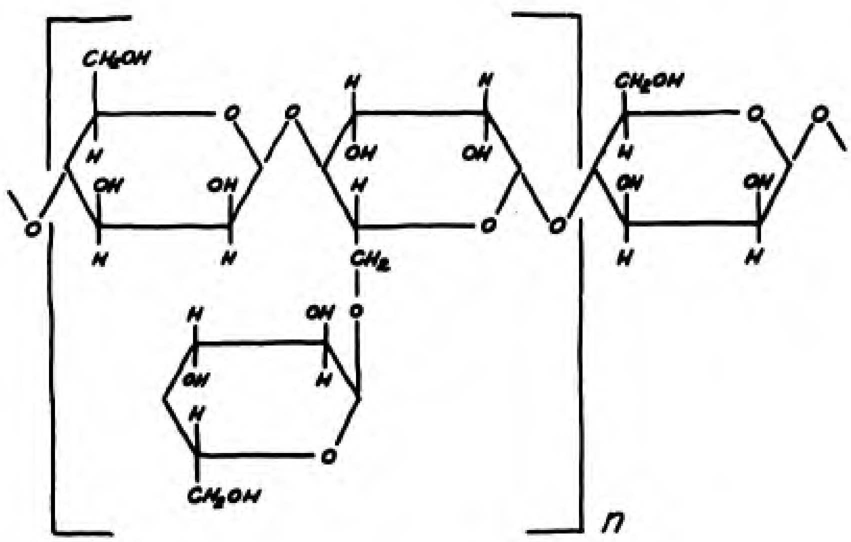

Guar

Fig. 4 - Chemical formulas of two effective additives

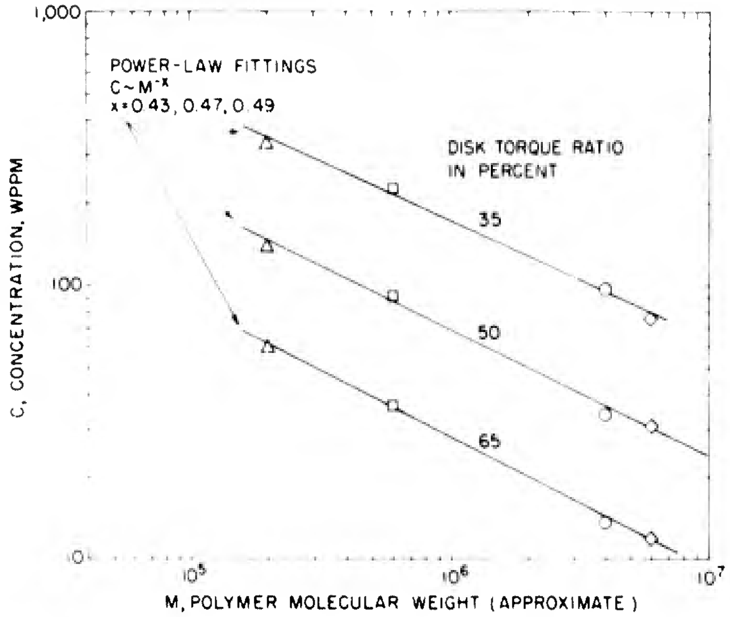

Fig. 5 - Dependence of required concentrations for various disk torque ratios on molecular weight of poly(ethylene oxide)

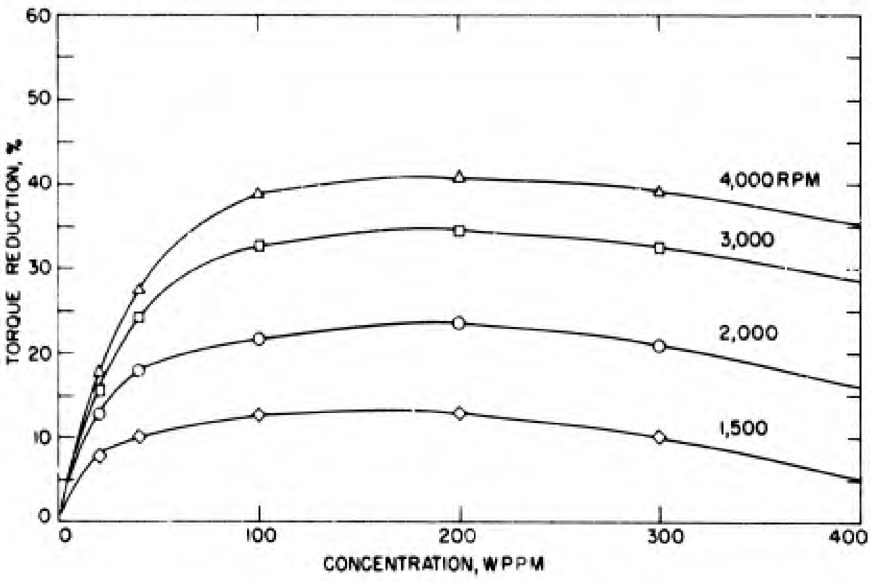

Fig. 6 - 7.6 cm disk torque reduction vs guar gum concentration

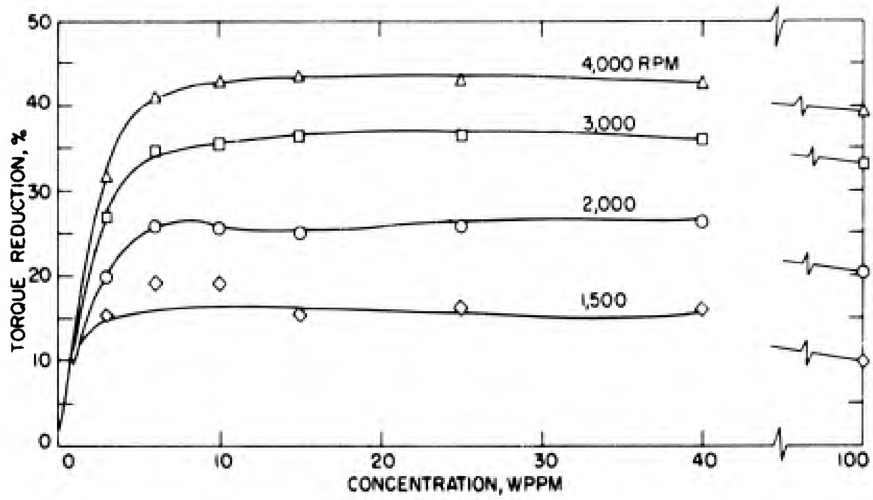

Fig. 7 - 7.6 cm disk torque reduction vs poly(ethylene oxide) concentration

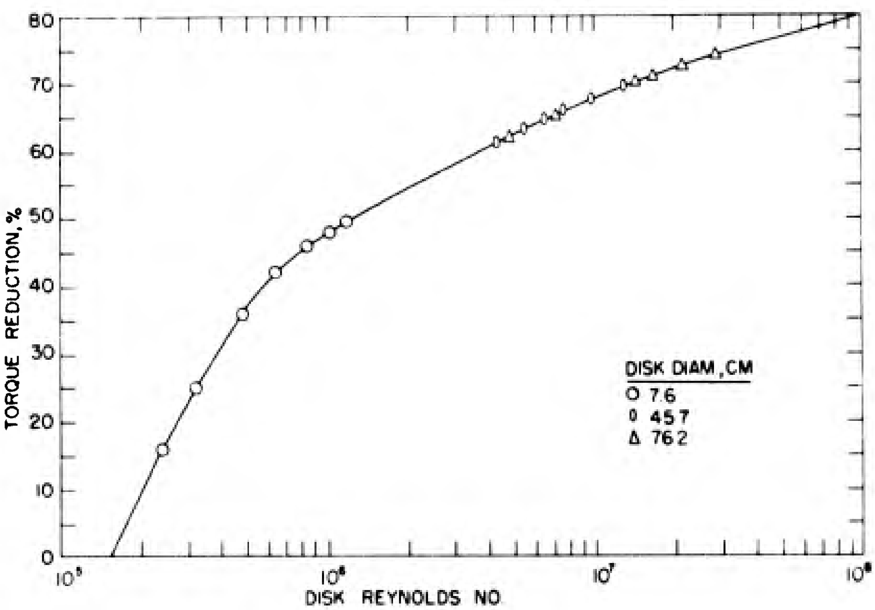

Fig. 8 - Maximum torque reduction as a function of Reynolds number

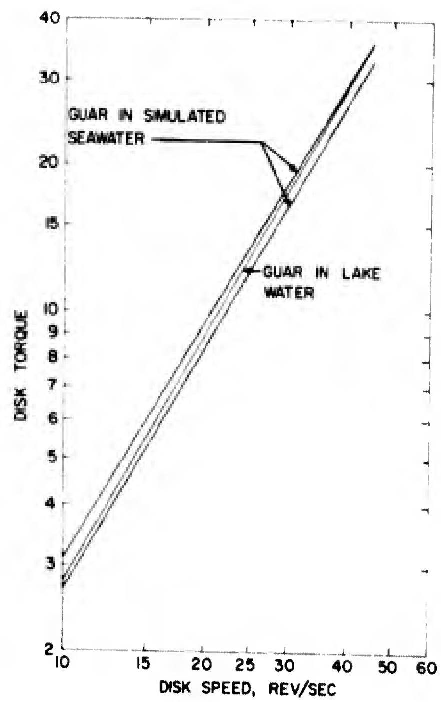

Fig. 9 - Effect of seawater on guar solution

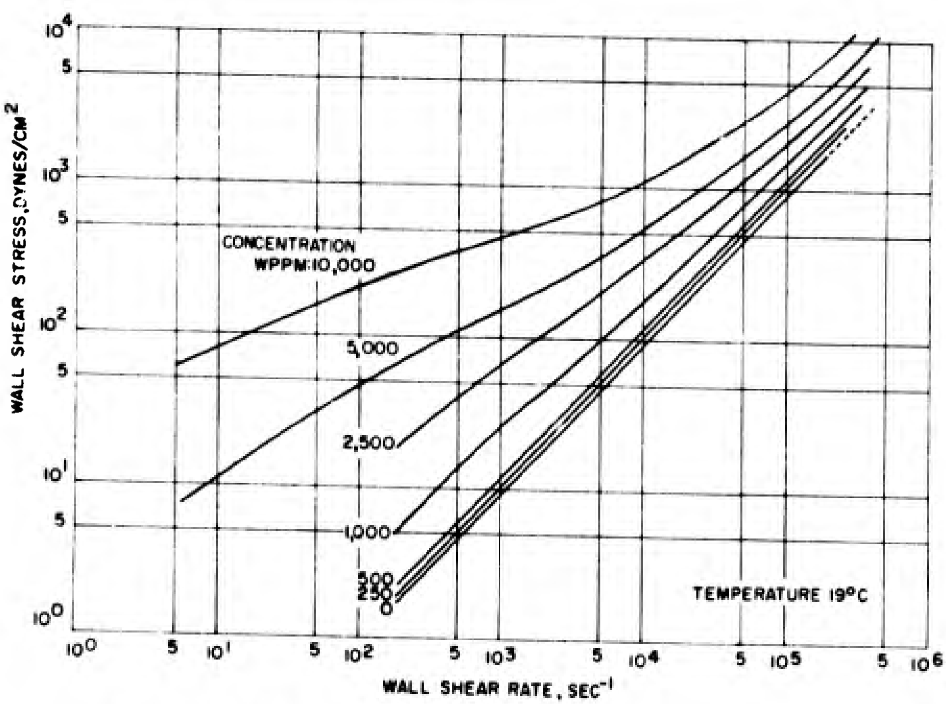

Fig. 10 - Rheogram for guar additive in water at 19°C

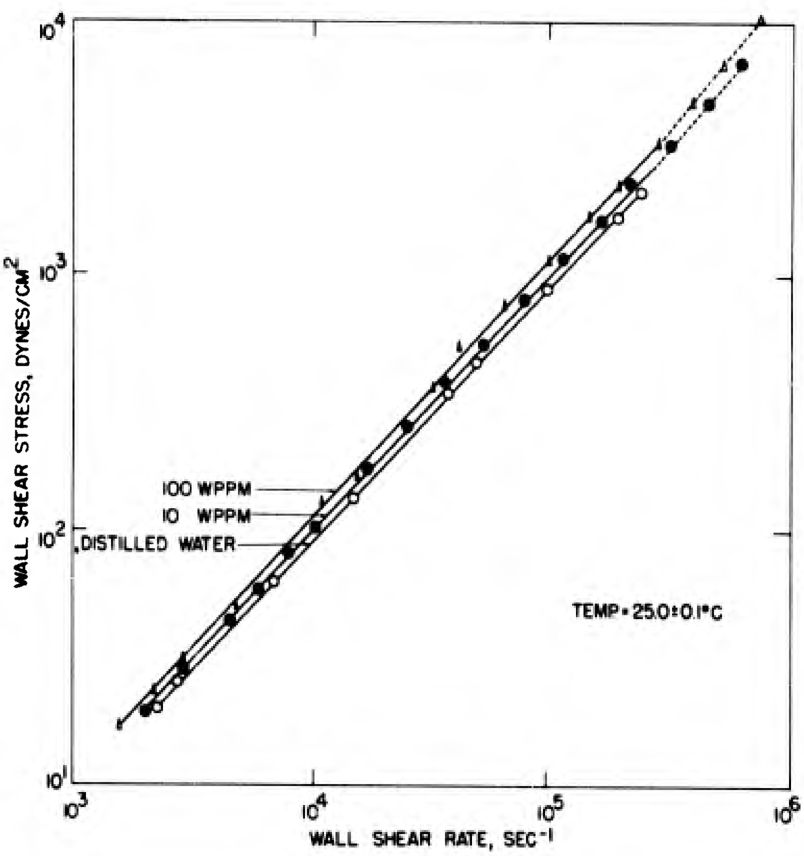

Fig. 11 - Rheogram of poly(ethylene oxide) of 4 million molecular weight in water

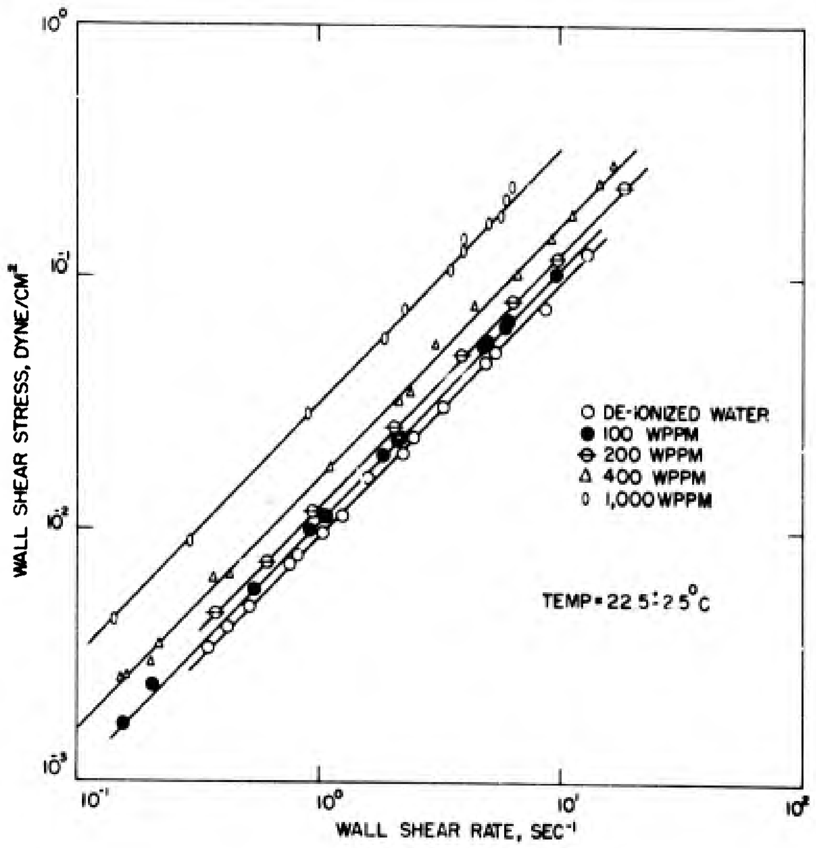

Fig. 12 - Rheogram for poly(ethylene oxide) of 4 million molecular weight at low shear rates

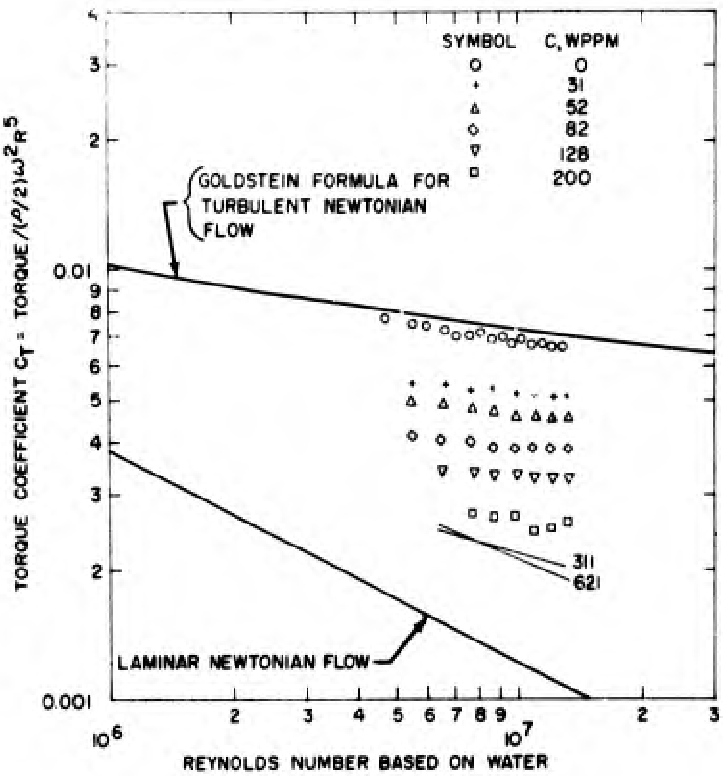

Fig. 13 - Torque coefficient as a function of Reynolds number

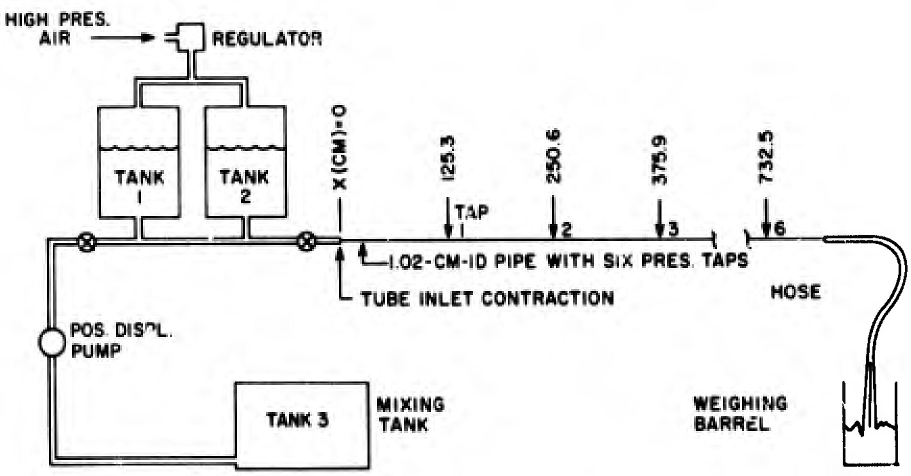

Fig. 14 - Schematic diagram of blowdown pipe apparatus

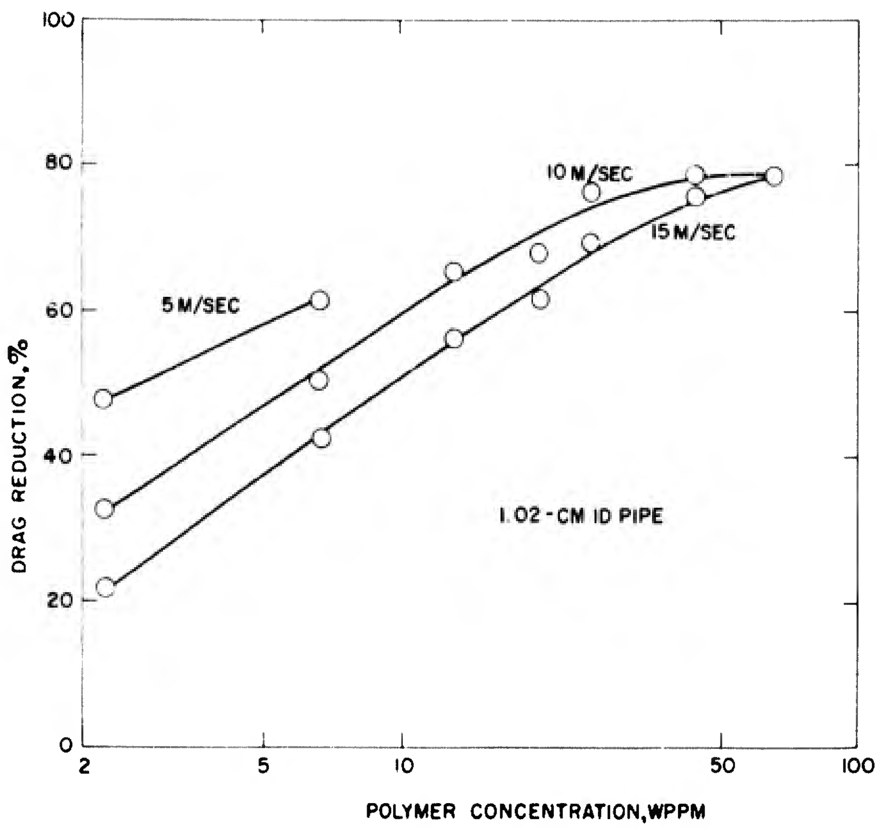

Fig. 15 - Drag reduction curves for poly(ethylene oxide in blowdown pipe apparatus

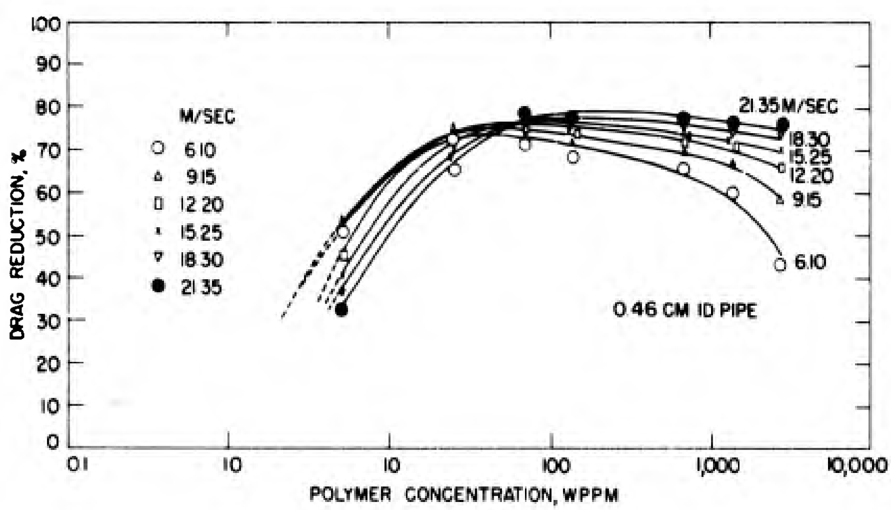

Fig. 16 - Friction reduction curves for poly(ethylene oxide) in pipe-flow apparatus

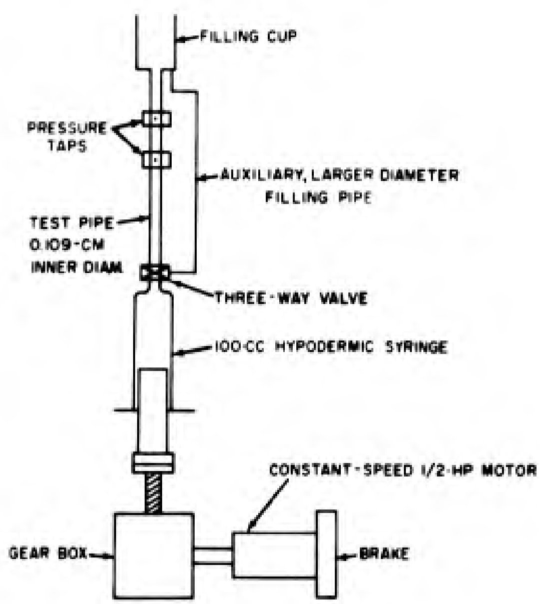

Fig. 17 - Turbulent-flow rheometer

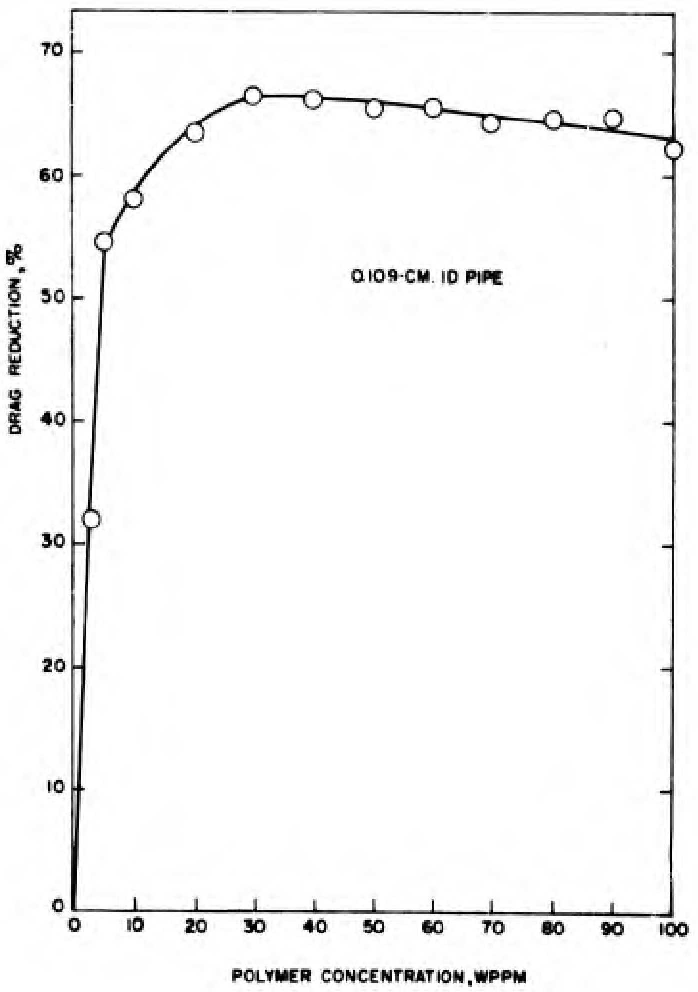

Fig. 18 - Turbulent-flow rheometer data for poly(ethylene oxide)

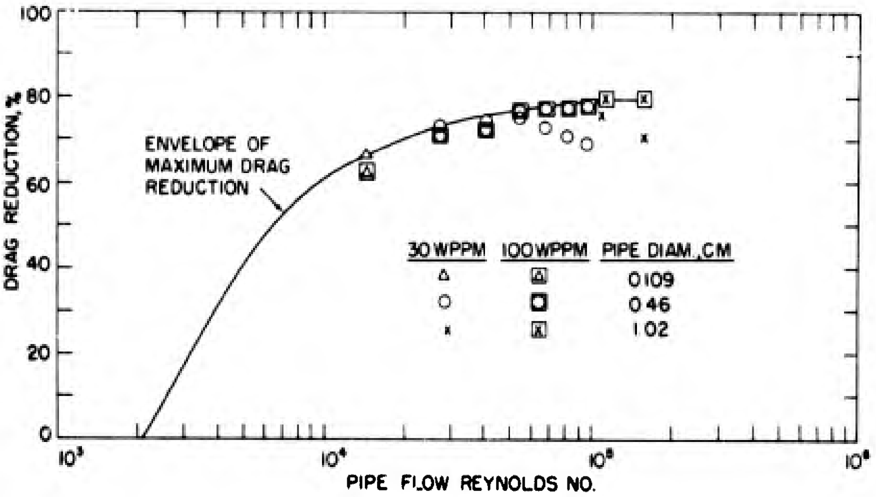

Fig. 19 - Reynolds number correlation for pipe flow

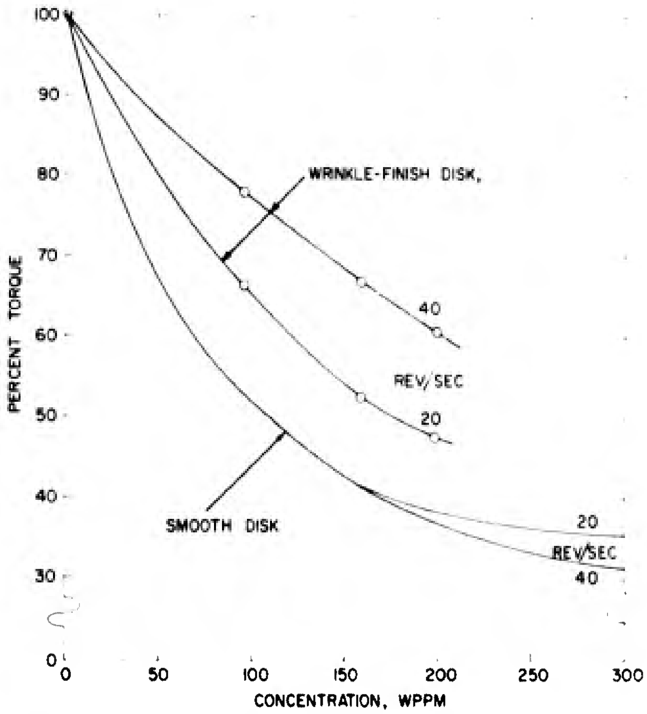

Fig. 20 - Effect of high surface roughness on the percent torque reduction with the 45.7 cm diameter disk

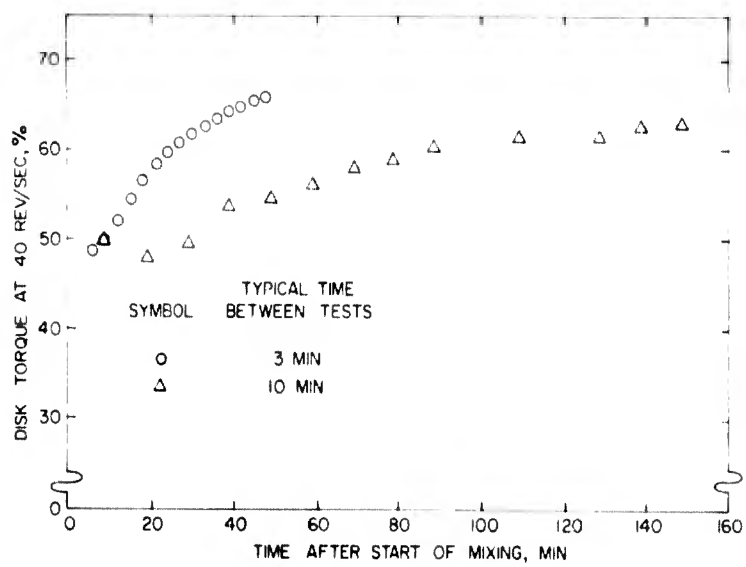

Fig. 21 - Rapid mechanical degradation of a dilute poly(ethylene oxide) solution of 15 wppm concentration, seen in disk tests

* * *

AN EXPERIMENTAL INVESTIGATION OF THE EFFECT OF ADDITIVES INJECTED INTO THE BOUNDARY LAYER OF AN UNDERWATER BODY

W. M. Vogel and A. M. Patterson
Pacific Naval Laboratory
Victoria, British Columbia, Canada

ABSTRACT

The effects of injecting solutions of three linear, high molecular weight polymers into the boundary layer of a three-dimensional streamlined model are being investigated. The following are the preliminary results of this experiment:

(a) The drag of the body decreased with increasing molecular weight of the polymer.

(b) The drag decreased as the concentration of the polymer solutions increased. At concentrations above 500 ppm for the highest molecular weight polymer used, the amount of drag reduction decreased.

(c) For increased flow rates of the polymer solution, the drag reduction increased.

(d) The flow rate of the solution injected into the boundary layer, and not the injection flow velocity, was the controlling factor at the injection velocities used.

(e) Turbulence and average velocity measurements in the wake of the body indicated two effects when the polymer solution is injected: a change in the mean square of the turbulence velocities, and a change in the velocity profile.

INTRODUCTION

B. A. Toms (1949) pointed out that, in turbulent pipe flow, dilute solutions of linear polymers reduced the pressure drop along the pipe to a value below that of the solvent. Since then there has been a growing body of literature on the flow of polymer solutions which exhibit non-Newtonian characteristics. Experimentally, most of the studies have been concerned with the rheological characteristics of the fluid, or with pipe friction. The work by Shaver (1957) showed that in some cases the addition of a long molecule polymer to a liquid resulted in higher friction losses at low flow rates and lower friction losses at high flow rates. This is analogous to the behaviour observed by Daily and Bugliarello (1961) in wood fibre suspensions in smooth pipes. Shaver and Merrill (1959) observed the velocity profiles of dilute polymer solutions in circular pipes and found that at high flow rates the profiles were sharper than for a corresponding Newtonian flow. This did not check with Dodge and Metzner's (1958) prediction of profiles blunter-than-Newtonian. This disagreement was attributed by Dodge and Metzner to the possible presence of elastic effects in the fluids used by Shaver and Merrill.

Recently Fabula, Hoyt and Crawford (1963) investigated about twenty-five water-soluble polymers. They discovered that whenever the polymer had both a high molecular weight and a linear molecule, significant reduction in friction occurred in the high Reynolds number flows ($Re > 10^5$). This phenomenon was first observed with a rotating-disc apparatus and later confirmed using a pipe flow apparatus. The very dilute solutions studied were often superficially indistinguishable from plain water, and their apparent viscosities for the high shear rates involved were nearly that of water.

One of the polymers tested in the rotating disc apparatus, poly(ethylene oxide), gave about a 70% torque reduction for a .01% solution (Hoyt and Fabula 1964). In the pipe flow apparatus, cases of 50% pipe friction reduction were found for very dilute solutions of poly(ethylene oxide) in water (Fabula, 1963). Because of these large changes in the turbulent flow produced by very low concentrations of poly(ethylene oxide) in water, it was proposed to study the effect of these polymer solutions when they were injected into the boundary layer of an underwater body.

EXPERIMENTAL APPARATUS

There are a number of variables which should be considered when a fluid is injected into the boundary layer of a body. These are:

1. Type of polymer solution
2. Concentration of the polymer solution
3. Velocity of injection of the solution
4. Position of the injection slot
5. Tunnel velocity

A body of revolution (Fig. 1) was chosen as the most convenient to use for these exploratory experiments. Because our low-turbulence water tunnel has a working section 35cm by 35cm, the maximum diameter of the body was limited to about 5cm so that tunnel blockage would be minimized. The body as finally constructed was 41.3cm long and had a maximum diameter of 5.08cm. Five slots were made in the body; the positions of the slots are shown in Fig. 2. The section

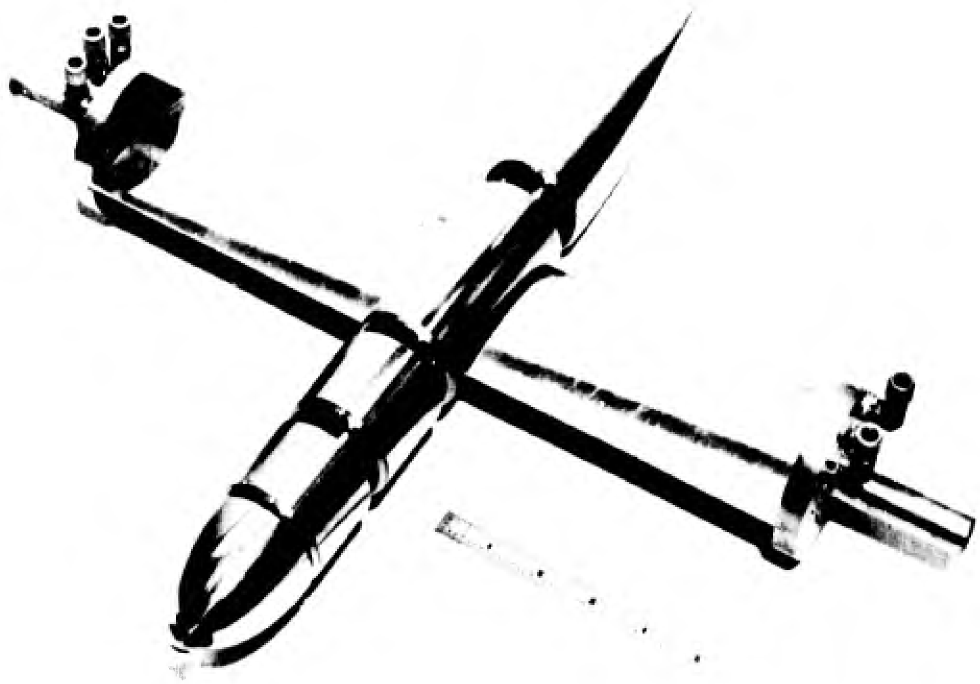

Fig. 1 - Model used for drag reduction experiments

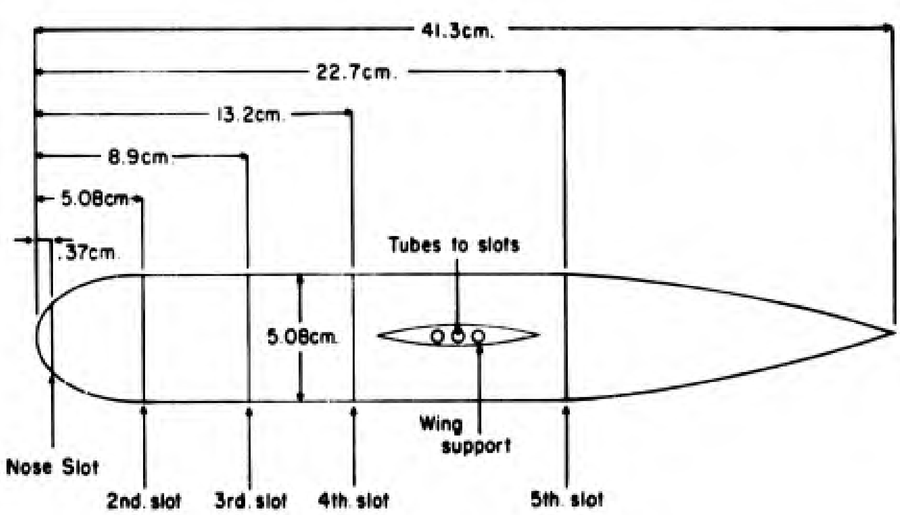

Fig. 2 - Schematic of model

up to the second slot is elliptical in shape, the section from the second to the fifth slot is cylindrical and the tail section is faired to a pointed trailing edge. Each slot can be individually adjusted, and the polymer solution can be injected through each slot independent of the flow through the other slots. Only the nose slot was used for this work.

The wings are elliptical sections symmetrical about the line joining the leading and trailing edges. They are mounted on the body so that the planes of symmetry of each wing pass through the centre-line of the body. The wings serve two purposes: to support the body in the three-component force balance, and to act as a shield for the lines running to the slots. Three lines are in one wing and two lines in the other.

The pumping system and tunnel set-up are shown in Fig. 3. In order to minimize the possibility of degrading the fluid before it is injected into the boundary layer it was decided to use air pressure as the pumping force. When the fluid is mixed it is drawn into the pump by reducing the air pressure in the pump. To inject the fluid into the boundary layer a known positive pressure is applied to the pump. The pressure is adjusted until the desired flow rate is achieved. The flow rate is determined by using a stopwatch to measure the time required for a known volume of the fluid to leave the pump.

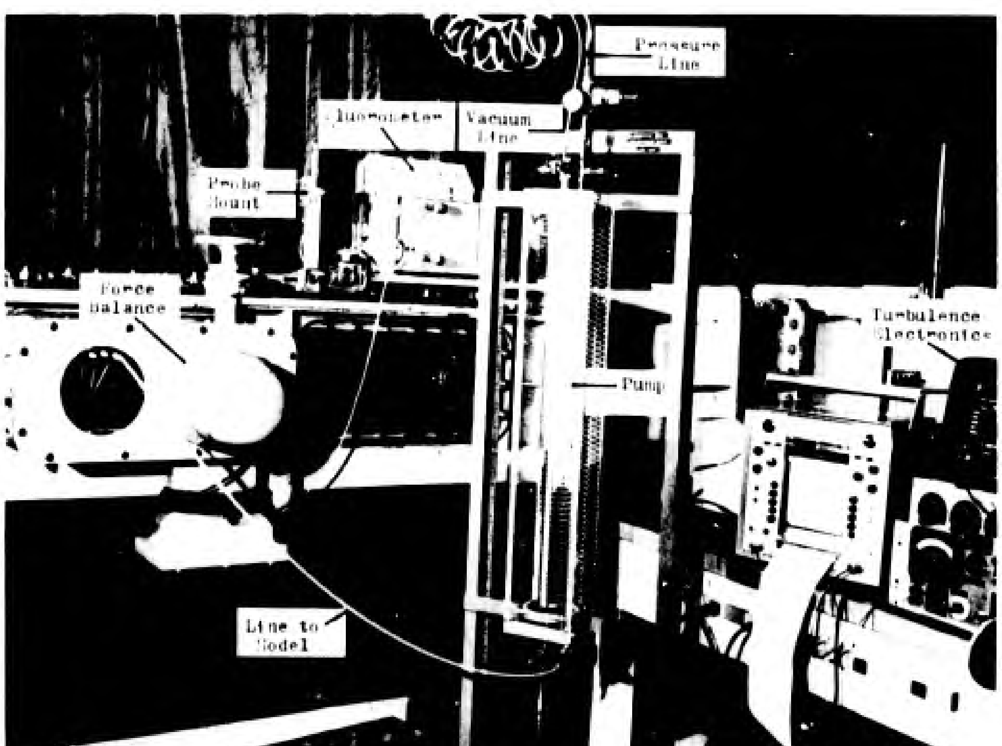

Fig. 3 - Water tunnel and equipment used for drag reduction experiments

POLYMER SOLUTION

Three types of poly(ethylene oxide) were used; these are manufactured by the Union Carbide Chemicals Company and are designated: POLYOX WSR-35, which has a weight-average molecular weight of several hundred thousand, POLYOX WSR-205, which has a weight-average molecular weight of about 500,000 and POLYOX WSR-301, which has a molecular weight of about 4 million. POLYOX resins are made up of very long linear molecules which are completely soluble in water at room temperatures. At concentrations of 1% or more, aqueous solutions of poly(ethylene oxide) with a molecular weight of a million or more exhibit a stringy consistency and are classed rheologically as "shear thinning" (Powell and Bailey, 1960). For very dilute solutions, however, the rheological properties are indistinguishable from water (Fabula et al, 1963).

Because previous work (Hoyt and Fabula, 1964) indicated that the reduction in friction was very sensitive to polymer molecular weight and to mechanical degradation, a standard mixing technique was employed to minimize and to standardize the degradation. The solutions were mixed in 4000 ml amounts, using a standard laboratory stirrer rotating at about 5 revs/sec. A large propeller with cylindrical blades was used to reduce the chopping of the molecules, which could occur with a sharp edge propeller. The poly(ethylene oxide) was used as received from the manufacturer and was slowly added to the water to prevent lumps forming. The length of the mixing was between 30 seconds and one minute, depending on the concentration being mixed. In order to ensure that the polymer was fully hydrated, the solution was left at least four hours before it was used. Usually the solution was left standing overnight. Before being put into the pump the solution was gently stirred to make certain that none of the polymer had settled out.

APPEARANCE OF THE SOLUTION

Concentrations of up to 250 ppm of POLYOX WSR-35 and WSR-205 were used for these tests. They were easily mixed, and at the 250 ppm concentration had a slippery feel but did not exhibit any stringiness. POLYOX WSR-301 was easily mixed up to concentrations of 500 ppm but at higher concentrations the material had a tendency to form lumps which, at the highest concentration used, (2,500 ppm) sometimes did not disperse even after the solution had been left standing for several days. In these cases the solution was re-mixed with the stirrer, with no apparent adverse effect. At about 400 ppm the WSR-301 solution began to exhibit stringiness; this stringiness increased markedly as the concentration was increased. Concentrations up to 2,500 ppm of the WSR-301 were used in these tests and it was found that, once mixed, these solutions were readily diluted, which indicated that even the highest concentration would mix with t boundary layer fluid when it was injected.

DRAG REDUCTION

A series of runs was carried out to examine the state of the boundary layer at different tunnel velocities. In order to ensure that the boundary layer would be turbulent over the body even at the lowest tunnel speeds used, it was decided to use a trip ring made of 0.09 cm diameter wire placed 1.43 cm from the nose of the body (between the nose slot and the 2nd slot). Observations using threads attached to the body indicated that at tunnel speeds above 150 cm/sec the boundary layer was completely turbulent from the trip ring to the tail. It is uncertain whether the boundary layer from the nose slot to the trip ring is completely turbulent at the lower speeds used.

Before the drag runs were made the body was aligned by measuring the lift and pitching moment on a three component force balance (Kempf and Remmers, Hamburg) and rotating the body vertically until these forces were zero. The balance holds the model so that the centre-line of the wing section is horizontal and at right angles to the centre-line of the tunnel.

Figure 4 shows the drag of the body-wing combination with the trip ring vs the tunnel velocity used for this work. The Reynolds numbers, based on the length of the body, are 6.5×10^5 for 150 cm/sec and 2.6×10^6 for 625 cm/sec.

SOURCES OF ERRORS IN DRAG MEASUREMENTS

There are several sources of error in determining the drag of the body. Fluctuations in tunnel velocity during the run gave rise to fluctuations in the drag reading by as much as plus or minus 1 to 2 grams. This error was minimized during the runs with the polymer injection by reading the drag reduction when the fluid was injected, and the drag increase when the fluid was stopped. If there was a marked difference between the two readings the run was repeated. Another source of error is a reading error of the meter recording the drag; this is about plus or minus 0.25 grams. A third source of error is the gradual buildup of the concentration of the polymer in the tunnel. The drag of the body was measured before each run and if there was a difference between it and the data in Fig. 4 the tunnel was drained and refilled with water. On only one occasion was it necessary to drain the tunnel for this reason; the usual procedure was to drain the tunnel after each day's runs when the higher concentrations were being used. At the lower concentrations the tunnel was drained after three day's runs. The tunnel holds 23,000 litres of water. Most of the drag data reported is an average of the data recorded for at least two runs, and the estimated error is plus or minus 1 gram.

EFFECT OF POLYMER CONCENTRATION AND MOLECULAR WEIGHT

A series of runs was carried out to determine the effect of polymer concentration on the drag reduction for the three polymers. The fluid was injected into the boundary layer through the nose slot which was 0.25 mm wide. Although the nose slot is at right angles to the centre-line of the body, the fluid when injected flows back over the body and does not appear to disturb the flow in the boundary layer.

Figures 5 to 7 show the drag reduction vs tunnel velocity obtained with the three polymers when they are injected into the boundary layer at a rate of 30 ml/sec. The average velocity through the slot would be 200 cm/sec. These figures are replotted in Figs. 8 to 12 to show the effect of polymer concentration on the drag reduction for different tunnel velocities. It is usual when plotting drag reduction to plot the percentage reduction. However, in this work we have

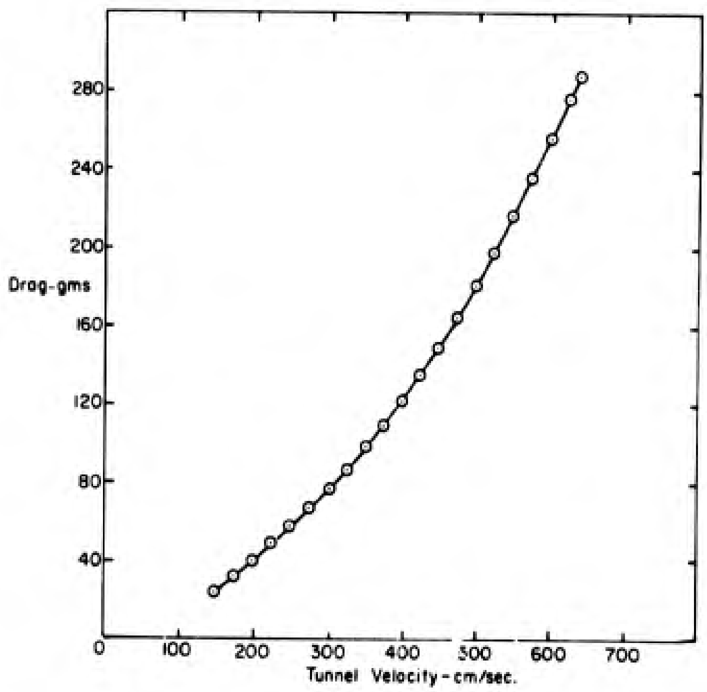

Fig. 4 - Drag of body plus wing supports and trip wire at nose

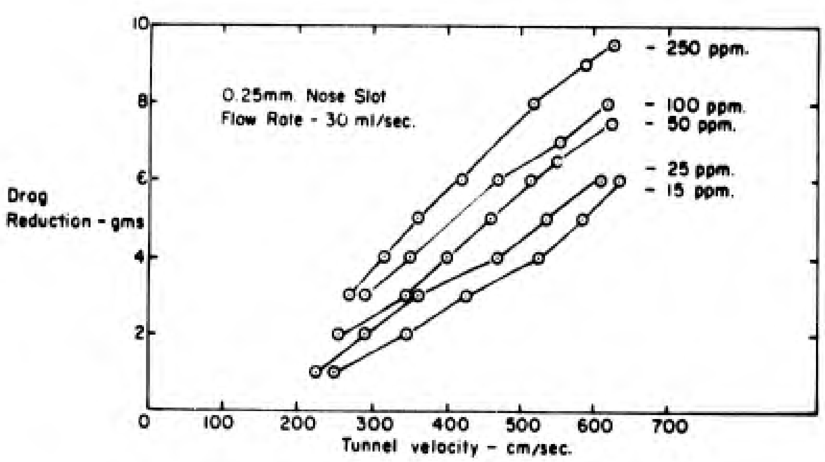

Fig. 5 - Drag reduction using POLYOX WSR-35

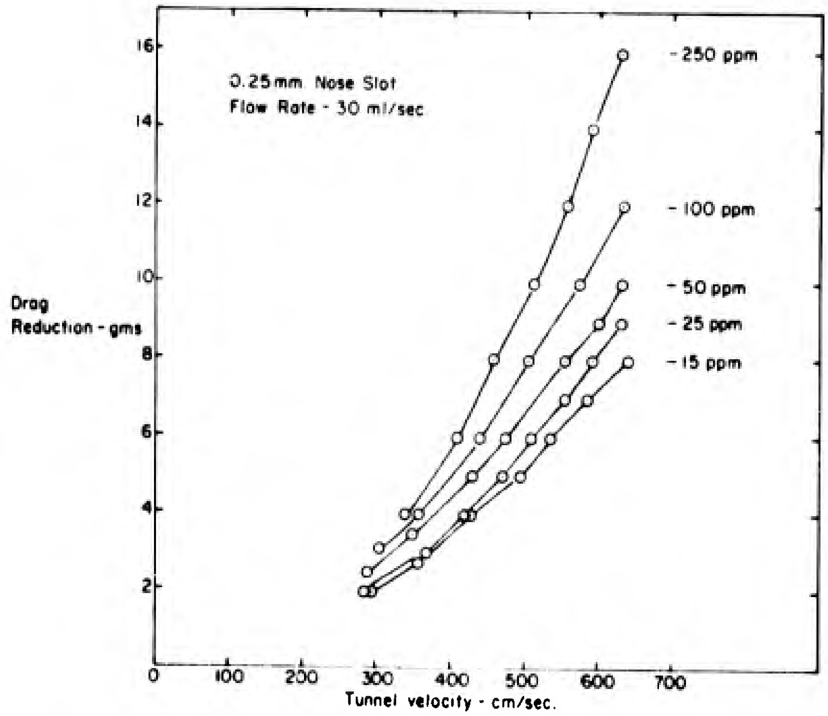

Fig. 6 - Drag reduction using POLYOX WSR-205

not separated the body and wing drag, and as the drag reduction takes place essentially over the body it was felt that plotting in terms of the actually drag reduction would give a clearer picture of the effect of additive injection. The increase in the effectiveness of the polymer as the concentration is increased is clearly shown. Figures 7 and 12 also show that a peak in the drag reduction curve is reached somewhere between a concentration of 500 ppm and 1,000 ppm. A similar peak occurred in the rotating-disc work carried out by Hoyt and Fabula (1964). Complete agreement is not likely as there is a large unknown dilution of the additive in our case. The increased drag reduction as the molecular weight is increased is shown in Figs. 9 to 10.

Figure 13 shows two sets of runs at a lower polymer flow rate of 13 ml/sec (average velocity through the slot would be 87 cm/sec). These curves also show that there is a decrease in the effectiveness of the polymer solution as the concentration is increased above about 500 ppm. Runs were also done injecting water of flow rates of 30 ml/sec and greater; no drag reduction was observed over the tunnel velocity range of 150-625 cm/sec.

VELOCITY OF INJECTION OF THE SOLUTION

Figure 14 shows the effect of increasing the flow rate of the polymer through the nose slot. Although this effect is plotted for only 500 ppm of WSR-301 it was also observed for other concentrations of the three polymers. Runs at other

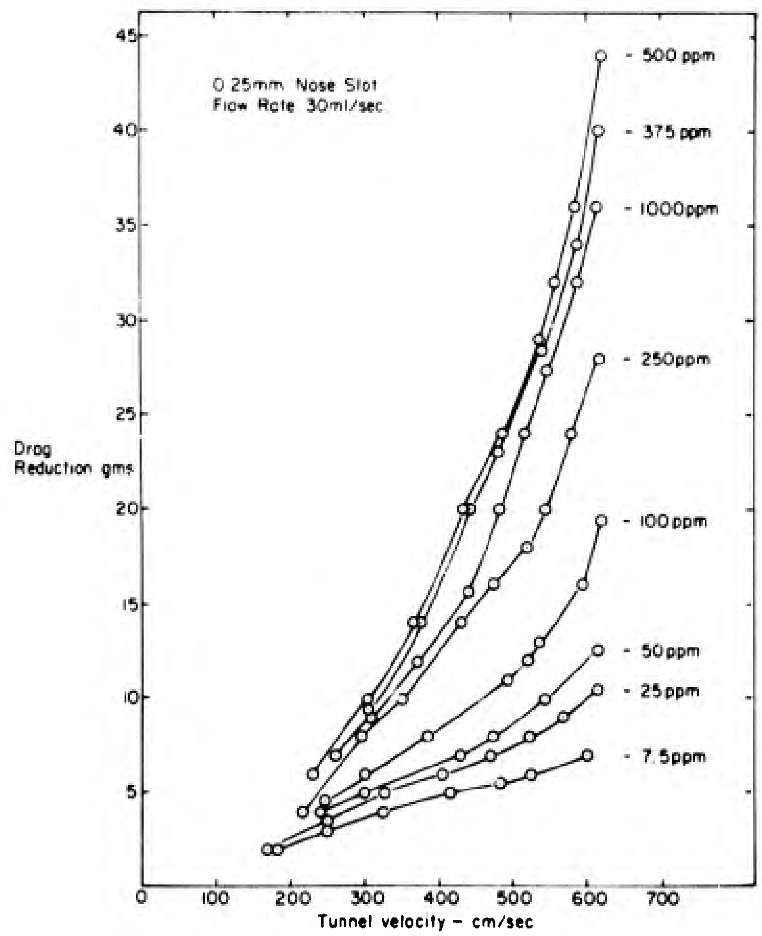

Fig. 7 - Drag reduction using POLYOX WSR-301

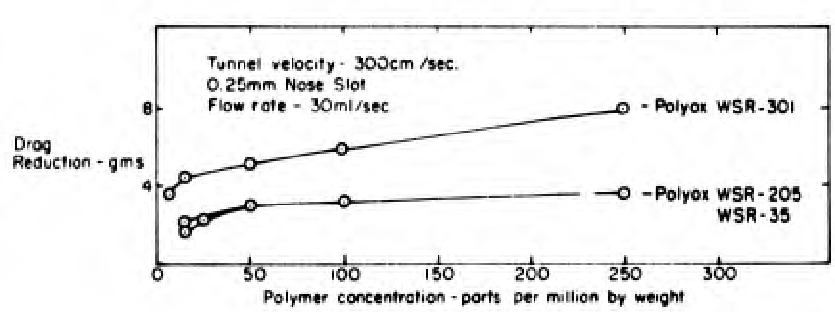

Fig. 8 - Drag reduction vs polymer concentration

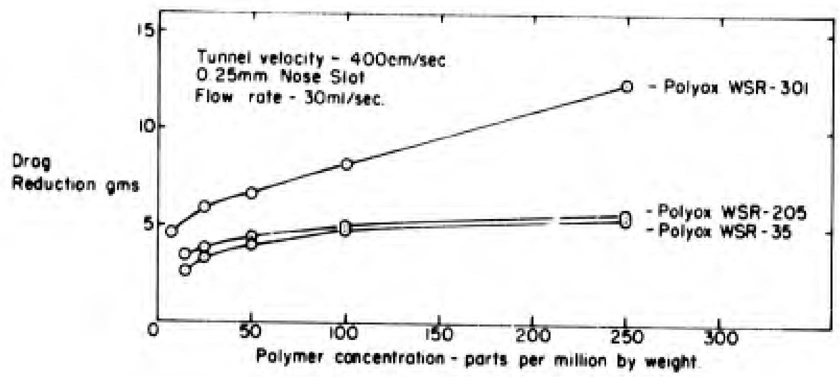

Fig. 9 - Drag reduction vs polymer concentration

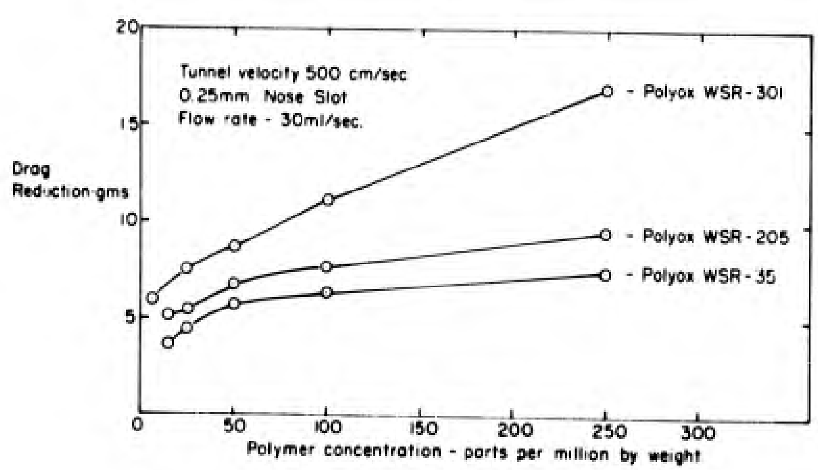

Fig. 10 - Drag reduction using polymer concentration

concentrations were carried out to a flow rate of 50 ml/sec and the drag reduction was still increasing with increasing flow rate. There was some indication that at flow rates higher than this a plateau was reached in the drag reduction. Whether this is a real effect in the boundary layer or a limitation in the flow through the tubes to the slot has not been determined. It has also been suggested that increased turbulence in these tubes could degrade the polymer.

The average velocities through the nose slot for these flow rates are; 87 cm/sec for 13 ml/sec, 154 cm/sec for 23 ml/sec, 200 cm/sec for 30 ml/sec, and 335 cm/sec for a flow rate of 50 ml/sec. These injection velocities are comparable to the tunnel velocities at which these tests were run.

Figure 15 shows the effect of increasing the slot width from 0.25 mm to about 0.9 mm. Four flow rates were used with each slot opening, and although

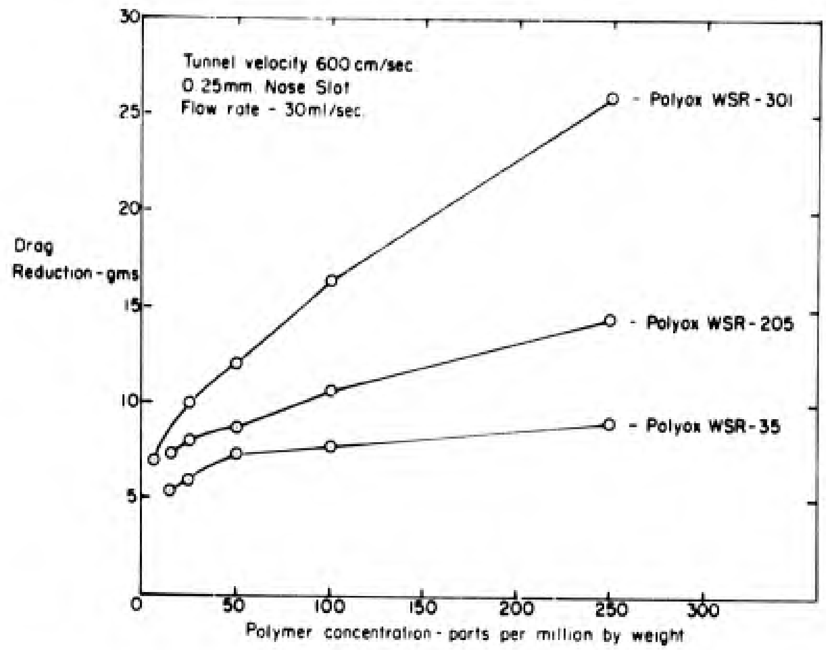

Fig. 11 - Drag reduction vs polymer concentration

there is some scatter in the data which could indicate that there is some degradation of the fluid at the smallest slot opening, the main conclusion drawn is that at these flow rates the important parameter is not the flow rate but the quantity of the fluid injected.

DEGRADATION OF THE POLYMER SOLUTION

On several occasions a solution was mixed and for some reason left standing for three or four days in a metal container. A brown deposit was usually found in the bottom of the container, and when the solution was used it was noted that the drag reduction was less than that obtained with solutions which had been standing less than 24 hours. These runs were not included in the foregoing figures. To determine the magnitude of this effect we did runs with a standard and with a degraded solution; the results are shown in Fig. 16. No analysis of the brown deposit was carried out.

No experiments were carried out to determine the mechanical degradation of the polymer solutions.

DYE-INJECTION STUDIES

In order to determine whether the gross structure of the boundary layer was affected when the polymer solutions were injected, it was decided to dye the fluid

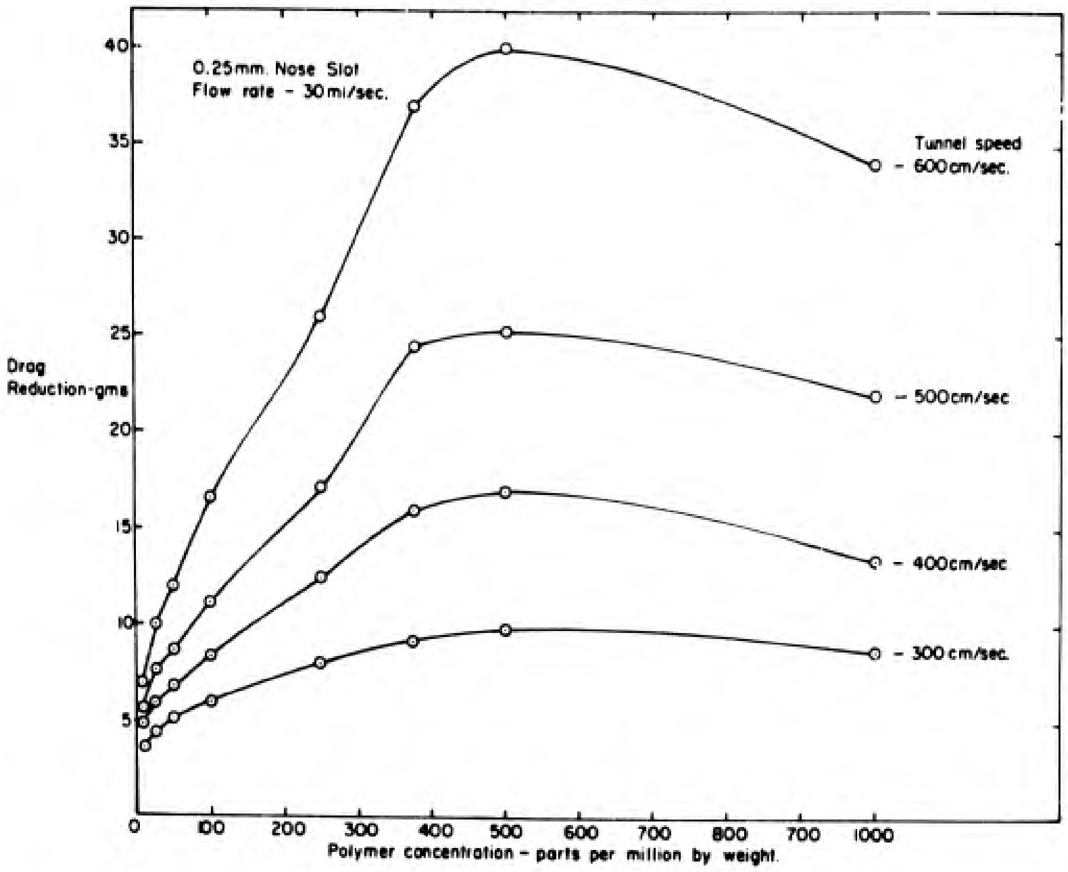

Fig. 12 - Drag reduction vs polymer concentration
for POLYOX WSR-301

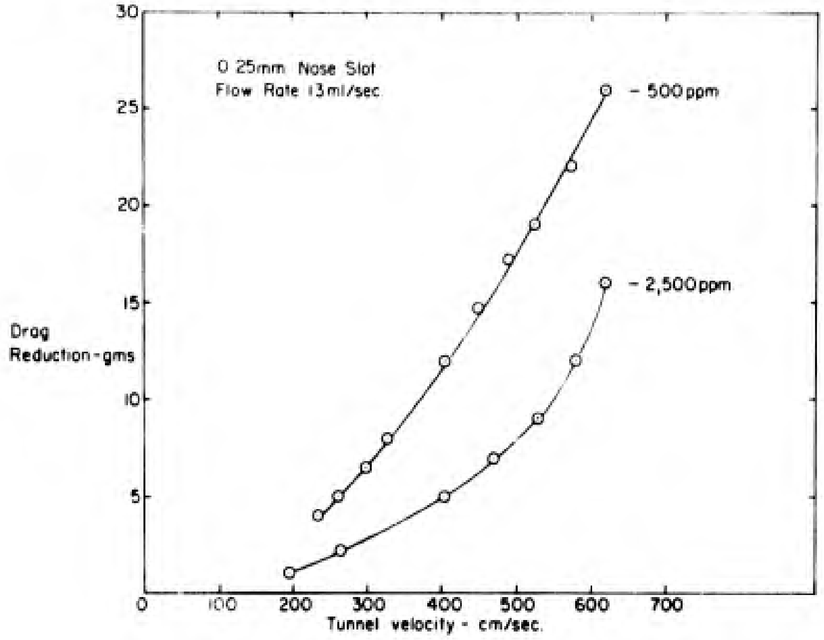

Fig. 13 - Drag reduction using POLYOX WSR-301

being injected and to monitor the dye concentration in the wake of the body. A series of runs was carried out at 450 cm/sec, using pure water and a 100 ppm solution of POLYOX WSR-301. The dye used was Rhodamine 'B', which is detectable to about 1 part in 10^{11} by a fluorometer (Model 111, G. K. Turner, Palo Alto, Calif.). The initial concentration of the dye in the fluids was 1 part in 10^{4}. The flow rate through the slot was 30 ml/sec.

Visual observations of the flow over the body indicated that the dye was almost immediately mixed into the boundary layer. The boundary layer thickness at the downstream end of the cylindrical section of the body was about 0.3 cm. Separation occurred over the tail section of the body, and the boundary layer at the trailing edge appeared to be about 2.5 cm thick. The dye measurements were made 7 cm downstream from the tail of the body. At this location the boundary layer appeared to have about the same diameter as the cylindrical portion of the body.

The total head pressure in the working section of the tunnel, which is about 0.7 kilograms per square inch above atmospheric pressure, was used to draw the fluid from the wake through a conical pitot probe, with a 2 mm opening, to the fluorometer. The probe was mounted on a holder which could be continuously moved across the wake and could be placed vertically in accurately measured steps. When the dye was injected the probe was moved at a known speed through the wake and the output was recorded on a paper chart. The probe was then moved vertically and the process repeated. The dye did not affect the properties of the polymer solution, because the drag reduction was the same as obtained for previous runs.

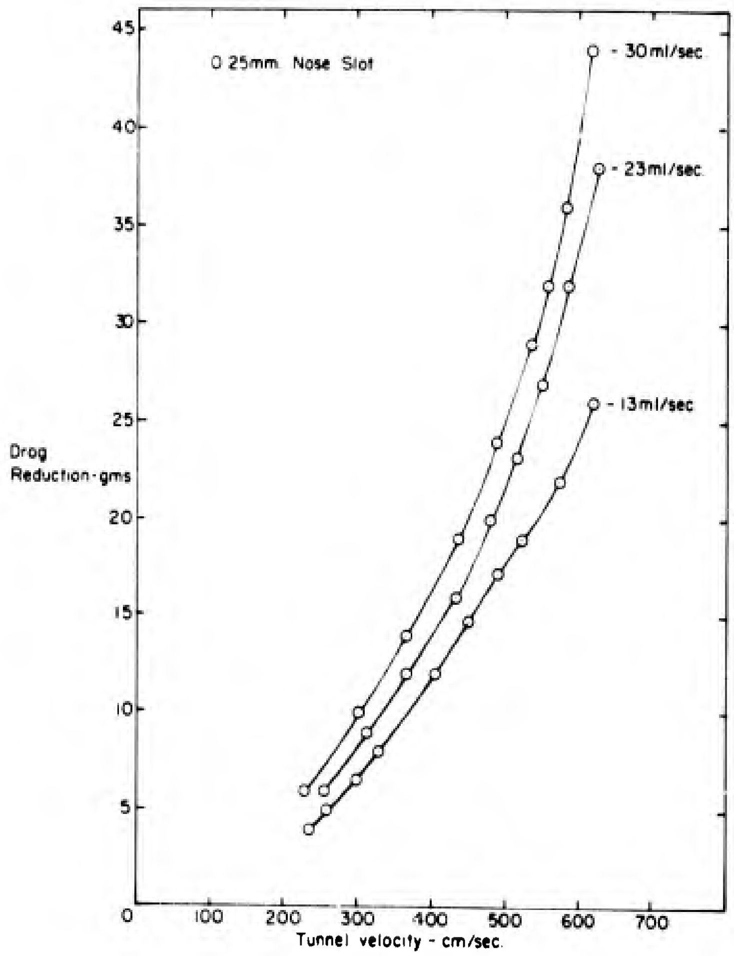

Fig. 14 - Drag reduction vs polymer injection flow for 500 ppm. POLYOX WSR-301

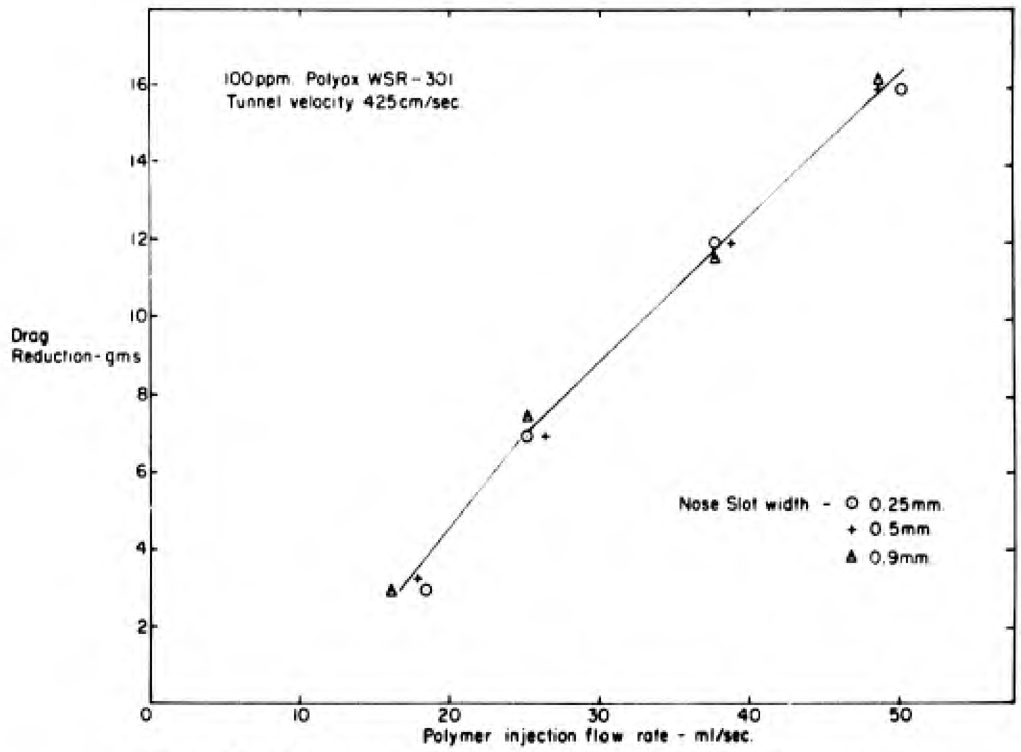

Fig. 15 - Drag reduction vs polymer injection flow rate

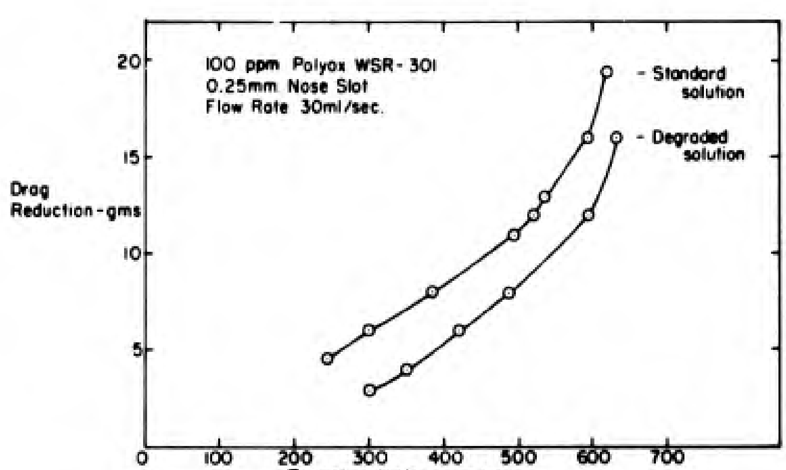

Fig. 16 - Effect of polymer degradation on drag reduction

Figure 17 shows the results of these runs. It is apparent from the dye concentration contours that the centre of the wake is between 1 cm and 1.5 cm above the centre-line of the body. This means that the body had become misaligned with the flow by about 1.75° for these runs. For the most part the distribution of the dye is very much the same for both the water and the polymer.

There appears to be a slight increase in the concentration of the dye at the centre of the wake for the polymer injection. The maximum reading for the water was 95 parts in 10^8, while for the polymer it was 97.5 parts in 10^8. The differences in shape at the outer portion of the wake are more likely the effect of the misalignment of the body than the effect of injecting the polymer solution. These runs do indicate that the solution is diluted appreciably in the boundary layer. At the centre of the wake the dilution is about 100:1, while at the edge of the wake it is at least 10,000:1.

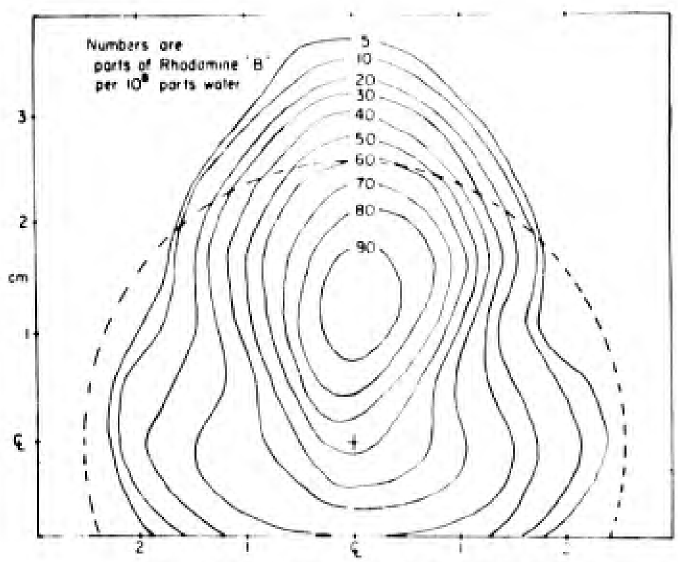

CROSS-SECTION OF WAKE 7cm DOWNSTREAM OF BODY-
NO POLYMER INJECTED

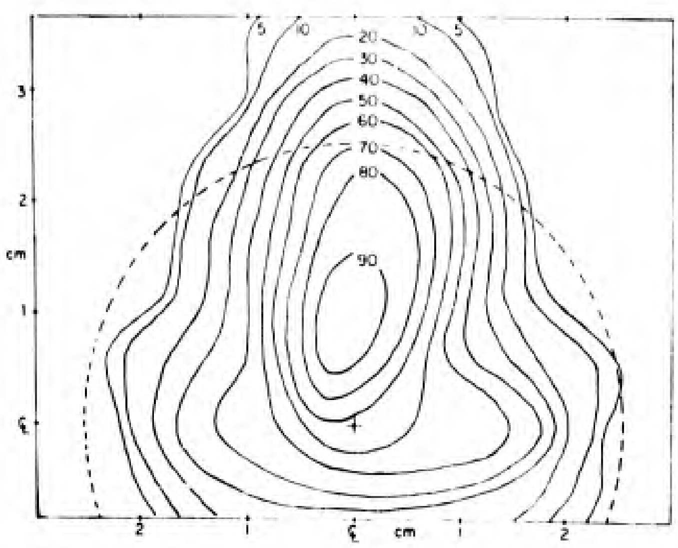

CROSS-SECTION OF WAKE 7cm DOWNSTREAM OF BODY-
WITH 100ppm POLYOX WSR-301 INJECTED FROM NOSE SLOT

Figure 17

TURBULENCE STUDIES OF THE WAKE

To obtain more detailed information on the effect of the injection of a polymer solution on the drag, a study of the turbulence in the wake was made using two concentrations of POLYOX WSR-301, 100 ppm, and 500 ppm. A tunnel velocity of 400 cm/sec and an injection flow rate of 30 ml/sec through the 0.25 mm nose slot were used for all the runs.

A hot-film probe was used to measure the turbulence and the average velocity in the wake. The sensitive element is a thin platinum film, mounted near the tip of the conical nose of the probe, which is maintained at a constant temperature by appropriate electronics (Evans, 1963). This type of probe essentially responds to the turbulence fluctuations in the direction of the mean velocity in the tunnel (Ling, 1955). The probe was mounted in the same holder as used for the dye work, with the platinum film 7 cm behind the tail of the model. This is the same position as used for the dye runs. The frequency response of the probe is reasonably flat to about 1000 cps, and the average velocity output of the equipment was adjusted so that it had a linear response over the velocity range encountered in the wake.

The procedure in each set of runs was to record the turbulence signal for about a minute starting at the centre of the wake without a polymer solution in the boundary layer. The polymer solution was then injected, and the turbulence again recorded for about a minute. The average velocity at that position in the wake was read from a meter, and any changes in the velocity when the polymer solution was injected were recorded. After each run the probe was moved up 0.5 cm and the procedure repeated until the probe was out of the wake.

The recorded turbulence signal was passed through a digitizer with a sampling rate of 2500 samples/sec, and the resulting digital tape was processed on our Packard-Bell PB-250 computer to obtain the mean square of the turbulence velocities, and the power spectrum of the turbulence at the probe positions in the wake.

Figures 18 and 19 show the average velocity profiles and the mean square of the turbulence velocities for the wake with no fluid injection, and with 100 ppm, and 500 ppm solutions of POLYOX WSR-301 injected at 30 ml/sec. The tunnel velocity for these runs was about 400 cm/sec. Two effects of the polymer solution injection are shown. For the 100 ppm solution the mean velocity increased and the turbulence level decreased; for the 500 ppm solution, the mean velocity increased markedly, but the turbulence level also increased. There is a reading error of about plus or minus 2 cm/sec in the average velocity curves. The significance of the differences shown in Fig. 19 for the probe positions between 2 cm and 3 cm above the wake centre-line is not known.

Figure 20 shows a set of spectrum of the turbulence taken 0.5 cm above the wake centre-line for the 100 ppm solution. Figure 21 shows three sets of spectra for the 500 ppm solution taken at the centre-line of the wake, 1.5 cm above the centre-line, and 3 cm above the centre-line. These curves are plots of log ϕ vs log k where ϕ is the mean square of the turbulence velocity per unit wave number k, and $k = 2\pi$ (frequency of the turbulence signal) divided by the average velocity passed the probe.

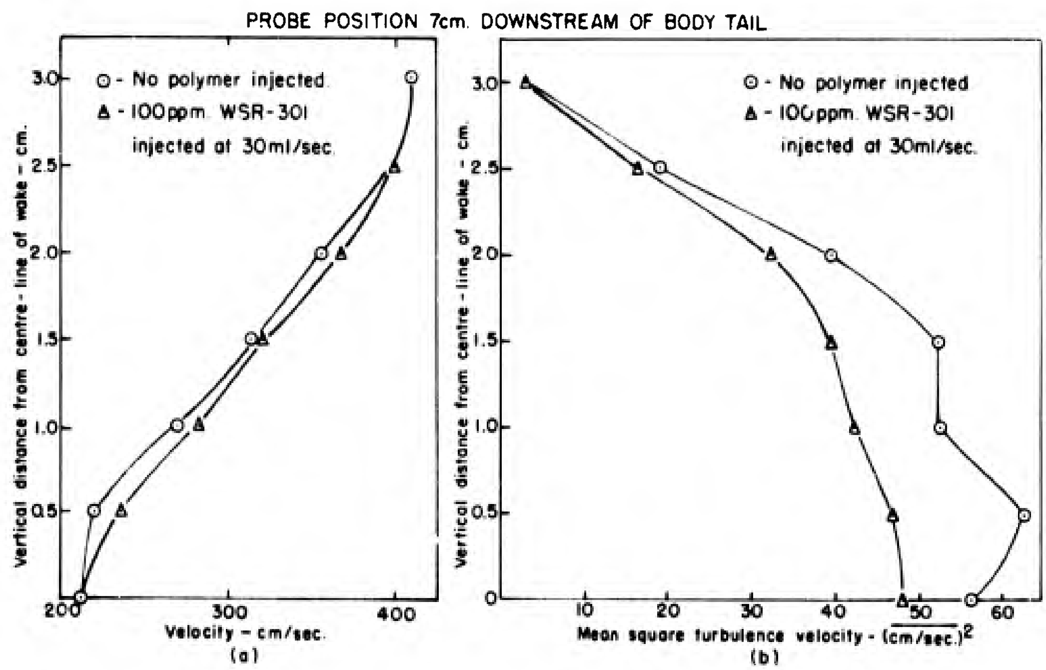

Fig. 18 - (a) Average velocity, (b) mean square turbulence velocity through wake

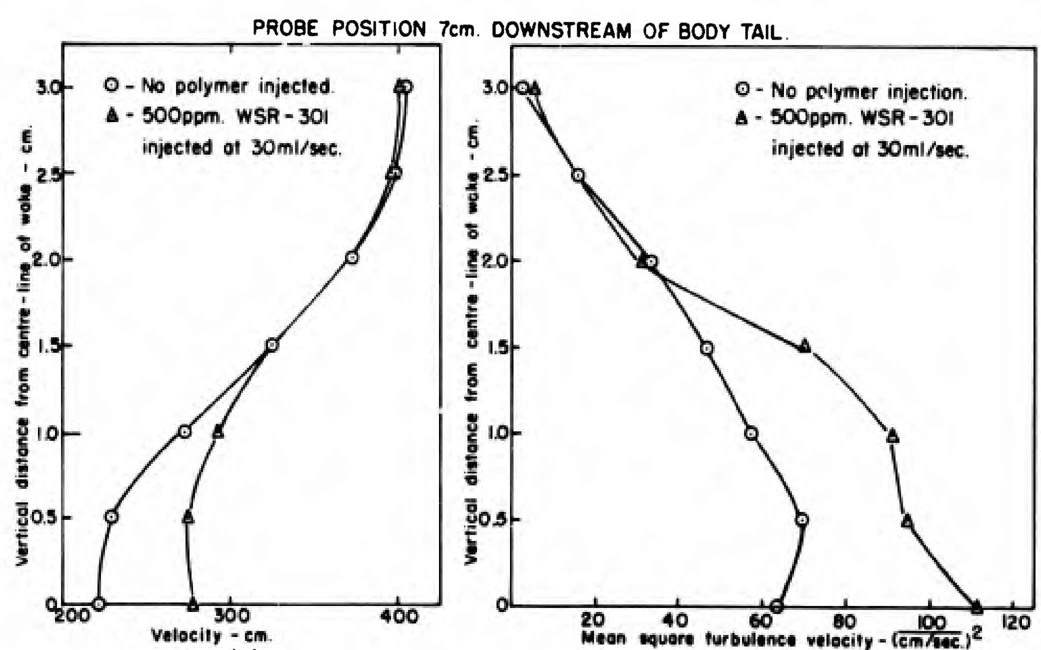

Fig. 19 - (a) Average velocity, (b) mean square turbulence velocity through wake

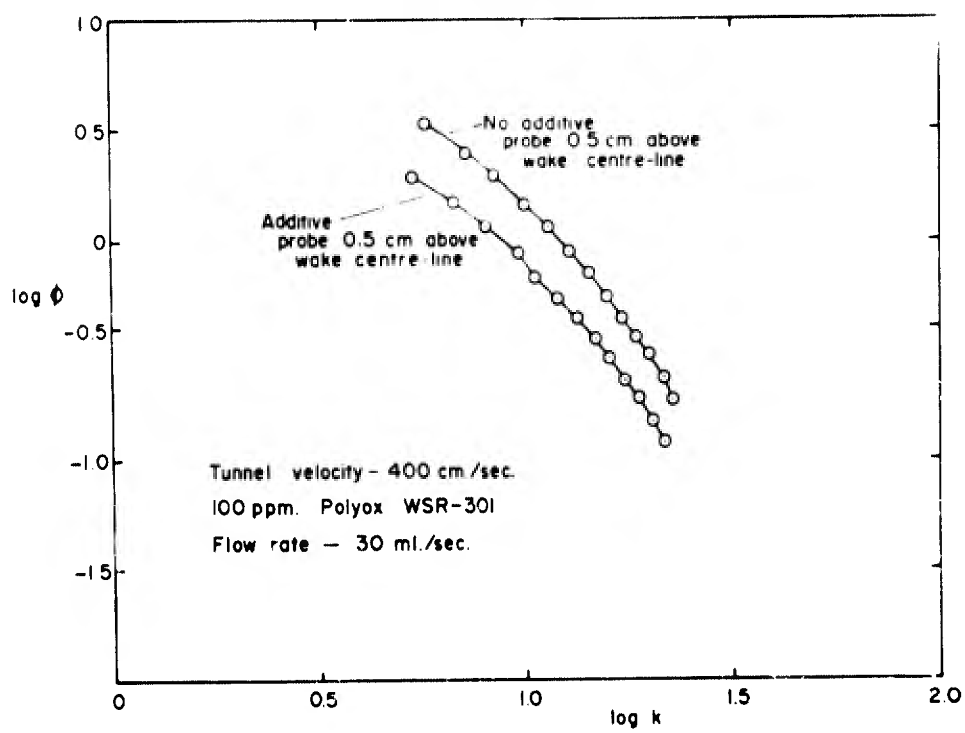

Fig. 20 - Turbulent velocity power spectra

The curves in Fig. 20 show that the injection of the polymer solution reduced the turbulence intensity over the frequency band analyzed. The highest frequencies used for this analysis are about 1200 cycles per second because tl frequency response of the hot-film probe falls off in this regio . In Figure 21 the curves for the probe at the centre-line of the wake show that, for the smal wave numbers, the turbulence energy is increased when the fluid is injected, b as the wave number increases the curve for the additive crosses the other cur and the energy at the higher wave numbers is less for the polymer in the boun ary layer. For the 1.5 cm position, the additive curve is again higher, and the point at which the curves appear to cross over is at a higher wave number tha for the centre-line case. With the probe 3 cm above the centre-line of the wal the character of the signal, as observed on an oscilloscope, contains many lar spikes which indicate that the wake turbulence is intermittent in this position. The curve for the additive case are still higher than for the wake without the a ditive but the slope of the curve indicates that a cross-over might occur at a wave number larger than for the 1.5 cm case.

DISCUSSION OF EXPERIMENTAL RESULTS

This is essentially an exploratory experiment which attempts to add to th knowledge of the behavior of polymer solutions in reducing the friction of a fl along a solid surface. Previous work by Fabula et al (1963) had shown that th

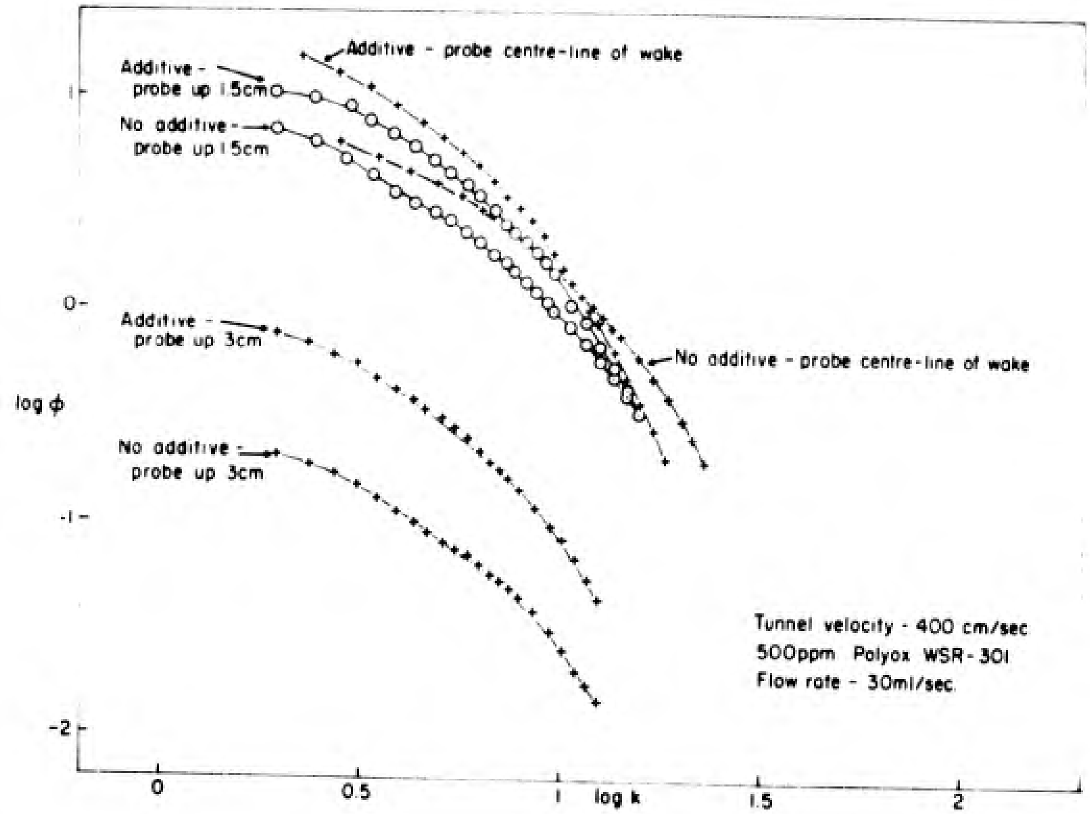

Fig. 21 - Turbulent velocity power spectra

best reduction in friction was obtained by a linear, high molecular weight molecule. The three POLYOX resins gave very good results in pipe-flow and rotating-disc experiments (Fabula, 1963; Hoyt and Fabula 1964) and were chosen for this work because of the amount of information available on some of their characteristics. Limiting ourselves to POLYOX limits the number a variables of the polymer characteristics to that of molecular weight.

All the runs were carried out with the polymer solutions and the water in the tunnel at a temperature of between 19.5° and 21°C so that if there are any temperature effects on the drag reduction they would not show up in this work. The use of standard mixing techniques should give solutions which if degraded, will have a constant degradation for each concentration of each polymer used. It is proposed in future to measure the molecular weights of the polymers after they have been mixed so that any degradation can be determined.

Increasing the molecular weight of the polymer gave increasing drag reduction as has been demonstrated by Fabula et al. It is difficult to relate our results directly to those of Hoyt and Fabula as we have an unknown but large dilution of the polymer solution when it is injected into the boundary layer. Measurements in the wake using a 100 ppm POLYOX WSR-301 solution indicate that a dilution of 100:1 takes place at the centre of the wake 7 centimetres behind the body. A rough calculation based on the observed boundary layer thickness at the downstream end of the cylindrical portion of the body showed that the dilution through the boundary layer would be of this order. The boundary layer is too thin to probe so no direct measurements in the boundary layer have been made.

The effect of increasing the polymer concentration has been shown for the three polymers used. For POLYOX WSR-301 a peak in the drag reduction curve is reached somewhere between a concentration of 500 ppm and 1,000 ppm. It is suggested that polymer molecular entanglement and interaction at the higher concentration is responsible for this effect. It is possible that the time interval the fluid is flowing over the body is too short for the molecules to become untangled even though the fluid is being diluted as it flows over the body. In extending this work we plan to carry out more dye runs at the higher concentrations to determine whether the fluid is being mixed through the boundary layer or concentrating near the body.

The turbulence studies in the wake have indicated that both the mean velocity and the turbulence level are being affected by the injection of the polymer solution into the boundary layer. We have not measured these parameters at other distances downstream nor in the boundary layer of the body itself so do not know whether the measurements are only applicable at this one position. Also the turbulence probe measures only the component of the turbulence in the direction of the mean flow. It would appear though that the polymer is interacting with the turbulence and with the shear stresses. The increase in the turbulence level for the low wave numbers for the 500 ppm solution of WSR-301 could be a result of the interaction of the polymer with the turbulence components in the two directions not measured and energy being fed into the downstream component. It could also be a result of the change in the shear stresses which occur with the change in the average velocity profile.

The one spectrum shown for the 100 ppm solution and the high wave number portions of the 500 ppm solution spectra indicate that the polymer does interact with the downstream component of the turbulence. Further information is required before a more definite statement on the significance of these results can be made.

In order to obtain more detailed information we are in the process of investigating the wake of a cylinder at right angles to the flow. The polymer solution is injected into the wake through holes in the rear of the cylinder and measurements of the effect of the polymer on the turbulence and mean flow of the wake are being investigated. Because the wake of a cylinder is quite well known it is hoped that some of the questions raised with this experiment will be answered.

SUMMARY OF RESULTS

The effects of injecting solutions of three linear, high molecular weight polymers into the boundary layer of a three-dimensional streamlined model are being investigated. The following are the preliminary results of this experiment:

1. The drag of the body was decreased as the molecular weight of the polymer was increased. At tunnel velocities of 300 cm/sec and 400 cm/sec the results for the two lower molecular weight polymers, POLYOX WSR-35 and -205, were almost the same. At 500 cm/sec and 600 cm/sec the differences were greater. POLYOX WSR-301 was at least twice as effective as WSR-205 at all tunnel speeds used.

2. The drag of the body was decreased as the concentration of the polymer solution was increased. However, for POLYOX WSR-301, the amount of drag reduction decreased at concentrations above 500 ppm. No runs were carried out with concentrations greater than 250 ppm for the other two polymers.

3. For increased polymer flow rates, the drag reduction increased. There was some indication that a plateau in the drag reduction was reached at flow rates greater than 50 ml/sec. Whether this is a limitation of the experimental equipment or a real effect in the boundary layer was not determined.

4. The flow rate of the polymer solution injected into the boundary layer, and not the injection flow velocity, was the controlling factor at the injection velocities and polymer concentrations used.

5. Dye-injection studies indicated that for a concentration of 100 ppm of POLYOX WSR-301 the fluid was quickly mixed through the boundary layer. The dilution of the injected fluid appeared to be at least 100:1 and was found to be 10,000:1 at the edge of the wake 7 cm downstream of the body.

6. Turbulence and mean velocity measurements were made in the wake 7 cm downstream of the body. These preliminary measurements showed that:

(a) For the 100 ppm solution of POLYOX WSR-301, the average velocity increased and the mean square of the turbulence decreased when the polymer was injected. Both these effects were distributed across the full width of the wake. Previous runs with dye had indicated that the polymer solution was distributed through the whole wake. The power spectra of the turbulence signal measured 0.5 cm above the centre-line of the wake, indicated that the decrease in turbulence energy occured over the wave number range measured.

(b) For the 500 ppm solution of POLYOX WSR-301, the average velocity was markedly increased over the central portion of the wake, but was not changed very much in the outer portion of the wake. The turbulence level increased over the central portion of the wake but was not changed very much in the outer portion of the wake. No dye measurements were carried out to determine if the polymer solution was concentrated in the central portion. The power spectra of the turbulence signals indicated that for the small wave numbers the curves for the polymer flow were higher than the curves for no additive. At the centre-line of the wake, the curves crossed, indicating that at the higher wave numbers the energy in the turbulence was reduced when the polymer solution was injected. With the probe 3 cm above the wake centre-line, the additive curve was again higher, but the curves appeared to cross at the limit of the wave number range analyzed.

REFERENCES

1. Daily, J. W. and Bugliarello, G., "Basic Data for Dilute Fiber Suspensions in Uniform Flow with Shear," 1961.

2. Dodge, D. W. and Metzner, A. B., "Turbulence in Non-Newtonian Systems," Report, Univ. of Delaware, 1958.

3. Evans, D. J., "An Instrument for the Measurement of Ocean Turbulence," Pacific Naval Laboratory Technical Memorandum 63-8, 1963.

4. Fabula, A. G., "The Toms Phenomenon in the Turbulent Flow of Very Dilute Polymer Solutions," "Fourth International Congress on Rheology," Brown Univ., Interscience Div., John Wiley, 1963 (in press)

5. Fabula, A. G., Hoyt, J. W. and Crawford, H. R., "Turbulent Flow Characteristics of Dilute Aqueous Solutions of High Polymers," Bull. Amer. Phy. Soc. 8 p. 430, 1963.

6. Hoyt, J. W. and Fabula, A. G., "The Effect of Additives on Fluid Friction." Paper presented at the Fifth Symposium on Naval Hydrodynamics, Bergen, Norway, 1964.

7. Powell, G. M., III and Bailey, F. E., Jr., "Poly(ethylene Oxide)," Encyclopedia of Chemical Technology Second Supplement Volume, Interscience Encyclopedia, New York, p. 597, 1960.

8. Shaver, R. G., "Turbulent Flow of Pseudoplastic Fluids in Straight Cylindrical Tubes," Sc.D. Thesis in Chem. Eng., MIT, 1957.

9. Shaver, R. G. and Merrill, E. W., "Turbulent Flow of Pseudoplastic Polymer Solutions in Straight Cylindrical Tubes," A.I.Ch.E. Journal 5 (2), p. 181, 1959.

10. Toms, B. A., "Some Observations on the Flow of Linear Polymer Solutions Through Straight Tubes at Large Reynolds Numbers," Proc. 1st Internal. Rheol. Congr., North-Holland Pub. Co., Amsterdam, Vol. II, p. 135, 1949.

DISCUSSION

T. G. Lang
Naval Ordnance Test Station
Pasadena, California

In the analysis of data from tests of the type described by Dr. Patterson, the question of the effect of additives on boundary layer separation and wake flow arises. As a preliminary study in investigating such effects, we constructed a small tank 7 ft high and 1 ft by 1 ft in cross-section in which we dropped 25 different bodies in water and also in water with 200 and 1000 parts per million of Polyox 301 additive. Most of the bodies were cones or spheres. The drag of the bodies was obtained through the photographic measurement of their terminal velocities using a darkened room and a strobe light for illumination. Separate photographs of the boundary layer separation and wake shape were obtained in a similar series of drop tests in which particles of potassium permanganate were attached to the aft end of each body. Figure 1 is a photograph of the wake flow behind a 2-inch sphere in plain water and in 200 and 1000 ppm Polyox solutions. Note that the point of boundary layer separation has been shifted rearward. Figure 2 is a typical photograph of the multiple images of a falling cone produced by the strobe-light technique.

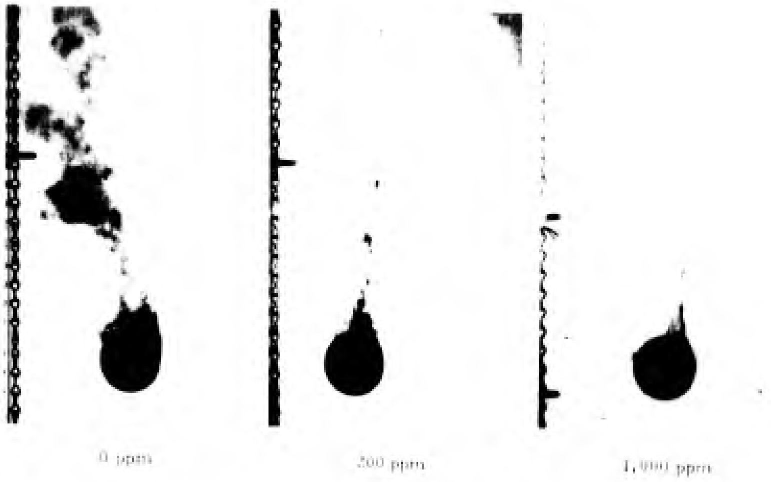

Figure 1

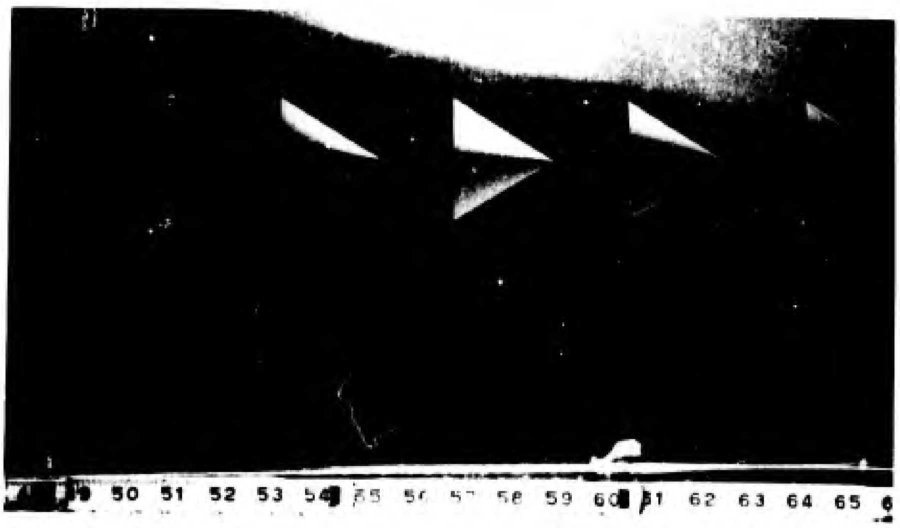

Figure 2

The drag data on spheres from 0.25 inch to 2 inches in diameter showed that Polyox reduced drag in all cases. The amount of drag reduction increased with sphere diameter up to a maximum of 69 percent. The results on the stable cones showed little or no drag reduction or change in wake shape due to the Polyox additive. In the tests on the unstable bodies that were tested, such as cylinders and the flatter cones, the Polyox had a small effect on stabilizing the trajectories.

* * *

REPLY TO THE DISCUSSION

W. M. Vogel and A. M. Patterson
Pacific Naval Laboratory
Victoria, B. C.

The discussion by Dr. Eringen* on his theory of simple micro-fluids was very interesting. We have not had time to assimilate the material presented in his referenced report, but if this theory can be used to predict the behaviour of dilute polymer solutions it will be a major step in our understanding of these fluids.

With reference to Mr. Lang's comments we have carried out some experiments with a cylinder mounted across our water tunnel. We have not measured the drag but when dilute polymer solutions are injected from the trailing edge of the cylinder major modifications to the structure of the wake occur.

* * *

*See discussion by Eringen on the paper by Lumley (p. 944).

AN EXPERIMENTAL STUDY OF DRAG REDUCTION BY SUCTION THROUGH CIRCUMFERENTIAL SLOTS ON A BUOYANTLY-PROPELLED, AXI-SYMMETRIC BODY

Barnes W. McCormick, Jr.
The Pennsylvania State University
University Park, Pennsylvania

ABSTRACT

This paper presents the analysis, design, and results of testing performed to date on TRI-B, a buoyantly-propelled body incorporating boundary layer control by suction through circumferential slots. This body is designed to maintain a nearly, full-length laminar boundary layer at a length Reynolds number of 39×10^6. Although the expected performance has not yet been achieved in the field with the free-running body, nearly full-length laminar flow has been measured in wind tunnel tests at lower Reynolds numbers. From the results of an analysis based on the Karman-Pohlhausen method, it is believed that transition is occurring ahead of the first suction slot at the higher Reynolds number.

INTRODUCTION

The purpose of this paper is to report on the TRI-B program currently in progress at the Ordnance Research Laboratory. Specifically, the method by which TRI-B, a buoyantly-propelled body with boundary layer control, was designed together with an analysis of the experimental results obtained to date will be presented.

A diagram of TRI-B is shown in Fig. 1. It has an overall length of 93 inches, a diameter of 12.75 inches and displaces 294 lbs. Beginning 6 inches back from the nose and spaced every 2 inches are circumferential slots having a thickness of .007 inches through which the boundary layer is removed. The suction is accomplished by means of an axial-flow pump driven by a hydraulic motor. The motor is supplied with hydraulic fluid under pressure from a piston driven from an accumulator capable of being pressurized to 5000 psi with nitrogen.

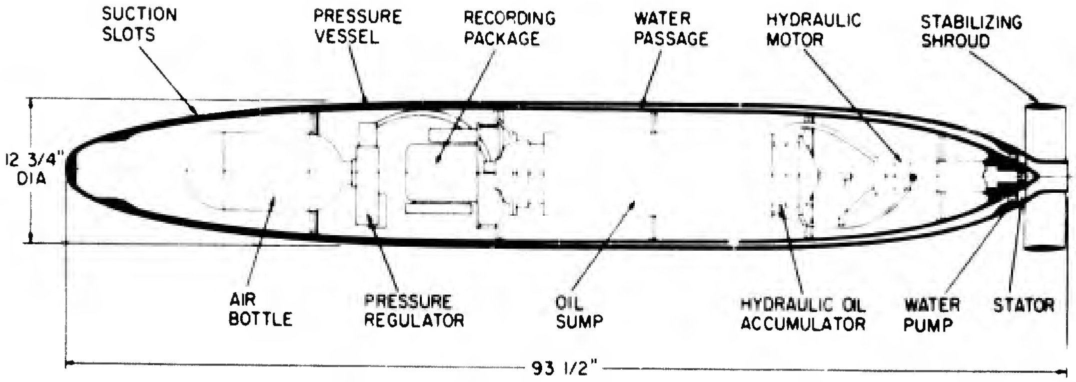

Fig. 1 - Section of TRI-B body

The purpose of removing the boundary layer is to stabilize the laminar layer and prevent it from becoming turbulent. The slots and suction flow quantity were chosen to prevent the Reynolds number based on the thickness of the laminar boundary layer from exceeding a critical value. This prescribed value and the means by which the slot geometry was chosen were based on the findings of Loftin and Burrows as reported in Ref. 1.

For testing, TRI-B is placed in a protective launching tube, lowered to a depth of 400 ft and released. Its buoyancy of approximately 84 lbs propels it vertically upward attaining a velocity at the surface of approximately 30 to 50 fps depending on whether or not laminar flow is achieved.

HYDRODYNAMIC DESIGN OF BODY

The method used to design the suction slots, i.e., their axial spacing, slot width and suction flow quantity was based on the semi-empirical approach proposed in Ref. 1. This reference relates experimentally the change in Reynolds number, based on the boundary layer thickness, across a suction slot to the amount of boundary layer flow removed through the slot.

If ΔQ is the flux removed per unit length of slot, then Ref. 1 has determined experimentally the ratio of δ immediately after the slot, δ_o to δ immediately before the slot, δ_1.

$$\frac{\delta_o}{\delta_1} = 1 - 1.6\,\frac{\Delta Q}{Q_{BL}} \qquad \frac{\Delta Q}{Q_{BL}} \leq .275 \tag{1}$$

Q_{BL} is the flux per unit width of fluid in the boundary layer.

Again from the experimental results of Ref. 1, the power required for the suction flow was calculated from an expression for the head loss across each suction slot. According to the reference,

$$\frac{\Delta H}{q_1} = 1.0 + \frac{\Delta Q}{Q_{BL}} (2.26\, K' - 1.26) \tag{2}$$

where

$$K' = 1.0 \text{ for } \frac{\Delta Q}{Q_{BL}} \leq .045$$

$$K' = 1.0 + 1.48\left(\frac{\Delta Q}{Q_{BL}} - .045\right) \text{ for } \frac{\Delta Q}{Q_{BL}} > .045$$

g_1 = local velocity head outside boundary layer.

According to the reference for laminar stability, the Reynolds number based on u_1, the local velocity outside the boundary layer, and the boundary layer thickness should not exceed approximately 3400. In this case, the boundary layer thickness was defined as the value of δ for which $u/u_1 = 0.707$.

A velocity profile through the boundary layer of the form

$$\frac{u}{u_1} = 2\eta - \eta^2$$

was assumed. In lieu of calculating the actual boundary layer profile, this seemed to be a reasonable choice since when based on the displacement thickness, this profile lies between that of Blasius and the asymptotic suction profile.

These results were then substituted into the Karman momentum integral equation and the boundary layer thickness obtaining by numerically integrating along the length of the body for different values of $\Delta Q/Q_{BL}$.

At each increment in length, x, along the body the value of the boundary layer Reynolds number was compared to the critical value quoted by Ref. 1.

If R_δ equalled, or possibly slightly exceeded 3400, the value of x was printed out and Q through the slot at the X location calculated from

$$Q = 2\pi\, r_o \left(\frac{\Delta Q}{Q_{BL}}\right) Q_{BL}. \tag{3}$$

δ immediately after the slot was calculated from Eq. (1) and the numerical integration continued to the next slot location where R_δ once again reached a value of 3400. In this manner the slots were located along the body and the total suction flow requirement determined as the sum of all the Q's obtained from Eq. (3).

After a series of trial designs, a value of $\Delta Q/Q_{BL}$ of 0.17 was selected. This resulted in slots 0.007 inches thick spaced every 2 inches starting 6 inches back from the nose. These continue back to within 7 inches from the tail at which point the axial flow pump is installed. On the recommendation of Ref. 1, the slot thickness was chosen equal to the boundary layer thickness. The required suction flow quantity was calculated to be 1.37 cfs for a design velocity of 50 fps. The pump was estimated to require 8.34 hp.

In order to integrate the Karman momentum equation it is necessary to know the body radius and static pressure distribution. The body shape of TRI-B is composed of three parts: (a) a modified ellipsoid nose, (b) a parallel mid-section and (c) the afterbody of the DTMB series 4166 body. The final shape is similar to a Reichardt constant pressure body.

For this shape, the pressure is nearly constant over 80% of its length beginning 5% back from the nose. The measured pressure distribution obtained from wind tunnel tests is presented in Fig. 2. Included on the figure are empirical expressions which were used in the numerical integration.

At 50 fps, the laminar skin-friction drag on the body was estimated to be 11.7 lbs. The drag of the ring tail was estimated at 29.4 lbs giving a total drag of 41.1 lbs.

If laminar flow were not achieved, the body drag was estimated to be 132 lbs giving a total drag of 173.1 lbs. The pump was designed to eject the suction flow at 50 fps; hence in evaluating the drag from the terminal velocity, thrust (or drag) from the pump must be considered. In terms of equivalent flat plate area, $f = D\ q$, f was predicted to be equal to 0.069 for a turbulent boundary layer and 0.0164 for a laminar one.

The method by which the body was designed has been presented only briefly because of various shortcomings in the method which became obvious as the project progressed. These will be discussed later in the paper.

TESTING OF TRI-B

The first tests of TRI-B began October 1962 at the U.S. Naval Torpedo Station, Keyport, Washington. Over a period of two months, 12 runs were performed of which 7 yielded valid data. A photograph showing the body exiting from the water is presented in Fig. 3. For these runs, only the velocity as a function of time was measured. From the results, the disappointing conclusion was reached that the expected laminar flow had not been achieved.

The fact that the boundary layer with the pump operating was turbulent was substantiated by running with a trip ring on the nose for which the body attained the same terminal velcoity as without the ring.

There were several possible reasons at this time why laminar flow was not being achieved. First, a calibration of the suction pump showed that at the design hydraulic pressure of 2000 psi, it was delivering only 0.85 cfs instead of the design value of 1.37 cfs. Secondly, the suction slots were not continuous around the circumference, instead they were interrupted by small, structural, carry-through bridges. Finally, the body exhibited a tendency to depart from the vertical in its travel to the surface.

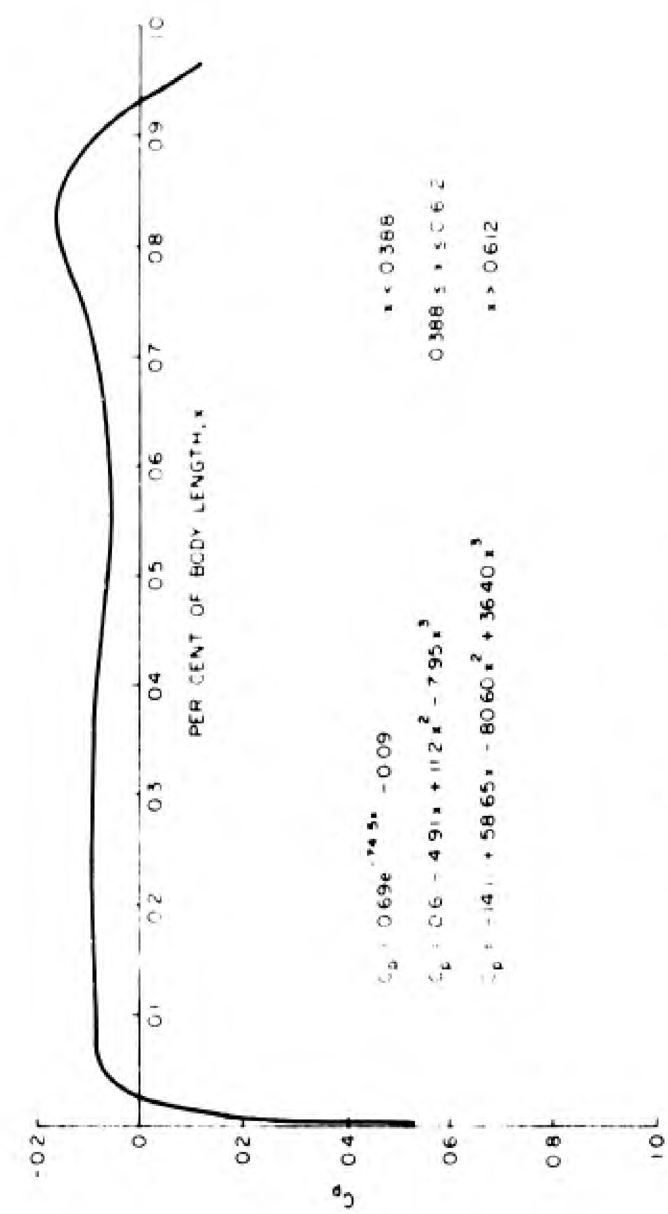

Fig. 2 - Pressure distribution for TRI-B

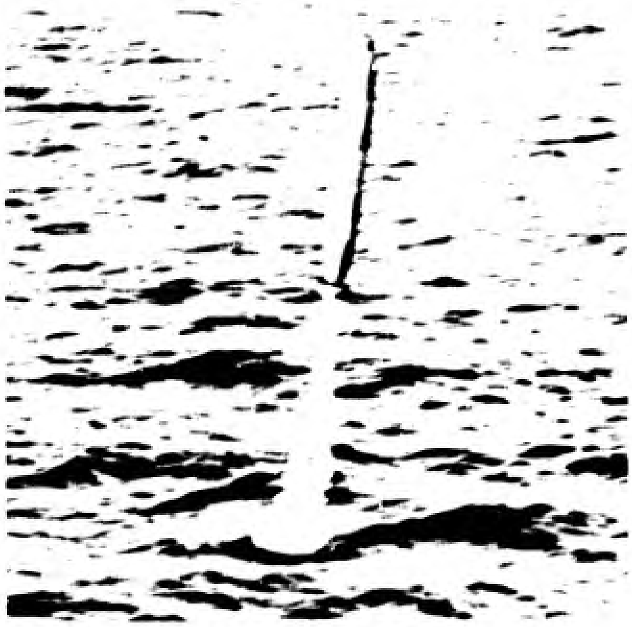

Fig. 3 - TRI-B body exiting from water

In view of these questions, the program at NTS was temporarily suspended and the body returned to ORL for modification and laboratory tests. Tests were conducted in the low turbulence wind tunnel at the Garfield Thomas Water Tunnel, a division of ORL, which showed that even at a length Reynolds number of approximately 4.5×10^6, lower than the design value by a factor of 8, extensive laminar flow could not be achieved. In light of these results, the suction slots were modified to assure a continuous suction around the circumference. When this was done, laminar flow was achieved at the low Reynolds number over approximately 90% of the body as determined by listening to the noise of the boundary layer with a total head tube connected to a stethescope. Hence it appeared that the interruptions to the slots were the cause of the difficulties.

At this time, tests were run to determine the suction coefficient, c_Q, required to maintain full-length laminar flow for different length Reynolds numbers. c_Q is defined as

$$c_Q = \frac{Q}{U_o S_w}$$

where S_w is the wetted area. For uniform suction c_Q is simply the ratio of suction velocity to free-stream velocity.

Transition Reynolds number for different length Reynolds numbers are presented in Fig. 4 as determined experimentally in the wind tunnel. The design value of C_Q at 50 fps is 12.3×10^{-4}. This value is appreciably higher than an extrapolation of Fig. 4 to the design length Reynolds number of 39×10^6 would indicate is necessary. This was the first indication that the design method was not sufficient.

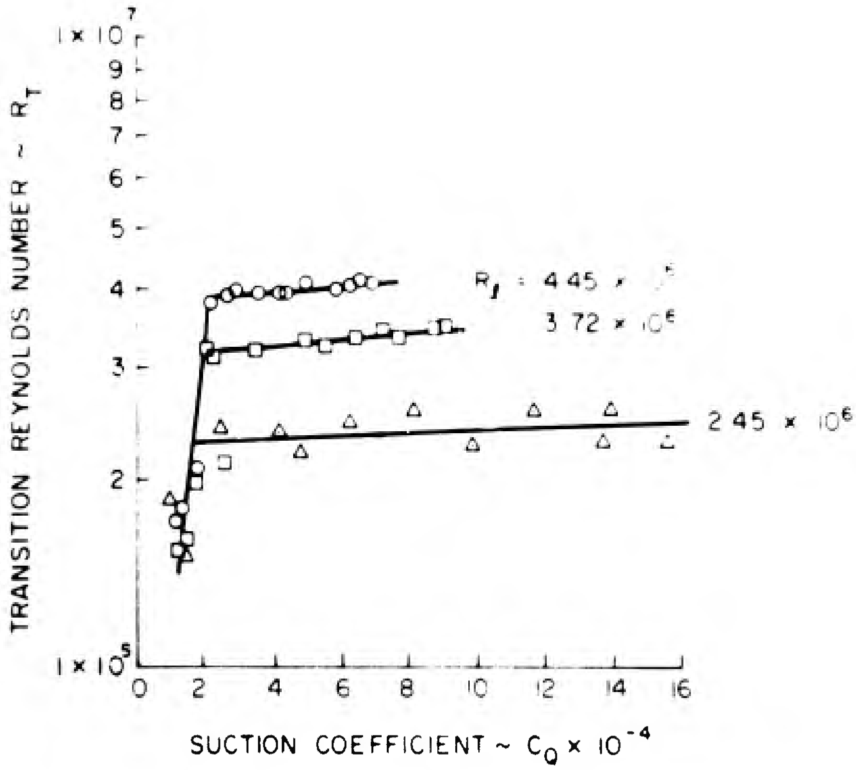

Fig. 4 - Transition Reynolds number vs suction coefficient

Field testing of TRI-B was resumed at NTS in March 1964. In addition to having the slots modified, the body incorporated more refined instrumentation. 10 channels of information were recorded on a galvanometer; measured were the velocity, depth, pressure across the pump, time, pump rpm, velocities at the tail at 3 different radial locations, and the deviation from the vertical in two mutually perpendicular planes.

The project was plagued with instrumentation difficulties throughout the second series of tests. This included the failure of pressure transducers, the sensitivity of differential transducers to change in temperature and absolute pressure and shifting in the zero settings of the bridge outputs, possibly the result of a mechanical hysteresis in the transducers.

Though somewhat inconsistent, the data: namely, the time history of the velocity, did point to the fact that laminar flow was still not being achieved with TRI-B even though the slots were now modified. However, the tilt traces and visual observations of its surfacing confirmed the fact that the body was undergoing violent excursions during its rise to the surface. This had been experienced to a lesser degree during the first series of tests and had apparently been cured by adding 10 lbs of lead in the tail. For the second series of tests the CG was even slightly behind that of the configuration with the lead. At this point, it was realized that the contribution of the hydrodynamic forces on the tail to the slope of the pitching moment curve completely overshadows that due to the displacement between the CG and the center-of-buoyancy above about 10 fps. Hence on a buoyant, vertically-rising body, moving the CG aft improves the stability at low speeds but, due to the shortening of the tail moment arm, is detrimental at higher speeds.

At this point in the program wind tunnel tests of a model of TRI-B showed it to be statically unstable, contrary to calculations of its dynamic stability made early in its design. These same tests indicated that an increase in the chord of the tail from 4 inches to 6 inches would provide static stability. Hence a new tail was made and shipped to the field. Successive runs with the new tail showed the stability problems to be solved. The body repeatably rose with no indication on the tilt traces of any deviations from the vertical.

Unfortunately, solving the stability problem did not result in a reduction in the drag according to the terminal velocity. Thus in the latter part of May, the body was returned to ORL for additional laboratory studies. It is planned to test this body in the Garfield Thomas Water Tunnel at the design Reynolds number. However, these tests must await the installation of a honeycomb in the tunnel designed to reduce the turbulence in the test section to a level acceptable for such tests.

ANALYSIS BASED ON KARMAN-POHLHAUSEN METHOD

The analysis on which the design was based was felt to be inadequate for several reasons. The assumed velocity profile was too approximate. In addition the stability limit having a fixed value did not consider the dependence of the stability of a laminar layer on the shape of velocity profile. Also there was no means to calculate the change in velocity profile across the slot.

An exact prediction of the stability of laminar boundary layers involves the solution of the eigen-value problem defined by the Orr-Sommerfeld equation. Fortunately, enough cases, with and without suction have been investigated so that one is able to specify a stability limit, $R_{\delta^*_{crit}}$, as a function of some measure of the shape of the velocity profile. Figure 5 taken from Ref. 2, presents $R_{\delta^*_{crit}}$ as a function of the shape parameter H, the ratio of displacement thickness to momentum thickness. More recently Tollmein in Ref. 3, presented the curve shown in Fig. 6. Here, the shape parameter used is related to the curvature at the wall measured in terms of displacement thickness. Qualitatively both criteria are in agreement. A profile having a relatively higher velocity at the wall will have a greater value of K and a smaller value of H.

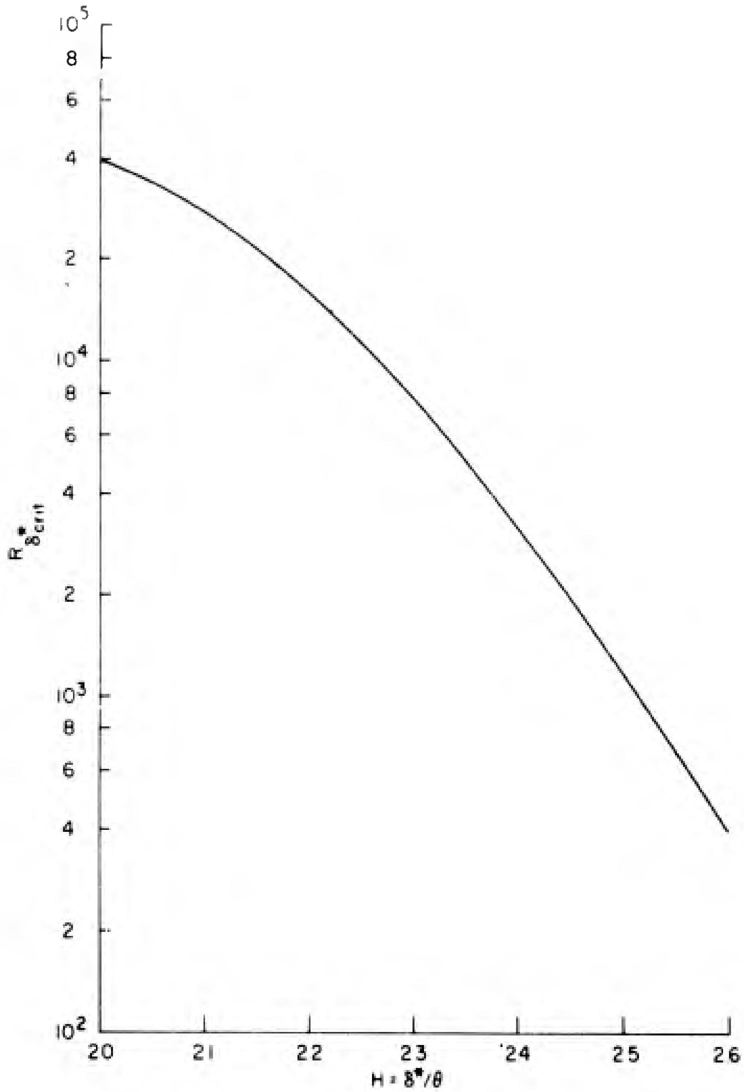

Fig. 5 - Stability limit R_{δ^*} vs shape parameter H

Hence the problem is reduced to calculating the boundary layer growth over the body and, at each location along the body, comparing R_{δ^*} to $R_{\delta^*_{crit}}$ obtained from Figs. 5 or 6.

To do this, the Karman-Pohlhausen method modified to account for suction at the walls was used. A brief outline of the method follows.

The velocity profile is represented by a fourth order polynomial

$$\frac{u}{U_1} = a\eta + b\eta^2 + c\eta^3 + d\eta^4 \qquad (4)$$

221-249 O - 66 - 65

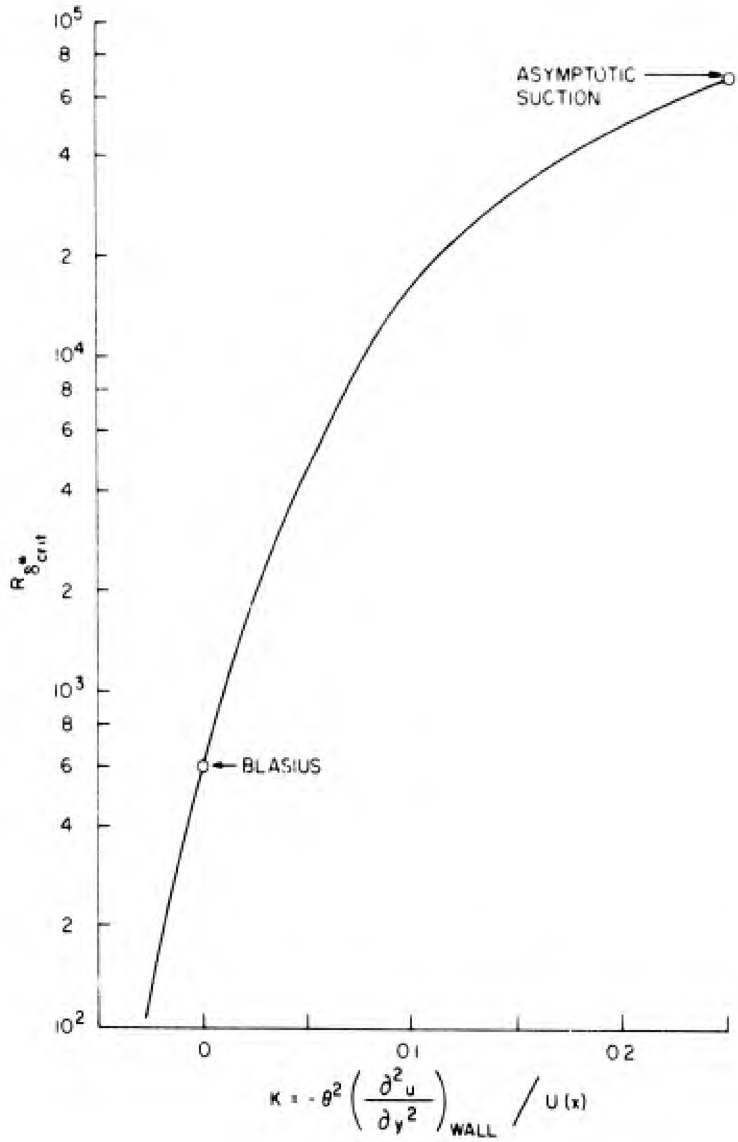

Fig. 6 - Stability limit R_{δ^*} vs shape parameter K

where

$$\eta = \frac{y}{\delta}.$$

The boundary conditions to be satisfied for a suction velocity of v_o are:

$$\text{At} \quad y = o, \; u = o, \; -v_o \frac{\partial u}{\partial y} = -\frac{1}{\rho}\frac{dp}{dx} + \nu \frac{\partial^2 u}{\partial y^2} \tag{5}$$

$$\text{At} \quad y = \delta, \; u = u_1, \; \frac{\partial u}{\partial y} = 0, \; \frac{\partial^2 u}{\partial y^2} = 0.$$

From the above it can be found that:

$$a = \frac{12 + \Lambda}{6 + \sigma} \qquad b = \frac{6\sigma - 3\Lambda}{6 + \sigma}$$
$$c = \frac{-12 - 8\sigma + 3\Lambda}{6 + \sigma} \qquad d = \frac{6 + 3\sigma - \Lambda}{6 + \sigma} \tag{6}$$

where

$$\Lambda = \frac{\delta^2}{\nu}\frac{du_1}{dx} \qquad \sigma = \frac{v_o\delta}{\nu}.$$

The displacement thickness δ^* can be expressed as:

$$\delta^* = \delta\left[1 - \frac{a}{2} - \frac{b}{3} - \frac{c}{4} - \frac{d}{5}\right] \tag{7}$$

while the momentum thickness is given by:

$$\theta = \delta^* - \delta\left[\frac{a^2}{3} + \frac{ab}{2} + \frac{(2ac + b^2)}{5} + \frac{(ad + bc)}{3} + \frac{(2bd + c^2)}{7} + \frac{cd}{4} + \frac{d^2}{9}\right]. \tag{8}$$

The shape parameter K can be calculated from

$$K = -\frac{\theta^2}{\delta^2}\, 2b. \tag{9}$$

For an axi-symmetric body with suction, the Karman momentum integral equation is written as

$$u_1^2 \frac{d\theta}{dx} + (2\theta + \delta^*)\, u_1 \frac{du_1}{dx} + u_1^2 \frac{\theta}{r}\frac{dr}{dx} + v_o u_1 = \frac{\tau_o}{\rho u_o^2} \tag{10}$$

r_o is the body radius at any x.

In the above all velocities are dimensionless with respect to the free-stream velocity U_o and all distances with respect to a reference distance. The dimensionless shearing stress $\tau_o/\rho U_o^2$ can be determined from

$$\frac{\tau_o}{\rho U_o^2} = \frac{u_1 a}{\delta R_R}. \tag{11}$$

The dimensionless velocity u_1 is found from the static pressure distribution,

$$u_1 = \sqrt{1 - C_P}$$

$$\frac{du_1}{dx} = -\frac{1}{2u_1}\frac{dC_P}{dx} \tag{12}$$

where C_P, the pressure coefficient is defined by

$$C_P = \frac{P - P_o}{\frac{1}{2}\rho U_o^2} .$$

The numerical integration is started close to the nose by estimating δ^* on the basis of the exact solution of viscous flow near a stagnation point. δ is then assumed to be equal approximately to 3 δ^*. Actually the ensuing integration depends very little on the initial choice of δ. Knowing δ, $C_P(x)$ and specifying v_o, one can now integrate Eq. (10) numerically along x with the aid of Eqs. (6), (7) and (8).

This integration has been carried out for the two Reynolds numbers of 2.3×10^6 and 39×10^6 and for C_Q values from 0 to .0003. The lower Reynolds number is typical of the wind tunnel tests while 39×10^6 represents the design value. The results of these calculations are presented in Figs. 7 and 8. In each case the suction was assumed distributed uniformly over the body starting 6 inches back from the nose. Also included on each figure are the stability limits predicted from Figs. 5 and 6.

These results are very interesting and in agreement with the experimental observations. From Fig. 7 for zero suction, the transition point is predicted to lie between 8 inches to 14 inches back from the nose. With a C_Q of .0001, the shape parameter H predicts transition 33 inches from the nose while K predicts it at 9.5 inches. Finally for a C_Q of .0002 both criteria predict laminar flow over nearly the entire length of the body. Observe that the lines of critical R_{δ^*} and actual R_{δ^*}, as C_Q increases, become nearly parallel. Hence as C_Q is increased slightly above some value close to .0002, the transition point shifts suddenly from the nose rearward. This predicted behavior was observed experimentally. It should be noted also that the flow is stable at a C_Q of .0002 not simply because the suction is inhibiting the growth of the boundary layer but, equally as important, because the suction is causing the profile to become more stable.

Now consider the predictions of Fig. 8 made at the design Reynolds number. Both shape criteria predict transition before the first suction slot at 3 or 4 inches from the nose. Thus it appears that transition may be occurring before the suction can take effect. In fact it appears as if the velocity would have to be reduced to about 17 fps in water to move the transition point behind the first suction slot. However, calculations, not presented here, have shown that a C_Q starting 3 inches back from the nose would be sufficient to prevent transition.

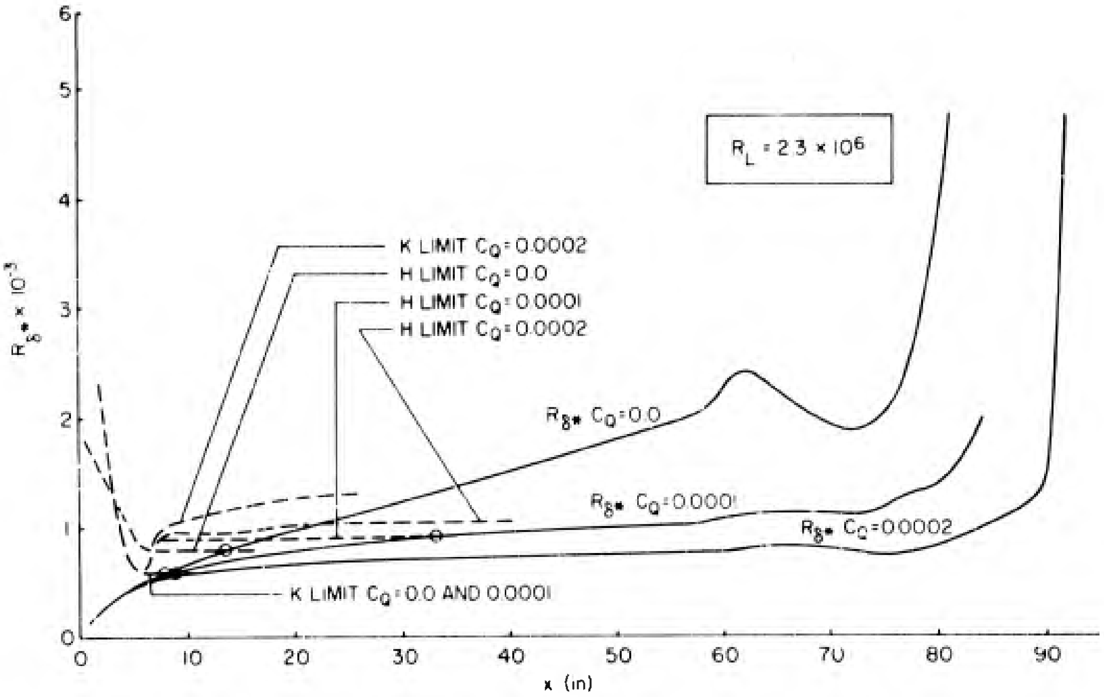

Fig. 7 - Calculated boundary--layer thickness and stability limits for TRI-B according to Karman-Pohlhausen method for low Reynolds number

CONCLUSIONS

It is concluded from the results of the Karman-Pohlhausen method that the probable reason why TRI-B has not yet achieved full-length laminar flow at 50 fps is due to transition occurring before the first suction slot. Wind tunnel experiments at low Reynolds number and predictions based on the Karman-Pohlhausen method were found to be in close agreement. This method assumes the suction to be continuously distributed over the surface. A method, based on calculating the decrease in δ across a slot, did not prove fruitful.

It was found experimentally that, even at low Reynolds number, continuous suction in the circumferential direction was necessary to the maintenance of a laminar layer. Interruption of the slots probably results in secondary flows or streamwise vortices which cause instabilities.

This paper would not be complete without pointing out the experience which has been gained in handling a body of this type in the field. It is very important to provide for proper handling equipment in the planning of such a program. All dollies and packaging equipment must be lined with soft coverings. Field personnel, particular ordinary seamen, must be impressed with the importance of not allowing the slightest scratch on the surface. This is not as easy as it may sound. A navy diver bobbing up and down with the body along side the ship is naturally more concerned with his own skin than with the skin of the body. It

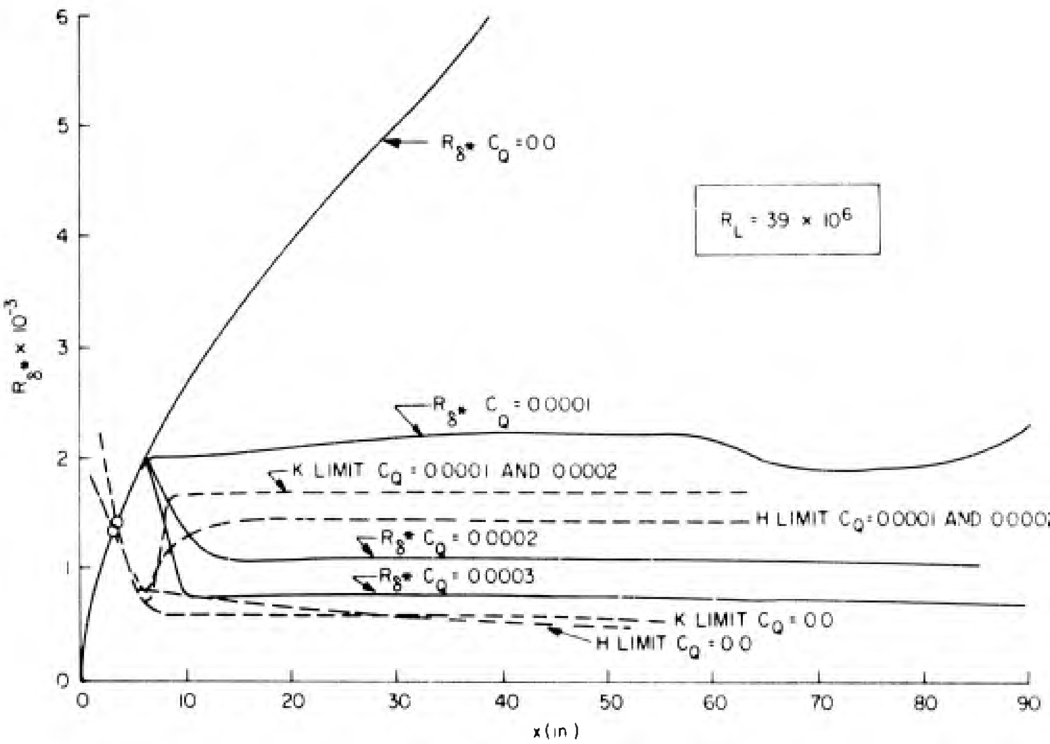

Fig. 8 - Calculated boundary--layer thickness and stability limits for TRI-B according to Karman-Pohlhausen method for high Reynolds number

was also necessary to have fresh water available on board the ship in a quantity sufficient to wash the body thoroughly immediately upon recovery. Not only was the external surface washed but the slots were flushed from the inside by inserting a hose in the tail.

ACKNOWLEDGMENTS

This program is being carried out by personnel at the Ordnance Research Laboratory of The Pennsylvania State University under contract to the U.S. Naval Bureau of Weapons. In particular the author would like to acknowledge the efforts of Dr. Thomas Peirce and Messers. Harry F. Wegener, Charles Holt, Fred Ott and Robert Woods in contributing to the project. Also, the assistance of the Naval Torpedo Station at Keyport, Washington, is gratefully acknowledged; in particular Mr. Ken McClure of that facility whose hospitality made life a little more tolerable for four engineers 3000 miles from home. Finally, our thanks go to Dr. Werner Pfenninger and Mr. Lloyd Gross of the Northrop Corporation for many stimulating discussions, recommendations and constructive criticisms concerning the project.

REFERENCES

1. Investigations Relating to the Extension of Laminar Flow by Means of Boundary-Layer Suction Through Slots, Loftin, J. K. and Burrows, Dale L., NACA TN 1961, Oct. 1949.

2. Boundary Layer Theory, Schlichting, H., 4th edition, McGraw-Hill, 1960.

3. Boundary Layer and Flow Control, Vol. II, edited by Lachmann, G. V., Pergamon Press, 1961.

* * *

DISCUSSION

T. G. Lang
Naval Ordnance Test Station
Pasadena, California

I would like to compliment Dr. McCormick on developing a relatively simple system for testing bodies with boundary layer control in a variety of open-water conditions. Using this system, such problems as clogging due to plankton and transition caused by natural turbulence can be investigated. A few years ago, we experimented on the susceptibility to clogging of several types of permeable materials. Samples of sea water, tap water, lake water with suspended particles, and distilled water were used in a small water tunnel specially designed to provide a high-speed laminar boundary layer over a small test plate to which suction was applied. The results of our limited tests showed that slots greater than 0.002 in. in width were relatively free from clogging, as were perforated plates with holes greater than 0.002 in. in diameter. Test plates made of sintered spheres clogged very rapidly while samples of porous fibrous material could be used for 5 to 10 minutes before clogging to the point where their permeability was reduced by a factor of two. Also, it was found that backflushing for about one second cleared the material. Perhaps if Dr. McCormick encounters problems due to clogging that the backflush technique would be of help.

* * *

Saturday, September 12, 1964

Afternoon Session

DRAG REDUCTION

Chairman: T. Inui

University of Tokyo
Tokyo, Japan

PROBLEMS RELATING TO THE SHIP FORM OF MINIMUM WAVE RESISTANCE

Hajime Maruo
National University of Yokohama
Yokohama, Japan

INTRODUCTION

The problem, to find a ship form which presents minimum resistance under a certain condition imposed by the practical requirement, is one of the aims of the ship designer. Experiments of methodical series of ship models have been considered as the most reliable method to find the best form. On the other hand recent developments in ship hydrodynamics urges the mathematical analysis of components of ship resistance, and attempts were made to find out the ship form of minimum resistance by means of the hydrodynamic theory. When the resistance of a ship is separated into a component due to viscosity and that due to wave-making, both of them have some correlation with the ship's form. As the effect of the form upon the viscous resistance is not only the effect on the wetted area but gives much influence to the boundary layer separation, our knowledge is not enough to make a full analysis of the relationship between the viscous resistance and the ship form. On the other hand, an analytical representation of the wave resistance is made possible by virtue of the assumption of the inviscid fluid and the technique of linearization of the fluid motion. The wave resistance of a thin ship is given by celebrated Michell's integral. The problem of minimizing Michell's integral has been a stimulating interest of theorists since Weinblum first published his calculation in 1930 [1]. When the wave resistance is represented by a functional of a function which gives the equation of the ship's surface, to minimize the wave resistance becomes a purely mathematical problem, that is the calculus of variations. The method of solution employed by Weinblum and his successors is a sort of approximation usually called Ritz's method. It assumes a type of solution involving some unknown coefficients which are determined by the condition of maxima or minima. It gives a reasonable approximation provided the problem has a solution of the specified type. Doubts were thrown with respect to the existence of the solution. The ship form of minimum wave resistance or, exactly speaking, minimum Michell's integral, can be expressed by a solution of an integral equation. Recently mathematical investigations were made into the nature of the integral equation and the controversy with respect to the existence of the solution seems to be nearly settled.

Because of the fact that the numerical results for the above problem were limited, attempts to apply the theory of minimum wave resistance to the practical ship design are quite scarce. However some shipbuilders have begun to show interest in the application of the above theory in recent years. It is not at all simple to realize its direct application because the theory of wave resistance is not necessarily an approximation accurate enough to describe the actual phenomenon. The exclusion of viscosity should be the most serious defect. Nevertheless a great utility of the above theory can be anticipated. The present paper is prepared in order to place emphasis on the feasibility of the theoretical result on the ship form of minimum wave resistance.

SIDE CONDITIONS AND EXISTENCE OF THE SOLUTION

The problem of minimum wave resistance can be considered only when some side condition is imposed, because without any restriction, there is a solution which makes no wave. It does not necessarily mean the trivial conclusion that no ship makes no wave. In fact, a class of singularities was found which are not accompanied with any wave term in the linearized potential of fluid motion. These wave-free singularities were found first by Krein [2] and later by Bessho [3] independently. The latter considered an application to the practical ship design problem. An important nature of the wave-free singularity is that the total sum of the dipole singularities is zero. This fact can be interpreted to Michell's theory that the linearized volume of the wave-free ship is zero. Bessho's application of the wave-free singularity is the method of changing the ship's form without any change in wave resistance. The theoretical result has been proved by experiments.

It can be easily understood that the restriction with respect to the volume is one of the necessary side conditions mentioned before. However a constant volume can not become a sufficient condition. The draft may become another restriction, otherwise the volume can be placed infinitely downward, resulting the wave resistance to be reduced to any extent. Therefore the problem of minimum wave resistance is usually considered under the conditions of constant volume and constant draft. However the existence of the wave-free singularity distribution invalidates the solution of the problem of this kind, because one can obtain an infinite set of the solution by addition or subtraction of the wave-free singularities. There is another difficulty. When the draft is fixed, or the lower boundary of the singularity distribution is prescribed, the body can be reduced to a fully submerged body, and Bessho [4] showed the wave resistance of submerged singularity distribution to have no solution of minimum problem. Hence the minimum problem of ships of given draft and constant displacement has no solution.

The minimum problem which has been usually considered is not such a general one, but a problem to find out a longitudinal distribution of displacement which makes the wave resistance minimum when the shape of the frame line is given by a prescribed equation.

Take the x-axis along the longitudinal axis of the ship, the y-axis athwart ships and the z-axis draftwise downwards. Write the equation of the ship's surface by the form like

$$y = f(x, z) . \tag{1}$$

Weinblum considered a case in which the function $f(x, z)$ is a product of a function of x only and that of z only, such as

$$f(x, z) = X(x)\, Z(z) \tag{2}$$

and called it an elementary ship. The problem now becomes to choose the function $X(x)$ in such a way that the wave resistance becomes minimum when the function $Z(z)$ is given. He published a number of numerical examples.

The simplest case is the wall-sided ship of infinite draft or the infinite strut for which $Z(z)$ is constant throughout the whole range of the positive z. The condition of the constant displacement is interpreted into the word "constant area of the water plane." When the equation of the waterline is

$$y = f(x) . \tag{3}$$

Michell's integral for the infinite strut of length 2ℓ moving with a uniform speed U becomes

$$R = \frac{4\rho U^2}{\pi} \int_1^\infty \frac{d\lambda}{\lambda^2 \sqrt{\lambda^2 - 1}} \int_{-\ell}^{\ell} \int_{-\ell}^{\ell} \frac{df(x)}{dx} \frac{df(x')}{dx'} \cos\,[\kappa\lambda(x - x')]\, dx\, dx' \tag{4}$$

where $\kappa = g/U^2$.

The area of the water plane is given by the integral

$$\begin{aligned} A_w &= 2 \int_{-\ell}^{\ell} f(x)\, dx \\ &= -2 \int_{-\ell}^{\ell} \frac{df(x)}{dx}\, x\, dx \end{aligned} \tag{5}$$

since $f(\pm\ell) = 0$.

The determination of the function $f(x)$ so as to minimize Michell's integral (4) for a fixed value of A_w leads to the equation derived by the theory of calculus of variations,

$$\int_1^\infty \frac{d\lambda}{\lambda^2 \sqrt{\lambda^2 - 1}} \int_{-\ell}^{\ell} \frac{df(x')}{dx'} \cos\,[\kappa\lambda(x - x')]\, dx' + kx = 0 . \tag{6}$$

Sretenski [5] concluded that no solution could exist among square-integrable functions, but there is some doubt in his reasoning as was pointed out by Wehausen [6]. Karp, Kotik and Lurye [7] has proved explicitly that the integral equation has really no solution except a trivial case $df(x)/dx = 0$ when $k = 0$. Being integrated by parts with respect to x and x' remembering that $f(\pm\ell) = 0$, Eq. (4) becomes

$$R = \frac{4\rho g^2}{\pi U^2}\int_1^\infty \frac{d\lambda}{\sqrt{\lambda^2-1}}\int_{-\ell}^{\ell}\int_{-\ell}^{\ell} f(x)\, f(x')\cos\left[\kappa\lambda(x-x')\right] dx\, dx'. \tag{7}$$

From this equation, the condition of the minimum wave resistance for a fixed water plane area gives the integral equation

$$\int_1^\infty \frac{d\lambda}{\sqrt{\lambda^2-1}}\int_{-\ell}^{\ell} f(x')\cos\left[\kappa\lambda(x-x')\right] dx' + k = 0. \tag{8}$$

Because of the integral representation of the Bessel function of the second kind, the kernel is expressed by a known function.

$$\frac{\pi}{2}\int_{-\ell}^{\ell} f(x')\, Y_0\left[\kappa(x-x')\right] dx' = k. \tag{9}$$

This equation was dealt numerically by Pavlenko [8] without regard of the existence of the solution. Wehausen pointed out that the solution of the integral equation has a type of

$$\frac{U(x)}{\sqrt{\ell^2 - x^2}}$$

where $U(x)$ is bounded. Karp, Kotik and Lurye calculated the function $U(x)$ numerically for several Froude numbers. It was found that $U(x)$ did not vanish at $x = \pm\ell$, so that the solution becomes singular at both ends. If $f(x)$ gives the ordinate of the surface, infinite horns appear and the condition $f(\pm\ell) = 0$ is violated. A similar situation appears in the case of finite draft because of the logarithmic singularity still existing in the kernel. As far as original Michell's assumption is employed, there is no admissible solution of the present problem.

However the formula of the wave resistance may have a different interpretation from the definition of original Michell's integral. It can be shown that the Eq. (7) gives the wave resistance of a distribution of x-directed dipoles over the vertical plane $y = 0$. Then $f(x)$ does not mean the shape of the strut but gives the density of the dipoles. Karp and others calculated the boundary streamline when such a dipole distribution was placed in a uniform stream.

The integral Eq. (9) belongs to the family of equations of the type

$$\int_{-\ell}^{\ell} f(x')\, Y_0\left[\kappa(x-x')\right] dx' = g(x) \tag{10}$$

which was solved by Dörr [9]. By the change of variables

$$x = -\ell\cos\theta, \qquad x' = -\ell\cos\theta'$$

Eq. (10) is converted into

$$\int_0^\pi \sigma(\theta') \, Y_0 [\kappa_0 \ell (\cos\theta' - \cos\theta)] \, d\theta' = \varphi(\theta) \tag{11}$$

where $\kappa_0 = g/U^2$. Dörr has shown that

$$\lambda_n \int_0^\pi ce_n(\theta', q) \, Y_0 [2\sqrt{q} \, (\cos\theta' - \cos\theta)] \, d\theta' = ce_n(\theta, q) \tag{12}$$

where $ce_n(\theta, q)$ is the even Mathieu function of the integral order. As ce_n is orthogonal in the interval $(0, \pi)$, the functions $\sigma(\theta)$ and $\varphi(\theta)$ can be expressed by Fourier series of ce_n. If $\varphi(\theta)$ is expressed by

$$\varphi(\theta) = \sum_{n=0}^{\infty} a_n \, ce_n(\theta, q) \tag{13}$$

the solution of the integral equation becomes

$$\sigma(\theta) = \sum_{n=0}^{\infty} a_n \lambda_n \, ce_n(\theta, q) \, . \tag{14}$$

Then the optimum dipole distribution $f(x)$ takes the form

$$(\ell^2 - x^2)^{-1/2} \, \sigma\left(\cos^{-1} \frac{x}{\ell}\right) .$$

Bessho [10] calculated the eigenvalues λ_n and showed numerical results for the solution of Eq. (9) at various Froude numbers. The function $\sigma(\theta)$ does not vanish at $\theta = 0$ and π, so that the singularity in the dipole distribution always appears, but becomes less remarkable at lower Froude numbers. The best form has blunt cylindrical nose and tail, but the radius of the cylinder decreases rapidly according to the decreasing Froude number. Though the solutions at higher Froude numbers show so to speak dog-bone shapes and are hardly regarded as practical, the shape appears quite plausible at moderate and lower Froude numbers. It can be noted that negative ordinates which have appeared often at approximate solutions by Pavlenko and others never appear. Therefore the problem to minimize the wave resistance of infinite struts under a single condition of constant sectional area always has a solution, if a slight deviation from Michell's original assumption is allowed. The similar situation holds in the case of elementary ships of finite draft. Though the kernel of the integral equation cannot be expressed by known functions and eigenfunctions which are given in the case of infinite struts are not known, a numerical solution is possible. A few results at Froude number 0.4 were published by Kotik [11]. Weinblum's investigation has assumed not only the condition of constant volume but also other side conditions such as the fixed beam. For elementary ships, the constant beam together with the constant volume means a constant block coefficient. To seek the best form among those of constant block coefficient seems to have greater importance from the practical side because the solution under a single condition of constant volume often presents a ship form of too small block coefficient. However Bessho has proved for the infinite strut that there is no solution under such dual condition. This situation is similar for the elementary ship of finite draft.

The wave resistance of an elementary ship is expressed by a general form as

$$R = \frac{2\rho g^2}{\pi U^2}\int_{-\ell}^{\ell} f(x)\,dx \int_{-\ell}^{\ell} f(x')\,K(x-x')\,dx' \tag{15}$$

where $y = f(x)$ is the equation of the load water line and the kernel $K(x-x')$ depends upon the shape of the frame line. Change of the variables

$$x = -\ell\cos\theta\,, \qquad x' = -\ell\cos\theta'$$

and substitution of the expression for the solution, remembering that the optimum form is symmetric,

$$f(x) = \frac{b}{\sin\theta}\left(a_0 + a_2\cos 2\theta + a_4\cos 4\theta + \cdots\right) \tag{16}$$

lead to the equation such as

$$R = 2\rho U^2 b^2 \nu_0^2 \sum_{n=0}^{\infty}\sum_{m=0}^{\infty} a_{2n}a_{2m}M_{2n,2m} \tag{17}$$

where

$$M_{2n,2m} = \int_0^{\pi} d\theta \int_0^{\pi} \cos 2n\theta \cos 2m\theta'\,K(\ell\cos\theta' - \ell\cos\theta)\,d\theta' \tag{18}$$

b being the half breadth of the ship. The condition of the constant volume is

$$a_0 = \text{constant} = C \tag{19}$$

while the half beam which is also assumed constant is

$$b = b\sum_{n=0}^{\infty}(-)^n a_{2n}\,. \tag{20}$$

Now let us determine the coefficients a_{2n} in such a way that the right hand side of Eq. (17) becomes minimum. Consider a function

$$T(a_0, a_2, \ldots, k) = \sum_{n=0}^{\infty}\sum_{m=0}^{\infty} a_{2n}a_{2m}M_{2n,2m} + k\left[1 - \sum_{n=0}^{\infty}(-)^n a_{2n}\right], \tag{21}$$

In order to make the wave resistance minimum under the condition of Eqs. (19) and (20), the coefficients a_{2n} and k should satisfy the following equations.

$$\frac{\partial T}{\partial a_2} = 0\,, \quad \frac{\partial T}{\partial a_4} = 0\,, \;\ldots\; \frac{\partial T}{\partial k} = 0 \tag{22}$$

together with Eq. (19). These are equivalent to the simultaneous equation

$$2\sum_{m=0}^{N} a_{2m} M_{2n,\,2m} = k(-1)^n\,, \qquad n = 1, 2, \ldots\,. \tag{23}$$

If the infinite series of Eq. (16) is truncated at Nth term, Eq. (23) together with Eqs. (19) and (20) presents $N+1$ equations for $N+1$ unknowns. The coefficients can be determined provided the characteristic determinant is non-zero. Assume that the coefficients of the Fourier series, Eq. (16), satisfy the Eq. (23) and substitute in the integral

$$\int_{-\ell}^{\ell} f(x')\, K(x-x')\, dx'\,.$$

Making use of the Eq. (18), it is easily found that

$$\begin{aligned}\int_{-\ell}^{\ell} f(x')\, K(x-x')\, dx' &= b\ell \int_0^{\pi} \varphi(\theta')\, K[\ell(\cos\theta' - \cos\theta)]\, d\theta' \\ &= b\ell k\left[\frac{1}{2} + \sum_{n=1}^{N} (-)^n \cos 2n\theta\right]\end{aligned} \tag{24}$$

where

$$f(x) = \frac{b\,\varphi(\theta)}{\sin\theta}\,.$$

When one tends N toward infinity, Eq. (24) will give an integral equation which the minimal solution $f(x)$ or $\varphi(\theta)$ should satisfy. However there is a relation

$$\frac{1}{2} + \sum_{n=1}^{N} (-)^n \cos 2n\theta = \frac{(-)^N \cos\,(2N+1)\theta}{2\cos\theta}$$

and the right hand side of Eq. (24) does not converge to a continuous function. Bessho has proved that the solution diverges in the case of infinite strut. For the infinite strut, the solution is expanded into a series of eigen-functions as mentioned before. The coefficients can be determined analytically. By virtue of the asymptotic behavior of Mathieu functions, a few terms at the beginning of the series becomes dominant when the speed parameter γ_0 increases. Though the minimal solution gives a diverging series, the latter may be regarded as an asymptotic expression for small Froude number. According to the numerical results, the asymptotic value obtained by taking first three terms gives a reliable approximation of the present problem, if the speed parameter γ_0 is greater than 5. Instead of the condition of constant beam, Bessho proposed another side condition as a substitute. That is a condition of constant moment of inertia of the water plane with respect to the transverse axis.

$$I = 2\int_{-\ell}^{\ell} f(x)\, x^2 dx = \text{constant} . \tag{25}$$

In this case, the integral equation satisfied by the minimal solution becomes

$$\int_{-\ell}^{\ell} f(x')\, K(x - x')\, dx' = k_1 + k_2 x^2 . \tag{26}$$

The solution exists and is unique. If the solution of the problem with a single condition of constant volume is designated by $f_0(x)$, the solution with dual condition is expressed as

$$f(x) = f_0(x) + \beta f_1(x) \tag{27}$$

where β is the difference between the given midship beam and $f_0(0)$. Bessho published the function $f_1(x)$ for the dual condition involving the constant moment of inertia. Figure 1 shows a comparison between the asymptotic approximation for constant beam and Bessho's substitute.

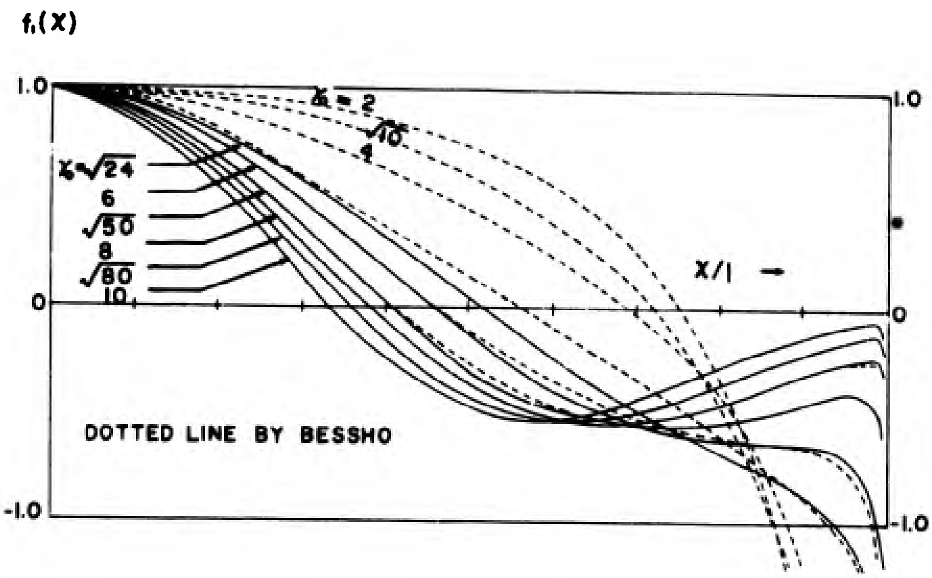

Figure 1

It has been shown that the best form does not exist under a single side condition of constant volume unless the elementary ship with prescribed vertical distribution is assumed. However Krein pointed out that a solution could exist if another side condition such as a fixed area of the wetted surface would be added. From the mathematical point of view, the solution under this dual condition is equivalent to the ship form for which the sum of the wave resistance and the skin friction becomes minimum. Lin, Webster and Wehausen [12] computed the ship form of minimum total resistance, which was assumed as the sum of Michell's integral and the frictional resistance according to Schoenherr's mean line. Their results are quite plausible except undulating lines which seem to be a consequence of an improper choice of the series used for the expansion of the solution.

According to Froude's hypothesis, the frictional resistance of a ship is equivalent to the frictional resistance of a flat plate of same length and same area. However the frictional resistance of a curved surface is an integration of the longitudinal component of the tangential stress. If the local frictional coefficient C_f' at a point where the normal to the surface makes an angle α to the longitudinal axis, x say, the total friction is given by

$$R_f = \frac{1}{2}\rho U^2 \iint C_f' \sin\alpha \, dS . \tag{28}$$

When the surface is expressed by an equation, $y = f(x, z)$, one can put

$$\cos\alpha = \frac{\dfrac{\partial f}{\partial x}}{\sqrt{1 + \left(\dfrac{\partial f}{\partial x}\right)^2 + \left(\dfrac{\partial f}{\partial z}\right)^2}}$$

$$dS = 2\sqrt{1 + \left(\frac{\partial f}{\partial x}\right)^2 + \left(\frac{\partial f}{\partial z}\right)^2} \, dx\, dz .$$

Therefore the frictional resistance becomes

$$R_f = \rho U^2 \iint C_f' \sqrt{1 + \left(\frac{\partial f}{\partial z}\right)^2} \, dx\, dz . \tag{29}$$

Taking the mean value of the local friction, one may write

$$R_f = \rho U^2 C_f \iint \sqrt{1 + \left(\frac{\partial f}{\partial z}\right)^2} \, dx\, dz \tag{30}$$

where C_f is regarded as the frictional resistance coefficient of the ship. The area

$$S_e = 2 \iint \sqrt{1 + \left(\frac{\partial f}{\partial z}\right)^2} \, dx\, dz \tag{31}$$

is called the effective area which is the product of the length and the mean girth. Let us consider a dual condition of constant displacement and constant effective area. Let us start with the formula for the wave resistance of a ship of length $2l$ and draft T as

$$R = 2\rho U^2 \nu^4 \int_{-l}^{l}\int_{-l}^{l}\int_{0}^{T}\int_{0}^{T} f(x,z)\, f(x',z')\, K(z+z',\, x-x')\, dx\, dx'\, dz\, dz' \qquad (32)$$

where

$$K(z+z',\, x-x') = \frac{2}{\pi}\int_{1}^{\infty} e^{-\nu\lambda^2(z+z')} \cos[\nu\lambda(x-x')] \frac{\lambda^4 d\lambda}{\sqrt{\lambda^2-1}} \qquad (33)$$

which is obtained by the integration by parts of Michell's integral. According to the principle of the calculus of variations, the minimization of the wave resistance under the conditions of constant volume of displacement

$$\nabla = 2\iint f(x,z)\, dx\, dz = \text{constant} \qquad (34)$$

and of the constant effective area

$$S_e = 2\iint \sqrt{1+\left(\frac{\partial f}{\partial z}\right)^2}\, dx\, dz = \text{constant} \qquad (35)$$

gives a non-linear integro-differential equation as

$$\int_{-l}^{l}\int_{0}^{T} f(x',z')\, K(z+z',\, x-x')\, dx'\, dz' = k_1 + k_2 \frac{\partial}{\partial z} \frac{\dfrac{\partial f}{\partial z}}{\sqrt{1+\left(\dfrac{\partial f}{\partial z}\right)^2}} \qquad (36)$$

where k_1 and k_2 are constants. Integrating with respect to z, one obtains

$$\int_{-l}^{l}\int_{0}^{T} f(x',z')\, K^{(1)}(z+z',\, x-x')\, dx'\, dz' = k_1 z + k_2 \frac{\dfrac{\partial f}{\partial z}}{\sqrt{1+\left(\dfrac{\partial f}{\partial z}\right)^2}} + \varphi_1(x) \qquad (37)$$

where

$$K^{(1)}(z+z',\, x-x') = -\frac{2}{\pi\nu}\int_{1}^{\infty} e^{-\nu\lambda^2(z+z')} \cos[\nu\lambda(x-x')] \frac{\lambda^2 d\lambda}{\sqrt{\lambda^2-1}} \qquad (38)$$

and $\varphi_1(x)$ is an arbitrary function of x only. Since the Eq. (37) is non-linear, an iterative method is employed. In the first place, the vertical gradient of the surface $\partial f/\partial z$ is assumed as small. Then a linearization of the integro-differential equation is made by the exclusion of the non-linear term $(\partial f/\partial z)^2$.

$$\int_{-\ell}^{\ell}\int_{0}^{T} f(x', z')\, K^{(1)}(z+z', x-x')\, dx' dz' = k_1 z + k_2 \frac{\partial f}{\partial z} + \varphi_1(x) . \tag{39}$$

Integrating again with respect to z, one may obtain a linear integral equation as

$$\int_{-\ell}^{\ell}\int_{0}^{T} f(x', z')\, K^{(2)}(z+z', x-x')\, dx' dz' = \frac{1}{2} k_1 z^2 + k_2 f(x, z) + z\varphi_1(x) + \varphi_2(x) \tag{40}$$

where

$$K^{(2)}(z+z', x-x') = \frac{2}{\pi\gamma^2}\int_1^{\infty} e^{-\gamma\lambda^2(z+z')} \cos[\gamma\lambda(x-x')] \frac{d\lambda}{\sqrt{\lambda^2 - 1}} \tag{41}$$

and $\varphi_2(x)$ is another arbitrary function of x only. Since $K^{(2)}(z+z', x-x')$ is absolutely integrable in the domain $-\ell \leq x \leq \ell$, $0 \leq z \leq T$, one can write

$$\int_{-\ell}^{\ell}\int_{0}^{T} |K^{(2)}(z+z', x-x')|\, dx' dz' \leq M .$$

M is the maximum of the integral in this domain. Now assume that

$$\frac{1}{2} k_1 z^2 + z\varphi_1(x) + \varphi_2(x)$$

is bounded. Then the Neumann series for the integral Eq. (40) converges uniformly if $|k_2| > M$. Therefore the linearized integral Eq. (40) has a solution, and the latter is unique except for the arbitrary constants k_1 and k_2 and the arbitrary functions $\varphi_1(x)$ and $\varphi_2(x)$. These unknowns are determined by side conditions. There are already two of them, the given volume and the given effective area. However the solution is still indeterminate owing to the functions $\varphi_1(x)$ and $\varphi_2(x)$. Two other conditions are necessary in order to determine the solution. It is understood easily that the vanishing ordinate at the keel line, i.e.,

$$f(x, T) = 0 \tag{42}$$

can become one of the required conditions. The other can be a condition imposed on the shape at the water line $z = 0$. As the integral on the left hand side of Eq. (39) is bounded in the domain $-\ell \leq x \leq \ell$, $0 \leq z \leq T$, one may have

$$\int_{-\ell}^{\ell}\int_{0}^{T} f(x, z')\, K^{(1)}(z', x-x')\, dx' dz' = k_2 \left(\frac{\partial f}{\partial z}\right)_{z=0} + \varphi_1(x) . \tag{43}$$

Therefore $\varphi_1(x)$ can be determined by giving the slope of the surface $\partial f/\partial z$ at $z = 0$. The vertical sides for instance corresponds to $\partial f/\partial z = 0$ at $z = 0$. This condition is equivalent to the implicit assumption employed by Lin, Webster and Wehausen in their calculation. As the non-linear factor has always a non-zero denominator $\sqrt{1 + (\partial f/\partial z)^2}$, the integral equation at any stage of the iteration has a solution. It can be shown by the Eq. (40) that $f(x, z)$ is finite (or zero) at both ends $x = \pm\ell$.

ASYMPTOTIC FORM OF THE OPTIMUM ELEMENTARY SHIP FOR VANISHING DRAFT

It has been shown that the elementary ship of given vertical distribution has a minimal solution for modified Michell's integral under the single condition of constant displacement. The wave resistance is given by

$$R = 2\rho U^2 \nu^4 \int_{-\ell}^{\ell} \int_{-\ell}^{\ell} \int_0^T \int_0^T X(x)\, Z(z)\, X(x')\, Z(z')\, K(z+z', x-x')\, dx\, dx'\, dz\, dz' . \tag{44}$$

Letting

$$\int_0^T \int_0^T Z(z)\, Z(z')\, K(z+z', x-x')\, dz\, dz' = K(x-x') \tag{45}$$

and writing $f(x)$ in place of $X(x)$, one obtains

$$R = 2\rho U^2 \nu^4 \int_{-\ell}^{\ell} \int_{-\ell}^{\ell} f(x)\, f(x')\, K(x-x')\, dx\, dx' . \tag{46}$$

Therefore the optimum form is given by a solution of an integral equation such as

$$\int_{-\ell}^{\ell} f(x')\, K(x-x')\, dx' = k . \tag{47}$$

As mentioned before, the above integral equation have a solution which can be determined only by a numerical way. Though there have been some examples, the solving procedure requires very tedious and extensive calculation any way.

As the basic assumption of Michell's theory is that the beam of the ship is very small in comparison with the length, it applies to the thin ship. However actual ships have draft which is smaller than the beam. The slender ship stands on the idea that the draft length ratio is of the same order of amount as the order of the beam length ratio which is much smaller than unity. The linearization is achieved by means of these parameters. Attempts have been made to find out a slender ship form of minimum wave resistance [13]. They seem not to be successful from the practical point of view. The reason is that the solution involves only ship forms of a very restricted class and is by no means the best among whole admissible ship forms.

Results which will be reported here deviate from the original slender ship assumption. The basic idea is to return to Michell's integral and to look for an asymptotic form of the minimal solution when the draft becomes infinitesimal.

The solution to minimize Michell's integral for elementary ships under a single condition of constant volume exists as mentioned before. Assume an elementary ship, $f(x,z) = X(x)\,Z(z)$, and write Michell's integral

$$R = 2\rho U^2 \kappa^4 \int_{-\ell}^{\ell}\int_{-\ell}^{\ell} X(x)\, X(x')\, K(x-x')\, dx\, dx' \tag{48}$$

where

$$K(x-x') = \frac{2}{\pi}\int_1^{\infty} \cos\left[\kappa\lambda(x-x')\right]\left[\int_0^T Z(z)\, e^{-\gamma\lambda^2 z}\, dz\right]^2 \frac{\lambda^4\, d\lambda}{\sqrt{\lambda^2-1}} . \tag{49}$$

The integral equation to determine the minimal solution is

$$\int_{-\ell}^{\ell} X(x')\, K(x-x')\, dx' = k . \tag{50}$$

Since the kernel has a logarithmic singularity at $x = x'$, the solution takes the form

$$X(x) = \frac{U(x)}{\sqrt{\ell^2 - x^2}} . \tag{51}$$

If $U(x)$ is finite at $x = \pm\ell$, the function $X(x)$ becomes singular at both ends. Now let us consider the asymptotic behavior of the wave resistance when the draft T tends to zero. The simple slender ship theory expands the integral

$$\int_0^T Z(z)\, e^{-\gamma\lambda^2 z}\, dz$$

by an ascending power series of T and takes the first term that makes the kernel $K(x-x')$ have the order of T^2. Though the kernel has a higher singularity at $x = x'$, the integral with respect to x and x' is regarded as the finite part due to Hadamard. Then Eq. (48) becomes finite only when $dX(x)/dx = 0$, otherwise the integral diverges. Since the finite part of the integral is taken, the singularity of the kernel does not matter except at the end points $x = \pm\ell$. Therefore the infinity appears from the behavior of the integrand at the ends. This phenomenon may be called the end effect. It has been shown that the end effect gives a term of the order of $T^2 \ln T$ when $dX(x)/dx$ is finite there. The order of the end effect can be evaluated if $Z(z)$ is assumed as a simple function such as $Z(z) = 1$ and the behavior of the resulting integral is examined at the limit of zero draft. It can be proved that the end effect has the order of $T^{1/2}$ when the water line function takes the form of Eq. (51). Since the volume is proportional to T, the resistance per unit volume increases infinitely when the draft decreases. It seems to be natural that this case is excluded from the admissible solution. The case that $X(x)$ is finite at both ends is also excluded by the same reason because the order of the end effect is $T \ln T$. Therefore the only case that the width of the water plane vanishes at both ends is taken as the asymptotic form of the optimum ship. Then the left hand side of the integral Eq. (50) is integrated by parts

$$\int_{-\ell}^{\ell} \frac{dX(x')}{dx'} K^{(1)}(x-x')\,dx' = k \tag{52}$$

where $K^{(1)}$ is an integral of Eq. (49) with respect to x. Integrating Eq. (52) three times with respect to x, and taking account of the fact that $dX(x')/dx'$ is an odd function of x' and $K(x-x')$ is symmetric, one obtains

$$\int_{-\ell}^{\ell} \frac{dX(x')}{dx'} K^{(4)}(x-x')\,dx' = \frac{1}{6} kx^3 + k'x \tag{53}$$

where

$$K^{(4)}(x-x') = \frac{2}{\pi\gamma^4}\int_1^{\infty} \cos[\gamma\lambda(x-x')] \left[\int_0^T Z(z)\,e^{-\gamma\lambda^2 z}\,dz\right]^2 \frac{d\lambda}{\sqrt{\lambda^2-1}} . \tag{54}$$

$K^{(4)}$ has an asymptotic form when T tends to zero as follows:

$$\begin{aligned} K^{(4)}(x-x') &\simeq \frac{2}{\pi\gamma^4}\int_1^{\infty} \cos[\gamma\lambda(x-x')] \left[\int_0^T Z(z)\,dz\right]^2 \frac{d\lambda}{\sqrt{\lambda^2-1}} \\ &= -\frac{1}{\gamma^4} Y_0[\gamma(x-x')] \left[\int_0^T Z(z)\,dz\right]^2 \end{aligned} \tag{55}$$

where Y_0 is the Bessel function of the second kind. By putting

$$A(x) = 2X(x)\int_0^T Z(z)\,dz \tag{56}$$

that means the area of the transverse section, Eq. (53) becomes

$$-\frac{1}{2\gamma^4}\int_0^T Z(z)\,dz \int_{-\ell}^{\ell} \frac{dA(x')}{dx'} Y_0[\gamma(x-x')]\,dx' = \frac{1}{6} kx^3 + k'x . \tag{57}$$

This is an asymptotic form of the integral equation. If the condition

$$\frac{dA(x)}{dx} = 0 \tag{58}$$

at $x = \pm\ell$ is employed, the end effect does not exist and the minimum wave resistance is given by

$$R_{min} = 2\rho U^2 \ell^4 k \int_{-\ell}^{\ell} X(x)\,dx \;. \tag{59}$$

This is the case of a simple slender ship theory. The method of solution and numerical results are given in literature [13]. In order to solve the integral equation, let us employ the dimensionless coordinates

$$x = -\ell \cos\theta \;, \qquad x' = -\ell \cos\theta' \;. \tag{60}$$

The sectional area is non-dimensionalized and to facilitate the solution, one may put

$$\frac{dA(x)}{dx} = \frac{\nabla}{2\ell^2}\,\frac{\sigma(\theta)}{\sin\theta} \;. \tag{61}$$

Then Eq. (57) is equivalent to the following integral equation:

$$\int_0^{\pi} \sigma(\theta')\, Y_0\left[\kappa_0 \ell(\cos\theta - \cos\theta')\right] d\theta' = k_1 \cos\theta + k_2 \cos 3\theta \tag{62}$$

where $\kappa_0 = g/U^2$. The displacement becomes

$$\nabla = -\int_{-\ell}^{\ell} \frac{dA(x)}{dx}\, x\,dx$$

$$= \frac{\nabla}{2}\int_0^{\pi} \sigma(\theta)\cos\theta\, d\theta$$

so that

$$\int_0^{\pi} \sigma(\theta)\cos\theta\, d\theta = 2 \;. \tag{63}$$

The integral Eq. (62) can be solved by means of Fourier expansion by Mathieu functions. There is a relation for even Mathieu functions $ce_n(\theta, q)$, that

$$\lambda_n \int_0^{\pi} ce_n(\theta', q)\, Y_0\left[2\sqrt{q}\,(\cos\theta - \cos\theta')\right] d\theta' = ce_n(\theta, q) \;.$$

Since $ce_n(\theta, q)$ makes an orthogonal system such as

$$\frac{2}{\pi}\int_0^{\pi} ce_n(\theta, q)\, ce_m(\theta, q)\, d\theta = 0 \qquad n \neq m$$

$$= 1 \qquad n = m$$

any function can be expanded into Fourier series of ce_n. As $A(x)$ is an even function of x, the expansion for $\phi(\theta)$ contains odd terms only.

$$\phi(\theta) = a_1\, ce_1(\theta, q) + a_3\, ce_3(\theta, q) + a_5\, ce_5(\theta, q) + \cdots .$$

There is also a relation

$$\cos(2r+1)\theta = \sum_{r=0}^{\infty} A_{2r+1}^{(2n+1)}\, ce_{2n+1}(\theta, q)$$

where $A_{2r+1}^{(2n+1)}$ is the Fourier coefficient of ce_{2n+1}, such as

$$ce_{2n+1}(\theta, q) = \sum_{n=0}^{\infty} A_{2r+1}^{(2n+1)} \cos(2r+1)\theta .$$

Substituting these relations in Eq. (62), the following equation is obtained:

$$\sum_{n=0}^{\infty} a_{an+1}\, ce_{2n+1}(\theta, q)\, \lambda_{2n+1} = \sum_{n=0}^{\infty} \left(k_1 A_1^{(2n+1)} + k_2 A_3^{(2n+1)}\right) ce_{2n+1}(\theta, q) .$$

Therefore the unknown coefficients are determined as

$$a_{2n+1} = \lambda_{2n+1}\left(k_1 A_1^{(an+1)} + k_2 A_3^{(2n+1)}\right) . \tag{64}$$

The condition (63) gives

$$\sum_{n=0}^{\infty} a_{2n+1} A_1^{(2n+1)} = \frac{4}{\pi} \tag{65}$$

and together with the condition $\phi(\theta) = 0$ at $\theta = 0$ and π the arbitrary constants k_1 and k_2 are determined. Since

$$k = -\frac{6k_2 \nabla}{\nu_o^4}\int_0^T Z(z)\, dz \tag{66}$$

the wave resistance is given by

$$R_{min} = \frac{6k_2 \rho U^2 \nabla^2}{\ell^4} . \tag{67}$$

Necessary coefficients for the calculation of Mathieu functions have been given by Bessho and the optimum forms of simple slender ships are calculated. Figure 2 gives the best curves of sectional area of the simple slender ship. It has been found that the minimum wave resistance of the simple slender ship given by Eq. (67) is not the minimum of the asymptotic value of Michell's integral for vanishing draft, as a result of comparison of it and the wave resistance of a slender ship with vertical stem. In the latter case, dA/dx or [illegible] does not vanish at the ends. If the condition Eq. (58) is discarded, one of the two coefficients in Eq. (62) becomes undetermined unless another side condition is introduced. Then solutions of the integral Eq. (62) give a family of curve of sectional area by which the wave resistance excluding the end effect is minimum for a constant displacement. One may have a doubt since the above indeterminateness seems to contradict with the fact that the minimal solution for Michell's integral of finite draft is unique. By a proper choice of the midship ordinate, k_2 can be eliminated. Then the principal part of the wave resistance given by Eq. (67) vanishes. Though difficult is it to identify the true asymptote, the above solution may be regarded as the asymptotic form of the minimal solution with the single condition of constant volume for vanishing draft. Figure 3 shows a comparison between the curve of sectional area obtained from the above method and the dipole distribution for the optimum infinite strut. The difference between them is small especially at lower Froude numbers. Kotik calculated the optimum form of the elementary ship of finite draft at Froude number 0.4, one of which concerned a 4th power vertical section and the other concerned a wall-sided section. His results with respect to a draft-length ratio 0.05 are plotted in Fig. 3 for comparison. They fall between the result for a infinite strut at Froude number 0.397 and that of the aforementioned approximation. When finite value of k_2 is retained, a family of solutions with various midship section area is obtained. As mentioned before, there is no minimal solution for dual condition of constant volume and constant midship section. Then the above results seem to correspond to the asymptotic solution for the condition of constant volume and constant moment of inertia. Figures 4-12 give the asymptotic optimum curve of sectional area at various speed coefficient $\nu_0 = g/U^2$ with prismatic coefficient φ as a parameter. In some of the figures Weinblum's results [14] are given by dotted lines. Difference is not remarkable except the case of $\nu_0 = 2$ where the polynomial representation employed by him seems to lose its accuracy. In Fig. 6, curves of forebody sectional area of the Taylor Standard Series (T.S.S.) are shown for comparison. There is a surprising agreement between the T.S.S. and the theoretically optimum form for medium prismatic coefficient at Froude number 0.25. On examining the chart of residuary resistance coefficient, one may find out that T.S.S. shows an excellent behavior at Froude number near 0.25, if the prismatic coefficient is around 0.60 where the best agreement is obtained. It is of some interest to observe that a hump appears at Froude number 0.25, if the prismatic coefficient is reduced to 0.48 or raised to 0.68 where deviation from the optimum curve becomes remarkable. At Froude numbers other than 0.25, T.S.S. does not agree with the optimum curve. Therefore better results than those of T.S.S. can be expected by employing the theoretical curve of sectional area.

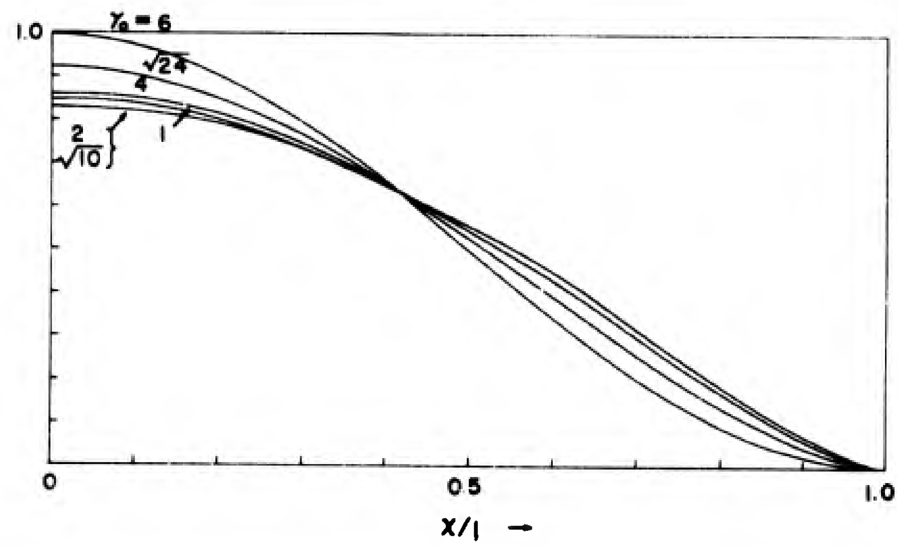

Figure 2

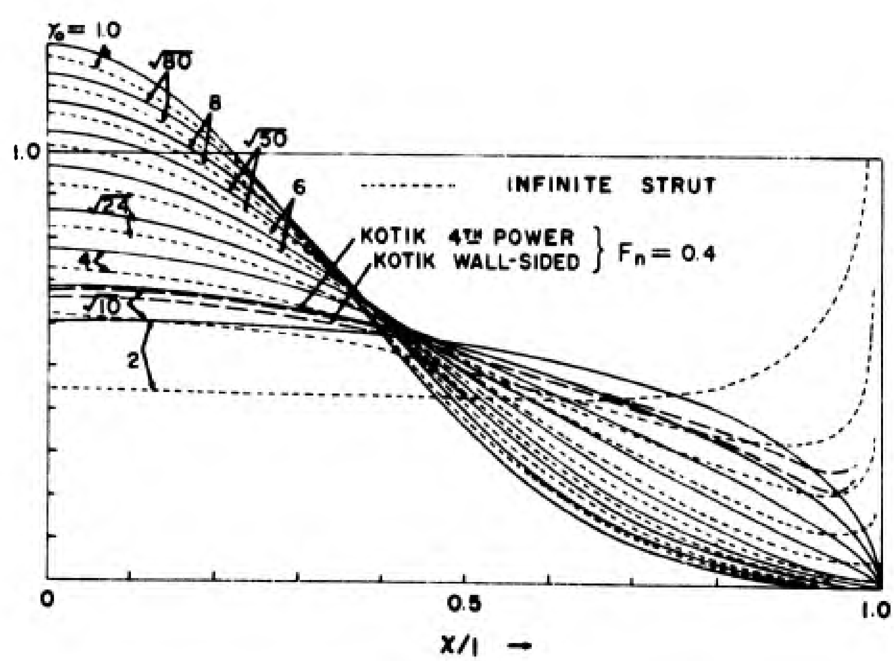

Figure 3

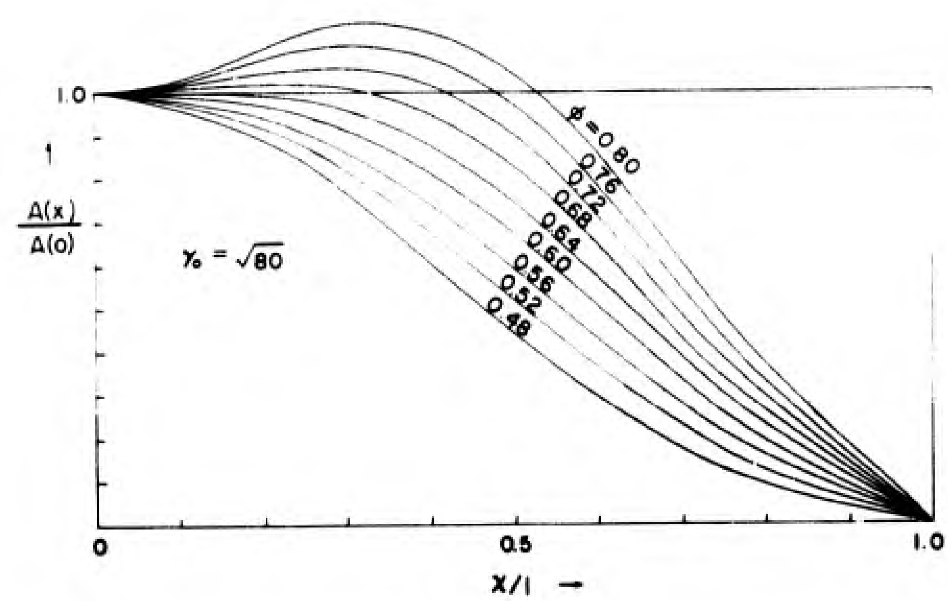

Figure 4

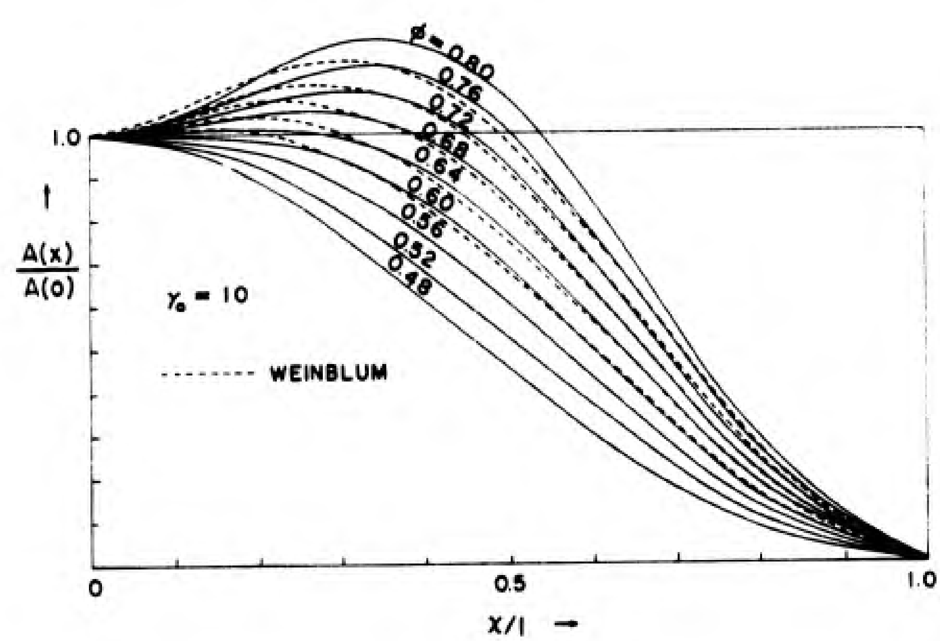

Figure 5

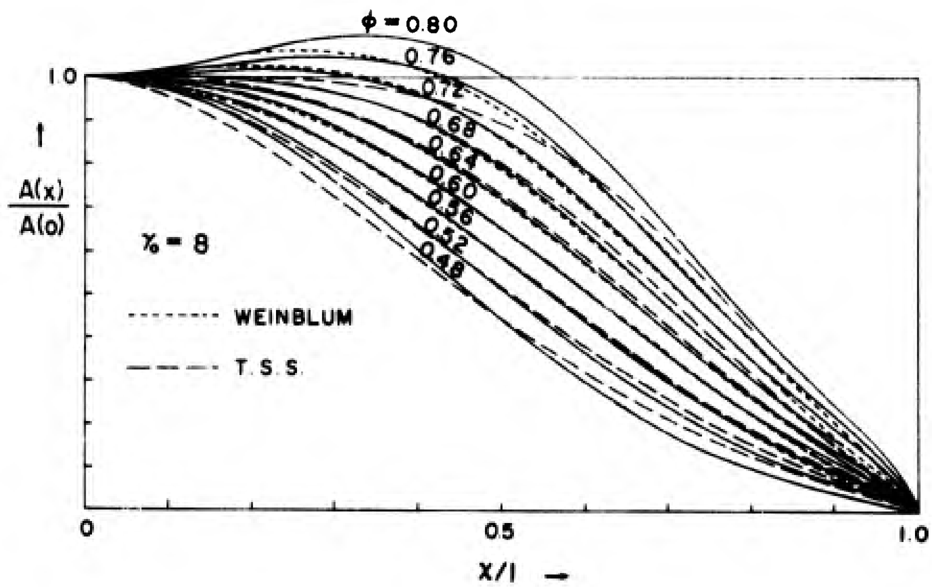

Figure 6

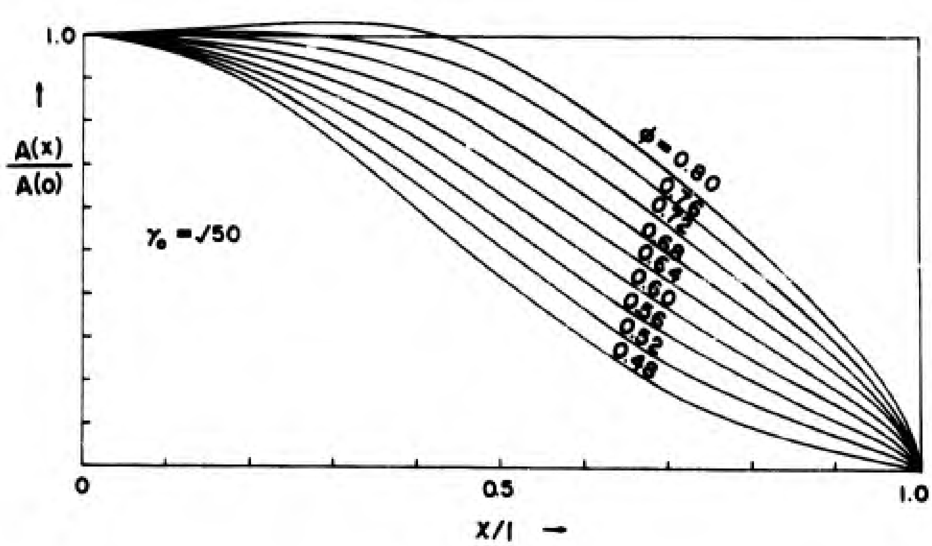

Figure 7

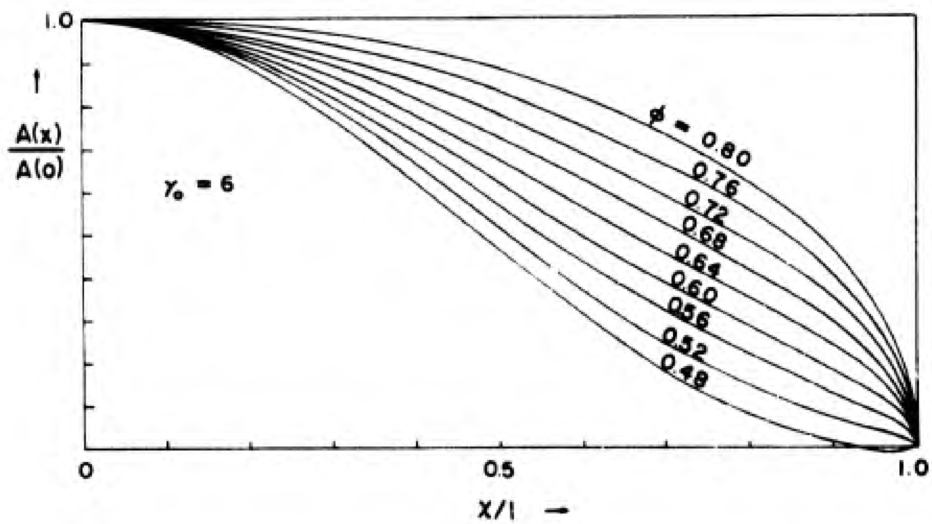

Figure 8

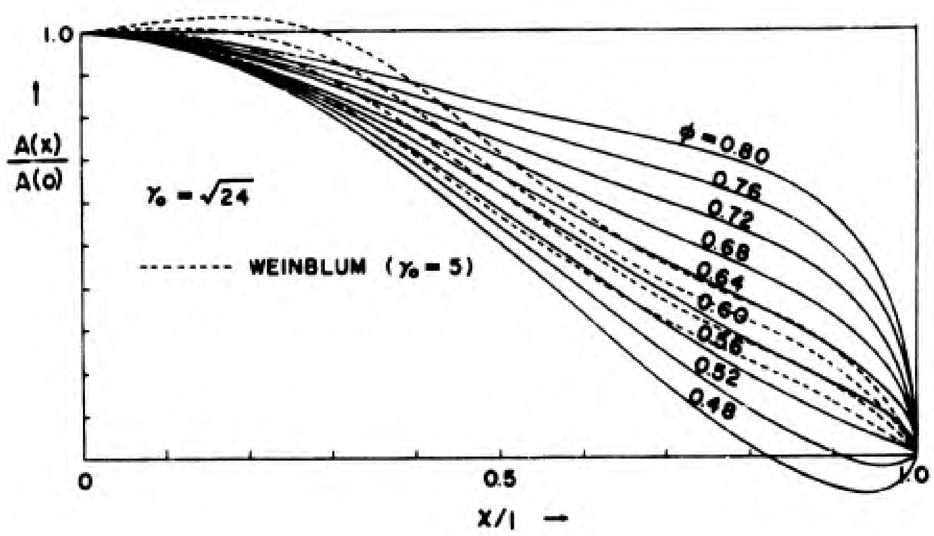

Figure 9

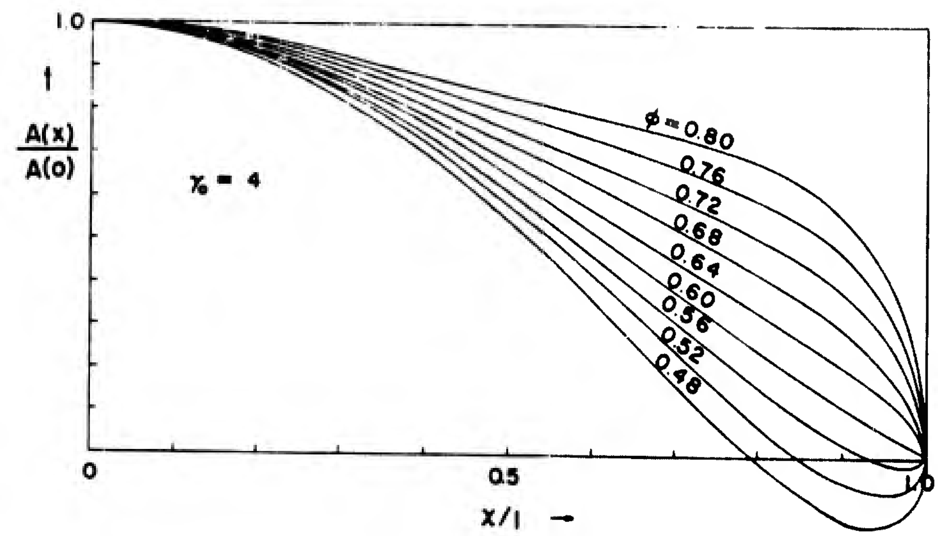

Figure 10

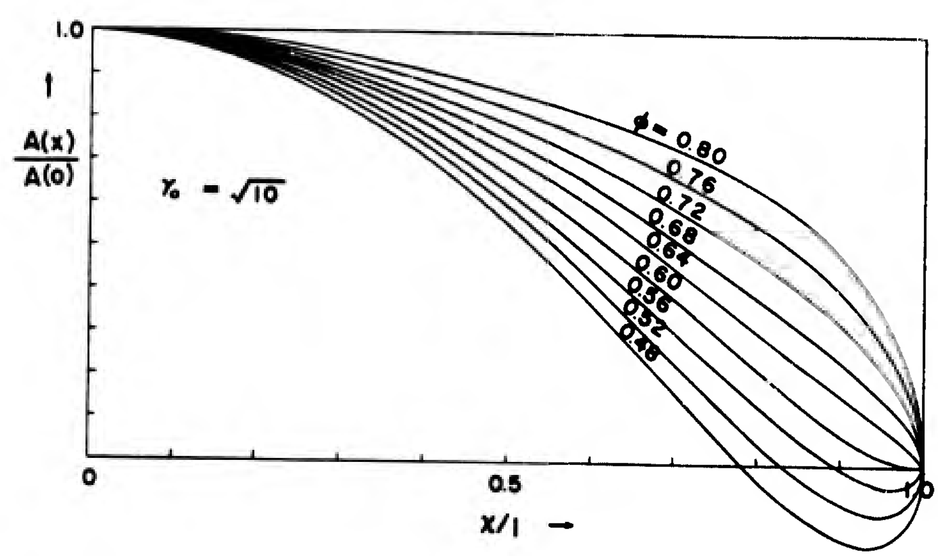

Figure 11

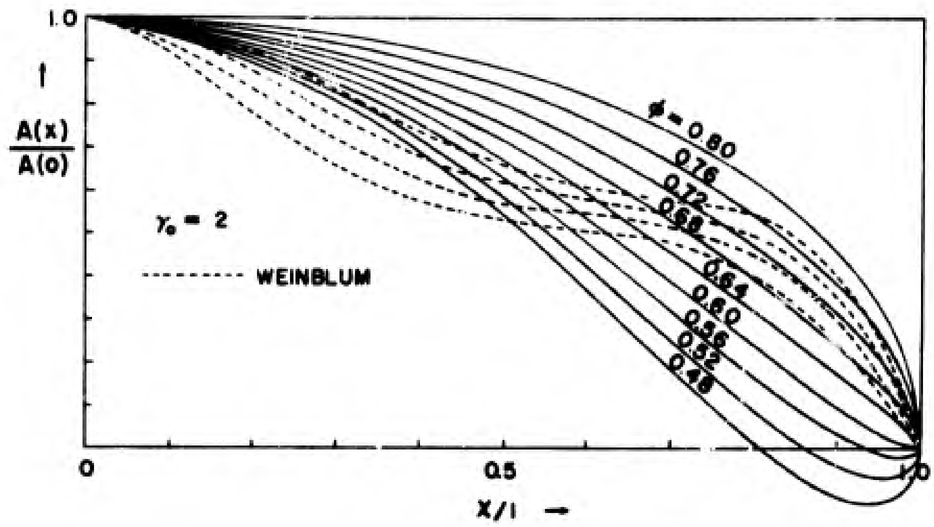

Figure 12

SOME CASES OF SMALL WAVE RESISTANCE

As shown by Krein and Bessho, there is no definite solution of the problem to minimize Michell's integral for a given volume. This fact suggests that the theory of minimum wave resistance discussed so far is not the only way to obtain a ship form of small wave resistance. Inui [15] has shown that the wave resistance can be reduced to a great extent by addition of a bulb at the bow which enables the cancellation of the wave generated by the main hull. This method was refined by Yim [16]. He considered a combination of a source distribution representing the ship's hull and a distribution of dipoles along a vertical line of infinite length at the bow. According to him, the wave resistance can be eliminated when a suitable choice is made in the combination of sources and dipoles. The vertical dipole distribution of Yim's model shows a vertical cylinder of infinite length at the bow. Instead of it, one may consider a source distribution on the vertical line. In fact, it is possible to make the wave resistance vanish by a suitable choice of source distribution along a horizontal line and those along vertical lines at both ends of the horizontal distribution. As the simplest example, let us consider a source distribution along a horizontal line of length $L = 2\ell$ on the free surface. Choose the density of sources given by the following equation:

$$\sigma_1(x) = m_1 \sin\left(\frac{\pi x}{\ell}\right), \qquad -\ell \le x \le \ell . \tag{68}$$

If a distribution of sources along an infinite vertical line at $x = \ell$ and that of sinks along a vertical line at $x = -\ell$ have density distribution given by

$$\sigma_2(z) = m_2 \exp\left(\frac{\pi^2 z}{\gamma \ell^2}\right), \qquad 0 \le z < \infty \tag{69}$$

the wave resistance becomes

$$R = 8\pi\rho\gamma^2 \int_{-\pi/2}^{\pi/2} P^2 \sec^3\theta \, d\theta \tag{70}$$

where

$$P = \int_{-\ell}^{\ell} \sigma_1(x) \sin(\gamma x \sec\theta) dx + 2 \sin(\gamma_0 \sec\theta) \int_0^{\infty} \sigma_2(z) \exp(-\gamma z \sec^2\theta) dz . \tag{71}$$

Substituting Eqs. (68) and (69) in (71) and carrying out the integration, one obtains

$$R = 64\pi\rho\gamma_0^4 \left(m_2 - \frac{\pi m_1}{\gamma_0}\right)^2 \int_0^{\pi/2} \left[\frac{\sin(\gamma_0 \sec\theta)}{\gamma_0^2 \sec^2\theta - \pi^2}\right]^2 \sec^3\theta \, d\theta \tag{72}$$

if $\gamma_0 > \pi$. If there is a relation

$$m_2 = \pi m_1/\gamma_0 \tag{73}$$

the wave resistance vanishes. Though Krein and Bessho have shown that wave-free distribution of sources gives zero linearized volume, the wave-free distribution without negative ordinates does exist if the draft is allowed to be infinite. The horizontal distribution corresponds to a half immersed body of revolution with cross sectional area given by the equation

$$A(x) = \frac{8\ell m_1}{U} \cos^2 \frac{\pi x}{2\ell} . \tag{74}$$

The vertical distribution corresponds to a vertical strut of infinite depth, the horizontal section of which is the Rankine oval. The resultant shape is a combination of them and is so to speak a yacht shaped ship with infinite vertical keel. As the infinite keel cannot be realized, it must be truncated at a finite depth. The truncation invalidates the perfect cancellation of the waves generated by each system of sources. Figure 13 shows the results of calculation of wave resistance when the vertical keel is truncated at a depth 0.25L and 0.1L, when the designed Froude number at which the wave resistance vanishes for the infinite keel is 0.316 or $\gamma_0 = 5$. Though the truncation of the vertical keel does not matter much at lower Froude numbers, it weakens the cancellation of the wave at high Froude number especially when the vertical keel is truncated at smaller depth because of the practical requirement. In order to compensate the weakened effect of the vertical keel, the strength of the vertical distribution should be augmented considerably. An investigation has been made so as to find out the vertical distribution which makes the resultant wave resistance minimum. According to the result, a remarkable peak appears at the bottom of the vertical source distribution. This fact suggests that the best form has a concentration of the source at the bottom. Instead of pursuing the best distribution along the vertical lines, a discrete source and a sink are assumed at the depth

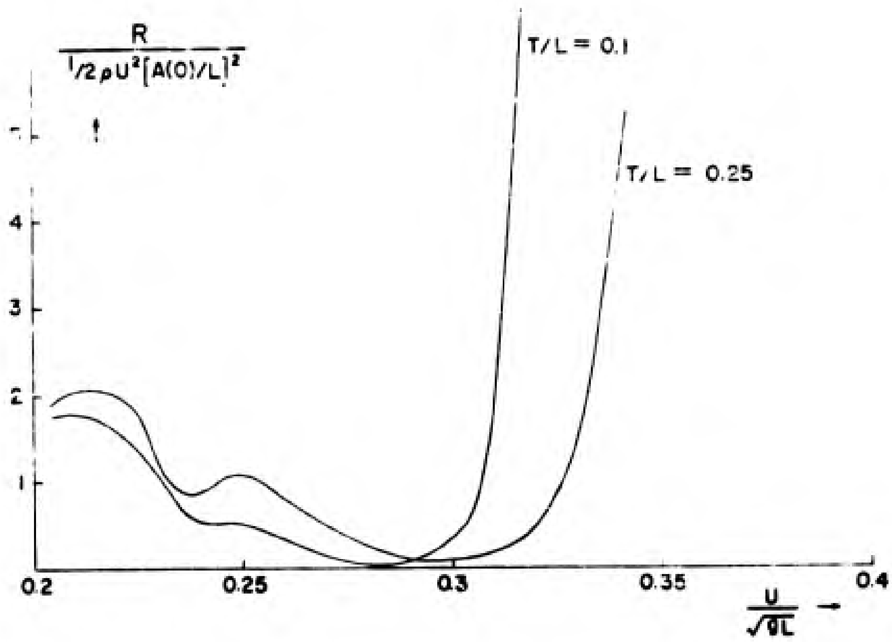

Figure 13

of the bottom. Then the system of sources is the combination of a discrete source at the forward end of the bottom and a discrete sink at the after end together with the horizontal distribution. The source and the sink form the so-called Rankine ovoid, and the resulting shape is the combination of a submerged ovoid and a surface piercing hull. At a lower Froude number, the surface piercing part is much greater than the submerged part, so that the former can be regarded as the main hull, while the latter forms bulbs on both sides. At higher Froude numbers on the other hand, the submerged part becomes the main hull, while the upper part is like the super-structure or bridge of a half submerged submarine. Such a type of ship as this may be called a semi-submerged ship which has been discussed from time to time [17]. If the strength of the submerged source at the point $x = \ell$, $z = f$, is designated by m_0 and an equal sink is placed at the point $x = -\ell$, $z = f$, the wave resistance when combined with the horizontal source distribution given by Eq. (68) becomes

$$R = 64\pi\rho\gamma_0^2 \int_0^{\pi/2} \left[m_0 \exp\left(-\gamma_0 \frac{f}{\ell} \sec^2\theta\right) + \frac{m_1 \pi}{\pi^2 - \gamma_0^2 \sec^2\theta}\right]^2 \sin^2(\gamma_0 \sec\theta) \sec^3\theta \, d\theta. \quad (75)$$

Write the area of the midsection of the Rankine ovoid as A_0 and that of the bridge by A_1. Then there is approximate relations due to a linearized theory such as

$$m_0 = \frac{UA_0}{4\pi\ell} \quad \text{and} \quad m_1 = \frac{UA_1}{8\ell}. \quad (76)$$

Then the wave resistance can be written as

$$R \quad \frac{4}{\ } \ g \frac{A_o^{\ 2}}{\ } \ _o \int_0^{\ \ 2} \left[\exp\left(- \ _o \frac{f}{\ } \sec^2 \right) + \frac{\ }{\ ^2 - \ _o^{\ 2} \sec^2 } \right]^2 \sin^2(\ _o \sec \ ) \sec^3 \ d \tag{77}$$

where

$$\frac{m_1}{m_o} \quad \frac{\ }{2} \frac{A_1}{A_o} \ . \tag{78}$$

The ratio λ can be chosen in such a way that the resulting wave resistance becomes minimum. If the volume of the submerged part is kept constant, it is merely given by the equation

$$\frac{\partial R}{\partial \ } \quad 0 \ . \tag{79}$$

Calculation has been carried out for cases of $f = 4$ and 5. Models for tank experiment were prepared as shown in Fig. 14. Figure 15 shows some of the results of the experiment together with the computed curves. The designed speed at which the relation Eq. (79) holds is indicated by the arrow. As the experimental value is the residuary resistance coefficient, some difference exists between the experimental curves and the theoretical wave resistance coefficient. However, the general feature of the curves is similar. There are also shown theoretical curves of wave resistance coefficient when the submerged body, the Rankine ovoid, moves alone under the water surface, and one can observe how the wave resistance is reduced by the interference between two parts.

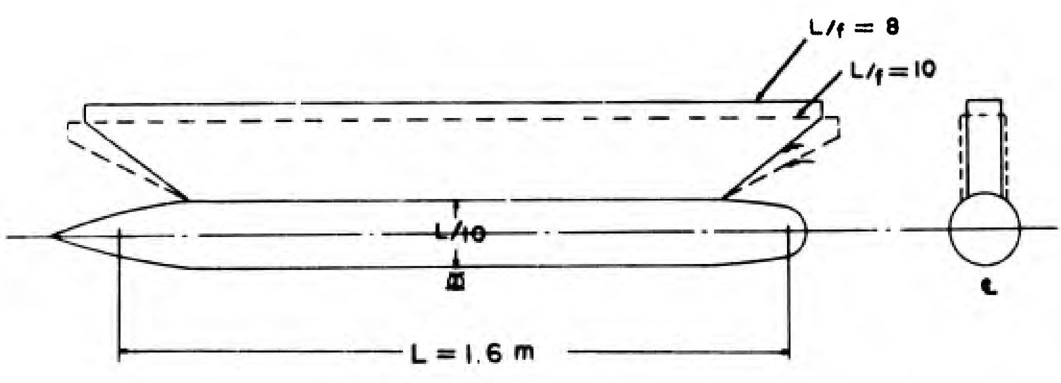

Figure 14

Kotik calculated the value of minimum wave resistance of elementary ships at Froude number 0.4. For a wall-sided ship of draft length ratio 0.1, the wave resistance coefficient defined by

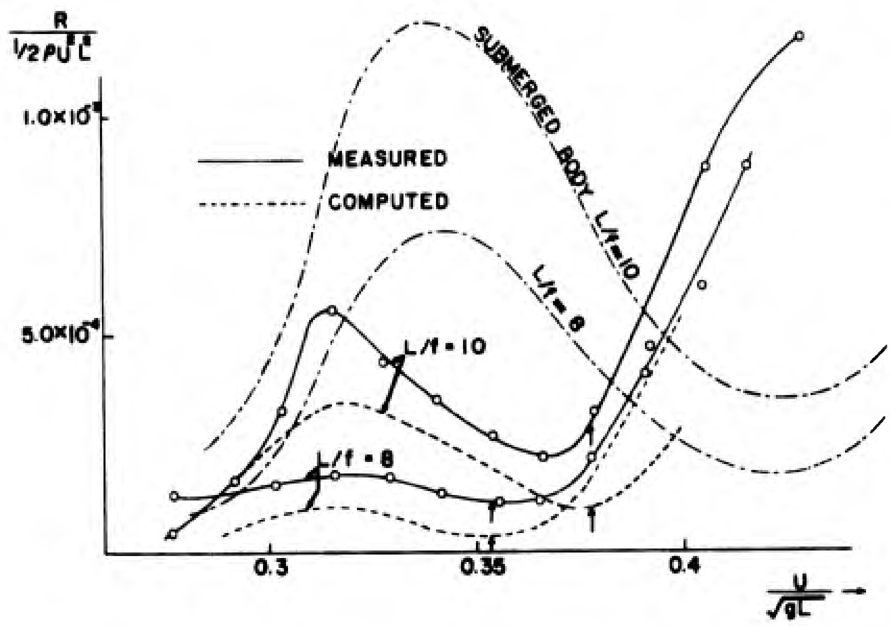

Figure 15

$$C_w = R\Big/\frac{1}{2}\rho U^2 \bar{B}^2$$

where $2\bar{B}$ is the mean breadth, becomes 0.32612 and for a ship with 4th power section, it is 0.35665. The corresponding value for a semi-submerged ship of minimum wave resistance at Froude number 0.4 was calculated. It was found to be 0.08837, and a considerable reduction of the wave resistance is achieved.

The experiment of the semi-submerged ship was conducted under a financial support by Uraga Heavy Industry Co. Ltd. The author wishes to express his gratitude.

REFERENCES

1. Weinblum, G., "Schiffe geringsten Widerstandes," Proc. 3rd Internat. Congr. Appl. Mech. Stockholm (1930)

2. Krein, M. G., Doklady Akademi Nauk SSSR, Vol. 100, No. 3, 1955

   Kostchukov, A. A., "Theory of Ship Waves and Wave Resistance," Leningrad, 1959

3. Bessho, M., "Wave-free Distributions and Their Applications," International Seminar on Theoretical Wave Resistance, University of Michigan (1963)

4. Bessho, M., "On the Problem of the Minimum Wave Making Resistance of Ships," Memoirs of the Defence Academy, Japan, Vol. II, No. 4 (1963)

5. Sretenskii, L. N., "Sur un Probleme de Minimum Dan la Theorie du Navire," C. R. (Dokl.) Acad. Sci. URSS(N.S.)3(1935)

6. Wehausen, J. V., "Wave Resistance of Thin Ships," Proc. of the Symposium on Naval Hydrodynamics Publication 515 (1957)

7. Karp, S., Kotik, J., and Lurye, J., "On the Problem of Minimum Wave Resistance for Struts and Strut-Like Dipole Distributions," Third Symposium on Naval Hydrodynamics, Scheveningen, September 1960

8. Pavlenko, G. E., "Theoretical Ship Forms of Least Wave Resistance," Proc. 4th Internat. Congr. Appl. Mech. Cambridge (1934)

9. Dorr, J., "Zwei Integralgleichungen erster art, die sich mit Hilfe Mathieuscher Funktionen Losen lassen," Z.A.M.P. 3 (1952)

10. Bessho, M., "On the Minimum Wave Resistance of Ships with Infinite Draft," International Seminar on Theoretical Wave Resistance, University of Michigan (1963)

11. Kotik, J., "Some Aspects of the Problem of Minimum Wave-Resistance," International Seminar on Theoretical Wave Resistance, University of Michigan (1963)

12. Lin, W. C., Webster, W. C , and Wehausen, J. V., "Ships of Minimum Total Resistance," International Seminar on Theoretical Wave Resistance, University of Michigan (1963)

13. Maruo, H., "Calculation of the Wave Resistance of Ships, the Draught of Which is as Small as the Beam," Journal of Zosen Kiokai, 112 (1962)

14. Weinblum, G., Wustrau, D., and Vossers, G., "Schiffe geringsten Widerstandes," J.S.T.G. 51 (1957)

15. Inui, T., "Wave-Making Resistance of Ships," Trans. SNAME, 70 (1962)

16. Yim, B., "On Ships with Zero and Small Wave Resistance," Internat. Seminar on Theoretical Wave Resistance, University of Michigan (1963)

17. Lewis, E. V. and Breslin, J. P., "Semi-Submerged Ships for High Speed Operation in Rough Seas," 3rd Symposium on Naval Hydrodynamics, Scheveningen, September 1960

* * *

EXPERIMENT DATA FOR TWO SHIPS OF "MINIMUM" RESISTANCE

Wen-Chin Lin, J. Randolph Paulling
and J. V. Wehausen
University of California
Berkely, California

ABSTRACT

This report presents the results of towing-tank tests carried out on two of the models of minimum "total" resistance described in an earlier report by Lin, Webster and Wehausen (1963). One model was symmetric fore and aft, the other asymmetric with a prescribed afterbody. Each was supposed to be optimum within its class for a Froude number 0.316 and a Reynolds number 1.18×10^9. Although the forms showed resistance qualities near the design speed as good as the equivalent forms for Taylor's Standard Series, they were not significantly better. The occurrence of separation behind the stern bulb of the symmetric model may have masked possible superior wave-making qualities as indicated by a rather small surface disturbance.

INTRODUCTION

In a paper presented at the International Symposium on Theoretical Wave Resistance in Ann Arbor in 1963 (Lin, Webster and Wehausen, 1964)* two different minimization problems for ship resistance were considered. In each problem an estimated "total" resistance consisting of the equivalent flat-plate frictional resistance plus the wave resistance as given by Michell's integral was minimized for selected values of the Froude number. In one of the problems, only the volumetric coefficient $C_V = V/L^3$ and the ratio H/L were fixed. The resulting optimum hull-form was necessarily symmetric about the midship section. In the other problem, H/L and a particular afterbody were prescribed, and an optimum forebody was found. In each case the class of hull shapes within which an optimum was sought was limited to a 6×6 double Fourier series:

$$f(x, z) = \sum_{m=1}^{6} \sum_{p=1}^{6} a_{mp} \cos \frac{1}{2} (2m-1) \pi x \cos \frac{1}{2} (2p-1) \pi z.$$

*References are identified by author(s) and date and collected at the end.

Here the variables have been made dimensionless by measuring distances in the x, y, z directions by $\frac{1}{2}L$, $\frac{1}{2}B_o$ and H, respectively, where B_o is not the true beam but is fixed at $3H$ for this purpose.

The optimum forms which were obtained for the symmetric ship for values of the parameter $\gamma_o = gL/2v^2$ varying from 5 to 10 were reasonably shiplike in appearance except for some waviness in the lines and two small areas at the waterline near the bow and stern where the ordinates became slightly negative. The waviness seems almost certainly to be a result of the limited number of trigonometric functions used to describe the hull. The amount of negativeness was so small that these regions could be deformed to zero without significantly altering the lines. The wave resistance at design speed for each of these forms, as predicted by Michell's integral, was very small compared with the frictional resistance, in fact, negligible for the forms corresponding to γ_o = 6 to 10. Figure 1 shows the wave-resistance coefficient $R_M/\rho g V$ for each of these optimum forms as predicted by Michell's integral for Froude numbers between 0.18 and 0.50.

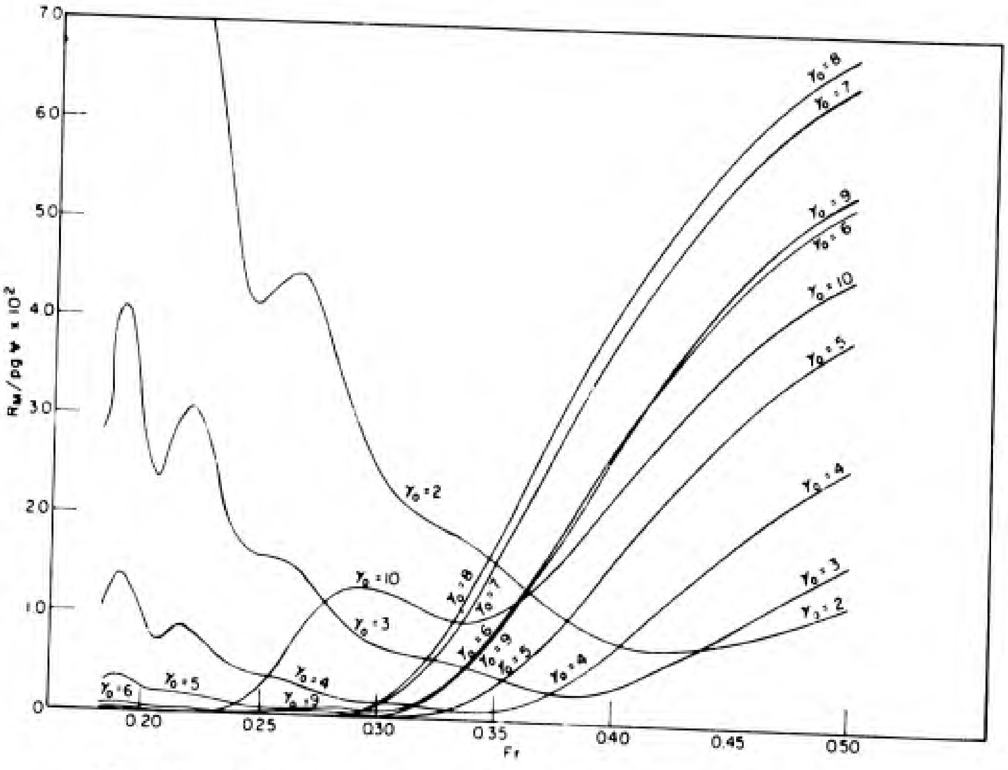

Fig. 1a - Michell resistance for optimum symmetric forms

The results obtained in the problem with the fixed afterbody were not as satisfactory as those described above. With the exception of the forebody obtained for γ_o = 5 (Fr = 0.316) the forebodies were generally unacceptable as ships. Partly this was a result of the occurrence of negative offsets of substantially

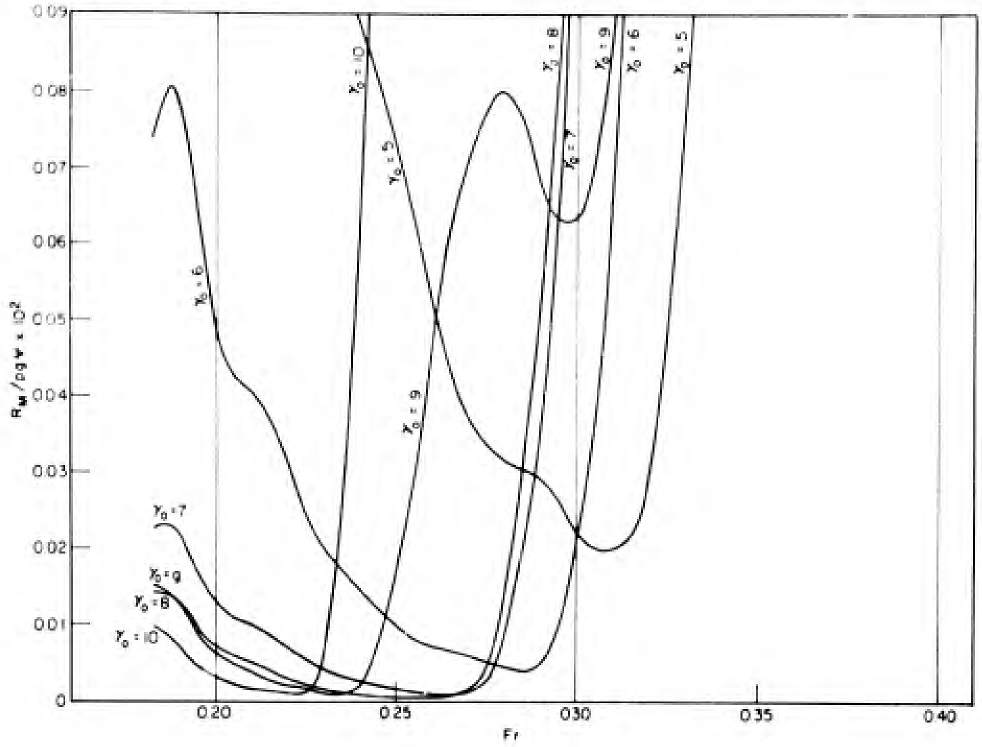

Fig. 1b - Michell resistance for optimum symmetric forms

larger amount than for the symmetric bodies, partly it was the result of excessive waviness in the waterlines. In the present context the latter was objectionable not because of the practical difficulty of fabricating such shapes but because of the great liklihood of boundary-layer separation behind the bellies. As was stated in the cited paper, imposition of restraints like $0 \le f(x,z) \le M$, $-C \le f_x(x,g) \le D$, which would have prevented the excessive waviness, presents a much more difficult problem in computation. The wave resistance for these forms, again as predicted by Michell's integral, is no longer negligible compared with the frictional resistance for comparable forms. For example, at the design speed the coefficient $R_M/\rho g V$ for the form corresponding to $\gamma_0 = 5$ is approximately half the coefficient $R_r/\rho g V$ for the equivalent ship from Taylor's Standard Series, and about one third the frictional resistance coefficient $R_f/\rho g V$.

Following the obtaining of these results, several courses of action seemed open: there were mathematical questions to be resolved; the effect of increasing the number of Fourier components upon the waviness of the waterlines could be studied; a feasible method of incorporating inequalities among the constraints could be devised. However, more important than any of these seemed having some experimental evidence that the optimum forms derived from theory did, in fact, have good resistance characteristics. The main purpose of this paper is to report the results of testing two of the forms.

Some preliminary comments with regard to possible expectations seem in order. As noted above, for the symmetric forms the Michell wave resistance at, and for some interval below, the design speed is generally negligibly small compared with the frictional resistance. If the "real" wave resistance does in some sense approximate this, any attempt to observe it experimentally will be plagued by the uncertainty in estimation of the "viscous part" of the total resistance. In particular, a region of boundary-layer separation or even an excessive form drag may have the effect of masking completely the quantity being measured. In addition, one must bear in mind that Michell's integral is based upon linearization of the boundary conditions and represents the first term in a perturbation series in B/L. However, the fact that this first term is very small for a particular form does not imply that the second-order term is also very small for this form. Under such circumstances it may, in fact, be considerably larger, although still of second order. Consequently, there may exist an appreciable wave drag in an inviscid fluid even though the linearized theory predicts practically none.

CHOICE AND CONSTRUCTION OF MODELS

One hull form was selected from each of the two series. For each, the form optimum for $\gamma_0 = 5$ (Fr = 0.316) was selected. As has been mentioned above, the choice $\gamma_0 = 5$ for the hull with prescribed afterbody was hardly a free one. For the symmetric ship this form was chosen because 0.316 was the largest Froude number for which the corresponding optimum ship had waterlines of small enough slope so that boundary-layer separation did not seem likely to occur and thus render invalid the fundamental assumptions underlying the computation. Figure 2 shows the section curves, waterlines and area curve for the optimum symmetric ship for $\gamma_0 = 5$. Figure 3 shows the prescribed afterbody, both as designed and as represented by the Fourier series. Figure 4 shows the optimum forebody for $\gamma_0 = 5$.

The models as actually constructed differed slightly from those designed by the computer. For the symmetric model the lines in the neighborhood of the regions of negative ordinates were modified slightly so that the ordinates were zero in these regions. In effect, this created a submerged protruding bulb, as in some of Inui's optimum forms, but not as deeply submerged. The optimum forebody as shown in Fig. 4 has rather noticeable wiggles in the midship section and in the section just ahead of it, a result of trying to fit a U-shaped section with only six terms of a Fourier series. In this case the afterbody was built as originally designed and not as approximated, and the forebody was modified slightly near the midsection to make it join smoothly to the afterbody. Figure 5 shows photographs of each model.

CRITERIA AND STANDARDS OF COMPARISON

One way to judge the performance of a proposed hull form is to compare it with others of acknowledgedly good performance. Of the usual measures of performance the dimensionless ratio $R_t/\rho g V$ at and near the design Froude and Reynolds numbers seems most appropriate and has been used in this paper. The

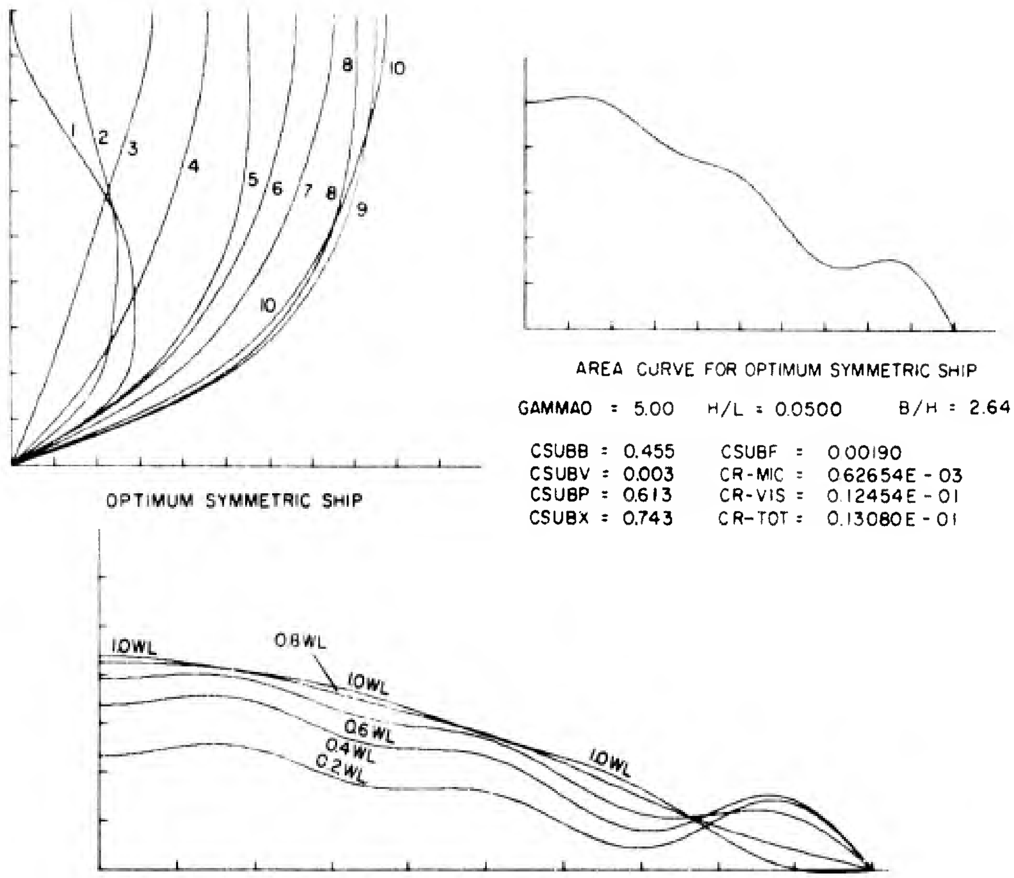

Figure 2

coefficient $R_t / \frac{1}{2} S v^2$, although convenient for working up model data, has several obvious disadvantages as a figure of merit for comparing different hull shapes.

Of the available standards of comparison, the two which have been used here are Taylor's Standard Series and Series 60. The "equivalent" hull in each case has been taken as the one with the same prismatic and volumetric coefficients and the same ratio B/H. Other geometric parameters such as H/L and the block coefficient cannot be kept constant in this comparison. Furthermore, an equivalent hull for the ship with prescribed afterbody did not seem to be available in Series 60. Table 1 below gives various geometric parameters for the two optimum hulls and the equivalent ones. The sources of data for Taylor's Standard Series have been Gertler (1954) and for Series 60 have been Todd (1963).

There is a second method by which a comparison can be made with Taylor's Standard Series. One can try to carry out within the series the same minimization problem as was formulated for the symmetric ships, i.e., with $C_v = 0.003$ and $L/H = 20$ fixed, one can look for a Taylor-Standard-Series hull which

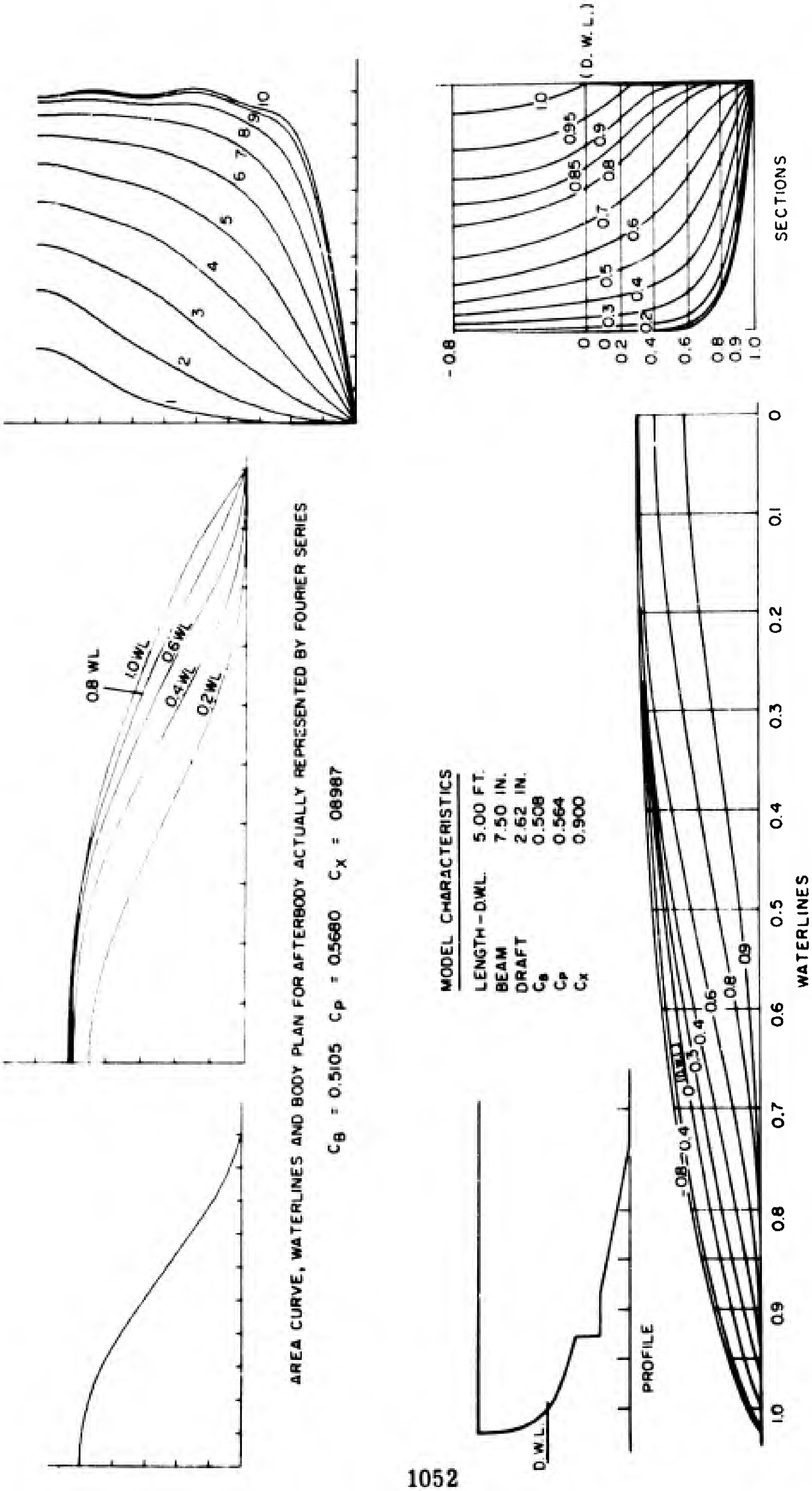
AREA CURVE, WATERLINES AND BODY PLAN FOR AFTERBODY ACTUALLY REPRESENTED BY FOURIER SERIES
C_B = 0.5105 C_P = 0.5680 C_X = 0.8987
0.8 WL
1.0 WL
0.6 WL
0.4 WL
0.2 WL
MODEL CHARACTERISTICS
LENGTH - D.W.L. 5.00 FT.
BEAM 7.50 IN.
DRAFT 2.62 IN.
C_B 0.508
C_P 0.564
C_X 0.900
PROFILE
D.W.L.
WATERLINES
SECTIONS
(D. W. L.)

Figure 3

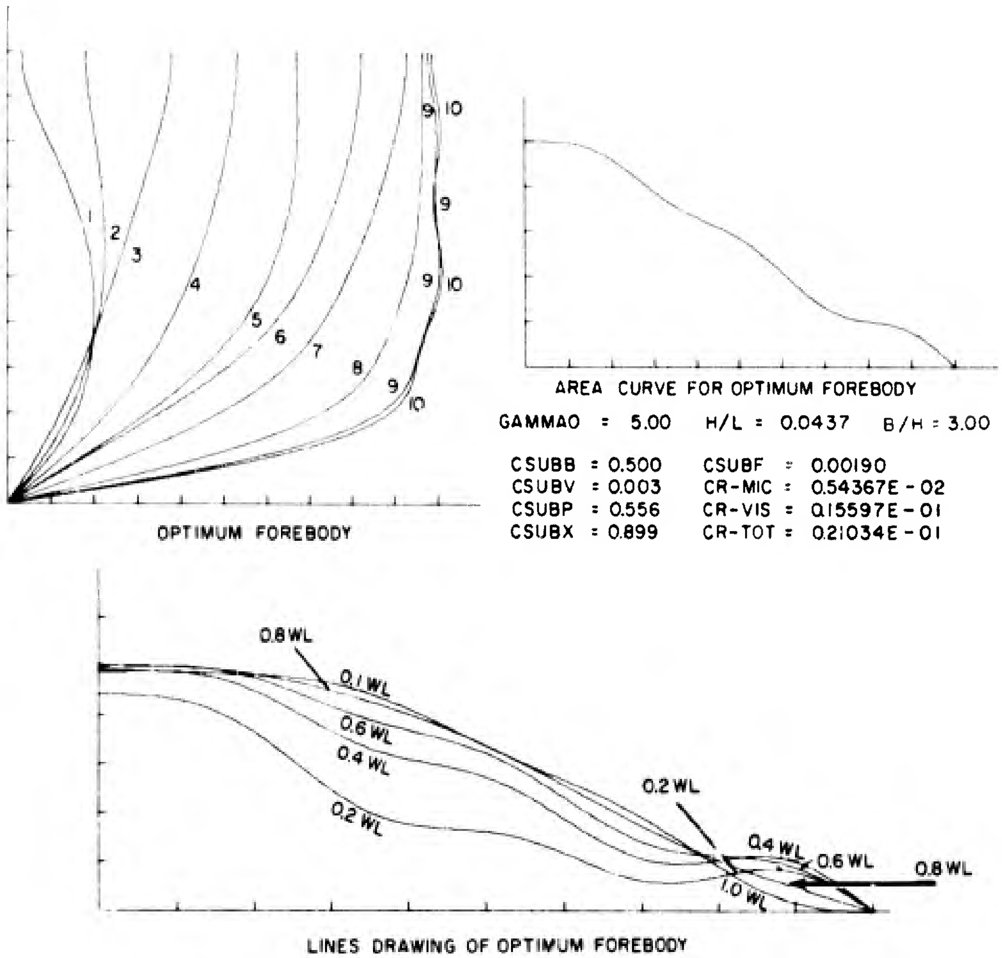

Figure 4

Table 1
Geometric Parameters

	Opt. Symm. Ship	Taylor's St. Series	Series 60	Opt.-Forebody Ship	Taylor's St. Series
B/H	2.64	2.64	2.64	3.00	3.00
L/H	20.0	20.0	23.0	22.9	20.7
C_V	3.00×10^{-3}	3.00×10^{-3}	3.00×10^{-3}	2.87×10^{-3}	2.87×10^{-3}
C_P	.613	.613	.614	.556	.556
C_B	.455	.567	.60	.500	.515

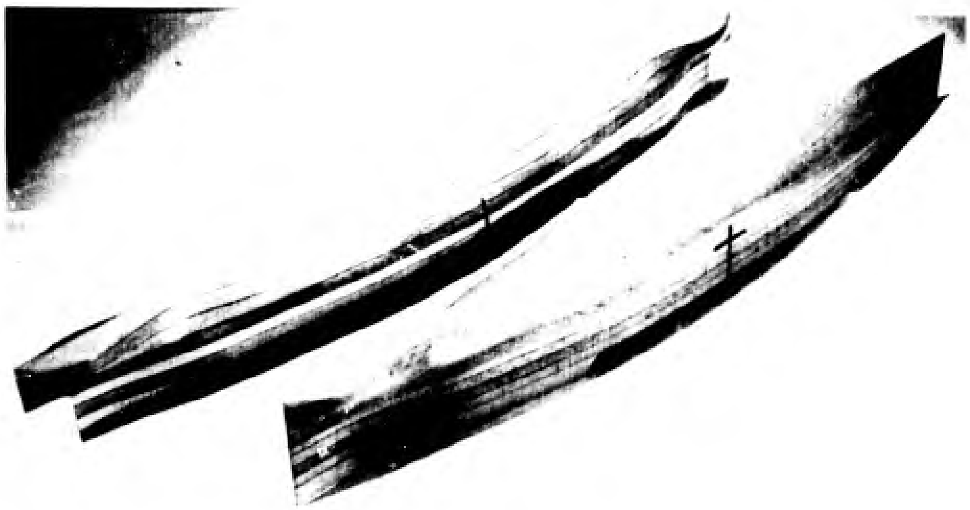

Fig. 5 - Photograph of the two models tested

minimizes $R_t/\rho g \nabla$ for the design Froude and Reynolds numbers. The various steps required are incorporated in Table 2 and are explained below. The successive lines in the table are obtained as follows. Fixing L/H fixes L/B for each of the three available values of B/H. Then C_p is fixed by the given value of C_V [see Gertler (1954), pp. 10-12]. Since there is no hull form with $B/H = 3.75$, $L/H = 20$, $C_V = 0.003$, this column now drops out. The associated values of $C_s = SL^{-2}C_V^{-1/3}$ and of $C_r = R_r/\frac{1}{2}\rho Sv^2$ are read directly from Gertler [1954]. The value of $C_f = R_f/\frac{1}{2}\rho Sv^2$ is the Schoenherr coefficient for $Re = 1.182 \cdot 10^9$, corresponding to a 400' ship in salt water at 63°F. with a ship's speed corresponding to $\gamma_0 = 5$. Then $C_t = C_r + C_f$ and

$$\frac{R_t}{\rho g \nabla} = \frac{1}{2} C_t Fr^2 C_s C_V^{-1/3} = \frac{1}{4} C_t \gamma_0^{-1} C_s C_V^{-1/3} .$$

The hull with $B/H = 3$ and $C_p = 0.536$ is evidently the best within Taylor's Standard Series which meets the constraints $L/H = 20$ and $C_V = 0.003$. Although this is not an "equivalent" hull, it does seem to be also a legitimate one to use in a comparison with the optimum symmetric ship for $\gamma_0 = 5$.

TEST PROCEDURE

The models were each tested in the Ship Towing Tank of the University of California. The models were attached to the dynamometer so that they were free to both heave and trim. Figure 6 shows the symmetric model being towed at a Froude number of 0.316.

Each model was tested both with and without a tripwire. In the region for which data are presented there was a small constant difference in the resistance coefficients $R_t/\frac{1}{2}\rho Sv^2$ with and without the tripwire. This was taken as evidence

Table 2
Optimization Within Taylor's Standard Series

B/H	2.25	3.00	3.75
L/H	8.89	6.67	5.34
C_P	0.580	0.536	--
C_S	2.557	2.524	
C_r	1.24×10^{-3}	1.03×10^{-3}	
C_f	1.90×10^{-3}	1.90×10^{-3}	
C_t	3.14×10^{-3}	2.93×10^{-3}	
$R_t/\rho g \nabla$	0.734×10^{-2}	0.676×10^{-2}	

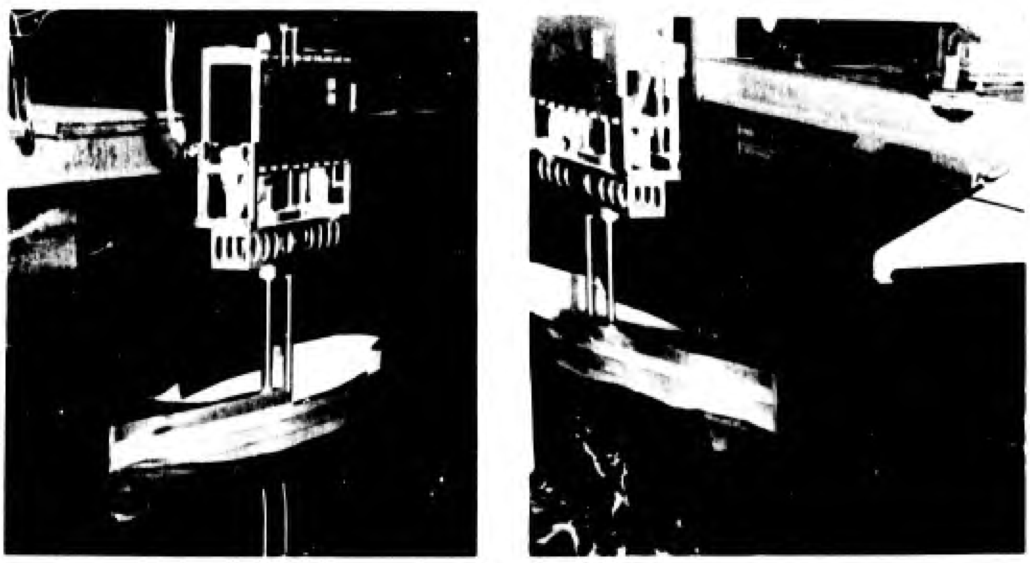

Fig. 6 - Symmetric model being tested at FR = 0.316

that the region of laminar flow was confined to the region ahead of the tripwire. The data were appropriately corrected for the added resistance of the tripwire where necessary.

In order to test for separation of the flow behind the bow and stern bulbs of the symmetric model, thread tufts were attached to the model and observed visually. There was no evidence of separation behind the bow bulb. However, behind the stern bulb there appeared to be separation at all speeds tested. This will, of course, cause an added resistance associated with viscosity which is not taken into account in the expression used for $R_f/\rho g V$. Furthermore, it contravenes to some extent the fundamental assumption of streamline flow upon which Michell's integral is based.

TEST RESULTS

Figure 7 shows $R_t/\rho g V$ for the symmetric model extrapolated to a 400' ship by using Schoenherr's friction coefficients and a roughness allowance 0.0004. On the same figure is shown the same resistance coefficient for the equivalent ships in Taylor's Standard Series and Series 60 and for the "optimum" ship in Taylor's Standard Series, as explained earlier. The results speak for themselves. The optimum symmetric ship is slightly but insignificantly better than either of the "equivalent" ships near the design speed but is not as good as the optimum Taylor's-Series ship.

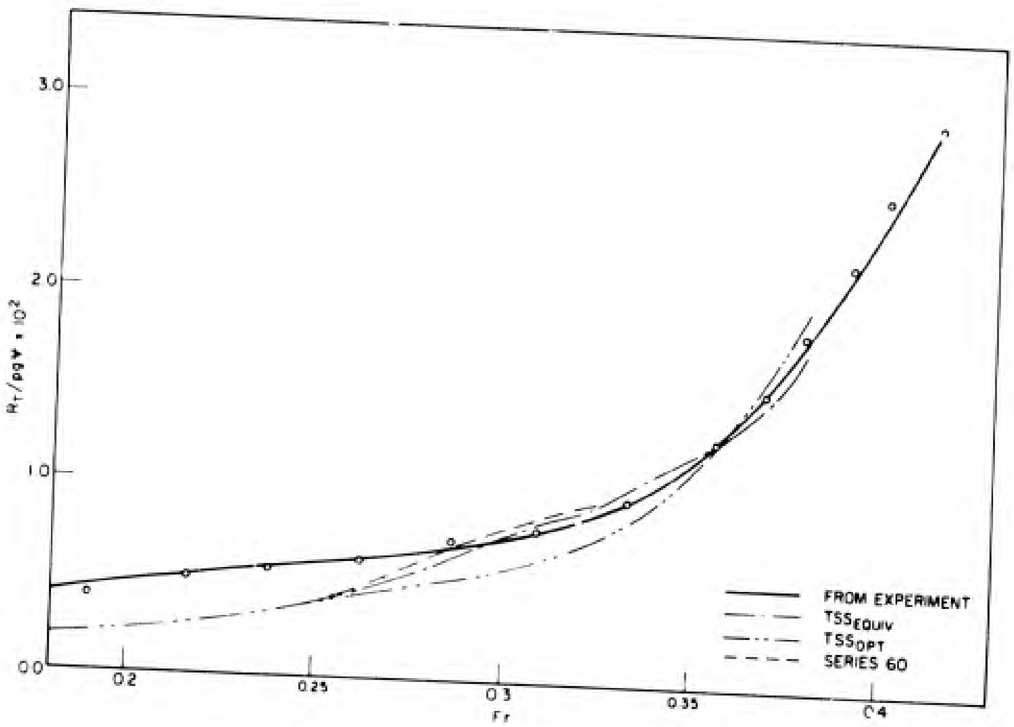

Fig. 7 - Total resistance coefficients for symmetric model and equivalent models

Figure 8 shows the residary-resistance coefficient $R_r/\rho g V$ for the symmetric ship and the equivalent Taylor's-Series ship, and also the Michell wave resistance $R_M/\rho g V$. It is evident that the residuary resistance of the model is much greater than its Michell wave resistance in the neighborhood of the design speed, but that the two become more nearly equal both below and above this speed. On

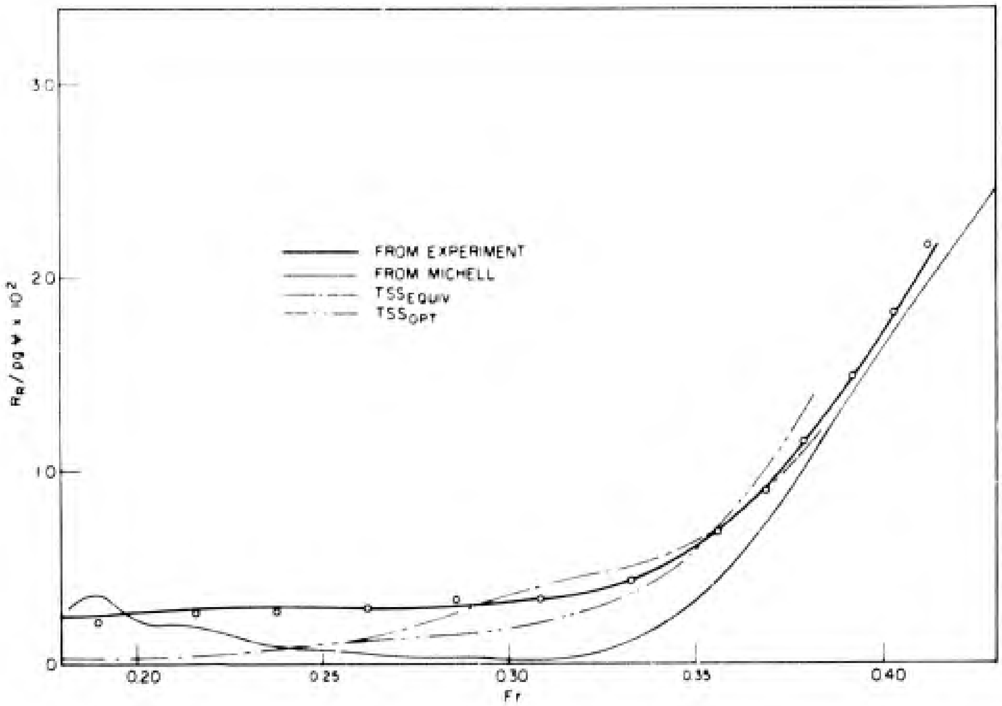

Fig. 8 - Residuary and Michell resistances for symmetric model. Residuary resistance for equivalent models.

the other hand, observation of the water surface during test runs near design speed shows remarkably little surface disturbance. This leads one to suspect that the residuary-resistance coefficient in this region may contain a significant amount of form resistance, a suspicion partly confirmed by the observed separation behind the stern bulb.

Figure 9 shows $R_t/\rho g\nabla$ for the optimum-forebody model, and for the equivalent Taylor's-Series ship, both extrapolated to a 400' ship. Over the range from $Fr = 0.25$ to 0.35 the two are practically indistinguishable.

Figure 10 shows the residuary resistance $R_r/\rho g\nabla$ for this model together with the Michell wave resistance $R_M/\rho g\nabla$. It is evident that the agreement is much better here than it was for the symmetric ship.

SOME CONCLUSIONS

As is evident from the foregoing, the "optimum" computer-designed ships have not shown any dramatic improvements in resistance properties over the equivalent ones in Taylor's Standard Series. In fact, they are hardly distinguishable. For the ship with prescribed afterbody this should cause no surprise, for the predicted improvement was a fairly modest part of the whole. The situation is somewhat different with the symmetric ship. Here the predicted

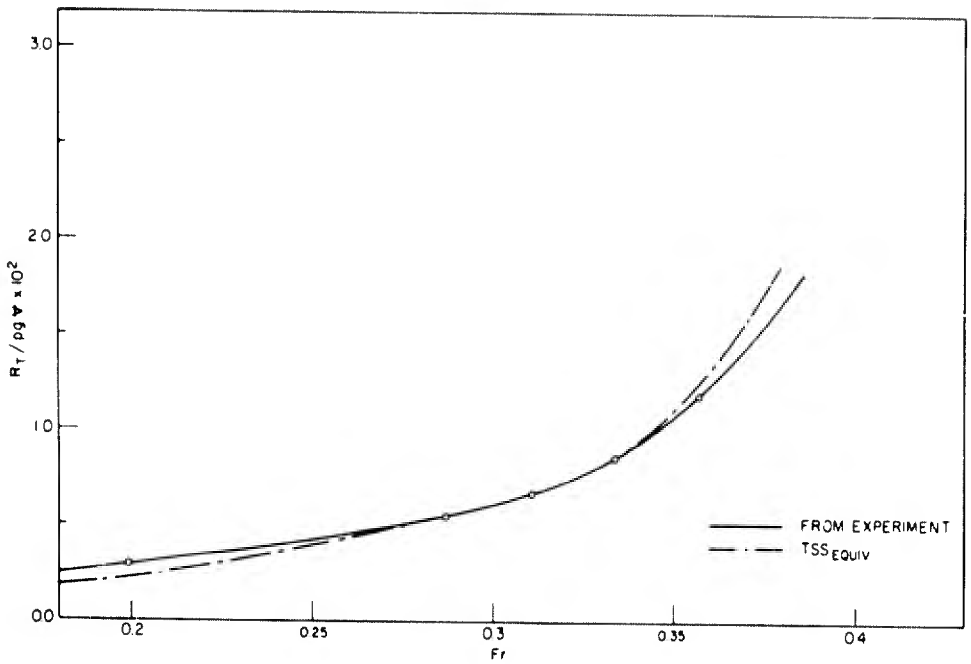

Fig. 9 - Total resistance coefficient for optimum-forebody model and for equivalent model

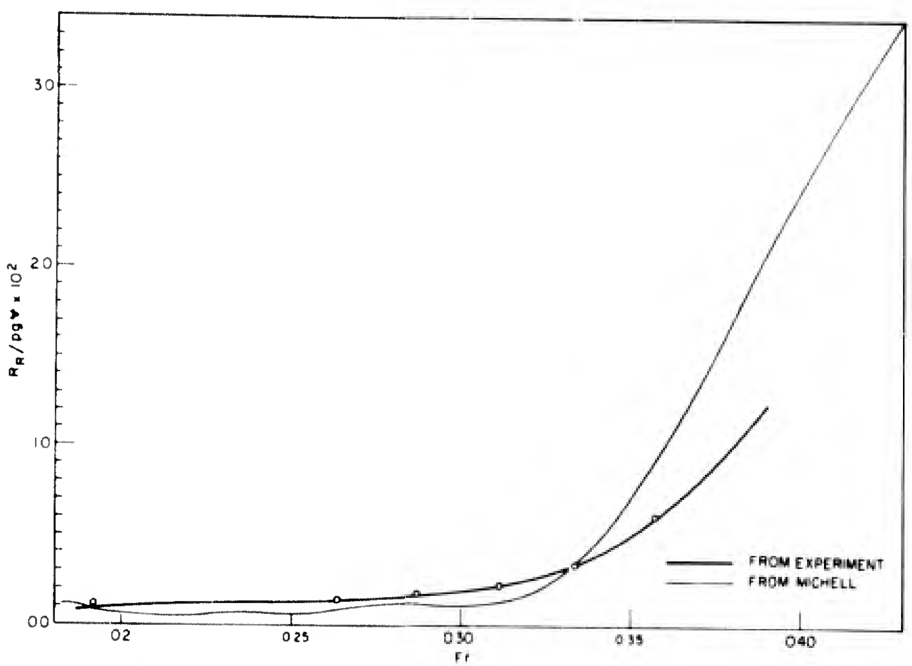

Fig. 10 - Residuary and Michell resistance for optimum-forebody ship

improvement was substantial and has not been realized. Unfortunately, for the present purpose, the reasons are not clear-cut and one cannot ascribe the failure entirely to unreliability of the linearized theory in a situation where it predicts unusually small values of the wave resistance. As has already been mentioned, there was, in fact, remarkably little disturbance of the free surface at and near the design Froude number, so that a small value of the residuary resistance might have been expected. It seems possible that the contribution of the observed boundary-layer separation behind the stern bulb to the residuary resistance may have increased this so much that the favorable wave-resistance properties of the hull were lost. With the wisdom of hindsight it seems evident that for our first symmetric model we should have chosen the one designed to be optimum for $\gamma_0 = 6$ ($Fr = 0.289$) or $\gamma_0 = 9$ ($Fr = 0.236$) instead of $\gamma_0 = 5$. Their Michell wave resistances are negligible in the Froude number range 0.2 to 0.3 (see Fig. 1) and their maximum waterline slopes at the stern are smaller, about 16° and 11°, respectively.

Even though the two computer-designed ships have not shown any marked superiority in resistance qualities, there is another sense in which the attempt to let certain over-all requirements and the optimization procedure design the ship can be said to have been successful. All forms have been designed without aid of the naval architect's practiced and expert eye and yet the two tested ones have performed as well as the equivalent Taylor's-Series hulls. This in itself is encouraging and seems to indicate that it is worth the trouble to refine the method, in particular, to devise computational procedures for taking into account more complicated kinds of restraints.

SYMBOLS

R_t	Total resistance
R_f	Frictional resistance
R_r	Residuary resistance
R_M	Wave resistance according to Michell
C_P	Prismatic coefficient
C_B	Block coefficient
$C_\forall$	Volumetric coefficient $= \forall/L^3$
C_s	Area coefficient $= SL^{-2}C_\forall^{-1/3}$
C_t	$R_t/(\frac{1}{2}\rho Sv^2)$
C_r	$R_r/(\frac{1}{2}\rho Sv^2)$
C_f	$R_f/(\frac{1}{2}\rho Sv^2)$

REFERENCES

1. Lin, Wen-Chin; Webster, W. C.; Wehausen, J. V. - Ships of minimum total resistance. Proceedings, International Symposium on Theoretical Wave Resistance, Ann Arbor, 1963.

2. Gerter, Morton - A reanalysis of the original test data for the Taylor Standard Series. David Taylor Model Basin Report 806 (1954).

3. Todd, F. H. - Series 60. Methodical experiments with models of single-screw merchant ships. David Taylor Model Basin Report 1712 (1963).

* * *

DISCUSSION

P. C. Pien
David Taylor Model Basin
Washington, D. C.

This paper gives us the theoretical and experimental results of two minimum resistance models. It is quite clear as to how these results have been obtained. However, it is not easy to digest these results.

Why the theoretically predicted low resistance has not been obtained experimentally? Why are the relative resistance qualities of these two models just opposite to the theoretical predictions? In explaining the results of the symmetrical model the authors suggested the possibility of the second term in the perturbation series being greater than the first term. If it is so then this second term would also be much larger than the first term of the asymmetrical model since the experimental results show that the symmetrical model has much greater resistance than the asymmetrical model. This is not likely to be the true situation.

Based on Professor Inui's important research work, we know the linearized ship-surface condition is not accurate for the beam value used in the paper. Therefore the theoretical model of singularity distribution used in the wave-making resistance computation is not in correspondence with the physical model used in the experiment. In such situations, we should not be surprised to see that the agreement between the theoretical and experimental resistance values is not good.

Based on the experience of Professor Inui as well as our own, I believe a much better agreement between theoretical and experimental wavemaking resistance results can be obtained, especially for the symmetrical case where the free-surface disturbance is small and the Froude number is not too low, if a higher order approximation is applied on the ship-surface. It would be interesting to see the experimental results of a new model which is more exactly corresponding to the theoretical model used in the wavemaking resistance computation. Even though it means additional work it is a rather essential step. I would like to know the authors' views on doing this additional experiment.

* * *

DISCUSSION

Lawrence W. Ward
Webb Institute of Naval Architecture
Glen Cove, Long Island, New York

This is a very interesting paper following the Ann Arbor paper and significant in including model tests of the forms. I would like to quote a sentence from the paper and then make a comment on it. In the last part of the "Abstract" we read:

> The occurrence of separation behind the stern bulb of the symmetric model may have masked possible superior wavemaking qualities as indicated by a rather small surface disturbance.

Thus, the authors clearly recognize that the residual resistance is not a good measurement of wave resistance in that it is not based on the waves in a direct way. I suggest at the least one should take a qualitative look at the wave pattern as is done by Inui, using stereo-camera pairs. Better yet, one should make quantitative measurements by means of a wave survey according to methods such as the ones which have been proposed by Dr. Eggers at Hamburg, Hogben and Gadd at NPL, or myself. Such methods are not as difficult to use as some might think, and while subject to certain approximations they should form a much more accurate means of obtaining the wave resistance in cases such as those in this paper.

* * *

DISCUSSION

G. P. Weinblum
Institut für Schiffbau der Universität
Hamburg, Germany

The discusser has tried to popularize the application of polynomials for the determination of hull forms of low wave resistance. There were two reasons for this preference: the theorem of Weyerstrass from a mathematical point of view and the attempt of using the wisdom of art embodied by "spline curves." The "ugly" wiggled forms obtained by the authors justify my dislike of trigonometrical series as long as a relatively small number of terms is admitted. Exact solutions (Karp, Maruo, Kotik, etc.) indicate that the wiggles are not significant results but an outcome of the use of the functions mentioned. In the meanwhile it follows from a kind information by Prof. Wehausen that the wiggles are smoothed out when a larger number of terms dependent upon x is used.

Notwithstanding the offense against beauty committed by the authors the theoretical investigation has furnished valuable information on the

(a) low magnitude of resistance up to relatively high F when a large number of terms is used,

(b) influence of vertical displacement distribution on resistance, and

(c) dependence of resistance upon number of form parameters.

In agreement with my experience when testing forms of extremely low wave resistance (by calculation) the authors are disappointed by their experimental results. The high resistance measured may be due (a) principally to the fact that viscosity destroys the calculated favorable interference effects. This applies even to fine streamlined forms in the afterbody (compare our tests with a model $C_p = \varphi = 0.52$, communicated at Ann Arbor Proceedings 1963, (b) to separation and excessive viscous form drag due to the stern bulb. The author's decision to test a more normal form is commended, further, forms with bow bulb alone could be tested. But in the light of our earlier experiments (Schiffbau (1936) point (a) may be more decisive than (b)), (c) the authors point out at the possibility that second order terms in the resistance integral may become important when developing optimum forms based on first order theory. This is a new idea which may be checked by evaluating a second approximation using Sisov's formula. Such work is going on under the guidance of Dr. Eggers at the Institut für Schiffbau, University Hamburg.

* * *

REPLY TO THE DISCUSSION

Wen-Chin Lin, J. Randolph Paulling
and J. V. Wehausen
University of California
Berkeley, California

First of all we should like to state that we are pleased that Dr. Pien has found it quite clear how our results were obtained, even though their significance may remain cloudy. It seemed particularly important for these tests that this should be the case and that there be no question of finagling with data in order to "improve" it.

The authors cannot agree with Dr. Pien's statement that the "relative resistance qualities are just opposite to the theoretical predictions." For both models the residuary resistance is greater than the Michell resistance at the design Froude number 0.316. This is, in fact the usual occurrence at this Froude number for hulls with these prismatics. The only thing which really seems out of the ordinary is the very low ratio of Michell to residuary resistance for the symmetric model, but here there are no similar experiments to compare with. However, it is because of the extremely low Michell resistance in this case that we called attention to the necessity of considering the possibility that the second-order term overpowers the first-order term. This necessity does not seem so pressing for the asymmetrical model. An accurate assessment of the effect of viscosity is also correspondingly more important for the symmetric model.

Although Dr. Pien might appear to have deprecated the importance of the second-order approximation, he is, in fact, also proposing that we take it into account. He states, "... we know the linearized ship-surface condition is not accurate for the beam value ...." Indeed, we know much more, for we know that the linearized approximation is not accurate for either the hull shape or the wave surface. In a paper by one of the authors presented at the Ann Arbor Symposium in 1963 it was shown that the more important error is associated with this phenomenon in a related situation. Dr. Pien's argument that, in cases where the first-order resistance is very low, it is legitimate to use the linearized free-surface condition together with the exact body boundary condition is tempting, but assumes that low wave resistance is associated with small surface disturbance everywhere. However, it is still possible that the local disturbance is substantial and it is just in this locality where the inaccuracy is most important.

With regard to further experiments, it is our own opinion that the influence of viscosity should be clarified before any attempts to improve the approximation are made, and, in particular, that one should have a more reliable experimental determination of the wave resistance. This also appears to be the import of Prof. Ward's remarks. It is a pleasure to add that he has later volunteered to undertake an investigation of the wave resistance of the symmetric model according to his method.

Prof. Winblum states that he has preferred polynomial representations for hulls partly on mathematical grounds because of Weierstrass's Theorem. We hope he will take it as good-natured malice if we point out that there are two Weierstrass approximation theorems. One states the uniform approximability of continuous functions on closed intervals by polynomials, the other by trigonometric sums. Thus there is no mathematical reason for preferring polynomials. The advantage of the trigonometric sums lies in the orthogonality of the expansion functions, which results in smaller coefficients for higher harmonics. The same can, of course, be achieved with Legendre or Chebyshev polynomials (Prof. Maruo worked out the details for the latter during a visit to Berkeley), but now the numerical computation becomes somewhat more complicated.

With regard to the unaesthetic aspect of our wavy forms we are pleased to report the following. Since the forms from which the tested models were made were computed, we have extended the computations from $M \times P = 6 \times 6$ to $M \times P = 10 \times 4$, 12×4 and 15×4 for the symmetric model. The numerical evidence suggests that the 15×4 form is already quite close to the limit with $P = 4$. The improvement in resistance is negligible. However, there is a quite noticeable change in form as one proceeds from 6×4 to 15×4, and, although the latter form is no longer wavy, it does not "smooth" the wavy lines of a 6×4 form, and it would have been misleading, if not even somewhat dishonest, to have drawn smooth curves through the wavy ones on this basis. It may be of interest to note the following. In going from 6×4 to 10×4 the beam decreases, the middle sections become more U-shaped and the ends much bulbier. In going from 10×4 to 15×4 the middle sections remain practically the same, but the bulbiness continues to increase, although the difference between 12×4 and 15×4 is slight. If one keeps M fixed at 10 and lets P be successively 2, 3, and 4, the section-area curve hardly changes, the sections near the ends change little, but the middle sections become more U-shaped.

The authors thank the discussers for their interest in and comments on their paper.

SOME RECENT DEVELOPMENTS IN THEORY OF BULBOUS SHIPS

B. Yim
Hydronautics, Incorporated
Laurel, Maryland

INTRODUCTION

The history of the bulbous bow on ships may start in the early 19th century with submerged rams on combatant vessels projecting forward along the waterline at the stem, or with the projecting underwater hulls of many old French warships built about the same time. Later, the British armored cruiser Leviathan had such a projecting ram bow. D. W. Taylor suspected that this ram bow played a definite part in the ships superior performance, and he based the parent model for his famous Standard Series (D. W. Taylor 1911 or 1943) upon the lines of Leviathan. Systematic bulb bow experiments were made by E. F. Eggert in the early 1920's and the general data were reported upon by D. W. Taylor (1923). It had been generally understood that the decrease of resistance due to a bulbous bow is a wavemaking phenomenon, such as a decrease in bow wave height due to a bulb wave. This understanding was more strongly supported when Havelock (1928) calculated the surface wave due to a doublet immersed in a uniform stream. A deeply submerged sphere is equivalent to a doublet. Hence according to his calculation, a sphere moving through water at a constant speed causes the surface wave to start with the trough just aft of the sphere. It is natural to imagine that this trough has something to do with the bow wave crest which is seen to start just aft of the bow in ordinary ships. However there was also some other suspicion that the bulb effect is due to a change in the effective ship length owing to the alteration by the bulb of the position of the bow wave. This suspicion was removed by Wigley's mathematical and experimental investigation (1936). He used Havelock's formula for wave resistance (1934) in terms of the regular wave heights due to the ship hull and a point doublet. He separated the wave resistance into three parts: the hull wave resistance, the bulb wave resistance and the interference resistance of the hull and bulb. The most favorable case occurred when the negative interference resistance was largest. He derived the following six rules for the bulbous bow as the conclusion of his investigation (W. C. S. Wigley, 1936):

"(1) The useful speed range of a bulb is generally from $V/\sqrt{L} = 0.8$ to $V/\sqrt{L} = 1.9$ (or in Froude numbers based on ship length, from 0.238 to 0.563), V being the speed in knots and L the ship's length in feet.

(2) The worse the wavemaking of the hull itself is, the more gain may be expected with the bulb and vice versa.

(3) Unless the lines are extremely hollow the best position of the bulb is with its center at the bow, that is, with its nose projecting forward of the hull.

(4) The bulb should extend as low as possible consonant with fai: ness in the lines of the hull.

(5) The bulb should be as short longitudinally and as wide laterally as possible, again having regard to the fairness of the lines.

(6) The top of the bulb should not approach too nearly to the water surface; as a working rule it is suggested that the immersion of the highest part of the bulb should not be less than its own total thickness."

G. Weinblum (1935) dealt with this same problem by expressing the form of a ship with a bulbous bow in terms of a polynomial according to Michell's thin ship approximation. His theory was also supplemented by model experiments. He expressed a different view from Wigley's, concerning the best vertical position of a bulb (Wigley's rule [4] and [6]). According to Weinblum's result for an extremely hollow form of ship, a uniformly distributed bulb along the stem line was superior (taking into account the wave resistance only without considering other effects like spray) to the bulb located near the keel, both having the same sectional area. However neither Weinblum or Wigley suggested any optimum variation of bulb size with the speed.

Since then, some experimental investigations on bulbous bows were performed by Lindblad (1944) in calm water and by Dillon and Lewis (1955) in smooth water and in waves. However, after Wigley (1936) and Weinblum (1935), no significant theoretical development on bulbous ships seems to have been made, until Takao Inui and his colleagues made a great contribution on this subject. This will be discussed in a later section in some detail.

In this report, first the necessity of a bulb for minimizing wave resistance will be discussed, followed by a brief review on Inui's explanation of the bulb effect. Inui, using the concept of Havelock's elementary surface waves brought us a clear understanding of the mechanism of bulbs and an easy approach to their design.

Yim (1963) found the ideal bulb or the doublet distribution on a semi-infinite vertical stem line which completely cancels the sine regular waves starting from the stem of a given ship. For the cosine waves from the ship bow, a source line or a quadrupole line are considered. The separation of waves and the wave resistance into the components as in the diagram of Fig. 1, simplified the analysis of the bulb effect at the bow or the stern of a ship. The size and the form of the bulb, which are functions of ship shapes and Froude numbers, are supplied extensively. The location of the bulb is of course related to the ship shape and the type of bulb. However, the higher order effect is found to be non-negligible. These are discussed in the next sections.

Throughout this report, inviscid, homogeneous, incompressible, and potential flow around a fixed ship is considered. The origin of the right handed Cartesian coordinate system is located on the bow of the ship and on the mean free

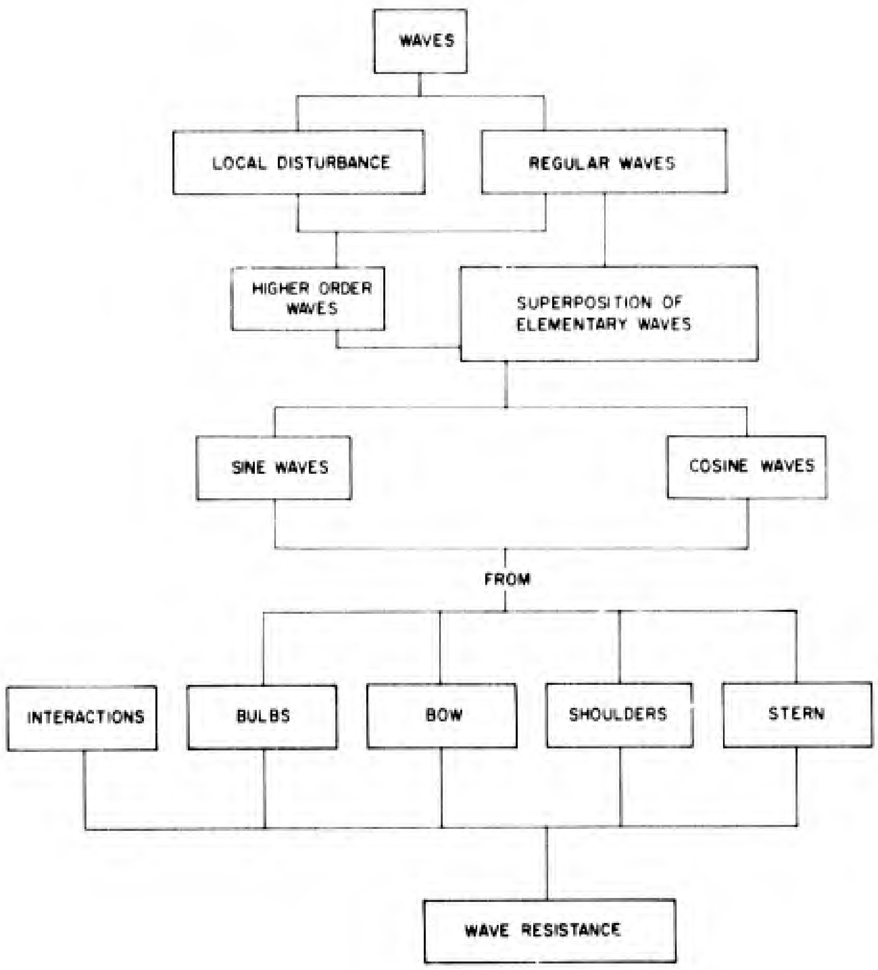

Fig. 1 - Diagram for the characteristics of ship waves

surface. The intersection of the ship's center plane and the mean free surface is taken as the x axis, with the z axis perpendicular to the free surface, positive upward. The flow at $x = -\infty$ is considered to be uniform with the velocity V parallel to the x axis in the positive x direction (see Fig. 2).

SHIPS OF MINIMUM WAVE RESISTANCE AND BULBOUS SHIPS

Since Michell's wave resistance formula (1898) was found, problems of finding the Michell's linearized ship which has the minimum wave resistance have been attacked by many hydrodynamists in various forms and ways. Sretenskii (1935), Pavlenko (1937), Karp, Votik and Lurye (1958) and Maruo and Bessho (1962) treated symmetric infinite vertical struts. Weinblum (1930, 1957), Krein (1955) and Martin (1961) dealt with three-dimensional symmetric ship

Fig. 2 - Schematic diagram for a surface ship and the coordinate system

with a given vertical distribution of volume. In their solution, they all found either some singularities in the functions representing hull shapes at the ends of ships, or bulblike forms around the bows and the sterns. Wehausen, Webster, and Lin (1962) treated the optimum forebodies of ships with a given afterbody as well as three-dimensional symmetric ships without any restriction on the vertical distribution of volume. However they took the ship surface area into account to minimize the wave and friction resistance, and they too found big bulblike forms near the bottom of bows for higher Froude numbers.

Havelock's wave resistance formula (1934) from the regular waves due to the singularity distribution on the center plane of a ship is essentially the same as Michell's, as long as the linear relation of the ship hull form with the singularity distribution

$$m(x, z) \quad \frac{V}{2} \frac{df}{dx}(x, z) \tag{1}$$

is used, where $m(x, z)$ is the source strength and $f(x, z)$ is the ship hull form.

Inui (1957) calculated an exact hull form (body streamlines of a double model) from a given source distribution for zero Froude number (flat free surface), and he used this hull form for his model experiment to test waves and the wave resistance. He compared his experimental results with his calculated wave heights and the wave resistance due to the source distributions. He found that the calculation agrees better with his experiment on his model than the corresponding Michell's model satisfying (1). The way Karp, Lurye, and Kotik (1958) interpreted their result to a ship form of infinite draft is similar to the idea of Inui's which we have just described. The singular behavior of Michell's ship hull can be easily treated by reinterpreting Michell's ship hull as the distribution of various singularities like sources or doublets either distributed or concentrated.

Krein (1955) proved in a rigorous manner the existence of a lower bound for the Michell's resistance of ships with a given center plane, a given velocity, a given displacement, and a given vertical distribution of volume. However he concludes that the lower bound of the wave resistance due to a submerged ship is obtained only with generalized functions (i.e., linear combinations of Dirac delta functions) of a ship hull shape; and for floating bodies the wave resistance achieves a lower bound but only for functions of hull shapes having integrable singularities at the ends of the ship.

In the Michell's ship hull representation (1), it is easy to see that the hull shape $f(x, z)$ is proportional to the doublet strength distributed on a given center plane of the ship. Therefore, if we consider the body streamlines due to the doublet distribution in the uniform stream instead of considering $f(x, z)$ as a hull shape, we may be readily convinced that the ship form of minimum wave resistance has a bulbous bow. In addition, it is worthwhile to note here that, the Dirac delta function of the distributed doublet at the bow is the concentrated line doublet, and the integrable singularity of the doublet distribution at the bow may also be interpreted as a doublet concentrated around the bow.

ELEMENTARY WAVES AND THE WAVE RESISTANCE FORMULA

By Lord Kelvin (1887), it was found that the surface wave due to a point disturbance in a uniform stream consists of two parts: the local disturbance which is limited to the neighborhood of the point disturbance and the regular wave which propagates far aft of the point, mainly restricted to the sector of $|\theta| < 19°30'$. This is a mathematical solution of the equation for the potential ϕ perturbed by the disturbance,

$$\nabla^2 \phi = 0 \tag{2}$$

with linear boundary conditions at the mean free surface $z = 0$, considering the wave height is small compared to the wave length,

$$\frac{\partial^2 \phi}{\partial x^2} + k_o \frac{\partial \phi}{\partial z} = 0 \tag{3}$$

where $k_o = g/V^2$ (g = acceleration of gravity) and at $x \to -\infty$ and $z \to -\infty$,

$$\nabla \phi = 0 . \tag{4}$$

Now it is well known that a point source of strength m located at a point $(x_1, o, -z_1)$, where $z_1 > 0$, produces a regular wave height ζ at a large x

$$\zeta \sim 4k_o \int_{-\pi/2}^{\pi/2} m \exp(-k_o z_1 \sec^2\theta) \sec^3\theta$$

$$\times \cos\left[k_1 \sec^2\theta \{(x - x_1)\cos\theta + y \sin\theta\}\right] d\theta \tag{5}$$

where

$$k_1 \quad \frac{Lg}{V^2} , \qquad k_o \quad \frac{Hg}{V^2} . \tag{6}$$

L is the ship length,

H is the ship draft,

m is nondimensionalized with respect to LHV,

$x, x_1, y,$ is nondimensionalized with respect to L,

$-z_1 \; z$ is nondimensionalized with respect to H.

For a distribution of sources at a ship center plane $S_o(y \; 0, \; 0 \; z \; -1, \; 0 \; x \; 1)$ represented by a series

$$\left.\begin{aligned} m(x, z) &\quad m_1(x) \; m_2(z) \\ m_1(x) &\quad \sum_{n=0} a_n x^n \\ m_2(z) &= 1 \end{aligned}\right\} \tag{7}$$

the wave height will be, by the integration of (5) with (7) in the domain S_o,

$$_s \quad _{sB} + \; _{ss} \tag{8}$$

$$_{sB} \quad 4 \int_{2}^{2} \{1 - \exp(-k_o \sec^2 \;)\} \left[S_1(0) \sin \;(0) + S_2(0) \cos \;(0)\right] d \tag{9}$$

$$_{ss} \quad -4 \int_{2}^{2} \{1 - \exp(-k_o \sec^2 \;)\} \left[S_1(1) \sin \;(1) + S_2(1) \cos \;(1)\right] d \tag{10}$$

where

$$\left.\begin{aligned} (a) &\quad k_o \sec^2 \; [(x - a) \cos \; + \; y \sin \;)] \\ S_1(a) &\quad \sum_{n=0} \frac{(-1)^n}{k_1(k_1} \frac{m^{(2n)}(a)}{\sec \;)^{2n}} \\ S_2(a) &\quad \sum_{n=0} \frac{(-1)^{n+1}}{k_1(k_1} \frac{m^{(2n+1)}(a)}{\sec \;)^{2n+1}} \end{aligned}\right\} \tag{11 (Cont.)}$$

$$m^{(n)}(a) = \left(\frac{\partial^n m(x)}{\partial x^n}\right)_{x=a} . \qquad (11)$$

According to the theory developed by Havelock, ζ_{sB} and ζ_{sS} are understood as bow waves and stern waves respectively.

The regular wave heights (5), (9) and (10) all have a form

$$\zeta = \int_{-\pi/2}^{\pi/2} S(\theta) \sin\left[k_1 \sec^2\theta \{(x-a)\cos\theta + y\sin\theta\}\right] d\theta$$

$$+ \int_{-\pi/2}^{\pi/2} C(\theta) \cos\left[k_1 \sec^2\theta \{(x-a)\cos\theta + y\sin\theta\}\right] d\theta . \qquad (12)$$

Havelock (1934a) showed that the integrands in (12) indicate one-dimensional waves propagating from the point $(a, o, 0)$ with the speed $V\cos\theta$ in the direction θ.

Indeed it can be easily understood if we recognize:

$$(x-a)\cos\theta + y\sin\theta = r \qquad (13)$$

is the equation of the straight line $\ell(r, \theta)$ on the plane $z = 0$ with the distance, r, from the point $(a, o, 0)$ to the line ℓ, and the angle between the normal to the line ℓ and the x axis, θ; the wave speed $C = V\cos\theta$ in the deep sea satisfies

$$C^2 = \frac{\lambda g}{2\pi} = V^2 \cos^2\theta \qquad (14)$$

where λ is the wavelength. Hence the one-dimensional wave in the direction angle θ is

$$\zeta_o = A \sin \frac{2\pi}{\lambda}(r - Ct)$$

$$= A \sin\left[\frac{V^2}{g} \sec^2\theta \{(x-a)\cos\theta + y\sin\theta - Vt\cos\theta\}\right] .$$

If we replace $x - Vt$ by x and nondimensionalize by L

$$\zeta_o = A \sin\left[k_1 \sec^2\theta \{(x-a)\cos\theta + y\sin\theta\}\right] . \qquad (15)$$

Therefore these Kelvin regular surface waves are a superposition of the one-dimensional sine and cosine waves with the respective amplitude $S(\theta)$ and $C(\theta)$ in the direction $-\pi/2 \leq \theta \leq \pi/2$. He named these one-dimensional waves "elementary waves" and $S(\theta)$ and $C(\theta)$, amplitude functions. We may omit the word "elementary" in this report except to avoid ambiguities.

He further considered (1934b) the energy carried away by regular waves far aft of a ship in connection with the wave resistance, and he derived the wave resistance formula related to the regular waves (8). From (9) and (10), (8) can be rearranged as

$$\zeta_s = \int_0^{\pi/2} \left[A_1(\theta)\sin(k_1 x\sec\theta) \cdot A_2(\theta)\cos(k_1 x\sec\theta)\right]\cos(k_1 y\sin\theta\sec^2\theta)\,d\theta \tag{17}$$

where

$$A_1(\theta) = 8\left[1-\exp(-k_0\sec^2\theta)\right]\left[S_1(0) - S_1(1)\cos(k_1\sec\theta) - S_2(1)\sin(k_1\sec\theta)\right] \tag{18}$$

$$A_2(\theta) = 8\left[1-\exp(-k_0\sec^2\theta)\right]\left[S_2(0) + S_1(1)\sin(k_1\sec\theta) - S_2(1)\cos(k_1\sec\theta)\right]. \tag{19}$$

Then Havelock's wave resistance formula is

$$R = \frac{1}{2}\int_0^{\pi/2}\left[A_1^2(\theta) + A_2^2(\theta)\right]\cos^3\theta\,d\theta \tag{20}$$

where R is related to the wave resistance R_o by

$$R = \frac{R_o}{\pi\rho g L^2 V^2}.$$

Since the integrand of (20) is positive definite, R is zero if and only if

$$A_1(\theta) = A_2(\theta) = 0, \quad \text{for } 0 \le \theta \le \pi/2. \tag{21}$$

The wave resistance (20) can be written as

$$R = R_B + R_s + R_{Bs} \tag{22}$$

R_B = bow wave resistance

$$= \frac{1}{2}\int_0^{\pi/2}\left[S_1^2(0) + S_2^2(0)\right]K^2\cos^3\theta\,d\theta \tag{23}$$

R_s = stern wave resistance

$$= \frac{1}{2}\int_0^{\pi/2}\left[S_1^2(1) + S_2^2(1)\right]K^2\cos^3\theta\,d\theta \tag{24}$$

R_{Bs} = stern bow interference resistance

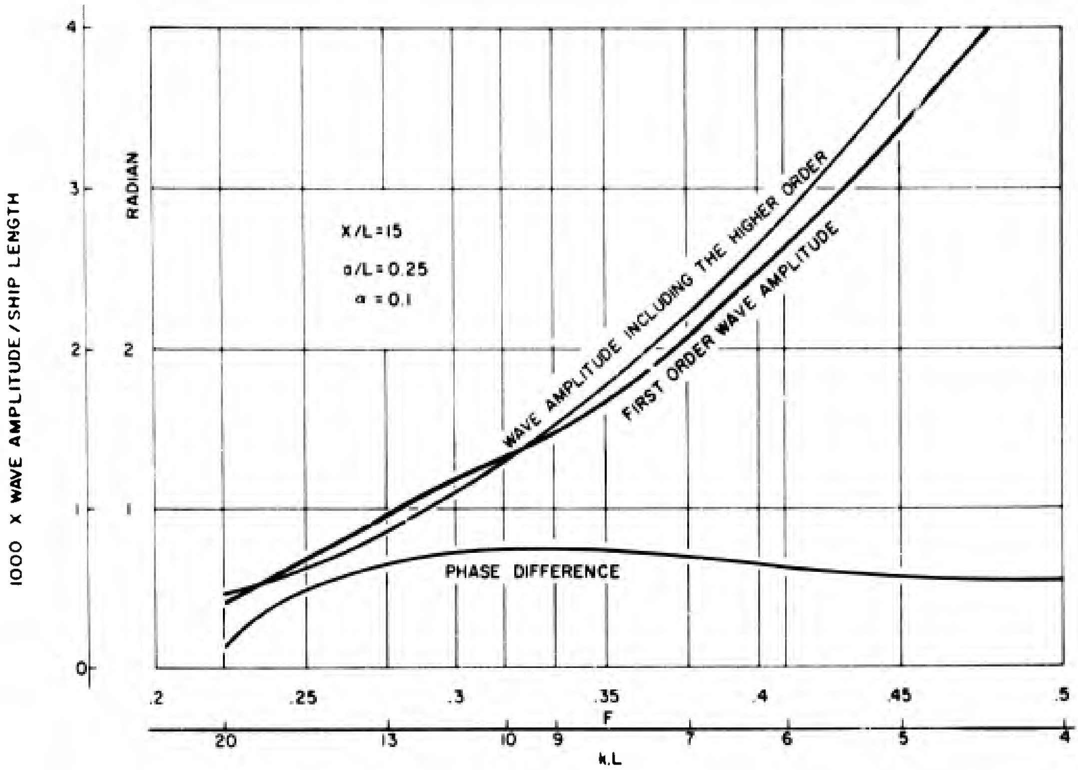

Fig. 12 - Comparison of the first order wave and the total wave (α = 0.1 rad)

We notice that when we cancel the regular wave by the bulb, the line integral due to this wave will be also cancelled.

This study of the line integral (50) has just started. However it seems to be quite promising for furtherance of a proper understanding of ship waves and of their reduction.

CONCLUDING REMARKS

Theory and experiment are always stimulating and helping each other. Although this report is on the theoretical side, it does not mean that the influence of experiments are underestimated. This report is merely intended to further appreciation of our great predecessors, Michell, Havelock, Wigley, Weinblum and Inui for the theories related to the bulbous bowed ship, and to add a slight theoretical illumination to them.

The mechanism of the bulb at the ship bow (or stern) is completely clarified. The type of bulb for a given ship hull, and the size and the vertical area distribution of bulb for a given Froude number are derived. The higher order influence is known to be the major reason for the phase shift of the regular

221-249 O - 66 - 71

waves. Although the stern problem in the non-viscous fluid is exactly the same as the bow problem, it should be studied separately due to the large influence of viscosity, wakes, propellers, etc. Because of these influences, the bow waves are more important in practice than the stern waves. The humps and hollows of the curve of the wave resistance due to a ship without a bulb may be applied to that for the ship with the bulb without any considerable error. The bulb has an effect of smoothing out the humps and hollows of the resistance curve to a considerable extent (Yim 1962) in the vicinity of the designed speed or for larger speeds. Pien (1962) seems to have obtained this effect using the principle of wave cancellation by distributed singularities rather than concentrated ones. Naturally, a ship with a bulbous bow would have much the better performance if it has a better stern. At the present time, shapes like the transom stern seem to attract the interest of many naval architects for high speed ships.

The higher order effect and the influence of viscosity are extremely difficult to analyze, yet they should and will be gradually exploited in the near future. The theoretical study on the seaworthiness of the bulbous ships remains to be done, although it is known from experiments that bulbous bows are still effective in waves.

ACKNOWLEDGMENT

This work was kindly sponsored by the Office of Naval Research, Department of the Navy under Contract No. Nonr-3349(00), NR 062-266. Thanks are due to Mr. M. P. Tulin for his helpful discussions.

NOTATION

a = Length of run of wedge strut

a_n = Coefficients of polynomial representing source distribution for a ship

b_n = Coefficients of polynomial representing concentrated singularity distributions for a bulb

B = Beam

$f(x, z)$ = Ship hull form

F_H, F_L = Froude numbers with respect to draft and length respectively

g = Acceleration of gravity

H = Draft of ship

H_n = Struve function

k_0 = gH/V^2

k_1 = $gL\ V^2$

L = Length of ship

m = Nondimensional source strength

R = Nondimensional wave resistance

V = Uniform velocity at x

x, y, z = Right handed rectangular coordinate system with z positive upward, x in the direction of the uniform velocity V, and the origin on the mean free surface

Y_n = Bessel function of the second kind

= Half entrance angle

$_1$ = First order wave height

= Second order wave height

= Coordinate system equivalent to 0 − x, y, z

= Nondimensional doublet strength

= Nondimensional quadrupole strength

( ) = (x −) cos + y sin .

REFERENCES

1. Bessho, M., "On the Wave Resistance Theory of a Submerged Body," 60th Anniversary Series, Vol. 2, SNAJ, 1957.

2. Bessho, M., "On the Minimum Wave-Resistance of Ships with Infinite Drafts," Proceedings of International Seminar on Theoretical Wave-Resistance, University of Michigan, 1962.

3. Dillon, E. S. and Lewis, E. V., "Ships with Bulbous Bows in Smooth Water and in Waves," Trans. SNAME, Vol. 63, 1955.

4. Havelock, T. H., "The Wave Pattern of a Doublet in a Stream," Proc. Roy. Soc., A 121, pp. 515-23, 1928.

5. Havelock, T. H., "Ship Waves: the Calculation of Wave Profiles," Proc. Roy. Soc., A 135, pp. 1-13, 1932.

6. Havelock, T. H., "Wave Patterns and Wave Resistance," TINA. Vol. 76, pp. 430-443, 1934a.

7. Havelock, T. H., "The Calculation of Wave Resistance," Proc. Roy. Soc., A 144, pp. 514-21, 1934b.

8. Havelock, T. H., "The Forces on a Circular Cylinder Submerged in a Uniform Stream," Proc. Roy. Soc., A 157, pp. 526-34, 1936.

9. Inui, T., "Wave Making Resistance of Ships," Trans. SNAME, Vol. 70, pp. 283-353, 1962.

10. Inui, T., Takahei, T., and Kumano, M., "Wave Profile Measurements on the Wave-Making Characteristics of Bulbous Bow," SNAJ (Translation from University of Michigan), 1960.

11. Karp, S., Kotik, J., and Lurye, "On the Problem of Minimum Wave-Resistance for Struts and Strut-Like Dipole Distributions," Third Symposium on Naval Hydrodynamics, ONR, Department of the Navy, 1960.

12. Kostchukov, A. A., "Theory of Ship Waves and the Wave-Resistance," Leningrad, 1959.

13. Krein, M. G., Koklady Akademi Nauk, SSSR, Vol. 100, No. 3, 1955.

14. Kelvin Lord (Sir W. Thomson), "On the Waves Produced by a Single Impulse in Water of any Depth, or in a Dispersive Medium," Proc. Roy. Soc. of London, Set A 42, pp. 80-85, 1887.

15. Lindblad, A., "Experiments with Bulbous Bows," Publication No. 3 of the Swedish State Shipbuilding Experimental Tank, 1944.

16. Lunde, J. K., "On the Linearized Theory of Wave Resistance for Displacement Ships in Steady and Accelerated Motion," Trans. SNAME, 1951.

17. Lunde, J. K., "On the Theory of Wave-Resistance and Wave Profile," Skipsmodelltankens, Meddeleke Nr. 10, 1952.

18. Martin, M. and White, J., "Analysis of Ship Forms to Minimize Wavemaking Resistance,' Stevens Inst. of Tech. R-845, May 1961.

19. Maruo, H., "Experiments on Theoretical Ship Forms of Least Wave-Resistance," The International Seminar on Theoretical Wave Resistance, University of Michigan, 1963.

20. Micheli, J. H., "The Wave Resistance of a Ship," London, Dublin and Edinburgh, Philosophical Magazine, Ser 5, Vol. 45, 1898.

21. Pavlenko, G. E., "The Ship of Least Wave Resistance," Trudy Vsesoyuz Nanch-Inzhen-Tekhn. Obshch. Sudostroen, 2, No. 3, 28-62, 1937.

22. Pien, P. C. and Moore, W. L., "Theoretical and Experimental Study of Wave-Making Resistance of Ships," Proc. of the International Seminar on Theoretical Wave-Resistance, Michigan, 1963.

23. Sisov, V., Isvestiya Akadem Nauk, SSSR, Mechanics and Engineering No. 1, 1961.

24. Stoker, J. J., "Water Waves," Interscience Publishers, Inc., New York, N.Y., 1957.

25. Sretenskii, L. N., "Sub un Probleme de Minimum dans la Theorie du Navire," C. R. (Dokl) Acad. Nauk, USSR 3, 247-248, 1935.

26. Takahei, T., "A Study on the Waveless Bow," SNAJ (Trans. from University of Michigan), 1960.

27. Taylor, D. W., "The Speed and Power of Ships," 3rd U.S. Gov't Printing Office, Washington, D.C., 1943.

28. Taylor, D. W., Marine Engineering and Shipping Age, pp. 540-548, Sept. 1923.

29. Wehausen, J. V., "An Approach to Thin-Ship Theory," Proc. of the International Seminar on Theoretical Wave Resistance, The University of Michigan, 1963.

30. Wehausen, J. V., Webster, W. C., and Lin, W. C., "Ships of Minimum Total Resistance," Proc. of the International Seminar on Theoretical Wave Resistance, The University of Michigan, 1913.

31. Weinblum, G., "Schiffe geringsten Widerstands," Proc. Third International Congr, Appl. Mech., Stockholm, pp. 449-458, 1930.

32. Weinblum, G., "Die Theorie der Wulstschiffe," Der Gesellschaft fur Angervandte, Mathematik, 1935.

33. Weinblum, G., "Schiffe geringsten Widerstandes," Jahrbuch der Schiffbautechnischen Gesellschaft, V. 51, 1957.

34. Wigley, W. C. S., "Ship Wave Resistance," Trans. N.E.C.I.E.S., Vol. XLVII, pp. 153-196, 1931.

35. Wigley, W. C. S., "The Theory of the Bulbous Bow and its Practical Application," Trans. N.E.C.I.E.S., Vol. LII, pp. 65-88, 1936.

36. Yim, B., "Analysis of the Bulbous Bow on Simple Ships," HYDRONAUTICS, Incorporated Technical Report 117-1, 1962.

37. Yim, B., "On Ships with Zero and Small Wave Resistance," Proc. of the International Seminar on Theoretical Wave Resistance, The University of Michigan, 1963.

38. Yim, B., "The Higher Order Effect on the Waves of Bulbous Ships," HYDRONAUTICS, Incorporated Technical Report 117-5, 1964.

* * *

THE SHIP BULB

Ata Nutku
Technical University
Istanbul, Turkey

The merits of the ship bulb as a resistance reducing mean has first been detected by Admiral D. W. Taylor. However, a great amount of testing has since been carried out to utilize it as an improving medium of ship form. The testing has been confined to minor changes on its size and form, and no attempt has been made towards a scrutiny on its basic concept or characteristic function.

As a matter of fact, the bulb today stands as we have inherited it from our forefathers who designed and used it for ramming the enemy ships during action. The original form of the bulb has been conservatively retained with only minor changes, which has satisfied its experimenters within the limits of 2 percent to 5 percent gain in total resistance of a ship. Some of the explanations for the action of the bulb may be summarized as:

(a) lowering centre of pressure zone at bow,
(b) displacing the bow wave to forward, consequently changing the phase of the wave system as to their order of synchronization, and
(c) causing a suction on the surface wave phenomena.

All the above will consequently cause change of flow pattern at bow.

The section of the bulb has attracted my attention from the observations made on the behaviour of a submerged circular streamlined body towed near the surface at different depths, and from the analysis of the results of its resistance and trimming moments. The purpose of these tests, conducted in the years 1956-57 has been purely academic, parallel to Wigley's and Gawn's experiments with fish form bodies.

I acknowledge the help and directives given by Prof. Dr. Günther Kempf, who was then a visiting professor in İ.T.Ü.

A circular streamlined body of L D = 4 has been used as a basic model which has later been utilized for different purposes as: the submerged body of a hydrofoil supported catamaran ship, as the ballast keel of sailboat tests and later as a bulb for Turkish fishing boat model tests.

Bulbs as large as one third the length of the model were tried and interesting results were obtained, which however not published has served to inspire the visitors to Turkish Tank, to promote new strides in chapters of wave resistance of ships with bulbs.

The action of the bulb as to its characteristic of producing suction can be visualized by the head-on trim it causes on the surface ship. This suction becomes highly distinctive when it is towed under a flat bottomed pontoon, or near the water surface.

The pictures of a fish form circular body of L D = 3 taken at different speeds are shown in Fig. 1.

Fig. 1 - Fish form circular body

It is noted that, at speeds lower than (the critical Froude number for depth), a wave trough is produced immediately after the bow wave of the fish, which moves aft as the speed is increased. This trough, the focal point of suction when coincides with the bow wave of the ship is swallowed in it. The effect becomes more pronounced as the bulge nears the surface. At greater speeds a sheet of water covers the top and the centre of the suction moves further aft over the tail.

The ships which are sensible to trim, when fitted with bulbs, have sometimes indicated increased resistances, at certain speeds, due to dive in of their bow, resulting from the suction produced by their bulbs, consequently increased bow waves, instead of reduced ones. This will mean a wrong shape, size and position of the bulb. This complex interaction of bulb and ship necessitated systematic testing with bulbs fitted as separate appendages at the fore end of the ship.

Unconventional means and methods were tried to assess the behaviour and interaction. For this purpose, geometrical bodies like spheres, cones, cylinders, etc., were included in the programme (Figs. 2a, 2b, 2c, 2d, and 2e).

The science of hydrodynamics already reveals the individual resistances of geometrical bodies, also when they are towed in tandem formation at different spacings between them. In choosing the unusual devices, the aim has been to study their comparative interactions with the hull, rather than their direct adoption as a resistance reducing mean.

The circular streamlined axisymmetric body has been selected as the nearest geometrical contemporary to the existing ship bulbs. Two ship models: one of a coastal tanker and the other of a motor launch were selected to be subjected to systematic testing. Some of the devices as fitted are shown in the accompanying photographs. The devices as tried may be subdivided into the following categories according to their functions:

(a) interference effect,
(b) bow wave suction or flow deviation,
(c) wave suppressors, and
(d) wave scrapers or spears.

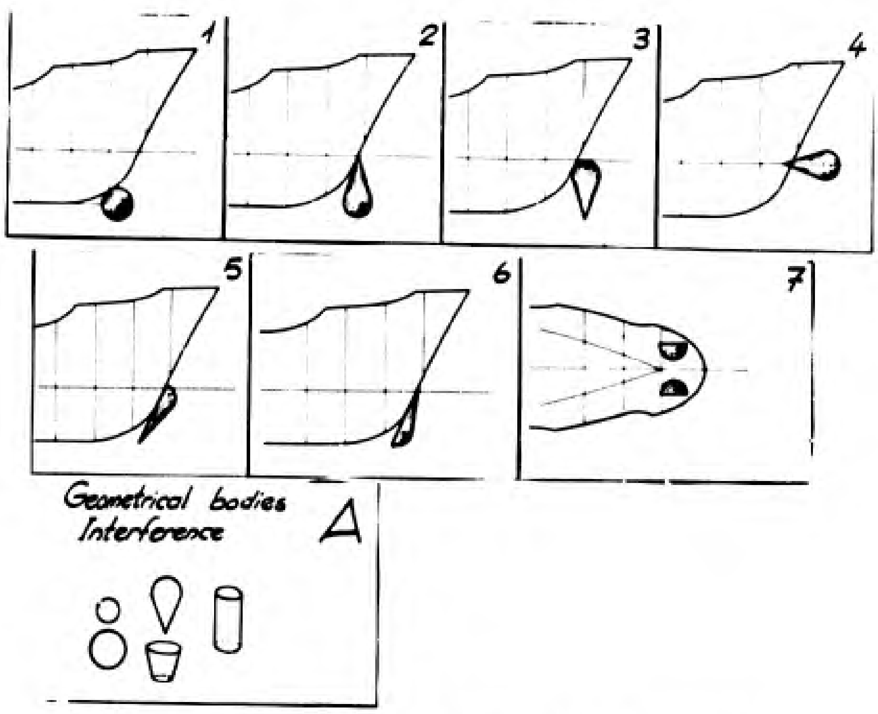

Fig. 2a - Passive means — geometrical bodies interference

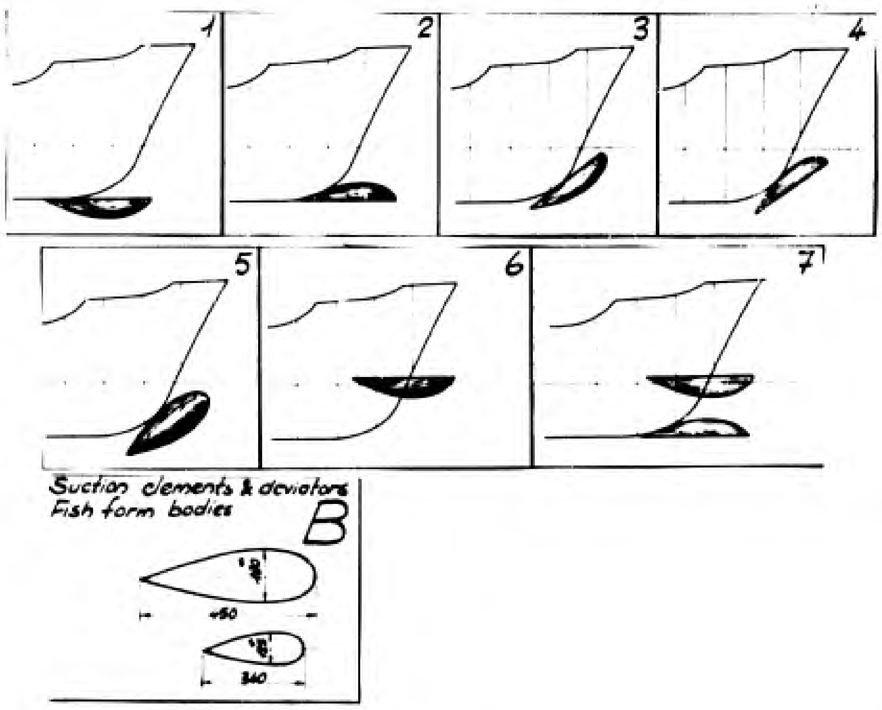

Fig. 2b - Passive means — suction elements
and deviators — fish form bodies

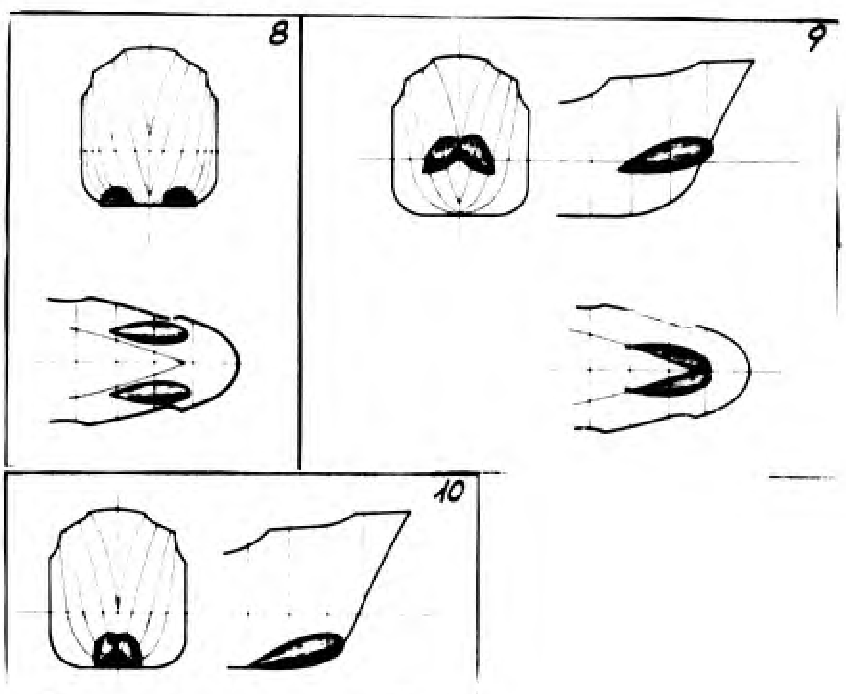

Fig. 2c - Passive means — suction elements
and deviators — fish form bodies

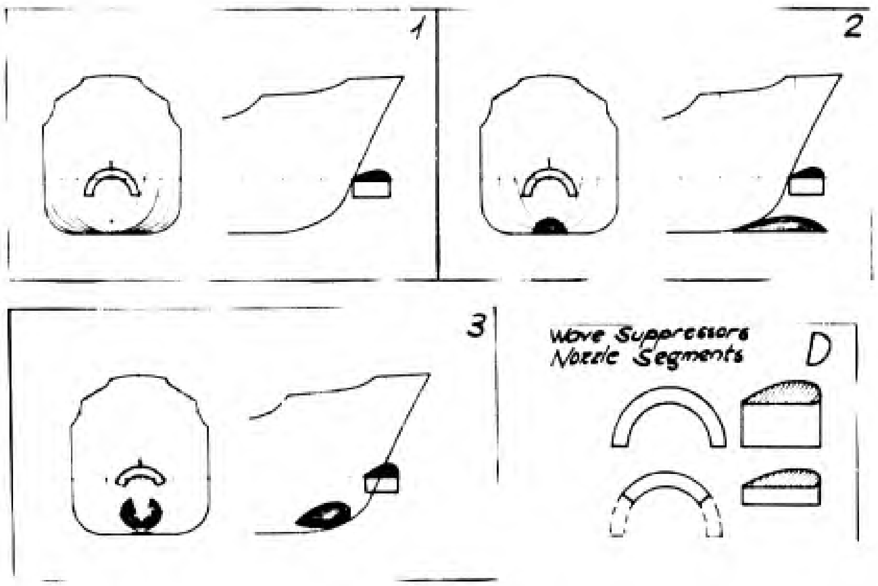

Fig. 2d - Passive means — wave suppressors — nozzle segments

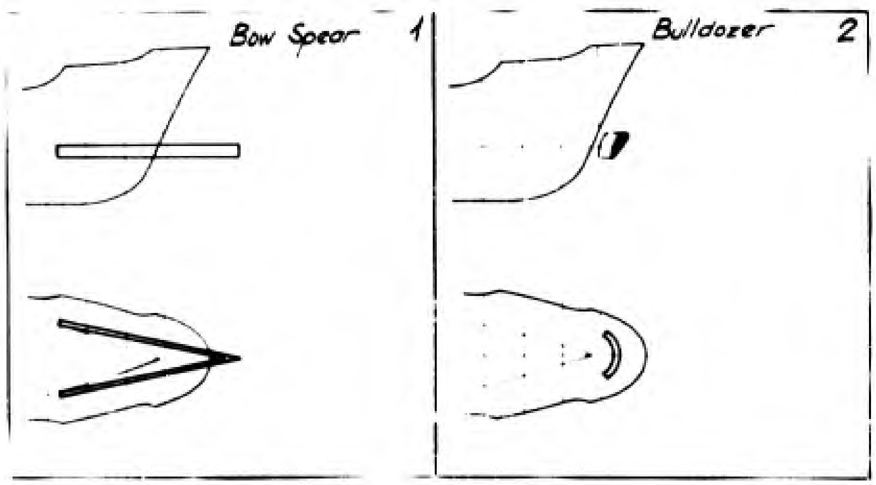

Fig. 2e - Passive means — wave scrapers

The axisymmetric fish form body has been split into two and has been fitted in different positions on the ship as shown in Fig. 3.

The comparative curves of resistances of the original naked model and that of a composite configuration having a bulb fitted at stem on the designed waterline in combination with a circular segmental suppressor of hydrofoil section (curved on top, Fig. 4). This model with (WL bulb plus suppressor) has shown itself of having less resistance after a model speed of $v = 1.60$ m sec approximately equivalent to $F_1 = 0.217$, $F = 0.292$ and a V $L = 1.00$.

Fig. 3 - Axisymmetric fish form body

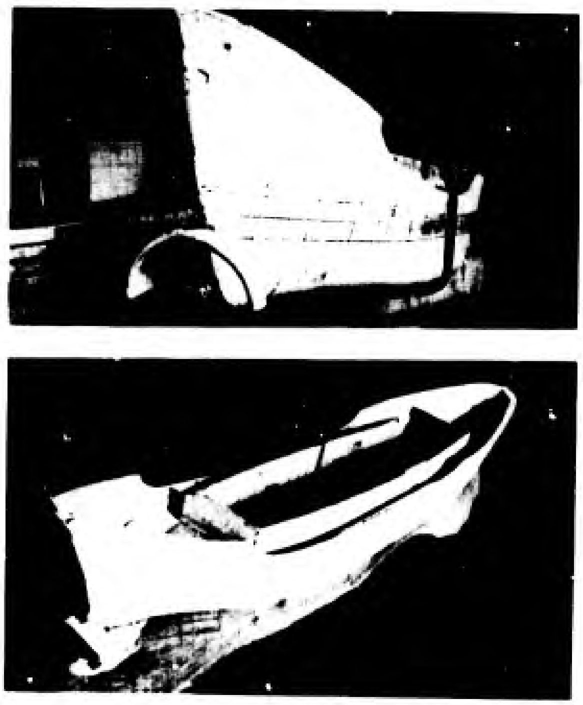

Fig. 4 - Naked bulb and bulb with circular segmented suppressor

It has shown a 17.5 percent gain in total resistance at maximum speed of $v_m = 1.75$ m/sec and up to higher speeds (from $V \quad L = 1.10$ upwards). Comparative wave formations at certain speed ranges are shown in Fig. 5.

It may be concluded that, the ordinary ship bulb as fitted near the keel does not perform as well as a bulb fitted at the designed waterline. The wave formation being a surface phenomena, the surface bulb becomes more effective, in taking the core of the bow wave, transforming thus the original solid bow wave into a sheet wave.

The water at the trailing edge is accelerated at its lower edge, trailing aft. Submerged bulbs of greater sizes may similarly influence the downwash, but the penalty paid for their extra resistances, due to their bulkiness thwarts off the advantage brought by their adoption. A badly designed bulb, is therefore, worse than having no bulb at all.

The bulb is destined to kill the bow wave which is the father wave and once it is killed, next of kin will not be as predominant. However, the effect of shoulder wave does still retain its place of importance and however the use of shoulder bulbs were also resorted to, it still needs careful considerations. calculations and a good programme of experimenting, to find its proper shape and place. It might be a denting instead of bulbing.

The devices shown in Fig. 2 as wave suppressors, scrapers or spears are impressive and effective in quenching or suppressing the waves, which is demonstrated by smoothed surface around the hull, yet their resistances are so high that their use for calm water alone may not be justifiable. Therefore, the term (waveless form) should not essentially implicate a form of least resistance, in every case.

The type, form, size and placement of the bow devices have to be decided according to the designed speed/length ratio, angle of entrance and other form characteristics of the ship. Some of the tests carried out with the model of a motor launch and the placement of the bulb or spear and the resulting wave formations are shown in Figs. 6, 7 and 8. The spear, solely an experimental device, piercing the water with a finer angle of entrance is also seen at speed.

The waterline bulb may invite suspicion of many of us as conservative naval architects, also due to its higher resistances up to the cruising speed range. Yet, apart from the fact that the part of the resistance curve we are most interested in, is in the high speed ranges, we may well go to introduce inflated rubber bulbs or appendages to suit the different speed ranges of the ship. Nearly every modern vehicle, from cars to ground effect machines are benefitting from its advantages. We may thus inflate it only at the speed ranges we want.

Naval architects of today trying to design sea kindly ships with solid walls of steel are preoccupied with problems of seakeeping and slamming. A bulb properly designed and fitted at design waterline may be a better antipitching device than its submerged contemporary, also insuring less loss of power in a seaway.

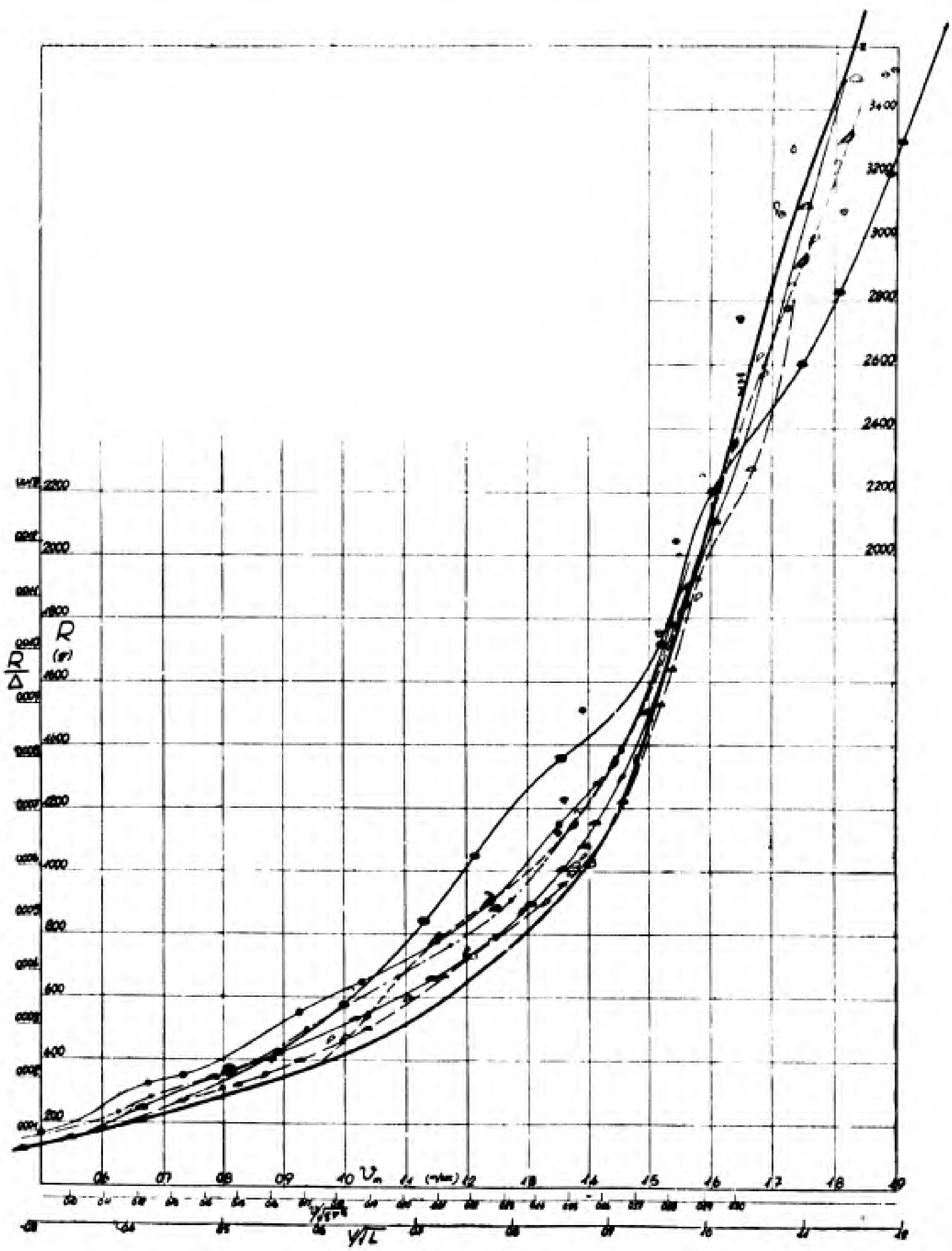

Fig. 5 - Comparative wave formations at certain speed ranges

Fig. 6 - Spear placement

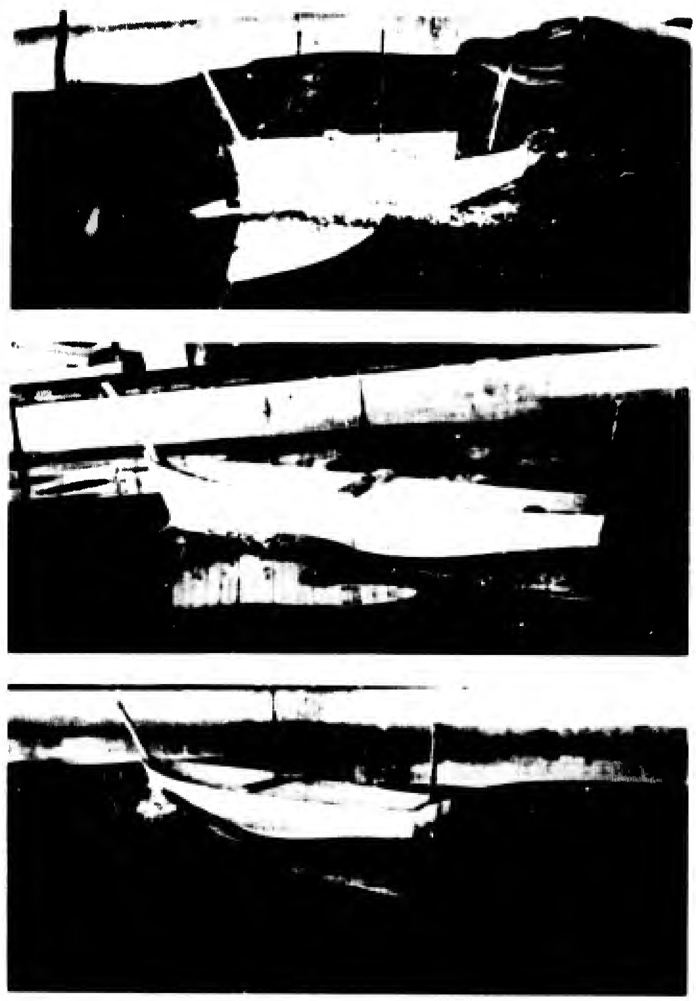

Fig. 7 - Spear placement

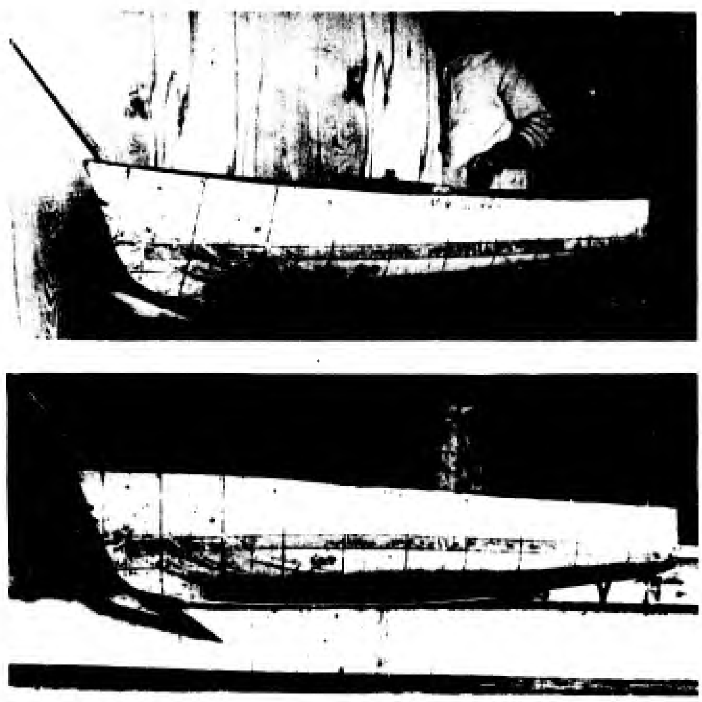

Fig. 8 - Mounted bulb and ship

*   *   *

THE APPLICATION OF WAVEMAKING RESISTANCE THEORY TO THE DESIGN OF SHIP HULLS WITH LOW TOTAL RESISTANCE

Pao C. Pien
David Taylor Model Basin
Washington, D.C.

ABSTRACT

Despite its limitations, the existing wavemaking resistance theory can be applied effectively to the design of better hull forms with practical proportions. Proper application of the theory can produce not only the direct benefit of reducing wave drag but also an indirect gain in viscous drag. Most of the numerical work involved in such application has been programmed into the 7090 IBM high-speed computer. Some numerical results obtained by using computing programs are shown. A ship design example to show how we can reduce both wave and viscous drags is also included.

INTRODUCTION

The total resistance of a ship consists of two parts, wavemaking resistance and viscous resistance. If wavemaking resistance theory can be used to minimize the wave drag of a ship, we can not only have the direct benefit of low wave drag but also a great possibility of reducing viscous drag.

It has often been said that the application of this theory to ships currently designed to operate at low Froude numbers holds little promise because wave drag is a very small portion of the total drag. It is true that we cannot reduce the total drag of a ship very much in such cases even if we can eliminate the wave drag entirely. However, if the length of a ship is reduced, the wetted surface will be reduced, and as a result, the viscous drag will be decreased. If ship length is decreased, and speed and displacement volume are kept constant, the operating Froude number will be increased. Any experienced ship designer will agree that the increase in wave drag will far exceed the decrease in viscous drag. If the wavemaking resistance can be kept low through the application of the wavemaking resistance theory, then reducing the ship length will achieve a great gain in total resistance as well as a reduction of construction costs. This

221-249 O - 66 - 72

concept of applying the wavemaking resistance theory to reduce the total resistance of ships can be applied advantageously in the design of "practical" ships, i.e., ships with practical L/B and B/H ratios.

To date, numerous attempts to utilize this theory have had disappointing results. However, this lack of success is not necessarily due to the limitations of the theory. It is my belief that, despite its defects, the existing theory can be used in the design of practical ships with low resistance. The justification for this view is fully discussed in this paper.

In the belief that much better forms can be obtained by using this theory, I have undertaken a hull form research project at the David Taylor Model Basin. The first part of this project has been to program for automatic computation all the numerical work involved in the application of the theory to ship design work. Once this has been done, the application of the theory becomes a fruitful, enjoyable task rather than tasteless, tedious labor. The second part of this project is devoted to the actual application of the theory to the design of ships. Models will be designed according to the theory and then tested, and the model experiment results can be applied immediately to the shipping industry. After sufficient theoretical and experimental data have been gathered, further improvement in the present wavemaking resistance theory can be expected.

The first part of this project has already been accomplished. Two computing programs have been developed. The first is used either to compute the wavemaking resistance and free-wave amplitudes of a given singularity distribution or to optimize a singularity distribution to fulfill a ship design problem. The second is used to compute the hull geometry from a given singularity distribution.

With these two computing programs, the second part of this project becomes relatively simple and easy. One model has already been designed and is under construction. The theoretical results for this model are given.

This paper is essentially a progress report of the present hull form research project. The second part of this project has just been started. Another paper will be published upon completion of this phase.

JUSTIFICATION FOR APPLYING THE WAVEMAKING RESISTANCE THEORY TO THE DESIGN OF PRACTICAL SHIPS

Two important assumptions are involved in the development of the existing wavemaking resistance theory; these must be carefully considered if the theory is applied to ships with practical L/B and B/H ratios:

1. The free-surface disturbances created by a moving ship are small, and so wave height will be small in comparison to wave length. This assumption justifies linearizing the free-surface condition.

2. The viscosity effect is negligible and the potential theory can be used in the study of ship-created waves.

The first assumption is usually satisfied by selecting a beam that is very small in comparison with the length and the draft. Such ships are called thin ships. Since a thin ship has no practical value, the theory has also been applied to ships with practical beams in the hope that some good may result despite the limitations of the theory.

Fortunately, while a small beam is a sufficient condition for a small free-surface disturbance, it is not a necessary one. If a practical (thick) ship can be designed which disturbs the free surface as little as a thin ship, the linearization of the free-surface condition should be applicable to this practical ship as well. Since the main portion of the free-surface disturbance is due to the free waves which cause the wavemaking resistance, the theory should be applicable to thick ships of low wave drag as well as to thin ships. Therefore, the pertinent question to be asked with regard to the linearization of the free-surface condition is whether or not the wavemaking resistance is small rather than whether or not the beam is small. If we limit our study only to hull forms with very small wavemaking resistance, the theory is valid so far as the assumption about the free surface is concerned.

In later sections, a procedure will be given for obtaining low wave-drag ships under the restraint of practical design conditions. Let us first examine more carefully the argument for using the theory to design low wave-drag practical ships. For this purpose, the comparisons made in the past between theoretical and experimental results have been carefully re-examined. Unfortunately, most of these comparisons have severe defects except those of Inui. He has clearly shown that the linearized condition on the ship surface is not accurate enough to obtain the singularity distribution of a given hull geometry for thick ships, or vice versa. If this situation is not improved, the theoretical model (singularity distribution) and the experimental model are not equivalent. Inui has been criticized by many people for employing a higher than first-order approximation on the ship surface while keeping the first-order approximation on the free-surface condition. His approach has been fully justified by the important results he has so obtained.

Since at this point we are examining only the consequence of the linearized free-surface condition, our study is confined to the comparison in the Froude number range where the viscosity effect is relatively small. In many cases, due to the fact that the theoretical and experimental models are not equivalent, such comparisons are rather confusing. Generally speaking, the percentage differences between theoretical and experimental results are smaller when the level of wavemaking resistance is lower. Emerson's paper [1], based on Wigley's experimental work, definitely shows this tendency. Fortunately, we have the comparisons of the S-series models made by Inui [2]. In each of these cases, the theoretical model and the experimental model are equivalent. Table 1 gives the theoretical and the experimental wavemaking resistance coefficients and the corresponding Froude numbers taken from Inui's published curves. Some geometrical parameters of these models are also listed. Figure 1 shows a simple comparison of the theoretical and experimental wavemaking resistance

Table 1

Model	B/L	H/L	M_o	K	C_w	C'_w	C_w	C'_w	C_w	C'_w
					F = 0.40		F = 0.45		F = 0.50	
S-101	0.0748	0.0806	0.4	0.13	0.00058	0.00053	0.00089	0.00082	0.00094	0.00089
S-201	0.1229	0.0979	0.8	0.18	0.0023	0.00147	0.0036	0.00243	0.00378	0.00294
S-102	0.0839	0.1356	0.4	0.13	0.00144	0.00118	0.0024	0.00206	0.00272	0.00235
S-202	0.1454	0.1562	0.8	0.20	0.00576	0.00256	0.0096	0.00551	0.0108	0.0076

Notes:

1. M_o is the surface source density at the end. It is proportional to the entrance angle of waterlines.
2. K is the form factor used with Hughes friction lines.
3. C_w is the computed wavemaking resistance coefficient.
4. C'_w is the measured wavemaking resistance coefficient.

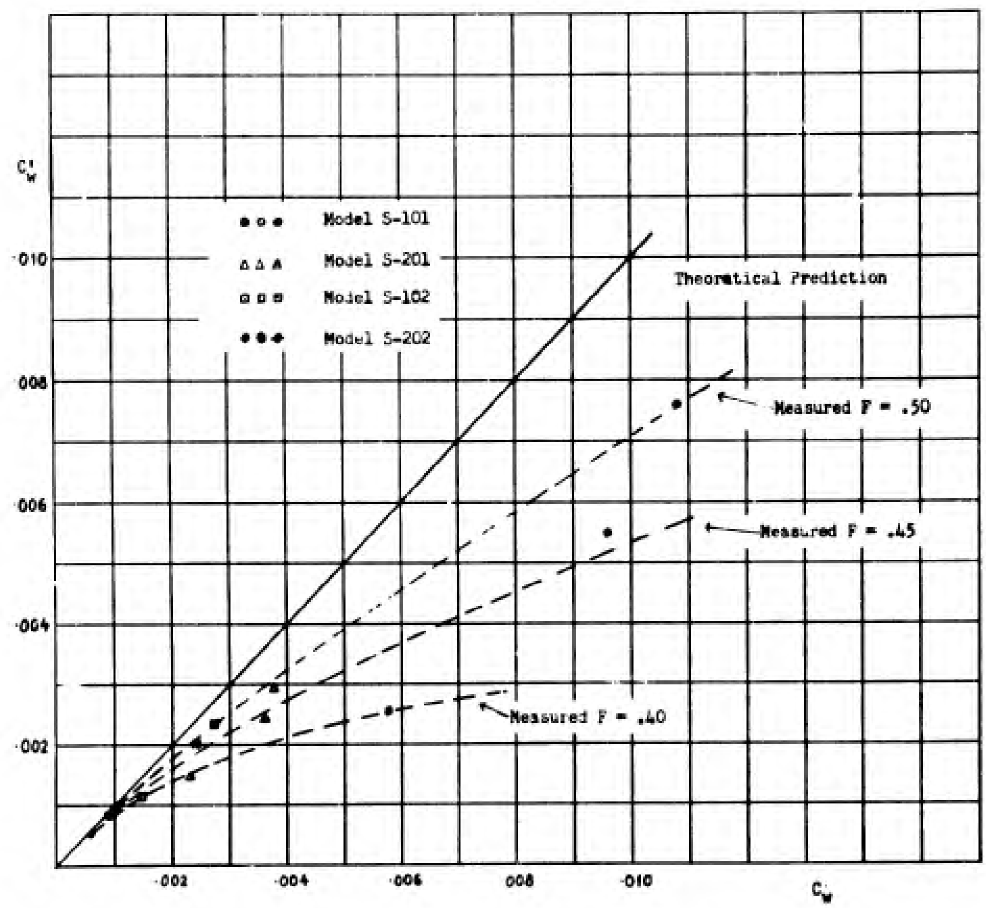

Fig. 1 - Comparison of theoretical and experimental C_w values of S-series models

coefficients. All the curves show a rather well-defined trend. Near the origin, the linearized theory gives quite accurate results. As the wavemaking resistance increases, the experimental values deviate more and more from the linearized theoretical results. At higher Froude numbers the experimental values are closer to the theoretical predictions. The theory always overestimates the experimental values. This is a rather familiar experience when using linearized theory for nonlinear problems.

In view of the fact that these four models vary greatly in beam, draft and angle of entrance, Fig. 1 is rather an interesting plot from which the following remarks can be made:

1. If the wavemaking resistance theory is applied to the forebody only, where the viscosity effect is small, the theoretical prediction will be an upper limit to the possible experimental wavemaking resistance values; and

2. the theory based on the linearized free-surface condition is more accurate when the level of the wavemaking resistance is very low (disregarding the value of beam) and when a higher order of ship surface condition approximation has been made. In such a case, the linearized free-surface condition is sufficient even though the ship-surface condition must have a higher than first-order approximation for practical beam values. Therefore, Inui's approach is both logical and practical even though it may seem inconsistent.

The second defect in the existing theory is that the viscosity effect has been neglected. At the present time there is no reliable method of estimating this, and the existing theory cannot predict the wavemaking resistance of a given hull form accurately. However, this fact should not prevent us from using the theory to search for forms with good wavemaking resistance qualities. The statements may seem to be self-contradictory, but it is hoped to show in what follows that they are quite consistent.

Because, for practical purposes, the viscosity effects can be neglected on the forebody and because the linearized free-surface condition will always overestimate the wavemaking resistance, we can use the theory to compute the upper limit of the wavemaking resistance of a forebody alone. This is equivalent to that of an infinitely long prismatic form fitted to the after end of the forebody. Since the forebody contributes most of the wavemaking resistance, the capability of the present theory to predict the upper limit of the forebody wavemaking resistance immediately gives the theory a very important role in the search for hull forms with low resistance.

The most frequent use made of the theory in ship design problems is to optimize the wavemaking resistance of a whole ship without checking the forebody free-surface disturbance alone. It is conceivable that the optimum value so obtained might be attributable not to the fact that both the bow and stern produce very small free waves but rather to the favorable theoretical interference effect of large bow and stern free-wave systems. Due to the viscosity effect, the existing theory cannot accurately predict either the amplitude or the phase of the stern free waves, so that the favorable interference effect as predicted by the theory may not always be realized in practice, thus leading to a large wavemaking resistance. Therefore, it is rather important to minimize the forebody free-surface disturbance.

It will be shown later that by proper application of the existing theory, we can obtain hull forms with theoretical wavemaking resistance values much less than those of existing designs. Due to these low levels of wavemaking resistance, such theoretical predictions will be quite accurate, any remaining errors no longer being of great practical significance. In concluding this section, I feel that the present wavemaking resistance theory can and should play an important role in the design of future ships.

NUMERICAL COMPUTATIONS

Theoretical Representation of a Hull Form — Singularity Distribution

For theoretical analysis of the wavemaking resistance of a given hull form, the latter is theoretically represented by a singularity distribution. Since our aim is to obtain a hull form with low wavemaking resistance rather than to predict the wavemaking resistance of a given hull form, the singularity distribution has been chosen as the starting point. After a suitable distribution has been found, the hull form is then generated from it.

A distribution of singularities in space is defined by their location as well as their density. Our ultimate objective is to find an optimum singularity distribution which will generate a hull form with low resistance and practical proportions, and at the same time is convenient for theoretical analysis.

It is obvious that a central plane distribution cannot yield practical hull proportions, and it must be discarded. On the other hand, if we choose the hull surface as the location (as has been done in Ref. 3), the density is automatically fixed. In such cases, even though we can always choose a satisfactory hull geometry to start with, we have no room left for improvement of the wavemaking resistance. A logical choice of the location is somewhere between the central plane and the hull surface.

The gross overall ship dimensions can be effectively controlled by the location of the singularity distribution. Our procedure is to select this location first and then to determine the density distribution on the chosen location such that the wavemaking resistance will be kept low. Let ξ, η, and ζ be the nondimensional coordinates normalized by one-half of the ship length. The origin is located at the midship section on the undisturbed free surface. The positive directions of ξ, η, and ζ are in the forward, port, and upward directions respectively.

Equation (1) defines an η-surface on which our singularity distribution is placed.

$$\eta = \pm B(\xi)\,[1-(1-a-b)\,\bar{x}^{3n} - a\bar{x}^{2n} - b\bar{x}^{n}] \qquad (1)$$

with

$$\bar{x} = \frac{\xi}{P_b(\zeta)} \qquad \text{For} \quad 0 \le \xi \le P_b(\zeta)$$

and

$$x = \frac{-\xi}{P_s(\zeta)} \qquad \text{For} \ -P_s(\zeta) \le \xi \le 0$$

where $B(\zeta)$, $P_b(\zeta)$, and $P_s(\zeta)$ define the midship section, bow profile and stern profile of the η-surface, respectively. Parameters a, b, and n are needed to obtain a large family of η surfaces. At present, $B(\zeta)$, $P_b(\zeta)$, and $P_s(\zeta)$ are chosen to be constant. Later, if necessary, the general case will be examined.

We choose Eq. (2) as the expression for the singularity density, which is defined as the singularity strength per unit velocity of a moving ship.

$$M(\xi,\zeta) = \sum_i \sum_j a_{ij} \xi^i \zeta^j \quad \text{for } -1 \leq \xi \leq 1,\ -T \leq \zeta \leq 0 \tag{2}$$

These surface singularities can be either source or doublet. For the purpose of generating a bulb, a line source and line doublet located at the end of the η-surface are also included in our scheme. Equations (3) and (4) define the line source and line doublet strength, respectively.

$$\text{line source } S(\zeta) = \sum_j s_j \zeta^j \tag{3}$$

$$\text{line doublet } D(\zeta) = \sum_j d_j \zeta^j \tag{4}$$

To obtain a flat keel line or a flat bottom, an additional surface source and doublet are placed on the horizontal bottom of the η-surface.

Theoretical Analysis of Wavemaking Resistance

We first assume that our hull form, theoretically represented by Eqs. (1) through (4), has a very low level of wavemaking resistance. Under this assumption, the theory can be used to analyze wavemaking resistance characteristics of the forebody of a hull form quite accurately. If, at the end, the theoretical wave-resistance level of the hull form under consideration is not low, we reject such singularity distributions.

We are interested in two different kinds of theoretical analysis. First we must obtain the theoretical wavemaking resistance curve as well as the free-wave amplitudes of a given singularity distribution. Second we must find the optimum singularity distribution under a set of design conditions. A computing program has been developed to perform both kinds of theoretical analysis.

The general scheme and procedure for performing the double integrations for free-wave amplitudes and triple integrations for wavemaking resistance numerically have been fully discussed in Ref. 4. Computing the free-wave amplitudes and wavemaking resistance curve of a given singularity distribution is a relatively straightforward procedure. To find the optimum singularity distribution under a given set of design conditions is more complicated. Our aim in such theoretical analysis is to develop a hull form with both low wavemaking resistance and a satisfactory hull geometry. It should be emphasized here that the wavemaking resistance theory is used to obtain a hull form with low wavemaking resistance rather than to predict the wavemaking resistance. The wavemaking resistance of a final design is obtained by model experiments. It should also be mentioned that when we write down a set of design conditions, we have to forego the usual way of specifying a number of hull proportions and hull coefficients intended for good resistance characteristics based on past experience. Basically, the chief objective of a design is to produce a ship which is safe to operate and economical to build and run, to carry a specified displacement at a specified operating speed. The conditions imposed in any design problem should not include any hull form coefficients related to the resistance. They are not to be spelled out as design conditions, but rather are to be determined in the process of design.

In our design problem, the objective is not to obtain the optimum hull form among the family covered by our theoretical representation scheme, but rather to find one hull form in this family which satisfies the design requirements and has an acceptable low level of wavemaking resistance. From a practical point of view, further reduction in wavemaking resistance has no great significance after such a level has been reached.

Our theoretical representation of hull forms is rather general, and the design conditions to be specified vary from one problem to another. In order to have a computing program that will cover a large variety of design conditions and perform the optimization, we split the surface source distribution in Eq. (2) into four elements. Equation (2) can be viewed as a polynomial of ζ with coefficients as functions of ξ. Each of the ζ terms is considered as a singularity distribution element. These elements are denoted by E_1, E_2, E_3, and E_4 respectively, corresponding to the zero, first, second, and third power terms of ζ in the case of surface source distribution. Similarly, E_5, E_6, E_7, and E_8 represent the four elements of surface doublet distribution. The line source distribution is denoted by E_9 and the line doublet is denoted by E_{10}. Altogether, we have ten independent singularity distribution elements.

Consider E_1 as an example. It is expressed as follows:

$$E_1(\xi) = a_{10}\xi + a_{20}\xi^2 + a_{30}\xi^3 + a_{40}\xi^4 + a_{50}\xi^5 \tag{5}$$

with $E_1(-\xi) = -E_1(\xi)$ and define:

$$V_1 = \int_0^1 E_1(\xi) \times \xi \, d\xi \tag{6}$$

$$B_1 = \int_0^1 E_1(\xi) \, d\xi \tag{7}$$

$$T_1 = E_1(1) . \tag{8}$$

Equations (6) to (8) define three possible restraints to be imposed on the element E_1. They are grossly related to the displacement volume, the midship area, and the entrance angle of the waterline. Similar restraints are defined for the rest of the nine elements. In the case of the surface doublet distribution, the first restraint is related to the ICB position of a half body and the second one is related to the displacement volume. In the case of the line source or line doublet, the first restraint is related to the VCB and the second one is related to the volume of a bulb. In any specific design problem, we can choose any number of the ten elements and impose any number of the three available restraints on each of the chosen elements.

The computing program performs basically one operation. The free-wave amplitude is computed from all the elements specified in the input data. Then a chosen element which is not specified in the input is determined under the specified restraints so that the resultant free-wave amplitudes of this particular element and that specified in the input will yield a minimum wavemaking resistance at the design Froude number. If no element is specified other than those in the input, the program simply computes the wavemaking resistance and the free-wave amplitudes of the singularity distribution given in the input at the specified Froude number range and interval.

To obtain a singularity distribution with a low level of wavemaking resistance, only two or three elements are required for a main hull form. The remaining surface singularity distribution elements are provided mainly for the purpose of meeting the hull geometrical requirements.

The computing program is very flexible. We can start either with the design of main hull form alone and later consider the size and shape of the bulb, or we may first specify a bulb and then design a main hull form in conjunction with this bulb.

A number of interesting theoretical analyses have been performed by using the computer program. The results are given in later sections.

Hull Form Tracing From a Given Singularity Distribution

A second computer program has been developed which can be used to develop a set of hull lines from a given singularity distribution. This program is an important link between a theoretical model and its corresponding experimental model. The basic assumption made here is that the free surface can be replaced by a rigid plane. Inui has shown in Ref. 2 that in the low Froude number range, the error resulting from this assumption is not serious so far as developing hull lines is concerned. Therefore, at the same Froude number, the less the wavemaking resistance, the closer the free surface will approach the rigid plane assumption. That means if we limit ourselves only to hull forms of low wavemaking resistance, the error involved in the rigid plane assumption will be even less serious.

The input data for this program specify all the singularity distribution elements involved in the theoretical representation of the hull form under consideration. The first item the program computes is the additional bottom surface singularity distribution required for obtaining flat keel line or flat bottom. The program will trace a specified number of streamlines generated by all the singularity distributions involved. The output of this program consists of a table of offsets which define a hull geometry. The details of this computation are given in Refs. 2 and 4.

If the hull geometry so obtained is not satisfactory, we may either introduce additional singularity distribution elements with the necessary restraints or modify the restraints on the original singularity distribution elements. Based on the gross effects of either modifying the restraints of a particular element or introducing a new element to the singularity distribution, we may decide what modifications should be made on the restraints or which additional elements should be introduced and then make corresponding changes in the input data for the first computer program. The output will give a new singularity distribution optimized with new elements or with new restraints. The iteration between these two programs is necessary in order to obtain a good compromise between hull resistance and hull geometry.

NUMERICAL EXAMPLES IN WAVEMAKING RESISTANCE

In the previous sections two computing programs have been described. The first one is used to obtain an optimum singularity distribution for a ship design problem or to compute wavemaking resistance curve and free-wave amplitudes of a given singularity over a specified range of Froude numbers. The second program is used to compute the hull geometry generated by a given singularity distribution. This section gives a few numerical results obtained from these programs.

The first example is intended to show that a thick ship can produce less free-surface disturbance and wavemaking resistance than a thin ship. The question of whether a ship is thin or not is a relative matter, and so is not easy to define. It may be thin enough at high Froude numbers and yet not be considered thin at low Froude numbers. Model S-101 of Ref. 2 is arbitrarily considered to be thin for Froude numbers greater than 0.30, based on the fact that the theoretical and experimental wavemaking resistance values are then in reasonably good agreement, as shown by the comparison of the computed and measured C_w curves in Fig. 2. This model is generated by a surface source distribution on a central plane having the following density expression:

$$M(\xi, \zeta) = 0.4\xi \tag{9}$$

with $-1 \leq \xi \leq 1$, and $-0.10 \leq \zeta \leq 0$. The body plan is shown in Fig. 4. The L/B ratio is 13.37.

We can now show that a model can be found with much smaller L/B ratio and much greater displacement-length ratio, but with less wavemaking resistance

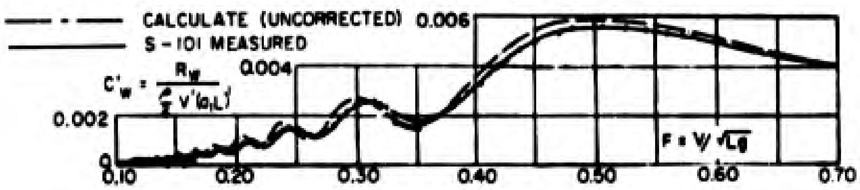

Fig. 2 - The computed and measured C_w curves of Model S-101

than Model S-101 at $F = 0.30$. At first, as in the case of Model S-101, only one singularity distribution element E_1 over the same distribution area as in Model S-101 is used. Only the restraint of a certain displacement volume requirement is imposed on the optimization of E_1 at $F = 0.30$. The E_1 so obtained is shown below:

$$E_1(\xi,\zeta) = 3.5127\xi - 5.4415\xi^2 + 13.3125\xi^3 - 24.4694\xi^4 + 13.6865\xi^5 \tag{10}$$

Figure 3 gives the plot of the corresponding density distribution.

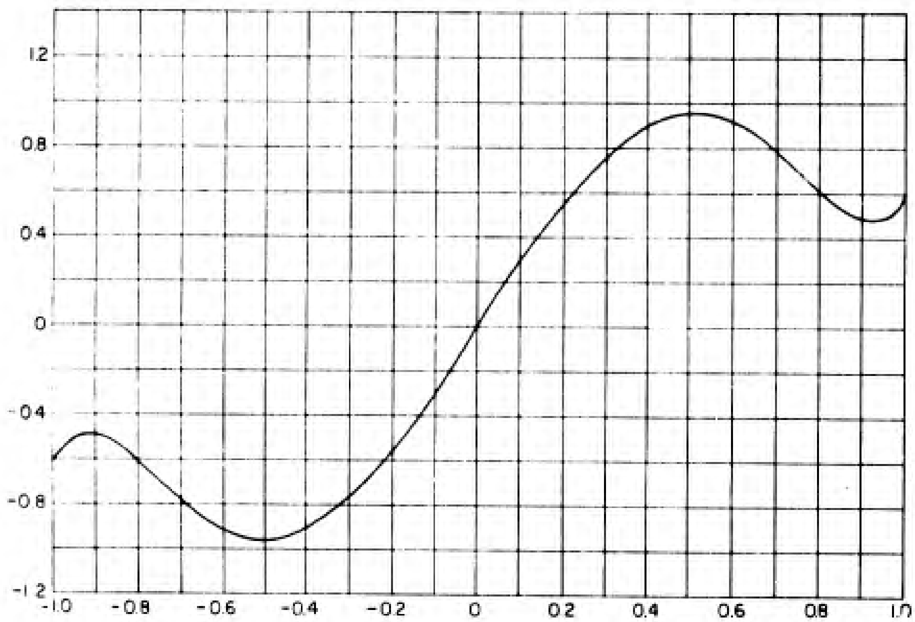

Fig. 3 - Surface source density distribution of Model A

The body plan of the model generated by E_1 is shown in Fig. 4. It is denoted as Model A. It has a L/B ratio of 6.06 which is less than half that of Model S-101.

Figure 5 shows the comparison of C_W curves of Models A and S-101. Up to a Froude number of 0.31, Model A actually has less wavemaking resistance than Model S-101. This result proves the point that a thick ship can have less wavemaking resistance than a much thinner ship.

If a singularity distribution is uniform in the draft direction, the free waves produced by layers of singularities at various depths are all in phase even though the magnitude is reduced as the depth is increased. There is no cancelling effect between them. To obtain favorable interference, the density distribution should vary with depth. To demonstrate this idea, a new singularity distribution element, say E_3, is added to the singularity distribution of Model A. Let us

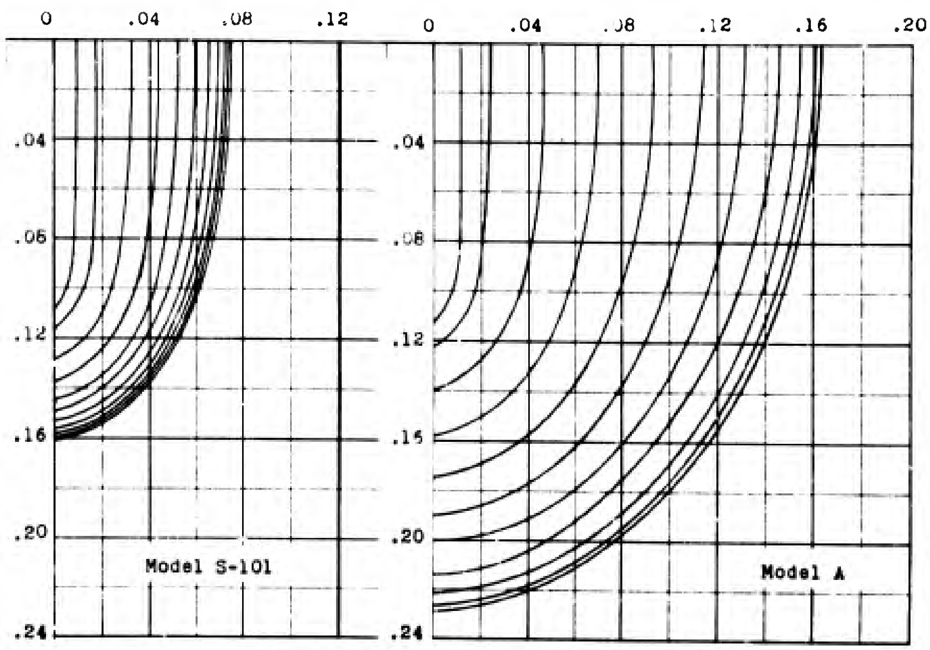

Fig. 4 - Body plans of Models A and S-101

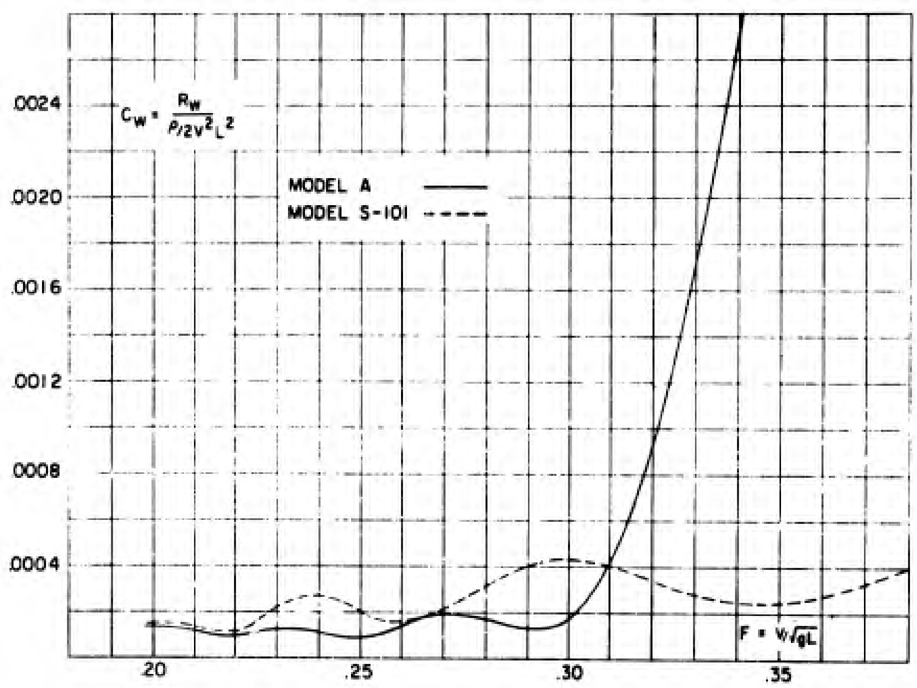

Fig. 5 - Comparison of theoretical C_w curves of Models A and S-101

assume that the only restriction put on E_3 is that the displacement volume of Model A should be increased by one-third. The optimum E_3 so obtained is shown below.

$$E_3 = [15.977\xi - 137.8429\xi^2 + 441.3259\xi^3 - 575.0504\xi^4 + 259.4315\xi^5]\zeta^2 \qquad (11)$$

This is derived in such a manner that the wavemaking resistance due to the combined singularity distributions of E_1 and E_3 is an optimum at $F = 0.3$. Let us denote the model, generated by E_1 and E_3, as Model B. Figure 6 shows the comparison between the C_w curves of Models A and B. Despite the fact that Model B has one-third more displacement volume than Model A, it has less wavemaking resistance at $F = 0.3$.

To illustrate the importance of section shape upon the wavemaking resistance, let us consider a third case, Model C, which has the following singularity distribution:

$$M(\xi, \zeta) = 3E_1\zeta^2 + E_3/3\zeta^2 \qquad (12)$$

where E_1 and E_3 are defined in Eqs. (10) and (11), respectively.

It is obvious that to the first order of approximation Models B and C have the same sectional area curve. Figure 7 shows the comparison of the C_w curves of Models B and C. The differences between these curves are quite large. This

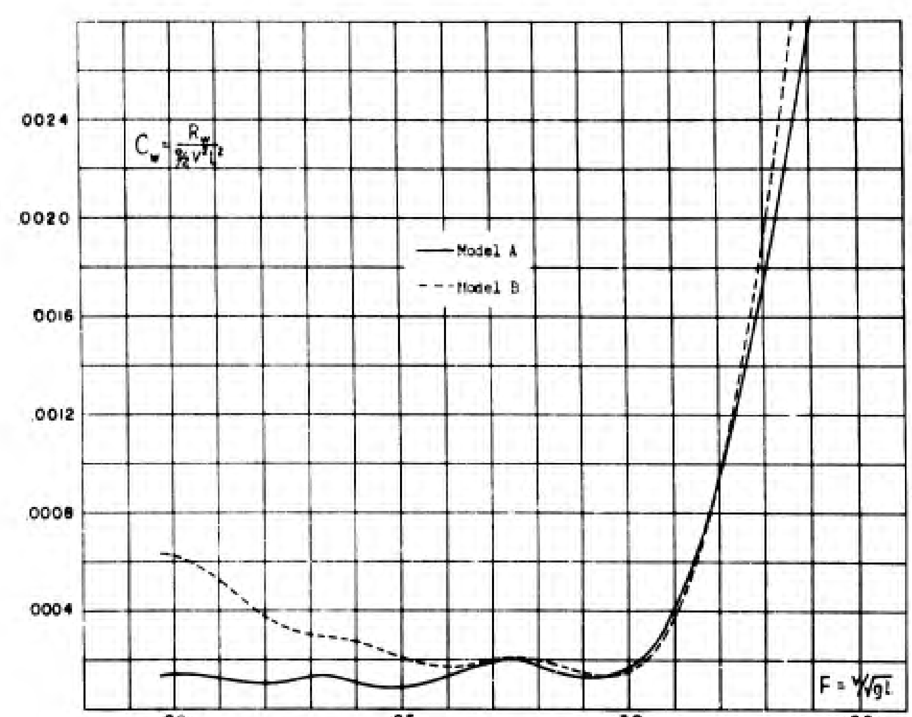

Fig. 6 - Comparison of C_w curves of Models A and B

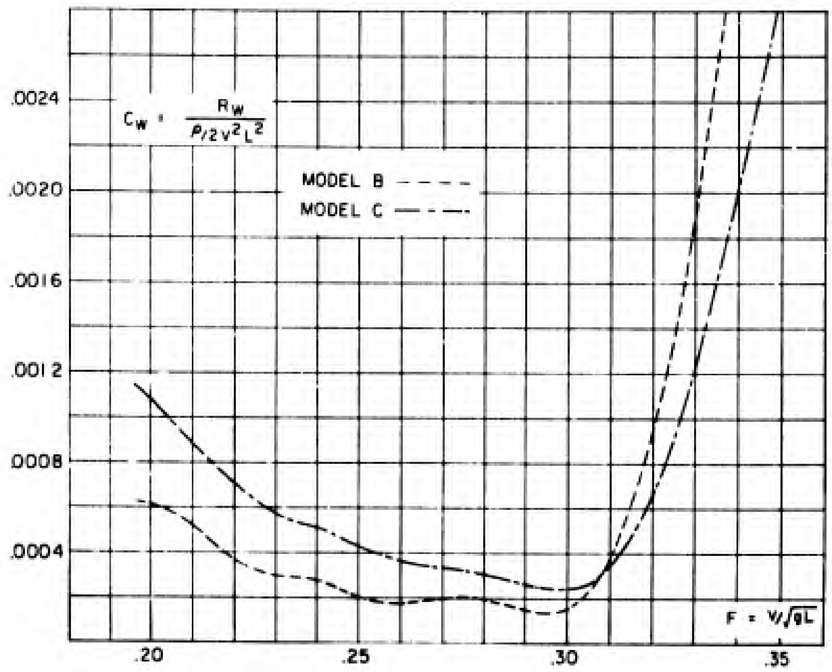

Fig. 7 - Comparison of theoretical
C_w curves of Models B and C

figure also indicates that a good vertical displacement-volume distribution at low Froude numbers may not necessarily be good at higher Froude numbers.

In Fig. 8, C_W curves are given for three cases with $M(\xi,\zeta) = \xi$, $4/3\,\xi^2$, and $7/3\,\xi^5$, respectively. To a first approximation, all three cases have the same displacement volume. At low Froude numbers, the differences between the three curves are amazingly large, mainly due to changes in angle of entrance. It is also interesting to note that in the case of $M(\xi,\zeta) = 7/3\,\xi^5$, the last hump is much less pronounced than the preceding ones.

REDUCTION OF VISCOUS DRAG

The viscous drag constitutes a major portion of the total resistance of a ship. A great potential, therefore, exists for reducing total resistance by decreasing the viscous drag, which is mainly a function of wetted surface and Reynolds number. However, if not designed properly, the hull form can produce large eddies, resulting in a large form drag. Therefore, to reduce the viscous drag, we have to reduce both the wetted surface and the form factor.

We know how to shape a hull to keep down viscous drag for a deeply submerged body, but such information cannot be directly applied to designing a ship hull subject to free-surface effects. In ship design, the principal dimensions

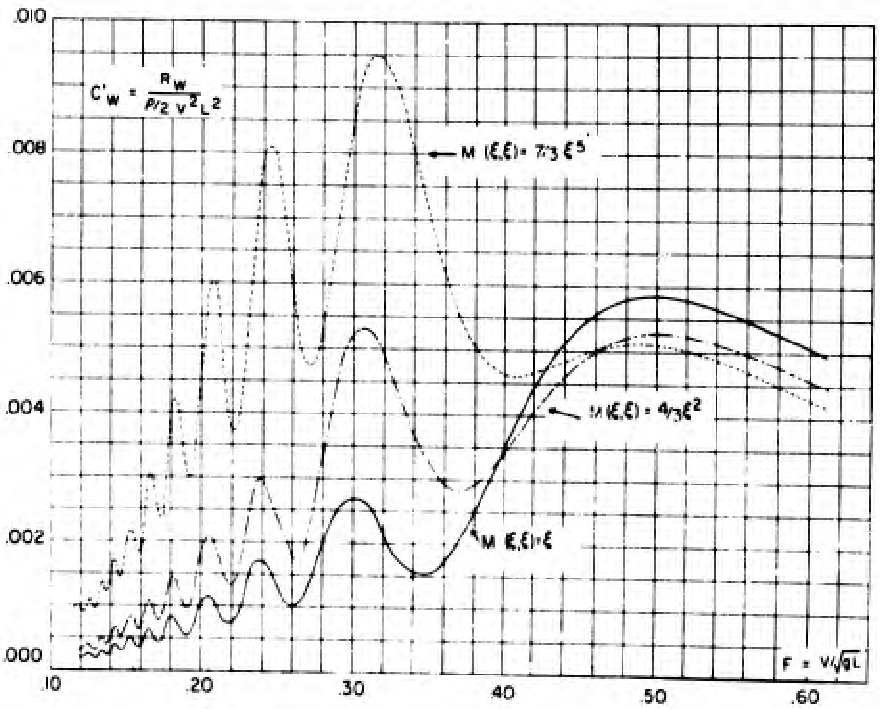

Fig. 8 - Theoretical c_w curves of $M(\xi,\zeta) = \zeta,\ 4/3\,\zeta^2,\ 7/3\,\zeta^5$, respectively

are chosen to give a proper balance between the viscous and wave drag, rather than for optimum viscous drag.

Knowing how to keep the wave drag at a low level, as previously described, we can select principal dimensions without the danger of increasing wavemaking resistance materially. This fact immediately opens the way to reducing the wetted surface.

As an example, let us consider Model 4210 of Series 60. It was designed for $V/\sqrt{L} = 0.9$ and has the following characteristics:

$$L/B = 7.5$$

$$B/H = 2.5$$

$$\Delta/(L/100)^3 = 122\,.$$

Assuming the length to be reduced by 20 percent, and the displacement and ship speed kept the same, $V/\sqrt{L}$ becomes about unity and $\Delta/(L/100)^3$ becomes 190.6. The reduction in wetted surface is of the order of 16 percent. For this model, such a change in length will greatly penalize the performance, the increase of wave resistance being much greater than the gain in viscous drag. If, based on theory, we can design a hull form of these proportions and displacement, with very low wave drag at $V/\sqrt{L} = 1.0$, such a gain in viscous drag can be realized without the penalty of increased wave drag.

This idea of reducing the wetted surface through the application of wavemaking resistance theory is quite useful. However, this is not the only way the theory can be used to reduce viscous drag — the form drag can also be reduced, as described below.

Ever since the comparison of the results of Models 4946 and 4953 (reproduced here as Fig. 9) were published (Ref. 4), some uneasiness has been felt. The body plans are given in Fig. 10. Model 4953 has 28 percent less displacement and 7 percent less wetted surface than Model 4946, and yet has greater total resistance at the lower Froude numbers. It was thought that this was mainly due to the wavemaking resistance, but considering the fact that the difference between these two models is confined to areas much below the free surface, it should not produce a big difference in wavemaking resistance, especially at lower Froude numbers.

One possible explanation for the larger total resistance of Model 4953 is a greater form drag. Due to the flat bottom, large eddies may be created in the water which flows over the bilge to reach the flat bottom. Such eddies are not likely to be created in the case of Model 4946 because of its rounded bottom. However, the turn of the bilge in the case of Model 4953 is not particularly hard. If large eddies do exist under the flat bottom of this model, it is likely that a majority of flat bottom models have the same drawback.

In searching for evidence of eddies beneath a flat bottom model, the wake survey results behind a smaller version of Model 4210, reported by Wu (Ref. 5), have been studied with great interest. Some of the figures of Ref. 5 have been reproduced here as Fig. 11. This model has a draft of only 0.53 ft and yet the wake is still quite strong at a depth of 0.7 ft. This cannot happen without the presence of large eddies underneath the flat bottom.

It is quite possible that although Model 4953 has less displacement volume and wetted surface than Model 4946, it may have a stronger wake belt trailing behind it. It would be very desirable to conduct wake surveys behind these models, but these are quite tedious and expensive, and it was thought that a flow visualization test might give a general picture of the flow near the bilge and bottom. Such tests have been conducted on both Models 4953 and 4946 in the circulating water channel.

Figures 12 and 13 show the corresponding pictures of these two models. Ink was introduced at nearly the same longitudinal stations. All the photographs were taken at a speed of 3 knots. It is quite clear from these pictures that large eddies do exist in Model 4953. These may account for a large portion of the increased total resistance. The bottom picture in Fig. 13 shows the ink flow near the stern of Model 4946. The ink was introduced at the bow, and there was no noticeable change in the thickness of ink marks as viewed from the other side of the model. If there is strong eddying, the diffusion of ink is very great, as observed in a similar test on Model 4953. (Unfortunately, the corresponding picture was not successful.)

221-249 O - 66 - 73

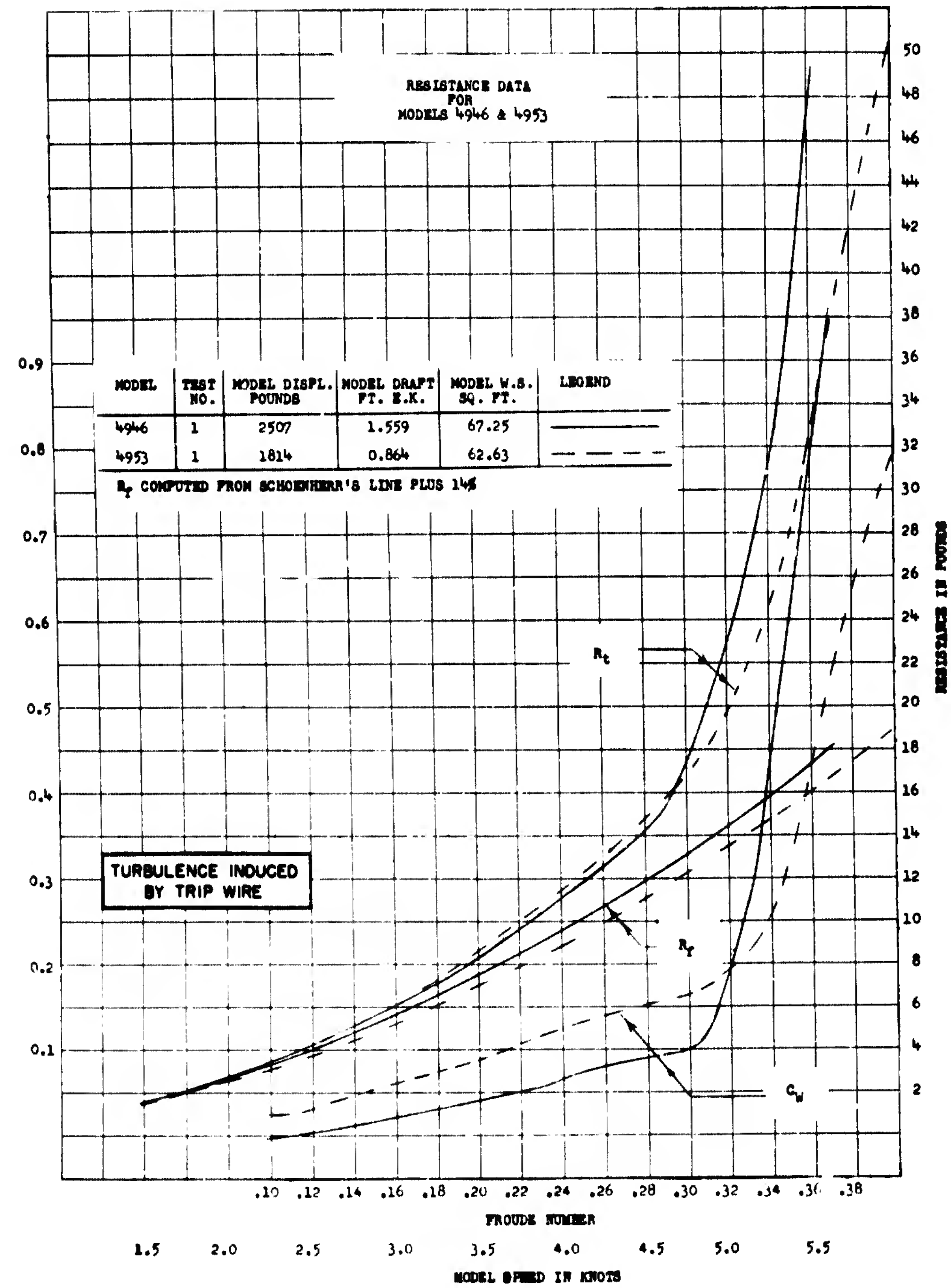

Fig. 9 - R_t and C_w comparisons for Models 4946 and 4953

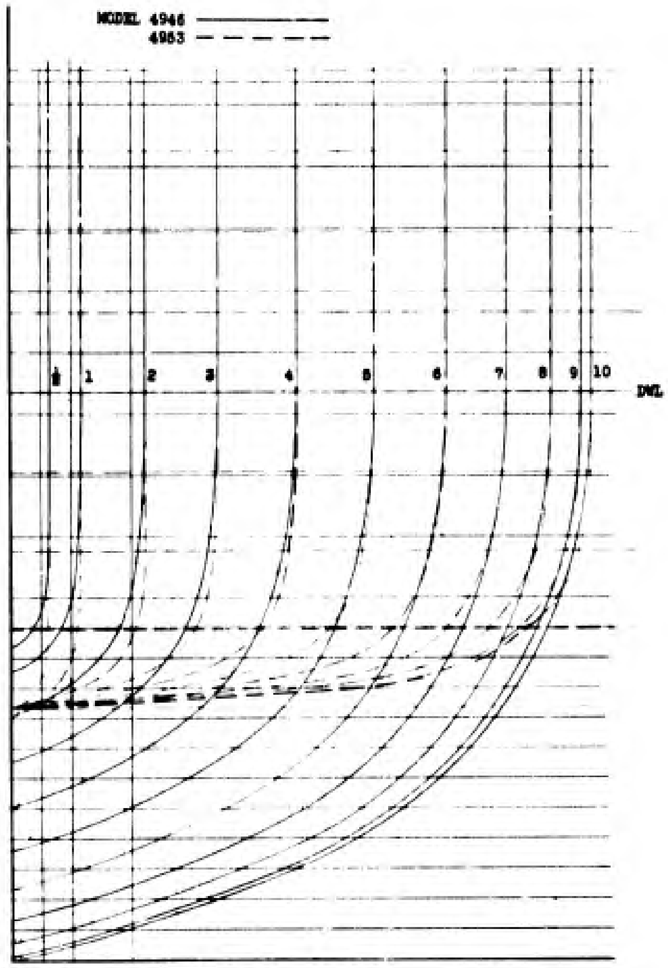

Fig. 10 - Body plans of Models 4946 and 4953

It is obvious from the foregoing that if water is prevented from flowing across the bilge, as in the case of Model 4946, formation of eddies can be avoided. However, the round bottom of Model 4946 is not practical, and we have to search for other means. A sizable bulb can be used for such a purpose. Starting from the stagnation point, the water can be guided in all directions by a bulb, so that it is properly channeled toward the flat bottom from the very beginning rather than spilling over the bilge to reach the bottom at a later stage.

A bulb can be used in this way to prevent the formation of eddies and thus reduce the form drag. However, the total resistance will not necessarily be reduced. If not properly matched to the main hull form, a bulb will produce a large wave drag, and any gain in form drag may well be exceeded by the penalty of wave-drag increment. Again the wavemaking resistance theory can be used to great advantage in this situation. To start with, we may choose a proper sized bulb and place it at a correct location based on the consideration of

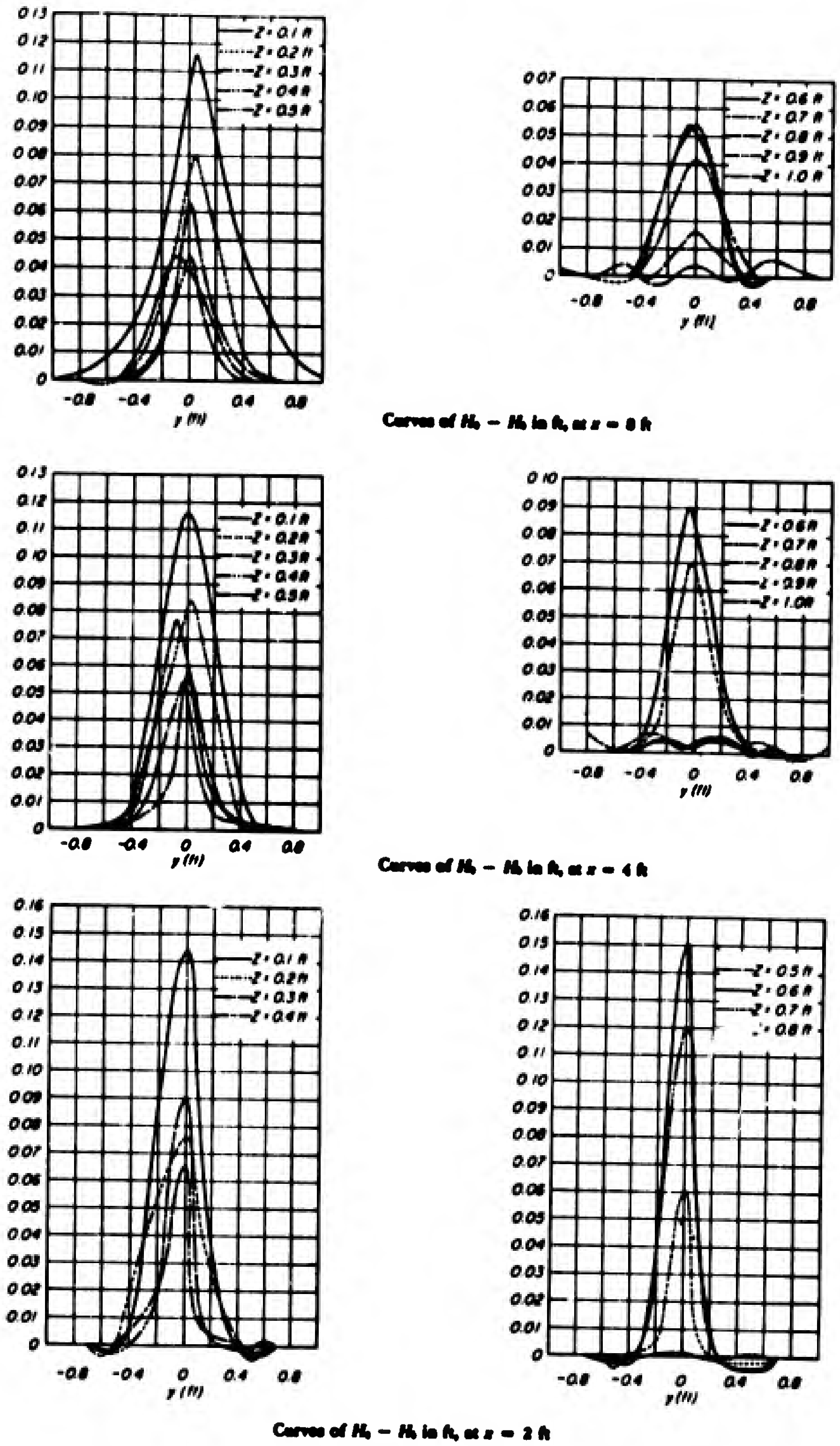

Fig. 11 - Curves of $H_o - H_b$ in ft at various distances behind Model 4210

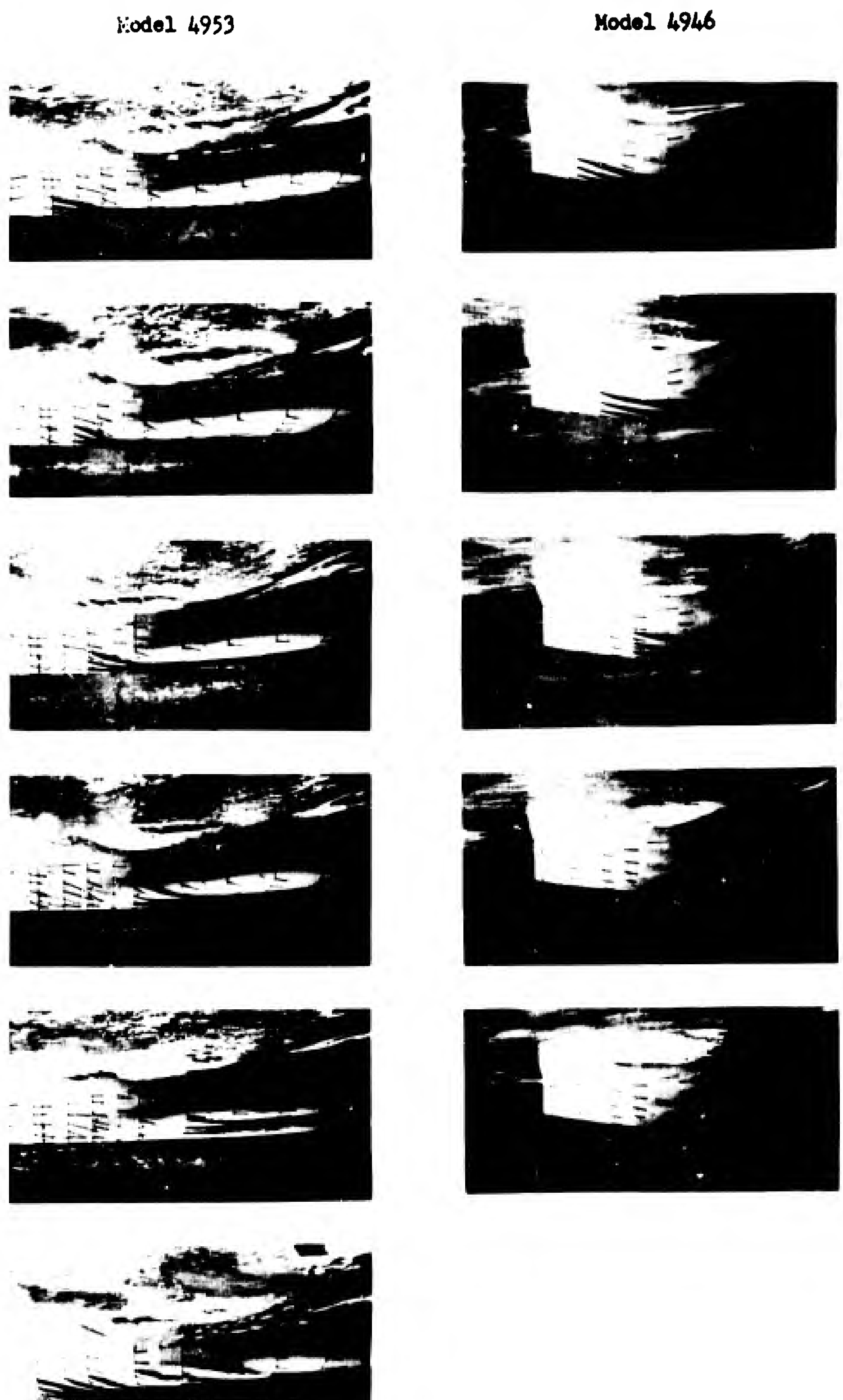

Fig. 12 - Pictures of flow on the forward end of Models 4946 and 4953

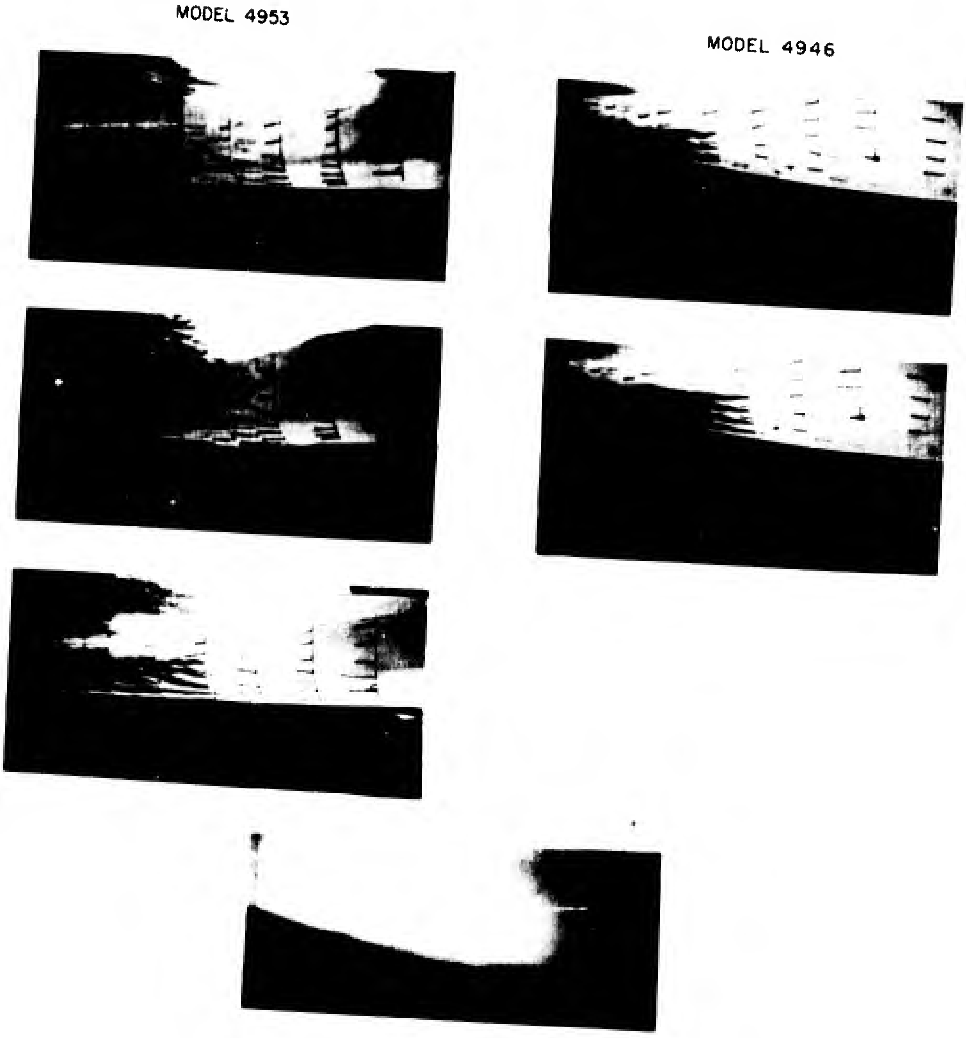

Fig. 13 - Pictures of flow on the after end of Models 4946 and 4953

reducing form drag. Then the matching main hull is designed by using the wavemaking resistance theory to ensure that the combination of the two will produce very low wavemaking resistance. Only in this manner is a bulb effective in reducing the total resistance of a ship by reducing the form drag. This may explain the reason why placing a large bulb on tanker models can result in a great reduction in total resistance at relatively low Froude numbers.

It is believed that the application of wavemaking resistance theory may have more practical value in the reduction of viscous drag than in the reduction of wavemaking resistance itself. From this point of view, the wavemaking resistance theory can always be used to reduce the total resistance of a ship regardless of its design speed.

SHIP DESIGN AND MODEL EXPERIMENT

Having finished the ground work in the first part, we now proceed to the second part of this research project. A number of ships will be designed and their models will be built and tested for resistance as well as self-propulsion. In each design problem, two models will be designed and built. The first one will have a simple stern profile. It will be tested for resistance only. The theoretical wavemaking resistance curve will be computed for comparison with the experimental curve. The second model will be obtained from the first one by modifying the afterbody for the purpose of self-propulsion tests in such a way as to obtain better propulsive characteristics. However, the original afterbody sectional area curve will be kept intact as much as possible.

One ship design has been started already, and the first model is now under construction. Perhaps it is worthwhile to discuss some of the thoughts incorporated in the design of this model.

The design conditions are very broad. It is required to develop a fast cargo ship with a displacement of 21,500 tons and a designed speed of 24 knots. A ship length of 550 ft will give a $V/\sqrt{L}$ value of 0.98 and a $\Delta/(L/100)^3$ value of 129. If normal practice is followed, a ship length of more than 550 ft would be chosen. Based on the idea of reducing viscous drag, we limit the ship length to 500 ft. This will increase the designed speed-length ratio from 0.98 to 1.07 and the displacement-length ratio from 129 to 172.

A bulb of moderate size has been adopted for the purpose of reducing eddying underneath the flat bottom. This bulb is placed above the base line so that the keel line is bent upward toward the bow. In doing so it is hoped that the favorable flow condition on the bottom of Model 4946 will also exist on this design. We have thus shaped the bow first entirely from the consideration of reducing eddying. Then the main hull is optimized in conjunction with the chosen bulb such that the forebody free-surface disturbance is very small.

To start with, only E_9 shown below is used to generate the bulb.

$$E_9 = .01 + .05\zeta^2 + .08\zeta^3 \qquad (13)$$

with $-0.8 \leq \zeta \leq 0$. E_{10} has not been included here in order to avoid excessive narrowing between the bulb and the main hull.

The next item to be considered is the η-surface. It has been found that satisfactory results can be obtained by approximating the η-surface waterline to the sectional area curve of a Standard Series Model with about the same prismatic coefficient as the model under consideration. The width and the depth of η-surface as well as the singularity distribution placed on it determine the L/B and B/H ratios of the design. To start with, the width and depth of η-surface are estimated. Satisfactory solution is obtained by trial and error.

From the eight available singularity distribution elements, we arbitrarily chose E_1 and E_3 for the main hull. The only restraint imposed upon the optimization is the required displacement volume. However, if the midship section area so obtained is too big, we can add one more restraint on the design condition so that a desirable prismatic coefficient can be obtained.

From the experience obtained from Model 4946 and many models tested by Inui at the University of Tokyo, we can anticipate a phase shift between theoretical and measured wavemaking resistance curves. The experimental curve is always shifted to the right of the theoretical curve. Therefore, in this design the optimization is done at $F = 0.28$ rather than 0.32.

At this point the computer programs are used to carry out the lengthy, tedious numerical computations. After a few trials and errors, we obtain the following singularity distribution for our final design.

$$\eta = \pm[.013\xi^6 + .04813\xi^4 - .16113\xi^2 + .1] .$$

On the side of η-surface we have

$$E_1 = [6.5504\xi - 29.0186\xi^2 + 67.4020\xi^3 - 74.7203\xi^4 + 30.2692\xi^5]$$

$$E_3 = [10.9934\xi - 61.3783\xi^2 + 158.8456\xi^3 - 183.8859\xi^4 + 75.0307\xi^5]\zeta^2 .$$

or

$$M(\xi, \zeta) = E_1 + E_3 .$$

On the end of η-surface we have

$$E_9 = .008 + .04\zeta^2 + .04\zeta^3 .$$

On the bottom of η-surface we have surface source

$$\begin{aligned} M_s(\xi, \bar{\eta}) = {} & [-.1882\xi - 2.3841\xi^2 + 15.9590\xi^3 - 28.8343\xi^4 + 13.6760\xi^5] \\ & + [2.2616\xi - 5.3769\xi^2 - 625.5772\xi^3 + 163.9480\xi^4 - 82.5272\xi^5]\bar{\eta} \\ & + [-13.3743\xi + 107.5863\xi^2 - 208.1482\xi^3 + 151.7266\xi^4 - 88.7849\xi^5]\bar{\eta}^2 \\ & + [12.2606\xi - 121.1156\xi^2 + 338.7764\xi^3 - 419.1692\xi^4 + 232.2801\xi^5]\bar{\eta}^3 \end{aligned}$$

surface doublet

$$\begin{aligned} M_d(\xi, \bar{\eta}) = {} & [.1131\xi - .4594\xi^2 + 1.5838\xi^3 - 2.7567\xi^4 + 1.6938\xi^5] \\ & + [-2.5399\xi + .9383\xi^2 - 4.1500\xi^3 + 7.5077\xi^4 - 5.1727\xi^5]\bar{\eta} \\ & + [-.3740\xi + 2.4491\xi^2 - 8.8036\xi^3 + 12.8106\xi^4 - 5.2930\xi^5]\bar{\eta}^2 \\ & + [.4157\xi - 3.4692\xi^2 + 1.3092\xi^3 - 20.3145\xi^4 + 1.0316\xi^5]\bar{\eta}^3 \end{aligned}$$

with $-0.08 \leq \zeta \leq 0$ and $0 \leq \xi \leq 1$, where $\bar{\eta}$ is the nondimensional distance from the central plane as normalized by the local offsets of η-surface.

The afterbody has been chosen as the mirror image of the forebody. This model is denoted as Model 4996.

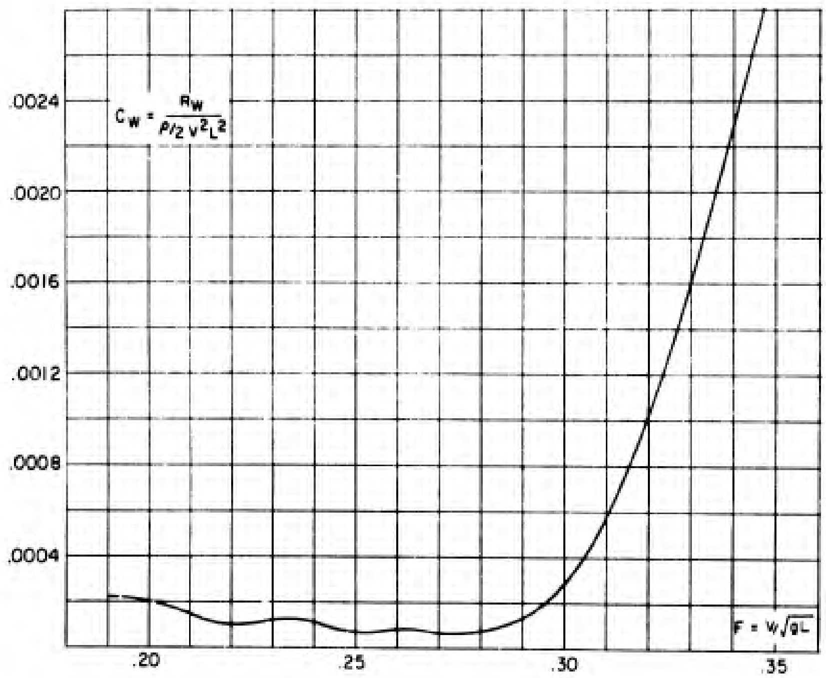

Fig. 14 - Theoretical c_w curve of Model 4996

The theoretical c_w curve for this design is given in Fig. 14 and the body plan and waterline endings are shown in Fig. 15. Due to certain limitations in the second computer program, we cannot obtain a true flat bottom. Some hand fairing is necessary at the present time. However, such fairing is limited to the bottom portion of a model only. In the case of Model 4996 as shown in Fig. 15, such fairing is done below the 0.3' W.L. An effort is being made to eliminate this shortcoming in the computer program.

Model 4996 has a B/H ratio of 2.64, a L/B ratio of 5.82, $\Delta/(L/100)^3$ ratio of 172.2. These proportions are very desirable, especially the large displacement-length ratio which has a large influence on the per ton construction cost. The experimental result of Model 4996 is anxiously awaited.

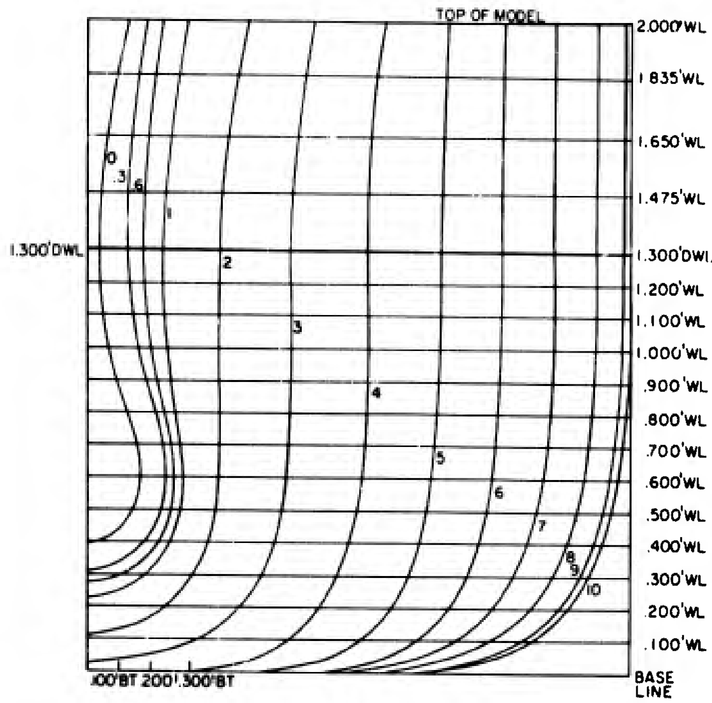

(a)

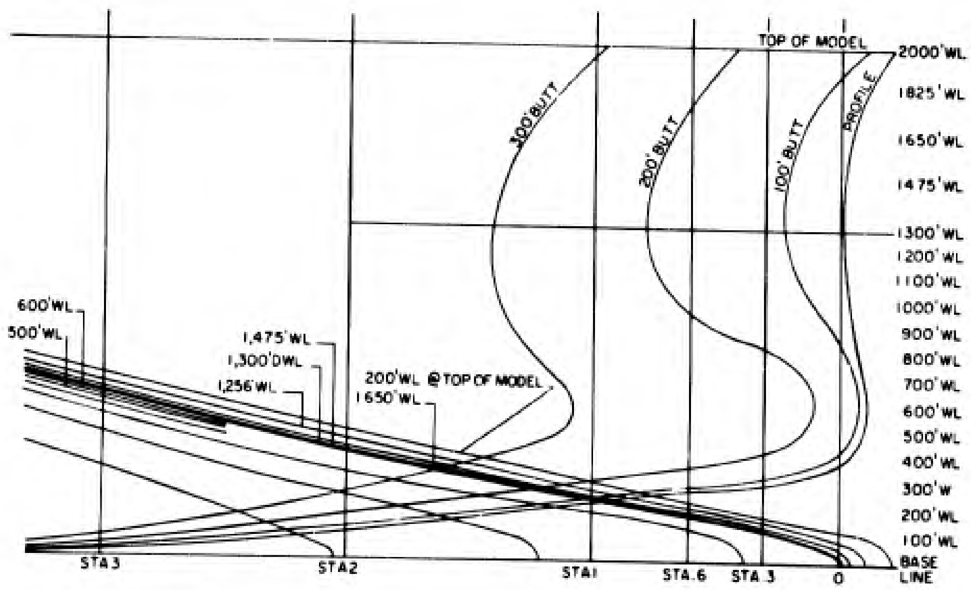

(b)

Fig. 15 - Body plan and waterline endings of Model 4996

CONCLUDING REMARKS

While fully aware of the limitations of the existing theory, we believe that useful results have been achieved without exceeding these limitations. By restricting the analysis to forms of absolute low-wavemaking we have not unduly violated the linearization at the free surface, and by recognizing the relative importance of forebody wavemaking we have avoided some of the problems of viscosity.

The idea of reducing the viscous drag of a ship through the application of the wavemaking resistance theory is rather interesting. It may have an important influence in the design of future ships.

However, even though the arguments used in this paper to support our views and ideas are quite logical and plausible, the final proof of the validity of these arguments rests on model experiments to be carried out in the very near future.

ACKNOWLEDGMENT

The author wishes to thank Mr. Louis F. Mueller of the Applied Mathematics Laboratory for his help in the computer work.

NOTATION

a, b, n	Three parameters defining η-surface
a_{ij}	General coefficient in Eq. (2)
B	Ship beam
B_1	Defined by Eq. (7)
C_t	Total resistance coefficient
C_W	Wavemaking resistance coefficient
d_j	General coefficient in Eq. (4)
$D(\zeta)$	Strength of a line doublet
E_1, E_2, E_3, E_4	Surface source distribution elements
E_5, E_6, E_7, E_8	Surface doublet distribution elements
E_9	Line source distribution element
E_{10}	Line doublet distribution element
F	Froude number

g Gravitational constant

H Ship draft

H_b Total head referring to the undisturbed condition

H_b Total head referring to the behind condition

K Form factor used with Hughes friction line

L Ship length

$M(\xi, \zeta)$ Density of surface singularity distribution

M_o Surface source density at $\xi = 1$

R_t Total resistance

R_W Wavemaking resistance

s_j General coefficient in Eq. (3)

$S(\zeta)$ Strength of a line source

T Depth of singularity distribution

T_1 Defined by Eq. (8)

V Ship speed

V_1 Defined by Eq. (6)

ξ, η, ζ Coordinates

Δ Displacement.

REFERENCES

1. Emerson, A., "The Application of Wave Resistance Calculations to Ship Hull Design," INA (1954) pp. 268-275

2. Inui, Takao, "Study on Wavemaking Resistance of Ships," 60th Anniversary Series of the Society of Naval Architects of Japan, Vol. 2, pp. 173-355

3. Breslin, J. P. and Eng, K., "Calculation of the Wave Resistance of a Ship Represented by Sources Distributed over the Hull Surface," Davidson Laboratory Report No. 972 (July 1963)

4. Pien, P. C. and Moore, W. L., "Theoretical and Experimental Study of Wavemaking Resistance of Ships," Internation Seminar on Theoretical Wave Resistance, University of Michigan, Ann Arbor, Michigan (August 1963)

5. Wu, J., "The Separation of Viscous from Wavemaking Drag of Ship Forms," Journal of Ship Research, Vol. 6, No. 1 (June 1962)

* * *

DISCUSSION

G. P. Weinblum
Institut für Schiffbau
University of Hamburg
Hamburg, Germany

Leaving aside basic theoretical considerations in the field of wave resistance, we consider Dr. Pien's recent proposal a valuable contribution following which bodies are generated in a uniform flow by distributing singularities over a suitably chosen skeleton surface instead of over the central plane. By these "Pienoids" a serious difficulty has been mitigated when investigating hull forms of least or low wave resistance; the recent trend to study flow conditions by determining singularities over a prescribed body surface makes an optimisation of the latter obviously impossible.

In the present paper an attempt has been made to apply theory to the solution of a rather general engineering problem, the determination of hull forms of low total resistance (instead of low wave resistance, etc.). The exposition of this important task is in my opinion slightly impaired by some global and deprecating statements made by the author. Some aspects of the problem have been clearly described by D. W. Taylor in his "Speed and Power of Ships"; cf., his famous sketch representing the total rest and frictional resistance R_t, R_r and R_f of a given dimensionless form and V = const. as function of the length. The essential difficulty consists in finding the wave and viscous drag components leading to an optimum.

It is typical and unavoidable that one has to face the viscous resistance problem when dealing with the wave resistance. The author asserts that we know how to shape a deeply submerged body of low viscous drag. This is correct as long only as a qualitative reasoning is concerned. Reference is made to the pertaining formulas

$$C_v = (1 + n)C_{f0}$$

with

$$n \doteq 2.2\ B/L + \ldots$$

for a cylinder;

$$n \doteq 0.6\ D\ L + \ldots$$

for a body of revolution;

$$n \doteq 19(C_B B\ L)^2$$

Granville's formula for shiplike bodies.

The primitive character of these relations indicates that quite a bit of research work should be done before the author's optimistic statement can be accepted, e.g., with regard to dependency of the drag of full forms upon proportions. Contrary to his optimism, Dr. Guilloton has recently expressed the opinion (Bull. Ass. Technique Maritime, 1964) that our knowledge of viscous drag as function of the hull form is almost nil.

The difference in the total resistance R_t of Model 4946 and Model 4953 can be explained by viscous as well as by wave effects. The former are estimated by R_{total} at low F (as pointed out by the author), the latter by the intersection of resistance curves at $F = 0.30$. The difference in the prismatic coefficients is helpful for such a phenomenological discussion.

The author emphasizes as a new result that the wave drag of a fat ship can be smaller than for a thin ship. In the light of Taylor's findings (and those deduced from theory) this may be trivial in a range where R_W depends strongly upon the prismatic coefficient. Examples based on theoretical calculations have been frequently given; some caution, however, in the quantitative application is advisable.

The shift of the measured wave drag curve to higher F as compared with theory has been firmly established by Wigley and Havelock.

The author asserts that in the field of comparison between theory and facts almost only the work done by Prof. Inui counts. Although I am an admirer of the valuable contributions made by our distinguished chairman the author's statement is in my opinion erroneous; the most valuable experiments are those by Mr. Wigley (TINA 1924) and the TMB Report where the so-called friction plate furnished by mistake the ideal thin ship model.

It is erroneous to assume that wave resistance results by computation are always larger than those derived by experiment; this certainly does not apply to hull forms which by theory are extremely advantageous (due to strong interference effects which may be destroyed by viscosity).

The hull form proposed by the author appears to be promising for medium Froude numbers ($c_p = \varphi = 0.58$, moderate bulb, gentle turns of bilge). The raised bulb, however, may be unfavorable in a seaway, especially under ballast conditions.

The attempt of applying theoretical reasoning to actual design problems is highly appreciated.

DISCUSSION

K. Eggers
Institut für Schiffbau
University of Hamburg
Hamburg, Germany

I have to make a general remark concerned with the method by which Dr. Pien and other colleagues find hull forms for which certain singularity distributions are considered representative for calculation of wave resistance.

We know that by the Hess-Smith procedure we can determine source distributions on surface of these hull forms, and that wave resistance for such distributions then can be calculated along the lines developed in the paper of Breslin and Eng.

I declare that there is definitely no convincing argument for the assumption that resistance calculations for these alternative singularity distributions should, precise numerical methods assumed, lead to identical values.

Furthermore, we can create systems of arbitrary high wave resistance, which still generate the same flow around the double body under infinite gravity, just by proper linear combination of both kinds of distributions!

Which wave resistance then is to be considered the 'correct' one, assuming now the form to be given? We could select the lower limit from the class of all distributions representing the form under infinite gravity and constant speed at infinity. But probably this value is not attained by a single distribution over the whole range of Froude numbers.

It is easily shown that for any form of nonzero volume there must exist more than one distribution to represent it in infinite fluid. We can, for instance, at any interior point add a source layer of constant strength on a surrounding sphere, compensated by a corresponding sink layer on an exterior concentric sphere such that there is no resulting flow outside.

In case of a submerged body this will not change the wave resistance. In case of a floating body, however, only the part of the additional system below the undisturbed free surface will contribute within linear theory. The flow due to this lower part only will in general not vanish outside and will thus induce additional waves.

Take the case of a semi-submerged spheroid. This can be represented by volumetric dipole distributions in any confocal spheroid, equivalent to source layers on the surfaces. As a limiting case we get a line dipole distribution between the foci. This latter gives the largest, i.e., infinite resistance.

For a singularity distribution found by analytical methods to be optimal within a certain class, we may determine some associated body form by tracing stream lines. But if the body is piercing the undisturbed free surface, why should just this distribution be selected for calculation of wave resistance?

Intuitively, I would prefer the combined source-dipole layer on the surface used in Green's theorem, as this has minimal, i.e., zero-inner kinetic energy. In any case we have to formulate proper restrictions for the flow within a ship's waterplane area to keep variation of resistance calculated in reasonable limits.

* * *

DISCUSSION

J. N. Newman
David Taylor Model Basin
Washington, D.C.

There has been considerable discussion this afternoon concerning the relative importance of nonlinearities in the free surface condition, and now Dr. Pien has advanced the suggestion that the linear free surface condition is valid for "fat" ships if they are ships of low wave resistance, or that fat ships of minimum wave resistance are equivalent to thin ships, as far as the free surface condition is concerned. This may in fact be a valid analogy from the engineering standpoint, but I hope that it will not be confused with a rigorous mathematical development.

A necessary condition for the linearized free surface assumption is that the elevation of the free surface is everywhere small, compared to the wave length of a characteristic wave. This is clearly true for a thin ship since (in an ideal fluid) the fluid disturbance and free surface elevation can be made arbitrarily small by making the ship sufficiently thin. The free waves or far-field disturbance associated with a ship of minimum resistance will also be small because wave resistance implies wave energy radiation, but the free surface disturbance near the ship will not necessarily be small since this is a local disturbance and is essentially independent of the wave resistance of the ship. An obvious example is the waveless (infinite draft) ship discussed by Dr. Yim; for this case there will be no free waves and the linearized free surface condition will clearly be justified in the far-field, but close to the ship there will be a local disturbance which can be made arbitrarily large simply by increasing the singularity strength. In other words, a ship of low wave resistance will satisfy the linear free surface condition over most of the free surface, but not necessarily close to the ship.

Please let me emphasize that my objection is based upon the rationality of the theory, and not upon practical considerations. For practical purposes I would encourage the use of the linear theory, as long as it gives satisfactory results. Intuitively I would agree with Dr. Pien that a ship of small wave resistance will probably have less associated nonlinear effects from the free surface than another ship of the same principal dimensions but larger wave resistance.

* * *

DISCUSSION

Lawrence W. Ward
Webb Institute of Naval Architecture
Glen Cove, Long Island, New York

Dr. Pien has presented a very stimulating paper and one which I feel is essentially correct, but I would like to take this opportunity to discuss two points which I feel are of importance in connection with this work and with some of the other papers given this afternoon as well.

The first point is that of the question of the definition of wave resistance which is essentially that of the definition of wave resistance in real fluid since in the case of an ideal fluid all definitions seem to lead to the same result. There are a number of definitions possible, depending on the use to which the definition is to be put; and I would like to review this matter with you at the risk of boring those who were at Ann Arbor with the help of a table similar to one shown at that time (Fig. 1). Since the theory of wave resistance in a real fluid

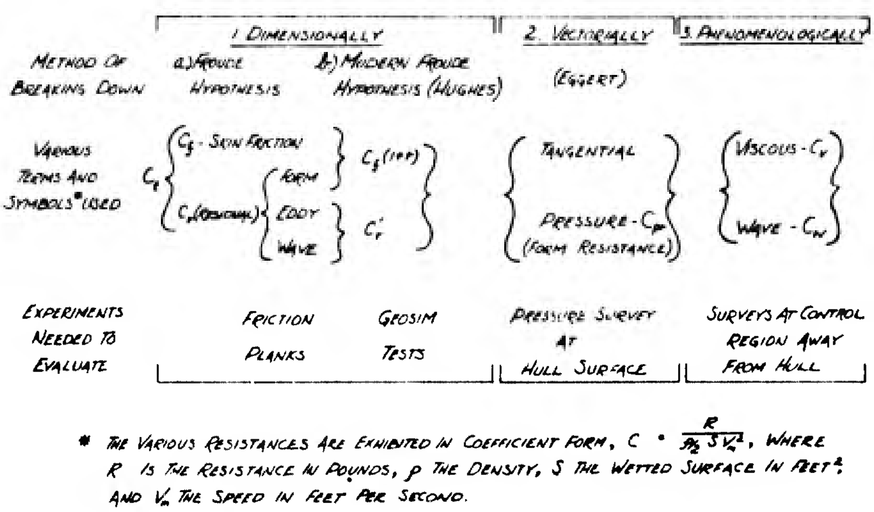

Fig. 1 - Various breakdowns of ship resistance into components

has not been developed to any useful extent, I have included only those definitions which can be related to experiments in some way.

In Fig. 1 various breakdowns of ship resistance into components are shown in historical order from left to right. First we have (1-a) Froude's hypothesis and (1-b) the modernization thereof by Hughes. Here the goal is mainly that of model scaling, and the breakdown into frictional and residual components is done on the basis of dimensional analysis, that is, Buckingham's Pi Theorem. Froude's original hypothesis was that the total resistance could be separated into a "residual" part, C_r, depending on the Froude number and a frictional part depending on the Reynolds number. In practice, the latter was estimated as being the skin friction, C_f, of a plank of the same length and wetted area. This results in the residual resistance including some viscous effects due to separation. These are sometimes termed "form" and "eddy" resistance. Hughes added the concept of a form effect $(1+r)$ on C_f derived from tests of geometrically similar models (Geosim tests), this being a practical improvement only if such factors do not depend strongly on the Froude number and can be estimated without recourse to such tests. By assuming no Froude number dependence, the form resistance can also be estimated on the basis of the resistance at low Froude numbers where the wave resistance is expected to be negligible. The corrected residual resistance, C_r', includes the wave resistance but also an undefined portion of the eddy and form resistance, probably that part which is Froude number dependent.

The second listed breakdown is with respect to the vectorial nature of the local fluid stresses at the hull boundary, i.e., tangential shear and normal pressure. The latter are determined from a pressure survey over the entire hull and then are integrated in conjunction with the known hull surface slopes to give a resultant pressure drag component, C_{pr}. This can then be subtracted from the measured total drag to deduce the integration of tangential viscous shear stresses. It should be pointed out that the major effects of viscous separation are not included in this force component but in the normal pressure drag component. The required experiments and analysis, originally done by Eggert and more recently by Townsin and Hogben are quire extensive. While historically interesting, this has not yet proved to be a practical means of meeting any important goal.

The third breakdown is with respect to the physical phenomena involved, i.e., the formation of waves and the development of a viscous shear wake. Here the question of breakdown reduces to that of separating the total momentum survey around a closed control volume away from the hull into (a) that portion involving the viscous wake and (b) that due to wave orbital velocities, and then integrating these to obtain C_v and C_w, respectively. The experimental techniques available to measure the wave resistance, C_w, are therefore either (a) a direct momentum survey of the waves making a proper correction in the wake region or (b) a valid viscous wake survey adjusted for the presence of waves which is then subtracted from the measured total resistance. The latter method, which has been employed for example by Landweber, is less direct and might suffer from inaccuracies due to the process of taking differences of large numbers. In addition, one must assume that there is no third mechanism of energy dissipation present, which has not been proven yet. It is the third breakdown of total resistance that I tend to favor. The wave resistance is in this way defined in terms of the energy actually going into the wave system in the real fluid (not for example what might be the energy going into the wave system of the same ship in an ideal fluid). It is evident that no direct relationship between the wave resistance, C_w so defined, and the pressure resistance, C_{p_r}, or the residual resistance, C_r (or C_r'), need necessarily exist, and this is the p‹›nt I wish to make. Recognition of this can eliminate pointless arguments as to which method of measuring wave resistance is correct.

My second point deals with the various statements by Dr. Pien on pages 1110-1116 and the results given in Table 1 and Fig. 1 of Dr. Pien's paper. The statements which I refer to and which seem to be backed up by comparison of theory and experiment are those which infer that the theory approaches the experimental values in some monotonic way (a) as the Froude number gets larger and (b) as the wave resistance gets smaller and furthermore that Michell's prediction forms an upper bound to the experimental wave resistance. I find it hard to believe that the situation in general is that simple and would like to point out some evidence to the contrary. The first involves experimental results I obtained in the Webb tank from direct measurement of the wave pattern using the "XY" method of analysis. The first (Fig. 2) shows this result for the ATTC Standard Model which is also the parabolic form Wigley tested and reported in 1926-7 in the INA. It can be seen that there is in fact a region where Michell's estimate is less than the wave survey result, and it would also be less than the residual resistance with a suitable Hughes form factor. The second result (Fig. 3) is a series of tests using the same method on the Series 60, 0.60 block model carried out to very high Froude numbers and while there is some question of the circular cylinder used in the method being large enough at the high Froude number end of the curve, it is obvious that a very major adjustment in the data would be required to bring theory and experiment together in this range.

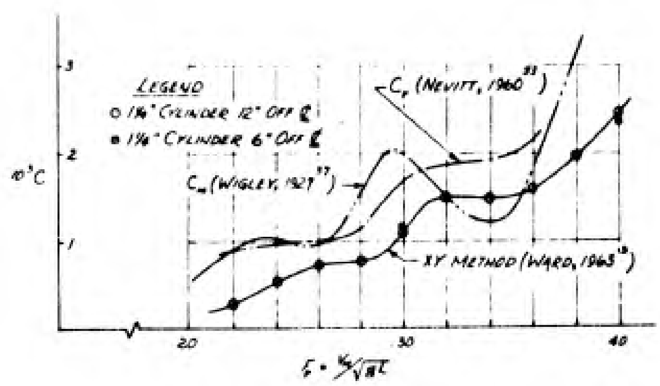

Fig. 2 - Experimental wave resistance of the ATTC standard model (L = 5 ft 4 in.)

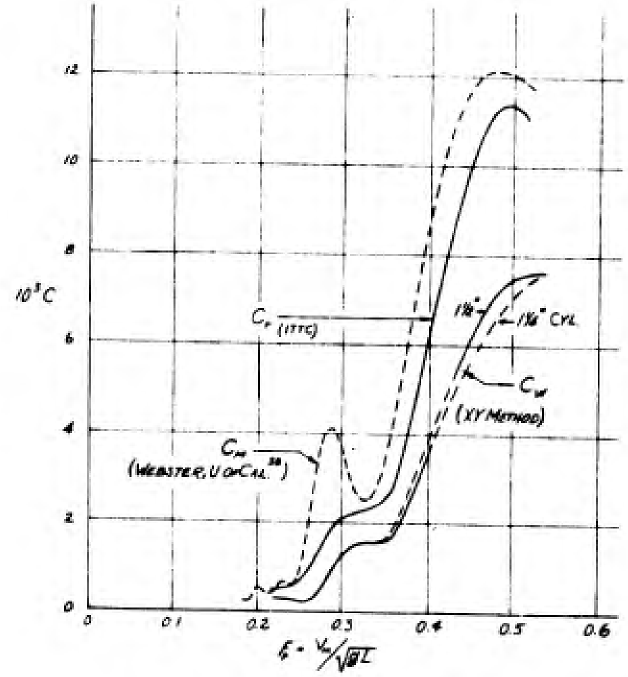

Fig. 3 - Experimental wave resistance of the 5 ft 0 in. Series, 60 Model (0.60 Block)

Finally, I should like to say in reference to the suggested improvement in agreement of theory and experiment as either value becomes small, Wigley himself as most of us know tested two models of the parabolic form of 3/4 and 1/2 the beam of the original, which was already quite a thin ship, with no such improvement in agreement between the experimental values obtained and the Michell's calculation which, of course, remained constant (on a coefficient basis). I do not mean to imply that Dr. Pien's results are not correct but that they should not be looked at as being general.

* * *

DISCUSSION

A. Silverleaf
National Physical Laboratory
Teddington, England

Dr. Pien's work in applying wavemaking resistance theory to ship design is held in the highest regard at N.P.L., and this latest progress report contains many fruitful ideas. A general programme of research into low resistance hull forms is now being undertaken at N.P.L.; this includes experiments to examine Pien's suggestion that the double model approximation should give closer agreement between calculated and measured resistances for source distributions having low wave resistance than for resistful forms. Two bodies are being designed from wave source theory, each consisting of a bow shape followed by a long parallel afterbody, and an attempt will be made to measure their head resistances alone. One of these forms does not have a particularly low calculated wave resistance, but the second has been optimised following the same general principles as those adopted by Pien. If good agreement between theory and experiment is obtained for this second form, we believe that it will aid significantly in using wave source theory as a practical design tool in the way indicated in this paper.

The assessment of the results of any such study of calm water resistance effects depends on the establishment of a recognised yardstick or resistance criterion. In assessing wave resistance alone, this criterion should preferably involve only the displacement, speed and length. Displacement and speed are the primary specified operational requirements, and length may be regarded as a primary limiting parameter. The hydrodynamic criterion of quality should be based on the maximum immersed length, thus imposing a penalty on a device, such as a projecting bulbous bow, which reduces resistance at the expense of increased underwater length. Not all comparisons have been made on this basis and it is more than possible that this has influenced the conclusions drawn from them.

* * *

DISCUSSION

S. W. W. Shor
Bureau of Ships
Washington, D.C.

In commenting on Dr. Pien's paper I first wish to congratulate him on the persistence with which he has pursued his search for a practical solution to the problem of reducing the total resistance of a ship's hull. The fact that this search seems verging on a successful result with even more general applicability than we had dared hope is most gratifying.

As to the details of his paper, I wish to invite attention particularly to two of his statements which are corroborated by my own work.

First, Dr. Pien is quite correct that the best approach within the confines of existing ship wave theory is to optimize the shape of the forebody of the ship, and then to design the stern separately. This means that he does not count on using the stern waves to cancel the bow waves, but instead sees to it that the forebody does not generate bow waves. This approach is suggested by Inui's work. We may recall that Inui found that bow wave amplitudes are close to those predicted by theory, particularly if they are small, but that stern wave amplitudes are significantly smaller than those predicted. The ratio of observed to predicted stern wave amplitude is Inui's parameter β, and it becomes quite small at low Froude numbers. At the Froude numbers around 0.3, for which Dr. Pien has designed his models, the value of β for Inui's Model S-201 is under 0.7, and for S-202 is even smaller, just above 0.5. This means that the stern waves, which by theory for these double-ended hulls should be as big as the bow waves, are in reality only a little over half as big and so cannot do much to cancel the bow waves. Worse, they are generated in the frictional wake which moves in the same direction as the ship, and so their transverse components must have a shorter wave length than the transverse components of the bow wave if the stern wave pattern is to move with the ship. Waves must both move in the same direction and have the same wave length if they are to cancel. It is therefore evident that in practice we cannot expect cancellation of the transverse portions of the bow wave by the transverse portions of the stern wave even to the extent suggested by the existence of non-zero values of β. It is possible to show, also, that transverse components of the bow wave should not penetrate into the wake at all, but should be reflected from its boundary so that cancellation becomes impossible. This, of course, can also be deduced from Inui's experimental observation of the wave-shadow effect. Because of this we should not expect complete cancellation of bow waves by stern waves even at Froude numbers much higher than 0.3 where the value of β approaches unity much more closely.

Actually, it is possible not only to provide an explanation for Inui's semi-empirical parameter β from the fact that viscosity causes water to be dragged along with the ship, but an estimate of how much this reduces the velocity of water relative to the stern. As a result of viscosity the stern waves are generated by water moving at a velocity relative to the hull which is somewhat less than that of the water which generates the bow waves. How much less can be deduced by working backwards from Inui's results. This has been done in Fig. 1, where the ratio c_r/c is that ratio of relative speed of ship and water at the stern to the forward speed of the ship which is required to fit Inui's curves of β vs Froude number. As shown in Fig. 1, the ratio does not change much over a wide range of speeds. Although the bow, as Pien points out, should be optimized at a speed close to the speed of the ship (he optimized at $F = 0.28$ for a ship with actual speed $F = 0.32$), it follows from the data shown in Fig. 1 that the stern should be optimized for a much lower speed. For example, referring to the figure, if we were to optimize the stern of hull S-202 to operate at a ship speed of $F = 0.32$, we should optimize the stern at a Froude number (c_r/c) $(0.32) = (0.66)\ (0.32) = 0.21$.

A second point which Dr. Pien makes is that the conventional hull form parameters must be disregarded when hull forms are optimimized. Certainly I find this to be true. I have just finished a calculation using the method of steep descent to decrease the wave resistance of a destroyer type ship intended to operate at 30 knots, and in the calculation I held constant the sectional area curve as well as the load waterline, the sound dome, and the draft. The calculation, which started with a hull designed by a good naval architect, had to make auxiliary functions arising from each term obtained by squaring the left-hand side of Eq. (2) are analogous to his functions tabulated in TMB Report 886. The main difference is that Eq. (2) is used to express the singularity distribution which will generate the hull form rather than to express the hull form directly. With this remark, I shall attempt to answer a number of points raised by him as follows:

It would indeed be erroneous to make a general statement that wavemaking resistance values as computed are always larger than those obtained experimentally. Remark 1 in the justification of application section of my paper was based on the observation of Fig. 1 that if the wavemaking resistance theory is applied to the forebody only, where the viscosity effect is small, the theoretical prediction based on Professor Inui's method will be an upper limit to the possible experimental wavemaking resistance values. I am fully aware of the fact that strong favorable interference effect may not be realized due to the viscosity effect. I mentioned this fact as a source of difficulty when the wavemaking resistance theory is applied to a whole ship. Hence the importance of minimizing the forebody free-surface disturbance has been advocated.

In the past, many comparisons have been made between the theoretical and experimental wavemaking results. No consistent conclusion has been reached from these comparisons. One of the main causes is due to the fact that the theoretical model and the experimental model are not "exact" as explained clearly by Inui in Ref. 2. Therefore it is extremely important to know whether the theoretical and the experimental models are equivalent or not, when we study the comparisons. To illustrate this important point, let us study the comparisons of three models made by Mr. Wigley in 1927.

Figure A is a replot of a portion of Mr. Wigley's original comparisons. In this figure, C_w versus Froude number (and $V/\sqrt{L}$) curves are plotted instead of Ⓒ$_w$ versus Ⓟ as in the original figure. Models 825, 829 and 755 are identical except in beam scale. Model 825 has the smallest beam and its theoretical prediction at high Froude number, where the viscosity effect is small, should be closer to the experimental curve than in the cases of the other models. However, this figure does not show this fact. This apparently puzzling situation had been cleared by Professor Inui thirty years later in Ref. 2. Figures B and C are taken from Ref. 2. Figure B shows how the singularity distribution per unit beam varies with beam instead of being constant as in the Michell's thin ship theory. Figure C shows how the wavemaking resistance coefficient $R_w/\frac{1}{2}\rho v^2 B^2$ varies with beam rather than independent of beam as Michell's theory asserts. Even though both of these figures are for the case of infinite draft, it is quite obvious that the theoretical wavemaking resistance curves computed according to Professor Inui's method would be higher than the experimental curves at high Froude number range for all of these three models. The overestimation by the theory varies depending upon the level of wavemaking resistance: the higher the wavemaking resistance level, the larger the overestimation. This agrees with remark 2 made in the justification of application section of the paper.

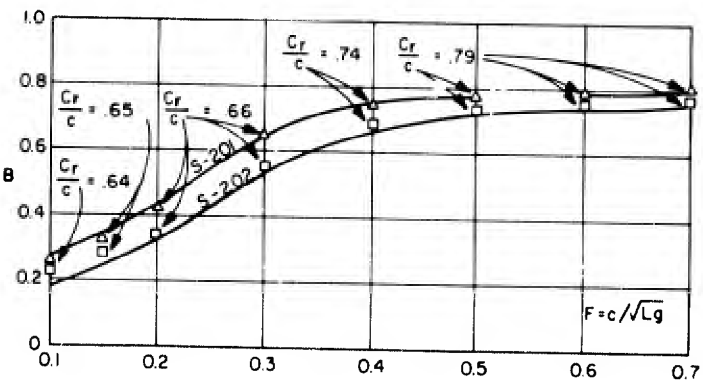

Fig. 1 - The parameter β for Models S-201 and S-202, with calculated values for the ratio c_r, c varying with speed. Curves are Inui's experimental values. Triangles are values calculated for Model S-201 and squares for Model S-202.

a considerable change in hull shape within the given constraints to work a one percent decrease in the wave resistance. It was obvious from some of the intermediate quantities computed that with less constraint much more improvement could have resulted from the same amount of departure from the given hull form. The calculation was therefore repeated with the constraint that increases but not decreases in hull volume could be accepted. Under this constraint, which is much less rigid than one which holds the sectional area constant, the same amount of calculation as used before resulted in a forty percent decrease in the wavemaking resistance instead of the one percent achieved under the constraint of constant sectional area.

* * *

REPLY TO THE DISCUSSION

Pao C. Pien
David Taylor Model Basin
Washington, D.C.

PROFESSOR WEINBLUM

Professor Weinblum's comment has been studied with great admiration. His work has greatly influenced my thinking in carrying out the work reported in the paper. For instance, the surface singularity distribution expressed by Eq. (2) is quite similar to his polynomials representing ship surface. Likewise,

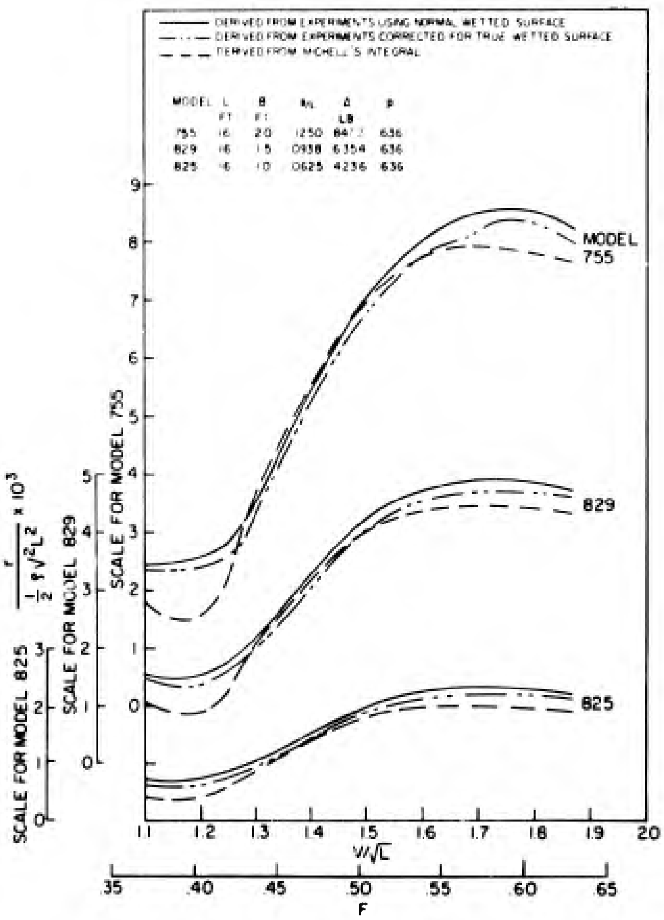

Fig. A - A comparison of the theoretical and experimental wavemaking resistance results of Models 755, 825, and 829

From the above discussion, then, it should not be unduly criticized for th fact that only Professor Inui's comparisons have been shown in Fig. 1 of the paper.

The fact that a fat ship can have smaller wave drag than a thin ship has r been stated in the paper as a new result. It is merely used to make the argument that the existing theory can be applied to a fat ship with very small wav drag as well as to a thin ship. The term "fat" has been used to indicate a lar displacement-length ratio rather than a large beamlength ratio.

In the light of Taylor's findings, R_w may seem to depend strongly upon th prismatic coefficient. However, our experience based on the experimental re sults of models derived according to the method described in the paper is tha the prismatic coefficient may not always be the dominating factor upon the wa resistance. For example, our most recent experimental results of a model w

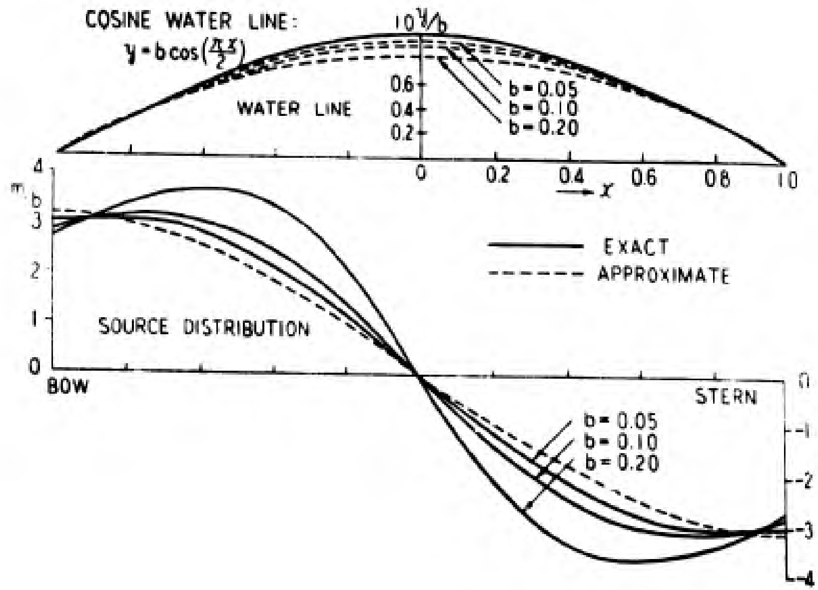

Fig. B - Comparison in waterline
and in source distribution

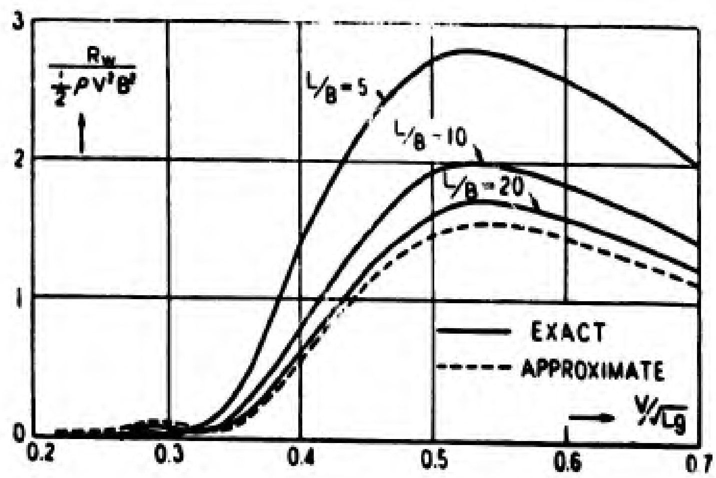

Fig. C - Comparison in wavemaking resistance
at high speeds (cosine waterline)

a prismatic coefficient of 0.64 showed that the C_T value of this model at $V/\sqrt{L} = 1.1$ is almost the same as that of a Taylor's Standard Series Model with the same beam-draught and displacement-length ratios, but with a much smaller prismatic coefficient value of 0.59.

Another point mentioned in Professor Weinblum's comment is related to the viscous drag which is much more complicated than wave drag. Our knowledge of viscous drag as functions of the hull form may be almost nil from the scientific viewpoint. But for practical ship design, it may not be a too difficult task to shape a form with a constant volume such that its viscous drag can be kept within reasonable limits. Besides these formulae quoted by him, there are thousands of models having been tested at Froude number ranges where the wave drag is very small in comparison with the viscous drag. Additional practical information as to the reduction of viscous drag of ship hulls may be extracted from this source.

DR. EGGERS

Dr. Eggers' comment is very interesting. It is indeed true that for a given body in infinite fluid there are many possible singularity distributions to represent that body. But for a given singularity distribution, we have a quite different situation. In this case, we should determine the body correctly by including the free-surface effects. Since such procedures are very time consuming, a double model technique has been used in the paper. Then the logical question is, how much difference is there between these two bodies so obtained. Such difference depends upon the singularity distribution under consideration. As mentioned in the paper, if it disturbs the free surface very little, such difference would also be little. Since we are interested in singularity distributions which produce very small free-surface distributions, we may not need to be too seriously concerned with the point raised by Dr. Eggers. In the meantime, we are considering the possibility of tracing the streamline by including the free surface effect.

DR. NEWMAN

Dr. Newman points out that a ship of low wave resistance will satisfy the linear free surface condition, but not necessarily close to the ship. Since the wavemaking resistance depends on the far field free surface disturbance only, it would be interesting to know, in such case, to what extent the local disturbance influences the accuracy of the computed wavemaking resistance.

In general, when we deal with ship-shape forms such a situation is not likely to occur. Professor Inui and his students in Tokyo University have computed many wave profiles along the side of ships. The local disturbance seems to be always much smaller than the free wave disturbance.

PROFESSOR WARD

Professor Ward gives a clear picture as to how the ship resistance has been divided into its components in many different ways. At the present time, the "Modern Froude hypothesis (Hughes)" has been used until the technique of obtaining the wavemaking resistance more directly is perfected.

Another point raised by Professor Ward is related to my remarks on the theoretical and experimental wavemaking resistance comparisons. I believe this point has already been covered in my reply to Professor Weinblum's comment.

MR. SILVERLEAF

Mr. Silverleaf's comment has been studied with great interest. The results from their experiment with two bows, one having low wave resistance and the other having resistful form, with a long parallel afterbody would be very revealing. I hope he will publish these results when they are available.

Mr. Silverleaf has suggested that in assessing wave resistance alone, the criterion should preferably involve only the displacement, speed, and length. The basic aim of any ship design is to obtain a hull form to carry a specified payload at a specified speed, safely and economically. The principal dimensions, especially the length, should be kept as small as possible so that the hull weight and building cost can be kept low. On the other hand, the smaller the length, the higher the $V/\sqrt{L}$ value and consequently, the higher the wave resistance. For a chosen length, smaller beam and draft values would result in a higher prismatic value. In the range of Froude number from, say, 0.9 to 1.2, increase in prismatic may also have a detrimental effect upon wave resistance. Higher resistance means higher machinery weight, fuel weight, and fuel consumption. Therefore, a final design is always a compromise between these contradictory factors. Then how could we assess the merit of any design on wave resistance alone, fairly? In view of the fact that the principal dimensions and the prismatic coefficient are decided upon by many factors besides wave resistance, we cannot assess the merit of such decision purely from the resistance standpoint. Therefore, for a fair comparison of wave resistance or total resistance, we have to compare with forms of same principal dimensions and prismatic coefficient. For this purpose, an equivalent Taylor's Standard Series form can be used as a yardstick.

CAPTAIN SHOR

Captain Shor's explanation of the parameter β as used by Professor Inui is quite interesting. At present, even though a few semi-empirical parameters, as used by Professor Inui, can bring the theoretical wavemaking resistance curve into good agreement with an experimental curve, the values of these parameters cannot be predicted accurately before the experiment is conducted. The flow near the stern of the ship is greatly complicated by the viscosity effects. It is very difficult to estimate the wavemaking ability of the afterbody of a ship. For this reason we cannot expect the theory to give an accurate prediction. The theory is used in the paper for obtaining relatively good hull forms.

In conclusion, I would like to thank all the discussers for their valuable comments.

* * *

AUTHOR INDEX

U.S. GOVERNMENT PRINTING OFFICE : 1966 O - 221-249